

Lecture Notes in Civil Engineering

Vito Ferro · Giuseppe Giordano ·
Santo Orlando · Mariangela Vallone ·
Giovanni Cascone ·
Simona M. C. Porto *Editors*

AIIA 2022: Biosystems Engineering Towards the Green Deal

Improving the Resilience of Agriculture,
Forestry and Food Systems in
the Post-Covid Era

 Springer

Lecture Notes in Civil Engineering

Volume 337

Series Editors

Marco di Prisco, Politecnico di Milano, Milano, Italy

Sheng-Hong Chen, School of Water Resources and Hydropower Engineering,
Wuhan University, Wuhan, China

Ioannis Vayas, Institute of Steel Structures, National Technical University of
Athens, Athens, Greece

Sanjay Kumar Shukla, School of Engineering, Edith Cowan University, Joondalup,
WA, Australia

Anuj Sharma, Iowa State University, Ames, IA, USA

Nagesh Kumar, Department of Civil Engineering, Indian Institute of Science
Bangalore, Bengaluru, Karnataka, India

Chien Ming Wang, School of Civil Engineering, The University of Queensland,
Brisbane, QLD, Australia

Lecture Notes in Civil Engineering (LNCE) publishes the latest developments in Civil Engineering—quickly, informally and in top quality. Though original research reported in proceedings and post-proceedings represents the core of LNCE, edited volumes of exceptionally high quality and interest may also be considered for publication. Volumes published in LNCE embrace all aspects and subfields of, as well as new challenges in, Civil Engineering. Topics in the series include:

- Construction and Structural Mechanics
- Building Materials
- Concrete, Steel and Timber Structures
- Geotechnical Engineering
- Earthquake Engineering
- Coastal Engineering
- Ocean and Offshore Engineering; Ships and Floating Structures
- Hydraulics, Hydrology and Water Resources Engineering
- Environmental Engineering and Sustainability
- Structural Health and Monitoring
- Surveying and Geographical Information Systems
- Indoor Environments
- Transportation and Traffic
- Risk Analysis
- Safety and Security

To submit a proposal or request further information, please contact the appropriate Springer Editor:

- Pierpaolo Riva at pierpaolo.riva@springer.com (Europe and Americas);
- Swati Meherishi at swati.meherishi@springer.com (Asia—except China, Australia, and New Zealand);
- Wayne Hu at wayne.hu@springer.com (China).

All books in the series now indexed by Scopus and EI Compendex database!

Vito Ferro · Giuseppe Giordano · Santo Orlando ·
Mariangela Vallone · Giovanni Cascone ·
Simona M. C. Porto
Editors

AIIA 2022: Biosystems Engineering Towards the Green Deal

Improving the Resilience of Agriculture,
Forestry and Food Systems
in the Post-Covid Era

 Springer

Editors

Vito Ferro
Department SAAF
University of Palermo
Palermo, Italy

Giuseppe Giordano
Department SAAF
University of Palermo
Palermo, Italy

Santo Orlando
Department SAAF
University of Palermo
Palermo, Italy

Mariangela Vallone
Department SAAF
University of Palermo
Palermo, Italy

Giovanni Cascone
Di3A
University of Catania
Catania, Italy

Simona M. C. Porto
Di3A
University of Catania
Catania, Italy

ISSN 2366-2557

ISSN 2366-2565 (electronic)

Lecture Notes in Civil Engineering

ISBN 978-3-031-30328-9

ISBN 978-3-031-30329-6 (eBook)

<https://doi.org/10.1007/978-3-031-30329-6>

© The Editor(s) (if applicable) and The Author(s), under exclusive license
to Springer Nature Switzerland AG 2023, corrected publication 2023

This work is subject to copyright. All rights are solely and exclusively licensed by the Publisher, whether the whole or part of the material is concerned, specifically the rights of translation, reprinting, reuse of illustrations, recitation, broadcasting, reproduction on microfilms or in any other physical way, and transmission or information storage and retrieval, electronic adaptation, computer software, or by similar or dissimilar methodology now known or hereafter developed.

The use of general descriptive names, registered names, trademarks, service marks, etc. in this publication does not imply, even in the absence of a specific statement, that such names are exempt from the relevant protective laws and regulations and therefore free for general use.

The publisher, the authors, and the editors are safe to assume that the advice and information in this book are believed to be true and accurate at the date of publication. Neither the publisher nor the authors or the editors give a warranty, expressed or implied, with respect to the material contained herein or for any errors or omissions that may have been made. The publisher remains neutral with regard to jurisdictional claims in published maps and institutional affiliations.

This Springer imprint is published by the registered company Springer Nature Switzerland AG
The registered company address is: Gewerbestrasse 11, 6330 Cham, Switzerland

Contents

Part I: Challenges in Hydraulic and Hydrological Processes, Sustainable Water Resources Management, Stream Rehabilitation and Soil Conservation Strategies Towards the Green Deal

A Remote Sensing Based Hydrological Modelling Approach to Estimate Daily Actual Evapotranspiration	3
Hassan Awada, Mirko Castellini, Simone Di Prima, Filippo Giadrossich, Costantino Sirca, Serena Marras, Donatella Spano, and Mario Pirastru	
Experimental Tests to Validate a Simple Procedure to Design Dual-Diameter Drip Laterals on Flat Fields	15
Giorgio Baiamonte, Mustafa Elfahl, and Samuel Palermo	
An Innovative Soil Bioengineering Technique by Waste Materials: The RiVite Project	27
Giorgio Baiamonte, Roberta Calvo, Gianluigi Pirrera, Samuel Palermo, and Francesco D’Asaro	
Monitoring of Irrigation Water Use in Italy by Using IRRISAT Methodology: The INCIPIT Project	41
O. R. Belfiore, A. Castagna, G. Longo-Minnolo, M. Ippolito, A. Bavieri, A. Comegna, and G. D’Urso	
Treatment of Steep and Clayey Soils with Olive Pruning Residues for Conservation Purposes: Hydrological Monitoring and Modelling Approaches	51
Giuseppe Bombino, Daniela D’Agostino, Pietro Denisi, José Alfonso Gomez, Demetrio Antonio Zema, and Santo Marcello Zimbone	

Macroscopic Root Water Uptake Modelling Using High-Throughput Screening (HTS) Systems: Design and Validation . . .	61
Lorenzo Bonzi, Fatma Hamouda, Àngela Puig-Sirera, Andrea Sbrana, Damiano Remorini, Lorenzo Cotrozzi, and Giovanni Rallo	
Testing the Effect of the Rill Channel Slope on the Correction Factor of Surface Velocity	71
F. G. Carollo, C. Di Stefano, A. Nicosia, V. Palmeri, V. Pampalone, and V. Ferro	
Monitoring Rainfall Erosivity in the Sparacia Experimental Area by an Optical Disdrometer	81
F. G. Carollo, C. Di Stefano, A. Nicosia, V. Palmeri, V. Pampalone, and V. Ferro	
Testing an Automatic Approach for Rill Network Extraction to Measure Rill Erosion by Terrestrial Photogrammetry	89
F. G. Carollo, C. Di Stefano, A. Nicosia, V. Palmeri, V. Pampalone, and V. Ferro	
Assessing Path Tortuosity on Rill Flow Resistance	97
F. G. Carollo, C. Di Stefano, A. Nicosia, V. Palmeri, V. Pampalone, and V. Ferro	
Assessing Daily ERA5-Land Reanalysis Data to Estimate Actual Evapotranspiration of Olive Orchards in Sicily	105
Dario De Caro, Ippolito Matteo, and Giuseppe Provenzano	
Field Study on Multifunctional Irrigation of Vineyards	117
C. Gandolfi, S. Cazzaniga, D. Ferrari, D. Masseroni, and B. Ortuani	
Productive Response of a Pear Orchard (<i>Pyrus Communis</i>, L.) to the Precision Irrigation Conducted Through a Decision Support System (DSS)	125
Fatma Hamouda, Àngela Puig-Sirera, Lorenzo Bonzi, Damiano Remorini, Giuseppe Provenzano, and Giovanni Rallo	
Assessing Potential Water Savings Implementing Variable Rate Sprinkler Irrigation in a Maize Farm in Northern Italy	133
Alice Mayer, Bianca Ortuani, and Arianna Facchi	
Monitoring and Predicting Irrigation Requirements of Tree Crops in Eastern Sicily as a Tool for Sustainability	143
Salvatore Pappalardo, Enrico Antonio Chiaradia, Giuseppe Longo-Minnolo, Daniela Vanella, and Simona Consoli	

The Vaia Event: Primary Impacts of the Storm and Subsequent Evolution of the Malgonera Stream (Dolomites)	153
Giacomo Pellegrini, Lorenzo Martini, Riccardo Rainato, Lorenzo Picco, and Mario Aristide Lenzi	
Analysis of Bedload Mobility in an Andean Stream	161
Riccardo Rainato, Luca Mao, and Mario Aristide Lenzi	
Hydraulic Roughness Estimation Induced by Riparian Vegetation in Tuscany Rivers for Management Purposes	169
Matteo Rillo Migliorini Giovannini, Andrea Dani, Rossana Saracino, Andrea Signorile, and Federico Preti	
The Effect of Soil and Vegetation Spatial Variability on Modelling Hydrological Processes for Irrigation Optimisation at Large Scales	181
Shawkat B. M. Hassan, Giovanna Dragonetti, Alessandro Comegna, Asma Sengouga, Nicola Lamaddalena, and Antonio Coppola	
Conceptual Interpretation of Infiltration Under Sealing Process by Membrane Fouling Models	191
Francesca Todisco, Lorenzo Vergni, and Rita Ceppitelli	
Adapting P-k-C* Model in Mediterranean Climate for Organic Removal Performance in Horizontal Treatment Wetlands	201
D. Ventura, F. Licciardello, L. Sciuto, M. Milani, S. Barbagallo, and G. L. Cirelli	
Influence of the Rainfall Time Step on the Thresholds for Separating Erosive and Non-erosive Events	211
L. Vergni, A. Vinci, and F. Todisco	
Quantifying Irrigation Volumes Using Sentinel-1 Soil Moisture Data in Central Italy	221
L. Vergni, J. Dari, F. Todisco, M. Vizzari, C. Saltalippi, S. Venturi, S. Casadei, and L. Brocca	
Hydrological and Erosive Effects of Prescribed Fire and Mulching with Fern Residues in a Mediterranean Pine Forest	229
Demetrio Antonio Zema, Manuel Esteban Lucas-Borja, Bruno Gianmarco Carrà, Giuseppe Bombino, Daniela D'Agostino, Pietro Denisi, and Santo Marcello Zimbone	
Part II: Applications in Smart Agriculture and Forestry, Post-harvest Logistics and Food Chain, Energy, Waste and By-Products Smart Use, Big Data and Machine Learning in Biosystems Engineering	
Uranine as a Tracer for Rapid Detection of Spray Deposition	241
Antonio Altana, Lorenzo Becce, Paolo Lugli, Luisa Petti, and Fabrizio Mazzetto	

Development of an Investment Decision Tool for Biogas Production from Biowaste in Mediterranean Islands	251
Antonio Ascianto, Martina Agosta, George Attard, Antonio Comparetti, Carlo Greco, and Michele Massimo Mammano	
Evaluation of Precision Technologies Approach for the Management of an Experimental Field in Organic Fruit Growing	263
Alberto Assirelli, Federica Brandi, Fiorella Stagno, Maura Sannino, Salvatore Faugno, Salvatore Musio, Gianluca Baruzzi, and Giancarlo Rocuzzo	
Potential Bioenergy and Biofertiliser Production from Livestock Waste in Mediterranean Islands Within Circular Bioeconomy	271
George Attard, Noel Azzopardi, Antonio Comparetti, Carlo Greco, Anthony Gruppeta, and Santo Orlando	
Sustainable Livestock Waste Treatment Technologies: Survey on a Group of Italian Farms	285
Giorgia Bagagiolo, Lucia Vigoroso, Giulia De Paolis, Federica Caffaro, Eugenio Cavallo, and Niccolò Pampuro	
Blockchain Technology for Food Supply Chain Traceability and Authentication	295
Paolo Barge, Matteo Antonio Angelo Franchetto, Valeria Maritano, Cristina Tortia, Paolo Gay, Claudio Schifanella, and Federica Cena	
Agroforestry Innovations Lab Activities on Sprayer Performance and Certification	305
Lorenzo Becce, Giovanni Carabin, and Fabrizio Mazzetto	
Analysis of Spraying Equipment Performances in Olive Orchards	315
Souraya Benalia, Giuseppe Zimbalatti, Lorenzo M. M. Abenavoli, Antonio Fazari, and Bruno Bernardi	
Different Strategies to Alleviate Soil Compaction Risk During Tillage Operations	323
Marco Benetti and Luigi Sartori	
Statistical Control of the Quality of Decaners Used for the Continuous Virgin Olive Oil Extraction	335
Biagio Bianchi, Michele Dassisti, Michela Orsino, Alessandro Bianchi, and Claudio Perone	
Spray Swath Study in Relation to Canopy Deposition During UAV Spray Applications in Vineyards	345
Alessandro Biglia, Marco Grella, Lorenzo Comba, Alessandro Sopegno, Leandro Eloi Alcatrão, Davide Ricauda Aimonino, and Paolo Gay	

Digital Technologies for the Sustainable Management of the Olive Orchards in Central Italy: The Farmers' Perception	353
Marcello Biocca, Pietro Gallo, Stefano Canali, and Elena Testani	
Work Time Study, Productivity and Costs of Felling Trees in Urban Areas	363
Marcello Biocca, Pietro Gallo, and Giulio Sperandio	
Automatic Feeding Systems for Cattle in Italy: State of the Art and Perspectives	373
Carlo Bisaglia, Andrea Lazzari, Simone Giovino, and Massimo Brambilla	
Preparatory Activities for the Care and Maintenance of Historic Parks and Gardens: A Case Study	383
Lucia Bortolini and Lorenzo Guerrini	
Pig Farming in the Abruzzo Region and Hepatitis E Virus Detection in Swine Slurries	393
M. Brambilla, C. Bisaglia, P. Mancini, C. Veneri, G. Bonanno Ferraro, M. Iaconelli, E. Suffredini, and G. La Rosa	
Enhancement of Mediterranean Greenhouses Facilities: Heat Power Pump Assessment for Bedding Plant Production by Coaxial Basal Heating	401
Sonia Cacini, Alessandro Orlandini, Gianluca Burchi, Maurizio Cutini, Massimo Brambilla, Carlo Bisaglia, Daniele Massa, and Marco Fedrizzi	
Drivers of Adoption of Sustainable Practices and Technologies for Soil Protection Among Vine-Growers in North-West Italy	411
Federica Caffaro, Eugenio De Gregorio, Giorgio Capello, Lucia Vigoroso, Giorgia Bagagiolo, Eugenio Cavallo, and Marcella Biddoccu	
The Direct Costs for Cover Crops Cultivation: Comparison Between Different Agronomical Practices	421
Aldo Calcante, Daniele Manenti, and Roberto Oberti	
Development and Experimental Evaluation of a Tractor Roll-Over Stability Model	429
Giovanni Carabin, Lorenzo Bece, and Fabrizio Mazzetto	
The MAGIC Project: A Tool for Promoting Safety in Agriculture During COVID-19 Pandemic	437
Pietro Catania, Giuseppe Aiello, Antonella Certa, Massimo Vincenzo Ferro, Santo Orlando, and Mariangela Vallone	

Assessment of Vine and Cover Crop Vegetation Indices Using High-Resolution Images Acquired by UAV Platform 447
 Pietro Catania, Massimo Vincenzo Ferro, Eliseo Roma, Santo Orlando, and Mariangela Vallone

Evaluation of Different Flight Courses with UAV in Vineyard 457
 Pietro Catania, Massimo Vincenzo Ferro, Eliseo Roma, Santo Orlando, and Mariangela Vallone

Olive Tree Canopy Assessment Based on UAV Multispectral Images ... 469
 Pietro Catania, Massimo Vincenzo Ferro, Eliseo Roma, Santo Orlando, and Mariangela Vallone

Development of a Test Bench for Vibration Measurements of Hand-Held Harvesters for Olives 479
 Emanuele Cerruto, Giuseppe Manetto, and Domenico Longo

Thermogravimetric Analysis for the Evaluation of Coffee Grounds in Combustion and Gasification Processes 489
 Colantoni Andrea, Leonardo Bianchini, Enrico Paris, Monica Carnevale, Beatrice Vincenti, Adriano Palma, and Francesco Gallucci

Convolutional Neural Network Based Detection of Chestnut Burrs in UAV Aerial Imagery 501
 Lorenzo Comba, Alessandro Biglia, Alessandro Sopegno, Marco Grella, Emilio Dicembrini, Davide Ricauda Aimonino, and Paolo Gay

Evaluation of Precision Sprayer Technologies Practical Application ... 509
 Maurizio Cutini, Elio Romano, Alberto Assirelli, Carlo Bisaglia, and Massimo Brambilla

New Technologies and Safety in Agriculture: SAFETY AR 517
 Valerio Di Stefano, Leonardo Bianchini, Riccardo Alemanno, and Andrea Colantoni

Waste Heat from District Heating Plants for Forage Drying in the Camonica Valley 523
 Marco Fiala, Luca Nonini, and Leonardo Colnago

Remote Sensing Imagery for Mapping and Monitoring High Nature Value Farmland Area (HNVF) 533
 Costanza Fiorentino, Angelo R. Donvito, Paola D’Antonio, Domenico Conte, Vincenzo Scalcione, and Francesco Toscano

Design of a System for the Mechanization of Subsoil Compost Tea Distribution 543
 Ester Foppa Pedretti, Alessio Ilari, Riccardo Scuppa, Carmine De Francesco, and Daniele Duca

Environmental Impact of Real Gaseous Pollutants Emission of Agricultural Tractors	555
L. E. Galli, D. Facchinetti, M. Gibin, and D. Pessina	
A Method for Energy Efficiency Rating of Low-Power Tractors Based also on Intensity of Use	565
L. E. Galli, D. Facchinetti, and D. Pessina	
Design, Setup and Virtual Test of a Three-Section Foldable Rear Rollbar for a Low-Power Tractor	575
D. Gattamelata, V. Laurendi, L. Vita, L. E. Galli, and D. Pessina	
Microclimatic Conditions at the Interior of Small-Sized Insect-Proof Nethouses with Tomato Cultivation	587
Anastasios Giannoulis, Nikoleta-Georgia Papardaki, Antonis Mistriotis, and Demetres Briassoulis	
The Effect of Adjuvants in Reducing Potential Spray Drift	597
Marco Grella, Paolo Marucco, Marco Resecco, Claudio Bozzer, Alessandro Biglia, Lorenzo Comba, Paolo Balsari, and Fabrizio Gioelli	
Whole-Body Vibration for Tractor Drivers	605
Rino Gubiani, Nicola Zucchiatti, and Ugo Da Broi	
A Facilitating Machine for Silkworm Rearing	615
Rino Gubiani and Nicola Zucchiatti	
Intermittent Drying of Walnuts: Evaluations of Warm Air Consumption on a Thin Layer	625
Lorenzo Guerrini, Andrea Pezzuolo, Giovanni Ferrari, Giovanni Pippa, and Francesco Marinello	
Open Field Geometric Primitives' Representation by a 2D Low-Cost LIDAR for Vineyard Sprayer Application Under Different Conditions	633
Alessio Ilari, Fabrizio Favi, Francesco Zingaretti, Luana Centorame, and Ester Foppa Pedretti	
Valorizing Agro-Industry Residues to Improve the Environmental Sustainability of Frozen Products	645
Ilari Alessio, Boakye-Yiadom Kofi Armah, Duca Daniele, and Foppa Pedretti Ester	
Requirements and Challenges in the Design and Potential of Smart and Efficient Winch Assisted Forestry Machinery	657
S. Leitner, M. Perez, G. Carabin, M. Renzi, R. Vidoni, and F. Mazzetto	

Feasibility of Two MEMS-NIR Spectrophotometers for Characterizing Different Biofuel Origin 667
 Elena Leoni, Manuela Mancini, Alberto Assirelli, Sara di Stefano, and Giuseppe Toscano

A Prototype of Photovoltaic Dryer for Nutraceutical and Aromatic Plants 677
 Michele Massimo Mammano, Antonio Comparetti, Salvatore Ciulla, Carlo Greco, and Santo Orlando

A Model of Sicilian Environmentally Friendly Multifunctional Farm for Soil Protection 687
 Michele Massimo Mammano, Antonio Comparetti, Carlo Greco, and Santo Orlando

LLL Strategies for New Educational Approaches in Smart Agriculture from an Agricultural Engineering Perspective in Italy 697
 Andreas Mandler, Giovanni Carabin, Lorenzo Becce, Sandro Liberatori, Heinz Bernhardt, Maximilian Treiber, Christina Paulus, Andreas Gronauer, Anders Herlin, and Fabrizio Mazzetto

First Results of Digestate Spreading Trials in Mediterranean Crops ... 705
 Giuseppe Manetto, Emanuele Cerruto, Rita Papa, and Roberta Selvaggi

Preliminary Trials to Investigate the Effect of Sprayer Setting for Ozonated Water Spray Applications to Improve Plants Disease Control Efficacy 717
 Marco Sozzi, Alessandro Zanchin, Franco Gasparini, Francesco Marinello, and Luigi Sartori

Evaluation of Potential Fuel Saving of Tractor Electrification Layouts Using Real-World Data 725
 Michele Mattetti, Giovanni Molari, and Massimiliano Varani

Technological Solutions for Implementing Sustainable Cereal-Based Value-Chains in High Mountain Areas 733
 Fabrizio Mazzetto, Giovanni Carabin, Lorenzo Becce, Andreas Mandler, and Pasqualina Sacco

Energy Valorization of Fruit Shells and Stones Deriving from the Food Industry 743
 Alessio Mencarelli, Raffaele Cavalli, Gina Marano, Marco Povo, and Rosa Greco

Improving Combine Harvester Management Through CANBUS Data Analyses 753
 Michielan Enrico, Mattetti Michele, and Molari Giovanni

Hazelnut Harvesting Machines: Recent Advances and New Trends	763
Danilo Monarca, Riccardo Alemanno, Gianmarco Rigon, and Pierluigi Rossi	
CANBUS Data for Site-Specific Tractor Performance Analysis and Prediction	775
Danilo Monarca, Riccardo Alemanno, Pierluigi Rossi, Gianmarco Rigon, Leonardo Bianchini, and Massimo Cecchini	
A Deep Learning Artichoke Plants Identification Approach for Site-Specific UAV Spraying	783
Jacopo Motta, Alberto Sassu, Alessandro Deidda, Luca Ghiani, Alberto Carlevaro, Giovanni Garibotto, and Filippo Gambella	
Forestry Machinery Chain Productivity in Stands Hit by the Vaia Storm: First Results for the Camonica Valley	793
Luca Nonini and Marco Fiala	
Can a Variable-Rate Sprayer Be Efficient and Economic? Testing and Economic Analysis in Viticulture	805
Andrea Pagliai, Daniele Sarri, Carolina Perna, and Marco Vieri	
Performance Analysis of a Harrowing Implement of New Concept	817
Simone Pascuzzi, Volodymyr Bulgakov, Iaroslav Gadzalo, and Volodymyr Nadykto	
Concept of a Foldable Transmission Chain Used Inside Tobacco Leaves Harvesting Machine	827
Simone Pascuzzi, Katarzyna Łyp-Wrońska, Francesco Santoro, and Francesco Vicino	
Assessment of Soil and Vegetation Index Variability in a Traditional Olive Grove: A Case Study	835
C. Perna, D. Sarri, A. Pagliai, S. Priori, and M. Vieri	
Microclimatic Monitoring and Analysis in a Hydroponic Greenhouse	843
Claudio Perone, Michela Orsino, Pasquale Catalano, Biagio Bianchi, Ferruccio Giametta, and Giovanna La Fianza	
Optimization of a New Knife Crusher to Increase Olive Oil Quality . . .	851
Claudio Perone, Antonia Tamborrino, Antonio Berardi, Roberto Romaniello, and Alessandro Leone	
Effect of Image Binarization on Drop Diameters Measurement	861
Salvatore Privitera, Emanuele Cerruto, Domenico Longo, and Giuseppe Manetto	

Application of Spectral Indices for the Evaluation of Conservative Techniques in Crops Management 871
 Elio Romano, Federico Calcagno, Carlo Bisaglia, Nicola Furnitto, Giampaolo Schillaci, and Sabina Failla

Big Data for Farm Machines: An Algorithm for Estimating Tractors’ Operating Costs 881
 Pierluigi Rossi, Gianmarco Rigon, Riccardo Alemanno, Leonardo Bianchini, Massimo Cecchini, and Danilo Monarca

Obstacle Avoidance Safety System for Agricultural Tractors and Autonomous Vehicles Based on Bluetooth and Passive RFID 891
 Pierluigi Rossi, Filippo Cossio, Massimo Cecchini, and Danilo Monarca

Sustainability Performance of Mountain Food Value Chains 901
 P. Sacco, D. Don, L. Becce, G. Carabin, A. Mandler, and F. Mazzetto

Combining Smart Glasses and Thermal Imaging as a Tool for Water Stress Detection in Greenhouses: A Preliminary Study 909
 Gabriele Sara, Giuseppe Todde, Daniele Pinna, and Maria Caria

A Smart Automation System for the Management and Control of a Medium Scale Digester Plant 917
 Luigi Scarcello, Souraya Benalia, Giuseppe Zimbalatti, Antonio Fazari, and Bruno Bernardi

Using Multiple Correspondence Analysis to Evaluate Milking Parlour Performance 927
 Francesco M. Tangorra and Annamaria Costa

Effect of Automatic Feeding System (AFS) on Dairy Cows Feeding Activity 933
 Francesco M. Tangorra and Aldo Calcante

Use of Heavy Metals Contaminated Industrial Hemp (Cannabis Sativa L.) for Bioenergy Production 941
 Giuseppe Todde, Gianluca Carboni, Serena Marras, Maria Caria, and Costantino Sirca

Smart Glove: Development and Testing of a Wearable RFID Reader Connected to Mixed Reality Smart Glasses 949
 Giuseppe Todde, Gabriele Sara, Daniele Pinna, Valentino Artizzu, Lucio Davide Spano, and Maria Caria

Experimental Analysis of Chainsaw Emissions in Chestnut Wood Operations 957
 Francesco Toscano, Paola D’Antonio, Carmen D’Antonio, Nicolino De Iorio, Felice Modugno, and Costanza Fiorentino

Quantity and Type of Logging Residues Following Cut-to-Length and Full-Tree Salvage Logging Systems in Damaged Mountain Forests	967
Alberto Udali, Lorenzo Garollo, Raffaele Cavalli, and Stefano Grigolato	
Concerning the Relationship Between Tilled Soil Aggregates Dimension and Power Harrow Energy Requirements	979
Massimiliano Varani, Michele Mattetti, Alessandro Biglia, Lorenzo Comba, and Giovanni Molari	
“Green” Investments in Sustainable Farming Systems: A Survey Among Italian Enterprises	987
Lucia Vigoroso, Giorgia Bagagiolo, Giulia De Paolis, Niccolò Pampuro, Eugenio Cavallo, and Federica Caffaro	
Characterization of a Multispectral Camera for Abiotic and Biotic Stress Detection in Greenhouse	997
Alessandro Zanchin, Marco Sozzi, Tiziano Valentini, Leonardo Piacentino, Francesco Marinello, Alberto Pozzebon, and Carlo Duso	
Low Dose Precision Distribution with Micro-Granules Fertilizer Using Different Spreader Machines	1007
N. Zucchiatti and R. Gubiani	
Part III: Smart Engineering Techniques, Design and Planning of Resilient Land and Built Systems	
Local community’s Perception of Agrobiodiversity as Cultural Heritage and the Role of <i>Ceratonia Siliqua</i> L. in Characterizing the Rural Landscape Identity of Modica and Rosolini (Sicily-Italy)	1019
Abbate Rosaria, Menconi Maria Elena, and Grohmann David	
Spatial Variability of Microclimatic Parameters in a Closed Compost-Bedded Pack Barn for Dairy Cows with Tunnel Ventilation	1029
Rafaella Resende Andrade, Ilda de Fátima Ferreira Tinôco, Gabriel Araújo e Silva Ferraz, Valentina Becciolini, Giuseppe Rossi, and Matteo Barbari	
Landscape Valorization and Rural Tourism Development: A Mobile Application for the Promotion of the Lauretana Way in Tuscany Region (Italy)	1039
Gianluca Bambi, Giuseppe Rossi, Matteo Barbari, Lorenza Gasparella, and Serena Savelli	

Real-Time Measurements of Gaseous and Particulate Emissions from Livestock Buildings and Manure Stores with Novel UAV-Based System	1049
V. Becciolini, L. Conti, G. Rossi, D. Bedin Marin, M. Merlini, G. Coletti, U. Rossi, and M. Barbari	
Detecting Coffee Leaf Nitrogen with UAV-Based Vegetation Indexes and Machine Learning	1057
Diego Bedin Marin, Gabriel Araújo e Silva Ferraz, Matteo Barbari, Giuseppe Rossi, and Leonardo Conti	
Mapping and Disposal of Irrigation Pipes for a Sustainable Management of Agricultural Plastic Waste	1065
Ileana Blanco, Giuliano Vox, Fabiana Convertino, and Evelia Schettini	
Buildings for Citrus Juices and Essential Oil Manufacturing: The Floor Design	1075
Giuseppe Davide Cardinali and Francesco Barreca	
Evaluation of the Efficacy of a Radial Flow Settler for Aquaculture Wastewater Treatment	1087
Bibbiani Carlo, Guidi Christian, and Rossi Lorenzo	
IoT Technologies for Herd Management	1097
Giulia Castagnolo, Dominga Mancuso, Francesca Valenti, Simona M. C. Porto, and Giovanni Cascone	
Assessing Application Potential of Species Distribution Models to the Case Study of Citrus in Eastern Sicily	1107
G. A. Catalano, F. Maci, F. Valenti, P. R. D'Urso, and C. Arcidiacono	
Simulation of the Heating Load in a NZEB Winery Building	1115
Antonino Ciappa, Giovanni Puglisi, Fabiana Convertino, Ileana Blanco, Giuliano Vox, and Evelia Schettini	
Green Façade to Improve Building Energy Performance in Summer and Winter	1125
Fabiana Convertino, Ileana Blanco, Giuliano Vox, and Evelia Schettini	
Assessing Setups of a Multigas Analyser for Noxious Gas Monitoring in an Open Dairy Barn	1133
D'Urso Provvidenza Rita, Arcidiacono Claudia, and Cascone Giovanni	
Agricultural By-Products for Biomethane Production: Opportunities for a Sustainable Bioenergy Conversion	1143
Giovanni Ferrari, Francesco Marinello, and Andrea Pezzuolo	

Heating from Biogas Plants: An Areal Approach for Enhanced Environmental Sustainability	1153
Giovanni Ferrari, Lorenzo Guerrini, and Andrea Pezzuolo	
Plant Factory with Artificial Lighting: Innovation Technology for Sustainable Agriculture Production	1163
Luigia Mandriota, Ileana Blanco, and Giacomo Scarascia-Mugnozza	
Multispectral UAV-Based Monitoring of Behavior of Different Wheat and Barley Varieties	1173
Gaetano Messina, Giuseppe Badagliacca, Salvatore Praticò, Giovanni Preiti, Michele Monti, and Giuseppe Modica	
Physical and Mechanical Characterization of a Low-Quality Sheep Wool Fiber	1183
Monica C. M. Parlato, Giusi Midolo, Simona M. C. Porto, and Francesca Valenti	
Historic Agricultural Landscape Characterization: First Attempt of Historic Landscape Characterization (HLC) to Costa Viola Terraced Landscape (Calabria, Italy)	1193
Salvatore Praticò, Francesco Solano, Salvatore Di Fazio, and Giuseppe Modica	
Recycled Plastics Used in the Production of Agricultural Nets for Crop Protection	1203
Roberto Puglisi, Giuseppe Cillis, Dina Statuto, and Pietro Picuno	
Efficiency of Plastic Nets for Greenhouse Shading	1211
Roberto Puglisi, Marco Lippolis, Giuseppe Starace, Paolo Arrigoni, and Pietro Picuno	
Multi-Temporal Satellite Imagery for Monitoring Productivity Trend in Mediterranean Coastal Forest Ecosystems: The Study Case of the State Natural Reserve "Duna Feniglia" (Italy)	1219
Francesco Solano, Salvatore Praticò, Giuseppe Modica, Giovanni Quilghini, and Gianluca Piovesan	
Assessing Differences in Land Productivity Trends to Climatic Data in Arid and Semi-arid Zones: A Study Case in Northern Mozambique	1229
Francesco Solano, Salvatore Praticò, Maria Nicolina Ripa, and Giuseppe Modica	
Impact of Agricultural Plastics on Rural Landscape: A Case Study in the "Metapontino" Agri-Food District (Southern Italy)	1237
Dina Statuto, Giuseppe Cillis, and Pietro Picuno	

Geospatial Tools Applications for the Analysis of Attractive Sources Related to Airport Wildlife Strike 1247
Trifulò Domenico, D.'Urso Provvidenza Rita, and Arcidiacono Claudia

Contribute of Digital Information Modelling to Territorial Governance and Airport Safety Interaction Management 1257
Trifulò Domenico, Ragusa Eliana, Alessandro Di Graziano, and Arcidiacono Claudia

Correction to: Can a Variable-Rate Sprayer Be Efficient and Economic? Testing and Economic Analysis in Viticulture C1
Andrea Pagliai, Daniele Sarri, Carolina Perna, and Marco Vieri

**Part I: Challenges in Hydraulic
and Hydrological Processes, Sustainable
Water Resources Management, Stream
Rehabilitation and Soil Conservation
Strategies Towards the Green Deal**

A Remote Sensing Based Hydrological Modelling Approach to Estimate Daily Actual Evapotranspiration



Hassan Awada, Mirko Castellini, Simone Di Prima, Filippo Giadrossich, Costantino Sirca, Serena Marras, Donatella Spano, and Mario Pirastru

Abstract Evapotranspiration (ET) is an important variable in the soil–plant–atmosphere (SPA) continuum. The quantification of the spatiotemporal dynamics of ET flows in natural vegetation is of fundamental importance for efficient water resource management and environmental modelling, particularly in the semi-arid areas of the Mediterranean. Satellite remote sensing-based surface energy balance (SEB) techniques have emerged as a very useful tool for quantifying actual evapotranspiration (ET_a) at various temporal and spatial scales. Remote sensing (RS) offers free and long-time series of data that is characterized by a relatively high spatio-temporal resolution. Such data can be an added value for SEB modelling of ET_a , however, discontinuous data acquisitions of thermal remote sensing data due to the platform temporal resolution and/or gaps in image acquisition due to cloud cover can limit RS utility. This study proposes a model-based approach for the construction of daily actual evapotranspiration between the Landsat 8 acquisition days. The proposed model integrates actual evapotranspiration obtained by the Surface Energy Balance Algorithm for Land (SEBAL) model on Landsat-8 acquisition days, RS retrieved vegetative biomass dynamics, on-field measurements of potential evapotranspiration and a hydrological modeling approaches of soil moisture in the root zone by using the transient flow Richards equation. Results shown that the proposed

H. Awada (✉) · S. Di Prima · F. Giadrossich · C. Sirca · S. Marras · D. Spano · M. Pirastru
Department of Agricultural Sciences, University of Sassari, Viale Italia 39, 07100 Sassari, Italy
e-mail: hassan_awada1987@live.com

M. Castellini
Council for Agricultural Research and Economics-Agriculture and Environment Research Center (CREA-AA), Via Celso Ulpiani 5, 70125 Bari, Italy

C. Sirca · S. Marras · D. Spano
Euro-Mediterranean Centre On Climate Change (CMCC) Foundation, Via de Nicola 9, 07100 Sassari, Italy

H. Awada · C. Sirca · S. Marras · D. Spano · M. Pirastru
National Biodiversity Future Center (NBFC), 90133 Palermo, Italy

M. Pirastru
Desertification Research Group, NRD, University of Sassari, Viale Italia 57, 07100 Sassari, Italy

approach was well suited for modelling the dynamics in the SPA continuum that occurs between 2 Landsat acquisitions to estimate the daily time series of ET_a .

Keywords Remote sensing · Temporal Upscaling · SEBAL · Actual Evapotranspiration · Eddy covariance

1 Introduction

Water resources scarcity is recognized as a major threat that humanity will face in the coming decades [48]. Unsustainable water management, deteriorating freshwater quality and quantity, over-consumption and increasing water demand, and water pollution, combined with climate change and water scarcity situations is increasing the pressure on water resources and can result in severe impacts on both nature and society [44]. Evapotranspiration (ET) constitutes to the combined loss of water from the stomata openings of the vegetative surface known as transpiration (T), and evaporation (E) from the surrounding bare soil [42]. In semi-arid and arid regions, evapotranspiration (ET) is the leading loss term in the soil water budget [38, 11]. Efforts have been invested in estimating ET in these ecosystems, yet the contribution of each ET component to its seasonal dynamics (e.g., tree and grass transpirations, bare soil evaporation), especially during dry periods, are often poorly quantified [11, 42].

Low-cost remote sensing techniques can be used to retrieve the space–time variability of numerous physical variables needed in the applications of the ET_a modeling ([12, 23, 29, 32, 35]. For example, surface energy balance (SEB) based approaches can benefit from data operating in the visible and near-infrared (VIS/NIR) regions of the electromagnetic spectrum and those acquired in the thermal infrared (TIR) for the estimation of ET_a as a residual of the SEB equation, after quantifying the rest of the instantaneous fluxes [26, 46, 17, 31, 33]. Various satellite-based SEB models have been applied and validated extensively in various parts of the world [9, 6, 16, 17, 31, 43]. Such modelling approaches has been widely applied in irrigation management [6, 13, 15, 41], water accounting [34], assessing irrigation system performance [3, 4, 8], assessing agricultural water productivity [18, 49], groundwater management [2, 1, 39], and hydrological modelling [20, 28, 36]. Remote sensing-based energy balance (RSEB) approaches applied on satellite data can capture large geographical extents and provide ET_a estimations at different spatial and temporal scales, however this same benefit can be a constraint for certain applications since the retrieved data is limited to clear-sky satellite overpasses and to the platform spatial and temporal resolution [10]. For example, the AATSR/ENVISAT, the MODIS and the Sentinel-3 satellites have a short revisit time (1 day) but a 1000 m spatial resolution of the thermal infrared. The use of these data in ET_a modelling is limited to the spatial extent of the TIR data and is not recommended in fragmented and heterogeneous areas, especially when the parcels considered are smaller than the TIR pixel. As an alternative, relatively high spatial resolution TIR imagery (from 60 to 120 m)

can be obtained from platforms such as Landsat and ASTER, however such images are only available every 16 days, provided that clear sky conditions were available at the overpass time. Most of the RSEB-related applications that use relatively high spatial resolution satellite data estimates ET_a on image acquisition days. Actual daily evapotranspiration retrievals based on periodically acquired snapshots can be operational in diverse applications, nevertheless water resources management requires the retrieval of a continuous time series of daily ET_a and over extended time intervals.

This paper proposes a crop actual evapotranspiration ($ET_{c\text{ act}}$) construction approach that accounts for the dynamics of meteorological variables, vegetation biomass changes and/or plant stress caused by soil water restriction between different Landsat acquisitions. The soil moisture dynamics in the root zone is obtained by hydrological modeling by using the transient flow Richards equation and is used to derive the dimensionless weighed stress index (K_s) and the soil water evaporation (E_s). The $ET_{c\text{ act}}$ construction approach is applied on a complex natural Mediterranean ecosystem northwest Sardinia island.

2 Materials and Methods

2.1 The Study Site

The study site is located inside a natural reserve called “Le Prigionette”, Northwest Sardinia, Italy. The climate is Mediterranean, semi-arid with a warm summer, mild winter, and a high-water deficit from May through September. The mean annual temperature is 15.9 °C, the minimum and maximum temperature is 7 °C and 28 °C, respectively. Precipitation is mainly concentrated from autumn to spring and the annual mean is 588 mm. The soil is 0.3–0.4 m deep Lithic Xerorthent. The ecosystem is a typical coastal Mediterranean maquis. The mean vegetation height ranges between 0.93 and 1.43 m. Ground cover varies between 42 and 91%.

2.2 Micrometeorological and Eddy Covariance Measurements

Eddy Covariance (EC) data were collected by the micro-meteorological station (IT-Noe), installed in the study area as part of the CARBOEUROPE flux monitoring network (Pastorello et al., 2020). The monitoring site is located at the Le Prigionette natural reserve (lat: 40.61, lon: 8.15, 25 m of elevation above sea level) (Fig. 1). The IT-Noe station consists of Eddy Covariance (EC) system with a sonic anemometer (CSAT3, Campbell Scientific, Logan, UT, USA) and an open path gas analyzer (LiCOR 7500, Lincoln, NE, USA), placed within the maquis at 3.5 m above the ground for measuring the latent heat flux (λE) and the sensible heat flux (H). The

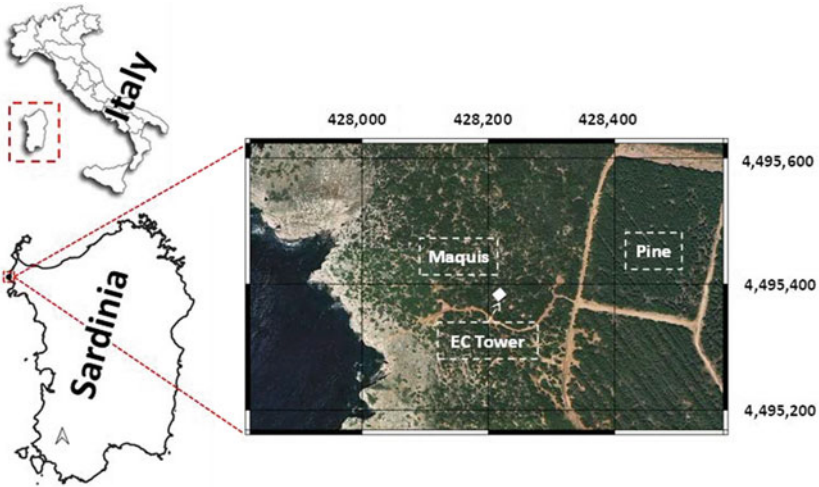


Fig. 1 Geographic location of the micro-meteorological IT-Noe station in the Le Prigionette natural reserve, Italy. Coordinates EPSG:32,632 (WGS 84/UTM zone 32N). The white square indicates the position of eddy covariance tower

station also measures the soil heat flux (G) by thermocouples and 4 heat flux plates (HFP01SC, Hukseflux, Delft, NL), installed at the 0.08 m of soil depth. The station also acquires downward and upward short and long wave radiation, air temperature, air humidity, precipitation, wind speed, and surface pressure at 2 m above the ground. EC data were processed using the software (EOLO) developed at University of Sassari. The software provides H and λE turbulent fluxes, net radiation (R_n) and G at half-hour time step.

2.3 *Vegetation Indices and the Surface Energy Balance Algorithm for Land (SEBAL) Model*

The Normalized Difference Vegetation Index (NDVI) is obtained from the Landsat 8 near-infrared (ρ_{NIR}) and the red (ρ_{Red}) spectral reflectance data as $\rho_{NIR} - \rho_{Red} / \rho_{NIR} + \rho_{Red}$ [40]. The canopy fractional cover f_c was estimated from NDVI as proposed by Gutman and Ignatov, [27] and the leaf area index (LAI) was estimated from f_c as proposed by the Choudhury [22]. NDVI, f_c and LAI were obtained as mean values over the studied field at the selected acquisition days. For the non-acquisition days, the indices were estimated by linear interpolation between each 2 Landsat acquisitions.

The Landsat images, accompanied by a 10 m digital elevation model (DEM) (<http://www.sardegnageoportale.it/>) and meteorological inputs, were used to produce the SEBAL data layers (i.e., land surface temperature, surface albedo, and surface emissivity). The SEBAL model was used to retrieve the instantaneous net surface

radiation flux, soil heat flux and the sensible heat flux [14]. Then the SEBAL model retrieves the instantaneous latent heat flux as a residual of the surface energy balance and upscales to actual evapotranspiration on the image acquisition day ($ET_{a\text{eb}}$) by utilizing the evaporative fraction (Λ) as an integration parameter [14] and the net daily radiation estimated by the procedure outlined in the FAO Irrigation and Drainage Paper [7].

2.4 The Canopy Water Interception, Soil Water Dynamics, Soil Water Evaporation and the Stress Factor

The actual canopy water interception (I_c) is modeled by an hourly water balance. Precipitation is assumed to be stored on the surfaces of overstory and understory vegetation until maximum interception storage capacities (C) is reached. The canopy water interception storage is filled by precipitation and is depleted by ET. When C is reached, excess precipitation is generated and provides an input for the FAO-56 soil water evaporation model. C (mm) was determined from the Leaf Area Index (LAI) as proposed by Dickinson et al., [24].

In this research, it is assumed that the water movement in the unsaturated soil is predominantly vertical and can be represented by a single dimension soil water modelling approach. A one-dimensional soil water content dynamic model based on the Richards equation was used to simulate the dynamics of the water content status [37]. The water content status was simulated at multiple layers on half hourly basis as expressed below

$$\frac{\partial \theta(z, t)}{\partial t} = \frac{\partial}{\partial z} \left[K(\theta, z) \frac{\partial h(\theta, z)}{\partial z} \right] - \frac{\partial K(\theta, z)}{\partial z} - S_w(z, t) - E_s(\theta, t) \quad (1)$$

where z is vertical coordinate (positive upward) [L], t is time [T], θ is soil water content [$L^3 L^{-3}$], h is soil water pressure head [L], K is hydraulic conductivity [$L T^{-1}$], S_w is root water extraction [$L^3 L^{-3} T^{-1}$] and E_s is evaporation from the topsoil [$L^3 L^{-3} T^{-1}$].

The numerical solution of Richards equation requires estimating soil water retention curve, $\theta(h)$, and the hydraulic conductivity function, $K(h)$. The model uses the Van Genuchten [45] parametric function for $\theta(h)$ and the Brooks and Corey [19] relation for $K(h)$:

$$\theta(h) = \begin{cases} \theta_r + \frac{\theta_s - \theta_r}{[1 + |\alpha h|]^m} & h < 0 \\ \theta_s & h \geq 0 \end{cases} \quad (2)$$

$$K(\theta) = K_{\text{sat}} \left(\frac{\theta - \theta_r}{\theta_s - \theta_r} \right)^\eta \quad (3)$$

where θ_s and θ_r are saturated and residual soil moisture content [L^3L^{-3}] respectively, α [L^{-1}], n [-], m [-] and η [-] are shape parameters that depend on soil type, K_{sat} is saturated hydraulic conductivity [LT^{-1}].

The shape parameters are deduced using specific pedo-transfer functions (PTF) based on PSD and infiltration experiments [30]. The K_{sat} and α parameters are derived from the analysis of cumulative water infiltration data using the BEST Slope-method [30]. The evaporation from soil surface depends on fraction of surface vegetation cover f_c [-], on ET_0 , and on surface soil moisture θ_{sur} through a restricting coefficient β computed by a simple linear method [21]:

$$E_s = \beta \cdot (1 - \text{veg}) \cdot ET_0/dz_1 \quad (4)$$

$$\begin{cases} \beta = 1 & \theta_{sur} \geq \theta_{fc} \\ \beta = \frac{\theta_{sur} - \theta_w}{\theta_{fc} - \theta_w} & \theta_{fc} < \theta_{sur} \leq \theta_w \end{cases} \quad (5)$$

where θ_{fc} and θ_w are water evaporation thresholds.

On image acquisition days, the transpiration component $T_{a\text{ eb}}$ [LT^{-1}] that represents water uptake by plants was obtained from SEBAL retrieved actual evapotranspiration ($ET_{a\text{ eb}}$) after subtracting the E_s and I_c components. On non-acquisition days, the actual transpiration component was removed from the root zone through the sink term S_w , which at a given depth and for a prescribed water pressure head was defined as:

$$S_w(h, z) = \frac{K_s(h) \cdot r_d(z)}{\int_0^{L_r} K_s(h) \cdot r_d(z) dz} \cdot T_{a\text{ eb}} \quad (6)$$

where $K_s(h)$ is a dimensionless plant water stress term [25], $r_d(z)$ is a root distribution function and L_r is the thickness of the root zone.

The water stress function $K_s(h)$ is evaluated as:

$$K_s(h, z) = \begin{cases} 0, & h > h_{ns} \\ 1, & h_{ns} \geq h > h_d \\ 1 - \frac{h-h_d}{h_w-h_d}, & h_d \geq h > h_w \\ 0, & h_w \geq h \end{cases} \quad (7)$$

where h_{ns} , h_d and h_w are water tension stress thresholds.

The plant roots were considered to be exponentially distributed with depth by the following relationship:

$$r_d(z) = \frac{\exp(-z/L_{rd})}{L_{rd}} \quad (8)$$

where L_{rd} [m] is the depth above which 63% of plant root density is located.

2.5 The Daily $ET_{c\ act}$ Construction Procedure

As shown in the equations below, the $ET_{c\ act}$ construction approach integrates the SEBAL retrieved $ET_{a\ be}$ with the temporal dynamics of daily ET_0 , NDVI, the root zone soil moisture dynamics by water stress coefficients K_s , E_s , and the water interception component, I_c . $ET_{c\ act}$ is obtained forwardly starting from each one of the acquisition days as shown in the following equation.

$$T_{c\ act,j} = T_{a\ eb,A.D.} \cdot \frac{ET_{0,j}}{ET_{0,A.D.}} \cdot \frac{NDVI_j}{NDVI_{A.D.}} \cdot \frac{K_{s,j}}{K_{s,A.D.}} \quad (9)$$

$$ET_{c\ act,j} = T_{c\ act,j} + E_{s,j} + I_{c,j} \quad (10)$$

where the subscript A.D. indicate the acquisition days and j the rest of the days of the studied period.

3 Results

The EC measured actual evapotranspiration ($ET_{a,EC}$) values were used as a reference for evaluating the performance of the SEBAL model and the integrated $ET_{c\ act}$ construction model. Although the results of this investigation are preliminary and were aimed to show the integrated modelling procedure potential in simulating $ET_{a,EC}$, our findings showed a good agreement between the SEBAL estimations and observed $ET_{a,EC}$ on the satellite acquisition days. The comparison on image acquisition days returned an overall average estimation error of 17%, a coefficient of determination (R^2) of 0.96, a mean absolute error (MAE) of 0.31 mm d⁻¹ and a root mean square error (RMSE) and 0.19 mm d⁻¹. The $ET_{a,EC}$ estimation errors were within the error bounds of the state-of-the-art ET measuring instruments and energy balance closure discrepancy from the ideal closure (± 15 to 30%) [5, 47].

In this paper we also compared the results of the daily $ET_{c\ act}$ construction integrated approach to the daily observed $ET_{a,EC}$ from the 7th of June 2013 (DOY 158) to the 1st of November 2014 (DOY 305). As shown in Fig. 2, the general trend of constructed $ET_{c\ act}$ slightly underestimated the observed data with an R^2 of 0.9, a MAE of 0.37 mm d⁻¹ and an RMSE of 0.21 mm d⁻¹. The temporal dynamics of $ET_{c,act,j}$ and $ET_{a,EC}$ and precipitation are plotted in Fig. 3(a). The proposed procedure reproduced accurately the general $ET_{a,EC}$ trend. The modeled and observed actual ET show similar patterns of variability. The integrated approach allowed adequately simulating actual ET under contrasting dry and wet conditions. Moreover, as shown in Fig. 3(b) the proposed integrated modeling approach returned good estimations of soil water content as compared to 0–40 cm measured soil moisture.

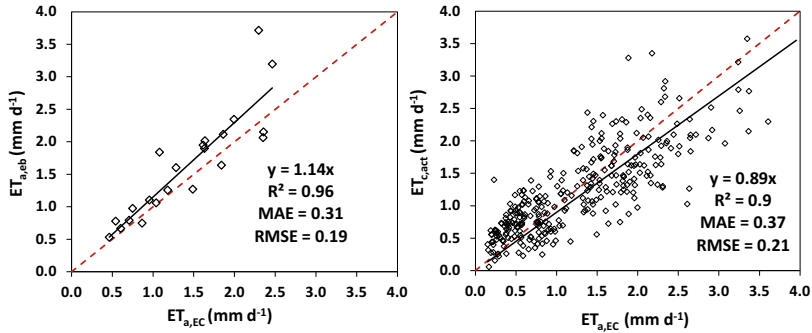


Fig. 2 Comparison of daily observed $ET_{a,EC}$ and SEBAL modeled $ET_{a,eb}$ on the Landsat image acquisition days and the daily constructed $ET_{c,act,j}$ on the studied period

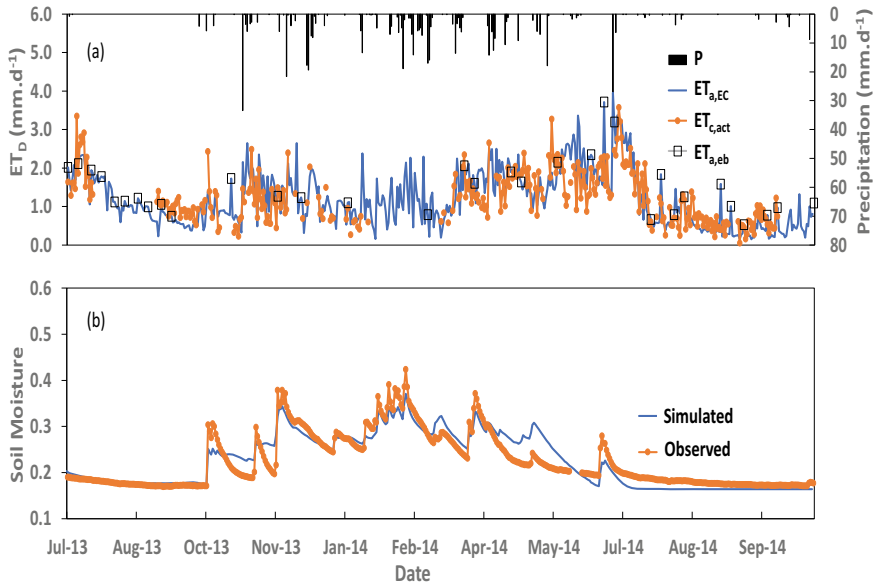


Fig. 3 a Daily time series of observed ($ET_{a,EC}$) and constructed actual evapotranspiration ($ET_{c,act,j}$), with the indication of the SEBAL estimated $ET_{a,eb}$ and observed precipitation (P). b Daily time series of observed and simulated soil moisture content

4 Discussion and Conclusions

The integrated daily $ET_{c,act}$ construction procedure efficiently reproduced the observed daily values of $ET_{a,EC}$ during the annual cycle of a Mediterranean maquis. In this study, the interactions between soil, vegetation and atmosphere is represented by coupling a hydrological model for water budgets, surface energy budget, RS

retrieved vegetation dynamics and meteorological variability. The temporal analysis of the modeled daily ET data-stream emphasized the importance of integrating a soil water evaporation model in the daily $ET_{c\ act}$ construction approach particularly in the period after significant rain events. The model simulated relatively high evapotranspiration values supported by adequate soil water availability after rainfall events. The distinguished performance of the integrated $ET_{c\ act}$ construction approach during the rainy spring period, where evaporative fluxes are significant, supported the importance of integrating a soil water evaporation model in the construction procedure. In this application NDVI values were retrieved from Landsat 8. Since NDVI values were interpolated between two Landsat scenes, it only permits a historical analysis. However, nowadays several available free or low-cost satellite platforms can provide NDVI scenes with a range of few days (e.g., Sentinels 2) supporting the near real-time monitoring of vegetation dynamics at a relatively high spatial resolution (10 m). The inclusion of a stress coefficient is required for considering the variation of plant transpiration due to soil moisture changes between acquisition days. The relatively good performance of the integrated approach in reproducing actual ET fluxes in the dry season emphasize the importance of considering plants stress. Moreover, it was important to account for the effect of soil moisture changes on plant transpiration, this is shown in Fig. 3(a), i.e., when using $ET_{a\ eb}$ obtained before significant soil moisture changes that occurs due to rainfall like that obtained on 27th of September 2013 or that occurs directly before an image acquisition like the $ET_{a\ eb}$ estimated on 17th of June 2014. The proposed construction approach is well suited for the modelling of daily $ET_{c\ act}$, which is of great importance in water management. For other type of applications, the simulation of near real-time and robust $ET_{c\ act}$ estimates at plot scale can be of a great value for agricultural water management and irrigation. The application of the proposed $ET_{c\ act}$ construction procedure in irrigation scheduling is a priority to realize soon.

References

1. Ahmad, M.-D., Bastiaanssen, W.G.M., Feddes, R.A.: A new technique to estimate net ground-water use across large irrigated areas by combining remote sensing and water balance approaches, Rechna Doab, Pakistan. *Hydrogeol. J.* **13**, 653–664 (2005). <https://doi.org/10.1007/s10040-004-0394-5>
2. Ahmad, M.D., Kirby, M., Islam, M.S., Hossain, M.J., Islam, M.M.: Groundwater use for irrigation and its productivity: status and opportunities for crop intensification for food security in Bangladesh. *Water Resour. Manag.* **28**, 1415–1429 (2014). <https://doi.org/10.1007/s11269-014-0560-z>
3. Akbari, M., Toomanian, N., Droogers, P., Bastiaanssen, W., Gieske, A.: Monitoring irrigation performance in Esfahan, Iran, using NOAA satellite imagery. *Agric. Water Manag.* **88**(1–3), 99–109 (2007). <https://doi.org/10.1016/j.agwat.2006.10.019>
4. Al Zayed, I.S., Elagib, N.A., Ribbe, L., Heinrich, J.: Spatio-temporal performance of large-scale Gezira irrigation scheme, Sudan. *Agric. Syst.* **133**, 131–142 (2015). <https://doi.org/10.1016/j.agry.2014.10.009>

5. Allen, R.G., Pereira, L.S., Howell, T.A., Jensen, M.E.: Evapotranspiration information reporting: I. Factors governing measurement accuracy. *Agric. Water Manage.* **98**(6), 899–920 (2011)
6. Allen, R.G., Tasumi, M., Trezza, R.: Satellite-based energy balance for mapping evapotranspiration with internalized calibration (METRIC)—model. *J. Irrig. Drain. Eng.* **133**(4), 380–394 (2007)
7. Allen, R.G., Pereira, L.S., Raes, D., Smith, M.: Crop evapotranspiration: Guidelines for computing crop water requirements. *Irr. Drain. Paper 56*. UN-FAO, Rome (1998)
8. Awada, H., Ciraolo, G., Maltese, A., Provenzano, G., Hidalgo, M.A.M., Côrcoles, J.I.: Assessing the performance of a large-scale irrigation system by estimations of actual evapotranspiration obtained by Landsat satellite images resampled with cubic convolution. *Int. J. Appl. Earth Obs. Geoinf.* **75**, 96–105 (2019)
9. Awada, H., Di Prima, S., Sirca, C., Giadrossich, F., Marras, S., Spano, D., Pirastru, M.: Daily actual evapotranspiration estimation in a Mediterranean ecosystem from Landsat observations using SEBAL approach. *Forests* **12**(2), 189 (2021)
10. Awada, H., Di Prima, S., Sirca, C., Giadrossich, F., Marras, S., Spano, D., Pirastru, M.: A remote sensing and modeling integrated approach for constructing continuous time series of daily actual evapotranspiration. *Agric. Water Manag.* **260**, 107320 (2022)
11. Baldocchi, D.D., Xu, L., Kiang, N.: How plant functional-type, weather, seasonal drought, and soil physical properties alter water and energy fluxes of an oak–grass savanna and an annual grassland. *Agric. for. Meteorol.* **123**(1–2), 13–39 (2004)
12. Bastiaanssen, W.G.M.: SEBAL-based sensible and latent heat fluxes in the irrigated Gediz Basin, Turkey. *J. Hydrol.* **229**, 87–100 (2000). [https://doi.org/10.1016/S0022-1694\(99\)00202-4](https://doi.org/10.1016/S0022-1694(99)00202-4)
13. Bastiaanssen, W.G.M., Brito, R.A.L., Bos, M.G., Souza, R.A., Cavalcanti, E.B., Bakker, M.M.: Low cost satellite data for monthly irrigation performance monitoring: benchmarks from Nilo Coelho, Brazil. *Irrig. Drainage Syst.* **15**(1), 53–79 (2001)
14. Bastiaanssen, W.G.M., et al.: A remote sensing surface energy balance algorithm for land (SEBAL): part 2: validation. *J. Hydrol. (amst)* **212**, 213–229 (1998)
15. Bastiaanssen, W.G.M., Van der Wal, T., Visser, T.N.M.: Diagnosis of regional evaporation by remote sensing to support irrigation performance assessment. *Irrig. Drain. Syst.* **10**(1), 1–23 (1996)
16. Bastiaanssen, W.G.M., Menenti, M., Feddes, R.A., Holtslag, A.A.M.: A remote sensing surface energy balance algorithm for land (SEBAL): 1. Formul. *J. Hydrol.* **212–213**(1998), 198–212 (1998b)
17. Bhattarai, N., Shaw, S.B., Quackenbush, L.J., Im, J., Niraula, R.: Evaluating five remote sensing based single-source surface energy balance models for estimating daily evapotranspiration in a humid subtropical climate. *Int. J. Appl. Earth Obs. Geoinf.* **49**, 75–86 (2016)
18. Blatchford, M.L., Karimi, P., Bastiaanssen, W.G.M., Nouri, H.: From global goals to local gains—a framework for crop water productivity. *ISPRS Int. J. Geo-Inf.* **7**(11), 414 (2018). <https://doi.org/10.3390/ijgi7110414>
19. Brooks, R.H., Corey, A.T.: Hydraulic properties of porous media. Hydrology paper No. 3, Colorado State Univ., Fort Collins (1964)
20. Cammalleri, C., Agnese, C., Ciraolo, G., Minacapilli, M., Provenzano, G., Rallo, G.: Actual evapotranspiration assessment by means of a coupled energy/hydrologic balance model: validation over an olive grove by means of scintillometry and measurements of soil water contents. *J. Hydrolog.* **392**, 70–82 (2010). <https://doi.org/10.1016/j.jhydro.2010.07.046>
21. Chen, X., Hu, Q.: Groundwater influences on soil moisture and surface evaporation. *J. Hydrol.* **297**(1–4), 285–300 (2004)
22. Choudhury, B.J.: Relationships between vegetation indices, radiation absorption, and net photosynthesis evaluated by a sensitivity analysis. *Remote Sens. Environ.* **22**(2), 209–233 (1987)
23. D’Urso, G.: Simulation and Management of On-Demand Irrigation Systems: a combined agro-hydrological approach. Ph.D. Dissertation, Wageningen University, p. 174, ISBN 90-5808-399-3 (2001)

24. Dickinson, R.E., Henderson-Sellers, A., Rosenzweig, C., Sellers, P.J.: Evapotranspiration models with canopy resistance for use in climate models, a review. *Agric. for Meteorol.* **54**(2–4), 373–388 (1991)
25. Feddes, R.A., Kowalik, P.J., Zaradny, H.: Water uptake by plant roots. In: Feddes, R.A., Kowalik, P.J., Zaradny, H. (Eds.) *Simulation of Field Water Use and Crop Yield*, pp 16–30. John Wiley & Sons, Inc., New York (1978)
26. Gowda, P.H., Chávez, J.L., Howell, T.A., Marek, T.H., New, L.L.: Surface energy balance based evapotranspiration mapping in the Texas high plains. *Sensors* **8**(8), 5186–5201 (2008)
27. Gutman, G., Ignatov, A.: The derivation of the green vegetation fraction from NOAA/AVHRR data for use in numerical weather prediction models. *Int. J. Remote Sens.* **19**(8), 1533–1543 (1998)
28. Immerzeel, W.W., Droogers, P.: Calibration of a distributed hydrological model based on satellite evapotranspiration. *J. Hydrol.* **349**, 411–424 (2008). <https://doi.org/10.1016/j.jhydrol.2007.11.017>
29. Kustas, W.P., Norman, J.M., Anderson, M.C., French, A.N.: Estimating subpixel surface temperatures and energy fluxes from the vegetation index-radiometric temperature relationship. *Remote Sens. Environ.* **85**, 429–440 (2003)
30. Lassabatère, L., Angulo-Jaramillo, R., Soria Ugalde, J.M., Cuenca, R., Braud, I., Haverkamp, R.: Beerkan estimation of soil transfer parameters through infiltration experiments—BEST. *Soil Sci. Soc. Am. J.* **70**(2), 521–532 (2006)
31. Maltese, A., Awada, H., Capodici, F., Ciralo, G., La Loggia, G., Rallo, G.: On the use of the eddy covariance latent heat flux and sap flow transpiration for the validation of a surface energy balance model. *Remote Sens.* **10**(2), 195 (2018)
32. Menenti, M.: Evaporation. In: Schultz, G.A., Engman, E.T. (eds.) *Remote Sensing in Hydrology and Water Management*, pp. 157–196. Springer, Heidelberg (2000). https://doi.org/10.1007/978-3-642-59583-7_8
33. Minacapilli, M., Cammalleri, C., Ciralo, G., Rallo, G., Provenzano, G.: Using scintillometry to assess reference evapotranspiration methods and their impact on the water balance of olive groves. *Agric. Water Manag.* **170**, 49–60 (2016)
34. Molden, D., Sakthivadivel, R.: Water accounting to assess use and productivity of water. *Int. J. Water Resour. Dev.* **15**(1–2), 55–71 (1999). <https://doi.org/10.1080/07900629948934>
35. Morse, A., Tasumi, M., Allen, R.G., Kramber, W. J.: Application of the SEBAL methodology for estimating consumptive use of water and streamflow depletion in the Bear River Basin of Idaho through remote sensing. In: Final report submitted to the Raytheon Systems Company, Earth Observation System Data and Information System Project, by Idaho Department of Water Resources and University of Idaho (2000)
36. Muthuwatta, L.P., Ahmad, M.-D., Bos, M.G., Rientjes, T.H.M.: Assessment of water availability and consumption in the Karkheh river basin, Iran—using remote sensing and geostatistics. *Water Resour. Manag.* **24**, 459–484 (2010). <https://doi.org/10.1007/s11269-009-9455-9>
37. Pirastru, M., Niedda, M.: Field monitoring and dual permeability modelling of water flow through unsaturated calcareous rocks. *J. Hydrol.* **392**(1–2), 40–53 (2010)
38. Reynolds, J.F., Kemp, P.R., Tenhunen, J.D.: Effects of long-term rainfall variability on evapotranspiration and soil water distribution in the Chihuahuan desert: a modeling analysis. *Plant Ecol.* **150**(1), 145–159 (2000)
39. Rodell, M., Velicogna, I., Famiglietti, J.S.: Satellite-based estimates of groundwater depletion in India. *Nature* **460**, 999–1002 (2009). <https://doi.org/10.1038/nature08238>
40. Rouse, J.W., Haas, R.H., Schell, J.A., Deering, D.W., Harlan, J.C.: Monitoring the vernal advancement and retrogradation (green wave effect) of natural vegetation. In: NASA/GSFC Type III Final Report, Greenbelt, Maryland, p. 371 (1974)
41. Senay, G.B., Schauer, M., Friedrichs, M., Velpuri, N.M., Singh, R.K.: Satellite-based water use dynamics using historical Landsat data (1984–2014) in the southwestern United States. *Remote Sens. Environ.* **202**, 98–112 (2017)

42. Stoy, P.C., et al.: Reviews and syntheses: turning the challenges of partitioning ecosystem evaporation and transpiration into opportunities. *Biogeosciences* **16**(19), 3747–3775 (2019)
43. Timmermans, W.J., Kustas, W.P., Anderson, M.C., French, A.N.: An intercomparison of the surface energy balance algorithm for land (SEBAL) and the two-source energy balance (TSEB) modeling schemes. *Remote Sens. Environ.* **108**(4), 369–384 (2007)
44. Tsakiris, G.: The status of the European waters in 2015: a review. *Environ Process* **2**(3), 543–557 (2015)
45. Van Genuchten, M.T.: A closed-form equation for predicting the hydraulic conductivity of unsaturated soils. *Soil Sci. Soc. Am. J.* **44**(5), 892–898 (1980)
46. Wagle, P., Bhattarai, N., Gowda, P.H., Kakani, V.G.: Performance of five surface energy balance models for estimating daily evapotranspiration in high biomass sorghum. *ISPRS J. Photogramm. Remote. Sens.* **128**, 192–203 (2017)
47. Wilson, K., et al.: Energy balance closure at FLUXNET sites. *Agric. for. Meteorol.* **113**(1–4), 223–243 (2002)
48. World Economic Forum 2021: World Economic Forum, The Global Risks Report 2021: 16th Edition (2021). http://www3.weforum.org/docs/WEF_The_Global_Risks_Report_2021.pdf. Accessed 4 May 2022
49. Zwart, S.J., Bastiaanssen, W.G.M., de Fraiture, C., Molden, D.J.: A global benchmark map of water productivity for rainfed and irrigated wheat. *Agric. Water Manag* **97**, 1617–1627 (2010). <https://doi.org/10.1016/j.agwat.2010.05.018>

Experimental Tests to Validate a Simple Procedure to Design Dual-Diameter Drip Laterals on Flat Fields



Giorgio Baiamonte , Mustafa Elfahl , and Samuel Palermo 

Abstract Multiple-diameter laterals reduce the total cost in microirrigation systems, however, the length of each sublateral should be determined carefully to assure appropriate performance of emitter flow rates. The most accurate method is the numerical trial and error, which is time-consuming. A series of research efforts have been made to propose simple analytical design procedures. By using the power-law form of the Darcy-Weisbach formula, and equal emitters spacing for the sublaterals, Sadeghi et al. (Sadeghi et al. in *J Irrig Drain E-ASCE* 142:04,016,020, 2016) extended a previously introduced design solution for one-diameter laterals to tapered laterals. Recently, a simplified procedure to design dual-diameter drip laterals has been introduced, providing relative errors in pressure heads less than 0.5%, and allowing to set different Hazen-Williams coefficients, flow rates and emitter interspaces for each sublateral. Moreover, this analytical procedure easily detects the required commercial emitter characteristics. The objective of this paper is to experimentally test this solution for drip sublaterals with different lengths, flow rates and emitter interspaces. Drip laterals of a major manufacturer (IRRITEC S.p.A) with diameters of 16 and 20 mm and given emitter characteristics were used in the experiments.

Keywords Dual-diameter drip laterals · Tapered lateral · Flow rate experimental measurements · Analytical solutions

G. Baiamonte (✉) · M. Elfahl · S. Palermo
Department of Agricultural, Food and Forest Sciences, University of Palermo, 90128 Palermo,
Italy
e-mail: giorgio.baiamonte@unipa.it

M. Elfahl
Department of Water Relations and Field Irrigation, Institute of Agricultural and Biological,
National Research Centre, 33 ELBohouth St., Dokki, Giza 12622, Egypt

© The Author(s), under exclusive license to Springer Nature Switzerland AG 2023
V. Ferro et al. (eds.), *AIIA 2022: Biosystems Engineering Towards the Green Deal*,
Lecture Notes in Civil Engineering 337,
https://doi.org/10.1007/978-3-031-30329-6_2

1 Introduction

Because of the climate change, water availability and food security are an issue of great concern, therefore an increasing use of irrigation systems is expected to be able to optimize the water use efficiency and to meet global food needs [2]. The limited availability of water for agriculture determined the need for a more prudent management of water. Moreover, among the criticalities, there is a general but certainly not negligible, rising energy costs.

In the irrigation field, the energy used to pump water has a fundamental importance and it is often consumed in large quantities. Compared to conventional irrigation methods, microirrigation offers a good opportunity to obtain substantial savings on energy and water consumption. For this reason, in recent decades, there has been an increasing interest in the microirrigation systems.

However, drip irrigation systems to be efficient, need that the water distribution uniformity is high enough. The distribution uniformity of water along the laterals is negatively affected by high pressure heads variation. Limitation of the pressure head variations depends on how accurate the design performed and on the accepted flow rate variability of the emitters installed along the laterals.

The use of tapered laterals allows reducing pressure variation along the lateral and water and energy consumption. Many efforts have been made to identify design procedures for tapered laterals. For equal flow rate and emitter spacing in the sublaterals, Valiantzas [3] introduced a new analytical continuous-uniform outflow approach that considers the effect of the number of outlets on the multidiameter lateral hydraulics. The latter is the extension to the previous modified energy-line approaches [4, 5] based on the two previous basic assumptions for designing multi-diameter irrigation laterals. The latter method was presented for the case of obtaining the general solution by the direct calculation and reported that this method is valid for all varying outlet discharge exponents.

In order to prevent trial and error and to use fewer head-loss equations, Sadeghi et al. [6] by maintaining the assumption of constant emitter spacing in the two sublaterals, and by considering the Hazen-Williams equation, introduced the factor H , demonstrating the advantage of using this factor over the approaches of Hart [7], Anwar [8] and Yitayew [9].

Recently, Sadeghi et al. [1] has extended for dual diameter lateral the analytical procedure to simulate the energy grade line along trickle laterals suggested by Valiantzas [10]. The authors used the Darcy-Weisbach formula to estimate the friction losses and then focused the effects of the different design parameters by making a comparison between the analytical method proposed and the numerical method step-by-step highlighting a high precision of the method.

However, an issue little covered in the past is detecting the commercial emitter characteristics that exactly match those corresponding to the design variables. The large number of commercially available products partly compensates this issue, but even small differences between commercial and design parameters can produce significant errors, frustrating the accuracy of the method.

The objective of this paper is to develop a simplified procedure to design tapered laterals and experimentally test it for drip sublaterals with different lengths, flow rates and emitter interspaces.

2 Materials and Methods

2.1 Simplified Procedure to Design Dual-Diameter Drip Laterals

Consider the sketch of a dual-diameter lateral laid on a horizontal field, displayed in Fig. 1. According to what commonly accepted, with respect to the flow direction, the Sublateral I ($j < N_I$) is characterized by a lower diameter, D_I (L), than that of the sublateral II, D_{II} (L).

Emitters are numbered from right to left, so that N_I and N_{II} are the number of emitters of sublateral I and II that are installed along the sublaterals with lengths, L_I (L) and L_{II} (L), respectively. Emitters flow rates, $q_{n,I}$ ($V T^{-1}$) and $q_{n,II}$ ($V T^{-1}$) can be different in both sublaterals, and also the emitters spacing, denoted by S_I (L) and S_{II} (L), respectively, which make it possible to determine the total lateral length, L , as illustrated in the Fig. 1. Moreover, the material of each sublateral can also be different, and it is described by the Hazen-Williams friction coefficient, according to C_I and C_{II} . However, in this work a common value for polyethylene pipe, $C_I = C_{II} = 135$, will be considered [11]. The local losses due to the integrated in-line emitters were considered, and the fraction coefficients of the kinetic head, $\alpha_I = 0.537$ and $\alpha_{II} = 0.332$, were assumed for the sublateral I and II, respectively [12].

Once the geometry of the dual-diameter lateral was established, for the hydraulic design the same procedure followed by Baiamonte [13] was applied, in order to suggest an easy to apply method to design tapered laterals, according to and established set of commercial emitter characteristics. The design procedure could be

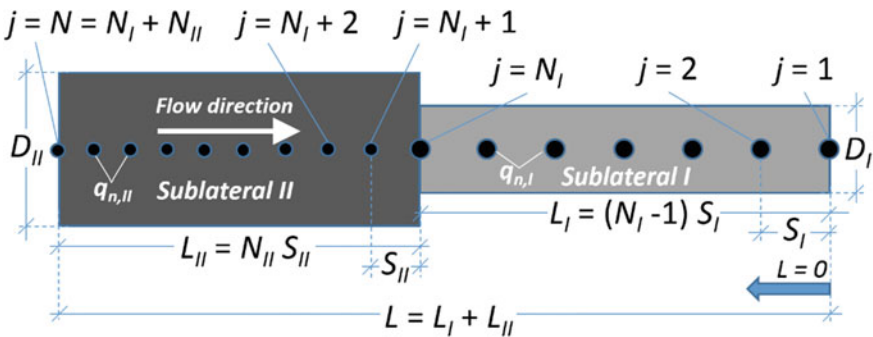
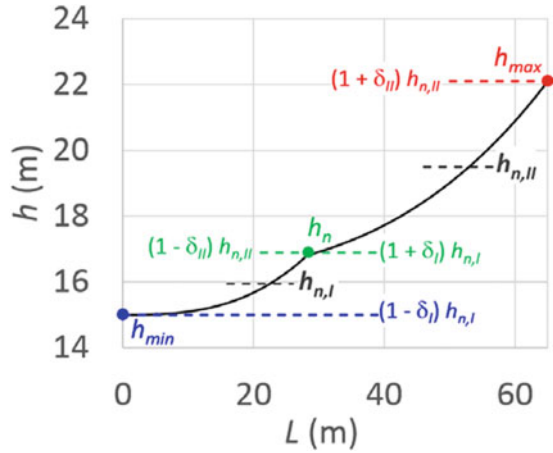


Fig. 1 Sketch of the considered dual-diameter drip lateral

Fig. 2 Example of pressure head distribution (PHD) of the dual-diameter lateral, where the characteristic pressure heads h_{min} , $h_{n,I}$, h_n , $h_{n,II}$ and h_{max} values are indicated



applied for two or more sublaterals, but for a simplified description of the procedure only two sublaterals will be considered here.

Figure 2 shows an example of pressure head distribution corresponding to a dual-diameter lateral, where the characteristic pressure heads are indicated. In particular, h_{min} is the minimum pressure head at $j = 1$ (Fig. 1), $h_{n,I}$, is the mean pressure head for the sublateral I, h_n is the maximum pressure head of the sublateral I that matches with minimum pressure head of the sublateral II, $h_{n,II}$ is the mean pressure head for the sublateral II, and h_{max} is the maximum pressure head of the dual-diameter drip lateral. We need to refer to Fig. 2 for describing the energy balance equations that can be written for the sublaterals I and II.

For the sublateral I ($j < NI$), following Baiamonte [13], under the assumption to neglect the emitter flow rate variation, the energy balance equation accounting for friction and local losses, can be written:

$$h_j = h_{min} + K_I L S_I \sum_{j=1}^j (j-1)^r + \alpha_I \frac{8q_{n,I}^2}{g\pi^2 D_I^4} \sum_{j=1}^j (j-1)^2 \quad (1)$$

where $h_j(L)$ is the pressure head at the emitter j , $h_{min}(L)$ is the minimum pressure head at the emitter $j = 1$, $q_{n,I}$ ($V T^{-1}$) is the emitters flow rates, corresponding to $h_{n,I}$, S_I is the emitter spacing, α_I is the fraction coefficient of the kinetic head, and K_I is the unit hydraulic gradient. For the selected Hazen-Williams resistance equation, K_I depends on the pipe diameter, $D_I(L)$, and emitter flow rate, $q_{n,I}$ ($V T^{-1}$), and on the numerical coefficients, $r = 1.852$ and $s = 4.871$:

$$K_I = \frac{10.675 q_{n,I}^r}{C_I^r D_I^s} \quad (2)$$

Dividing both sides by L , Eq. (1) can be rewritten:

$$h_{*j} = h_{*min} + K_I S_{*I} \sum_{i=1}^j (i-1)^r + \alpha_I K_{*L,I} \sum_{i=1}^j (i-1)^2 \quad (3)$$

where h_{*j} and h_{*min} are the pressure heads normalized with respect to L , whereas $K_{*L,I}$ and S_{*I} are, respectively:

$$K_{*L,I} = \frac{4^2 q_{n,I}^2}{2g(\pi D_I^2)^2 L} = \frac{8q_{n,I}^2}{g\pi^2 D_I^4 L} \quad (4)$$

$$S_{*I} = \frac{S_I}{L} \quad (5)$$

Equation (3) can be rewritten by using the generalized harmonic number truncated at the emitter j , in power $-r$ [14] and the Faulhaber's formula [15], respectively:

$$H(j-1, -r) = \sum_{i=1}^j (j-1)^r /; Re(r) > 1 \quad (6)$$

$$H(j-1, -2) = \sum_{i=1}^j (j-1)^2 = P_j = \frac{1}{6} j(j-1)(2j-1) \quad (7)$$

Substituting Eqs. (6) and (7) into Eq. (3) provides:

$$h_{*j} = h_{*min} + K_I S_{*I} H(j-1, -r) + \alpha_I K_{*L,I} P_j \quad (8)$$

Of course, for $j = N_I$, $h_{*j} = h_{*n}$:

$$h_{*n} = h_{*min} + K_I S_{*I} H(N_I - 1, -r) + \alpha_I K_{*L,I} P_{N_I} \quad (9)$$

Equation (9) can be rewritten by denoting as $Y_{Fr,I}$ and $Y_{L,I}$ the friction losses and the minor losses terms, respectively:

$$h_{*n} = h_{*min} + \Psi_{Fr,I} + \Psi_{L,I} \quad (10)$$

On the other hand, the normalized pressure heads, h_{*min} and h_{*n} , can be also expressed as a function of the pressure head tolerance of the sublateral I, d_I (Fig. 2):

$$h_{*min} = h_{*n,I}(1 - \delta_I) \quad (11)$$

$$h_{*n} = h_{*n,I}(1 + \delta_I) \quad (12)$$

that are linked by the following relationship:

$$h_{*n} = h_{*min} \frac{1 + \delta_I}{1 - \delta_I} \quad (13)$$

Substituting Eq. (13) into Eq. (10), yields:

$$h_{*min} \frac{1 + \delta_I}{1 - \delta_I} = h_{*min} + \Psi_{Fr,I} + \Psi_{L,I} \quad (14)$$

that can be solved with respect to δ_I :

$$\delta_I = \frac{\Psi_{Fr,I} + \Psi_{L,I}}{2h_{*min} + \Psi_{Fr,I} + \Psi_{L,I}} \quad (15)$$

For the Sublateral II ($j > N_I$), by maintaining a notation like that considered for the Sublateral I, the energy balance equation can be written:

$$h_{*j} = h_{*n} + K_{II} S_{*j,II} [H(j-1, -r) - H(N_I - 1, -r)] + \alpha_{II} K_{*L,II} (P_j - P_{N_I}) \quad (16)$$

where P_j and P_{N_I} are the Faulhaber's formula [15] associated with j and N_I (Eq. 6), respectively. Of course, for $j = N$, Eq. (16) provides the maximum normalized pressure head of the dual-diameter drip lateral:

$$h_{*max} = h_{*n} + K_{II} S_{*j,II} [H(N-1, -r) - H(N_I - 1, -r)] + \alpha_{II} K_{*L,II} (P_N - P_{N_I}) \quad (17)$$

whereas P_N the Faulhaber's formula [15] associated to the total number of emitter $N = N_I + N_{II}$:

$$P_N = \frac{1}{6} N(N-1)(2N-1) \quad (18)$$

Similar to the sublateral I, for $j = N = N_I + N_{II}$, Eq. (17) provides h_{*max} :

$$h_{*max} = h_{*n} + \Psi_{Fr,II} + \Psi_{L,II} \quad (19)$$

where:

$$\Psi_{Fr,II} = K_{II} S_{*II} [H(N-1, -r) - H(N_I - 1, -r)] \quad (20)$$

$$\Psi_{L,II} = \alpha_{II} K_{*L,II} (P_N - P_{N_I}) \quad (21)$$

On the other hand, the normalized pressure heads, h_{*n} and h_{*max} , can be also expressed as a function of the pressure head tolerance of the sublateral II, δ_{II} (Fig. 2):

$$h_{*n} = h_{*n,II} (1 - \delta_{II}) \quad (22)$$

$$h_{*max} = h_{*n,II} (1 + \delta_{II}) \quad (23)$$

that makes it possible to express h_{*max} as a function of h_n :

$$h_{*max} = h_{*n} \left(\frac{1 + \delta_{II}}{1 - \delta_{II}} \right) \quad (24)$$

Substituting Eq. (13) into Eq. (24), a relationship between h_{*max} and h_{*min} can be derived:

$$h_{*max} = h_{*min} \left(\frac{1 + \delta_I}{1 - \delta_I} \right) \left(\frac{1 + \delta_{II}}{1 - \delta_{II}} \right) \quad (25)$$

Substituting Eq. (25) into Eq. (19), yields:

$$h_{*min} \left(\frac{1 + \delta_I}{1 - \delta_I} \right) \left(\frac{1 + \delta_{II}}{1 - \delta_{II}} \right) = h_{*min} \frac{1 + \delta_I}{1 - \delta_I} + \Psi_{Fr,II} + \Psi_{L,II} \quad (26)$$

where h_{*min} can be made explicit:

$$h_{*min} = \frac{(1 - \delta_I)(1 - \delta + \delta_I)}{2((\delta - \delta_I) + \delta_I(\delta - \delta_I))} (\Psi_{Fr,II} + \Psi_{L,II}) \quad (27)$$

Substituting Eq. (15) into Eq. (27), and solving with respect to δ , yields:

$$\delta = \frac{2(h_{*min} + \Psi_{Fr,I} + \Psi_{L,I})(\Psi_{Fr,I} + \Psi_{L,I} + \Psi_{Fr,II} + \Psi_{L,II})}{(2h_{*min} + \Psi_{Fr,I} + \Psi_{L,I})(2(h_{*min} + \Psi_{Fr,I} + \Psi_{L,I}) + \Psi_{Fr,II} + \Psi_{L,II})} \quad (28)$$

The characteristics of the commercial drip laterals emitters considered in the present investigation are made by IRRITEC S.p.A. and are reported in Table 1.

In particular, for the corresponding h_{min} , D_I , C , S , α_I , for the sublateral I, and for D_{II} , and α_{II} , for the sublateral II, Fig. 3a shows the pressure head tolerance of sublateral I, δ_I (Eq. 15), whereas Fig. 3b shows the pressure head tolerance of the dual diameter sublateral, δ (Eq. 28), as a function of the number of the emitter N_I , with the emitter flow rate as a parameter.

As expected, both δ_I and δ increase at increasing N_I , and for fixed N_I increase at increasing the emitter flow rate, q_n . The figures also show the dots corresponding to run #1 that will be selected for the applications that will be performed later.

2.2 Determining the Characteristics of the Emitter for Sublaterals I and II

As previously observed, the emitter flow rate – pressure head relationship is compulsory to be considered when designing according to non-pressure compensated emitters [16]. In this context, where the mean flow rate of the dual sublateral is assumed

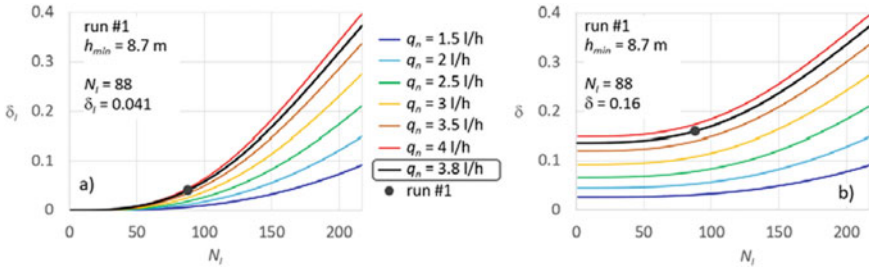


Fig. 3 For run #1 (Table 1), pressure head tolerance a) of the sublateral I, δ_I , and b) of the dual-diameter lateral, δ , vs. the number of emitters in the sublateral I, N_I , by varying q_n . For $q_n = 3.8$ l/h, the selected N_I value is indicated

“constant”, the emitter characteristics (k and x) of the flow rate – pressure head relationship, have to be determined with reference to the mean pressure head value of each sublateral, $h_{n,I}$ and $h_{n,II}$ (Fig. 2).

$$k_{e,I} = 3.610^6 q_n \left(\frac{(1 - \delta_I^2)}{L h_{*min} (1 + \delta_I)} \right)^{x_I} \tag{29}$$

$$k_{e,II} = 3.610^6 q_n \left(\frac{(1 - \delta_I)(1 - \delta + \delta_I)}{L h_{*min} (1 + \delta_I)} \right)^{x_{II}} \tag{30}$$

Equation (29) and Eq. (30) can be applied together with the pressure head tolerance relationships (δ_I , Eq. 15, and δ Eq. 28) versus N_I , to detect the emitters characteristics that match the commercial ones (Table 1). Towards this aim, for run #1, Fig. 4 shows Eq. (29) and Eq. (30), with q_n as a parameter, together with the horizontal lines indicating the commercial emitters characteristics (solid-dots), making possible to detect the commercial emitters that better fit the simplified analytical design procedure.

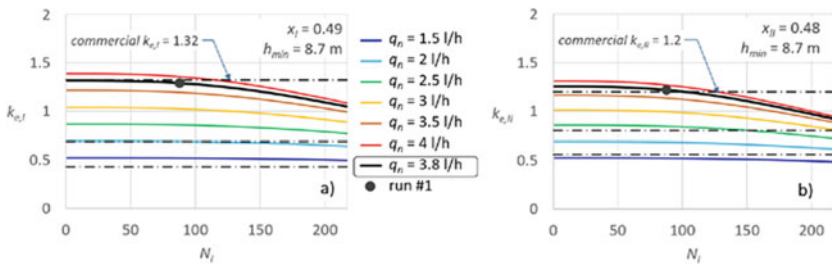


Fig. 4 For run #1 (Table 1), emitter scale parameter $k_{e,I}$, a) of the sublateral I, $k_{e,I}$, and b) of the sublateral II, $k_{e,II}$, vs. the number of emitters in the sublateral I, N_I , by varying q_n . For $q_n = 3.8$ l/h, the selected N_I value is indicated. Solid-dot lines refer to the commercial emitters

3 Experimental Results

The results obtained by the experimental campaign consist in comparing the experimental emitter pressure derived by the emitter flow rates, according to the pressure head – flow rates relationship, with those derived by the simplified design procedure (Eq. 8 and Eq. 16).

For run #1, run #2 and run #3 (Table 1), Fig. 5 shows the pressure head distribution (PHD) line obtained by the simplified procedure (Eq. 8 and Eq. 16, red line) and the PHD obtained by the exact SBS procedure (black line). Figure 5 also shows the range of variability of pressure heads, according to the considered $CVT = \pm 3\%$, applied to the SBS PHD. As can be observed in the figure, the experimental pairs (L, h) lay in between the considered range, validating the suggested simplified procedure.

Furthermore, it is noteworthy that the differences between pressure heads derived the SBS procedure and those derived by the simplified procedure are much lesser than the above-mentioned range of variability based on CVT.

Analogously to Table 1, for each sublateral, Table 2 reports the results of the experimental applications, together with the coefficient of variation in pressure head CV, the corresponding flow rate tolerance (δ_q), the detected pressure head tolerances (δ_I , δ_{II} and δ), and finally the characteristic pressure heads, h_{min} , $h_{n,I}$, h_n , $h_{n,II}$, and $h_{max} \equiv h_{in}$. The results reported in Table 1 and Table 2 can be compared.

Of course, the slight differences between the pressure head and flow rate tolerances have to be ascribed to the assumption of neglecting flow rate variation in the simplified procedure, but also to the assumed CVT, which undoubtedly plays an important role in determining the experimental flow rate and pressure tolerances.

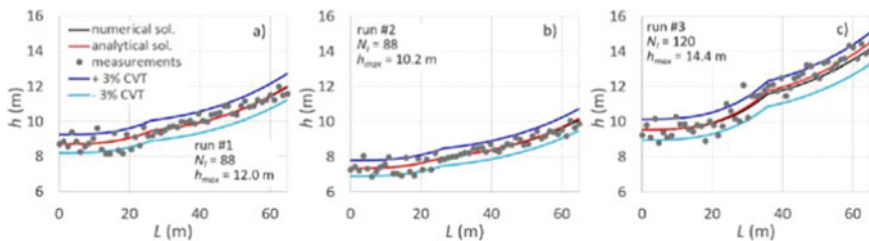


Fig. 5 For runs #1, 2 and 3, comparison between the “dual” PHD obtained by the suggested design procedure and that by the numerical method (SBS). The figure also illustrates the corresponding pressure heads determined by the measured emitter flow rates, and the range of pressure heads by assuming the manufacturing coefficient of variation $CVT = \pm 0.03$

Table 2 Parameters associated with the experimental procedure corresponding to the applications performed

run #	Sublat	D (mm)	S_I, S_{II} (m)	N_I, N_{II}	L_I, L_{II} (m)	q_{in} (l/s)	q_{av} (U/h)	$q_{av,I}, q_{av,II}$ (U/h)	σ_I, σ_{II}	CV_I, CV_{II}	CV	δ_q	δ_I, δ_{II}	δ	$h_{av,I}, h_{av,II}$ (m)	$h_{min}, h_{in}, h_{max} \equiv h_{in}$ (m)	EU (%)
1	I	13.8	0.3	88	26.1	0.228	3.75	3.83	0.10	0.026	0.035	0.071	0.073	0.218	8.79	8.14	89.17
	II	17.7	0.3	129	38.7			3.70	0.12	0.034			0.144		10.48	9.15	
2	I	13.8	0.3	88	26.1	0.210	3.45	3.53	0.10	0.027	0.035	0.070	0.075	0.217	7.43	6.87	89.79
	II	17.7	0.3	129	38.7			3.41	0.11	0.032			0.142		8.79	7.80	
3	I	13.8	0.3	120	35.7	0.248	4.10	4.08	0.18	0.043	0.038	0.078	0.125	0.233	10.05	8.79	89.92
	II	17.7	0.3	97	29.1			4.11	0.13	0.031			0.108		13.03	11.82	
																14.44	

4 Conclusions

In recent years, among the research activities carried out at the Department of Agricultural, Food and Forest Sciences of the University of Palermo, the microirrigation system design was deeply addressed. The activity focused on finding simplified design procedures for one-diameter laterals, aimed at maximizing water and energy saving, in place of the common numerical design methods that require many trial-and-error attempts and time-consuming iterations. In this paper the simplified procedure was extended to the design of tapered laterals and different experimental tests to validate this procedure were presented.

Of course, this is only the first step, since the proposed solutions need to be extended to drip laterals laid on sloping fields and to the manifolds, where the use of more than one diameter could be a convenient choice from an energy saving point of view.

References

1. Sadeghi, S.H., Peters, T., Shelia, V.: Energy grade line assessment for tapered microirrigation laterals. *J. Irrig. Drain E-ASCE* **142**(7), 04016020 (2016)
2. Madramootoo, C.A., Morrison, J.: Advances and challenges with microirrigation. *Irrig. Drain* **62**, 255–261 (2013)
3. Valiantzas, J.D.: Hydraulic analysis and optimum design of multi-diameter irrigation laterals. *J. Irrig. Drain E-ASCE* **128**(2), 78–86 (2002)
4. Valiantzas, J.D.: Analytical approach for direct drip lateral hydraulic calculation. *J. Irrig. Drain E-ASCE* **124**(6), 300–305 (1998)
5. Valiantzas, J.D.: Continuous outflow variation along irrigation laterals: effect of the number of outlets. *J. Irrig. Drain E-ASCE* **128**(1), 34–42 (2002)
6. Sadeghi, S.H., Mousavi, S.F., Sadeghi, S.H.R., Abdolali, M.: Factor H for the calculation of head loss and sizing of dual-diameter laterals. *J. Agric. Sci.* **14**, 1555–1565 (2012)
7. Hart, W.E.: *Irrigation System Design*. Lecture Note, Dept. of Agricultural and Chemical Engineering, Colorado State Univ., Fort Collins, CO (1975)
8. Anwar, A.A.: Factor G for pipelines with equally spaced multiple outlets and outflow. *J. Irrig. Drain E – ASCE*. **125**(1), 34–38 (1999)
9. Yitayew, M.: Simplified method for sizing laterals with two or more diameters. *J. Irrig. Drain E – ASCE*. **135**(1), 111–114 (2009)
10. Valiantzas, J.D.: Modified Hazen-Williams and Darcy-Weisbach equations for friction and local head losses along irrigation laterals. *J. Irrig. Drain E-ASCE* **131**(4), 342–350 (2005)
11. Moghazi, H., ElDin, M.: Estimating Hazen-Williams coefficient for polyethylene pipes. *J. Transp. Eng.* **124**, 197–199 (1998)
12. Provenzano, G., Pumo, D.: Experimental analysis of local pressure losses for microirrigation laterals. *J. Irrig. Drain E-ASCE* **130**(4), 318–324 (2004)
13. Baiamonte, G.: Advances in designing drip irrigation laterals. *Agr. Water Manage* **199**, 157–174 (2018)
14. Abramowitz, M., Stegun, I.A.: *Handbook of Mathematical Functions*. Dover Publications, New York (1972)
15. Bazsó, A., Pintér, Á., Srivastava, H.M.: A refinement of Faulhaber’s theorem concerning sums of powers of natural numbers. *Appl. Math. Lett.* **25**, 486–489 (2012)
16. Baiamonte, G.: Simple relationships for the optimal design of paired drip laterals on uniform slopes. *J. Irrig. Drain E-ASCE* **142**(2), 04015054 (2016)

An Innovative Soil Bioengineering Technique by Waste Materials: The RiVite Project



Giorgio Baiamonte , Roberta Calvo , Gianluigi Pirrera, Samuel Palermo , and Francesco D'Asaro 

Abstract This paper describes the RiVite project granted by the Italian Ministry of Economic Development according to the JUMP (Joint Universities Program for PoC) program for patents enhancement, proposed by Sant'Anna School, Scuola Normale and the University of Palermo. The patent (Calvo, R., D'Asaro, F., Baiamonte, G.: Metodo per la realizzazione di un'opera costruttiva modulare per la protezione del territorio e detta opera. Attestato di Brevetto per Invenzione Industriale, n° 102,017,000,141,369, Ministero dello Sviluppo Economico, Roma, 27/02/2020.) consists of an advanced soil bioengineering work providing anti-erosion function, consolidating and stabilizing of slopes, thus for land protection. The technique is based on modular elements construction (Roll Modular Fascine, RFM, 40 cm × 60 cm) made with the residues of vine pruning collected with specialized agricultural machines. The RFMs are filled with a pre-seeded cultivation substrate, consisting of a mixture of beached *Posidonia oceanica* (L.) Delile, seeds of autochthonous species and coolant fluids. The wooden part of the work resists only for the time to rooting and development of the native species, after which the resistant action will be exerted by the root systems. The final work was realized connecting longitudinally the RFMs with cables or wire meshes. Differently from the common works, thanks to the assembling system, the proposed patented work is less time consuming, and reduces CO₂ emissions because of reusing waste materials. The project was based on different prototypes, and the JUMP program made it possible to implement four prototypes in two areas near Etna volcano (Nicolosi, Giarre).

Keywords Soil bioengineering technique · Vine shoots · Vine pruning · *Posidonia oceanica* residues

G. Baiamonte (✉) · S. Palermo
Department of Agricultural, Food and Forest Sciences, University of Palermo, 90128 Palermo, Italy
e-mail: giorgio.baiamonte@unipa.it

R. Calvo · F. D'Asaro
Associazione Italiana per L'Ingegneria Naturalistica, 90139 Palermo, Italia

G. Pirrera
Biocity Engineering s.r.l., Palermo, Italy

1 Introduction

Because of multiple environmental problems, the need to operate in a sustainable way is increasingly manifested, thus trying to adopt the guidelines of the Circular Economy (economic system that can regenerate itself by ensuring eco-sustainability) [2]. Environmental engineering, as a technical-scientific discipline, studies the use of the living plant component associated with other eco-compatible materials, and is based on several principles:

- 1) the reuse of waste materials and their release into the production cycle;
- 2) the use of renewable resources;
- 3) the eco-sustainability and environmental adequacy of the proposed soil bioengineering technique.

The basic element of the RiVite project is a modern version of the fascines that, as well known, is the collection of branches of small size, of ancient origin. The project describes the idea behind the soil bioengineering technique patented by the University of Palermo and the subsequent implementation of four prototypes.

The innovative technique suggested of the RiVite project is based on the formation of modular construction elements, made with organic waste materials (pruning residues of the vine, that is the vine shoots, and beached *P. oceanica*), and the low-cost assembly system for the formation of the work [1].

The implementation process is consistent with the economic policies of the European Union, for which the economy is circular when a system preserves the value of products, materials, and economic resources for as long as possible, by supplementing reuse, the repair, regeneration, or recycling of products and thereby reducing the generation of waste.

Moreover, this approach respects the DNSH (Do No Significant Harm) principle established by Regulation (EU) 2020/852 of 18 June 2020 on the establishment of a framework (Taxonomy Regulation) that favors and defines "sustainable investment" economic activities contributing to an environmental objective and/or a social objective, provided, however, that such investments "do not cause significant damage". The proposed artifact takes into account the life cycle of the vine shoots and the services provided by the wine-growing activities, setting as objectives to be achieved those set out in the Taxonomy Regulation, namely: a) the mitigation of climate change; b) adaptation to climate change; c) sustainable use and protection of water and marine resources; d) circular economy, including waste prevention and recycling; c) prevention and reduction of air, water or soil pollution; f) the protection and restoration of biodiversity and ecosystems.

2 Materials and Methods

The patent of the soil bioengineering technique, on which the RiVite project is based, concerns the method and the building materials used for the realization of the work

itself. More precisely, an innovative technique is advanced that involves the formation of modular construction elements, made with organic waste materials at low cost, and the assembly system for the formation of the work. The research on the reuse of organic waste materials in the field of soil bioengineering works, led to the development of the construction technique for modules of a fascines, denoted as Roll Modular Fascines (RFM) [3].

The basic idea of the patent is therefore the recovery of organic waste materials. At the same time, beached biomass, suitably treated, which are destined to the constitution of the cultivation substrate for the growth of native species in the body of the work. The pruning residues of the vine, that is the vine shoots, and those of the beached *P. oceanica* (Fig. 1) constitute therefore the two biomasses employed in the construction of the soil bioengineering work.

The basic element of the work (module) is a vine pruning residues mechanically assembled with specialized agricultural machines and currently on the market. The mechanical assembly of the modules (RFM), involving the improvement of the production process, compared to traditional works (fascines), resulting in an increase in productivity, a reduction in costs and construction times.

The new product, made with local and renewable waste materials, responds to the growing demand of the market in terms of defense and protection of the environment, against a framework of supply of similar products of import and higher cost (e.g. coconut fiber, biorollers, etc.).

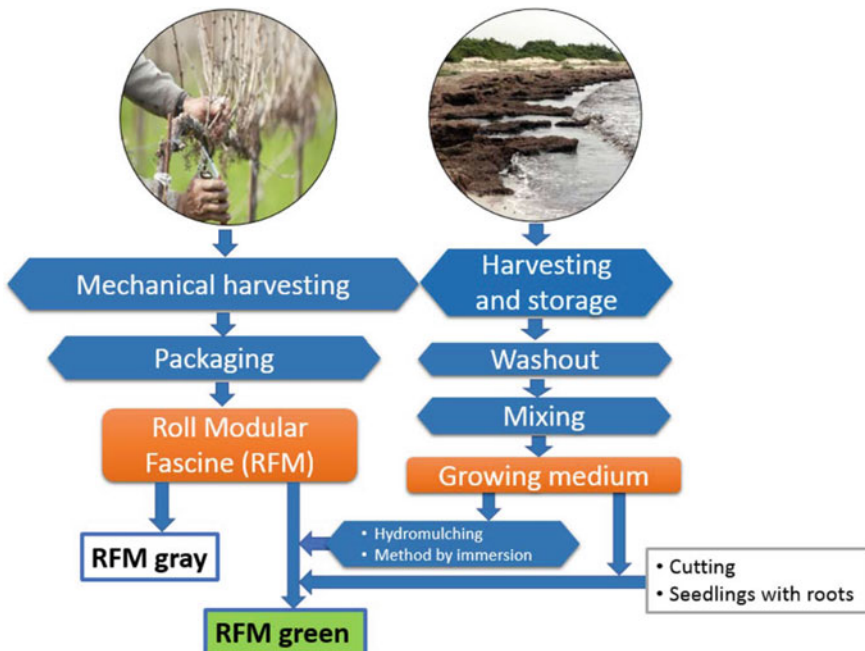


Fig. 1 Basic idea for the construction of the Roll Modular Fascines (RFM)

2.1 Materials Used in the Soil Bioengineering Work

The pruning residues of vines have many advantageous characteristics that make them suitable for the construction of the soil bioengineering works i) have a cost practically negligible, ii) are easy to find in the national country, iii) constitute a renewable resource on an annual scale. The reuse of this material, as an alternative to its burning, or to its burial or its transfer in rubbish dumps, is a considerable advantage both from the ecological and the economic point of view.

Analysis of the mechanical characteristics of the vine shoots, aimed at testing the resistance and durability of the material, showed values of the breaking stresses ranging from 35 to 55 MPa depending on the cultivar. The vine shoots are then collected mechanically for the establishment of the RFM. In the RiVite project, the CAEB International QUICKPOWER 1230 round bale wrapping machine (Fig. 2) was used, operating on rows larger than 160 cm, capable of completing the entire processing cycle:

- loading of vine shoots in the machine (up to 30 mm diameter);
- tying the RFM with natural fiber twine;
- automatic unloading from the rear door in a few minutes (Fig. 2).



Fig. 2 a Vine shoots collecting and Roll Modular Fascine (RFM) production with the CAEB International QUICKPOWER 1230 round bale wrapping machine, b weight collecting of RFM, c low density RFM (100 kg/m^3)

The size of the RFM produced is: 40 cm in diameter and 60 cm height. The machine harvests along rows of 200×80 cm where the pruning residues must be previously arranged perpendicular to the direction of machine motion.

Mechanized packaging significantly increases the apparent density of RFMs from 40–80 kg/m³ of conventional fascines to 100–300 kg/m³ for RFMs. By acting on a device, the compression adjustment in the wrapping chamber of the RFM, allows varying the RFM density.

The beached *P. oceanica* residues, previously washed out, instead have optimal characteristics for the constitution of the growing medium of the RFMs, in substitution of the soil. The RFMs, packaged at low density, in fact allow their filling with a substrate with a growing medium consisting of *P. oceanica* residues, composted organic vegetable residues and a mixture of native seeds.

The beaching of *P. oceanica* residues is a natural phenomenon that annually occurs in all countries of the Mediterranean basin and therefore represents a high renewable source of biomass. The removal and subsequent use therefore have a threefold advantage: the use of the beach, solving the waste disposal problem and the creation of new local and low-cost products, reusable in the field for the environmental rehabilitation.

The formation of a fertile substratum is fundamental for the rooting and the development of the vegetation inside the RFMs and it is useful to counteract the growing phenomenon of desertification. Moreover, the high degree of porosity of the residues reduces the phenomenon of radical asphyxia, allowing a good drainage [4] and creating the optimal conditions for the seedlings rooting and vegetative growth [5].

2.2 *Assembling the RFM Modules*

The soil bioengineering work is realized by connecting the RFMs with a mounting system that makes the structure resistant. This then allows the resulting RFM, in the initial pre-greening phase, to support the earth pressure exerted by the soil upstream. A connection example is described in Fig. 3. The connection could be made with textile or metal cables passing longitudinally inside or outside the RFM. The RFMs, so connected and bound on discrete points to the ground, therefore increase their degree of mechanical resistance, and react to earth pressure well (Fig. 3). However, for the four prototypes described below different assembling procedures will be considered and then implemented in the field.

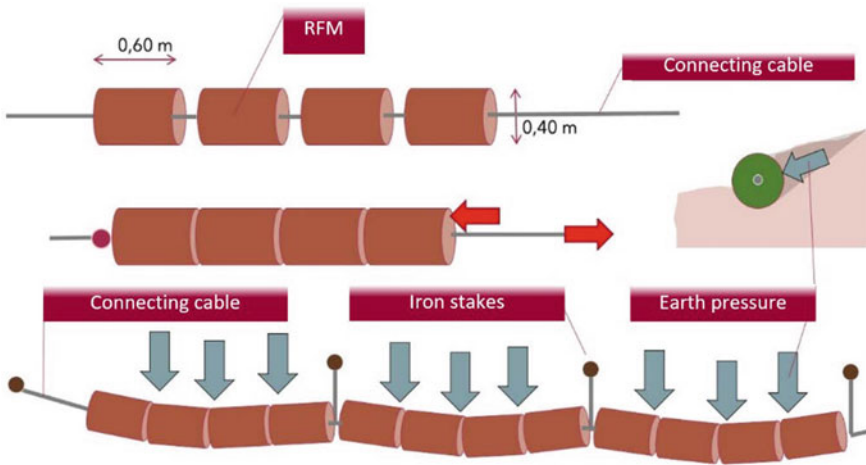


Fig. 3 Example of RFMs assembling

3 Sites Description and Prototypes

The realization of the soil bioengineering work described above allowed the achievement of the Technology Readiness Level (TRL) 5, with the technology of the patent idea that has been validated in the field. A further increase in technological development was achieved at the end of the project, reaching TRL 7 (Demonstration of a system prototype in the operating environment).

The project RiVite financed by the MISE therefore envisaged the design of the experimental plant of prototypes of the soil bioengineering work, in line with the idea of patenting, its implementation and subsequent monitoring in order to highlight its effectiveness.

The working team is composed of the proposers and the co-funding company Jonica 2001 Soc. Coop. ARL, Giarre (CT), which has carried out the intense activities in the field.

3.1 Sites Description

The prototypes of the soil bioengineering work have been realized in two adjacent areas to the park of the Etna volcano, having rather different pedoclimatic characteristics (Fig. 4).

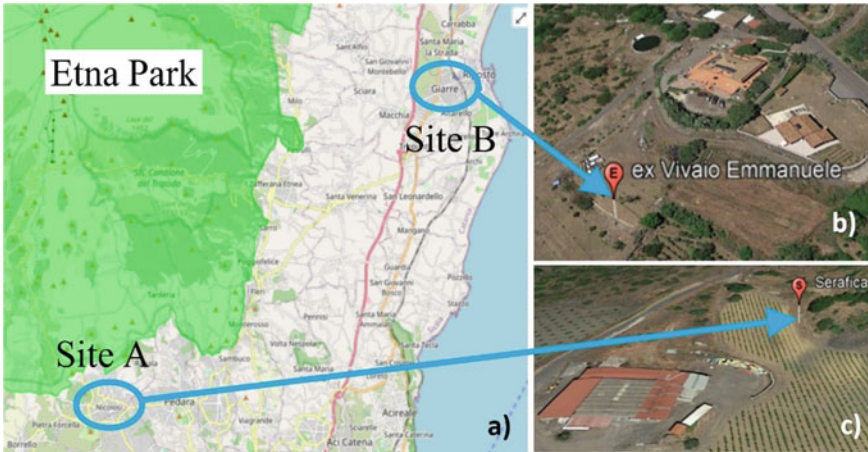


Fig. 4 a Sites location; b site A (Nicolosi, CT) Google earth V 7.1.2.2600 (May 24, 2020). Nicolosi, Italy. 37°36'17.74" N, 15°00'44.48" E, Elev. 664 m., c site B (Giarre, CT). Google earth V 7.1.2.2600 (May 24, 2020). Giarre, Italy. 37°43'57.07" N, 15°09'07.74" E, Elev. 319 m. <https://earth.google.com>

The first site, denoted A in the project, is located in the municipality of Nicolosi at an altitude of about 670 m s.l.m. The second site, denoted B, is in the municipality of Giarre at an altitude of about 320 m s.l.m.

3.2 Prototypes

Four prototypes, diversifying in RFM assembling and implementation, reproducing different static characters of the linear bioengineering work, were designed, and implemented in the field. The height of the work has always been less than one meter.

The two prototypes, called A1 and A2, were located upstream of the Azienda Serafica. The other two prototypes, denoted B1 and B2, were arranged inside the Azienda Vivai Emmanuele. The prototypes A1 and A2 were arranged on the same line, along a total length of 60 m, at the edge of the existing vineyard. The prototype A1, 30 m long, of overall height above ground 80 cm, consists of a fence of sharp wooden stakes with reinforcement crosspieces formed by two overlapping rows of RFM not connected (Fig. 5). The fence consists of chestnut stakes 1 m high above ground, interspaced 60 cm (the RFM size) connected by a rail at half height. Transversal stakes, arranged at 50° on the horizontal, one for each 1.8 m, were also arranged. In this scheme the RFMs have no static function. Figure 6 shows the implemented prototype A1.

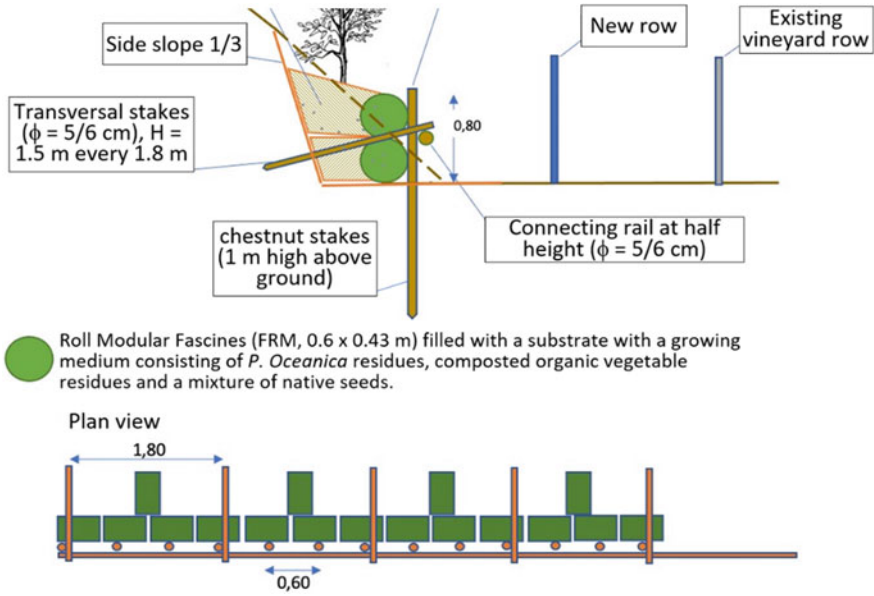


Fig. 5 Sketch of the prototype A1 (section and plan view)



Fig. 6 The implemented prototype A1

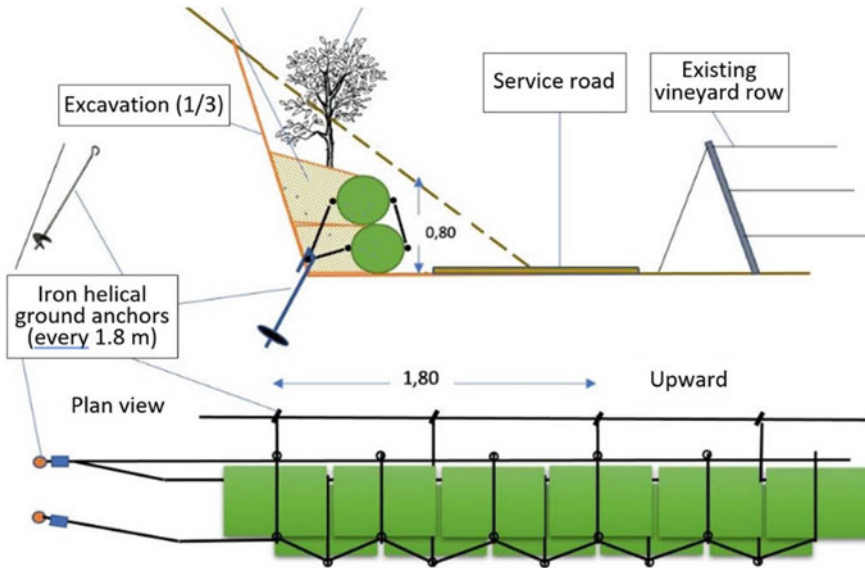


Fig. 7 Sketch of the prototype A2 (section and plan view)

The A2 prototype, on the other hand, provides a full static function of the fascines consisting of two overlapping rows of RFM (Fig. 7). The individual rows are connected by two longitudinal connecting cables, tied, and fixed at the ends and in intermediate points of the bioengineering work with iron helical ground anchors. The frontal face of the bioengineering work is reinforced by a steel cable that binds the two overlapping rows with a zig-zag pattern. As a whole the structure reacts to the earth as a catenary constrained in discrete points. Figure 8 shows the implemented prototype A2.

The smaller B1 and B2 prototypes (4.2 m and 5.4 m) were arranged along the upper edge of a terracing in stone wall which collapsed in several places. Thus, the intervention consisted in "weeding" of the existing wall by reconstructing two missing sections.

The B1 prototype consists of two steps made by two RFM fans with double height closed by galvanized loose metal mesh fixed to the ground by metal pegs (Fig. 9). The resulting gabions are supported downstream by metal pegs 1 m above ground, interspaced 0.60 m. The static pattern is a mixture of that of the armed land and that of the gabions. The overall height difference of the work reaches 1.70 m for a width of steps equal to about 2 m. Figure 10 shows the implemented prototype B1.



Fig. 8 The implemented prototype A2

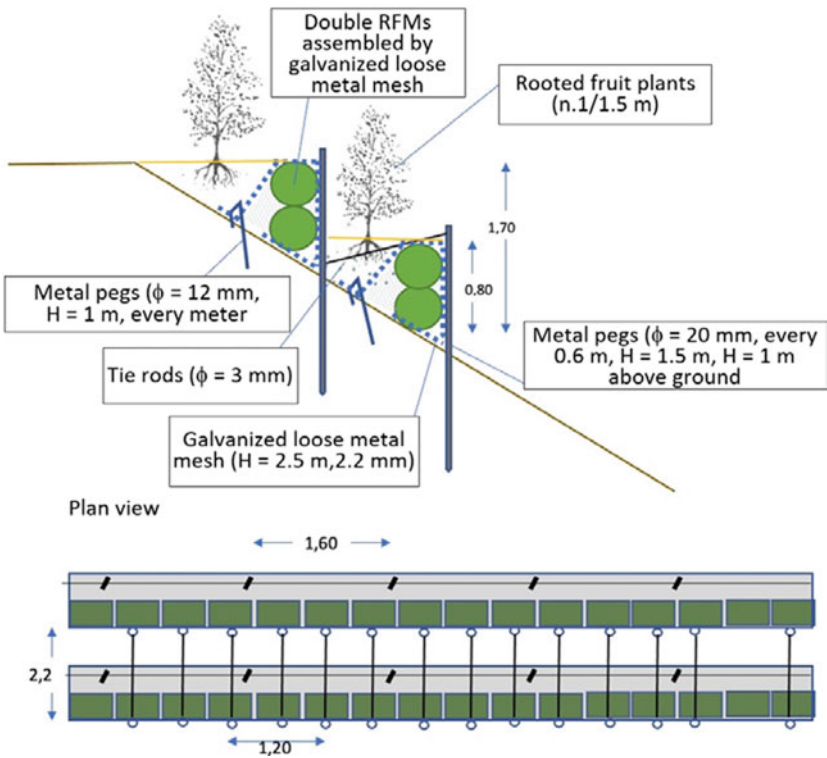


Fig. 9 Sketch of the prototype B1 (section and plan view)



Fig. 10 The implemented prototype B1

The B2 prototype is conceived as a terrace consisting of three distinct rows of RFM placed at a distance of 1.7 m along the slope (Fig. 11). Each row is connected by two side current cables bound to metal pegs at the ends and in intermediate points. The overall height difference of the work reaches 1.5 m for a total width of about 6 m. Figure 12 shows the implemented prototype B1.

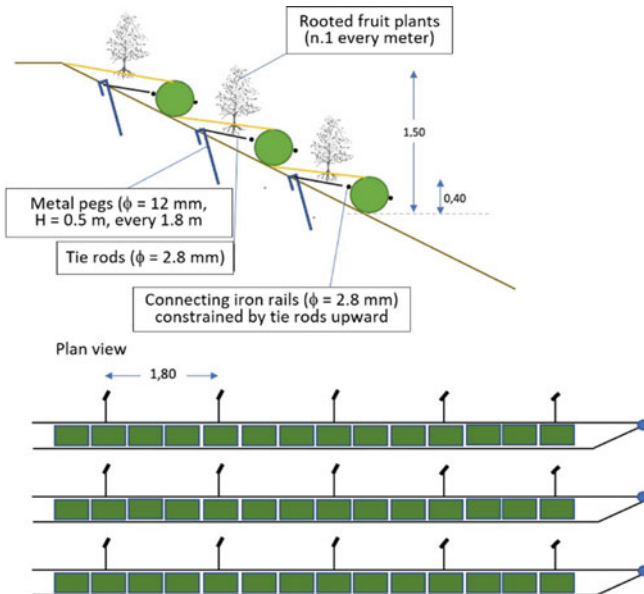


Fig. 11 Sketch of the prototype B2 (section and plan view)



Fig. 12 The implemented prototype B2

4 Conclusions

This work describes the RiVite project that is based on the patent issued to the University of Palermo [1] consisting of an advanced soil bioengineering technique to stabilize the slopes. The soil bioengineering work is made with generally waste materials: i) the vine shoots, which give life to the so-called rotofascine module (RFM), basic elements of the work and ii) the beached *P. oceanica*, which is a component of the substrate of growth.

The Jump-Poc Project, funded by the Ministry of Economic Development, then made it possible to implement the patent idea and the implementing of four different prototypes, which differ in the RFMs connections the and in the greening, in two different sites close to the Etna Park (Nicolosi and Giarre).

The characteristics of the soil bioengineering work is certainly of high ecological value due to the eco-compatibility of employed materials and the efficient use of resources, fits well into the environmental mission of the recent PNRR (Italy).

Moreover, the use of the techniques exhibited in vineyards would show the sign of the productive characteristic of the same area (the vine shoots), counteracting against the degradation induced by tillage and mainly by the erosive problems due to the establishment of new plants (excavations, bush clearing, earth movements, etc.).






Of course, the implementation of the suggested bioengineering work is in the early stages and only in the future you will see the beneficial effects of the greening.

References

1. Calvo, R., D'Asaro, F., Baiamonte, G.: Metodo per la realizzazione di un'opera costruttiva modulare per la protezione del territorio e detta opera. Attestato di Brevetto per Invenzione Industriale, n° 102017000141369, Ministero dello Sviluppo Economico, Roma, 27 February 2020
2. Preti, F., Capobianco, V., Sangalli, P.: Soil and Water Bioengineering (SWB) is and has always been a nature-based solution (NBS): a reasoned comparison of terms and definitions. *Ecol. Eng.* **181**, 106687 (2022)
3. Calvo, R.: Reutilización de residuos de poda de la vid y de *Posidonia oceanica* en las obras de Bioingeniería del paisaje, pp. 1–95. Ph.D. thesis. University of Palermo. (2018a)
4. Baiamonte, G., D'Asaro, F., Calvo, R.: Gravity-driven infiltration and subsidence phenomena in *Posidonia Oceanica* residues. *J. Hydrol. Eng.* **24**(6), 04019016 (2019). [https://doi.org/10.1061/\(ASCE\)HE.1943-5584.0001791](https://doi.org/10.1061/(ASCE)HE.1943-5584.0001791)
5. Calvo, R.: Thermal insulation role and possible exploitation of *Posidonia oceanica* detritus in the Mediterranean area. *Bocconea* **28**, 321 (2018)

Monitoring of Irrigation Water Use in Italy by Using IRRISAT Methodology: The INCIPIT Project



O. R. Belfiore , A. Castagna, G. Longo-Minnolo , M. Ippolito ,
A. Bavieri, A. Comegna , and G. D'Urso 

Abstract The INCIPIT project (INtegrated Computer modeling and monitoring for Irrigation Planning in ITaly) focuses on the development of a methodological framework to monitor irrigation water uses at different spatial scales and under different hydro-meteorological conditions in six Italian regions (Apulia, Campania, Emilia Romagna, Lombardia, Sardinia, and Sicily). The objective of the INCIPIT project is to fill the wide gap between research and application in order to meet the requirements of sustainable water-related policies – such as the Water Framework Directive

O. R. Belfiore (✉) · G. D'Urso
Department of Agricultural Sciences, University of Napoli Federico II, Via Università 100, 80055 Portici, NA, Italy

e-mail: oscarrosario.belfiore@unina.it

G. D'Urso

e-mail: URSO@unina.it

A. Castagna

Department of Agricultural and Environmental Sciences, University of Milano, 20133 Milano, MI, Italy

e-mail: alessandro.castagna1@unimi.it

G. Longo-Minnolo

Department of Agriculture, Food and Environment, University of Catania, 95123 Catania, CT, Italy

e-mail: giuseppe.longominnolo@phd.unict.it

M. Ippolito

Department of Agricultural, Food and Forest Sciences, University of Palermo, 90133 Palermo, PA, Italy

e-mail: matteo.ippolito@unipa.it

A. Bavieri

Department of Agricultural and Food Sciences, University of Bologna, 40127 Bologna, BO, Italy

e-mail: alberto.bavieri3@unibo.it

A. Comegna

School of Agricultural Forestry Food and Environmental Sciences (SAFE), University of Basilicata, 85100 Potenza, PZ, Italy

e-mail: alessandro.comegna@unibas.it

(WFD), and the MIPAAF Ministry Decree of July 31, 2015- where a specific set of obligations of measurement and estimation of the irrigated areas and irrigation water volumes is defined. For this purpose, the ESA Sentinel-2 (S2) satellites provide a very valuable source of information for mapping irrigated areas and estimating spatially-distributed irrigation water requirements. This study illustrates the results achieved using the IRRISAT methodology. In detail, the quantification of the irrigation water abstraction was achieved using the one-step approach, based on the Penman–Monteith equation, and properly adapted with canopy parameters namely crop height, Leaf Area Index (LAI), and surface albedo derived from S2 data. The quantification of the irrigated areas was performed by using pre-existing maps, unsupervised (clustering), and supervised classification (Machine Learning Algorithms) applied to dense temporal series of vegetation indices.

The analysis was performed for the irrigation seasons 2019 and 2020 in seven irrigated areas, which differ in size, type of irrigation schemes, farm delivery, irrigation methods, and crop types.

Keywords Crop evapotranspiration · Irrigated areas · Irrigation water requirements · IRRISAT · Sentinel-2

1 Introduction

Agriculture is the main user of water resources. This sector accounts for 66% of the total water used in Europe and 80% in the Mediterranean region, where from 2002 to 2014 the total irrigated area increased by 12%, while the total agricultural production harvested decreased by 36% [1]. In Europe, the Water Framework Directive (WFD, 2000/60/EC) defines the main objectives in relation to the management of water resources using a sustainable and integrated approach [2]. In Italy, from 31 July 2015, the declaration on the measurements and estimates of water consumption in agriculture is regulated by the Decree of the Ministry of Agricultural, Food and Forestry Policies (Mipaaf). For the purposes of the most effective application of this decree, and considering the heterogeneity of Italian irrigation systems, it is necessary to develop appropriate methodologies for the evaluation of the temporal evolution of irrigated areas and the irrigation water abstraction in compliance with the WFD.

In this context, the INCIPIT (INtegrated Computer modeling and monitoring for Irrigation Planning in ITaly) project (funded by Italian Min. Univ. and Research) is focused on the development of a methodological framework to monitor irrigation water uses at different spatial scales and under different hydro-meteorological conditions in six Italian regions (Apulia, Campania, Emilia Romagna, Lombardia, Sardinia, and Sicily) [3].

This study illustrates the results achieved using the IRRISAT methodology, the first satellite-based irrigation advisory service developed in Italy and operating in the Campania region [4]. In detail, the quantification of the irrigation water abstraction was achieved using the “one-step approach”, based on the Penman–Monteith equation, and properly adapted with canopy parameters namely crop height (hc), Leaf Area Index (LAI), and surface albedo derived from Sentinel-2 (S2) data. The

quantification of the irrigated areas was performed by using pre-existing maps, unsupervised (clustering), and supervised classification (Machine Learning Algorithms) applied to dense temporal series of vegetation indices. The analysis was carried out for the irrigation seasons 2019 and 2020 in seven irrigated areas, which differ in size, type of irrigation schemes, farm delivery, irrigation methods, and crop types.

2 Materials and Methods

2.1 Pilot Areas

In the INCIPIT project we compare results for irrigation water abstraction in seven irrigation districts in different conditions of availability of hydrometric and meteorological data in six Italian regions (Apulia, Campania, Emilia Romagna, Lombardia, Sardinia, and Sicily).

In Northern Italy, we consider two areas within the Po Valley: the first one, in the Lombardia Region, is the Adda river basin with more than 100,000 hectares served by an open channel network from April to September. In the Adda pilot areas the main crops are maize, forage crops, and vegetables irrigated mainly by the surface irrigation method. The second one, in Emilia-Romagna Region, is “Bonifica Renana” managed by the Water User Association (WUA) “Consorzio di Bonifica Renana” (CBR), where we selected seven irrigation districts (about 5,100 ha), four served by open channel, and three with a pressurized irrigation network. The irrigation season extends from April to September for crops such as maize, sorghum, vegetables, fruit trees, and vineyards. The most common irrigation methods are surface and sprinkler irrigation for herbaceous crops and localized irrigation for tree crops.

In Southern Italy, we consider two pilot areas: The first one is the “Basso Volturno”, in Campania Region, which is managed by the WUA “Consorzio Generale di Bonifica del Bacino Inferiore del Volturno” (ConsBIV). This study area is divided into three irrigation districts (about 13,300 ha) served by pressurized network, with irrigation guaranteed from April to October. The main crops are maize, tomato, alfalfa, tobacco, fruit trees, and greenhouse crops such as vegetables and strawberries. The most common irrigation method for herbaceous crops is the sprinkler, while localized irrigation prevails for trees. The second one is the “Sinistra Ofanto”, in Apulia Region, which is managed by the WUA “Consorzio di Bonifica della Capitanata” (CBC), where we select the “District n.10” (about 1,700 ha) served by pressurized irrigation network from April to November. The main crops are vineyards and olives watered with drip irrigation, and to lesser extent vegetables irrigated with sprinkler method.

In insular regions, we consider three pilot areas: the first one, in Sardinia Region, is the “Sardegna Centrale”, managed by the WUA “Consorzio di Bonifica Sardegna Centrale” (CBSC), where two artificial reservoirs feed two irrigation districts (about 12,000 ha) served by means a pressurized distribution system. The main crops are meadows, pastures, alfalfa, maize, sorghum, vegetables, and tree crops such as vineyards, olives, and, citrus. The most common irrigation method is sprinkler and micro-sprinkler for herbaceous crops and drip for tree crops. Irrigation is guaranteed for twelve months per year, with an intensification of the water demand during the

spring–summer irrigation season (from April to September). The second one, in Sicily Region, is the “Castelvetro” district (about 3,000 ha), managed by the WUA “Consorzio di Bonifica Sicilia Occidentale” (CBSOc), where two artificial reservoirs feed a pressurized distribution network from June to September. The area is mainly dedicated to the cultivation of olives and vineyards watered with drip irrigation, and to a lesser extent, citrus orchards and vegetables.

The third one, located in the eastern part of the Sicily Region, is the “Piana di Catania” (about 5,100 ha), managed by the WUA “Consorzio di Bonifica Sicilia Orientale” (CBSOr), and served by an open channel network. The irrigation season extends generally from May to October. The main crops are citrus, olives, and other fruit trees mainly irrigated by using localized irrigation and micro-sprinkler.

2.2 Map of Irrigated Areas

For the assessment of the irrigation water volumes at the district scale, the detection of the irrigated areas is required. Often this information is not available to water managers, who have also to deal with unauthorized water withdrawals for irrigation. For this purpose, the detection of the irrigated areas was performed for each pilot area by using different data sources and approaches. In detail, for the Adda and Castelvetro pilot areas the quantification of the irrigated areas was performed by using pre-existing land use land cover (LULC) maps, derived respectively by [5], and [6] enhanced with photointerpretation analysis. In the case of the Renana and Sinistra Ofanto pilot areas, for both the 2019 and 2020 irrigation seasons, the maps of the irrigated areas were derived from the farmers’ declarations on a cadastral basis, while for the Piana di Catania pilot area, an unsupervised classification algorithm [7] was applied to dense temporal series of vegetation indices. For the Sardegna Centrale and Basso Volturno pilot areas, where ground truth data are available for both irrigation seasons, the detection of the irrigated areas is performed by using a time-series of NDVI (Normalized Difference Vegetation Index) maps and rainfall data as input data in a supervised classification process [8]. In detail, the first assumption is that, in conditions of hydrological deficit, typical of the summer period in arid and semi-arid environments (like the Mediterranean area), crop growth is possible only with irrigation. In other words, high trends of vegetation indicate irrigated crops when the precipitation and/or the rise from groundwater are not sufficient to provide the water supplies required for their growth, in reverse for the rainfed crops (Fig. 1) [9].

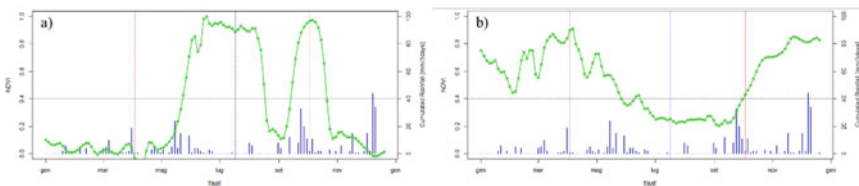


Fig. 1 Examples of the NDVI temporal pattern labelled as irrigated crop (a) and rainfed crop (b)

The pre-processing is related to the atmospheric correction of S2 data, executed by using the MAJA (MACCS ATCOR Joint Algorithm) processor, and the cloud masking and gap-filling process carried out by means of the Whittaker smoother (WS), proposed by [10] and implemented in the MODIS package into the R environment [11]. In particular, the time series filtering was performed on the NDVI maps, replacing clouds and shadows derived with the Multi-Temporal Cloud Detection method (MTCD) implemented in the MAJA processor [12]. Subsequently, the smoothed and gap-filled NDVI maps and three-day cumulated rainfall data derived from Persiann dataset [13] are considered as input data for supervised classification. In detail, six Machine Learning Algorithms (MLA) as Random Forest (RF), Support Vector Machine (SVM), Boosted Decision Tree (BDT), Single Decision Tree (SDT), Artificial Neural Network (ANN), k-Neighbour Neighbour (k-NN) were tested by using the R studio CARET package [14]. In the Sardegna Centrale pilot area, the VIS–NIR–Rainfall assumption is not sufficient, given that many pastures and tree crops such as olives and vineyards are irrigated occasionally during the dry periods. In detail, in winter-spring and autumn for the pastures, and in the summer for the tree crops. For this reason, from the “rainfed” and “tree crops” classes it was necessary to derive further classes, such as irrigated winter-spring and autumn crops and distinguish irrigated and not-irrigated tree crops. To this end, the VIS–NIR–SWIR–Rainfall domain is tested by using the OPTical TRAppezoid Model (OPTRAM) [15], properly adapted by [16]. The OPTRAM model is based on the pixel distribution within the Shortwave Infrared Transformed Reflectance (STR)-NDVI space, where the STR index [17], computed with the S2 SWIR band (Band 12- 2190 nm), is linearly related to the water content of the soil-canopy ensemble. As shown in Fig. 2 in the STR-NDVI space, the upper limit represents the position of pixels corresponding to wet conditions in the soil–plant ensemble (“wet edge”), and the lower the drier (“dry edge”). Dividing the region between the two extreme edges in four sub-sections, and selecting S2 images acquired in dry periods without significant rainfall, the pixels previously detected as rainfed and tree crops located in the upper wet regions of the scatterplot are considered as irrigated. In reverse, those pixels included in the dry subsection are labeled as not irrigated.

2.3 Crop Evapotranspiration and Crop Irrigation Water Requirements

The crop evapotranspiration (ET) is computed by using the Penman–Monteith (PM) equation based on the “one-step approach” implemented in the IRRISAT© methodology [4]. The ET modeling is carried out by deriving canopy parameters, hemispherical albedo (α) [18], and Leaf Area Index (LAI) [19] by using S2 data, [20, 21], while the crop height (h_c) is fixed at 0.4 m for the herbaceous crops and 1.2 m for tree crops, assuming that the influence of h_c on the estimation of ET is negligible during the irrigated season compared to the incoming solar radiation, as reported by [4]. The agro-meteorological input data (solar radiation, wind speed, air temperature, dew point temperature, atmospheric pressure, and precipitation) were derived

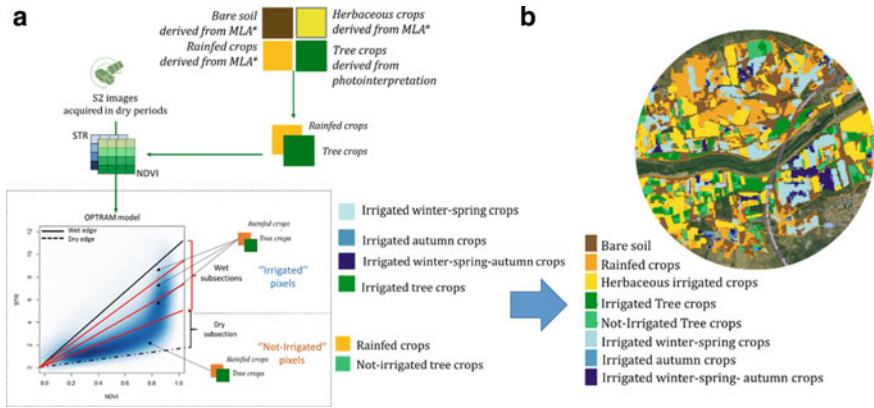


Fig. 2 a OPTRAM model adaptation for the detection of irrigated areas. b Detail of the map of irrigated areas (2020) for “Sardegna Centrale” pilot area.

from the reanalysis data provided by the Copernicus ERA5 single level dataset (horizontal resolution: $0.25^\circ \times 0.25^\circ$). This dataset, along with the ERA5-Land dataset, represents a valid data source for the estimation of ET in irrigation water management applications in Italy [21, 22], especially when the availability of ground-based stations is limited [23]. The crop irrigation water requirements (IWR) were computed on a daily basis (mm day^{-1}) by subtracting from the ET the effective precipitation (P_e), derived by using a semi-empirical model of interception of total precipitation (P), [24]. In conclusion, the gross irrigation water requirements (GIWR) were derived by dividing the IWR by irrigation method efficiency, assuming the following values: i) 45% for surface irrigation, ii) 75% for sprinkler, and iii) 85% for drip irrigation (Fig. 3).

In the case of the Adda pilot area, considering the wide extension of the district ($>100,000$ ha) served with open channels, a distribution efficiency coefficient of 40% was assumed. For the study areas as “Piana di Catania”, “Castelvetrano”, and “Sinistra Ofanto”, where drip irrigated tree crops are predominant, the IWR estimation was performed taking into account only the crop transpiration rate, derived from crop ET by using the approach proposed by [25]. In addition, for the “Piana di Catania” pilot area preliminary tests were performed using the approach proposed by [26], where the canopy resistances were modulated in the function of the water content of the soil-canopy ensemble defined by using the OPTRAM model (Fig. 4).

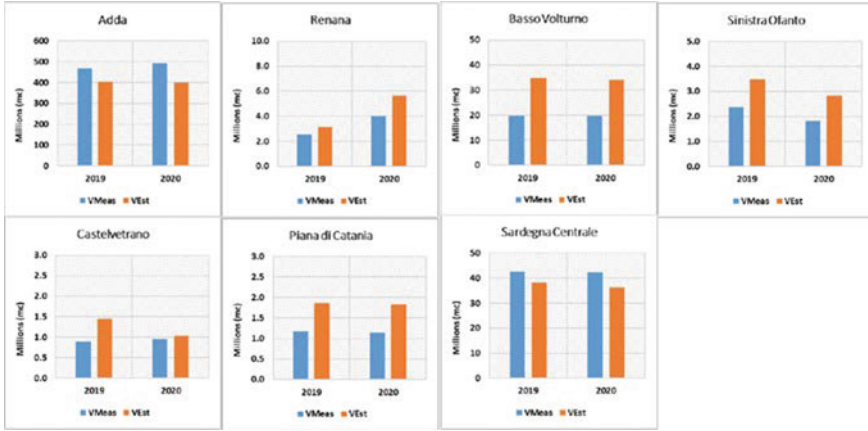


Fig. 3 Comparison between measured (V_{Meas}) and irrigation seasonal volumes estimated from EO data ($V_{Est} = GIWR$) for the irrigation seasons 2019 and 2020

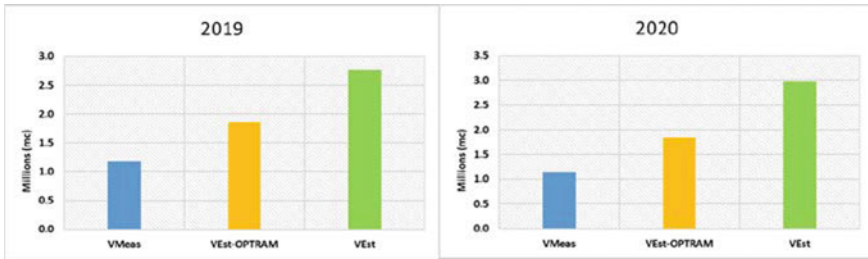


Fig. 4 Comparison between measured (V_{Meas}) and IRRISAT irrigation seasonal volumes estimated with ($V_{Est-OPTRAM}$) and without (V_{Est}) the modulation of the canopy resistances

3 Discussion and Conclusions

The preliminary results of the INCIPIT project confirm the reliability of the Earth Observation data in the mapping of irrigated areas and in the estimation of irrigation water abstraction. The high revisiting time of the two ESA Sentinel-2A and Sentinel-2B sensors and the high geometric resolution allow for constant monitoring of the development of irrigated crops, also in the typical agricultural land fragmentation of the Mediterranean areas. The IRRISAT methodology provides reliable estimates of the irrigated volumes with good agreements for most of considered pilot areas, despite the different sources of uncertainty for the measured values: i) unknown distribution efficiency of the irrigation networks, ii) water abstraction from non-measurable sources (irrigation wells, open channels, irrigation tanks), iii) water abstraction for non-irrigation use (i.e. livestock farms, recreational green spaces); while the thematic accuracy of the map of irrigated areas and the lack of suitable field data (i.e. flux

tower data) could affect the validation of the estimated volumes. In conclusion, the results obtained demonstrate the effectiveness of the proposed framework as a valid tool for water managers in an operative context, providing valuable information in compliance with the requirements of the WFD.

Acknowledgements This paper brings together the results of studies performed within the project PRIN 2017 INCIPIT with the support of the M.I.U.R (Italian Ministry of University and Research).

References

1. European Environment Agency, Water use and environmental pressure. <https://www.eea.europa.eu/themes/water/european-waters/water-use-and-environmental-pressures>. Accessed 25 Sep 2022
2. Wriedt, G., Van der Velde, M., Aloe, A., Bouraoui, F.: Estimating irrigation water requirements in Europe. *J. Hydrol.* **373**(3–4), 527–544 (2009)
3. INCIPIT Project. www.principit2017.it. Accessed 25 Sep 2022
4. Vuolo, F., D’Urso, G., De Michele, C., Bianchi, B., Cutting, M.: Satellite-based irrigation advisory services: a common tool for different experiences from Europe to Australia. *Agricultural Water Management*, vol. 147, pp. 82–95. Elsevier (2015). <https://doi.org/10.1016/j.agwat.2014.08.004>
5. ERSAF. <https://www.ersaf.lombardia.it/>. Accessed 25 Sep 2022
6. Land Monitoring Service. <https://land.copernicus.eu/pan-european/corine-land-cover/clc2018>. Accessed 25 Sep 2022
7. Ball, G.H., Hall, D.J.: ISODATA, a novel method of data analysis and pattern classification. Stanford research inst Menlo Park, CA (1965)
8. Falanga, B.S., Pasolli, E., Belfiore, O.R., De Michele, C., D’Urso, G.: Harmonized Landsat 8 and Sentinel-2 time series data to detect irrigated areas: an application in Southern Italy. *Remote Sens. MDPI* **12**(8), 1275 (2020). <https://doi.org/10.3390/rs12081275>
9. Ozdogan, M., Yang, Y., Allez, G., Cervantes, C.: Remote sensing of irrigated agriculture: opportunities and challenges. *Remote Sens. MDPI* **2**, 2274–2304 (2010). <https://doi.org/10.3390/rs2092274>
10. Eilers, P.H.C.: A perfect smoother. *Anal. Chem.* **75**, 3631–3636 (2003)
11. Mattiuzzi, M., Verbesselt, J., Hengl, T., Klisch, A., Evans, B., Lobo, A.: MODIS: MODIS download and processing package. In: Processing Functionalities for (Multi-Temporal) MODIS Grid Data. First International Workshop on “Tem-poral Analysis of Satellite Images, Mykonos Island, Greece, pp. 23–25 (2012)
12. Hagolle, O., Huc, M., Pascual, D.V., Dedieu, G.: A multi-temporal method for cloud detection, applied to FORMOSAT-2, VEN μ S, LANDSAT and SENTINEL-2 images. *Remote Sens. Environ.* **114**(8), 1747–1755 (2010)
13. CHRS Data Portal. <https://chrsdata.eng.uci.edu/>. Accessed 25 Sep 2022
14. Kuhn, M., et al. Caret: Classification and Regression Training. R Package Version 6.0–86 (2016)
15. Sadeghi, M., Babaeian, E., Tuller, M., Jones, S.B.: The optical trapezoid model: a novel approach to remote sensing of soil moisture applied to Sentinel-2 and Landsat-8 observations. *Remote Sens. Environ.* **198**, 52–68 (2017)
16. Belfiore, O.R., Falanga Bolognesi, F., D’Urso, G., De Michele, C.: D2.4 Data products validation report. Zenodo. <https://doi.org/10.5281/zenodo.3600256> (2020). Accessed 25 Sep 2022

17. Sadeghi, M., Jones, S.B., Philpot, W.D.: A linear physically-based model for remote sensing of soil moisture using short wave infrared bands. *Remote Sens. Environ.* **164**, 66–76 (2015). <https://doi.org/10.1016/j.rse.2015.04.007>
18. D'Urso, G., Calera Belmonte, A.: Operative approaches to determine crop water requirements from Earth Observation data: methodologies and applications. In: AIP Conference Proceedings. American Institute of Physics, 2006. pp. 14–25 (2006)
19. Weiss, M.; Baret, F.: Sentinel-2 ToolBox Level 2 Products: LAI, FAPAR, FCOVER, Version 1.1; European Space Agency: Noordwijk, The Netherlands (2016). https://step.esa.int/docs/extra/ATBD_S2ToolBox_L2B_V1.1.pdf. Accessed 25 Sep 2022
20. Pasqualotto, N., et al.: Retrieval of evapotranspiration from sentinel-2: comparison of vegetation indices, semi-empirical models and SNAP biophysical processor approach. *Agronomy* **9**(10), 663 (2019)
21. Er-Rami, M., D'Urso, G., Lamaddalena, N., DAgostino, D., Belfiore, O.R.: Analysis of irrigation system performance based on an integrated approach with Sentinel-2 satellite images. *J. Agric. Eng.* **52**(2), 1–14 (2021). <https://doi.org/10.4081/jae.2021.1170>
22. Vanella, D., et al.: Comparing the use of ERA5 reanalysis dataset and ground-based agrometeorological data under different climates and topography in Italy. *J. Hydrol. Reg. Stud.* **42**, 101182 (2022)
23. Pelosi, A., Terribile, F., D'Urso, G., Chirico, G.B.: Comparison of ERA5-Land and UERRA MESCAN-SURFEX reanalysis data with spatially interpolated weather observations for the regional assessment of reference evapotranspiration. *Water* **12**(6), 1669 (2020)
24. Braden, H.: Ein Energiehaushalts- und Verdunstungsmodell für Wasser- und Stoffhaushaltsuntersuchungen landwirtschaftlich genutzter Einzugsgebiete. *Mitteilungen der Deutschen Bodenkundlichen Gesellschaft* **42**, 294–299 (1985)
25. Ritchie, J.T.: Model for predicting evaporation from a row crop with incomplete cover. *Water Resour. Res.* **8**(5), 1204–1213 (1972)
26. D'Urso, G., et al.: Determining evapotranspiration by using combination equation models with sentinel-2 data and comparison with thermal-based energy balance in a California irrigated Vineyard. *Remote Sens.* **13**(18), 3720 (2021). <https://doi.org/10.3390/rs13183720>

Treatment of Steep and Clayey Soils with Olive Pruning Residues for Conservation Purposes: Hydrological Monitoring and Modelling Approaches



Giuseppe Bombino, Daniela D'Agostino, Pietro Denisi, José Alfonso Gomez, Demetrio Antonio Zema, and Santo Marcello Zimbone

Abstract This study evaluates and models the hydrological response of a steep and clayey olive grove of Southern Italy under three Soil Management Practices (SMPs, mechanical tillage “MT”, mulching with 3500 kg/ha of pruning residues “M”, and standard protection of soil “SP”). The saturated hydraulic conductivity, K_{sat} , surface runoff and soil loss have been evaluated after 26 natural rainfalls at the plot scale throughout two years. Moreover, the accuracy of the SCS-CN and USLE-M models in predicting runoff volume and soil loss has been evaluated for the three SMPs. The MT showed the lowest K_{sat} (on average 45%, compared to SP), and the highest runoff coefficient (+9%) and soil loss (+130%). M increased the K_{sat} by 26%, and reduced runoff coefficients and soil loss (−13% and −43%, respectively) compared to SP. The SCS-CN model was accurate in predicting runoff for all SMPs, and its performance increased after CN calibration. The erosion predictions using USLE-M running with default C-factors were inaccurate. Calibration of this parameter gave a good prediction performance, especially in M plots.

Keywords Surface runoff · Soil loss · Soil cover · Soil management practices · SCS model · USLE-M model

1 Introduction

In the Mediterranean area, olives are often cultivated on steep slopes, where erosion rates can be high, mainly because of the specific climatic conditions (heavy and infrequent storms with intense and often destructive floods). Mechanical tillage, when

G. Bombino · D. D'Agostino · P. Denisi (✉) · D. A. Zema · S. M. Zimbone
Department “Agraria”, Mediterranean University of Reggio Calabria, Località Feo di Vito, 89122
Reggio Calabria, Italy
e-mail: pietro.denisi@unirc.it

J. A. Gomez
Agronomy Department, Institute for Sustainable Agriculture (IAS-CSIC), Avenida Menendez
Pidal S/N, 14004 Córdoba, Spain

intensive, may result in worsening of the soil structure and thus in increased runoff and erosion, particularly during the wet periods [13]. Soil management practices (SMPs), such as mulching and cover crops with seeded or spontaneous species, are beneficial for erosion reduction, water conservation and fertility maintenance (e.g., [13, 6]).

Although several studies have analysed the hydrological effects of these practices in olive groves, very few studies have been published about the effect of soil mulching with pruning residues on the hydrological response of soils in olive groves over steep slopes. These effects can be predicted by using the most common hydrological models at the hillslope scale, but, also by this approach, more research is needed to validate the prediction capacity of the models in these environments. To the best authors' knowledge, no studies have explored the capacity of the SCS-CN and USLE-M models to predict surface runoff and soil loss in soils treated with mulching using pruning residues in steep and clayey olive groves.

To fill these gaps, this study evaluates: (i) the water infiltration, surface runoff and soil loss in steep and clayey plots of an olive grove of Southern Italy under three SMPs: standard protection, mechanical tillage, mulching with pruning residues (at dry matter dose of 3500 kg/ha); (ii) the performance of SCS-CN and USLE-M models in predicting these variables in the same experimental conditions.

2 Material and Methods

2.1 Study Area and Experimental Site

The experimental site is an olive grove located in Locri (Calabria, Southern Italy) at a mean altitude of 114 m a.s.l. (Fig. 1a). The climate is semi-arid hot summer Mediterranean. The annual average rainfall and minimum/maximum temperatures are 1350 mm and 11/28 °C, respectively.

The olive grove, planted with trees of *Olea europaea* at 6 × 6 m spacing, was 10–12 years old (Fig. 1b). The slope was uniform (20%), and the soil was an Eutric

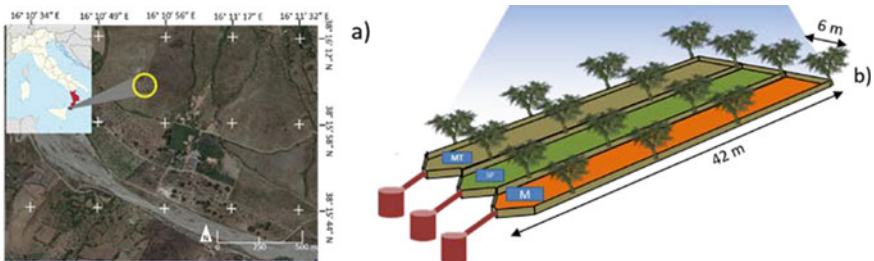


Fig. 1 Location and aerial map a, and layout of the experimental equipment b for hydrological monitoring of the experimental site (Locri, Calabria, Italy)

cambisol with prevalent clayey texture (28% of sand, 28% of silt and 44% of clay, w/w). In this olive grove, three plots (42-m long and 6-m wide, area of 252 m²) were hydraulically isolated (Fig. 1b). Each plot simulated one of the following SMPs: (i) standard protection of soil (assumed as control, SP); (ii) mechanical tillage (MT) and (iii) no tillage and soil mulching with pruning residues (M). The standard protection, which is the ideal cover for soil protection, was created by keeping the plot covered by spontaneous or seeded vegetation. MT was carried out in autumn and spring by a rotary tiller. The soil of the M plot was covered every spring with pruning and grass residues at a dose of 3500 kg/ha.

2.2 Monitoring and Statistical Processing of the Hydrological Variables

The hydrological variables (rainfall depth and intensity, saturated hydraulic conductivity of soil, K_{sat} , runoff volume, and soil loss) were measured from January 2016 to June 2018. Rainfall depth and intensity were recorded at a gauging station that was 1 km far from the experimental site. The K_{sat} was measured following the NRCS Survey NRCS Soil survey manual [11] immediately after each precipitation by a double cylinder infiltrometer in three points per plot (upper, medium and lower part). The ratio between the water depth (20 mm) and the time recorded for water infiltration until complete soil saturation gave the K_{sat} . The choice of this method for evaluating the K_{sat} was also supported by the experiences of Fatehnia and Tawfiqa [4]. Runoff and soil loss were monitored after 26 erosive rainfalls (depths between 16.6 mm and 183 mm). For each event, the runoff water was stored in tanks and samples of 0.5 L were collected and dried. The sediment of each sample was then weighted, to estimate the soil loss. The used method for measuring soil loss, although widely used, could be affected by underestimation due to non-homogeneous dispersion of sediment into the tanks. However, the sampling process was performed by mixing accurately the tank content, and sampling at three different depths.

The runoff coefficient was the ratio between the runoff and rainfall depths.

The statistical significance of differences in K_{sat} , runoff coefficient and soil loss among the different SMPs was analyzed using Kruskal–Wallis test (at p-level < 0.05) and Dunn's procedure with Bonferroni's correction.

2.3 Model Implementation, Calibration and Evaluation

The SCS-CN and USLE-M models were implemented in the experimental plots according to the guidelines of the USDA-SCS [14] and Wischmeier and Smith [15] with subsequent literature updates. In short, for the SCS-CN model, the AMC was derived from the antecedent 5-day rainfalls, the hydrological group was assumed

according to the Soil Map of Calabria, and the default CN values (CN) were derived from the original tables of USDA. For the USLE-M model, the runoff coefficient was input, while, for estimating the R-factor, the method proposed by Renard et al. [12] was adopted based on the kinetic energy and the maximum intensity for a rainfall duration of 30 min. The LS factor was estimated from the morphometric characteristics of the plots; the K-factor was calculated using the nomograph of Wischmeier and Smith [15], the C-factor, which depends on the management practice applied to the soil, was related to the tree density canopy diameter, and ground cover of the plots. In this study, this USLE C-factor was calculated following the study by Bombino et al. [1], who proposed an empirical equation based on canopy cover and aboveground biomass. Finally, C and K factors were adapted (indicated as K_{UM} and C_{UM} .) according to the guidelines by Kinnel and Risse [8]. The P-factor was always set to one.

The model predictions were analysed for “goodness-of-fit” with the corresponding observations, adopting the coefficient of efficiency [9]. NSE is variable between $-\infty$ and 1, and the model accuracy is good if $E \geq 0.75$, satisfactory if $0.36 \leq E \leq 0.75$, and unsatisfactory if $E \leq 0.36$ [16].

The two models were calibrated by adjusting the CNs (for the SCS-CN model) and the C factor (for the USLE-M) of each SMP. Particularly, a qualitative (by comparing observed and simulated values in scatterplots) and a quantitative (using statistics and a set of indexes, commonly used in hydrological modelling) procedure was adopted to calibrate the CNs and C factor up to reach the optimal values of simulation.

3 Results

3.1 Monitoring of the Hydrological Variables

The K_{sat} of MT (3.58 ± 2.75 mm/h) and M (4.82 ± 4.99 mm/h) plots were significantly lower (-44.6% and -25.5% , respectively) compared to the SP soil (6.47 ± 4.79 mm/h) (Fig. 2). The K_{sat} of M plot was higher by 34.5% compared to the MT soil, although not significantly.

The runoff coefficient of the M plot ($49.6 \pm 13.7\%$) was lower compared to both the SP ($56.7 \pm 15\%$) and MT soils ($61.8 \pm 15.4\%$) (Fig. 2). The differences in runoff coefficients in M soil were equal to 12.6% compared to SP (not significantly) and 19.8% compared to MT (significantly).

The highest soil loss was measured in the MT plot (0.04 ± 0.06 tons/ha, $+130\%$ compared to SP), while the lowest value was observed in the M soil (0.01 ± 0.01 tons/ha, -43.2%). The reciprocal differences in soil loss among the three SMPs were not significantly different (Fig. 2).

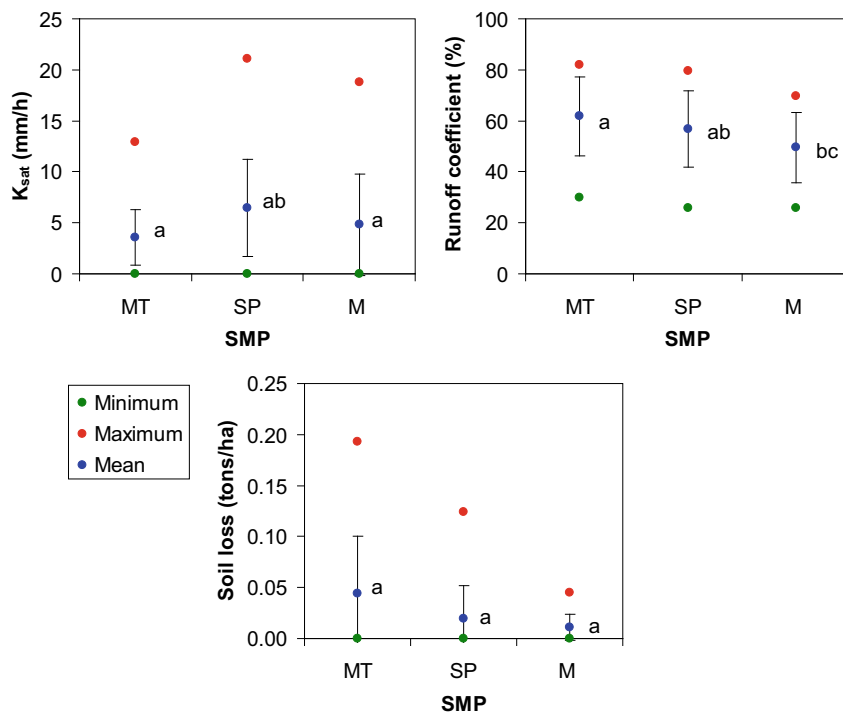


Fig. 2 Soil hydraulic conductivity (K_{sat}), runoff coefficient, and soil loss measured in the experimental plots subjected to three soil management practices (SMP) (Locri, Southern Italy). Notes: MT = mechanical tillage; SP = standard protection; M = mulching. Significant differences, at $p < 0.05$ are indicated by different letters among SMPs

3.2 Hydrological Modeling

Runoff predictions using the SCS-CN model with default CNs (88 for MT, 79 for SP, and 90 for M plots) were acceptable, but not optimal ($NSE < 0.71$ with a minimum of 0.49). To improve the model reliability, the default CNs were decreased to 85 (MT), 70 (SP), and 75 (M) during the calibration, and this noticeably improved the prediction capability of the model. Calibration gave runoff predictions closer to the corresponding observations for all the investigated SMPs (Fig. 3), and the NSE increased up to 0.91 (MT), 0.94 (SP), and 0.85 (M).

Simulations of soil erosion by the USLE-M model running with default C-factors (0.08 for MT, 0.04 for SP, and 0.02 for M) showed a poor prediction capacity ($NSE < -0.18$) for the soil loss measured under all the three SMPs. The default model always overestimated the observed soil loss, and therefore the C-factors were decreased to 0.06 (MT), 0.02 (SP), and 0.01 (M). Calibration reduced the model's tendency to soil loss overestimation, and noticeably increased the prediction accuracy of the model.

However, a tendency to erosion underprediction still remained. The NSE coefficients of the calibrated model running with C-factors were 0.87 for MT, 0.90 for SP, and 0.83 for M (Fig. 4).

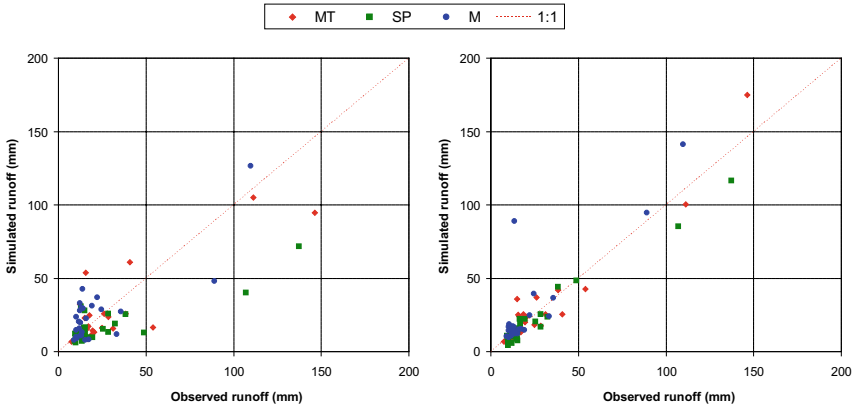


Fig. 3 Scatterplots of observed vs. simulated run-off using the SCS-CN model in the plots simulating three soil management practices (Locri, Southern Italy) with default (left) or calibrated CNs (right). Notes: MT = mechanical tillage; SP = standard protection; M = mulching

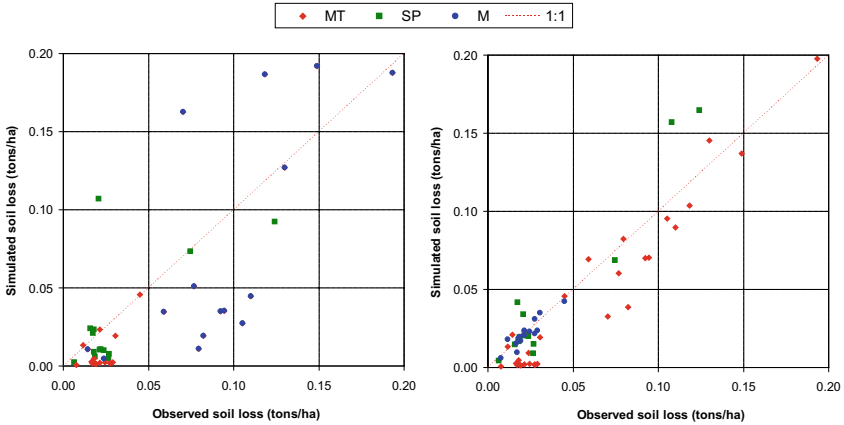


Fig. 4 Scatterplots of observed vs. simulated soil loss using the SCS-CN model in the plots simulating three soil management practices (Locri, Southern Italy) with default (left) or calibrated CNs (right). Notes: MT = mechanical tillage; SP = standard protection; M = mulching

4 Discussion

4.1 *Monitoring of the Hydrological Variables*

The MT produced the highest runoff and erosion rates, since the soil was left without vegetal cover and the machinery worsened the water infiltration capacity of the soil. Soil mulching with pruning residues resulted in lower runoff rate and erosion. This reduction can be attributable to the higher K_{sat} , as compared to MT, but also to the interception of precipitation and increase in surface roughness, which simultaneously increased water storage and reduced overland flow velocity. It is well known that K_{sat} is influenced by the root system of plants that creates preferential pathways for water infiltration [2, 5]. Moreover, the presence of the intricate mesh of wood sticks branches and grass on the ground in the M plots (absent in SP) probably increased the surface roughness, maximising the impact of these processes [3].

The reduction in soil losses detected in M soil is mainly associated to the general decreased in surface runoff, as compared to MT. A reduction of splash, rill and interrill erosion might be also an important reason for the decrease in erosion in M and SP plots. This can be due to the soil protection by the different synthetic and organic materials as well as to living vegetation, which prevented surface sealing observed after intense rainfalls in the MT plot [6]. Although not directly measured in this experiment, the soil organic matter could have played a great influence on soil loss, which is associated to increasing vegetation and mulch covers. Moreover, in soil with the cover of pruning residues, the high density of grass with thick and high stems (which was lower in SP plot) prevented the complete and spontaneous burying of the pruning residues, due to the weather agents. Unburied residues limit the soil loss in the early stage of the runoff process.

4.2 *Hydrological Modeling*

This study has indicated an acceptable (using default CNs) and good (after calibration) runoff prediction capacity of the SCS-CN model in the experimental conditions, which are typical of many olive groves of Southern Italy. The suggested values of CN should be used instead of the standard SCS values for runoff predictions in olive groves of the Mediterranean region with similar soils, climate, and management conditions. However, this model should be further validated in the same climate using further experimental data on rainfall-runoff relationships in olive groves with different soils and slopes. More research is also needed for a broader use of this model in agricultural areas of the Mediterranean environment, for instance by the analysis of the model's performance at the catchment scale or the evaluation of the effect of various soil moisture accounting systems.

The USLE-M model, running with default C-factors, was inaccurate to predict erosion in the experimental conditions. This forced the modellers to calibrate the

model, decreasing the default C-factors, which resulted in very good predictions of soil loss under all the studied SMPs. Other modelling experiences highlighted that the applications of USLE-family models in different contexts can both over- or under-predict soil loss. The residual underprediction of USLE-M detected in this study is in contrast with the usual behaviour of USLE-family models, which generally overpredict the lower soil loss [10]. The estimation of the site-specific C-factors using locally measured data, as in our study, increased the erosion prediction accuracy of USLE-family models. Therefore, the results may not be compatible with other sites, unless the model is validated in other environmental conditions or supported by external parameters. Modellers frequently propose C-factors based on poor understanding of the methodological and geographical origin of these values and often without a description of the specific crop management systems. However, bearing in mind the limitation of our study, the C-value proposed for mulched plots could be reliable at least for steep and clayey soils of Mediterranean conditions and fills the lack of similar values for mulching applications in the literature. Further improvements of the USLE-family models could consider the use of a sub-factor, which introduce the modification of the erosion risk due to changes in the soil moisture content, and the evaluation of the effects of management on soil conditions, to improve the understanding of the system and to predict its temporal changes (Gomez et al., 2003).

5 Conclusion

The hydrological monitoring of mulched plots in comparison with mechanically tilled soils and standard protection has shown that the use of pruning residues as mulch cover seems to be the best strategy to protect clayey soils in olive groves in steep areas. In contrast, our study has clearly demonstrated the need to minimise tillage operations as much as possible, since this management practice may worsen the runoff and erosion rates in these environmental conditions.

The modeling exercise has shown the feasibility of SCS-CN and USLE-M models in predicting surface runoff and soil loss under the experimental conditions, provided that both models are calibrated by the setup of the initial CNs and C-factors, respectively. For olive orchards with a steep slope and clayey soil of Southern Italy, the following two sets of CNs and C-factors values can be suggested for applications of the SCS-CN and USLE-M models, respectively: 95 (MT), 70 (SP), and 85 (M) for runoff modelling; 0.4 (MT), 0.2 (SP), and 0.1 (M) for soil loss predictions.

Acknowledgements This work was supported by the Spanish Government (PID2019-105793RB-I00) and Italian Ministry of University, Education and Research (PON03 PE00090_2).

References

1. Bombino, G., Porto, P., Zimbone, S.M.: Evaluating the crop and management factor C for applying RUSLE at plot scale. In: 2002 ASAE Annual Meeting (p. 1). American Society of Agricultural and Biological Engineers (2002)
2. Cui, Z., Wu, G.L., Huang, Z., Liu, Y.: Fine roots determine soil infiltration potential than soil water content in semi-arid grassland soils. *J. Hydrol.* **578**, 124023 (2019)
3. DíazRaviña, M., Martín, A., Barreiro, A., Lombao, A., Iglesias, L., DíazFierros, F., Carballas, T.: Mulching and seeding treatments for post-fire soil stabilisation in NW Spain: short-term effects and effectiveness. *Geoderma* **191**, 31–39 (2012)
4. Fatehnia, M., Tawfiq, K., Ye, M.: Estimation of saturated hydraulic conductivity from double-ring infiltrometer measurements. *Eur. J. Soil Sci.* **67**(2), 135–147 (2016)
5. Ghestem, M., Sidle, R.C., Stokes, A.: The influence of plant root systems on subsurface flow: implications for slope stability. *BioScience* **61**(11), 869–879 (2011). <https://doi.org/10.1525/bio.2011.61.11.6>
6. Gholami, L., Sadeghi, S.H., Homaei, M.: Straw mulching effect on splash erosion, runoff, and sediment yield from eroded plots. *Soil Sci. Soc. Am. J.* **77**(1), 268–278 (2013)
7. Gómez, J.A., InfanteAmate, J., GonzálezdeMolina, M., Vanwallegem, T., Taguas, E.V., Lorite, I.: Olive cultivation, its impact on soil erosion and its progression into yield impacts in Southern Spain in the past as a key to a future of increasing climate uncertainty. *Agriculture* **4**, 170–198 (2014)
8. Kinnell, P.I.A., Risse, L.M.: USLE-M: empirical modeling rainfall erosion through runoff and sediment concentration. *Soil Sci. Soc. Am. J.* **62**(6), 1667–1672 (1998)
9. Nash, J.E., Sutcliffe, J.V.: River flow forecasting through conceptual models. Part I. a discussion of principles. *J. Hydrol.* **10**, 282–290 (1970)
10. Nearing, M.A.: Evaluating soil erosion models using measured plot data: accounting for variability in the data. *Earth Surf. Proc. Land.* **25**(9), 1035–1043 (2000)
11. NRCS Soil Survey Manual. In: C. Ditzler, K. Scheffe, & H. C. Monger (Eds.), USDA handbook 18. Government Printing Office, Washington, D.C (2017)
12. Renard, K.G., Foster, G.R., Weesies, G.A., Porter, J.P.: RUSLE: revised universal soil loss equation. *J. Soil Water Conserv.* **46**(1), 30–33 (1991)
13. Sastre, B., Marques, M.J., García-Díaz, A., Bienes, R.: Three years of management with cover crops protecting sloping olive groves soils, carbon and water effects on gypsiferous soil. *CATENA* **171**, 115–124 (2018)
14. USDA, Soil Conservation Service: National Engineering Handbook. Hydrology, Section 4: 548. Washington, D.C. (1972)
15. Wischmeier, W.H., Smith, D.D.: Predicting rainfall erosion losses: a guide to conservation planning, vol. 537. Department of Agriculture, Science and Education Administration (1978)
16. Van Liew, M.W., Arnold, J.G., Garbrecht, J.D.: Hydrologic simulation on agricultural watersheds: choosing between two models. *Trans. ASAE* **46**, 1539 (2003)

Macroscopic Root Water Uptake Modelling Using High-Throughput Screening (HTS) Systems: Design and Validation



Lorenzo Bonzi, Fatma Hamouda, Àngela Puig-Sirera, Andrea Sbrana, Damiano Remorini, Lorenzo Cotrozzi, and Giovanni Rallo

Abstract Climate change and the widespread intensive agriculture are responsible for the increasing frequency and intensity of abiotic stresses consequent to water scarcity. At present, there is the need to select and release, in short time, plants adaptable to the current environmental conditions and resistant to biotic and/or abiotic stress. In this work we designed and validated a High-Throughput Screening (HTS) system for the continuous and simultaneous monitoring of plant drought stress response in a semi-controlled environment. Structurally, the HTS-system consists of three hardware segments for high-frequency detection of the agrometeorological forcing variables (i.e., atmometry), the weights (i.e., gravimetry), and the soil water content, SWC, (i.e., time domain reflectometry, TDR) of sixteen pots in which the medicinal crop *Salvia officinalis* L (sage) was grown.

Two irrigation treatments, which were based on soil water deficit conditions, were applied and an automated micro-irrigation system was designed to manage water by following a feedback control irrigation scheduling protocol.

The system was able to model the sage water stress function following the root water uptake macroscopic approach. The threshold of soil water status below which crop water stress occurred was also identified. The gravimetric-based daily evapotranspiration (ET_a) and the time domain reflectometry (TDR) -based root water-uptake (RWU) rates showed a high correlation, which allowed validating RWU indicators based on soil moisture sensors to estimate the ET_a fluxes.

Keywords Agro-hydrological modeling · High-throughput systems · Root water uptake · Sage · Water stress function

L. Bonzi (✉) · F. Hamouda · À. Puig-Sirera · A. Sbrana · D. Remorini · L. Cotrozzi · G. Rallo
Department of Agriculture, Food and Environment (DAFE), AgroHydrological Sensing and Modelling Lab., University of Pisa, Via del Borghetto, 80, 56124 Pisa, Italy
e-mail: lorenzo.bonzi@phd.unipi.it

D. Remorini · L. Cotrozzi · G. Rallo
CIRSEC, Centro Interdipartimentale di Ricerca per lo Studio degli Effetti del Cambiamento Climatico dell'Università di Pisa, 56124 Pisa, Italy

© The Author(s), under exclusive license to Springer Nature Switzerland AG 2023
V. Ferro et al. (eds.), *AIIA 2022: Biosystems Engineering Towards the Green Deal*,
Lecture Notes in Civil Engineering 337,
https://doi.org/10.1007/978-3-031-30329-6_6

1 Introduction

HTS systems are non-destructive and non-invasive tools that continuously detect the crop response to soil and/or atmospheric conditions. In this context, the accuracy of HTS allows the detection and comparison of small changes in specific eco-physiological behaviours associated to the plant response to environmental constraints, such as drought conditions [2, 13].

The general objective of this study was to present a HTS system integrated into a platform that combines a gravimetric weighing system with soil and atmospheric sensors for high-resolution and high-throughput diagnostic-screening, which aimed at the macroscopic modelling of the crop water stress function. The system was used on sage (*Salvia officinalis* L.), a medicinal crop largely cultivated for its important biological properties and high tolerance level against abiotic stresses [5] cultivated in pots under greenhouse conditions. Moreover, the specific objectives consisted of i) compare the gravimetric-based and the soil moisture-based approaches to measure the actual evapotranspiration fluxes and ii) perform a specific crop water stress function following the root water uptake macroscopic approach.

2 Materials and Methods

2.1 Description of the HTS-System and Experimental Setup

Experimental activities were conducted in the field station of San Piero a Grado owned by the Department of Agriculture, Food and Environment (DAFE) of the University of Pisa (Italy; 43°40'48'' N, 10°20'46'' E, 2 m a.s.l.), whereas the HTS-system was designed by the AgroHydrological Sensing and Modeling (AgrHySMo) laboratory of DAFE. The HTS-system was installed in a semi-controlled environment, where it was possible to control the solar radiation through shading sheets, the air temperature and relative humidity through a fan and/or active cooling system. The greenhouse, oriented in the East–West direction, is 15 m length, 8 m width, and 3 m height.

The plants developed under natural radiative and wind speed conditions during the initial phases of growth. Then, they were moved in the greenhouse in which the experiment was carried out from 12th September to 5th November 2019.

Structurally, the HTS-system consists of three hardware segments for high-frequency detection of the agrometeorological forcing variables (i.e. atmometry), the weights (i.e. gravimetry), and the soil water content (i.e. time domain reflectometry, TDR) of sixteen pots in which sage was seeded (Fig. 1).

An automated micro irrigation system was designed to manage water by following a feedback control irrigation scheduling protocol. The three monitoring segments and the irrigation system control were implemented in an algorithm written in CR-Basic programming language. The elementary module of the HTS-system consisted of a



Fig. 1 The sixteen modules of the HTS platform integrated with the Time Domain Reflectometry (TDR) and the gravimetric (Lysimetry) segments, irrigated with the drip irrigation system

5.0 l pot filled with sandy-soil and included 4-month-old sage seedlings; each pot container was integrated with a load cell and a TDR system used, respectively, to detect the weight [g] and the volumetric soil water content [$\text{m}^3 \text{m}^{-3}$]. The weights and/or the volumetric water content measured in each module represented the feedback control variables used to manage irrigation events.

Data acquisition and the control system used Campbell scientific Inc. (Loughborough, UK) technologies. A data logger CR1000 implemented a TDR200 with two levels of multiplexers (model SDM80X) and 16 TDR probes. The CR1000 also managed a multiplexer for differential voltage (DiffVolt) channels (model AM16/32), used for the load cells data acquisition, and a relay controller (model SDM16AC) to open and close the electrovalves controlling irrigation.

The main climate variables were measured with a standard agrometeorological station, model ATMOS-41, connected to a data logger model ED50 of the METER Group (Pullman, WA, USA). The meteorological measurements allowed the calculation of reference evapotranspiration (ET_0) using the Penman–Monteith model proposed by Allen et al. [1].

The gravimetric segment used a high-resolution load cell (LC) to weight (W) each module. For each module, three LCs model U2D1-3 K (NMB-Minebea Ltd, Bangkok, Thailand), were fixed over a steel beam triangle and allowed reaching a maximum load capacity of 9 kg. At this aim, a voltage regulator/stabilizer circuit was designed and built to power the three load cells per module with the same constant voltage of 10 V. The gravimetric segment was preliminarily calibrated based on standard metrology protocols [4].

The TDR probe installed in each pot was designed based on a multi-wire configuration (hexagonal geometry) to maintain the electrical field inside the soil volume. In particular, the soil monolith was 130 mm height, and the active part of the TDR probe covered a profile of 125 mm, being its head fixed at the bottom of the pot. The TDR segment was programmed to acquire a waveform (WF) in each pot every 15 min, for

a total of 16 WFs. A specific CRBasic instruction allowed extracting the probe bulk length used to calculate the soil dielectric permittivity. The volumetric soil water content (θ) was finally calculated according to the universal equation proposed by Topp et al. [12].

Two treatments were implemented and carried out based on different levels of imposed soil water deficit. 8 modules of the HTS-system were maintained under soil water deficit conditions (SAGE-DI), by maintaining the soil water content below the critical point, whereas the other 8 modules of the HTS-system (SAGE-FI) were maintained under full irrigation, in the range of soil water contents between the field capacity and the critical point.

2.2 *Determination of the Soil Hydrological Properties and Irrigation Scheduling Protocol*

The soil hydraulic properties were obtained using the approach of Polak and Wallach [7]. At the beginning of the experiment all the pots were watered until observing water from the bottom and monitored at high frequency during the drying process. Initially, a rapid decrease of θ was observed, mainly due to the free drainage process (FD). Then, a significantly slower extinction process occurred, due to the combination of drainage (D) and root water uptake (RWU) processes. Finally, when the gradients of total soil water potential become negligible, the dynamics of the drying process only depended on RWU. The points obtained by intersecting the tangent lines characterizing the three hydrological processes allowed identifying the soil field capacity (θ_{fc}) and the critical water content (θ^*). The soil wilting point (θ_{min}) was assumed corresponding to the minimum value of θ measured during the investigated period [6]. The irrigation management followed a feedback control protocol, which allowed to identify the irrigation timing based on two thresholds of θ . For the SAGE-DI treatment, irrigation timing was set to maintain the soil water status in the range of soil water content between θ^* and θ_{min} whereas, for the SAGE-FI treatment the soil water content was maintained in the range between θ_{fc} and θ^* .

2.3 *Procedure to Assess the Indicators of Soil and Crop Water Status*

Once determined the values of θ_{fc} and θ_{min} , it was possible to evaluate the fraction of water available for transpiration (*FTSW*) [11] corresponding to each actual soil water content (θ_i) used to quantify the soil water status conditions:

$$FTSW = \left(\frac{\theta_i - \theta_{min}}{\theta_{fc} - \theta_{min}} \right) \quad (1)$$

Actual evapotranspiration (ET_a) of each module was determined by a differential analysis based on the series of pot weights, W [g]. The weight loss between two consecutive weightings ($k = 15$ min), was equal to the crop evapotranspiration, including the instantaneous irrigation amount (I_k) and assuming the absence of biomass accumulation and drainage during short and soil drying periods respectively, was calculated as:

$$ET_a = - \left[\frac{dW}{dt} \right]_k \approx I_k - \frac{W_k - W_{k-1}}{t_k - t_{k-1}} \quad (2)$$

The 24-h integral of Eq. (2) returned the daily amount of ET_a .

The RWU was as well determined by finite element analysis of the soil moisture values, θ_k , by inverting:

$$- \frac{\theta_k - \theta_{k-1}}{t_k - t_{k-1}} V_s = I_k - E_k(\theta) - RWU_k(\theta) - D_k(\theta) \quad (3)$$

where I_k is the irrigation rate, $E_k(\theta)$ is the soil evaporation, $D_k(\theta)$ is the drainage and V_s is the volume of the soil in the pot. Assuming the absence of free drainage and soil drying period, the 24-h integral of Eq. (3) allowed estimating the daily amount of root water uptake which included the evaporation term.

The relative evapotranspiration (RET) was obtained by normalizing the daily ET_a for the corresponding value of the atmospheric water demand (ET_0). The root water uptake model (i.e. water stress function, WSF), describing the dependence between RET and $FTSW$, was represented by means of a logistic model:

$$RET = \frac{a}{1 + be^{-cFTSW}} \quad (4)$$

where a , b and c are the shape parameters of the model.

3 Results and Discussion

3.1 Agro-Meteorological Characteristics

During the experimental period there was a certain variability in the daily dynamics of the agro-meteorological variables. The values of hourly Rg were characterized by a wide range of peaks, from 400 W m^{-2} to 70 W m^{-2} at the beginning and end of the experimental period, respectively, with a decreasing trend during the last month of observation. Similarly, the maximum values of hourly RH , T_{air} , VPD , and u_2 showed decreasing trends from the end of September to November. Consequently, the distribution of hourly reference evapotranspiration, ET_0 , showed the highest peak of 0.37 mm h^{-1} in September, whereas the lowest of 0.05 mm h^{-1} was recorded in November.

3.2 *Preprocessing of the Crop and Soil Water Status Data Series*

The SAGE-DI treatment showed lower average ET_a [$\text{g h}^{-1} \text{m}^{-2}$] intensity than the SAGE-FI treatment, with more marked differences around midday. The hourly ET_a series for both treatments resulted strongly variable. Even the dynamic of θ showed a strong intra-treatment variability, for both treatments.

However, the adopted irrigation protocol allowed to maintain the θ in the pre-defined ranges (i.e., between θ_{fc} and the critical point θ^* for SAGE-FI and from the critical point θ^* to θ_{min} for the SAGE-DI treatment).

The total amount of supplied irrigation was equal to 2200 and 1100 g for the SAGE-FI and SAGE-DI treatments, respectively. Consequently, a total evapotranspiration of 1836 g and 1437 g was measure for the SAGE-FI and SAGE-DI treatments, respectively.

The variability observed in water fluxes (irrigation amount and ET_a) could be associated to the variability of θ occurring among the treatments. Because irrigation timing was based on the soil water status, an intra-treatment variability of θ has consequently caused a phase shift on irrigation timing among different plants of the same treatment.

3.3 *Soil–Plant Water Relation and Root Water Uptake Modelling*

A high correlation ($R^2 = 0.77$, p-value < 0.0001) between gravimetric-based daily ET_a and TDR-based RWU rates was obtained for the DI treatments. While a lower correlation ($R^2 = 0.35$, p-value < 0.0001) was found between the two methods for the FI treatments. The minor correlation on the FI could be explained by the fact that the TDR-based approach is not able to capture the variations of water status derived from the evaporation processes in the surface soil layers (i.e., first 5 cm depth), as the TDR metal rods were installed at the bottom of the pot and did not reach the first 5 cm of topsoil. Therefore, the TDR-based approach is not able to estimate the ET_a accurately when the irrigation volumes applied are more frequent and higher, which is translated into higher evaporation fluxes.

A deeper analysis of the dataset showed the effect of the ET_o on the crop evapotranspiration process, which was more marked for higher values of $FTSW$ (Fig. 2). On the contrary, the effect of ET_o appeared more attenuated for lower values of $FTSW$ because the evapotranspiration fluxes are more dependent on soil water status. Therefore, solar radiation and vapour pressure deficit are the main forcing controlling the plant transpiration processes when soil water is not limiting (10).

The nonlinear regression analysis allowed to fit the logistic model (Eq. 4) that was parameterized by fixing $a = 1$, and estimating the other two parameters, whose values resulted equal to $b = 8.93$ and $c = 8.57$ ($R^2 = 0.6$; p-value < 0.0001). The

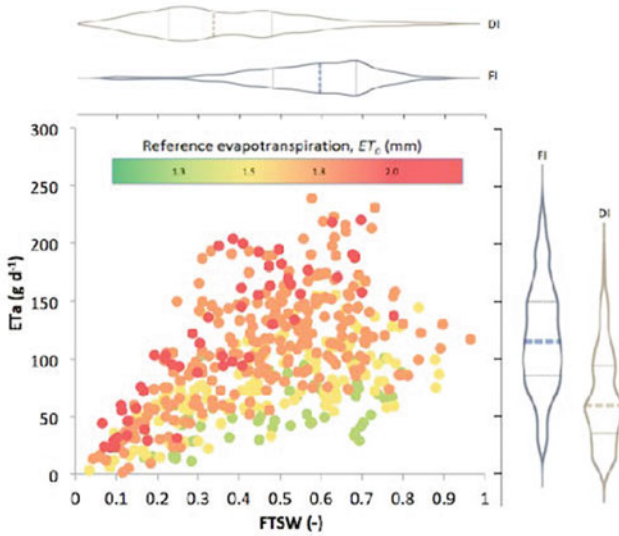
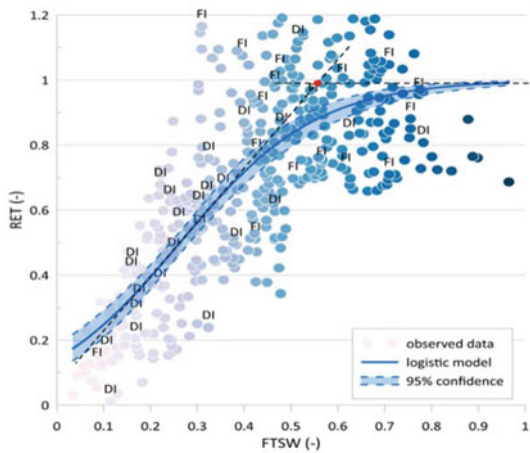


Fig. 2 Screening of the agro-hydrological data expressed as actual plant actual evapotranspiration (ET_a) versus soil water status ($FTSW$) and atmospheric evaporative demand (ET_0)

critical soil water status ($FTSW^*$), which marks the transition to the water deficit condition, was determined as the intersection between the plateau and the tangent line through the inflection point of the curve (Fig. 3).

This schematization suggests that at decreasing $FTSW$, the value of RET remains around the unit until a critical water status is reached ($FTSW^* = 0.52$) and then decreases in response to the lower soil water availability.

Fig. 3 Relative transpiration, RET , as a function of the fraction of soil water available for transpiration, $FTSW$. The root water uptake model is expressed with a three parameters logistic function with the 95% of the confidence interval is also shown



The complexity of the spatial distribution of the root water uptake patterns allows the plant to compensate the effects due to the spatial variability of the soil water contents. Thus, the roots located in the wetter soil volume can extract greater amount of water from the soil, compensating for the reduced activity of the roots located in the soil volume with lower water content [3].

4 Conclusions

The current study presents a simple and robust High-Throughput Screening (HTS) system allowing the continuous measurement of the plant responses to stress and non-stress conditions. The system was built by combining a pot gravimetric system with TDR-based soil moisture sensors and placed in a greenhouse environment.

Two irrigation treatments, full and deficit, were set using a feed-back control of irrigation scheduling with the aim to understand the sage response to water deficit conditions. The full irrigation treatment, as expected, evidenced generally higher soil water content (θ) and plant evapotranspiration (ET_a), than the deficit treatment. The large intra-treatment variability observed for ET_a and irrigation amount could be related to the different root water uptake (RWU) intensity of each plant of the treatment, due to the feed-back irrigation control, which was based on the soil water content threshold.

The RWU process was represented by a nonlinear (logistic) relationship between the RET and $FTSW$, which allowed identifying the critical threshold of $FTSW$ defining the incipient occurrence of water deficit conditions for the sage crop. The RET values above the critical threshold of $FTSW$ showed a relatively higher variability than that beyond the threshold, evidencing the plant roots ability to compensate the spatial heterogeneity of soil moisture under higher soil water contents.

References

1. Allen, R., Pereira, L., Raes, D., Smith, M.: Crop Evapotranspiration, Guideline for Computing Crop Water Requirements. FAO Irrigation and Drainage Paper No. 56, 2008th edn. FAO, Rome (1998)
2. Gosa, S.C., Lupo, Y., Moshelion, M.: Quantitative and comparative analysis of whole-plant performance for functional physiological traits phenotyping: new tools to support pre-breeding and plant stress physiology studies. *Plant Sci.* **282**, 49–59 (2019). <https://doi.org/10.1016/j.plantsci.2018.05.008>
3. Guswa, A.J., Celia, M.A., RodriguezIturbe, I.: Effect of vertical resolution on predictions of transpiration in water-limited ecosystems. *Adv. Water Resour.* **27**, 467–480 (2004). <https://doi.org/10.1016/j.advwatres.2004.03.001>
4. IMCCP 2011: Institute of Measurement and Control Code of Practice. A Code of Practice for the Calibration of Industrial Process Weighing Systems (2011). ISBN 0 904457 23 0

5. Marchica, L., Cotrozzi, L., Nali, P., Remorini, E.: Early detection of sage (*Salvia officinalis* L.) responses to ozone using reflectance spectroscopy. *Plants* **8**(9), 346 (2019). <https://doi.org/10.3390/plants8090346>
6. Pellegrino, A., Goz , E., Lebon, E., Wery, J.: A model-based diagnosis tool to evaluate the water stress experienced by grapevine in field sites. *Eur. J. Agron.* **25**(1), 49–59 (2006)
7. Polak, A., Wallach, R.: Analysis of soil moisture variations in an irrigated orchard root zone. *Plant Soil* **233**, 145–159 (2001). <https://doi.org/10.1023/A:1010351101314>
8. Rallo, G., Gonz lezAltozano, P., ManzanoJu rez, J., Provenzano, G.: Using field measurements and FAO-56 model to assess the eco-physiological response of citrus orchards under regulated deficit irrigation. *Agric. Water Manag.* **180**, 136–147 (2017). <https://doi.org/10.1016/j.agwat.2016.11.011>
9. Sinclair, T.R.: Theoretical analysis of soil and plant traits influencing daily plant water flux on drying soils. *Agron. J.* **97**, 1148–1152 (2005). <https://doi.org/10.2134/agronj2004.0286>
10. Sinclair, T.R.: Early partial stomata closure with soil drying. In: Sinclair, T.R. (ed.) *Water-Conservation Traits to Increase Crop Yields in Water-Deficit Environments*, pp. 5–9. Springer, Cham (2017). https://doi.org/10.1007/978-3-319-56321-3_2
11. Sinclair, T.R., Ludlow, M.M.: Influence of soil water supply on the plant water balance of four tropical grain legumes. *Aust. J. Plant Physiol.* **13**, 329–341 (1986). <https://doi.org/10.1071/PP9860329>
12. Topp, G.C., Davis, J.L., Annan, A.P.: Electromagnetic determination of soil water content: measurement in coaxial transmission lines. *Water Resour. Res.* **16**, 574–582 (1980)
13. Walter, A., Liebisch, F., Hund, A.: Plant phenotyping: From bean weighing to image analysis. *Plant Methods* **11**, 1–11 (2015). <https://doi.org/10.1186/s13007-015-0056-8>

Testing the Effect of the Rill Channel Slope on the Correction Factor of Surface Velocity



F. G. Carollo , C. Di Stefano , A. Nicosia , V. Palmeri ,
V. Pampalone , and V. Ferro 

Abstract The knowledge of flow velocity is necessary for studying rill hydraulics and the related soil erosion processes. The dye tracer technique to measure surface flow velocity V_s is based on the measurement of the travel time of a tracer needed to cover a known distance. The measured V_s must be corrected to obtain the mean flow velocity V using a correction factor $\alpha_v = V/V_s$ which is generally empirically deduced and can vary in different flow conditions. Experiments were performed by a fixed-bed sloping flume simulating a rill channel. Two different bed arrangements (smooth flume, and flume covered by sieved soil) were tested. The measurements were carried out for four slope values (9, 11, 13, and 15%) and different discharges. For each slope-discharge combination, 20 measurements of V_s were carried out using a Methylene blue solution. The travel time of the leading edge of the dye cloud was measured by a chronometer. For both the arrangements, the frequency distributions of V_s/V_m resulted independent of slope and discharge. All measurements resulted normally distributed, with a mean equal to one, and featured a low variability, demonstrating that V_m can be considered representative of surface flow velocity. The results highlighted that α_v is not correlated with the Reynolds number, the Froude number, and the channel slope.

Keywords Soil erosion · Interrill flows · Rill flows · Flow velocity · Dye method · Correction factor

1 Introduction

The knowledge and measure of flow velocity, which is a key hydrodynamic variable influencing channelized (rill and gully) and interrill erosion processes, allow for developing and testing process-based soil erosion models [1]. Many methods to

F. G. Carollo · C. Di Stefano · A. Nicosia (✉) · V. Palmeri · V. Pampalone · V. Ferro
Department of Agricultural, Food and Forestry Sciences, University of Palermo, Viale Delle Scienze, Building 4, 90128 Palermo, Italy
e-mail: alessio.nicosia@unipa.it

measure flow velocity in interrill and rill flows are available, but the dye-tracer technique [2] is one of the most common. This technique requires the measurement of the travel time of a tracer [3] needed to cover a known distance from the injection point to a given section. However, this technique gives the measurement of surface flow velocity V_s , which must be corrected with a correction factor α_v to obtain the mean flow velocity V [2]:

$$\alpha_v = V/V_s \quad (1)$$

This correction is due to the circumstance that, for open channel flows, local velocity varies along the vertical, is equal to zero at the bed, and reaches the maximum value at or below the water surface, depending on whether the effect of channel walls is negligible or not, respectively [4]. The correction factor is influenced by the shape of the vertical velocity profile, which depends on the flow hydraulic characteristics and the interaction with the channel roughness. Consequently, reliable measurements of the mean flow velocity are necessary to determine an appropriate correction factor α_v for different hydraulic conditions. In the literature, many studies, which explore different conditions and determine different correction factor values, are available. However, the results obtained in the literature are various and reinforce the idea that the determination of an appropriate correction factor is a relevant problem in studying rill flow hydraulics. Unfortunately, there is a lack of measurements performed for the rill flow scale [5] since the majority of the available investigations regarding the correction factor were carried out for flume and overland flow.

Di Stefano et al. [6] performed an experimental investigation using a small flume with fixed smooth bed and walls, slope s values ranging from 0.1% to 8.7%, and clear discharge ranging from 0.3 to 0.87 L s⁻¹. Each experimental run was characterized by a sample of 20 measurements of surface velocity V_s , having a mean value V_m , and was carried out with fixed values of slope and discharge. The sample mean V_m was representative of surface flow velocity. The authors also found that α_v is independent of Reynolds number Re , while two relationships with a Froude number $F_s = V_m / \sqrt{(g h)}$ and s were established.

Nicosia et al. [7] performed experiments with clear water flowing over a fixed rough bed in a flume simulating a rill to compare, for two different roughness conditions, the measurements of surface flow velocity. Also for a rough bed, these authors found that the sample mean V_m was representative of surface flow velocity, while no trends were detected between the correction factor and Re , F_s , and s , even if the analysis of the empirical frequency distributions of the α_v demonstrated a slope effect.

In this investigation, experiments were performed with clear water flowing over a fixed smooth or rough bed in a flume to i) extend the slope range investigated by Di Stefano et al. [6] and Nicosia et al. [7], ii) test slope effect on α_v , and iii) analyze the relationships between α_v and Re , F_s , and s for slope values ranging from 9 to 15%0.8

2 Materials and Methods

The experiments were carried out using a flume (5 m long, 0.079 m wide and 0.04 m high). The setup is the same used by Di Stefano et al. [6] and Nicosia et al. [7]. Water entered the flume by a small pipe, and an inflow device with wire meshes was used allow the flow to span the entire flume width and dissipate flow turbulence. Experimental runs were carried out using two different arrangements. For the first one, the flume was left smooth in its bed and walls (Fig. 1).

The second one was obtained by fixing, by waterproof vinyl glue, a sieved soil ($d_{50} = 0.014$ mm, clay 32.7%, silt 30.9%, and sand 36.4%) (Fig. 2) to the flume bed and walls. For both arrangements, the measurements were performed for four s values (9, 11, 13, and 15%). For each slope, five values of discharge Q (from 0.3 to 0.88 L s⁻¹), were used. Consequently, each run was characterized by fixed values of slope s , discharge Q , and water depth h . Discharge values were measured by the volumetric technique, while the water depth h was measured from the bottom of the flume bed by a point gauge (measurement accuracy of ± 0.1 mm) placed in the flume axis at 2 m from the inlet section. For each run, the flow cross-section area was calculated by the flow depth h , and the mean flow velocity V was determined as the ratio between Q and the flow cross-section area. The Froude number F of the flow was calculated as $F = V/(g h)^{0.5}$, where g is the gravitational acceleration.

The velocity V_s was measured using a Methylene blue solution as a dye-tracer (Fig. 1). A small volume (2 mL) of the solution was sprayed by a pipette to avoid changes in water properties. The tracer injection section was placed 4.3 m upstream from the end of the flume. The travel time of the leading edge of the dye cloud



Fig. 1 Views of the flume for the smooth arrangement

Fig. 2 View of the flume covered by glued sieved soil



was measured by a chronometer. For each run, the measurement of V_s was repeated 20 times obtaining 20 values of the correction factor α_v . For a given run, V_m , the corresponding correction factor $\alpha_v = V/V_m$, and F_s were also calculated. This last hydraulic variable was used to test the reliability of the relationship between $\alpha_v (= V/V_m)$ and F_s , which would allow estimating the correction factor by the measured surface velocity. 420 and 400 measurements were carried out for the smooth and soil arrangement, respectively.

3 Results and Discussion

3.1 Measurements of Flow Surface Velocity

Figures 3a (smooth) and 3b (soil) show, as an example for $s = 11\%$, the empirical cumulative frequency distributions of the V_s/V_m ratio corresponding to the examined discharges. Each empirical frequency distribution is referred to a sample of twenty measurements of V_s , carried out in the same experimental condition (given values of slope and discharge), having a mean value V_m . This figure shows that the distribution of the ratio V_s/V_m can be considered independent of discharge.

For each experimental condition, the empirical distribution of the V_s/V_m values was plotted for fixed slope (Fig. 4). In this figure, the data covering the slope range from 0.1 to 8.7%, obtained by Di Stefano et al. [6] for the smooth arrangement and by Nicosia et al. [7] for the soil one, are also represented. For both the arrangements, the overlapping of the five empirical frequency distributions suggested that V_s/V_m can be assumed independent of slope.

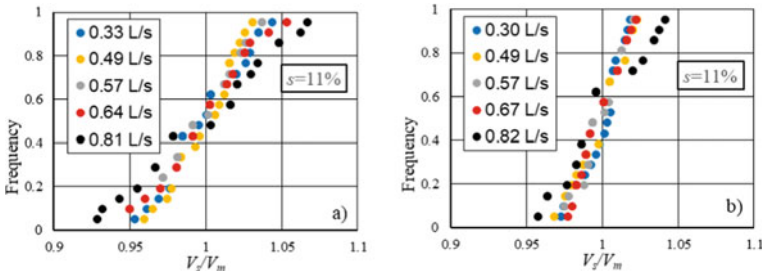


Fig. 3 Example of empirical cumulative frequency distributions of the V_s/V_m ratio corresponding to the investigated discharges for the smooth (a) and soil (b) arrangement

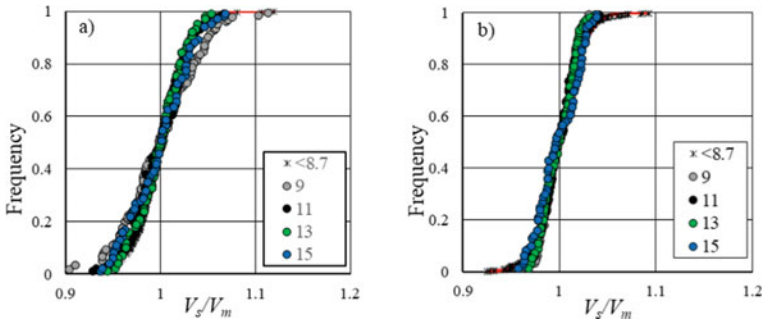


Fig. 4 Empirical cumulative frequency distributions of the V_s/V_m ratio corresponding to the investigated slopes for the smooth (a) and soil (b) arrangement

The results shown in Figs. 3 and 4 agree with those obtained by Di Stefano et al. [6] and Nicosia et al. [7] for experiments carried out on the same flume with smooth bed and walls and covered with soil, respectively. These findings allow stating that the distribution of the V_s/V_m ratio is independent of slope and discharge, i.e., the mean value V_m accounts for the effects of both slope and discharge on surface flow velocity. Since the V_s/V_m ratio was independent of slope and discharge, all samples corresponding to different bed conditions belong to a single population. Consequently, a single frequency distribution of the V_s/V_m ratio was considered (Fig. 5). This figure also highlights the normal distribution, with a mean value of V_s/V_m equal to 1, having a standard deviation equal to 0.027 for the smooth bed and 0.022 for the soil arrangement. Since each distribution is sub-vertical and characterized by V_s/V_m values close to 1, the mean value V_m can be considered representative of the flow velocity for each experimental run. This finding also agrees with that obtained by Di Stefano et al. [6] for the smooth flume case and Nicosia et al. [7] for the soil arrangement.

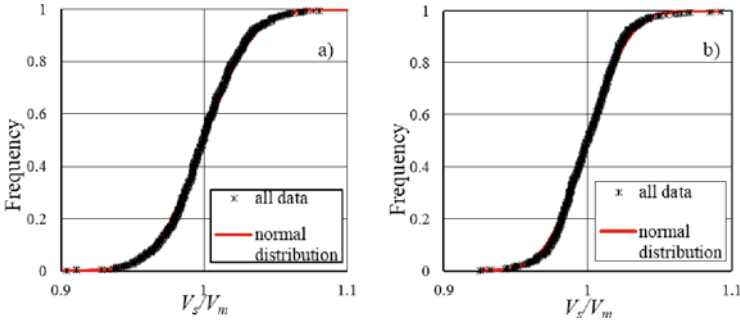


Fig. 5 Empirical cumulative frequency distributions of the V_s/V_m ratio for the smooth (a) and soil (b) arrangement

For analyzing the variability of the surface velocity V_s for the two roughness conditions, for each experimental run, the coefficient of variation $CV(V_s)$ was calculated. Figure 6 shows the relationship between $CV(V_s)$ and F for smooth (Fig. 6a) and soil (Fig. 6b) arrangement.

Figure 6 shows that $CV(V_s)$, for the smooth arrangement (Fig. 6a), except for $s = 9\%$ (data pairs enclosed by an ellipse in Fig. 6a), the $CV(V_s)$ increases almost linearly with F , probably due to a less measurement accuracy for higher flow velocities. Instead, for the soil arrangement, $CV(V_s)$ does not depend on F . The measurement variability is comparable ($1\% \leq CV(V_s) \leq 4\%$) for the two investigated arrangements. This result confirms that the dye-tracer technique is reliable for both arrangements.

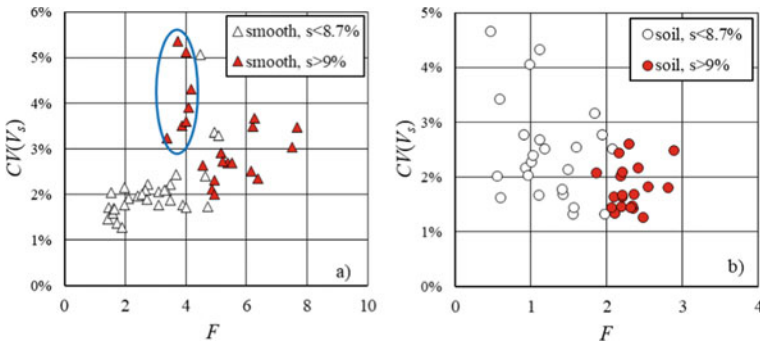


Fig. 6 Relationship between F and $CV(V_s)$ for the smooth (a) and soil (b) arrangement

3.2 Determining the Correction Factor for Rill Flows

Figures 7a (smooth) and 7b (soil) show the (Re, α_v) pairs, with $\alpha_v = V/V_m$, for the two investigated conditions. To extend the investigated slope range, also the data by Di Stefano [6] (Fig. 7a) and Nicosia et al. [7] (Fig. 7b) were considered. For both cases, the investigated channelized flows are turbulent ($3532 \leq Re \leq 9799$ for the smooth arrangement and $3462 \leq Re \leq 10,155$ for the soil one). For the slope range 9–15%, α_v is also independent of Re for both arrangements.

The result shown in this figure confirms that the correction factor is not influenced by Re , as already demonstrated, for the same experimental setup and a lower slope range (0.1–8.7%), by Di Stefano et al. [6] the smooth arrangement and by Nicosia et al. [7] for the soil one.

Figure 8 shows the relationship between the correction factor α_v and F_s , highlighting that these variables are not correlated, as already found by Di Stefano et al. [6] and Nicosia et al. [7] for a slope range varying from 0.1 to 8.7% and the same experimental setup.

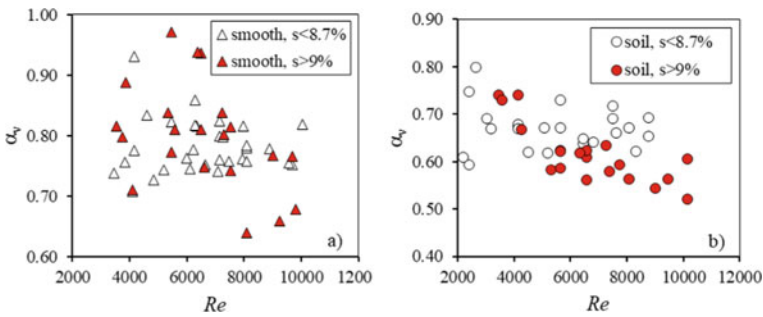


Fig. 7 Relationship between Re and α_v for the smooth (a) and soil (b) arrangement

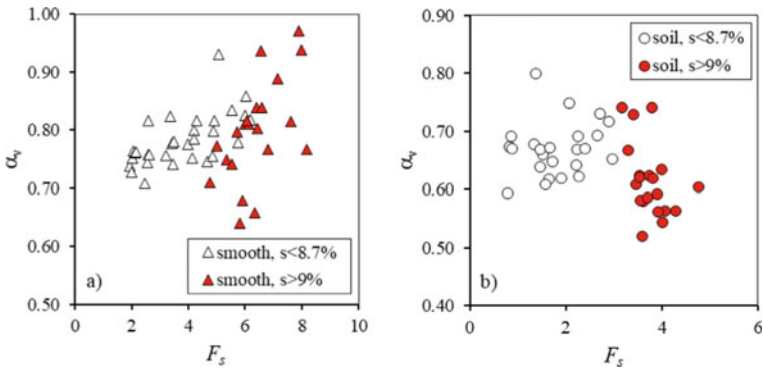
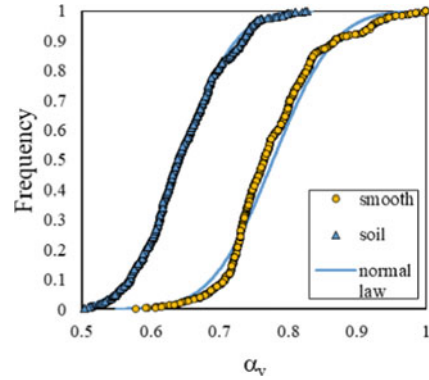


Fig. 8 Relationship between F_s and α_v for the smooth (a) and soil (b) arrangement

Fig. 9 Empirical frequency distribution of the α_v values for the smooth and soil arrangements



The empirical frequency distribution of the α_v values (Fig. 9), for the whole s investigated range (0.1–15%), shows that the correction factors for the smooth arrangement are higher than those of the soil one and that both the curves are normally distributed. Consequently, the mean values, equal to 0.78 ($CV = 0.091$) for the smooth arrangement, and 0.645 ($CV = 0.095$) for the soil one, can be considered representative for the investigated conditions.

4 Conclusive Remarks and Research Needs

The dye-tracer technique is a reliable method that requires an appropriate correction factor α_v for different hydraulic and bed conditions to obtain the mean flow velocity from the measured surface velocity V_s . In this paper, experiments were performed to study the applicability of the dye-tracer technique in a small flume. The obtained results allow stating that for both the smooth and the soil arrangement a single surface velocity measurement is, on average, representative of this kinetic variable. Moreover, in accordance with previous results obtained with the same experimental setup, the developed analysis on the correction factor confirmed that, also for higher slope values, α_v is not correlated with the Reynolds number, the Froude number F_s , and the channel slope. Finally, the analysis demonstrated that α_v is higher for the smooth arrangement and, for a given experimental condition, its mean value can be considered representative.

Considering the obtained results, new experiments should be carried out to explore different flume roughness and other values of channel slope. Moreover, another interesting challenge might be to study the effect on the correction factor deriving from the sizes of the flume.

References

1. Takken, I., Govers, G., Ciesiolka, C.A.A., Silburn, D.M., Loch, R.J.: Factors influencing the velocity-discharge relationship in rills. *Model. Soil Erosion, Sediment Transp. Closely Related Hydrological Process.* **249**, 63–69 (1998)
2. Zhang, G., Luo, R., Cao, Y., Shen, R., Zhang, X.C.: Correction factor to dye-measured flow velocity under varying water and sediment discharges. *J. Hydrol.* **389**, 205–213 (2010)
3. Ventura, E., Jr., Nearing, M.A., Norton, L.D.: Developing a magnetic tracer to study soil erosion. *CATENA* **43**, 277–291 (2001)
4. Ferro, V., Baiamonte, G.: Flow velocity profiles in gravel-bed rivers. *J. Hydraul. Eng. ASCE* **120**(1), 60–80 (1994)
5. Yang, D.M., Fang, N.F., Shi, Z.H.: Correction factor for rill flow velocity measured by the dye tracer method under varying rill morphologies and hydraulic characteristics. *J. Hydrol.* **591**, 125560 (2020)
6. Di Stefano, C., Nicosia, A., Palmeri, V., Pampalone, V., Ferro, V.: Flume experiments for assessing the dye-tracing technique in rill flows. *Flow Meas. Instrum.* **77**(2), 101870 (2021)
7. Nicosia, A., Di Stefano, C., Palmeri, V., Pampalone, V., Ferro, V.: Roughness effect on the correction factor of surface velocity for rill flows. *Hydrol. Process.* **35**, e14407 (2021)

Monitoring Rainfall Erosivity in the Sparacia Experimental Area by an Optical Disdrometer



F. G. Carollo , C. Di Stefano , A. Nicosia , V. Palmeri ,
V. Pampalone , and V. Ferro 

Abstract The kinetic power of rainfall plays a fundamental role in soil erosion processes. Kinetic power can be determined by knowing both drop size distribution (DSD) and drop falling velocity.

This paper reports the results obtained by the DSDs detected by an optical disdrometer installed in two Sicilian sites. In particular, the disdrometer was installed at Palermo in the period June 2006 – May 2014 and at Sparacia experimental station in the period March 2017 – December 2019. The DSDs, that are detected using a sampling time equal to 1 min, after aggregation by rainfall intensity classes, are presented highlighting the differences on DSDs characteristics for the two experimental sites.

The rainfall kinetic power was calculated by combining DSDs and the falling velocity obtained by the relationship suggested by Ferro (Ferro, V.: *Tecniche di misura e monitoraggio dei processi erosivi. Quaderni di Idronomia Montana* (21/2), 63–128 (2001)). The reliability of the empirical relationships estimating kinetic power by only rainfall intensity proposed by Wischmeier and Smith (Wischmeier, W.H., Smith, D.D.: *Predicting Rainfall Erosion Losses-A guide to conservation planning. Agriculture Handbook: United States Department of Agriculture, Washington, DC; 537* (1978).) and Brown and Foster (Brown, L.C., Foster, G.R.: *Storm erosivity using idealized intensity distribution. Trans. ASAE* **30**, 379–386 (1987). <https://doi.org/10.13031/2013.31957>), is firstly verified. Furthermore, the relationship theoretically deduced by Carollo et al. (Carollo, F.G., Ferro, V., Serio, M.A.: *Reliability of rainfall kinetic power-intensity relationships. Hydrol. Process* **31**, 1293–1300 (2016). <https://doi.org/10.1002/hyp.11099>), which allows to estimate the kinetic power by rainfall intensity and a characteristic diameter (median volume diameter), is tested.

Finally, the comparison between the relation kinetic power – intensity detected in the two sites is presented.

F. G. Carollo (✉) · C. Di Stefano · A. Nicosia · V. Palmeri · V. Pampalone · V. Ferro
Department of Agricultural, Food and Forestry Sciences, University of Palermo, Viale delle Scienze, Building 4, 90128 Palermo, Italy
e-mail: francescogiuseppe.carollo@unipa.it

Keywords Soil loss · Rainfall erosivity · Rainfall kinetic power · Drop size distribution

1 Introduction

The rainfall erosivity is one of the most important parameters of erosion processes and it can be evaluated the rainfall kinetic power, P_n , i.e. the kinetic energy per unit time and area.

There are numerous empirical relationships that use rainfall intensity, I , and have various mathematical formulations to estimate the kinetic power. The relationship suggested by Wischmeier and Smith [7] is the one that is most frequently used to estimate P_n ($\text{J m}^{-2} \text{s}^{-1}$):

$$P_n = \begin{cases} (11.9 + 8.73 \log I)I & \text{for } I \leq I_t \\ (11.9 + 8.73 \log I_t)I & \text{for } I > I_t \end{cases} \quad (1)$$

According to Eq. (1), P_n/I , i.e. the kinetic energy per unit rainfall volume, increases for $I \leq I_t$ and becomes constant for rainfall intensity greater than I_t . They justify the threshold value, I_t , considering that the median volume diameter, D_0 , stops to continue to increase when I exceed 76 mm h^{-1} .

Kinnell [5] described the same trend proposing the following relationship:

$$P_n = a(1 - b \exp(-cI))I \quad (2)$$

and Eq. (2) was introduced in RUSLE model with $a = 29 \text{ J m}^{-2} \text{ mm}^{-1}$, $b = 0.72$ and $c = 0.05 \text{ h mm}^{-1}$ [1].

On the other hand, the knowledge of drop size distribution (DSD) and the relationship between raindrop terminal velocity and drop diameter allow to calculate the rainfall kinetic power by adding the contribution of all raindrops. Carollo and Ferro [2], considering the falling velocity relationship proposed by Ferro [4] and the Gamma distribution [6], obtain the following theoretical expression of the kinetic power

$$P_n = 10^{-6} \frac{9.5^2 \rho}{7.2} \left[1 - \frac{2\Lambda^{4.67}}{(6 + \Lambda)^{4.67}} + \frac{\Lambda^{4.67}}{(12 + \Lambda)^{4.67}} \right] I \quad (3)$$

in which Λ and μ represents two parameters of Gamma distribution [6]. Carollo et al. [3] demonstrated that if the exponential distribution is applicable, from Eq. (3) the following relationship can be deduced

$$P_n = 10^{-6} \frac{9.5^2 \rho}{7.2} \left[1 - \frac{2}{(6 \frac{D_0}{4.34} + 1)^{4.67}} + \frac{1}{(6 \frac{D_0}{2.17} + 1)^{4.67}} \right] I \quad (4)$$

which establishes that the ratio P_n/I depends only on D_0 value. In other words, Eq. (4) establishes that the median volume diameter D_0 is representative of the entire DSD for calculating rainfall kinetic power.

This paper presents the DSDs measured by an optical disdrometer at Sparacia experimental area in the period March 2017 – December 2019. The DSDs were aggregated into rainfall intensity classes and they were used to deduce the kinetic power values and evaluate the reliability of the above relationships Eqs. (1), (2) and (4). All the results are compared with those obtained by the same instrument in Palermo in the period June 2006 – March 2014.

2 Materials and Methods

A unique optical disdrometer (Eigenbrodt model ODM 70) was used to detect the DSDs at two experimental Sicilian sites (Fig. 1).

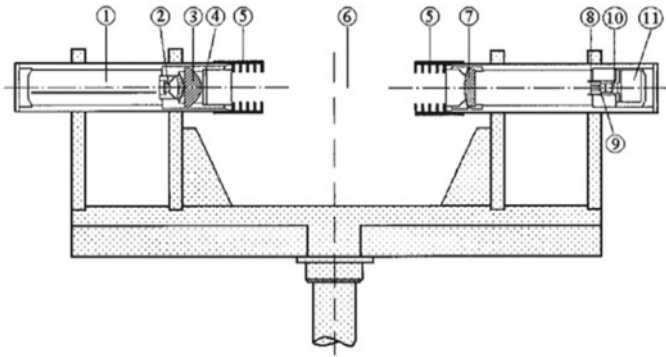
The measure of drop diameter is based on the light damping due to the passage of the drop in the control volume between two diodes (Fig. 2). Dividing the diameter range into 128 classes of width of 0.005 cm, the disdrometer measures drop diameters between 0.035 and 0.6 cm. The instrument reports, for each record minute, the number of drops falling into each class.

The Sparacia Area is located in western Sicily at 415 m a.s.l., (Fig. 3). The Palermo experimental site, about 100 km north of Sparacia area, is located in the Department of Agricultural, Food and Forest Sciences of the University of Palermo, at an altitude of 40 m a.s.l (Fig. 4).

The disdrometer monitored 544 rainy days in the period June 2006-April 2014 at Palermo experimental site, and 318 rainy days at Sparacia in the period March 2017 - December 2019.

Fig. 1 Location of the experimental areas





1) electronics, 2) light-emitting diode, 3) lens system, 4) window, 5) baffles, 6) sensitive volume, 7) achromatic collector lens, 8) optical blend, 9) ocular, 10) photo diode, and 11) electronics compartment.

Fig. 2 Sketch of optical disdrometer

Fig. 3 Sparacia experimental area



Fig. 4 Palermo experimental area



3 Results and Discussion

Only DSDs characterized by $I > 0.5$ mm/h and a number of not empty diameter classes greater than 20 were considered. With these limitations low erosive rainfalls and DSDs with small sample sizes were excluded. Therefore, 45,802 DSDs for Palermo ($I < 203$ mm/h) and 25,928 DSDs ($I < 504$ mm) for Sparacia were considered.

The single DSDs detected at Palermo and Sparacia were aggregated into intensity classes with a different range in order to better illustrate how rainfall intensity affects rainfall energetic properties. The intensity class range was specifically established at 1 mm/h for $I < 30$ mm/h, 2 mm/h for $30 \leq I < 50$ mm/h, 5 mm/h for $50 \leq I < 100$ mm/h and 10 mm/h for $I \geq 100$ mm/h. The average of the intensities of the DSDs falling into each class was used to identify the rainfall intensity of the aggregated DSD of that class. 59 aggregated DSDs for Palermo and 71 for Sparacia were obtained.

The comparison between drop diameter, D_{xx} , corresponding to xx -th percentile ($xx = 25, 50, 75$), of the aggregated DSDs and rainfall intensity was reported in Fig. 5. Figure 6 shows the pairs (I, D_0) measured in the two sites.

For a given I value, the precipitations observed in the two sites present $DSDs$ with similar values of D_{25} and D_{50} . While, For D_{75} , instead, Fig. 5 shows that, for $I > 50$ mm/h, the DSDs detected at Sparacia present lower diameter values than Palermo

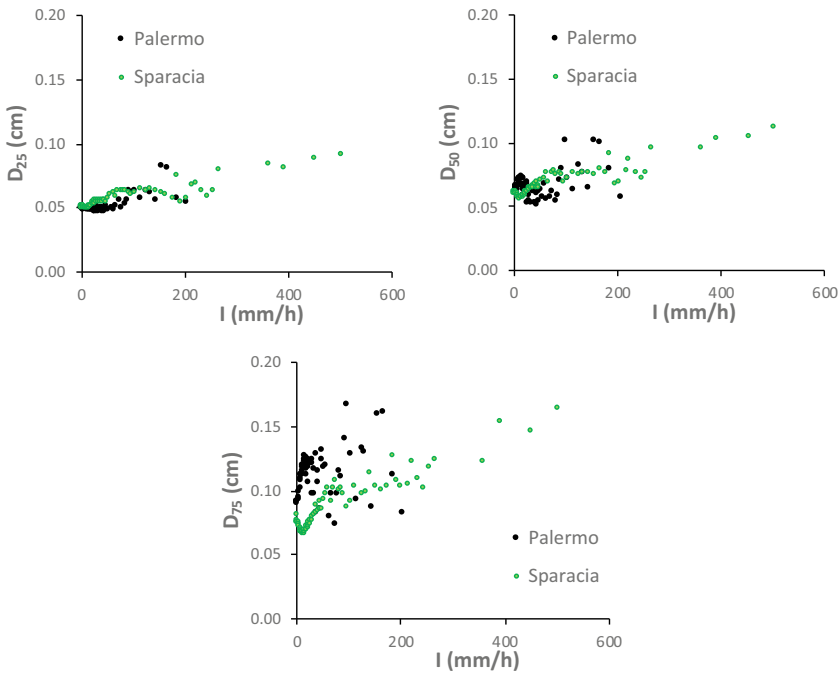
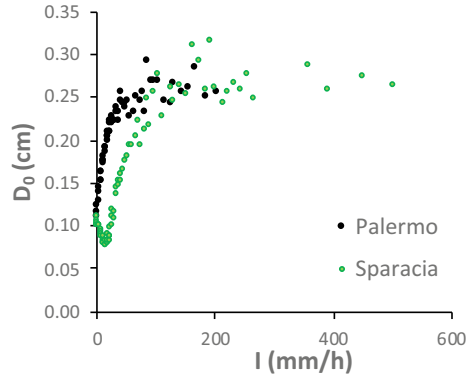


Fig. 5 Drop diameter's 25th (D_{25}), 50th (D_{50}), 75th (D_{75}) percentiles of the aggregated DSDs versus rainfall intensity

Fig. 6 Measured D_0 values versus rainfall intensity for the aggregated DSDs detected in the two sites



ones. For $I > 50$ mm/h, this trend is not more appreciable. As consequence, for a given rainfall intensity, different DSDs for $I < 50$ mm/h and similar DSDs for $I > 50$ mm/h characterize the two experimental sites.

As shown in Fig. 6, for $I < 17$ mm/h, the Sparacia DSDs are characterized by a decreasing trend of median volume diameter with I . While, for $I > 17$ mm/h, the relation D_0 - I is not different to Palermo one and for $I > 100$ mm/h, the values of D_0 registered in the two sites can be considered equal.

The kinetic power of each aggregated DSD was calculated by combining each diameter with its terminal velocity obtained by the relationship proposed by Ferro [4].

Figure 7 highlights that the pairs $(I, P_n/I)$ detected at Palermo and Sparacia are roughly overlapped for $I > 100$ mm/h while, for $I < 100$ mm/h, the pairs relative to Palermo stay above Sparacia ones. However, for $I > 17$ mm/h, the relation $P_n/I - I$ for the two datasets is similar since P_n/I increases with rainfall intensity until $I = I_t$ ($I_t = 40$ mm h⁻¹ for Palermo and $I_t = 100$ mm/h for Sparacia). Above these limits, P_n/I varies around the constant value of 27 J m⁻² mm⁻¹ which is near to the asymptotic values given by Eq. (1) (28.3 J m⁻² mm⁻¹) or Eq. (2) (29 J m⁻² mm⁻¹). Anyway, according to Fig. 7, the relation $P_n/I - I$ depends on the location of the site and the rainfall intensity can not be the only predictive variable. Therefore, relationships such as Eq. (1) or Eq. (2), are not reliable everywhere (Fig. 8).

Figure 9 reports the pairs $(D_0, P_n/I)$ for both datasets highlighting that they are overlapped for $D_0 > 0.17$ cm and near to the curve of Eq. (4). For $D_0 < 0.17$ cm the Palermo P_n/I values are greater than Sparacia ones. In this case, only for the Sparacia dataset, use of Eq. (4) determines a P_n/I systematic underestimation.

The above considerations suggest that the validity of the hypotheses on which Eq. (4) is based is reliable for whole Palermo dataset and is limited to $D_0 > 0.17$ cm for Sparacia dataset.

Fig. 7 Kinetic power per unit volume of rainfall versus rainfall intensity for the aggregated DSDs detected in the two sites

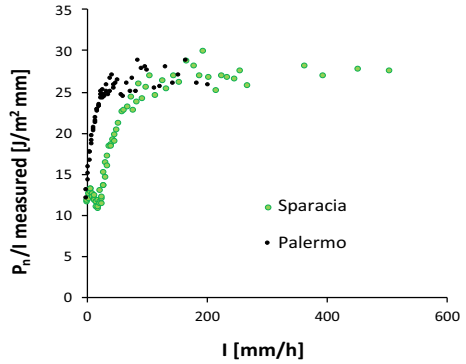


Fig. 8 Reliability of Eqs. (1) and (2) to Palermo and Sparacia datasets

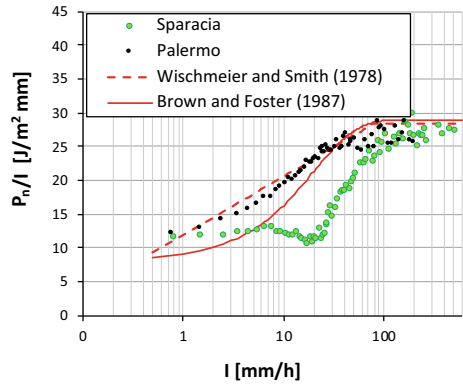
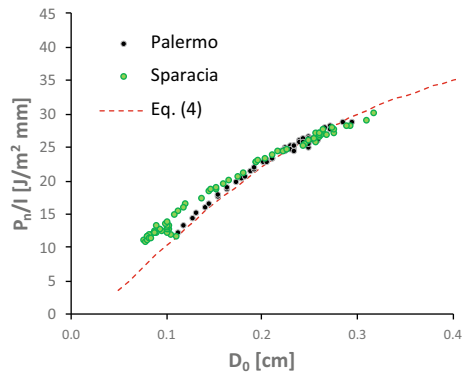


Fig. 9 Kinetic power per unit volume of rainfall, P_n/I , versus median volume diameter D_0 , for the two datasets



4 Conclusive Remarks and Research Needs

In this study, the DSDs recorded by the same optical disdrometer at two Sicilian experimental sites (Palermo and Sparacia) were compared. Even though the two

sites are situated in a comparable geographical environment, the DSDs registered at Palermo differ from Sparacia ones.

Fixing rainfall intensity, the kinetic power per unit volume of rainfall registered in the two sites can be considered roughly similar only for rainfall intensity greater than 100 mm h^{-1} .

This study showed that the relation $P_n/I - I$, such as Eq. (1) and Eq. (2), is not applicable anywhere because the rainfall intensity is not the only predictive variable. In other words, knowing only the rainfall intensity does not allow to estimate accurately its erosivity.

The Eq. (4) deduced by Carollo et al. [3] is reliable for the Palermo dataset while, for Sparacia dataset, its reliability is limited to $D_0 > 0.17 \text{ cm}$ because for $D_0 < 0.17 \text{ cm}$, a systematic underestimation of P_n/I is detected.

For verifying the above results, further investigations in other climatic contexts are needed.

References

1. Brown, L.C., Foster, G.R.: Storm erosivity using idealized intensity distribution. *Trans. ASAE* **30**, 379–386 (1987). <https://doi.org/10.13031/2013.31957>
2. Carollo, F.G., Ferro, V.: Modeling rainfall erosivity by measured drop-size distributions. *J. Hydrol. Eng.* **20**(6), C4014006 (2015). [https://doi.org/10.1061/\(ASCE\)HE.1943-5584.0001077](https://doi.org/10.1061/(ASCE)HE.1943-5584.0001077)
3. Carollo, F.G., Ferro, V., Serio, M.A.: Reliability of rainfall kinetic power-intensity relationships. *Hydrol. Process* **31**, 1293–1300 (2016). <https://doi.org/10.1002/hyp.11099>
4. Ferro, V.: Tecniche di misura e monitoraggio dei processi erosivi. *Quaderni di Idronomia Montana* **21**(2), 63–128 (2001)
5. Kinnell, P.I.A.: Rainfall intensity-kinetic energy relationship for soil loss prediction. *Soil Sci. Soc. Am. Pro.* **45**, 153–155 (1981). <https://doi.org/10.2136/sssaj1981.03615995004500010033x>
6. Ulbrich, C.W.: Natural variations in the analytical form of the raindrop size distribution. *J. Clim. Appl. Meteorol.* **22**, 1764–1775 (1983)
7. Wischmeier, W.H., Smith, D.D.: Predicting Rainfall Erosion Losses-A guide to conservation planning. *Agriculture Handbook: United States Department of Agriculture, Washington, D.C.* 537 (1978)

Testing an Automatic Approach for Rill Network Extraction to Measure Rill Erosion by Terrestrial Photogrammetry



F. G. Carollo , C. Di Stefano , A. Nicosia , V. Palmeri ,
V. Pampalone , and V. Ferro 

Abstract In a recent investigation, the applicability of close-range photogrammetry to measure rill erosion was positively tested on two plots with a length of 22 m and steepness of 22% and 26% at the Sparacia experimental area (Sicily, Southern Italy). An objective method, based on the convergence index, was applied to delineate the rill network from the Digital Elevation Models (DEMs) and measure the eroded channel volume, accordingly.

For the erosion event of September 2017, rills also formed on the 14.9% slope of the experimental area and were surveyed on a 44 m-long plot with a series of photographs taken from the ground. Rills were characterized by clear differences in the cross-section geometry as compared to those previously detected on the more sloped plots, inasmuch they were wider and shallower. The present investigation aimed to check the effects of the rill cross-section morphology on the proposed procedure to measure rill erosion. The three-dimensional (3D) Digital Terrain Models and DEMs were obtained by an image-processing software using the Structure from Motion technique. The rill channels detected by a method based on the combination of a drainage algorithm and the convergence index were separated into contributing and non-contributing to the total soil loss measured in the tanks downstream of the plots. The rill density and frequency, and the soil loss due to contributing rills were obtained. Finally, the sediment weight measured by the contributing rills was compared with the weight of the sediment stored in the tanks that was assumed as reference value. The low measurement errors (−14%) obtained by image based technique supported the validity of the assumptions made to detect the contributing rill network and further confirmed the reliability of the SfM technique to measure rill erosion.

Keywords Rill erosion · Digital terrain models · Structure from motion technique

F. G. Carollo · C. Di Stefano · A. Nicosia · V. Palmeri (✉) · V. Pampalone · V. Ferro
Department of Agricultural, Food and Forest Sciences, University of Palermo, 90128 Palermo,
Italy
e-mail: vincenzo.palmeri02@unipa.it

© The Author(s), under exclusive license to Springer Nature Switzerland AG 2023
V. Ferro et al. (eds.), *AIIA 2022: Biosystems Engineering Towards the Green Deal*,
Lecture Notes in Civil Engineering 337,
https://doi.org/10.1007/978-3-031-30329-6_9

1 Introduction

Water erosion is one of the most important soil degradation processes and rill erosion contribution to total soil loss is usually dominant as compared to interrill erosion [1, 9]. Measurement of rill channels can be carried out by direct and indirect methods. The direct method is time consuming and invasive because the operator carrying out the survey walks inside the rilled area. The indirect methods, such as terrestrial laser scanner (TLS), and the three-dimensional-photo reconstruction (3D-PR) techniques, overcame these limitations and provide accurate 3D models of the investigated area. The 3D-PR techniques, such as the coupled use of Structure from Motion (SfM) and Multi View-Stereo (MVS) workflows [10], use images acquired from uncalibrated and non metric cameras coupled with photogrammetric software packages [4] for creating a 3D - point cloud representing the surveyed surface. Using the 3D point cloud, a 2.5D surface (i.e., Digital Elevation Model, DEM) can be generated. In a recent investigation [5], the applicability of close-range photogrammetry to measure rill erosion was positively tested on two plots with a length of 22 m and steepness of 22% and 26% at the Sparacia experimental area (Sicily, Southern Italy). An objective method, based on the convergence index, was applied to delineate the rill network from the Digital Elevation Models (DEMs) and measure the eroded channel volume, accordingly.

The general aim of this investigation is the measurement of plot rill erosion using the SfM technique for rill digital reconstruction from terrestrial image sources. In particular, a survey was carried out for measuring rills occurred in a plot located at the Sparacia experimental area due to a natural intense rainfall event. The specific aims are: i) comparing some morphological variables (depth, h , and width, w) of the rill cross section measured in this investigation with those measured by Di Stefano et al. [5], ii) testing the method based on the combination of a drainage algorithm and the convergence index at the rill scale; iii) comparing some morphometric parameter of the rill network obtained using three different thresholds of the segment length producing the rill interruption, iv) comparing soil loss measurements carried out by the image based technique using these three different thresholds with the actual soil loss measured in the sediment storage system located downstream of the plot.

2 Materials and Methods

For the severe erosion event of September 24, 2017, which was characterized by a total rainfall amount of 33 mm and an erosivity index [13] equal to $517.4 \text{ MJ mm ha}^{-1} \text{ h}^{-1}$, both total erosion and rill erosion were measured on a $8 \text{ m} \times 44 \text{ m}$ plot, with steepness, s , of 14.9% located at the Sparacia experimental area. The Sparacia experimental station for soil erosion measurement of the Department of Agriculture Food and Forest Sciences of Palermo University is located in western Sicily, southern Italy, approximately 100 km south of Palermo (Fig. 1).

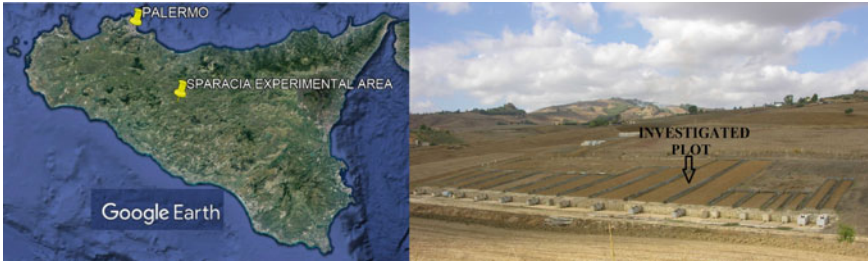


Fig. 1 Location of the experimental area and view of the investigated plot

In this experimental area 22 USLE-type plots, varying in length from 11 to 44 m, in width from 2 to 8 m and in steepness from 9 to 26%, are established. All plots are subjected to natural rainfall, and are continuously in fallow. Runoff and associated sediments from each plot are intercepted by a gutter placed at the lower end of the plot, and collected into a storage system consisting of tanks of known geometric characteristics, each having a capacity of approximately 1 m^3 , that are arranged in series at the base of each plot. In this investigation, the 12 MP GoPro Hero4 Silver camera was used for terrestrial image acquisition. The camera was fixed to the tip of a telescopic pole to capture high centred perspectives of the plot by following a walking itinerary around the plot. The average object distance H was equal to 2.4 m and a total number of about 325 images were taken to cover the plot. Eight GCPs were deployed on the plot perimeter and their (x, y, z) coordinates were collected with a geodetic total station. The GCPs consisted of $15 \text{ cm} \times 15 \text{ cm}$ black and white wooden targets. The image processing software Photoscan Professional (by Agisoft, St. Petersburg, Russia) was used for obtaining the 3D model by an automatic process which couples SfM and MVS techniques. Then, using the point cloud of the 3D model a DEM having a pixel size equal to 5 mm was generated by Photoscan.

Various methods have been used in different studies to extract channel network from a DEM such as the landform curvature method [11], the slope analysis, the Broscoe's method [2] and the Canny operator [3, 7]. In this investigation, the method based on the combination of a drainage algorithm and the convergence index was applied.

The CI index is defined by the following relationship [5, 12],

$$CI = \left(\frac{1}{n-1} \sum_{i=1}^{n-1} \theta_i \right) - 90 \quad (1)$$

where n is the number of kernel cells, and for each external cell i , θ_i is the angle, in degrees, between the aspect of cell i and the direction of the vector joining the centre of cell i and the centre of the kernel [12]. The convergence index ranges from -90° to 90° . Positive values relate to divergent areas, negative values relate to convergent areas, and null values represent areas without curvature as planar slopes.

Tarolli et al. [11] suggested that the kernel size for topographic parameter calculation has to be related to the size of the feature to be detected. In the present investigation, a moving window of 23 cm, having a size equal three times the spatial extent of the investigate feature, was used.

To determine significant cells, i.e. which should actually correspond to the rill channel, an objective threshold CI_T , beyond which the CI values could be considered significantly different from a plane landform, was applied. In particular, the threshold was set equal to two times the standard deviation, σ , of CI . The choice of this threshold value was supported by the findings of Pirotti and Tarolli [8] concerning channel network extraction. Taking into account that only negative CI values relate to convergent areas, significant flow convergence cells were characterized by convergence index values less than or equal to -2σ .

At the end of this step, the disconnected convergent areas were identified and considered as rill features. To achieve the connection, the flow accumulation algorithm was weighted with the threshold convergence grid according to Thommeret et al. [12]. A GRID representing the rill thalweg was obtained.

Considering that only some rill channels were connected to the rill network reaching the plot outlet, according to Di Stefano et al., [5] and Rejman and Brodowski, [9] the rills were separated into contributing, which were connected to this network and contributed to total soil loss measured at the plot outlet, and non-contributing rills which were interrupted within the plot. To identify the contributing rills, the automatic procedure by Di Stefano et al. [5] was applied. The procedure allows obtaining a raster of deepening, h_d , respect to the maximum elevation in a given neighborhood of the pixel.

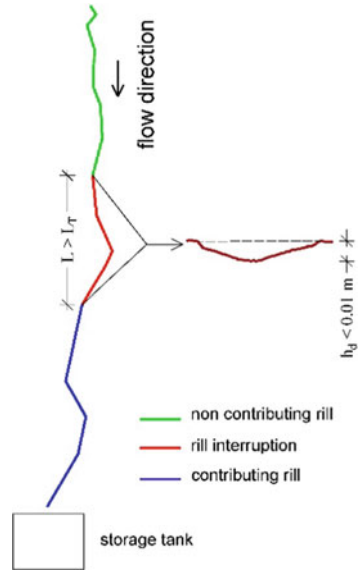
From the obtained raster of deepening values, rill interruptions were localized where the pixel values were lower than a given deepening threshold, h_T , and this condition persisted at least for a rill segment length, L , greater than a threshold L_T . A single h_T value, equal to 1 cm, and three different L_T values (10, 12 and 15 cm) were used. In other words, if the deepening value was lower than 1 cm and this condition occurred for a rill of at least 10–12–15 cm, then the rill was interrupted and the upstream rill reach was classified as non-contributing. Figure 2 shows, schematically, the criterion for the determination of contributing and non-contributing rills.

To measure the total volume V , each contributing rill was divided into segments, each of them bounded by two 0.30 m long transects perpendicular to the rill thalweg and with a distance interval, d , of 0.3 m. The extraction of the cross section profile was carried out in correspondence of the transects from the point cloud of the 3D model by Cloud Compare software. The surface width, w , the depth, h , calculated using the rill thalweg as reference, and the cross section area σ were measured by AutoCad. The rill segment volume $V_{r,s}$ was calculated by the following relationship:

$$V_{r,s} = 0.5 (\sigma_i + \sigma_{i+1}) d \quad (2)$$

where σ_i and σ_{i+1} are the upslope and downslope cross section areas of the rill segment, respectively. The total volume V was obtained by adding the rill segment

Fig. 2 Sketch concerning the criterion adopted for the determination of non-contributing and contributing rills



volumes. The total rill volume V was converted into weight using the bulk density mean value equal to 1200 kg m^{-3} .

To measure the actual soil loss, the direct method (DM), was adopted. In particular, the total weight of the stored suspension (liquid and solid fractions) into each tank was measured and a representative sample from the free surface to the bottom of the tank was extracted by a cylindric sampler to measure the water content in the suspension. The sample was oven-dried at $105 \text{ }^\circ\text{C}$ for 48 h and the solid material was weighed.

3 Results and Discussion

The cumulative frequency distributions of both w and depth h plotted in Fig. 3 show that width values detected in this investigation are significantly higher than those measured by Di Stefano et al. [5] while for h no significant differences are appreciated with the available data for plot steepness, $s = 22\%$. This result can be explained by the lower slope of the investigated plot.

Figure 4 shows, as an example, a representative cross-section of rill surveyed by Di Stefano et al. [5] (a), and in this investigation (b).

Figure 5 shows the total length, L_R , and drainage frequency, F_k , values by three different L_T for non-contributing and contributing rills.

L_R of non-contributing rills were, on average, higher than those of contributing rills. Moreover, for non-contributing rills the total length decreases as L_T increases, while for contributing rills L_R decreases as L_T decreases. The L_R values of

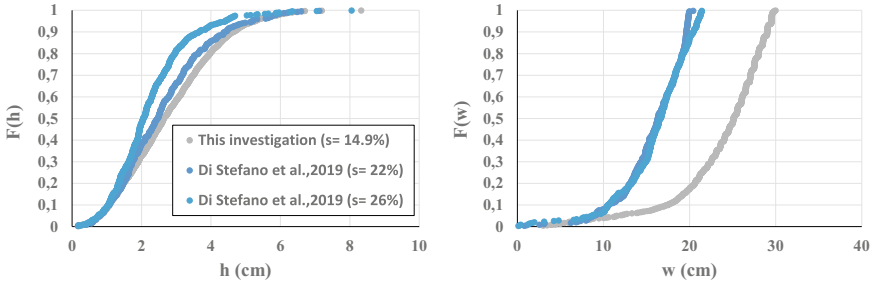


Fig. 3 Cumulative frequency distributions of w and h

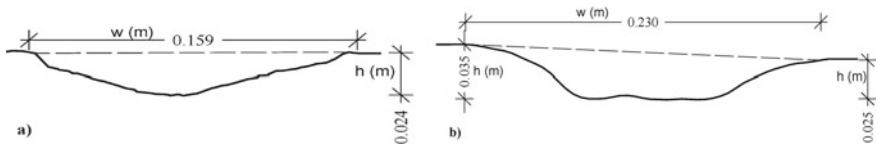


Fig. 4 Representative cross-section profile of rill surveyed by Di Stefano et al. [5] a, and in this investigation b

contributing rills were equal to 48%, 42% and 34% of the total length of all rills for $L_T = 10$ cm, 12 cm and 15 cm, respectively. F_k , obtained from the three different values of L_T were similar (Fig. 5b) both for the non-contributing and contributing rills, and the highest values of F_k were detected for non-contributing rills. For contributing rills the drainage density D_k was 0.65 m m^{-2} ($L_T = 10$ cm), 0.80 m m^{-2} ($L_T = 12$ cm) and 0.90 m m^{-2} ($L_T = 15$ cm) while, for those not contributing, it was equal to 1.24 m m^{-2} ($L_T = 10$ cm), 1.10 m m^{-2} ($L_T = 12$ cm) and 0.99 m m^{-2} ($L_T = 15$ cm).

For both non-contributing and contributing rills the drainage frequency was less sensitive to the threshold L_T than total length and the drainage density. This result suggested that L_T affects the total length of rills while does not affect the number of rills. Therefore, for contributing rills, the increase of L_T yields almost exclusively an increased total length of the contributing rill network.

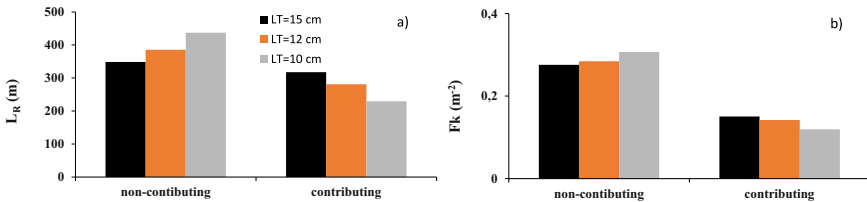


Fig. 5 L_R and F_k values by three different L_T values for non-contributing and contributing rills

Fig. 6 Comparison of soil loss measurement by 3D model with that obtained by DM

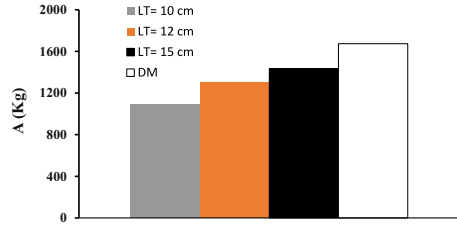


Figure 6 shows the comparison of soil loss measurement by 3D model using three different L_T values with that obtained by DM. These measurements were affected by an error equal to -35% for $L_T = 10$ cm, -22% for $L_T = 12$ cm and -14% for $L_T = 15$ cm. Therefore the most reliable value of soil loss due to rill erosion, i.e., closest to that obtained by DM method, was obtained by setting $L_T = 15$ cm.

The low measurement errors (-14% for $L_T = 15$ cm)) was close to both obtained by Di Stefano et al. [6] (ranging from -6.4% to 16.8%) and by Di Stefano et al. [5] (ranging from -6% to 13%). The underestimation of soil loss for all three L_T thresholds can be explained by the fact that the DM also takes into account the contribution of the interrill component. However, the low measurement errors obtained by image based technique supported the validity of the assumptions made to detect the contributing rill network and further confirmed the reliability of the SfM technique to measure rill erosion.

4 Conclusions

This paper reported the results of the comparison between rill surveys that were conducted for three different plots at the Sparacia experimental area for two different rainfall event. In all cases the acquired data were processed using SfM technique. Furthermore, in this investigation the results of the comparison between some morphometric parameters and rill erosion measures, obtained by three different values of rill interruption length, L ; were reported. The technique performed in the present investigation allowed to establish that i) the plot steepness affects the surface width of the rill cross section ii) the L_T values affects the total length of rills while does not affect the number of detected rills iii) the combination of a drainage algorithm and the convergence index, and the adopted criterion to detect the contributing rill network leads to reliable results. Further studies are necessary to choose a L_T value which can be used in absence of measured data allowing its calibration.

References

1. Borrelli, P., et al.: An assessment of the global impact of the 21st century land use change on soil erosion. *Nat. Commun.* **8**, 1–13 (2017)
2. Broscoe, A.J.: Quantitative analysis of longitudinal stream profiles of small water-sheds. Technical report 389–042. Department of Geology, Columbia University, New York (1959)
3. Canny, J.: A computational approach to edge detection. *IEEE Trans. Pattern Anal. Mach. Intell.* **8**, 679–698 (1986)
4. Castillo, C., Pérez, R., James, M.R., Gómez, J.A.: SF3M software: 3-D photo-reconstruction for non-expert users and its application to a gully network. *Soil* **1**, 583–594 (2015)
5. Di Stefano, C., Palmeri, V., Pampalone, V.: An automatic approach for rill network extraction to measure rill erosion by terrestrial and low-cost unmanned aerial vehicle photogrammetry. *Hydrol. Process.* **33**, 1883–1895 (2019)
6. Di Stefano, C., Ferro, V., Palmeri, V., Pampalone, V.: Measuring rill erosion using structure from motion: a plot experiment. *CATENA* **156**, 383–392 (2017)
7. Eltner, A., Baumgart, P., Maas, H.G., Faust, D.: Multi-temporal UAV data for automatic measurement of rill and interrill erosion on loess soil. *Earth Surf. Proc. Land.* **40**(6), 741–755 (2015). <https://doi.org/10.1002/esp.3673>
8. Pirotti, F., Tarolli, P.: Suitability of LiDAR point density and derived landform curvature maps for channel network extraction. *Hydrol. Process.* **24**(9), 1187–1197 (2010). <https://doi.org/10.1002/hyp.7582>
9. Rejman, J., Brodowski, R.: Rill characteristics and sediment transport as a function of slope length during a storm event on loess soil. *ESP Landforms* **30**, 231–239 (2005)
10. Seiz, S.M., Curless, B., Diebel, J., Scharstein, D., Szeliski, R.: A comparison and evaluation of multi-view stereo reconstruction algorithms. In: *IEEE Conference on Computer Vision and Pattern Recognition*. IEEE Computer Society, New York (2006)
11. Tarolli, P., Sofia, G., Dalla, F.G.: Geomorphic features extraction from high-resolution topography: landslide crowns and bank erosion. *Nat. Hazards* **61**, 65–83 (2012)
12. Thommeret, N., Bailly, J.S., Puech, C.: Extraction of thalweg networks from DTMs: application to badlands. *Hydrol. Earth Syst. Sci.* **14**, 1527–1536 (2010)
13. Wischmeier W.H., Smith D.D.: Predicting rainfall erosion losses. A guide to conservation planning, USDA Agriculture Handbook. N. 282 (1978)

Assessing Path Tortuosity on Rill Flow Resistance



F. G. Carollo , C. Di Stefano , A. Nicosia , V. Palmeri ,
V. Pampalone , and V. Ferro 

Abstract The departure of the thalweg from a straight path is accounted for by the tortuosity t , a parameter of rill morphology. Few research has been done on how t affects flow resistance for rills. The analyses of a plot investigation reported in this study are finalized calculating the tortuosity parameter and evaluating the reliability of a theoretical flow resistance equation. The Structure from Motion algorithm was used to generate a three-dimensional Digital Terrain Model. First, an approximation of the thalweg was obtained by photo-interpretation for the four investigated rills. A calculation routine was then applied to identify the cross sections perpendicular to this rill thalweg, with a fixed distance d , and determine the relative lowest points. The real rill thalweg resulted from the line connecting these points. Among the several investigated distances, the value of 0.075 m was selected for tortuosity calculation. The detected non-monotonic relationship of the Darcy-Weisbach friction factor f against t was attributed to the three additive components resulting from sediment transport, bed roughness, and localized energy losses caused by curves. In fact, compared to the third component, the first two have the opposite influence on f . The theoretical approach gave an accurate and t -dependent estimation of f .

Keywords Tortuosity · Rill erosion · Flow velocity profile · Flow resistance

1 Introduction

The rill component of soil erosion is frequently dominant relative to the interrill one [2, 9]. Rills are likely to occur when severe rainfalls hit bare soils [3].

The mean flow velocity, V , is a fundamental hydraulic variable for studying and modeling rill erosion processes since it affects sediment detachment and transport [7]. Uniform flow equations, such as Darcy-Weisbach, Manning, or Chezy [5, 11], developed for river hydraulics, are used in many soil erosion models. The latter are

F. G. Carollo · C. Di Stefano · A. Nicosia · V. Palmeri · V. Pampalone (✉) · V. Ferro
Department of Agricultural, Food and Forest Sciences, University of Palermo, 90128 Palermo,
Italy
e-mail: vincenzo.pampalone@unipa.it

applicable to turbulent and uniform flows, which differ from rills for the geometrical scale, interactions between flow and the eroding channel, and tortuosity. This last parameter of rill morphology represents how much the thalweg deviates from a straight line.

A common definition of rill tortuosity still lacks [10, 11]. In this investigation, the rill tortuosity t is calculated as the ratio between the actual and the straight thalweg length, following Strohmeier et al. [11].

Although investigations about the impact of path geometry on flow resistance for meandering channels have been conducted, studies for rills are lacking in the literature. This is a challenge as rills in field can be characterized by a level of tortuosity. This may be important, for instance, in areas with sparse and irregularly spaced plants, where runoff is naturally directed between plants by vegetation. In fact, runoff is compelled to flow between patches because the soil supporting vegetated patches is frequently higher relative to the surrounding environment [8]. Since 1984, numerous experimental studies have been conducted to develop relationships that predict rill flow velocity [3]. To the best of our knowledge, however, only one study, conducted by Strohmeier et al. [11], examined the relationship between rill tortuosity and rill roughness, measured by the Manning–Strickler coefficient k_{st} . Their experimental runs were performed for two discharge values (0.145 and 0.170 L s⁻¹) and both rills freely developing on a sloping bed and rills forced to have a straight direction. The former experiments were characterized by tortuosity values ranging from 1.051 to 1.109, while the latter ones had values approximately equal to 1.000 (1.000–1.017).

Di Stefano et al. [2] proposed a theoretical rill flow resistance equation, which is obtained by integrating the power velocity profile:

$$f = 8[(\delta + 1)(\delta + 2)/(2^{1-\delta} Re^\delta)]^{2/(1+\delta)} [1/\Gamma]^{2/(1+\delta)} \quad (1)$$

where f is the Darcy-Weisbach friction factor, $\delta = 1.5/\ln Re$, Re is the Reynolds number, and Γ is the velocity profile parameter. The Γ parameter can be estimated by the following power equation

$$\Gamma = a F^b / s^c \quad (2)$$

where F is the Froude number, s is the bed slope, and a , b and c are coefficients to be experimentally determined. Equation (2) was parameterized by measurements obtained only for straight rills, with flat or step-pool beds, and with or without sediment transport [3]. A tortuous rill prevents uniform flow from occurring. In comparison to straight channels, the flow structure in this situation is more complicated, as all the three components of flow velocity are relevant. For this reason, specific measurements are needed to calibrate and assess the predictive capability of flow resistance equations, such as Eq. (1).

Given the obvious fractal nature of the rill length, the adopted accuracy level of the measurement technique has a clear impact on the tortuosity value. Additionally, the flow velocity obtained by the dye-tracing technique [7], and consequently flow resistance, are affected by the measured rill length.

This paper presents the findings of a plot research conducted to determine how rill tortuosity affects flow resistance. Firstly, the adequate accuracy of the rill thalweg measurement for establishing t was identified, and then applied to study rill flow resistance. The tests broadened the range of the tortuosity values adopted in the study by Strohmeier et al. [11].

2 Materials and Methods

The experimental runs were performed on a $2\text{ m} \times 7\text{ m}$ plot, placed at the Department of Agriculture, Food and Forest Sciences of the University of Palermo. A soil having a clay percentage of 32.7%, silt of 30.9%, and sand of 36.4%, was used to fill the plot to a slope of 18%. Four different values of tortuosity, approximately equal to 1 (straight rill), 1.08, 1.16, and 1.30 (Fig. 1a) were set manually incising four mobile bed rills, where a low clear flow discharge ($Q = 0.1\text{ L s}^{-1}$) initially ran. Then, during the experiments, a constant inflow discharge $Q = 0.32\text{ L s}^{-1}$ shaped the rill channel. At the end of each run, the three-dimensional Digital Terrain Model (3D-DTM) was constructed through about 70 photographs, acquired with a digital camera, and was used to define the rill channel geometry and ascertain the real tortuosity value. Considering that the 3D algorithm operates with convergent photos, these images were taken to ensure that each point of the surveyed area was included in at least three photos. Structure from Motion (SfM) and MultiView Stereo algorithms were combined automatically by Agisoft Photoscan Professional to create the 3D model [3]. Then, using photo-interpretation, an approximation of the rill thalweg was identified. A calculation routine was then applied to identify the cross sections perpendicular to this rill thalweg, with a fixed distance d , and determine the related lowest points. The real rill thalweg resulted from the line connecting these points. Each rill channel was split into nine longitudinal segments, each bordered by ten transects having a distance of 0.624 m and perpendicular to the steepest slope of the plot (Fig. 1a). The rill segment between a certain transect-thalweg intersection and the rill ending was referred to as a rill reach.

The measurements of water depth h , hydraulic radius R , mean flow velocity V , and bed slope s were performed at the reach scale and were used to calculate the Darcy-Weisbach friction factor $f = 8gRs/V^2$, where g is acceleration due to gravity, the Froude number $F = V/(gh)^{0.5}$, and the Reynolds number $Re = Vh/\nu$, in which ν is the kinematic water viscosity.

For each run, a newly established approach [4], that combines the ground survey of the rill channel from the SfM with the survey of the wetted surface highlighted by a dye solution, was used to calculate R and h . Specifically, a Methylene blue solution injected in the flow (Fig. 1b) colored the rill channel to survey the wetted lateral surface SL_{rr} using the GIS functions “real surface” (SAGA 7.0.0) and “zonal statistics” (ARCGIS 10.5).

The ARCGIS-tool developed by Băcovà et al. [1] allows for building the water surface and measure the related area W_{rr} using the vector polygon matching to the

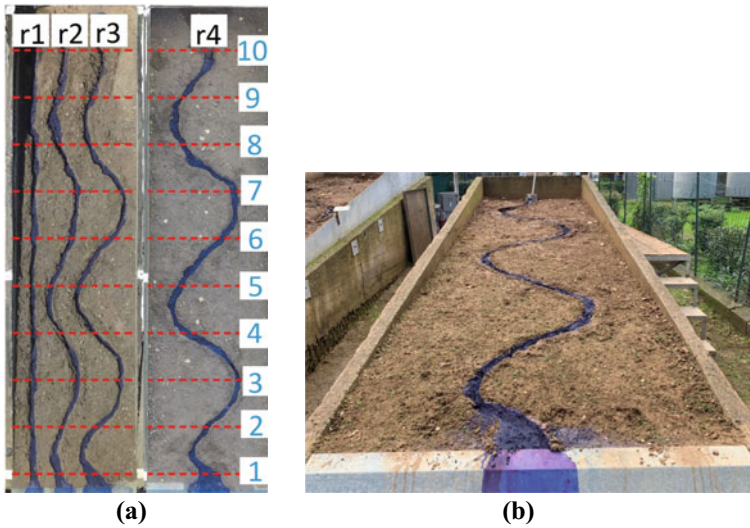


Fig. 1 View of the (a) four investigated rills (r1-r4) characterized by different tortuosity values and (b) the marked wetted surface of the rill

rill tracks. The difference between the DEM of the rebuilt water surface and that of the eroded channel was used to calculate the channel volume V_{rr} . The equations $R = V_{rr}/SL_{rr}$ and $h = V_{rr}/W_{rr}$ provide the mean hydraulic radius R and depth h [4].

By averaging the data collected in the rill reach thalweg obtained by 3D-DTM, the reach's slope steepness was determined.

A sensitivity analysis of t to d was carried out for the four entire rills (reaches 10–1) and cross-section spacing of 0.005, 0.01, 0.025, 0.05, 0.075, 0.10, and 0.15 m. The tortuosity values were calculated for all rill reaches using $d = 0.075$ m, which was selected as stated below. When compared to the differences between the four whole rills, the variability of these tortuosity values for each rill in relation to that of the entire rill channel was modest. As a result, the tortuosity values obtained for the whole rills were also assigned to all the nested reaches.

Using a Methylene blue solution as a tracer, the dye-tracing method [6] was applied to determine the mean rill flow velocity V . The flow velocity was calculated by timing the progression of the leading edge of the dye cloud over the reach distance after a modest quantity of tracer was injected at the transect-thalweg intersection. The surface velocity V_s of the leading edge of the dye cloud was calculated as the ratio of the reach length to the travel time. In this study, the reach length was calculated along the thalweg and was d -dependent, as shown below. For the conversion of V_s to the mean flow velocity V , a correction factor equal to 0.8 was used.

3 Results and Discussion

Figure 2 plots t versus d , as an example for rills 3 and 4. For smaller d values, the expected diminishing relationships clearly display a quick variation and reach a practically constant value for $d \geq 0.075$ m. Thus, the flow velocity is unaffected by the section spacing for $d \geq 0.075$ m, but it dramatically rises for the lowest values of d as observed rill length grows. Nevertheless, the highest velocities would correspond to flow paths with unrealistic continuous changes in direction. The distance $d = 0.075$ m was selected and employed in subsequent analyses as it was deemed to be physically sound. The resulting tortuosity values were 1, 1.10, 1.18, and 1.29, which are quite similar to the values established with the manual rill incision.

For the whole rill channels, the changes of slope gradient s , Darcy-Weisbach friction factor f , and flow velocity V with tortuosity t are shown in Fig. 3. For a certain difference in elevation, the slope declines due to the lengthening of the thalweg from 16.8% for the straight rill channel ($t = 1.04$) to 13.8% for $t = 1.29$. The friction factor exhibits a non-monotonic relationship with t , with decreasing values up to $t = 1.18$ and an increased value (1.44) for $t = 1.29$, which is nearly identical to that (1.45) of the straight channel. For $1.04 \leq t \leq 1.18$, the velocity is roughly constant (0.33 m s^{-1}), but it decreases to 0.28 m s^{-1} for the maximum tortuosity value of 1.29.

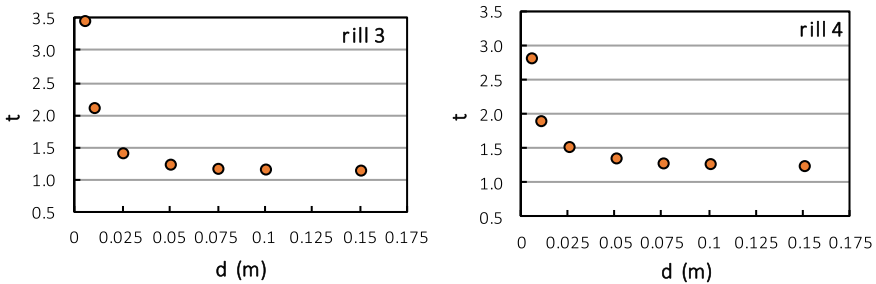


Fig. 2 Plot of the tortuosity t against the section spacing d for rills 3 and 4

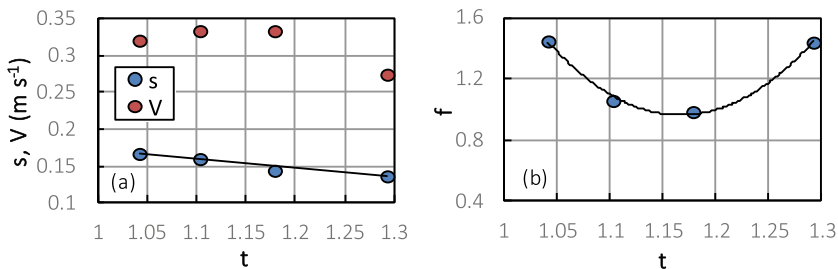


Fig. 3 Variations of (a) slope gradient s and mean flow velocity V and (b) Darcy-Weisbach friction factor f , with t for the four whole rills

Three additive components produced by bed roughness, sediment load, and localized energy losses caused by the curves may be postulated to give the friction factor. For straight rill channels, the latter leads to minor local friction effects. When the slope declines, the erosion rate also diminishes, resulting in less sediment transport and smoother beds. As a result, these two components of f diminish for rising t values (see Fig. 3a), whereas the local friction effects caused by the curves become increasingly significant. For $1.04 \leq t \leq 1.18$, the plot of f versus t (Fig. 3b) indicates that the components owing to bed roughness and sediment load exceed those due to curves, but the inverse is true for higher t values. For $t > 1.18$, the existence of sharp curves causes flow velocity to be lower, while the found constant flow velocity for $1.04 \leq t \leq 1.18$ (Fig. 3a) is compatible with the occurrence of a feedback mechanism [6].

The (Re, F) pairs related to rill reaches reveal that the flow is supercritical for 6 out of 29 cases with 4 out of 6 supercritical flows occurring for $t = 1.10$, while the flow is subcritical in the majority of cases. Moreover, the flow is constantly turbulent, and as tortuosity grows, the Reynolds number tends to fall. Many studies have been done on the relation between the Reynolds number and f for straight rill channels. If the flow depth is significantly higher than the size of the roughness elements, the drop in f with increasing Re is well recognized. For example, Gilley et al. [5] obtained a $f - Re$ decreasing power relationship. Figure 4b displays the (Re, f) measurements identified by the tortuosity t values investigated here and confirms the occurrence of a decreasing power relationship between f and Re .

The least-squares method was used on the entire dataset to estimate the coefficients of Eq. (2) that are $a = 0.449$, $b = 1.065$, and $c = 0.536$. Equations (1) and (2) with these numerical values, give accurate f predictions, characterized by a mean absolute error of 2.9% and absolute errors less than $\pm 5\%$ for 89.7% of measurements. Nevertheless, for $t = 1.04$ and 1.29 , the f predictions slightly but systematically underestimate the friction factor, whereas for $t = 1.18$, systematically overestimate f as indicated in Fig. 5a. Fixing $b = 1.065$ and $c = 0.536$, the a coefficient was determined for each value of the tortuosity. In this case, the estimation performance was better than that of the previously parameterized equation because it was characterized by a mean

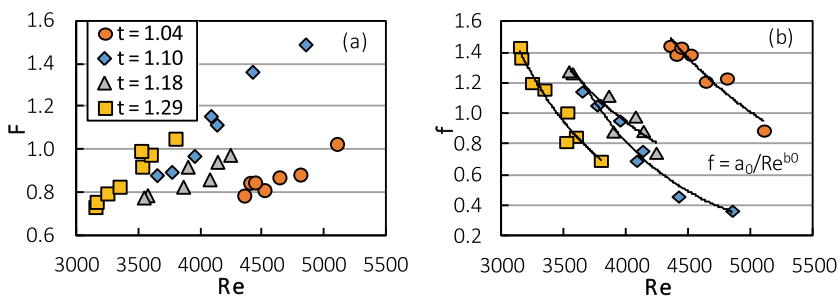


Fig. 4 Plot, for the investigated values of tortuosity and the measurements carried out in the rill reaches, of the Reynolds number Re against (a) the Froude number F and (b) the friction factor f and the best-fit curves having a power form

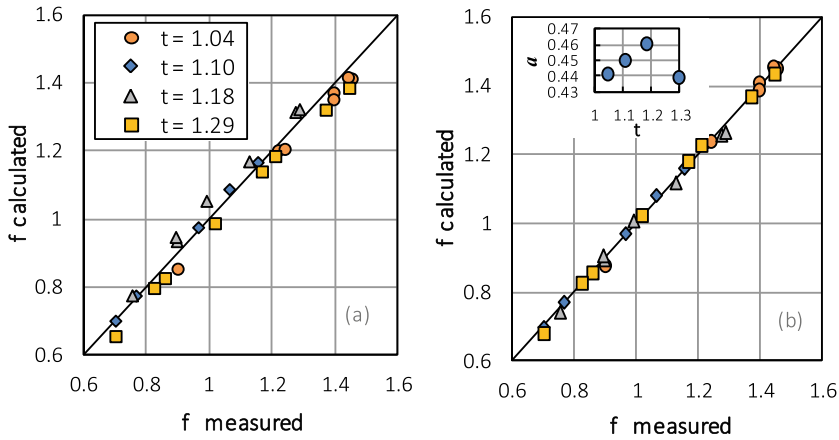


Fig. 5 Comparison between the measured f values in the rill reaches and the calculated f values by Eqs. (1) and (2) with (a) $a = 0.449$, $b = 1.065$, and $c = 0.536$, and (b) $b = 1.065$, $c = 0.536$ and a estimated for each t value

absolute error of 1.1%, estimate errors that are less than $\pm 5\%$, and predictions that are unaffected by bias for all t values (Fig. 5b). The tested flow resistance equation with the non-monotonic a - t relationship (Fig. 5b) can agree with the non-monotonic f - t relationship shown in Fig. 3b.

4 Conclusions

A level of tortuosity characterizes the rills that naturally occur in hillslopes. Tortuous rills have not been studied nearly as much as straight rills, therefore, there is no common tortuosity definition yet, and the reliability of the widely used flow resistance equations has not been examined in this particular situation. The results of the current study highlighted that the extraction of the rill thalweg and the determination of the tortuosity parameter can be obtained using a distance interval of 0.075 m between two consecutive cross sections, and the opposing effects of rill surface roughness plus soil particle load and of the changes in the flow direction cause the flow resistance to decrease initially and then increase as the tortuosity increases. The presented theoretical approach allows for accurately estimating the friction factor, even though additional measurements are needed to broaden the investigated experimental ranges.

References

1. Báčová, M., Krása, J., Devátý, J., Kavka, P.: A GIS method for volumetric assessments of erosion rills from digital surface models. *Eur. J. Remote Sens.* **52**(sup1), 96–107 (2019)

2. Di Stefano, C., Ferro, V., Palmeri, V., Pampalone, V.: Flow resistance equation for rills. *Hydrol. Process* **31**, 2793–2801 (2017)
3. Di Stefano, C., Nicosia, A., Palmeri, V., Pampalone, V., Ferro, V.: Rill flow velocity and resistance law: a review. *Earth Sci. Rev.* **231**, 104092 (2022)
4. Di Stefano, C., Nicosia, A., Pampalone, V., Palmeri, V., Ferro, V.: New technique for measuring water depth in rill channels. *CATENA* **181**, 104090 (2019)
5. Gilley, J.E., Kottwitz, E.R., Simanton, J.R.: Hydraulics characteristics of rills. *Trans. ASAE* **27**, 797–804 (1990)
6. Govers, G.: Relationship between discharge, velocity and flow area for rills eroding loose, non-layered materials. *Earth Surf. Process Landf.* **17**, 515–528 (1992)
7. Nicosia, A., Di Stefano, C., Palmeri, V., Pampalone, V., Ferro, V.: Roughness effect on the correction factor of surface velocity for rill flows. *Hydrol. Process* **35**, e14407 (2021)
8. Nouwakpo, S.K., Williams, C.J., AlHamdam, O.Z., Weltz, M.A., Pierson, F., Nearing, M.A.: A review of concentrated flow erosion processes on rangelands: fundamental understanding and knowledge gaps. *Int. Soil Water Conserv. Res.* **4**, 75–86 (2016)
9. Rejman, J., Brodowski, R.: Rill characteristics and sediment transport as a function of slope length during a storm event on loess soil. *Earth Surf. Process Landf.* **30**(2), 231–239 (2005)
10. Shen, H., Zheng, F., Wen, L., Lu, J., Jiang, Y.: An experimental study of rill erosion and morphology. *Geomorphology* **231**, 193–201 (2015)
11. Strohmeier, S.M., Nouwakpo, S.K., Huang, C.H., Klik, A.: Flume experimental evaluation of the effect of rill flow path tortuosity on rill roughness based on the Manning-Strickler equation. *CATENA* **118**, 226–233 (2014)

Assessing Daily ERA5-Land Reanalysis Data to Estimate Actual Evapotranspiration of Olive Orchards in Sicily



Dario De Caro , Ippolito Matteo , and Giuseppe Provenzano 

Abstract Accurate estimations of actual crop evapotranspiration are of utmost importance to evaluate crop water requirements and optimize water use efficiency. The objective of this work was to assess the suitability of ERA-5 Land (ERA5-L) reanalysis data to estimate the actual evapotranspiration (ET_a) of an olive orchard (cv. “Nocellara del Belice”) located in southwest Sicily, Italy. After examining the errors associated with daily precipitation and crop reference evapotranspiration deduced from the ERA5-L products and verifying the reliability of the FAO-56 model, the comparison between daily ET_a predicted by introducing in model simulation the reanalysis data and the corresponding measured on the ground was carried out. Experiments were implemented for three irrigation seasons (2009–2011) in a 13 ha olive orchard characterized by 3.5 m height trees spaced 5 m \times 8 m. An Eddy Covariance tower (EC) was installed in the orchard to measure, at a sub-hourly time step, air temperature and relative air humidity, wind speed and direction, net solar radiation, and, finally, sensible and latent heat fluxes. A meteorological station of the Sicilian Agrometeorological Information Service (SIAS) to monitor the climatic variables used to estimate crop reference evapotranspiration was also installed about 500 m apart from the study area. The hourly values of reanalysis climatic variables, including rainfall, were finally deduced from the ERA5-L product, characterized by a spatial resolution of about 9 km. For the three examined seasons, the application of the FAO-56 model with climate data measured on the ground produced fairly good estimations of ET_a , with values of root mean square error (RMSE) ranging between 0.40 and 0.69 mm d⁻¹ and mean bias error (MBE) from -0.24 to 0.10 mm d⁻¹. Suitable results were also obtained when model simulations included the reanalysis data, with RMSE and MBE respectively in the range 0.46 \div 0.65 and -0.13 \div 0.07 mm d⁻¹.

Keywords Climate variables · Eddy covariance · FAO-56 model

D. De Caro (✉) · I. Matteo · G. Provenzano
Department of Agriculture Food and Forest Sciences, University of Palermo, Viale Delle Scienze,
Bld 4, 90128 Palermo, Italy
e-mail: dario.decaro01@community.unipa.it

© The Author(s), under exclusive license to Springer Nature Switzerland AG 2023
V. Ferro et al. (eds.), *AIIA 2022: Biosystems Engineering Towards the Green Deal*,
Lecture Notes in Civil Engineering 337,
https://doi.org/10.1007/978-3-031-30329-6_11

105

1 Introduction

Evapotranspiration (ET) is one of the most important components in the hydrologic cycle. ET is the sum of the two different components: evaporation (E) from the soil and transpiration (T) from the plant canopy. In particular, the latter can allow identifying crop water requirements. To assess the plant water demand and optimize irrigation water use, the agro-hydrological models (AM) [1] and surface energy balance (SEB) models [2] have been developed. Several authors have studied the reliability of these models [3–5] highlighting that they can be a suitable solution to assess crop water status and improve irrigation water management. If on one hand, the AM and SEB models can represent powerful tools, on the other, their application depends on the availability of data input.

In general, to implement AMs is necessary to calculate the atmospheric evaporative demand which, as suggested in the FAO-56 paper [1], can be represented by the reference crop evapotranspiration, E_{To} . Despite numerous methods to calculate E_{To} have been proposed [6], the Penman–Monteith equation is largely applied when standard climate data (air temperature, global solar radiation, wind speed, and relative air humidity) are available [1]. Climate data used as input in the AMs are generally acquired by weather stations installed on the ground. In some cases, the poor maintenance of weather stations and extraordinary climatic events can damage the installed instruments with consequent data loss or the presence of sporadic outliers in the time series.

When ground weather stations are absent, reanalysis data can be a suitable solution to compensate for the missing weather variables. Reanalysis data are the result of a retrospective analysis of past historical data, developed using the most recent computational resources and a recent version of numerical weather prediction (NWP) models. In the last two decades, several authors have investigated the potential of the reanalysis data to compute E_{To} or to fill gaps in the temporal series of climate data [7–9]. As an example, Negm et al. [7] stated that the climate variables acquired from the NASA-POWER reanalysis database, are a suitable data source to assess E_{To} in areas characterized by a complex morphology like Sicily.

The last generation of global reanalysis databases is represented by the ERA5 and ERA5-Land (ERA5-L) database, released in 2019 by the European Centre for Medium-Range Weather Forecasts (ECMWF) in the frame of the Copernicus Climate Change Service. A detailed description of both databases can be found in Vanella et al. [9]. Recently, Muñoz-Sabater et al. [10] published a review that shows the state of the art referred to the use of ERA5-L for land and environmental applications, evidencing the qualities of ERA5-L compared to those of ERA-Interim and ERA5. Despite several authors indicating that the ERA5-L is suitable for land and environmental applications, the performance of this database has not been evaluated when the climate variables are used to run agro-hydrological models to estimate actual crop evapotranspiration (ET_a).

The main objective of this paper was to assess the suitability of the ERA-5 Land reanalysis database to estimate actual evapotranspiration (ET_a) of an olive orchard (cv. “Nocellara del Belice”) located in the southwest of Sicily, Italy.

2 Materials and Methods

2.1 Description of the Experimental Layout

The study area (Fig. 1), located inside a larger irrigation district in the South-West of Sicily (Italy) at about 5 km from the town of Castelvetro, is characterized by a flat landscape and a rather homogeneous soil type. The main crops in the district are represented by olive (cv. “Nocellara del Belice”) (70%), vineyards (24%), and citrus (2.6%), being other horticultural (3.4%) crops limitedly present. The climate of the area is the Mediterranean, characterized by moderate rainfall during autumn and winter and quite high air temperatures and low precipitations in summer.

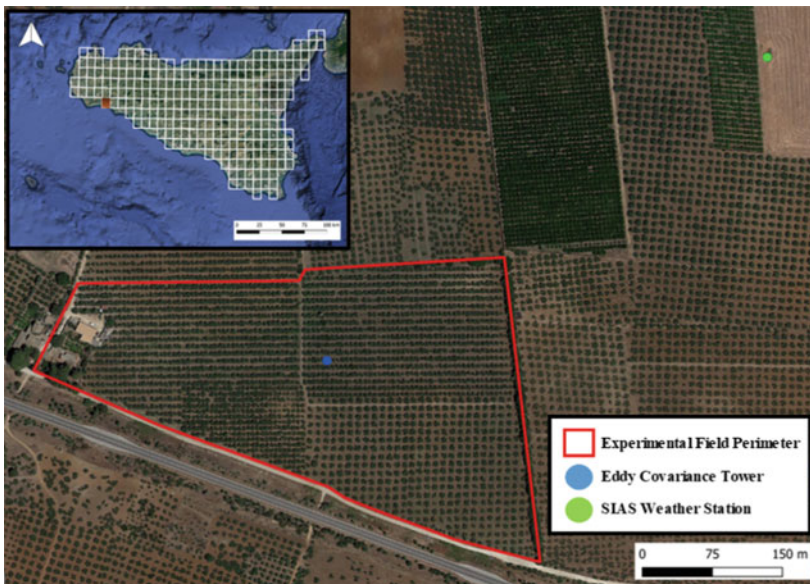


Fig. 1 Study area with the position of the flux tower (EC) and the SIAS weather station. The top left is represented Sicily island with the ERA5-Land (ERA5-L) grid; the cell containing the study site is marked in orange (Basemap: Google Hybrid (obtained through QuickMapServices QGIS plugin), Map data ©2015 Google)

The experimental field has an extension of about 13 ha; the plants, having a height of about 3.5 m, are spaced according to a regular grid of 5×8 m (density of 250 plants ha^{-1}). The analysis involved three irrigation seasons, from 2009 to 2011. Irrigation volumes, scheduled by the farmer according to the ordinary management of the area, resulted in quite diverse during the 3 years. In 2009, the seasonal irrigation dose was 80 mm distributed in three waterings, while in 2010 and 2011 were supplied respectively 33 mm in a single watering and 150 mm divided into five events. The irrigation depth was computed by considering a wetted fraction of the soil surface of 0.70 [11]. The soil textural class, according to the USDA classification, is classified as silty clay loam with average clay, silt, and sand contents of 24, 16, and 60%, respectively [11].

2.2 Climate and Micrometeorological Data

A weather station of the Sicilian Agro-meteorological Information Service (SIAS) is installed nearby the experimental field. This weather station provides hourly data of air temperature, T [$^{\circ}\text{C}$], relative air humidity, RH [%], wind speed, W_s [m s^{-1}] and direction [$^{\circ}$] measured at 2 m above the ground, global solar radiation, R_s [W m^{-2}] and precipitation height, P [mm]. An Eddy Covariance (EC) tower is also installed to acquire the main components of the surface energy balance. More details regarding the equipment of the EC tower are reported in Cammalleri et al. [11].

The raw data acquired by the EC tower were processed by using the processing software developed by Manca [12], which allowed the heat fluxes estimation with a 30 min time step. Finally, the ET_a fluxes data, retrieved from the latent heat fluxes (LE), were aggregated at a daily time scale. The quality of surface energy balance closure was evaluated based on the Closure Ratio (CR) suggested by Prueger et al. [13] only for the subset of hourly data characterized by $R_n \geq 100 \text{ W m}^{-2}$.

An ERA5-L database of hourly data of air temperature, T [$^{\circ}\text{C}$], global solar radiation, R_s [W m^{-2}], dew-point temperature, T_{dew} [$^{\circ}\text{C}$], and wind speed measured at 10 m above the ground, W_{s10} [m s^{-1}], was also downloaded from the Copernicus climate change service portal (<https://cds.climate.copernicus.eu/cdsapp#!/home>).

Being the values of hourly relative air humidity, RH [%], not available in the ERA5-L reanalysis database, they were calculated based on actual vapour pressure e_a (T_{dew}) and saturated vapour pressure e_s (T) expressed as a function of the dew-point, T_{dew} , and actual air temperature, T , respectively [1].

Moreover, the ERA5-L hourly wind speed at 2 m above the ground, W_s [m s^{-1}], was calculated from the ERA5-L wind speed at 10 m, based on the assumption of a logarithmic wind profile [1]. Finally, all hourly climate data, from the SIAS weather station and ERA5-L, were aggregated at a daily time step.

Table 1 Values of the variables used to run the FAO-56 model simulations

Model variables	Units	Value	Data source
SWC_{fc}	$[cm^3/cm^3]$	0.32	Cammalleri et al. (2013)
SWC_{wp}	$[cm^3/cm^3]$	0.08	Cammalleri et al. (2013)
SWC_0	$[cm^3/cm^3]$	0.32	Fixed
SWC^*	$[cm^3/cm^3]$	0.18	Allen et al. (1998)
Z_r	[m]	0.80	Fixed
K_c	[-]	0.45	Rallo et al. (2021)

2.3 FAO-56 Model Parameterization

As suggested by Allen et al. [1], daily crop reference evapotranspiration, ET_0 , was evaluated by the PM equation and both the climate databases (SIAS and ERA5-L).

Based on the single crop coefficient approach [1] the daily ET_a values were obtained by multiplying ET_0 by the crop coefficient, K_c , and the water stress coefficient, K_s . The first coefficient accounts for the differences between the bio-physical characteristics of the reference crop (canopy properties, ground cover, aerodynamic resistance) and the specific crop. On the other hand, the second depends on the soil water content. The model FAO-56 was implemented through a specific Matlab script. Table 1 summarized the values of the data input used to run the simulations and the relative data source.

2.4 Statistical Analysis for Model Validation

The model performance was assessed based on the following goodness-of-fit indicators used to evaluate the matching between measured and estimated actual evapotranspiration: i) Root Mean Square Error (RMSE) whose target value is zero when there are no differences between simulated and observed values; ii) Mean Bias Error (MBE), whose target value is zero; a positive value indicates that simulated values are overestimated, while a negative value indicates the model underestimation [14]; iii) percent bias (PBIAS), whose target value is zero; positive values are associated with the model underestimation, while negative values indicate the model overestimation; iv) coefficient of determination (R^2 , dimensionless) whose unitary target indicates that the variance of the observed values is explained by the model [15] and v) regression coefficient (b), whose target value is one, representing the angular coefficient of the regression line between simulated and observed variables forced through the origin.

3 Results and Discussion

For the period of observation (2009 to 2011) Fig. 2a,b shows the scatterplots between daily precipitation, P , and crop reference evapotranspiration, ET_o obtained by considering the reanalysis database and ground measurements. The colored bar indicates the day of the year (DOY).

As can be observed, the angular coefficient (b) of the straight line referred to as the daily precipitation depth, equal to 0.57, indicates an average underestimation of the measured values. Other authors [16] indicated for Sicily an underestimation of about 25%, while similar results were obtained by Tarek et al. [17] in North America. When considering the three irrigation seasons (from June to September), the cumulative rainfall reported by ERA5-L resulted in 48, 85, and 25 mm, while the corresponding SIAS, resulted in 108, 118, and 9 mm, respectively. However, in both databases, the occurrence of rainfall was generally concentrated in September.

Crop reference evapotranspiration, calculated by the PM equation with reanalysis climate variables estimated fairly well the corresponding obtained with the SIAS database, with a slope of regression line passing through the origin equal to 0.98.

Similar performances of the reanalysis database to evaluate crop reference evapotranspiration based on the PM equation were obtained in other sites of Sicily [7, 9, 18]. These results support the assumption that for Sicily the ERA5-L reanalysis database of weather variables can be considered a good surrogate of ground data. The database of actual crop evapotranspiration ET_a measurement, used in this work was previously processed by Cammalleri et al. [11] who obtained, for the years 2009 and 2010, values of CR equal to 0.90 and 0.92 respectively. For 2011, the CR value resulted equal to 1.02 [19]. Even other authors considered acceptable the values of CR ranging between 0.80 and 0.90 obtained in three different orchards [20], or equal to 1.08 and 1.03, as evaluated by Er-Raki et al. [21] in two citrus orchards located in south Morocco, characterized by a semi-arid Mediterranean climate.

The temporal dynamics of measured daily actual evapotranspiration (red dots) and daily precipitation (blue bars) are shown in Fig. 3. The gaps in the time series of

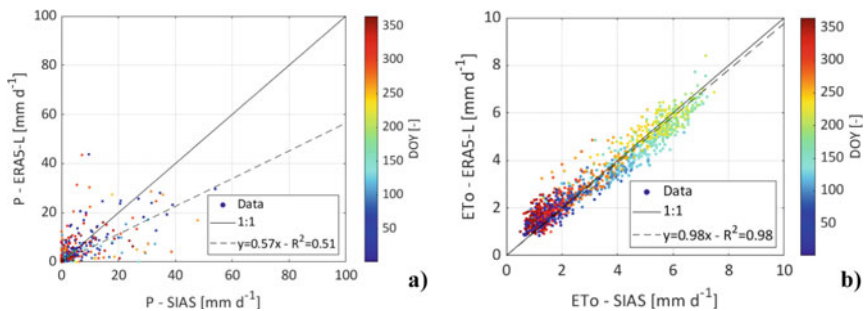


Fig. 2 Comparison between daily precipitation (a), P , and crop reference evapotranspiration (b), ET_o obtained from the reanalysis database and ground measurements

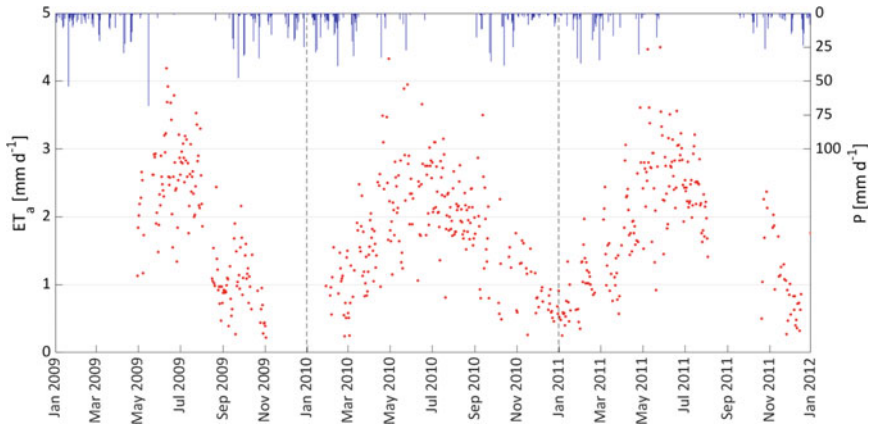


Fig. 3 Temporal dynamics of actual crop evapotranspiration (red dots), ET_a , and precipitation (blue bars), P during the three years of observation

ET_a are generally due to malfunctions of the instruments and/or sporadic faults of the battery. The missing values are generally scattered during the three years, even if there is a lack of data from November 2009 to March 2010 and from August to November 2011. Moreover, the values of ET_a recorded during the 92 days in which rainfall height was equal to or higher than 2.5 mm were excluded from the following analysis. A total of 573 ET_a measurements resulted available out of 1095 days of observations (52.3%).

The temporal dynamic of daily actual evapotranspiration follows a seasonal pattern, with maximum values registered during summer and minimum during winter.

During the three years, the patterns of ET_a resulted quite similar, with a maximum slightly higher than 4.0 mm d^{-1} and a minimum lower than 0.5 mm d^{-1} . Sporadic values, higher than 3.5 mm d^{-1} , resulted in days immediately after the rain events.

As an example, Fig. 4 shows the result of the FAO-56 model simulation for irrigation season 2009 (from June 1 to September 30). The upper graph illustrates the comparison between measured ET_{a_meas} (red dots) and simulated ET_{a_sim} (dashed line) when the model was run based on the SIAS weather data. On the other hand, the lower graph shows the results of similar simulations in which ERA5-L weather data replaced the corresponding measured. As can be observed, in both cases, the values of estimated actual evapotranspiration followed the dynamic of the measured values. For the three examined years (2009–2011) Table 2 summarizes the values of the statistical indicators used to assess the model performance.

Based on the statistical indicators, when using the weather variables measured on the ground, the estimated values of actual crop evapotranspiration resulted characterized by RMSE ranging between 0.40 and 0.69 mm d^{-1} , with a slope of the regression line passing through the origin, b , always higher than 0.87 . On the other hand, when the climate data are replaced by the ERA5-L variables, despite the differences observed in the seasonal rainfall, which occurrence was generally concentrated

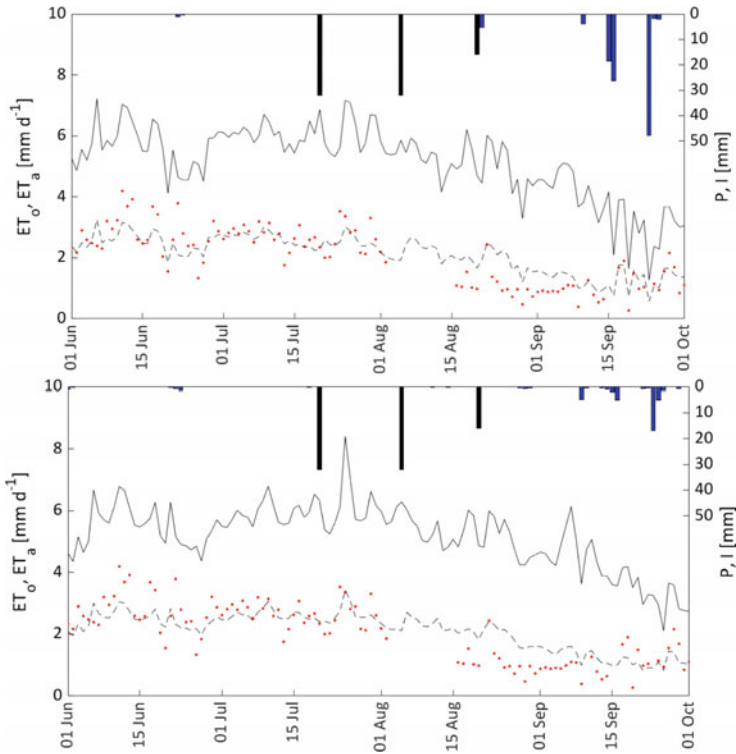


Fig. 4 Temporal dynamics of crop reference evapotranspiration, ET_o , as well as simulated (black line) and measured (red dots) actual evapotranspiration, ET_a . In the secondary axes are reported the precipitation (blue bars), P , and the amount of irrigation (black bars), I

Table 2 Results of the statistical analysis to assess the FAO-56 model performance

	<i>RMSE</i>	<i>MBE</i>	<i>PBIAS</i>	R^2	<i>b</i>
	[mm d ⁻¹]	[mm d ⁻¹]	[%]	[–]	[–]
SIAS					
2009	0.53	0.10	–4.83	0.74	0.96
2010	0.69	–0.24	11.41	0.23	0.87
2011	0.40	0.07	–2.98	0.35	1.01
ERA5-L					
2009	0.57	0.07	–3.29	0.67	0.95
2010	0.65	–0.13	6.13	0.18	0.91
2011	0.46	–0.01	0.21	0.16	0.97

at the end of the simulations, the results were still fairly good, with RMSE in the range 0.46–0.65 mm d⁻¹ and b values variable between 0.91 and 0.97.

The carried analysis confirmed the suitability of the FAO-56 model to estimate daily actual evapotranspiration, as well as the potential of using, as a valid alternative, the reanalysis data in the absence of ground measurements of weather variables.

4 Conclusion

In this study, the potential of using weather variables retrieved from the ERA5-L reanalysis database to assess actual evapotranspiration was investigated in an olive orchard during three years of observation from 2009 to 2011. The comparison between daily precipitation and crop reference evapotranspiration retrieved from the reanalysis database and the corresponding obtained from the SIAS weather station installed nearby the study area was initially carried out. When referring to the entire period, the comparison showed a certain underestimation of daily precipitation with a slope of the regression line passing through the origin, b, equal to 0.57. However, limiting the analysis to only the irrigation seasons, it was observed that the main differences in the rainfall height generally occurred in September, being the other months quite dry. On the other hand, the comparison between ETo calculated by measured weather data and the corresponding obtained from the reanalysis database was characterized by a fairly good agreement, with both b and R² equal to 0.98.

The FAO-56 model was then implemented for the three irrigation seasons to estimate actual daily evapotranspiration, by considering both the ground and the reanalysis databases. When using the ground measurements, the RMSE values associated with actual crop evapotranspiration ranged between 0.40 to 0.69 mm d⁻¹, whereas assuming the reanalysis data, the corresponding values ranged from 0.46 to 0.65 mm d⁻¹. In both cases, despite the differences observed in the rainfall heights, the model was characterized by fairly good performances, confirming that for the examined area, the use of the ERA5-L reanalysis database, in the absence of measured weather data, can be considered a valid alternative to estimate daily actual crop evapotranspiration for irrigation scheduling purposes.

References

1. Allen, R., Pereira, L., Raes, D., Smith, M.: Crop evapotranspiration - Guidelines for computing crop water requirements. FAO Irrigation and drainage paper No. 56. Food and Agriculture Organization of the United Nations. Rome, Italy (1998). ISBN: 92-5-104219-5
2. Bastiaanssen, W.G.M., Menenti, M., Feddes, R.A., Holtslag, A.A.M.: A remote sensing surface energy balance algorithm for land (SEBAL). 1. Formulation. *J Hydrol.* **212–213**, 198–212 (1998). [https://doi.org/10.1016/S0022-1694\(98\)00253-4](https://doi.org/10.1016/S0022-1694(98)00253-4).

3. Paredes, P., de Melo-Abreu, J.P., Alves, I., Pereira, L.S.: Assessing the performance of the FAO AquaCrop model to estimate maize yields and water use under full and deficit irrigation with focus on model parameterization. *Agric. Water Manag.* **144** 81–97 (2014)
4. Bhattarai, N., Shaw, S.B., Quackenbush, L.J., Im, J., Niraula, R.: Evaluating five remote sensing based single-source surface energy balance models for estimating daily evapotranspiration in a humid subtropical climate. *Int. J. Appl. Earth Obs. Geoinf.* **49**, 75–86 (2016). <https://doi.org/10.1016/j.jag.2016.01.010>
5. Suleiman, A.A., Tojo Soler, C.M., Hoogenboom, G.: Evaluation of FAO-56 crop coefficient procedures for deficit irrigation management of cotton in a humid climate. *Agric. Water Manag.* **91**, 33–42 (2007). <https://doi.org/10.1016/j.agwat.2007.03.006>
6. Djaman, K., et al.: Evaluation of sixteen reference evapotranspiration methods under sahelian conditions in the Senegal River Valley. *J. Hydrol. Reg. Stud.* **3**, 139–159 (2015). <https://doi.org/10.1016/j.ejrh.2015.02.002>
7. Negm, A., Jabro, J., Provenzano, G.: Assessing the suitability of American National Aeronautics and Space Administration (NASA) agro-climatology archive to predict daily meteorological variables and reference evapotranspiration in Sicily. *Italy. Agric. For. Meteorol.* **244–245**, 111–121 (2017). <https://doi.org/10.1016/j.agrformet.2017.05.022>
8. de Araújo, C.S.P., e Silva, I.A.C., Ippolito, M., de Almeida, C.D.G.C.: Evaluation of air temperature estimated by ERA5-Land reanalysis using surface data in Pernambuco, Brazil. *Environ. Monit. Assess.* **194** (2022). <https://doi.org/10.1007/s10661-022-10047-2>
9. Vanella, D., et al.: Comparing the use of ERA5 reanalysis dataset and ground-based agrometeorological data under different climates and topography in Italy. *J. Hydrol. Reg. Stud.* **42**, 101182 (2022). <https://doi.org/10.1016/j.ejrh.2022.101182>
10. Muñoz-Sabater, J., et al.: ERA5-Land: a state-of-the-art global reanalysis dataset for land applications. *Earth Syst. Sci. Data* **13**, 4349–4383 (2021). <https://doi.org/10.5194/essd-13-4349-2021>
11. Cammalleri, C., Rallo, G., Agnese, C., Ciraolo, G., Minacapilli, M., Provenzano, G.: Combined use of eddy covariance and sap flow techniques for partition of et fluxes and water stress assessment in an irrigated olive orchard. *Agric. Water Manag.* **120**, 89–97 (2013). <https://doi.org/10.1016/j.agwat.2012.10.003>
12. Manca, G.: Analisi dei flussi di carbonio di una cronosequenza di cerro (*Quercus cerris* L.) dell'Italia centrale attraverso la tecnica della correlazione turbolenta Ph.D. Dissertation Thesis. Università degli Studi della Tuscia, Viterbo, 225 pp (2003). (in Italian)
13. Prueger, J.H., et al.: Tower and Aircraft Eddy covariance measurements of water vapor, energy, and carbon dioxide fluxes during SMACEX. *J. Hydrometeorol.* **6**, 954–960 (2005). <https://doi.org/10.1175/JHM457.1>
14. Kennedy, J.B., Neville, A.M.: *Basic Statistical Methods for Engineers and Scientists*, 3rd edn., Harper and Row Publisher, New York (1986). ISBN :978-0060436339
15. Eisenhauer, J.G.: Regression through the origin. *Teach Stat.* **25**, 76–80 (2003). <https://doi.org/10.1111/1467-9639.00136>
16. Longo-Minnolo, G., Vanella, D., Consoli, S., Pappalardo, S., Ramírez-Cuesta, J.M.: Assessing the use of ERA5-Land reanalysis and spatial interpolation methods for retrieving precipitation estimates at basin scale. *Atmos Res.* **271** (2022). <https://doi.org/10.1016/j.atmosres.2022.106131>
17. Tarek, M., Brissette, F.P., Arseneault, R.: Evaluation of the ERA5 reanalysis as a potential reference dataset for hydrological modelling over North America. *Hydrol. Earth Syst. Sci.* **24**, 2527–2544 (2020). <https://doi.org/10.5194/hess-24-2527-2020>
18. Pelosi, A., Chirico, G.B.: Regional assessment of daily reference evapotranspiration: can ground observations be replaced by blending ERA5-Land meteorological reanalysis and CM-SAF satellite-based radiation data? *Agric. Water Manag.* **258** (2021). <https://doi.org/10.1016/j.agwat.2021.107169>
19. Autovino, D., Minacapilli, M., Provenzano, G.: Modelling bulk surface resistance by MODIS data and assessment of MOD16A2 evapotranspiration product in an irrigation district of Southern Italy. *Agric. Water Manag.* **167**, 86–94 (2016). <https://doi.org/10.1016/j.agwat.2016.01.006>

20. Kustas, W.P., Zhan, X., Jackson, T.J.: Mapping surface energy flux partitioning at large scales with optical and microwave remote sensing data from Washita '92. *Water Resour. Res.* **35**, 265–277 (1999). <https://doi.org/10.1029/98WR02094>
21. Er-Raki, S., Chehbouni, A., Guemouria, N., Ezzahar, J., Khabba, S., Boulet, G., Hanich, L.: Citrus orchard evapotranspiration: comparison between eddy covariance measurements and the FAO-56 approach estimates. *Plant Biosyst.* **143**, 201–208 (2009). <https://doi.org/10.1080/11263500802709897>

Field Study on Multifunctional Irrigation of Vineyards



C. Gandolfi , S. Cazzaniga , D. Ferrari , D. Masseroni ,
and B. Ortuani 

Abstract In recent decades, worldwide wine-growing regions have been increasingly exposed to the effects of climate change, such as summer heat waves and late spring frosts, as well as long period of droughts during the growing season. In this context, it is necessary to develop innovative adaptation strategies: particularly, this study explored a multifunctional approach in vineyard irrigation, to provide hydric nutrition when needed and to counter the negative effects of excessively high summer temperatures and of late spring frosts. The experimental activities were conducted during the 2020 and 2021 agricultural seasons, in a Chardonnay vineyard located in Cavriana, in the area of Garda Colli Mantovani DOC (Italy). An irrigation system equipped with drippers and mini-sprinklers (the latter to protect from both spring frosts and summer high temperature events) was set up. In particular, eight plots were designed to compare four different irrigation strategies: i) automated drip irrigation; ii) automated drip and sprinkler irrigation; iii) traditional drip irrigation, iv) no irrigation. Results obtained during the two seasons highlight the potential of the automated, multifunctional irrigation in protecting vines from thermal stress and in increasing water use efficiency.

Keywords Multifunctional irrigation · Vineyard · Heat stress · Spring frost · Hydric nutrition

1 Introduction

Due to climate change, grapevine is increasingly exposed to both thermal stress and water stress, that affect the physiological activity and the phenological stages of vine. In particular, high temperature can accelerate ripening, involving in excessive sugar accumulation and high alcohol in the wine, reducing the total acidity due to a faster degradation of organic acids [5]. Beside the technological ripening, the temperature

C. Gandolfi (✉) · S. Cazzaniga · D. Ferrari · D. Masseroni · B. Ortuani
Department of Agricultural and Environmental Sciences, University of Milan, 20133 Milan, Italy
e-mail: claudio.gandolfi@unimi.it

© The Author(s), under exclusive license to Springer Nature Switzerland AG 2023
V. Ferro et al. (eds.), *AIIA 2022: Biosystems Engineering Towards the Green Deal*,
Lecture Notes in Civil Engineering 337,
https://doi.org/10.1007/978-3-031-30329-6_12

117

increase also affects the synthesis and the accumulation of polyphenols, vitamins, and aromatic compounds in berries [9]. The effect of the warming conditions is aggravated by the increasing exposure of vines to water stress, due to decreasing trend of rainfall during spring and summer. Depending on the level and the phenological stage, water stress reduces the yield and affects the quality of grapes [11]. The warming trend not only affects grape ripening, determining an impact on grape and wine quality, but also induces an anticipation in the sprouting phases of the vine, increasing the risks caused by late spring frosts. Low temperature during sprouting can involve to the loss of buds and shoots [10], reducing the production of grape.

Different adaptation strategies could be adopted in viticulture to counter the emerging problems related to climate change, including both long-term measures (e.g., changes in vineyard locations) and short-term ones (e.g., use of tolerant varieties, of shading systems, of delayed pruning). Smart irrigation strategies are also an option and, in this study, we explored a multifunctional approach to vineyard irrigation, capable to counter the negative effects of excessively high summer temperatures and of late spring frosts, as well to provide hydric nutrition when needed. The capacity of evaporating water to achieve the canopy and berry cooling has been well studied from 1970s [1]. The first studies considered overhead cooling sprinkler systems, that mainly water the outer canopy layer and only partially the bunch zone. More recently micro-sprinkler cooling system inside the canopy at the bunch level were also applied [4]. Over-vine sprinklers have been widely applied also for protection from frosts, allowing to form a layer of ice over vines that keeps the temperature slightly above the critical values and preventing damages of buds and shoots [10].

As climate change negatively affects grape growing, this study explores the effectiveness of multifunctional irrigation systems in facing the extreme weather events. Particularly, the use of mini-sprinklers was explored to supply irrigation facing both late spring frost and summer high temperature events. Moreover, different setups for sprinkler irrigation system (over-vine vs under-vine) were studied, to assess the optimal solution in term of efficacy and efficiency of water use. Finally, this study assesses also the irrigation management protocols (i.e. rules for irrigation scheduling, assessment of water amounts, and, in case of cooling irrigation, distribution over time of the water) as tools to improve the reliability of the irrigation system to counter the critical conditions as water stress, heat stress and frost, at the same time limiting the water consumptions.

2 Methods

2.1 *Experimental Site*

This study was conducted during the 2020 and 2021 agricultural seasons, in a commercial vineyard located in Cavriana, south Lake Garda, in northern Italy, at 135 m a.s.l. in the viticultural area of Garda Colli Mantovani DOC. The grapevine

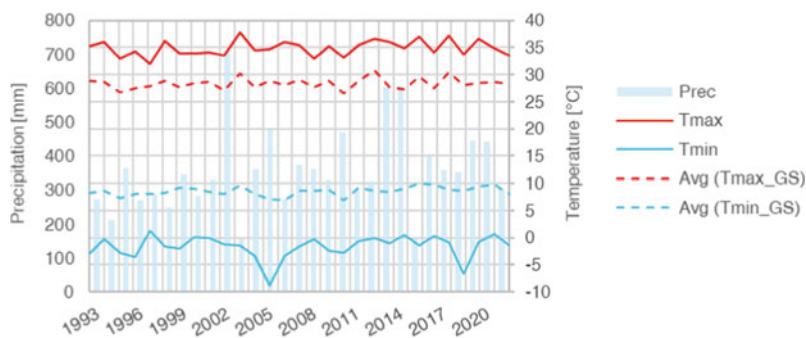


Fig. 1 Temperature and precipitation extracted from the ERA5 dataset, evaluated for the vine growing season, from 1993 to 2021: minimum and maximum daily temperature (light blue and red solid lines), average of the minimum and maximum daily temperature (light blue and red dashed lines) and cumulated precipitation (light blue bars)

variety is Chardonnay, grafted on rootstock 420A; the vines are trained using Guyot system, with distance on the row of 0.8 m and distance between rows of 2.5 m. Soil between rows is grass-covered with periodic mowing.

According to the ERA5 dataset (developed by the European Centre for Medium-Range Weather Forecasts, based on the fifth generation of European ReAnalysis, considering a combination of forecast model data and worldwide observations with 9 km horizontal resolution), the precipitation in the 2020 growing season had a 23% higher precipitation with respect to the average value in the period 1993–2021, while the 2021 seasons was 15% drier (Fig. 1). The maximum temperature in July and August 2020, and in June 2021 were respectively 1.1, 1.6 and 0.5 °C hotter than the average value in the period 1993–2021 of the maximum temperature in July, August, and June. Moreover, the minimum temperature in April 2021 was 2.5 °C cooler than the average value in the period 1993–2021 of the April minimum temperature.

2.2 Irrigation System and Experimental Design

An irrigation system was realised within the experimental vineyard to separately manage the plots with four different irrigation strategies. As the soil-crop system conditions in the plots should be affected only by the different irrigation managements, the plots were located where no significant differences in soil properties (monitored through a geophysical survey measuring soil electrical conductivity) occurred. In particular eight plots (two repetitions for each irrigation strategy) were designed (Fig. 2) considering: i) automated drip irrigation (DI), providing water supply by drippers, mainly for water plant nutrition and secondarily to protect the vine from excessively high summer temperatures; ii) automated drip and sprinkler irrigation (DSI), providing water supply by drippers for water plant nutrition and by sprinklers

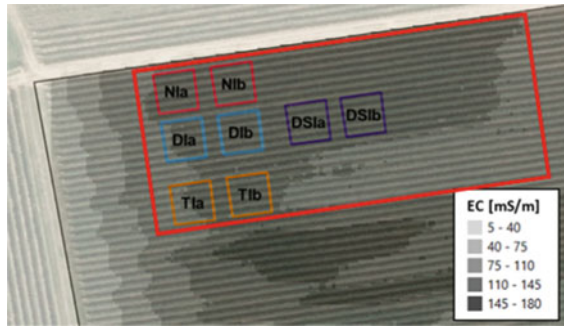


Fig. 2 The experimental plots located within an area (red box) where soil electrical conductivity (EC) referring to soil depth 0–80 cm varies from 75 to 110 mS/m: DI, drip irrigation; DSI, drip and sprinkler irrigation; TI, traditional irrigation; NI, no irrigation. In transparency the orthophoto with the vineyard rows

to protect the vine from temperature-related stresses, due to late spring frosts or excessively high summer temperatures; iii) traditional drip irrigation (TI), operated by the farmer with drippers, based on farmer's usual practices; iv) no irrigation (NI), providing no water supply at all and used as control plot.

Each plot is a square of 11.5×11.5 m over 5 rows, with about 14 vines on each row.

DI, DSI and TI plots were equipped with a drip irrigation system, with 1 m distance between drippers and irrigation rate of 1.6 mm/h. Moreover, the DSI plots were equipped with an additional irrigation line, to supply a sprinkler irrigation system. Sprinklers with drop size suitable for both cooling and late spring frost irrigation, were chosen. In the latter case, the drop size has to be sufficiently big in order to reduce the evaporative process, thus maintaining a thin ice layer around the buds at temperature about 0°C [3]. In the case of cooling irrigation during heat events, the drop size has to be small enough to easily evaporate, in order to reduce air and grape temperature [2].

In 2020, an over-vine 360° sprayer system was set up in both DSI plots, installing sprinklers at 4 m distance with an irrigation rate of 4 mm/h. This solution requested a lot of manpower for maintenance, therefore in 2021 two different types of alternative emitters were set up. Over-vine sprinklers, with pop-up nozzles, were installed in the DSIa plot, at 4 m distance and with an irrigation rate of 15 mm/h. In the DSIB plot, under-vine 180° micro-sprayers were installed at 2 m distance, directly nested in the dripline, with an irrigation rate of 10.6 mm/h. Each sprinkler is characterized by a water stream directed upward and localized at bunch level.

A soil-air-plant monitoring station was set up in DIa, T1b and NIa plots and in both the DSI plots, to check the different performances of the pop-up over-vine and under-vine sprinkler systems. Moreover, an agro-meteorological station was installed just outside the field, nearby the vine rows of the experimental plots.

Irrigation Management Protocols. Drip irrigation (in both DI and DSI plots) was managed to primarily optimize the water supply according to the vine phenological stage, by activating irrigation only when SWC is below a water stress threshold; secondarily, to contrast the effects of summer high temperature events, by providing water during the previous night, in order to increase the SWC easily available for plants [12].

The water stress threshold was assessed considering the hydrological soil properties measured on soil samples collected at 30 and 60 cm depths, in DI and DSI plots, as well as the vine phenological stages [6], considering a greater susceptibility to water stress during the flowering and véraison stages rather than during the ripening stage. When SWC was below the threshold value, the water amount supplied by irrigation increased the SWC up to the field capacity. Nightly drip irrigation was activated if temperature higher than 35 °C and no precipitation were forecasted for the following day. In order to reduce water consumption, irrigation was applied only when the SWC condition was below a proper threshold.

Sprinkler irrigation in DSI plots was managed according to two different protocols. In case of spring frost, irrigation was activated when the air wet bulb temperature was below 1 °C (a cautionary value to avoid water freezing into pipes). The water was continuously supplied and the irrigation was stopped when the air temperature was higher than 2 °C [8], with an increase of 1 °C at least in the previous hour [3]. In case of extreme high temperature in summer, sprinkler irrigation was activated when the air temperature rose above a threshold temperature for heat stress insurgence. Severe stress may occur when the temperature is higher than 35 °C [7]; in this field study, lower threshold values were considered (33 °C for 2020 and 34 °C for 2021) to reduce water consumption. Moreover, continuous and pulsed water applications, respectively in 2020 and 2021 seasons, were tested and compared. Particularly, in 2020 the sprinklers were continuously activated for 1 h when the air temperature was higher than 33 °C; in 2021, when the air temperature of the lower canopy was higher than 34 °C, 1-min sprinkler activation was followed by 2-min break.

3 Results

3.1 Drip Irrigation

For both the seasons, the adopted protocol allowed to significantly reduce the water application with respect to the water amounts distributed in TI plots (59 mm in 2020 and 86 mm in 2021). In DI plots the water depth applied was 14 mm in 2020 while in 2021 irrigation was not activated (Fig. 3).

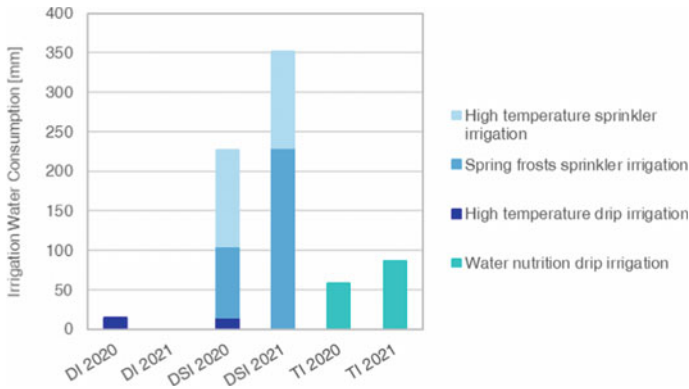


Fig. 3 Yearly irrigation water application [mm] for DI, DSI and TI plots in 2020 and 2021

3.2 Spring Frost Sprinkler Irrigation

Sprinkler irrigation was activated two times both in 2020 and 2021, with water application of 91 mm in 2020 and 229 mm in 2021 (Fig. 3).

Figure 4a shows the effects of irrigation on the air temperature during the frost in the night of 25–26 March 2020. The irrigation was activated when the temperature measured in NIa plot was about 4 °C, while it was 3.5 °C in DSIB plot; this gap in temperature was kept until the temperature measured in NIa plot fell below 0 °C, when the temperature in DSIB plot was up to 1 °C higher than in NIa plot.

3.3 Evaporative Cooling Sprinkler Irrigation

Sprinkler irrigation was activated in 2020 for about 23 h distributed in 10 days from mid-July to end-August, with a total water application of 121 mm; in 2021 it was activated for 7.5 h distributed in 11 days from end-June to mid-August, with a total water application of 125 mm (Fig. 3).

The highest temperature in 2020 (36.7 °C) was reached on 1 August. Five 1-h sprinkler irrigation were provided, determining a decreasing trend in the lower-canopy air temperature (Fig. 4b), with values on average 3 °C lower than those ones measured in NIa plot.

In 2021, daily maximum temperature up to 36 °C were recorded on 15 August. Particularly, sprinkler irrigation was activated 76 times (Fig. 4c). During the first sparse activations, the cooling effect was comparable in DSIB plot and in DSIA plot. The lower-canopy temperature in DSIA and DSIB plots was on average respectively 3 and 1.5 °C lower than that in NIa plot. On the other hand, as irrigations became more frequent, the above-canopy irrigation in DSIA plot resulted in an increasing temperature gap from the temperature in NIa plot, with a more intense cooling effect

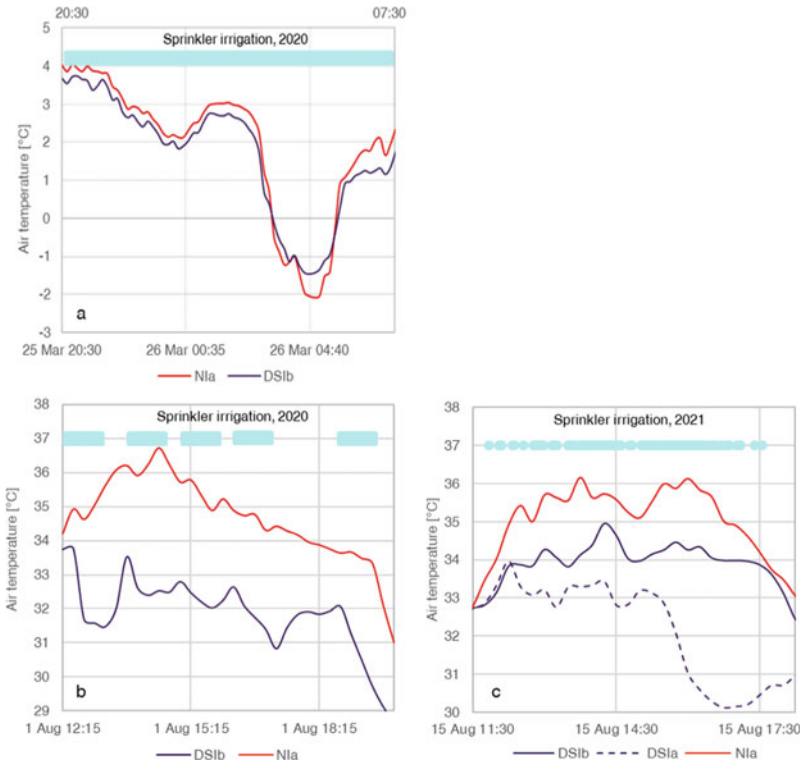


Fig. 4 Sprinkler irrigation, effect on air temperature in the lower canopy. **(a)** Spring frost: temperature recorded during the night of 25–26 March 2020, in DSib and Nia (red line) plots. The irrigation was continuously activated for 11 h, from 20:30 to 07:30. Summer heat events: **(b)** temperature recorded on 1 August 2020 in DSib and Nia plots. Five 1-h sprinkler irrigations were applied, at 12:15, 13:45, 15:00, 16:15, 18:45; **(c)** temperature recorded on 15 August 2021 in DSib, DSia and Nia plots. Seventy-six 1-min sprinkler irrigations were applied, from 11:51 to 17:34.

than in DSib. This behavior in DSia plot was probably due to the thermo-hygrometers wetting, because of the irrigation applied over-vine and with higher flowrate than that of the under-vine 180° micro-sprayers in DSib plot.

4 Conclusions

The study compared four irrigation strategies (traditional drip irrigation, automated drip irrigation, automated sprinkling, no irrigation) employed to protect the vineyards from both water stress and thermal stresses caused by late spring frosts and high temperature summer events. The results showed that irrigation application can

be considerably reduced, through an optimized management supported via automation by a monitoring system to assess the crop-soil water status. Moreover, harvesting measurements showed that this automated strategy allowed to decrease water application even for drip irrigation, without reducing the vine yield. Also the results relative to sprinkler irrigation showed the effectiveness of this strategy. Indeed, the vineyard was equipped with sprinklers suitable for both protection irrigation during late frosts and evaporative cooling irrigation during high temperature summer events. The sprinkler irrigation demonstrated to properly control the air temperature to create optimal conditions for buds, during late frosts, and for grapes, during the growing season. Moreover, harvesting measurements and physiological measurements during the growing season showed how sprinkler irrigation positively influenced grape production and quality.

Finally, the studied irrigation strategies seem to be effective innovative tools to support vineyard resilience to both water and thermal stresses due to climate change.

References

1. Aljibury, F.K., Brewer, R., Christensen, P., Kasimatis, A.N.: Grape response to cooling with sprinklers. *Am. J. Enol. Vitic.* **26**(4), 214–217 (1975)
2. Anconelli, S., Solimando, D., Letterio, T., Morandi, B.: Impianti climatizzanti soprachiuma contro le ondate di calore. *Rivista di frutticoltura e di ortofloricoltura* **82**(2), 40–45 (2018)
3. ARPAE Emilia Romagna: Nota tecnica di difesa attiva antibrina – dai risultati del progetto DISGELO (2004). <https://www.arpae.it/it/temi-ambientali/meteo/previsioni-meteo/previsioni-agrometeo/nota-tecnica-difesa-gelate>. Accessed 8 Jan 2021
4. Caravia, L., Pagay, V., Collins, C., Tyerman, S.D.: Application of sprinkler cooling within the bunch zone during ripening of Cabernet Sauvignon berries to reduce the impact of high temperature. *Aust. J. Grape Wine Res.* **23**(1), 48–57 (2017)
5. De Orduna, R.M.: Climate change associated effects on grape and wine quality and production. *Food Res. Int.* **43**(7), 1844–1855 (2010)
6. Deloire, A., Carbonneau, A., Wang, Z., Ojeda, H.: Vine and water: a short review. *OENO One* **38**(1), 1–13 (2004)
7. Greer, D.H., Weedon, M.M.: Does the hydrocooling of *Vitis vinifera* cv. Semillon vines protect the vegetative and reproductive growth processes and vine performance against high summer temperatures? *Funct. Plant Biol.* **41**(6), 620–633 (2014)
8. Jorgensen, G., Escalera, B.M., Wineman, D.R., Striegler, R.K., Zoldoske, D., Krauter, C.: Microsprayer Frost Protection in Vineyards. CATI Publication 960803 (1996)
9. Keller, M.: Managing grapevines to optimise fruit development in a challenging environment: a climate change primer for viticulturists. *Aust. J. Grape Wine Res.* **16**, 56–69 (2010)
10. Poling, E.B.: Spring cold injury to winegrapes and protection strategies and methods. *HortScience* **43**(6), 1652–1662 (2008)
11. Shellie, K., Cragin, J., Serpe, M.: Performance of alternative European wine grape cultivars in southwestern Idaho: cold hardiness, berry maturity, and yield. *HortTechnology* **24**(1), 138–147 (2014)
12. Webb, L., Watt, A., Hill, T., Whiting, J., Wigg, F., Dunn, G. et al.: Extreme heat: managing grapevine response. GWRDC and University of Melbourne (2009)

Productive Response of a Pear Orchard (*Pyrus Communis*, L.) to the Precision Irrigation Conducted Through a Decision Support System (DSS)



Fatma Hamouda, Àngela Puig-Sirera, Lorenzo Bonzi, Damiano Remorini, Giuseppe Provenzano, and Giovanni Rallo

Abstract In this study, a soil moisture-based wireless sensor network (SM-WSN) was transferred to support the reduction of irrigation water consumption. Our sensor was designed and validated in a commercial pear orchard during three growing seasons (2019–2021) in which the smart irrigation strategy was implemented and applied. Initially, the micro irrigation system was assessed based on its performance in terms of water distribution uniformity (DU), which was evaluated with field measurements of emitter flow rates. Then, a zoning analysis was carried out to divide the orchard into homogeneous areas according to the normalized difference vegetation index (NDVI) that was detected with unmanned aerial vehicle (UAV) and GIS tools. The effect of DU on the vigor of the trees has been identified assuming that the zoning outcome was only associated with the soil spatial variability. Moreover, unlike the ordinary irrigation scheduling applied in the farm, the smart system allowed maintaining the soil water content within a pre-defined optimal range, in which the upper and lower limits corresponded respectively to the soil field capacity and the threshold below which water stress occurs. In this way, the smart irrigation management saved up to 50% of the total water supplied with the ordinary scheduling during the three growing seasons. Moreover, the fruits sizes were in line with the standard required by the farmer. Consequently, the adoption of the new technology, which aims at identifying the most appropriate irrigation management, has the potential to generate positive economic returns and to reduce the environmental impacts.

Keywords Normalized difference vegetation index (NDVI) · Soil moisture-based wireless sensor network (SM-WSN) · Unmanned aerial vehicle (UAV) · Water distribution uniformity (DU)

F. Hamouda (✉) · À. Puig-Sirera · L. Bonzi · D. Remorini · G. Rallo
Department of Agriculture, Food and Environment (DAFE), Agro Hydrological Sensing and Modelling Lab, University of Pisa, Via del Borghetto, 80 56124 Pisa, Italy
e-mail: f.hamouda@studenti.unipi.it

G. Provenzano
Dipartimento Scienze Agrarie, Alimentari E Forestali, Università Degli Studi Di Palermo, Viale Delle Scienze 12 Blg. 4, 90128 Palermo, Italy

1 Introduction

Increasing Water Use Efficiency (WUE) has been identified as the key factor for the improvement of agricultural water resource management [1, 2]. Moreover, by implementing efficient irrigation techniques and protocols such as drip irrigation with specific water saving strategies, it could be possible to control water inputs (timing and volumes) and reduce water losses by 50% [3]. In this context, technologies concerning integrated telecommunication systems together with sensor technology which represent an innovative tool to support precision agriculture [4], have enabled the development of efficient decision support systems (DSS). The DSS aims to provide methodologies to facilitate business decision making, it combines human evaluation and optimization technologies based on information processing.

The main objectives of this paper were to design, calibrate and validate the Soil Moisture-Wireless sensor network (SM-WSN) for an expert irrigation management in pear (*Pyrus* spp.) orchards; and to transfer the DSS to the farmer to achieve a better productive performance.

After carrying out the different methodological steps to install the DSS, this work presents the results on the hydraulic, hydrological and agronomic performance of three pear orchards cultivated with medium- to high-density planting systems, drip-irrigated and equipped with a DSS based on feedback irrigation control.

2 Materials and Methods

2.1 Site Description and Evaluation of the Irrigation Plant

The technology transfer of the DSS was carried out at the Illuminati Frutta Consortium Company during three experimental years 2019–2021. The farm is in the Val di Chiana Aretina (Arezzo, Italy), covering 350 ha with cultivated varieties of apples, pears, peaches, and plums crops. The experimental field (727244 m E; 4807237 m N: 250 m.a.s.l) was 7 ha cultivated with pears of the Carmen, Williams and Conference varieties. The three orchards are managed with a bibaum training system and with the trees spaced 3.31×1 m inter-row and intra-row respectively.

The drip irrigation system is specific for each variety and the water sources were the Montedoglio dam and the company well (artesian). The farm's ordinary irrigation protocol consists in an irrigation frequency of 2–3 days with a duration of about 6 hours. The field irrigation uniformity was evaluated using the low quarter distribution uniformity coefficient, DU_{lq} , which is quantified based on field measurements of 200 emitter flows. The DU_{lq} rating scale proposed by the ASAE standards (1999) [5] was used for the qualitative evaluation of the irrigation plant. The operating hydraulic pressure was imposed equal to that usually settled by the farmer, which were 2.4 bar for the Conference, 2.0 bar for the Williams and 3.0 bar for the Carmen.

2.2 *Soil Moisture Sensors Calibration and Implementation in WSN*

The simplified protocol [6] was followed to carry out the soil-specific calibration of the drill & drop FDR sensor [7]. The protocol uses undisturbed soil monoliths taken in two sites where different extreme vigor values were observed. Two undisturbed soil monoliths were collected for each layer of the soil 0–0.2 and 0.3–0.50 m on each site. Operatively, the procedure consists of acquiring at the same time the two target variables for the calibration analysis: the soil water content (SWC), measured by a weighing lysimeter, and the Scaled Frequency (SF), detected by the FDR sensor.

The design of the WSN followed a zoning process based on the spatial variability of the Normalized Difference Vegetation Index (NDVI) quantified with remote sensing techniques. The remote sensing service was provided by the Dronebee company (Flor- ence, Italy), using a Zephyr EXOS hexacopter with a Parrot Sequoia multispectral cam- era. The NDVI images were analyzed and mapped using Quantum GIS (QGIS) suite. The AgriNET Decision Support System (DSS) was transferred to the farmer, which implements a WSN of multi-level FDR sensors [7].

The DSS acquires soil moisture every 0.1 m depth up to 0.6 m. Each node communi- cates with the transceiver through which sends the data to an internet gateway and, therefore, into a MYSQL database managed by AgriNET platform (Tuctronics). Through any internet connection, it will be possible to interrogate the different nodes by operating on the smartphone AgriNet application (www.agrinet.us).

The irrigation thresholds, which are needed for a feedback control irrigation, were ob- tained using the approach proposed by Polak et al. (2001) [8] and Thompson et al. (2007) [9]. This approach allowed to derive the soil field capacity (SWC_{fc}) and the critical soil water content (SWC^*), respectively implemented to settled upper and the lower irrigation thresholds.

2.3 *Crop Ecophysiological and Fruit Yield and Quality Measurements*

The midday stem water potential (MSWP) was measured with the Scholander chamber following the Turner and Jarvis protocol (1982).

The amount of fruit produced on the harvest date was determined for each pear tree using the bin units, equal to 240 kg of fruit. The historical production data for the period 2015–2018 was used to evaluate the performance of the new irrigation management system transferred to the farm.

The irrigation efficiency (IWUE) was determined as the ratio of total production (kg) to the irrigation plus rainfall volume (m^3).

The biometric fruit analysis consisted in fruit diameter measurements using a capiler rule. The diameters were measured in the wider part of the pear, in two perpendicular directions.

Three control plots of each variety were selected that were similar in age, canopy management and irrigated with the ordinary farm protocol.

3 Results and Discussion

3.1 Audit of the Micro-Irrigation Plants and Setting of the WSN

The distribution uniformity of the irrigation plant was exceptional in Conference and Williams irrigation plant ($DU_{Iq} > 85\%$), while was very good ($70\% > DU_{Iq} > 74\%$) in Carmen.

The three irrigation plants showed a statistically significant differences of the emitter flow rates ($p\text{-value} < 0.0001$). The highest average flow rate was delivered by the Conference plant, followed by the Williams and Carmen irrigation plant. Figure 1 shows the spatial distribution of emitter flow rates within each sector. From the pattern analysis, it can be observed that the Carmen displays the lowest flow rates with higher spatial variability than the Williams and Conference irrigation plants.

Figure 2a shows the pilot field with the NDVI data of each row. There was a gradient of the NDVI spectral index that moved from West to East of the field and with higher values in the Conference plot. The analysis by single plot shows a strong NDVI variability especially for the Carmen variety, which agrees with what found on the variability of the emitter flow rates. Consequently, the NDVI pattern seems to

Fig. 1 Spatial variability of the flow rates measured within the three irrigation plants

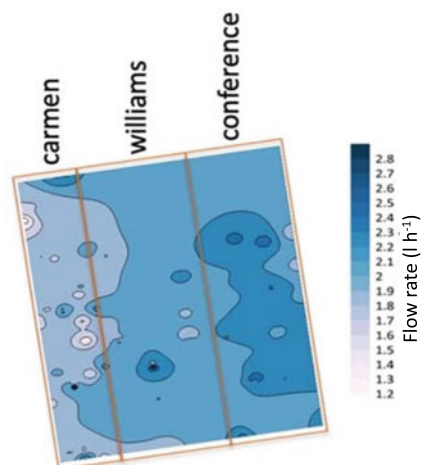
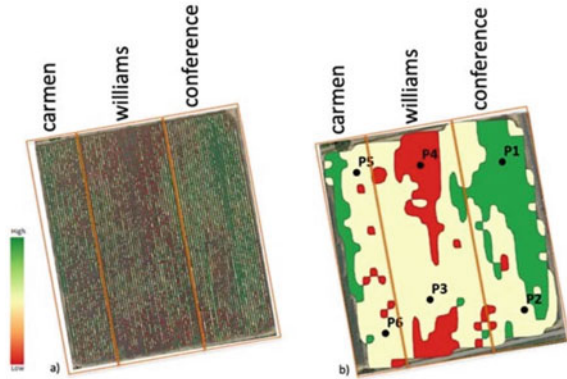


Fig. 2 (a) NDVI map of each crop row and (b) the three homogeneous areas (red: low vigor; yellow: medium vigor; green: high vigor) identified by the zoning analysis.



depend on the emitter flow spatial distribution (Fig.1). The higher the vigor of the pear tree, the higher emitter flow rate was delivered by the relative irrigation plant.

Figure 2b shows the three homogeneous zones identified and mapped using QGIS soft- ware, where within them two nodes of the network were installed to monitor the SWC dynamics.

Figure 3 shows the pairs of SWC vs SF values for the two lysimeters taken at two depths (SUP: 0.0–0.2 m; INF: 0.3–0.5 m) and falling in the two field zones with the highest and lowest NDVI zones. There was not significant difference between the measured and estimated data by the model suggested by the manufacturer (RMSE= 3%) and thus we used the calibration equation proposed by the latter.

Figure 4 shows the distribution of wetting events (rain and irrigation) and the dynamics of the SWC as an averaged of the FDR data collected in the 0.1–0.4 m layer for the three experimental years. The background of the udograms shows the spatial distribution of the SWC according to the soil depth. In addition, the stem water potential values (MdSWP), measured the day before of the irrigation event, are shown.

The analysis, extended from June to September, showed that the transferred expert ir- rigation protocol was able to keep the SWC within the optimal range, delimited by the field capacity ($SWC_{fc} = 34\%$) and the critical ($SWC^* = 25\%$) water content.

The MdSWP measurements confirmed that the adopted feedback control strategy avoided severe water stress conditions. The values were below 15 bar, which is the threshold for severe water stress conditions in pears [10, 11].

In terms of watering duration, a significant reduction has been observed, from 6–7 hours scheduled by the farmer to 3 h, as suggested by the new protocol.

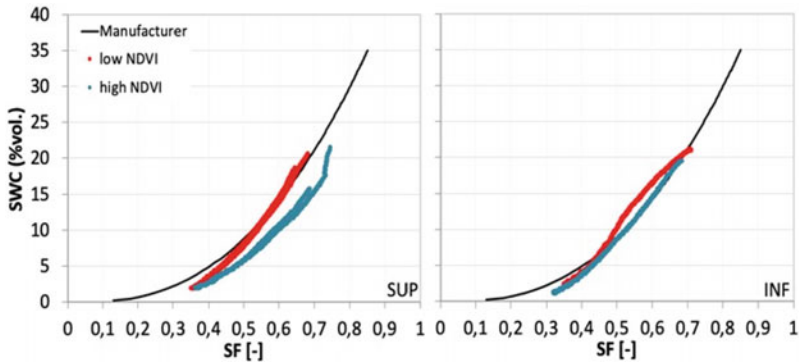


Fig. 3 Calibration function of the FDR sensor suggested by the manufacturer and experimental data acquired in two different depths on each site. Hydrological and Hydraulic performances of the WSN

3.2 *Production and Quality Performance of the New Irrigation Protocol*

The fruit yield of all varieties was maintained within the confidence interval of the previous five years. However, in 2021, there was a yield decreased for the whole farm because of an early frost damage and lack of pollinators.

The Williams and Conference orchards depicted a higher water use efficiency (IWUE) than the Carmen orchard. Specifically, IWUE was very good with values above 5 kg m^{-3} in 2019 and 2020.

Regarding the fruit diameter, the William showed a similar distribution to its control plot, where irrigation followed the ordinary protocol (Fig. 5). The curve appears shifted to the right, demonstrating that fruit with diameters greater than the commercial reference (60 mm) were mainly produced to be considered in the extra category. The Conference showed similar behavior, even if for the 2020 season the production focused on diameters smaller than 60 mm.

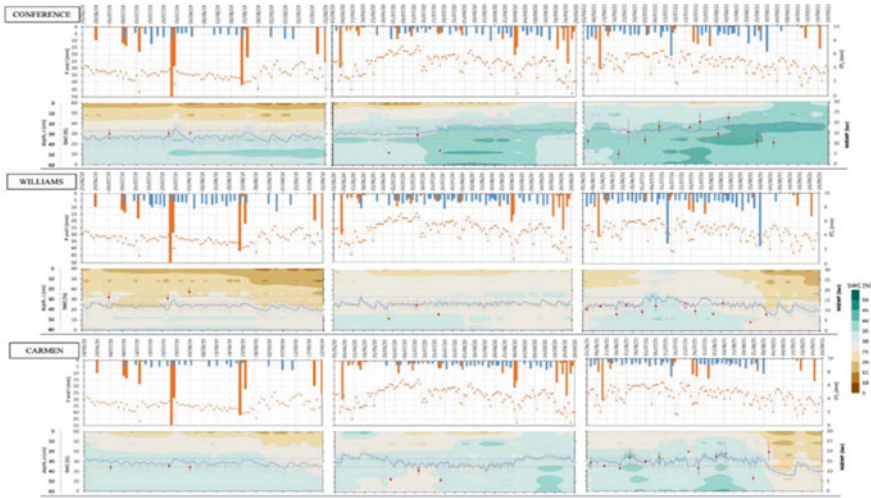


Fig. 4 Distribution of rainfall (blue bar), irrigation (orange bar) and the dynamics of the 0.1–0.4 m averaged soil water content. The background shows the spatio-temporal distribution of the soil water contents. In addition, the midday stem water potentials values are presented (red dots)

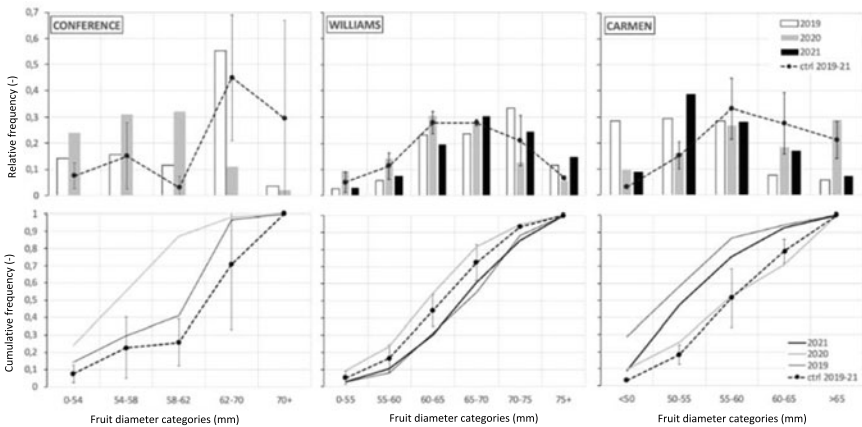


Fig. 5 Distribution of fruit diameter measured at harvest for the three orchards studied. In addition, the average distribution of fruit diameters measured on the control plots is reported. Vertical bars indicate the standard deviation of the acquired measurements for the 2019–2021 experimental period.

4 Conclusions

In this paper, important topics in precision agriculture have been addressed, concerning the design, calibration, and validation of a wireless sensor network (WSN) for an expert management of irrigation in fruit orchards.

The DSS performance was evaluated in terms of production, hydraulic and hydrology parameters during three years 2019–2021. The latter showed significant results, since the application of the DSS reduced the duration of a single watering to about 3 hours, which corresponded to half of the ordinary protocol. Consequently, lower number of waterings per irrigation season were delivered that turned into 50% water savings and the relative energy needed for irrigation pumping. In this way, the irrigation water use efficiency (IWUE) values were positive during the experimental period, especially for the Conference cultivar where the best results were found.

The fruit yield was maintained in comparison with the yield average of the previous five years. Moreover, fruit size in William and Conference were like those obtained for control plots.

Finally, the farmer was able to acquire awareness about the use of the water resources through the DSS adoption. He was able to check regularly the DSS application to identify the optimal moments to start and end an irrigation event.

References

1. Mpanga, I.K., Gaikpa, D.S., Koomson, E., Dapaah, H.K.: Innovations in Water management: agriculture. In: Gliński, J., Horabik, J., Lipiec, J. (eds) *The Palgrave Handbook of Global Sustainability*. Palgrave Macmillan, Cham (2011). https://doi.org/10.1007/978-3-030-38948-2_33-1
2. Navarro-Hellín, H., Martínez-del-Rincon, J., Domingo-Miguel, R., Soto-Valles, F., Torres-Sánchez, R.: A decision support system for managing irrigation in agriculture. *Comput. Electron. Agric.* **124**, 121–131 (2016)
3. Pereira, L.S., Cordery, I., Iacovides, I.: Improved indicators of water use performance and productivity for sustainable water conservation and saving. *Agric. Water Manag.* **108**, 39–51 (2012)
4. Čulibrk, D., Vukobratovic, D., Minic, V., Fernandez, M.A., Osuna, J.A., Crnojevic, V.: *Sensing Technologies for Precision Irrigation*. Springer, New York (2014)
5. ASAE Standards: EP 458: Field Evaluation of Micro-irrigation Systems, pp. 918–924. ASAE, Michigan (1999)
6. Provenzano, G., Rallo, G., Duarte Guedes Cabral de Almeida, C., Gomes de Almeida, B.: Development and validation of a new calibration model for diviner 2000® probe based on soil physical attributes. *Water* **12**, 3414 (2020)
7. Sentek Environmental Technologies: Calibration of the Sentek Pty Ltd Soil Moisture Sensors (2001)
8. Polak, A., Wallach, R.: Analysis of soil moisture variations in an irrigated orchard root zone. *Plant Soil* **233**, 145–159 (2001)
9. Thompson, R.B., Gallardo, M., Valdez, L.C., Fernández, M.D.: Determination of lower limits for irrigation management using in situ assessments of apparent crop water uptake made with volumetric soil water content sensors. *Agric. Water Manag.* **92**(1–2), 13–28 (2007)
10. Marsal, J., Stockle, C.: Use of CropSyst as a decision support system for scheduling regulated deficit irrigation in a pear orchard. *Irrig. Sci.* **30**, 139–147 (2012)
11. Shackel, K., Lampinen, B., Sibbett, S., Olson, W.: The relation of midday stem water potential to the growth and physiology of fruit trees under water limited conditions. *Acta Hort.* **537**, 425–430 (2000)

Assessing Potential Water Savings Implementing Variable Rate Sprinkler Irrigation in a Maize Farm in Northern Italy



Alice Mayer , Bianca Ortuani , and Arianna Facchi 

Abstract In recent agricultural seasons, many areas of the Po plain have experienced periods of water scarcity; to cope with this situation, farmers are introducing water saving technologies which would be more effective if supported by appropriate tools. Specifically, agro-hydrological models and soil moisture probes can support farmers in the irrigation management. In this study, an agro-hydrological model and soil water content measurements were used to optimize the water management in two irrigation sectors characterised by different soils under a center-pivot in a maize farm. When compared to the management operated by the farmer, a water use reduction of 17 and 23% was achieved in the coarse and fine soil sectors, respectively; this water saving was obtained respecting the constraints imposed by the farmer. The same modelling approach, applied to simulate variable rate irrigation for all the sprinkler systems of the farm (covering about 300 ha) in the period 2016–2020, resulted in an average water saving of 18%. This translates to a proportional energy saving at the farm level.

Keywords Precision irrigation · Maize · Agro-hydrological model · Weather forecast · Energy saving

1 Introduction

The Po Valley in Italy is characterized by a strong agricultural and zootechnical vocation: in the plain areas of Lombardy, the utilized agricultural area (UAA) is 700,000 hectares, 70% of which are irrigated [1]. The prevailing crops are cereals, dominated by maize, which covers about half of the regional UAA. Thanks to the historical availability of water in many areas, irrigation methods are often gravity-fed, with a prevalence of border irrigation. This technique, adopted by farmers for

A. Mayer · B. Ortuani · A. Facchi (✉)

Department of Agricultural and Environmental Sciences - Production, Landscape, Agroenergy,
Università degli Studi di Milano, 20133 Milan, Italy
e-mail: arianna.facchi@unimi.it

centuries, has an irrigation efficiency ranging between 30 and 60% as a function of the soil type, the groundwater table depth, and the irrigation practices adopted.

In the coming years, as a consequence of the climate change, the decrease in water availability in many geographical areas, including north of Italy, will increase water scarcity problems for all sectors, including agriculture [2–4].

In the most recent agricultural seasons, water scarcity periods in many areas of the Lombardy plain increased their frequency, which, combined with the enhanced competition for water resources between agriculture and other sectors, pushed farmers to introduce more efficient irrigation methods in their farms, in order to meet crop water needs and at the same time preserve the water resource.

This process has been supported in the last years by the RDP 2014–2020 of the Lombardy Region (Operation 4.1.03 “Incentives for investments aimed at modernizing or converting irrigation systems”). However, even with the most efficient irrigation technologies (sprinkler and drip irrigation), the irrigation management must be supported by appropriate tools aimed at providing optimal irrigation volumes at the right moment, to avoid water losses due to surface runoff and deep percolation below the root zone. This is one of the key points of Precision Agriculture [5], aimed at developing procedures and tools for the distribution of inputs (including water) in an optimized and time-variant mode not only in time, but also in space within the agricultural fields, if this is required by the spatial heterogeneity of the soil-crop system.

In this study, a precision irrigation approach was developed and applied to a center-pivot in the core of one of the most productive maize areas in Lombardy. The approach was based on: (1) characterization of the within field soil variability through an EMI sensor; (2) decision about when and how much irrigation to apply with the support of soil moisture probes and an agro-hydrological model; (3) distribution of variable rate irrigation through a center-pivot. Moreover, with the use of remotely sensed phenometrics and crop parameters to describe the crop evolution, the VR approach was simulated in the whole farm (La Canova, 300 ha) for the period 2016–2020.

2 Materials and Methods

2.1 Study Area

The study was carried out during the agricultural season 2021 at La Canova farm in Gambara (Brescia), a large livestock farm (about 300 ha). Seven sprinklers (pivot and lateral move sprinkler systems, Fig. 1 left) irrigate the majority of the farm agricultural surface; small areas not reached by the sprinkler systems are irrigated through border irrigation or hose reel irrigators. Irrigation is typically applied by the farmer in a uniform mode, with irrigation depth of about 25–32 mm and turns of 4–5 days, depending on the crop stage and the year.

Fig. 1 The seven irrigation systems of La Canova farm (left panel), and the 29 irrigation sectors considered for the farm scale simulations (right panel)



During the 2021 crop season, the irrigation of two sectors under a pivot covering an area of about 15 hectares was carried out in a variable-rate mode, with irrigation depths diversified according to the soils characteristics, and predicted by using soil moisture probes and an agro-hydrological model.

2.2 *EMI Survey and Soil Mapping*

For all the fields in La Canova farm, the soil variability under the sprinkler irrigation systems was investigated through an electromagnetic induction (EMI) sensor (CMD-MiniExplorer, GFS Instruments) pulled by a quad-bike. The EMI sensor measures the soil electrical resistivity (ER), which is related to the physical and hydrological properties of soils. ER is therefore an indirect measure of the soil properties, and it is used to investigate the in-field soil spatial heterogeneity.

The EMI sensor acquired ER values at three depths in points positioned along parallel acquisition lines. These data were interpolated to obtain ER maps which were successively processed through advanced statistical techniques (cluster analysis) to delineate areas including homogeneous soils, whose characteristics were investigated through laboratory analysis carried out on soil samples collected in each area. Finally, a soil map was derived for the whole farm.

2.3 *Design of the Variable-Rate Irrigation Sectors in the Pilot Pivot*

Consistently with the soil distribution identified, the area under the pilot pivot was divided into four sectors, two of which including mainly coarse soils and other two with a prevalence of medium-fine soils. For each sector, FDR (frequency domain

reflectometry) soil water content probes (Netsens TerraSense) were installed in two points at 20 and 40 cm depth, to explore the rooted soil profile, which, under sprinkler irrigation, was found to be within the first 50 cm from the soil surface.

Soil water content probes were connected wirelessly to a master station transmitting the acquired data at hourly time step to a server, which can be consulted remotely (from PC or mobile devices) through a web portal.

In two out of four sectors (one for each soil type), named “VR (variable-rate) sectors”, the irrigation was managed through an agro-hydrological model calibrated through soil water content measurements, while in the other two sectors, named “control sectors”, it was managed according to the practices adopted in the farm in 2021 (25 to 30 mm of water every 4 days, depending on the crop stage).

Even for the VR sectors, the farmer imposed some constraints: 1) to maintain the 4-day irrigation turn (only the last irrigation of the season could be skipped); 2) a minimum irrigation depth of 25–22 mm at the beginning of the season and 22–18 mm from July onwards had to be provided at each irrigation turn; 3) three fertigation of 30 mm were provided in all the irrigation systems.

2.4 SWAP Model and Irrigation Management in the Pilot Pivot

SWAP (Soil Water Plant Atmosphere model, [6]) is an agro-hydrological model that simulates vertical water movements in the soil-crop system by solving the 1D Richard’s equation. It has been used to optimize the irrigation management for many crops, including maize [7, 8]. SWAP requires input data related to agrometeorological variables, vertical soil discretization and hydraulic properties, crop parameters and groundwater table depth. To obtain all the needed data, an agrometeorological weather station (Netsens MeteoSense) and two piezometers were installed in the farm. The van Genuchten–Mualem soil hydraulic properties used in SWAP were derived by applying the ROSETTA pedo-transfer functions [9] to the collected soil data.

Due to the water availability, the 7 irrigation systems must operate alternately, thus, to allow an effective organization of the farm irrigation, farmer requires the irrigation depth to be distributed in the different sprinkler systems (or in the sectors under each system) in advance.

After each irrigation turn, by feeding the agro-hydrological model with 7-days weather forecast data (ABACO; www.abacofarmer.com) it was possible to simulate the soil water content dynamics till the next irrigation turn, and thus to identify in advance the optimal irrigation depths to be provided to the VR sectors of the pilot pivot. In particular, for each VR sector, the irrigation depth needed to replenish the soil water content in the root zone up to field capacity was calculated. Since two simulations were run for every VR sector (one for each soil type), the irrigation depth

was calculated as the average of the two values weighted for the relative surface of each soil type within the sector.

Before the 2021 irrigation season, a new panel was mounted on the pilot pivot, allowing VR irrigation by regulating the pivot speed. Once the decision on the irrigation depth to be distributed in the next irrigation turn was taken, it was uploaded in the panel by the farmer.

2.5 Farm Scale Simulations

A modelling framework was developed in MATLAB to apply SWAP at the farm scale for the period 2016–2020, following a semi-distributed approach. The same procedure used for the pilot pivot was applied to the 7 irrigation sprinkler systems in the farm. Starting from the soil map, 29 irrigation sectors were identified, each one containing two prevailing soil types (one coarse and one fine). Sentinel-2 images of the study area were processed for the period from 2016 to 2021 to retrieve maize growth stages and LAI pattern for each sector [10].

Simulations for every irrigation sector were run maintaining the same fixed irrigation dates used in the actual farm management, while optimizing the water depth as explained for the pilot pivot. A sequence of simulations was run in a cycle, each one ending in a day when the actual irrigation took place; in every step two simulations were launched for every sector, one for each soil type. At the end of the two simulations the deficit with respect to the soil field capacity was calculated and the higher value was applied in that irrigation turn (therefore, compared to the approach used in the pilot pivot, a cautionary approach was adopted for the farm simulations).

3 Results and Discussion

3.1 Irrigation Management in the Pilot Pivot

The SWAP model simulates the soil water content for the whole soil profile, thus the values measured by the soil water content probes installed at 20 and 40 cm depths could be compared with the simulated values at the same depths. Particularly, the measurements were used to calibrate the model by fine tuning some crop parameters, namely the root density and the soil evaporation coefficient.

An example of the processed model outputs used to calculate the optimal irrigation depth is reported in Fig. 2; the red line represents the root zone water content, while the blue and yellow lines represent field capacity and wilting point values, respectively. The grey box identifies the period in which the simulations are run in a provisional mode.

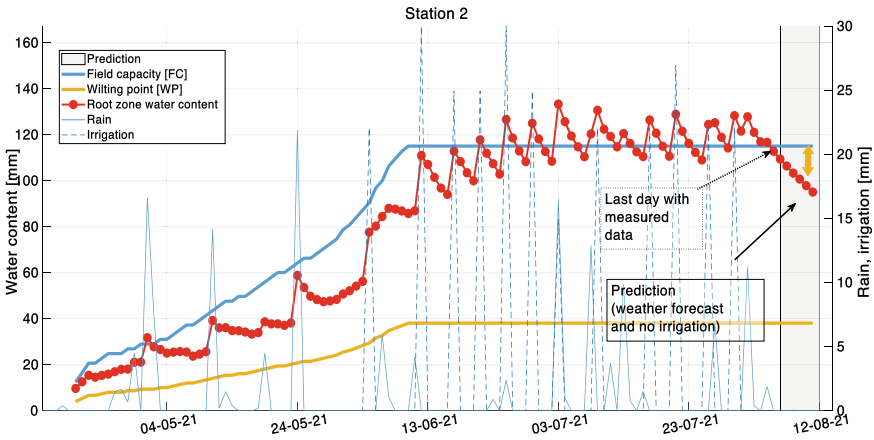


Fig. 2 Example of model output processed to identify the optimal irrigation depth to be provided

For every irrigation turn, the difference between field capacity and soil water content in the irrigation day was calculated (yellow arrow). Water content in Fig. 2, often above field capacity, can be explained considering the constraints imposed by the farmer (Sect. 2.3).

Total irrigation was 391 and 360 mm for the coarse and the fine sectors, respectively, while in the control sectors 469 mm were provided, thus resulting in a water saving of 17 and 23% for the two sectors.

At the end of the crop season the fields under the pilot pivot were harvested with a combine harvester provided by a yield monitor and a grain moisture sensor, allowing to obtain the maps reported in Fig. 3.

Results for the four sectors are synthesized in Table 1, showing no differences in yield between VR-managed and control sectors, while grain moisture resulted to be lower in VR sectors.

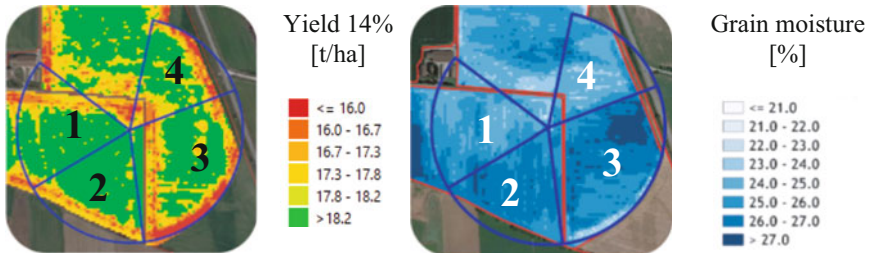


Fig. 3 Yield (left panel) and grain moisture (right panel) maps for the pilot pivot area

Table 1 Yield mean values calculated for the four sectors under the pilot pivot

Sector	Management	Average yield [t/ha]
1	VR	18.34
2	VR	18.43
3	Control	18.78
4	Control	18.24

3.2 Farm Scale Simulations

Results for the VR irrigation simulated in the 7 irrigation sprinkler systems are reported in Table 2, illustrating the mean/min/max irrigation depth for the single sprinkler systems in the years in which they were cropped with maize (for systems 3 and 7: 2016–2018–2020, for the other systems: 2017–2019). In the table, simulated results and actual irrigation depths are compared.

The results for the sprinkler systems were processed to obtain yearly water consumptions for the whole farm; these results, expressed in m^3 , are reported in Table 3. For the period 2016–2020, the approach adopted to simulate an optimised VR irrigation at the farm scale led to a water saving ranging from 6 to 27%, depending mostly on the rainfall amount and distribution during the summer months.

The mean water saving for the 5-years period is 18%; since the reduction in water consumption led to a proportional decrease in irrigation time, an average energy saving (for water pumping and sprinkler system handling) of 18% could be achieved by La Canova if the proposed irrigation management were adopted.

Table 2 Total irrigation (actual and simulated) provided for the 7 sprinkler systems in the period 2016–2020 (mean, min, max)

Irrig. plant	Actual irrig.- mm (mean, min, max)	Optimized irrig. – mm (mean, min, max)	% Var
1	440 (410, 470)	330 (281, 379)	–25.0
2	486 (479, 493)	396 (373, 418)	–18.6
3	460 (396, 501)	374 (359, 401)	–18.7
4	486 (479, 493)	389 (371, 407)	–20.0
5	501 (466, 535)	353 (324, 383)	–29.4
6	514 (493, 535)	377 (350, 404)	–26.6
7	421 (357, 456)	370 (345, 404)	–12.0

Table 3 Total irrigation (actual and optimized) provided at the farm scale for maize fields (2016–2020)

Year	Actual irrigation – m ³	Optimized irrigation – m ³	Variation – m ³	% Var
2016	437,251.20	341,381.74	–95,869.46	–21.9
2017	617,352.40	493,007.00	–124,345.40	–20.1
2018	352,182.90	331,245.33	–20,937.57	–5.9
2019	590,065.40	428,423.14	–161,642.26	–27.4
2020	447,973.50	379,966.58	–68,006.92	–15.2
Mean				–18.1

4 Conclusions

In this study, the water saving achievable by adopting a VR irrigation strategy in a maize farm with 7 sprinkler irrigation systems (linear and center pivots) in northern Italy was assessed; the PA (precision agriculture) approach was developed and experimented in a center pivot and then extrapolated at the farm scale through simulations.

An EMI survey was used to identify homogeneous soil zones. Starting from them, the area under each sprinkler system was divided in sectors which were the base for the VR irrigation management.

For the pilot pivot, the SWAP model was implemented for two VR-managed sectors, achieving a water saving of 17% and 23% (for the coarse and fine soils, respectively) if compared to the control sectors. These results were obtained by respecting some constraints imposed by the property, the absence of which would probably have led to higher savings. While average yields in the VR sectors were comparable with those of the control sectors; grain moisture was lower in the VR sectors, leading to a consequent energy saving during the grain drying operation.

The same modelling framework was applied to the whole farm for the period 2016–2020, obtaining water savings for the single sprinkler system ranging from 12 to 29%, and for the whole farm from 6 to 27% (average value: 18%), well in line with the results observed for the pilot pivot.

Since the energy used to pump water from the farm wells, and for the handling of the sprinkler systems, is proportional to the amount of water provided, an average energy saving of 18% is expected at the farm level.

Acknowledgements We wish to thank Regione Lombardia for funding the SOS-AP project (<https://www.sos-agricolturadiprecisione.it/>), and La Canova farm (<http://lacanovasrl.it/>) for hosting the experimental activities.

References

1. Gandolfi, C.: Acqua e irrigazione per nutrire il pianeta. La realtà della pianura Padana lombarda. INCONTRI (2017). <https://doi.org/10.4081/incontri.2017.308>
2. Moonen, A.C.: Climate change in Italy indicated by agrometeorological indices over 122 years. *Agric. Forest Meteorol.* **111**, 13–27 (2002)
3. Costa, J.M.: Modern viticulture in southern Europe: vulnerabilities and strategies for adaptation to water scarcity. *Agric. Water Manag.* **164**, 5–18 (2016)
4. Pachauri, R.K.: Climate change 2014: synthesis report. Contribution of working Groups I, II and III to the Fifth Assessment Report of the Intergovernmental Panel on Climate Change. IPCC, Geneva (2014)
5. Blasi, G.: Linee guida per lo sviluppo dell'agricoltura di precisione in Italia. Ministero delle Politiche Agricole Alimentari e Forestali **78** (2017)
6. Kroes, J.G., et al.: Alterra - soil, water and land use, soil physics and land management, Wimek, et al. SWAP version 4. Wageningen Environmental Research, Wageningen (2017)
7. Bonfante, A.: LCIS DSS—An irrigation supporting system for water use efficiency improvement in precision agriculture: a maize case study. *Agric. Syst.* **176**, 102646 (2019)
8. Jiang, J.: Irrigation management for spring maize grown on saline soil based on SWAP model. *Field Crop Res* **196**, 85–97 (2016)
9. Zhang, Y., Schaap, M.G.: Weighted recalibration of the Rosetta pedotransfer model with improved estimates of hydraulic parameter distributions and summary statistics (Rosetta3). *J. Hydrol.* **547**, 39–53 (2017)
10. Mayer, A., et al.: Use of satellite-based phenometrics, geophysical soil data and a semi-distributed agro-hydrological model for the scheduling of irrigation in a maize farm in northern Italy. In: MetroAgriFor2022, Perugia 3–5 November 2022, Submitted

Monitoring and Predicting Irrigation Requirements of Tree Crops in Eastern Sicily as a Tool for Sustainability



Salvatore Pappalardo, Enrico Antonio Chiaradia, Giuseppe Longo-Minnolo, Daniela Vanella, and Simona Consoli

Abstract The irrigated agriculture of Southern Italy, managed by the reclamation consortia, generally lacks the necessary information and tools which can allow to improve water management and achieve the necessary sustainability of the irrigation systems. In this context, the objective of the study was to provide an effective tool for monitoring tree crop water needs at the irrigation district level.

The study was carried out in Eastern-Sicily (Italy) during the years 2019–2020. An object-based classification using the Random Forest (RF) algorithm was applied to map the main tree crops of the area. The RF model was built using a temporal stack of green (B2), red (B3), and near-infrared (B8) bands of 24 selected Sentinel-2 images and 503 ground-truth sample points. The accuracy was assessed by determining the out-of-bag (OOB) error and kappa coefficient. The irrigation water requirements (IWR) were determined with the IdrAgra model (www.idragra.unimi.it) over the identified tree crop areas using the dual crop parameters provided by the FAO-56 paper and validated at 5 reference farms. The obtained IWR at the district scale were compared with the irrigation volumes distributed by the reclamation consortium.

The results show the potential of hydrological simulation models coupled with remote sensing-based land use classification techniques for improving water management of tree crops and increasing the sustainability of irrigated agriculture under semi-arid conditions.

Keywords Random Forest · Water needs · FAO-56 · GIS · Sustainable irrigation management

S. Pappalardo · G. Longo-Minnolo (✉) · D. Vanella · S. Consoli
Dipartimento di Agricoltura, Alimentazione e Ambiente (Di3A), Università degli Studi di Catania, Via S. Sofia, 100, 95123 Catania, Italy
e-mail: giuseppe.longominnolo@phd.unict.it

E. A. Chiaradia
Department of Agricultural and Environmental Sciences, University of Milan, 20133 Milan, Italy

1 Introduction

In the last 20 years, many countries of the Mediterranean basin have suffered from prolonged drought periods [4]. Moreover, in a climate change context where more frequent and severe droughts are expected to occur, water scarcity is destined to become worse [9]. Because water represents the most important input for the agricultural sector, improvements in water management are necessary to enhance the sustainability of irrigated agriculture, especially in the Mediterranean areas, where water shortage is a limiting factor for crop production [7, 14]. In terms of production, among tree crops, citrus is one of the most important in the world [17]. In 2018, the production of citrus fruits corresponded to millions of dedicated hectares, with a large contribution of oranges (75 million tons), followed by clementines, mandarins, lemons and limes (19 million tons), and grapefruits and pummelos [13]. 48% of world citrus production comes from the Mediterranean basin [2]. In these environments, the efficiency of citrus production largely depends on adequate irrigation. Therefore, it is essential to manage water availability sustainably to optimize crop productivity and, at the same time, improve their adaptation to water scarcity conditions [15]. In this context, hydrological simulation models can be very useful in supporting water-resources planning and management decisions. Additionally, these models are efficient when combined with multiple supervisory classification algorithms, such as Random Forest (RF) [11].

The general aim of this study was to monitor the irrigation water requirements (IWR) of the main Mediterranean tree crops (i.e. citrus, olive, and grapevine; [12] in Eastern Sicily (Italy) during the reference period 2019–2020, and specifically to evaluate the water management of a reclamation consortium, at the district level, by using a remote sensing-based method for land use classification and water balance model for crop water needs estimation.

2 Materials and Methods

2.1 Study Area

The study was carried out at the irrigation district “Quota 102.5” located in Eastern Sicily (Italy), managed by the “Consorzio di Bonifica Sicilia Orientale” (CBSO) (Fig. 1). The irrigation district “Quota 102.50” is characterized by a total and irrigated surface of about 5,050 and 2,300 ha, respectively. It consists of 102 sub-districts and more than 1,220 farms. The altitude ranges between 15 to 180 m above the sea level (a.s.l.), with an average value of 106 m a.s.l. and a slope of 4.4%. It is mainly cultivated with citrus (95%), olives, and fruit (5%) groves. The climate of the area is typical Mediterranean with annual average air temperature, relative humidity, cumulative precipitation, and reference evapotranspiration (ET_0) values of 18 °C, 64%, 586 mm, and 1,209 mm, respectively (data, referring to the period 2002–2020,

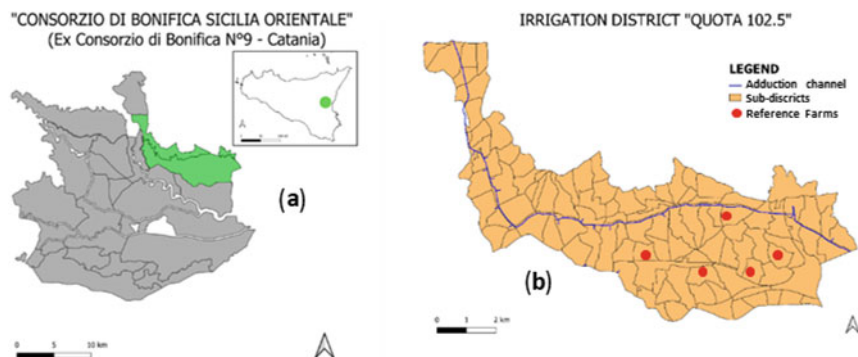


Fig. 1 Location of CBSO **a** and characterization of the irrigation district "Quota 102.50" with the localization of the reference farms used in the study **b**

are provided by the Sicilian Agro-meteorological Information Service, SIAS, www.sias.regione.sicilia.it.

The irrigation district is served by open and pressure channels. The irrigation management is based on turn planning criteria, within the irrigation season (commonly from May to October). The principal adduction channel has a length of about 20 km and an average discharge of $1.8 \text{ m}^3\text{s}^{-1}$. Each farm receives about $520 \text{ m}^3/\text{ha}$ during each turn, for a total of 3–4 turns during the irrigation season. On-farm irrigation methods include sprinkler and drip irrigation systems.

2.2 Estimation of the Irrigation Water Requirements

In order to determine the IWR, a preliminary supervised classification was applied for mapping the main tree crops of the irrigation district "Quota 102.50". Specifically, the Random Forest (RF) algorithm was computed using a stack-layer of green (B2), red (B3), and near-infrared (B8) bands of 24 Sentinel-2 images (<https://sentinel.esa.int/web/sentinel/missions/sentinel-2>) and 503 ground truth sampling points collected at the study area. The classification map obtained was used as input of the hydrological model, named IdrAgra ("Idrologia Agraria" in Italian), specifically designed for water needs estimation in agricultural areas.

IdrAgra (www.idragra.unimi.it, [6]) is a conceptual model with spatially distributed parameters, based on the FAO-56 method of double crop coefficient (K_c), which simulates the distribution of IWR in agricultural areas and estimates the daily hydrological balance. Specifically, it computes the daily crop evapotranspiration (ET_c) estimates, using the original dual K_c approach [1], on the basis of ET_0 , by separating the K_c into the basal crop coefficient (K_{cb}), which describes the crop transpiration, and the evaporative coefficient (K_e), which accounts for soil evaporation:

$$ET_c = (K_{cb} + K_e) * ET_0 \quad (1)$$

In this study, crop parameters from the FAO-56 paper were used and daily ET_0 values were calculated using Penman–Monteith equation [1]:

$$ET_0 = \frac{0.408\Delta(R_n - G)\gamma \frac{37}{T+273}u_2(e_s - e_a)}{\Delta + \gamma(1 + 0.34u_2)} \quad (2)$$

where, R_n is the net radiation at the reference crop surface ($\text{MJ m}^{-2} \text{h}^{-1}$); G is the soil heat flux density ($\text{MJ m}^{-2} \text{h}^{-1}$); T is the mean hourly air temperature T_{air} ($^{\circ}\text{C}$); Δ is the slope of saturation vapour pressure curve at T_{air} ($\text{kPa } ^{\circ}\text{C}^{-1}$). γ is the psychrometric constant ($\text{kPa } ^{\circ}\text{C}^{-1}$); e_s is the saturation vapour pressure at T_{air} (kPa); e_a is the average hourly actual vapour pressure (kPa); u_2 is the average hourly wind speed at 2 m height (m s^{-1}).

The IWR (mm) is defined by the following equation:

$$IWR = ET_c - P_e \quad (3)$$

where, P_e (mm) is the effective rainfall.

The irrigation volume is calculated by multiplying the IWR for the irrigated surface (ha). The agrometeorological data used in this study were collected by four weather stations (Catania, Lat. 37.44° , Log. 15.07° ; Paternò, Lat. 37.51° , Log. 14.85° ; Lentini, Lat. 37.34° , Log. 14.92° ; and Riposto, Lat. 37.68° , Log. 15.16°) managed by SIAS.

2.3 Validation

In order to validate the result of the RF algorithm, the out-of-bag (OOB) accuracy and the kappa coefficient were calculated. The OOB is an unbiased estimate of the true prediction error [10], and the kappa coefficient is an index to express the accuracy of image classification. Kappa values range between 0 and 1, showing the highest agreement for values close to 0.75 and the lowest agreement for values close to 0.4 [5].

The absolute error (AE) and the relative error (RE) were determined for validating IdrAgra, by comparing the outputs of the model (IWR_{IdrAgra}) with the IWR provided by five reference farms (IWR_{farm}) located at the irrigation district “Quota 102.50”. Since the irrigation water supplied by the reclamation consortia is not enough for satisfying the IWR, these farms use also their own water sources. The main characteristics of the reference farms, in terms of crop/soil types and used irrigation methods, are reported in Table 1.

Finally, the IWR outputs calculated at the district scale were compared with the irrigation volumes distributed by the CBSO.

Table 1 Main characteristics of the reference farms used for the validation of IdrAgra

Ref. farm	Crop	Area (ha)	Soil type	Irrigation method
Farm 1	citrus	3.7	silty clay loam	full drip irrigation
Farm 2	citrus	26.0	silty clay loam	
Farm 3	citrus	15.0	silty clay loam	
Farm 4	citrus	35.0	sandy loam	70% drip irrigation, 30% other methods
	olive	1.7	silty clay loam	
	grape	5.2	silty clay loam	
Farm 5	citrus	50.0	silty clay loam	60% drip irrigation, 40% other methods
	olive	8.18	silty clay loam	
	grape	0.32	silty clay loam	

3 Results

Figure 2 shows the land cover map obtained by applying RF classification at the irrigation district “Quota 102.50”.

The OOB accuracy was of 87% with a kappa coefficient of 0.85, showing a very good agreement between the land cover classes obtained by RF and the sample points. Table 2 shows the comparison between the irrigation volumes obtained by applying the IdrAgra model and those supplied at the reference farms during the period 2019–2020.

The best performance of IdrAgra model was observed in simulating the irrigation volumes of citrus crops, with average AE values of 11,56 and 11,14 m³, during 2019

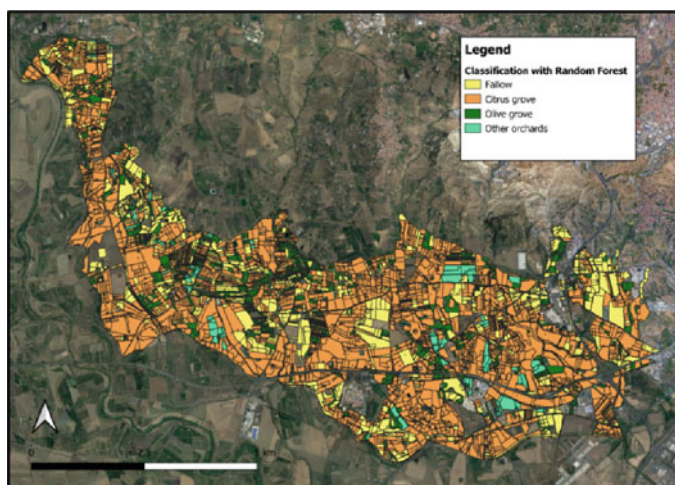


Fig. 2 Land cover map obtained by applying RF classification at the irrigation district “Quota 102.50”

Table 2 Comparison between the irrigation volumes obtained by applying the IdrAgra model and those supplied at the reference farms, during the period 2019–2020 (IWR = irrigation water requirements, AE = absolute error, RE = relative error)

Reference farm	Crop	2019					2020				
		IWR _{farm} (m ³)	IWR _{IdrAgra} (m ³)	AE (m ³)	RE (%)	IWR _{farm} (m ³)	IWR _{IdrAgra} (m ³)	AE (m ³)	RE (%)		
Farm 1	citrus	38,102	33,263	4,839	-12.70	38,102	34,189	3,913	-10.27		
Farm 2	citrus	244,972	248,221	3,249	1.33	244,972	252,427	7,455	3.04		
Farm 3	citrus	138,209	139,660	1,451	1.05	138,209	144,514	6,305	4.56		
Farm 4	citrus	280,057	288,928	8,871	3.17	280,057	283,179	3,122	1.11		
	olive	10,597	12,983	2,386	22.52	10,597	14,497	3,900	36.81		
	grape	29,407	43,978	14,571	49.55	29,407	43,816	14,409	49.00		
Farm 5	citrus	409,514	448,917	39,403	9.62	409,514	444,446	34,932	8.53		
	olive	25,483	60,403	34,920	137.03	25,483	68,617	43,134	169.27		
	grape	2,400	3,030	630	26.24	2,400	3,050	650	27.08		

and 2020, respectively. The maximum error was observed at reference Farm 5, with overestimations of 9.62% and 8.53%, and at reference Farm 1, with underestimations of 12.70% and 10.27%, for the years 2019 and 2020, respectively.

IdrAgra model was less performing in simulating the irrigation volumes of the grapevine, with average AE values of 23.50 and 23.43 m³, during the years 2019 and 2020, respectively. Average overestimations of 37.90% and 38.04% were observed during the years 2019 and 2020, respectively.

The worst performance was instead observed for olive crops, with average AE values of 36.69 and 41.56 m³, with the maximum error observed at Farm 5, with overestimations of 137.03% and 169.27% during 2019 and 2020, respectively.

By running the IdrAgra model at the district scale, irrigation volumes of 27,513,890 and 27,915,680 m³ were determined for the irrigation season 2019–2020, respectively. Whereas, the irrigation volumes declared by the CBSO were of 1,198,112 and 1,124,672 m³ for the same years, highlighting large overestimations.

4 Discussion and Conclusion

In this study, the use of a hydrological model based on FAO-56 dual K_c approach, i.e. IdrAgra coupled with a remote sensing-based method for land use classification, was evaluated for estimating IWR at district scale in Sicily, during the reference period 2019–2020. The framework was first validated at 5 reference farms.

The results show the reliability of the IdrAgra model for simulating the water needs of citrus crops. Several studies applied this method for calculating ET_c estimates of citrus orchards. For instance, [3] found an overestimation of about 77% using the dual K_c approach with tabulated crop parameters over an irrigated citrus orchard under drip and flood irrigation methods in Marrakech (Morocco). Conversely, in this study lower overestimates/underestimates were found, even using tabulated K_c values.

The results obtained at the district scale are critical due to the large difference observed between the irrigation volumes declared by the CBSO and those estimated by the IdrAgra model. However, it should be noticed that the farmers often use their own water sources since the amount of water provided by the consortium is not enough for proper crop irrigation. In Sicily, autonomous irrigation managed by single farm owners is quite widespread and prevails in many areas compared with collective irrigation, with the abstraction of water from small reservoirs and/or wells [18].

In conclusion, IdrAgra can be considered a promising model for simulating the water needs in the Mediterranean area and specifically for citrus crops. However, future research outlooks are needed for enhancing the performance of the proposed approach by applying the remote sensing technology also for deriving crop parameters and using climate reanalysis data, as meteorological input of the IdrAgra model instead of ground-based agro-meteorological observations [8, 16].

Acknowledgements This study was supported by the Research Project of National Relevance (PRIN 2017) entitled “INtegrated Computer modeling and monitoring for Irrigation Planning in Italy - INCIPIT” and “Miglioramento delle produzioni agroalimentari mediterranee in condizioni di carenza di risorse idriche – WATER4AGRIFOOD”. Cod. progetto: ARS01_00825; cod. CUP: B64I20000160005, “PON “RICERCA E INNOVAZIONE” 2014–2020, Azione II – Obiettivo Specifico 1b.


References

1. Allen, R.G., Pereira, L.S., Raes, D., Smith, M.: Crop evapotranspiration guidelines for computing crop water requirements-FAO irrigation and drainage paper 56. Fao, Rome **300**(9), D05109 (1998)
2. Catalano, C., et al.: Biotechnological approaches for genetic improvement of lemon (*Citrus limon* (L.) burm. f.) against mal secco disease. *Plants* **10**(5), 1002 (2021)
3. Er-Raki, S.A.L.A.H., Chehbouni, A., Guemouria, N., Ezzahar, J., Khabba, S., Boulet, G., Hanich, L.: Citrus orchard evapotranspiration: comparison between eddy covariance measurements and the FAO-56 approach estimates. *Plant Biosyst.* **143**(1), 201–208 (2009)
4. FAO. Global forest resources assessment 2005: report on fires in the Mediterranean region. Fire Management Working Paper, Rome (2006)
5. Foody, G.M.: Explaining the unsuitability of the kappa coefficient in the assessment and comparison of the accuracy of thematic maps obtained by image classification. *Remote Sens. Environ.* **239**, 111630 (2020)
6. Gandolfi, C., Facchi, A., Maggi, D.: Comparison of 1D models of water flow in unsaturated soils. *Environ. Model. Softw.* **21**(12), 1759–1764 (2006)
7. Hsiao, T.C., Steduto, P., Fereres, E.: A systematic and quantitative approach to improve water use efficiency in agriculture. *Irrig. Sci.* **25**(3), 209–231 (2007)
8. Longo-Minnolo, G., Vanella, D., Consoli, S., Pappalardo, S., Ramírez-Cuesta, J.M.: Assessing the use of ERA5-Land reanalysis and spatial interpolation methods for retrieving precipitation estimates at basin scale. *Atmos. Res.* **271**, 106131 (2022)
9. Mancosu, N., Snyder, R.L., Kyriakakis, G., Spano, D.: Water scarcity and future challenges for food production. *Water* **7**(3), 975–992 (2015)
10. Matthew, W.: Bias of the random forest out-of-bag (OOB) error for certain input parameters. *Open J. Stat.* **2011** (2011)
11. Monsalve-Tellez, J.M., Torres-León, J.L., Garcés-Gómez, Y.A.: Evaluation of SAR and optical image fusion methods in oil palm crop cover classification using the random forest algorithm. *Agriculture* **12**(7), 955 (2022)
12. Motisi, A., Rossi, F., Consoli, S., Papa, R., Minacapilli, M., Rallo, G., Cammalleri, C., D’Urso, G.: Eddy covariance and sap flow measurement of energy and mass exchanges of woody crops in a Mediterranean environment. *Acta Hort.* **951**, 121–127 (2012)
13. Poles, L., Licciardello, C., Distefano, G., Nicolosi, E., Gentile, A., La Malfa, S.: Recent advances of in vitro culture for the application of new breeding techniques in citrus. *Plants* **9**(8), 938 (2020)
14. Singh, S., Boote, K.J., Angadi, S.V., Grover, K.K.: Estimating water balance, evapotranspiration and water use efficiency of spring safflower using the CROPGRO model. *Agric. Water Manag.* **185**, 137–144 (2017)
15. Vanella, D., et al.: Long-term monitoring of deficit irrigation regimes on citrus orchards in Sicily. *J. Agric. Eng.* **52**(4) (2021)
16. Vanella, D., et al.: Comparing the use of ERA5 reanalysis dataset and ground-based agrometeorological data under different climates and topography in Italy. *J. Hydrol. Region. Stud.* **42**, 101182 (2022)

17. Salonia, F., Ciacciulli, A., Poles, L., Pappalardo, H.D., La Malfa, S., Licciardello, C.: New plant breeding techniques in citrus for the improvement of important agronomic traits a review. *Front. Plant Sci.* **11**, 1234 (2020)
18. Zucaro, R., et al.: Atlas of Italian irrigation systems. Politiche per l'ambiente e l'agricoltura. Risorse idriche (2014)

The Vaia Event: Primary Impacts of the Storm and Subsequent Evolution of the Malgonera Stream (Dolomites)



Giacomo Pellegrini , Lorenzo Martini, Riccardo Rainato, Lorenzo Picco, and Mario Aristide Lenzi

Abstract Large infrequent disturbances (LIDs) increasingly affect mountain basins, but secondary impacts are often disregarded although their understanding would provide advice to river managers. The following work aims at investigating primary and secondary impacts of the Vaia storm on the channel morphology and large wood (LW) load of a reach of Malgonera Stream (6,025 m²). To achieve the objectives, remote sensing and field data were exploited. Remote sensing data were used to compute two DoDs: the first investigated the Vaia impact (2010–2019) while the second the subsequent evolution (2020–2021). LW field data, combined with remote sensing surveys, were collected to compute the LW load entailed by Vaia and the subsequent fluctuations (2020–2021). The net sediment volume after the event was $-2,025 \text{ m}^3$. The area of erosion was 2,659 m², while the deposition covered 1,222 m². The recent DoD (2020–2021) featured a net sediment volume of 15.79 m³, showing irrelevant geomorphic changes. After the Vaia storm, 96.3 m³ha⁻¹ of LW was detected inside the study area. Around 83 logs per ha were classified as single elements while the remaining as jams' components. Between 2020 and 2021, the LW load increased up to 102 m³ha⁻¹, for a total of 485 elements per ha due to cantilever failures of unstable banks. This work (i) underlines the capability of LIDs to rearrange the morphology of mountain streams, (ii) providing first evidence on secondary processes of LW recruitment along unstable mountain streams and (iii) highlighting how changes in the LW load are detached from morphological changes.

Keywords Vaia storm · Alpine stream · Morphological changes · LW load · LW recruitment

G. Pellegrini (✉) · L. Martini · R. Rainato · L. Picco · M. A. Lenzi
Department of Land, Environment, Agriculture and Forestry, University of Padova, Viale dell'Università 16, 35020 Legnaro, PD, Italy
e-mail: giacomo.pellegrini@unipd.it

© The Author(s), under exclusive license to Springer Nature Switzerland AG 2023
V. Ferro et al. (eds.), *AIIA 2022: Biosystems Engineering Towards the Green Deal*,
Lecture Notes in Civil Engineering 337,
https://doi.org/10.1007/978-3-031-30329-6_16

153

1 Introduction

Large Infrequent Disturbances (hereinafter LIDs) can overturn the entire drainage basin of a river triggering new sediment sources as well as increasing new material (sediment and wood) within the channel network [1, 2]. The disturbances, which typically cause the LIDs, are: hurricanes, tornados and windthrows [3], wildfires [4], floods, glacial lake outburst floods (GLOFs), volcanic eruptions, and earthquakes. Apart from the immediate consequence, worth highlighting is the chain of processes that is started when one of the LIDs occurs. At present, this concept is defined as “cascading process” [5] whose functioning is explained by the “domino effect”: when a piece falls, the following pieces fall too. With climate change, unpredictable large disturbances seem to become more frequent and for this reason, new strategic plans and monitoring are needed worldwide. The case of the Vaia storm event that recently affected the Northeast Alpine area of Italy is a clear example. Thousands of hectares of forest rapidly blown down [6–8], hundreds of roads eroded, roofs-raised, huge volumes of sediment and wood recruited and transported along the rivers and millions of euros of damages to the aqueducts and to the electric systems took place. This first step, which resulted evident to everyone’s eyes, will unavoidably lead to seconds step consequences. The breakdown of the natural equilibrium will presumably cause active dynamics on the sediment yield and on the large wood (LW) loads affecting directly the morphology, stability and safety [9] of mountain basins. For this reason, disturbance-affected areas need continuous monitoring for both didactical-research and risk-related purposes. Moreover, the LW dynamics, its recruitment from the hillslopes and its interaction with the sediment are still worldwide poorly understood [10] due to the deficiency of direct field observations [11]. Progresses on this new branch of river science is needed, both to improve the limited information present until now and to cover the evident existing lack of knowledge in order to give some tips for future strategic and management plans. Therefore, the following work aims at investigating the primary impacts of the Vaia storm event (27th–31st October 2018) and the subsequent evolution of the channel morphology and large wood loads of a small Alpine stream (Malgonera).

2 Study Area

The Malgonera basin (1 km²) is a sub-catchment of the Tegnans Torrent Basin and is located in the Northeast Italian Alps (Veneto Region) (Fig. 1). The Malgonera basin exhibits a prevalent nivo-pluvial runoff regime while the average annual precipitation is around 850 mm. Overall, norway spruce (*Picea abies*) forests, and pastures cover the basin. The channel bed-forms defining the Malgonera Stream morphology are boulder-cascade and step-pool. The mean slope is around 19% and the grain size distribution is characterized by a D₅₀ of 60 mm and a D₉₀ of around 406 mm. The area of interest of this study (Fig. 1b) is 6,025 m².

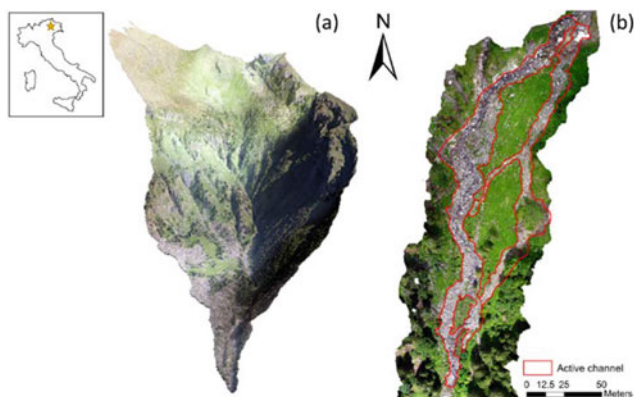


Fig. 1 **a** Localization of the Malgonera basin in Italy and its 3D map. On the right **b** the active channel of interest where the data were collected is represented

Between 27th and 31st October 2018, the entire basin was affected by the Vaia storm. The discharge and precipitation measured at the outlet of the Tegnias Torrent basin [12] were $548 \text{ mm } 72 \text{ h}^{-1}$ and $173 \text{ m}^3 \text{ s}^{-1}$, respectively. Both values exceeded 100 years of recurrence interval. Nonetheless, several hectares of forests were blown down due to wind gusts exceeding 200 km h^{-1} .

3 Materials and Methods

To achieve the objectives, remote sensing (LiDAR; UAV) and field data were exploited. Remote sensing products were used to compute two Dem Of Difference (DoD): the first investigated the Vaia impact (pre vs post Vaia; 2010–2019) and the second monitored the evolution of the channel (post vs post-post Vaia, 2020–2021). Field data of LW, combined with the LiDAR and UAVs surveys, were collected to compute both the LW load entailed by Vaia and the subsequent LW fluctuations and recruitment (2020–2021).

3.1 The GCD Tool for DoDs Computation

The Geomorphic Change Detection (GCD) software has the objective of detecting the topographic changes in rivers. In order to identify and detect the changes in time, the tool needs at least two raster-based surfaces. The volumetric change in storage is calculated from the difference in surface elevations from digital elevation models (DEMs) derived from repeated topographic surveys [13].

As each DEM has an uncertain surface representation, the detection of the changes between two surveys is highly dependent on the surface representation uncertainties inherent in the individual DEMs [13]. Therefore, the uncertainties are computed independently in each DEM and then propagated to the DEM of difference. To do so, in the following work the Fuzzy Inference Systems for modelling the errors [14] was used. Such technique captured the potential source of elevation uncertainty driven by different parameters such as point density, slope and roughness [13, 15, 16]. Thus, according to the topographic characteristics of the study area under assessment and the available data (i.e., LiDAR and UAV), a set of rules to compute the surface error were applied (more info in [12]). In this way, the GCD output quantified the volumes of sediment displaced during and after the Vaia storm event, highlighting the main areas of deposition and erosion and ignoring those affected by error.

3.2 Large Wood Surveys Using Field and Remote Sensing Data

All the woody elements longer than 1 m and with a diameter larger than 0.1 m are defined as LW [14, 17, 18]. To identify the LW, every log was measured and tagged.

The LW was classified as single element or as jam forming log, with wood jam defined as at least two logs were touching each other [19]. The LW diameter and length were measured based on UAVs high-resolution orthophotos interpretation, using the ArcGIS software. The wood volume was computed applying the formula of the cylinder to each element.

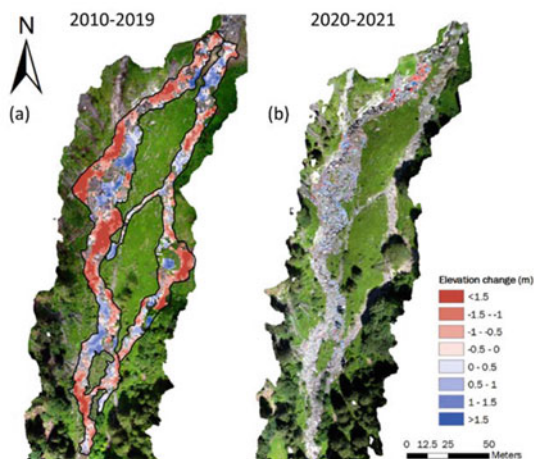
The total LW load was computed by summing the total elements detected in each survey (post Vaia and post-post Vaia) both in terms of number (elements and elements per ha) and volumes (m^3 and $\text{m}^3 \text{ha}^{-1}$). The recruited LW was detected by subtracting the load of the most recent survey with the oldest and by validating it with the new UAV survey through orthophotos interpretation. Overall, the basic statistical analysis was run taking advantage of the R Studio software.

4 Results

4.1 Morphological Changes

The DoD 2010–2019 (Fig. 2) shows significantly how erosion prevailed on deposition. In fact, the net sediment volume after the Vaia storm event was estimated around $-2,025 \text{ m}^3$. The area of total erosion was $2,659 \text{ m}^2$, while the deposition covered $1,222 \text{ m}^2$. Notably, the average depth of surface lowering was deeper than 1 m. Particularly, the deepest eroded areas were detected on the riverbanks and by the curves of the Malgonera Stream (Fig. 2a). For what concerns the depositional areas,

Fig. 2 Visual representation of the **a** pre-post Vaia DoD and **b** of the post-post post Vaia DoD. Red colour indicates erosion while blue the deposition



instead, most of them were found either in the internal part of the curves or in those areas where the vegetation was creating, presumably, a functional disconnection to the channel (i.e., shrub patches, standing trees).

On the contrary, the most recent DoD (2020–2021) featured 138.28 and 122.58 m^3 of deposition and erosion, respectively. Overall, the sediment net volume was computed as 15.79 m^3 (Fig. 2b), highlighting a balanced condition and almost irrelevant geomorphic changes.

4.2 Large Wood Loads and Recruitment

The LW load detected after the Vaia storm event was 58 m^3 ($96.3 \text{ m}^3 \text{ ha}^{-1}$) for a total amount of 279 (463 elements per ha) wood elements. 50 logs were classified as single elements while the remaining as elements composing wood jams. The LW length ranged between 1 and 20.2 m while the median and mean values were 2.38 m and 3.43 m, respectively (Fig. 3a). The LW diameter, instead, ranged between 0.1 and 0.76 m. The median diameter was 0.19 m (Fig. 3b).

Between 2020 and 2021 the LW load increased up to a volume of 61.50 m^3 ($102 \text{ m}^3 \text{ ha}^{-1}$), increasing the number of elements to 292 (485 elements per ha). However, changes neither in the ranges of the length and diameters nor in the mean and median values of the “after event” survey were detected.

Interestingly, 13 new elements were identified inside the channel. The total load of the recruited material was 3.5 m^3 ($5.7 \text{ m}^3 \text{ ha}^{-1}$) (Fig. 3c). The length and diameter ranged between 1.23 and 8.55 m, 0.13 and 0.57 m, respectively. On the one hand, the median diameter was 0.17 m, while the mean was 0.23 m. On the other, the median and mean length were 3.15 and 3.7 m, respectively.

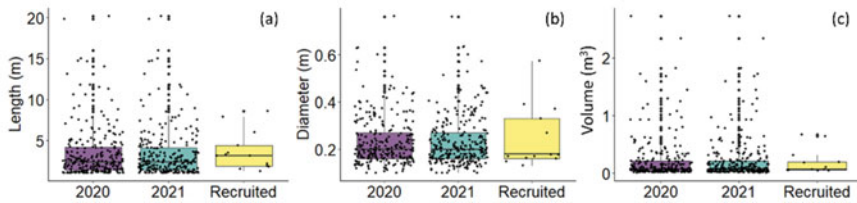


Fig. 3 Boxplot representing the **a** length, the **b** diameter and the **c** volume distribution of the LW detected in 2020 (purple), in 2021 (blue) and of the recruited material (yellow)

5 Discussions

This work provides (i) a geomorphological assessment of the intensity by which the Vaia storm affected a small alpine stream located in the Northeast of Italy and (ii) a preliminary analysis on the ongoing cascading processes related to LW dynamics and channel morphological changes. On the one hand, during Vaia the Malgonera Stream featured significant geomorphic changes along the entire active channel, causing both planimetric (i.e., channel widening) and longitudinal variations that, as seen in other similar environments [20, 21], have led to the complete removal of the armored layer. On the other hand, during the two years after the event, morphological changes seem not to have been started. For this reason, further analyses are required soon in order to (i) implement the data with longer time monitoring to catch a larger magnitude range of floods and to (ii) see whether a formative flood to trigger changes in the channel has yet to come.

As far as the LW is concerned, worth noting is the huge load of material produced during the Vaia event. The LW came both from the neighboring and upstream-forested areas and was entirely composed by norway spruce (*Picea abies*) due to its surficial root ward that was not capable of resisting to such kind of wind gusts disturbances [22, 23]. Additionally, the large ranges of length, diameter and volumes showed an overall heterogeneity of the LW dimensions confirming that the Vaia event has left no way out to all stages of the standing spruce trees.

Worth mentioning are the $5.7 \text{ m}^3 \text{ ha}^{-1}$ that were recruited between 2020 and 2021. This value demonstrates how an environment affected by a large disturbance is still fragile and vulnerable three years after the storm event. Besides, it underlines the fact that cascading processes concerning LW recruitment are ongoing and detached from the changes in the channel morphology since the new LW input was entirely sourced by cantilever failures of small portions of the unstable forested banks. For sure, in such environments, is important to pay attention both to the large event itself and to the upcoming secondary processes that may occur without, apparently, an intense triggering factor.

6 Conclusions

This work underlines how the availability of high-resolution remote sensing data, such as aerial images and LiDAR, can be an effective tool to identify and characterize the impact and the subsequent evolution of a mountain stream affected by a large disturbance, both in terms of morphological changes and large wood loads. Nonetheless, this work underlines the capability of LIDs to affect and rearrange the morphology of mountain streams (i) providing first evidence on secondary processes of LW recruitment along an unstable mountain stream affected by a storm and (ii) highlighting how changes in the LW are detached from limited changes in the channel morphologies. Nonetheless, although this approach needs further investigations, the results are promising for implementing cost-efficient and low time-consuming analyses for managing the risk of vulnerable areas such as mountain areas.

Acknowledgements This work was funded by the Veneto Region in the frame of Vaia-Land (OCDPC 558/2018) project.

References

1. Pierson, T.C., Major, J.J.: Hydrogeomorphic effects of explosive volcanic eruptions on drainage basins*. *Annu. Rev. Earth Planet Sci.* **42**, 469–507 (2014)
2. Ulloa, H., Iroumé, A., Picco, L., et al.: Spatial analysis of the impacts of the Chaitén volcano eruption (Chile) in three fluvial systems. *J. South Am. Earth Sci.* **69**, 213–225 (2016). <https://doi.org/10.1016/j.jsames.2016.04.008>
3. Rich, R.L., Frelich, L.E., Reich, P.B.: Wind-throw mortality in the southern boreal forest: effects of species, diameter and stand age. *J. Ecol.* **95**, 1261–1273 (2007). <https://doi.org/10.1111/j.1365-2745.2007.01301.x>
4. Schulte, L.A., Mladenoff, D.J.: Severe wind and fire regimes in Northern forests: historical variability at the regional scale. *Ecology* **86**, 431–445 (2005)
5. Mazzorana, B., Picco, L., Rainato, R., et al.: Cascading processes in a changing environment: Disturbances on fluvial ecosystems in Chile and implications for hazard and risk management. *Sci. Total Environ.* **655**, 1089–1103 (2019)
6. Chirici, G., Giannetti, F., Travaglini, D., et al.: Forest damage inventory after the “Vaia” storm in Italy. *Forest@ - Rivista di Selvicoltura ed Ecologia Forestale* **16**, 3–9 (2019). <https://doi.org/10.3832/efor3070-016>
7. Costa, M., Marchi, N., Bettella, F., et al.: Biological legacies and rockfall: the protective effect of a windthrown forest. *Forests* **12** (2021). <https://doi.org/10.3390/f12091141>
8. Marangon, D., Marchi, N., Lingua, E.: Windthrown elements: a key point improving microsite amelioration and browsing protection to transplanted seedlings. *Forest Ecol. Manage.* **508** (2022). <https://doi.org/10.1016/j.foreco.2022.120050>
9. Montgomery, D.R., Buffington, J.M.: Channel-reach morphology in mountain drainage basins. *Bull. Geol. Soc. Am.* **109**, 596–611 (1997). [https://doi.org/10.1130/0016-7606\(1997\)109%3c0596:CRMIMD%3e2.3.CO;2](https://doi.org/10.1130/0016-7606(1997)109%3c0596:CRMIMD%3e2.3.CO;2)
10. Ravazzolo, D., Mao, L., Picco, L., et al.: Geomorphic effects of wood quantity and characteristics in three Italian gravel-bed rivers. *Geomorphology* **246**, 79–89 (2015). <https://doi.org/10.1016/j.geomorph.2015.06.012>

11. Macvicar, B., Piégay, H.: Implementation and validation of video monitoring for wood budgeting in a wandering piedmont river, the Ain River (France). *Earth Surf Process Landf.* **37**, 1272–1289 (2012). <https://doi.org/10.1002/esp.3240>
12. Pellegrini, G., Martini, L., Cavalli, M., et al.: The morphological response of the Tegnas alpine catchment (Northeast Italy) to a large infrequent disturbance. *Sci. Total Environ.* **770** (2021). <https://doi.org/10.1016/j.scitotenv.2021.145209>
13. Wheaton, J.M., Brasington, J., Darby, S.E., Sear, D.A.: Accounting for uncertainty in DEMs from repeat topographic surveys: improved sediment budgets. *Earth Surf. Process Landf.* **35**, 136–156 (2010). <https://doi.org/10.1002/esp.1886>
14. Pellegrini, G., Martini, L., Rainato, R., Picco, L.: Large wood mobilization and morphological changes in an alpine river following the release of an ordinary experimental flood from an upstream dam. *Catena (Amst)* **216** (2022). <https://doi.org/10.1016/j.catena.2022.106398>
15. Cavalli, M., Goldin, B., Comiti, F., et al.: Assessment of erosion and deposition in steep mountain basins by differencing sequential digital terrain models. *Geomorphology* **291**, 4–16 (2017). <https://doi.org/10.1016/j.geomorph.2016.04.009>
16. Neverman, A.J., Fuller, I.C., Procter, J.N.: Application of Geomorphic Change Detection (GCD) to quantify morphological budgeting error in a New Zealand gravel-bed river: a case study from the Makaroro River Hawke's Bay. *J. Hydrol. (New Zealand)* **55**(1), 45–63 (2016)
17. Schenk, E.R., Moulin, B., Hupp, C.R., Richter, J.M.: Large wood budget and transport dynamics on a large river using radio telemetry. *Earth Surf Process Landf.* **39**, 487–498 (2014). <https://doi.org/10.1002/esp.3463>
18. Tonon, A., Picco, L., Rainato, R.: Test of methodology for developing a large wood budget: a 1-year example from a regulated gravel bed river following ordinary floods. *Catena (Amst)* **165**, 115–124 (2018). <https://doi.org/10.1016/j.catena.2018.01.035>
19. Comiti, F., Lucía, A., Rickenmann, D.: Large wood recruitment and transport during large floods: a review. *Geomorphology* **269**, 23–39 (2016). <https://doi.org/10.1016/j.geomorph.2016.06.016>
20. Rainato, R., Martini, L., Pellegrini, G., Picco, L.: Hydrological, geomorphic and sedimentological responses of an alpine basin to a severe weather event (Vaia storm). *Catena (Amst)* **207** (2021). <https://doi.org/10.1016/j.catena.2021.105600>
21. Pellegrini, G., Rainato, R., Martini, L., Picco, L.: The morphological evolution of a step–pool stream after an exceptional flood and subsequent ordinary flow conditions. *Water (Switzerland)* **13**, 3630 (2021). <https://doi.org/10.3390/w13243630>
22. Motta, R., Ascoli, D., Corona, P., et al.: Selvicoltura e schianti da vento. Il caso della “tempesta Vaia.” *Forest@ - Rivista di Selvicoltura ed Ecologia Forestale* **15**, 94–98 (2018). <https://doi.org/10.3832/efor2990-015>
23. Picco, L., Rainato, R., Pellegrini, G., et al.: An extraordinary event changed the (morphological) appearance of a famous Alpine stream. In: *Proceedings of the River Flow 2020—10th Conference on Fluvial Hydraulics*, Delft, The Netherlands, 7–10 July 2020, pp. 1653–1658. CRC Press: Boca Raton (2020)

Analysis of Bedload Mobility in an Andean Stream



Riccardo Rainato , Luca Mao, and Mario Aristide Lenzi

Abstract High gradient streams form the majority of the mountain drainage network and the sediment dynamics that occur here influence the features of sediment delivered downstream. In this sense, the bedload is the transport process that regards the coarser particles, which are mobilized by rolling, sliding, and saltation on the channel bed. In mountain streams, bedload can be the main sediment transport process, therefore, its analysis and quantification are crucial. However, the importance of bedload contrasts with the fact that it is difficult and impractical to monitor due to its impulsive nature. Different direct and indirect methods were used during the last decades to cover this gap. One of these is the bedload tracing method. In this work, bedload tracing was used to analyze the sediment dynamics in a high-gradient Andean stream, the Estero Morales, located in central Chile. The Estero Morales stream exhibits an average slope of 14.0% and a $D_{50} = 59$ mm. The basin (27 km²) extends between 1780 and 4497 m a.s.l., hosting the San Francisco glacier (1.8 km²) that strongly affects the hydrological regime. In January 2016, 197 clasts tracers were seeded along the Estero Morales stream and their mobility was monitored by 9 surveys between January and March 2016. During this study period, the tracers experienced an average transport distance equal to 12.0 m, while the average diameter mobilized was 95.0 mm. However, the mobility observed was not clearly related to the hydraulic forcing, stressing the complex transport dynamics of a mountain stream.

Keywords Glaciers · Mountain streams · Andes · Bedload · Tracers

R. Rainato (✉) · M. A. Lenzi
Department of Land, Environment, Agriculture, and Forestry, University of Padova, Padova, Italy
e-mail: riccardo.rainato@unipd.it

L. Mao
School of Geography, University of Lincoln, Lincoln, UK

© The Author(s), under exclusive license to Springer Nature Switzerland AG 2023
V. Ferro et al. (eds.), *AIIA 2022: Biosystems Engineering Towards the Green Deal*,
Lecture Notes in Civil Engineering 337,
https://doi.org/10.1007/978-3-031-30329-6_17

161

1 Introduction

In mountain streams, the sediment dynamics are driven by the interplay of different factors such as geological-lithological structure, topographic setting, climatic conditions, hydrological forcing, and sedimentological configuration, which can act at both basin and river network scales [1–3]. Then, the sediment dynamics acting in these high gradient streams influence the features of sediment delivered downstream, particularly by controlling the timing of sediment fluxes and the amounts and size of material released to the lowland rivers [4–6]. In mountain streams, the main sediment transport processes are suspended sediment transport and bedload transport. The bedload occurs under high hydraulic forcing conditions (flood events) and consists of the transport of coarse sediments. This coarse material can be supplied by source areas located along the hillslopes or the river network [7]. In light of this, the bedload analysis is crucial for several aspects, including hazard assessment, understanding the morphodynamics of higher-order channels, and managing reservoir sedimentation. In this sense, a better understanding of bedload, and the transport processes in general, became particularly important in light of the alterations induced to the river systems by the increased frequency of droughts and large and infrequent floods [8–10]. In the last decades, several direct and indirect methods were used to analyze bedload transport. Of these, bedload tracing was widely used, initiating with the pioneering works based on simply painted particles up to the more recent ultra-high frequency radio frequency identification tags (UHF RFID tags) used effectively in gravel-bed rivers [11, 12]. Over the years, the tracing method permitted to analyze the bedload mobility acting in mountain basins, being applied both on the hillslopes [13] and on different portions of the river network [14]. Particularly, the bedload tracing permitted to investigate different aspects related to the mobility of the coarse streambed material such as the initiation of motion [15], the displacement [16], the active layer depth [17], and the propagation velocity [18]. In this sense, the aim of this work is the analysis of the bedload mobility in a high-gradient Andean stream. Particularly, the mobility expressed by the coarse streambed material as a consequence of high-frequency floods was investigated by means of the bedload tracing method.

2 Methods

2.1 Study Site

The Estero Morales basin (Fig. 1) extends 27 km² into the Provincia de Cordillera (Region Metropolitana, Chile). It ranges between 1780 to 4497 m a.s.l and is part of a protected CONAF (Corporación Nacional Forestal) reserve. Mediterranean climatic

conditions lead to an average annual precipitation of about 550 mm, with the predominance of snowfall to rainfall [19]. About 1.8 km² of the basin is covered by glacierized areas, primarily belonging to the San Francisco glacier [20]. Due to the glacier, the runoff regime is mainly dominated by snow and glacier melt in summer, while rainfall events prevail in late spring. Particularly, during the melt period (December–March) the San Francisco glacier induces daily floods along the channel network, with different bedload transport rates associated. Such a condition represents the ideal scenario for monitoring bedload transport under a wide range of hydraulic forcing. In this sense, the Estero Morales stream is a typical high-gradient channel 7 m wide and characterized by an average slope = 14.0% and D_{16} , D_{50} , D_{84} of stream bed material equal to 20, 59, 318 mm. These conditions result in the alternation of boulder-cascade, step-pool, and plane bed morphologies.

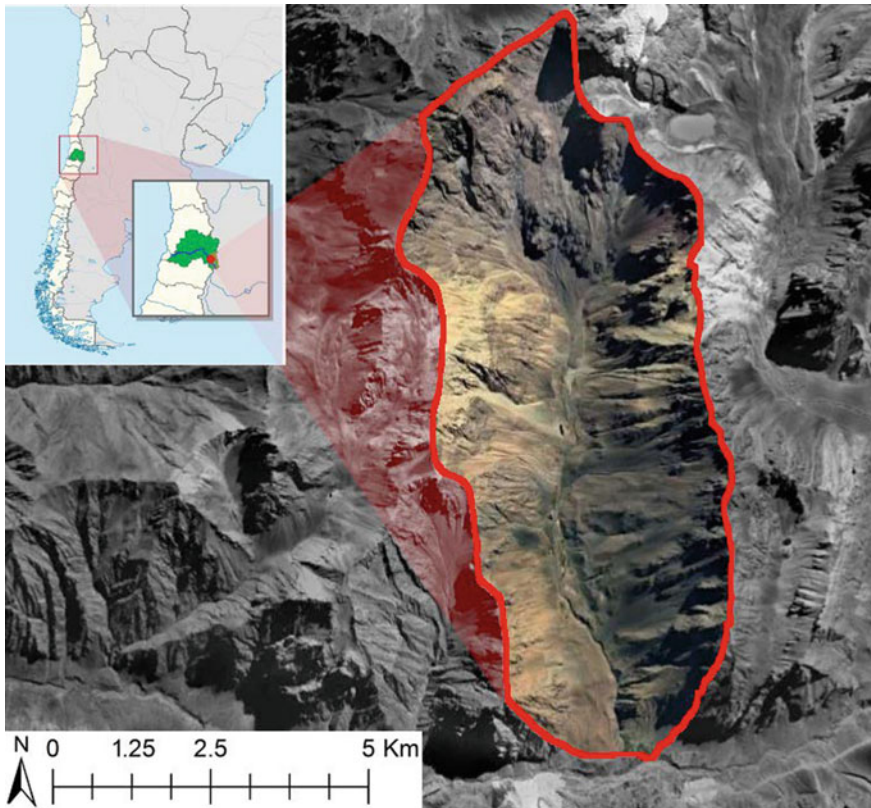


Fig. 1 Estero Morales basin (in red) and its position in the Region Metropolitana, Chile (in green) (Color figure online)

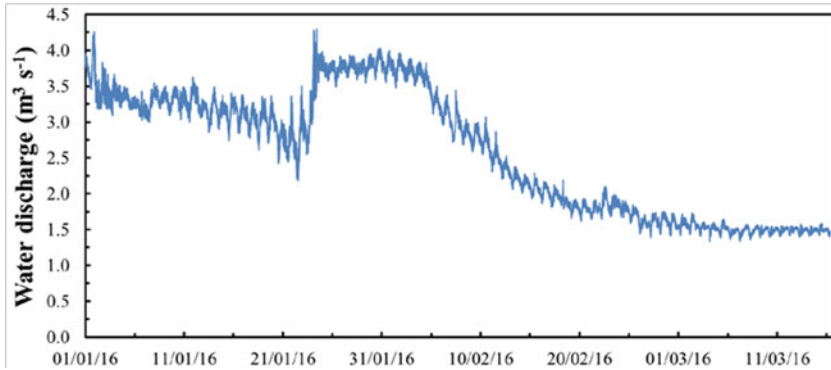


Fig. 2 Water discharge measured in the Estero Morales during the study period

2.2 Bedload Tracing

To analyze the bedload mobility, 197 clasts equipped with Passive Integrated Transponders were progressively seeded along the Estero Morales stream starting from January 2016. Specifically, 45 of these tracers were released on January 5, 60 on January 21, 44 on February 4, 30 on February 5, and 18 on February 17. These clasts were collected from the Estero Morales streambed material and featured a b-axis between 30 and 280 mm. The dispersion of the tracers was investigated along a reach of 745 long and through 9 field surveys (inventories) realized between January and March 2016. These tracer inventories were realized by two operators following the approach already used by [19, 21]. Specifically, to identify the position of the tracers a mobile Oregon RFID antenna was used, while a laser rangefinder was used to measure the travel distance. In this sense, 32 stable cross sections were identified along the study reach, and from these, the displacements were measured.

During the study period, the water stages were measured every 10 min through a pressure transducer sensor and, then, converted into water discharge using the stage-discharge rating curve established in the Estero Morales by [20]. Between January and March 2016, the water discharge exhibited evident daily fluctuations (Fig. 2), ranging overall between 1.34 and 4.28 $\text{m}^3 \text{s}^{-1}$. The mean water discharge over the study period was 2.59 $\text{m}^3 \text{s}^{-1}$.

3 Results

The 9 field surveys were organized to define different extents of intra-survey periods, which ranged from 1 day (e.g., 04–05/02/16) to 14 days (e.g., 07/01/16–21/01/16). This led to the investigation of a wide range of hydraulic forcing conditions. In fact, in terms of peak of water discharge (Q_p), the tracers experienced values between

1.60 and 4.28 m³ s⁻¹ over the intra-survey periods (Table 1). In this sense, a certain variability was observed also in terms of mean water discharge (Q_{MEAN}), which spanned from 1.52 to 3.58 m³ s⁻¹. Interestingly, the peak of unit discharge (q_P) was constantly over 0.20 m² s⁻¹ during the study period, exhibiting its maximum in the first and third inventories through a value of 0.61 m² s⁻¹. The methodology used has led to a progressive increase in the number of tracers over the study period, starting with 45 tracers in the first survey and ending with 197 tracers at the end of the field campaign. The linear increase in the number of tracers was not accompanied by an augment in the tracer recovery rate (R_r). In fact, R_r exhibited large fluctuations over the 9 tracer inventories, remaining, however, always below 25% (Table 1). Large fluctuations were observed also in terms of mean transport distance expressed by the tracers (L_{MEAN}), which ranged over two orders of magnitude (Table 1). Differently, the median b-axis mobilized (D_{MED}) appeared quite constant over the study period, ranging between 58.5 and 76.0 mm.

To better comprehend the conditions driving the bedload mobility, the relationships between the variables related to hydraulic forcing conditions (i.e., Q_P , Q_{MEAN} , q_P) and those concerning the tracer mobility (i.e., L_{MEAN} , D_{MED}) were investigated. None of these relationships expressed a coefficient of determination (R^2) > 0.60 except for the $Q_P - D_{MED}$ relationship, which resulted statistically significant ($R^2 = 0.684$, p-value <0.05).

Table 1 Hydraulic forcing conditions and bedload mobility observed over the study period. *Survey* identifies the date of the tracer inventory; Q_P , Q_{MEAN} and q_P describe, respectively, the peak of water discharge, the mean water discharge, and the peak of unit discharge that occurred in the intra-survey period; $N_tracers$ is the number of tracers present in the Estero Morales streambed at the time of the survey; R_r is the tracer recovery rate achieved, L_{MEAN} is the mean transport distance exhibited by the tracers (including those that did not move), while D_{MED} is the median b-axis mobilized (including only the tracers entrained)

<i>Survey</i>	Q_P (m ³ s ⁻¹)	Q_{MEAN} (m ³ s ⁻¹)	q_P (m ² s ⁻¹)	$N_tracers$ (n)	R_r (%)	L_{MEAN} (m)	D_{MED} (mm)
07/01/16	4.26	3.42	0.61	45	24	5.0	76.0
21/01/16	3.62	3.17	0.52	45	16	22.7	69.0
04/02/16	4.28	3.55	0.61	105	9	36.4	75.0
05/02/16	3.82	3.58	0.55	149	13	13.6	76.0
11/02/16	3.50	2.96	0.50	179	19	52.7	76.0
17/02/16	2.86	2.22	0.41	179	15	1.5	73.5
02/03/16	2.19	1.75	0.31	197	24	39.5	58.5
03/03/16	1.73	1.57	0.25	197	5	125.0	66.0
04/03/16	1.60	1.52	0.23	197	24	6.5	62.0

4 Discussion

The field campaign realized in 2016 in the Estero Morales stream permitted to obtain valuable data about the bedload mobility in a high-gradient stream. Particularly, the tracing method allowed to analyze the response of the coarse streambed material to the hydraulic forcing conditions acting during the glacier-melting season. In this sense, the sediment dynamics of glacierized basins are only partially understood [22] and this is especially evident for the bedload transport [23]. Such an issue contrasts with the ongoing climate change that is severely affecting the glacial and periglacial areas, triggering dynamics unobserved until now [24]. In this sense, the bedload tracing realized in 2016 was part of a longer monitoring program started in the Estero Morales basin in 2014, the results of which were also presented in [20, 25]. Interestingly, the hydraulic forcing conditions investigated in 2016, while ordinary, exhibited a certain variability. Particularly, in terms of Q_P , a slightly larger range (1.60–4.28 m³ s⁻¹) than that analyzed in the Estero Morales in 2014 (3.44–4.68 m³ s⁻¹) and 2015 (1.70–3.77 m³ s⁻¹) by [19, 26] was investigated. These flow conditions were somehow reflected in the recovery rates achieved. In fact, in the bedload tracing performed in 2014 (14 surveys) and 2015 (15 surveys) average R_r equal to 50% and 45% were obtained, respectively. Differently, in 2016 the average R_r was 16%. This difference seems to be associated with the most varied hydraulic forcing conditions analyzed but also with the manifestly lower number of tracers used. In fact, 197 tracers were seeded along the Estero Morales stream in 2016, while 461 and 395 were used in 2014 and 2015, respectively. Therefore, although an $R_r = 16\%$ appears in line with what was reported in other bedload tracing studies [16, 17, 27, 28], it led to a certain uncertainty in the results obtained that must be carefully considered. In this sense, the bedload mobility documented in the Estero Morales stream during 2016 resulted comparable to what was observed in other study cases. In fact, the range obtained in terms of L_{MEAN} (1.50–125.0 m) was in line with the 6.5–185.3 and 3.1–162.0 m documented in the Estero Morales in 2014 and 2015, respectively [26]. However, the results seem to suggest also a high transport efficiency. In particular, for flow conditions featuring $q_P \leq 0.31$ m² s⁻¹, an average L_{MEAN} of 57.0 m was observed in the Estero Morales. Under the same conditions, in the Rio Cordon (Italian Alps) the average L_{MEAN} was 0.2 m [21]. Interestingly, the variables related to hydraulic forcing conditions overall poorly described the bedload mobility. The only significant relationship documented was Q_P-D_{MED} . On one hand, this result supports the effectiveness of Q_P in describing the sediment dynamics, on the other hand, it stresses the high complexity of the same [1, 2].

5 Conclusion

In January 2016, the Estero Morales stream was equipped with 197 tracers in order to investigate the bedload mobility triggered by high-frequency floods. Particularly,

the tracers' dispersion was analyzed by 9 surveys realized during the glacier melting season (January–March). The bedload mobility observed was not clearly related to the hydraulic forcing conditions experienced by the tracers, which were mobilized for travel distances >300 m. In this sense, the results seem to suggest a certain control of flow conditions on the grain size entrained (Q_{P-MED} relationship) rather than mobility (L_{MEAN}). However, the low recovery rates achieved during the surveys (average $Rr = 16\%$) and the pretty short study period could have influenced the results obtained. Nevertheless, the result stressed the complexity of the sediment dynamics acting in the high-gradient streams and, especially, in the glacier-fed ones.

References

1. Duvert, C., et al.: Towards prediction of suspended sediment yield from peak discharge in small erodible mountainous catchments (0.45–22 km²) of France, Mexico and Spain. *J. Hydrol.* **454–455**, 42–55 (2012)
2. Pagano, S.G., Rainato, R., Garcia-Rama, A., Gentile, F., Lenzi, M.A.: Analysis of suspended sediment dynamics at event scale: comparison between a Mediterranean and an Alpine basin. *Hydrol. Sci. J.* **64**(8), 948–961 (2019)
3. Pellegrini, G., Rainato, R., Martini, L., Picco, L.: The morphological evolution of a step–pool stream after an exceptional flood and subsequent ordinary flow conditions. *Water* **13**(24), 3630 (2021)
4. Hinderer, M., Kastowski, M., Kamelger, A., Bartolini, C., Schlunegger, C.: River loads and modern denudation of the Alps – a review. *Earth Sci. Rev.* **118**, 11–44 (2013)
5. Picco, L., Ravazzolo, D., Rainato, R., Lenzi, M.A.: Characteristics of fluvial islands along three gravel bed-rivers of North-Eastern Italy. *Cuadernos de Investigacion Geografica* **40**(1), 53 (2014)
6. Tenorio, G.E., Vanacker, V., Campforts, B., Alvarez, L., Zhiminaicela, S., Vercruysse, K., Molina, A., Govers, G.: Tracking spatial variation in river load from Andean highlands to inter-Andean valleys. *Geomorphology* **308**, 175–189 (2018)
7. Recking, A.: Influence of sediment supply on mountain streams bedload transport. *Geomorphology* **175–176**, 139–150 (2012)
8. Goode, J.R., Luce, C.H., Buffington, J.M.: Enhanced sediment delivery in a changing climate in semi-arid mountain basins: implications for water resource management and aquatic habitat in the northern Rocky Mountains. *Geomorphology* **139**, 1–15 (2012)
9. Pellegrini, G., Martini, L., Cavalli, M., Rainato, R., Cazorzi, A., Picco, L.: The morphological response of the Tegnass alpine catchment (Northeast Italy) to a Large Infrequent Disturbance. *Sci. Total Environ.* **770**, 145209 (2021)
10. Rainato, R., Martini, L., Pellegrini, G., Picco, L.: Hydrological, geomorphic and sedimentological responses of an alpine basin to a severe weather event (Vaia storm). *CATENA* **207**, 105600 (2021)
11. Takayama, S.: Bedload movement in torrential mountain streams. *Tokyo Geograph. Paper* **9**, 169–188 (1965)
12. Cassel, M., Dépret, T., Piégay, H.: Assessment of a new solution for tracking pebbles in rivers based on active RFID. *Earth Surf. Proc. Land.* **42**, 1938–1951 (2017)
13. Oss Cazzador, D., Rainato, R., Cavalli, M., Lenzi, M.A., Picco, L.: Integrated analysis of sediment source areas in an Alpine basin. *CATENA* **188**, 104416 (2020)
14. Oss Cazzador, D., Rainato, R., Mao, L., Martini, L., Picco, L.: Coarse sediment transfer and geomorphic changes in an alpine headwater stream. *Geomorphology* **376**, 107569 (2021)
15. Church, M., Hassan, M.: Mobility of bed material in Harris Creek. *Water Resour. Res.* **38**(11), 1237–1249 (2002)

16. Ivanov, V., Radice, A., Papini, M., Longoni, L.: Event-scale pebble mobility observed by RFID tracking in a pre-alpine stream: a field laboratory. *Earth Surf. Proc. Land.* **45**(3), 535–547 (2020)
17. Schneider, J.M., et al.: Scaling relationships between bed load volumes, transport distances, and stream power in steep mountain channels. *J. Geophys. Res. Earth Surf.* **119**, 533–549 (2014)
18. Milan, D.J.: Virtual velocity of tracers in a gravel-bed river using size-based competence duration. *Geomorphology* **198**, 107–114 (2013)
19. Mao, L., Toro, M., Carrillo, R., Brardinoni, F., Fraccarollo, L.: Controls over particle motion and resting times of coarse bed load transport in a glacier-fed mountain stream. *J. Geophys. Res. Earth Surf.* **125**(4), e2019JF005253 (2020)
20. Mao, L., Carrillo, R.: Temporal dynamics of suspended sediment transport in a glacierized Andean basin. *Geomorphology* **287**, 116–125 (2017)
21. Rainato, R., Mao, L., Picco, L.: The effects of low-magnitude flow conditions on bedload mobility in a steep mountain stream. *Geomorphology* **367**, 107345 (2020)
22. Beylich, A.A., Laute, K.: Sediment sources, spatiotemporal variability and rates of fluvial bedload transport in glacier-connected steep mountain valleys in western Norway (Erdalen and Bødalen drainage basins). *Geomorphology* **228**, 552–567 (2015)
23. Comiti, F., Mao, L., Penna, D., Dell’Agnese, A., Engel, M., Rathburn, S., Cavalli, M.: Glacier melt runoff controls bedload transport in Alpine catchments. *Earth Planet. Sci. Lett.* **520**, 77–86 (2019)
24. Carrillo, R., Mao, L.: Coupling sediment transport dynamics with sediment and discharge sources in a glacial Andean basin. *Water* **12**, 3452 (2020)
25. Mao, L., Carrillo, R., Escauriaza, C., Iroume, A.: Flume and field-based calibration of surrogate sensors for monitoring bedload transport. *Geomorphology* **253**, 10–21 (2016)
26. Bertoncetto, P.: Monitoraggio del trasporto solido di fondo in un bacino Andino (Estero Morales, Cile) tramite metodologia bedload tracing. Tesi Magistrale per Corso di Laurea in Scienze Forestali ed Ambientali. Università degli Studi di Padova (2016)
27. Haschenburger, J.K., Church, M.: Bed material transport estimated from the virtual velocity of sediment. *Earth Surf. Proc. Land.* **23**, 791–808 (1998)
28. Vázquez-Tarrió, D., Menéndez-Duarte, R.: Bedload transport rates for coarse-bed streams in an Atlantic region (Narcea River, NW Iberian Peninsula). *Geomorphology* **217**, 1–14 (2014)

Hydraulic Roughness Estimation Induced by Riparian Vegetation in Tuscany Rivers for Management Purposes



Matteo Rillo Migliorini Giovannini, Andrea Dani, Rossana Saracino, Andrea Signorile, and Federico Preti

Abstract Riparian vegetation and its management on vegetated bank and floodplains can affect hydraulic and hydrologic characteristics of the river flow and can reduce or increase hydraulic risk, especially in downstream urban areas in small catchments.

In the present work, roughness estimation has been carried out by applying models that take into account relatively simple descriptive parameters, i.e. the diameter d (m) and the spatial density of plants m (N_p/m^2). Vegetation density was gauged on homogeneous areas by using forest-related field surveys on river bank and floodplain on Tuscan rivers and creeks: Albegna river, Arbia stream, Ombrone Grossetano river, Ombrone Pistoiese stream and Tevere river. An alternative field survey method based on the MOTI app, developed by the School of Agricultural, Forest and Food Sciences HAFL of Zollikofen for forest environments, was tested to evaluate its performance in the riparian zone. This speditive approach can provide basal area, number of plants per hectare by using relascope and optical theory to obtain the needed parameters for the most widespread roughness estimation models. Significant results were obtained for the $m = f(d)$ relations, which lead to estimates of roughness and associated hydraulic risk, useful for management purposes.

Keywords Riparian vegetation · Roughness · Hydraulic modeling · Flood risk · Best management practices

1 Introduction

Riparian zones are the buffers between terrestrial and aquatic ecosystems along watercourses, that affect and is affected by the presence of water [1]. In the landscape they function as corridors with flowing energy, material and biodiversity for

M. Rillo Migliorini Giovannini (✉) · A. Dani · R. Saracino · A. Signorile · F. Preti
Dipartimento di Scienze E Tecnologie Agrarie, Alimentari, Ambientali e Forestali, Università
Degli Studi di Firenze, Firenze, Italy
e-mail: matteo.rillomigliorini@unifi.it

adjacent ecosystems. Riparian vegetation has the capacity to deliver an high amount of Environmental Services relative to their extent in the landscape [2]. Among them stabilization and erosion control; flow attenuation; flood protection.

Hence, vegetation along watercourses has a significant influence on resistance, velocity distribution and turbulence intensity, features that significantly depend on the vegetation properties, consistency and distribution patterns [3]. Moreover, plant form can have a significant effect on the mean flow field and, therefore, potentially influence riverine and wetland system management strategies [4].

Previous studies asserted that locally vegetation reduces flow rate, consequently increasing flow resistance [5, 6]. However, it should also be considered that for water section-to-height ratio (B/H) greater than $10 \div 15$, the effect of riverbank vegetation on the flow is negligible, except on vegetated strips [7].

Among riparian woody species, there are some species, mainly belonging to *Salicaceae* and *Betulaceae*, which can survive to flooding events [8–11]. These species exhibit a set of adaptive traits that allowed them to sustain their population within naturally disturbed riverine environments [12]. However, anthropogenic pressure and disturb have advanced the spread of invasive alien species, above all *Robinia pseudoacacia*.

Vegetation preservation is significant in the ecology of natural and artificial system, specifically along water courses [13]. Nevertheless, riparian vegetation preservation practices have not been often encouraged because of increased flow resistance and decreased flood discharge efficiency compared to unvegetated regions [14]. Under human controlled river ecosystems riparian woody vegetation is managed by coppicing, often with the main purpose to enhance the discharge capacity of the rivers and thus mitigate the flood hazards [8, 15]. Different silvicultural management strategies should also be applied according to spatial distribution of trees in the riparian zone, to reconcile the need of mitigating flood hazards with the need of preserving the ecology of the water systems [16]. Thus, managing riparian vegetation's growth is fundamental in mitigating the flood risk in urban and rural areas [17, 18]. Usually flood peak has been controlled by adopting solutions based on civil engineering, aimed at reducing flow peak discharge and water levels through traditional hydraulic structures and infrastructures that affect natural development of riparian ecosystems over time [19, 20].

Estimation of flow resistance and, therefore, of roughness coefficient is a fundamental factor in constructing river stage-discharge curves, especially during flood events [21].

As a matter of fact, several studies have proposed different formulae to calculate flow resistance of vegetation, due to its great importance in river management and significant effects on channel conveyance [14, 21–32]. The flow–vegetation drag mainly depends on morphological properties and elastic behavior of plants when subjected to the hydrodynamic load of the river flow [14]. Pasquino et al. (2018) pointed out that in a previous study, Aberle and Järvelä (2013) found that the frontal area of a fully submerged willow (*Salix spp.*) progressively reduces to 82% of its original value in “still air” (i.e., not loaded by hydrodynamic forces) as the flow velocities increase up to 1 m/s, without further reduction for velocities above 1 m/s

[8, 14]. Sellin and van Beesten (2003) pointed out that the resistance coefficient in their study varies both annually and with seasons due to the annual cycle of vegetation growth that conducted to a corresponding reduction in whole channel mean velocity as the resistance coefficient increases during the growing season [33]. In several studies it is also affirmed that whenever the vegetation cover of the embankments is kept elastic, it bends with the increase of the water current, reducing its volume and flow resistance until it is finally crushed on the ground at moments of maximum flow [4, 22, 34]. In this way the flow velocity close to the ground surface can be sufficiently reduced and at the same time the maximum flow rate guaranteed. Too rigid plant elements cause turbulence and erosive phenomena. Hence, some previous studies showed that most of the typically riparian species decreases their bending capacity significantly when the stems reach a diameter >4 cm, indicating that care and management interventions are appropriate starting from a diameter of approximately 4 cm [5, 35, 36]. This ensures that the vegetation behaves flexibly during floods, can cover and protect the soil and thus prevent erosion processes as much as possible. Therefore, this implies the need for a coppice cut also to restore the flow capacity of the section. Also Pasquino et al. (2018) in their study concluded that a diameter of 3 cm can be identified as a threshold value above which stems behave as almost rigid elements for a reference flow velocity of 1 m/s, with a significant impact on the flow resistance and the river bank stability [8]. The larger is the basal diameter, the lower is height reduction relative to the stem height.

The aim of the present study is to find a correlation between age, diameter and roughness of riparian vegetation, so that land managers could assess intervention to take under control the flow resistance caused by plants, without unnecessarily harvesting, preserving riparian ecosystems.

2 Material and Methods

2.1 Study Area

The subject of this work is the riparian vegetation that grows along the banks of Tuscan streams and rivers. In particular the watercourses are: Arbia stream, Ombrone Pistoiese stream, Ombrone Grossetano river, Albegna river and Tevere river. Tracts of low and high plains have been identified by the presence of hydrophilic vegetation, mainly *Populus spp.*, *Salix spp.* and *Alnus spp.*, and also invasive alien species such as *Robinia pseudoacacia*. The tree stands are mostly managed by coppicing and the ordinary vegetation maintenance is carried out by local authorities in accordance with the Tuscany Regional Law on water courses management and protection and conservation of the Tuscan ecosystem [37] (Fig. 1)



Fig. 1 Watercourses (blue lines) and samples (red dots) localization

2.2 Methods for Field Surveys

As above mentioned, there are several different formulae to calculate vegetation roughness, mainly depending on the water surface level and on the characteristics of vegetation, but the most appropriate for our investigation has been considered that of Baptist et al. (2007), as a proposal for the flow resistance caused by non-submerged rigid vegetation [27, 38]:

$$n = \sqrt{\frac{mC_D D Y}{2}} \left(\frac{Y^{\frac{1}{6}}}{g^{\frac{1}{2}}} \right) \quad (1)$$

where m (m^{-2}) is the density expressed as the number of trees per unit area, C_d the average drag coefficient, d (m) the average diameter of the trees and Y (m) the water level.

In our further calculations it has been considered a constant water depth (Y) of 1 m, to guarantee non-submersion of surveyed riparian vegetation.

In order to obtain parameters to analyze roughness with Baptist's formula, it was necessary to carry out field surveys, in which we collected the diameter and the number of plants, that, once processed, returned average diameter d and density m . To calculate roughness coefficient n , using the (1), the data collection methodology is described below.

Thus, tree stands with different ages and diameters have been identified along the banks of the Tuscan water courses.

A new methodology was also tested for acquiring data in the field more quickly by using the MOTI smartphone application [39].

Once a vegetational representative area has been identified, the tracing of the test area was carried out. Therefore, within this area, the diameters of each tree stem, the age of different plants are recorded on a pedestal to estimate the average age of the riparian tree stand and, for a better understanding of the cenosis, the average height of the riparian forest.

The diameters were measured with the dendrometer stand, the ages were measured with the Pressler gimlet and the heights with the Suunto hypsometer. The collected data are subsequently reported on a spreadsheet and the average diameter (m) and the density of the tree stand (N_p/ha and N_p/m^2) were calculated.

In addition to the above-mentioned traditional field survey, a virtual field survey method was performed on some test areas, using the MOTI open source smartphone application, which bases its technology on relascope theory and on optical theory for the survey of forest stands [40]. The app is the result of a project carried out by the University School of Agronomic, Forestry and Food Sciences (BFH-HAFL) in collaboration with the Technical and Informatic Department of the Bernese Specialized University School (BFH-TI). Specifically, MOTI is able to detect essential dendrometric measurements in a simple, fast and reliable way, such as the basal area, the number of trees per hectare, the dendrometric height and the cormometric commission [41].

After calibrating the application, the first step involves establishing the size of the circular test area (depending on average size of plant diameter) which for this study was 300 m² or with a radius of about 10 m.

Once this area has been designated and its coordinates have been detected, in order to establish whether or not a plant falls within the virtual area, it is necessary to establish a numbering factor appropriate to the type of tree stand. This factor affects the viewing angle of the mobile phone and determines the “weight” of the basal area of each tree on the total population [42].

The tree stands examined in this study are mainly governed by high density coppice with diameters belonging mainly to classes below 20 cm; therefore, it was used a numbering factor (φ) equal to 1. A tree is virtually counted within the area if its diameter is wider than the pointers (which simulate the width of the relascope band).

Subsequently, all the individuals within the virtual area are counted, and finally the application returns an interface with the dendrometric results.

3 Results and Discussion

Different vegetation scenarios generate different effects on the hydraulic characteristics of the watercourse. Therefore, each scenario translates into a relative roughness coefficient n .

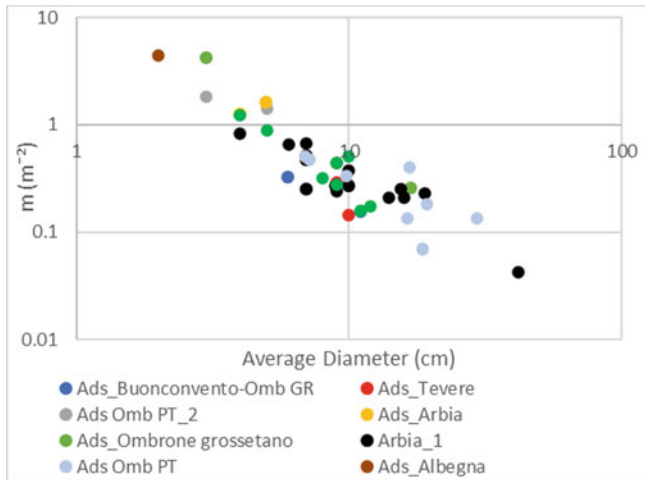


Fig. 2A Correlation between density (m) and average stem diameter (d)

Figures 2A and 2B were constructed to analyze vegetation evolution over time. Hence, they show the correlation between density and average diameter. For these curves it was necessary to detect, on the banks of various Tuscan water courses, the main parameters of the tree vegetation:

- m = number of plants per unit area (N_p/ha and N_p/m^2);
- dg = average diameter (m);
- *average age* of the stand (years).

Surveyed data shows variability due to the different environmental characteristics of water courses; the numerosity of the sample analyzed and its localization on only a few river courses, does not allow, at the moment, to consider a regression reliable; in fact, the purpose is to highlight the method and the variability in the calculation of roughness with the proposed formulas; the collected parameters fit into the roughness formula proposed by Baptist et al. (2007) useful for hydraulic modeling and, consequently, for choosing the best maintenance approach [27]. In Fig. 2B, data were also compared to other studies on herbaceous vegetation [43–45].

This relationship follows the trend of the data obtained from the study by Van Velzen et al. (2003) and is in agreement with other international case studies [5; 46]. The greater is the average diameter of a stand, the smaller is the number of plants per surface unit.

The correlation between m and *age* follows the same previous trend, also visible in Fig. 3, derived from the fact that, in the surveyed tree stands with a maximum age of about 15–18 years, the average annual increase was equal, in average, to about one centimeter.

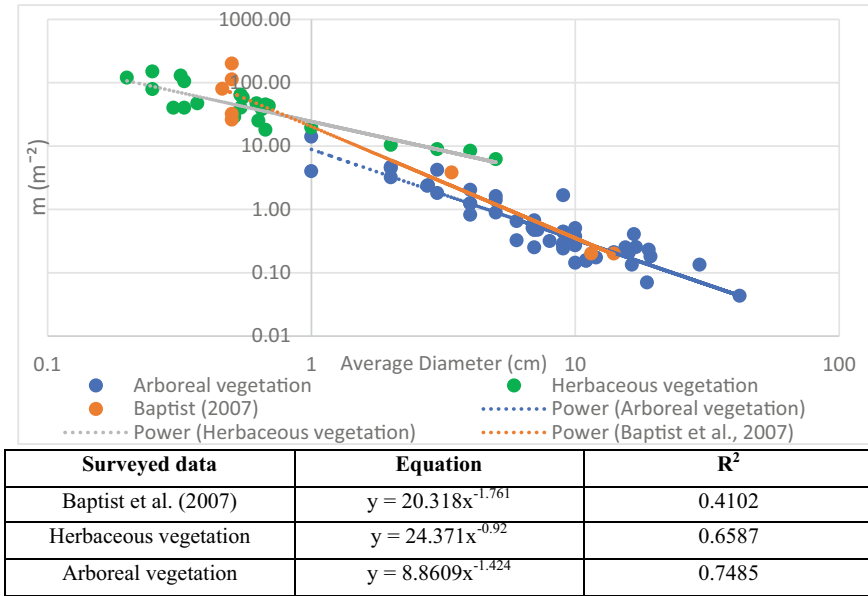


Fig. 2B. Comparison between Baptist et al. (2007), arboreal and herbaceous vegetation data. In the table are shown trend equations and their R²

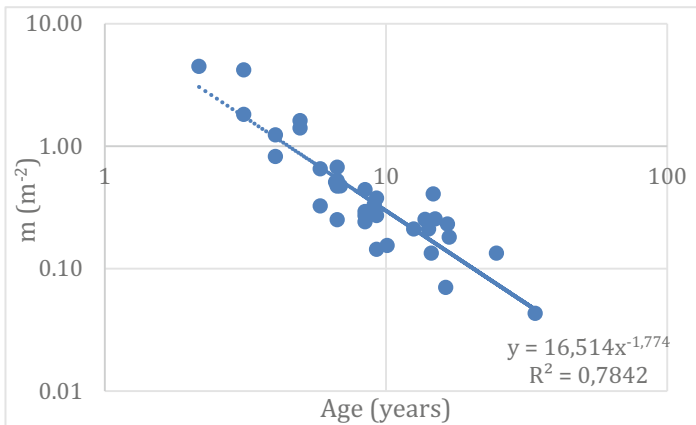


Fig. 3 Correlation between density *m* and average age

This preliminary result will be further investigated: indeed, the impression from the first analysis that the origin (gamic or agamic) of the stem, does not decisively affect the variation in hydraulic roughness, must be confirmed.

Figure 4 shows the correlation between roughness coefficient and average diameter of surveyed tree stands, all managed by coppicing. It has been considered a

constant water depth (Y) of 1 m, in order to guarantee non-submersion of surveyed riparian vegetation. It is also shown, as a comparison, roughness calculated using Järvelä formula (2), with Leaf Area Index (LAI) chosen from literature, variable between 5 and 3.7 as a likely value for floodplain covered by poplars [31], as well as black poplar specific parameters Cd_χ , χ and u_χ , while we set u_m , i.e. the cross sectional mean flow velocity, estimated equal to 1.6 m/s for rivers along which vegetation has been surveyed [14, 23–25, 30–32].

$$n = \sqrt{\frac{Cd_\chi * LAI * \left(\frac{u_m}{u_\chi}\right)^\chi}{2}} \left(\frac{Y^{\frac{1}{6}}}{g^{\frac{1}{2}}}\right) \tag{2}$$

In the first section (orange dots), is showed the sudden raise of the roughness coefficient strictly connected with tree stand density increase, simulating the vegetation scenario following a clear cut starting from diameter = 0 cm and Manning’s $n = 0.035$ up to the diameter of 3 cm. The roughness then decrease due to an ever decreasing in the number of plants per surface unit such as to create lower resistance to the motion of the flow. The second section (blue dots) shows the Manning’s n coefficient between 3 and 10 cm diameter. Roughness coefficient has a decrease probably due to the continuative natural competition of the tree sprouts. This leads to an even more decrease in the number of plants per unit of surface and an increase in the average diameter of the stand. The third section (grey dots) shows a stable slightly increasing trend in the roughness coefficient, justified by the stabilization in

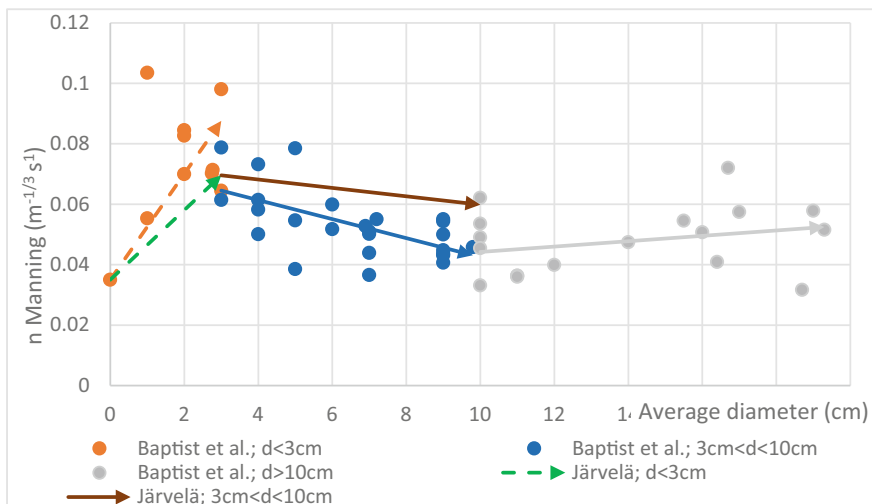


Fig. 4 Correlation between Manning’s n and diameter calculated with Baptist et al. and Järvelä formulae [24, 27]

the density of the stand with an increase in its average diameter and therefore by the loss of flexibility of the woody vegetation that opposes against water flow.

However, to reach a more accurate Manning's n value using Järvelä and also Nepf formulae for partially submerged vegetation, further investigations should be conducted on flexible vegetation height and streamlining, parameters not so easy to determine because variable according to the biomechanical characteristics of the stems [23–26, 29, 30, 38].

4 Conclusions

Plants of a smaller diameter (younger shoots) are more flexible, and better suitable for riverbanks stabilization, regardless of species, in accordance with Suttili et al. [6]. The flexibility of the stems and branches decrease over the time, but 10 years after harvesting, roughness coefficient stabilizes, and plants behave even more as rigid elements. Maintaining an high flexibility means that plants in flood conditions are able to bend down reducing turbulence effects and acting as a protection layer against bank erosion, instead of potentially causing hydraulic blockage in case of breaking. This target could be achieved with a more frequent maintenance in order to preserve its “flexibility function”.

However, statistical reliability of the previously proposed methods are still being tested and analyzed, and will be presented in future studies.

According to Pasquino et al. [8] it could be useful to evaluate the maximum tolerable plant size from a hydraulic perspective, that will bring, from a vegetation management perspective, to identifying a threshold value of the diameter above which plants must be coppiced.

This type of management should be taken into account along water courses next to inhabited areas, in order to maintain the plant community with that certain age and diameter, and, thus, the optimal roughness, without drastic clear-cuts. On the other hand, when there is no risk for public safety, it is possible to leave free plant growth and evolution for naturalistic purposes.

These results can be utilized for identifying objective hydrodynamic criteria to be adopted by land managers, e.g. land reclamation authorities, for coppice management of riparian vegetation in human influenced river ecosystems, in order to plan vegetation harvesting along water courses.

References

1. Naiman, R.J., Decamps, H., McClain M.E.: *Riparia: Ecology, Conservation, and Management of Streamside Communities*. Elsevier, London (2010)

2. González, E., Sher, A.A., Tabacchi, E., Masip, A., Poulin, M.: Restoration of riparian vegetation: a global review of implementation and evaluation approaches in the international peer-reviewed literature. *J. Environ. Manage.* **158**, 85–94 (2015)
3. Xia, J., Nehal, L.: Hydraulic features of flow through emergent bending aquatic vegetation in the Riparian Zone. *Water* **5**, 2080–2093 (2013)
4. Wilson, C.A.M.E., Stoesser, T., Bates, P.D., Batemann Pinzen A.: Open channel flow through different forms of submerged flexible vegetation. *J. Hydraul. Eng.* **29**, 847–853 (2003)
5. Weitzer, Ch., Doppler, F., Florineth, F.: Untersuchungen über die Wirksamkeit von Pflanzen in Einzugsgebieten des Forsttechnischen Dienstes der Wildbach- und Lawinerverbauung. Forschungsbericht, im Auftrag des BM:LF und der Universität f. Bodenkultur Wien, p. 81 (1998)
6. Sutili, F.J., Denardia, L., Durlob, M.A., Rauch, H.P., Weissteiner, C.: Flexural behaviour of selected riparian plants under static load. *Ecol. Eng.* **43**, 85–90 (2012)
7. Preti, F., Guarnieri, L.: Criteri per la manutenzione della vegetazione ripariale di corsi d'acqua collinari e montani. Convegno AIIA2005: Catania, 27–30 giugno 2005 - L'ingegneria agraria per lo sviluppo sostenibile dell'area mediterranea (2005)
8. Pasquino, V.: Hydrodynamic behaviour of European black poplar (*Populus nigra* L.) under coppice management along Mediterranean river ecosystems. *River Res. Applic.* **34**, 586–594 (2018)
9. Camporeale, C., Perucca, E., Ridolfi, L., Gurnell, A.M.: Modeling the interactions between river morphodynamics and riparian vegetation. *Rev. Geophys.* **51**, 379–414 (2013)
10. Corenblit, D., Steiger, J., Tabacchi, E., González, E., Planty-Tabacchi, A.-M.: Ecosystem engineers modulate exotic invasions in riparian plant communities by modifying hydrogeomorphic connectivity. *River Res. Appl.* **30**(1), 45–59 (2014)
11. Gurnell, A.: Plants as river system engineers. *Earth Surf. Proc. Land.* **39**(1), 4–25 (2014)
12. Glenz, C., Schlaepfer, R., Iorgulescu, I., Kienast, F.: Flooding tolerance of Central European tree and shrub species. *For. Ecol. Manage.* **235**(1–3), 1–13 (2006)
13. López, F., García, M.: Mean flow and turbulence structure of open channel flow through non-emergent vegetation. *J. Hydraul. Eng.* **127**, 392–402 (2001)
14. Aberle, J., Järvelä, J.: Flow resistance of emergent rigid and flexible floodplain vegetation. *J. Hydraul. Res.* **51**, 33–45 (2013)
15. Darby, S.E.: Effect of Riparian vegetation on flow resistance and flood potential. *J. Hydraulic Eng.* **125**, 443–454 (1999)
16. Tabacchi, E., Lambs, L., Guilloy, H., Planty-Tabacchi, A., Muller, E., Decamps, H.: Impacts of riparian vegetation on hydrological processes. *Hydrol. Process.* **14**, 2959–2976 (2000)
17. De Paola, F., Ranucci, A.: Analysis of spatial variability for stormwater capture tank assessment. *Irrig. Drain.* **61**, 682–690 (2012)
18. Večeřa, M., et al.: Mapping species richness of plant families in European vegetation. *J. Veg. Sci.* **32**(3), 13035 (2021)
19. Chanson, H., Gualtieri, C.: Similitude and scale effects of air entrainment in hydraulic jumps. *J. Hydraul. Res.* **46**, 35–44 (2008)
20. Lama, G.F.C., et al.: Hydraulic efficiency of green-blue flood control scenarios for vegetated rivers: 1D and 2D unsteady simulations. *Water* **13**, 2620 (2021)
21. Fathi-Maghadam, M., Kouwen, N.: Nonrigid, Nonsubmerged, Vegetative Roughness on Floodplains. *J. Hydraul. Eng.* **23**(1) (1997)
22. Stone, M.C.: Bending of submerged woody riparian vegetation as a function of hydraulic flow conditions. *River Res. Appl.* **29** (2011)
23. Järvelä, J.: Flow resistance of flexible and stiff vegetation: a flume study with natural plants. *J. Hydrol.* **269**, 44–54 (2002)
24. Järvelä, J.: Determination of flow resistance caused by non-submerged woody vegetation. *Int. J. River Basin Manag.* **2**(1), 61–70 (2004)
25. Jalonen, J., Järvelä, J., Aberle, J.: Leaf Area Index as vegetation density measure for hydraulic analyses. *J. Hydraul. Eng.* **139**(5), 461–469 (2013)
26. Nepf, H.M.: Hydrodynamics of vegetated channels. *J. Hydraul. Res.* **50**, 262–279 (2012)

27. Baptist, M.J., Babovic, V., Rodríguez, U.J., Keijzer, M., Uittenbogaard, R.E., Mynett, A., Verwey, A.: On inducing equations for vegetation resistance. *J. Hydraul. Res.* **45**, 435–450 (2007)
28. Kouwen, N., Li, R.-M., Simons, D.B.: Flow resistance in vegetated waterways. *Trans. ASAE* **24**, 684–690 (1981)
29. Luhar, M., Nepf, H.M.: From the blade scale to the reach scale: a characterization of aquatic vegetative drag. *Adv. Water Resour.* **51**, 305–316 (2013)
30. Box, W., Järvelä, J., Västilä, K.: Flow resistance of floodplain vegetation mixtures for modelling river flows. *J. Hydrol.* **601** (2021)
31. Antonarakis, A.S., Richards, K.S., Brasington, J., Muller, E.: Determining leaf area index and leafy tree roughness using terrestrial laser scanning. *Water Resour. Res.* **46**, W06510 (2010)
32. Antonarakis, A.S., Richards, K.S., Brasington, J., Bithell, M.: Leafless roughness of complex tree morphology using terrestrial Lidar. *Water Resour. Res.* **45**, W10401 (2009)
33. Sellin, R.H.J., van Beesten D.P.: Conveyance of a managed vegetated two-stage river channel. *Water Manag.* 157(WMI), 21–33 (2003)
34. Tyminski, T., Kaluza, T.: Investigation of mechanical properties and flow resistance of flexible Riverbank vegetation. *Pol. J. Environ. Stud.* **21**(1), 201–207 (2012)
35. Florineth, F.: Pflanzen statt Beton. *Handbuch zur Ingenieurbiologie und Vegetationstechnik*. Patzer Verlag, Berlino – Hannover (2004)
36. Weitzer-Bruckner, Ch., Doppler, F., Florineth, F.: Untersuchungen über die Wirksamkeit von Pflanzen in Einzugsgebieten des Forsttechnischen Dienstes der Wildbach- und Lawinverbauung. *Wildbach und Lawinverbauung* **142**, S.7–27 (2000)
37. D.G.R.T 1315/2019. Direttive regionali per la manutenzione dei corsi d'acqua e per la protezione e conservazione dell'ecosistema toscano - art. 24 bis l.r. 80/2015 - art. 22, comma 2, lettera b) l.r. 79/2012. Sostituzione della d.g.r. 293/2015
38. Solari, L., Paris, E., De Cicco, P.N., Piccoli F., Francalanci, S., Gabellini, F.: Accordo Collaborazione Scientifica Regione Toscana–E Dipartimento Di Ingegneria Civile E Ambientale Dell'universita' Di Firenze Per Attivita' Di Ricerca Per La Mitigazione Del Rischio Idraulico Nella Regione Toscana. *Relazione Tecnica Finale Attività E-1'*: Interazione vegetazione in alveo e corrente: studi sperimentali e indirizzi operativi. (2014)
39. <http://www.moti.ch/drupal/?q=it>
40. Bitterlich, W.: The Relascope Idea: Relative Measurements in Forestry. *Commonwealth Agricultural Bureaux*, p. 242 (1984)
41. Noiret, O.: Les smartphones au service de la forêt. *Silva Belgica mai-juin* **2016**, 10–14 (2016)
42. La Marca, O.: *Elementi di dendrometria*. Patron Editore, Bologna (2004)
43. Errico, A.: The effect of flexible vegetation on flow in drainage channels. Field surveys and modelling for roughness coefficients estimation. Ph.D. Thesis. Università degli Studi di Firenze (2016)
44. Lama, G.F.C., Errico, A., Francalanci, S., Chirico, G.B., Solari, L., Preti, F.: Comparative analysis of modeled and measured vegetative Chézy flow resistance coefficients in a drainage channel vegetated by dormant riparian reed. In: *IEEE International Workshop on Metrology for Agriculture and Forestry (MetroAgriFor)* - Portici, Italy 24–26/10/2019, pp. 180–184 (2019)
45. Errico, A., Lama, G.F.C., Francalanci, S., Chirico, G.B., Solari, L., Preti F.: Validation of global flow resistance models in two experimental drainage channels covered by *Phragmites australis* (Common reed). In: *E-proceedings of the 38th IAHR World Congress 1–6 September 2019*, Panama City, Panama (2019)
46. Van Velzen, E.H., Jesse, P., Cornelissen, P., Coops, H.: *Stromingsweerstand vegetatie in uiterwaarden*. Handboek. Part 1 and 2. RIZA Reports 2003.028 and 2003.029, Arnhem, The Netherlands. (2003)

The Effect of Soil and Vegetation Spatial Variability on Modelling Hydrological Processes for Irrigation Optimisation at Large Scales



Shawkat B. M. Hassan, Giovanna Dragonetti, Alessandro Comegna, Asma Sengouga, Nicola Lamaddalena, and Antonio Coppola

Abstract Spatial variability of soil and vegetation parameters are crucial in agro-hydrological models concerned with optimizing irrigation volumes at large scales. Measuring aforementioned parameters can be time consuming and laborious, so it is more efficient to aggregate their spatial variability without significantly affecting the optimal irrigation fluxes at large scales. The main purpose of this paper is to study the effect of spatial variability of soil hydraulic parameters and vegetation indices (i.e., leaf-area index, LAI, and crop coefficient, K_c) and soil profiles' hydraulic parameters on the optimal irrigation volumes. Here we analyse the effect of aggregating the spatial variability of soil and vegetation parameters on a 140-ha irrigation sector in "Sinistra Ofanto" irrigation system in Apulia Region, Southern Italy. Five soil profiles were excavated and their hydraulic parameters were measured. Remote sensing applications were used to obtain LAI and K_c using European space agency's Sentinel-2 images. Optimal irrigation volumes were calculated using FLOWS-HAGES agro-hydrological model at field scale using variable vegetation and soil inputs. Then, a sensitivity analysis was carried out by aggregating soil and vegetation parameters into sector scale. Aggregating vegetation parameters was carried out while preserving soil parameters variability. Aggregating soil parameters variability was carried out five times by applying each of the five measured profiles while preserving vegetation parameters. Aggregating vegetation parameters did not significantly change the optimal irrigation volumes and the resulting deep percolation volumes. However, aggregating soil parameters variability significantly affected the optimal irrigation volumes and the corresponding deep percolation volumes. Aggregating soil vegetation parameters is possible to facilitate irrigation management provided that soil parameters variability is preserved and the cropping pattern is relatively uniform.

S. B. M. Hassan (✉) · A. Comegna · A. Sengouga · A. Coppola
School of Agricultural, Forestry, Food and Environmental Sciences (SAFE), University of Basilicata, Viale Dell'Ateneo Lucano, 10, 85100 Potenza, PZ, Italy
e-mail: shawkat.hassan@unibas.it

G. Dragonetti · N. Lamaddalena
CIHEAM - Mediterranean Agronomic Institute of Bari IT, 70010 Valenzano, BA, Italy

© The Author(s), under exclusive license to Springer Nature Switzerland AG 2023
V. Ferro et al. (eds.), *AIIA 2022: Biosystems Engineering Towards the Green Deal*,
Lecture Notes in Civil Engineering 337,
https://doi.org/10.1007/978-3-031-30329-6_19

181

Keywords Spatial variability · Soil hydraulic parameters · Vegetation indices · Optimal irrigation volumes · Agrohydrological modelling

1 Introduction

Irrigation management, as many other agricultural and environmental issues, is more and more dealt with using physically-based agro-hydrological models [4, 6]. These models use mechanistic approaches to calculate water flow and solute transport in a soil–plant–atmosphere system [3, 9, 11]. Such models can be used as decision support tools to quantify and schedule optimal irrigation volumes at different spatial scales using soil, vegetation and meteorological parameters as inputs. However, the challenges lie in the spatial variability of different inputs when applied at large district or sector scales [4, 10]. In order to overcome these spatial variability challenges, input parameters may be aggregated to obtain parameters effective at the larger applicative scale of concern. As for soil parameters, geostatistical methods [13] and/or more or less complex averaging procedures [14, 15] can be used. In any case, this remains a difficult task, due to the nonlinearity of flow equations [14]. As for vegetation, similar approaches may be used. However, the effect of using different schemes for averaging vegetation parameters (Leaf Area Index, Root parameters, ...) on predicting water fluxes in the soil–vegetation–atmosphere is not immediate as it depends on the way the vegetation is accounted for in different agrohydrological models.

With these premises, the aim of this paper is to study the effect of aggregating the spatial variability of soil and vegetation parameters on optimising irrigation volumes for a 140-hectare irrigation sector in Apulia Region, Southern Italy. For this purpose, surface soil hydraulic parameters were obtained using tension infiltration experiments at 90 locations. Five excavation pits were dug in the sector to measure the soil hydraulic parameters for the subsurface soil layers using tension infiltration experiments. Also, remote sensing applications using Sentinel-2 satellite images were utilized to obtain the vegetation parameters (e.g., leaf-area index, LAI, and crop coefficient, K_c) for the year 2020.

Based on these data, FLOWS-HAGES model [4] was used to optimise the irrigation fluxes in the study area using the soil and vegetation spatially variable inputs. Then, two aggregation scenarios were used to analyse the effect of aggregating input parameters at sector scale on calculating the optimal irrigation fluxes by the model: 1) aggregating the spatial variability of vegetation parameters while preserving the spatial variability of soil hydraulic parameters, and 2) aggregating the spatial variability of soil hydraulic parameters and vegetation parameters. The simulation results were then compared in terms of optimal irrigation and deep percolation fluxes.

2 Materials and Methods

2.1 FLOWS-HAGES Agrohydrological Model

The agrohydrological simulations aiming at optimizing irrigation fluxes at different scales were carried out using FLOWS-HAGES model [4]. FLOWS-HAGES is a 1D vertical transient water flow model that numerically solves 1D Richards equation.

The model has two configurations to simulate irrigation: 1) introducing irrigation fluxes as an input, or 2) computing optimal irrigation fluxes by the model. In the first case, the model can be used to analyse irrigation fluxes actually applied by the farmers and their effect on agrohydrological processes in the root zone. In the second configuration, it can be used to optimise the irrigation fluxes taking into account the farmers' behaviour. The model computes the optimal irrigation fluxes and its timing based on the average soil water pressure head in the root zone, h_{av} , as shown in Fig. 1.

Irrigation starts when h_{av} becomes smaller than h_{crit} . The irrigation depth is calculated so that the water content at each depth is brought to field capacity (Fig. 1b). The critical head, h_{crit} , and irrigation depth, z_c , can be defined from the simulations using irrigation fluxes as input to analyse the farmers' behaviour.

As for the hydraulic properties, the surface layer of the soil profiles was assumed to have bimodal hydraulic properties, which were described by using the Durner water retention model [5]. The subsurface layers were assumed to have unimodal porous media. In this case, [12] soil water retention model was used. The unsaturated hydraulic conductivity, $K(h)$, was described using Mualem model [7] for both layers.

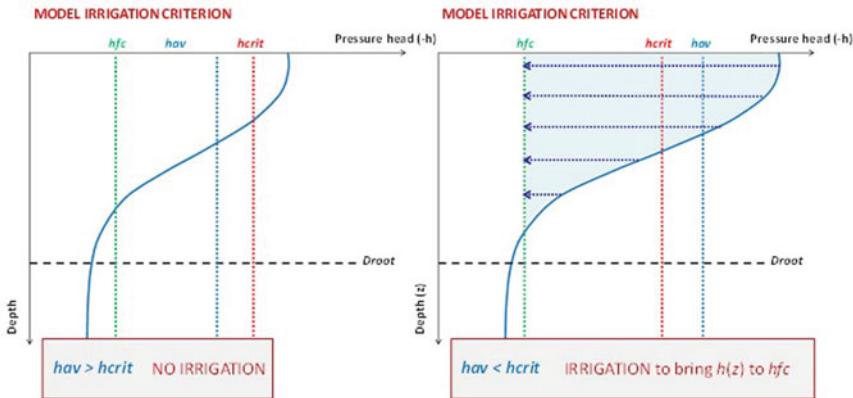


Fig. 1 Graphical view of the on which the model is based to compute the time and volume of irrigation. **a** h_{av} higher than h_{crit} , no irrigation is required; **b** h_{av} lower than h_{crit} , irrigation is required to bring the pressure head at the field capacity, h_{fc}

2.2 Study Area and Soil Database

The study area is sector 6 in district 10 in “Sinistra Ofanto” irrigation system in Apulia region, Southern Italy. Ninety locations were selected to measure surface bimodal hydraulic properties. Subsurface hydraulic properties were measured at 5 locations using 1-m-deep excavation pits. The study area was divided into 90 Thiessen polygons based on the 90 surface measurement sites using geographic information system (ArcGIS) (Fig. 2a). Each Thiessen polygon was assigned the surface hydraulic properties of its corresponding point. Subsurface hydraulic properties were assigned to each Thiessen polygon according to the nearest excavation pit. The sector is predominantly cropped with wine grapes (58% of the area) and the second predominant crop is peach (19% of the area) (Fig. 2b).

At each of the 5 excavation pits, a complete pedological description was carried out. At each of the 90 surface measurement sites, Durner’s bimodal and van Genuchten unimodal hydraulic parameters were obtained by using cumulative infiltration data coming from tension infiltrometer measurements [1, 3]. These cumulative infiltration data were then used as input in the HYDRUS 3D software to estimate hydraulic parameters by an inverse solution of the Richards 3D [8, 9]. Tension infiltration experiments were also carried out for the subsurface layers in the 5 excavation pits.



Fig. 2 The study area. On the left, the solid border represents sector 6, the dashed borders represent Thiessen polygons, the solid circles represent the 90 surface measurement sites, and the red triangles represent the excavation pits. On the right, the cropping pattern of the sector with wine grapes being the predominant crop occupying 58% of the area

2.3 Obtaining Vegetation and Irrigation Parameters for FLOWS-HAGES Simulations Using Geographic Information Systems and Remote Sensing Applications

European Space Agency's (ESA) Sentinel-2 satellite images with 10-m resolutions were utilized. Two satellite images were downloaded for each month in 2020. LAI was obtained at each pixel using ESA's SNAP software. K_c was then obtained at each pixel using the equation proposed by [2]. Zonal statistics tool on ArcGIS was then used to obtain the mean values of K_c and LAI for each Thiessen polygon for each image representing a day of the year. Time series of the evolution of K_c and LAI, along the year 2020, were created for each polygon using linear interpolation. Time series were then checked to remove the outliers.

As for the root system and the irrigation periods, we opted for assuming a single crop for each polygon. ArcGIS was used to create an intersection between the cropping pattern and the Thiessen polygons corresponding to the soil measurement sites. If a crop type occupied more than 70% of the Thiessen polygon area (dominant crop), which was the case for most Thiessen polygons, the Thiessen polygon was assumed to be cultivated with the dominant crop type. If else (no crop > 70%), a theoretical crop type was created with: 1) the weighted average of the root depth and 2) the irrigation period of the crop with the longer-lasting irrigation period.

2.4 Agrohydrological Simulations Using FLOWS-HAGES Model

In order to optimise irrigation fluxes in the study area, simulations were carried out first on the first configuration by introducing the registered irrigation fluxes as an input. The purpose of those simulations was to understand the farmers' irrigation management parameters. The output of these simulations was analysed in terms of the mean soil–water pressure head at different depths in the root zone. The irrigation fluxes and the pressure heads were plotted in order to graphically observe: 1) the irrigation periods of each crop type 2) the critical pressure head value, h_{crit} , the farmers tend on average to not overcome with their irrigation behaviour (in terms of volumes and timing) at each irrigation event, and 3) the depth z_c at which h_c is guaranteed by the farmer irrigation behaviour. The total number of simulations using this configuration is 90, corresponding to the 90 Thiessen polygons in the sector.

The second step was to carry out the simulations under the second configuration to optimise the irrigation fluxes. In this case, the irrigation periods, the critical pressure head, h_{crit} , and the critical depth, z_c , obtained by analysing the farmer behaviour under the first configuration, were used as input in the second configuration simulations. This allowed to optimise irrigation volumes by still accounting for the real farmer irrigation behaviour. Similar to the first configuration, the total number of simulations in this case was 90 simulations representing the Thiessen polygons.

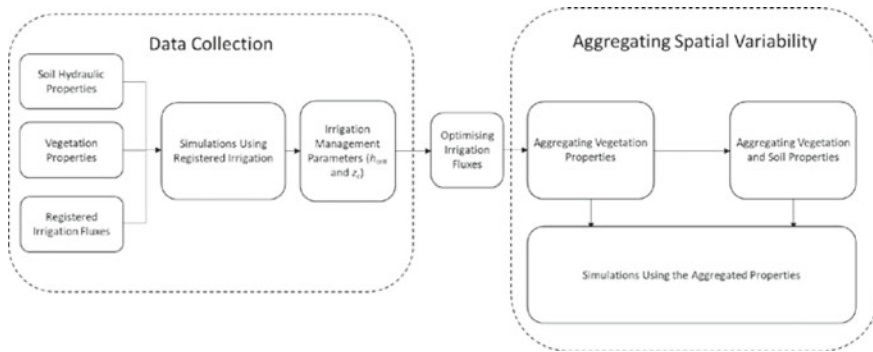


Fig. 3 A schematic view of the steps taken for agrohydrological simulations using spatially variable and aggregated soil and vegetation properties

In the third step, two aggregation scenarios were assumed: 1) aggregated vegetation parameters with spatially variable soil properties, and 2) aggregated soil properties and vegetation parameters. For the first case, irrigation fluxes were optimised for the 90 Thiessen polygons by using 90 different hydraulic parameters vectors, one for each polygon. As for the vegetation, a so called “virtual macrocrop” was assumed whose parameters were obtained by averaging the daily values of LAI and K_c over the entire sector. Therefore, a total of 90 simulations were carried out. In the second case, the vegetation parameters variability was aggregated into the macrocrop, while using a representative soil profile for the entire sector. This process was repeated 5 times for each of the 5 soil profiles excavated in the study area (Fig. 2a), for a total of 5 simulations. Figure 3 shows a schematic view of the data collected and the steps taken for running the agrohydrological simulations using spatially variable and aggregated soil and vegetation properties.

3 Results and Discussions

3.1 *Optimising Irrigation Fluxes for Spatially Variable Soil and Vegetation Parameters*

Figure 4 shows a comparison between the optimal irrigation fluxes obtained using FLOWS-HAGES model in m^3/ha and the registered irrigation fluxes in m^3/ha for each of the Thiessen polygons in 2020 as colour-graduated maps. The mean optimal irrigation fluxes were lower than the registered ones with the mean values of 1360 m^3/ha and 1693 m^3/ha , respectively. The deep percolation fluxes were also calculated using FLOWS-HAGES model for both the irrigation optimisation or using the registered irrigation fluxes as inputs. The deep percolation fluxes were negligible

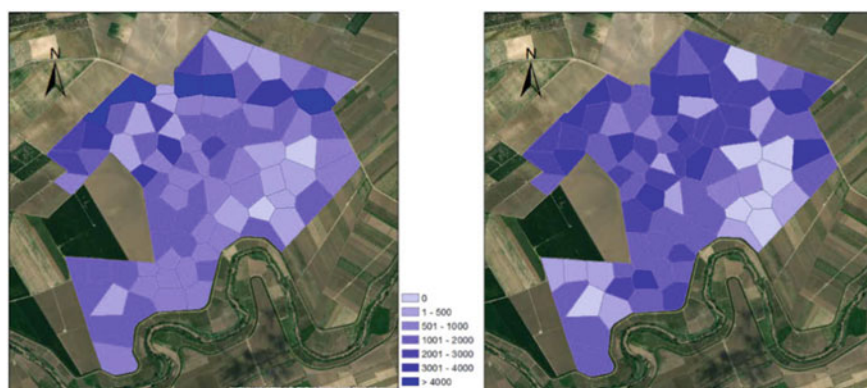


Fig. 4 The optimal irrigation fluxes obtained using FLOWS-HAGES model in m^3/ha (on the left) compared to the registered irrigation fluxes in m^3/ha (on the right) for each of the Thiessen polygons as colour-graduated maps. The legend in the middle shows the colour for each range of fluxes

with the values of $44 \text{ m}^3/\text{ha}$ and $43 \text{ m}^3/\text{ha}$ resulting from the optimal and registered irrigation fluxes respectively.

3.2 Aggregating Spatial Variability of Soil and Vegetation Parameters

Figure 5 shows the mean irrigation fluxes and the mean deep percolation fluxes obtained from three simulation scenarios: the registered irrigation, the optimal irrigation fluxes accounting for the spatial variability of different input parameters, and the optimal irrigation fluxes for the macrocrop while preserving soil parameters spatial variability. Figure 6 shows the mean irrigation and deep percolation fluxes obtained from registered irrigation and from five scenarios of aggregating soil parameters spatial variability.

Looking at Fig. 5 and Fig. 6, aggregating the vegetation parameters spatial variability does not significantly affect the optimal irrigation fluxes as it underestimated the optimal irrigation fluxes by only 2.2% while aggregating soil parameters variability drastically changes the optimal irrigation fluxes. This indicates the importance of soil parameters variability in agro-hydrological modelling.

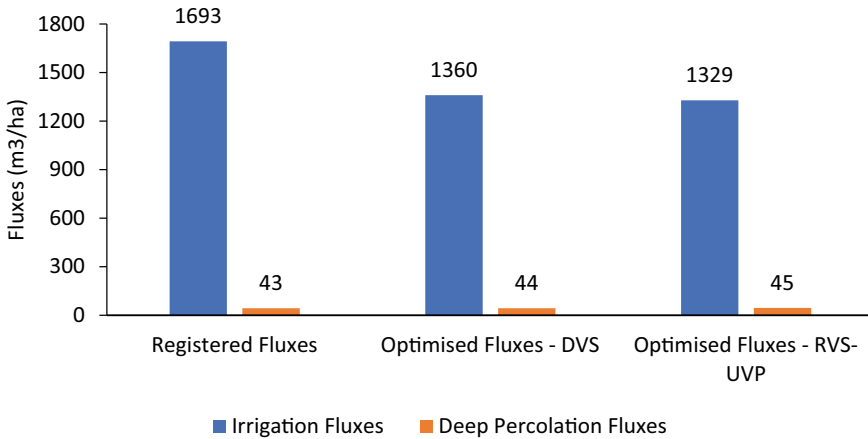


Fig. 5 The mean irrigation fluxes (blue bars) and the mean deep percolation fluxes (orange bars) obtained from three simulation scenarios: the registered irrigation, the optimal irrigation fluxes accounting for the spatial variability of different input parameters, and the optimal irrigation fluxes for the macrocrop while preserving soil parameters spatial variability. All the fluxes are in m³/ha

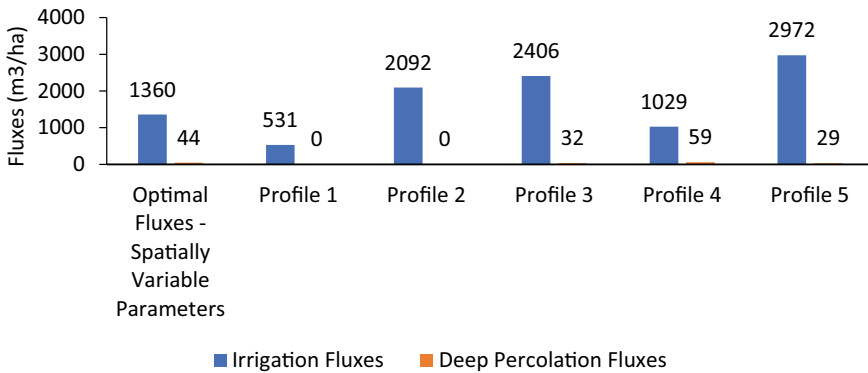


Fig. 6 The mean irrigation fluxes (blue bars) and the mean deep percolation fluxes (orange bars) obtained from registered irrigation fluxes and from 5 scenarios of aggregating soil parameters spatial variability. For each of the five scenarios, one of five excavation pits was considered representative of the entire sector

4 Conclusions

The main purpose of this study was to study the effect of soil and vegetation properties' spatial variability on optimising irrigation volumes at large scales. The results showed that accounting for the soil spatial variability is crucial in agro-hydrological models concerned with water flow and irrigation optimisation. Aggregating soil parameters spatial variability from local to sector scale proved to significantly affect

the model outputs in terms of optimal irrigation fluxes and the subsequent deep percolation fluxes. Also, the results showed that changing the soil hydraulic parameters would lead to completely different optimal irrigation fluxes.

On the other hand, aggregating vegetation parameters spatial variability into a sector scale did not affect those outputs significantly. This would facilitate irrigation management at large scale by reducing the number of input datasets regarding vegetation indices, such as LAI and K_c .

References

1. Ankeny, M.D., Kaspar, T.C., Horton, R.: Design for an automated tension infiltrometer. *Soil Sci. Soc. Am. J.* **52**(3), 893–896 (1988)
2. Beerli, O., et al.: K_c and LAI estimations using optical and SAR remote sensing imagery for vineyards plots. *Remote Sens.* **12**(21), 3478 (2020)
3. Coppola, A., et al.: Hydrological behaviour of microbiotic crusts on sand dunes: example from NW China comparing infiltration in crusted and crust-removed soil. *Soil Tillage Res.* **117**, 34–43 (2011)
4. Coppola, A., et al.: Identifying optimal irrigation water needs at district scale by using a physically based agro-hydrological model. *Water* **11**(4), 841 (2019)
5. Durner, W.: Hydraulic conductivity estimation for soils with heterogeneous pore structure. *Water Resour. Res.* **30**(2), 211–223 (1994)
6. Kroes, J.G., et al.: SWAP version 4. Wageningen Environmental Research (2017)
7. Mualem, Y.: A new model for predicting the hydraulic conductivity of unsaturated porous media. *Water Resour. Res.* **12**(3), 513–522 (1976). <https://doi.org/10.1029/WR012i003p00513>
8. Rassam, D., Šimůnek, J., Van Genuchten, M.: Modelling variably saturated flow with HYDRUS-2D. ND Consult, Brisbane (2003)
9. Šimůnek, J., Martinus, T., Genuchten, M.S.: Development and applications of the HYDRUS and STANMOD software packages and related codes. *Vadose Zone J.* **7**(2), 587–600 (2008). <https://doi.org/10.2136/vzj2007.0077>
10. Sposito, G.: Scale Dependence and Scale Invariance in Hydrology. UK Cambridge University Press, Cambridge (1998)
11. Van Dam, J.C., et al.: Theory of SWAP version 2.0; Simulation of water flow, solute transport and plant growth in the soil-water-atmosphere-plant environment. DLO Winand Staring Centre, Wageningen (1997)
12. van Genuchten, M.T.: A Closed-form equation for predicting the hydraulic conductivity of unsaturated soils. *Soil Sci. Soc. Am. J.* **44**(5), 892–898 (1980)
13. Warrick, A.W., Nielsen, D.R.: Spatial variability of soil physical properties in the field. In: Hillel, D. (ed.) *Applications of Soil Physics*, pp. 319–344. Academic Press, New York (1980)
14. Zhu, J., Mohanty, B.P.: Spatial averaging of van Genuchten hydraulic parameters for steady-state flow in heterogeneous soils: a numerical study. *Vadose Zone J.* **1**(2), 261–272 (2002)
15. Zhu, J., Young, M.H., van Genuchten, M.T.: Upscaling schemes and relationships for the Gardner and van Genuchten hydraulic functions for heterogeneous soils. *Vadose Zone J.* **6**(1), 186–195 (2007)

Conceptual Interpretation of Infiltration Under Sealing Process by Membrane Fouling Models



Francesca Todisco, Lorenzo Vergni, and Rita Ceppitelli

Abstract In the paper, the filtration membrane fouling models (Hermia, J.: Constant pressure blocking filtration laws-application to power law non-newtonian fluids, *Trans. of the Institution of Chemical Engineers*, 60,183–187. (1982).; Bolton, G., Kuriyel, R., LaCasse, D.: Combined models of membrane fouling: development and application to microfiltration and ultrafiltration of biological fluids, *Journal of Membrane Science*, 277, pag. 75–84 (2006).;), adapted to simulate the infiltration of overland flow through porous soils under seal formation, were tested. The validation dataset, provided by the SERLAB (Soil Erosion LABORatory, Italy), consists of runoff and infiltration rates measured at 5 min intervals in a sequence of four simulated rainfall (70 mm/h intensity), following initial tillage and lasting until the steady runoff is reached. As a porous medium, the soil is assumed to be the filter. The soil infilling that occurs during structural seal formation is assimilated to the membrane fouling process, and the turbid fluid is the flow enriched in fine particles due to the illuviation of the soil particles detached by raindrop impact and overland flow. The combination of two basic models, intermediate pore blocking (IPB) and standard pore blocking (SPB), yields the best fit. IPB brings about progressive superficial pore clogging and particle accumulation at the surface; in SPB, the particles illuviated by water accumulate inside the media on the walls of straight cylindrical pores. The results indicate the efficacy of models able to simulate multiple mechanisms participating in the structural modification of soil. Also, IPB model alone, contrary to SPB, provides reasonable estimates. This indicates that the dynamics of the soil surface hydrological properties remain active. At the same time, the pore constriction seems to run out quickly with the cumulative infiltration from tillage.

F. Todisco (✉) · L. Vergni

Department of Agricultural, Food and Environmental Sciences, University of Perugia, Borgo XX Giugno 74, 06121 Perugia, Italy
e-mail: francesca.todisco@unipg.it

R. Ceppitelli

Department of Mathematics and Informatics, University of Perugia, Via L. Vanvitelli, 1, 06123 Perugia, Italy

Keywords First order differential equations · Darcy's equation · Mathematical models · Soil crusting · Structural crust · Particle mobilization in soil · Rainfall sequences

1 Introduction

During rainfall, part of the sealing process [3] is caused by the surface compaction due to the drop impacting energy [4, 5], and part is due to the deposition within the soil profile of the fine particles mobilized by raindrop impact and overland flow and vertically transported by water [6]. The process of fine particles infilling the pores is typically not accounted for in the infiltration models under crust formation. The paper's objective is to evaluate if models, where infiltration is driven only by fine particles infilling of pores, pores obstruction and particles accumulation in the soil surface can describe the behaviour of the infiltration data. To this purpose, the filtration membrane fouling models [1, 2, 7], typically used to describe industrial filtration, are adapted and tested. In the filtration models, the fouling can occur by various basic mechanisms such as pore blocking, pore constriction, caking, or a combination of these. Fouling models do not reproduce the mechanical processes occurring during soil seal formation but reproduce their effect on the soil surface structure, such as the reduction of the porosity area, A , at the soil surface and an increase in resistance, R , to infiltration flow both for the crust formation and for the underneath pores obstruction by infilling fine particles. Explicit mathematical equations were derived [8] during a constant pressure operation for the dynamics of the free surface pores area for infiltration, $A(t)$, the resistance of the infiltration porous medium, $R(t)$, the infiltration rate, $Q(t)$, the cumulative infiltration volume, $V(t)$, and the saturated hydraulic conductivity, $K_s(t)$. These models were adapted to simulate the infiltration in the soil experiencing overland flow, erosion and crust formation. The soil infilling that occurs during structural seal formation is assimilated to the membrane fouling process. The soil is assimilated to the filter, and it is assumed to be rigid, and the turbid fluid is the flow enriched in fine particles due to the illuviation of the soil particles detached by raindrop impact and overland flow. In [8], the validation dataset was collected in rainfall simulation experiments consisting in a sequence of three simulated rainfalls following initial tillage. An initial wetting preceded the rainfalls. In this paper, a new validation database is used. The data were collected during experimental trials consisting of four simulated rainfalls following initial tillage without any wetting.

2 Materials and Methods

2.1 Materials

The data were provided by the SERLAB (Soil Erosion LABORatory, 42°59'34"N 12°17'27"E, Italy, [9, 10] of the University of Perugia), and derived from an experiment (E2021) on bare silty-clay loam soil (16% sand, 51% silt and 34% clay), carried out in a micro-plot (1 m width \times 0.92 m length and slope 16%). The experiment consists of a sequence of four simulated rainfalls (from now on I, II, III and IV) carried out over a few weeks. Before the experiment, the soil was manually harrowed to obtain a fine seedbed (almost 10 cm deep and with clods smaller than 5 cm). The rainfall simulator [11] installed over the micro-plot provides a constant rainfall intensity of about 70 mm/h and a kinetic energy rate of 14.5 J/(mm \cdot m²). The entire runoff volume was sampled every 5 min to determine the hydrographs at the down-most section of the plot. The corresponding infiltration rate was computed as the difference between the rainfall intensity and the measured runoff. The runoff samples were also analysed to obtain the soil sediment concentration dynamics. The dataset consists of 50 observations of rainfall, runoff and infiltration. The mean porosity varies between 60 and 65%, the mean bulk density at the soil surface is 1050 (kg/m³), mean runoff is 3.56 mm (minimum 2.9 mm in the I rainfall and maximum 3.8 in the IV) and the mean concentration is 10.45 g/l (minimum 5.2 g/l in the I rainfall and maximum and maximum 12.6 g/l in the IV). The models cannot simulate the sediment load dynamics and the compaction due to impinging drops as the porous media is assumed to be rigid, in analogy with the membrane. Therefore, sediment load concentration in the flow and dimensional characteristic of the particles were assigned according to the sediment concentration measures. The independent variable in each rainfall episode is the initial soil surface condition (porous medium structural characteristics), which is progressively modified by the drop impact, the surface flow, and generally by the structural modification of the porous medium [5].

2.2 Methods

The Hermia models [1] derive from Darcy's law, which estimates the flow rate Q (m³/s) as a function of the medium resistance R (1/m) and the free surface area A (m²) for infiltration as follows

$$Q = PA/R\mu \quad (1)$$

with P (N/m²), trans-membrane pressure that in Darcy's equation corresponds to the hydraulic gradient and μ (Ns/m²) is the solution viscosity.

The Darcy's equation, usually adopted in the infiltration processes in a porous medium, is

$$Q = A_0 K_s \Delta P / (\varphi L') \quad (2)$$

with φ (N/m^3), fluid specific weight; L' (m), distance; K_s (m/s), saturated hydraulic conductivity. Comparing the Eqs. (2) and (1) it is possible to express K_s as a function of the variables involved in the Hermia's and Bolton's models as follows:

$$K_s(t) = (A(t)\varphi L') / (A_0 \mu R(t)) \quad (3)$$

In soil moisture conditions close to saturation with the prevalence of the gravitational component over the capillary one, the ΔP can be considered constant and equal to the atmospheric pressure.

Two models (IPB, SPB), based on different hypotheses on the behaviour of A and R , were tested. The combined model IPB + SPB was also tested. Table 1 shows the explicit mathematical equations, derived in [8] for basic and combined models, of the dynamics during sealing of the: free surface pores area, $A(t)$, porous media resistance, $R(t)$, infiltration rate, $Q(t)$, cumulative infiltration volume, $V(t)$ and saturated hydraulic conductivity, $K_s(t)$. The IPB model is based on the premise that the particles larger than the pore size seal off the surface, and the smaller particles accumulate on top of other deposited particles. The model estimates $A(t)$, assuming a constant $R(t) = R(0) = R_0$. Denoted by Q_0, A_0, R_0 the initial data with $R = R_0$ for every $t > 0$, from Darcy's equation, we get $Q/Q_0 = A/A_0$. This model uses a successive approximation method to estimate the reduction of A . The portion of surface area occupied and blocked in a given interval of time is assumed to be proportional to the filtered volume as follows $A_{t+\Delta t} = A_t - \sigma(V_{t+\Delta t} - V_t)A_t/A_0$, where the probability that the particles in the filtered volume $\Delta V_{t+\Delta t} = V_{t+\Delta t} - V_t$ occupy a portion of the free surface is A_t/A_0 . Making the limit as Δt tends to zero with, $Q = dV/dt$, $Q/Q_0 = A/A_0$, and integrating, we get eqs. in Table 1.

Table 1 Models for the dynamic in time t (s) of free surface area for infiltration, A (m^2); infiltration rate, Q (m^3/s); medium resistance to flow, R (1/m) and infiltration volume, V (mm); corresponding initial data, Q_0, R_0, A_0 ; coefficients of the models k_i and k_p ($1/\text{m}^3$); the volume of particles deposited per unit of filtered volume, C (kg/m^3); diameter of the particles, d (m); length of each pore, L (m); density of the turbid fluid, γ_s (kg/m^3); density of the solid particles, γ_0 (kg/m^3); mass fraction of the solids in the suspension, s (-)

Model				
IPB	$A(t) = \frac{A_0}{(1+k_i Q_0 t)}$	$Q(t) = \frac{Q_0}{(1+k_i Q_0 t)}$	$V(t) = \frac{Q_0 t}{\ln(1+k_i Q_0 t) / k_i}$	$k_i = \sigma / A_0$ $\sigma = 1.5 \gamma_s \frac{s}{d \gamma_0}$
SPB	$R(t) = R_0 \left(1 + \frac{k_p Q_0 t}{2}\right)^2$	$Q(t) = \frac{Q_0}{\left(1 + \frac{k_p Q_0 t}{2}\right)^2}$	$V(t) = \left(\frac{k_p}{2} + \frac{1}{Q_0 t}\right)^{-1}$	$k_p = \frac{2C}{L A_0}$
IPB + SPB	$Q(t) = \frac{Q_0}{\left[\left(1 + Q_0 t \left(k_i + \frac{k_p}{2}\right)\right)\left(1 + \frac{k_p}{2} Q_0 t\right)\right]}$		$V(t) = \frac{1}{k_i} \ln\left(1 + \frac{2k_i Q_0 t}{2 + k_p Q_0 t}\right)$	

To evaluate, σ let: d , be the diameter of the particles (assumed to be spherical); $\frac{\pi d^3}{6}$, the volume of the particle; $\frac{\pi d^2}{4}$, the surface projected onto the membrane; $V \gamma_s \frac{s}{\gamma_0}$, the volume of particles contained in the filtered volume V , where γ_s is the density of the turbid fluid, γ_0 is the density of the solid particles, and $s(-)$ is the mass fraction of the solids in the suspension. Now the surface of the totality of the particles projected on the filter membrane is: $\sigma V = \left(\frac{6}{\pi d^3}\right) \left(\frac{\pi d^2}{4}\right) \left(\frac{V \gamma_s s}{\gamma_0}\right)$, simplifying we get the equation for σ given in Table 1.

The SPB model assumes that particles accumulate inside membranes on the walls of straight cylindrical pores; thus, the pore volume decrease is proportional to the filtered volume. The pores are assumed to have a constant diameter and length. The radius, r (m), of the pores decreases due to the solid matter that accumulates on the pore walls. In SPB the A is assumed to be constant, $A(t) = A(0) = A_0$. In the model, SPB, the increasing of the resistance becomes more important, and with the hypothesis of constantly available surface area $A = A_0$ for every $t > 0$, from Darcy's equation, we get $Q/Q_0 = R_0/R$. The reduction of the pore section as a function of the infiltrated volume, in Hermia (1982) is expressed as $N^*(-2\pi r dr)L = CdV$, where r is the pore radius, $N^*(-)$ is the number of pores, L , the length of each pore, supposed to be equivalent to the thickness of the soil layer affected by structural modifications, and $C(-)$ the volume of particles deposited per unit of filtered volume. Integrating with the initial data $V(r_0) = 0$, using the constant pressure Poiseuille equation to express the flow rate as a function of the pore radius, combining the equations and integrating, we get eqs. in Table 1. The parameters of the eqs. in Table 1. are calculated as follows: γ_s , mass of fluid + the mass of solid per unit of volume (density of water + measured average concentration of the solids in the runoff); s , the ratio between the measured mean concentration of the solid in the runoff and the density of the fluid; γ_0 , solid particle density, equal to 2650 kg/m³; d , selected according to the observed dynamics of the sediment granulometry; A_0 , was assumed to be 0.65 m² in test I and then 0.6151, 0.6152 and 0.6075 m², in tests II, III and IV, respectively based on the measured mean porosity; L , assumed to be constant and equal to 0.0005 m; C , average of the ratio of the measured concentration of the solid in the runoff divided by γ_0 .

3 Results

The models were applied starting from the measured data. The model that, on average, provides the most accurate estimates of the infiltrated rate, $Q(t)$, is IPB + SPB (with a Nush-Sutcliffe efficiency, NS = 0.94 in the III rainfall and a mean NS = 0.88, Table 2). Among the basic models, the IPB is more efficient than SPB.

Figure 1 shows that the combined model, considering both the pore clogging and the increase in the resistance of the porous medium, tends to underestimate the infiltration rate data. Still, in general, it provides an excellent prediction. The simple

Table 2 Coefficient of efficiency (Nash and Sutcliffe, NS) of Intermediate Pore Blocking (IPB), Standard Pore Blocking (SPB) and combined model in estimating infiltration rate. The results refer to four rainfall simulations (I, II, III and IV)

Rainfalls	Models		
	IPB	SPB	IPB + SPB
I	0.95	0.03	0.92
II	0.92	0.41	0.75
III	0.81	0.14	0.94
IV	0.82	0.18	0.92
mean	0.88	0.19	0.88

models overestimate the measures. The best results are obtained with the IBP model, which provides a slight overestimation.

Figure 2 shows the boxplots of the percentage errors relative to the entire dataset (50 observations of infiltration rate). The combined model provides the lowest mean absolute percentage error (24% for the IPB + SPB). The error in 75% of the cases is lower than 38% for IPB + SPB. Furthermore, the combined model presents lower variability as quantified by the lower interquartile range and shorter whiskers. IPB, among the basic models, provides the best performance with an error that in 75% of the cases, remains lower than 40%.

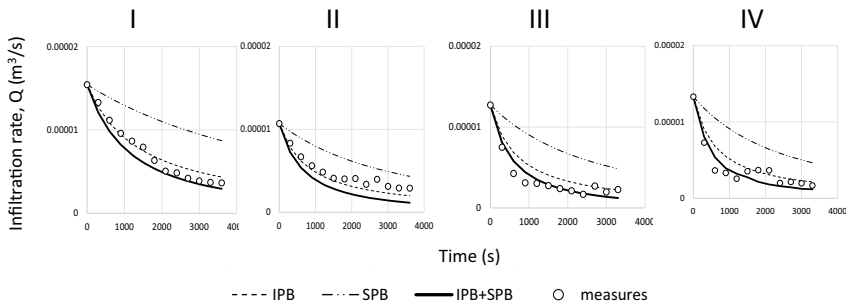
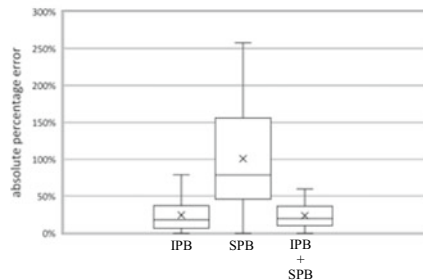


Fig. 1 Measured and estimated infiltration rate during the rainfall simulations I, II, III, IV

Fig. 2 Boxplots of the models' absolute percentage errors in estimating the infiltration rate, calculated as the absolute value of the ratio between the absolute errors (predicted – observed) and observed values



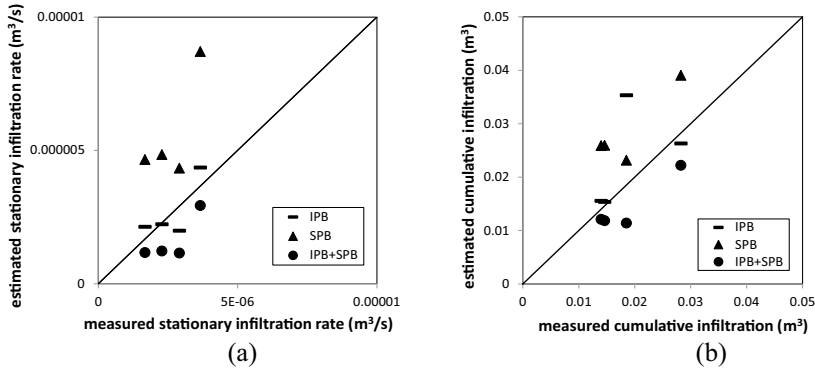


Fig. 3 Stationary infiltration rate **a** and cumulated infiltration volumes **b** measured and estimated with the single and combined models, for the four rainfall simulations

The comparison of the measured and estimated final stationary infiltration rate (Fig. 3a), confirms the overestimation of SPB and the slight underestimation of the combined model. The best model for forecasting the final infiltration rate is the IPB. The overestimation of SPB and the slight underestimation of the combined model are also confirmed in the prediction of the cumulative infiltration volume (Fig. 3b),

4 Discussion and Conclusions

The IPB model provides good results because the reduction of the surface area of the pores is an actual process occurring during seal formation. The coefficient k_i depends on the diameter, d , of the soil particles, on γ_s and s that, in this application, have been estimated from the observed concentration data.

In the SPB model, only the increase in the resistance of the filter medium is considered, and the porous surface area is assumed to be constant. These hypotheses are less effective in reproducing the actual dynamics (Fig. 2). In the real process, the structural and depositional crust determine both the increase of the surface resistance (due to compaction) and the reduction of surface pore area (due to reallocation). The SPB model provides the worst result.

A global sensitivity analysis [12] was performed to evaluate the robustness of one of the best-performing models (i.e., the combined model IPB + SPB). The results show that the model's output is always in a physically sound range. The $Q(t)$ distribution shows a left shift with time that is consistent with the progressive pores obstruction due to particles deposition inside the soil profile and in the soil surface during structural crust formation. The diameter of solid particles d is the most influential independent variable. The positive correlation exhibited by $Q(t)$, slightly decreases with time. The fact that d has a determining role in the model output agrees with the processes simulated by the IPB + SPB model, both in the soil

profile and in the soil surface. The positive correlation is justified by the mathematical formulation of the model (Eq.s Table 1) and is physically consistent, given that the probability of forming occluding layers decreases with increasing particle size. The s , γ_s , and C , all related to the sediment concentration in the suspension, are also important variables. The negative correlation appears consistent with the simulated process since, other factors being equal, lower infiltration values are expected as the suspension concentration increases. The variables A_0 and L (related to the porosity and thickness of the surface soil layer, respectively) show a positive correlation with $Q(t)$, in accordance with the role played in the process. The contribution of the initial infiltration rate Q_0 also appears consistent with the expectations. Indeed, it shows a relatively high positive correlation in the initial phases of the process, but subsequently, its importance becomes negligible.

In conclusion, the combined model, IPB + SPB provides the best results because it accounts for the dynamics of the resistance and the surface pores area. In this model, all the parameters of the basic models involved are present and maintain the same functional role. For IPB + SPB model, the mathematical formulation of the $K_s(t)$ dynamics with time are rational functions of degree -3 depending on the dynamics of both the infiltration area, $A(t)$, and the medium resistance, $R(t)$.

The success of the filtration models suggests that in soils where the silt and clay content is relatively abundant (20% or more), the processes driving the infiltration dynamics need to be parameterized separately from the processes immediately due to raindrop impacts. In modelling, this means that the equations describing the decrease of porosity [5] need an additional cause of variation due to the infilling of fine particles.

References

1. Hermia, J.: Constant pressure blocking filtration laws-application to power law non-newtonian fluids. *Trans. Inst. Chem. Eng.* **60**, 183–187 (1982)
2. Bolton, G., Kuriyel, R., LaCasse, D.: Combined models of membrane fouling: development and application to microfiltration and ultrafiltration of biological fluids. *J. Membr. Sci.* **277**, 75–84 (2006)
3. Muallem, Y., Assouline, S., Rohdenburg, H.: Rainfall induced soil seal (A) a critical review of observations and models. *CATENA* **17**(2), 185–203 (1990)
4. Rousseva, S., Torri, D., Pagliai, M.: Effect of rain on the macroporosity at the soil surface. *Eur. J. Soil Sci.* **53**(1), 83–94 (2002)
5. Todisco, F., Vergni, L., Vinci, A., Torri, D.: Infiltration and bulk density dynamics with simulated rainfall sequences. *Catena*, Forcoming (2022)
6. Biielders, C.L., Baveye, P.: Processes of structural crust formation on coarse-textured soils. *Eur. J. Soil Sci.* **46**, 221–232 (1995)
7. Ceppitelli, R., Marconi, O.: Mathematical models on milk, coffee and beer. In: *Proceedings APLIMAT 2018 - 17th Conference on Applied Mathematics, Bratislava, Slovakia 2018*, pp. 205–216, ISBN 978-80-227-4765-3 (2018).
8. Todisco, F., Vergni, L., Ceppitelli, R.: Modelling the dynamics of seal formation and pore clogging and its effect on infiltration using membrane fouling models. (under revision)

9. Todisco, F., Brocca, L., Termitte, L.F., Wagner, W.: Use of satellite and modeled soil moisture data for predicting event soil loss at plot scale. *Hydrol. Earth Syst. Sci.* **19**(9), 3845–3856 (2015)
10. Bagarello, V., Ferro, V., Giordano, G., Mannocchi, F., Todisco, F., Vergni, L.: Statistical check of USLE-M and USLE-MM to predict bare plot soil loss in two Italian environments. *Land Degrad. Dev.* **29**(8), 2614–2628 (2018)
11. Vergni, L., Todisco, F., Vinci, A.: Setup and calibration of the rainfall simulator of the Masse experimental station for soil erosion studies. *CATENA* **167**, 448–455 (2018). <https://doi.org/10.1016/j.catena.2018.05.018>
12. Cariboni, J., Gatelli, D., Liska, R., Saltelli, A.: The role of sensitivity analysis in ecological modelling. *Ecol. Model.* **203**, 167–182 (2007)

Adapting P-k-C* Model in Mediterranean Climate for Organic Removal Performance in Horizontal Treatment Wetlands



D. Ventura , F. Licciardello , L. Sciuto , M. Milani , S. Barbagallo ,
and G. L. Cirelli

Abstract The P-k-C* is considered as the most suitable in modeling treatment wetland (TW) performance providing a good compromise between accuracy and computational simplicity to assess the degradation processes for selected pollutants. However, there is a need to test the model in different climate conditions due to its high sensitivity to temperature. This study aims at demonstrating the applicability of P-k-C* model to describe the response of horizontal TWs (H-TWs) for domestic and agro-industrial wastewater treatment, and evaluating key design parameters for the model optimization in Mediterranean semi-arid conditions. In particular, kA_{20} (m year^{-1}) and θ values were assessed in two H-TWs in Eastern Sicily, characterized by different organic loads and hydraulic and design features. The model was evaluated for simulating BOD5 and COD effluent concentrations at the outlet of the H-TW units. Calibration parameters, kA_{20} and θ , were found by summing and minimizing the squared differences between measured and modeled data, obtained by simultaneous adjustment of kA_{20} and θ for all samples ($25 < n < 27$). The coefficient of determination, R^2 , the Nash–Sutcliffe efficiency, NSE, and the root mean square error, RMSE, were used as statistical performance measures. Results showed a good reliability of the model to describe water quality response in terms of BOD5 and COD effluent concentrations. Most important finding was that a $\theta < 1$ should be used from practitioners to optimize H-TW design in Mediterranean conditions.

Keywords Horizontal treatment wetland · P-k-C* model · Semi-arid climate

1 Introduction

Treatment wetlands (TWs) are systems increasingly used worldwide to treat different types of wastewaters by removing mineral and organic pollutants. These systems are

D. Ventura · F. Licciardello (✉) · L. Sciuto · M. Milani · S. Barbagallo · G. L. Cirelli
Dipartimento Di Agricoltura, Alimentazione E Ambiente (Di3A), Università Di Catania, Via S.
Sofia 100, 95123 Catania, Italy
e-mail: feliciana.licciardello@unict.it

particularly suited to remove organic matter (i.e. COD and BOD₅) and, in general, chemical compounds such as nitrate, ammonia, phosphate, etc., and microbiological organism through a natural combination of miscellaneous processes contributing to enhance the wastewater (WW) quality. In order to understand and identify the main removal mechanisms acting in the TWs, several models have been proposed by literature [2], to simulate, among others, NO₃⁻, COD and microbiological removal. For a comprehensive understanding of TWs treatment processes, concurrent pollutant degradation and hydraulic behavior require to be considered. To this aim the relaxed version of TIS (tank-in-series) model [4], also known as PTIS or P-k-C* model, seems to be the most suitable in representing TWs performance [2], Dotro et al., 2017). Up-to-date, there are several studies on P-k-C* application worldwide [1, 2, 4–6], while there is a lack of information about its applicability in Mediterranean area, especially utilizing observed data from TWs treating different type of WW. Therefore, the aim of this study is to demonstrate the applicability of the model to describe the response of horizontal TWs (H-TWs) treating different type of WW in Mediterranean climate conditions and to validate it by assessing main design parameters. In particular, k_{A20} (m year⁻¹), θ and P values were assessed in two H-TWs, respectively 5 and 9 years-operating, treating WW produced by a winery and a farmhouse, both located in Eastern Sicily (Italy).

2 Material and Methods

2.1 Case Studies

Marabino Winery TW. The Marabino winery WW (about 3 m³ day⁻¹) are treated by a coarse screening, an Imhoff tank, an equalization tank (5 m³) and a multistage TW (Milani et al., 2020). The TW (Fig. 1) has a total surface area of about 230 m² and is made of a vertical subsurface flow (VF) bed, followed by a horizontal subsurface flow (HF) bed and then by a free water (FW) system. Every four hours, a timer activates a pump installed in the equalization tank for a cycle of five minutes to distribute the WW on the top of VF bed. The HF and FW TWs have a nominal hydraulic retention time (HRT) of about 110 and 90 h, respectively. The TW was planted with: *Phragmites australis* (VF), *Cyperus Papyrus var. Siculus* and *Canna Indica* (HF), *Iris pseudacorus*, *Nymphaea alba* and *Scirpus lacustris* (FWS).

Valle dei Margi (VDM) Farmhouse TW. The TW was designed for the secondary treatment of WW produced by toilets, food area and wellness centre of the VDM farmhouse, with a maximum flow rate of about 30 m³ day⁻¹. The preliminary and primary treatment plant is made of two parallel lines, each one consisting of a degreaser unit and an Imhoff tank (Fig. 2). TW includes an HF bed followed by a FW unit, with a surface area of about 350 m² and 180 m², respectively. The nominal HRT is about 64 h in HF and 115 h in FW TW. The HF bed was vegetated with *Canna*

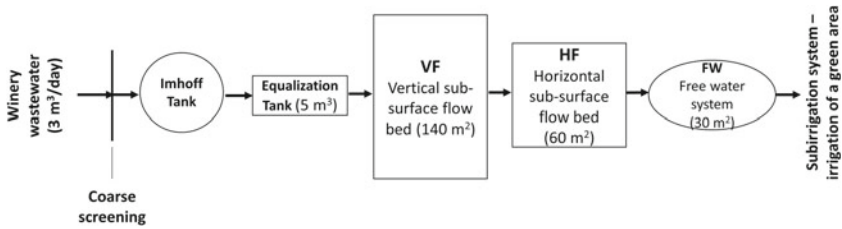


Fig. 1 Layout of wastewater treatment plant in Marabino winery

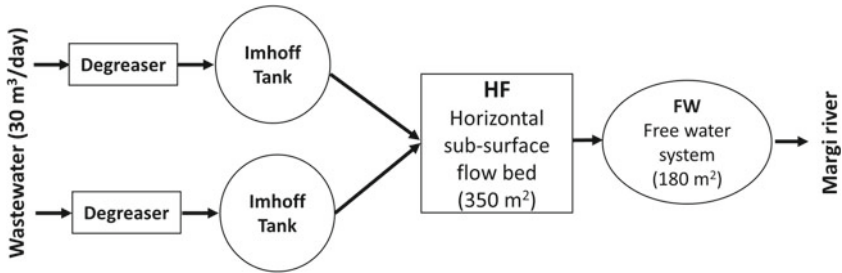


Fig. 2 Layout of wastewater treatment plant in Valle dei Margi farmhouse

Indica, *Cyperus papyrus* and *Iris pseudacorus* while the FW banks was planted with *Phragmites australis*.

Study sites are located in a semi-arid climate area characterized by an average annual precipitation of about 500 mm, and summer air temperature values reaching 40 °C. The climatic data, for two sample years, respectively for Marabino and VDM sites, showed a similar temperature trend with the highest values in July–August (with some peaks in September and the lowest in December–March (data not shown). Temperature values varied from a minimum of -1.6 at VDM (mid-February) °C and -1.7 at Marabino (mid-January) to a maximum of 42 °C at Marabino (beginning of August) and 41.6 at VDM (mid-August). As expected, rain is concentrated in the period September–March with a maximum value of around 40 mm day⁻¹ observed in November. The water temperature of collected samples was close to the daily average air temperature due to the high thermic capacity of the water (data not shown).

2.2 Water Quality Database

The simulation procedure was conducted for COD and BOD₅ data collected in 2018–2020 in the Marabino TW (n = 25 samples) and in 2019–2020 in the VDM TW (n = 27 samples). The sampling points were located at the inflow and outflow of each TW using manual water samplers. WW samples were collected in 500 mL

plastic bottles and stored at 4 °C during the transport to the laboratory. Analyses were carried out according to Standard Methods (APHA 1998; APHA-AWWA-WEF, 2005). A portable water quality probe (Multiparametric Hanna probe, USA) was used to measure temperature and electrical conductivity (EC). The flow was recorded by an on-site flowmeter. Meteorological variables, such as rainfall and air temperature, were provided by the SIAS (Sicilian Agro-meteorological Informative System) reference stations. For each TW configuration, the loading mass rate (LR) and mass removal rate (MR) parameters were calculated [2], as also reported by [1].

2.3 *P-k-C* Model Application*

The fundamentals of the P-k-C* model are based on first order removal rate coefficients (k-rates), non-zero background concentrations (C*), and non-ideal hydraulics [2], while assuming steady-state conditions: no infiltration, no evapotranspiration, and constant flow in the system. The pollutant concentration at outlet (C_o calculated) was calculated by Eq. 1.

$$C_{o\text{ calculated}} = C^* + \frac{C_i - C^*}{\left(1 + \frac{k_{A20}\theta^{(T-20)}}{Pq}\right)^P} \quad (1)$$

The first order areal removal rate constant (k_A) indicates how fast the pollutant degradation process is and depends on water temperature through the theta factor (θ) [2], deriving from the Arrhenius equation. The non-zero background concentration C* [7] represents the lowest effluent concentration (i.e. regarding certain pollutant loads) at the TW outlet. Moreover, P is a fitted parameter that accounts for apparent tanks-in-series, since it merges both, the hydraulic efficiency of the reactor (number of tanks in series, N) and the pollutants “weathering”. The parameters P, k_{A20} and θ (Eq. 1) were optimized to minimize the sum of the square of the errors (SSE) between C_o observed and calculated [3–5]. The minimization process was carried out following [1]. Calibration and validation goodness of P-k-C* kinetic equation was evaluated by calculating the root mean squared error, RMSE (mg L⁻¹), the coefficient of determination, R², and Nash–Sutcliffe efficiency, NSE, between calculated and measured concentration values (for each quality parameter and in individual TWs). With the aim to demonstrate the applicability of the model in the Mediterranean climate to design and to manage TWs for different WW, NSE and RMSE were evaluated for all TWs together.

3 Results

3.1 TWs Characterization and Model Fit Parameters

Mean quality parameter concentrations measured at the inlet (C_i , mg L^{-1}) and at the outlet of TW systems (C_o , mg L^{-1}) and flow rates at the inlet (q_i , m d^{-1}) are reported in Table 1. Evapotranspiration (ET), evaluated as in Consoli et al. (2018), reduced the flow at the inlet (q_i) of about 4% on average in both TWs (with a minimum value of 1% in winter, and a maximum 20% in summer). Mean mass removal rates, considering COD and BOD₅ for each TW were equal to 51% and 50% for Marabino TW and 85% and 86% for VDM TW (Table 1).

Model fitting (reaction rate) parameters, K_{A20} and θ , optimized for the calibration dataset of COD and BOD₅ in each TW are summarized in Table 2. The apparent number of TIS (P) was set equal to 8.3, a median value derived by 35 studies [2] for both COD and BOD₅ and both TWs; the calibration process of this parameter did not improve the simulations.

Mean and standard deviation EC values observed in different periods of the year for the TWs are reported on Table 3. Mean EC values showed an increase of about 15% between April-September (summer season) and October - March (winter season) probably due to the higher ET in the hottest period.

Table 1 Number of samples, mean quality parameters concentration measured at the inlet and outlet of TW systems and their standard deviation (SD), and flow rates at the inlet (q_i , m day^{-1}). C* was fixed as the lowest outlet concentration observed

TWs	n	Parameter	C_i (mg L^{-1})		C_o (mg L^{-1})		C^* (mg L^{-1})	q_i (m day^{-1}) Nominal	MR (%)
			Mean	SE	Mean	SE			
Marabino	25	BOD ₅	121	7	38	2	3	0.05	50
	25	COD	221	12	74	4	3		51
VDM	21	BOD ₅	513	8	77	3	3	0.09	86
	27	COD	712	10	107	3	3		85

Table 2 Model fit parameters k_{A20} and θ (m year^{-1}) for BOD₅ and COD measured in each TW

TWs	COD k_{A20} (m year^{-1})	θ	BOD ₅ k_{A20} (m year^{-1})	θ
Marabino	169.7	0.744	132.2	0.803
VDM	59.9	0.965	41.4	1.018
Mean	114.8	0.855	86.8	0.910

Table 3 Electrical conductivity (EC) measured in HF effluents in different seasons

TWs	EC ($\mu\text{S cm}^{-1}$)		EC ($\mu\text{S cm}^{-1}$)		Difference
	October - March		April - September		
	Mean	SD	Mean	SD	
Marabino	885.6	50.1	1049.5	29.2	18.5
VDM	2765.2	40.3	3101.0	20.7	12.1
Mean	1825.4		2075.3		15.3

Table 4 Calibration Statistical Evaluations: R^2 , NSE, RMSE (mg L^{-1})

TWs	COD				BOD ₅			
	n	R^2	NSE	RMSE	n	R^2	NSE	RMSE
Marabino	15	0.93	0.91	32.1	15	0.85	0.80	22.0
VDM	16	0.71	0.54	50.6	13	0.84	0.81	29.1

Table 5 Validation Statistical Evaluations: R^2 , NSE, RMSE (mg L^{-1})

TWs	COD				BOD ₅			
	n	R^2	NSE	RMSE	n	R^2	NSE	RMSE
Marabino	10	0.96	0.67	66.3	10	0.91	0.48	39.3
VDM	11	0.51	0.32	56.9	8	0.92	0.71	24.6

3.2 Calibration and Validation Results

Statistical evaluations were carried out for calibration and validation datasets for each pollutant and TW (Tables 4 and 5, respectively).

Mean R^2 values (considering both TWs) varied between 0.73 (COD) and 0.92 (BOD₅) for both calibration and validation dataset. Mean NSE values (considering both TWs) varied from 0.59 to 0.81 (respectively for validation and calibration set of BOD₅) and from 0.73 to 0.82 (respectively for validation and calibration set of COD). Mean RMSE values varied between 32.0 (BOD₅) and 61.6 (COD) for both calibration and validation dataset. After calibration/validation process carried out separately for each TW, the observed/predicted values were recompiled for an overall calculation of RMSE and NSE. The statistical metrics of both TWs for each pollutant are summarized in Table 6. As expected, model prediction strength varied between calibration and validation, being for the first dataset higher (between 0.76 and 0.86 for COD and BOD₅ respectively) than the second one (between 0.58 and 0.63 for BOD₅ and COD respectively).

Table 6 Statistical metrics for pollutants observed in all TWs

Pollutant	Calibration (both H-TWs)			Validation (both H-TWs)		
	n	NSE	RMSE (mg L ⁻¹)	n	NSE	RMSE (mg L ⁻¹)
COD	31	0.76	56.54	21	0.63	72.84
BOD ₅	28	0.86	30.21	18	0.58	39.52

4 Discussion

The calibration/validation procedure confirmed the ability of the P-k-C* model to represent BOD₅ and COD kinetic degradation in different H-TWs operating in semi-arid Mediterranean climate. After the calibration of k_{A20} and θ parameters for COD and BOD₅, accordingly with [8], the performance of the model evaluated for all the TWs together was very good for the calibration step, good for the validation set. [9], following a similar model calibration approach (first for a single TW and then considering all TWs together), found similar NSE values (0–72–0.91). k_{A20} optimized values ranging from 41.4 to 169.7 m year⁻¹, considering the two investigated pollutants (COD and BOD₅) in the present study, are in the range of those found in literature [2], they are higher than those generally found in temperate areas [3, 6] and very similar to those found in another study in semi-arid areas [1]. The fact that θ was < 1 in most cases (with the exception of BOD₅ for VdM) was found in literature for a study carried out in Ethiopian arid climate [5] besides another one carried out in Sicily [1]. In particular, optimized K_{A20} and θ parameters allowed the following considerations. A value of $\theta < 1$, means that temperature increases in the summer season caused a reduction in the K_{A20} and the kinetic degradation in all the cases, as observed by [5] under African arid conditions, and by [1] under Sicilian semi-arid conditions.

This behaviour could be explained by two compensation factors, in contrast with the general idea that temperature increases cause K_{A20} increases (Vymazal et al., 2021). First of all, generally, the temperature increase causes the increase of kinetic degradation rate and therefore of k_{A20} value, since “seasonal variations of some biotic and abiotic factors” occur [12]. In spite of this, in summer period in semiarid region, very high temperatures and consequent ET increases can act predominantly causing a higher concentration of effluent pollutants than expected, and so, determining a reduction of k_{A20} [2]. Also, a correlation between the increased water salinity and the TW treatment effectiveness reduction, due to plants and microbial function inhibition, was reported by [11]. In our case, this effect could be contributing as confirmed by higher EC values observed during April–September season. On the other hand, the second compensation condition occurs in winter season, when rain dilutes pollutants concentration in TW outlet, increasing the k_{A20} , being also ET almost neglectable and the effect of temperature not relevant. However, the preponderance of literature (Stein et al., 2006) evidence suggests that BOD₅ removal is not improved with higher wetland water temperatures.

5 Conclusion

The P-k-C* model calibration/validation procedure carried out in the present study, confirms the applicability of the model to describe the simulation of H-TWs treating different type of WW and characterized by different design, and hydraulic and organic load in Mediterranean climate conditions. Very good values of R^2 , NSE and RMSE reached in most of cases indicated the good performance of the model. Therefore, optimized data of k_{A20} and θ , confirming those already found in arid and semiarid areas of the world, could be considered a contribute for P-k-C* model application in typical Sicilian climate, and, in general in Mediterranean weather conditions. In particular, the calculated k_{A20} values were generally higher than those showed in the case of TWs located in temperate climate zone and for all the pollutants considered, the θ values were generally lower than 1. This means that temperature increase in the summer reduces the k_{A20} and the kinetic degradation in all cases.

Acknowledgements This research was funded by PON RICERCA E INNOVAZIONE 2014–2020, Azione II—Obiettivo Specifico 1b—Progetto “Miglioramento delle produzioni agroalimentari mediterranee in condizioni di carenza di risorse idriche—WATER4AGRIFOOD”, cod. progetto ARS01_00825, and by the University of Catania-PIA no di inCentivi per la Ricerca di Ateneo 2020/2022—Linea di Intervento 3 “Starting Grant”. The author Delia Ventura conducted this work within the activities of the RTD-A contract co-funded by PON “Ricerca e Innovazione” 2014-2020 (PON R&I FSE-REACT EU), Azione IV.6 “Contratti di ricerca su tematiche Green”.

References

1. Ventura, D., et al.: Application of first-order kinetic removal models on constructed wetlands under Mediterranean climatic conditions. *Ecol. Eng.* **175**, 106500 (2022)
2. Kadlec, R.H., Wallace, S.D.: *Treatment Wetlands*, 2nd edn. CRC Press, Boca Raton, Florida (2009)
3. Nivala, J., Knowles, P., Dotro, G., Gara, J., Wallace, S.: Clogging in subsurface flow treatment wetlands: measurement, modeling and management. *Water Res.* **46**(6), 1625–1640 (2012). <https://doi.org/10.1016/j.watres.2011.12.051>
4. Nivala, J.: *Effect of Design on Treatment Performance, Plant Nutrition and Clogging in Subsurface Flow Treatment Wetlands*. PhD Thesis. Aarhus University, Department of Bioscience, Aarhus, Denmark (2012)
5. Ayano, K.K.: *Effect of Depth and Plants on Pollutant Removal in Horizontal Subsurface Flow Constructed Wetlands and their Application in Ethiopia*. PhD Thesis. Berlin University (2014)
6. Vymazal, J.: Is removal of organics and suspended solids in horizontal sub-surface flow constructed wetlands sustainable for twenty and more years? *Chem. Eng. J.* (2019). <https://doi.org/10.1016/j.cej.2019.122117>
7. IWA: *Constructed Wetlands for Pollution Control. Processes, Performance, Design and Operation* (2000). <https://www.iwapublishing.com/sites/default/files/ebooks/9781900222051.pdf>. Accessed 2 Sept 2021
8. Moriasi, D.N., Arnold, J.G., Van Liew, M.W., Binger, R.L., Harmel, R.D., Veith, T.: Model evaluation guidelines for systematic quantification of accuracy in watershed simulations. *Trans. ASABE* **50**, 885–900 (2007). <https://doi.org/10.13031/2013.23153>.

9. Merriman, L.S., Hathaway, J.M., Burchell, M.R., Hunt, W.F.: Adapting the relaxed tanks-in-series model for stormwater wetland water quality performance. *Water* **9**, 691 (2017). <https://doi.org/10.3390/w9090691>
10. *Ecol. Eng.* **26**, 100–112. <https://doi.org/10.1016/j.ecoleng.2005.07.001>
11. Liang, Y., et al.: Constructed wetlands for saline wastewater treatment: a review. *Ecol. Eng.* **98**, 275–285 (2017). <https://doi.org/10.1016/j.ecoleng.2016.11.005>
12. Zhu, Y., Cui, L., Li, J., Wang, R., Vymazal, J., Li, W., Lei, Y., Zhang, M., Hao, T., Wei, J.: Long-term performance of nutrient removal in an integrated constructed wetland. *Sci. Total Environ.* **779**, 146268 (2021). <https://doi.org/10.1016/j.scitotenv.2021.146268>

Influence of the Rainfall Time Step on the Thresholds for Separating Erosive and Non-erosive Events



L. Vergni , A. Vinci , and F. Todisco 

Abstract In previous work [1] Todisco et al. (2019), Todisco et al. (2019) analyzed 522 rainfall events from 2008 to 2017 at the Masse experimental station (central Italy) to define and evaluate several thresholds of rainfall characteristics able to classify non-erosive and erosive events. The analysis was performed based on a 5-min rainfall dataset. In this study, working on the same dataset, we evaluated how the value and performance of the thresholds change when their determination is made based on rainfall records at different time steps. In particular, the original 5-min data were aggregated at 30 min, one of the typical timesteps of the data provided by the Hydrographic Services and that required for calculating the USLE erosivity factor. The results indicate that some rainfall characteristics maintain effectiveness, passing from a 5-min to a 30-min rainfall dataset. However, only the total event rainfall has a threshold (~ 15 mm) that is almost independent of the resolution, while for other effective variables (e.g., Maximum duration of an individual run and the Maximum rainfall amount in a burst), the thresholds change significantly. Moreover, some variables dependent on the number of runs or showers during the event become entirely ineffective when switching to the 30-min resolution due to the consequent flattening of the internal dynamics of the hyetographs.

Keywords Hyetograph · Rainfall erosivity · Rainfall characteristics · Rainfall classification

1 Introduction

The identification of thresholds of simple and practical determination capable of operating a separation between non-erosive and erosive rains has considerable importance from both a practical and scientific point of view [1, 2]. It reduces the work necessary

L. Vergni (✉) · A. Vinci · F. Todisco

Department of Agricultural, Food and Environmental Sciences, University of Perugia, Borgo XX Giugno, 74 06124 Perugia, Italy
e-mail: lorenzo.vergni@unipg.it

to manage and process erosive events and provides useful information to determine the triggering of erosion processes of different entities and nature and consequently to understand their dynamics better. A well-known threshold is certainly that proposed by [3], which indicated as erosive the rainfalls having more than 12.7 mm or at least 6.35 mm in 15 min. More recent studies [1, 2, 4] have been aimed at determining whether the variables that describe the internal structure of rain events (e.g., presence and duration of high-intensity showers), can be effective in classifying non-erosive and erosive events, and even in separating erosive events that produce sheet or rill erosion [1]. In particular, in [1], the 5-min hyetographs of 522 rainfall events from 2008 to 2017 at the Masse experimental station (central Italy) were analyzed, identifying the most effective variables and their threshold value.

Here, the same dataset is re-analyzed with the specific aim of evaluating how the values of the best thresholds change when their determination is based on 30-min rainfall records. This application has a practical interest since the 30-min time resolution is that typical of the rainfall time series provided by the Regional Hydrographic Service and is the minimum required for calculating the USLE erosivity factor according to [3].

2 Materials and Methods

2.1 Rainfall Data and Rainfall Event Classification

The study was based on the data collected at the SERLAB station (central Italy, 42° 59' 34" N 12° 17' 27" E), an experimental site equipped for the monitoring and characterization of erosive processes at plot scale. A brief description of this experimental station is provided below; more details on the technical and environmental characteristics and on the measurement procedures can be found in previous studies [5, 6].

The station has 10 Wischmeier-type plots of various sizes, with a 16% slope, kept in cultivated fallow through frequent tillage operations to remove any spontaneous vegetation and to obliterate the presence of any rills formed during erosive events. Each plot is equipped in its terminal part with a channel that conveys the solid and liquid runoff into collection tanks. After each erosive event, the runoff and soil loss are measured with a specially calibrated sampling technique [7] and the tank is emptied and cleaned to be ready to receive the runoff of a new event.

The weather station in operation at SERLAB includes, among other instrumentations, a tipping bucket rain gauge set to record rainfall depths with a 5-min time step.

The rainfall database was analysed to identify the individual storms, i.e., the rain events preceded and followed by 6 h or more of no rain (in accordance with [3]).

Each individual storm was therefore classified as erosive if a measurable soil loss was found in the collection tanks, while it was considered non-erosive if it did not produce runoff or if the soil loss was so irrelevant that it cannot be measured [7].

Sometimes, due to the impossibility of measuring runoff and soil loss of individual events very close to each other, the information refers to a sequence of individual storms. In this case, the individual storms included in a sequence were classified as non-erosive (erosive) if their rainfall depth was lower (higher) than the minimum depth observed for the individual erosive rainfalls.

For the study, we used the rainfall data and the corresponding rainfall event classification from 01–01-2008 to 31–12-2017.

As explained in the introduction, the analysis was conducted in parallel both based on rainfall amounts, p , collected every 5 min (original time resolution) and at 30 min. The latter was obtained by cumulating the rainfall depths of the corresponding 5-min records.

2.2 *Rainfall Variables*

We considered 23 rainfall variables describing both overall and pattern characteristics of storms (Table 1).

As the name suggests, overall variables don't take into account the internal structure of the hyetograph, while pattern variables do. The internal storm structure is described by the characteristics (number, duration, severity, etc.) of both bursts (i.e., intervals of continuous rain) and runs (i.e. intervals of continuous rain exceeding a predetermined truncation value $p0$). The identification of the truncation level, $p0$, for both the 5-min and 30-min rainfall datasets, was based on the frequency analysis of rainfall records by excluding zero values. The selected $p0$ value is that corresponding to a cumulative frequency of 95% [4], which gives $p0_5 = 0.8$ mm in 5 min (9.6 mm/h) and $p0_{30} = 3$ mm in 30 min (6 mm/h).

2.3 *Procedure for Determining Thresholds for Separating Erosive and Non-erosive Events*

The procedure to determine suitable and practical thresholds for separating erosive and non-erosive rainfall events is the same described in [1] and [2]. The following steps summarize the procedure: a) calculation of the rainfall erosivity EI30 for each storm using the method described by [3]; b) sum of the EI30 of all erosive storms, named EI30_t (i.e., target EI30); c) sort of all storms (both erosive and not erosive) in decreasing order of the selected variable X, along with the corresponding EI30 values; d) sum of the EI30 values from the highest value of the selected variable up to the one where the cumulative value, EI30_c, equals or approximates by excess the target

Table 1 Variables considered for the characterization of individual storms

Variable	Symbol and unit
Total rainfall amount	P (mm)
Total duration	D (h)
Wet duration	D_wet (h)
Dry duration	D_dry (h)
Rainfall amount above truncation level p0	P_run (mm)
Rainfall duration above truncation level p0	D_run (h)
Rainfall erosivity	R (MJ mm ha ⁻¹ h ⁻¹)
Rainfall kinetic energy	E (MJ ha ⁻¹)
Maximum intensity over 30 min	I30 (mm h ⁻¹)
Mean intensity	I (mm h ⁻¹)
Mean wet intensity	I_wet (mm h ⁻¹)
Number of runs	N_run (-)
Maximum duration of an individual run	Max_D_run (h)
Maximum rainfall amount of an individual run	Max_P_run (mm)
Maximum peak of the run (p-p0)	Max_peak_run (mm)
Maximum rainfall depth cumulated from the start of the storm to the run	Max_P_pre_run (mm)
Maximum slope of the rising limb of a burst	Max_slope_burst (%)
Maximum mean run intensity	Max_I_run (mm h ⁻¹)
Number of bursts in a storm	N_burst (-)
Maximum rainfall amount in a burst	Max_P_burst (mm)
Maximum burst duration	Max_D_burst (h)
Maximum rainfall depth cumulated from the start of the rainfall event to the burst	Max_P_pre_burst (mm)
Maximum mean burst intensity	Max_I_burst (mm h ⁻¹)

EI30; e) the value of the variable X_t corresponding to the cumulative value EI30_c is identified as the threshold for the selected variable. Finally, the identified threshold is used to classify the rainfall events (i.e., if $X \geq X_t$ the storm is considered erosive, otherwise non-erosive). Compared to the work of [1], here the energy calculation was done according to the USLE formulation [3] instead of RUSLE [8]. This modification was made because the kinetic energy calculation of the USLE is judged to be more reliable than that of RUSLE [9]. However, the effect of this change on the threshold values is not relevant in most cases.

For each variable, the threshold performance was evaluated by the Correct Selection Index (CSI) and the Wrong Selection Index (WSI). CSI is defined as:

$$CSI = \frac{N_{Se}}{N_e} \quad (1)$$

where N_{Se} is the number of storms selected as erosive and N_e is the actual number of erosive storms. CSI (%) assumes the maximum value of 100 when all erosive events are selected.

WSI is defined as

$$WSI = \frac{N_{Sn}}{N_s} \quad (2)$$

where N_{Sn} is the number of non erosive storms selected as erosive and N_s is the number of storms selected. WSI is 0 when all the selected storms are correct.

In general, a well-performing threshold must present a good compromise between high CSI and low WSI.

3 Results

3.1 Characteristics of Individual Storms and Rainfall Variables

Based on the 5-min database, we identified 528 individual storms (of which 158 erosive) while in the 30-min dataset, the individual storms were 522 (of which 156 erosive). These small differences are due to the fact that a few events (very close to each other but actually separated by more than 6 h) were not perceived as distinct on the basis of the coarser acquisition time. Therefore, this is a first, but moderate difference arising from the analysis of the same rainfall data using a different timestep.

The rainfall events common in both databases were then considered to compare the changes in the statistical characteristics of the 23 variables in the transition from the 5-min scale to the 30-min one. Figure 1 shows, for each variable, the boxplot comparison of 5-min and 30-min datasets.

The analysis of Fig. 1 shows that, except for P, the dataset resolution always has an influence, more or less evident, on the statistical properties of the rainfall variables. Some variables (D, P_run, R, E, I30, I, Max_P_run, Max_P_burst, Max_P_pre_burst) appear more robust, i.e., they are moderately affected by the time resolution. The rest of the variables show considerable differences in the statistical indices, both in dispersion and central tendency.

A further comparison between the two datasets is given in Fig. 2, which shows, for each variable, the slope coefficients of the regression lines of 30_min- on 5_min-derived variables, obtained by forcing the intercept to zero.

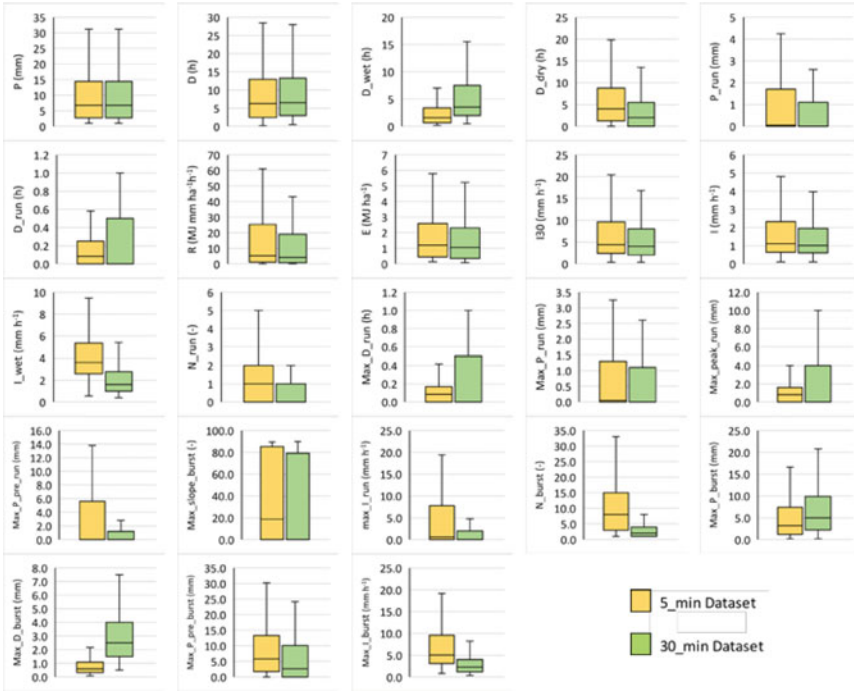


Fig. 1 Boxplot comparison of the samples of the 23 variables computed on the 5-min and 30-min datasets. See Table 1 for the definition of the acronyms used for the variables

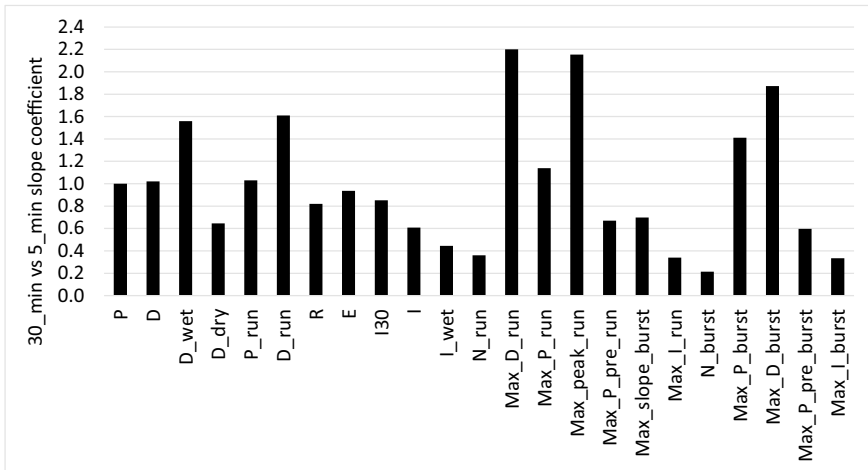


Fig. 2 Slope coefficients of the regression lines of 30_min- on 5_min-derived variables, obtained by forcing the intercept to zero. See Table 1 for definitions and units of the variables

Table 2 Threshold values of different variables for the separation between erosive and non-erosive events, based on 5-min and 30-min rainfall datasets. The thresholds marked with an asterisk meet the minimum efficiency criterion (Correct Selection Index, CSI \geq 60% and Wrong Selection Index, WSI \leq 40%)

Variable	5-min			30-min		
	Threshold	CSI (%)	WSI (%)	Threshold	CSI (%)	WSI (%)
P (mm)	14.8*	60.1	24.6	15.2*	60.9	23.4
D_run (h)	0.3	58.9	24.4	0.5*	67.9	29.3
R (MJ mm ha ⁻¹ h ⁻¹ year ⁻¹)	33.2	56.3	16.0	24.7*	60.3	13.0
N_run (-)	1	68.4	41.3	1*	68.6	34.0
Max_D_run (h)	0.2*	60.1	34.9	0.5*	68.6	33.6
Max_P_pre_run (mm)	2.0*	75.2	36.3	–	–	–
Max_slope_burst	78.2	62.7	53.5	68.5*	66.0	36.8
Max_I_run (mm h ⁻¹)	5.4	58.2	39.9	1.9*	60.3	29.3
Max_P_burst (mm)	7.6*	65.2	20.2	10.2*	64.7	21.1
Max_P_pre_burst (mm)	11.2*	69.6	26.7	–	–	–

3.2 Thresholds for Separating Erosive and Non-erosive Events

The procedure described in Sect. 2.3 was applied to each of the 23 variables, computed on the 5-min and 30-min datasets. To focus the analysis only on the most effective variables, an arbitrary minimum performance criterion was applied, consisting of a CSI greater than 60% and a WSI less than 40%. This criterion enabled the identification of 5 and 8 best-performing thresholds on the 5-min and 30-min datasets, respectively (Table 2). Only 3 variables (i.e., P, Max_D_run, Max_P_burst) satisfy the established efficiency criterion regardless of the temporal resolution of the dataset. In this regard, however, it is noted that the well-performing thresholds at 5-min are also good at 30-min (and vice versa) even though they do not strictly satisfy the imposed minimum criteria of CSI = 60% and WSI = 40%.

The variables Max_P_pre_run and Max_P_pre_burst are an exception: while in the 5-min dataset, they are well-performing, at 30-min they are ineffective at all in the separation between erosive and non-erosive events.

4 Discussion and Conclusion

The coefficients provided in Fig. 2 can be interpreted as correction (or calibration) factors required to convert the 5-min-derived variables into the corresponding 30-min variables. Similar information in the literature can only be found for well-known

variables such as R. For example, in [10], to convert the 5-min-derived R to the 30-min derived one, a factor of 0.7984 is proposed. Here, we obtained a value of 0.8209, almost equal to the factor (0.8205) indicated [10] to switch from the 10-min-derived R to the 30-min-derived one.

In general (Fig. 2), in the passage from the 5-min to the 30-min dataset, there is a reduction of the variables relating to the number (number of runs, number of bursts) and an increase in those relating to the durations (both of the showers and of the runs), precisely because of the more “blurry” view of the hyetograph obtained by the dataset with lower temporal resolution. It follows that the variables that quantify the different types of intensities (e.g., mean intensity, run intensity, burst intensity) tend to decrease significantly in the transition from higher resolution datasets to less detailed ones.

As regards the variables effective in separating erosive and non-erosive events, it was found a good performance of the total rainfall, P, confirming what was already indicated by [3]. The threshold value found (about 15 mm) is slightly higher than that proposed by Wischmeier and Smith (12.7 mm) and is almost independent of the temporal resolution of the rainfall dataset. Valid alternatives are the Maximum duration of an individual run (Max_D_Run) and the Maximum rainfall amount in a burst (Max_P_burst), with performances similar to or higher than that of P. These variables are effective in both the 5-min and 30-min datasets but have the drawback of very different threshold values in the two datasets (Table 2). It has been verified that the coefficients that allow the conversion of the variables at 5 min into those at 30 (Fig. 2), can be used with good approximation also for the conversion of the thresholds. However, this doesn't work for discrete variables (such as N_run). Finally, some variables are definitely to be discarded for this type of evaluation (e.g., Max_P_pre_run, Max_P_pre_burst) as they are effective for the high-resolution dataset but completely ineffective at coarser resolutions. These two variables quantify the maximum amount of rainfall detected before a run or a burst, respectively. At 30-min resolution, many events have 1 burst or 1 run only because dry intervals of less than 30 min during rainfall are not detected. This fact greatly flattens the possibility of differentiating events based on these variables. In particular, the procedure indicated in Sect. 2.3 leads to thresholds = 0, which is evidently completely ineffective for any classification of rainfall events.

References

1. Todisco, F., Vergni, L., Vinci, A., Pampalone, V.: Practical thresholds to distinguish erosive and rill rainfall events. *J. Hydrol.* **579**, 124173 (2019)
2. Xie, Y., Liu, B., Nearing, M.A.: Practical thresholds for separating erosive and nonerosive storms. *Trans. Am. Soc. Agric. Eng.* **45**(6), 1843–1847 (2002)
3. Wischmeier, W.H., Smith, D.D.: Rainfall erosion losses-a guide to conservation planning. Agricultural Handbook No. 537. United States Department of Agriculture, Washington D.C. (1978)

4. Todisco, F.: The internal structure of erosive and non-erosive storm events for interpretation of erosive processes and rainfall simulation. *J. Hydrol.* **519**(PD), 3651–3663 (2014)
5. Di Stefano, C., Pampalone, V., Todisco, F., Vergni, L., Ferro, V.: Testing the universal soil loss equation-MB equation in plots in central and South Italy. *Hydrol. Process.* **33**(18), 2422–2433 (2019)
6. Vergni, L., Todisco, F., Vinci, A.: Setup and calibration of the rainfall simulator of the Masse experimental station for soil erosion studies. *CATENA* **167**, 448–455 (2018)
7. Todisco, F., Vergni, L., Mannocchi, F., Bomba, C.: Calibration of the soil loss measurement method at the masse experimental station. *CATENA* **91**, 4–9 (2012)
8. Renard, K.G., Foster, G.R., Weesies, G.A., McCool, D.K., Yoder, D.C.: Predicting soil erosion by water: a guide to conservation planning with the Revised Universal Soil Loss Equation (RUSLE). Agriculture Handbook No. 703, United States Department of Agriculture (1997)
9. Nearing, M.A., Yin, S., Borrelli, P., Polyakov, V.O.: Rainfall erosivity: an historical review. *CATENA* **157**, 357–362 (2017)
10. Panagos, P., Borrelli, P., Spinoni, J., et al.: Monthly rainfall erosivity: conversion factors for different time resolutions and regional assessments. *Water* **8**, 119 (2016)

Quantifying Irrigation Volumes Using Sentinel-1 Soil Moisture Data in Central Italy



L. Vergni , J. Dari , F. Todisco , M. Vizzari , C. Saltalippi ,
S. Venturi , S. Casadei , and L. Brocca 

Abstract In this work, surface soil moisture (SSM) datasets at different spatial resolutions (1 km and plot-scale), derived from Sentinel-1 observations, are used as input into the soil moisture (SM)-based inversion algorithm to retrieve information on irrigation volumes. The method is applied over an agricultural area of about 7000 ha falling within the Upper Tiber River valley (central Italy). For this area, information about irrigation water consumption in the period 2017–2020 is used as a benchmark. A district-scale analysis is carried out by comparing the performances of three different SSM datasets: two 1 km resolution products (Copernicus and RT1), and the S2MP, a plot-scale product developed by merging Sentinel-1 and Sentinel-2 observations. At the district level, the best performances are obtained through the Copernicus SSM, providing a median yearly relative error of 17.5%. RT1 SSM shows an overestimation lower than 30% compared to the actual irrigation volumes for two of the four considered irrigation seasons. The lowest performances are found for the S2MP dataset, with irrigation estimates much larger than the actual irrigation amounts. At the plot scale, overestimates (BIAS = 19.75 mm/14-day) and underestimates (BIAS = 14.88 mm/14-day) are obtained in the irrigation seasons of 2017 and 2018, respectively.

Keywords Soil moisture · remote sensing · irrigation volumes · water balance model

L. Vergni (✉) · F. Todisco · M. Vizzari
Department of Agricultural, Food and Environmental Sciences, University of Perugia, Perugia, Italy
e-mail: lorenzo.vergni@unipg.it

J. Dari · C. Saltalippi · S. Venturi · S. Casadei
Department of Civil and Environmental Engineering, University of Perugia, Perugia, Italy

J. Dari · L. Brocca
National Research Council, Research Institute for Geo-Hydrological Protection, Perugia, Italy

1 Introduction

The efficient use of water resources in agriculture represents a strategic objective, particularly in areas like central and southern Italy, where crops are strictly dependent on irrigation, and deficit phenomena are more likely. This objective must be pursued through technical and infrastructural improvements of irrigation systems and management optimization. A reliable and effective management strategy requires the availability of updated and detailed data on the actual extension of irrigated areas and water consumption, as required by the EU directive on water (2000/60 EC). The most interesting perspective for obtaining this information is represented by satellite data, particularly those providing information on soil moisture.

However, the use of satellite soil moisture data for this purpose is still an open challenge, especially in agricultural contexts where a mismatch exists between the spatial resolution of satellite-retrieved information and the extent of the irrigated fields [1].

In this study, three different Sentinel-1-derived surface soil moisture (SSM) products have been used to force the SM-based inversion approach [2–4] and to evaluate their performances in retrieving the amounts of water used for irrigation practices. The considered products are the Copernicus SSM [5], the RT1 SSM [6], and the S2MP SSM [7]. The latter is a plot-scale dataset developed by merging Sentinel-1 and Sentinel-2 observations, while the others have a spatial resolution of 1 km. Two experiments have been carried out over an agricultural area of about 7000 ha falling within the Upper Tiber River valley (central Italy) and hereafter defined as the “Tevere I” district. The first is a district-scale experiment in which the SSM datasets have been averaged over the whole district. The second experiment is a plot-scale application over an experimental field; in this case, only the S2MP SSM product at its native resolution has been considered.

2 Materials and Methods

2.1 Study Area and Irrigation Data

The study refers to an almost flat irrigation district called Tevere I (~70 km²) located in the Upper Tiber river basin, central Italy (Fig. 1). The area has a typical Mediterranean climate with hot summers and cold winters. The wettest season is autumn, and the driest is summer. The agricultural fields, both because of the complex surrounding orography and for historical reasons, are very fragmented. Most herbaceous crops grown in the spring–summer period (mainly maize, vegetables, and tobacco), and fruit trees, require irrigation due to the relevant imbalance between precipitation and evapotranspiration. The most relevant distribution of irrigation volumes (i.e., the irrigation season) occurs between June and August [8, 9].

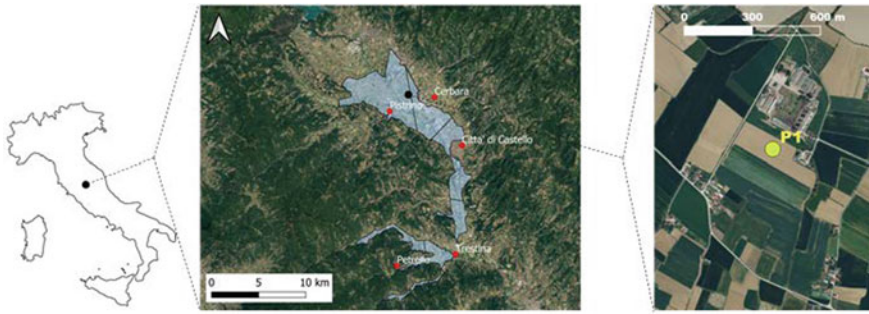


Fig. 1 Position map of the Tevere I district and P1 field. Red points and blue shaded areas indicate the weather stations and the corresponding Thiessen polygons, respectively

The main water supply is the Montedoglio reservoir. The irrigation distribution network of the Tevere I district is managed by the Regional Forestry Agency (AFOR), which annually stipulates supply contracts with farmers.

The methodology has been applied considering large and small spatial scales: the first is represented by the whole irrigation district Tevere I, whilst the latter refers to a specific field of about 10 ha, named P1 (Fig. 1). For Tevere I, AFOR provided, upon request, the irrigation volumes distributed from 2017 to 2020. For the P1 field, AFOR provided data about the crop types and irrigation (volumes and dates) for 2017 and 2018. This ground-truth information has been used to assess the reliability of the estimated irrigation volumes.

2.2 The SM-Based Inversion Approach

The procedure for quantifying irrigation volumes from remotely sensed moisture data is based on a modified version of the SM2RAIN algorithm, initially developed to derive rainfall estimates from moisture data [10]. In brief, the SM-based inversion algorithm [2–4] solves the following soil water balance equation:

$$IR(t) = Z^* \frac{dS(t)}{dt} + aS(t)^b + PET(t)S(t)F - P(t) \tag{1}$$

where $IR(t)$ [mm/day] is the output variable (i.e., the irrigation volume), $S(t)$ [–] is the relative soil moisture or saturation degree, t [day] is the reference time scale, Z^* [mm] is the actual soil water capacity, $aS(t)^b$ [mm/day] is the drainage expressed by a power law depending on $S(t)$ and the parameters a and b , the term $PET(t)S(t)F$ [mm/day] is the actual evapotranspiration ET, expressed as a function of the potential evapotranspiration $PET(t)$, relative soil moisture and an adjustment factor, F , while the $P(t)$ term indicates the rainfall rate [mm/day].

The use of Eq. (1) implies that runoff is considered negligible. The following iterative procedure is applied to calibrate the model parameters a , b , Z^* , and F . First, the model is run in periods not including the irrigation season (i.e., from June to August), for which it can be assumed $IR(t) = 0$. This first calibration involves the a , b , and Z^* parameters which are optimised against the observed rainfall rates $P(t)$, while F is assumed equal to 1. Then the model is run during the irrigation season, calibrating only the evapotranspiration parameter F against the irrigation volumes. Lastly, the calibrated F parameter is used in the first step to re-calibrate the parameters a , b and Z^* . The procedure is summarised in Fig. 2. It is noteworthy that yearly irrigation rates have been considered in the district-scale analysis, while daily irrigation doses have been used for the plot-scale experiment. In both district- and plot-scale analysis, the benchmark irrigation volumes have been divided by the area of interest to obtain equivalent mm to be directly compared with the output of Eq. (1). Water distribution efficiency was not taken into account due to a lack of specific information on irrigation methods.

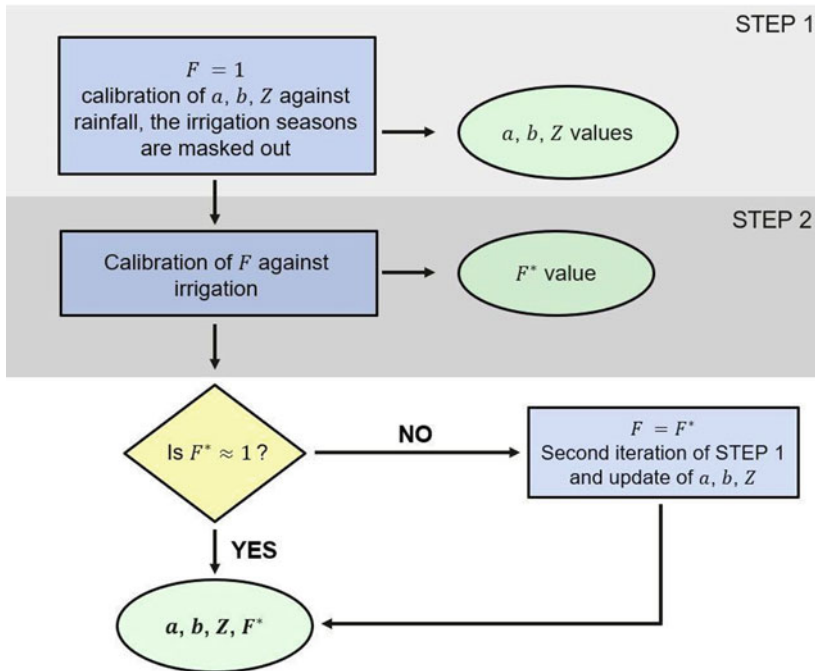


Fig. 2 Flow chart showing the adopted calibration strategy for estimating the parameters of the SM-based inversion algorithm

2.3 Data Collection

The application of Eq. (1) requires relative soil moisture, potential evapotranspiration, and precipitation data. The method has been implemented with three different Sentinel-1-derived SSM products. Two have a spatial resolution of 1 km, namely the Copernicus SSM [5] and the RT1 SSM [6] datasets. The third considered product is S2MP [7], developed by the National Research Institute of Agriculture, Food and Environment (INRAE); it is a plot-scale dataset that merges Sentinel-1 and Sentinel-2 observations and is delivered by the Theia Pole through the catalogue available at: <https://thisme.cines.teledetection.fr/#!/home>.

The potential evapotranspiration PET has been obtained from the MODerate resolution Imaging Spectroradiometer (MODIS) observations at a spatial resolution of 500 m. Specifically, the product MOD16A2 was used. Spatially averaged time series of SSM and PET have been used for the district-scale analysis.

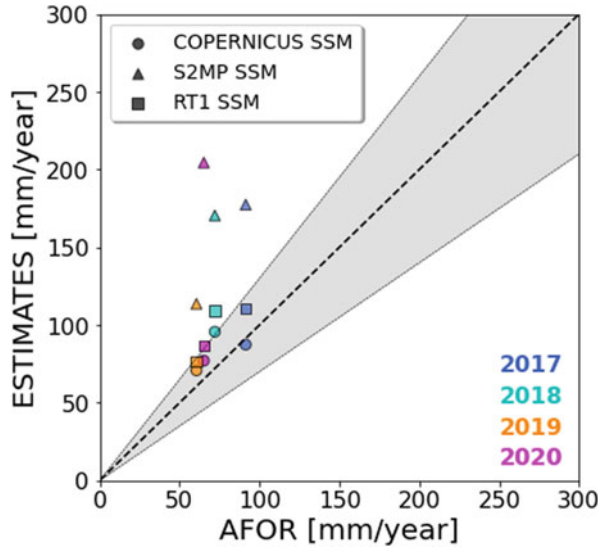
Daily rainfall data from 2017 to 2020 have been retrieved from the Regional Hydrographic Service of the Umbria Region for the five stations shown in Fig. 1, i.e., Cerbara, Città di Castello, Petrelle, Pistrino, and Trestina. The spatially averaged rainfall, used in the district-scale experiment, has been obtained by the Thiessen Polygons method (Fig. 1). Rainfall rates recorded by the closest station to the P1 field (Pistrino) have been instead used for the plot-scale application.

3 Results

The results of the district-scale analysis are summarised in the scatter plot of Fig. 3, where the x-axis indicates the observed yearly irrigation volumes from AFOR and the y-axis the yearly amounts estimated through the proposed approach. Different markers and colours indicate different SSM products and irrigation seasons, respectively. The shaded area delineates a relative error of $\pm 30\%$. The estimated volumes are generally higher than those observed, except for the irrigation rates retrieved by Copernicus SSM in 2017. Regarding the 1 km resolution products, the most performing one is Copernicus SSM, with a median relative error of 17.5%, while for RT1 SSM, the analogous value is 30%. Both products, however, outperform S2MP SSM, whose median relative error is 115.3%

The irrigation estimates provided by Copernicus and RT1 SSM products are consistent. For both products, the highest overestimates are recorded in the irrigation season of 2018. Moreover, the 14-day aggregated time series of irrigation amounts retrieved through the two 1 km products evaluated here are strongly correlated with each other. In fact, the Pearson correlation coefficient, r , between the Copernicus-SSM- and the RT1-SSM-derived irrigation estimates during the considered irrigation seasons is equal to 0.91, while lower values are found between Copernicus SSM and S2MP SSM ($r = 0.62$) and between RT1 SSM and S2MP SSM ($r = 0.51$).

Fig. 3 Comparison between estimated and observed (AFOR) irrigation volumes at the district level during the period 2017–2020 and based on different SSM products: Copernicus SSM, RT1 SSM, and S2MP SSM



The S2MP SSM has also been tested in a plot-scale experiment. In this case, a single time series referring to the P1 experimental field has been used; the benchmark irrigation data has been used to infer the irrigation season, in which the retrieved estimates have been evaluated. The results, provided in Fig. 4, show overestimates in the irrigation season of 2017 (RMSE = 28.30 mm/14-day and BIAS = 19.75 mm/14-day), when tobacco was cultivated and slight underestimates during 2018 (RMSE = 22.39 mm/14-day and BIAS = -14.88 mm/14-day), when the crop was maize.

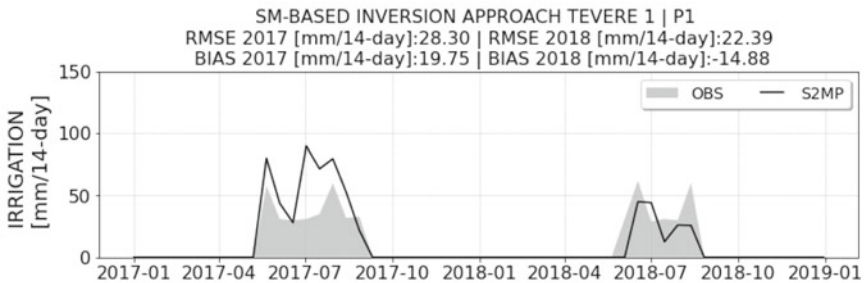


Fig. 4 14-day aggregated time series of benchmark irrigation doses (gray shaded area) and of S2MP-SSM-derived estimates over the P1 pilot field

4 Discussion and Conclusion

In this study, preliminary analyses on the potential of different SSM products relying on Sentinel-1 observations in retrieving irrigation amounts at different spatial scales over an agricultural area in central Italy have been carried out. The district-scale experiment reveals better performances of the 1 km resolution products compared to S2MP SSM, with the Copernicus operational product resulting in the best-performing one. The slight but systematic irrigation overestimates of 1-km products could, in part, find justification in the fact that the AFOR data, used as the benchmark, don't include the volumes (albeit limited) coming from private sources (wells and ponds). Instead, the reason for the non-negligible overestimates retrieved through S2MP SSM in the larger scale experiment lies in the district-aggregated SSM time series used in input. In fact, while the SSM data referring to the Copernicus and RT1 product are in strong agreement during the considered irrigation seasons ($r = 0.93$), the S2MP SSM time series shows different behaviour, resulting in r values equal to 0.74 and 0.59 with Copernicus SSM and RT1 SSM, respectively. The S2MP SSM series shows a higher number of SSM increases in time compared to the coarser resolution products. As a result, when using such data in Eq. (1), there are fewer $\frac{dS(t)}{dt}$ contributions lower than zero, resulting in more water entering the soil. In fact, negative $\frac{dS(t)}{dt}$ values in the absence of rainfall or irrigation events are necessary to solve the balance expressed by Eq. (1) and thus equilibrate the positive contributions coming from the drainage and evapotranspiration terms, representing a consumption of the available SSM [3]. During the investigated irrigation seasons, the percentage of negative $\frac{dS(t)}{dt}$ terms compared to the total has been 35.7% for S2MP SSM, while the analogous percentage of 43.1% and 46.2% have been found for Copernicus SSM and RT1 SSM, respectively. This issue is likely attributable to the lower temporal resolution of the S2MP product compared to the coarser spatial resolution datasets, in combination with the NDVI threshold equal to 0.7 adopted in the data processing chain, which eliminates the lowest SSM values [7]. Moreover, merging many field-scale SSM data to obtain a single district-scale SSM could lead to a further loss of accuracy [7].

The plot-scale experiment provides contrasting results, with overestimates in the irrigation season of 2017 and slight underestimates in 2018, when the result is, however, satisfactory, and the evaluation metrics (RMSE and BIAS) are consistent with similar experiments [4, 11]. The small dataset considered here does not allow for a robust analysis of the factors (e.g., cultural, technical-agronomic, climatic) that can influence the model's performance.

This study sheds light on the potential use of Sentinel-1-derived SSM products for retrieving irrigation amounts at different spatial scales. The collection of reference irrigation data for a higher number of irrigation seasons over the considered pilot field and more pilot sites is foreseen for deepening the finer scale analysis, thus understanding the actual capabilities of high-resolution SSM datasets. In particular, detailed information on the irrigation methods will allow an evaluation of their

influence on the reliability of the estimates. Improvements in the algorithm configuration, such as implementing crop-specific calibration for the ET adjustment factor or adopting different modelling approaches or data sources for the ET term, are also foreseen.

References

1. Massari, C., et al.: A review of irrigation information retrievals from space and their utility for users *Remote Sens.* **13**(20), 4112 (2021)
2. Brocca, L., et al.: How much water is used for irrigation? A new approach exploiting coarse resolution satellite soil moisture products. *Int. J. Earth Obs. Geoinf.* **73**, 752–766 (2018).
3. Dari, J., Brocca, L., Quintana-Seguí, P., Escorihuela, M.J., Stefan, V., Morbidelli, R.: Exploiting high-resolution remote sensing soil moisture to estimate irrigation water amounts over a Mediterranean region. *Remote Sens.* **12**, 2593 (2020).
4. Dari, J., et al.: Irrigation estimates from space: Implementation of different approaches to model the evapotranspiration contribution within a soil-moisture-based inversion algorithm. *Agric. Water Manag.* **265**, 107537 (2022a).
5. Bauer-Marschallinger, B., et al.: Towards global soil moisture monitoring with Sentinel-1: harnessing assets and overcoming obstacles. *IEEE Trans. Geosci. Remote Sens.* **57**, 520–539 (2019).
6. Quast, R., Albergel, C., Calvet, J.C., Wagner, W.: A Generic first-order radiative transfer modelling approach for the inversion of soil and vegetation parameters from scatterometer observations. *Remote Sens.* **11**(3), 285 (2019).
7. Bazzi, H., Baghdadi, N., El Hajj, M., Zribi, M., Belhoucette, H.A.: Comparison of two soil moisture products S2 MP and copernicus-SSM over Southern France. *IEEE J. Sel. Top. Appl. Earth Obs. Remote Sens.* **12**, 3366–3375 (2019).
8. Vergni, L., Vinci, A., Todisco, F., Santaga, F.S., Vizzari, M.: Comparing Sentinel-1, Sentinel-2, and Landsat-8 data in the early recognition of irrigated areas in central Italy. *J. Agricul. Eng.* **52**(4), 1265 (2021).
9. Dari, J., et al.: Double-scale analysis on the detectability of irrigation signals from remote sensing soil moisture over an area with complex topography in central Italy. *Adv. Water Resour.* **161**, 104130 (2022b).
10. Brocca, L., et al.: Soil as a natural rain gauge: estimating global rainfall from satellite soil moisture data. *J. Geophys. Res. Atmos.* **119**, 5128–5141 (2014).
11. Modanesi, S., et al.: A comparison between satellite- and model-based approaches developed in the ESA Irrigation+ project framework to estimate irrigation quantities. In: 2021 IEEE International Workshop on Metrology for Agriculture and Forestry (MetroAgriFor), pp. 268–272 (2021)

Hydrological and Erosive Effects of Prescribed Fire and Mulching with Fern Residues in a Mediterranean Pine Forest



Demetrio Antonio Zema, Manuel Esteban Lucas-Borja, Bruno Gianmarco Carrà, Giuseppe Bombino, Daniela D'Agostino, Pietro Denisi, and Santo Marcello Zimbone

Abstract This study has evaluated the short-term effects of prescribed fire and post-fire mulching using fern on soil hydrology in a pine forest of Southern Italy. Water infiltration (by rainfall simulations) and soil water repellency (SWR) were estimated immediately and one year after fire. Surface runoff volume and soil loss due to rainsplash erosion have been measured in experimental plots under natural precipitations throughout one year. The prescribed fire reduced the infiltration rates compared to the unburned soils. Mulching was not able to contrast this reduction, which, however, vanished over time. Immediately after the fire, the runoff (+375%) and erosion (+900%) significantly increased. The pre-fire runoff and erosion rates restored after about five months. Soil mulching with fern was effective to limit these increases (reductions in the runoff coefficients and soil losses by 60–90%, respectively). The prescribed fire induced SWR, which disappeared after one year. Overall, in a Mediterranean pine forest, post-fire management actions with a cheap mulch materials, as fern, are needed to control the hydrological impacts of prescribed fires in the short term.

Keywords Water infiltration · Soil water repellency · Surface runoff · Soil erosion · Soil hydrological response · Post-fire management

1 Introduction

Prescribed fire, the planned use of low-intensity fire to remove or reduce the fuel that can generate high-severity fires, is considered as a primary option to reduce the

D. A. Zema (✉) · B. G. Carrà · G. Bombino · D. D'Agostino · P. Denisi · S. M. Zimbone
Department "Agraria", Mediterranean University of Reggio Calabria, Località Feo di Vito, 89122
Reggio Calabria, Italy
e-mail: dzema@unirc.it

M. E. Lucas-Borja
School of Advanced Agricultural and Forestry Engineering, Department of Agroforestry
Technology and Science and Genetics, Castilla La Mancha University, Campus Universitario s/n,
02071 Albacete, Spain

wildfire risk in forests. However, this technique removes forest litter and vegetation, leaving the soil bare in the so-called “window of disturbance” of forest soils [12] that lasts from some months to one year after fire application. Moreover, in spite of the low temperature of soil during heating, some changes in soil properties may be noticed (for instance, reductions in organic matter content and soil aggregate stability) [1], and soil hydrophobicity may be induced [5]. The latter effects of prescribed fire may result in reduced water infiltration, and, therefore, in increased runoff and erosion. In the Mediterranean forests, these increases may be even more intense, since the soils are generally shallow and show low aggregate stability. Despite an ample literature about the impacts of fire on soils, the studies on the hydrological effects of prescribed fire are not exhaustive and often contrasting [3]. Increases in runoff and erosion by two orders of magnitude may be observed compared to unburned areas [3]. In contrast, minimal erosion after prescribed fire is sometime recorded [10, 17].

In order to reduce the soil’s susceptibility to runoff and erosion after a wildfire, several treatments have been proposed [16]. Soil mulching is one of the most common post-fire management options [9], since the mulch protects the soil and improves its quality. Agricultural straw is often used as mulch cover in fire-affected areas, but its residues can be displaced by wind in some areas, leaving the hillslopes bare, or accumulated in other areas, with possible reductions in the post-fire emergence of vegetation [13]. Moreover, straw may contain seeds, chemicals and parasites, which can be the sources of non-native vegetation and plant diseases. Fern - *Pteridium aquilinum* (L.) Kuhn – is widely available in forests, does not carry non-native seeds or chemical residues, and is more resistant to wind displacement [13]. Therefore, its residues as mulching material in burned forests may be preferable to straw. However, to the authors’ best knowledge, no evaluations about the use of fern to protect the burned soil from runoff and erosion impacts are available in literature, and, in this sense, this is the main novelty of the present study.

To fill these research gaps, this study has evaluated the hydrological and erosive response of soils in a forest of Calabria (Southern Italy) after a prescribed fire, with or without a mulching treatment with fern residues, in comparison to the unburned soils. More specifically, water infiltration has been estimated in rainfall simulations, and surface runoff and soil loss due to rainsplash erosion were measured after natural precipitations throughout one year after fire.

2 Material and Methods

2.1 Study Area

The study was carried out in a pine forest site close to the municipality of Samo (Calabria, Southern Italy, Fig. 1). The climate of the area is typical of the semi-arid environment (“Csa” class, “Hot-summer Mediterranean” climate, according to Köppen classification [6]. The minimum temperature is -4.3 °C, while the maximum

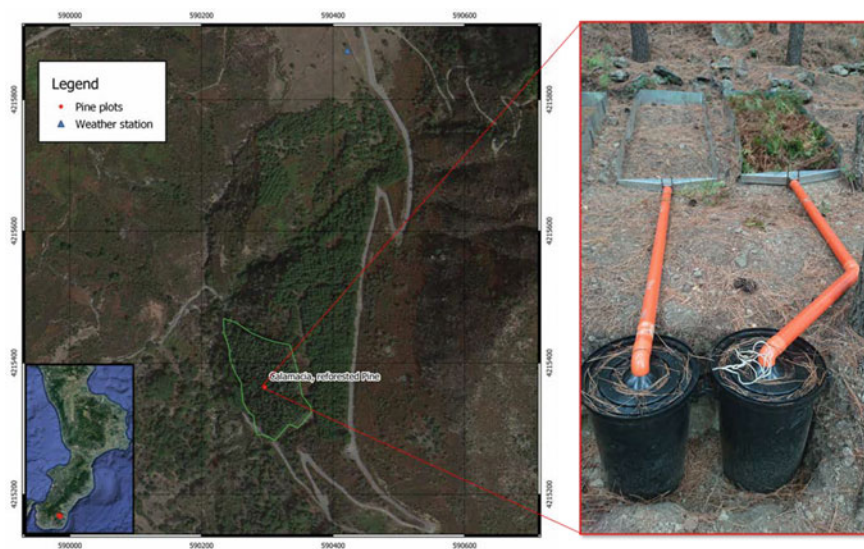


Fig. 1 Location of the experimental site (Samo, Calabria, Italy)

is 43.1°C. The altitude ranges between 650 and 700 m a.s.l. and the local slope is $20.0 \pm 0.82\%$. The texture of soil burned by prescribed fire was loamy sand, while the unburned area was sandy loam. The main tree and shrub species are Pine (*Pinus pinaster* Aiton) and *Quercus ilex* L., *Rubus ulmifolius* S., respectively.

2.2 Prescribed Fire Operations and Mulching Application

In early June 2019 the prescribed fire was applied in the forest site by the Environmental Regional Agency under proper weather conditions (no wind and/or humidity over 50%). The mean soil temperature, measured by thermocouples, was about 25 °C with a peak of 29 °C. Immediately after the prescribed fire, a part of the burned areas was covered with fern residues as mulch material. The plants were cut in the same forest and manually shredded in small pieces (3–5 cm) at a dose of 200 g/m² of dry matter, to form a mulch layer 2–3-cm thick.

2.3 Experimental Design

In the experimental site, three series of plots were installed on hillslopes. Three plots were located in the unburned soils (considered as control). Six other plots were in the burned area, of which three plots were not treated and three plots were mulched with

fern. Overall, the experimental design consisted of three soil conditions (unburned, burned and not treated, and burned and mulched) \times three replicates. Each plot was 3-m long and 1-m wide, and covered an area of 3 m². In order to prevent the inflow of surface water, the plots were hydraulically isolated using metallic sheets that were inserted below the ground surface. A transverse channel and a longitudinal pipe, installed downstream of each plot, intercepted the flows of water and sediments, which were collected into 100-L tanks.

2.4 Monitoring of the Hydrological and Erosive Variables

The water infiltration rate (IR) was determined using a portable Eijelkamp® rain simulator. The simulator reproduced a rainfall with a height and intensity of 18 mm and 360 mmh⁻¹, respectively, over a surface area of 0.3 m \times 0.3 m. The soil water repellency (SWR) was estimated using the Water Drop Penetration Test (WDPT) method [7, 15], and classified according to the values of WDPT proposed by [2]. Fifteen drops of distilled water were released on the soil surface, using a pipette. The time needed by the drops to penetrate the soil was measured, in order to estimate the WDPT. The SWR was measured at the natural soil water content (SWC) using a probe. The SWR measures differing in the same point for a SWC by over 10% were discarded, in order to avoid the SWR being biased by different SWC values, which noticeably influences SWR. IR, SWR and SWC were measured immediately after the prescribed fire and at one year in three randomly selected points per plot, and the three measures were then averaged.

The measurements of surface runoff and soil loss under natural precipitations started immediately after site installation and were carried out throughout until June 2020. Precipitation depth, duration, and intensity were measured by a tipping bucket rain gauge (measuring 5-min data) at a weather station with that was located 1 km from the experimental site. Surface runoff (SR) and sediment concentration were measured after rainfalls over 13 mm, which can be considered as “erosive events” according to [14]. The runoff water in the tank was stirred to achieve a good suspension, and three separate samples were collected, totaling about 0.5 L. The samples were oven-dried at 105°C for 24 h in laboratory. Then, the dried sediments were weighted and sediment concentration was determined, to calculate the soil loss (SL).

2.5 Statistical Analyses

One-way ANOVA with repeated measures (one for each rainfall-runoff event) was applied to IR, SWR, SR, and SL (response variables), assuming as factor the soil condition (unburned, burned and not treated, and burned and mulched). The pairwise comparison by Tukey’s test (at $p < 0.05$) was also used to evaluate the statistical significance of the differences in the response variables. In order to satisfy the

assumptions of the statistical tests (homogeneity of variance and normal distribution), the data were subjected to normality test or were square root-transformed whenever necessary. All the statistical tests were carried out by with the XLSTAT software.

3 Results and Discussion

Prescribed fire reduced IR by 46% compared to the unburned sites. Mulching was not able to limit this reduction (−51%) (Fig. 2a). Moreover, fire increased the slight SWR of unburned soil, which became strongly repellent (Fig. 2b). The significant reduction in IR is due to the synergistic effects of increased SWR, removal of vegetation and presence of ash that clogs the soil pores [18]. One year after the fire, the SWR disappeared and all soils became non-repellent (Fig. 2b). The IR of burned soils slightly increased compared to the value measured one day after the fire (+20%), while this increase was 55% in the mulched soils (Fig. 2a). This shows the positive effect of the post-fire treatment on the hydrological properties of burned soils.

Throughout the monitoring period, seven rainfalls were classified as erosive events. The depth of these events was in the range of 22.4–156 mm, while their duration varied between 7 and 41 h. The maximum absolute intensity was 26.2 mm/h, while the highest mean intensity was 4.90 mm/h. Runoff and erosion significantly increased after the two rainstorm events occurred immediately after fire. In more detail, compared to the unburned plots, the runoff volume measured in the burned soils increased by over 375% in the first event and from zero to 11 mm in the second rainstorm. About five months after burning, the pre-fire runoff generation capacity practically restored, and surface runoff in the burned soils was similar as in the unburned conditions (Fig. 3a). Soil loss due to rainsplash erosion followed the same pattern as runoff, with increases in burned plots up to 900% on occasion of the first erosive event. Soil erosion progressively decreased over time (Fig. 3b). This means that the negative impacts on the hydrological and erosive response in burned soils are limited to four-five months after burning. The first rainfall events, when fire has almost thoroughly removed the vegetation cover and the litter, noticeably increase runoff and erosion [8]. This is in close accordance with the majority of studies, which showed that prescribed fire generates noticeably more runoff and soil loss compared to the unburned areas in the short term after fire (e.g., [4, 10]).

In the short term, soil mulching with fern residues was effective at limiting the increase in the hydrological and erosive response of the burned soils, surface runoff and soil loss due to rainsplash erosion being lower by 60–70% and 80–90%, respectively, compared to the burned and untreated plots. The changes in runoff and erosion rates were associated to the variations in the infiltration rates and water repellency immediately after fire. The slight differences in soil texture may have amplified these changes among the three soil conditions. The recovery of the pre-fire IR and the disappearance of the SWR gained importance over time, and the incorporation of mulch residues became beneficial in driving the short-term hydrological and erosive response of the burned soils. The effectiveness of fern mulching on soil hydrology

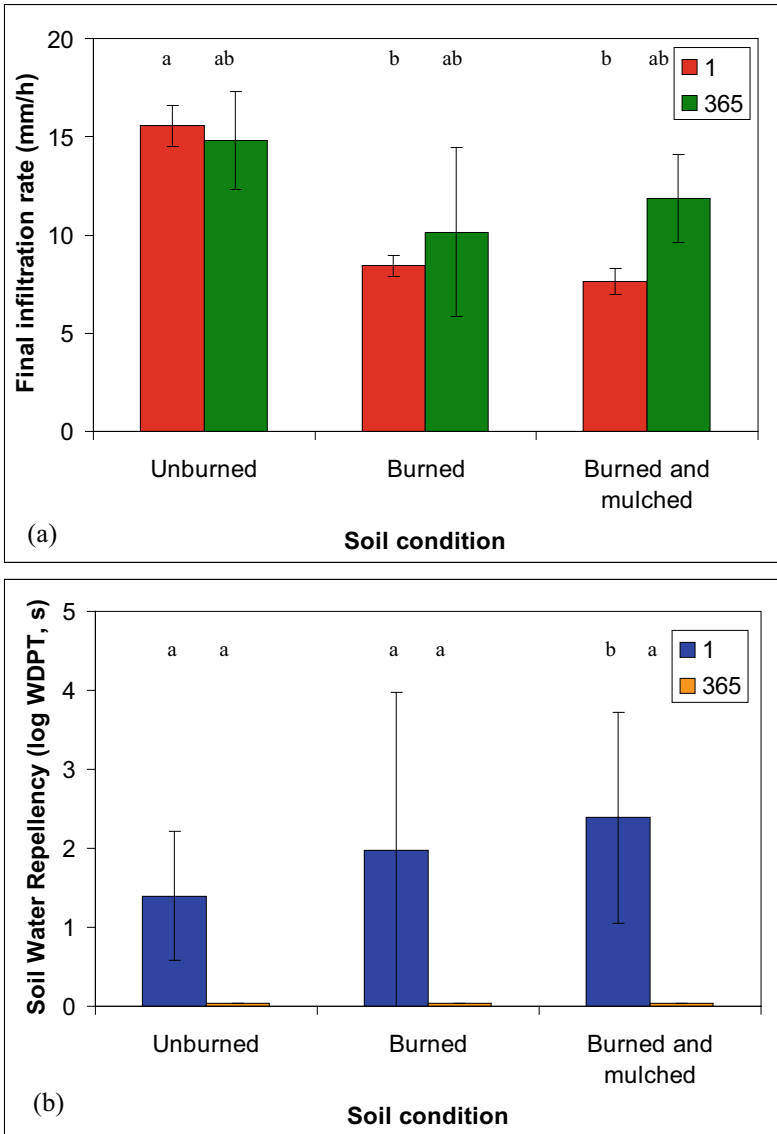


Fig. 2 Water infiltration rate (a) and soil water repellency (b) after prescribed fire and soil mulching with fern residues in the experimental site (Samo, Calabria, Italy). Note: different letters indicate significant differences in the interaction between soil conditions and time after fire, respectively, after Tukey's test ($p < 0.05$); bars report mean \pm std. dev. ($n = 3$)

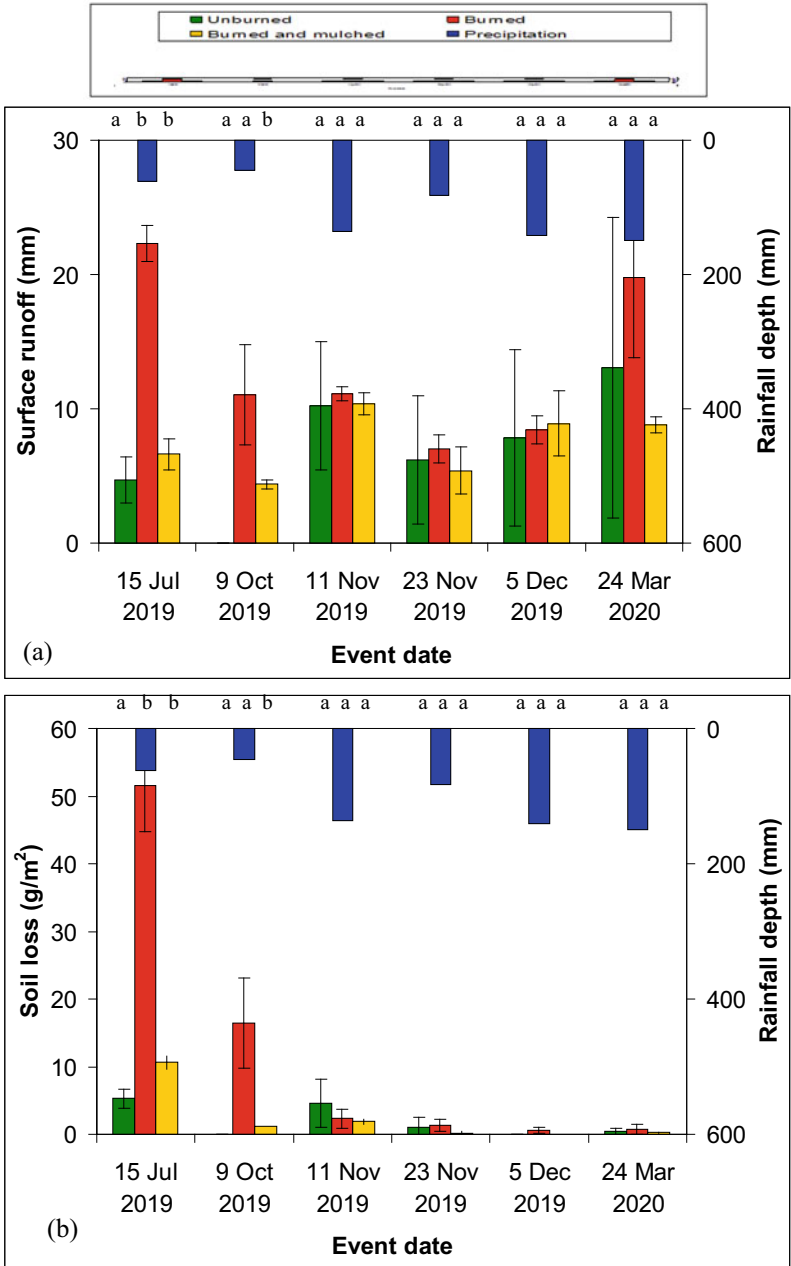


Fig. 3 Precipitation, runoff coefficients (a) and soil loss (b) measured in plots under natural precipitations after prescribed fire and soil mulching with fern residues (Samo, Calabria, Southern Italy). Note: different letters indicate statistically significant differences after Tukey’s test ($p < 0.05$)

shown in our study is higher compared to other relevant investigations (reductions between 40 to 60% compared to the runoff observed in unburned conditions, e.g. [11, 13]).

4 Conclusion

The experimental investigation has shown that, in a Mediterranean pine forest, post-fire management actions, such as the soil cover with a fern residues, are needed to control the short-term increases in surface runoff and soil erosion after prescribed fires. Further research is needed (i) to validate the results at the plot scale through upscaling to hillslopes (which should consider all erosion forms other than rainsplash) or better catchments, and (ii) to explore the influence of the physico-chemical properties of soil on its hydrological and erosive response under burned conditions with and without treatments.

Acknowledgements Bruno Gianmarco Carrà was supported by the Ph.D. fellowship “Programma Operativo Nazionale Ricerca e Innovazione 2014-2020, Fondo Sociale Europeo, Azione I.1 “Dot-torati Innovativi con Caratterizzazione Industriale” granted by the Italian Ministry of Education, University and Research (MIUR) 2018-2021. We cordially thank the management and staff of “Consorzio di Bonifica Alto Ionio Reggino” and “Calabria Verde” (Reggio Calabria, Italy), and the National Corp of Firefighters (“Vigili del Fuoco”) for their valuable support in prescribed fire application and monitoring of the forest sites.

References

1. Alcañiz, M., Outeiro, L., Francos, M., Úbeda, X.: Effects of prescribed fires on soil properties: a review. *Sci. Total Environ.* **613**, 944–957 (2018)
2. Bisdom, E.B.A., Dekker, L.W., J.F.Th., Schoute: Water repellency of sieve fractions from sandy soils and relationships with organic material and soil structure. *Geoderma* **56**, 105–118 (1993). [https://doi.org/10.1016/0016-7061\(93\)90103-R](https://doi.org/10.1016/0016-7061(93)90103-R)
3. Cawson, J.G., Sheridan, G.J., Smith, H.G., Lane, P.N.J.: Effects of fire severity and burn patchiness on hillslope-scale surface runoff, erosion and hydrologic connectivity in a prescribed burn. *For. Ecol. Manage.* **310**, 219–233 (2013)
4. de Dios, B.-S., MacDonald, L.H.: Measurement and prediction of post-fire erosion at the hillslope scale, Colorado Front Range. *Int. J. Wildland Fire* **14**, 457–474 (2005)
5. DeBano, L.F.: Water repellent soils: a state-of-the-art. US Department of Agriculture, Forest Service, Pacific Southwest Forest and ... (1981)
6. Kottek, M., Grieser, J., Beck, C., et al.: World map of the Köppen-Geiger climate classification updated (2006)
7. Letey, J.: Measurement of contact angle, water drop penetration time, and critical surface tension (1969)
8. Lucas-Borja, M.E., Parhizkar, M., Zema, D.A.: Short-term changes in erosion dynamics and quality of soils affected by a wildfire and mulched with straw in a mediterranean forest. *Soil Syst.* **5**, 40 (2021)

9. Lucas-Borja, M.E., Plaza-Álvarez, P.A., Gonzalez-Romero, J., et al.: Short-term effects of prescribed burning in Mediterranean pine plantations on surface runoff, soil erosion and water quality of runoff. *Sci. Total Environ.* **674**, 615–622 (2019)
10. Morris, R.H., Bradstock, R.A., Dragovich, D., et al.: Environmental assessment of erosion following prescribed burning in the Mount Lofty Ranges. Australia. *Int. J. Wildland Fire* **23**, 104 (2014). <https://doi.org/10.1071/WF13011>
11. Prats, S.A., Wagenbrenner, J.W., Martins, M.A.S., et al.: Hydrologic implications of post-fire mulching across different spatial scales. *Land Degrad. Develop.* **27**, 1440–1452 (2016). <https://doi.org/10.1002/ldr.2422>
12. Prosser, I.P., Williams, L.: The effect of wildfire on runoff and erosion in native Eucalyptus forest. *Hydrol. Process.* **12**, 251–265 (1998)
13. Robichaud, P.R., Jordan, P., Lewis, S.A., et al.: Evaluating the effectiveness of wood shred and agricultural straw mulches as a treatment to reduce post-wildfire hillslope erosion in southern British Columbia, Canada. *Geomorphology* **197**, 21–33 (2013). <https://doi.org/10.1016/j.geomorph.2013.04.024>
14. Wischmeier, W.H., Smith, D.D.: Predicting rainfall erosion losses: a guide to conservation planning. Department of Agriculture, Science and Education Administration (1978)
15. van't Woudt, B.D.: Particle coatings affecting the wettability of soils. *J. Geophys. Res.* **64**, 263–267 (1959)
16. Zema, D.A.: Post-fire management impacts on soil hydrology. *Current Opinion in Environmental Science & Health* 100252 (2021)
17. Keesstra, S.D., Maroulis, J., Argaman, E., Voogt, A., Wittenberg, L.: Effects of controlled fire on hydrology and erosion under simulated rainfall. *Cuadernos de Investigación Geográfica* **40**(2), 269–294 (2014). <https://doi.org/10.18172/cig.vol40iss2>. <https://doi.org/10.18172/cig.2532>
18. Cawson, J.G., Sheridan, G.J., Smith, H.G., Lane, P.N.J.: Surface runoff and erosion after prescribed burning and the effect of different fire regimes in forests and shrublands: a review. *Int. J. Wildland Fire* **21**(7), 857 (2012). <https://doi.org/10.1071/WF11160>

**Part II: Applications in Smart Agriculture
and Forestry, Post-harvest Logistics
and Food Chain, Energy, Waste
and By-Products Smart Use, Big Data
and Machine Learning in Biosystems
Engineering**

Uranine as a Tracer for Rapid Detection of Spray Deposition



Antonio Altana , Lorenzo Becce , Paolo Lugli , Luisa Petti ,
and Fabrizio Mazzetto 

Abstract While being virtually mandatory to any sustainable agricultural activity, plant protection products pose sensible risks due to the side effects of improper application techniques.

Monitoring of the application parameters is therefore of paramount importance. In particular, one of the most interesting parameter to monitor is the deposition pattern, whose sampling is reportedly time-consuming and unreliable due to uncontrollable test conditions [9]. In this paper, we investigated a simplified deposition assessment strategy involving uranine, a non-toxic and low cost fluorescent tracer widely used in other fields [7], to minimize the measurement uncertainties exploiting the well known phenomenon of optical absorbance, thanks to the identification of a linear proportionality regime between concentration and absorption peak with coefficient of determination $R^2 = 99\%$. A nozzle evaluation bench has been set up to deposit the fluorescent solution on a matrix of Petri dishes, which were then oven-dried to redissolve the residuals in a fixed amount of water. Spectrophotometry was used to retrieve the mass of deposited solution. After careful calibration against known uranine concentrations, the method yielded results very well correlated to the weight measurements performed prior to drying and allowed to trace back an approximate deposition curve. The complete evaporation of the deposited solvent allows to get rid of the unpredictable atmospheric conditions during the test, while the flexibility of the solution enables an easy tailoring of the technique to different application volumes, deposition rates or collector configurations without losing accuracy.

Keywords Plant protection · Spray drift · Vineyard sprayers · Spray nozzles · Uranine

A. Altana (✉) · P. Lugli · L. Petti · F. Mazzetto
Faculty of Science and Technology (Fa.S.T.), Free University of Bozen-Bolzano (unibz), Bozen,
Italy
e-mail: lorenzo.becce@unibz.it

L. Becce · L. Petti · F. Mazzetto
Competence Centre for Plant Health, Free University of Bozen-Bolzano (unibz), Bozen, Italy

1 Introduction

Plat protection products (PPP) are transported away from target area by several mechanism during their administration to crops, leading to unwanted contamination of natural sites, urban settlements and water bodies. The ISO 22866 standard [1] regulates the test to estimate drift distance on the field, laying out all the test requirements, providing rules for positioning the material collectors that will be used to estimate the distance reached by the sprayed material and the tracer solution requirements employed for the test. In particular, the tracer solution must not induce hazards or contaminations and must have physical properties representative of the PPP, therefore it is suggested to use a surfactant in water solution. The most commonly used tracers involve dissolving in water colour dyers such as yellow tartrazine [8] or brilliant sulfoflavine (BSF) [10]; however, these substances entail problems with residual dye material after the experiment and long processing times to acquire the information about the deposition pattern, as reported by [3]. Aim of this work is to investigate the use of Uranine (fluorescein sodic salt) in water as a tracer, with the purpose of reducing the elaboration and post-cleaning workload during the ISO 22866-compliant spray drift assessment test; issues about the compatibility with other chemical compounds and large-scale measurements will be addressed in following studies.

2 Current Uses and Properties of Uranine

Uranine is widely used in various field, such as ophthalmology and optometry for the identification of blood vessels in the eye [5]. In agriculture and earth sciences, due to its property of changing colour depending on concentration, uranine is used in evaporation experiments [11], applied to identify leaks in pipelines [12], as flow tracer for surface and groundwater [6], and in flow-through systems to quantify the retention of PPPs in surface water [13] and to consequently optimize the application techniques to achieve stable day-scale exposures [14]. Uranine is found in the solid state as red crystals; when dissolved in water, it acquires a green colour dependent on the solution concentration and becomes fluorescent when exposed to UV light, as shown in Fig. 1. Its absorbance peak is around 490 nm, but its intensity and wavelength are affected by the pH of the solution and subject to photodecay over time [7]. In this work, the employment of uranine as a drift tracer is investigated through laboratory analysis, with the aim to identify its optimal concentration range for this specific application and subsequently to estimate the spatial distribution of deposited material from a dedicated test bench.

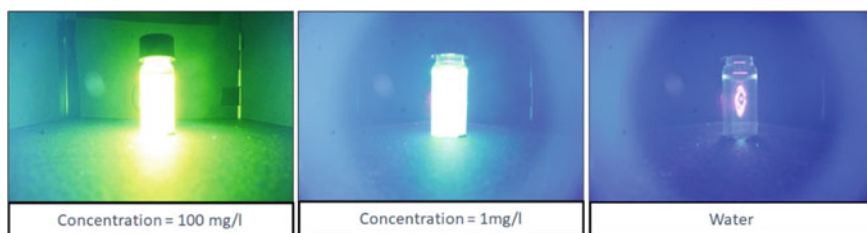


Fig. 1 Fluorescent solutions at different concentration and water, exposed to UV light

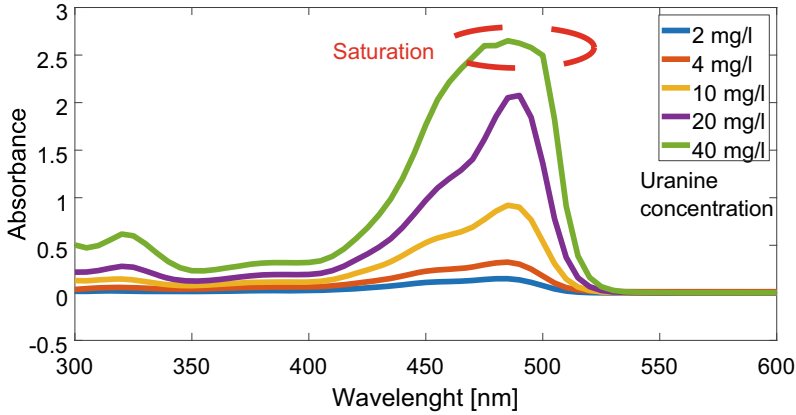
3 Materials and Methods

3.1 Solution Preparation and Absorbance Measurement

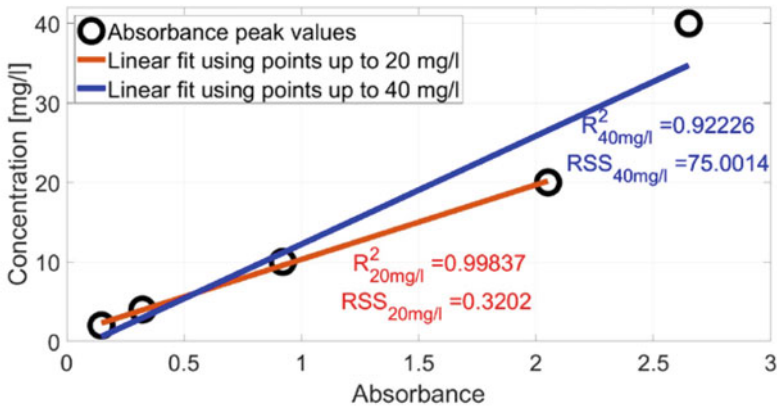
First, has been identified the range of uranine concentration in which peak absorbance varies linearly with respect to concentration. The solution has been obtained by adding the calculated amount of Uranine powder (Trotec GmbH) in fresh deionized water (DI). The absorption spectrum was measured by an Agilent Cary 60 UV–V is spectrophotometer, equipped with 1 ml disposable polystyrene cuvettes, from 300 to 600 nm so that the entire curve around the peak was within the measured spectrum.

3.2 Linear Regime Investigation

Different solutions of uranine from 1 mg/l to 100 mg/l have been tested, and the absorption spectrum analyses are summarised in Fig. 2a, where it can be noted how, with the instrument used, the absorbance peak measurement saturates for concentration above 40 mg/l, where a broadening of the spectrum around the peak is noticeable. The concentration of 20 mg/l of uranine in water has been selected as reference concentration for the subsequent experiments, this is the highest concentration that would avoid visible saturation in the spectrum, and results in a better coefficient of determination R^2 and lowest residual error RSS (Residual Sum of Squares, indicating the deviation of the predicted values from the actual empirical data), calculated in the linear fitting of the correlation between absorbance peak and concentration, displayed in Fig. 2b.



(a) Absorption spectrum for different concentrations of uranine in aqueous solution



(b) Relation between concentration of uranine in water and absorbance peak value, with coefficient of determination R^2 and residual error RSS for solution up to 20mg/l and 40mg/l

Fig. 2 Measurements to identify the regime where absorbance peak changes linearly with concentration of uranine. **a** Absorption spectrum for different concentrations of uranine in aqueous solution. **b** Relation between concentration of uranine in water and absorbance peak value, with coefficient of determination R^2 and residual error RSS for solution up to 20 mg/l and 40 mg/l

3.3 Deposited Material Estimation Method

After spraying, the procedure for estimating the deposited material involves the complete drying of the liquid in each collector for 18 h at 60 °C, and the redissolution of the dry residue in 25 ml DI water; thus the final uranine concentration for each collector will be proportional to the initially deposited material, which can

be estimated by measuring the peak absorbance value of the solution and using the calibration equation obtained with known solutions and concentrations.

4 Deposition on Test Bench

4.1 Description of the Test Bench and Patternator Setup

The test bench is a modification of the one described in [4] at the Agroforestry Innovations Lab (AFI-Lab) of unibz and consists of a pump that leads the test solution, at a maximum pressure of 10 bars, from a reservoir to a conventional nozzle holder. The holder was held at 45° from the horizontal by a simple elbow joint attached to the original structure. The nozzle and joint can be observed in Fig. 3.

The patternator is a conventional field drift test stand (Salvarani s.r.l., IT), of which a 5 m section was placed in front of the nozzle, parallel to the spraying direction. The bench is composed of a series of housings for Petri dishes, one every 0.5 m. The first slot of the system was placed at 0.7 m horizontal distance from the nozzle, with the Petri 0.5 m below the nozzle orifice, due to the construction constraints of the setup and the patternator.

For completeness, two hollow-cone nozzles were used for the tests: a type TXB8002 and an air-induction AITXB8002; both are made by TeeJet and have 80° cone aperture. However, differentiating the performance of the nozzles is beyond the scope of this study. Before the tracer deposition experiment, all the pipes in the system were flushed with DI water for about a minute and rinsed using the same uranine solution, to reduce the dilution due to water in the pipes. Each spray repetition lasted 1 min and in total 8 Petri were exposed for each experiment up to a distance of 4.2 m.

Fig. 3 The nozzle holder and its support



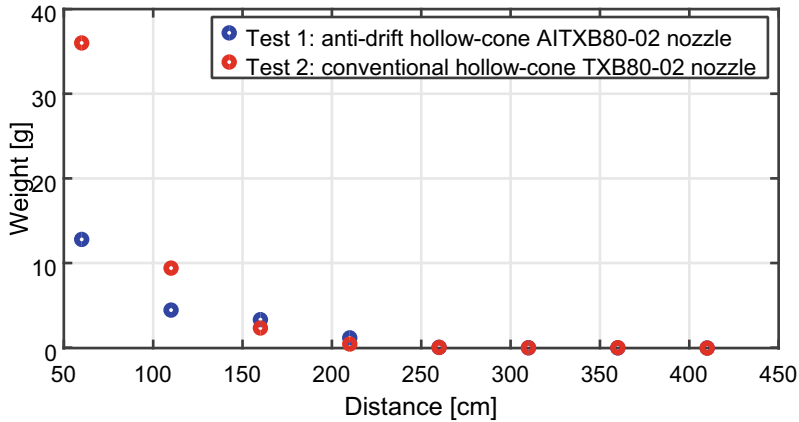


Fig. 4 Spatial distribution of the sprayed solution, indicated by its weight

4.2 Experiment Results

The accuracy of the method was estimated against the weight of material deposited in each container immediately after spraying: since the time between spraying and weighting was minimal, thanks to the small number of samples, the disturbance introduced by the uncontrollable variables was also minimal. Clearly, under large-scale testing conditions, water re-evaporation could not be considered negligible. The spatial distribution of the material can be seen in the graph in Fig. 4.

The calibration curve has been calculated by depositing a known amount of the sprayed solution, from 1 to 25 ml, and adding DI water to reach the fixed volume of 25 ml used for redissolving the material in the other containers. The obtained calibration curve, such that of Fig. 5, was used to estimate the amount of deposited spray, using the peak absorbance of each solution, previously calculated from the measured absorption spectrum after over-drying and subsequent redissolving of residual material in each collector.

Figure 6 and 7, for the first and second tests respectively, compare the measured weights after spray to the estimated weights and their relative error; it can easily be observed how the estimated and measured weights share the same trend.

4.3 Results Discussion

Both tests have the same amplitude behaviour in the estimate error. The Petri dishes with the largest deposition showed a higher estimation error, which may be due to the fact that the resulting solution approaches a regime of non-linearity of the absorbance peak value in relation to the concentration and begins to saturate, as described in Fig. 2a. In Figs. 6, 7, the negative values for the estimated curve around zero are due

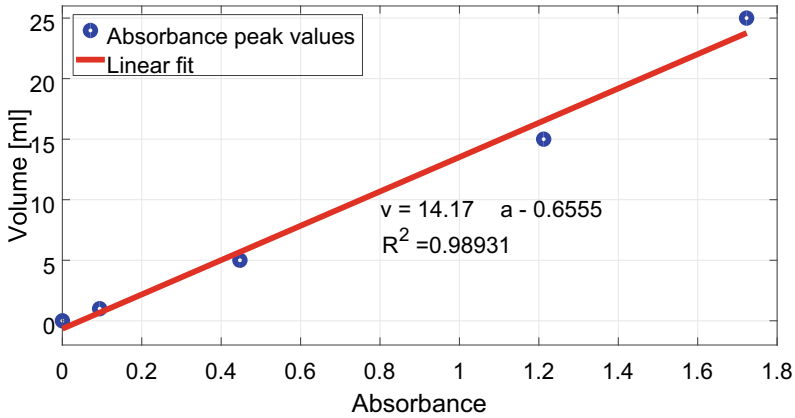


Fig. 5 Calibration curve obtained by depositing fixed volumes of uranine solution. Where v is the volume in millilitres and a is the absorption

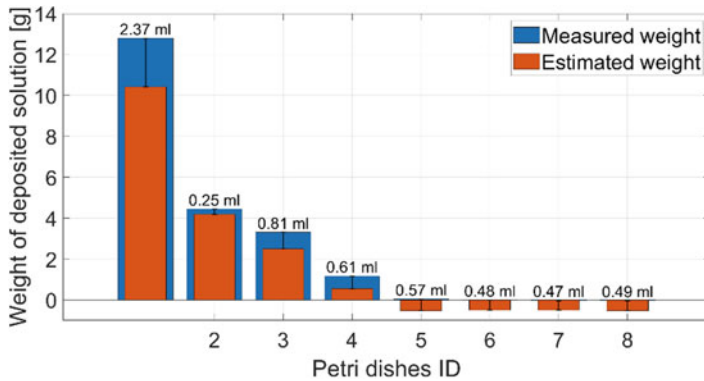


Fig. 6 Comparison Petri by Petri, between the weight measurement, used as a reference, and the estimated deposited material. Test 1: using the anti-drift hollow cone AITXB80 02 nozzle

to the intercept in the calibration equation; however, this numerical artefact has little relevance, as it is possible to indicate a threshold of deposited material, and identify the minimum distance over which a given amount of deposition has occurred, as per indicated in the standard. The calibration curve calculation can be improved using concentration points that ensure a linear regime, or it could be divided in multiple regimes to which apply dedicated, piecewise linear calibration curves better fitting for the estimated material. Besides the numerical factors, the material properties themselves could lead to deviation from linearity: as a matter of fact, even the pH of the dilution water could vary and shift the absorption peak, as well as the ageing of the solution over time, all factors which can lead to a decay of the properties.

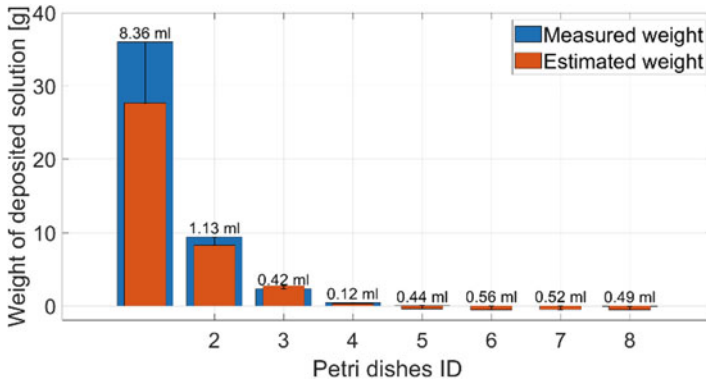


Fig. 7 Comparison Petri by Petri, between the weight measurement, used as a reference, and the estimated deposited material. Test 2: using the conventional hollow-cone TXB80-02 nozzle

5 Conclusion and Outline

Uranine, extensively used in other fields, has been preliminarily investigated as a tracer for estimating spray drift deposition. Two trials were carried out with a test bench, that ensures both compatibility with real agricultural equipment and repeatability of the process under laboratory conditions. The results indicate a linear behaviour between uranine concentration and absorbance peak value, coherent with other studies performed in controlled experimental conditions employing the same tracer in a grid pattern [2]. Further studies are needed to refine the test procedure and the use of the solution, investigating the interaction with other typical solutes in the sprayer tank, including agrochemicals, but from these results it is evident how the use of a solution of uranine in water enables a quick estimate of the amount of material deposited during spraying.

References

1. Equipment for crop protection—Methods for field measurement of spray drift. Standard ISO 22866:2005, International Organization for Standardization, Geneva, CH (2005)
2. Altana, A., Becce, L., Avancini, E., Lugli, P., Petti, L., Mazzetto, F.: Cost-effective tracing techniques for the rapid characterization of spray deposition and drift through electrical conductivity and fluorescence. In: 2022 IEEE Workshop on Metrology for Agriculture and Forestry (MetroAgriFor), pp. 164–168. IEEE (2022)
3. Balsari, P., et al.: Field-crop-sprayer potential drift measured using test bench: Effects of boom height and nozzle type. *Biosys. Eng.* **154**, 3–13 (2017). <https://doi.org/10.1016/j.biosystemeng.2016.10.015>
4. Becce, L., Amin, S., Carabin, G., Mazzetto, F.: Preliminary spray nozzle characterization activities through shadowgraphy at the AgroForestry innovation lab (AFI-lab). In: 2022 IEEE Workshop on Metrology for Agriculture and Forestry (MetroAgriFor), pp. 136–140. IEEE. <https://doi.org/10.1109/MetroAgriFor55389.2022.9965106>

5. Cai, S., Liu, T.: The role of ultra-widefield fundus imaging and fluorescein angiography in diagnosis and treatment of diabetic retinopathy. *Curr. Diab. Rep.* **21**(9), 1–6 (2021)
6. Flury, M., Wai, N.N.: Dyes as tracers for vadose zone hydrology. *Rev. Geophys.* **41**(1) (2003)
7. Gerke, K.M., Sidle, R.C., Mallants, D.: Criteria for selecting fluorescent dye tracers for soil hydrological applications using uranine as an example **61**(4), 313–325. <https://doi.org/10.2478/johh-2013-0040>
8. Gil, E., et al.: Determination of drift potential of different flat fan nozzles on a boom sprayer using a test bench. *Crop Prot.* **56**, 58–68 (Feb2014). <https://doi.org/10.1016/j.cropro.2013.10.018>
9. Gil, E., Llorens, J., Gallart, M., Gil-Ribes, J.A., Miranda-Fuentes, A.: First attempts to obtain a reference drift curve for traditional olive grove's plantations following ISO 22866 **627**, 349–360. <https://doi.org/10.1016/j.scitotenv.2018.01.229>
10. Gregorio, E., et al.: Measurement of spray drift with a specifically designed lidar system. *Sensors* **16**(4), 499 (2016). <https://doi.org/10.3390/s16040499>
11. Kass, W.: *Tracing Technique in Geohydrology*. Routledge (2018)
12. Phillips, A.J., et al.: Potential CO₂ leakage reduction through biofilm-induced calcium carbonate precipitation. *Environ. Sci. Technol.* **47**(1), 142–149 (2013)
13. Stang, C., et al.: Role of submerged vegetation in the retention processes of three plant protection products in flow-through stream mesocosms. *Chemosphere* **107**, 13–22 (2014)
14. Wiczorek, M.V., et al.: Reference scenarios for exposure to plant protection products and invertebrate communities in stream mesocosms. *Sci. Total Environ.* **545**, 308–319 (2016)

Development of an Investment Decision Tool for Biogas Production from Biowaste in Mediterranean Islands



Antonio Ascuito, Martina Agosta, George Attard, Antonio Comparetti, Carlo Greco, and Michele Massimo Mammano

Abstract Biomethane is the Renewable Energy Source (RES) derived from the purification of biogas produced from Anaerobic Digestion (AD) process using biomass. Biomethane can be injected into the natural gas grid, thereby contributing towards satisfying the energy demands of society. The aim of this work is to test an investment decision tool for assessing the financial feasibility of an AD plant using biowaste for producing biogas and, then, biomethane, as well as digestate and, then, compost.

The first Sicilian AD plant aimed at producing biomethane was built in the province of Caltanissetta in 2021. The innovative Enersi Sicilia plant treats 56,000 t of Organic Fraction of Municipal Solid Waste (OFMSW) per year to generate 499.22 Sm³h⁻¹ of biomethane. This plant yields a yearly total of 4,168,483 Sm³ of biomethane, thereby replacing 8,450 t of oil equivalent and avoiding the emission of 6,126 t of fossil CO₂ into the atmosphere. The solid fraction of digestate is recovered and processed into compost, that corresponds to approximately 25–30% of the original feed in biomass weight. This compost is classified as a “mixed composted soil conditioner”, that can be used in agriculture, within Circular Bioeconomy (CBE). The financial feasibility of AD plant case study was assessed through Cost-Benefit Analysis (CBA), by assuming a reference period of 20 years, both with and without the financial subsidy provided by the Italian government to those who market biofuels,

A. Ascuito (✉) · M. Agosta · A. Comparetti
Department of Agricultural, Food and Forest Sciences, University of Palermo, Viale delle Scienze, Building 4, 90128 Palermo, Italy
e-mail: antonio.asciuto@unipa.it

G. Attard
Institute of Earth Systems, Department of Rural Sciences and Food Systems, University of Malta, Msida MSD 2080, La Valletta, Malta

Agency for the Governance of Agriculture Bio-Resources, Ministry for Agriculture, Fisheries and Animal Rights, Triq Antonio Cassar, Marsa, Malta

C. Greco · M. M. Mammano
Council for Agricultural Research and Economics (CREA), Research Centre Protection and Certification, Bagheria (Palermo), Italy

i.e. certificate of introduction in consumption. The reliability and robustness of CBA results were verified through the Sensitivity Analysis (SA).

Even without the subsidy, the AD plant proved to be a good financial investment, without taking into consideration all its social and environmental benefits. The financial feasibility of the investment would be preserved up to an 8.21% yearly increase of the operational costs.

The production and use of biomethane and other renewable gases in existing infrastructures would allow EU to achieve the climate objectives of Paris Agreement, i.e. to save € 140 billion a year by 2050. The interest of the growing market in biomethane mobility demonstrates the great potential of alternative uses of this gas.

Keywords Anaerobic digestion · Biogas · Biomethane · Digestate · Compost · Circular Bioeconomy (CBE)

1 Introduction

The severe energy satiation challenge faced by some developing as well as developed countries to meet the demand for domestic and industrial use has recently been further aggravated by the geopolitical conflict that has resulted in a surge in international market prices for Liquefied Petroleum Gas (LPG) as well as for chemical fertilizer. Concurrently, the amount of household kitchen biowaste, constituting the Organic Fraction of Municipal Solid Waste (OFMSW), is steadily increasing [1–3]. Under such a scenario, the Anaerobic Digestion (AD) technology, that has the capacity of producing biogas and digestate would address both issues. Biogas can be used for the co-generating of electric and thermal bioenergy or alternately, the it can be scrubbed into biomethane to be used as a biofuel. Additionally, the digestate, the final by-product of the AD process, can be used either as a liquid bio-fertiliser or further transformed through aerobic composting into a solid bio-fertiliser. Thus, the AD technology could be a cost-effective and clean process capable of addressing some of the society's energy demands [1]. This technology is a proven and widely used process for the conversion of organic waste into usable biogas, thereby alleviating the dependence on fossil fuels and in so doing, reduces Greenhouse Gases (GHGs) emissions [4].

The first Sicilian AD plant aimed at producing biomethane (a purified form of biogas) to be used as a biofuel or alternatively injected into the regional natural gas grid, was commissioned in 2021 by “Enersi Sicilia Srl”, and built in the province of Caltanissetta in 2021. The yearly inputs of this innovative plant comprise of 56,000 t of OFMSW, with a disposal gate fee of € 65–70 t⁻¹; and 10,500 t of woodchips that is co composted with the digestate to produce a structured compost matrix. The yearly outputs include 7,551,600 m³ of biogas that following proper scrubbing results in 4,168,483 Sm³ of biomethane (499.22 Sm³ h⁻¹), and 19,200 t of compost, to be used as bio-fertiliser. The biomethane has the capacity of replacing and estimated 8,450 t of oil equivalent, and in so doing eliminates the emission of approximately 6,126

t of fossil CO₂ into the atmosphere. The compost to approximately 25–30% of the original feed in biomass weight is classified as a “mixed composted soil conditioner”, that can be used in agriculture within Circular Bio Economy (CBE) concept.

While the technical efficiency parameters for the selected plant are well known and established, the financial parameters may not be so easily defined. In projects with such a magnitude of investment, different criteria guide the decision of implementing an investment on whether the economic entity involved is private or public [5]. In the case study is a private entity, thus according to the hedonistic principle, the decision of implementing the investment must be based on direct costs and benefits, which “can actually be converted into money” [5].

A recent study by [6] on bibliometric mapping of Cost Benefit Analysis (CBA) highlighted that the “Energy fuels and geosciences” is one of the most important research topics where this analysis was applied during the last 30 years. The CBA is a tool for quantifying and comparing costs and benefits, has been used since the nineteenth century to establish whether a project is cost-effective or not [7]. In order to assess the desirability of an investment, a wide and straightforward view analysing the perspective cash flows is needed. Thus, the effects of the investment can be examined, but this implies the evaluation of all relevant costs and benefits associated with the implementation of the project. CBA is aimed at helping the decision-makers [8], as it is an investment decision tool able to establish communications between economists, policymakers, and citizens on the opportunity of implementing projects [9]. The robustness of CBA can be verified through the Sensitivity Analysis (SA) that examines the elements of the analysis that can be uncertain or controversial. This procedure illustrates results’ sensitivity to changes in these values [10]. The Discounted Cash Flow (DCF) analysis provides, initially, a time period (i.e., number of years) during which the investment consequences, traduced into cost and benefit flows, are expected to occur. Subsequently, the CBA requires the calculation of a series of indicators useful to establish the financial viability of the project, i.e., Net Present Value (NPV), Internal Rate of Return (IRR), Payback Period (PP) and Benefit Cost ratio (B_0/C_0).

Many authors [11–30] have relied on CBA for assessing the economic or financial feasibility of AD plants, by calculating economic indicators such as NPV, B_0/C_0 ratio, IRR and PP and by implementing SA. These studies often consider the availability of subsidies in an attempt to understand whether the financial feasibility of the project is strictly bound to the subsidies. As evident from the surveyed literature, at a time when the struggle to mitigate against climate change has a crucial role, the priority is to promote innovative projects and methods that increase energy production from renewable sources. In order to better evaluate these proposals, all the aspects that the implementation of this kind of investment can involve need to be examined and evaluated. With this perspective, the aim of this study is the application of an investment decision tool for assessing the financial feasibility of an AD plant located in Caltanissetta (Sicily, Italy) that utilises OFMSW and woodchips into biomethane and a mixed compost.

2 Materials and Methods

The AD plant case-study could provide a solution not only for the sustainable management and disposal of OFMSW, whose costs cannot be supported anymore by local institutions but also for producing bioenergy from renewable sources and, therefore, reducing GHGs emissions in the atmosphere. Thus, this work is part of CBE concept, aimed at safeguarding the environment for the next generations.

The financial feasibility of AD plant case-study was therefore assessed through CBA based on the technical-economic data used in the project Business Plan (BP), dating 2018 and provided by the company that manages this AD plant.

In general terms the different criteria that guide the decision of implementing an investment depend on whether the economic entity involved is private or public [5]. In the case study, the involved entity is private so that, according to the hedonistic principle, the decision of implementing the investment must be based on direct costs and benefits, which “can actually be converted into money” [5].

The technical data of the plant, indicated in the BP, include the input amounts, i.e. OFMSW and wood chips, the feeding plan and the output amounts, i.e. biomethane and compost, that was defined as a “mixed composted soil conditioner”.

The economic data consist of yearly revenues and costs.

The costs are classified in investment costs (CAPEX), that are further divided into total plant cost, development costs and technical know-how, as well as yearly operational costs (OPEX).

The revenues are divided into three categories:

- 1) money flow from biomethane, that is in turn disaggregated in the revenue obtained from its sale (applying the unit market price of $\text{€ } 0.27 \text{ Sm}^3 \text{ }^{-1}$) and in the financial subsidy provided by the Italian government to those who market biofuels, i.e. certificate of introduction in consumption (“Certificato di Immissione in Consumo” - CIC), calculated by multiplying the unit market price of CIC ($\text{€ } 0.59 \text{ Sm}^3 \text{ }^{-1}$) per the yearly subsidised production of biomethane;
- 2) revenues generated by the gate fee from the disposal of feedstocks (i.e. OFMSW and wood chips in the case study) at the plant, calculated by multiplying the yearly OFMSW amount disposed per the unit value of $\text{€ } 60 \text{ t}^{-1}$, according to agreement protocols signed with the local municipalities (as well as a prudential unit value of $\text{€ } 30 \text{ t}^{-1}$ was used for wood chips);
- 3) sale of compost (applying the unit price of 30 € t^{-1}), as this is a quality soil conditioner, suitable for both traditional and organic agriculture.

With regard to cost items, the CAPEX consists of the expenses needed from purchasing to commissioning the whole AD plant. These cost items are distributed over a period of 1.5 years and also include the costs of development and technical skills, i.e. intangible fixed assets, such as administrative burdens, specialist advice, publications, printing, executive design, work management and corresponding safety coordination.

The CAPEX also includes the cost for the purchase of the land where the plant was built up and an item including the potential unforeseen occurrences, equal to 1% of the total investment cost.

The OPEX includes all the costs needed for carrying out the yearly production activity, e.g. ordinary and extraordinary maintenance needed in each phase of the production process (pre-treatment, biogas production, upgrading and composting), materials used in this process (e.g. chemicals and activated carbons), cost for consumption of electric energy and general costs (e.g. disposal, reusable fractions, insurance, employees, technical management, administration, and local taxes).

The assessment of financial viability of the investment was carried out through CBA, by assuming the duration of the subsidy of 20 years as reference period.

The estimated cash flows were actualised, by using a discount rate of 5%, identified on the basis of the Weighted Average Cost of Capital (WACC), in relation to the risk profile identified by the investor.

Moreover, although the Business Plan hypothesised a 2% yearly increase, both in the price of biomethane and in the operational costs, it was considered appropriate to keep the yearly cash flows (operational costs and revenues) constant during the reference period (20 years).

The yearly changes of the above items were taken into account in SA, described in “Results and Discussion” section.

The Discounted Cash Flow (DCF) analysis provides, initially, a time period (i.e. number of years) during which the investment consequences, traduced into cost and benefit flows, are expected to occur.

Subsequently, the CBA requires the calculation of a series of indicators useful to establish the financial viability of the project, i.e. NPV, DBCR, IRR and PP, which are those usually utilised in literature.

NPV (€) represents the present value of the future cash flows concerning the economic activity in the considered time period. Positive values indicate that the investment is financially justifiable, while negative results show a non-profitable investment. It can be calculated as follows (Eq. 1):

$$NPV = \sum_{t=0}^n \frac{Net\ Benefit}{(1+r)^t} \quad (1)$$

where:

Net Benefit is the yearly difference between revenues and costs (€);

r is the discount rate (%);

t is the time period from 0 to n years.

DBCR is the ratio between the discounted future revenues and the corresponding costs (Eq. 2). Values equal to and higher than 1 indicate that the discounted costs are more than compensated by the discounted benefits, hereby justifying the investment decision.

$$DBCR = \frac{B_0}{C_0} \quad (2)$$

where:

B_0 and C_0 are the discounted benefits and costs, respectively.

IRR (%) is the interest rate at which NPV reduces to 0 (Eq. 3). The investment will result cost-effective only for IRR values higher than the discount rate (5%).

$$\sum_{t=0}^n \frac{Net\ Benefit}{(1 + IRR)^t} = 0 \quad (3)$$

PP represents the number of years needed for the total recovery of the initial investment cost and is calculated by the ratio of the total cost of AD plant (€) to the yearly operational gross margin (€ year⁻¹), as it is reported in Eq. 4.

$$PP = \frac{Total\ investment\ cost}{Annual\ net\ benefit} \quad (4)$$

In order to test the robustness of CBA results, SA was carried out for recalculating the above indicators, by varying the trend of the operational costs in the 20-year reference period.

The different levels of yearly increase of the operational costs assumed for the SA were +2%, +5%, +10% and +15%.

Moreover, the hypothesis of the absence of the CIC was formulated and, under this condition, the financial feasibility of the AD plant was tested for different levels of yearly increase in the operational costs (+2%, +5%, +10% and +15%).

The decision to apply the SA only to the operational costs is based on two reasons: 1) the available technical-economic data are provisional and aggregated, as they were aimed at the project approval; 2) the revenues of AD plant (biomethane, compost, OFMSW and wood chips) are unlikely to be subject to market price reductions in the short and medium term for the strategic role that they play in the search for RES.

3 Results and Discussion

The general assumptions useful for the financial analysis, in terms of revenues and costs, are described in detail in “Materials and Methods” section, hence only the numerical results concerning the average yearly balance (revenues and operational costs) and the total investment cost are here discussed.

The investment costs are structured as summarised in Table 1.

The total investment costs are assumed to be equal to € 17,200,000, where 91.4% is related to total plant cost, 5.2% includes expenses for development and technical skills, 2.3% is considered for the purchase of land and 1.1% is for contingencies and rounding up.

The distribution of the yearly revenues, on a total equal to € 7,835,896, is shown in Table 2.

Table 1 Investment costs (CAPEX)

CAPEX	€	%
Total plant cost	15,720,000	91.4
Land purchase	400,000	2.3
Contingencies and rounding up	192,600	1.1
Development and technical skills	887,400	5.2
Total	17,200,000	100.0

Table 2 Yearly revenues

Yearly revenues	€	%
Biomethane injected into the natural gas grid	1,125,490	14.4
CIC	2,459,405	31.4
Disposal of OFMSW and wood chips	3,675,000	46.9
Sale of compost	576,000	7.3
Total	7,835,896	100.0

The revenues from biomethane, that resulted € 3,584,896, are disaggregated into two items:

- 1) sale of biomethane when it is injected into the natural gas grid, resulting in € 1,125,490, equal to 14.4% of total revenue;
- 2) revenue obtained from the financial subsidy provided by the Italian government (CIC), that is quite significant in absolute terms, i.e. € 2,459,505 (corresponding to 31.4% of total plant revenue).

The revenue from gate fee for waste disposal, that is the amount of money paid by the municipalities of the territory surrounding the AD plant to the company managing it for the disposal of OFMSW and wood chips, plays a paramount role within the profitable entries of the yearly financial report of the company itself. In fact, its total amount (€ 3,675,000, equal to 46.9% of the total plant revenue) is comparable to the above revenue obtained from biomethane, proving to be an actual strength in the financial profitability of the examined plant. The revenue from OFMSW is nevertheless more relevant, since it is 91.4% of total amount, whereas wood chips correspond in money terms to the remaining 8.6% of this item.

The revenue from the sale of compost is less significant in money terms rather than the other items, accounting for € 576,000, which represent just 7.3% of total yearly revenue of the AD plant.

The operational costs of the process, whose structure is summarised in Table 3, are equal to € 1,787,500 and are divided in three categories:

- 1) expenses for ordinary and extraordinary maintenance, including costs for spare parts and external assistance during each phase of the production process, chemicals and activated carbons used in the AD plant and in the upgrading phase, as

Table 3 Yearly operational costs (OPEX)

OPEX	€	%
Maintenance	481,000	26.9
Consumption of electric energy	352,500	19.7
General costs	954,000	53.4
Total	1,787,500	100.0

well as accounting for approximately one quarter (26.9%) of total operational costs;

- 2) costs for the consumption of electric energy, that is purchased from the grid network, within the electricity self-produced through the photovoltaic generator, and is equal to € 352,500 (calculated by multiplying the unit value of € 0.15 kWh⁻¹ per the estimated net consumption of electric energy, i.e. 2,350,000 kWh per year) and, therefore, accounts for 19.7% of total operational costs;
- 3) general costs, i.e. diversified group of expenses, including insurance, personnel and technical management, administration, local taxes and disposal of reusable fractions, whose amount is € 954,000, so that they represent the most significant cost category, with a percentage of 53.4% of total operational costs.

Based on the above data, the financial feasibility of the AD plant was challenged and tested. The first CBA was carried out in the current scenario, taking into account the subsidy (CIC) for plant management.

The financial indicators obtained from the cash flow analysis at a discount rate of 5% showed an excellent performance of the AD plant.

NPV of the investment resulted € 55,406,719, which is quite satisfactory for the AD plant. The DBCR resulted 2.47, which means that € 1 of discounted cost produces € 2.47 of discounted benefits. The PP resulted 2.84 years and, therefore, in less than three years the capital cost would be repaid by the net benefits of the AD process, despite a 20-year investment period. Finally, the IRR of the investment resulted over 35%, i.e. much higher than the discount rate (5%) chosen according to the opportunity cost of the investment. The CBA and SA results with reference to CIC scenario are summarised in Table 4.

Table 4 Results of CIC scenario

Yearly increase of OPEX	NPV (€)	IRR (%)	DBCR	PP (years)
+0.0% (baseline)	+55,406,719	35.08	2.47	2.8
+2.0%	+51,156,079	34.22	2.22	3.0
+5.0%	+42,573,882	32.63	1.84	3.6
+10.0%	+19,112,472	28.40	1.26	7.8
+15.0%	-24,561,761	–	0.79	>20.0
+13.5%	0	5.00	1.00	20.0

Table 5 Results of no-CIC scenario

Yearly increase of OPEX	NPV (€)	IRR (%)	DBCR	PP (years)
+0.0% (baseline)	+26,215,956	20.35	1.70	4.8
+2.0%	+21,965,962	18.98	1.52	5.4
+5.0%	+13,383,766	15.92	1.27	7.6
+10.0%	-10,077,644	-	0.86	>20.0
+8.2%	0	5.00	1.00	20.0

The SA showed a good stability in the results of the financial analysis. In fact, only a severe yearly increase (+13.5%) in the plant operational costs would cause the NPV to fall to zero, the DBCR to drop to 1 and the PP to extend to 20 years.

The robustness of the above financial results was tested by repeating the CBA with the exclusion of the CIC-related revenue from the cash flow analysis.

Even without the economic support of CIC, the AD plant proved to be a good investment in financial terms, without taking into consideration all its social and environmental benefits that would be quantified through a CBA carried out by a public investor.

Without CIC (Table 5), even if the plant NPV goes down from over € 55,000,000 ca. to € 26,000,000 ca., from a financial point of view, the new scenario would not be worrying at all. The PP becomes longer rather than that calculated in the previous scenario: in less than 5 years (4.79) the plant investment costs are repaid, i.e. in a short time period to refund the invested capital. The DBCR, which is a CBA indicator more neutral rather than the NPV (usually biased in large investment projects), still expresses (value equal to 1.70) a high capacity of the plant to produce benefits, in relation to the incurred costs. The IRR is lower (20.35%) than that obtained in a CIC scenario but still represents an interest rate much higher than that expressing the opportunity cost of a comparable investment under the same risk profile.

The SA applied to this scenario shows that a 8.21% yearly increase in the total plant operational costs, approximately one quarter (26.9%), is needed for making to decrease the NPV to 0 and the DBCR to 1, while the PP would lengthen to the whole 20-year period. The financial feasibility of the investment would be preserved up to an 8.21% yearly increase of the operational costs, hereby showing the stability of the investment decision.

Although the literature analysis produced a considerable number of recent papers [11–30] where CBA was applied to AD plant investment, no study was found in order to compare the obtained results with those ones of the present work.

In fact, not only studies including extremely diversified scenarios and research objectives but also a large number of combinations of technical variables, e.g. plant size, biomethane yield, other process outputs, nature and amounts of feedstocks and catchment area, different from those of the analysed AD plant, were found.

4 Conclusions

Results indicate that, despite the substantial investment cost involved to have the case study AD plant built up and running for the conversion of OFMSW and wood chips into biomethane and compost, it is possible to deduce that:

- 1) this investment is financially feasible, both with and without CIC subsidy, as it is shown by the positive values of NPV and by other calculated indicators (DBCR, IRR and PP);
- 2) the investment continues to be profitable even in the worst study case scenario, where operational costs undergo yearly increase up to 13.5%, during the AD plant lifetime of 20 years, as it is shown by the satisfactory SA results.

Moreover, even when assuming the most prudential scenario, i.e. without the subsidy and with the yearly increase of operational costs up to 8.21%, the NPV continues to be positive, proving the financial convenience of building up the AD plant.

Furthermore, the strength of this plant is the use of OFMSW and wood chips, i.e. feedstocks that represent an additional revenue, besides that deriving from the sale of biomethane. In fact, the company does not support any cost for the purchase of the above feedstocks needed for plant operation as it is the case of other plants using other raw materials and, therefore, charge a disposal gate fee.

On the other hand, the only scenario which might give rise to an apparent negative performance of the AD plant is a prospective political decision of withdrawing subsidy (CIC) and waste disposal gate fee. In fact, the yearly income from sale of bioenergy and compost would not be enough to cover plant operational costs. This consideration might cause a rethinking with regard to an investment decision in an AD plant by a private entity but only in a long-term view, where the current economic situation might lead to a stoppage of subsidies and gate fees. Besides the economic viability of an AD plant, an alternative way to appreciate this technology is to look at the maximisation of the social well-being instead of the private income.

A limitation of this work is that the economic data used in the analysis are forecast, as the plant was triggered just a few months ago, so that the related cost and revenue items are not sufficiently disaggregated, hereby not allowing more pertinent considerations.

More accurate data, that would allow to perform a more detailed assessment, will be obtained after the first years of plant operation.

Thus, the production and use of biomethane and other renewable gases in existing infrastructures would allow EU to achieve the climate objectives of Paris Agreement, i.e. to save € 140 billion a year by 2050.

On the other hand, the interest of the growing market in biomethane mobility demonstrates the great potential of alternative uses of this renewable gas.

References

1. Rajendran, K., Aslanzadeh, S., Johansson, F., Taherzadeh, M.J.: Experimental and economical evaluation of a novel biogas digester. *Energy Convers. Manage.* **74**, 183–191 (2013)
2. Comparetti, A., et al.: Biogas yield from Sicilian kitchen waste and cheese whey. X Convegno Nazionale di Ingegneria Agraria, Viterbo, 8–12 settembre 2013. *J. Agric. Eng.* **XLIV**(s2) (2013)
3. Greco, C., Comparetti, A., Orlando, S., Mammano, M.M.: A contribution to environmental protection through the valorisation of kitchen biowaste. In: Biocca, M., Cavallo, E., Cecchini, M., Failla, S., Romano, E. (eds.), *Safety, Health and Welfare in Agriculture and Agro-food Systems*. SHWA 2020. *Lecture Notes in Civil Engineering (LNCE)*, vol. 252, pp. 411–420 (2022).
4. Wang, Y., et al.: Reactor performance and economic evaluation of singular, binary, and ternary mixing of feedstocks for anaerobic digestion. *Environ. Technol.* (2019).
5. Michieli, M., Cipolotti, G.B.: *Trattato di estimo. Generale, immobiliare, agrario, forestale, ambientale, legale (Treaty of Evaluation. General, real estate, agricultural, forestry, environmental, legal)*. Ed. Edagricole - New Business Media, Series University & training, Edition 8 (2018)
6. Majerova, I., Abdrazakova, A.: A bibliometric mapping of cost-benefit analysis - three decades of studies. *Economies (MDPI)* **9**, 110 (2021)
7. Torriti, J., Ikpe, E.: Cost-benefit analysis, pp. 1–14 (2014)
8. Prest, A.R., Turvey, R.: XII Cost-benefit analysis: a survey. *The American Economic Association, Surveys of Economic Theory Volume III, The Royal Economic Society and the American Economic Association*, pp. 155–156 (1966)
9. Persky, J.: Cost-benefit analysis and the classical creed. *J. Econ. Perspect.* **15**(4), 199–208 (2001)
10. Hadley, D.: Sensitivity analysis within cost benefit analysis. Spicosa (Science Policy Integration for Coastal Systems Assessment), Project Report, University of East Anglia CSERGE, Norwich, UK, Integrated Project funded by The European Community Under the Sixth Framework Programme Priority 1.1.6.3 Global Change and Ecosystems (2011)
11. Karellas, S., Boukis, I., Kontopoulos, G.: Development of an investment decision tool for biogas production from agricultural waste. *Renew. Sustain. Energy Rev.* **14**(4), 1273–1282 (2010)
12. Hublin, A., Schneider, D.R., Džodan, J.: Utilization of biogas produced by anaerobic digestion of agro-industrial waste: energy, economic and environmental effects. *Waste Manage. Res.* **32**(7), 626–633 (2014)
13. Cucchiella, F., D’Adamo, I., Gastaldi, M., Miliacca, M.: A profitability analysis of small-scale plants for biomethane injection into the gas grid. *J. Clean. Prod.* **184**, 179–187 (2018)
14. de Brito, R.C., Barros, R.M., dos Santos, I.F.S., Tiago Filho, G.L., da Silva, S.P.G.: Municipal solid waste management and economic feasibility for electricity generation from landfill gas and anaerobic reactors in a Brazilian state. *Environ. Technol. Innov.* **22**, 101453 (2021)
15. Silva, S.T.S., Barros, R.M., dos Santos, I.F.S., de Cassia Crispim, A.M., Tiago Filho, G.L., Lora, E.E.S.: Technical and economic evaluation of using biomethane from sanitary landfills for supplying vehicles in the Southeastern region of Brazil. *Renew. Energy* **196**, 1142–1157 (2022)
16. Anaya-Reza, O., Altamirano-Corona, M.F., Castelán-Rodríguez, G., García-González, S.A., Durán-Moreno, A.: Techno-economic and environmental assessment for biomethane production and cogeneration scenarios from OFMSW in Mexico. *Waste Biomass Valoriz.* **13**(2), 1059–1075 (2022)
17. Akbulut, A., Arslan, O., Arat, H., Erbaş, O.: Important aspects for the planning of biogas energy plants: Malatya case study. *Case Stud. Thermal Eng.* **26**, 101076 (2021)
18. Zhang, D., Zhang, B., Zheng, Y., Zhang, R., Liu, P., An, Z.: Economic assessment and regional adaptability analysis of CCHP system coupled with biomass-gas based on year-round performance. *Sustain. Energy Technol. Assess.* **45**, 101141 (2021)

19. Lim, Y.F., et al.: Evaluation of potential feedstock for biogas production via anaerobic digestion in Malaysia: kinetic studies and economics analysis. *Environ. Technol.* **43**(16), 2492–2509 (2022)
20. Campello, L.D., Barros, R.M., Tiago Filho, G.L., dos Santos, I.F.S.: Analysis of the economic viability of the use of biogas produced in wastewater treatment plants to generate electrical energy. *Environ. Develop. Sustain.* **23**(2), 2614–2629 (2021).
21. Cañote, S.J.B., et al.: Energy and economic evaluation of the production of biogas from anaerobic and aerobic sludge in Brazil. *Waste Biomass Valoriz.* **12**(2), 947–969 (2021)
22. Jellali, S., Charabi, Y., Usman, M., Al-Badi, A., Jeguirim, M.: Investigations on biogas recovery from anaerobic digestion of raw sludge and its mixture with agri-food wastes: application to the largest industrial estate in Oman. *Sustainability* **13**(7), 3698 (2021)
23. Martín-Pascual, J., Fernández-González, J.M., Ceccomarin, N., Ordoñez, J., Zamorano, M.: The study of economic and environmental viability of the treatment of organic fraction of municipal solid waste using Monte Carlo simulation. *Appl. Sci.* **10**(24), 9028 (2020)
24. Teghammar, A., Forgács, G., Horváth, I.S., Taherzadeh, M.J.: Techno-economic study of NMMO pretreatment and biogas production from forest residues. *Appl. Energy* **116**, 125–133 (2014)
25. Boffardi, R., De Simone, L., De Pascale, A., Ioppolo, G., Arbolino, R.: Best-compromise solutions for waste management: Decision support system for policymaking. *Waste Manage.* **121**, 441–451 (2021)
26. Gupta, R., Miller, R., Sloan, W., You, S.: Economic and environmental assessment of organic waste to biomethane conversion. *Biores. Technol.* **345**, 126500 (2022)
27. Cudjoe, D., Nketiah, E., Obuobi, B., Adu-Gyamfi, G., Adjei, M., Zhu, B.: Forecasting the potential and economic feasibility of power generation using biogas from food waste in Ghana: evidence from Accra and Kumasi. *Energy* **226**, 120342 (2021)
28. Padilha, J.L., Mesquita, A.L.A.: Waste-to-energy effect in municipal solid waste treatment for small cities in Brazil. *Energy Convers. Manage.* **265**, 115743 (2022)
29. Gwavuya, S.G., Abele, S., Barfuss, I., Zeller, M., Müller, J.: Household energy economics in rural Ethiopia: a cost-benefit analysis of biogas energy. *Renew. Energy* **48**, 202–209 (2012)
30. Adeoti, O., Ilori, M.O., Oyebisi, T.O., Adekoya, L.O.: Engineering design and economic evaluation of a family-sized biogas project in Nigeria. *Technovation* **20**(2), 103–108 (2000)

Evaluation of Precision Technologies Approach for the Management of an Experimental Field in Organic Fruit Growing



Alberto Assirelli , Federica Brandi , Fiorella Stagno ,
Maura Sannino , Salvatore Faugno , Salvatore Musio ,
Gianluca Baruzzi , and Giancarlo Rocuzzo 

Abstract Understanding the main growing crop parameters is the key factor in precision and sustainable agriculture, therefore, the use of remote geophysical measurement systems has increased. Criteria for the adoption of precision agriculture are slowly affecting a growing number of farms managed generically according to the principles of conventional and integrated agricultural systems. Organic farming experiences, for which CREA has been active at the Italian area, are still limited. In order to start a rational process of setting up activities, this work focused on the characterization of an experimental organic field of CREA's fruit species breeding program. In this work, the Automatic Resistivity Profiling approach (ARP) was tested with the application of the Top Soil Mapper (TSM) system. The results obtained were used for discrimination of homogeneous zones and for considerations of the subsequent set of targeted management operations. The test in the CREA field was carried out in March 2021 and the data obtained were evaluated. Two types of soil have been identified and the reasons for this difference were evaluated in detail and reported. The main advantages of TSM are optimization of machines use, reduction of fuel consumption and working times. With this technology, already known especially for extensive crops, can be mutated adopted for in organic orchards with more protection of soil structure through appropriate tillage, fuel savings and sustainable yield optimization.

Keywords TSM · precision agriculture · soil compaction · auto-guidance · sustainable management

A. Assirelli · F. Brandi (✉) · F. Stagno · S. Musio · G. Baruzzi · G. Rocuzzo
CREA Council of Agricultural Research and Economics, Via della Navicella 2/4, 00184 Roma (Rm), Italy
e-mail: federica.brandi@crea.gov.it

M. Sannino · S. Faugno
Department of Agricultural Sciences, University of Naples Federico II^o, Via Università 100, 80055 Portici (Na), Italy

© The Author(s), under exclusive license to Springer Nature Switzerland AG 2023
V. Ferro et al. (eds.), *AIIA 2022: Biosystems Engineering Towards the Green Deal*,
Lecture Notes in Civil Engineering 337,
https://doi.org/10.1007/978-3-031-30329-6_27

1 Introduction

Precision agriculture is rediscovering a new prospect for development due to the now increasing digitization in different production processes with real benefits in different sectors even in initial applications [1]. Until a few years ago, the prevailing interest had always been indicated toward ordinary, commodity-based production, while today advantages are also perceivable in the canopy evaluation of orchards for their management [2]. The growing field of conservation agriculture and soil management is beginning to deliver results [3] and to find meeting points with the latest technologies in interfile orchards management [4].

Many of the techniques used so far for ordinary crops can profitably be extended to the organic sector as from the positive experiences conducted on mulberry [5]. The dissemination of these new techniques and technologies to the agricultural sector requires careful planning even initially starting with soil characterization possibly using indirect methodologies [6] from which targeted crop water management strategies can then be derived [7] with insights into the water footprint in arboriculture [8]. Precise characterization of soils can also enable detailed profiling of moisture itself or groundwater tables to support irrigation strategies [9]. Early experiments in pushing automation and robotization of production cycles, studied in the livestock sector [10] also show valuable insights for mechanical and repetitive field operations such as thinning and inter-row checks. However, the diffusion of these technologies and more generally of precision agriculture is encountering not a few difficulties by identifying very diverse paths and often linked to local production realities understood both as land and technological availability, which greatly condition its inclusion and the development of digital agriculture in Italian agriculture [11].

As part of the CREA “Council for agricultural Research and Economics” fields, managed by Research Center for Olive, Fruit and Citrus Crops (OFA), there are one certified organic area with the aim of fostering the dissemination of innovation; at the Forlì site, Emilia-Romagna region, Italy and with the support of Research Center for Engineering and agrofood processing (CREA-IT), a path has been undertaken for the gradual introduction of precision agriculture technologies in the organically managed field, starting with soil characterization using innovative systems based on ARP technology (Automatic Resistivity Profiling), a new rapid and non-invasive survey method that allows continuous detection of the apparent electrical resistivity of soil (in Ohm*m), which can be compared with soil parameters such as texture, moisture, organic matter, mineral content.

In this paper, the first experiences of characterization by TSM of the CREA-OFA-Forlì test field soils, are reported as a start of the introduction of new indirect and non-invasive soil characterization technologies for subsequent targeted management of crop operations and technical means.

2 Material and Methods

The study was carried out in 3.8 ha an organically managed field located in Magliano (FC) of the CREA-OFA (44°9' N, 12°5' E, 32 m altitude). In the experimental area pear, apple and peach trees are cultivated, in the framework of breeding activities (crossing combinations to increase tolerance to biotic and abiotic stresses). The Topsoil Mapper is an integrated geophysical measurement system for determining different soil parameters. Using modern geophysical measurement technology and automated data analysis methods, the top layers of the rootable soil are measured accurately and with high resolution. To this end, the TSM relies on the principle of electromagnetic induction for conductivity measurement in the soil. The depth of exploration is about one meter (3.5 feet). The sensor sends a low-voltage electric current to the soil and, thanks to a complex system of receiving sensors, is able to measure and record characteristic parameters of the reference soil. The system is able to measure the electrical conductivity in different layers: 0–20, 0–40, 0–60, 0–80 cm depth soil moisture, depth first characterizing layer (plowed sole, rock, boulders, etc.). With the aim to identify the main key variable classes in soil management as in [13]. Soil mapping provides a thorough understanding of the soil in space and time as detailed in [14]. The TSM system is composed by different elements: external detector from which transmission emitted and received soil signal, a GPS (Global Positioning System) antenna for detailed georeferencing data, a data logger with internal processor for data storage, processing and archiving, an external monitor for operator with the aim to managing the detection phase and operation according to the manufacturer's instructions, intermediate checks and instant evaluation of processing data. Overall, it is very versatile and easy to install on any self-propelled vehicle with the availability of a 12 V electrical socket, not necessarily agricultural but also of another kind of All Terrain Vehicles (ATV).

The information is displayed on a map, the soil conductivity map, to improve information for better field management (eg. fertilization, irrigation, weeds control). The experimental field currently managed by CREA appears to be planted to tree species with 4–4.5-m row spacing depending on the species.

The system, installed at the rear of a farm tractor (Fig. 1), followed a well-defined and detailed path that allowed precise characterization of the plot. Initially, a perimeter routing (Fig. 2) of the entire plot was followed then followed by a precise routing of all the inter-rows.

The field was managed with regular mowing of the herbaceous wild essences, in some inter-row areas trials on cover cropping are currently carried out. The contemporary three samples were run for each identified soil type and the sub samples were pooled and sent to a laboratory for chemical and physical analyses.

In soil sampling the following parameters were analyzed: pH, electrical conductivity extract (EC), cationic exchange capacity (CEC) obtained with NH_4Ac [15], particle-size (texture), nitrogen (N) quantification determined in according to the Dumas method [16]; available phosphorus (P) using Olsen's method [17]; organic matter with Walkley Black method [18], and Extractable Micronutrients using DTPA



Fig. 1 Inter-row scanning with TSM (Top Soil Mapper) technology



Fig. 2 The first part of the analysis at the Magliano experimental fields involved identifying the perimeter within which to do the surveys and identification of soil zones based on electrical conductivity

Extraction (Zn, Mn, Cu, Fe) [19]. In compliance with the regional organic production regulations and the certification and control body, the soil characterization of TSM with specific analysis will be analysed in order not to incur management penalties which in detail include the integrated production specification of the Emilia Romagna region, physical–chemical parameters for soil classification are showed in Tables 1 and 2.

Table 1 Endowments of exchangeable P (ppm); Emilia-Romagna Region - Integrated production regulations 2010 - General rules

Endowments of exchangeable P (ppm)		
Judgment	Olsen P-value	Class endowment for standard cards
Very low	<5	Very poor
Low	5–10	Poor
Medium	11–15	Normal
High	16–30	Normal
Very high	>30	High

Table 2 C/N ratio
Emilia-Romagna Region -
Integrated production
regulations 2010 - General
rules

C/N ratio		
<9	Low	Fast mineralization
9–12	Medium	Normal mineralization
>12	High	Slow mineralization

3 Results

The system has initially identified the shape field (Fig. 2) and homogeneous soil zones by electrical conductivity from which it also extrapolates and indicates soil characterizing points responsible for the different electrical conductivity detected will be identified.

The system identified two prevailing soil area, both of which are characterized by the clay soil type, medium C/N ratio variable from 10.4 to 11.8 a medium–high content of organic matter variable from 3.10% to 3.36%: a low boron content variable from <0.50 to 0.50 mg/kg. The main variable that emerged from two soil type concerns the assimilable phosphorus content found to be significantly different between the two soil types identified from low-medium to very high P content (Table 1). Based on these results, it is possible to make interesting observations about the soil analyzed with this technology. The importance of fruit tree Phosphorus fertilization of has received much less attention than nitrogen (N) and potassium (K) fertilization, although some studies have shown that a phosphorus supply, distributed in a single annual intervention at flowering, in apple trees results in increased production without compromising Soluble Solid Content (SSC) and without altering organoleptic characteristics [20]; beneficial effects related to fertilization with this element have also been recorded in other species, such as melon and peach tree.

In soil, Phosphorus is considered a stable element because of its low solubility; Phosphorus is an indispensable element because of the many processes in which it is involved: it plays a primary role in energy transfers (recall, in fact, that Phosphorus is one of the components of Adenosine-triphosphate or ATP); it is essential for seed germination; it is part of photosynthetic processes; it contributes to the formation of, it is involved in all metabolic processes of the plant; and, finally, it is one of the constituents of the cell walls of nucleic acids (DNA-RNA).

Phosphorus is also the constituent responsible for the robustness and stability of tissues: a toughening of tissues in turn results in greater plant re-strength to attacks by pathogenic organisms and pests. Some studies have highlighted its role in determining the organoleptic characteristics of fruits [21].

The two soil types are characterized by analysis showed in Table 3 where not only P content is different but also texture and organic matter.

As can be seen from the comparative analysis of the two types of soils surveyed by the TSM, the instrument in a single step has allowed to identify an important variable that will modify in every way the management system followed up to now. The organic management of the field showed also to highlight an organic substance content, common in the two prevailing soil types, but more than twice the average

Table 3 Main soil characteristics, sampled in the two zones identified by the TSM

Analisis codes	S-21/025590	S-21/025591
Soil physical property		
Texture	Clay	Clay
Sand (%)	14	19
Silt (%)	37	30
Clay (%)	49	51
Chemical composition		
EC (dS/m 20 °C)	0.140	0.146
pH (extract 1:2,5)	7.84	7.77
Organic Matter (g/kg)	33.6	31.0
N (g/kg)	1.653	1.736
C/N ratio	11.8	10.4
Available Phosphorus (mg/kg)	11	46.6
Active limestone (% CaCO ₃)	3.1	2.53
Micro elements		
B (mg/kg)	<0.50	0.50
Fe (DTPA) (mg/kg)	19.5	19.2
Mn (DTPA) (mg/kg)	21.8	27.8
Cu (DTPA) (mg/kg)	12.3	13.6
Zn (DTPA) (mg/kg)	1.24	1.39
Exchange capacity		
Mn (meq/100 g)	1.33	1.46
K (meq/100 g)	0.68	0.78
Na (meq/100 g)	<0.05	<0.05
CEC (meq/100 g)	30.8	29.5
Saturations	98.8	0.995

content of the neighboring soils where it is difficult to exceed 1.5%. As for the phosphorus between one type of soil and another, the content of available P ranges from 11 to over 40, denoting an important consideration for future practices for at least a few years it will be necessary to target fertilizations only to products, authorized in organic crops, with low or no phosphorus content with direct economic advantages being the second macro-element of fertility.

4 Conclusion

This first test in organic experimental orchards of remote characterization of soils conducted on the CREA test field showed a types of soils rather homogeneous, only two main types characterized prevalently for the P content, important aspects also for allow to lay the foundations to future experiments on rootstocks allowing, through suitable test protocols, to evaluate the management, development and response in two environments differing and introduction of targeted techniques identified may lay the groundwork for a introduction of digital agriculture concepts also for experimentation purpose in organic orchards.

References

1. Scarfone, A., et al.: Semi-automatic guidance vs. Manual guidance in agriculture: a comparison of work performance in wheat sowing. *Electronics*, MDPI **10**(71), Article number 825 (2021)
2. Assirelli, A., Romano, E., Bisaglia, C., Lodolini, E., Neri, D., Brambilla, M.: Canopy index evaluation for precision management in an intensive olive orchard. *Sustainability* (Switzerland) **13**(151), Article number 8266 (2021)
3. Maetens, W., Poesen, J., Vanmaercke, M.: How effective are soil conservation techniques in reducing plot runoff and soil loss in Europe and the Mediterranean? *Earth Sci. Rev.* **115**, 21–36 (2012)
4. Assirelli, A., Liberati, P.: Simulation modelling of mechanical systems for intra-row weeding in a precision farming approach. *Spanish J. Agricul. Res.* **20**(14), Article number e0201 (2022)
5. Giora, D., et al.: Preliminary study on the application of a commercial LAI ceptometer for estimation of leaf production on low vigour mulberry trees. In: 2021 IEEE International Workshop on Metrology for Agriculture and Forestry, MetroAgriFor 2021 - ProceedingsPages 416 - 4212021 3rd IEEE International Workshop on Metrology for Agriculture and Forestry, MetroAgriFor 2021Virtual, Online3 November 2021 through 5 November 2021Code 175226 (2021)
6. Islam, M.M., Meerschman, E., Saey, T., De Smedt, P., Van De Vijver, E., Van Meirvenne, M.: Comparing apparent electrical conductivity measurements on a paddy field under flooded and drained conditions. *Precision Agric.* **13**, 384–392 (2012)
7. James, I.T., Godwin, R.J.: Soil, water and yield relationships in developing strategies for the precision application of nitrogen fertiliser to winter barley. *Biosys. Eng.* **84**, 467–480 (2003)
8. Salmoral, G., Aldaya, M.M., Chico, D., Garrido, A., Llama, M.R.: The water footprint of olives and olive oil in Spain. *Span. J. Agric. Res.* **9**, 1089–1104 (2011)
9. Martínez, G., Vanderlinden, K., Espejo, A.J., Giraldez, J.V., Muriel, J.L.: Field-scale soil moisture pattern mapping using electromagnetic induction. *Vadose Zone J.* **9**, 871–881 (2010)
10. Tangorra, F.M., Calcante, A., Vigone, G., Assirelli, A., Bisaglia, C.: Assessment of technical-productive aspects in Italian dairy farms equipped with automatic milking systems: a multivariate statistical analysis approach. *J. Dairy Sci.* **105**(9), 7539–7549 (2022)
11. Linee Guida sviluppo agricoltura di precisione in Italia, decreto ministeriale n.33671 del 22/12/2017. <https://www.politicheagricole.it/flex/cm/pages/ServeBLOB.php/L/IT/IDPagina/12069>
12. Martínez, G., Vanderlinden, K., Pachepsky, Y., Espejo, A., Giraldez, J.V.: Estimating topsoil water content of clay soils with data from time-lapse electrical conductivity surveys. *Soil Sci.* **177**, 369–376 (2012)

13. Van Meirvenne, M., Islam, M.M., De Smedt, P., Meerschman, E.V., De Vijver, E., Saey, T.: Key variables for the identification of soil management classes in the aeolian landscapes of north-west Europe. *Geoderma* **199**, 99–105 (2013)
14. Viscarra Rossel, R.A., Adamchuk, V.I., Sudduth, K.A., McKenzie, N.J., Lobsey, C.: Proximal soil sensing: An effective approach for soil measurements in space and time. *Adv. Agron.* **113**, 237–282 (2011)
15. Rich, C.I.: Removal of excess salt in cation-exchange-capacity determinations. *Soil Sci.* **93**, 87–94 (1962)
16. Dumas, J.B.A.: Procédes de l'Analyse Organique. *Ann. Chim. Phys.* **247**, 198–213 (1831)
17. Olsen, S.R., Cole, C.V., Watanabe, F.S., Dean, L.A.: Estimation of available phosphorus in soils by extraction with sodium bicarbonate. United States Department of Agriculture Circular 939, Washington, DC, 19 pp (1954)
18. Walkley, A., Black, I.A.: An examination of the Degtjareff method for determining soil organic matter and a proposed modification of the chromic acid titration method. *Soil Sci.* **37**, 29–38 (1934)
19. Lindsay, W.L., Norvell, W.A.: Development of a DTPA soil test for zinc, iron, manganese, and copper. *Soil Sci. Soc. Amer. J.* **42**, 421–428 (1978)
20. Martuscelli, M., Di Mattia, C., Stagnari, F., Specca, S., Pisante, M., Mastrocola, D.: Influence of phosphorus management on melon (*Cucumis melo* L.) fruit quality. *J. Sci. Food Agricul.* **96**(8), 2715–2722 (2016)
21. Neilsen, G.H., Neilsen, D., Toivonen, P., Herbert, L.: Annual bloom-time phosphorus fertigation affects soil phosphorus, apple tree phosphorus nutrition, yield, and fruit quality. *HortScience* **43**(3), 885–890 (2008)

Potential Bioenergy and Biofertiliser Production from Livestock Waste in Mediterranean Islands Within Circular Bioeconomy



George Attard, Noel Azzopardi, Antonio Comparetti, Carlo Greco, Anthony Gruppetta, and Santo Orlando

Abstract The livestock sector can generate a steady stream of manure biomass, that can be subjected to different transformation technologies. Moreover, EU must also play an important role in developing a policy framework for the Mediterranean islands, in order to offer equality of development opportunities to all its territories, by designing and implementing adequate measures for reducing their dependency on fossil fuels. Therefore, this study evaluates the potential biogas and digestate production through the Anaerobic Digestion (AD) process of livestock manure on a selection of Mediterranean islands, sharing characteristics such as the costs of waste management and energy production, that are much higher than in mainland Europe: Balearic Islands, Corsica, Sardinia, Sicily, Malta, Crete and Cyprus.

The potential manure generation from cattle and pigs was estimated by using available livestock statistical data, so that the potential biogas, bioenergy and digestate production was quantified by applying established conversion factors.

It was possible to estimate a yearly potential generation of 10.9 million t of livestock manure, that corresponds to a potential biogas production of 269.28 million m³, equivalent to a total bioenergy of 5234.77 thousand GJ. The bioenergy generated from livestock manure in Sardinia and Sicily can potentially satisfy 17.20 and 9.18% of the energy demand, respectively. Moreover, it was possible to estimate a yearly potential

G. Attard

Institute of Earth Systems, Department of Rural Sciences and Food Systems, University of Malta, Valletta, Malta

G. Attard · N. Azzopardi · A. Gruppetta

Agency for the Governance of Agriculture Bio-Resources, Ministry for Agriculture, Fisheries and Animal Rights, Triq Antonio Cassar, Marsa, Malta

A. Comparetti · S. Orlando

Department of Agricultural, Food and Forest Sciences, University of Palermo, Viale delle Scienze, Building 4, Palermo, Italy

C. Greco (✉)

Council for Agricultural Research and Economics (CREA), Research Centre Protection and Certification, Bagheria (Palermo), Italy

e-mail: carlo.greco@crea.gov.it

production of 4.69 million t of digestate, that can be separated into a liquid fraction, to be used as biofertiliser, instead of conventional inorganic/mineral/chemical fertilisers, and a solid fraction, to be used as growing substrate for the soilless cultivation of Mediterranean crops, instead of peat, according to Circular Bioeconomy (CBE) principles.

The islands of Malta and Corsica, having high livestock population and low availability of Utilised Agricultural Area, will have to deal with an oversupply of nitrogen equivalent to a double and triple, respectively, rather than the amount that can be applied to soils. Therefore, AD needs to be complimented with other technologies to process the excess nitrogen inside the digestate, i.e. combustion and pyrolysis.

Keywords Anaerobic Digestion · Animal manure · Biogas · Digestate · Nitrogen balance · Renewable Energy Sources

1 Introduction

The Mediterranean islands have a significant market share of global tourism, equivalent to more than 400 million of International Tourists Arrivals (ITAs) in 2019, being one of the most popular destinations in the world [1]. This is beneficial for the respective local economies but it also places a high burden on the local infrastructures, especially those for waste management practices [2]. The majority of these islands experience seasonal mass tourism, making the energy, water and food demand also extremely seasonal [3, 4], characterised by intense peaks during the summer months and a moderate demand during the rest of the year. Therefore, the Mediterranean islands have a series of shared but unique challenges, that distinguishes them from the European mainland.

Despite the above challenges, these islands also present a series of locally available potential Renewable Energy Sources (RES) such as biomass [5], that can be utilised to contribute towards satisfying their energy demand [6] and, thus, resulting in the instauration of a self-sufficient and sustainable internal economy [7]. Through the application of the correct technology, many Mediterranean islands may achieve 100% supply [8], by replacing fossil fuels with RES [9].

Therefore, the EU has to engage in a leading role in developing a policy framework for the Mediterranean islands, by designing and implementing adequate measures aimed at reducing their dependency on fossil fuels, thereby providing for equality of development opportunities at par across all its territories,.

In this perspective, the use of renewable energy has been included in the agenda of many small islands [10]. In fact, the recommendations of the Committee on Energy, Environment and Water deriving from the 8th Plenary Session of the Parliamentary Assembly of the Union of the Mediterranean [11] focused on the potential use of biomass in the Mediterranean countries and suggested to carry out applied research, aimed at adapting solutions to the Mediterranean basin (on a country/region specific

basis) [12], by taking into consideration also the high amounts of agricultural and livestock waste [13].

The impact of the ongoing geopolitical conflict in Ukraine has exposed the vulnerability of sovereign nations on their dependence on imported gas, fertilisers and grain. This situation is causing disastrous effects on the energy and food security in mainland Europe and even more so in some Mediterranean islands (e.g. Malta), where water security is intimately dependant on energy security. In an attempt to secure alternative supplies, the EU is focusing on Southern and Eastern Mediterranean countries to increase energy imports [14]. However, this scenario means exchanging one dependency for another, since these countries are also characterised by unstable geopolitical episodes of civil unrest and uprising.

In May 2022, the European Commission presented the REPowerEU Plan in response to the hardship and global energy markets disruption caused by Russia's invasion of Ukraine [15]. This plan also proposes to increase the target for RES use from 40 to 45% by 2030, thereby creating a framework for other initiatives, including a Biomethane Action Plan. The technology for the conversion of biomass into bioenergy in the form of biogas is well established, especially in the Northern European countries, while the Mediterranean basin is severely lagging far behind. Anaerobic Digestion (AD) is a process by which microorganisms break down biodegradable biomass and recover bioenergy in the form of biogas, which mainly consists of biomethane. This process generates a by-product, i.e. digestate, that has a significant amount of macro- and micronutrients, making it an excellent biofertiliser. Hence, within the context of this study, AD addresses issues of energy, fertiliser and water security.

The vulnerability of islands is due to their particular social, political and economic features, i.e. small area, insufficient productivity, infrastructures and competences, as well as geographic isolation and ecological fragility [16]. These conditions, together with their potential exposure to natural catastrophes [17], make Mediterranean islands a particular case to be studied, especially when they are important tourist destinations.

Therefore, this study is aimed at evaluating the potential biogas and digestate production through the AD process of livestock manure [18] found on a selection of European Mediterranean islands: Balearic Islands, Corse, Sardinia, Sicily, Malta, Crete and Cyprus (home to estimated 10.4 million residents).

2 Materials and Methods

The potential manure biomass generation from cattle and pigs was estimated using publicly available livestock statistical data for the different selected islands. The numerical data on cattle and pig populations were retrieved from reports published by the National Statistics Offices of Spain (for Balearic Islands), France (for Corsica), Italy (for Sardinia and Sicily) and Greece (for Crete), as well as Eurostat (for Malta and Cyprus). The 2018 data were taken as the basis platform for this study. The mass

of manure produced by each livestock species was computed according to Comparetti et al. [19].

The potential biogas production (B_m) from livestock manure was determined according to Eq. (1):

$$B_m = b_m m_m \quad (1)$$

where:

b_m specific biogas yield of manure mass unit, m^3t^{-1} ;
 m_m manure mass of each animal species, t.

The B_m was computed using the b_m of cattle at $80 \text{ m}^3\text{t}^{-1}$ and that for pigs at $15 \text{ m}^3\text{t}^{-1}$ [20].

The possible available m_m was estimated using the conversion factors provided by Petersen [21].

The potential biogas and digestate production quantities, together with the potential electrical and thermal bioenergy to be generated through Combined Heat and Power (CHP) plants were quantified by applying the established conversion factors, that are reported in this section.

The yearly potential electrical and thermal bioenergy production was calculated using the following efficiency of energy conversion process:

- i. 90% for cogeneration (by means of CHP plants);
- ii. 31.5% for electrical energy generation;
- iii. 58.5% for thermal energy generation [20].

The yearly potential electrical bioenergy production from livestock manure E_{em} was determined according to Eq. (2):

$$E_{em} = B_m e_{eb} \quad (2)$$

where:

e_{eb} electrical value of biogas (efficiency of energy conversion process) [22], depending on the concentration of biomethane within the biogas, kWhm^{-3} .

The yearly potential thermal bioenergy production from livestock manure E_{tm} was determined according to Eq. (3):

$$E_{tm} = B_m e_{tb} \quad (3)$$

where:

e_{tb} thermal value of biogas (efficiency of energy conversion process) [22], depending on the concentration of biomethane within the biogas, kWhm^{-3} .

The yearly estimated production of digestate was computed according to Du Pont Pioneer [20].

When calculating the nitrogen balance resulting from the application of digestate as biofertiliser on soils, the following assumptions were made:

- i. the total nitrogen contained in the digestate is equal to that included in the animal manure used in AD plants, since the AD process does not reduce nor increase the amount of this nutrient;
- ii. milking cows make up 40% of the total bovine population, expressed in Livestock Units (LU);
- iii. breeding sows make up 15% of the total swine population, expressed in LU;
- iiii. the digestate can be applied on that portion of Utilised Agricultural Area which is used for forage and cereal production [23];
- iiiii. the nitrogen uptake by forage and cereal crops is equivalent to the requirement for this nutrient by wheat.

The total nitrogen excreted by cattle was estimated by using Eq. (4):

$$ENC = LU \left(NDC \frac{0.4}{100} + NOC \frac{0.6}{100} \right) \quad (4)$$

where:

ENC total nitrogen excreted by cattle;

LU population of cattle, expressed in Livestock Units;

NDC yearly nitrogen excretion rate of dairy cattle in Western Europe, according to IPCC (Intergovernmental Panel on Climate Change) methodology, i.e. 150 kg/animal;

NOC yearly nitrogen excretion rate of other cattle in Western Europe, according to IPCC methodology, i.e. 51 kg/animal.

Similarly, the total nitrogen excreted by pigs was estimated by using Eq. (5):

$$ENP = LU \left(NBS \frac{0.4}{100} + NMS \frac{0.6}{100} \right) \quad (5)$$

where:

ENP total nitrogen excreted by pigs;

LU population of pigs, expressed in LU;

NBS yearly nitrogen excretion rate of breeding sows in Western Europe, according to IPCC methodology, i.e. 30.35 kg/animal;

NMS yearly nitrogen excretion rate of market swine in Western Europe, according to IPCC methodology, i.e. 9.3 kg/animal.

The Utilised Agricultural Area used for forage and cereal production was taken from publicly available data (Eurostat, 2013).

The nitrogen uptake by wheat was assumed to be equivalent to 158 kg ha^{-1} , which is the average requirement for this nutrient by this cereal crop according to publicly available information and studies.

3 Results

The numerical data of the livestock population and the yearly potential manure generation by species in the surveyed Mediterranean islands are shown in Figs. 1 and 2, respectively.

Results indicate that an estimated 10.90 million t of livestock manure is generated every year, of which 10.27 million t originate from cattle and 0.62 million t from pigs.

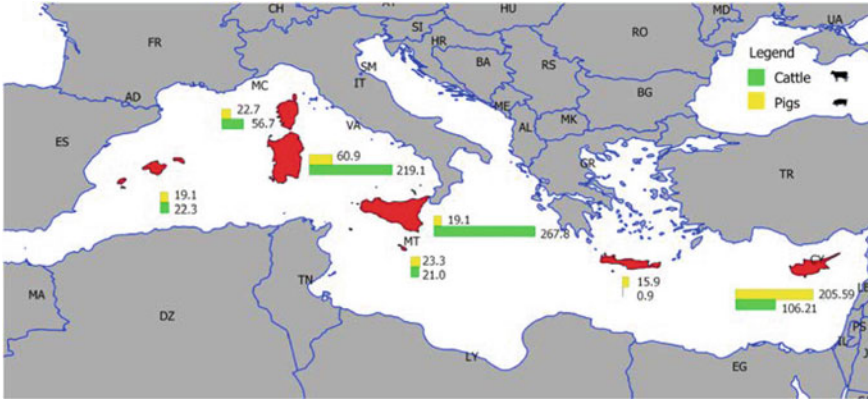


Fig. 1 Livestock population by species (10³) in the selected Mediterranean islands

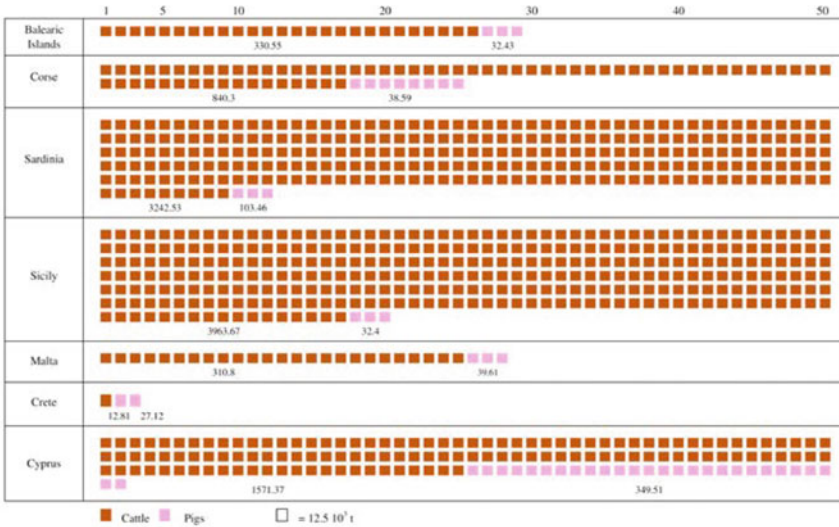


Fig. 2 Yearly potential manure generation by livestock species in the selected Mediterranean islands

Table 1 Yearly potential biogas and digestate (biofertiliser) production through the Anaerobic Digestion (AD) of livestock manure in the selected Mediterranean islands

Islands	Manure (10 ³ t)	Biogas (10 ⁶ m ³)	Digestate (10 ³ t)
Balearic Islands	362.98	8.91	156.09
Corsica	878.89	21.78	377.93
Sardinia	3,345.99	83.13	1,438.78
Sicily	3,996.07	99.74	1,718.31
Malta	350.41	8.56	150.68
Crete	39.92	0.86	17.17
Cyprus	1,921.48	46.29	826.24
Total	10,895.75	269.28	4,685.17

This corresponds to a yearly potential conversion into biogas production of 269.28 million m³ (Table 1), of which 256.82 million m³ originate from cattle manure and 12.46 million m³ from pig manure.

The highest yearly potential biogas production is on the islands of Sicily (99.74 million m³), Sardinia (83.13 million m³) and Cyprus (46.29 million m³).

Furthermore, the yearly potential production of digestate is 4.69 million t, of which 4.42 million t originate from cattle manure, while 0.27 million t from pig manure. This yearly potential biogas production is equivalent to a cogeneration of 1832.17 thousand GJ of electrical bioenergy and 3402.60 thousand GJ of thermal bioenergy, so that the bioenergy generation resulted 5234.77 thousand GJ (Table 2).

Table 2 Yearly potential electrical and thermal bioenergy production through the co-generation from biogas in the selected Mediterranean islands

Islands	Electrical bioenergy (10 ³ GJ)	Thermal bioenergy (10 ³ GJ)	Bioenergy (10 ³ GJ)	Bioenergy/energy demand (%)	Bioenergy (Tons of Oil Equivalent - TOE)	Bioenergy (TOE/inhabitant)
Balearic Islands	60.64	112.62	173.26	0.80	4,138	3.48
Corsica	148.19	275.20	423.39	1.83	10,112	29.83
Sardinia	565.63	1,050.46	1,616.09	17.20	38,599	23.53
Sicily	678.63	1,260.31	1,938.94	9.18	46,311	9.54
Malta	58.26	108.19	166.45	0.77	3,975	7.71
Crete	5.87	10.90	16.77	0.15	400	0.63
Cyprus	314.95	584.91	899.86	0.02	21,492	18.07
Total	1,832.17	3,402.60	5,234.77	-	125,030	12.07

Table 3 Nitrogen from the AD of livestock manure, agricultural area utilised for forage and cereal production and satisfaction of nitrogen requirement by wheat in the selected Mediterranean islands (yearly data)

Islands	Nitrogen from cattle (t)	Nitrogen from pigs (t)	Agricultural area utilised for forage and cereal production (ha)	Nitrogen from AD/nitrogen requirement (%)
Balearic Islands	2,023.10	238.50	92,230	15.52
Corsica	5,144.27	283.75	9,540	360.11
Sardinia	19,849.55	760.75	342,280	38.11
Sicily	24,264.49	238.25	527,390	29.41
Malta	1,902.60	291.25	5,647	245.89
Crete	78.82	199.37	12,580	14.00
Cyprus	9,622.63	2,569.87	97,612	79.06
Total	62,885.46	4,581.75	1,087,279	39.27

The highest yearly potential bioenergy generation was found on the islands of Sicily (1938.94 thousand GJ), Sardinia (1616.09 thousand GJ) and Cyprus (899.86 thousand GJ). The yearly potential bioenergy generation was divided by the energy (both electrical and thermal) demand for each island or archipelago. Thus, it is interesting to note that the bioenergy generated from livestock manure in Sardinia and Sicily can potentially satisfy 17.20 and 9.18% of the energy demand, respectively, while this bioenergy has a very low potential in the other islands. Yet, the highest bioenergy generation per inhabitant was found on the islands of Corsica (29.83 TOE/inhabitant), Sardinia (23.53 TOE/inhabitant) and Cyprus (18.07 TOE/inhabitant).

The nitrogen from the AD of livestock manure, the agricultural area utilised for forage and cereal production and the ratio nitrogen from AD/nitrogen requirement by wheat crop for the selected islands are shown in Table 3.

Figure 3 shows the estimated nitrogen balance, assuming that the digestate obtained from the AD of cattle and pig manure would be applied on soils used for forage and cereal production.

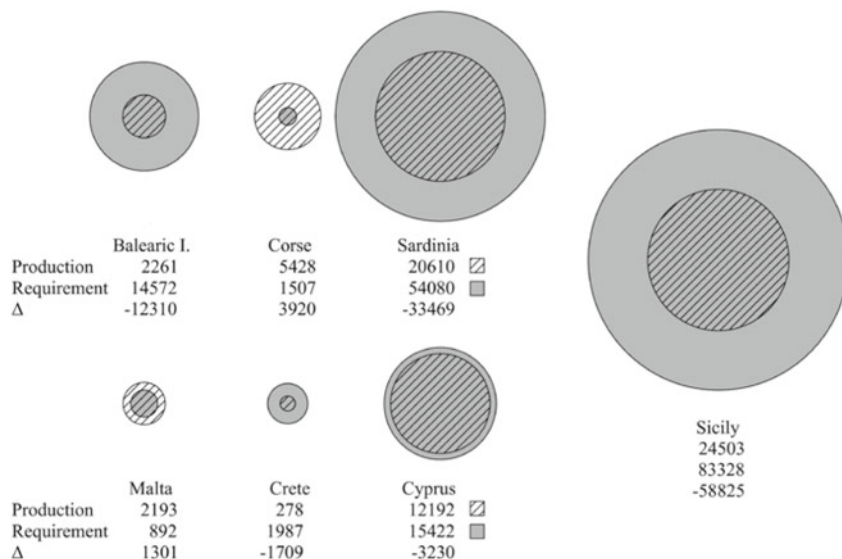


Fig. 3 Nitrogen balance resulting from applying digestate on soils used for forage and cereal production in the selected Mediterranean islands (yearly data)

4 Discussion

AD process could face challenges in Mediterranean environments, due to the particularities of livestock diets and manure handling protocols. In fact, the main principle of animal nutrition is based on the least cost formulation of diets, that allows the expression of the animal genetic potential for growth or milk production. Thus, the main role of feed ingredients is to satisfy the animal requirements, rather than ending up with a manure composition that maximises biogas generation. On the other hand, the use of the generally low quality locally produced roughage would not only compromise the digestion process but it would also result in manure that is not suitable for biogas production. For instance, the biogas produced from cattle manure in the island of Malta cannot reach the amount estimated in this work, due to the utilisation of locally produced high lignin roughage in ruminant diets. Nonetheless, the computed results indicate that the bioenergy generated from livestock manure alone can contribute to satisfy the energy demand in the selected islands, especially in Sardinia and Sicily. This could be further augmented if AD technology would be used to process other biomass, e.g. household and catering waste, that is usually made up of kitchen scraps and food waste, especially during the summer period, due to the tourist influx. However, prudence is called for ensuring that the resulting digestate does not cause challenges when it is applied on soils as a biofertiliser.

The results from this empirical study uncover a phenomenon that is rarely surveyed within the research community, i.e. the potential limitation of AD technology. AD is

often presented as a stand-alone technological solution for the sustainable management of biomass, often assuming the availability of adequate soils for the application of the digestate that has a high fertiliser value. However, this is not always the case, as shown in Table 3: the islands of Malta and Corsica will have to deal with an oversupply of nitrogen equivalent to a double and triple, respectively, rather than the amount that can be applied to soils. The amount of this nutrient inside manure tends to be higher than that the soils can absorb. Thus, in disagreement with sustainable principles, the nutrient amounts that are not absorbed by cultivated plants risk being leached into aquifers and, therefore, contributing to water pollution. Hence, in the case of Malta, Corsica and generally in islands having high livestock population and low availability of Utilised Agricultural Area, AD needs to be complimented with additional technology to process the excess nitrogen inside the digestate. Different technologies are available besides AD such as combustion and pyrolysis. However, a limitation of these technologies is that they require that the feedstock is completely dry. Instead, livestock manure may be still too wet to be directly burnt and may need to be dried by mixing it with dry bedding materials or by using heat from the combustion process to remove its water content.

5 Conclusions

The potential biogas production from cattle and pig manure on the islands of Sardinia, Sicily and Crete is substantial, while the application of digestate on soils may be a greater challenge for the islands of Corsica and Malta [23]. This study shows that these two islands do not have enough Utilised Agricultural Area available for forage and cereal production, where the digestate can be applied within the maximum amount of manure to be applied per unit of agricultural area set by EU Nitrates Directive, i.e. 91/676/EEC [24], regulating also the manure storage conditions. Yet, using or disposing this surplus of nitrogen in a sustainable way involves further expensive processing, so that the overall feasibility of AD plants results unfavourable in Corsica and Malta, as this process does not mitigate the excess of this nutrient. Yet, the revised EU Renewable Energy Directive, i.e. 2018/2001/EU [25], promotes the use of RES, as well as the development and implementation of manure treatment technologies, in order to increase the use of this biomass, as a renewable energy and nutrient source, as well as to decrease its surplus in areas having high animal density [26, 27].

This work demonstrates that the production of RES, i.e. electrical and thermal bioenergy, from organic waste allows to extract an added value, as well as reduce the production costs, by replacing inorganic/mineral/chemical fertilisers with digestate, that is not only rich of nutrients but also able to improve the soil structure [28]. This is particularly relevant for Sardinia and Sicily, that have the potential to satisfy 17.20 and 9.18% of the energy demand, respectively, as well as enough land available to dispose the digestate in a sustainable way.

Thus, this work contributes to:

- reduce the dependency on fossil energy sources and develop alternative technologies for the production of bioenergy from renewable carbon neutral sources;
- reduce the polluting emissions and leachate from stored livestock manure;
- reduce energy production costs;
- process livestock waste through an environmentally friendly method;
- develop new profit sources for farmers, through the bioenergy production from the residual biomass in the Mediterranean islands;
- reduce the dependency on inorganic/mineral/chemical fertilisers and increase the availability of organic ones, e.g. digestate, that can improve both the chemical and physical soil parameters [23];
- emphasise the compatibility of AD process with the zero-landfill concept, i.e. the minimum or null disposal of waste in landfills.

The livestock manure management method proposed in this study can be applied also to other islands, where animal husbandry is not land based, landfills are limited and the removal of manure by means of transport overseas would be very expensive and not economically feasible.

References

1. Fosse, J., et al.: The future of Mediterranean tourism in a (post) covid world - Back to Mass Tourism or leapfrog towards Sustainability. Eco-med briefing 01/21. Eco-union (2021). https://www.ecounion.eu/wp-content/uploads/2021/04/Nota_Thefuture_mediterranean_tourism_03.pdf
2. Kuang, Y., et al.: A review of renewable energy utilization in islands. *Renew. Sustain. Energy Rev.* **59**, 504–513 (2016)
3. Comparetti, A., Febo, P., Greco, C., Orlando, O.: Current state and future of biogas and digestate production. *Bulg. J. Agric. Sci.* **19**(1), 1–14 (2013). <https://doi.org/10.1146/annurev.earth.32.101802.120435>
4. Michalena, E., Hills, J., Amat, J.-P.: Developing sustainable tourism, using a multicriteria analysis on renewable energy in Mediterranean Islands. *Energy Sustain. Dev.* **13**, 129–136 (2009)
5. Michalena, E., Tripanagnostopoulos, Y.: Contribution of the solar energy in the sustainable tourism development of the Mediterranean islands. *Renewable Energy* **35**, 667–673 (2010)
6. Attard, G., Comparetti, A., Febo, P., Greco, C., Mammano, M.M., Orlando, S.: Case study of potential production of renewable energy sources (RES) from livestock wastes in Mediterranean Islands. *Chem. Eng. Trans.* **58**, 1–6 (2017). <https://doi.org/10.3303/CET1758093>
7. Bloomfield, J., Copsey, N., Rowe, C.: Renewable energy in the Mediterranean. Aston Centre for Europe - Aston University, European Union (2011). <https://cor.europa.eu/en/engage/studies/Documents/renewable-energy-mediterranean.pdf>
8. Maxoulis, C.N., Kalogirou, S.A.: Cyprus energy policy: the road to the 2006 world renewable energy congress trophy. *Renewable Energy* **33**(3), 355–365 (2008)
9. Krajačić, G., Martins, R., Busuttill, A., Duić, N., da Graça Carvalho, M.: Hydrogen as an energy vector in the islands' energy supply. *Int. J. Hydrogen Energy* **33**(4), 1091–1103 (2008). <https://doi.org/10.1016/j.ijhydene.2007.12.025>
10. Garcia, A., Meisen, P.: Renewable Energy Potential of Small Island States. GENI (Global Energy Network Institute). August 2008 (2008). <http://www.geni.org/globalenergy/library/technical-articles/generation/small-island-nations/renewable-energy-potential-of-small-island-states/Renewable%20Energy%20Potential%20of%20Small%20Island%20States1.pdf>

11. United Nations - Department of Economic and Social Affairs - Division for Sustainable Development. Trends in sustainable development: Small Island Developing States (SIDS). New York, NY, USA (2010). <https://www.preventionweb.net/publication/trends-sustainable-development-small-island-developing-states>
12. Committee on Energy, Environment and Water deriving from the 8th Plenary Session of the Parliamentary Assembly of the Union of the Mediterranean, Rabat, Morocco (2012)
13. Ezeah, C., Fazakerley, J., Byrne, T.: Tourism waste management in the European Union: lessons learned from four popular EU tourist destinations. *Am. J. Clim. Change* **4**, 431–445 (2015). <https://doi.org/10.4236/ajcc.2015.45035>
14. Hadjigeorgiou, I., Zervas, G.: Evaluation of animal production systems on species rich Mediterranean islands: a case study on the Island of Rhodes. In: Porqueddu, C., Ríos, S. (eds.) *The Contributions of Grasslands to the Conservation of Mediterranean Biodiversity. Options Méditerranéennes: Série A. Séminaires Méditerranéens n. 92*. CIHEAM/CIBIO/FAO/SEEP, Zaragoza, Spain, pp. 35–38 (2010)
15. Alberici, S., Grimme, W., Toop, G.: Biomethane production potentials in the EU - Feasibility of REPowerEU 2030 targets, production potentials in the Member States and outlook to 2050 - A Gas for Climate report, July 2022. *Gas for Climate - A path to 2050*. Guidehouse Netherlands B.V. (2022). https://www.europeanbiogas.eu/wp-content/uploads/2022/07/GfC_national-biomethane-potentials_070722.pdf
16. United Nations - Department of Economic and Social Affairs: World Population Prospects: The 2017 Revision (2017). <https://www.un.org/development/desa/publications/world-population-prospects-the-2017-revision.html>
17. Akçali, E., Görmüş, E., Özel, S.: Energy Transitions and Environmental Geopolitics in the Southern Mediterranean. IAI Commentaries (22/17 April 2022). IAI (Istituto Affari Internazionali - International Affairs Institute) (2022). <https://www.iai.it/sites/default/files/iaicom2217.pdf>
18. Howarth, R.: *The Environmental Vulnerability of SIDS (United Nations Development Programme)* (2002)
19. Comparetti, A., Febo, P., Greco, C., Orlando, S., Navickas, K., Venslauskas, K.: Sicilian potential biogas production. *J. Agric. Eng.* **44**(2s) (2013). <https://doi.org/10.4081/jae.2013.345>
20. Du Pont Pioneer: Servizio Agronomico Pioneer Italia. Gruppo, E.F., Technologie Srl, Gadesco Pieve Delmona (Cremona), Italy (2016)
21. Petersen, J.B.: Manure nutrient credit worksheet. In: Kelling, K.A. (ed.) *Managing Manure and Waste*, vol. 3411, pp. 1–6. University of Wisconsin-Extension, Cooperative Extension Service (1987)
22. EU: Intelligent Energy Europe: IEE Project ‘BiogasIN’. Highlights of potential renewable energy from biogas in 28 target regions. D.2.3, WP2, Ilze Dzene, Ekodoma, November 2010, This Project (Contract No. IEE/09/848 SI2.558364) (2010)
23. Mantovi, P., Moscatelli, G., Piccinini, S., Bozzetto, S., Rossi, L.: Microfiltered digestate to fertigation: a best practice to improve water and energy efficiency in the context of biogas-doneright™. In: Naddeo, V., Balakrishnan, M., Choo, K.-H. (eds.) *Frontiers in Water-Energy-Nexus—Nature-Based Solutions, Advanced Technologies and Best Practices for Environmental Sustainability: Proceedings of the 2nd Water Energy NEXUS Conference*, November 2018, Salerno, Italy, pp. 497–499. Springer International Publishing, Cham (2020). https://doi.org/10.1007/978-3-030-13068-8_124
24. EU: Council Directive 91/676/EEC of 12 December 1991 concerning the protection of waters against pollution caused by nitrates from agricultural sources, 91/676/EEC. In: *Official Journal*, L 375, 31/12/1991, pp. 1–8 (1991)
25. EU: Directive (EU) 2018/2001 of the European Parliament and of the Council of 11 December 2018 on the promotion of the use of energy from renewable sources (Text with EEA relevance), PE/48/2018/REV/1, 2018/2001/EU. In: *Official Journal*, L 328, 21/12/2018, pp. 82–209 (2018)
26. Menzi, H., Oenema, O., Burton, C.: Impacts of intensive livestock production and manure management on the environment. In: Steinfeld, H., Mooney, H.A., Schneider, F., Neville, L.E. (eds.) *Livestock in a changing landscape, drivers, consequences, and responses*, pp. 139–164. Island Press (2010)

27. Vinnerås, B.: Sanitation and hygiene in manure management. In: Sommer, S.G., Christensen, M.L., Schmidt, T., Jensen, L.S. (eds.) *Animal Manure Recycling: Treatment and Management*, Chapter 6, pp. 91–104. John Wiley & Sons, Chichester, UK (2013)
28. Karellas, S., Boukis, I., Kontopoulos, G.: Development of an investment decision tool for biogas production from agricultural waste. *Renew. Sustain. Energy. Rev.* **14**, 1273–1282 (2010). <https://doi.org/10.1016/j.rser.2009.12.002>

Sustainable Livestock Waste Treatment Technologies: Survey on a Group of Italian Farms



Giorgia Bagagiolo , Lucia Vigoroso , Giulia De Paolis, Federica Caffaro , Eugenio Cavallo , and Niccolò Pampuro 

Abstract The present study focuses on the expected benefits and drivers that may influence the adoption of sustainable waste treatment technologies in the livestock sector, as well as enterprises' provision for future investments pursuing sustainability. Forty-seven livestock enterprises were administered a questionnaire investigating: i) the adoption and intention to adopt strategies and technologies to reduce the environmental impact of livestock waste, ii) the expenses they incurred, iii) the frequency of exposure to various information sources, and iv) the perceived drivers and benefits. The results showed that 66% of the respondents adopted sustainable technology solutions to manage livestock waste aimed at recovering nutrients or reducing GHG emissions. The expected benefits in adopting sustainable technologies are firstly "the improved soil fertility and soil organic matter content". For those enterprises that do not adopt any of the proposed technologies, the rising prices of mineral fertilizers and the possibility of producing on-farm bioenergy would be the main drivers to adoption. The average expense for initial investment is 20–50 k€, primarily funded by enterprises' own capital and secondarily by rural development programs. Forty-three percent of the respondents expressed their intention to continue investing in the

G. Bagagiolo · L. Vigoroso (✉) · E. Cavallo · N. Pampuro
Institute of Sciences and Technologies for Sustainable Energy and Mobility (STEMS), National Research Council of Italy (CNR), Strada delle Cacce, 73-10135 Torino, Italy
e-mail: lucia.vigoroso@stems.cnr.it

G. Bagagiolo
e-mail: giorgia.bagagiolo@stems.cnr.it

E. Cavallo
e-mail: eugenio.cavallo@stems.cnr.it

N. Pampuro
e-mail: niccolo.pampuro@stems.cnr.it

G. De Paolis · F. Caffaro
Department of Education, University of Roma Tre, via del Castro Pretorio 20, 00185 Rome, Italy
e-mail: gju.depaolis3@stud.uniroma3.it

F. Caffaro
e-mail: federica.caffaro@uniroma3.it

future, primarily on “high-precision distribution systems for slurry on-field application” and “automated systems for the management of waste within the livestock house”. Results from the present survey are a valuable baseline to develop and disseminate targeted information on implications and opportunities for sustainable livestock treatment systems, addressing policy makers, farmers’ trade associations, and technology providers.

Keywords Animal waste-treatment technologies · Mitigation measures · Survey · Technology adoption

1 Introduction

Within the husbandry sector, the evolution of larger and more concentrated livestock operations has accentuated the problems related to the management of animal waste [1, 2]. Indeed, animal waste represents an environmental concern in many European countries both in terms of air pollution by greenhouse gas (GHG) emissions and water pollution by nutrients leaching [3]. According to the most recent data [4], a large component of GHG emissions from the Italian agricultural sector (46%), refers to CH₄ and N₂O levels due to the enteric fermentation from livestock and to the ammonia (NH₃) from the management of animal waste. In particular, the greatest contribution comes from the dairy cattle breeding (producing about 56% of emissions expressed in CO₂ equivalent), followed by other cattle (18%) and pigs (12%). Though in recent years, a downward trend of total GHG emissions (−13.0%) has been observed, mainly driven by the European Common Agricultural Policy (CAP) measures, much still needs to be done to comply with the “Effort Sharing” regulation and the long-term strategies of European Union aiming at climate-neutral economy by 2050 [5].

Furthermore, intensive breeding may lead to excessive animal waste soil application, causing nitrogen surpluses, NH₃ emissions and nitrate leaching in both surface and ground waters, especially in areas classified as Nitrate Vulnerable Zones (NVZs) in accordance with European Regulation (91/676/EEC) [6]. In particular, in Italy, the total area of the NVZs is approximately 4 million hectares, equivalent to approximately 13.4% of the national territory and approximately 29.7% of the total agricultural area [7].

Under these premises, technological solutions for animal waste treatment play a pivotal role in the transition toward sustainable management of the livestock sector, turning the environmental issues into an opportunity for nutrients recovery. In recent years, livestock waste management technologies have been rapidly changing [2] and several methods of animal waste processing have been developed for various purposes, including environmental protection, ease in handling, energy production or soil amelioration [8]. Moreover, processing of organic waste can improve its nutrient availability and content, and thereby increases the agricultural value of the waste when used as a fertilizer, while contributing to a more bio-based, ‘circular’ economy

[9]. However, though many technological innovations aimed at mitigating the effects of animal husbandry on the environment are already on the market, the diffusion of such technologies is often slow, entailing low adoption rates [10, 11]. In the light of the imperatives set by climate change and associated policy goals, increasing our knowledge about the main factors affecting diffusion and adoption rates of more sustainable technologies is essential. Such understanding could hopefully contribute to the design and implementation of targeted interventions that can overcome barriers to the adoption of animal waste treatment technologies.

2 Materials and Methods

2.1 Instrument and Participants

Forty-seven livestock farms took part in the study. The sample showed a high rate of male participants (83.0%) with an average of 13 years of education (high school) and a mean age of 48.9 (SD = 12.7). The participants were mainly farmers with medium/large-sized farms; 74.5% of them have a utilized agricultural area (UAA) higher than 20 ha, and of this, 38.3% has an extension greater than 50 ha. Most participants declared an annual turnover of more than 100 k€ (59.6%).

Participants were administered an online questionnaire that was aimed at investigating the expected benefits and drivers that may influence the adoption of sustainable waste management technologies in livestock farming, as well as predicting future investments by enterprises pursuing sustainability.

The study was conducted by the Institute of Science and Technology for Sustainable Energy and Mobility of the National Research Council (CNR Stems) in collaboration with the Department of Education (DSF) of the University of Roma Tre University and was advertised in an Italian well-known farming magazine. The different sections and items of the questionnaire were designed based on previous instruments [12, 13].

The questionnaire included seven sections investigating the most important barriers and motivating factors for innovative practices and technologies aimed at mitigating the environmental impact of agri-food models, namely practices aimed at promoting sustainable development and efficient management of natural resources such as water, soil and air, including advanced technologies ascribable to precision agriculture and Agriculture 4.0.

For the aims of this contribution, not all the variables included in the questionnaire were analyzed, but only those items aimed at investigating the adoption of strategies and technologies to reduce the environmental impact of animal waste: the intention to adopt them, the expenses incurred, willingness for future investments, frequency of exposure to various information sources, expected benefits and drivers. These last were rated by respondents on a four-point Likert scale (1 = not at all /never, 4 = completely/often). The frequency of exposure to information was computed as

a mean of the scores regarding the frequency of exposure to different sources of information: journals/advertisements/internet, demonstrations/exhibitions, training courses, discussions with peers/relatives, and discussions with consultants/trade organizations.

Ten sustainable strategies and technologies were investigated, namely: i) sewage and digestate drying systems; ii) anaerobic digestion plants; iii) chemical-biological treatment systems (e.g., acidification, nitrification/denitrification, urease, etc.); iv) advanced systems for relaying and cleaning the stables; v) solid-liquid separation plants for sewage and digestate; vi) solid fractions of sewage and digestate composting; vii) storage tanks covering; viii) on-field effluents distribution systems (e.g., equipment for directly injecting animal waste beneath the soil surface or equipment with variable rate dosing system); ix) stables ventilation regulating systems; x) stripping and scrubbing systems for the treatment of exhausted air.

3 Results

3.1 Adoption Rates and Expected Benefits

More than half of the surveyed farms (63.8%) had already adopted at least one of the investigated strategies and technologies for animal waste management aimed at recovering nutrients or reducing greenhouse gas emissions. In particular, the most implemented strategies were mainly aimed at containing ammonia emissions to the atmosphere including on-field effluents distribution systems (equipment for directly injecting animal waste beneath the soil surface or equipment with variable rate dosing system) and monitoring systems adjusting fresh air flow and temperature in the stables (both adopted by 46.7% of the respondents). These were followed by “storage tanks covering” and “solid fraction composting” (both adopted by 33.3% of respondents). None of the investigated farms adopted “stripping and scrubber systems”. The results showed that altogether the initial investment made was higher than 10 k€ for 83.3% of the respondents. In particular, in most cases, the average initial investment ranged from 20 to 50 k€ (30.0%), followed by 20.0% of the enterprises who invested 10–20 k€ and another 20.0% who invested 50–100 k€. The economic sources of the initial investment may be combined but they mainly derived from owned capital (60.0%) and secondarily from EU programs for rural development (36.7%), while only a quarter of respondents (26.7%) benefited of loans from private financial institutions.

With regard to the expected benefits (Fig. 1), the greatest advantage recognized by respondents from the adoption of the investigated technologies is “the improvement of soil fertility” and “the improvement of soil organic matter content”, both with a mean score of 3.4 out of 4. In particular, the improvement of fertility and organic matter quality of the soil were considered either “important” or “very important” respectively by 91.5% and 89.4% of the respondents.

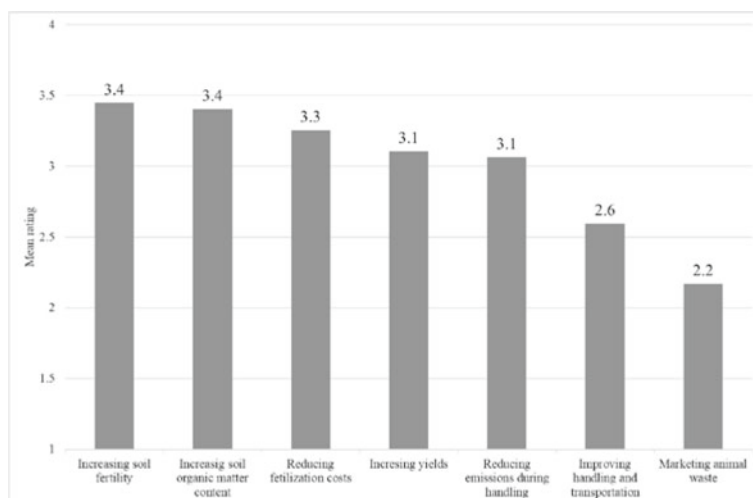


Fig. 1 Mean ratings of expected benefits from the adoption of sustainable animal waste management technologies

3.2 Potential Users and Perceived Drivers to Adoption

The remaining part of the enterprises (36.2%) did not adopt any of the proposed technologies. The results showed that, on average, the main drivers for the future adoption of these technologies were the “increasing prices of mineral fertilizers” with a score of 2.8 out of 4 and the “possibility of on-farm bio-energy production” with a score of 2.6 out of 4.

In detail, the “increasing prices of mineral fertilizers” and the “possibility of bioenergy production”, were considered either “important” or “very important” respectively by 70.6% and 58.8% of respondents.

3.3 Future Investments

Overall, only 42.6% of the entire sample of participants expressed the intention to invest in the future in livestock waste management technologies. They would mainly invest in solutions such as ‘high precision distribution systems for slurry application in the fields’ (21.9%) and stables ventilation regulating systems (18.8%), followed by solid-liquid separation plants (15.6%). The results showed that 45% of the enterprises intended to invest from 20 to 50 k€ also in the future, followed by 15% who would invest 5–10 k€ and another 15% who would invest 50–100 k€. The propensity to invest in the future was correlated to expected benefits in terms of emission reduction and farms’ turnover (Table 1).

Table 1 Pearson correlations between farm characteristics, frequency of exposure to different sources of information, expected benefits and intention to invest in the future

Variables	Turnover	UAA	Freq. of info	B1	B2	B3	B4	B5	B6	B7	Future invest
Turnover	1										
UAA	0.337*	1									
Freq. of info	0.035	0.143	1								
B1	-0.039	0.227	0.120	1							
B2	-0.105	0.232	0.080	0.893**	1						
B3	-0.045	0.121	0.154	0.561**	0.520**	1					
B4	-0.092	0.023	0.045	0.533**	0.453**	0.634**	1				
B5	0.193	0.369*	0.105	0.511**	0.494**	0.509	0.466**	1			
B6	0.126	0.009	0.427**	0.336*	0.221	0.294*	0.437**	0.454**	1		
B7	0.031	0.018	0.411**	0.224	0.210	0.305*	0.260	0.158	0.643**	1	
Future invest	0.323*	0.197	0.100	0.004	-0.004	0.200	0.149	0.437**	0.187	0.104	1

B1=Increasing soil fertility; B2 = Increasing soil organic matter; B3 = Reducing fertilization costs; B4 = Increasing yields; B5=Reducing emissions during handling; B6 = Improving handling and transportation; B7 = Marketing animal waste. Note: * p < .05, ** p < .01, *** p < .001.

3.4 Frequency of Exposure to Information Sources

The mean score for the overall frequency of exposure to information sources was 2.7 out of 4. The most frequently used information channels were journals/advertisements/internet (95.7% of farmers reporting to use from sometimes to very often) followed by demonstrations/exhibitions (63.8%) and discussions with peers/relatives/colleagues (59.6%). A positive correlation was found between the exposure to information sources and two expected benefits: improving handling and transportation and marketing animal waste (Table 1).

4 Discussion

Livestock waste may cause air quality degradation from emissions, soil quality detriment and water pollution issues from nutrient runoff to the water bodies. Despite the significant environmental benefits deriving from the sustainable management of these organic materials, the present survey revealed an overall adoption of practices predominantly aimed at mitigating the effect of emissions. On the contrary, the recovery of value-added products from livestock waste was not current practice, probably due to the high investment costs required and the low market values being offered for the recovered products [14]. Poor adoption was also observed for treatments like air stripping and scrubbing, probably because of more innovative and less well-known systems or higher investments and specific machinery required.

Compared to other solutions for animal stables and waste storage, the adoption of precision systems for slurry application in the fields may not be the most efficient in terms of emissions reduction, but such technology can combine air pollution reduction with efficient nutrient recycling. This is a possible motivation for the higher rate of adoption and the high interest for future investments. Responses related to expected benefits seemed to confirm that farmers gave greater importance to nutrient recovery, in particular to fertility and organic matter improvement from animal waste distribution.

Following the classification proposed by [15, 16] the most important driver was external to the farm and it was “market pull” being linked to increasing prices of mineral fertilizers. On the contrary, “regulatory push/pull” drivers seemed to be less effective among the surveyed farms. Hence, the results related to both expected benefits and drivers revealed that when speaking of sustainable technologies adoption farms from the livestock sector are more profit-driven rather than compliance-driven. Nonetheless, environmental awareness is rapidly increasing among farm managers and in future studies it could be considered a potential driver [17]. The second most rated driving factor (“technology push driver”) is the perspective of on-farm energy production. This result is mirrored by the significant increase in biogas plants for the production of electricity and heat, contributing to the reduction of total emissions, observed in the last years [18]. Finally, there was a low interest among the participants

in new business opportunities from by-products (e.g., selling compost or digestate) probably due to difficulties in undertaking consortium initiatives.

Perspectives on future investments pointed out a substantial continuity with the present situation, indeed, as observed by a number of studies [19–21] some categories of farmers, based on socio-economic characteristics, personal variables and behaviors, may be skeptical towards innovation. To overcome this, a bottom-up approach, where mechanisms of innovation are no longer considered a simple transfer of technology, but the exchange of knowledge and information between actors, should be adopted. Such an approach is reflected by the Agricultural Knowledge and Information System (AKIS) [21] promoted within the new rural development programs and it is supported by the relatively high frequency of use of different communication channels and its relation with perceived benefits of animal waste management technologies pointed out in the present study.

5 Conclusions

Notwithstanding the small sample size, the results from the present survey represent a useful baseline to develop targeted information campaigns on implications and opportunities for sustainable livestock treatment systems addressing policymakers, farmers trade associations and technology providers.

Long-term planning is needed for the management of livestock residue in order to guarantee farm survival and environmental conservation. Hence, the issues addressed in the present contribution will need to be further developed, researched and implemented. The adoption of sustainable technologies should be promoted through demonstration events or seminars addressing farmers. Scholars, advisers and technology providers should focus on the following items: clarifying how technologies work, highlighting both the improvements in terms of environmental and economic sustainability, demonstrating how recovered nutrients may become a valuable alternative to chemical fertilizers and even become the opportunity for a new business. With this regard, the development of cooperative economic models to improve the production and marketing of specific innovative fertilizers whose composition is controlled and well-known should be encouraged. For these specific issues, the study demonstrated that being exposed to sources of information makes it possible to appreciate the benefits.

References

1. Martinez, J., Dabert, P., Barrington, S., Burton, C.: Livestock waste treatment systems for environmental quality, food safety, and sustainability. *Biores. Technol.* **100**, 5527–5536 (2009)
2. Wang, L.K., Wang, M.-H., Hung, Y.-T., Shammass, N.K. (eds.): *Handbook of Environmental Engineering*, vol. 17. Springer, Cham (2016). <https://doi.org/10.1007/978-3-319-26800-2>

3. Hjorth, M., Christensen, K.V., Christensen, M.L., Sommer, S.G.: Solid-liquid separation of animal slurry in theory and practice. A review. *Agron. Sustain. Dev.* **30**, 153–180 (2010)
4. ISPRA (Istituto Superiore per la Protezione e Ricerca Ambientale) Italian Greenhouse Gas Inventory 1990–2018, Roma (2020)
5. European Commission. Contributing to climate action to meet commitments under the Paris Agreement, 2021, vol. COM (2021)
6. Council of the European Communities COUNCIL DIRECTIVE of 12 December 1991 concerning the protection of waters against pollution caused by nitrates from agricultural sources (91/676 /EEC) (1991)
7. Rete Rurale Nazionale L'Italia e la Pac post 2020 - Policy Brief 5 OS 2.2: Favorire lo sviluppo sostenibile e un'efficiente gestione delle risorse naturali come l'acqua, il suolo e l'aria (2019)
8. Pampuro, N., Bagagiolo, G., Priarone, P.C., Cavallo, E.: Effects of pelletizing pressure and the addition of woody bulking agents on the physical and mechanical properties of pellets made from composted pig solid fraction. *Powder Technol.* **311**, 112–119 (2017)
9. Case, S.D.C., Oelofse, M., Hou, Y., Oenema, O., Jensen, L.S.: Farmer perceptions and use of organic waste products as fertilisers – a survey study of potential benefits and barriers. *Agric. Syst.* **151**, 84–95 (2017)
10. Long, T.B., Blok, V., Coninx, I.: Barriers to the adoption and diffusion of technological innovations for climate-smart agriculture in Europe: evidence from the Netherlands, France, Switzerland and Italy. *J. Clean. Prod.* **112**, 9–21 (2016). <https://doi.org/10.1016/j.jclepro.2015.06.044>
11. Kemp, R., Volpi, M.: The diffusion of clean technologies: a review with suggestions for future diffusion analysis. *J. Clean. Prod.* **16**, S14–S21 (2008)
12. Caffaro, F., Roccatò, M., Micheletti Cremasco, M., Cavallo, E.: An ergonomic approach to sustainable development: the role of information environment and social-psychological variables in the adoption of agri-environmental innovations. *Sustain. Dev.* **27**, 1049–1062 (2019)
13. Bagagiolo, G., Vigoroso, L., Pampuro, N., Cavallo, E.: The role of social interaction and personal characteristics in affecting the adoption of compost from organic fraction of municipal solid waste in Italy. *Agronomy* **12**(2), 445 (2022). <https://doi.org/10.3390/agronomy12020445>
14. Sampat, A.M., Hicks, A., Ruiz-Mercado, G.J., Zavala, V.M.: Valuing economic impact reductions of nutrient pollution from livestock waste. *Resour. Conserv. Recycl.* **164**, 105199 (2021)
15. Parker, C.M., Redmond, J., Simpson, M.: A review of interventions to encourage SMEs to make environmental improvements. *Eviron. Plann. C. Gov. Policy* **27**, 279–301 (2009)
16. Marin, G., Marzucchi, A., Zoboli, R.: SMEs and barriers to Eco-innovation in the EU: exploring different firm profiles. *J. Evol. Econ.* **25**, 671–705 (2015)
17. Burton, R.J.F., Farstad, M.: Cultural lock-in and mitigating greenhouse gas emissions: the case of dairy/beef farmers in Norway. *Sociol. Rural.* **60**, 20–39 (2020)
18. Nevzorova, T., Kutcherov, V.: Barriers to the wider implementation of biogas as a source of energy: a state-of-the-art review. *Energ. Strat. Rev.* **26**, 100414 (2019)
19. Pampuro, N., Caffaro, F., Cavallo, E.: Reuse of animal manure: a case study on stakeholders' perceptions about pelletized compost in northwestern Italy. *Sustainability* **10**, 2028 (2018)
20. Caffaro, F., Cavallo, E.: The effects of individual variables, farming system characteristics and perceived barriers on actual use of smart farming technologies: evidence from the piedmont region, northwestern Italy. *Agriculture* **9**, 111 (2019)
21. Vecchio, Y., Agnusdei, G.P., Miglietta, P.P., Capitanio, F.: Adoption of precision farming tools: the case of Italian farmers. *Int. J. Environ. Res. Public Health* **17**, 869 (2020)

Blockchain Technology for Food Supply Chain Traceability and Authentication



Paolo Barge , Matteo Antonio Angelo Franchetto, Valeria Maritano ,
Cristina Tortia , Paolo Gay , Claudio Schifanella , and Federica Cena 

Abstract To enhance food quality and value, transparent traceability systems, also proofed by authentication methods, are used to give information about the product from the primary production stages to the selling point. Nowadays, information is accessed in multi- or omni- channel (websites, mail, app, social media). Data analytics and Artificial Intelligence can then highly enhance marketing strategies. Furthermore, there is a high demand of proof of authenticity systems able to certify high-value food credential attributes. Thus, in this paper a blockchain-based system is proposed to manage and certify traceability information and, therefore, the authenticity of food products.

In the context of the PININ project, the traceability of dairy supply chains has been considered. A decentralized application (DApp) has been developed for the registration of the collected traceability data in a consortium blockchain, where a limited number of actors can submit transactions and access data. The DApp also allows the publication of recorded data in a regional blockchain to render them publicly available. A mobile application has been developed to connect the physical products with their digital twins. By means of a QR code printed on labels, certified data are then available to food supply chain public and private stakeholders.

Electronic collars equipped with GPS and Bluetooth systems have been also developed to geo-referencing cattle in mountain pastures. The acquired data, recorded in the blockchain, allow competent authorities to securely verify the position of the animals for the correct disbursement of European funds to farmers, thus preventing frauds.

Keywords Blockchain · Traceability · Cheese · Pasture · NFC

P. Barge · M. A. A. Franchetto · V. Maritano · C. Tortia (✉) · P. Gay
DISAFA, Department of Agricultural, Forest and Food Sciences, Università degli Studi di Torino,
Largo Paolo Braccini 2, 10095 Grugliasco, TO, Italy
e-mail: cristina.tortia@unito.it

C. Schifanella · F. Cena
DI Department of Computer Science, Università degli Studi di Torino, Corso Svizzera 185,
10149 Torino, Italy

1 Introduction

The blockchain is a disruptive technology for the secure recording and distribution of digital information in several fields, such as financial sector (Bitcoin).

The blockchain is a distributed database shared among several nodes of a computer network that involves a sequence of interconnected blocks containing transactions that are secured by means of public-key encryption and that are verified by the network members. As this technology is based on distributed ledgers controlled and validated by several different users, every time a transaction is added to the pre-existent chain of blocks it cannot be subsequently modified. The security of the blockchain relies on the fact that any modification of the recorded data requires the consensus of most of the network participants which is very difficult to reach [1]. Moreover, each block of the chain contains two key security elements: a hash, resulting from an algorithm calculated on the previous block and allowing the concatenation, and a timestamp, a digital signature that certifies the exact moment of creation and validation of the block in the blockchain. The three essential features of the blockchain technology (decentralization, security and data immutability) make it a powerful tool for the improvement of transparency, trust and reliability in sharing information between numerous players in complex systems.

Depending on the management of the central authority, which is distributed and decentralized, three different types of blockchains can be identified: private, consortium and public.

Public blockchains are also known as “permissionless” since they are open to everyone and there is no need for anyone to grant permission to participate. Given the decentralized structure, the control over the network by a central authority is not needed, and anyone can become a user to participate in the main activities using a defined cryptography protocol that certifies the transactions. Public blockchains are therefore in the form “read all, write all”.

In private, or “permissioned”, blockchains each participant has to be admitted by a central authority, which can grant permission to other network users, adding restrictions and exercising control over the system. Private blockchain are useful in certain contexts where organizations deal with extremely sensitive documents or can be exposed to competitors. Private blockchains have authentication processes which authorize an entry into the system, enhancing security and protecting against criminal activity.

Consortium blockchains can be considered as hybrids between public and private blockchains. They contain some cryptographic features similar to those of their public counterpart, but, the centralized authority guarantees a greater control on the network. The consensus is neither in the hands of a single node, nor totally distributed on the network, but can be handled by multiple organizations which have both access and authority.

The blockchain is a tool capable of self-regulating and self-correcting without the intervention of third parties thanks to consensus algorithms. The protocols are necessary to ensure consistency between the registers stored in the different nodes

to reach consensus. Three main consensus mechanisms exist: Proof of Work (PoW), Proof of Stake (PoS), and Proof of Authority (PoA).

Proof of Work is the protocol used by several blockchain systems (such as Ethereum) to confirm transactions and produce the new blocks of the chain. The PoW algorithm requires continuous work by the miners who compete to solve the cryptographic problem to validate the transactions. The block validation implies a reward, therefore new digital currencies are created continuously. One important drawback of the continue mining process is the requirement of very fast hardware systems and high energy consumption.

The Proof of Stake protocol represents an energy-saving alternative to the PoW algorithm. In this case the creator of a new block is chosen based on the participation fee (deposit blocked in the network). A group of validators participates in a consensus algorithm to vote for the next block to be mined. The reward is not created in cryptocurrency in the moment of the block validation, but the payment is acquired only after the validation by a sum defined as “fee”.

Proof of Authority is a type of permissioned consensus algorithm that provides a practical and effective solution for current blockchain systems, especially for consortium blockchains [2]. PoA is based on a limited number of authority nodes (sealers), to perform consensus procedures. Blocks and transactions must be verified by these eligible nodes. The design of a small size committee enables fast confirmation of transactions and easy management of involved members.

The main blockchain applications involve financial technology (e.g. Bitcoin) but progressive increase in non-financial projects such as logistics, production and traceability is observed [3]. The blockchain technology is taking hold in the food sector especially for the management of traceability since it allows the secure and transparent registration of information and their sharing among the numerous supply chain actors [4]. The blockchain could allow traceability at different levels of physical aggregation of the product (item-level, packages, or lots), and the level of detail of the information flow: expiring date, production methods, certifications, details on ethics, sustainability, requirements related to ethnic and religious group, nutritional information, composition, and presence of allergens, etc., as well other information that can also be used in marketing strategies and against counterfeiting.

Furthermore, there is a high demand of proof of authenticity systems able to certify high-value food credential attributes [5]. Thus, in this paper a blockchain-based system is proposed to manage and certify traceability information and, therefore, the authenticity of food products.

2 Case Study: The PININ Project

The PININ (PIemuNt chèINa, <https://www.pinin-project.eu/>) started in 2019 in Piedmont Region and was financed by the POR/FESR project 2014/2020. Its main objective is to propose and validate distributed and decentralized models for potential use of blockchain in the regional agri-food context. In the whole project the following

aspects were considered: control of the regional financial aids for pastures, cattle geo-localization in mountain pastures, cheese and meat traceability, artificial intelligence and big data in the agri-food system, external parameters monitoring by IoT sensors paired to blockchain (e.g. temperature), new services for supply chain stakeholders, including the consumer and new technologies to contrast food frauds.

This paper regards the models regarding cheese traceability as well as the control of the financial aids for mountain pastures. Both are developed on a common platform, using a similar architecture.

2.1 PININ Blockchain Model Architecture

The architectural system adopted in the context of the PININ Project is composed by three different blockchain typologies:

- Project blockchain: is a consortium blockchain (Ethereum PoA based on the Clique algorithm) designed for the project. Within this blockchain, all users authorized for the network access can freely read and write transactions using no currency. This blockchain enables to operate on the consortium data and smart contracts; it is composed by five Ethereum Geth nodes, three of which are “sealer” nodes and two are nodes of exposure to HTTP JSON/RPC services (Fig. 1a).
- Regional blockchain: public Ethereum PoA blockchain. All the accounts can freely read the data, but they need currency to perform writing. It is composed by 3 Ethereum Hyperledger Besu nodes providing exposure to HTTP JSON/RPC services (Fig. 1b).
- Public blockchain: Ethereum blockchain based on PoW consensus algorithm. It is public and involves the use of currency for writing operations by the accounts.

The smart contracts developed for the interaction with the blockchain are organized based on 3 layers:

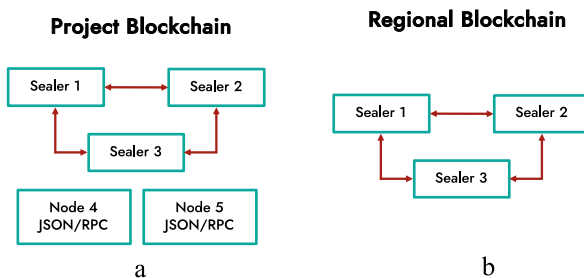


Fig. 1 Blockchain architectures: a) Project blockchain without currency. Read all, write all. Five Ethereum Geth nodes (3 sealers and 2 JSON for access control); b) Regional blockchain with currency. Read all, write some. Three Ethereum Hyperledger Besu nodes

- Platform Layer: set of contracts at the base of the architecture. They guarantee a robust system against eventual data manumission, as well as enable the simplification of traceability data handling and easiness in the interaction with the blockchain.
- Service Layer: contracts that contribute to satisfy the project requirements and support the certification and the checkpoint systems.
- Business Layer: contracts that define business logic. They are strictly connected with the underlying platform level in order to exploit its potential (persistent storage, access control, contracts and events census).

A Decentralized Application (DApp), accessible through the web and interacting with the blockchain, has been developed. It enables authorized users to log in by means of a private key and to register products traceability data in the consortium blockchain by means of smart contracts. The DApp also allows the partners to read the recorded data and to retrieve information about their authors. Moreover, data verification is possible: records are read by smart contracts that verify their formal validity and their accordance with data previously registered. The fourth main function of the DApp is to process data entered in the consortium blockchain and to publish them into the regional one.

A mobile application was developed to provide consumers with certified product traceability information. Consumers are able to discover the history of the product they are buying by scanning the QR code on the food label and retrieving information directly from the blockchain.

2.2 Cattle Tracking for Pasture Funds Control

The disbursement of European funds dedicated to the breeding of cattle in mountain pastures is often the protagonist of multiple scams. The payment of economic support for breeders is based on the number of heads which are displaced in the mountain pastures and are fed mainly with grass during the summer season.

The breeder self-compiles a fund request declaring the animals which are moved to the pasture. Data of each bovine is then recorded by the Regional Funding Office. The cattle movements are recorded in the National Bovine Database, when the cows are effectively moved to the pasture. Frauds are based on false declaration of cattle movements to obtain funds.

To monitor the effective movements of cattle in pastures in relation to the real use of land systems, the precise identification of the animals with their own pasture code and the relative association to the cadastral parcel relating to that code could be useful.

It is indeed fundamental to project new IoT systems to geo-locate cattle in pastures to facilitate controls. The additional implementation of a blockchain system is helpful to keep a secure record of the collected information and allows to increase their truthfulness and authenticity value.

Fig. 2 Primary collar used for the geolocation of cattle in pastures



The geo-location system developed in the context of the PININ project involved the use of smart collars, provided with an autonomous tracking system, that have been worn by the animals during the mountain pasture period (May–October).

The smart collars are based on a set of primary collars and secondary collars which communicate through Bluetooth Low Energy (BLE) communication protocol that uses Beacon technology. Primary collars (Fig. 2) mount a GPS, while the secondary collars are geo-located as they transmit their position through the BLE connection with the primary collar worn by neighboring animals every few seconds. The primary collar is geo-located at regular settable intervals and the unique codes of the nearby Bluetooth modules are associated to its position.

For the transmission of data to the server, 4G technology was used as it involves reduced energy consumption and an advantageous cost/Kbyte ratio compared to satellite transmission. Primary collars were therefore equipped with a 4G SIMCOM7600 modem, enabled to transmit through the pay-per-use ThingsMobile operator which relies on the Vodafone and Wind-Tre networks that cover the pasture area with 2-3-4G frequencies.

Primary collars were equipped with a 3.2 V lithium-iron-phosphate battery, that must have sufficient capacity to power the system for the entire period of pasture and must have an acceptable size and weight to be transported easily by the animals.

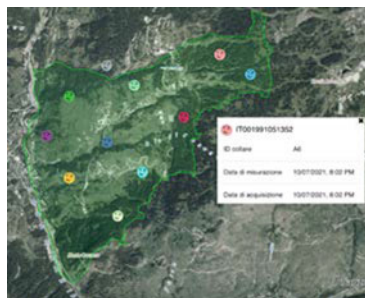
Data that has to be send to the server and recorded in the blockchain are: collar ID (unequivocal), GPS coordinates (latitude, longitude, precision), timestamp of secondary collars detection (year:month:day:hour:minute:second), RSSI (Receive Signal Strenght Indicator), and the battery voltage (in Volt).

A web dashboard was developed to visualize and navigate between all the positions of cattle certified in the blockchain and to filter them by individual cattle and/or by a reference time interval (Fig. 3).

2.3 Use Case of Cheese Traceability

Three types of artisanal dairy products (ripened Toma cheese, pasteurized milk and yogurt) have been considered for experimental trials in two Piedmontese farms which

Fig. 3 Detail of the dashboard developed for visualizing the positions of the cattle in mountain pastures recorded by the collars



have been involved in the project (May 2021–May 2022). Data about 1480 milk lots and 425 production lots were registered in the blockchain.

Starting from the production flows, the traceable units to be registered in the blockchain have been defined: “milk lot”, related to a single milking process and “production lot”, related to the finished product that is obtained using one or more milk lots.

The recording of each traceability lot data in blockchain was performed using the DApp described in Sect. 2.1. The information registered in blockchain were the tax code of the cattle breeder, the code of the stable of the breeding farm (retrieved from the National Bovine Database), the code of the place of cows feeding (stable or pasture), the ID code of the lot (4-digits in length), the quantity of milked milk, and the date of milking. For each production lot, the following data have been entered in the blockchain: the tax code of the cattle breeder, the code of the stable of the breeding farm, the typology of considered dairy product, the IDs of the milk lots from which it is made, the ID code of the production lot (numeric or alphanumeric), a timestamp (generated automatically by the DApp system based on the time and date of data entry into the blockchain), the total quantity of milk used for the specific production, and the production date. Once published in the public blockchain, the certified data can be consulted by final consumers thanks labels placed on the products and the specially developed application for smartphones. The identification labels, autogenerated by the DApp, were designed to contain a QR code specific for each dairy product lot. The use of NFC tags placed directly on the cheese wheel during moulding and reporting the same code has been also hypothesized, in the case automation in the inventory and logistic phases is requested. Two scenarios for the application of the identifiers to the final products were proposed, each tested in one of the two considered farms. In the first scenario the identification labels (Fig. 4) were applied to the packaging of the products exposed to sale (milk bottles, yogurt pots, and wrappers containing Toma slices portioned over the counter). In this case, the matching of physical materials and traceability information registered in the blockchain must be guaranteed by other identification devices (e.g. by a stamp on the cheese wheel crust) both during processing and warehousing, which can lead to errors. In the second scenario, instead, the Toma cheese wheels were identified during the forming phase by using the QR code labels applied on a plastic circular device inserted directly into the cheese wheel

Fig. 4 Identification label with the QR code applied to a yogurt pot



Fig. 5 Toma cheese during ripening phase with the circular identifier with the QR code label



Fig. 6 The NFC tag under the plastic identifier



(Fig. 5). The NFC tag was placed under the plastic device (Fig. 6). At the end of the seasoning (more than three months) both the QR code as well as the tag placed directly on the cheese crust were readable.

Besides allowing the production lot identification, the QR code label enables final consumers to discover the history and the traceability data of the dairy products they are buying. This is possible thanks to the specially developed mobile application, available both for iOS and Android devices, through which the user can scan the QR code and retrieve certified information about the specific lot directly from the blockchain. The application, in addition to providing data about the milk origin (cattle breeding methods and places), production processes, and supply chain details, offers also the access to a social network (FirstLife, <https://www.firstlife.org/>) for sharing social contents on an interactive map. Information and opinions on farms, restaurants, markets, cultural heritage, traditions, recipes, etc. enhance the experience during both selling and post-selling phases, adding supply chain value.

3 Conclusions

A distributed, decentralized and scalable infrastructure based on blockchain for food supply chain traceability has been proposed. The three level BC architecture maintains low transactional costs by reducing the use of currency. The system can be used to put-in-place anti-counterfeit strategies to protect brand reputation as well as quality and origin certifications. Proves of financial frauds can be indisputably detected to improve control bodies efficiency. The public blockchain allows all citizens to access information during the buying experience by means of their smartphone. The authenticated traceability information can be coupled to other credential attributes which can be shared on the social media and websites, thus enhancing the available alternatives in multichannel marketing and allowing e-commerce functionalities. The PININ model could be used to provide new services for farmers and citizens in a supply chain paradigm where the quality concept is conceived as a participative process. This approach allows to include also the small producers which are often excluded from business opportunities, leading to territory valorisation, tradition preservation and to the reduction of mountain area population decline.

Funds and Acknowledgments This work was supported by the project “PININ - PiemuNt chèINa” (POR FESR 2014–2020 - Piattaforma Bioeconomia - Piedmont Region). We thank the owners and personnel of the farms involved in this study Bermond Daniele (San Sicario, TO) and Cibrario Marco (Chiomonte, TO).



References

1. Seebacher, S., Schüritz, R.: Blockchain technology as an enabler of service systems: a structured literature review. In: Za, S., Drăgoicea, M., Cavallari, M. (eds.) *Exploring Services Science*. LNBI, vol. 279, pp. 12–23. Springer, Cham (2017)
2. Wang, Q., Li, R., Wang, Q., Chen, S., Xiang, Y.: Exploring unfairness on proof of authority: order manipulation attacks and remedies. In: *Proceedings of the 2022 ACM on Asia Conference on Computer and Communications Security*, Nagasaki, Japan, pp. 123–137 (2022)
3. Caldarelli, G., Rossignoli, C., Zardini, A.: Overcoming the blockchain oracle problem in the traceability of non-fungible products. *Sustainability* **12**, 2391 (2020)
4. Feng, H., Wang, X., Duan, Y., Zhang, J., Zhang, X.: Applying blockchain technology to improve agri-food traceability: A review of development methods, benefits and challenges. *J. Clean. Prod.* **260**, 121031 (2020)
5. Cena, F., Boella, G., Cordero, A., Guffanti, A., Rapp, A., Schifanella, C., Ambrosini, S., Gay, P., Tortia, C., Barge, P., Comba, L., Biglia, A.: Blockchain and Artificial Intelligence for quality food protection and advanced consumer services. In: *I-Cities 2019, 5th Italian Conference on ICT for Smart Cities and Communities*, Pisa, Italy, pp. 1–2 (2019)

Agroforestry Innovations Lab Activities on Sprayer Performance and Certification



Lorenzo Becce , Giovanni Carabin , and Fabrizio Mazzetto 

Abstract Plant protection treatments are of paramount importance to the food supply chain, especially with a growing world population. However, they pose serious risks to the health of operators, bystanders and ecosystems, so the products have to be very carefully administered in order to reduce the dispersion to the environment, which also represents a loss of income for the farmer. The extent of the problem calls for an increased awareness by all stakeholders and new solutions of growing complexity. This, in turn, raises the demand for (i) base research toward new, performance-oriented solutions, (ii) a certification system to guarantee the adoption of good practices to protect functionality and human and environmental health, and (iii) the tailoring of specialized solutions to various operating contexts such as alpine areas. Within this framework, the Agroforestry Innovations Lab (AFI-Lab) is launching a research branch dedicated to sprayer performance and certification in synchrony with local stakeholders, both industrial partners and farmer communities. Aim of this work is to present the equipment that has been developed in aid of this activity, and some preliminary results obtained, with particular attention to the realization of a wind tunnel for the investigation of atmospheric spray drift, mainly through optical instruments. The tunnel measures $6 \times 10 \times 30$ m (W, H, L) and allows airflows of up to 5 m/s. Within it, vertical and horizontal patternators can be accommodated to characterize the deposition performance of orchard sprayers during simulated treatments with advanced tracing solutions. A laser Particle/Droplet Image Analysis system is also installed within a dedicated test bench for the characterization of nozzles. The work is closed with a roadmap of the activities and a panoramic of the potential side applications of the facility.

Keywords Spray Drift · Plant Protection · Wind Tunnel · Droplet Size · Orchard Sprayers

L. Becce (✉) · F. Mazzetto

Competence Centre for Plant Health, Free University of Bozen-Bolzano (unibz), Bolzano, Italy
e-mail: lorenzo.becce@unibz.it

G. Carabin · F. Mazzetto

Faculty of Science and Technology (Fa.S.T.), Free University of Bozen-Bolzano (unibz), Bolzano, Italy

1 Introduction

Monitoring the performance of agricultural sprayers, especially in the field, has always proven difficult due to the high number of involved parameters and their random variability: wind, solar radiation, air temperature and humidity, to mention a few, hinder the repeatability and reliability of field tests. The authors of [1] clearly outlined this problem while implementing the current spray drift measurement standard (ISO 22866).

To cut out the effect of the wind, an experiment similar to that of ISO 22866 was replicated indoors at the newly-instituted Agroforestry Innovations Laboratory (AFI-Lab) of the Free University of Bozen-Bolzano (unibz) together with members from the Department of Agricultural, Forest and Food Sciences (DiSAFA) of the University of Torino [2], thus laying the groundwork for the research on sprayers at the AFI-Lab.

Orchards and vineyards, even in the mountains, play a key role in the local economy of South Tyrol, where unibz is operating, and the drift of Plant Protection Products (PPP) constitutes a large problem, widely felt by all the stakeholders (including the general public). This highlights the necessity to tailor specific solutions to the local scenario, staying up-to-date with the global advancements in the field while keeping close contact with local farmers. To gain insight into the problem, a wind tunnel has been built in order to study the spray drift phenomena typical of the regular treatments of orchards on real-scale, field-worthy equipment. Local machine constructors and end-users show a great interest in the facility, which allows to carry out the trials in semi-controlled environment.

Despite wind tunnels being extensively used across and beyond Europe, they are usually built to test single nozzles, and not the entire machine in its operational conditions. Examples include the investigation of the deposition pattern and drift potential of nozzles at Universitat de Lleida (Spain) and Université de Montpellier (France) [3], at the Silsoe Spray Applications Unit (UK) [4]; and recently, of the performances of Unmanned Aerial Systems for crop spraying at the Julius Kühn Institute (Germany) [5].

The presented document will briefly describe this branch of research activities, with a focus on the realization of the wind tunnel, and will close with a brief look at the opportunities enabled by this facility.

2 The Research Activity

2.1 Aims of the Research

The rationales under the institution of the facility are (i) the investigation of repeatability and practicality of performance measurement techniques to bypass the influence of environmental factors and, possibly, to develop and propose more effective, representative or practical testing procedures, both in functional inspection and certification; (ii) the development of specialized solutions tailored around mountain agriculture; and finally (iii) to understand the drift phenomena and the efficacy of drift reduction techniques.

The activities start from the analysis of nozzle performance and aim at investigating the primary/secondary drift mechanisms (off-target movement and aerosol generation) during PPP application, with a possibility to extend the scope to atmospheric transport phenomena in partnership with other research groups.

2.2 Nozzle Performance

Due to their role in the overall performance of the sprayer, key nozzle performances such as particle size statistics need to be thoroughly evaluated before any test. The laboratory is equipped with a Particle/Droplet Image Analysis (PDIA) system (Oxford Lasers N60), mounted in an experimental test bench where a pump forces water into a conventional nozzle holder spraying downward, whose position relative to the instrument's field of view can be adjusted manually. Figure 1 shows a typical result from a comparative study of two hollow-cone nozzles (HCI80-01 and 02, ASJ s.r.l.) operated at 8 bar pressure. Some preliminary results of this thread are described in [6].

2.3 Wind Tunnel Testing

The idea behind the wind tunnel is to perform simulated treatments (hence without any active principle) with real machinery while controlling the environment as much as possible, to assess the distribution on target surfaces and dispersion in air of representative test solutions using intercepting surfaces and optical devices, currently under investigation. A wind tunnel enables the simulation of treatments under steady winds, but is also important during experiments in still-air to rid the test chamber of leftover aerosols between measurements.

Figure 2 illustrates a typical application, with the machine crossing the flow perpendicularly and spraying in the downwind direction.

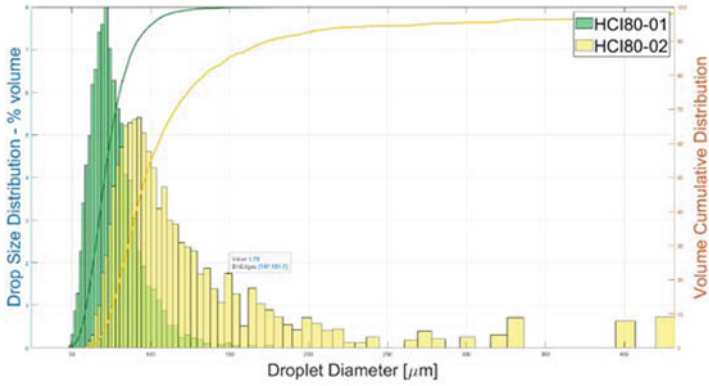


Fig. 1 Droplet spectra from HCI80 nozzles. The histogram of the drop size distribution is complemented by the continuous line, representing the cumulative distribution. The graph was obtained in Matlab from N60 raw data as per [6]

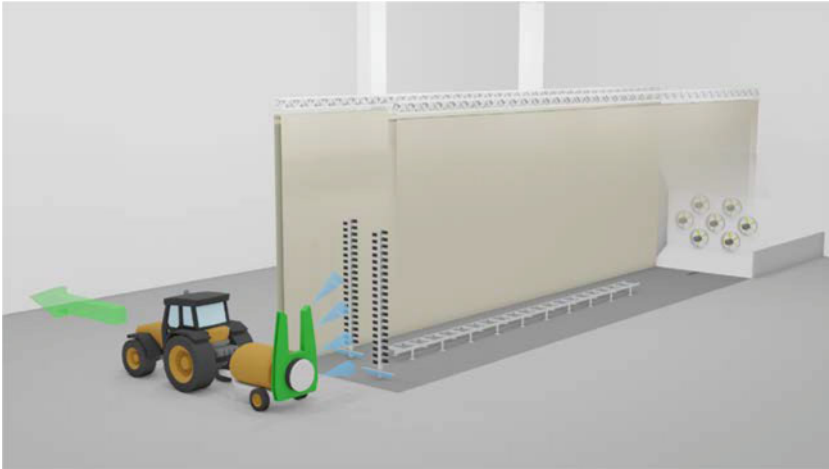


Fig. 2 Concept of the typical foreseen test: the test solution is sprayed inside the wind tunnel, appropriately instrumented to intercept the solution in the points of interest. The right-side walls are transparent for visibility. Rendering: Blender 3.2.2

An airtight design was rejected from the start for being excessively complex, volume- and energy-intensive. Since it would require enclosing the whole test area with manoeuvre space for the tractor, a compromise was struck in favour of an open channel, which enables the reasonable control of key variables with respect to the open-field testing, chiefly wind and solar radiation.

3 The Wind Tunnel

3.1 Design and Realization of the Wind Tunnel

The design and realization activities, carried out jointly between CUBIT s.c.a.r.l. (Consortium Ubiquitous Technologies, Cascina (Pisa), Italy) and the Free University of Bolzano-Bozen, consisted of a (i) CFD analysis of the channel flow, (ii) the structural design and selection of the vertical walls materials, (iii) the design of the ventilation system and (iv) of the sensor system for flow control, and finally (v) a cost estimate.

Requirement Analysis. A maximum wind speed of 5 m/s was deemed sufficient to replicate any operative weather condition and to clean the air volume between tests. The flow must be uniform across the width of the channel.

The facility is inserted into the existing B5 building at NOI Techpark, so the dimensions were constrained by structural and organisational limits: the channel is 6 m wide, 10 m high and spans 30 m in length. As will be discussed, it was decided for collapsible channel walls, in order to save space for other activities when not in use.

Aerodynamic Flow Analysis. A 20-million-cell Reynolds Averaged Navier–Stokes (RANS) CFD simulation has been employed to analyse the ideal flow as well as the different configurations which kept the physical limitations of the building into consideration. The investigation started from the ideal required flow and progressively evolved the solution by implementing elements and constraints of the real situation; for relevance, however, these intermediate steps are not represented and emphasis will be put on the final configuration. All the CFD visualisations are provided by CUBIT.

Ideal Flow and First Iterations. The ideal situation, analysed for reference with the practical proposals, would foresee air entering the hall uniformly at 5 m/s from a large door at the southern end of the building, then proceed through the channel and vent outside through an exit perfectly aligned with the entrance, which is impossible due to the existence of a second building hall at the end of the channel. The side walls were idealized so as to perfectly enclose the flow without leaking air. Figure 3 clearly shows the non uniformity of the flow even in this case, with the uniform 5 m/s region thinning in both dimensions throughout the longitudinal evolution. The sequence of simulations that followed gradually added details and refined the design: it was shown how the original idea of placing the fans at the entrance creating intense turbulence at the tunnel entrance, that is where the experiments are to be carried out. A suction system drawing air at 5 m/s from the channel exit was then schematized so as to analyse the forced flow. Finally, to overcome the spatial limitations of the building, an outlet on the roof was proposed, which was however deemed impractical to realise, albeit very promising.

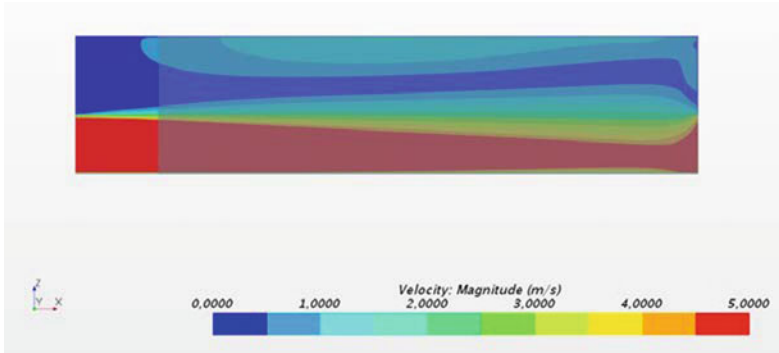


Fig. 3 Side view of the ideal flow at the centerline

Final Configuration. The compromise solution takes advantage of the side windows of the hall for venting. Figure 4 shows a velocity profile compatible with the roof-based solution, with the added benefit of a simpler realization.

Fans. The final steps implemented the fan system and investigated different configurations: from an initial 3×3 fan disposition, the calculations established a $2 + 3 + 2$ configuration to be sufficient. The outlet duct leads the airflow through a window, with an estimated pressure drop of 208 Pa, further refined to 158.5 Pa by employing two windows.

Walls. The main requirement for lateral walls is to isolate as best as possible the internal channel space, especially to protect the longitudinal flow from potential crossing air streams, while being removable when not in use to save space. The installation of the whole system should be as quick as possible (ideally less than an hour): thus rigid walls, due to their size (10×30 m), would be impractical and were

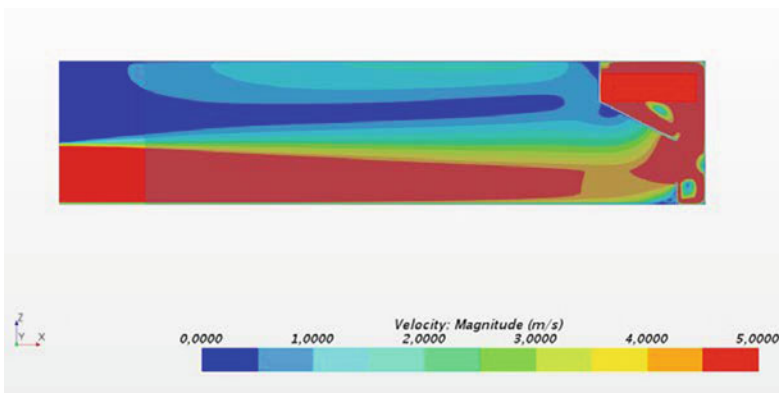


Fig. 4 Section view of the flow at the centreline with outlet at the windows, in the upper right corner

excluded from the start. A similar domain of application are the collapsible walls in sport halls, so a custom solution was sought from companies operating in the sector.

Particular attention had to be paid to the rigidity of the walls, so as to avoid deformations due to the slight underpressure caused by airflow: therefore, each wall is made of two layers, interconnected and ballasted in several points across the height so as to keep the right tension, also with the aid of ground fixing points. A system of electric motors ensures a quick deployment and retirement of the walls.

Requirements for Flow Control and Measurement. The flow control system, currently under realisation, shall be able to: (i) verify the functioning of the facility, particularly the main parameters of the airflow, to be verified in several points across the channel, and of the fans (rotational speed, flow rate, absorbed electrical power); (ii) verify the liquid and airflow distribution performance of the sprayer, via optical and physical instruments; (iii) quantify the aerosol concentration in several positions at different heights (2–5 m, secondary drift) and deposited concentrations on specific interceptors on the ground (primary drift).

Patternators. As for the liquid distribution, horizontal patternators up to 20 m can be deployed, as well as two 4.5 m vertical patternators which can characterize the vertical distribution pattern of the machine with a 10 cm resolution. The equipment, provided by Salvarani s.r.l. (Poviglio, IT), is to be used in certification and testing activities as well. Figure 5 shows the wind tunnel instrumented with both kinds of patternators. The green boxes represent the tools, some of which have been presented, instrumental to the areas in the light blue boxes. Dashed lines are reserved for planned activities and tools.



Fig. 5 View of the wind tunnel with the walls deployed from the entrance. The vertical patternators are on the foreground, and the horizontal one runs along the length. In the background, the fan array can be seen

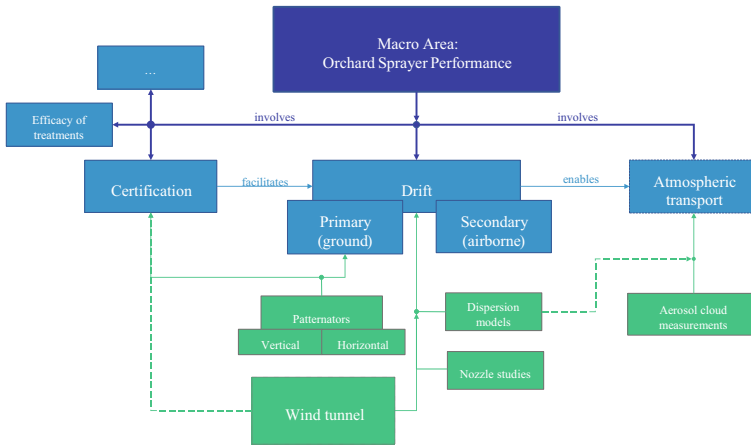


Fig. 6 Conceptual map of the AFI-Lab activities on sprayer performance

4 Conclusions and Future development

The presented facility opens several possibilities: (i) understanding of formation and short-range transport dynamics of drift, (ii) the assistance to machine designers in product development, (iii) the search for new forms of certification for new machinery, and finally, (iv) the testing of rotary-wing Unmanned Aerial Systems (UAS, [7, 8]), in particular in terms of flight stability against wind gusts.

Figure 6 presents the current and foreseen research sub-threads on sprayer performance. The next steps involve the investigation of optical systems to quantify the concentration of aerosols in the confined spaces of the channel; a related activity, currently yielding interesting results, is the search for advanced tracers for reliable, repeatable and cost-effective measurements of spray deposition, presented in [9, 10].

Acknowledgements The tractor in Fig. 2 by Igor Bistriski, licensed under Creative Commons Attribution (<https://skfb.ly/6YZQ9>). Credits for the CFD views: CUBIT s.c.a.r.l.

References

1. Gil, E., Llorens, J., Gallart, M., Gil-Ribes, J.A., Miranda-Fuentes, A.: First attempts to obtain a reference drift curve for traditional olive grove's plantations following ISO 22866. *Sci. Total Environ.* **627**, 349–360 (2018). <https://doi.org/10.1016/j.scitotenv.2018.01.229>
2. Grella, M., Marucco, P., Manzone, M., Gallo, R., Mazzetto, F., Balsari, P.: Indoor test bench measurements of potential spray drift generated by multi-row sprayers. In: 2021 IEEE International Workshop on Metrology for Agriculture and Forestry (MetroAgriFor), Trento-Bolzano, Italy, pp. 356–361, November 2021. <https://doi.org/10.1109/MetroAgriFor52389.2021.9628652>

3. Torrent, X., Gregorio, E., Douzals, J.-P., Tinet, C., Rosell-Polo, J.R., Planas, S.: Assessment of spray drift potential reduction for hollow-cone nozzles: Part 1. Classification using indirect methods. *Sci. Total Environ.* **692**, 1322–1333 (2019). <https://doi.org/10.1016/j.scitotenv.2019.06.121>
4. Kuster, C.J., Hewitt, N.J., Butler Ellis, C., Timmermann, C., Anft, T.: Measurements of the dermal exposure to bystanders from direct off-crop drift during the application of plant protection products. *Ann. Appl. Biol.* **179**(1), 123–133 (2021). <https://doi.org/10.1111/aab.12686>
5. Wang, C., et al.: Spray drift characteristics test of unmanned aerial vehicle spray unit under wind tunnel conditions. *Int. J. Agric. Biol. Eng.* **13**(3), 13–21 (2020). <https://doi.org/10.25165/j.ijabe.20201303.5716>
6. Becce, L., Amin, S., Carabin, G., Mazzetto, F.: Preliminary spray nozzle characterization activities through shadowgraphy at the AgroForestry Innovation Lab (AFI-Lab). In: 2022 IEEE Workshop on Metrology for Agriculture and Forestry (MetroAgriFor), Perugia, Italy, pp. 136–140, November 2022. <https://doi.org/10.1109/MetroAgriFor55389.2022.9965106>
7. Becce, L., Bloise, N., Guglieri, G.: Optimal path planning for autonomous spraying UAS framework in precision agriculture. In: 2021 International Conference on Unmanned Aircraft Systems (ICUAS), Athens, Greece, pp. 698–707 (2021). <https://doi.org/10.1109/ICUAS51884.2021.9476690>
8. Bloise, N., Carreno Ruiz, M., D'Ambrosio, D., Guglieri, G.: Wind tunnel testing of remotely piloted aircraft systems for precision crop-spraying applications. In: 2021 IEEE International Workshop on Metrology for Agriculture and Forestry (MetroAgriFor), Trento-Bolzano, Italy, pp. 378–383, November 2021. <https://doi.org/10.1109/MetroAgriFor52389.2021.9628600>
9. Altana, A., Becce, L., Lugli, P., Petti, L., Mazzetto, F.: Uranine as a tracer for rapid detection of spray deposition. presentato al AIIA 2022: Biosystems Engineering Towards the Green Deal, Palermo (2022)
10. Altana, A., Becce, L., Avancini, E., Lugli, P., Petti, L., Mazzetto, F.: Cost-effective tracing techniques for the rapid characterization of spray deposition and drift through electrical conductivity and fluorescence. In: 2022 IEEE Workshop on Metrology for Agriculture and Forestry (MetroAgriFor), Perugia, Italy, pp. 164–168, November 2022. <https://doi.org/10.1109/MetroAgriFor55389.2022.9964955>

Analysis of Spraying Equipment Performances in Olive Orchards



Souraya Benalia, Giuseppe Zimbalatti, Lorenzo M. M. Abenavoli, Antonio Fazari, and Bruno Bernardi

Abstract This paper reports the outcomes of a study dealing with the evaluation of the equipment used to spray plant protection products in olive groves. We performed experimental tests in an intensive olive orchard situated in the province of Reggio Calabria to determine under field conditions according to machine operating parameters 1) foliar deposition, from both quantitative and qualitative point of view, and 2) ground losses. Hence, we applied a solution of a food dye on olive trees as to simulate a plant protection product mechanical distribution. Spray quantitative analysis was determined according to the colorimetric method using a bench spectrophotometer, while, image analysis of water-sensitive paper allowed qualitative analysis. A significant effect of the trial conditions was found at the $p < .05$ level on both normalized foliar deposit D_n ($\mu\text{L}\cdot\text{cm}^{-2}$), [$F(2, 65) = 8.58$, $p = 0.0005119^{***}$] as well as on ground losses [$F(2, 25) = 3.931$, $p = 0.00328^*$].

Keywords Foliar deposit · Ground loss · Olive growing · Plant protection product · Sustainability

1 Introduction

The growing consciousness of consumers regarding health properties of olive products has manifested, in recent years, through an increase in the consumption of olives and olive oil even in those countries where their use was not usual until recent years. The International Olive Council (COI) has, in fact, estimated for the 2021/2022 campaign a consumption of more than 3.2 million tons of olive oil and 2.7 million tons for table olives, globally [1, 2]. This scenario undoubtedly offers great investment margins to meet market demand and guarantee requests from both quantitative and qualitative points of view. However, production fluctuations that olive and olive oil

S. Benalia (✉) · G. Zimbalatti · L. M. M. Abenavoli · A. Fazari · B. Bernardi
Department of Agriculture, University Mediterranea of Reggio Calabria, Località Feo Di Vito,
Snc, 89122 Reggio Calabria, RC, Italy
e-mail: soraya.benalia@unirc.it

sector suffered in recent years, because of the effects of climatic trends on the spread of diseases and pests, engendered the intensification of crop protection interventions, to guarantee profitable levels.

Crop protection represents a key intervention without which it would be difficult to achieve production objectives. Although progress, strategies and tools have reached a remarkable technological level, particularly regarding the formulations, it is quite difficult to affirm the same concept regarding the implemented equipment for the application of plant protection products. Indeed, most of the times, only a part of the mixture containing the active substance can reach the target, while applying a treatment. The remaining part is lost on the ground or due to drift with considerable risks for the environment [3]. This low effectiveness of application is often due to obsolete, malfunctioning or incorrectly calibrated and adjusted equipment.

Considering the Directive 2009/128/EC [4], it becomes clear that machines used for the distribution of pesticides play a strategic role to guarantee treatment effectiveness, operator safety and environmental preservation.

In this context, this work focuses on the evaluation of spraying equipment performances in olive orchards. Particularly, quantitative and qualitative analysis of the foliar deposit and losses on the ground were determined under field conditions according to machinery operating parameters.

2 Material and Methods

2.1 Field Description

Experimental trials were conducted in a private olive farm located in the province of Reggio Calabria (38° 23'16.02 "N, 16° 4'19.31" E). Three tests were carried out in three different plots of about 1,000 to 1,300 m², grown with *Olea europaea* L. cv. 'Carolea' having a planting layout of mostly 6 m × 8 m. The following Table 1 shows the dimensional characteristics of the plants.

Table 1 Field and tree dimensional features

Planting layout (m)	Tree age (year)	Trunk height (m)	Canopy volume (m ³)	Tree height (m)	Branch number
6 × 8 / 6 × 4	30	1.3	78.5	5	3



Fig. 1 The sprayer used in experimental trials

2.2 Equipment Description

Experimental trials based on the application of a dye solution on olive trees were performed by using the DSM Turbo spray 1500, towed by a NEW HOLLAND 82–86 tractor (Fig. 1). The sprayer, which tank capacity is 1,500 L, is equipped with a centrifugal fan and n. 7 + 7 active nozzles with a ceramic plate having 1.5 mm hole.

2.3 Spray Distribution and Quantitation in the Field

As previously mentioned, a dye solution, particularly a tartrazine yellow (E102, 85%) solution at $10 \text{ g}\cdot\text{L}^{-1}$, was sprayed using the above-described sprayer in three different plots (Fig. 2), considering different configurations (Table 2), to assess spray distribution from both quantitative and qualitative points of view as performed in Benalia et al. [5].

Once the solution was applied, the samples were collected and stored individually in hermetic containers until subsequent analysis as performed by Bernardi et al. [6]. Particularly, olive tree leaves were collected to determine the foliar deposition, Petri dishes, previously placed between the rows, were used as collectors to determine losses on the ground and water sensitive paper, previously put into olive tree canopies were used for spray qualitative evaluation. Leaf sampling considered three vertical and two horizontal sections in the canopy as shown in Fig. 3.

Subsequently, we applied the colorimetric method to determine foliar deposit and losses on the ground. This included: 1) washing each sample with a known amount of demineralized water, 2) analyzing each recovered solution with the spectrophotometer to determine the concentration of tartrazine yellow in it, 3) determining the



Fig. 2 Tartrazine solution application in olive orchard for spray assessment

Table 2 Machinery characteristics implemented in field trials

	Trial 1	Trial 2	Trial 3
Engine speed (rpm)	1,800		
Power take-off (rpm)	540		
Nozzle number	14		
Advancing speed (km·h ⁻¹)	2.34	3.46	3.01
Exercise pressure (MPa)	1.5	1.3	1.5
Observed area (m ²)	1,124	1,008	1,296
Application rate (L·ha ⁻¹)	1,307.19	1,190.48	1,543.21

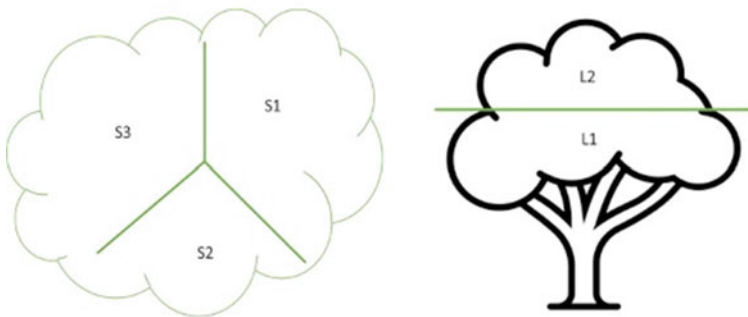


Fig. 3 Leaf sampling positions considered for the trial purposes

volume of the solution intercepted by each sample, 4) measuring sample area and express the deposit in terms of $\mu\text{L}\cdot\text{cm}^{-2}$.

2.4 Data Analysis

Prior to data analysis, performed using the software R (version 3.3.1), spray foliar deposit and losses on the ground values were first normalized to $1,000 \text{ L}\cdot\text{ha}^{-1}$ according to the following formula “Eq. (1)”:

$$D_n = \frac{V_n}{V_d} \times D_{ef} \quad (1)$$

With

D_n : normalized deposit value ($\mu\text{L}\cdot\text{cm}^{-2}$);

V_n : normalized application rate equal to $1,000 \text{ L}\cdot\text{ha}^{-1}$;

V_d : application rate in field ($\text{L}\cdot\text{ha}^{-1}$);

D_{ef} : effective deposit value ($\mu\text{L}\cdot\text{cm}^{-2}$).

While, scanned images of water-sensitive papers were processed using ImageJ 1.45 s software with Java (1.6.0–20).

3 Results and Discussion

According to the considered operating conditions, the spray application rate was of $1,307.19 \text{ L}\cdot\text{ha}^{-1}$ in trial 1; $1,190.48 \text{ L}\cdot\text{ha}^{-1}$ in trial 2; and $1,543.21 \text{ L}\cdot\text{ha}^{-1}$ in trial 3.

The determination of spray application rate depends on several factors such as, crop features (species, layout, training, and vegetation characteristics), the biotic agent to be controlled, the chemical to be used as well as climatic conditions. Application rate recommended by Calabrian authorities [7] when applying a plant protection product in olive growing is $1,200 \text{ L}\cdot\text{ha}^{-1}$, with maximum values not exceeding $1,500 \text{ L}\cdot\text{ha}^{-1}$. Such amounts of plant protection products aim at ensuring a high biological efficacy, however, they also engender huge product loss [8].

Application rate slightly exceeded the maximum threshold in trial 3, while operating parameters considered in trial 2 enabled to keep it around the advised one. Godoy-Nieto et al. [9] applied similar spraying volumes in conventional olive orchard, while in intensive orchards; the application rate was slightly lower.

Normalized foliar deposit (D_n) values, expressed as $\mu\text{L}\cdot\text{cm}^{-2}$, were statistically analysed by performing a two-way analysis of variance. A significant effect of trial conditions was found at the $p < 0.05$ level [$F(2, 65) = 8.58, p = 0.0005119***$]. However, no effect due to leaf sampling height was encountered in all trials (Table 3). Figure 4 (Fig. 4) shows normalized foliar deposit mean values. These values

Table 3 Results of a two-way analysis of variance applied on normalized foliar deposit results

	Sum Sq	Df	F value	Pr(>F)
Trial	96.04	2	8.5838	0.0005119 ***
Leaf sampling height (LSH)	1.95	1	0.3485	0.5571032
Trial * LSH	4.85	2	0.4336	0.6501512
Residuals	346.85	62		

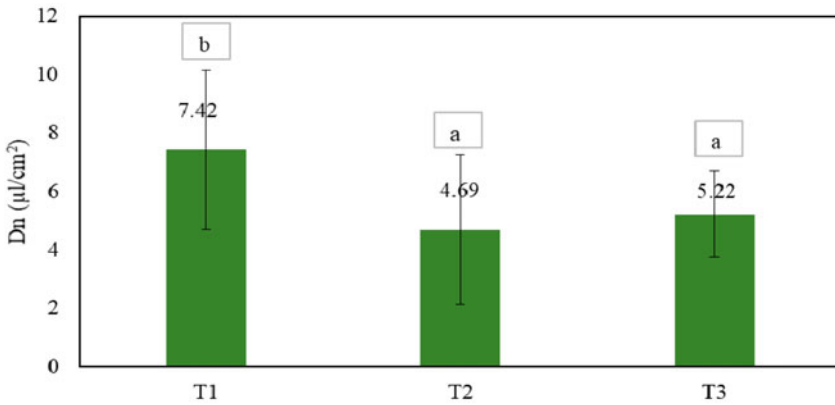


Fig. 4 Normalized foliar deposit mean values in the performed trials

are higher than those obtained by Godoy-Nieto et al. [9] are, in intensive olive orchards. The coefficient of variation (CV) was equal to 45.32%, 59.02%, and 41.63% respectively in trials 1, 2, and 3.

From qualitative point of view, spray distribution parameters, obtained through image analyses of water sensitive paper, reveal a very heterogeneous distribution, considering the number of spots (impacts) per unit area, which varied from 168 up to 1,987, as well as the percentage of area covered with spots, which ranged between 34% and 52.5%. These parameters were very different between trials and within each trial (Fig. 5).

Trials conditions also had a significant effect on the losses on the ground at the $p < 0.05$ level [$F(2, 25) = 3.931, p = 0.00328^*$]. Figure 6 reports losses on the ground mean values. They amounted to 39.25% in trial 1, 15% in trial 2 and 22% in trial 3.

Fig. 5 Water sensitive paper obtained in trial 2 used for spray qualitative analysis

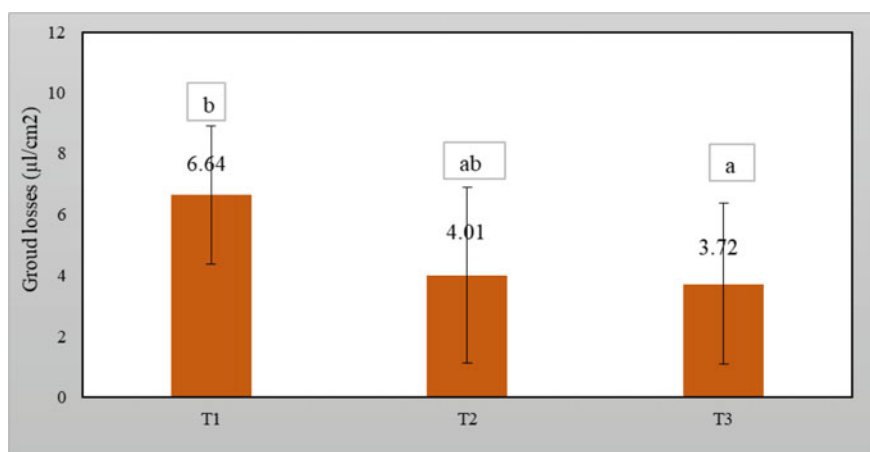
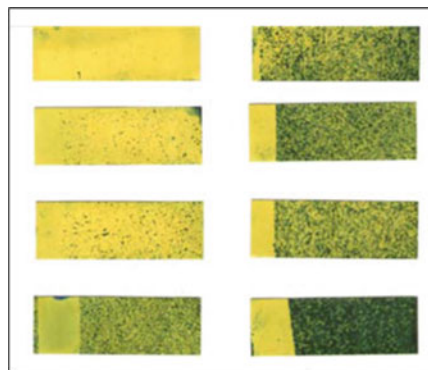


Fig. 6 Normalized losses on the ground mean values in the performed trials

4 Conclusions

According to the obtained results, we can state that spray vertical distribution was quite homogeneous, as we did not register any significant difference according to foliar sampling height.

Spray application rate and consequent foliar deposit, as well as losses on the ground were higher than those obtained in other studies were. In addition, qualitative evaluation of the spray suggests performing PPP application considering equipment adjustments according to crop features and operating conditions.

Acknowledgements The present activity was realized in the framework of the project “Controllo ecosostenibile dei fitofagi dell’olivo –CEbiOl, funded by the Italian Ministry of Agricultural, Food and Forestry Policies.

References

1. COI: Olive oil consumption. <https://www.internationaloliveoil.org/wp-content/uploads/2021/12/HO-W901-17-12-2021-C.pdf>. Accessed Sept 2022
2. COI: Table olive consumption. <https://www.internationaloliveoil.org/wp-content/uploads/2021/12/OT-W901-07-12-2021-C.pdf>. Accessed Sept 2022
3. Garcera, C., Moltó, E., Izquierdo, H., Balsari, P., Marucco, P., Grella, M., Gioelli, F., Chueca, P.: Effect of the airblast settings on the vertical spray profile: implementation on an on-line decision aid for citrus treatments. *Agronomy* **12**, 1462 (2022). <https://doi.org/10.3390/agronomy12061462>
4. EU (European Parliament, Council of the European Union): Directive 2009/128/CE of the European Parliament and of the council of 21 October 2009 establishing a framework for community action to achieve the sustainable use of pesticides. *Off. J. Eur. U.*, L **309**, 71–82 (2009)
5. Benalia, S., Violi, L., Barreca, P., Zimbalatti, G., Bernardi, B.: Analysis of spray behavior using different sprayers in citrus groves. In: Biocca, M., Cavallo, E., Cecchini, M., Failla, S., Romano, E. (eds.) *Safety, Health and Welfare in Agriculture and Agro-Food Systems*. SHWA 2020. *Lecture Notes in Civil Engineering*, vol. 252. Springer, Cham (2022). https://doi.org/10.1007/978-3-030-98092-4_41
6. Bernardi, B., Benalia, S., Panuccio, M.R., Zimbalatti, G.: Assessing the “Special-Serre” sprayer for pesticide application to a greenhouse chrysanthemum crop. In: *Acta Horticulturae*, vol. 1170, pp. 603–610 (2017). <https://doi.org/10.17660/ActaHortic.2017.1170.75>
7. Regione Calabria: *Disciplinari di Produzione Integrata 2019: difesa fitosanitaria e controllo delle infestanti*. https://www.arsacweb.it/wp-content/uploads/2019/06/DISCIPLINARI__2019_PARTE_DIFESA_E_DISERBO_aggiornati_ad_aprile_definitivo_ok.pdf. Accessed Sept 2022
8. Miranda-Fuentes, A., Llorens, J., Rodríguez-Lizana, A., Cuenca, A., Gil, E., Blanco-Roldán, G.L., Gil-Ribes, J.A.: Assessing the optimal liquid volume to be sprayed on isolated olive trees according to their canopy volume. *Sci. Total Environ.* **568**, 296–305 (2016)
9. Godoy-Nieto, A., Miranda-Fuentes, A., Grella, M., Blanco-Roldán, G.L., Rodríguez-Lizana, A., Gil-Ribes, J.A.: Assessment of spray deposit and loss in traditional and intensive olive orchards with conventional and crop-adapted sprayers. *Agronomy* **12**, 1764 (2022). <https://doi.org/10.3390/agronomy12081764>

Different Strategies to Alleviate Soil Compaction Risk During Tillage Operations



Marco Benetti and Luigi Sartori

Abstract Compaction causes soil degradation, but different strategies can help to mitigate this phenomenon, such as increasing soil strength under traffic and decreasing soil stress due to equipment features. Controlled traffic farming enhances soil compaction mitigation by confining all equipment transit to the traffic lane. Crop seedbeds remain undisturbed, improving crop performance and increasing yield. Controlled traffic needs equipment standardization for all operations, from tillage to harvest, which can overcomplicate equipment travel on public roads and use of contractors. This study investigates three strategies to alleviate soil compaction risk during tillage: Random traffic with tracks, with wheels and controlled traffic farming. Three scenarios were compared by using the following traffic indexes: Rut Length, Traffic Intensity, Mechanization Degree, and Field Load Index. Soil stresses in specific scenarios were calculated with the Terranimo[®] model. Collecting soil bulk density, penetrometer resistance, working time analysis, field traffic analysis and fuel consumption with telemetry was completed on a real scale thanks to a 19 ha field test on a farm in northeast Italy. The soil stress is higher in the Controlled traffic than in the other two random traffic scenarios due to the narrow width of the wheels used to decrease the trafficked area. The field index Ruth Length shows a higher value in CT caused by a lower working width. On Mechanization Degree the RT scenario has a 47% increase compared to CT and 21% more than RW due to the high power used. Lower bulk density and Cone Index were found in CT seedbed. CT shows a decrease in fuel consumption and CO₂ emission due to higher traction efficiency.

Keywords Soil compaction · Controlled traffic farming · Tillage

M. Benetti (✉) · L. Sartori

Department of Land, Environment, Agriculture and Forestry, Università degli Studi di Padova, Agripolis, Viale dell'Università 16, 35020 Padova, Legnaro, Italy
e-mail: marcobenetti.agri@gmail.com

1 Introduction

Soil compaction due to machinery traffic is one of the causes of soil degradation [1, 2]. The intensity and spread of this phenomenon are increasing due to increased farm equipment weight and size that has occurred during the last decades [3]. Soil degradation due to compaction affects 33 million ha of farmland in Europe [4]. Compaction affects soil porosity resulting in poor water and gas communication and difficulties in root penetration. This could increase crop sensitivity to drought and wet conditions producing a yield drop. Tillage is an important operation to guarantee plant establishment and alleviate soil compaction but intensive and repetitive traffic could cause compaction and decrease soil strength. Different strategies were developed to mitigate soil compaction. Decrease soil stress by reducing vehicle mass and size [5], improve the driving system by tracks or double tires or low inflation tires, or adopt controlled traffic farming [6].

The aim of this study was to analyze three different soil compaction management strategies during seedbed preparation for processing tomato. To achieve this objective a one-year field test was planned that focused on mechanization performance, fuel efficiency and soil effect.

2 Materials

The field test was planned to analyse different soil compaction management systems focused on real fieldwork conditions. Three treatments were defined:

1. Random traffic with wheeled propulsion (standard work condition) (RW)
2. Random traffic with rubber track propulsion (RT)
3. Controlled Traffic (CT)

The treatments show three different farm mechanisation and management strategies to decrease soil compaction damage. These solutions were chosen because they are the most used; they could be introduced into the Italian farming system and lack a comparison between them. Three regular fields were found for the experiment for a total area of 19.5 hectares, split into 6.5 ha for the scenarios (44°53'12.2"N 11°56'21.9"E) to give the minimum size to allow the work of a tracked tractor and implement and measure the performance as close as possible to real use conditions (Table 1).

Table 1 Tractors and implements used in the field test

Brand and model	Power (kW)	Operation	Driving system	Thesis
JD 8370RT	276	Cultivation, seedbed preparation,	Rubber caterpillars	RT
JD7290R	216	Cultivation	Low inflation pressure Pneumatic wheels	RW
JD6120R	89	Cultivation, seedbed preparation, fertilizing	Rubber semi-caterpillars and Pneumatic wheels	CT, RT
JD6110RC	89	Seedbed preparation, fertilizing	Low inflation pressure Pneumatic wheels	RW
JD6155M	115	Seedbed preparation,	Double Pneumatic wheels	RW

Table 2 Soil texture and SOM on test field

		Clay			Silt			Sand			SOM		
Depth		0–5	15–20	40–45	0–5	15–20	40–45	0–5	15–20	40–45	0–5	15–20	40–45
CT	min	20.7	24.7	28.7	30.7	26.7	30.7	30.5	24.5	24.5	4.52	4.52	4.09
	max	38.7	38.7	44.7	34.7	38.7	32.7	48.5	48.5	38.5	5.04	4.92	4.61
RT	min	38.7	20.7	24.7	30.7	30.7	26.7	28.5	30.5	24.5	4.9	4.52	4.52
	max	38.7	38.7	38.7	32.7	34.7	38.7	30.5	48.5	48.5	5.11	5.04	4.92
RW	min	24.7	22.7	22.7	30.7	26.7	30.7	28.5	36.5	24.5	4.59	4.45	4.09
	max	40.7	24.7	44.7	34.7	38.7	36.7	40.5	48.5	40.5	5.04	4.61	4.45

Soil texture and soil organic matter (SOM) were analyzed by a disturbed sample collected simultaneously and close to the bulk density and penetrometer sampling zone (Table 2).

Bulk Density was analyzed by 36 undisturbed soil samples collected in the study area with a specific sampler (Eijkelkamp, Veesebek, NL) at three depths: 0–5 cm; 15–20 cm; 40–45 cm. The controlled traffic treatment was sampled twice, splitting tramline (CTFT) and seedbed zone (CTFS).

Volumetric water content (VWC) was calculated from wet and dry weight of soil bulk density sample. Wet soil samples after weight were dried in a 105 °C oven to constant weight.

Penetration resistance and CI was measured with a cone penetrometer to evaluate the effect of traffic conditions on soil. The cone penetrometer was inserted into the soil at a constant speed with a penetration rate of less than 2 cm s⁻¹. The cone used in the penetrometer had a base diameter of 12.83 mm and cone angle of 30°, as specified in ASAE Standards S313.3 and EP 542 (ASAE Standards, 1999, 2001). Three 18 m transects were done for every treatment orthogonally to row direction. A total number of 333 penetrometer points were sampled.

Traffic pattern was calculated after mapping all vehicle traffic in the field test. Vehicles positions were recorded on 1 Hz GPS RTK driving system. These position data were analyzed with GIS software in the following procedure:

1. Cleaning double points and outlier points from the dataset.
2. Converting point to line traffic patterns, one in the center of each axle of every machine.
3. Building a line for every wheel center following the previous traffic pattern
4. Building a polygon for every wheel/track traffic, observing the tire characteristics (tire width)
5. Creating a layer of traffic patterns polygon to every field operation
6. Rebuilding the history of traffic patterns thanks to adding all the involving layer at a certain analysis moment.
7. Calculating the number of overlapping layers that correspond to a Penetrometer sampling point.

Field traffic indices were estimated to understand and compare the intensity of field traffic. Indices were calculated using telemetry data collected from tractor GPS RTK driving systems and equipment specifications:

Rut length (RL) [7]

This parameter indicates the total rut length made by the rear wheel of a tractor that is pulling an implement. It is calculated with the equation:

$$RL = 20 / WW \quad (1)$$

where RL = Total rut length (km ha^{-1}); WW = working width of the implement
Traffic intensity (TI) [8]

$$TI = (10 / WW) WL \quad (2)$$

where: TI = Traffic Intensity ($\text{t km}^{-1} \text{ ha}^{-1}$); WW = Working width of implement (m); WL = Wheel Load (t).

Mechanisation Degree (MD) [9]

Amount of energy applied in the field

$$MD = EP \cdot FT \quad (3)$$

where: MD = mechanization degree (kWh ha^{-1}); EP = engine power (kW); FT = field time (h ha^{-1}).

Field Load Index (FLI) [10]

This formula provides the overall field loading:

$$FLI = W \cdot T \quad (4)$$

where: FLI = Field load index ($t\ h\ ha^{-1}$); W = weight of tractor plus implement (t); T = time of vehicle in the field ($h\ ha^{-1}$).

Soil Stress

Terranimo[®] were used to estimate different soil stresses using FRIDA model and Sohne function [11–13] for every equipment configuration using the data of every machine and soil measured in the test as input. The model returns the Mean Soil Stress every 10 cm soil layer.

Working capacity was calculated using the following formula [14].

Real Working capacity (RWC):

$$RWC = EWC \cdot Kr \quad (5)$$

where EWC = Effective working capacity ($Ha\ h^{-1}$); Kr = real use coefficient.

Effective Working capacity:

$$EWC = (EWW \cdot EWS)/10 \quad (6)$$

where EWW = Effective working width (m); EWS = Effective working speed ($km\ h^{-1}$)

Effective working width was calculated measuring field width and number of passages, for every piece of equipment.

Effective working speed was calculated with average of speed in field test, excluding headland and not working phase.

Real use coefficient Kr :

$$Kr = ET/OT \quad (7)$$

where ET = Effective time (s) as time needed to travel field length using the EWS; OT = Operating time (s), as sum of all working time: effective time, turning time and refueling/reloading time. Turning time and reloading time were measured using the position data, available thanks to GPS RTK system, as for the traffic patterns analysis.

Fuel consumption was measured with tractor telemetry system. Carbon dioxide emission due to the work of the internal combustion engine was estimated considering 1 kg diesel fuel as 2.6 $kgCO_2e$ [15].

Table 4 Traffic indices on tillage with cultivator

	Rut length (RL) (Frese, 1969)	Traffic intensity (TI) (Eriksson et al., 1974;	Mechanization Degree (MD)(Perdok and Van de Werken, 1983)	Field Load Index (FLI) (Kuipers, 1986)
	km ha ⁻¹	t km ⁻¹ ha ⁻¹	kWh ha ⁻¹	t h ha ⁻¹
RT	4.39	44.17	67.28	4.91
RW	3.97	30.64	57.08	4.07
CT	4.43	24.70	36.83	4.58

Table 5 Traffic indices on tillage during seedbed preparation

	Rut length (RL) (Frese, 1969)	Traffic intensity (TI)(Eriksson et al., 1974;	Mechanization Degree (MD)(Perdok and Van de Werken, 1983)	Field Load Index (FLI) (Kuipers, 1986)
	km ha ⁻¹	t km ⁻¹ ha ⁻¹	kWh ha ⁻¹	t h ha ⁻¹
RT	3.23	21.08	31.43	2.76
RW	3.80	15.75	22.63	1.91
CT	4.44	18.39	21.94	2.03

3.2 Field Traffic Indices

The Rut length (RL) [7] index shows important differences in seedbed preparation with a lower value in RT, due to the use of a wider implement. Traffic intensity (TI) [8] is higher in RT in comparison to CT in cultivation and RW in seedbed preparation due to the use of a heavier tracked tractor. Mechanization Degree (MD) [9] gives evidence of the power difference between systems, with a higher value in RT resulting in higher working capacity due to faster working speed and wider implements. Higher working capacity decreases the difference between scenarios on Field Load Index (FLI) [10] because a heavier machine stay in the field for less time. The CT system has low MD because only a 90 kW tractor was used with a cultivator. Efficient use of power was achieved by avoiding tillage on the tramline with power demand decreasing and maintaining working capacity (Tables 4, 5 and 6).

Table 6 Traffic pattern of all field operation until tomato BBCH 61

Tomato row	0	1	1	0	1	1	0	1	1	0	1	0	1	1	0	1	0	1	0	1	0	1	1	0	1	0
Sum distance	0	52.5	97.5	150	203	248	300	353	398	450	503	548	600	652	698	750	803	848	900							
Point number	1	2	3	4	5	6	7	8	9	10	11	12	13	14	15	16	17	18	19							
RT	1	1	0	6	1	1	5	0	1	1	1	1	18	0	1	6	11	0	4							
RT	2	3	2	1	5	2	0	6	1	0	0	1	2	2	0	5	1	2	2							
RT	3	1	1	10	4	1	2	13	1	0	2	1	8	5	0	6	2	0	1							
RW	1	5	0	5	20	5	2	4	11	6	5	1	0	8	4	2	0	0	2							
RW	2	2	4	5	6	0	2	8	2	6	0	12	6	10	0	15	3	3	0							
RW	3	2	0	1	9	2	2	7	0	5	9	2	15	6	6	7	14	1	3							
CT	1	0	0	0	8	0	0	8	0	0	0	6	18	0	0	17	0	0	0							
CT	2	0	0	0	8	0	0	8	1	0	0	0	20	0	0	12	15	0	0							
CT	3	0	0	0	20	0	0	20	6	0	0	0	8	0	0	8	0	0	0							

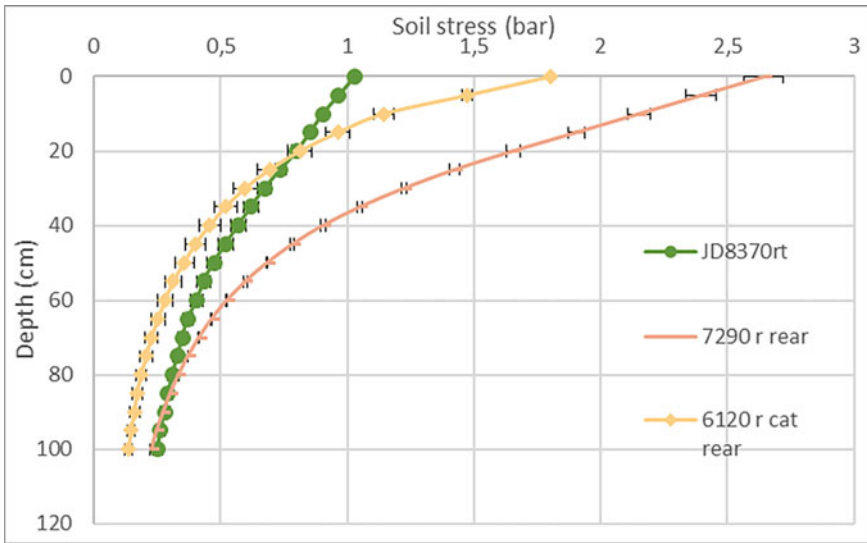


Fig. 1 Soil stress distribution on rear wheel calculated with Terranimo® considering equipment used in cultivation

Traffic pattern analysis shows clear differences between treatments, with a low number of traffic events spread on a different area in RW treatment, and a high number of traffic events in very small area in CT.

Soil stress confirms the CI and BD result with the same trend on tracked tractor with a low impact on the shallow layer and high impact on the deepest layer in comparison with other equipment. The narrow section, high pressure tire used in CT results in higher stress in shallow soil layers, but does not affect the crop zone due to traffic management (Fig. 1).

3.3 Working Capacity and Fuel Consumption

Table 7 shows RT had the highest working capacity in cultivation due to high power and tracked good maneuverability with linked implement. The high power tractor uses more fuel, but the high working capacity balances the hourly fuel consumption, resulting in low differences in fuel consumption per hectare between treatments.

Table 8 shows that the use of high tracked tractor with wide implement gains only a 25% increase in working capacity during seedbed preparation, with a 53% higher hourly fuel consumption. CT has lower fuel consumption and CO₂ emission during tillage probably due to the higher traction efficiency on a tramline.

Table 7 Working capacity, fuel consumption and CO₂ emission on tillage with cultivator

	Real working capacity	Hourly fuel consumption	Hectare fuel consumption	CO ₂ emission	CO ₂ emission
	ha h ⁻¹	l h ⁻¹	l ha ⁻¹	kg h ⁻¹	kg ha ⁻¹
RT	4.10	44.80	10.93	96.68	23.58
RW	3.79	51.03	13.47	110.12	29.06
CT	2.43	23.01	9.47	49.66	20.44

Table 8 Working capacity, fuel consumption and CO₂ emission on tillage during seedbed preparation

	Real working capacity	Hourly fuel consumption	Hectare fuel consumption	CO ₂ emission	CO ₂ emission
	ha h ⁻¹	l h ⁻¹	l ha ⁻¹	kg h ⁻¹	kg ha ⁻¹
RT	5.42	41.08	7.18	88.66	15.49
RW	4.34	25.64	5.88	55.33	12.70
CT	4.09	22.09	5.41	47.67	11.67

4 Conclusions

The test proves the benefits of CT in cultivation and seedbed preparation, especially on fuel consumption and CO₂ emission. The magnitude of benefits was limited on soil compaction by the efficiency of CT and the favorable conditions during the test that allowed good soil compaction management with random traffic treatment. Further study is suggested to complete the knowledge on resilience of soil compaction management system.

References

1. Batey, T.: Soil compaction and soil management - a review. *Soil Use Manage* (2009)
2. Soane, B.D., Van Ouwerkerk, C.: Soil compaction in crop production (1994)
3. Keller, T., Sandin, M., Colombi, T., Horn, R., Or, D.: Historical increase in agricultural machinery weights enhanced soil stress levels and adversely affected soil functioning. *Soil Tillage Res.* **194**, 104293 (2019)
4. Alaoui, A., Diserens, E.: Mapping soil compaction – a review. *Current Opin. Environ. Sci. Health* (2018)
5. McPhee, J.E., Antille, D.L., Tullberg, J.N., Doyle, R.B., Boersma, M.: Managing soil compaction – a choice of low-mass autonomous vehicles or controlled traffic?. *Biosyst. Eng.* (2020)
6. Antille, D.L., et al.: Review: soil compaction and controlled traffic farming in arable and grass cropping systems. *Agron. Res.* **17**(3), 653–682 (2019)
7. Frese, H.: Aktuelle Probleme der Bodenbearbeitung. *Present. Probl. soil tillage*). *Arch. Dtsch. Landwirtschafts Gesellschaft*, vol. 44, pp. 53–73 (1969)

8. Eriksson, J., Håkansson, I., Danfors, B.: The effect of soil compaction on soil structure and crop yields. Swedish Institute of Agricultural Engineering, Bull, no. 354 (1974)
9. Perdok, U.D., Van de Werken, G.: Power and labour requirements in soil tillage—a theoretical approach. *Soil Tillage Res.* **3**(1), 3–25 (1983)
10. Kuipers, H.: Soil compaction in arable farming (1986)
11. Schjønning, P., et al.: Driver-Pressure-State-Impact-Response (DPSIR) analysis and risk assessment for soil compaction—a european perspective. *Adv. Agron.* **133**, 183–237 (2015)
12. Schjønning, P., Lamandé, M., Tøgersen, F.A., Arvidsson, J., Keller, T.: Modelling effects of tyre inflation pressure on the stress distribution near the soil-tyre interface. *Biosyst. Eng.* **99**(1), 119–133 (2008)
13. Söhne, W.: Druckverteilung im Boden und Bodenformung unter Schleppereiffen. *Grundlagen der Landtechnik* **5**, 49–63 (1953)
14. Bodria, L., Pellizzi, G., Piccarolo, P.: *Meccanica e meccanizzazione agricola*. Edagricole New Business Media (2018)
15. Mantoam, E.J., Angnes, G., Mekonnen, M.M., Romanelli, T.L.: Energy, carbon and water footprints on agricultural machinery. *Biosyst. Eng.* **198**, 304–322 (2020)

Statistical Control of the Quality of Decaners Used for the Continuous Virgin Olive Oil Extraction



Biagio Bianchi, Michele Dassisti, Michela Orsino, Alessandro Bianchi, and Claudio Perone

Abstract It was set up a study of a diagnostic program by means of specific Quality Control Charts. The quality control was carried out on 14 AMENDUNI REX-250 two-phase decaners, according to ISO 20816-1: 2016 standards. The machines were studied at rotational speeds 3,000 rpm, 2,900 rpm, and 2,800 rpm. The tested decaners provided the best performance in terms of process controller-ship at 3,000 rpm. The machines that reported significant anomalies at the maximum number of revolutions were those balanced on lower rotation speeds which is usual in the extraction of virgin oil. It was possible to identify the most stressed sections of the machines at all speeds; these were the closest to the engine and on the left side of the basin (the side where the machine is set in rotation by the branch of the belt transmission). The possible causes of the anomalies are: unbalanced bowl, incorrect assembly of the bearings and, more rarely, defects and damages in the raceways, balls or rollers. The process carried out by the manufacturing company was adequately monitored, in accordance with current technical standards. On the top of the regulations, the statistical quality control of the balancing process shows to be free to the non-natural variability according to one of the criteria and seems that no further improvement to the process are needed. However, the control chart tool provides an efficient breakdown of the current state of quality of the process. Eventually, other criteria may be explored to fully determine the degree of control on the explored process.

Keywords Two-phase Decanter · Virgin Olive Oil Extraction · Rotation Speed

B. Bianchi · C. Perone

Department of Agricultural and Environmental Science (DISAAT), University of Bari Aldo Moro, Via Amendola 165/A, 70126 Bari, Italy

M. Dassisti · A. Bianchi

Department of Mechanics, Mathematics and Management, Polytechnic University of Bari, Via Orabona 4, 70125 Bari, Italy

M. Orsino (✉)

Department of Agricultural, Environmental and Food Sciences, University of Molise, Via Francesco De Sanctis, 86100 Campobasso, Italy
e-mail: m.orsino2@studenti.unimol.it

1 Introduction

The extraction process represents a crucial operation for the quality of extra virgin olive oil and has an important role in the energy efficiency of the mill. To this aim, continuous evolution in processing technology has been made to optimize every single phase of the process [1].

Control charts are tools used in statistics to monitor whether a KPI (Key Performance Indicator) of a process is under control. These tools are based primarily on the data collection and the subsequent analysis of samples. The analysis of the sample or samples allows to obtain useful information, for the sake of making considerations on the stability of the process that leads to those products and that, in some cases, could generate others [2, 3].

Currently, the most used control charts are: 1) P chart (defective fraction); 2) PN chart (number of defective shares); 3) C chart (number of defects); 4) U chart (number of defects per unit); 5) \bar{x} - R chart (mean value and range of variation); 6) \bar{x} chart (observed value); 7) Single measures chart [2]. Depending on the object of the check, two types of charts can be used: those related to “variables” and those to “attributes”. The control charts for variables are suitable for continuous series [4]. Both the control charts share the reference to some values (upper limit, lower limit, and average) used to compare with the value assumed by the variable examined, at the end of each process cycle or at a specific time. The central value is represented by the average value assumed by the monitored variable [5, 6]. The comparison between the value assumed by the variable examined, with the average value, allows to be aware of the degree of dispersion. The closer the values are to the average the greater the stability. Another element to control is the pattern drawn by the value, which should not be more than 3 points above average [7].

The purpose of this research was the inspection of a two-phase decanter for continuous virgin olive oil extraction measuring the vibrations, varying the rotation speed, and setting up a study for the realization of a diagnostic and prognostic program, using specific statistical control.

2 Materials and Methods

Experimental tests of quality control were carried out in an equipped area of the Amenduni S.p.A. workshop, Modugno (Ba), Via delle Mimose n. 3, on n. 14 REX-250: two-phase decanters with an operating capacity of 30.0–80.0 q/h and installed power of 45 kW, in compliance with ISO 20816-1: 2016 standard and ISO 1940: 2007.

In the first phase, the mechanical vibrations induced by the rotating parts at different rotation speeds were measured. A vibrometer-analyzer-balancer N.402 (nr. 1165-1999.01), of CEMB S.p.A. was used. This tool can to measure vibrations with a frequency from 1.5 to 8,000 Hz (from 90 to 480,000 cycles/min), with the following

measurement options: peak-to-peak, the maximum excursion of the wave (maximum stress, mechanical play); peak, the maximum positive or negative vibration excursion (short duration shocks); RMS (Root Mean Square = mean effective value), the most significant measure of amplitude, as it takes into account the history of the wave over time and gives an amplitude value directly related to the energy content of the vibration. The measurements were carried out with no load running and vibrations were measured in n. 6 positions of the frame: the 4 corners and the middle points. The rotation speeds of the rotating parts tested were: 2,800 rpm, 2,900 rpm, and 3,000 rpm, which are the most common in the extraction of virgin olive oil industrial production [8–10].

Once the measurement operation was completed, a comparison was made. The chart chosen that best represents the case study was the “single measures” because the sample size used to monitor the process was equal to 1; thus, each control chart was built by reporting the vibration measurements on each tested machine and for each rotation speed [4]. This operation consisted in writing n. 3 charts for each rotation speed (2,800–2,900–3,000 rpm) in each measuring position (Fig. 1): A (maximum distance from the right side engine), F (maximum distance from the left side engine), B (medium distance from the right side engine), E (medium distance from the left side engine), C (minimum distance from the right side engine), D (minimum distance from the left side engine).

For the drawing up of the chart, the “moving range” (MR_i) was calculated. It is defined as the absolute value of the difference between two successive observations ($X_{i+1} - X_i$):

$$MR_i = |X_{i+1} - X_i| \tag{1}$$

\bar{X} (Sample average) and \overline{MR} (moving range average) were calculated afterwards:

$$\bar{X} = \frac{\sum_{i=1}^n x_i}{n} \tag{2}$$

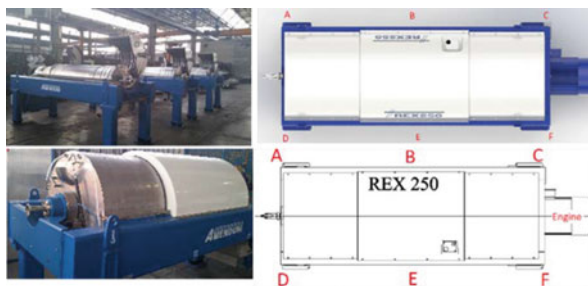


Fig. 1 Equipped area with tested decaners and frame’s positions scheme related to the vibrometer during the vibration tests within different rotation speeds.

$$\overline{MR} = \frac{\sum_{i=1}^{n-1} MR_i}{n - 1} \tag{3}$$

Eventually, both upper and lower control limits were calculated: Upper Control Line (*UCL*), Low Control Line (*LCL*), Center Line (*CL*):

$$UCL = B \overline{MR} = 3,267 \overline{MR}; \quad CL = \overline{MR}; \quad LCL = C \overline{MR} = 0 \tag{4}$$

3 Results and Discussion

In compliance with ISO 20816-1: 2016 and UNI ISO 1940: 2007 standards, the rotating groups of the tested machines are subjected to a vibration level (Tables 1, 2, and 3) that can be classified as: GOOD, up to 1.4 mm/s RMS; PERMISSIBLE, from 1.4 to 2.8 mm/s RMS; TOLERABLE, from 2.8 to 4.5 mm/s RMS. In depth, values above the threshold were highlighted (Tables 1, 2, and 3) but just for some specific machines with peculiar rotation speed. The study and the data processing related to the control charts allowed to analyze the machines on a qualitative level different from the simple compliance with the technical regulations in force.

Figures 2, 3, and 4 show the moving range of the vibration variations detected on the machines in the different positions, respectively 3,000 rpm, 2,900 rpm, and

Table 1 Results of the vibrometer’s test: position A (left), position F (right).

Sample	RMS (mm/s) at 2800 rpm	RMS (mm/s) at 2900 rpm	RMS (mm/s) at 3000 rpm	Sample	RMS (mm/s) at 2800 rpm	RMS (mm/s) at 2900 rpm	RMS (mm/s) at 3000 rpm
1	4.550	3.250	2.300	1	5.120	3.500	3.100
2	6.500	4.660	4.000	2	6.300	4.310	3.100
3	5.000	3.100	2.530	3	5.300	4.150	3.450
4	1.000	1.000	1.000	4	2.580	1.300	1.840
5	5.700	4.440	4.000	5	4.300	3.100	2.800
6	5.240	4.250	3.750	6	4.050	2.900	2.380
7	2.600	1.800	1.900	7	2.400	2.500	2.300
8	11.000	7.800	1.000	8	12.400	7.610	1.000
9	5.900	5.800	4.920	9	6.830	4.800	4.830
10	7.680	3.860	3.000	10	7.700	4.900	2.850
11	4.000	2.400	2.100	11	3.600	2.750	2.400
12	6.500	4.500	3.300	12	5.500	3.300	2.100
13	4.200	2.900	3.000	13	5.200	3.800	2.800
14	3.500	2.400	2.300	14	1.700	2.100	2.000

Table 2 Results of the vibrometer’s test: position B (left), position E (right)

Sample	RMS (mm/s) at 2800 rpm	RMS (mm/s) at 2900 rpm	RMS (mm/s) at 3000 rpm	Sample	RMS (mm/s) at 2800 rpm	RMS (mm/s) at 2900 rpm	RMS (mm/s) at 3000 rpm
1	2.400	2.180	2.140	1	1.530	1.540	1.590
2	2.970	2.520	2.650	2	1.600	1.520	2.000
3	1.600	1.400	1.870	3	1.260	1.520	1.840
4	1.030	1.000	1.400	4	1.040	1.150	1.340
5	2.100	2.600	3.000	5	2.000	2.000	2.400
6	1.700	1.600	1.600	6	1.700	1.720	1.980
7	1.450	1.700	2.000	7	1.600	1.510	1.700
8	1.000	1.000	1.000	8	1.000	1.000	1.000
9	4.250	4.900	4.460	9	4.400	3.900	4.300
10	1.600	1.000	1.700	10	2.500	1.400	1.580
11	1.240	1.100	1.000	11	1.100	1.000	1.100
12	3.200	2.500	2.800	12	2.300	2.200	2.700
13	2.700	2.000	2.200	13	2.100	1.700	1.700
14	1.100	0.900	0.700	14	1.600	1.700	1.400

Table 3 Results of the vibrometer’s test: position C (left), position D (right).

Sample	RMS (mm/s) at 2800 rpm	RMS (mm/s) at 2900 rpm	RMS (mm/s) at 3000 rpm	Sample	RMS (mm/s) at 2800 rpm	RMS (mm/s) at 2900 rpm	RMS (mm/s) at 3000 rpm
1	2.400	2.180	2.140	1	3.760	2.440	1.800
2	3.600	2.400	2.100	2	4,600	3,640	3,240
3	3.500	1.700	1.200	3	4.000	2.600	2.080
4	3.500	2.700	2.000	4	1.430	1.000	1.100
5	1.270	1.000	1.300	5	2.500	1.700	1.900
6	2.200	0.700	0.800	6	2.600	1.940	2.060
7	3.100	2.000	1.900	7	2.140	1.630	1.800
8	2.130	1.850	2.000	8	10.200	1.000	1.000
9	10.600	1.320	1.000	9	5.700	5.700	5.920
10	5.920	5.120	5.800	10	4.800	1.500	1.350
11	5.470	2.450	1.840	11	2.500	1.100	1.000
12	2.400	1.300	1.000	12	3.400	2.000	2.200
13	2.600	1.500	1.500	13	2.700	1.600	15.000
14	1.000	0.400	0.800	14	1.200	0.900	0.700

2,800 rpm. The variations of the vibrations are fluctuating but within the limits of control; thus, a uniform trend common to almost all machines can be identified. The rotation speed at which the tested decanters provided the best performance, in terms of control of the process, is 3,000 rpm. This value is the highest speed used by this type of machine for virgin olive oil extraction. Therefore, at the mentioned rotation speed, all moving ranges are within or in the proximity of the control limits; thus, the statistical trend of the vibration's variations is close to the central value for all the measured positions (Fig. 2A–B–C–D–E–F). Moreover, the upper control limits (UCL) are lower than the other rotation speeds for all the positions (Fig. 3 and 4) and only the samples n. 9 and n. 10 exceeded UCL limits (Fig. 2A–B–C–D–E–F).

On the other hand, all the other samples show a trend closer to the central value (Fig. 2). Around 2,900 rpm (Fig. 3), a trend similar to 3,000 rpm (Fig. 2) is highlighted. At this rotation speed, the more distant samples are still n. 9 and n. 10, whereas

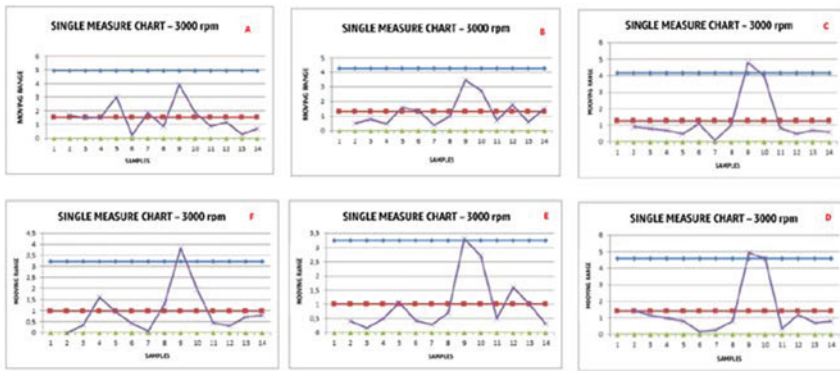


Fig. 2 Moving range of the vibrations detected on the machines in the different positions at 3,000 rpm.

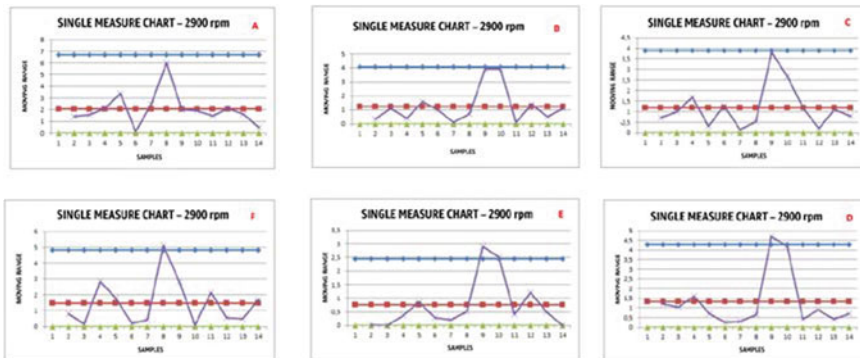


Fig. 3 Moving range of the vibrations detected on the machines in the different positions at 2,900 rpm

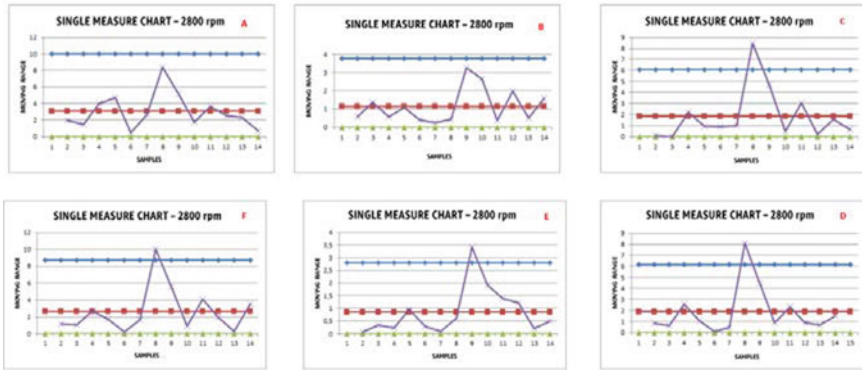


Fig. 4 Moving range of the vibrations detected on the machines in the different positions at 2,800 rpm.

sample 8 shows a significantly high value, close to the UCL in positions close to the engine (Fig. 3F), which is not at 3,000 rpm. Around 2,800 rpm (Fig. 4), a trend similar to 3,000 rpm and 2,900 rpm (Fig. 2 and 3) is highlighted. The highest discrepancies, at this rotation speed, are reported with samples 8 and 9, while sample n.10 does not show as high discrepancies as in the other rotation speeds. Moreover, differently from the other speeds tested, sample n. 8 showed high-level values in almost all the evaluated positions, including the ones far from the engine (Fig. 2C–D–E–F).

At all speeds, the most stressed parts are identified. These are the positions closest to the engine (Fig. 1 and Fig. 2, 3 and 4C, D) and on the left side of the frame (Fig. 1 and Fig. 2, 3 and 4D, F). In fact, the left side of the frame is rotated by the slack slides of the drive belts: the tight slide stretches due to the tractive load applied by the drive shaft and on the slack slides a lower load acts generating a lower torque. This situation is balanced by the elastic deformation of the belt which converts part of the resulting torque as vibration.

The values showing significant anomalies in the vibrations are n. 8, n. 9, and n. 10 (Tables 1, 2, and 3). These affect both the previous and following values of the moving range, this is why samples n. 8, 9, and 10 are on average the most out of the limits (Fig. 2, 3, and 4). The results obtained could be due to the fact that these samples were balanced at lower rotation speeds, which are frequently registered in the extraction of virgin oil to avoid the risk of overheating of the paste [10–12]; indeed, they have excellent performance at 2,600 rpm (Table 4). In general, the most common causes that determine higher vibrations are linked to a wrong balancing of the bowl due to errors during the assembly phase: for example, bolts not fastened enough, assembly of caps, plates, or straws heavier than the pre-fixed one (at a maximum of 2 g) or mounted at different heights different from those tolerated (17/18 mm). Another cause of misalignment could be due to bearings assembly (in particular main bearings), generating dangerous gap inside the machinery.

Table 4 Vibrations (mm/s) at lower rotation speeds for samples n. 8–9–10.

Position	2,600 rpm	2,700 rpm
A	1,000	10,900
B	1,000	1,000
C	1,000	6,700
D	1,000	8,000
E	1,000	1,000
F	1,000	8,870

In rare and exceptional cases, defects and damages may be found in the proximity of the rolling bearing, balls, or rollers. Other factors causing vibration peaks are the drive narrow cogged banded V-belts: they ensure silence and high power transmission performance, without slipping or breaking; on the contrary, these belts, even if not presenting assembly and construction defects, can lead to problems due to the not uniform elasticity. Indeed, as in the previous extent, too high or poor tractive load drives residual vibrations and high transmission noise, due to the misalignment of the pulleys, which could wear out and get damaged in the long run. Eventually, other causes could be the length of the belt, insufficient pressure on the cogs during idle operation, and insufficient lubrication.

Another aspect not to be underestimated is the decoupling between the bowl and the screw, which can also happen, at critical speeds, when the machine is in its stopping phase. In this case, fluctuations may occur other than those expected at the design stage. These vibrations are due to the different speeds of the two moving components, which have different stopping times, but these generally tend to disappear after a short phase. An imbalance due exclusively to the auger can be caused by errors in design, assembly, and connection to the gearbox [13].

The frame is made in external workshops and can be characterized by micro-cracks or cracks happening in the welding phase. Another aspect not to be overlooked is the flooring where the frame rests; in the tested models, the frame is equipped with wheels and is not fixed to the floor; therefore, it can be more affected by any irregularities.

With the consideration made on the anomalous machines and the possible causes for that, the same control charts have been re-calculated excluding samples 8, 9, and 10. The results show no values over the control limits.

4 Conclusions

Based on the study and the presented results, it is possible to conclude that the production process carried out is in the first stage of process control and aligned with the technical regulations in force.

As discussed, control charts are in all the cases in control according to one of the criteria used to determine whether a process is or is not “in control” meaning free from the non-casual variability [14]. For the next step, there are other criteria to

verify the full absence of not natural variability [14]; checking all of that, helps to understand if there are any patterns that, once analyzed, can lead to full control of the process.

Once highlighted the pattern, the process itself would be reviewed and in some cases, if possible, modified or re-engineered. Having full control is useful for the manufacturer to redirect the target of the KPI needed; e.g. reducing the percentage of machines discarded or re-equilibrated and deciding whether or not retargeting his quality delivers, up to specific quality values. Using other charts as well, it may be possible to predict the behavior of the machine over time and increase its “Expected useful life”. This tool, properly managed, would be a solution to any breakdown that during the olive oil season generates critical shortage costs and can compromise the turnover of a full year in an oil mill. This is a logical first step that regards a phase of “diagnosis” of the trend; the continuation of the study must be oriented towards a predictive maintenance program, developing a prognosis phase. At a company level, the proposed solution could be an added value in the context of the maintenance service offered to customers.

Acknowledgements Research carried out within the project: European Union—Next Generation EU—funding from Ministry for University and Research Decree 737/2021—research project “ECONomia circolare, Sostenibilità e profili di evoluzione Normativa nella produzione dell’Olio extravergine Di Oliva (ECOSNODO)” with Unique Project Code H91I21001700006.

References

1. Tamborrino, A., Servili, M., Leone, A., Romaniello, R., Perone, C., Veneziani, G.: Partial de-stoning of olive paste to increase olive oil quality, yield, and sustainability of the olive oil extraction process. *Eur. J. Lipid Sci. Technol.* **122**(11), 2000129 (2020)
2. Vadde, K.K., Syrotiuk, V.R., Montgomery, D.C.: Optimizing protocol interaction using response surface methodology. *IEEE Trans. Mob. Comput.* **5**(6), 627–639 (2006)
3. Dassisti, M.: HY-CHANGE: a hybrid methodology for continuous performance improvement of manufacturing processes. *Int. J. Prod. Res.* **48**(15), 4397–4422 (2010). <https://doi.org/10.1080/00207540801901840>
4. Benneyan, J.C.: Use and interpretation of statistical quality control charts. *Int. J. Qual. Health Care* **10**(1), 79–63 (1998)
5. Abbasia, A.R., Mahmoudi, M.R.: Application of statistical control charts to discriminate transformer winding defects. *Electric Power Syst. Res.* **191**, 106890, 1–11 (2021)
6. Dassisti, M., Jardim-Goncalves, R., Molina, A., Noran, O., Panetto, H., Zdravković, M.M.: Sustainability and interoperability: two facets of the same gold medal. In: OTM Confederated International Conferences “On the Move to Meaningful Internet Systems”, pp. 250–261. Springer, Heidelberg, September 2013. https://doi.org/10.1007/978-3-642-41033-8_33
7. Ali, S., Siegel, H.J., Maheswaran, M., Hensgen, D., Ali, S.: Representing task and machine heterogeneities for heterogeneous computing systems. *J. Appl. Sci. Eng.* **3**(3), 195–207 (2000)
8. Bianchi, B., Tamborrino, A., Santoro, F.: Assessment of the energy and separation efficiency of the decanter centrifuge with regulation capability of oil water ring in the industrial process line using a continuous method. *J. Agric. Eng.* **XLIV**(s1), e56, 278–282 (2013). [https://doi.org/10.4081/jae.2013.\(s1\):e56](https://doi.org/10.4081/jae.2013.(s1):e56)

9. Tamborrino, A., Leone, A., Romaniello, R., Catalano, P., Bianchi, B.: Comparative experiments to assess the performance of an innovative horizontal centrifuge working in a continuous olive oil plant. *Biosys. Eng.* **129**, 160–168 (2015). <https://doi.org/10.1016/j.biosystemseng.2014.10.005>
10. Tamborrino, A., Squeo, G., Leone, A., Paradiso, V., Romaniello, R., Summo, C., Pasqualone, A., Bianchi, B., Caponio, F.: Industrial trials on coadjutants in olive oil extraction process: effect on rheological properties, energy consumption, oil yield and olive oil characteristics. *J. Food Eng.* **205**, 34–46 (2017). <https://doi.org/10.1016/j.jfoodeng.2017.02.019>
11. Caponio, F., Squeo, G., Brunetti, L., Pasqualone, A., Summo, C., Paradiso, V.M., Catalano, P., Bianchi, B.: Influence of the feed pipe position of an industrial scale two-phase decanter on extraction efficiency and chemical-sensory characteristics of virgin olive oil. *J. Sci. Food Agric.* **98**, 4279–4286 (2018). <https://doi.org/10.1002/jsfa.8950>
12. Tamborrino, A., Perone, C., Catalano, F., Squeo, G., Caponio, F., Bianchi, B.: Modelling energy consumption and energy-saving in high-quality olive oil decanter centrifuge: numerical study and experimental validation. *Energies* **12**, 2592, 1–20 (2019). <https://doi.org/10.3390/en12132592>
13. Perone, C., Bianchi, B., Catalano, F., Orsino, M.: Experimental evaluation of functional and energy performance of pneumatic oenological presses for high quality white wines. *Sustainability* **14**, 8033, 1–13 (2022). <https://doi.org/10.3390/su14138033>
14. Montgomery, D.C.: *Introduction to Statistical Quality Control*, 7th edn. Wiley, New York (2012)

Spray Swath Study in Relation to Canopy Deposition During UAV Spray Applications in Vineyards



Alessandro Biglia , Marco Grella , Lorenzo Comba ,
Alessandro Sopegno , Leandro Eloi Alcatrão ,
Davide Ricauda Aimonino , and Paolo Gay 

Abstract Unmanned aerial vehicles (UAVs) have been rising interest for spray applications in 3D crops such as vineyards. When dealing with UAV broadcast spray applications, the preliminary study of the spray swath is a key factor. Indeed, an optimised fly path planned considering proper spray swath overlaps allows maximising the canopy spray deposition, avoiding under- or over-spray situations, and minimising off-target spray losses.

This paper presents the correlation between the spray swath, filters upholstered on polystyrene cubes and the canopy deposition during UAV spray applications in a vineyard. Three arrays of Petri dishes (140 mm diameter) and iron poles (0.8 m height), used to host cubes of 50 mm edge that were upholstered by filter papers (90 g m⁻² density), were set up outside the vine rows, while deposition in the canopy was measured using filter papers at three heights and depths per plant. Moreover, six configurations were tested based on the combination of different UAV flight modes (1way and 2way broadcast), nozzle type (conventional and air inclusion 110°, 03 and 015 size), and UAV cruise speeds (1 and 3 m s⁻¹).

Swath deposition and filters deposition on the cubes had a good correlation with the canopy deposition as the linear fitting curves had an R-square higher than 0.8. Also, the obtained spray swath allowed to optimise the UAV flight path planning, obtaining a distance between flight centerlines of 1.5 m.

Keywords Spray application · Aerial drones · Swath · Precision agriculture · Ground losses

A. Biglia (✉) · M. Grella · L. Comba · A. Sopegno · L. Eloi Alcatrão · D. Ricauda Aimonino · P. Gay
Department of Agricultural, Forest and Food Sciences (DiSAFA), Università degli Studi di Torino, Largo Paolo Braccini 2, 10095 Grugliasco, TO, Italy
e-mail: alessandro.biglia@unito.it

© The Author(s), under exclusive license to Springer Nature Switzerland AG 2023
V. Ferro et al. (eds.), *AIIA 2022: Biosystems Engineering Towards the Green Deal*,
Lecture Notes in Civil Engineering 337,
https://doi.org/10.1007/978-3-031-30329-6_35

345

1 Introduction

Pesticide applications in vineyards using conventional equipment such as airblast sprayers or knapsack sprayers are often featured by high amounts of agrochemicals losses in the atmosphere and on the ground, which originate severe environmental pollution [1]. The losses can account up to more than 90% of the applied volume at vine early growth stages and can still represent more than 50% at full growth stages [2]. The frequency of treatments, even higher than 15–20 per year in EU areas, together with the number of diseases and pests to control (e.g., downy mildew, powdery mildew, botrytis, moths, and other insects) imply the use of a relevant number of pesticides. As the EU path within Green Deal and Farm to Fork strategies is to drastically reduce pesticide consumption in the EU, at least by 50% by 2030, there is a need to improve spray application efficiency, while keeping adequate biological efficacy of treatments. To reach this goal, innovative pesticide application techniques and/or decision-making models have to be explored according to the different crop needs [3]. In vineyards, for example, one option may be represented using unmanned aerial vehicles (UAVs) for pesticide applications, which can offer several advantages in terms of timeliness of treatments, use of very low water volumes, no greenhouse gases emissions, and minimisation of operators' exposure to agrochemicals [4]. UAV-spray systems have been spreading on the market since several years and currently used at large scale especially in the Americas and in many Asian countries including China and India, working mainly on arable crops [5] but also on some arboreal crops [6]. Nevertheless, few studies are available concerning UAV-spray systems in vineyards [7, 8]. In Italy, spray applications from UAVs are forbidden according to article n. 13 of legislative decree n. 150/2012 but experiments aimed at the use of drones, also in consideration of the EU Parliament, which recognises the potential linked to the use of intelligent technology and precision agriculture to better manage plant protection products (PPPs) will be considered in the new national action plan for the sustainable use of PPPs [9].

Even if aerial treatments are currently discouraged in the EU due to their potential environmental impact, they represent the only alternative to hand-held sprayers in hilly areas where vineyards are featured by severe slope. Moreover, UAVs can fly very close to the canopy (< 1 m) keeping straight routes precisely planned, containing spray drift and dispersion risks. The point is to design and customise the spray system mounted on a UAV or several UAVs [10, 11], and to define the optimal operating parameters such as UAV cruise speed, flight altitude, spraying path (band or broadcast), spray quality, applied liquid volume (pressure, nozzles type), thus achieving a quality of spray distribution on the target able to ensure the biological efficacy of treatments. This latter aspect is strictly related to the selection of the most appropriate types and formulations of pesticides enabling to protect vineyards from pests and diseases when using UAV-spray systems, which usually apply ultra-low volumes. In this respect, the assessment of the plant protection products for vineyards more suitable to be sprayed using UAVs among those currently available on the market is mandatory.

This paper presents the correlation between the spray swath and the canopy deposition during UAV spray applications in a vineyard. In particular, six configurations were tested based on the combination of different UAV flight modes (1 way and 2way broadcast), nozzle type (conventional 110°, 03 and 015 size), and UAV cruise speeds (1 and 3 m s⁻¹).

2 Materials and methods

2.1 UAV-Spray System

The UAV used in the experimental campaign was a hexacopter DJI Matrice 600 Pro. The drone was equipped with a customised sprayer system of 2.8 kg and a RTK antenna connected to a ground station for navigation. The sprayer system consists of a 5 L polyethylene tank, two diaphragm pumps assembled in parallel and powered by an auxiliary battery (1800 mAh), two nozzle holders, one pressure regulator and one analogic pressure gauge (0–6 bar). The pressure was manually set before each flight, and a remote controller was used to turn the pumps on and off during the flights. The two nozzle holders were installed on two UAV arms at 910 mm from each other. Also, the nozzle holders were oriented straight-down at 175 mm from the rotor plane, and at 110 mm from the propeller axis [12].

2.2 Experimental Design

Six configurations were tested according to different operating conditions, which are two UAV flight modes, two nozzle types, and two UAV cruise speeds. Specifically, the UAV flew across the vine rows in one-way flights (named 1-way broadcast) or in round-trip flights on the same route (named 2-way broadcast). The UgCS software (SPH Engineering) was used to plan UAV flights and to automatically rotate the UAV nose to guarantee the nozzle holders being perpendicular to the flight direction, thus maximising the spray swath. Also, UgCS allows the flight altitude to be kept constant at 3 m above the ground in the trials. The selected ASJ nozzles were conventional and air inclusion flat fan nozzles with a spray angle of 110°, and a 03 (blue colour, ISO 2018 [7]) or 015 (green colour, ISO 2018 [7]) size in case of the 1-way or 2-way broadcast application. Different nozzle sizes were used to keep the spray application rate constant among the trials. Finally, the UAV cruise speeds were 1 and 3 m s⁻¹. Since, the spray pressure was fixed at 3 bar, the liquid flow rate was 1.2 or 2.4 L min⁻¹ according to the nozzle sizes, 015 and 03 respectively. Considering the UAV cruise speeds, the flow rate ranged between 133 and 400 μL per cm of UAV travelled space.

2.3 *Experimental Layout*

One experimental plot was set up next to the vineyard in a free-crop surface characterised by short grass to collect the spray deposition at ground level [13], and at 0.8 m above the ground (light blue areas named R1, R2 and R3 in Fig. 1). In every blue area shown in Fig. 1c, an array of 13 Petri dishes having a 140 mm diameter (collection surface of 153.86 cm²) and of 7 iron poles of 0.8 m height was arranged perpendicular to the UAV flight path, Petri dishes were located at 0.3 m distant from each other, and at 1 m from the iron poles. The distance between blue areas was 5 m. All Petri dishes were fixed on wooden boards to withstand the UAV-generated air flux. Regarding the spray deposition measurements at 0.8 m height above the ground, a polystyrene cube having an edge of 50 mm was stuck on the top of each pole [13]. The cube faces were upholstered with filter papers characterised by a density of 90 g m⁻², and a total collection surface equal to 125 cm². The above-described experimental layout was replicated three times as shown in Fig. 1. The UAV take-off point was set at 20 m before the first array, and the vineyard was also at 20 m from the last array. A second experimental plot was set up in the vineyard. In particular, measurements of spray deposition in the canopy were performed using filter paper discs (120 mm diameter, 90 g m⁻² density) at three locations, and at three heights and depths per vine canopy [7]. In order to correlate the spray swath, cubes, and the canopy deposition, two additional sampling points in the canopy were located at ± 1.6 m apart to UAV flight path (centre line) for each replicate using the same type of collectors (filter papers).

A Stonex S900A GNSS receiver was used to perfectly align the two experimental plots and the UAV take off point. A weather station was used to monitor and record (0.1 Hz) environmental conditions during the trials. It was equipped with a sonic anemometer at a 4 m height to measure wind speed and direction, and two thermohygrometer probes at 2 and 4 m heights to measure air temperature and relative humidity. The experiments were done in a vertical shoot position trellised vineyard (cv. Barbera) at growth stage BBCH 89 “Berries ripe for harvest” located in our facilities (Turin, Italy). The grapevines were spaced at 2.5 m and 0.8 m between and within rows respectively, thus resulting in a density of about 5,000 vines per hectare. A solution of water and E-102 tartrazine yellow dye tracer (85% w/w) was used in the UAV-spray system to evaluate spray deposits on the collectors. The collectors were then washed with deionised water to extract the tracer, and the washing solution analysed with a UV-1600PC VWR spectrophotometer as described in [7].

2.4 *Statistical and Data Analysis*

The correlation between the spray swath and the canopy deposition was evaluated using the Pearson coefficient and a linear interpolation in the SPSS software environment. Before the analysis, values were standardised (z-score) and the values $> |3|$

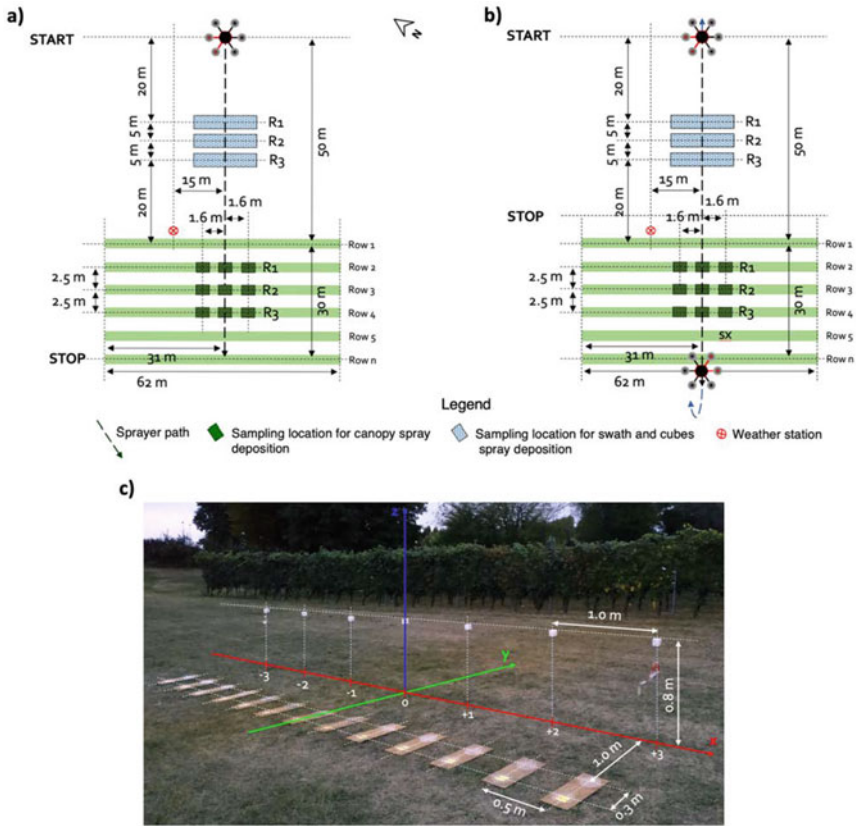


Fig. 1 Schematic of the experimental layout with the adopted UAV flight modes: a) one-way across the row (1-way broadcast), b) round-trip across the row (2-way broadcast), and, c) view of the experimental plot for swath evaluation

were excluded as considered to be outliers. We averaged the Petri dishes and cubes deposition values by grouping them into 3 classes according to their relative position with respect to the central one (UAV flight path).

3 Results and Discussion

The correlation between the deposition on the Petri dishes positioned on the ground (spray swath) outside the vineyard, and the one on the filters upholstered on the polystyrene cubes at 0.8 m height, with the canopy deposition is presented in this section.

Based on 468, 252, and 864 valid samples, collected on the Petri dishes, filters (cubes), and filters on the canopy respectively, the average deposition values in μL

per cm^2 were reported in Figs. 2 and 3. Different colours in Figs. 2 and 3 refer to different UAV-spray system configurations. Specifically, thesis T1 and T3-T5 (conventional and air inclusion at 1 m s^{-1} , and conventional and air inclusion at 3 m s^{-1} respectively) refer to 1-way broadcast applications while thesis T2 and T6-T8 refer to 2-way broadcast applications (conventional and air inclusion at 1 m s^{-1} , and conventional and air inclusion at 3 m s^{-1} respectively).

Figures 2 and 3 report the correlation between canopy deposition and swath deposition, and canopy deposition and cubes deposition respectively. It can be observed

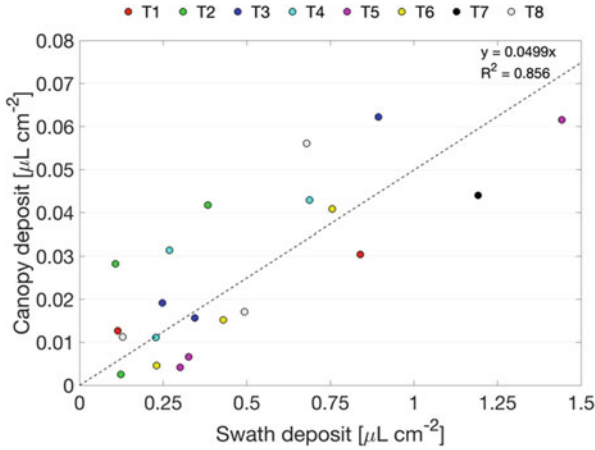


Fig. 2 Correlation between canopy and swath deposition. Colours refer to different UAV-spray system configurations

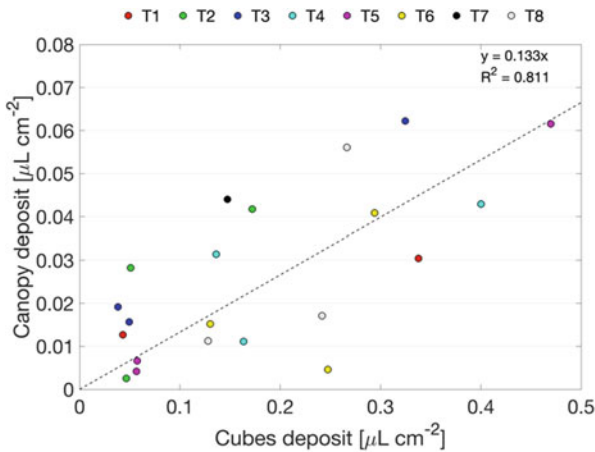


Fig. 3 Correlation between canopy and cubes deposition. Colours refer to different UAV-spray system configurations

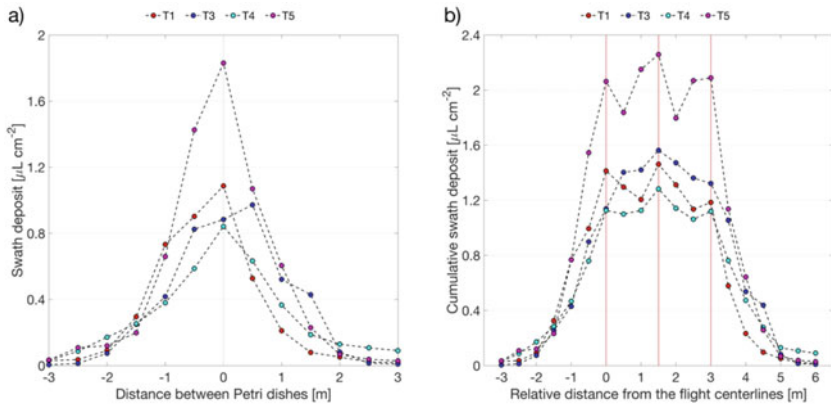


Fig. 4 Swath deposition for 1-way broadcast applications in a) and Cumulative swath deposition in b) with red lines representing the distance between hypothetical flight centerlines

that the fitting line has a good R-square value (0.856) in Fig. 2, while the one in Fig. 3 is slightly lower and equal to 0.811. This could be due to a lower number of samples collected in the case of the filters upholstered on the polystyrene cubes. Moreover, the Pearson coefficient resulted to be equal to 0.783 between canopy deposition and swath deposition and equal to 0.698 in case of canopy deposition and cubes deposition.

The results reported in Figs. 2 and 3, and the Pearson coefficients show a positive correlation with respect to the canopy deposition and swath and cubes. This means that the data collected outside the vineyard could provide us a preliminary indication about the canopy deposition. The idea of using the filters upholstered on the polystyrene cubes at 0.8 m height is because of their 3D shape which should better reflect the crop shape. Considering the 1-way broadcast application, Fig. 4a shows swath profiles, while Fig. 4b reports the cumulative swath profiles. It can be observed in Fig. 4b that a hypothetical flight centerline of 1.5 m, lower than the interrow distance, was obtained to have a good spray swath superposition. However, such a flight centerline depends on the nozzle type, flight altitude and flight speed.

4 Conclusions

The experimental campaigns were performed in a vineyard at full growth using a six-rotor UAV equipped with a customised spray application system; they allowed the correlation between canopy deposition and spray swath to be obtained. From the experimental results, it can be concluded that: (i) the swath deposition and the cube deposition have a positive correlation with the canopy deposition (> 0.65), and (ii) the distance between flight centerlines is 1.5 m, which is lower than the vineyard interrow.

Funding This research was partially funded by the Italian Ministry of University and Research (MUR), PRIN 2017 project “New technical and operative solutions for the use of drones in Agriculture 4.0” (Prot. 2017S559BB), and PRIN 2020 project “*DATA-BUS - Digital Agriculture Technology to Achieve data to Build User-friendly Sustainability indicators*” (Prot. 2020SCNF4L).

Declaration of Competing Interest The authors declare that they have no known competing financial interests or personal relationships that could have appeared to influence the work reported in this paper.

References

1. Grella, M., Marucco, P., Balsari, P.: Toward a new method to classify the airblast sprayers according to their potential drift reduction: comparison of direct and new indirect measurement methods. *Pest Manag. Sci.* **75**, 2219–2235 (2019)
2. Grella, M., Marucco, P., Zwertvaegher, I., Gioelli, F., Bozzer, C., Biglia, A., et al.: The effect of fan setting, air-conveyor orientation and nozzle configuration on airblast sprayer efficiency: Insights relevant to trellised vineyards. *Crop Prot.* **155**, 105921 (2022). <https://doi.org/10.1016/j.cropro.2022.105921>
3. Fedele, G., González-Domínguez, E., Delière, L., Díez-Navajas, A.M., Rossi, V.: Consideration of latent infections improves the prediction of Botrytis bunch rot severity in vineyards. *Plant Dis.* **104**, 1291–1297 (2020)
4. Wang, G., Han, Y., Li, X., Andaloro, J., Chen, P., Hoffmann, W.C., et al.: Field evaluation of spray drift and environmental impact using an agricultural unmanned aerial vehicle (UAV) sprayer. *Sci. Total Environ.* **737**, 139793 (2020)
5. Cavalaris, C., Karamoutis, C., Markinos, A.: Efficacy of cotton harvest aids applications with unmanned aerial vehicles (UAV) and ground-based field sprayers – a case study comparison. *Smart Agric. Technol.* **2**, 100047 (2022)
6. Meng, Y., Su, J., Song, J., Chen, W.H., Lan, Y.: Experimental evaluation of UAV spraying for peach trees of different shapes: effects of operational parameters on droplet distribution. *Comput. Electron. Agric.* **170**, 105282 (2020)
7. Biglia, A., Grella, M., Bloise, N., Comba, L., Mozzanini, E., Sopegno, A., et al.: UAV-spray application in vineyards: flight modes and spray system adjustment effects on canopy deposit, coverage, and off-target losses. *Sci. Total Environ.* **845**, 157292 (2022). <https://doi.org/10.1016/j.scitotenv.2022.157292>
8. Sarri, D., Martelloni, L., Rimediotti, M., Lisci, R., Lombardo, S., Vieri, M.: Testing a multi-rotor unmanned aerial vehicle for spray application in high slope terraced vineyard. *J. Agric. Eng.* **50**, 38–47 (2019)
9. <https://www.politicheagricole.it/flex/cm/pages/ServeBLOB.php/L/IT/IDPagina/14282>
10. Mammarella, M., Comba, L., Biglia, A., Dabbene, F., Gay, P.: Cooperation of unmanned systems for agricultural applications: a theoretical framework. *Biosys. Eng.* **223**, 61–80 (2022). <https://doi.org/10.1016/j.biosystemseng.2021.11.008>
11. Mammarella, M., Comba, L., Biglia, A., Dabbene, F., Gay, P.: Cooperation of unmanned systems for agricultural applications: a case study in a vineyard. *Biosys. Eng.* **223**, 81–102 (2022). <https://doi.org/10.1016/j.biosystemseng.2021.12.010>
12. Bloise, N., Carreño Ruiz, M., D’Ambrosio, D., Guglieri, G.: Wind tunnel testing of remotely piloted aircraft systems for precision crop-spraying applications. In: *IEEE International Workshop on Metrology for Agriculture and Forestry*, pp. 378–383 (2021)
13. International Organisation for Standardisation (ISO): ISO/DIS 23117-1. *Agricultural and forestry machinery—Unmanned aerial spraying systems—Part 1: Environmental requirements*

Digital Technologies for the Sustainable Management of the Olive Orchards in Central Italy: The Farmers' Perception



Marcello Biocca, Pietro Gallo, Stefano Canali, and Elena Testani

Abstract Digital agriculture offers a range of technologies to be implemented at different scales and for a multitude of objectives, supporting farmers and other key actors in decision making. In the olive oil production, which is at present mainly carried out implementing business as usual non-digital solutions, the growing availability and accessibility of specific digital technologies enable wide opportunities. This paper aims at investigating how much current and future advances in the so-called digital agriculture is known and perceived by the olive growers. A specific survey was conducted by means of a questionnaire divided into four main sections: (1) exploring the knowing of digital solutions and applicability; (2) actual use; (3) perception and ambitions in the field; (3) farm and farmer profiling. The questionnaire was responded by 96 farmers of Central Italy (Latium region). The results of the survey showed several aspects of the penetration and perception of the potential of digital agriculture in olive oil production. Among others, the interest of olive farmers in innovative digital technologies resulted high (average score of 4.3 out of 5). Anyway, most of the respondents did not show an exhaustive knowledge of the proposed technologies and only few of them already adopted some digital solutions in their own farm (11.4%). The sustainability of the implementation of the questioned innovation technologies is finally discussed.

Keywords Digital Agriculture · Innovative Technologies · Olive Oil · Precision Farming

M. Biocca (✉) · P. Gallo

CREA - Consiglio per la ricerca in agricoltura e l'analisi dell'economia agraria, Centro di ricerca Ingegneria e Trasformazioni Agroalimentari, Via della Pascolare, 16, 00015 Monterotondo (Rome), Italy
e-mail: marcello.biocca@crea.gov.it

S. Canali · E. Testani

CREA - Consiglio per la ricerca in agricoltura e l'analisi dell'economia agraria, Centro di ricerca Agricoltura e Ambiente, Via della Navicella, 2/4, 00184 Rome, Italy

1 Introduction

Latium (Central Italy) contributes about 4–5% to the national production of olive oil, with about 127,000 tons of olive harvested in 2021. In terms of surface, olive predominates among the woody crops with about 78,000 hectares, followed by the hazelnut and vineyards [1]. About 81% of the cultivation takes place in the hills, 15% in the inland mountains and only 4% in lowland land. The regional production of olive oil has recorded a progressive reduction in the overall yield over the last 15 years, going from 25,000 tons in 2006 to about 13,000 tons in 2020 [1]. The factors of the decline are many and are equally reflected in surveys on national production that indicate as main drivers the incidence of pathologies and pests and of the climate change effects. Olive growing in Latium is present above all in inland areas where there are small and medium-sized farms and is characterized by the predominant use of family work.

In this context digital innovation represents, according to FAO [2], a great opportunity. Through digitalization, all parts of the agri-food production chain should be modified, allowing for more efficient work, greater economic return, increased environmental benefits, and better working conditions in the field [3]. In recent years, advances in the fields of electronics, ICT (Information and Communication Technology) and satellite detection have made available reliable, robust and low-cost technologies [4] that include: (1) geographic positioning via satellite network (GPS, GLONASS, GNSS) and geographic information (GIS); (2) machines capable of implementing assisted/semi-automatic/automatic driving [5]; (3) the acquisition of specific data through multiple sensors (optoelectronic such as RGB, multispectral, thermal cameras, and humidity, temperature sensors, etc.) [6] which, depending on the carrier that transports them, can be remote (satellite or airborne) or proximal [7]; (4) operating machines capable of dosing the production factors on the basis of the above information (variable rate machines - VRT) and equipped with standardized information transmission systems (ISOBUS) [8]; (5) robots [9]; (6) systems of production traceability (infotracing) such as protocols based on the blockchain (Quadhash), RFID systems, or labels with QR-code [10]; (7) software with DSS (Decision Support Systems).

Understating the perception and the acceptance of these new technologies among actors of the production chain is the first step in their implementation [11, 12].

The aim of this work was specifically investigating how much current and future advances in the so-called digital agriculture is known and perceived by the olive growers.

2 Material and Methods

Data were collected using an ad-hoc questionnaire. The questionnaire structure was previously discussed in a focus group including olive growers, extension service technicians and the authors of the paper. Four main sections were identified, to explore: (1) knowing of digital solutions and applicability; (2) actual use; (3) perception and ambitions in the field; (3) farm and farmer profiles. A draft version of the questionnaire was formulated and then submitted to the focus group and to five additional selected researchers for validation. The questionnaire was reviewed and finalized according to their comments, resulting in 26 items (Table 1). The questionnaire was a close-ended structured instrument containing both objective contents and attitudinal/opinion questions (subjective content), multiple-choice questions and one open question. To gather the olive growers' opinions a five-point Likert scale was applied. The questionnaire was disseminated through the site www.agroambientelazio.it, which provides various technical assistance services to registered olive growers from Latium region. A small number of questionnaires were compiled during live interviews. Data collected were explored using descriptive statistics.

3 Results

The survey was answered by 96 olive growers who expressed satisfaction in the initiative with about 83% of responses that found the proposed questionnaire "interesting". The respondents were mainly men (94.8%) over the age of 51 (67%), with Diploma (36%) or Degree (35%), coming from all the provinces of Latium (57 municipalities), with a slight prevalence of the province of Rome (37%). As regards the production methods, about 39.6% adopted the organic, biodynamic regime or were in conversion, while 57.2% adopted conventional production; of the latter, about 25% adopted the voluntary integrated system.

The most frequent production address was the mixed olive-fruit one (around 40% of cases) while 33 farms (34.3%) claimed to be specialized in olive growing. The 43.8% of respondents had farms of 1 to 5 ha, 21.9% over 10 ha. The average altitude of the farms was around 266 m a.s.l.

On-farm direct transformation of the olives was carried out in about 28% of the cases.

The direct sales system in the company turned out to be the most common.

The most adopted harvesting system was that using pneumatic or electric facilitators (79%), only 2 farms use trunk shakers.



Most of the respondents (53%) access to the Internet through their personal computer, 36% through smartphones and 6% using a tablet; 4 respondents stated that they do not access the Internet or someone does it for them.

Table 1 List of the questionnaire questions

Question	Answer's options
1. What is the total size of your farm in hectares?	
2. What is your farm's average altitude above sea level (in meters)	
3. What production method do you use?	(1) Conventional (2) Integrated voluntary (3) In conversion to organic (4) Organic (5) Biodynamic (6) Mixed (7) Other
4. What is your production address?	(1) Specialized olive farm (2) Mixed olive + fruit (3) Mixed olive + herbaceous crops (4) Mixed olive + vegetables (5) Mixed olive + animal production (6) Mixed (7) Other:
5. In case of a mixed production address, indicate the area in hectares of the olive grove	(1) Less than 1 (2) from 1 to 5 (3) from 6 to 10 (4) from 11 to 30 (5) More than 30
6. Your farm produces (multiple choice allowed)	(1) Olive for oil (2) Table olives (3) DOP
7. Does your farm directly transform the entire production (or most of the production)?	(1) Yes (2) No
8. In case of on-farm direct transformation, what do you produce?	(1) Oil (farm oil mill) (2) Table olives (3) Both (4) Other
9. What are your farms's sales channels (multiple answers possible)	(1) Direct sales in the farm (2) Online selling (3) Buying groups (4) Sale to fruit and vegetable markets (5) Sale to large retailers (6) Wholesale (7) Other
10. How do you carry out the olive harvest?	(1) Manual (2) Hand-held equipment (3) Trunk shakers (4) Mixed
11. To browse the Internet, you mainly use	(1) Personal computer (2) Tablet (3) Smartphone (4) I do not browse the Internet or another person does it for me
12. Do you know or have you ever heard of these technologies for the management of fertilization and irrigation?	(1) Prescription maps from satellite or drone remote sensing for fertilization and irrigation management (2) Sensors for detecting soil moisture (3) Expert IT systems (SSD) for the management of treatments or fertilization (4) Meteorological shed with automatic data transmission (5) Software (dedicated programs) for fertilization management (6) Web platforms for consulting forecast models for planning irrigation needs, nutritional needs and plant health

(continued)

Table 1 (continued)

Question	Answer's options
<p>13. Do you know what is the object in the photo?</p> 	<p>(1) A trap for the mass capture of the olive fly (2) A trap that sends images of olive flies captured via cellular network (3) I do not know</p>
<p>14. Do you know or have you ever heard of these technologies for monitoring diseases and pests?</p>	<p>(1) Automatic insect traps (e.g. olive fly) (i.e. with remote control) (2) Websites with access to phytopathological bulletins (4) Expert IT systems (DSS) for the management of treatments (4) Biomolecular methods for the diagnosis of diseases (4) Other</p>
<p>15. For the management of soil and plants on the farm, do you know or have you ever heard of:</p>	<p>(1) Monitoring of plant health conditions through drone surveys (2) Portable optical instruments for determining the ripeness of olives (3) Variable rate sprayers and spreaders (4) Tractors with GPS and automatic driving (5) Spot spraying systems for weeds</p>
<p>16. Do you know what the object indicated by the arrow and mounted on the tractor cab is?</p> 	<p>(1) The tractor GPS antenna (2) The automatic driving system (3) The cabin air conditioning filter (4) I do not know</p>
<p>17. To facilitate the management of your business, do you know or have you ever heard of:</p>	<p>(1) Software (dedicated programs) for business accounting or management of the farm logbook (2) RFID systems for product traceability (3) Applications for product traceability using blockchain storage protocols (Quadhash) (4) Ultrasonic malaxing tanks (5) Expert IT systems for the assessment of environmental, economic and social sustainability</p>
<p>18. If you use one or more digital technologies in your company, can you indicate which one (s)?</p>	<p>Free text</p>
<p>19. Are you satisfied with the technology (s) you indicated in the previous question?</p>	<p>1 to 5 scale</p>

(continued)

Table 1 (continued)

Question	Answer's options
20. In case you don't use digital technologies in your company, can you state the reasons?	(1) I don't know of digital technologies that could be useful to me (2) I don't know how to access available digital technologies (3) The digital technologies available are all too expensive (4) Digital technologies are too complex and require special high-level training (5) I don't know, I don't want to answer
21. Do you think that digital technologies can help or can be a disadvantage in solving problems in the context of:	1 to 5 scale for: (1) Soil management, fertilization, irrigation (2) Management of crop protection (3) Support for the management of operations in the field (4) Business management support (5) Access to technical updates, funds, information exchange and networking with other producers/actors (6) Access to local market information (7) Relationship with the customer
22. Do you have any ideas about new technologies that you would like to be developed in relation to improving some aspects of your farm?	(1) No, I have no idea about it (2) No, I've never thought about it (3) Yes, my idea is the following
23. Your age	
24. Your gender	
25. Your educational qualification	
26. Thank you for participating in the questionnaire! Did you appreciate it?	(1) Interesting (2) Too long (3) Of little interest (4) Other

Pictures were proposed showing respectively the antenna of a GPS system mounted on the cab of a tractor and an automatic trap for the olive fly; about half of the respondents did not recognize the image or did not respond.

Only 11 farms claimed to use some technologies in their own farm. The perception was that the available solutions are too expensive (28%), uselessness in other 28% of cases, too much complexity/need for special high-level training and difficulties in accessing the digital technologies available (20%), the remaining did not answer.

In another question, space was left for the suggestion of ideas on technologies to be introduced, but 79.1% claimed that they never thought about it or had no ideas.

Respondents were asked to answer if they knew or had ever heard of specific technologies. For the management of fertilization and irrigation (question n. 12, Table 1) it turned out that nearly a third did not respond, 18% claimed to know all the six typologies, while around 21% said to know at least one. Sensors for the detection of humidity and the meteorological stations were the best-known technologies.

Regarding the knowledge of crop protection technologies (question n. 14, Table 1), only 9 respondents did not know any of the technologies, 42% knew at least one and 11% knew them all. The best-known technology turned out to be the website for the phytopathological bulletin.

In the field of technologies for the management of soil and plants in the farm (question n. 15, Table 1), nearly 30% of the respondents did not know any technology, while about 9% knew all of them. The best-known technology was the monitoring of plant health conditions through drone surveys (48%).

For business management (question n. 17, Table 1), almost a third of the respondents did not know any of the proposed technology while being all known only by 6%. The most cited technology was that of software for business accounting or the management of the farm logbook.

An opinion was requested to be expressed with a score from 1 to 5 on the usefulness of digital technologies in solving problems related to different management areas and value chain scales (question n. 21, Table 1). In this case, the digital technologies indicated as being of “great help” were those for points (1) Soil management, fertilization, irrigation; (2) Management of crop protection and (5) Access to technical updates, funds, information exchange and networking with other producers/actors, and of “helpful” (median score of 4) the other technologies.

4 Discussion and Conclusions

This paper gave insights on the factors influencing the diffusion and perceptions of digital technology in oliviculture.

In general, the questionnaire intercepted a number of producers representative of the different production methods in the Latium region, with a slight prevalence of organic farming compared to the national average.

Almost all the interviewees access the web, mainly using a personal computer. Olive growers seem very interested in innovative digital technologies. They indiscriminately attribute high approval scores to the various questions asking whether technologies can provide them with concrete help in solving problems. However, most of the sample did not show a good knowledge of the proposed technological systems and very few of them already adopt some digital technology in their farms. Furthermore, a large part of the sample showed a certain difficulty in approaching new technologies because they are perceived too expensive or difficult to use. It is indicative that one of the best-known technologies has turned out to be the issue of phytopathological bulletins on websites. In fact, most of the questionnaires were disseminated through the site agroambientelazio.it, which provides this service.

Another well-known technology was the monitoring of plant health conditions through drone surveys. This is likely due to the fact that a number of companies are now offering and massively advertising services based on drone surveys.

This paper has some limitations needing acknowledgment. We carried out the study in one Italian region, therefore results could be context-specific and may not be completely applicable in other areas with varied cultural milieus. However, some general considerations can be drawn. A weak point of our oliviculture is the delay in the implementation of technological innovations and in the application of the results

of scientific research. The average age of olive growers and other intrinsic characteristics of the agricultural system also fuel the existence of the so-called “digital divide” which makes it difficult to introduce digital technologies. With regard to the latter, it should be noted that both the 4G (and 5G) coverage, that is the mobile infrastructure that allows an adequate connection speed, and the various fixed connection technologies, cover a portion of the territory mainly limited to inhabited centers, while large rural areas do not have got coverage. Though, even a socio-technological system resistant to change is generally not completely uniform: innovation niches may appear, which tend to create a “space” partially isolated from the normal functioning of the system. These niches of innovation, operating with different rules, allow the affirmation of (micro) economic networks capable of supporting innovations, in the technical and/or organizational field, constituting the condensation nuclei for initiating transitions (the so-called areas of break-out). To facilitate the transition processes, these niches must form a structure capable of overcoming the endogenous resistance effects of the current socio-technological system and the process underlying the affirmation of an innovation niche requires a minimum level of coordination between the different actors. involved in the value generation chain.

References

1. ISTAT – Istituto Nazionale di Statistica. <http://dati.istat.it/Index.aspx?QueryId=33706>. Accessed 13 July 2022
2. FAO - Food and Agriculture Organization. Digital Agriculture. <http://www.fao.org/digitalagriculture/en/>. Accessed 13 July 2022
3. Shepherd, M., Turner, J.A., Small, B., Wheeler, D.: Priorities for science to overcome hurdles thwarting the full promise of the ‘digital agriculture’ revolution. *J. Sci. Food Agric.* **100**(14), 5083–5092 (2020)
4. Pallottino, F., Biocca, M., Nardi, P., Figorilli, S., Menesatti, P., Costa, C.: Science mapping approach to analyze the research evolution on precision agriculture: world, EU and Italian situation. *Precis. Agric.* **19**, 1011–1026 (2018)
5. Scarfone, A., Picchio, R., del Giudice, A., Latterini, F., Mattei, P., Santangelo, E., Assirelli, A.: Semi-automatic guidance vs. manual guidance in agriculture: a comparison of work performance in wheat sowing. *Electronics* **10**, 825 (2021). <https://doi.org/10.3390/electronics10070825>
6. Cisternas, I., Velásquez, I., Caro, A., Rodríguez, A.: Systematic literature review of implementations of precision agriculture. *Comput. Electron. Agric.* **176**, 105626 (2020)
7. Brambilla, M., Romano, E., Toscano, P., Cutini, M., Biocca, M., Ferré, C., Comolli, R., Bisaglia, C.: From conventional to precision fertilization: a case study on the transition for a small-medium farm. *AgriEngineering* **3**, 438–446 (2021)
8. Thomasson, J.A., Baillie, C.P., Antille, D.L., McCarthy, C.L., Lobsey, C.R.A.: Review of the state of the art in agricultural automation. Part II: on-farm agricultural communications and connectivity. In 2018 ASABE Annual International Meeting, p. 1. American Society of Agricultural and Biological Engineers (2018)
9. Biocca, M., et al.: Rovitis 4.0: an autonomous robot for spraying in vineyards. In: Biocca, M., et al. (eds.) *Safety, Health and Welfare in Agriculture and Agro-Food Systems*. SHWA 2020. Lecture Notes in Civil Engineering, vol. 252, pp. 176–185. Springer, Cham (2022). https://doi.org/10.1007/978-3-030-98092-4_19

10. Antonucci, F., Figorilli, S., Costa, C., Pallottino, F., Raso, L., Menesatti, P.: A review on blockchain applications in the agri-food sector. *J. Sci. Food Agric.* **99**(14), 6129–6138 (2019)
11. Pfeiffer, J., Gabriel, A., Gandorfer, M.: Understanding the public attitudinal acceptance of digital farming technologies: a nationwide survey in Germany. *Agric. Hum. Values* **38**(1), 107–128 (2021). <https://doi.org/10.1007/s10460-020-10145-2>
12. Bolfe, É.L., et al.: Precision and digital agriculture: adoption of technologies and perception of Brazilian farmers. *Agriculture* **10**(12), 653 (2020). <https://doi.org/10.3390/agriculture10120653>

Work Time Study, Productivity and Costs of Felling Trees in Urban Areas



Marcello Biocca, Pietro Gallo, and Giulio Sperandio

Abstract Various factors affect the care and the management of urban trees and felling of trees in town requires specific technical competences. To remove trees, operators dismantle the plant utilizing either an aerial lift or ascending the crown with ropes, the so-called “tree-climbing”. The study aimed at: (1) investigating technical and economic features of felling; (2) evaluating the productivity, the costs and the sustainability of the observed yards; (3) assessing the potential residual biomass. The felling operations were analyzed with work time studies in 18 work sites (8 yards in tree-climbing and 10 yards with aerial lift), for a total observation time of 88.4 h. Starting from the fuel consumption data, emissions of CO₂ and energy consumption were also calculated. The total residual biomass resulted in average equal to 4.4 Mg per tree (min. 0.5; max. 15.0 Mg). Cost calculation for each yard considered the fixed and the variable costs and the costs for the labor force. This paper can contribute improving tree maintenance methods in urban sites and assessing the potential residual wood biomass attainable from urban trees.

Keywords Urban Forestry · Tree Maintenance · Residual Biomass · Tree Removal

1 Introduction

Urban trees are key elements of green infrastructure and provide urban dwellers with a variety of essential ecosystem services and benefits. Therefore, the maintenance of trees plays a decisive role in the development of strategies aimed at maintaining urban forestry and biodiversity to improve human health and well-being [1].

In urban environment, various factors that are often absent in natural ecosystems, affect the care and the management of trees: the presence of numerous botanical

M. Biocca (✉) · P. Gallo · G. Sperandio

CREA - Consiglio per la ricerca in agricoltura e l'analisi dell'economia agraria, Centro di ricerca Ingegneria e Trasformazioni Agroalimentari, Via della Pascolare, 16, 00015 Monterotondo (Rome), Italy
e-mail: marcello.biocca@crea.gov.it

species (native species, naturalized and non-natives), the interference with building, roads and other “grey” infrastructure, the role of residents, the trees’ property, etc.

Felling of trees in town requires specific technical competences, based on interdisciplinary principles, that face the particular aspects of urban environments [2].

In the last years, the occurrence of tree felling has increased in our cities due to various reasons: the adverse effects deriving from climate change [3], which undermine the static stability of plants and incite decline [4], the spread of new pests and pathogens [5], the mismanagement (especially road maintenance and management of underground facilities) [6], the presence of many trees that are now old or senescent and the intensive urbanization.

Urban tree removal entails dismantling the plant, i.e., to cut into pieces from top to bottom. Felling can be carried out either utilizing an aerial lift or ascending the crown with ropes, commonly named “tree-climbing” [7]. The choice of the employed method largely depends on the tree’s accessibility and safety measures [8, 9]. Tree-climbing is chosen when trees are in confined areas where machinery cannot enter. In urban forestry, tree-climbing is frequently the only possible solution to maintain trees.

Tree removal produces considerable amounts of woody residual biomass, which can be potentially utilized at local level as a resource for wood products and bio-based fuels for power and heat generation [10, 11]. Furthermore, due to the neutral cycle of CO₂ in the chain, biomass is considered a sustainable energy source. It is also worth noticing that the residuals reuse allows the tree owner to save the disposal charge usually paid.

The purposes of this study were: (1) investigating technical and economic features of urban tree felling, (2) evaluating the productivity, the costs and sustainability of the observed yards and (3) assessing the potential residual biomass.

2 Material and Methods

This study analyzed works carried out in 18 work sites (with a total of 27 trees observed). The operations were carried out either with aerial platforms (10 yards) or by tree-climbing (8 yards). Trunk diameters (at 1.3 m from soil) and heights of trees were measured by means of a tree diameter tape and by a laser rangefinder (mod. TruPulse 360R, Laser Technology Inc), respectively. The size of the crown was assessed by measuring its projection on the soil.

The yards showed differences in site accessibility and in the characteristics of the area surrounding the tree place. For this aspect, a qualitative variable named “site” specifies the work easiness, ranging from 1 (difficult) to 5 (easy) (for details see reference [8]). The distance of the trees from the loading point of residual biomass ranged from 1 m (full accessibility, with the possibility to place a truck for loading very close to the tree) to 30 m (the collected biomass must be manually transported

from the tree's position to the stacking point). Dendrometric and site characteristics are shown in Table 1 and 2.

Table 1 Main dendrometric and site characteristics of the yards managed with aerial lift

Yard code	Species	Tree height [m]	D.b.h. ^a [cm]	Crown diameter [m]	Observed plants [N.]	Distance ^b [m]	Site ^c
AA1	<i>Pinus pinea</i>	27	100	15	1	10	1
AA2	<i>Pinus pinea</i>	25	99	12	1	2	1
BUS	<i>Pinus pinea</i>	22	67	12	1	1	2
CA1	<i>Ulmus</i> sp.	15	20	6	2	1	3.5
FAN	<i>Pinus pinea</i>	20	65	10	3	5	4
FRT	<i>Cupressus arizonica</i>	15	49	5	5	1	5
ITA	<i>Pinus pinea</i>	19	71	11	3	1	2
LQR	<i>Cedrus deodara</i>	20	84	7	1	2	3
TSC	<i>Eucaliptus</i> sp.	16	70	5	1	10	3.5
VLS	<i>Pinus pinea</i>	23	70	16	1	2	3
Average		20	69	10	19^d	4	3

^aTrunk diameter at 1.3 from the ground; ^bDistance of the tree to the loading point of residual biomass; ^cSee explanation in the text. ^dThe value is the sum

Table 2 Main dendrometric and site characteristics of the yards managed in tree climbing

Yard code	Species	Tree height [m]	D.b.h. ^a [cm]	Crown diameter [m]	Observed plants [N.]	Distance ^b [m]	Site ^c
ANA	<i>Pinus pinea</i>	16	80	11	1	1	4
BSP	<i>Pinus pinea</i>	17	56	8	1	2	4
CLS	<i>Pinus pinea</i>	15	42	7	1	1	5
LEM	<i>Pinus pinea</i>	11	49	7	1	1	2
PIG	<i>Pinus pinea</i>	15	60	9	1	15	3
QRM	<i>Pinus pinea</i>	15	70	8	1	5	3
SMC	<i>Cupressus sempervirens</i>	12	37	3	1	2	5
TRF	<i>Laurus nobilis</i>	12	45	6	1	30	4
Average		14	55	7	8^d	7	4

^aTrunk diameter at 1.3 from the ground; ^bDistance of the tree to the loading point of residual biomass; ^cSee explanation in the text. ^dThe value is the sum

Work time study was based on the identification and the separation of five work phases: (1) “setting and stacking” (which includes distinct phases, occurring at the beginning and at the end of the work, such as, for example: i) preparation of the work site, setting the signage for a safety perimeter, approaching of the aerial lift to the tree, mounting of a friction for the operations in tree-climbing, time to wear personal protective equipment, dismounting or protecting objects under the tree; ii) transport of residual biomass to the loading point, site’s cleaning, packing up tools and instruments); (2) “cutting”, (time during the operator does not move in the crown and it operates the branches or trunk cut); (3) “shift” (movement of the operator inside or around the tree’s crown, by either using ropes or moving the platform); (4) “delay time for avoidable time losses”: (5) “delay time for unavoidable time losses” [12, 13].

In this study the time (and the cost) for loading and transportation of the obtained biomass was not considered. The time elements were recorded by the same researcher using centesimal stopwatches and video recording.

Eight private companies, formed by experienced professional arborists, carried out the operations.

The residual biomass was either assessed by measuring the volume of wood stacked at the collection point or by weighing the wood with a hanging electronic weighing scale (Laumas, mod. Dten. 500/1). The volume data were converted into the fresh weights according to conversion tables [14].

The evaluation of the operating costs of each work yard was carried out by means of an analytical method, considering the fixed, the variable and the labor costs [15].

The following values were provided for the analyses: (1) gross time, the total time of work carried out per each tree (h tree^{-1}); (2) biomass productivity, the fresh weight of residual biomass obtained hourly (Mg h^{-1}); and (3) cost per tree, the total cost of work per each tree (€ tree^{-1}). The calculation of CO_2 emissions and of energy consumption of every mechanized yard was based on the fuel consumption (for details see reference [10]).

To compare average values among treatments, an ANOVA (Analysis of Variance) parametric test was performed, after checking the distribution of the given variables. Not normally distributed variables (Shapiro–Wilk test, p -value <0.05) were normalized according to the results of a Box-Cox test procedure, which showed that the best technique of data normalization for the selected variables was logarithmic transformation. The software R [16] was employed for the statistical analysis.

3 Results

Yards were observed during tree removal operations for a total time of 88.4 h.

Work time phases of each yard are shown in Fig. 1. The variability among yards in terms of total work time was particularly evident, both in yards operating with an aerial platform (min 0.74 – max 8.08 h) and in tree-climbing (min 1.88 – max 6.75 h).

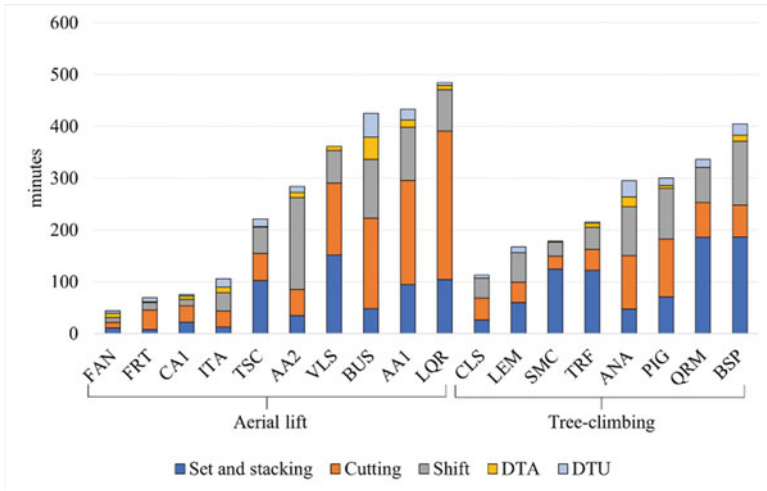


Fig. 1 Work time elements (in minutes) in yards carried out with aerial lift and tree-climbing

The average gross time of the two methods (Fig. 2) is comparable and not statistically different (Table 5), with a larger variability in yards operating with the aerial lift. Considering the single work elements (Fig. 2), in tree-climbing the time necessary for set the yard and stacking the residual biomass is longer than with an aerial lift, while the avoidable delay time is significantly greater with aerial lift (Table 5).

The gross time, the obtained biomass per tree, the productivity (biomass per hour) and the total costs per tree per each yard, are shown in Table 3 and 4.

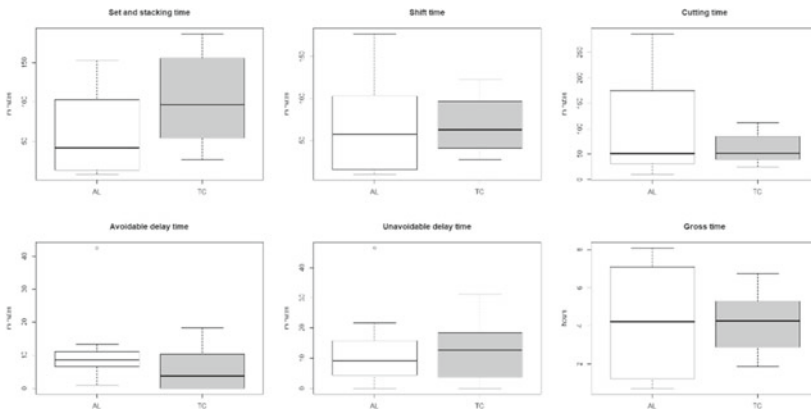


Fig. 2 Average times of the different work phases (in minutes) and of the gross time (in hours) in yards carried out with aerial lift (AL) and tree-climbing (TC) (treatments with the same letter are not significantly different ($p < 0.005$))

In general, the aerial lifts were preferred for bigger trees. In fact, dendrometric characteristics (Table 1) show that in the work sites operated with aerial lifts the trees showed an average height of 20.2 m and a d.b.h. of 0.694 m while trees worked in tree-climbing showed a height of 14.0 m and a d.b.h. of 0.549 m. Notably, only two trees (yard code AA1 and AA2) removed with aerial lift, contributed strongly to this difference.

Comparing the two methods, it is possible to note that they do not differ significantly in terms of productivity (Fig. 3 and Table 5), even if the average value of the biomass provided in yards with aerial lifts is greater.

As regards the total costs, it appears slightly higher in yards with aerial lifts (Fig. 3 and Table 5).

The yards carried out with the two methods differ for their environmental sustainability (Fig. 4) because the energy consumption and the CO₂ emissions are clearly higher in the yards with aerial lifts.

In terms of obtained biomass (Table 3), it was estimated that each removed tree provided an average of 4.4 Mg of biomass, with a large variability depending on size, species and physiological conditions (min 0.54; max 15 Mg per tree).

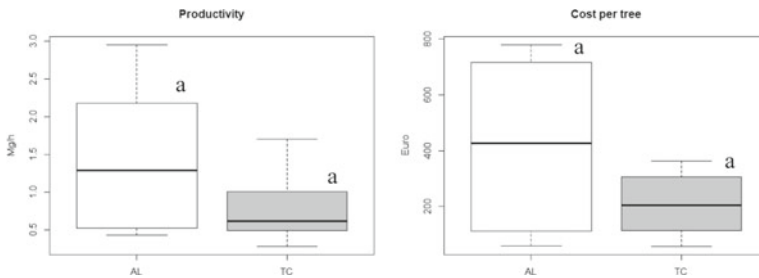


Fig. 3 Average productivity (Mg of biomass obtained per hour) and average total cost of observed yards (AL = aerial lift; TC = tree-climbing; treatments with the same letter are not significantly different ($p < 0.005$))

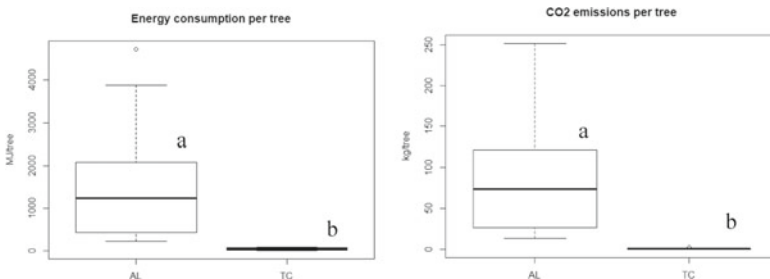


Fig. 4 Average energy consumptions (MJ per tree) and CO₂ emissions (Kg per tree) of observed yards (AL = aerial lift; TC = tree-climbing; treatments with the same letter are not significantly different ($p < 0.005$))

Table 3 Main parameters of the yards carried out with aerial lift

Yard code m.u.	Gross time h tree ⁻¹	Obtained biomass Mg tree ⁻¹	Productivity Mg h ⁻¹	Total cost € tree ⁻¹
AA1	7.2	15.0	2.1	779.9
AA2	4.7	14.0	3.0	745.9
BUS	7.1	5.4	0.8	546.6
CA1	1.3	0.5	0.4	138.8
FAN	0.7	1.6	2.2	58.0
FRT	1.2	2.0	1.7	84.2
ITA	1.8	4.2	2.4	110.9
LQR	8.1	4.2	0.5	715.0
TSC	3.7	1.6	0.4	347.8
VLS	6.0	5.1	0.8	503.6

Table 4 Main parameters of the yards carried out in tree-climbing

Yard code m.u.	Gross time h tree ⁻¹	Obtained biomass Mg tree ⁻¹	Productivity Mg h ⁻¹	Total cost € tree ⁻¹
ANA	4.9	4.2	0.9	219.0
BSP	6.8	4.0	0.6	271.9
CLS	1.9	0.8	0.4	66.6
LEM	2.8	1.6	0.6	161.5
PIG	5.0	1.4	0.3	341.3
QRM	5.6	3.6	0.6	363.3
SMC	3.0	5.1	1.7	56.1
TRF	3.6	4.2	1.2	192.0

Table 5 Results of ANOVA of the two methods (aerial lift and tree-climbing)

Variable	Degrees of freedom	<i>p</i> -values	Significance ⁽¹⁾
Set and stacking time	1	0.086	.
Shift time	1	0.44	
Cutting time	1	0.67	
Avoidable delay times	1	0.0359	*
Unavoidable delay times	1	0.888	
Gross time	1	0.521	
Productivity (hourly biomass per tree)	1	0.131	
Cost per tree	1	0.0963	.
Energy consumption per tree	1	< 0.0001	***
Emissions of CO ₂	1	< 0.0001	***

(1) Significance codes of *p*-values: 0 '***' 0.001 '**' 0.01 '*' 0.05 '.' 0.1 '.'

4 Discussion

In this paper yards for tree removal in urban areas were studied by means of time work analysis, which contribute to reveal technical and economic features of trees maintenance operations. In general, the observed yards showed a similar organization in terms of the sequence of the work phases and in the use of equipment, allowing to utilize the same time work elements for collecting the working time data and comparing the different methods employed.

Yards carried out in tree-climbing showed a longer phase of “setting and stacking” than with aerial lift. This is likely due to the time necessary to the operator for dressing the special personal protective equipment, the slings, etc. and to the time for launching the throwline (the first rope used to access the tree’s crown), that often requires several attempts to be successful. Furthermore, the distance between the tree and the loading point is greater in tree-climbing yards than in the aerial lift ones, increasing the total time of the “setting and stacking” phase. Tree climbing is, in fact, the favorite (and frequently the only possible) method to work in sites where the access to machines is not possible.

The tree-climbing yards showed a significant difference in terms of avoidable delay times, which were longer using an aerial lift. This is probably caused by the platform operator’s reduced view of the crown, that sometimes can lead to the aerial lift becoming stuck in the branches for a while. Moreover, to place the platform properly, the operator of the aerial lift spends more time briefing with the ground workers than the tree-climber, who tends to work more autonomously.

Depending on the method employed, the observed yards differed in terms of mechanization intensity. Therefore, the two methods clearly differ in terms of fuel consumption and in consequence of CO₂ emissions and energy consumption.

The difference in terms of total time needed to fell a tree was not statistically different between aerial lift and tree-climbing. Furthermore, in the observed yards, the cost of yards with aerial lifts was in average slightly higher than the ones in tree-climbing.

5 Conclusions

The choice between accessing the trees’ crown for their maintenance using an aerial lift or climbing with ropes, depends on several factors. For example, tree-climbing is often the best possibility in urban sites without access to aerial platforms, but it requires qualified and skilled personnel. At the same time, aerial lift is preferred when trees are not easily accessible by the climbers (i.e., hazardous trees with stability problems) and when plants are aligned in rows. Also, the cost of the two methods differs, but this aspect appears not generally applicable because of the high variability of total cost of each yard (especially among the yards of felling with aerial lift).

From an economic point of view, it was showed that the tree-climbing resulted less expensive because the method entails a low level of mechanization, even if this difference was not statistically significant. Furthermore, tree-climbing is clearly more sustainable from an environmental perspective because the emitted CO₂ and the energy consumption were markedly lower than the yards which employed an aerial lift.

As for the potential biomass available from urban trees, it is certainly an aspect to be deeply investigated and taken into greater consideration with respect to the current energy politics.

Acknowledgements This research was funded by the Italian Ministry of Agriculture (MiPAAF) under the AGROENER project (D.D. N. 26329, 1st April 2016) - <http://agroener.crea.gov.it/>. The authors are grateful to the following companies that carried out the works described in the paper: Ecologistica srl (Viterbo), Ecogeo srl (Roma), Ars Arborea sas (Guarda, TR), Il Giardino Malandrino srl (Roma), Verdeitalia srl (Roma), Garden Services srl (Roma), Floema Studio (Monterotondo, RM), Vivaio Talenti (Roma).





References

1. Escobedo, F.J., Kroeger, T., Wagner, J.E.: Urban forests and pollution mitigation: analysing ecosystem services and disservices. *Environ. Pollut.* **159**, 2078–2087 (2011)
2. Biocca, M., Bortolini, L.: *Macchine e tecniche per il verde urbano. Realizzazione, cura e manutenzione delle aree verdi. Consiglio per la ricerca in agricoltura e l'analisi dell'economia agraria – CREA (ed.), Roma, Italy, p. 234 (2019). ISBN: 9788833850108*
3. Yang, J.: Assessing the impact of climate change on urban tree species selection: a case study in Philadelphia. *J. Forest.* **9**, 364–372 (2009)
4. Burley, H., Beaumont, L.J., Ossola, A., Baumgartner, J.B., Gallagher, R., Laffan, S., Esperon-Rodriguez, M., Manea, A., Leishman, M.R.: Substantial declines in urban tree habitat predicted under climate change. *Sci. Total Environ.* **685**, 451–462 (2019). <https://doi.org/10.1016/j.scitotenv.2019.05.287>
5. Moricca, S., Bracalini, M., Croci, F., Corsinovi, S., Tiberi, R., Ragazzi, A., Panzavolta, T.: Biotic factors affecting ecosystem services in urban and peri-urban forests in Italy: the role of introduced and impending pathogens and pests. *Forests* **9**(2), 65 (2018). <https://doi.org/10.3390/f9020065>
6. Biocca, M., Motta, E., Lucatello, G., Dallari, D.: Aspects of the stability of the Italian Stone Pine (*Pinus pinea* L.) in Rome, Italy. In: *Proceedings of Second International Symposium on Plant Health in Urban Horticulture, Berlin, Germany, 27–29 August 2003*, pp. 228–229 (2003)
7. Anderson, D.L., Koomjian, W., French, B., Altenhoff, S.R., Luce, J.: Review of rope-based access methods for the forest canopy: safe and unsafe practices in published information sources and a summary of current methods. *Methods Ecol. Evol.* **6**, 865–872 (2015). <https://doi.org/10.1111/2041-210X.12393>
8. Biocca, M., Gallo, P., Sperandio, G.: Technical and economic evaluation of urban trees pruning by climbing arborists. In: *Lecture Notes in Civil Engineering*, vol. 67, pp. 653–660 (2020)
9. Biocca, M., Bianchini, L., Gallo, P., Caffaro, F., Cavallo, E., Cecchini, M.: A survey on safety among tree-climber professional arborists. In: Biocca, M., Cavallo, E., Cecchini, M., Failla, S., Romano, E. (eds.) *Safety, Health and Welfare in Agriculture and Agro-Food Systems. SHWA 2020. Lecture Notes in Civil Engineering*, vol. 252, pp. 357–364 (2022)

10. Biocca, M., Gallo, P., Sperandio, G.: Potential availability of wood biomass from urban trees: implications for the sustainable management of maintenance yards. *Sustainability* **14**, 11226 (2022). <https://doi.org/10.3390/su141811226>
11. Verani, S., Sperandio, G., Picchio, R., Marchi, E., Costa, C.: Sustainability assessment of a self-consumption wood-energy chain on small scale for heat generation in central Italy. *Energies* **8**, 5182–5197 (2015)
12. Spinelli, R., Visser, R.J.M.: Analyzing and estimating delays in wood chipping operations. *Biomass Bioenergy* **33**(3), 429–433 (2009). <https://doi.org/10.1016/j.biombioe.2008.08.003>
13. Olsen, E.D., Kellogg, L.D.: Comparison of time-study techniques for evaluating logging production. *Trans. ASAE* **26**(6) 1665–1668 (1983). <https://doi.org/10.13031/2013.33821>
14. Tabacchi, G., Di Cosmo, L., Gasparini, P., Morelli, S.: Stima del volume e della fitomassa delle principali specie forestali italiane. Equazioni di previsione, tavole del volume e tavole della fitomassa arborea epigea. CRA, Unità di Ricerca per il Monitoraggio e la Pianificazione Forestale, Trento, Italy, p. 412 (2011)
15. Miyata, E.S.: Determining fixed and operating costs of logging equipment. General technical report NC-55, Department of Agriculture, Forest Service, North Central Forest Experiment Station, St. Paul, MN, USA (1980)
16. R Core Team: R: A Language and Environment for Statistical Computing. R Foundation for Statistical Computing, Vienna, Austria (2013). www.R-project.org

Automatic Feeding Systems for Cattle in Italy: State of the Art and Perspectives



Carlo Bisaglia , Andrea Lazzari , Simone Giovinazzo ,
and Massimo Brambilla 

Abstract The AUTOFEED project (<https://autofeed.crea.gov.it>) is a farm management project aiming to point out the advantages and disadvantages of adopting automatic feeding systems (AFS) in cattle breeding. In this context, two surveys were carried out: one to investigate the market offer (in cooperation with manufacturers) and another to record the AFS user impressions to point out the driving variables of the purchase and installation. In parallel, the research group set up an interview for farmers already using AFS in their barns or considering adopting them.

The market research identified 38 AFS models by 20 manufacturers with highly variable features resulting in many installation potentials: this articulated offer meets the needs and requirements of most livestock breeding sites. In 2021, there were 101 AFS installations in Italy (63% self-propelled, 26% rail-suspended, 9% wheel-driven, and 2% belt-conveyed), mainly located in Northern Regions. The orography of the sites was the main affecting parameter of the installed AFS driving technology.

The interview provided fact-finding insights on the user feedback about AFS. Despite the still limited diffusion of AFS on the national territory, compared to a traditional mixer wagon, the resulting perceived advantages consider the various aspects of cattle breeding. Among them, farmers underlined the increase in animal welfare and performance, the transformation of workload towards managerial and decisional tasks and, finally, the energy and operating costs saving, which align with the goal of sustainable animal farming.

Keywords AFS · total mixed ration · farm management · online survey · animal welfare and cattle performance

C. Bisaglia · A. Lazzari · S. Giovinazzo · M. Brambilla (✉)

Research Centre for Engineering and Agro-Food Processing, Council for Agricultural Research and Economics, Via Milano, 43, 24047 Treviglio, BG, Italy

e-mail: massimo.brambilla@crea.gov.it

1 Introduction

Over time, bovine nutrition has undergone profound changes dictated by technological and scientific advances. The bovine ration as we know it today relies on the adoption of the total mixed ration (TMR or *unifeed*), which foresees the mixing of all the ration components to provide animals with a single "dish". The first scientific articles on the subject date back to 1966 when the mechanical equipment in farms began to intensify [1, 2]. The introduction of TMR in cattle breeding has resulted in numerous benefits to both animals and operators. However, the progressive growth of farm size, technological advancement, and the reduction of labour market offer in the livestock farming sector, have caused unifeed to become an essential technique. Therefore, providing automation for TMR preparation is a relieving action for the operators employed on this task [3, 4].

For the set-out reasons, and considering that the TMR's mechanical preparation is repetitive work very liable to human errors, automatic feeding systems (AFS) were born. They are smaller than a mixer wagon and can distribute the unifeed ration numerous times throughout the day compared to the classic wagon, commonly run for 1 or 2 daily distributions [5].

There are currently about 20 AFS manufacturers and more than 1250 robots sold worldwide [4], which can be classified into three different automation levels [6]:

- Level I: automation refers only to ration component shredding-mixing and distribution operations. Here, the mixer is stationary, and operators fill it with the single components of the TMR ration picked up from the storage facilities of the farm.
- Level II: automation extends to wagon filling from shredding-mixing and distribution operations. Wagons can also mix the TMR before distribution. In this case, the kitchen shall have sufficient space for a temporary deposit with a crane construction, feed grabber, or mechanically emptying storage bins that automatically feed the robot.
- Level III: the automation covers all the steps of TMR preparation, from ingredients loading and transport to their mixing and distribution to animals. It means that the wagon receives or withdraws the ration components directly from the silos; therefore, it is unnecessary to have a temporary deposit.

The AUTOFEED project fits into this modern context of bovine farming, trying to define the strengths and weaknesses of AFS technology. In this article, research was carried out on the websites of the various AFS owners to identify their market offer, and thanks to the support of the same manufacturers, it was possible to identify the quantity and type of AFS present in Italy. Finally, a survey was developed to collect the impressions of farmers using AFS robots.

2 Methodology

2.1 *The Market Offer*

The market research of the AFS models was carried out by monitoring the manufacturer's official websites and checking bibliographic resources. In addition, owners and resellers cooperated to analyze the AFS models available in Italy, providing the list of the machines sold and installed in Italy.

2.2 *The Survey*

The survey design aimed to find out farmers' impressions of this technology. The platform used for the development was Microsoft Forms®: the survey (in both Italian and English) was based on existing literature, and before administering it to the interviewees, it underwent testing on two farms to verify the correct functioning. The survey design allowed the administering both online and in the presence (e.g. during fairs and other farmers' events). Of course, the time required to complete the questionnaire represented an issue. Depending on the answers breeders provided, the completion time ranges from 5 to 10 min. Most of the answers were in the multiple-choice format; however, some couldn't help, requiring manual completion. The survey consisted of four parts: one standard introductory section (about the farm characteristics and the level of the technological supply) and three sets of questions addressing specifically:

1. *Farmers who currently have an AFS installed:* were asked about the characteristics of the installed system, the characteristics of the rationing before the AFS arrival, the strengths and weaknesses and, finally, a global assessment of the purchased technology.
2. *Farmers who intend to purchase an automatic feeding system:* were asked the reasons for their willingness to install an AFS and how much they are inclined to spend.
3. *Farmers who do not have the technology and that do not want to buy it.*

The questionnaire was open from 21 June 2021 until 31 May 2022. Its disclosure occurred through the AUTOFEED website (<https://autofeed.crea.gov.it>), the Facebook and LinkedIn® channels of the project, via known persons and interviewing farmers during meetings and fairs. During the publication period, a total of 100 responses were collected.

2.3 Data Processing

The data obtained were processed using the Microsoft Excel® software. Data processing foresaw the chi-square (χ^2) test for independence and calculated the Cramer's V index for contingency. V has the advantage of indicating the strength of the relationship between two categorical variables ranging between the two extreme values of 0 and 1: 0 means statistical independence, while 1 total dependence in the observed distribution [7].

3 Result and Discussion

3.1 AFS Models in the Market Offer

The research revealed 38 robot models and 20 manufacturing companies worldwide. The identified systems are highly flexible and adaptable to different conditions: following the work of Haidn [8], they have been classified into self-propelled, rail-suspended, wheel-driven, and belt-conveyed systems.

The rail-suspended AFSs (37%) consist of a track on which the robot rests and moves; two versions are available: a) chopper-mixing and distributing robots; b) only TMR distributing robots.

The self-propelled systems (34%) are electrically powered (batteries) and move in the barn following specific magnetic indicators placed within the paving. Even in this case, they provide for chopping-mixing and distribution functions or just distribution.

Belt conveyor systems (16%) distribute an already mixed ration (from a fixed mixer close to the barn where animals are grown) directly in the feeding trough using moving belts. In some models, the belt itself is the animals' feeding trough.

Lastly, wheel-driven systems (11%) foresee using a track/line as a direction and power source: a small steering wheel underneath the wagon allows them to discharge their weight on soil instead of the housing structure.

Besides distributing the TMR, rail-suspended, self-propelled and wheel-driven, also provide feed pushing when run outside the distribution times.

All the robots described above require human intervention in preparing the TMR: operators shall supply all the ingredients in a specific technical environment (the *kitchen*), usually placed close to the barn. However, fully automated models (2%, currently under development) may carry out all the ration preparation and distribution steps in complete autonomy without human intervention (Fig. 1):

The Italian Situation. Thanks to the collaboration with the AFS owners, it was possible to assess the number of AFSs distributed throughout Italy. The situation presents a total of 101 installations, where the self-propelled type is predominant



Fig. 1 Different models of AFS: a) rail-suspended only distributor; b) Wheel-driven; c) rail-suspended chopper-mixing and distributor; d, e, f) Self-propelled (pictures taken by the authors)

Table 1 Construction types of AFS by orography in Italy (%)

Orography	Rail-suspended	Self-propelled	Wheel-driven	Belt conveyor
Mountain	60.0%	22.5%	12.5%	5.0%
Lowland	4.0%	92.0%	4.0%	0.0%
Hill	0.0%	81.8%	18.2%	0.0%

(63%), followed by rail-suspended models (26%), wheel-driven models (9%) and finally, conveyor belt systems (2%).

The robot installation areas mainly concern northern Italy; however, the type installed differs significantly from area to area and strongly depends on the size of the farm and the territorial orography. A remarkable difference in the type of construction installed was observed following the orography of the area; in fact, the subdivision of the installations according to three parameters (mountain, lowland, hill) has shown that: in the mountain areas, there are more suspended AFSs, however, in the lowland areas the self-propelled robot is preferred (Table 1).

The statistical analysis assessed the significant strong connection between the installed type of AFS and the orography of the territory (Cramer's V index = 73%).

The farm size, on the other hand, does not influence the choice of the type of AFS; however, the survey indicated that larger farms are less prone to adopt rail-suspended systems because of the required high length of rail/line.

3.2 The Farmers' Perspective from the Survey

The introductory analysis of the breeder survey showed a strong male (89%) conduction compared to female (11%). A more specific analysis showed that even in farms

equipped with AFS, the sex of the handler remains unchanged in percentage, and no significant difference emerged between the sex of the owner and the presence/absence of the AFS. The situation regarding the age of the owner of the farm shows that most of them (85%) are under 60 years old, and a small part (15%) are over 60; however, the age of the farm owner was not connected with the purchase of an AFS meaning that there is no greater predisposition of younger breeders towards this technology.

Dairy farmers primarily participated in the survey (82%), and the remaining answers resulted equally from beef producers and farmers running mixed farming operations. The predominance of the farm interviewed is of medium-small size (<500 heads).

Despite the still low adoption rate of the robotic equipment, the survey pointed out that farmers having an AFS system installed are more receptive to other robotic systems such as self-feeders and milking robots. 29% of the interviewed farmers already used AFSs (mainly belonging to automation level II); the remaining belong to the level I. Automation level III, being still in the prototype or primordial installation phase, is not yet active in Italy.

The feed distribution methods before AFS adoption were various: most farms adopted a mixer wagon (self-propelled or trailed) to prepare and distribute the unifeed (69%); 21% of farms provided the manual distribution of the ration ingredients or made use of the machines just the distribution of single ingredients (10%).

According to the interviewees, transitioning from manual or partly mechanized distribution to automatic feeding has brought benefits in animal daily feed ingestion (on average +2.92 kg/d) with subsequent increases in milk production (+3.31 kg/d on average). Such a consistent increase results from farms previously performing manual distribution of the ration: following the transition to robotization, they have achieved exponential growth in production. Increased animal performance, however, resulted not only from the increases in TMR distribution but also from the increases registered for feed pushing activities (TMR distribution, from an average of 2 daily distributions, has reached up to 12 passages while feed pushing moved from about 4 daily passages to 12). The advantages of frequent distribution and pushing are now known and documented in the international bibliography [9].

According to farmers, using an AFS also led to significant savings in labor and energy. For example, for energy savings, 28% participants observed energy savings higher than 60%; 28% were unaware of the potential energy saving, and the remaining 44% achieved energy savings ranging between 0 and 50%. Concerning labor, AFS owners observed a net saving (higher than 40%) compared to the previous working condition, accompanied by a transformation of the workload towards managerial and decisional tasks. Figure 2 summarizes the reasons behind farmers' decision to install an AFS system.

The items concerning animal welfare, the accuracy of the ration and the flexibility of working hours obtained the highest marks in 76% and 66% of the farms interviewed, respectively. In fact, bibliographic sources have already shown how frequent distribution throughout the day increases animal welfare mainly due to always fresh and available ration and reduced competition between animals in the barn [10]. In addition, the absence of a fixed operator who repetitively performs the preparation of

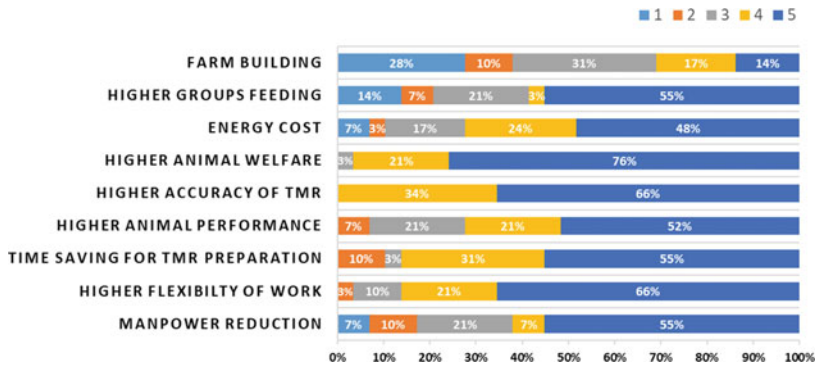


Fig. 2 Reasons for installing an AFS and level of agreement of the interviewed farmers (1: strongly disagree; 2: disagree; 3: neutral; 4: agree; 5: strongly agree)

the ration increased the breeder flexibility in line with the increase of AFS technological level [11]. The building category found a low rating for the interviewed farmers because the building interventions are often not required to install an AFS, demonstrating their strong adaptability. In conclusion, the breeders have shown complete general satisfaction with the AFS system and declare their propensity to make the same choice again.

The survey also included a special section for breeders who currently don't have an automatic system for unifeed but, in the future, intend to buy it. Again, the propensity to spend resulted quite variable; however, most (79%) have a medium–low investment, between 500 and 1500 €/head. Several reasons are behind their willingness to install an AFS (Fig. 3): the increase in animal welfare (89% grade greater than 4), increase in animal performance (79% grade greater than 4), and accuracy of the TMR (74% vote greater than 4) are the main reasons why farmers would choose to install an automatic unifeed system.

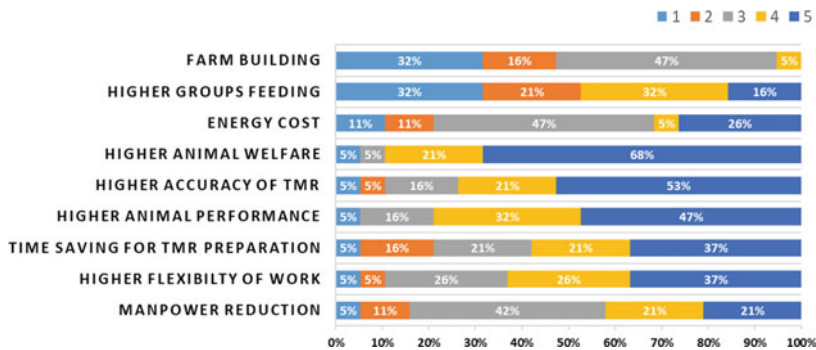


Fig. 3 Reasons for future installing an AFS and level of agreement of the interviewed farmers (1: strongly disagree; 2: disagree; 3: neutral; 4: agree; 5: strongly agree)

4 Conclusion

The market of AFS offers numerous models that perfectly adapt to each type of farm. As a result, the AFS spread in Italy has exited the embryonic phase. The analysis of the installed models made it possible to evaluate the strong adaptability of the systems to the different and various situations of Italian farms (e.g., number of heads, orography of the territory). Following the numerous advantages that the survey pointed out (i.e., energy saving, reduction of repetitive operations in rationing, workload transformation, improved animal welfare and performance), a substantial expansion of the market for such systems is expected in the future.

Acknowledgements The authors acknowledge the Lombardy Region that funded the project “*Feeding automation for cattle farms in Lombardy – AUTOFEED*”, in the framework of SUBMEASURE 16.1 – “Support for the establishment and the management of EIP Operative Group in the topic of agriculture’s productivity and sustainability” of the Rural Development Program 2014-2020.

The research is carried out within the PhD in Engineering for energy and environment - Biosystems and environment at the University of Tuscia.

References

1. Bisaglia, C.: Automazione della preparazione e distribuzione di razioni completamente miscelate (TMR) o unifeed per bovine da latte: possibilità tecnologiche e ricadute produttive, gestionali ed economiche. IRIS Institutional Research Information System - AIR Archivio Istituzionale della Ricerca. <https://air.unimi.it/>. Accessed 13 Sept 2022
2. Schingoethe, D.J.: A 100-year review: total mixed ration feeding of dairy cows. *J. Dairy Sci.* **100**(12), 10143–10150 (2017)
3. Oberschatzl, R., Haidn, B., Neiber, J., Nesper, S.: Automatic feeding systems for cattle – a study of the energy consumption of the techniques. In: XXXVI Ciosta Cigr V, Saint Petersburg (2015)
4. Tangorra, F.M., Calcante, A.: Energy consumption and technical-economic analysis of an automatic feeding system for dairy farms: results from a field test. *J. Agric. Eng.* **49**, 228–232 (2018)
5. Belle, Z., André, G., Pompe, J.: Effect of automatic feeding of total mixed rations on the diurnal visiting pattern of dairy cows to an automatic milking system. *Biosys. Eng.* **111**(1), 33–39 (2012)
6. Haidn, B., Leicher, C.: Automatisches Füttern-Neues aus Praxis und Forschung. In: Automatische Grundfuttermvorlage für Rinder. Bayerische Landesanstalt für Landwirtschaft, pp. 47–49 (2017)
7. Kearney, M.W.: Cramer’s V. In: Allen, M.R. (ed.) Sage Encyclopedia of Communication Research Methods. Sage Publisher (2017)
8. Haidn, B.: Automatisches Füttern bei Milchkühen – Verfahrenstechnik, Arbeitswirtschaft und Kosten. In: Automatisches Füttern im rinderhaltenden Betrieb. Bayerische Landesanstalt für Landwirtschaft, pp. 7–20 (2014)
9. Nabokov, V.I., Novopashin, L.A., Denyozhko, L.V., Sadov, A.A., Ziablitskaia, N.V., Volkova, S.A., Speshilova, I.V.: Applications of feed pusher robots on cattle farmings and its economic efficiency. *Int. Trans. J. Eng. Manag. Appl. Sci. Technol.* **11**(14), 1–7 (2020)
10. Schneider, L., Volkmann, N., Kemper, N., Spindler, B.: Feeding behavior or fattening bulls fed six times per day using an automatic feeding system. *Front. Vet. Sci.* **7**, 1–10 (2020)

11. Hohendiger, M., Stumpfenhausen, J., Treiber, M., Bernhardt, H.: Estimation of effects on the workload at dairy farms caused by automatization. In: 47th Symposium "Actual Tasks on Agricultural Engineering", pp. 1–9, Opatija (2019). Izvorni znanstveni rad Original scientific paper

Preparatory Activities for the Care and Maintenance of Historic Parks and Gardens: A Case Study



Lucia Bortolini and Lorenzo Guerrini

Abstract Historic parks and gardens are certainly an important part of the Italian cultural heritage and a fascinating resource for tourism. Historic parks and gardens are often composed by areas and areoles with different geometries and uses (e.g., lawns, parterres, groves, etc.) and the complexity and artistic and naturalistic value of these cultural assets require the highest level of professionalism and expertise, with maintenance work that must scrupulously respect the garden's original layout. In addition, in areas with similar uses, differences in fruition as well as in visibility by visitors could lead to large differences in the intensity of maintenance required. It is precisely the number and complexity of the tasks and the high-quality standards required that lead to high working hours and rising costs. Thus, the organisation of areas according to similarities in terms of operations and equipment could improve productivity in the required tasks with a reduction of costs and an improvement of the use of these assets.

The Miramare Park (Trieste, Italy) is an example of an artificial mixed planting of forest species, trees and shrubs, with large areas of lawn, combining a more typically romantic English style with areas of Italian garden near the castle. At present, it is a public park much frequented by tourists and locals, especially in the areas close to the castle, while other parts are almost unused or hardly accessible.

In this work the different areas of the park were firstly identified. Then, the maintenance requirements of each area were assessed and, finally, a zoning process was carried out by grouping areas according to similarities in management needs, considering both softscape and hardscape requirements. This preparatory work will make it possible to verify and quantify the presumed benefits of the proposed organisational approach and provide a good basis for future management improvements.

Keywords Urban greening · Zoning · Work planning

L. Bortolini (✉) · L. Guerrini

Department of Land, Environment, Agriculture and Forestry, University of Padova, Padua, Italy
e-mail: lucia.bortolini@unipd.it

1 Introduction

The 1981 Florence Charter defines the historic garden as “an architectural and horticultural composition of interest to the public from the historical or artistic point of view” [1] and emphasises that, in addition to being an architectural composition, it is also a living plant tissue [2]. For this reason, historic gardens should be considered natural monuments to which the principles of the Venice Charter should be applied [3], and must be preserved and their heritage protected. Their conservators must adopt detailed strategies with protection and conservation plans, directions for restoration, and procedures for making them available to the public [4].

Historic parks and gardens are certainly an important part of the Italian cultural heritage and a fascinating resource for tourism, and their popularity has grown steadily, making them fully part of that highly specialised and rather lucrative branch of ‘garden tourism’ [5].

Since they are green spaces, they can also provide many other benefits, among which urban heat island (UHI) mitigation [6], carbon sequestration [7] and oxygen production, habitat and biodiversity enhancement [8], and when accessible to citizens, they offer opportunities for their recreation and physical activity [9]. However, the benefits and the ecosystem services of historic parks and gardens are closely related to their quality standards.

Historic parks and gardens require a lot of efforts in terms of care and maintenance and their management usually involves qualified personnel, a large number of working hours and different types of equipment and machinery.

The care and conservation of these green areas, which are also artistic objects, is an expression of the culture of our societies [10], and only correct and careful maintenance can prevent their degradation and avoid irreversible damage [11].

Historic parks and gardens are often composed by areas and areoles with different geometries and uses (e.g., luxury lawns, utility lawns, *parterres*, groves, etc.) and the complexity and artistic and naturalistic value of these cultural assets require the highest level of professionalism and expertise, with maintenance work that must scrupulously respect the garden’s original layout. In addition, in areas with similar uses, differences in fruition as well as in visibility by visitors could lead to large differences in the intensity of maintenance required. However, it should not be forgotten that one of the cornerstones of maintenance is also to ensure safe work places for the workers with an approach that can be defined as “operator-oriented” [12].

It is precisely the number and complexity of the tasks and the high-quality standards required that lead to high working hours and rising costs. Thus, the organisation of areas according to similarities in terms of operations and equipment could improve productivity in the required tasks with a reduction of costs and an improvement of the use of these assets.

The aim of this work is to carry out a preliminary analysis of the care and maintenance activities in the Park of the Castle of Miramare, in order to verify which interventions are necessary for the conservation of the various functions of this important place of Italian culture. The preparatory work will make it possible to verify and

quantify the possible benefits of a given organisational approach in order to create a basis for assessing future management improvements.

2 Context and Methodology

The Miramare Park is located in the municipality of Trieste (North-eastern Italy) and has a total area of about 220,000 m². It was built in the mid-nineteenth century at the behest of Archduke Maximilian of Habsburg, on a karstic, almost bare area with only a few shrubs and thorny bushes. It is an example of an artificial mixed planting of forest species, trees and shrubs, with large areas of lawn, combining a more typically romantic English style with areas of Italian garden near the castle. Even today, the avenues and carriage roads appear to be original to the time when the layout of the park was conceived. Figure 1 shows the original map of the park.

At present, it is a public park much frequented by tourists and locals, especially in the areas close to the castle, while other parts are almost unused or hardly accessible.

In the eastern part, a reforestation of Austrian black pine (*Pinus nigra*) was carried out and used as an experimental station to understand whether the geo-morphological and climatic conditions were appropriate for the species. In addition, the planting allowed the *parterre* to be protected from the Bora winds, which are typical in

Fig. 1 Original map of the Miramare Castle Park (quitrieste.it/2014/02/carlotta-a-miramare/)



this area. Now, it is currently in a partially abandoned condition and is not particularly frequented by visitors. In fact, in this context, time and poor maintenance have imprinted a degraded structure of vegetation, which presents little landscape and consequently historical value, so that cultural, tourist and recreational use is practically absent.

In the western part of the park, a more geometric layout can be seen, which can be described as an ‘Italian garden’. In this area, there is also the *parterre*, with flowerbeds that have recently been upgraded by inserting new species such as *Araucaria araucana*, *Trachycarpus fortunei* and *Cortaderia selloana*, reminiscent of Central America, where Archduke Maximilian of Habsburg became Emperor of Mexico (Fig. 2).

The northern part of the area contains several species of European and non-European origin, showing that the purpose of the park was also the acclimatisation of various species collected during the Archduke’s travels and planted in this park. Among the most important species are *Sequoiadendron giganteum*, *Ginkgo biloba*, *Cedrus deodara* and *Cedrus atlantica*, as well as the presence of numerous conifers.

The maintenance of the greenery in the Miramare Castle park is one of the main priorities of the current administration. Major restoration work began in 2016 when special autonomy was granted by the Ministry of Cultural Heritage and Activities. At present, reports are periodically drawn up in which all ordinary and extraordinary maintenance works are recorded. On the basis of these reports, it was possible to draw up a list of the various works, grouping them by type and by the homogeneous areas into which the Park can be divided.



Fig. 2 The flowerbeds of the parterre in the ‘Italian garden’ of the western part of the park

3 Current Results and Discussion

The restoration/renewal activities affected several parts of the park and are still continuing. These activities have restored some characteristic elements of the park that were in a state of partial or complete decay. In Fig. 3 two orthophotos of the park are shown, highlighting the effects of some of these extraordinary maintenance works.

The new layout of the park makes it possible to better distinguish some zones, listed below and reported in Fig. 4.

The peculiar features of each zone were identified and described for the purposes of selecting the necessary maintenance work:

- the Central square: with high visibility, being in front of the Castle, it has flowerbeds with re-flowering roses around the central fountain, a large pergola with wisteria and areas with ornamental turf;
- the Marina area “Porticciolo”: area sloping towards the marina with turf and boxwood perimeter hedges, walls partially covered with a deciduous climber;
- the Avenue of holm oaks: zone with many holm oaks lining the entrance way and undergrowth with evergreen shrubs;
- the Stables: they host a popular museum, the outdoor area features several specimens of plane and oak trees and flower beds with seasonal blooms;
- the Orangery: it consists of 18 plants of various cultivars of *Citrus aurantium* in pots placed outdoors on an area with ornamental turf and low shrubs;
- the Parterre: recently redeveloped with mixed flowerbeds and boxwood borders and with an area sloping down towards the sea with turf and ground cover;
- the Wooded area: particularly large and heterogeneous area, characterised by the presence of what remains of the black pines of the original planting and with a large area of undergrowth left to natural evolution (among the most common species *Quercus ilex*, *Robinia pseudoacacia* and *Fraxinus ornus*);
- the Clearings with tree specimens: large lawn zone with some bulbous areas and tree elements, some of which are monumental;
- the Ex-nursery: terraced area with grass (originally hosted exotic plants to study their adaptability and later vegetable gardens and orchards).

As can be seen, the identified areas also constitute homogeneous zones in terms of ordinary maintenance needs. For this reason, on the basis of this subdivision, the main maintenance activities were identified using the classification proposed by Biocca and Bortolini [13]. The maintenance activities of the different homogeneous areas constituting the park were summarized and reported in the Table 1.

Some areas (i.e. the Central square, the Marina area, the Avenue of holm oaks, the Stables, the Orangery, the Parterre, the Clearings with tree specimens) have completed their restoration and have achieved full usability and historical value. The required ordinary maintenance activities will most likely remain those shown in Table 1.

Conversely, other areas of the park have been cleaned up and made safe but their final use has not yet been fully defined and are awaiting new planning. In



Fig. 3 Orthophotos of Miramare Park of June 2016 (top) and June 2021 (bottom)



Fig. 4 Map of the different areas identified in the Miramare Park

Table 1 List of the maintenance activities of the different homogenous areas of the Park

Park area	Maintenance activities
Central square	Weeding and pest control treatments, Fertilisation, Roses/shrub/arbour pruning, Grass cutting, Lawn renovation, Leaf clean-up, Irrigation
Marina or "Porticciolo"	Grass cutting, Lawn renovation, Irrigation, Leaf clean-up
Avenue of holm oaks	Pruning, Leaf clean-up, Undergrowth clean-up
Stables	Planting of annul plants, Weeding and pest control treatments, Surface soil tillage, Irrigation, Fertilisation
Orangery	Pest control treatments, Fertilisation, Pruning, Irrigation, Grass cutting, Lawn renovation
Parterre	Planting of annul plants, Weeding and pest control treatments, Surface soil tillage, Pruning of boxwood, Cleaning of dead plant parts
Wooded area	Tree pruning, Undergrowth clean-up, Felling of dead and dangerous trees
Clearings with tree specimens	Grass cutting, Tree pruning, Transplanting bulboses
Ex-nursery	Grass cutting with mulching

particular, the ex-nursery is a terraced area that is currently managed simply as grass with periodic mulching cuts, while for the wooded area a decision must be made whether to restore the original black pine planting or leave the natural evolution. This is the largest area that currently requires ordinary cleaning of the undergrowth, maintenance pruning and canopy cleaning, and annual monitoring of the stability of some historical trees.

Whatever the development of the park, maintenance activities must be taken into account in order to optimise resources so that the quality of interventions remains over time.

4 Conclusions

The zoning process carried out by grouping areas according to similarities in management needs should be considered as preparatory work to be carried out by those responsible for the maintenance of complex green areas, such as historical parks and gardens, in order to verify and quantify the possible limits and benefits of the proposed organisational approach and which can provide a good basis for future management improvements.

References

1. O'Donnell, P.M.: Florence charter on historic gardens. In: *Encyclopedia of Global Archaeology*, pp. 2812–2817. Springer, New York (2014)
2. Jagiełło, M.: Do we need a new Florence charter? The importance of authenticity for the maintenance of historic gardens and other historic greenery layouts in the context of source research (past) and taking into account the implementation of the sustainable development idea (future). *Sustainability* **13**(9), 4900 (2021)
3. Athanasiadou, E.: Historic gardens and parks worldwide and in Greece: principles of acknowledgement, conservation, restoration and management. *Heritage* **2**, 2678–2690 (2019)
4. Tieskens, K.F., Schulp, C.J., Levers, C., Lieskovský, J., Kuemmerle, T., Plieninger, T., Verburg, P.H.: Characterizing European cultural landscapes: accounting for structure, management intensity and value of agricultural and forest landscapes. *Land Use Policy* **62**, 29–39 (2017)
5. Bell, S., Fox-Kämper, R., Keshavarz, N., Benson, M., Caputo, S., Noori, S., Voigt, A.: *Urban Allotment Gardens in Europe*. Routledge, New York (2016)
6. Shishegar, N.: The impact of green areas on mitigating urban heat island effect: a review. *Int. J. Environ. Sustain.* **9**(1), 119–130 (2014)
7. Nowak, D.J., Crane, D.E.: Carbon storage and sequestration by urban trees in the USA. *Environ. Pollut.* **116**(3), 381–389 (2002)
8. Young, R.F.: Managing municipal green space for ecosystem services. *Urban Forest. Urban Greening* **9**(4), 313–321 (2010)
9. Bertram, C., Rehdanz, K.: The role of urban green space for human well-being. *Ecol. Econ.* **120**, 139–152 (2015)
10. Harney, M.: *Gardens and Landscapes in Historic Building Conservation*. Wiley-Blackwell, Chichester (2014)
11. Anthony, J.: Protection for historic parks and gardens. *Gard. Hist.* **24**(1), 3–7 (1996)

12. Bortolini, L., Cividino, S.R., Gubiani, R., Cecchini, M., Delfanti, L.M., Colantoni, A.: Urban green spaces activities: a preparatory groundwork for a safety management system. *J. Saf. Res.* **56**, 75–82 (2016)
13. Biocca, M., Bortolini, L.: *Macchine e Tecniche per il Verde Urbano*. CREA Ed., Roma, Italy (2019)

Pig Farming in the Abruzzo Region and Hepatitis E Virus Detection in Swine Slurries



M. Brambilla , C. Bisaglia , P. Mancini , C. Veneri ,
G. Bonanno Ferraro , M. Iaconelli , E. Suffredini , and G. La Rosa 

Abstract Hepatitis E virus (HEV) infection is a recognized emerging zoonosis, and sporadic autochthonous cases, unrelated to travel in endemic areas, are rising in industrialized countries. Pigs and wild boars are considered HEV main reservoirs. The ongoing *One Health* project “Improving understanding of autochthonous Hepatitis E transmission routes: a focus on foodborne and waterborne pathways” focuses on the Abruzzo Region, where a high prevalence of anti-hepatitis E IgG (48.9%) was detected among blood donors.

Abruzzo pig husbandry is mainly a family business, and pig farms often host a few animals. However, for most animals, rearing occurs in a few specialized structures mainly devoted to animal reproduction (open cycle) and fattening. A survey showed a heterogeneous distribution of the pig production structures in the territory, with 53% of the fattening pigs occurring in six municipalities, while three other municipalities host the largest part of the animals in reproduction facilities. Therefore, in this study, swine slurry samples taken from chosen representative specialized production sites underwent analysis to identify the presence of HEV strains.

Preliminary data on HEV occurrence suggests that, among the tested farming structures, the housing of animals in buildings with partly slatted floors, the presence of wild fauna and the use of slow manure removal technologies are associated with higher probabilities of HEV detection in slurries.

Keywords Foodborne viruses · waterborne viruses · zoonotic transmission · livestock building · Hepatitis E virus · Swine farming

M. Brambilla (✉) · C. Bisaglia

CREA - Council for Agricultural Research and Economics, Research Centre for Engineering and Agro-Food Processing, Via Milano, 43, 24047 Treviso, BG, Italy
e-mail: massimo.brambilla@crea.gov.it

P. Mancini · C. Veneri · G. B. Ferraro · M. Iaconelli · G. La Rosa

Department of Environment and Health, Istituto Superiore Di Sanità, 299, Viale Regina Elena, 00161 Roma, Italy

E. Suffredini

Department of Food Safety, Nutrition and Veterinary Public Health, Istituto Superiore Di Sanità, 299, Viale Regina Elena, 00161 Roma, Italy

1 Introduction

The hepatitis E virus (HEV) is a common causative agent of acute viral hepatitis. Usually silent or producing self-limiting icteric illness, HEV infection may, however, develop in fulminant liver failure in pregnant women (fatality rates may reach 25% in this group) as well as in patients with underlying chronic liver disease. In European Union countries, HEV is an important human infection [1]. A systematic World Health Organization (WHO) review reported HEV seroprevalence to range from 0.03% to 52% among blood donors in the WHO European Region [2], showing widespread exposure to HEV.

In Italy, the burden of disease and transmission pathways for autochthonous HEV have not been sufficiently defined yet, despite the reporting and the description of autochthonous cases in recent years [3]. HEV seroprevalence differs considerably depending on population, geographical area and the used serological assay, and there is evidence of “hot spots” of HEV infection in specific Regions of Italy (e.g., Abruzzo) ascribable to HEV occurrence in wild animals and local eating habits [4–7]. Consequently, great attention has been placed on wild boars, considering the local tradition of using their raw or undercooked meat for homemade food preparation [8, 9].

A study performed on the occurrence and diversity of HEV in swine slurry in Italy confirmed the presence of HEV strains in swine slurries from breeding operations [10], suggesting the need to deepen the risk factors connected with HEV entry in swine farming.

This study reports the preliminary results of long-term monitoring of HEV presence in swine farms in the Abruzzo region: after an initial assessment of Abruzzo’s swine farming characteristics, the monitoring activity considered slurry and water samplings in representative swine breeding units to underpin the factors increasing the exposure of animals (and, therefore, of operators) to HEV infection.

2 Material and Methods

2.1 Swine Farming Facilities in Abruzzo and Slurry Sampling

The records of the National Veterinary Registry Database (www.vetinfo.it) were used for a survey on the total number of reared animals and the facilities where they are grown. Further investigations on the resulting dataset revealed the main features and organization characteristics of the farming facilities: the location of the farms allowed the identification of the housing structures to be included in the slurry and water sampling plan for HEV detection.

Slurry sampling was performed in 19 swine farming units throughout the Abruzzo Region during three sampling campaigns (i.e., July 2021, November 2021 and May 2022). The choice of the sampling sites considered the number of reared animals and

Table 1 Localization and characterization of the sampling sites

NHS territorial unit	Territory	No. of sampled sites	Sampled wards
1	Avezzano-Sulmona-L'Aquila	3	Weaning, Fattening
2	Lanciano-Vasto-Chieti	4	Farrowing, Delivery, Weaning, Fattening
3	Pescara	9	Farrowing, Delivery, Weaning, Fattening
4	Teramo	3	Fattening

their production cycle. The local veterinary services of the National Health Service (NHS) supported identifying the most representative structures and the approach with the farmers (Table 1).

Slurry sampling was undertaken according to biosafety rules: operators avoided entering the structures during the rearing cycle, and, when possible, sampling occurred through the collection pits placed close to the barn to collect the effluent before entering the storage tank or lagoon. During sampling campaigns, farmers were interviewed to record the characteristics of the production site, the manure management system's features and the building structures hosting the animals. For each ward of the chosen farming units, 50 mL of fresh slurry were taken, placed in a laboratory test tube, and kept stored at 4 °C until the transfer to the National Institute of Health (Department of Environment and Health) for analysis. Overall, the sampling campaigns resulted in collecting 120 swine slurry samples.

2.2 Slurry Sample Processing

Swine slurries were concentrated using a standard PEG-centrifugation-based protocol [11]. Nucleic acid extraction was performed using magnetic silica beads with the MiniMag platform (bioMerieux). Broadly reactive primers targeting the ORF1 region were used to detect HEV by nested RT-PCR followed by amplicon sequencing. Typing in the ORF2 region with the RIVM HEV typing tool (<https://www.rivm.nl/mpf/typingtool/hev/>) was also performed for further subtyping [12].

2.3 Data Processing

Frequency analysis was applied to determine any possible connection between breeding site characteristics and the geographical location of the farm, using the Cramer's V index [13], which relies on the chi-square (χ^2) test for independence.

Data processing with the Jamovi software [14] assessed the relationship between the results of HEV detection assays (positive/negative nominal variable) and the features of the sampled sites (e.g., manure management, production, ventilation, housing, wild fauna) using binomial logistic regression (BLR) [15] and Bayesian contingency tables [16, 17].

3 Results and Discussion

3.1 Swine Farming Facilities in Abruzzo

Overall, the National Veterinary Registry Database recorded a total pig population of 69,793 pigs reared in 15,455 breeding facilities in the Abruzzo Region. Family-run breeding sites were the most widespread structures; however, they hosted just a minor part of the reared animals (11%), meaning that such production sites, albeit very frequent in the territory, host very few animals each. A significant part of swine breeding occurs in specialized structures (Fig. 1), which are mainly devoted to the open production cycle (49% fattening and 39% farrowing for piglet production); however, 1% of them have a closed production cycle.

The statistical survey on the possible connection between municipal territory and pig facilities (Fig. 1), carried out by calculating the Cramer's V index, showed the presence of a good connection regarding the number of reared animals ($V = 0.53$) and moderate connection for the number of farms ($V = 0.39$). It means that the micro-territory level tends to affect the distribution of the farming structures more than the NHS territoriality of the Abruzzo Region. Six municipalities (i.e., Corfinio, Atri, Arsita, Cupello and Civitaluparella) host 53.0% of animals reared in fattening structures; three municipalities (i.e., Sant'Omero, Silvi and Cupello) host 50.6% of the animals in open production cycle structures, and the province of Teramo hosts the majority of pigs reared in closed-cycle production facilities.

Fig. 1 Distribution of the animals reared in specialized rearing structures among the different NHS territorial units of the Abruzzo Region (processed data)

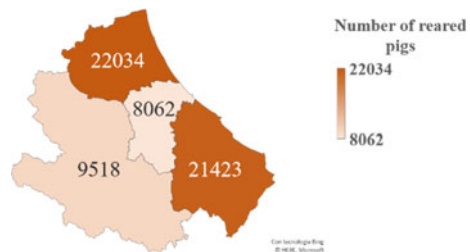


Table 2 Result of sample analysis for HEV presence

HEV	NHS 1	NHS 2	NHS 3	NHS 4	Total
Positive	4	5	7	4	20
Negative	10	43	34	43	100
Total	14	48	41	47	120

3.2 HEV Presence in the Monitored Farming Sites

Table 2 reports the results of the analysis for HEV detection in the sampled slurries and irrigation waters. Overall, 16.7% of the collected samples were positive for HEV, confirming a certain degree of virus circulation.

The results of the BLR pointed out that partly slatted floor housing, deep pit manure collection system (occurring with both overflow discharge systems and scrapers), and the presence of wildlife fauna are significant for the omnibus likelihood ratio test. The resulting model, overall, is significant ($\chi^2_{(3)} = 17.7$ and $p < 0.001$): the predictor set explains between 13.7% and 23.1% of the variance in the odds of HEV detection. Across both outcome categories, 82.5% of cases were accurately classified, with sensitivity higher than specificity. However, positive sample correct prediction occurred in 20.0% of cases compared to 95.0% of negative samples.

Table 3 reports the estimates and the significance of the considered predictors for the binomial logistic model and the results of the Bayesian contingency tables.

The BF_{10} values show that the presence of wildlife in the breeding site surrounds moderately relates to HEV detection in slurries, while the deep pit collection system is less related to HEV occurrence. Partly slatted floor housing (Fig. 2) and wildlife combined presence increase BF_{10} up to 13.02, which indicates that the combined occurrence of these factors acts strongly on the exposure of the animals and operators to excreta and, therefore, to HEV infection.

Such results, albeit preliminary, confirm the importance of housing conditions in HEV diffusion prevention. Furthermore, considering the proven faecal-oral transmission route of this virus [18], adopting best management practices in swine farming plays a fundamental role in limiting animal and operator infection, in particular during cleaning operations.

Table 3 Logistic regression results and BF_{10} values of the predictors

Predictor	Estimate*	p-value	BF_{10} Poisson
Wildlife presence	1.08	0.054	4.33
Partly slatted floor	1.56	0.026	0.47
Deep pit slurry collection	-18.65	0.991	1.19

* The estimates represent the log odds of “HEV = Negative” vs. “HEV = positive”. The reference category for all the predictors is 1 (presence).



Fig. 2 Examples of pigs housed on partly slatted floors

Building cleaning and disinfection usually occur after batches of livestock and manure have been removed (the cleaning frequency is at least equal to the number of production cycles per year), often using high-pressure washers. Such activity has an effect on operator health: Coffman et al. [19] found that operators tend to wear personal protective equipment (e.g., coveralls and facemasks) less consistently when experiencing worse barn conditions and have more contact with pigs and that increase in cleaning activities results in more consistent use of coveralls and facemasks.

In the specific case of HEV, farmer knowledge is relatively low [20]. Given the HEV spreading on pig farms without specific clinical signs in pigs or financial losses, farmers' awareness of the problem may remain low, with subsequent low motivation to take steps towards disease control and prevention [21]. Regarding the farmer's professional environment, several studies have shown that veterinarians and farming advisors play a significant role in spreading information and motivating farmers to adopt improved management practices [22, 23].

4 Conclusions

In Abruzzo, a significant part of reared swine is hosted in specialized structures; however, family-run breeding sites are the most widespread even though they accommodate just a minority of the overall reared animals.

The monitoring of a representative fraction of specialized swine farming structures throughout the Region resulted in a 16.7% prevalence of HEV, mainly ascribable to three housing characteristics: the presence of wildlife in the surrounding of the site, the housing of animals on partly slatted floors with the solid floor on more than 50% of the area, and the adoption of the deep pit for manure removal.

Such results show that: a) even in specialized farming structures, there is a non-negligible viral circulation in the swine population; b) good farming practices represent the first countermeasure to control HEV circulation (i.e., application of biosafety procedures, rapid manure removal from the pens).

Motivating farmers to adopt best management practices in animal housing would result in improved protection of the operators from HEV infection during rearing and cleaning operations. Further studies are, however, needed to highlight potential

barriers and preferred motivators for the implementation of on-farm risk mitigation strategies.

Acknowledgements This work was supported by the Italian Ministry of Health (Ricerca Finalizzata 2018 call) with the funding of the project “*Improving understanding of autochthonous Hepatitis E transmission routes: a focus on foodborne and waterborne pathways*”.

The authors acknowledge Mr Alex Filisetti (CREA-IT) for the valuable work performed in slurry sampling procedures and sampling equipment assembly and maintenance.

The authors acknowledge Dr Lidia Orlandi and Dr Claudia Del Giudice for their technical assistance in sample preparation and analysis.

The authors gratefully acknowledge the kind support of Dr Lino Antonini, Dr Enzo De Febis, Dr Germano Di Corinto, Dr Franco Ruggeri, Dr Antonio Di Matteo, Dr Patrizia Liberale, Dr Pietro Di Taranto, Dr Mario Mazzetti, Dr Nicola Pisegna and Dr Claudio Schiavo, veterinarians of the NHS territorial units of Abruzzo, in farming sites identification and monitoring.







References

1. Ricci, A., Allende, A., Bolton, D., Chemaly, M., Davies, R., et al.: Public health risks associated with hepatitis E virus (HEV) as a food-borne pathogen. *EFSA J.* **15**(7), 4886 (2017)
2. World Health Organization. <https://apps.who.int/iris/handle/10665/70513>. Accessed 20 July 2022
3. Romanò, L., Paladini, S., Tagliacarne, C., Canuti, M., Bianchi, S., Zanetti, A.R.: Hepatitis E in Italy: a long-term prospective study. *J. Hepatol.* **54**, 34–40 (2011)
4. Mauceri, C., Grazia Clemente, M., Castiglia, P., Antonucci, R., Schwarz, K.B.: Hepatitis E in Italy: a silent presence. *J. Infect. Public Health* **11**(1), 1–8 (2018)
5. Spada, E., et al.: Prevalence and risk factors for hepatitis E virus infection in blood donors: a nationwide survey in Italy, 2017 to 2019. *Eurosurveillance* **27**(22) (2022). pii=2100516
6. Garbuglia, A.R., et al.: Hepatitis E outbreak in the central part of Italy sustained by multiple HEV genotype 3 strains. *Viruses* **13** (2021)
7. Fonti, N., Pacini, M.I., Forzan, M., Parisi, F., Periccili, M., Mazzei, M., Poli, A.: Molecular and pathological detection of hepatitis E virus in Roe Deer (*Capreolus capreolus*) and Fallow Deer (*Dama dama*) in central Italy. *Vet. Sci.* **9**(3), 100 (2022)
8. Montone, A.M.I., et al.: Occurrence of HEV-RNA in Italian regional pork and wild boar food products. *Food Environ. Virol.* **11**(4), 420–426 (2019)
9. De Sabato, L., et al.: Novel subtypes and unexpected heterogeneity of hepatitis E viral strains in wild boar captured in a small area in central Italy. *Transboundary Emerg. Dis.* (2022). in press
10. La Rosa, G., et al.: Hepatitis E Virus (Genotype 3) in slurry samples from swine farming activities in Italy. *Food Environ. Virol.* **9**, 219–229 (2017)
11. Wu, F., et al.: SARS-CoV-2 titers in wastewater are higher than expected from clinically confirmed cases. *Msystems* **5**(4), e00614–20 (2020)
12. Iaconelli, M., et al.: Nine-year nationwide environmental surveillance of Hepatitis E virus in urban wastewaters in Italy (2011–2019). *Int. J. Environ. Res. Public Health* **17**(6), 2059 (2020)
13. Kearney, M.W.: Cramer’s V. In: Allen M.R. (ed.) *Sage Encyclopedia of Communication Research Methods*. Sage, Thousand Oaks
14. The jamovi project (2021). jamovi. (Version 1.6) [Computer Software]. <https://www.jamovi.org>.
15. Fox, J., Weisberg, S.: *Car: Companion to Applied Regression*. [R package] (2020). <https://cran.r-project.org/package=car>.
16. Morey, R.D., Roudier, J.N.: *BayesF* (2018)

17. actor: Computation of Bayes Factors for Common Designs. [R package]. <https://cran.r-project.org/package=BayesFactor>.
18. Gunel, E., Dickey, J: Bayes factors for independence in contingency tables. *Biometrika* **61**, 545–557 (1974)
19. Treagus, S., Wright, C., Baker-Austin, C., Longdon, B., Lowther, J.: The foodborne transmission of hepatitis E virus to humans. *Food Environ. Virol.* **13**, 127–145 (2021)
20. Coffman, V.R., et al.: Personal protective equipment use during industrial hog operation work activities and acute lung function changes in a prospective worker cohort, North Carolina 2014–2015. *Am. J. Ind. Med.* **64**(8), 688–698 (2021)
21. Teixeira-Costa, C., Andraud, M., Rose, N., Salines, M.: Controlling hepatitis E virus in the pig production sector: assessment of the technical and behavioural feasibility of on-farm risk mitigation strategies. *Prev. Vet. Med.* **175**, 104866 (2020)
22. Alarcon, P., Wieland, B., Mateus, A.L.P., Dewberry, C.: Pig farmers' perceptions, attitudes, influences and management of information in the decision-making process for disease control. *Prev. Vet. Med.* **116**, 223–242 (2014)
23. Mahon, M.M., Sheehan, M.C., Kelleher, P.F., Johnson, A.J., Doyle, S.M: An assessment of Irish farmers' knowledge of the risk of spread of infection from animals to humans and their transmission prevention practices. *Epidemiol. Infect.* **145**, 2424–2435 (2017)

Enhancement of Mediterranean Greenhouses Facilities: Heat Power Pump Assessment for Bedding Plant Production by Coaxial Basal Heating



Sonia Cacini , Alessandro Orlandini, Gianluca Burchi, Maurizio Cutini , Massimo Brambilla , Carlo Bisaglia , Daniele Massa , and Marco Fedrizzi 

Abstract Protected horticulture is a highly energy-consuming sector where optimizing energy use and cost for heating facilities is strategic to achieve high environmental and economic sustainability. The paper main aim is to present the use of a heat pump (HP) for basal heating as an alternative technology to produce bedding plants. The experimental test was carried out by bedding plant production for the early spring market. The adopted greenhouse, located in Tuscany, Central Italy, consisted of a frame made of galvanized iron, roofing in polycarbonate slabs, and walls of polyethylene sheets with a fully automatized opening system equipped with twelve concrete benches.

The benches were isolated from the ground with polystyrene and a substrate of volcanic lapilli. Then eight benches were provided with a basal heating system based on four couples of coaxial pipes circulating warm water, while four were not heated. Cuttings of *Impatiens Walleriana* ‘Buddha F1 Carmine’ were transplanted in 1.2 L pots and subsequently grown by comparing basal heating of 16 °C with no basal heating conditions for a total of 960 potted plants. According to requirements, all the plants underwent the same agronomic care (fertigation and pest control). The microclimatic conditions and the energy consumption were acquired. The experimental results show that the heat pump ensures suitable thermal conditions for such cultivation in the winter period, confirming the possibility of using a conventional heat pump in horticulture as a simple installation in an existing Mediterranean greenhouse.

S. Cacini · A. Orlandini · G. Burchi · D. Massa
Council for Agricultural Research and Economics, CREA Research Centre for Vegetable and Ornamental Crops, Via Dei Fiori 8, 51017 Pescia, PT, Italy

M. Cutini (✉) · M. Brambilla · C. Bisaglia
Council for Agricultural Research and Economics, CREA Research Centre for Engineering and Agro-Food Processing, Via Milano 43, 24047 Treviglio, BG, Italy
e-mail: maurizio.cutini@crea.gov.it

M. Fedrizzi
Council for Agricultural Research and Economics, CREA Research Centre for Engineering and Agro-Food Processing, Via Della Pascolare 16, 00015 Monterotondo, Rome, Italy

Keywords Energy saving · efficiency · greenhouse · controlled environment · horticulture

1 Introduction

Energy to heat greenhouses represents a significant expenditure: in cold Countries, it represents the second-largest cost item after workforce [1]. Therefore, research proposed strategies such as structural design, the use of energy-efficient covers, improved heating and ventilation systems, indoor micro-climates management, and renewable energy sources usage following greenhouses' location. However, the balance between the agronomic needs of plants and the energy-saving potential of each heating technique requires attention as well [2]. Among the energy-saving potential that renewable and sustainable solutions (e.g., photovoltaic modules, solar thermal collectors, wood pellet, ...) also heat pumps (HP), have found interest for greenhouse systems, but only in the case of geothermal source heat pumps, integrated systems [3–5]. There are many reasons, mostly deriving from traditional design in building experiences, why HP hasn't found great interest in protected agriculture applications. In fact, conventional heat pumps have the best efficiency with a relatively low temperature of supply water that can't exceed 45–50 °C, so they are thought to be efficient only in the case of well-isolated structures, mainly associated with low-temperature heating systems such as floor heating. The authors carried out previous studies on basal heating and the use of HP in the root zone [6, 7]; in this case, the innovative aim is to verify the applicability of a commercial air-to-water heat pump to provide basal heating to pot culture.

2 Materials and Methods

2.1 *The Greenhouse and the Growing Benches*

The trial took place in a greenhouse of the CREA Research Centre for Horticulture and Floriculture (Pescia, Italy, 43°53'13" N, 10°41'18" E; degree day: 1.877). The greenhouse had a total surface area of 200 m², a ridge height of 3.50 m and it is North/East to South/West longitudinally oriented. It consisted of a frame made of galvanized iron, roofing in polycarbonate slabs and walls of polyethylene sheets equipped with a fully automatized opening system. It bordered open spaces to the North, South and West and with another greenhouse eastward. Inside the greenhouse were 12 regular prismatic concrete benches (0.70 m width × 3.6 length m × 0.21 m height, with 3 cm thickness polystyrene panels coating on the walls and on the bottom) placed on cement blocks that raised them 0.35 m above the soil level. Figure 1 shows the schematic layout of the experimental greenhouse. The setting phase included:



Fig. 1 Global layout of the experimental greenhouse



Fig. 2 Detail of the coaxial pipes positioning and plant layout

- The coating of the internal part of the benches with polystyrene sheets for thermal insulation.
- The placing volcanic lapilli on the polystyrene-based, between the heated and irrigation pipes.
- The positioning of the heat pump pipes (Fig. 2), used for basal heating, on top of the polystyrene lining. The pipes were placed in 8 of the 12 total benches (4 control benches).
- Preparation of two irrigation lines.

2.2 Design of the Experiment

The experimental plan foresaw the use of two heating systems for the experimental benches: a heat pump (HP) with the engine outside the greenhouse (as commonly installed); a heat pump with the engine inside another greenhouse; and a third

unheated bench (NH) as reference. In addition, a diesel burner with an air-to-air heat exchanger was installed which only had the emergency function to prevent the temperature from dropping below the set point by 4° C.

The layout foresaw 12 benches: each one with 80 pots. Each pot had 2 plants, for a total of 1920 plants. Each bench was divided into 4 sections to account for the replications of a completely randomized design.

According requirements, all plants underwent the same agronomic cares (fertigation and pest control). Growing media composition was coconut/perlite e peat/perlite with 70:30 as volume. The chosen crop for the experiment was a small leafy crop: *Impatiens Walleriana* CV Buddha F1 Carmine.

The population resulted as follows:

1. Heated (8 benches = 640 pots = 1280 plants)
 - a. HP Engine position
 - i. inside
 - ii. outside
 - b. growing media
 - i. coconut/perlite
 - ii. peat/perlite
2. Not heated (4 benches = 320 pots = 640 plants)
 - a. growing media
 - i. coconut/perlite
 - ii. peat/perlite

2.3 The Heating Systems

The adoption of two identical HPs is based on the hypothesis that an adjacent greenhouse could work as heat accumulation and improve the HP efficiency allowing energy saving. Figure 3 reports a detailed layout of the experimental greenhouse.

The HP basal heating system was an Airmec HSI 140CT (Airmec, Italy; Table 1).

The thermostat for managing HP systems, set at 15° C, had the temperature probe placed inside the canopy, just above the center of the hydraulic line.

2.4 Instruments

The acquired data were: the air humidity and temperature inside and outside the greenhouse; the temperature inside the pots; the temperature at the canopy, and the electric consumption of the HP (kWh).

The detail and the number of the sensors is reported in Table 2.

The temperature (in °C) and humidity (percentage relative humidity) were monitored with the instruments TESTO 175 T2 (substrate temperature and canopy) and

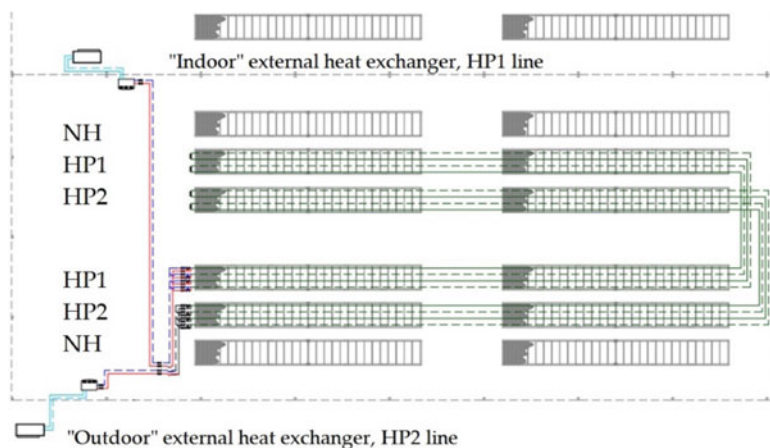


Fig. 3 Detailed layout of the experimental trial: in the left part the dashed and full lines represent the pipes used to heat the substrate

Table 1 Technical declared data of the heating systems

Heat pump		Airmec HSI 140CT
Maximum thermal power	kW	12.8
Maximum cooling capacity	kW	10.00
Maximum absorbed electrical power (external unit)	kW	5.2
Coefficient of performance (COP, radiators, external air $t = 7\text{ }^{\circ}\text{C}$, water in/out $t = 40/45\text{ }^{\circ}\text{C}$)		3.6

Table 2 Instruments

Brand/model	Unit	Position/purpose	n°
Testo 175 T1	Temperature	Growing media and canopy	12
Testo 175 T2	Temperature	Growing media and canopy	12
Testo 175 H1	Temp, Humidity	OAT, IAT	3
Orno OR-WE-505	Electricity consumption	HP	1

TESTO 175 T3 (temperature and humidity of the air), programmed to acquire data every 5 min. The consumption of diesel and energy was monitored with instruments directly present on the heating systems.

In total, 27 dataloggers were used: 24 distributed on the benches (2 for each bench), 2 positioned inside the greenhouses and 1 outside.

To investigate the effect of the different heating treatments, probes recorded internal greenhouse air and growing media temperatures. Growing media temperature monitoring was performed in each greenhouse area contemporarily using 24 Testo (Testo Spa, Italy) mod. 175 data loggers: 2 for each bench. Greenhouse temperature and relative humidity was monitored by installing a datalogger Testo mod. 175H1 at 2 m above ground level. The list of the adopted instruments is reported in Table 3.

2.5 Analysis and Data Processing

The experimental data underwent statistical processing with Minitab 17 statistical software [8] to calculate the descriptive statistics for each treatment (arithmetic mean \pm standard deviation). Data underwent analysis of variance (ANOVA) followed by post-hoc multiple comparisons (Tuckey HSD test – $p < 0.05$) to evaluate the statistically significant differences among the treatments.

3 Results

3.1 Environmental Temperatures

The main results regarding the environmental temperature conditions during the trial are reported in Table 3.

3.2 Canopy and Growing Media Temperatures

The main results regarding the temperature at the canopy for the different benches are reported in Table 4.

The main results regarding the temperature at the growing media for the different benches are reported in Table 5.

Table 3 Main temperatures of the experimental trial

Environment	Temperature (°C)		
	Mean	Daily minimum mean	Absolute minimum
External	13.0 \pm 5.2	6.9 \pm 3.3	0,5
Adjacent greenhouse	17.1 \pm 9.0	7.6 \pm 3.3	0.6
Experimental greenhouse	17.4 \pm 6.5	10.3 \pm 2.5	5.0

Table 4 Main temperatures at the crop's canopy

Benches	Temperature (°C)		
	Mean	Daily minimum mean	Absolute minimum
Not heated	16.7 ± 7.3	9.1 ± 2.8	2.6
HP1	17.9 ± 6.6	11.3 ± 2.8	3.6
HP2	17.6 ± 6.8	10.5 ± 2.6	4.5

Table 5 Main temperatures at the growing media

Benches	Temperature (°C)		
	Mean	Daily minimum mean	Absolute minimum
Not heated	15.4 ± 4.9	10.1 ± 2.6	3.3
HP1	17.9 ± 4.1	13.9 ± 2.8	4.6
HP2	17.9 ± 4.2	13.7 ± 2.7	6.3

Table 6 Harvested biomass statistical significance

Factor	PF-PG	PS-PG	PF-FL	PS-FL	PF-PA	PD-PA	PS-R
Heating	***	***	***	***	***	***	**
Grow media	ns	ns	ns	ns	ns	ns	ns
Heating x Grow media	ns	ns	ns	ns	ns	ns	ns

ns = not significant; asterisk = significance levels at 0.05 (*), 0.005 (**), or 0.001 (***)

3.3 Results of the Crop Harvest

The results regarding the harvested biomass are reported in Table 6. The analyzed parameters are: the fresh weight of the green part (PF-PG); the dry weight of the green part (PD-PG), the fresh weight of the flowers (PF-FL); the dry weight of the flowers (PD-FL), the total fresh weight of the aerial part (PF-PA), the total dry weight of the aerial part (PD-PA) and dry weight of the roots (PS-R).

3.4 Difference Between the HP Engine Position

The hypothesis that the adjacent greenhouse could work as an accumulation of heat to improve the efficiency of the heat pump has to be evaluated depending on the winter period. Indeed, on the coldest days, the HP with the engine in the adjacent greenhouse saved 20% of electricity. However, this saving is not completely clear because a higher temperature complying with the hypothesis was recorded only after

sunrise, in the first hours of the morning. For this reason, this result deserves further deepening in subsequent studies.

4 Discussion

This work focused on evaluating the thermal energy saving for leafy vegetable productions, characterized by reduced (small) canopies, in winter time.

The experiment compared two basal heating systems powered by an air-to-water heat pump with a not-heated bench. The HP heated benches resulted in higher productions than the not heated trial. Increasing soil/growing media temperature results in heat accumulation at the root zone level, which can be associated with increased yields [9]. These results confirm the possibility of using a conventional heat pump in agriculture as a simple installation in an existing greenhouse and their efficiency with respect to traditional heating systems [10]. In other layouts of cultivation or species, it shall be considered that underfloor or basal heating systems fed by moderate temperature (approximately 40 °C) engender a limitation on the heating output of the radiant system. Therefore, they may not cover all the heating requirements in cold periods, so they should be coupled to another heating system [11].

Funding This work was supported by the Italian Ministry of Agricultural, Food, Forestry and Tourism Policies, MIPAAFT) under the AGROENER project (D.D. n. 26329, 1 April 2016) - [http://agroener.crea.gov.it/](http://agroener.crea.gov.it)

References

1. Hemming, S., et al.: Innovations in greenhouse systems - energy conservation by system design, sensors and decision support systems. In: ISHS Acta Horticulturae 1170: International Symposium on New Technologies and Management for Greenhouses, GreenSys2015 (2015). <https://doi.org/10.17660/ActaHortic.2017.1170.1>
2. Paradiso, R., De Pascale S.: Effects of plant size, temperature, and light intensity on flowering of phalaenopsis hybrids in mediterranean greenhouses. *Sci. World J.* **2014**, 9 (2014). <https://doi.org/10.1155/2014/420807>
3. Fang, H., Yang, Q., Sun, J.: Application of ground-source heat pump and floor heating system to greenhouse heating in winter. *Trans. Chin. Soc. Agric. Eng.* (12) (2008). <https://doi.org/10.3969/j.issn.1002-6819.2008.12.030>
4. Anifantis, A.S., Colantoni, A., Pascuzzi, S., Santoro, F.: Photovoltaic and hydrogen plant integrated with a gas heat pump for greenhouse heating: a mathematical Study. *Sustainability* **10**, 378 (2018). <https://doi.org/10.3390/su10020378>
5. D'Arpa, S., Colangelo, G., Starace, G., Petrosillo, I., Bruno, D.E., Uricchio, V., Zurlini, G.: Heating requirements in greenhouse farming in southern Italy: evaluation of ground-source heat pump utilization compared to traditional heating systems 2016. *Energ. Effi.* **9**(5), 1065–1085 (2016). <https://doi.org/10.1007/s12053-015-9410-y>

6. Fedrizzi M., Cacini S., Burchi G.: Root zone heating optimization in ornamental plant production. In: Proceedings of IS on High Technology for Greenhouse Systems—GreenSys2009, *Acta Horticulturae*, pp. 389–395, no. 893 (2011). ISSN 0567–7572, ISHS 2011. <https://doi.org/10.17660/ActaHortic.2011.893.36>
7. Terrosi, C., Cacini, S., Burchi, G., Cutini, M., Brambilla, M., Bisaglia, C., Massa, D., Fedrizzi, M.: Evaluation of compressor heat pump for root zone heating as an alternative heating source for leafy vegetable cultivation. *Energies* **13**(3), 745 (2020). <https://doi.org/10.3390/en13030745>
8. Minitab: Minitab 17 statistical software. Minitab, State College (2010)
9. Elad, Y., et al.: Conditions influencing the development of sweet basil grey mould and cultural measures for disease management. *Crop Protect.* **64**, 67–77 (2014). <https://doi.org/10.1016/j.cropro.2014.06.006>
10. Fabrizio, E.: Energy reduction measures in agricultural greenhouses heating: envelope, systems and solar energy collection. *Energy Build.* **53**, 57–63 (2012). <https://doi.org/10.1016/j.enbuild.2012.07.003>
11. Goh, L.J., Othman, M.Y., Mat, S., Ruslan, H., Sopian, K.: Review of heat pump systems for drying application. *Renew. Sustain. Energy Rev.* **15**(9), 4788–4796 (2011). <https://doi.org/10.1016/j.rser.2011.07.072>

Drivers of Adoption of Sustainable Practices and Technologies for Soil Protection Among Vine-Growers in North-West Italy



Federica Caffaro , Eugenio De Gregorio , Giorgio Capello ,
Lucia Vigoroso , Giorgia Bagagiolo , Eugenio Cavallo ,
and Marcella Biddoccu 

Abstract The study aimed at investigating the drivers of adoption of good practices and technological innovations for soil protection in a group of vine-growers in the Piedmont region, Northwest Italy. Four focus groups have been conducted with 16 vinegrowers, to investigate: 1) perception of soil erosion and the role of the human factor in preventing/causing it, 2) adoption and intention to adopt good practices and technological innovations for soil protection and, 3) barriers and drivers for adoption. A questionnaire regarding vineyard management practices was also used to encourage the discussion. The results showed that soil erosion was perceived as a relevant issue by the majority of the participants. Wide use of machinery during vineyard plantation and management was acknowledged as affecting soil and water conservation. The adoption of sustainable practices and technological innovations appeared to be promoted by landscape protection, whereas tradition and habits were cited as barriers to adoption. To maximize the fit between farmers' needs and sustainable innovation, personal values and habitual processes should be targeted with awareness raising and education interventions. These interventions should be based on a participatory approach and the co-creation of tailor-made solutions to better support the transition toward a more sustainable farming paradigm.

Keywords Soil management · Mixed methods research · Sustainability · Vine-growers perception

F. Caffaro
Department of Education, Roma Tre University, Via del Castro Pretorio 20, 00185 Rome, Italy

E. De Gregorio
Link Campus University, Via del Casale Di San Pio V, 44, 00165 Rome, Italy

G. Capello · L. Vigoroso · G. Bagagiolo (✉) · E. Cavallo · M. Biddoccu
Institute of Sciences and Technologies for Sustainable Energy and Mobility (STEMS) of the
National Research Council of Italy (CNR), Strada Delle Cacce 73, 10135 Turin, Italy
e-mail: giorgia.bagagiolo@stems.cnr.it

1 Introduction

Over the last decades, there has been increasing attention toward ecosystem services (ES), which can be defined as “the direct and indirect contributions of ecosystems to human well-being” [1]. Regarding the agricultural compartment in general, on the one hand, previous research suggested that intensive agriculture and unsustainable practices have contributed to the loss of habitat and biodiversity, to the increase in soil erosion and nutrient runoff [2]. On the other hand, other studies showed that vineyard management practices that consider the presence of cover crops or natural vegetation positively impact ecosystem services and can help decrease runoff, sediment, and nutrient loss [3–7].

Management of the plantations, and in particular the orientation of the rows in relation to the slope lines of the field, is an additional measure able to limit the erosion phenomena. Practices adopted for vineyard management, including soil management, have an impact on both production (quality and quantity) and the environment. However, management decisions in tree crops such as orchards and vineyards are usually influenced not only by the area’s water availability and pedoclimatic conditions but also by the perception of benefits and drawbacks in adopting ES such as inter-row cover crops or natural grass cover.

Grass covering in vineyards has been comprised in the most relevant European policies for soil conservation, including the Standards of Good Agricultural and Environmental Condition (GAEC), established by Council Regulation No. 73/2009 (CEC, 2009). Grass covering measures have been supported also at a local level by Rural Development Programmes (RDPs) that are drawn up by Member States and regions addressing Common Agricultural Policy (CAP) EU priorities that include prevention of soil erosion and improvement of soil management. Concerning Italy and the Piedmont region, the measures envisaged during the 2007–2013 RDP for soil erosion prevention were essentially based on the grass covering of orchard and vineyard areas and involved more than 13,000 ha (15.4% of Piedmont’s agricultural area utilized for orchards and vineyards).

Spontaneous grass cover is nowadays widespread in Piedmont’s vineyards. However, its adoption is not always supported by awareness and knowledge about the effects on soil quality and its conservation. Soil erosion processes imply soil losses and soil degradation, nevertheless, vinegrowers are not always aware of what factors contribute to increase the risk of soil erosion and what techniques and management choices they can carry out to maintain healthy soil. In Piedmont, during recent years, the occurrence of very warm and dry vine-growing seasons led some vinegrowers to quit the adoption of permanent spontaneous grass cover. However, do they have adequate knowledge of what are the possible other choices and their advantages/disadvantages for both the crop and the soil, in relation to pedoclimatic conditions? The IN-GEST SOIL project [8] aims to reduce the soil erosion in hillslope vineyards in Piedmont, improving soil and vine quality through the introduction of improved best soil management practices.

Farmers' behavior has a significant impact on the environment, and this behavior is strongly influenced by their knowledge and perception of environmental issues and sustainable measures [9]. Many previous studies addressed soil conservation and degradation, but the points of view of vine-growers have not been frequently addressed. Particularly in Italy, little attention has been paid to farmers' perceptions of soil erosion and attitudes toward the adoption of soil conservation practices and technologies [10]. Understanding farmers' perceptions, intentions and needs could help in a better-suited implementation of measures for soil protection in vineyards. The present contribution reports the first results from the first phase of the IN-GEST SOIL project, in which the vinegrowers' perception of soil erosion risk, factors influencing it and possible solutions were investigated. The IN-GEST SOIL (Innovation in viticulture soil management through the adoption of good practices and tools to support field activities) project is funded within the frame of the EU EIP-AGRI Rural development 2014–2020 for Operational Groups programme, namely by the PSR Regione Piemonte 2014–2020, Misura 16.1. The main aim of INGEST-SOIL is the reduction of soil erosion in hillslope vineyards in Piedmont, Northwest Italy, by means of the introduction of three main innovations: 1) Improved best soil management practices, 2) Agro-meteorological monitoring, to improve water and soil management, 3) ICT tools for managing of monitored data and field observation to support the farmer in vineyard management and water-soil conservation. The Operational Group includes research institutions, vine farmers, vinegrowers and winemakers associations, SMEs dealing with ICT for agriculture and technical services for agriculture. In particular, the present study, carried out in the initial phase of the project, aimed at investigating the drivers of the adoption of good practices and technological innovations for soil protection in a group of vine-growers in the Piedmont region, Northwest of Italy.

2 Materials and Methods

2.1 Participants

Sixteen vinegrowers from the Piedmont region, Northwest Italy, took part in the study. Regarding their sociodemographic characteristics, all the involved participants were men, with a mean age of 48 years ($SD = 14.50$), and a mean of work experience in agriculture of 29.06 years ($SD = 17.49$). The participants were recruited by vinegrowers' associations: twenty-four vine-growers were contacted at first and then, those who were willing to take part in the study were contacted by telephone by the researchers to explain the aims of the study and collect their consent to participate.

2.2 *Instruments and Procedure*

Four online focus groups have been conducted in the spring of 2021 with the Microsoft Teams platform. Topics addressed in the focus groups were designed based on previous evidence [11–13] about the most critical factors involved in the adoption of soil conservation measures: the perception of soil erosion and the role of the human factor in preventing/causing it, adoption intention to adopt good practices and technological innovations for soil protection and, finally, barriers and drivers for adoption. Before each focus group, a questionnaire was emailed to the participants and the responses were then used to encourage discussion. The questionnaire assessed vineyard characteristics and management practices, and perceived causes of soil erosion. Based on [14], the procedure to be followed to design the focus groups, including invitations to participants and topics to be addressed and the questionnaires, were drafted and collected into a guidance document, to ensure consistency of responses across all the groups. The meetings were recorded and lasted about one hour each.

2.3 *Data Analysis*

Questionnaire responses were analyzed using descriptive statistics. The focus group transcripts were subjected to qualitative content analysis through a coding procedure for narrative themes [15]. Next, in each of the transcribed files, an attempt was made to identify emergent themes. In the tradition of the qualitative approach, a theme is important because it captures something significant about the data as it relates to the research questions [16]. We used ATLAS.ti software to perform computer-supported qualitative content analysis [17] to filter the structure of our transcripts and then code them. In the first step, major themes were identified through reading the transcripts. This led to the identification of the main content analysis categories (codes and code sets). Each segment featuring the above-described topics was (re)coded so as to detect, with greater precision, the specific theme around which the discourse of the participants was built; for each theme, the corresponding segment was identified and defined (coded). More dense segments (articulate, complex, polysemic) were coded with more than one code. The analysis procedure thus consisted of a sequence of steps from coding, that is, reading the transcripts of the responses, interpreting those responses and aggregating the topics of the responses into broader content areas, the themes. It involved working out concepts from the data, taking into account the theoretical dimensions underlying the data itself.

From the qualitative content analysis of the focus groups, 44 codes were identified and subsequently grouped into 6 themes. A detailed analysis of these themes answered the research questions. The themes were:

- good practice
- considerations on the problem of erosion

- methods and techniques of vineyard management
- obstacles to the implementation of the best erosion prevention solutions
- resources useful for implementing solutions
- geographic areas.

In this contribution, we examined in detail the obstacles and resources for the implementation of best practices. In addition to this, we tried to understand how much awareness the people who participated in the focus groups had of the problem of soil erosion and how willing they were to find innovative solutions.

3 Results

3.1 *Descriptive Statistics and Quantitative Data*

Concerning the vineyard characteristics, their size ranged between 4 and 56 hectares (mean = 17.44 ha, SD = 12.24) and the steep slopes ranged between 4 and 25% (mean = 16.23%). Concerning the vineyard management, in 9 cases vineyards had rows arranged along contour lines, 5 had rows along the slope, 1 had terraces and 1 was in a flat area; inter-rows were mainly managed with grass cover in every inter-row (adopted by 7 participants), followed by grass cover every two inter-rows (6 participants) and bare soil obtained by mechanical cultivation (3 participants).

Concerning the factors affecting soil erosion, climate change was perceived as the main cause, with a mean score of 3.25 (SD = 0.77), followed by soil management, topography and soil texture, with a mean score of 3.06 (SD = 0.85), 2.94 (SD = 0.85) and 2.68 (SD = 0.79) respectively.

Participants indicated “mechanical cultivation, resulting in bare soil in all inter-rows for the whole year” as the vineyard management technique that contributes most to the increase of soil erosion, whereas, “permanent grass cover in all inter-rows” was considered as the technique that contributes most to soil erosion reduction (Fig. 1).

3.2 *Thematic Maps and Qualitative Content Analysis*

As stated, we focused our attention on obstacles and resources for the implementation of preventive actions against soil erosion. Figure 2 shows the map of concepts connected to each other as causes or consequences of soil erosion, or as limits to the repair intervention. In the figure, the numbers corresponding to the letter G (Grounded) indicate the frequency of that code in the four focus groups. Based on this evidence, we note that according to the participants, climatic conditions, different types of tillage, and the use of tools/machines are the relevant obstacles in determining the difficulties in preventing soil erosion in the vineyards, as well as some cultural customs and practices.

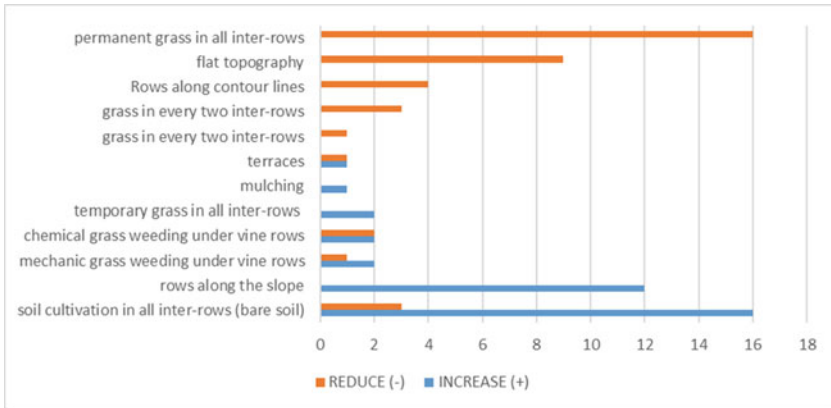


Fig. 1 Vineyard management techniques that contribute to increasing and reducing soil erosion

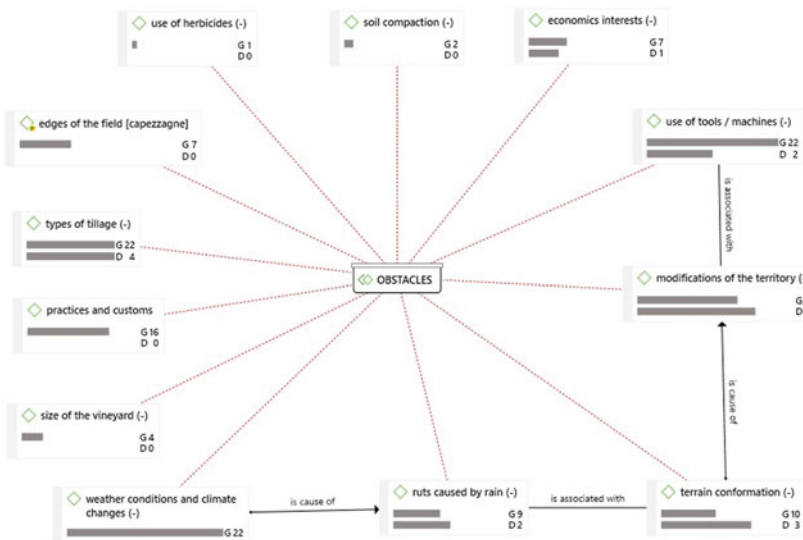


Fig. 2 Thematic map of obstacles and their links as detected by the narrative flow of the focus groups

Similarly, Fig. 3 shows the codes pertaining to the theme resources. Also, in this case, specific types of soil tillage are called into question, but with a meaning that characterizes them as resources, i.e., a useful procedure to prevent soil erosion.

Participants also suggested the use of some specific techniques or procedures. Among these, grassing was the one that characterized most of the debates in the four focus groups.

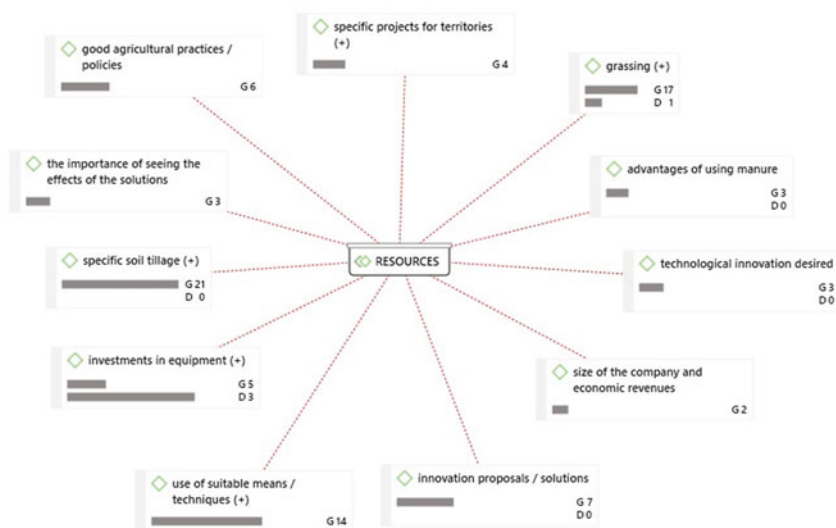


Fig. 3 Thematic map of resources and their links as detected by the narrative flow of the focus groups

It is evident that some concepts expressed by the participants can be used both as obstacles and as resources. We have seen that this is true for the types of tillage: if facilitated by agricultural machinery, it is a problem, but it can also be a resource when using traditional systems and benefiting from new technologies. We also considered that the contents expressed with respect to obstacles and resources were quite equivalent in terms of frequency. This gave us another type of information: the participants had a high awareness of the problem but also of the possible solutions.

As reported in Fig. 2, Traditions and cultural habits had a weight: this aspect was mentioned in 16 citations. Finally, we note that technological innovation (which in some cases is desired) did not find a broader consensus. We explain this data on the basis of two possible interpretations: the first is that some technological solutions are actually considered obstacles and not resources; the second possible interpretation, on the other hand, concerns solid roots in traditions.

4 Discussion and Conclusions

The present results showed that soil erosion was perceived as a relevant issue by most of the participants. Wide use of machinery during vineyard plantation and management was acknowledged as affecting soil and water conservation. The cost-benefit ratio appeared not to sufficiently capture the complexity of farmers' decision-making and behaviors, since the adoption of sustainable practices and technological innovations was more often related to place attachment and landscape protection.

Whereas tradition and habits appeared to play a role in hindering adoption. Some recommendations arise from the present study: to encourage the adoption of soil protection practices and technologies, access to economic support should be spread but it does not seem to be enough. Personal values and habitual processes emerged as critical variables that could be targeted with awareness-raising and education interventions. To maximize the fit between farmers' needs and sustainable innovation, these interventions should be based on a participatory approach and the co-creation of tailor-made solutions to better support the transition toward a more sustainable farming paradigm.

References

1. Sukhdev, P., et al.: The economics of ecosystems and bio-diversity: mainstreaming the economics of nature: a synthesis of the approach. *Concl. Recomm. TEEB* (333.95), E19 (2010)
2. Dunbar, M.B., Panagos, P., Montanarella, L.: European perspective of ecosystem services and related policies. *Integr. Environ. Assess. Manag.* **9**(2), 231–236 (2013)
3. Bagagiolo, G., Biddoccu, M., Rabino, D., Cavallo, E.: Effects of rows arrangement, soil management, and rainfall characteristics on water and soil losses in Italian sloping vineyards. *Environ. Res.* **166**, 690–704 (2018)
4. Ferreira, C.S.S., Keizer, J.J., Santos, L.M.B., Serpa, D., Silva, V., Cerqueira, M., Ferreira, A.J.D., Abrantes, N.: Runoff, sediment and nutrient exports from a Mediterranean vineyard under integrated production: an experiment at plot scale. *Agr. Ecosyst. Environ.* **256**, 184–193 (2018)
5. Gómez, J.A.: Sustainability using cover crops in Mediterranean tree crops, olives and vines—challenges and current knowledge. *Hung. Geog. Bull.* **66**(1), 13–28 (2017)
6. López-Vicente, M., Gómez, J.A., Guzmán, G., Calero, J., García-Ruiz, R.: The role of cover crops in the loss of protected and non-protected soil organic carbon fractions due to water erosion in a Mediterranean olive grove. *Soil Tillage Res.* **213**, 105119 (2021)
7. Winter, S., et al.: Effects of vegetation management intensity on biodiversity and ecosystem services in vineyards: a meta-analysis. *J. Appl. Ecol.* **55**(5), 2484–2495 (2018)
8. IN-GEST SOIL—Innovazione nella gestione dei suoli viticoli attraverso l'adozione di buone pratiche e strumenti di supporto alle attività di campo. <https://ec.europa.eu/eip/agriculture/en/find-connect/projects/gest-soil-innovazione-nella-gestione-dei-suoli>
9. Guo, R., Li, Y., Shang, L., Feng, C., Wang, X.: Local farmer's perception and adaptive behavior toward climate change. *J. Clean. Prod.* **287**, 125332 (2021)
10. Bechini, L., Costamagna, C., Zavattaro, L., Grignani, C., Bijttebier, J., Ruyschaert, G.: Drivers and barriers to adopt best management practices. survey among Italian dairy farmers. *J. Clean. Prod.* **245**, 118825 (2020)
11. Prosdocimi, M., Cerdà, A., Tarolli, P.: Soil water erosion on Mediterranean vineyards: a review. *Catena* **141**, 1–21 (2016)
12. Gómez, J.A., Montero, A.S., Guzmán, G., Soriano, M.A.: In-depth analysis of soil management and farmers' perceptions of related risks in two olive grove areas in southern Spain. *Int. Soil Water Conserv. Res.* **9**, 461–473 (2021)
13. Marques, M.J., Bienes, R., Cuadrado, J., Ruiz-Colmenero, M., Barbero-Sierra, C., Velasco, A.: Analysing perceptions attitudes and responses of winegrowers about sustainable land management in central Spain. *L. Degrad. Dev.* **26**, 458–467 (2015)
14. Daniels, N., Gillen, P., Casson, K., Wilson, I.: STEER: factors to consider when designing online focus groups using audiovisual technology in health research. *Int. J. Qual. Methods* **18** (2019)

15. Ryan, G.W., Bernard, H.R.: Techniques to identify themes. *field. Methods* **15**(1), 85–109 (2003)
16. Braun, V., Clarke, V.: *Thematic Analysis A Practical Guide*. Sage, London (2021)
17. Friese, S.: *Qualitative data analysis with ATLAS.ti*, 3rd edn. Sage, London (2019)

The Direct Costs for Cover Crops Cultivation: Comparison Between Different Agronomical Practices



Aldo Calcante , Daniele Manenti , and Roberto Oberti 

Abstract As it is known, cover crops are plants that cover the soil between the harvest of the main crop and the seeding of the later. They are herbaceous species that are not cultivated for their commercial value, but to obtain agronomical and environmental benefits. These species are inserted in the production processes with the primary aim to maintain soil covered by vegetation in periods when the same soil would remain lacking in every cultivation, and therefore subject to damaging effect from pedological point of view. The limits of cover crops are due to their nature. Indeed, since they are crops which do not have a commercial value, the most significant aspect is related to their production costs therefore the incidence of costs for the purchase of seed, for seeding and for the termination must be limited.

The goal of this study is to experimentally evaluate and analyze in details the fuel consumption, the main operative parameters (i.e. workability and hours necessary to carry out every single mechanized activity per hectare) and costs per unit of area for fuel, labor and agrochemical required for the cover crops cultivation, as a function of different agronomical practices applied. In particular, the study takes into account the following agronomical practices: 1) conventional tillage, 2) minimum tillage, 3) direct seeding and 4) no-tillage and, to destroy cover crop, the mechanical and the chemical termination.

Keywords Cover Crops · Mechanization Costs · Tillage · Termination

1 Introduction

Cover crops are plants that cover the soil between the harvest of the main crop and the seeding of the later. They are herbaceous species which are not considered “cash crops” since are not cultivated for their commercial value, but to obtain agronomical

A. Calcante (✉) · D. Manenti · R. Oberti

Department of Agricultural and Environmental Sciences, Università Degli Studi di Milano, Milan, Italy

e-mail: aldo.calcante@unimi.it

and environmental benefits. These species are inserted in the production processes with the primary aim to maintain soil covered by vegetation in periods when the same soil would remain lacking in every cultivation, and therefore subject to damaging effect from pedological point of view [1].

The introduction of a cover crop allows protecting soil from wind and rain erosion [2]. Root systems of cover crops carry out a real soil tillage airing it and contributing to improvement the soil structure [3]. Cover crops can increase water infiltration and retention and have an important role in controlling weeds [4].

Cover crops allow to increase the organic matter content of the soil since the vegetal biomass is not removed, but is bury [5], and are capable to retain nitrogen both present in zotechnical effluents. This reduces the nitrates losses up to 90% [1, 6]. Finally, the leguminous used as cover crops, thanks to symbiosis with nitrogen fixing bacteria, fixing atmospheric nitrogen converting it into organic nitrogen thus enriching the soil [7]. The limits of cover crops are due to their nature. Indeed, since they are crops which do not have a commercial value, the most significant aspect is related to their production costs [8]. Another limit is related to the achievement of the expected results that, often, are particularly uncertain [9].

The introduction of cover crops in farm production systems needs careful planning related to the mechanized operations, especially from the economical point of view, looking for the solution that minimize the production costs whenever it is possible. In this perspective, the agricultural techniques to cultivate cover crops can be of type conventional or conservative.

The techniques usually applied are: i) conventional tillage; ii) minimum tillage; iii) direct seeding; iv) no-tillage.

The peculiar aspect of cover crops is that, at the end of their growth, they must be terminated to allow the cash crop seeding. The termination by the cold is an effective method for those species so called “frost-sensitive” (e.g. white mustard). These categories of plants are devitalized as a result of a proper frost period in terms of duration and intensity. The chemical termination involves the use of non-selective herbicides (e.g. glyphosate) distributed on field using sprayer. Alternatively, cover crops can be destroyed with one or more mechanical operations. In this case, it can be possible to achieve two different results: 1) the vegetal biomass is buried into the ground and 2) the vegetal biomass remains on the field surface.

In the first case, in the context of conventional tillage, termination is carried out by means of ploughing. Conversely, in a context of conservative agriculture, operating machines equipped with anchors tools are used in case of low amount of vegetal biomass whilst, in case of abundant biomass, disks tools are preferred. In the second case, vegetal biomass remains on the field surface creating a mulch layer. To do this, the most used operations are the mowing and the chopping. A recent method of cover crop termination is the rolling by means of crimper rollers that crushes and creases plant stems so that growth is terminated [9].

The scientific literature is poor of studies related to mechanization cost analysis for cover crops cultivation. For this, the goal of the present study is to experimentally evaluate and analyze in details the fuel consumption, the main operative parameters (i.e. workability and hours necessary to carry out every single mechanized activity

per hectare) and costs per unit of area for fuel, labor and agrochemical required for the cover crops cultivation, as a function of different agronomical practices applied.

2 Materials and Methods

The present study was conducted in four farms located in Brescia Province (Northern Italy) that have introduced the cover crops in their farm production systems from several years. Every farm is characterized by the use of different agricultural practice both for tillage (conventional tillage, minimum tillage, direct seeding and no-tillage) and for termination (chemical and mechanical). The four farms have similar size (ave. 55 ± 11 ha) and the soils are deep, medium textured with presence of skeleton.

Table 1 shows the main technical parameters of equipment used for every considered agronomical practice.

The conventional tillage followed by Farm A included one 4 WD tractors coupled with a 4-share plough (Drt = 1.8 m); the same tractor was later coupled with a combine seed drill which, at the same time, prepared the seedbed using a 3 m rotary harrow. The cultivated cover crop was *Secale cereale* L. and the seeding rate was 130 kg/ha.

Table 1 Main technical parameters of the equipment and tractors used by the four farms

Farm	Agronomical Practice	Operation	4WD Tractor (Pn, kW)	Typology of Operating Machine	Drt (m)
A	Conventional tillage	Ploughing	110	4-share plough	1.8
		Harrowing + seeding	110	Rotary harrow + seed drill	3.0
	Termination	Mechanical	97	Crimper roller	3.0
B	Minimum tillage	Harrowing	118	Combined chisel with disk harrow and packer roller	3.0
		Seeding	88	Mechanical seed drill	3.0
	Termination	Chemical	68	Sprayer	12.0
C	Direct seeding	Seeding	110	Combined seed drill	3.0
	Termination	Mechanical	125	Coulter chisel with disk harrow and packer roller	3.0
D	No-tillage	Seeding	97	No-till seed drill	3.0
	Termination	Mechanical	118	Disk harrow with packer roller	3.0

Abbreviations: Pn: engine rated power; Drt: Theoretical working width.

Farm B has applied the minimum tillage using a 3 m combined chisel with disk harrow and packer roller coupled with a 118 kW 4WD tractor to create the seedbed. The seeding was carried out by a 3 m mechanical seed drill, and the cultivated cover crop was *Secale cereale* L. (seeding rate: 130 kg/ha).

Farm C used a combined seed drill (3.0 m disk harrow with mechanical seeder) coupled with a 110 kW 4WD tractor. In this case, the cover crop was tillage radish and the seeding rate was 6 kg/ha.

Finally, to carry out the no-tillage practice, Farm D used a no till-drill with Drt of 3 m, and the cover crop was *Sinapis alba* L. seeded with a seeding rate of 15 kg/ha.

The farms have used different type of termination, according to the typology of cultivated cover crop. Farms A and B have used mechanical termination carried out by a 3 m crimper roller and chemical termination carried out by a 12 m sprayer (distributed herbicide: glyphosate, with rate = 1.8 kg/ha) respectively. Farm C have used a 3 m coulter chisel with disk harrow and packer roller, whilst farm D has employed a 3 m disk harrow with roller.

All the agricultural machines (tractors and operating machines) were owned by the analyzed farms and they were consistent, from the operative point of view (i.e. engine power and working width), with the farm size.

Finally, it should be noted that every equipment used for the cultivation of cover crops (except crimper roller) is primarily used to allow the cultivation of the cash crops, that are the actual sources of income for the considered farms. So, in this study, the mechanization ownership costs were non considered because they are already included in the farm production costs; only the direct costs due to the cover crops cultivation were analyzed.

In order to calculate working time, main operative parameters and fuel consumption of every mechanized operation carried out by the single farm for cover crops cultivation, a field monitoring has been performed. The field observations have considered whole regular fields, or parts of them, with size between 5 and 22 ha, so that measured parameters were actually representative of mechanized operations performed and were possible to correctly compare obtained results.

The experimental protocol provided data recording related to: working depth (cm), working width (m), total work time (h), fuel consumption (L), cultivated area (ha). Working depth and working width were measured through a tape measure. About total work time, for every operation starting time and end time have been measured thanks to a digital chronometer and data recorded in a tablet. This allowed to obtain the total length of every mechanized activity, including turning times and any interruption during the work phase (i.e. refilling sprayer's tank).

Concerning the fuel consumption, after each operation, the volume of diesel consumed was measured by refilling the fuel tank of the tractor by using a graduated transparent container, and per hectare fuel consumption (kg/ha) was computed by using Eq. (1), [10]:

$$\text{Fuel consumption} = \rho_{\text{diesel}} \cdot x / A$$

where:

ρ_{diesel} = diesel density (0.835 kg/dm³)

x = volume of diesel consumed for each operation (dm³).

A = area processed by the equipment (ha).

For every agronomical practice and termination, cultivated areas were measured through a single frequency GPS receiver with decimetric precision (Mobile Mapper Pro, Thales, Cannes, France). Later, by using a GIS software (QGIS 3.10.2, Creative Commons, Mountain View, USA), it has been possible to obtain digital maps and to calculate the field sizes cultivated by each farm.

For every mechanized activity, the effective field capacity (C_a , ha/h), that is the actual rate of land processed per time unit has been calculated through Eq. (2), [11]:

$$C_a = A / wt$$

where:

A = area processed by the equipment (ha);

wt = total work time measured using the digital chronometer (h).

All data acquired during the field monitoring have been managed and elaborated using Microsoft Excel 2016 spreadsheet (Microsoft, Redmond, USA).

Finally, in order to compute the costs related to diesel, labor and herbicide (this latter used only for chemical termination) per unit of area (1 hectare), a price of 0.95 €/kg for diesel, 20 €/h for labor and 5 €/kg for herbicide were considered. The herbicide rate applied by farm B was 1.8 kg/ha.

3 Results and Discussion

Table 2 shows the fuel consumption and the working time of the various agricultural operations starting from data recorded during the field activities. In order to compare the different agricultural practices, the obtained parameters have been expressed per unit of area (1 hectare).

Note that the higher values of fuel consumption per 1 hectare of area were observed for farm A, that follows the conventional tillage practice. In this case, the ploughing and the seedbed preparation with contextual seeding required 19.8 kg/ha and 9.5 kg/ha of fuel respectively, for a total fuel consumption of 29.3 kg/ha. The minimum tillage, applied by Farm B, required 9.8 kg/ha of fuel for harrowing and 7.2 kg/ha for seeding, for a total fuel consumption of 17.0 kg/ha (less than 42% in comparison with conventional practice). Direct seeding (Farm C) required 6.9 kg/ha of fuel, whilst no-tillage required 8.4 kg/ha of diesel per 1 hectare of area. Compared to the conventional tillage, the saving amount to 76.4% and 71% respectively. Also, in respect of minimum tillage, direct seeding and no-tillage allow to obtain significant savings (−59.4% and −50%) confirming them as the less demanding agricultural practices from fuel consumption point of view.

Results confirmed that the reduction of the tillage intensity implies a significant reduction of fuel consumption, according to [10]. The same Table shows the fuel

Table 2 Effective field capacity, fuel consumption and work time for 1 hectare area measured during field operations

Farm	Agronomical Practice	Operation	C _a (ha/h)	Fuel consumption (kg/ha)	Work time per 1 ha area (h/ha)
A	Conventional tillage	Ploughing	0.95	19.8	1.05
		Harrowing + seeding	1.86	9.5	0.54
	Termination	Mechanical	3.10	2.6	0.32
B	Minimum tillage	Harrowing	1.93	9.8	0.52
		Seeding	2.20	7.2	0.45
	Termination	Chemical	6.48	1.2	0.15
C	Direct seeding	Seeding	2.43	6.9	0.41
	Termination	Mechanical	1.64	22.5	0.58
D	No-tillage	Seeding	1.71	8.4	0.59
	Termination	Mechanical	2.68	7.3	0.37

consumption related to chemical and mechanical termination. It is possible to note that chemical termination (Farm B) involves fuel consumption per hectare significantly lower than the use of coulter chisel with disk harrow and packer roller (Farm C, -94.7%), disk harrow equipped with packer roller (Farm D, -83.6%) and crimper roller (Farm A, -53.8%). This result is ascribable both to the larger surface area managed by sprayer per unit of time ($C_a = 6.48$ ha/h) because of its high working width (12 m) with respect the others operating machines, and the low energy required to distribute herbicide [12]. The crimper roller is an interesting solution, because its fuel consumption is low (2.6 kg/ha) due to the less energy required for termination [13] in comparison with termination by tillage, and the C_a is, however, remarkable (3.10 ha/h). Its limit is due to the fact that this operating machine can be used on a limited number of cover crops and, above all, in order to obtain the best effects of termination, the operation must be carried out at the correct phenological stage of plants [14].

Figure 1 left shows the direct costs to cultivate cover crops related to the four considered farms. Concerning the soil tillage and the seeding, the agricultural practice most expensive is the conventional tillage (27.8 €/ha of fuel costs and 31.9 €/ha of labor costs), followed by minimum tillage (16.2 €/ha of fuel costs and 19.4 €/ha of labor costs), no-tillage (6.8 €/ha of fuel costs and 11.7 €/ha of labor costs) and direct seeding (6.5 €/ha of fuel costs and 8.2 €/ha of labor costs). Bergtold et al. [15] reported seeding costs equal to 17.70 \$/ac (40 €/ha) for a mechanical seeding of different type of cover crops (hairy vetch, crimson clover, rye, oats). This value, although of the same order of magnitude, includes charges for machinery, power, fuel, and labor and so it is not fully comparable with our data, that are related only to fuel and labor costs excluding the ownership costs of agricultural machines. In our study, direct seeding is the most convenient agricultural practice because allows a saving of -75.4% with respect conventional tillage, -58.7 with respect minimum

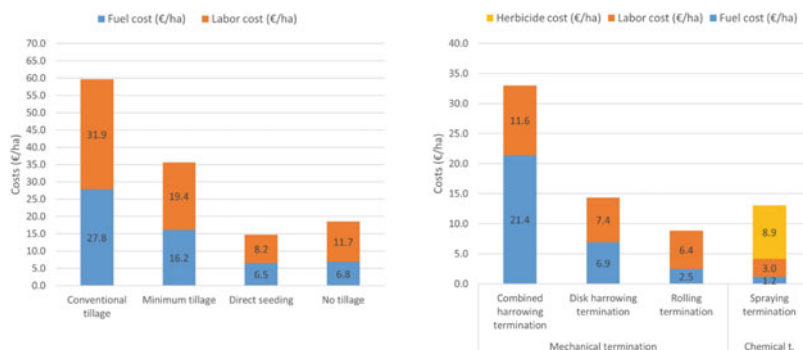


Fig. 1 Direct costs of the considered agricultural practices and the different typologies of termination

tillage and -20.5% with respect no-tillage that, in any case, represents an efficient alternative compared to conventional and minimum tillage. Figure 1 right shows direct costs related to cover crops termination. Also in this case, the operations that carrying out a soil tillage in order to terminate the cover crop are the most expensive in terms both of fuel costs and of labor costs. From the mechanical point of view, the spraying termination is the most convenient techniques, with savings of -87.3% with respect combined harrowing termination, -70.6% with respect disk harrowing termination and 52.8% with respect rolling termination. This is in accord with those reported by [13]. However, if cost of herbicide is considered, the cost of spraying termination is equal to 13.1 €/ha , 32% in more than rolling termination.

4 Conclusion

Much has been written about the benefits of cover crops about sustainability, fertility, impact on the cash crops, on the reduction on negative externalities such as soil erosion or chemical runoff, etc. By contrary, the scientific literature is poor of studies related to mechanization cost analysis for cover crops cultivation. The present study focused on the calculation of direct costs (fuel and labor) and working time necessary to cultivate cover crops according to four different agronomical practices and termination techniques. The results suggest that the most convenient and timely techniques are direct seeding and no-tillage. About cover crop destruction, results demonstrate, in absolute terms, that chemical termination is the timeliest operation (0.15 h/ha of working time), but is not the most cost-effective choice since, to direct costs, must be add the cost of the herbicide. The more convenient termination is that carried out using crimper rolling (8.9 €/ha), but this technique is only apply to a small number of cover crops with a specific phenological stage. Overall, the chemical termination appears as the more reliable option for economy, timely and efficacy; its limits are due to the environmental impact of agrochemicals and the risk of not obtaining, by

public institutions, the incentive to cultivate cover crops in case of adoption of this technique.

References

1. Justes, E.: *Cover Crops for Sustainable Farming*. Springer, Dordrecht (2017). <https://doi.org/10.1007/978-94-024-0986-4>
2. Kaspar, T.C., Radke, J.K., Laflen, J.M.: Small grain cover crops and wheel traffic effects on infiltration, runoff, and erosion. *J. Soil Water Conserv.* **56**(2), 160–164 (2001)
3. Restovich, S.B., Andriulo, A.E., Armas-Herrera, C.M., Beribe, M.J., Portela, S.I.: Combining cover crops and low nitrogen fertilization improves soil supporting functions. *Plant Soil* **442**(1–2), 401–417 (2019)
4. Shrestha, A., Knezevic, S.Z., Roy, R.C., Ball-Coelho, B.R., Swanton, C.J.: Effect of tillage, cover crop and crop rotation on the composition of weed flora in a sandy soil. *Weed Res.* **42**(1), 76–87 (2002)
5. Wulanningtyas, H.S., Gong, Y., Li, P., Sakagami, N., Nishiwaki, J., Komatsuzaki, M.: A cover crop and no-tillage system for enhancing soil health by increasing soil organic matter in soybean cultivation. *Soil Tillage Res.* **205**, 1–14 (2021)
6. Tonitto, C., David, M.B., Drinkwater, L.E.: Replacing bare fallows with cover crops in fertilizer-intensive cropping systems: a meta-analysis of crop yield and N dynamics. *Agr. Ecosyst. Environ.* **112**(1), 58–72 (2006)
7. Ding, G., Liu, X., Herbert, S., Novak, J., Amarasiriwardena, D., Xing, B.: Effect of cover crop management on soil organic matter. *Geoderma* **130**(3–4), 229–239 (2006)
8. Cai, Z., Udawatta, R.P., Gantzer, C.J., Jose, S., Godsey, L., Cartwright, L.: Economic impacts of cover crops for a Missouri wheat–corn–soybean rotation. *Agriculture* **9**(4), 1–13 (2019)
9. Bechini, L., Cabassi, G., Cavalli, D., Corti, M.: Impiego delle cover crop nella coltivazione del mais. AGF S.p.A., San Giuliano Milanese (2019)
10. Calcante, A., Oberti, R.: A technical-economic comparison between conventional tillage and conservative techniques in paddy-rice production practice in Northern Italy. *Agronomy* **9**, 1–14 (2019)
11. Tona, E., Calcante, A., Oberti, R.: The profitability of precision spraying on specialty crops: a technical–economic analysis of protection equipment at increasing technological levels. *Precision Agric.* **19**, 606–629 (2018)
12. Kornecki, T.S., Price, A.J., Raper, R.L.: Performance of different roller designs in terminating rye cover crop and reducing vibration. *Appl. Eng. Agric.* **22**, 633–641 (2006)
13. Goddard, T., Zoebisch M., Gan Y., Ellis W., Watson A., Sombatpanit S.: No-Till farming systems, special publication No. 3. In: World Association of Soil and Water Conservation. Funny Publishing, Bangkok (2008)
14. Ashford, D., Reeves, D.W.: Use of mechanical roller-crimper as an alternative kill method for cover crops. *Am. J. Altern. Agric.* **18**(1), 37–45 (2003)
15. Bergtold, J.S., Ramsey, M., Maddy, L., Williams, J.R.: A review of economic considerations for cover crops as a conservation practice. *Renew. Agric. Food Syst.* **34**(1), 62–76 (2019)

Development and Experimental Evaluation of a Tractor Roll-Over Stability Model



Giovanni Carabin , Lorenzo Becce , and Fabrizio Mazzetto 

Abstract The roll-over stability is one of the main issues that affects agricultural tractors/machinery, and earth-moving machines operating in hilly or mountainous environments. Indeed, on average, it causes more than 100 fatal accidents every year in Italy due to tractor roll-overs. In the best cases, when operators are not or only minimally injured, they cause considerable damage to the vehicles as well as the loss of income from missed work. Creating stability models to study the behaviour of existing vehicles operating in hazardous conditions results very important in the designing phase as well as they can then be integrated into the vehicles control systems. In this work the results of a model for determining the stability of an agricultural vehicle moving on slope terrain is compared and validated through a series of experimental test. They have been accomplished exploiting an innovative rig for testing the stability of vehicles available at the Agro-Forestry Innovation LABORatory (AFILAB) of the Free University of Bolzano.

Keywords Stability model · machinery stability · roll-over stability · static stability test · stability on sloping terrains

1 Introduction

One of the main issues that affects agricultural tractors/machinery, and earthmoving machines operating in hilly or mountainous environments is the roll-over stability. Indeed, on average, it causes around 110–140 fatal accidents every year in Italy [1]. In the best cases, when operators are not or only minimally injured, they cause considerable damage to the vehicles as well as the loss of income from missed work [2]. Therefore, creating stability models to study the behaviour of existing

G. Carabin (✉) · F. Mazzetto

Faculty of Science and Technology, Free University of Bozen-Bolzano, Bolzano, Italy
e-mail: giovanni.carabin@unibz.it

L. Becce · F. Mazzetto

Competence Centre for Plant Health, Free University of Bozen-Bolzano, Bolzano, Italy

© The Author(s), under exclusive license to Springer Nature Switzerland AG 2023
V. Ferro et al. (eds.), *AIIA 2022: Biosystems Engineering Towards the Green Deal*,
Lecture Notes in Civil Engineering 337,
https://doi.org/10.1007/978-3-031-30329-6_44

vehicles operating in hazardous conditions results very important, especially if they are designed to work on flat surfaces. These models can then be integrated into the vehicles control systems in order to warning the operator when instability is approaching, or to implement automatic countermeasures to prevent it [3, 4]. In the literature many works are related to the lateral roll-over stability, which represents the most critical problem [5–8]. Further works consider the study of stability for any orientation of the tractor to determine different machine operation conditions [2, 3, 9, 10] Generally, with some exceptions [7], these works are based on the definition of a model of the phenomena, which is then used to study the stability under different conditions. Typically, they focus on a specific tractor/platform configuration (e.g., tracked, 4-wheeled, rigid body, articulated-body, etc.). However, these works are often not accompanied by experimental validations, as it is complex to perform such tests due to the difficulty and cost of the necessary equipment.

In this work a basic model for determine the stability of a common agricultural vehicle configuration, i.e., rigid body and front pivoting axle, is considered. It is developed in Matlab environment, and it is based on the identification of the contact forces between wheels and ground. The approach can be adapted to different vehicle configurations such as conventional tractor, tractor with isodiametric wheels, tracked tractor, vehicles with rigid or articulated chassis, presence or not of implements, etc. Moreover, a multitude of slope conditions can be studied, evaluating for example the most common static lateral roll-over, or the helical motion of leaving a crop row and entering in the next one. In particular this work focuses on the roll-over stability problem. The model and the calculated results have been validated through a series of rollover experimental tests performed on a real. For this scope, a test-rig for evaluating the stability of vehicles developed in collaboration with De Pretto Industrie S.r.l. and available at the Agro-Forestry Innovation LABORatory (AFILAB) of the Free University of Bolzano has been exploited.

2 Materials and Methods

2.1 Rollover Stability Model

In this work a New Holland TN75V tractor has been considered. This is a common tractor frequently used in orchards due to its compact dimensions and in particular its narrow width compatible with orchard rows. It has 4 wheels drive transmission with a pivoting front axle. In order to study and simulate the behaviour of the tractor a simplified model of its kinematics has been developed based on the work of Previati et al. [9]. The kinematic model is based on the following hypothesis: (1) the tyre-terrain contact force has direction according to the action of gravity, (2) the tyre-terrain contact area is considered as a point located in the middle of tyre width, (3) the front axle is symmetric and (4) the front pivoting axle is friction-less.

With reference to Fig. 1 and Table 1, the normal components of the reaction forces acting on the tyres can be computed considering the momentum equilibrium around the axis r_1 of the front and rear part separately, and axis r_2 and r_3 . This corresponds to solve the following system of equations:

$$\begin{cases} \text{eq. } r_1 \text{ front : } (F_{FL,z} - F_{FR,z})\frac{ft}{2} + (F_{FL,y} - F_{FR,y})hf = 0 \\ \text{eq. } r_1 \text{ rear : } (F_{RL,z} - F_{RR,z})\frac{rt}{2} + (F_{RL,y} - F_{RR,y})hf + \\ \quad -mg_y(CoG_z - hf) + mg_zCoG_y = 0 \\ \text{eq. } r_2 \quad (F_{RL,z} - F_{RR,z})wb + mg_xCoG_z + mg_z(wb - CoG) = 0 \\ \text{eq. } r_3 \quad -(F_{FL,z} - F_{FR,z})wb + mg_xCoG_z - mg_zCoG_x = 0 \end{cases} \quad (1)$$

where $F_{i,j}$ is the component j of the contact force of the i -th wheel (i.e., FL - front left, FR - front right, RL - rear left, RR - rear right), wb is the wheelbase, ft the front track, rt the rear track, hf the front axle height, hr the rear axle height, m the tractor mass and CoG the position of the centre of gravity. Finally, g_x , g_y and g_z are the component of the gravity vector referred to the tractor reference system, that can be expressed in function of angles α and β as:

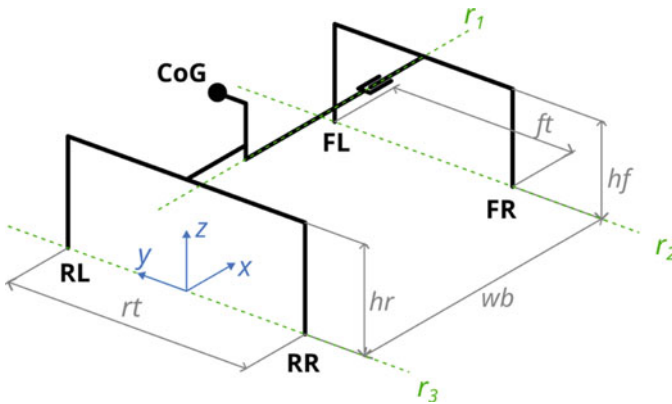


Fig. 1 Rigid model of a farm tractor with pivoting front axle

Table 1 New Holland NH-TN75V parameters

Mass	m	[kg]	2540
Wheelbase	wb	[m]	2.060
Rear axle height	hr	[m]	0.555
Front axle height	hf	[m]	0.360
Rear track	rt	[m]	0.860
Front track	ft	[m]	0.850

$$\mathbf{g} = (g_x, g_y, g_z) = g(-\sin \alpha \cos \beta, \sin \alpha \sin \beta, \cos \alpha) \quad (2)$$

where substituting Eq. (2) into system (1) and solving for the force components, a close solution can be determined. Here it is not reported for lack of space.

2.2 Stability Test-Rig

The experimental campaign has been conducted on a New Holland TN75V tractor exploiting the stability test-rig developed in collaboration with De Pretto Industrie S.r.l. and available at the Agro-Forestry Innovation LABORatory (AFILAB) of the Free University of Bolzano [11] and visible in Fig. 2a. It consists in a rotating platform, with a usable surface of $6.42 \times 4.46 \text{ m}$, capable of moving and orientate in a quasi-static way a machine positioned on it (up to a weight of 10 tons). The degrees of freedom are two rotations (Fig. 2b): (1) support plane tilting (angle α) and (2) support plane rotation around an axis normal to its surface (angle β). Moreover, the support plane can change its conformation by lowering and/or rising one or more of its four plates (Fig. 2c). In this way, uneven terrains with the presence of bumps or potholes can be simulated. A series of load cells, integrated into each of the support plane plate, measure in real-time the contact forces between wheels/tracks and the ground. The plates are covered with special metal grids fitted with a series of small reliefs (Fig. 2d). These fit into the tire rubber so as to prevent, or at least limit, the machine from sliding on steep slopes. For safety reasons, the machine is still anchored with a series of chains which are kept loose so as not to interfere with the measurement (e.g., they must allow the wheel to detach from the ground). By combining the different possible motions of the platform, different kind of test can be realized and certified on a machine, such as the rollover stability determination, the localization of the gravity centre, the study of the behaviour of a tractor passing through a hole or over an obstacle, the influence of implements over stability, etc.

2.3 Experimental Test

In this work, the lateral roll-over stability test has been considered. It consists in driving the platform so that the tractor rotates around its longitudinal axis (i.e., it tilts to one side) until it becomes unstable as one or more wheels loose the contact with the ground (Figs. 2f and 2g). In particular, the orientation angle β is set to 90° or -90° , while the tilting angle α is slowly increased. The wheel contact forces are then continuously monitored: as soon as one of them becomes zero or negative (i.e., instability initial phase), the platform motion stops. This motion can be better visualized in the first two charts of Fig. 3: starting from a horizontal position ($\alpha = 0^\circ$) and with the tractor oriented according to the platform's tilting direction ($\beta = 0^\circ$), the α angle is raised up to 13° so the tractor nose points down. Beyond this



Fig. 2 Experimental test: (a) Stability test-rig and New Holland TN75V tractor, (b) test-rig rotational degrees of freedom, (c) plane conformation, (d) plate special metal grid, (e) tractor anchoring with chains, (f)(g) roll-over instability

limit the platform can rotate freely without colliding with the access ramps. Thus, the orientation of $\beta = -90^\circ$ is reached and so the tractor is tilted sideways. From this moment, the α angle is increased up to the reaching of the instability.

3 Results and Discussion

One of the results of this experimental test concerns the trend of the four wheel contact forces as the slope and orientation angles change (Fig. 3). Firstly, it can be noted that the forces sum does not keep constant as the slope increase. This why it represents the normal component to the platform surface of the tractor weight force. Therefore, it decreases due to the cosine of the angle.

Analysing the behaviour of individual contact forces, as expected it can be seen that the downhill wheels (left tractor side in this test) exert an increasing weight, while the uphill wheels have an inverse trend. Again, the rear wheels show a huge variation in forces since it is where the greatest load is applied (i.e., the centre of gravity is nearest to the rear axle).

A graph of greater interest is shown in Fig. 4. The measured wheel-ground contact forces (continuous lines) are plotted as a function of the tilting angle α . The rear left wheel contact force (continuous blue line) decreases, and it reaches the null value when $\alpha = 26.5^\circ$. This point is identified as the initial phase of the roll-over instability.

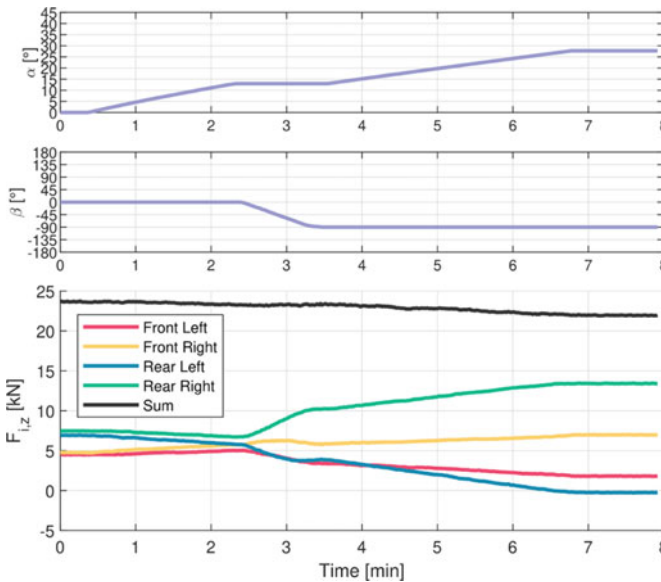


Fig. 3 Acquired data: (top) tilting angle, (middle) orientation angle, (bottom) Contact force of each wheel over the ground

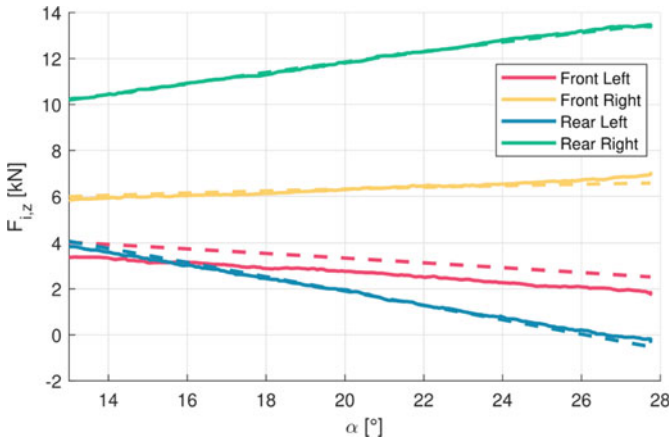


Fig. 4 Measured (continuous lines) and calculated (dashed lines) contact forces vs. tilting angle α

If the tilting angle is further increased, the wheel lift does not occur immediately but for larger α angles. As in this case where the test was manually stopped at 27.5° . This because the wheel detaching phenomena is partly hampered by the kinematics of the tractor and the elasticity of the tyres. In Fig. 4 the prediction of the four contact forces provided by the model presented in Sect. 2.1 are also reported (dashed lines). The model, although simplified, gives a good approximation of the trend of the phenomenon. In particular, the front right wheel trend (red line) presents an offset with respect to the measured data. It can be explained by the presence of a certain friction momentum in the front pivot axle and/or with the different tyre deformation due to the load variation. Anyway, in this work a more weight has been given to the potential of the test-rig system to calibrate models (e.g., identification of tractor parameters, such as the centre of gravity) and verify their validity using real machines.

4 Conclusions

In this work a basic model for determine the stability of a common agricultural vehicle with a rigid body and front pivoting axle, is considered. Based on the evaluation of the contact forces between wheels and ground, it has been used to study the roll-over stability problem. The effectiveness of the model has been evaluated through a series of experimental tests on a real tractor. For this scope, a test-rig for evaluating the stability of vehicles developed in collaboration with De Pretto Industrie S.r.l. and available at the Agro-Forestry Innovation LABORatory (AFILAB) of the Free University of Bolzano has been exploited. This latter has proven to be a valuable aid both in identifying parameters that cannot be measured directly (e.g., position of the centre of gravity) and in validating various stability models.

Acknowledgements This research has been carried out within the PNRR research activities of the consortium iNEST (Interconnected North-East Innovation Ecosystem) funded by the European Union Next-GenerationEU (Piano Nazionale di Ripresa e Resilienza (PNRR) Missione 4 Componente 2, Investimento 1.5 D.D. 1058 23/06/2022, ECS_00000043). This manuscript reflects only the Authors views and opinions, neither the European Union nor the European Commission can be considered responsible for them.

References

1. Facchinetti, D., Santoro, S., Galli, L.E., Pessina, D.: Agricultural tractor rollover related fatalities in Italy: results from a 12 years analysis. *Sustainability* **13**(8) (2021)
2. Bietresato, M., Mazzetto, F.: Stability tests of agricultural and operating machines by means of an installation composed by a rotating platform (the turntable) with four weighting quadrants. **10**(11), 3786 (2020)
3. Carabin, G., Gasparetto, A., Mazzetto, F., Vidoni, R.: Design, implementation and validation of a stability model for articulated autonomous robotic systems. **83**, 158–168 (2016)
4. Rondelli, V., Martelli, R., Casazza, C., Guarnieri, A.: Methodological approach to assess tractor stability in normal operation in field using a commercial warning device. **44**, 659–662 (2013)
5. Yang, H., et al.: Analysis of stability and dynamic model simulation of mountain tractor rollover. **512**(1) (2020). ISSN: 1755-1307
6. Franceschetti, B., Rondelli, V., Capacci, E.: Lateral stability performance of articulated narrow-track tractors. **11**(12) (2021)
7. Pessina, D., Facchinetti, D., Galli, L.E., Bisaglia, C., Cutini, M.: Survey on the lateral stability of wheeled narrow-track tractors. In: Biocca, M., Cavallo, E., Cecchini, M., Failla, S., Romano, E. (eds.) *Safety, Health and Welfare in Agriculture and Agro-food Systems*. SHWA 2020. Lecture Notes in Civil Engineering, vol. 252, pp. 457–467, Springer, Cham (2022). https://doi.org/10.1007/978-3-030-98092-4_47
8. Franceschetti, B., Lenain, R., Rondelli, V.: Comparison between a rollover tractor dynamic model and actual lateral tests. *Biosyst. Eng.* **127**, 79–91 (2014)
9. Previati, G., Gobbi, M., Mastinu, G.: Mathematical models for farm tractor rollover prediction. **64**, 280–303 (2014)
10. Vidoni, R., Bietresato, M., Gasparetto, A., Mazzetto, F.: Evaluation and stability comparison of different vehicle configurations for robotic agricultural operations on side-slopes. **129**, 197–211 (2015)
11. Bietresato, M., Mazzetto, F.: A novel facility for statically testing the stability of vehicles: technical features and possibilities. **6**(2), 107–121 (2022)

The MAGIC Project: A Tool for Promoting Safety in Agriculture During COVID-19 Pandemic



Pietro Catania , Giuseppe Aiello , Antonella Certa ,
Massimo Vincenzo Ferro, Santo Orlando , and Mariangela Vallone 

Abstract COVID-19 pandemic poses a threat to global health highlighting the importance of prevention and measures of social distancing. In agriculture, cultivation operations carried out in open field by farm workers represent a serious danger in this sense. Social distancing of the workers during the labor day is not always easy to be maintained, especially for the very close rows among the plants. In 2020, the researchers of the Mechanics Section of the Department of Agricultural, Food and Forest Sciences in collaboration with the Department of Engineering of the University of Palermo, presented a project entitled “Design of a real time Monitoring and control system for AGRicultural workers to limit the SARS-Cov-2 virus” (acronym MAGIC) to the Italian Ministry of University and Research. The aim of the project was the design of a real time monitoring and control system for workers in agriculture in order to monitor, record and control any violations of the distance among the workers. The system is based on the use of a small device equipped with a uniquely stored serial number that securely emits an alarm signal to both the worker and the manager when the distance between two employees is below the permitted threshold. A central manager perform a historical “track” that lists all the subjects with whom a person has come into close contact. The system was tested at a farm in Sicily during winter pruning in vineyard.

Keywords Bracelet · Distancing · Tracking · Wearable device

P. Catania (✉) · M. V. Ferro · S. Orlando · M. Vallone
Department of Agricultural, Food and Forest Sciences, University of Palermo,
Viale Delle Scienze, Ed. 4, 90128 Palermo, Italy
e-mail: pietro.catania@unipa.it

G. Aiello · A. Certa
Department of Engineering, University of Palermo, Viale Delle Scienze Ed. 9, 90128 Palermo,
Italy

© The Author(s), under exclusive license to Springer Nature Switzerland AG 2023
V. Ferro et al. (eds.), *AIIA 2022: Biosystems Engineering Towards the Green Deal*,
Lecture Notes in Civil Engineering 337,
https://doi.org/10.1007/978-3-031-30329-6_45

1 Introduction

Following the COVID-19 pandemic outbreak, social distancing has become an important method to prevent the infection and to contain the spread of the contamination. In agriculture, cultivation operations carried out in open field by farm workers represent a serious danger in this sense.

The importance of 1–2 m physical distancing for preventing the diffusion of respiratory diseases can be traced back in the seminal researches of Wells (1934) and Turner et al. (1941), in which most of the exhaled droplets ($>100 \mu\text{m}$) was found to land within a distance between 1 and 2 m. Coherently with such findings, during the COVID-19 Pandemic, the most relevant healthcare institutions issued specific recommendations in such regard. For example, the World Health Organization (WHO) has advised health care personnel to maintain a 3-foot (1-m) distance from persons showing symptoms of respiratory disease [1]. The US Centers for Disease Control and Prevention (CDC) recommended a 6-foot (2-m) separation [2], while other countries such as Australia and Germany established a 1.5-m distancing rule in public places [3]. As a direct consequence of such scientific evidences, almost all the governments on global scale to counteract the spread of the pandemic have enforced social distancing rules.

Despite the several Internet of Things (IoT) technologies potentially available for supporting the respect of voluntary or mandated social distancing measures, the effectiveness of social distancing systems and applications has been frequently questioned mainly because of the several technical issues which make the systems poorly reliable and effective [4, 5].

The specific working environment may significantly influence the effectiveness of a solution in counteracting the spread of the infection through self-distancing. In particular, a recent study [6] demonstrate that the COVID-19 incidence rate is significantly higher in regions with more agricultural workers; a 1% increase in the number of hired agricultural workers in a county is associated with a 0.04% increase in the number of COVID-19 cases per person and 0.07% increase in deaths per person. An explanation to such evidences can be found in the nature of agricultural jobs, which frequently requires the formation of teams working in close proximity to each other, thus being exposed to a higher risk for infection.

In such context, the objective of the proposed research is to develop and validate a technological system for social distancing specifically designed for agricultural workers, taking into account the specific issues related to the activities performed and the operating environment.

2 Materials and Methods

2.1 Description of the Research Project

In 2020, the researchers of the Mechanics Section of the Department of Agricultural, Food and Forest Sciences (SAAF) in collaboration with the Department of Engineering of the University of Palermo, presented a project entitled “Design of a real time Monitoring and control system for AGRicultural workers to limit the SARS-Cov-2 virus” (acronym MAGIC) to the Italian Ministry of University and Research. The aim of the project was the design of a real time monitoring and control system for workers in agriculture in order to monitor, record and control any violations of the distance among the workers.

The project goal was to develop a technological solution for risk prevention from COVID-19 in agricultural operations in open field, aimed at countering and containing the effects of any future pandemics. The system consists of tracing contacts in the workplace to selectively isolate employees at risk of COVID-19, allowing the rest of the farm to continue working safely.

The system is based on the use of a token, i.e. a small device (wrist/arm band) equipped with a securely stored unique serial number, which emits an alarm signal to the worker when the distance between two employees is at a minimum below the permitted threshold. A central manager can perform a historical “trace” that lists everyone with whom a person has had close contact (and for how long). This functionality is achieved through the construction of an archive in which proximity contact with other tokens is recorded in an anonymous and secure way and the ability to receive and process information on the tokens for which the user’s infection has been determined.

2.2 Tracking Device

The device for tracking the position of agricultural workers is shown in Fig. 1.

The device has dimensions $58 \times 96 \times 32$ mm and GPRS connection and Bluetooth 5.2. The battery is 200 mAh (Li-ion) whose duration covers the working day of 6.5 h. A Bluetooth 5.0 LE module is inserted (Fig. 2) with dimensions of $12.9 \times 15.0 \times 2.2$ mm, with a frequency of 2.4 GHz and TX Power + 19 dB, 32-bit 38.4 MHz ARM CPU, memory of 512 kB (flash program memory) and 64 kB RAM data memory. The temperature range is $-40 \text{ }^\circ\text{C} + 85 \text{ }^\circ\text{C}$.

Fig. 1 Device for tracking the position of agricultural workers



Fig. 2 Bluetooth module of the device

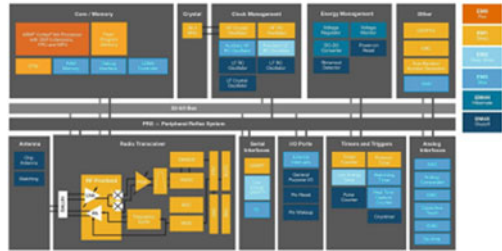
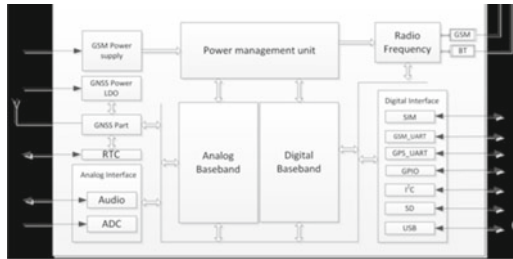


Fig. 3 GPRS-GPS module



The system is completed by a GPRS-GPS module (Fig. 3) with dimensions of $17.6 \times 15.7 \times 2.3$ mm, with a frequency of 850/900/1800/1900 MHz. The GPRS is multi-slot class 12/10, GSM compliant phase 2/2+ , low consumption battery, class B GPRS mobile station and 322 Mbit flash memory, 32 Mbit RAM. The GNSS multi constellation with GPS and GLONASS receiver has sensitivity tracking -167 dBm.

The system records the workers’ position in real time throughout the working day by sending the position data (latitude and longitude) to a cloud whose access is password protected. The signal is sent and recorded every 5 s, which allows for accurate tracking of movements. The bluetooth system registers close contact and, precisely, when the mutual distance between the operators is less than 1.5 m. The system can be worn both on the arm and on the operator’s side using a special belt. The system has been tested both in the laboratory and in the open field and the results obtained are very encouraging. The positions of close contacts among the employees have been archived on the cloud platform and are available for any checks in the event that COVID 19 infections occur among the employees.

The device had to be extremely easy to operate, with pre-established settings and no need for any action by the operator. Solution was thus to develop a smart-band involving NFC technologies (radio signals on the Bluetooth frequencies) with a unique identification code (ID) and capable of measuring the distance from another smart band. When two smartbands are in proximity, hence, an acoustic alert is generated, thus helping people respect the necessary safety distance. The device also records which other smartband wearers it has been in close contact with, thus enabling contact tracing in case of COVID-19 infection.

The system is finally connected to a cloud platform which allows to maintain an anonymous centralized database to perform risk-analysis and alerts notifications to

the managers (who is demanded the task to alert the workers in case of possible contagion). Thus, while contact tracing is based on a decentralized approach, the system also implements some centralized functions. To perform contact matching and notification by storing the contact information from the smartbands to de centralized database. In such system, only the data of potentially infected workers are shared with the centralized server, which only holds the anonymous codes of the smart bands, while the workers' names can only be associated knowing the restricted list of associations between the smartband and the workers. This allows more effective privacy policies compared to the centralized contact tracing solutions. The debate on the privacy and security aspects on the use of such systems has thus been addressed.

2.3 Field Tests

The experimental field tests were carried out in January 2022, on a vineyard in a farm located in the province of Palermo, during the manual pruning operations. The experimental site belongs to the Protected Designation of Origin (PDO) Alcamo winegrowing area, at an altitude of 300 m above sea level, with irregular orography. The variety is Catarratto Lucido, grafted onto a vigorous 1103P rootstock and drip-irrigated system. The vineyard is fifteen years old and has a total extension of 8 ha, the rows are 2.40 m apart, with 0.95 m between the vines in the rows, the orientation of the rows is NE-SW. The vines were trained on a vertical shoot positioned trellis and pruned to two buds per spur, spaced approximately 15 cm apart in a single cordon, in total each vine has 6 spurs.

The vineyard planting consists of steel-galvanised poles, 2.50 m long, which are placed at a depth of 0.90 m in the ground, with the remaining part (1.60 m) providing support for the vegetation, each pole is spaced in the row approximately 5 m apart from the other. Each pole supports three different types of metal wires, these are positioned at different heights. The vineyard is equipped with an irrigation system with in-line 4 L h⁻¹ pressure compensated emitters, spaced 0.95 m apart. The drip irrigation lines were placed approximately 50 cm above the ground.

Pruning operations consist of selecting the fruit buds to leave on the vine to provide grape production, these operations are divided into the cutting of shoots and the removal of shoot residues. To perform these operations the worker has first to select the two buds to be left on each spur and then cut the shoot, usually requiring about 2 min. Afterwards, the worker has to remove the pruning residues, an operation that takes about 2 min. Therefore, the total time required to prune each vine is about 4 min.

During the field tests, three devices were worn on the arm by the PhD students of the SAAF Department of the University of Palermo (Fig. 4).

The tests consisted in carrying out the pruning operations by simulating close contacts of the PhD students who wore the devices.

Fig. 4 Field tests during pruning operations in vineyard



3 Results

Figure 5 shows the tracking lines obtained throughout the field tests by the three devices during pruning operations in the vineyard. The red (worker A), blue (B) and green (C) dots represent the position of each operator wearing the device.

The close contact events among the operators are marked by asterisks. During these events, the alarm signal emitted by the device warned the operator that the distance limit had been reached.

Figure 6 shows the position of the single device registered by GPRS-GPS module as displayed by the software including day and time.

The hand-shape cursor on the right side of Fig. 7 allows to visualize the position and the information associated to the data.

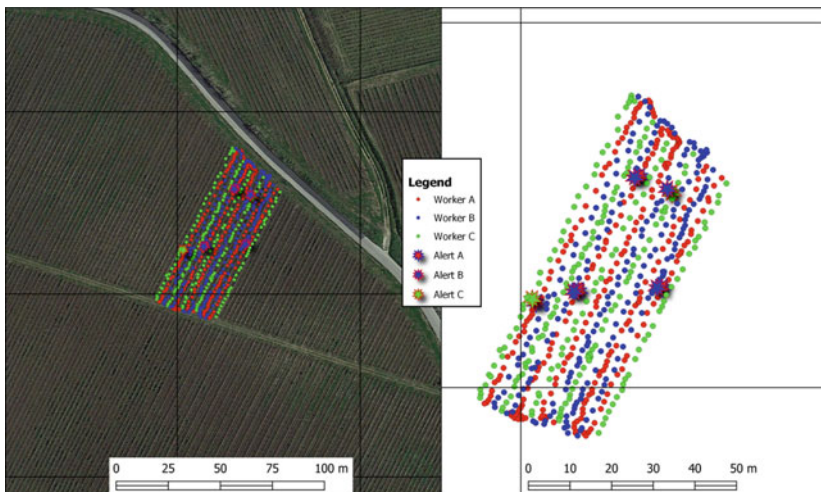


Fig. 5 Tracking lines obtained during the field tests by the three devices during pruning operations in the vineyard and close contact events among the operators (marked by asterisks)

The screenshot shows the 'Lettura Tracking' interface with a sidebar menu and a main data table. The table columns are: #, Terminale, Batteria, Lettura, Ricezione, and Posizioni. The data rows are as follows:

#	Terminale	Batteria	Lettura	Ricezione	Posizioni
1	40526466	80%	24/02/2022 11:35:48	24/02/2022 11:35:48	37.920192 013.072475
2	40526466	80%	24/02/2022 11:33:47	24/02/2022 11:33:58	37.920096 013.072273
3	40526466	80%	24/02/2022 11:32:43	24/02/2022 11:33:37	37.919832 013.075299
4	40526466	80%	24/02/2022 11:31:40	24/02/2022 11:31:45	37.919891 013.075242
5	40526466	80%	24/02/2022 11:29:39	24/02/2022 11:29:39	37.919806 013.075293
6	40526466	80%	24/02/2022 11:28:34	24/02/2022 11:28:39	37.919927 013.075271
7	40526466	70%	24/02/2022 11:27:37	24/02/2022 11:27:37	37.919896 013.075326

Fig. 6. Positions of the device registered by GPRS-GPS module as displayed by the software, including day and time

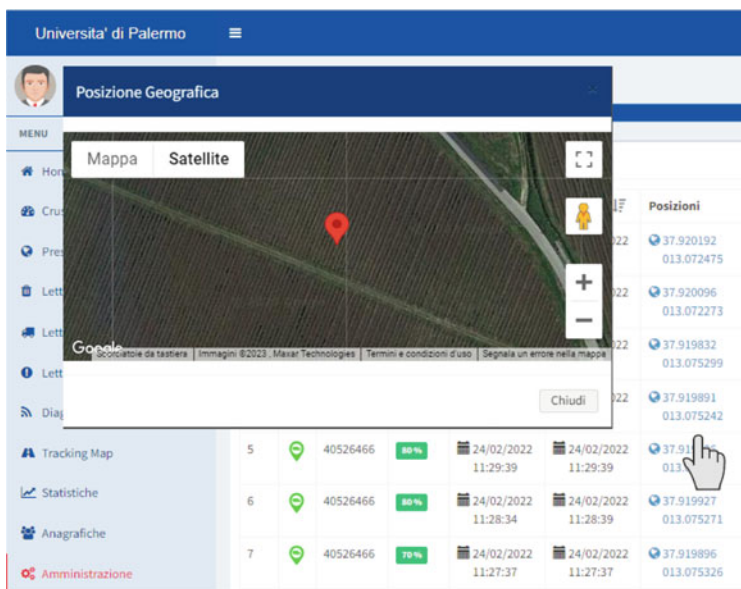


Fig. 7 Position of the device registered by GPRS-GPS module as displayed by the software when clicking on each data

#	Terminale	Batteria	Letture [F]	Ricezione [F]	Posizioni	Anomalia	Utente/Tag [F]
26	40526474	99%	04/02/2022 10:36:37	04/02/2022 10:36:41	38.107827 013.351049	Contatto	[User/Tag]
27	40526474	99%	04/02/2022 10:36:35	04/02/2022 10:36:45	38.107827 013.351049	Contatto	[User/Tag]
28	40526474	99%	20/01/2022 15:16:46	20/01/2022 15:16:59	Non disponibili	Contatto	[User/Tag]
29	40526474	99%	20/01/2022 14:45:57	20/01/2022 14:46:03	Non disponibili	Contatto	[User/Tag]
30	40526466	99%	20/01/2022 14:05:55	20/01/2022 14:08:41	41.470277 014.531810	Batteria	[User/Tag]
31	40526466	99%	20/01/2022 14:02:01	20/01/2022 14:02:08	41.469863 014.530466	Batteria	[User/Tag]

Fig. 8 Contact events among the operators and associated information

The close contact events among the operators are registered and can be displayed in a separate sheet of the software, as shown in Fig. 8, where day, time, position, irregularity and name of the device are reported.

4 Conclusions

The research project aimed at developing and validating a technological system for social distancing specifically designed for agricultural workers.

The first field tests allowed to test the devices in the real operating conditions, i.e. during pruning operations in the vineyard.

The designed system makes it possible to avoid the closure of the agricultural activity of the farm following the contacts of the workers with the colleagues eventually infected with COVID-19. This strategic objective is achieved thanks to the tracking of the positions of all the operators present in the workplace.

Funding: This research was funded by the Italian Ministry of University and Research, project acronym “MAGIC”, code FISR2020IP_03316.

References

1. World Health Organization (WHO): COVID-19: Occupational health and safety for health workers. Interim guidance Considerations for public health and social measures in the workplace in the context of COVID-19(2020). WHO reference number: WHO/2019-nCoV/Adjusting_PH_measures/Workplaces/2020.1. Accessed 20 Dec 2022

2. US Centers for Disease Control and Prevention (CDC) (2020). <https://www.cdc.gov/coronavirus/2019-ncov/hcp/infection-control-recommendations.html>. Accessed 20 Dec 2022
3. Qian, M., Jiang, J.: COVID-19 and social distancing. *Z Gesundh Wiss.* **30**(1), 259–261 (2022)
4. Murad, S.S., Yussof, S., Badeel, R.: Wireless technologies for social distancing in the time of COVID-19: literature review, open issues, and limitations. *Sensors* **22**(6), 2313 (2022)
5. De Fazio, R., Giannoccaro, N.I., Carrasco, M., Velazquez, R., Visconti, P.: Wearable devices and IoT applications for symptom detection, infection tracking, and diffusion containment of the COVID-19 pandemic: a survey. *Front. Inform. Technol. Electron. Eng.* **22**, 1413–1442 (2021)
6. Lusk, J.L., Chandra, R.: Farmer and farm worker illnesses and deaths from COVID-19 and impacts on agricultural output. *PLoS ONE* **16**(4), e0250621 (2021)

Assessment of Vine and Cover Crop Vegetation Indices Using High-Resolution Images Acquired by UAV Platform



Pietro Catania, Massimo Vincenzo Ferro, Eliseo Roma, Santo Orlando, and Mariangela Vallone

Abstract In recent years, there has been an increasing need to implement sustainability in agricultural systems, especially for the risks associated with soil degradation. Cover crops are widely recognised and adopted for sustainable vineyard management, reducing soil and water losses, restoring organic matter, and increasing soil fertility. Therefore, it is necessary to determine the biomass development of cover crops using alternative and innovative methods. High-resolution UAV-based (Unmanned Aerial Vehicle) multispectral images can be used for this purpose, giving significant information for monitoring the seasonal growth variation of crops. The aim of this research was to study the biomass vigour spatial variability of cover crops and vineyard evaluating the possible correlation between cover crop and vineyard vigour values. Cover crop biomass was monitored by sampling during flowering, measuring fresh weight and dry weight. The multispectral images were obtained with the use of a UAV before cover crops were buried (March); the spectral response of the vineyard was evaluated with UAV flights during the summer period. The analysis of the vigour maps obtained showed a degree of variability for the vegetation index examined. This variability was found both on the cover crop biomass development and on the vegetative growth of the vineyard. The results showed the applicability of remote sensing to monitor cover crop and vineyard biomass development, explaining the overall variability of the field. This information allows the application of the appropriate agronomic techniques to improve the quality of the production.

Keywords Precision viticulture · Spatial analysis · Sustainability · Vineyard management

P. Catania · M. V. Ferro · E. Roma (✉) · S. Orlando · M. Vallone
Department of Agricultural, Food and Forest Sciences, University of Palermo, Viale delle Scienze, Ed 4, 90128 Palermo, Italy
e-mail: eliseo.roma@unipa.it

© The Author(s), under exclusive license to Springer Nature Switzerland AG 2023
V. Ferro et al. (eds.), *AIIA 2022: Biosystems Engineering Towards the Green Deal*,
Lecture Notes in Civil Engineering 337,
https://doi.org/10.1007/978-3-031-30329-6_46

1 Introduction

Conventional agriculture through innovative agronomic practices and the efficiency of agricultural mechanization has improved crop yields in the semiarid environment of the Mediterranean. Recent reports estimate that by 2050 the population's demand for food is expected to double [1]. Agriculture is thus becoming increasingly competitive, but it is important to preserve the environment from intensive management of agricultural systems. Intensive management of agricultural systems and especially soil, causes an increase in the rate of mineralization of organic matter [2]. European guidelines have supported Good Agricultural Practices, which relate to the reduction of mineral fertilization or the cultivation of cover crops [3]. In order to monitor fertilizer management, in precision viticulture variable rate fertilizer application is practiced, which reduces spatial variability by increasing vineyard sustainability [4, 5]. In vineyard management, the introduction of legume cover crops improves soil physical and chemical properties and reduces the risk of soil erosion. The use of cover crops makes it possible to reduce the use of N external inputs, through the decomposition of biomass that is buried during winter and gradually releases nutrients [6]. So cover crops can satisfy the N needs of the vineyard [7]. Detection of biomass development is a very important agronomic aspect. The rapid and non-destructive monitoring is an important tool provided by smart precision agriculture practices [8, 9]. Recent remote sensing technologies, surveying the spectral response of cover crops, can rapidly estimate vegetative growth and the fraction of nutrients they release to the soil [10, 11]. The use of UAVs equipped with multispectral cameras allows the acquisition of high-resolution images over large areas with high flight flexibility in short time [12, 13]. There are different multispectral indices used to monitor the vegetation status. Among the most widely used indices, there is the normalized differential vegetation index (NDVI) [12]. Multispectral indices are well correlated with crop biomass development, [8] with a strong linear relationship between NDVI and cover crop biomass (kg ha^{-1}). The objective of this research was to evaluate the feasibility and accuracy of using UAVs to survey the growth variability of a typical cover crop used in Mediterranean vineyards to improve soil conditions. In addition, the spectral response of the vineyard with those of the cover crop, surveyed at two different times of the year were compared.

2 Materials and Methods

2.1 Study Area

The experimentation was performed in Camporeale (Palermo, Italy) at Tenute Rapi-talà farm. According to the Köppen–Geiger's classification, the climate of the area is classified as Mediterranean hot summer climates [14]. Climatic data recorded with a weather station positioned in the field showed a mean air temperature ranging from

18.3 to 24.6 °C and a mean annual rainfall from 700 to 820 mm in the growing season. The experiment was carried out in 2022 in a vineyard managed according to the ordinary practices of the area with drip irrigation system. In this area, cover crop species in the winter season is used. In our field beans (*Vicia faba* L.) was seeded, using a combined power harrow with a mechanical seed drill. Sowing was made in all the vineyard in the inter-row areas. The amount sown was of 90 kg ha⁻¹. The field has a total area of 8 hectare with an irregular orography. The layout planting is 2.4 × 1 m. The rows orientation is NE-SW with an angle of 22° from the North. The trellis system is a double cordon spur pruned. The vineyard was planted in 2007 with a traditional variety of the area, cv. Catarratto, in full productivity (Fig. 1).

2.2 Data Collection

During the winter season, while the vineyard was in the dormancy in DOY 55 (Day Of Year) the field samplings were carried out to investigate cover crop variability. In the same day, the flight was performed using the UAV platform described in Sect. 2.4. The sampling points were identified in areas with different vigour, excluding the most external part of the field. The sample area was identified using a square of 1 m² positioned in the center of the inter-row. A total number of 10 points was sampled. Each sample was represented by three sub-sampling. For each sub-sampling the fresh weight of the cover crop was measured using a digital balance. Subsequently, these samples were carried out to the laboratory to be dried and evaluate their dry weight.

2.3 Flight Scheduling and Multispectral Data Acquisition

A remote UAV platform equipped with a multispectral and RGB camera was used to investigate the spectral features of bean and vine. The UAV platform is a quad-copter model Phantom 4 (DJI, Shenzhen, China). Before the flight, 10 Ground Control Points (GCPs) were placed in the external and internal part of the field. They were georeferenced using the GNSS receiver S7-G by Stonex (Milano, Italy), equipped with a Stonex geodetic antenna [15, 16]. This instrument is able to use multiband signals from the main GNSS satellites such as Global Position System (GPS), GLONASS, BeiDou and SBAS. It can improve accuracy through the Real Time Kinematic (RTK) differential correction data. The coordinates of the different GCPs were acquired in RTK mode as an average of 60 measurements. The flight was carried out on DOY 55 and 195 at 12:00, with the best weather condition and the automatic guide following the set route and waypoints for bean and vine crop, respectively. Both flights presented the same setting characteristics. The flight height was of 70 m a.g.l. using Real Time Kinematic (RTK) differential corrections, obtaining a ground sample surface (GSD) of 3.7 cm. The image acquisition was performed at an average speed of 25 m * s⁻¹ in stop-and-go mode. The front and

Fig. 1 Study area site location



side overlap percentage between the image was 70%, while the gimbal pitch was set at 90° (downwards).

2.4 Data Processing and Analysis

Photogrammetric processing to obtain the orthomosaic was done using the main photogrammetric technique in the Agisoft Metashape version 1.7.3 software. The orthomosaic multi-bands was processed on QGIS version 3.2 to obtain the NDVI map and perform the analysis of the several layouts. The raw NDVI map was calculated using the near infra-red (NIR) and red reflectance map [17]. NDVI was calculated to identify the vigor level through the segmentation process [18] made using the K-means algorithm, choosing three classes in the SAGA library of QGIS. The interpolation Kriging method was used to create continuous maps from the point data of cover crop analysis. Statistical analysis was made using Minitab and Microsoft Excel software.

3 Results

The experimentation showed some variability of cover crop in the experimental field (see Fig. 2). This variability was investigated as NDVI value of whole plot area. The mean NDVI value was 0.61 ± 0.16 .

NDVI as able to determine the different vigor conditions of the cover crop. Indeed, the NDVI values were highly statistically significant with the vegetative values measured on the soil. In particular, the best correlation of cover crop NDVI values was observed with dry weight ($r = 0.95^{***}$, Fig. 3). With lower correlation

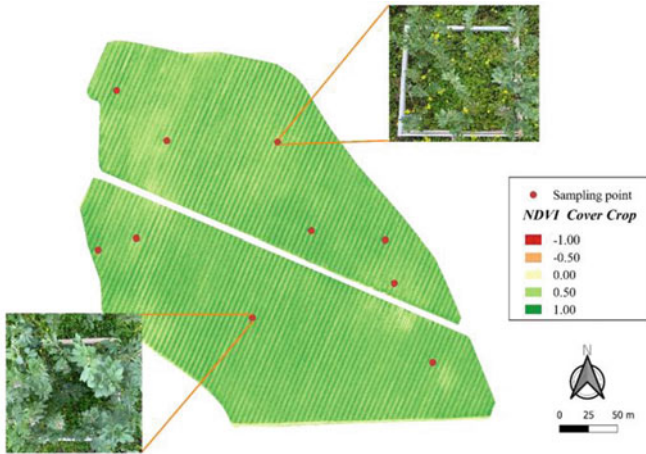


Fig. 2 NDVI map obtained from the flight of DOY 55. The red points represent the different positions of the cover crop samples. Images of real cover crop conditions were associated with these points

values also cover crop fresh weight showed a statistically significant correlation with NDVI ($r = 0.93^{***}$; data not show).

The vineyard growth also showed a good variability of NDVI value on the field. The average NDVI of the vineyard was 0.42 ± 0.16 with a ranging of -1 to $+1$ (Fig. 4).

The lower values corresponds to the soil pixels, while the other values corresponds to the vineyard.

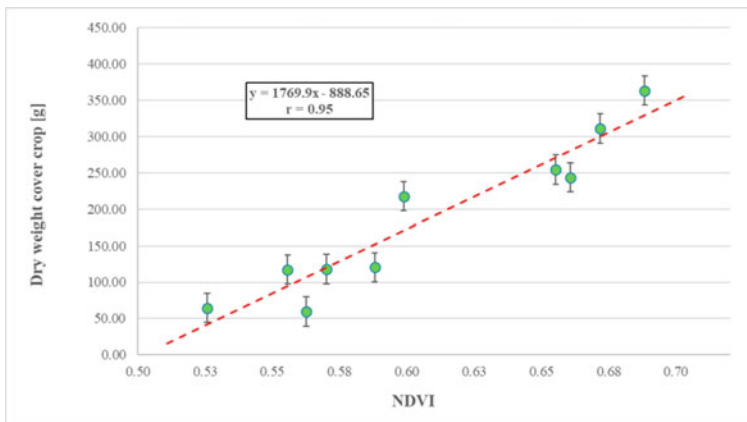


Fig. 3 Correlation between mean NDVI of the broad bean in the sampling square metre and dry weight

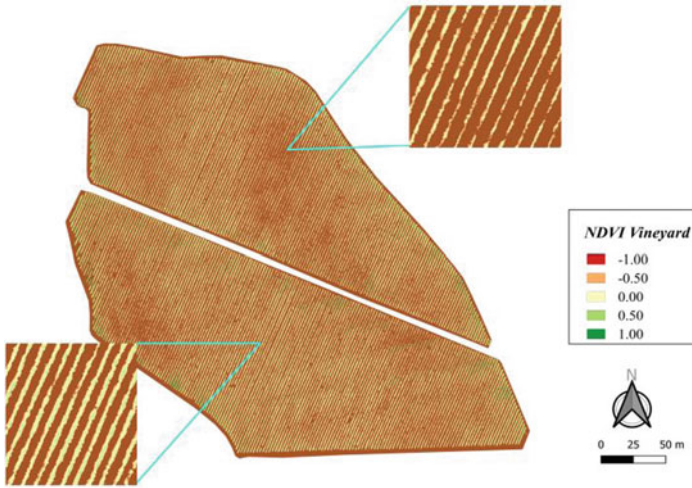


Fig. 4 NDVI map obtained from the flight of DOY 195. The zoom zone allows a better view of the vineyard conditions in terms of multispectral and canopy thickness

Interesting results emerge from the comparison of vineyard and bean multispectral data. Both crops showed the same trend vigor in the field (data not show). Indeed the vigor areas were similar. Comparing the multispectral two datasets, the experiments showed a statistically significant correlation ($r = 0.82^{***}$; Fig. 5).

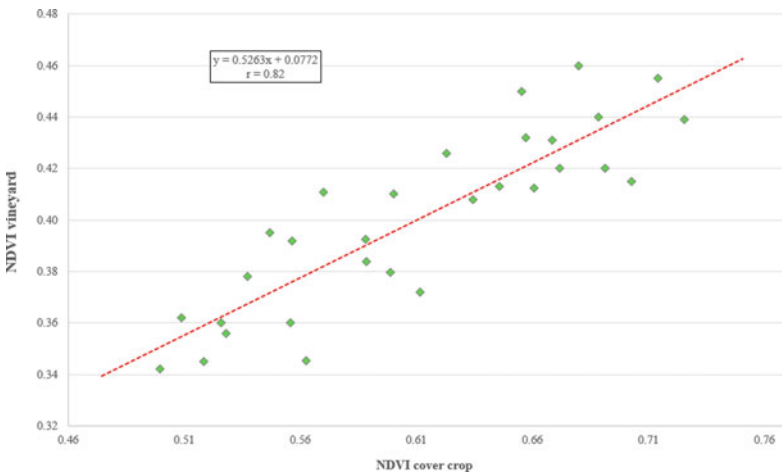


Fig. 5 Correlation between NDVI values of cover crop and NDVI values of vineyard determined from multispectral image sampling

4 Discussion

The experimentation showed the good capability of the multispectral images acquired from UAV to detect the growth spatial variability of cover crop and vineyard. Indeed, the NDVI values of cover crop presented good correlation with one of the main parameters of growth. In another study [19] similar results were found using NDVI index, confirming the good capabilities of such information for plants investigation. However, our study shows a better multispectral correlation with dry weight of cover crops. This result may be due to the optimal agronomic conditions that cover crops had at the time of the survey, indeed, it was a phenological stage prior to flowering. It is known that some multispectral indices under dense vegetation conditions or at specific phenological stages are more affected by saturation problems [20]. The surveys performed in our study were carried out with a high ground resolution of the images. Another reason could be attributed to the density of cover crop in our study, which, unlike other species, does not create an obvious index saturation effect. However, starting from the NDVI maps cleared from the soil and shadow pixels, it is possible to observe that the zone with high NDVI value has the highest thickness of the canopy. These results showed the possibility of multispectral images to detect the vigor maps and differentiate soil using NDVI [18].

The use of cover crops during the winter period provides several benefits to the vine, increases vineyard sustainability, and cover crops also promote soil conservation and reduce the impact of agronomic management on climate change [21, 22]. This experiment showed that crop development variability is always related to soil conditions [23]. Similarly, soil type is known to significantly influence vineyard development and vine vigor [24]. Vine growth variability or vigor is related to cover crop development and its spatial pattern of vigor. Large spatial variability in NDVI data of cover crops has been observed; quantifying this variability is an important step in understanding potential impacts on vineyard yield.

5 Conclusions

As a high-accuracy, flexible and non-destructive remote sensing system, UAVs have been widely used for agronomic monitoring. The application of UAVs in cover crop and vineyard monitoring was performed using a multispectral sensor. Normalized vegetation index was calculated for both cover crops and vineyard. Our study found that remote sensing methods using UAVs are useful for quantifying the spatial variability of cover crops at the field scale. With these sensing methods, cover crop management practices can be improved and objectives inherent in vineyard environmental sustainability can be increased. Cover crops play a central role in improving soil quality. Strong linear relationships were found between NDVI of cover crops and their dry weight. In addition, there were good linear relationships between NDVI of cover crops and those of the vineyard. The distribution of whole-plot vigor is

therefore closely associated with variability in soil conditions. The methodological approach performed in this study can contribute to improving and simplifying biomass sampling conducted in the field. In this way, the farmers can take advantage of cover crop vigor maps and move around the field following the spatial distribution of vigor, significantly reducing sampling time, while still obtaining accurate data of the produced biomass amount per hectare.

References

1. Niu, Y., Zhang, L., Zhang, H., Han, W., Peng, X.: Estimating above-ground biomass of maize using features derived from UAV-Based RGB imagery. *Remote Sens.* **11**, 1261 (2019)
2. Kemmitt, S., et al.: Mineralization of native soil organic matter is not regulated by the size, activity or composition of the soil microbial biomass—a new perspective. *Soil Biol. Biochem.* **40**, 61–73 (2008)
3. Galati, A., Gristina, L., Crescimanno, M., Barone, E., Novara, A.: Towards more efficient incentives for agri-environment measures in degraded and eroded vineyards. *Land Degrad. Dev.* **26**, 557–564 (2015)
4. Balafoutis, A.T., Koundouras, S., Anastasiou, E., Fountas, S., Arvanitis, K.: Life cycle assessment of two vineyards after the application of precision viticulture techniques: a case study. *Sustainability* **2017**, 9 (1997)
5. Sozzi, M., et al.: On-the-Go Variable Rate Fertilizer Application on Vineyard Using a Proximal Spectral Sensor, pp. 343–347. *IEEE* (2020)
6. García-Díaz, A., Bienes, R., Sastre, B., Novara, A., Gristina, L., Cerda, A.: Nitrogen losses in vineyards under different types of soil groundcover. a field runoff simulator approach in central Spain. *Agricul. Ecosyst. Environ.* **236**, 256–267 (2017)
7. Conradie, W.: Partitioning of Mineral Nutrients and Timing of Fertilizer Applications for Optimum Efficiency, pp. 69–81. *American Society for Enology and Viticulture* (2005)
8. Yuan, M., Burjel, J., Isermann, J., Goeser, N., Pittelkow, C.: Unmanned aerial vehicle-based assessment of cover crop biomass and nitrogen uptake variability. *J. Soil Water Conserv.* **74**, 350–359 (2019)
9. Barnes, M.L., Yoder, L., Khodaei, M.: Detecting winter cover crops and crop residues in the midwest us using machine learning classification of thermal and optical imagery. *Remote Sens.* **2021**, 13 (1998)
10. Yu, K., Li, F., Gnyp, M.L., Miao, Y., Bareth, G., Chen, X.: Remotely detecting canopy nitrogen concentration and uptake of paddy rice in the northeast china plain. *ISPRS J. Photogramm. Remote. Sens.* **78**, 102–115 (2013)
11. Swoish, M., Leme Filho, J.F.D.C., Reiter, M.S., Campbell, J.B., Thomason, W.E.: Comparing satellites and vegetation indices for cover crop biomass estimation. *Comput. Electron. Agricul.* **196**, 106900 (2022)
12. Pajares, G.: Overview and current status of remote sensing applications based on Unmanned Aerial Vehicles (UAVs). *Photogramm. Eng. Remote. Sens.* **81**, 281–330 (2015)
13. Matese, A., et al.: Intercomparison of UAV, aircraft and satellite remote sensing platforms for precision viticulture. *Remote Sens.* **7**, 2971–2990 (2015)
14. Kotteck, M., Grieser, J., Beck, C., Rudolf, B., Rubel, F.: *World Map of the Köppen-Geiger Climate Classification Updated* (2006)
15. Catania, P., et al.: Positioning accuracy comparison of GNSS receivers used for mapping and guidance of agricultural machines. *Agronomy* **10**, 924 (2020)
16. Catania, P., Orlando, S., Roma, E., Vallone, M.: Vineyard design supported by GPS application. *Acta Hortic.* **1314**, 227–234 (2021)

17. Rouse, J.W., Haas, R.H., Schell, J.A., Deering, D.W., Harlan, J.C.: Monitoring the Vernal Advancement and Retrogradation (Green Wave Effect) of Natural Vegetation. NASA/GSFC Type III Final Report, Greenbelt, Md, vol. 371 (1974)
18. Caruso, G., et al.: High-resolution imagery acquired from an unmanned platform to estimate biophysical and geometrical parameters of olive trees under different irrigation regimes. *PLoS ONE* **14**, e0210804 (2019)
19. Hunt, E.R., et al.: NIR-green-blue high-resolution digital images for assessment of winter cover crop biomass. *GIScience Remote Sens.* **48**, 86–98 (2011)
20. Zhou, X., et al.: Predicting grain yield in rice using multi-temporal vegetation indices from UAV-based multispectral and digital imagery. *ISPRS J. Photogramm. Remote. Sens.* **130**, 246–255 (2017)
21. Keesstra, S., et al.: The superior effect of nature based solutions in land management for enhancing ecosystem services. *Sci. Total Environ.* **610**, 997–1009 (2018)
22. Novara, A., Cerda, A., Barone, E., Gristina, L.: Cover crop management and water conservation in vineyard and olive orchards. *Soil Tillage Res.* **208**, 104896 (2021)
23. Colombi, T., Walter, A.: Genetic diversity under soil compaction in wheat: root number as a promising trait for early plant vigor. *Front. Plant Sci.* **8**, 420 (2017)
24. Hubbard, S.S., et al.: Estimation of soil classes and their relationship to grapevine vigor in a bordeaux vineyard: advancing the practical joint use of Electromagnetic Induction (EMI) and NDVI datasets for precision viticulture. *Precision Agric.* **22**, 1353–1376 (2021)

Evaluation of Different Flight Courses with UAV in Vineyard



Pietro Catania, Massimo Vincenzo Ferro, Eliseo Roma, Santo Orlando, and Mariangela Vallone

Abstract Precision farming has consolidated the use of Unmanned Aerial Vehicles (UAVs), which have confirmed their role as excellent tools for data acquisition and analysis. These systems have wide operational flexibility, good flight autonomy and excellent spatial resolution of multispectral images. They proved to be more competitive in data acquisition than satellite systems, especially on small areas typical of Italian viticulture. Unfortunately, there is little knowledge in literature about the flight course influence in the extraction of canopy spectral and biometric information. The aim of this work is to compare the different flight directions that can be performed with UAVs, to assess the differences in the acquisition of the spectral response of vineyard canopy and biometric characteristics. The vineyard is located in Camporeale, (Sicily, Italy); with a typical cultivar (Catarratto). The surface area of the experimentation field is 3.2 ha. Row orientation is NE-SW; the field can be divided into two different orographic area. In specific, one of them is flat and the other is hillside with medium-high slope. Remote images were acquired with a multicopter UAV, equipped with a camera with six multispectral bands, the RGB for visible light images and five monochrome narrow bands for multispectral images. The sensor has a field of view (FOV) of 62.7° and 90° downwards. Front and side over-lapping were 70%. Two flight courses were carried out, one perpendicular and the other parallel to the orientation of the rows. The results show differences in the reconstructions image that induced a variability in multispectral data.

Keywords Precision viticulture · Unmanned Aerial Vehicle (UAV) · Management zones

P. Catania · M. V. Ferro (✉) · E. Roma · S. Orlando · M. Vallone
Department of Agricultural, Food and Forest Sciences, University of Palermo,
Viale Delle Scienze, Ed 4, 90128 Palermo, Italy
e-mail: massimovincenzo.ferro@unipa.it

© The Author(s), under exclusive license to Springer Nature Switzerland AG 2023
V. Ferro et al. (eds.), *AIIA 2022: Biosystems Engineering Towards the Green Deal*,
Lecture Notes in Civil Engineering 337,
https://doi.org/10.1007/978-3-031-30329-6_47

457

1 Introduction

The use of unmanned aerial vehicles (UAV) is becoming increasingly important in precision viticulture. Therefore, there is a huge interest in generating orthophotos with high spatial resolution. UAVs are used in various fields and sectors due to their flexibility and ease of survey. The drones can be divided into horizontal take-off and landing (HTOL), vertical take-off and landing (VTOL) and hybrid drones [11]. Among them, VTOL-type multi-rotor drones are the most widely used in precision agriculture [9, 19]. This configuration benefits from vertical take-off and landing, which increases the operational flexibility [8]. The drones used in precision agriculture are semi-autonomous. This means that the UAV flies a specific flight path, following information obtained through waypoints and previously established altitudes. The UAV is equipped with a positioning measurement system, such as a Global Navigation Satellite System or GNSS, to find out its location in real-time from waypoints. It is also equipped with an altimeter to maintain a constant altitude. UAVs are used to produce images generated by various sensors, such as RGB, multi-spectral, hyperspectral, and thermal cameras, allowing to detect variability in crop growth and productivity [1, 6, 10, 13].

One of the main advantage of UAVs is the flexibility of carrying sensors that are able to capture images at closer or shorter distances from multiple viewing angles [2]. In particular, depending on the adjustment of the camera axis, either vertical or at a variable angle of inclination, the detail of the survey can be changed [20]. The accuracy of image acquisition performed by UAVs can be affected by several parameters and factors, which depend on the embedded characteristics of the sensor used, but especially on the configuration of flight operations. Field characteristics such as soil profile, hydrology, soil conditions can also influence the acquisition accuracy. In particular, soil profile can affect the spectral features due to the change in altitude [16]. The speed and direction of flight influence its duration, while varying other flight attributes such as height, the ground resolution of the images changes [12]. Variation in flight height affects some parameters of the spectral response of crops, influencing, for instance, a variation in NIR reflectance [22]. There are scientific references in the literature that defines how the flight path affects geometric resolution [25]. However, in the context of precision agriculture, no studies investigate the influence of different flight routes. The aim of this study was to evaluate the influence of two flight paths on the spectral response (in terms of Normalized Difference Vegetation Index, NDVI) and vigor area (expressed in m^2) in vineyard plot characterized by irregular orography using UAVs platform.

2 Materials and Methods

2.1 Study Area

The trial was performed in Camporeale (Palermo, Italy) in Tenute Rapitalà farm with centroid coordinates of Lat 37° 55′ 11.18″ N, Long 13°04′22.31″ E. According to the Koppen–Geiger’s classification, the climate of the area is classified as Mediterranean hot summer climates [14]. Climatic data were recorded by a weather station positioned in the field; the mean air temperature was from 18.3 to 24.6 °C and the mean annual rainfall from 700 to 820 mm in the growing season. The experiment was carried out in 2022 in a vineyard cultivated according to the ordinary management practices of the area with drip irrigation system. The field has a total area of 3.2 hect. with an irregular orography. The experimental plot was divided into two different sub plots according to soil profile, flat and slope condition. The flat area (F) had a surface of 1.7 hect. corresponding to 6,905 vines, the sloped area (S) had a surface of 1.5 hect. corresponding to 6,038 vines. The planting layout was 2.4×1 m for both plots. The rows orientation was NE-SW with an angle of 22° from the North. The trellis system was a double cordon spur pruned. The vineyard was planted in 2007 with cv. Catarratto, a typical cultivar of the area, in full productivity.

2.2 Flight Scheduling and Multispectral Data Acquisition

A remote UAV platform equipped with a multispectral camera was used to investigate the spectral features. The UAV platform used, was a quadcopter model Phantom 4 (DJI, Shenzhen, China). Before the flight, 12 Ground Control Points (GCPs) were located in the external and internal part of each sub area. They were georeferenced using the GNSS receiver S7-G by Stonex (Milan, Italy), equipped with a Stonex geodetic antenna [4, 5]. This instrument is able to use multiband signals from the main GNSS satellites and improve accuracy through the Real Time Kinematic (RTK) differential correction data. The coordinates of the different GCPs were acquired in RTK mode as an average of 60 measurements. The flight was carried out on DOY 195 at 12:00, with the sun rising at the zenith and under clear sky conditions and low wind speed, with the automatic guide following the set route and waypoints (Fig. 1).

A flight height of 30 m a.g.l. was set in the two flight configurations, using Real Time Kinematic (RTK) differential corrections, obtaining a ground sample surface (GSD) of 1.7 cm. The image acquisition was performed at an average speed of $10 \text{ m} \cdot \text{s}^{-1}$ in stop-and-go mode. The front and side overlap percentage between the image was 70%, while the gimbal pitch was set at 90° (downwards).

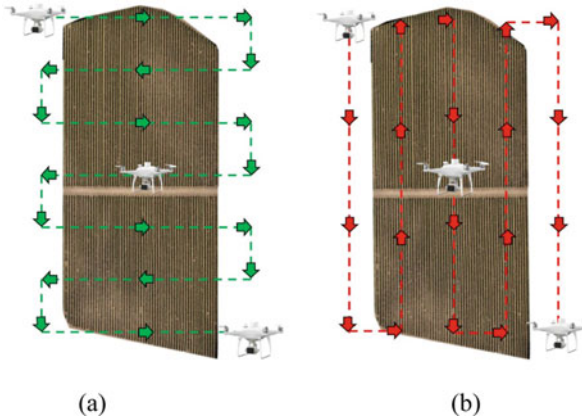


Fig. 1 Schematic representation of the flight paths. **(a)** Perpendicular flight path; **(b)** Parallel flight path (with reference to row orientation)

2.3 Processing and Data Analysis

Photogrammetric processing to obtain the orthomosaics was performed using Agisoft Metashape software, version 1.7.3. The orthomosaics were processed on QGIS (version 3.2) to obtain NDVI map and perform Kriging interpolation to identify homogeneous vigor areas. The raw NDVI map was calculated using the near infrared (NIR) and red reflectance map [21]. NDVI was calculated to identify the vigor level through the segmentation process [3]. The K-means algorithm from the SAGA library of QGIS was used; through this tool three classes of vigor were defined, low vigor (LV), medium vigor (MV) and high vigor (HV). Statistical analysis was performed using Minitab and Microsoft Excel software.

3 Results

The study area showed two different soil profile according to their slope values (Fig. 2a). Figure 2b shows the altitude curve for the entire plot. The first part of the curve refers to the flat subplot. It shows values ranging from 362 a.g.l. at the lowest point, to 365 a.g.l. at the highest, with an average slope value of 2.55%. The second section of the curve, referred to the sloped subplot, has values ranging from 363 a.g.l. at the highest point to 348 a.g.l. at the lowest point, with an average slope value of 10.55%.

The study area showed a good variability in the multispectral response. The NDVI raw map ranging from -1 to 1 from both flight configuration. The lowest NDVI value characterized the soil zone, while the highest NDVI value corresponded to vegetation. Through the segmentation analysis it was possible to remove the soil

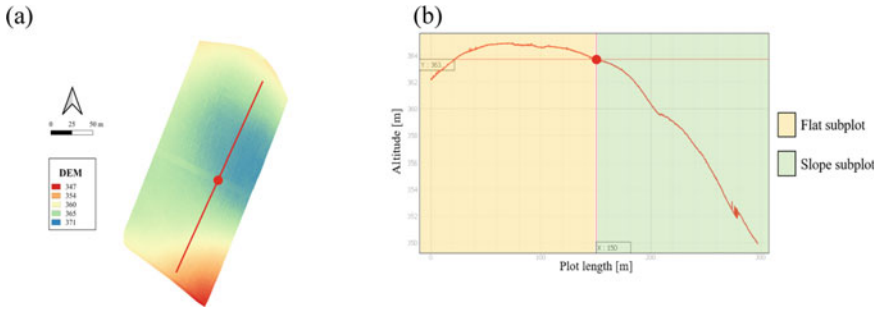


Fig. 2 (a) Digital Elevation Model (DEM) of the whole study area; (b) Graphical representation of the altitude of the two subplots

pixel value and to extract only the vegetation canopy value. After this processing, the average NDVI was 0.31 ± 0.19 and 0.48 ± 0.19 for parallel and perpendicular flight path respectively. Analyzing the entire study area, it was possible to assess the influence of the different slopes on vineyard vigor.

Figure 3 shows differences in terms of NDVI pixels frequency over the entire study area according to the flight path. In the flight perpendicular to the vineyard rows, a higher frequency of pixels shifted to higher NDVI values was observed, compared to the parallel flight path. Using an unsupervised clustering algorithm, the pixels of the NDVI rasters were classified into three different vigor classes: low, medium and high. For each of the three clusters obtained, the surface area was calculated. In the parallel flight path, the total low vigor area was 3,567 m², the medium was 18,173 m² and the high vigor area was 9,298 m². Among these areas, in the flat area the percentage of low vigor was 3.6%, the medium vigor was 34.19% and the high vigor was 10.91%. The sloped area showed a low vigor zone of 7.55%, a medium vigor zone of 21.09% and a high vigor zone of 18.00%, referred to the whole study area.

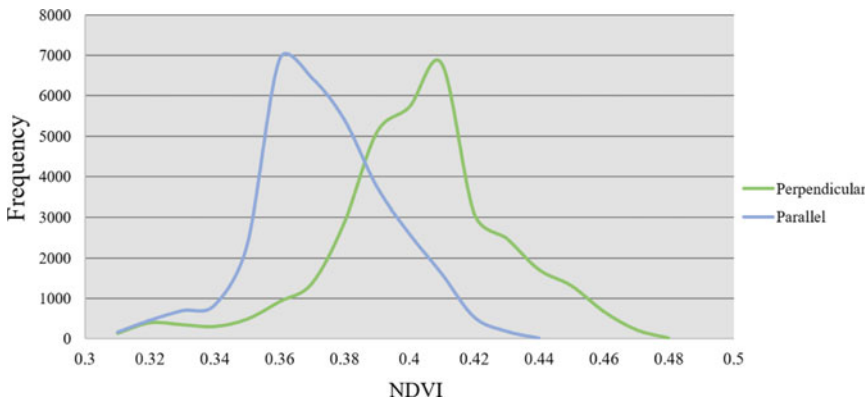


Fig. 3 NDVI frequency histogram of parallel and perpendicular flight paths rasters

In the perpendicular flight path, the total low vigor area was 4,390 m², the medium was 21,000 m² and the high vigor area was 7,580 m². Among these areas, in the flat area the percentage of low vigor was 6.3%, the medium vigor was of 37.61% and the high vigor was 8.71%. The sloped area showed a low vigor zone of 6.95%, a medium vigor zone of 25.91% and a high vigor zone of 14.24%. referred to the whole study area.

The results concerning the analysis of variance of the multispectral data showed statistical significance for the two flight paths (p value < 0.001) for all the three levels of vigor. A similar result was obtained for the NDVI data in the two topographical conditions (p value < 0.001). However, the analysis of variance showed zero significance in the interaction between the flight configurations and the two topographical conditions for NDVI data of medium and high vigor areas (p value = 0.483 and 0.045 respectively). The interaction was significant for low vigor areas (p value < 0.001).

3.1 Flat Subplot

In the flat plot and parallel flight path (Fig. 4a), the low vigor area was of 3,947 m², the medium area was 8,526 m² and the high vigor was 4,087 m² corresponding to 23.83%, 51.49% and 24.68% respectively. In the perpendicular flight configuration (Fig. 4b), the low vigor area was of 5,283 m², the medium area was 8,056 m² and the high vigor was 4,107 m² corresponding to 30.28%, 46.18% and 23.54% respectively.

Regarding multispectral data, there were statistically significant differences among the different flight paths and vigor levels (Fig. 5). The ANOVA test showed that high vigor level in the perpendicular flight and low vigor level in the parallel flight were statistically different with all the data (p value < 0.001). No statistically significant differences were found between the medium vigor level of the perpendicular flight and the high level vigor of the parallel flight according to the ANOVA test (p value < 0.001). No statistically significant differences were found between the

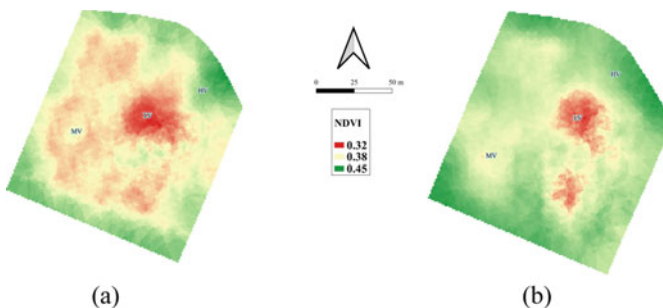


Fig. 4 Distribution of vigor classes in the flat plot; **(a)** Parallel flight path; **(b)** Perpendicular flight path; Low Vigor (LV), Medium Vigor (MV), High Vigor (HV)

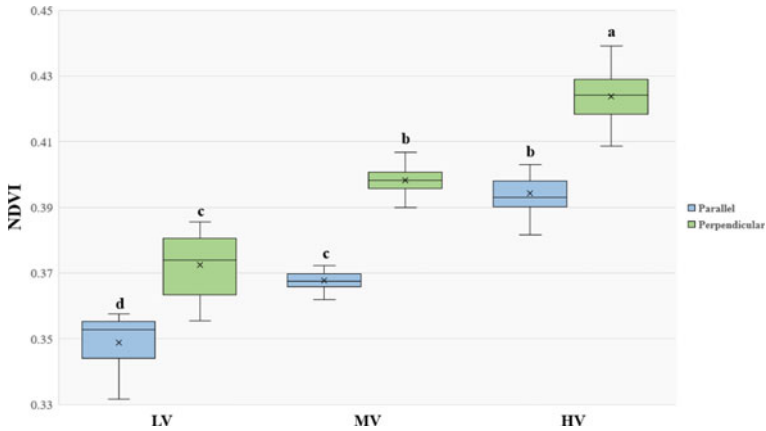


Fig. 5 Box plot and ANOVA test results of different vigor levels in the flat area for the two flight configurations

low vigor level of perpendicular flight and the medium level vigor of parallel flight according to the ANOVA test (p value < 0.001).

3.2 Sloped Subplot

In the sloped plot and parallel flight configuration (Fig. 6a), the low vigor area was 3,056 m², the medium area was 7,889 m² and the high vigor was 3,536 m² corresponding to 21.10%, 54.48% and 24.42% respectively. In the perpendicular configuration (Fig. 6b), the low vigor area was 2,112 m², the medium area was 9,667 m² and the high vigor was 3,758 m² corresponding to 13.59%, 62.22% and 24.19% respectively.

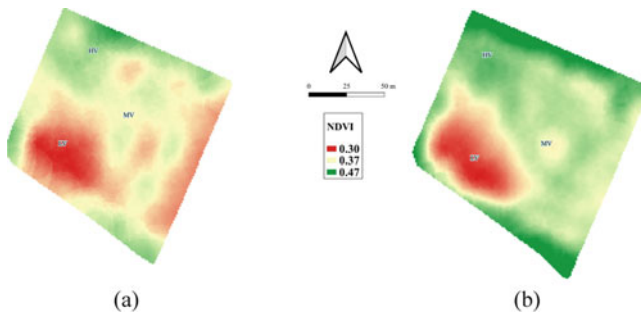


Fig. 6 Distribution of vigor classes in the sloped plot; (a) Parallel flight path; (b) Perpendicular flight path; Low Vigor (LV), Medium Vigor (MV), High Vigor (HV)

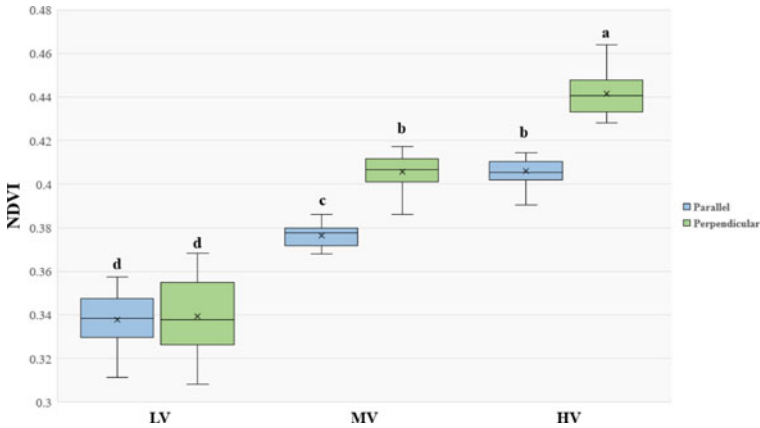


Fig. 7 Box plot and ANOVA test results of different vigor levels in the sloped area for the two flight configurations

Regarding multispectral data, there were statistically significant differences among the different flight paths and vigor levels (Fig. 7). The ANOVA test showed that high vigor level in the perpendicular flight and medium vigor level in the parallel flight were statistically different with all the data (p value < 0.001). No statistically significant differences were found between the medium vigor level of the perpendicular flight and the high vigor level of the parallel flight according to the ANOVA test (p value < 0.001). No statistically significant differences were found between the low vigor level of both flight paths according to the ANOVA test (p value < 0.001).

4 Discussion

The orography of the study area influenced the result of the experiments [7]. Indeed, it is commonly observed that sloped vineyards show several types of soil erosion processes bringing soil fertility in downhill [7, 16]. This process leads to the change of soil hydrological dynamics and increased sediment transport [18]. The impact of orography on the extension of the vigor areas and multispectral data was studied by means of the DEM. Previous studies had shown that the vine growth is closely correlated with soil differences [23, 24]. The experiment showed that the flat area in both path configurations was characterized by a larger extension of high vigor area than the sloped plot. The largest extension of medium vigor area was always in the sloped plot. The low vigor area was similar in the perpendicular path for both plots and slightly lower for the sloped plot in the parallel path. These results are different from that obtained in another study where soil fertility is higher in the downhill [17]. In this case, the effect can be explained taking into account that the sloped plot was not in the lowest altitude zone. In addition, the flat plot is not directly joined with

the sloped plot because there is the street that prevents the transport process. For this reason, the flat plot had a greater extension of the high vigor area.

The difference in the vigor areas has been detected in multispectral data as observed in previous studies [17, 23]. They found lower value of NDVI in the upper zone of the field than in the bottom zone. Instead, in our study for the same reason of vigor distribution, the higher NDVI values were concentrated in the flat plot. Therefore, the flat plot has not facilitated the elements transport process, while the sloped plot allowed it.

With reference to NDVI data, our study showed statistically significant differences between NDVI data in the two flight configurations. The values reported by the flight path performed perpendicular to the rows overestimate the NDVI for all three vigor levels. About that it is observed that in the flat plot the three vigor levels are all statistically different. Between the two flight paths, in the sloping plot there are statistically significant differences in medium and high vigor area unlike the low vigor data. This effect can be explained by taking into consideration the results obtained from the analysis of variance. The spectral response of the vineyard depends on both the slope effect and the flight configurations, thus their interaction was not significant. In the bibliography it is known that some pixels of the marginal parts of the vineyard canopy are mixed pixels, which in many cases are identified as shadow pixels and can affect the spectral response of the vineyard [15]. Due to this effect, we have noticed that in the low vigor areas it has not been discretized efficiently and probably the spectral response is flawed. On the other hand, in the areas of medium and high vigor, this effect was lower, discretizing the canopy more efficiently.

5 Conclusions

This study investigated the effects of different image acquisition procedures from UAV in two topographic configurations. The results obtained showed that the topography of the plot affects the spectral response data of the vineyard. Within each plot a different vigor distribution trend can be identified. In the flat zone there was a greater extension of the high vigor area, while in the sloped zone there was a greater extension of the low vigor area. In addition, we found that both flight paths influenced the spectral response data. Specifically, performing a flight perpendicular to the vineyard rows, it induces an overestimation of NDVI values. Our findings provide a better understanding of the influences of different flight paths in vineyard multi-spectral response, and further highlights that terrain orography plays a key role in the distribution of vegetation vigor. These preliminary results define the importance of setting a correct UAV flight path planning and further underline that the use of UAVs in precision viticulture allows to obtain vigor maps with high definition.

References

1. Adão, T., et al.: Hyperspectral imaging: a review on UAV-based sensors, data processing and applications for agriculture and forestry. *Remote Sens.* **9**, 1110 (2017)
2. Barba, S., Barbarella, M., Di Benedetto, A., Fiani, M., Gujski, L., Limongiello, M.: Accuracy assessment of 3D photogrammetric models from an unmanned aerial vehicle. *Drones* **3**, 79 (2019)
3. Caruso, G., et al.: High-resolution imagery acquired from an unmanned platform to estimate biophysical and geometrical parameters of olive trees under different irrigation regimes. *PLoS ONE* **14**, e0210804 (2019)
4. Catania, P., et al.: Positioning accuracy comparison of GNSS receivers used for mapping and guidance of agricultural machines. *Agronomy* **10**, 924 (2020)
5. Catania, P., Orlando, S., Roma, E., Vallone, M.: Vineyard Design Supported by GPS Application, pp. 227–234 (2019)
6. Catania, P., Roma, E., Orlando, S., Vallone, M.: Evaluation of multispectral data acquired from UAV platform in olive orchard. *Horticulturae* **9**, 133 (2023). <https://doi.org/10.3390/horticulturae9020133>
7. Comino, J.R., et al.: Understanding soil erosion processes in Mediterranean sloping vineyards (Montes de Málaga, Spain). *Geoderma* **296**, 47–59 (2017)
8. Czyba, R., Lemanowicz, M., Gorol, Z., Kudala, T.: Construction prototyping, flight dynamics modeling, and aerodynamic analysis of hybrid VTOL unmanned aircraft. *J. Adv. Transp.* (2018)
9. Darvishpoor, S., Roshanian, J., Raissi, A., Hassanalian, M.: Configurations, flight mechanisms, and applications of unmanned aerial systems: a review. *Prog. Aerosp. Sci.* **121**, 100694 (2020)
10. Fernández-Guisuraga, J.M., Sanz-Ablanedo, E., Suárez-Seoane, S., Calvo, L.: Using unmanned aerial vehicles in postfire vegetation survey campaigns through large and heterogeneous areas: opportunities and challenges. *Sensors* **18**, 586 (2018)
11. Hassanalian, M., Abdelkefi, A.: Classifications, applications, and design challenges of drones: a review. *Prog. Aerosp. Sci.* **91**, 99–131 (2017)
12. Hu, P., Guo, W., Chapman, S.C., Guo, Y., Zheng, B.: Pixel size of aerial imagery constrains the applications of unmanned aerial vehicle in crop breeding. *ISPRS J. Photogramm. Remote Sens.* **154**, 1–9 (2019)
13. Hunt, E.R., Jr., Hively, W.D., Fujikawa, S.J., Linden, D.S., Daughtry, C.S., McCarty, G.W.: Acquisition of NIR-green-blue digital photographs from unmanned aircraft for crop monitoring. *Remote Sens.* **2**, 290–305 (2010)
14. Kottek, M., Grieser, J., Beck, C., Rudolf, B., Rubel, F.: World map of the Köppen-Geiger climate classification updated (2006)
15. Lu, S., Xuan, J., Zhang, T., Bai, X., Tian, F., Ortega-Farias, S.: Effect of the shadow pixels on evapotranspiration inversion of vineyard: a high-resolution UAV-based and ground-based remote sensing measurements. *Remote Sens.* **14**, 2259 (2022)
16. Manandhar, R., Odeh, I.O.: Interrelationships of land use/cover change and topography with soil acidity and salinity as indicators of land degradation. *Land* **3**, 282–299 (2014)
17. Martínez-Casasnovas, J., Ramos, M., Balasch, C.: Precision analysis of the effect of ephemeral gully erosion on vine vigour using NDVI images. In: Stafford, J.V. (eds.) *Precision Agriculture 2013*, pp. 777–783. Springer (2013). https://doi.org/10.3920/978-90-8686-778-3_96
18. Novara, A., Keesstra, S., Cerdà, A., Pereira, P., Gristina, L.: Understanding the role of soil erosion on CO₂-C loss using ¹³C isotopic signatures in abandoned Mediterranean agricultural land. *Sci. Total Environ.* **550**, 330–336 (2016)
19. Roma, E., Laudicina, V.A., Vallone, M., Catania, P.: Application of precision agriculture for the sustainable management of fertilization in olive groves. *Agronomy* **13**, 324 (2023). <https://doi.org/10.3390/agronomy13020324>
20. Rossi, P., Mancini, F., Dubbini, M., Mazzone, F., Capra, A.: Combining nadir and oblique UAV imagery to reconstruct quarry topography: methodology and feasibility analysis. *Eur. J. Remote Sens.* **50**, 211–221 (2017)

21. Rouse Jr, J., Haas, R.H., Deering, D., Schell, J., Harlan, J.C.: Monitoring the vernal advancement and retrogradation (green wave effect) of natural vegetation (1974)
22. Stow, D., Nichol, C.J., Wade, T., Assmann, J.J., Simpson, G., Helfter, C.: Illumination geometry and flying height influence surface reflectance and NDVI derived from multispectral UAS imagery. *Drones* **3**, 55 (2019)
23. Tagarakis, A., Liakos, V., Fountas, S., Koundouras, S., Gemtos, T.: Management zones delineation using fuzzy clustering techniques in grapevines. *Precis. Agric.* **14**, 18–39 (2013)
24. Tardáguila, J., Baluja, J., Arpon, L., Balda, P., Oliveira, M.: Variations of soil properties affect the vegetative growth and yield components of “Tempranillo” grapevines. *Precis. Agric.* **12**, 762–773 (2011)
25. Zheng, X., Wang, F., Li, Z.: A multi-UAV cooperative route planning methodology for 3D fine-resolution building model reconstruction. *ISPRS J. Photogramm. Remote Sens.* **146**, 483–494 (2018)

Olive Tree Canopy Assessment Based on UAV Multispectral Images



Pietro Catania, Massimo Vincenzo Ferro, Eliseo Roma, Santo Orlando, and Mariangela Vallone

Abstract Unmanned Aerial Vehicle (UAV) is widely used to acquire data on the biometric and spectral characteristics of olive trees through multispectral cameras. Several flight parameters and image processing techniques can be applied in order to obtain this information. The aim of this work was to study the variability of the main biometric parameters and multispectral characteristics of olive trees through multispectral images acquired from a remote platform (UAV) at three different flight altitudes (30, 50 and 70 m), in two acquisition periods, with and without the use of differential coordinate correction (RTK), also applying different image segmentation techniques. Phantom 4 Multispectral UAV platform was used for the two flight campaigns. The photogrammetric processing was carried out using the software Agisoft Photoscan Professional, version 1.7.3. The biometric and multispectral data extraction processing was carried out through the software QGIS, version 3.2. Different segmentation techniques were applied on the acquired images, starting from the main vegetation indices maps as Normalized Difference Vegetation Index (NDVI) and the Modified Soil Adjust Index (MSAVI). The results showed that the olive tree canopy can be accurately studied using the canopy spectral information obtained by the UAV multispectral system.

Keywords Remote sensing · *Olea europaea* L. · Canopy · Unmanned aerial vehicle (UAV) · Vegetation Index

1 Introduction

Precision oliviculture continuously requires techniques and technologies capable of investigating the variability in the olive grove with high precision and accuracy in order to conveniently manage it [1]. The field variability can be detected using

P. Catania · M. V. Ferro · E. Roma · S. Orlando (✉) · M. Vallone
Department of Agricultural, Food and Forest Sciences, University of Palermo,
Viale Delle Scienze, Ed 4, 90128 Palermo, Italy
e-mail: santo.orlando@unipa.it

different sensors placed on different platforms. One of the most important platforms is the Unmanned Aerial Vehicle (UAV). There are several variables that can affect the final image resolution and consequently the information, such as the flight altitude, whereas the most used sensors are the multispectral and RGB. The image acquired with these technologies can determine the status of each tree starting from the multispectral and biometric characteristics. Different methodologies can be used in GIS programs to extract this information from the orthomosaic multiband. The first step is to identify the canopy of each plant with the aim of obtaining several biometric information strictly related to the vegetative activity. Subsequently, for each canopy it is possible to extrapolate the multispectral response to investigate the health status of the plant. A crucial phase is the segmentation of the images. It allows to obtain different non-overlapping zones that form the basis for the classification. Therefore, the proper implementation of this step is crucial to achieve correct plant identification. There are several methods to perform segmentation, the main one is the threshold clustering. This method can be applied to the Vegetation Index (VI) maps [2]. VIs can be used to differentiate the soil pixels from the vegetation pixels. Among them, the Normalized Difference Vegetation Index (NDVI) is the most important, while the Modified Soil Adjust Index (MSAVI) is an orthogonal vegetation index [3]; they are able to discriminate soil and non-pure pixels differently, as well as the resulting spectral information [4]. NDVI is the most widely used in olive and many other crops and was invented by Rouse et al. (1974). It is calculated from the normalisation of spectral information of the red (Red) and infrared (NIR) bands and can take values between -1 and 1 . It measures healthy vegetation using the highest absorption and reflectance regions of chlorophyll and is useful for characterising canopy growth or vigour [4]. Its main limitation is related to the high sensitivity of background factors, such as shade, canopy brightness of vegetation and soil. The MSAVI is a distance-based index and was invented by Qi et al. [5]. It was created to improve the spectral information of another distance-based index, the Soil Adjusted Vegetation Index (SAVI). The main feature of this category of indices is the high discrimination ability between vegetation and soil. In order to properly apply precision agriculture in olive growing, it is necessary to obtain accurate data on biometric and multispectral characteristics of the olive trees. The aim of this study was to verify whether multispectral images acquired from a remote platform (UAV) at three different flight altitudes (30, 50 and 70 m) and two different Vegetation Indices for image segmentation, can describe the variability of the canopy area and the multispectral characteristics of the olive orchard.

2 Materials and Methods

The experiment was conducted in 2021 in a 20-year-old olive grove cultivated according to ordinary management practices. The olive grove, cv. Cerasuola, is cultivated without irrigation system. The area under study is located in Segesta (Trapani,

Italy). The surface area covers 5,860 m² with a flat regular orography. The soil moisture regime is xeric, border with the aridic one, and the temperature regime is thermic. The soil texture is Franco-Sandy-Argillaceous, according to the USDA classification. It has a regular layout with a planting distance of 5 m. The total number of trees that was used for the experimentation was 211. In June 2021, the measure of the Trunk Cross Section Area (TCSA, m²) for each plant was registered to have an indicator for the real vigor condition. It was taken at 50 cm from the ground trying to decrease the influence of the stem ribs.

2.1 Workflow

The workflow that was applied for the achievement of the experiment included three main phases: UAV data planning and acquisition; pre-processing (photogrammetric reconstruction, orthorectification and mosaicking, spectral calibration of images, image georeferencing, topographic derivation); image processing and analysis (object-based image segmentation, vegetation index derivation, image classification, extraction of olive canopy area and spectral data).

2.2 Scheduling of Flight and Images Acquisition

Two flight campaigns were carried out on DOY (day of year) 189 (flight 1) and DOY 217 (flight 2) at 12 noon to minimise shadowing. Both days were characterised by excellent weather conditions with high light intensity and low wind speed. The planning was carried out using the official DJI software. The flights were carried out with the automatic flight configuration using the different flight path predetermined in Real Time Kinematic mode (RTK). Prior to the flight 1, harrowing was performed to remove weedy vegetation, which could have created problems in locating the pure canopies. For both flights, 5 Ground Control Points (GCPs) were placed evenly at the edges and centre of the plot on a solid platform. The GCPs were georeferenced using a GNSS instrument, specifically the Stonex S7-G, which has already been used in other experiments with excellent results [6, 7]. To improve accuracy, the coordinates of the different GCPs were acquired by mounting an external dual-frequency antenna (L1/L2; Stonex geodetic antennas), in RTK mode and averaging approximately 60 coordinate points.

The flights were carried out at three different flight heights: 30, 50 and 70 m a.g.l., obtaining a ground sample distance (GSD) of 1.6, 2.6 and 3.6 cm respectively. For all the flights, image acquisition was carried out at an average speed of 10 m * s⁻¹ with the stop-and-go mode. The image overlap ratio, front overlap ratio and side overlap ratio was 70% while the gimbal pitch was set at 90° (downwards). The schedule of the two flights (1 and 2) is summarised in Table 1.

Table 1 Flight characteristics

ID flight	DOY	Take-off time [UTC + 2]	Flight height a.g.l [m]	Speed [m*s ⁻¹]	Photographed area [m ²]	Duration [m' s'']	GSD [cm]	Photo [n]	Overlap [%]	Sidelap [%]	RTK
	–										–
1	189	12:00	30	10	532.48	12'52"	1.6	136	70	70	Yes
1			50		1406.08	6'19"	2.6	47			
1			70		2695.68	5'10"	3.6	27			
2	217	12:00	30	10	532.48	12'52"	1.6	136	70	70	Yes
2			50		1406.08	6'9"	2.6	47			
2			70		2695.68	5'10"	3.6	27			

2.3 Pre-processing of the Images

Once the multispectral images were acquired, they were pre-processed in order to obtain an orthomosaic. Data processing was carried out using a Structure for Motion (SFM) software, Agisoft Photoscan Professional version 1.7.3.

Image alignment was performed using the software and setting high accuracy, generic preselection, reference preselection and the sequential method. The number of key and tie point limits were left by default. Once the alignment had been carried out, the GCPs were entered using the WGS84 geographical coordinate system (EPSG: 4326). Then, the GCPs were identified on the different photos. After this step, the most accurate topographic transformation could be carried out, depending on the number of GCPs present. The calibration of the images was carried out by the software using the brightness data recorded by the sensor. The construction of the Dense Cloud was then carried out using very high accuracy; finally, the mesh was constructed and, through a process of orthorectification and mosaicking, the multiband orthomosaic was realized.

2.4 Images Processing and Analysis

Once the orthomosaic was obtained, it was processed in order to extrapolate the spectral and biometric data, using the open-source software QGIS version 3.16.6. The processing phase was carried out using the Geographic Object-Based Image Analysis (GEOBIA) methodology. The first processing phase of the orthomosaic was the image segmentation. In this study, we chose to carry out the image segmentation from the vigour map, as also carried out in other studies on olive grove [2]. In this case, the two main vegetation indices were considered: the Normalized Difference Vegetation Index (NDVI) [8] and the Modified Soil Adjusted Vegetation Index (MSAVI) [5]. From the VI map, a 2bit clustering of the image was performed using the K-means algorithm, which is one of the main clustering algorithms used. It was taken from Saga's Images analysis library.

Once clustered, the individual plant crowns were extracted through a polygonization process. Finally, from the single crowns, it was possible to extract the biometric 2D data of the crowns. By cross-referencing the multispectral raster images and the vector of the crowns, the spectral data of each individual plant was obtained.

2.5 Survey Equipment

The flight campaigns were carried out using the Phantom4 Multispectral drone (P4M, DJI). The multispectral camera has six 1/2.9" CMOS sensors, such as an RGB sensor for visible light imaging and five monochrome sensors for multispectral imaging.

Table 2 Multispectral sensor characteristics bands specification

Bands	Centre of band wavelength [nm]	Spectral Resolution [nm]
Blue	450	± 16
Green	560	± 16
Red	650	± 16
Red Edge	730	± 16
NIR	840	± 26

The lens has a FOV (field of view) of 62.7° , a focal length of 5.74 mm and an aperture of $f/2.2$. The maximum final image size is 1600×1300 . The spectral characteristics of the camera are summarised in Table 2.

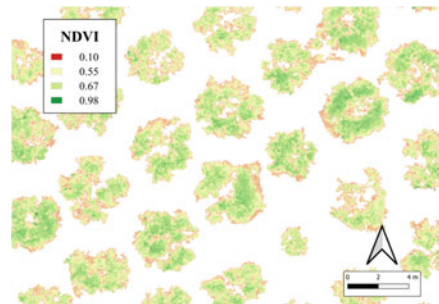
The drone is equipped with four rotary-wing (quadricopter) rotors capable of autonomously flying over the route predetermined by waypoints. It has a light sensor at the top, which enables to obtain pre-calibrated images. It is also capable of image position compensation as the relative positions of the CMOS sensor centres. The multi-frequency Global Navigation Satellite System (GNSS) positioning system is able to see and receive signals from the following satellites with their frequencies: GPS L1/L2; GLONASS L1/L2; BeiDou B1/B2; Galileo E1/E5.

3 Results

The variability of the whole plot was investigated in terms of canopy area and multispectral features (Fig. 1).

Both vegetation indices showed good mean values strictly related to the flights acquisition period and the real condition of the plants. Precisely, NDVI showed an average value of 0.60 and 0.62 for flight 1 and flight 2, respectively, while MSAVI showed an average value of 0.72 and 0.73 for flight 1 and flight 2, respectively (Fig. 2).

Fig. 1 NDVI values for each canopy extracted for the plants



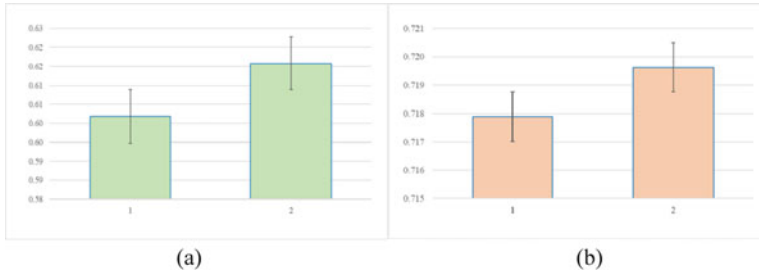


Fig. 2 Average values of NDVI (a) and MSAVI (b) in the two flight periods

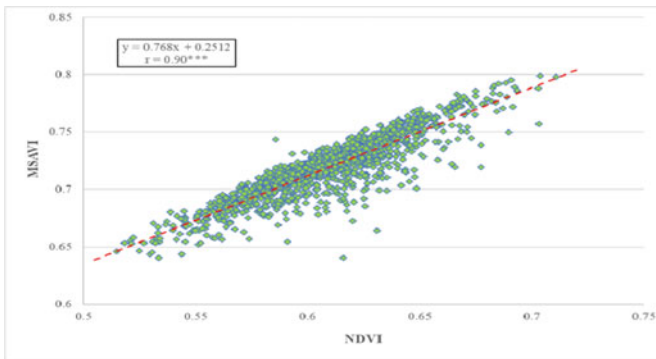


Fig. 3 Correlation between NDVI and MSAVI for all the plants of the study area

However, the two VIs had the same trend for each plant showing a high correlation between the datasets ($p_{value} < 0.001$; Fig. 3).

The canopy area variability showed a low relation with the flight altitude while resulted most correlated with the VI map used for the segmentation process (Fig. 4). Indeed, MSAVI and NDVI, using the ANOVA test, showed statically significant differences in all flight altitudes and periods. MSAVI always showed the highest value of canopy area, quantifiable at 1.55 m². There were no statistically significant differences between the two flight periods within each index. The average canopy area of MSAVI was 11.48 m² while for NDVI it was 9.93 m². NDVI showed no statistically significant differences, while MSAVI showed little statistically significant differences but no certain definite correlation with altitude or flight period.

All the VIs showed high correlation with the canopy area ($p_{value} 0.001$), but the NDVI values acquired at 70 m a.g.l. in flight 1 showed the best correlation (Fig. 5).

Comparing the Trunk Cross Section Area (TCSA values) with the values of canopy area the best correlation was obtained with the canopy area extracted from MSAVI image acquired at 70 m a.g.l. in flight 2 (Fig. 6).

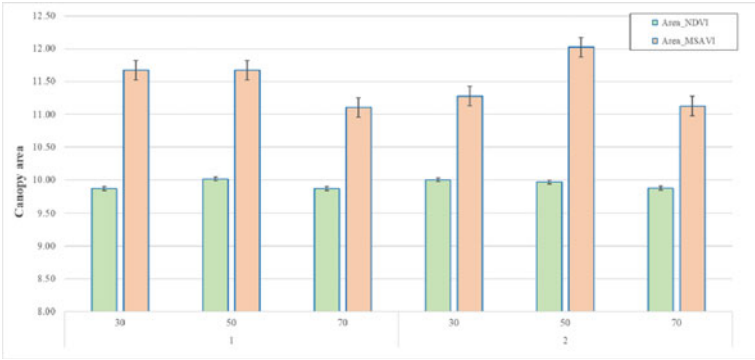


Fig. 4 Canopy area (m²) divided for flight acquisition periods and altitudes for both VIs

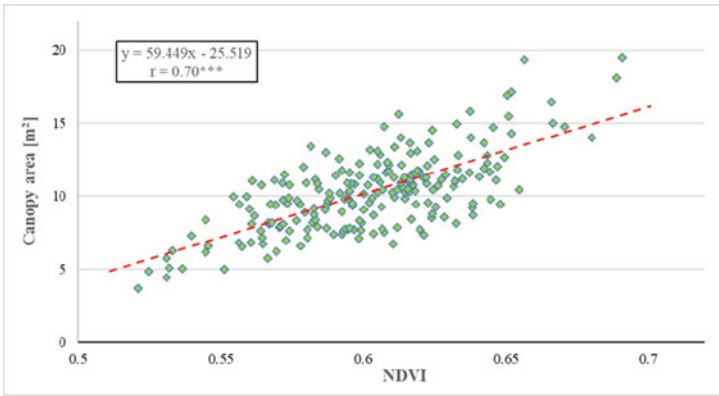


Fig. 5 Correlation between canopy area (m²) extracted from NDVI map of flight 1 at 70 m a.g.l. and average NDVI values of each plant

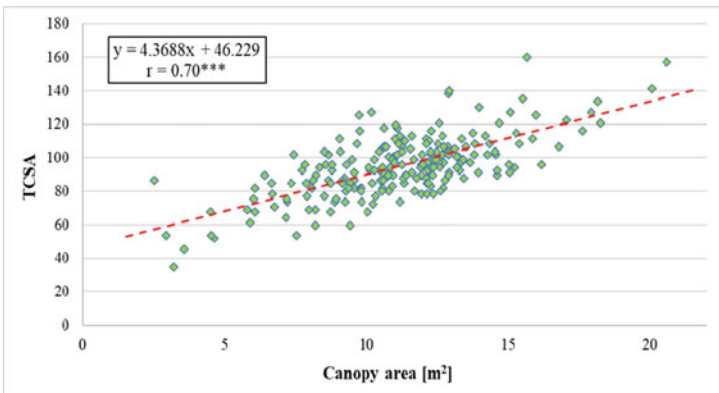


Fig. 6 Correlation between TCSA values and canopy area extracted from MSAVI of flight 2 at 70 m a.g.l

4 Discussion

The information provided by the used technique allows creating maps of olive orchard heterogeneity due to zones with different tree sizes. These maps help to understand the linkages between tree grown and field-related factors (soil properties, weed infestations, etc.) or to study the mutual relationship between nearby trees. In addition, these maps allow adopting a strategy for site-specific management of homogenous zones based on field spatial variability, which could increase farmer net economic advantage and environmental protection [9, 10].

In our study, both VI maps showed a good relationship in all the applications performed. The strong linear relationships between NDVI and MSAVI data confirms that the two datasets follow the same trend [11]. The indices were able to detect the whole vegetation status of the plants with high precision. NDVI confirmed its good relationship with the vigour characteristics, as reported in previous studies [2, 12]. Regarding the multispectral features, no differences were found within the same period between the different altitudes for both VIs. Little differences were found between the two acquisition periods in the multispectral feature due to the increase in the vegetative activity during the growth season, thanks to the higher photosynthetic efficiency, as obtained in [13]. Regarding the biometric data, our results are confirmed in literature. Johansen et al., [12] also found no statistically significant differences from flying at different heights in the quantification of canopy in terms of volume, perimeter and height of canopy. Indeed, Johansen et al., [12] also found the best correlation with the flying height of 70 m. There are clear management advantages to flying a UAV at a height of 70 m compared to 30 m, as it is possible to cover a larger area in a single flight, reduce the flying time for covering a set area, perform a flight mission more quickly and reduce the risk of shadow contamination. Also Torres-Sánchez et al., [14] mapped tree structural parameters of olive trees from UAV imagery acquired at 50 and 100 m a.g.l. and they did not observe reductions in their predicted mapping accuracies, while significantly reductions for the time of flight and the orthomosaic processing were obtained, with a reduction in the total required time.

5 Conclusions

The UAV platform was able to quantify the spatial variability of the olive grove at plant scale with high accuracy. The experimentation confirmed that this platform and its sensors have a good ability to describe the biometric and multispectral conditions of each plant. The flight carried out in two different periods was able to detect the physiological status of the plants and quantify the higher photosynthetic efficiency of the vegetation on the second date. Nevertheless, the flight period has no influence on the canopy area. The flight altitudes did not influence the multispectral data of the individual plants and the canopy area within the same indices. The segmentation

process with the MSAVI map resulted in a higher canopy area estimation than the NDVI. The indices considered were able to well estimate the canopy area and a vegetative parameter as TCSA, but the best results were obtained for NDVI at 70 m, confirming the close relationship between this index and the vegetative activity. All the canopy area values were well correlated with the vegetation parameter of TCSA, but the best results were obtained from the canopy extracted by segmentation with the MSAVI at 70 m, confirming its high ability to differentiate bare soil from canopy vegetation.

References

1. Roma, E., Catania, P.: Precision oliviculture: research topics, challenges, and opportunities—a review. *Remote Sens.* **14**, 1668 (2022)
2. Caruso, G., et al.: High-resolution imagery acquired from an unmanned platform to estimate biophysical and geometrical parameters of olive trees under different irrigation regimes. *PLoS ONE* **14**, e0210804 (2019)
3. Dorigo, W.A., Zurita-Milla, R., de Wit, A.J., Brazile, J., Singh, R., Schaepman, M.E.: A review on reflective remote sensing and data assimilation techniques for enhanced agroecosystem modeling. *Int. J. Appl. Earth Obs. Geoinf.* **9**, 165–193 (2007)
4. Xue, J., Su, B.: Significant remote sensing vegetation indices: a review of developments and applications. *J. Sens.* **2017** (2017)
5. Qi, J., Chehbouni, A., Huete, A.R., Kerr, Y.H., Sorooshian, S.: A modified soil adjusted vegetation index. *Remote Sens. Environ.* **48**, 119–126 (1994)
6. Catania, P., et al.: Positioning accuracy comparison of GNSS receivers used for mapping and guidance of agricultural machines. *Agronomy* **10**, 924 (2020)
7. Catania, P., Orlando, S., Roma, E., Vallone, M.: Vineyard design supported by GPS application. *Acta Hort.* **1314**, 227–234 (2021)
8. Rouse, J.W., Haas, R.H., Schell, J.A., Deering, D.W., Harlan, J.C.: Monitoring the Vernal Advancement and Retrogradation (Green Wave Effect) of Natural Vegetation. NASA/GSFC Type III Final Report, Greenbelt, Md, vol. 371 (1974)
9. Fountas, S., Aggelopoulou, K., Gemtos, T.A.: Precision agriculture: crop management for improved productivity and reduced environmental impact or improved sustainability. *Supply Chain Manage. Sustain. Food Networks* 41–65 (2015)
10. Van Evert, F.K., Gaitán-Cremaschi, D., Fountas, S., Kempenaar, C.: Can precision agriculture increase the profitability and sustainability of the production of potatoes and olives? *Sustainability* **2017**, 9 (1863)
11. Avola, G., et al.: Remotely sensed vegetation indices to discriminate field-grown olive cultivars. *Remote Sens.* **11**, 1242 (2019)
12. Johansen, K., Raharjo, T., McCabe, M.F.: Using multi-spectral UAV imagery to extract tree crop structural properties and assess pruning effects. *Remote Sens.* **10**, 854 (2018)
13. Jurado, J.M., Ortega, L., Cubillas, J.J., Feito, F.: Multispectral mapping on 3D models and multi-temporal monitoring for individual characterization of olive trees. *Remote Sens.* **12**, 1106 (2020)
14. Torres-Sánchez, J., López-Granados, F., Serrano, N., Arquero, O., Peña, J.M.: High-throughput 3-D monitoring of agricultural-tree plantations with Unmanned Aerial Vehicle (UAV) technology. *PLoS ONE* **10**, e0130479 (2015)

Development of a Test Bench for Vibration Measurements of Hand-Held Harvesters for Olives



Emanuele Cerruto, Giuseppe Manetto, and Domenico Longo

Abstract Olive harvesting is the most expensive activity among cultural operations, so its mechanization is essential to reduce production costs. For this reason, the use of hand-held vibrating harvesters is quite widespread where full mechanization is not possible. However, these machines expose operators to high vibration risks for the hand-arm system. The assessment of the effective risk requires direct measurement under real working conditions or the definition of standardized procedures able to provide reliable acceleration values. Although this need has long been known, a unified regulation for this purpose does not yet exist. To this end a test bench was designed and built at the Section of Mechanics and Mechanization of the Department of Agriculture, Food and Environment, to simulate in a reproducible way the load resistance the branches offer during harvesting. The test bench has an aluminum frame with a working area of about 1.5×1.5 m and allows testing all the main models of combo, beater or flap-type hand-held harvesters available on the market. The working area consists of vertical and horizontal nylon wires with adjustable spacing and tension to 2D-simulate the crown of the tree and to provide the load during the tests. The wires are stretched by means of springs and simultaneously about equally preloaded by moving a vertical and a horizontal bar of the frame. Fixing the preload and the distance between the wires, the load conditions for the machine under test are almost constant and measurements should be reproducible over time.

Keywords Safety · Health · Vibration exposure · Acceleration · HAV

E. Cerruto · G. Manetto (✉) · D. Longo
Department of Agriculture, Food and Environment (Di3A), University of Catania,
Via S. Sofia 100, 95123 Catania, Italy
e-mail: giuseppe.manetto@unict.it

© The Author(s), under exclusive license to Springer Nature Switzerland AG 2023
V. Ferro et al. (eds.), *AIIA 2022: Biosystems Engineering Towards the Green Deal*,
Lecture Notes in Civil Engineering 337,
https://doi.org/10.1007/978-3-031-30329-6_49

1 Introduction

Occupational exposure to mechanical vibrations was regulated for the first time in Italy by Legislative Decree 187/2005 [17], implementing the 2002/44/EC Vibration Directive [19]. Legislative Decree 187/2005 was subsequently incorporated into Legislative Decree 81/2008 [22], in which it appears as Chapter III of Title VIII on the protection of workers from the risks of exposure to mechanical vibrations. According to the Italian National Institute for Insurance against Accidents at Work [21], most of the professional diseases reported in the agricultural sector, such as biomechanical overload of upper limbs, lumbar herniated disc, diseases due to vibrations transmitted to the hand-arm system, noise-induced hearing loss, are strictly vibration-related. The problem is made even more serious by the growing level of mechanization that has affected many agricultural activities in the last decades. Due to the great multiplicity of agricultural tasks, vibration exposure may regard both the whole body, mainly when driving tractors [4, 10, 13, 16, 27, 30, 32, 34, 35] and the hand-arm system, mainly when using portable machines [2, 5, 8, 11, 26, 28, 31, 36].

The large use of portable harvesters in the olive sector, due to reduction in production costs they are able to guarantee when the traditional tractor-mounted or self-propelled shakers can't be used [1], exposes users, mainly interested in productivity rather than in ergonomic and safety aspects, to high level of vibrations for the hand-arm system (HAS) [6, 9, 25, 29]. Regular exposure to hand-arm vibration can result in symptoms and chronic disorders recognized by several names such as secondary Raynaud's phenomenon, vibration white finger, dead finger, traumatic vasospastic disease, collectively known as the hand-arm vibration syndrome (HAVS) [3, 7, 20, 33].

As it is well documented in the literature, the transmission and propagation of the vibration in the organism through the hand-arm system represent a very complex phenomenon and measured acceleration values depend on several factors, among which the features of machine (kinematics of the harvester head, rod material, its geometry and configuration), the working conditions (idling or full-load), the characteristics of the operator (weight, grip force, ability), the use of protective equipment (anti-vibration gloves). On the other hand, knowledge of the acceleration values is of great importance because, according to the 2006/42/EC Directive [18], the manufacturers have to declare them in the machine instruction manual. It is therefore necessary to have equipment and procedures that allow carrying out laboratory measurements under conditions that are as standardized and repeatable as possible, resulting in vibration values close to the field values.

A very simple device is described in Deboli et al. [14] for testing hook-type portable harvesters. It consists in a fork lift with wrapped elastic rope bound at the fork in such a way to have load and variable 'tree branch' height. Another device, able to test flat-type portable harvesters, is described in Deboli et al. [15]. It consists in a wooden framed device with multifilament polypropylene UV stabilized wires loaded with 1-kg iron masses.

In this study, another device is proposed, based on the model of Deboli et al. [15] and preliminary tests were carried out with one electric portable harvester, running both at idling and loaded with the test bench.

2 Materials and methods

2.1 Design of the Vibration Test Bench

The designed test-bench is an aluminum frame with a suitable pedestal (Fig. 1). It is realized using modular extruded aluminum bars from Bosch Rexroth 40×40 mm and related connecting element (brackets, nuts and so on). The working area is about 1.5×1.5 m at a height between 1.5 and 3 m above the ground to 2D-simulate the crown of the plant. It is constituted by two sets (horizontal and vertical) of nylon wires 0.5 mm diameter, applied by means of metal rings and nuts to the Bosh modular bar. One spring is mounted in series with each wire, in one end. The elastic constant of the springs used, measured by means of the dynamometer Sauter Fk 250 (KERN & SOHN GmbH, Balingen, Germany), is 0.135 N mm^{-1} , with coefficient of variation of 3.99%.

The working area has two fixed borders (that are parts of the structure itself) and two adjustable sides (one horizontal and one vertical) (Fig. 1). This allows to apply a known tension to wires and springs: in fact, springs, and so the wires, connected to each bar are almost equally and simultaneously preloaded by moving the bar along the frame. Finally, by fixing the space between the wires and their tension, the load conditions for the machine under test should be almost constant and the measurements

Fig. 1 The test bench with a detail of the movable bars to preload wires with springs

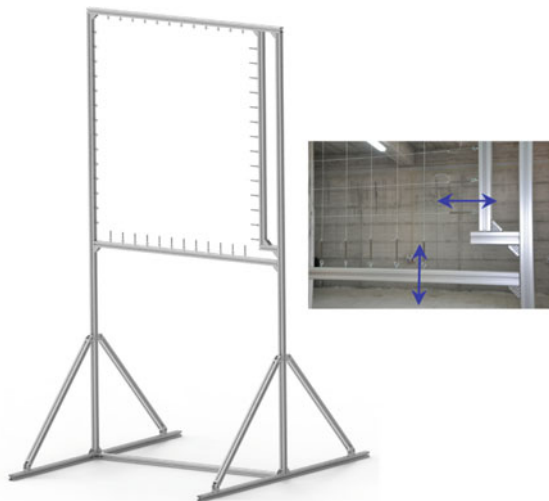
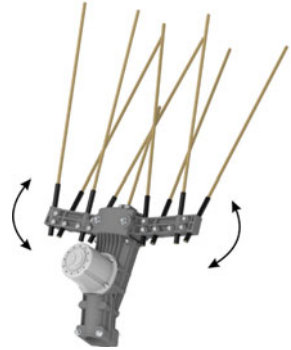


Fig. 2. 3D model of the harvesting head



should be reproducible over time. In this first test, the wires are spaced 10 cm both vertically and horizontally.

2.2 *The Portable Harvester*

Experimental tests were carried out by using one electric portable harvester produced by a local manufacturer. The harvesting head (Fig. 2) has a plastic box to which are connected two arms with opposing oscillations on a plane orthogonal to the motor shaft. Each arm, 121-mm long, carries 4 carbon fiber sticks, 360-mm long and with 5-mm diameter. Another stick, 180-mm long, is fixed in central position. The total width of the harvesting head is 300 mm.

The harvesting head is applied to an aluminum made telescopic rod, which diameters are 35 mm (external part) and 28 mm (internal part), both 1-mm thick. Total rod lengths, including the handle equipped with the activation switch (225 mm) and a rear handle extension (135 mm), are 1840 mm (minimum length) and 2630 mm (maximum length). The total mass (harvesting head, rod, handle, extension, and electric cable inside the rod), is 3.12 kg.

The harvesting head is driven by a 12 V DC brushless electric motor (maximum power of 800 W and nominal rotation speed of 6300 rpm, regulated by suitable electronic), powered by means of a lead-acid 12 V external battery. The motor shaft is connected to a transmission system that, with a gear ratio of 10:58, moves the arms with the sticks with an oscillating frequency of about 18 Hz.

2.3 *The Vibration Measurement System*

Vibration was measured near to the position of the hands: rear position (M1, near the handle with the activation switch) and front position (M2, on the rod). The distance between the two measuring points M1 and M2 was chosen 0.80 m.

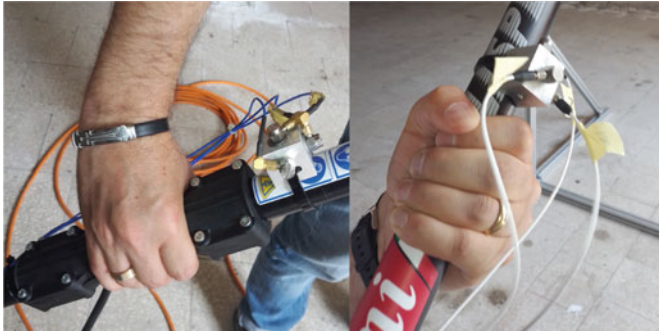


Fig. 3 The accelerometers applied to the rod near the position of the hands

Measurements were carried out contemporarily in the two points by using six mono-axial accelerometers (nominal sensitivity 10 mV g^{-1} , $1 \text{ g} = 9.81 \text{ m s}^{-2}$, the gravity acceleration), fixed on a custom-made aluminum block so as to constitute two tri-axial accelerometers and attached to the rod by means of plastic clamps. (Fig. 3). Accelerometers were oriented according to the basicentric coordinate system defined by the EN ISO 5349-1:2001 [23] regulation: x -axis perpendicular to the palm surface area, y -axis parallel to the longitudinal axis of the grip, and z -axis directed along the third metacarpus bone of the hand.

The accelerometer signals were sampled at 51.2 kHz and then recorded on the hard disk of a PC by means of a 12-channel PC-based acquisition unit, managed by the dBFA Suite software (01 dB-Metravib, Lyon, France). Subsequently, they were analyzed according to the ISO 5349-2:2001 [24] standard (one-third octave analysis in the frequency range 6.3–1250 Hz and frequency weighting) by using the post-processing module of the same dBFA Suite software. Total weighted acceleration a_{hw} was computed as the root-sum-of-squares of the three component values for the three reference axes:

$$a_{hw} = \sqrt{a_{hwx}^2 + a_{hwy}^2 + a_{hwz}^2} \quad (1)$$

2.4 The Experimental Activity

The portable harvester was used both at idling and at load conditions, operated by three peoples (mass ranging from 70 to 98 kg, height ranging from 1.70 to 1.76 m). Idling measurements were carried out with the rod inclined at about 45° with respect to the horizontal plane. Load tests were carried out by inserting the sticks of the harvester head into the frame of the test bench and, after 5–10 s, they were extracted and then re-inserted in a different position of the frame (Fig. 4). The springs of the test bench were elongated (in static conditions) of about 28 mm, so to provide a

Fig. 4 Load tests with the test bench



preload of around 3.7 N. In both conditions, the shortened configuration of the rod was used.

Each test condition was replicated 6 times and each measurement lasted about 60 s. The level of charge of the battery was periodically controlled by means of a multimeter and, when operator or test condition changed, the battery was recharged by a charger so to report the voltage at around 12 V. In addition, the intensity of the absorbed current was also measured, both at idling and at load conditions. Before and after the tests, the measurement chain was calibrated by means of a vibration exciter, which generated a sinusoidal output acceleration signal of 10 m s^{-2} (root mean square) at the frequency of 159.2 Hz.

Total weighted acceleration values were analyzed by applying the analysis of variance (ANOVA), considering test condition (idling and load) and measurement point (front and rear) as fixed factors and operator as random factor.

3 Results and Discussion

Table 1 summarizes the ANOVA results concerning acceleration values. The difference between the two measuring points was statistically significant, as well as the difference due to the interaction between measuring point and test condition. The difference between the two test conditions was not statistically significant.

On average, acceleration values were: 3.99 m s^{-2} in front position (M2) and 3.42 m s^{-2} in rear position (M1), difference statistically significant; 3.75 m s^{-2} at idling condition and 3.67 m s^{-2} at load condition, difference not statistically significant. The difference between the two measuring points confirms the results of previous researches, also obtained with different models of portable harvesters [11, 12]. The quite low difference between idling and load condition may be due to a low stiffness of the springs used to stretch the wires of the test bench. In previous researches [11, 37], these models of portable harvesters produced acceleration values

Table 1 ANOVA table of acceleration values

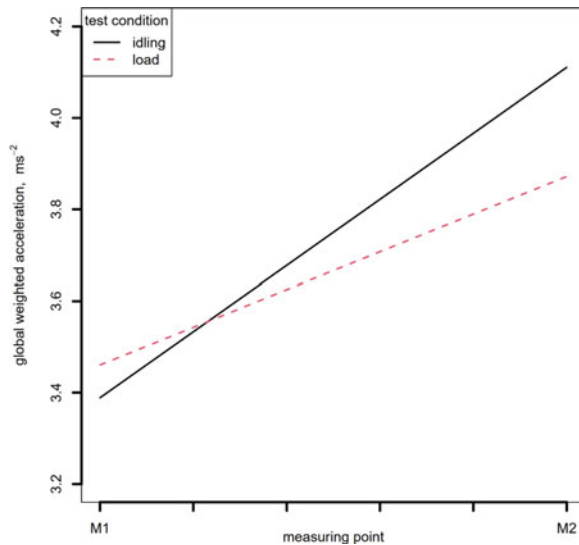
Source of variation	df	SS	MS	F value	Pr (>F)	Significance ^(a)
Test condition	1	0.126	0.126	1.293	0.2596	ns
Measuring point	1	5.774	5.774	59.329	<0.001	***
Interaction	1	0.434	0.434	4.459	0.0385	*
Residuals	66	6.424	0.097			

(a): *: significant at p-level = 0.05; ***: significant at p-level = 0.001; ns: not significant.

higher when they were used during olive harvesting rather than at idling conditions. In this study, the low difference between the two test conditions is also confirmed by the low difference in the current absorbed by the motor: about 2.5 A at idling condition and about 2.8 A at load condition. Finally, the Fast Fourier Transform (FFT) analysis of the acceleration signals showed a slight decrease in the first harmonic: 15.25 Hz at idling condition and 14.91 Hz at load condition. To be noticed that the measured frequency (around 15 Hz) was lower than the nominal one (around 18 Hz). These preliminary results suggest to modify the test bench by using springs with greater stiffness and/or decreasing the wire spacing so as to increase the resistance encountered by the sticks under load condition.

Figure 5 plots the interaction between measuring point (M1-rear and M2-front) and test condition (idling and load). The plot clearly shows the significance of the interaction: in point M1 acceleration was higher at load, whereas in M2 the acceleration was higher at idling.

Fig. 5 Interaction between measuring point and test condition



All results were quite reproducible: in fact, variability between operators was characterized by a coefficient of variation (CV) equal to 4.10% and the residual variability had $CV = 8.41\%$.

4 Conclusions

The study describes the design and construction of a test bench useful to standardize the measurement of the vibration transmitted to the hand-arm system by hand-held portable harvesters for olive harvesting. The test bench allows testing all the main models of combo, beater or flap-type (not hook-type) harvesters available on the market. The working area presents vertical and horizontal nylon wires with adjustable spacing and tension (fixed by means of springs) that 2D-simulate the crown of the tree and provide a constant load during the tests. The preliminary tests discussed in this research allow drawing the following conclusions:

- Portable harvesters similar to that used in this study produce acceleration values higher under load conditions and lower under idling conditions. However, in this study the difference between idling and load conditions (at the test bench) was not statistically significant. This result may be due to the low stiffness of the springs used to stretch the wires of the test bench.
- Low stiffness of the springs means low resistance encountered by the sticks of the harvester head. This is confirmed by the low difference between idling and load condition in the current absorbed by the motor and in the first harmonic frequency.
- These preliminary results suggest to increase the wire tension by using springs with greater stiffness and/or decrease the wire spacing. In addition, more frames could be applied to the same structure to simulate a 3D-model of the tree crown. These aspects will be investigated in future research developments.

Acknowledgements This research was funded by the University of Catania with the research projects “Sostenibilità ed innovazioni della ricerca in agricoltura, alimentazione e ambiente - WP 6: Monitoraggio ambientale, Meccanica e Meccanizzazione Sostenibile nell’Agricoltura Mediterranea”, premialità Linea 2 PIACERI and “Safe and Smart Farming with Artificial Intelligence and Robotics” (S2FAIR) - Programma Ricerca di Ateneo UNICT 2020-22 linea 2 PIACERI.

References

1. Aiello, G., Vallone, M., Catania, P.: Optimising the efficiency of olive harvesting considering operator safety. *Biosys. Eng.* **185**, 15–24 (2019). <https://doi.org/10.1016/j.biosystemseng.2019.02.016>
2. Bernardi, B., Quendler, E., Benalia, S., Mantella, A., Zimbalatti, G.: Occupational risks related to vibrations using a brush cutter for green area management. *Ann. Agricul. Environ. Med.* **25**(2), 255–258 (2018). <https://doi.org/10.26444/aaem/75684>

3. Bovenzi, M.: Health effects of mechanical vibration. *G Ital. Med. Lav. Ergon.* **27**(1), 58–64 (2005)
4. Caffaro, F., Micheletti, C.M., Preti, C., Cavallo, E.: Ergonomic analysis of the effects of a telehandler's active suspended cab on whole body vibration level and operator comfort. *Int. J. Ind. Ergon.* **53**, 19–26 (2016). <https://doi.org/10.1016/j.ergon.2015.10.009>
5. Çakmak, B., Saraçoğlu, T., Alayunt, F.N., Özarslan, C.: Vibration and noise characteristics of flap type olive harvesters. *Appl. Ergon.* **42**, 397–402 (2011). <https://doi.org/10.1016/j.apergo.2010.08.015>
6. Calvo, A., Deboli, R., Preti, C., De Maria, A.: Daily exposure to hand arm vibration by different electric olive beaters. *J. Agricul. Eng.* **45**(3), 103–110 (2014). <https://doi.org/10.4081/jae.2014.424>
7. Calvo, A., Romano, E., Preti, C., Schillaci, G., Deboli, R.: Upper limb disorders and hand-arm vibration risks with hand-held olive beaters. *Int. J. Ind. Ergon.* **65**, 36–45 (2018). <https://doi.org/10.1016/j.ergon.2018.01.018>
8. Calvo, A., Deboli, R., Preti, C.: Machines used in little olive groves: the hidden hand-arm vibration risk. *Int. J. Ind. Ergon.* **90**, 103326 (2022). <https://doi.org/10.1016/j.ergon.2022.103326>
9. Catania, P., Bono, F., Vallone, M.: Evaluation of the vibrations transmitted to the hand-arm system in the use of portable harvesters for olives. *Agric. Eng. Int. CIGR J.* **19**(2), 129–138 (2017)
10. Cerruto, E., Emma, G., Manetto, G.: Whole body vibrations of tractor driver in citrus orchard. In: International Conference on “Work Safety and Risk Prevention in Agro-food and Forest Systems”, Ragusa, Italy, 16–18 September (2010)
11. Cerruto, E., Manetto, G.: Vibration from electric hand-held harvesters for olives. *Appl. Sci.* **12**, 1768 (2022). <https://doi.org/10.3390/app12041768>
12. Cerruto, E., Manetto, G., Papa, R.: Hand arm vibration: comparison between laboratory and in field tests. *SHWA 2020. LNCE* **252**, 223–232 (2022). https://doi.org/10.1007/978-3-030-98092-4_24
13. Cutini, M., Brambilla, M., Bisaglia, C.: Whole-body vibration in farming: background document for creating a simplified procedure to determine agricultural tractor vibration comfort. *Agriculture* **7**, 84 (2017). <https://doi.org/10.3390/agriculture7100084>
14. Deboli, R., Calvo, A., Preti, C.: The use of a capacitive sensor matrix to determine the grip forces applied to the olive hand held harvesters. In: International Conference on “Innovation Technology to Empower Safety, Health and Welfare in Agriculture and Agro-food Systems”, Ragusa, Italy, 15–17 September (2008)
15. Deboli, R., Calvo, A., Preti, C., Inserillo, M.: Design and test of a device for acceleration reproducibility of hand held olive harvesters. *Int. J. Ind. Ergon.* **44**, 581–589 (2014). <https://doi.org/10.1016/j.ergon.2014.05.007>
16. Deboli, R., Calvo, A., Preti, C.: Whole-body vibration: measurement of horizontal and vertical transmissibility of an agricultural tractor seat. *Int. J. Ind. Ergon.* **58**, 69–78 (2017). <https://doi.org/10.1016/j.ergon.2017.02.002>
17. Decreto Legislativo n.187 del 19 agosto 2005. Attuazione della direttiva 2002/44/CE sulle prescrizioni minime di sicurezza e di salute relative all'esposizione dei lavoratori ai rischi derivanti da vibrazioni meccaniche. *Gazzetta Ufficiale* n. 220 del 21 settembre 2005
18. Directive 2006/42/EC of the European Parliament and of the Council of 17 May 2006 on machinery, and amending Directive 95/16/EC, Luxembourg
19. European Commission: Commission Decision of 6 July 2002 concerning minimum health and safety requirements regarding the exposure of workers to the risks arising from physical agents (vibration), 2002/44/EC. *Official Journal*, L 177, 06/07/2002, pp. 13–20 (2002)
20. Griffin, M.J.: Measurement, evaluation, and assessment of peripheral neurological disorders caused by hand-transmitted vibration. *Int. Arch. Occup. Environ. Health* **81**, 559–573 (2008). <https://doi.org/10.1007/s00420-007-0253-5>
21. INAIL: Malattie Professionali - Denunciate - Agricoltura - Caratteristiche malattia professionale (2022). <https://bancadaticsa.inail.it/bancadaticsa/bancastatistica.asp?cod=2>. Accessed 19 July 2022

22. Italian Directive: Application of the Italian Directive No. 81/2008. Attuazione dell' articolo 1 della legge 3 agosto 2007, no. 123, in materia di tutela della salute e della sicurezza nei luoghi di lavoro. *Gazzetta Ufficiale* No. 101, 30/4/2008, suppl. ord. No. 108 (2008)
23. ISO (International Organization for Standardization): ISO 5349–1, Mechanical Vibration—Measurement and Evaluation of Human Exposure to Hand-Transmitted Vibration—Part 1: General Requirements. ISO Publications, Geneva, Switzerland (2001)
24. ISO (International Organization for Standardization): ISO 5349–2, Mechanical Vibration—Measurement and Evaluation of Human Exposure to Hand-Transmitted Vibration—Part 2: Practical Guidance for Measurement at the Workplace. ISO Publications, Geneva, Switzerland (2001)
25. Lenzuni, P., Deboli, R., Preti, C., Calvo, A.: A round robin test for the hand-transmitted vibration from an olive harvester. *Int. J. Ind. Ergon.* **53**, 86–92 (2016). <https://doi.org/10.1016/j.ergon.2015.10.006>
26. Manetto, G., Cerruto, E.: Vibration risk evaluation in hand-held harvesters for olives. *J. Agricul. Eng.* **44**(s2), 705–709 (2013). <https://doi.org/10.4081/jae.2013.384>
27. Manetto, G., Cerruto, E., Papa, R.: Effects of rod and oscillating frequency on the vibrations transmitted to hand-arm system by four olive portable harvesters. *LNCE* **67**, 671–679 (2020). https://doi.org/10.1007/978-3-030-39299-4_73
28. Mehta, C.R., Tewari, V.K.: Seating discomfort for tractor operators - a critical review. *Int. J. Ind. Ergon.* **25**, 661–674 (2000). [https://doi.org/10.1016/S0169-8141\(99\)00054-2](https://doi.org/10.1016/S0169-8141(99)00054-2)
29. Monarca, D., et al.: Transmission of vibrations from portable agricultural machinery to the Hand-Arm System (HAV): risk assessment and definition of exposure time for daily action and exposure limits. In: International Conference on “Innovation Technology to Empower Safety, Health and Welfare in Agriculture and Agro-food Systems”, Ragusa, Italy, 15–17 September (2008)
30. Monarca, D., Cecchini, M., Colantoni, A.: Study for the reduction of vibration levels on an “olive electrical harvester”. In: Proceedings of the XXXII CIOSTA-CIGR Section V Conference “Advances in Labour and Machinery Management for a Profitable Agriculture and Forestry”, pp. 503–509. Nitra, Slovakia (2007)
31. Paddan, G.S., Griffin, M.J.: Effect of seating on exposures to whole-body vibration in vehicles. *J. Sound Vib.* **253**(1), 215–241 (2002). <https://doi.org/10.1006/jsvi.2001.4257>
32. Pascuzzi S., Santoro F., Panaro V.: Investigation of workers' exposure to vibrations produced by portable shakers. *Agricul. Eng. Int. CIGR Ejournal*, Manuscript MES 1127, **XI** (2009)
33. Pessina, D., Facchinetti, D., Bonalume, V.: Evaluation of vibration levels improves the efficiency of modern tracklaying tractors. *J. Agricul. Eng.* **43**(1), 43–47 (2012). <https://doi.org/10.4081/jae.2012.e7>
34. Ramos, D., Schoenmann, L., Scott, D., Trent, J.: The effects of vibration on workers. *Work* **6**, 127–132 (1996). <https://www.doi.org/10.3233/WOR-1996-6207>
35. Scarlett, A.J., Price, J.S., Stayner, R.M.: Whole-body vibration: evaluation of emission and exposure levels arising from agricultural tractors. *J. Terramech.* **44**, 65–73 (2007). <https://doi.org/10.1016/j.jterra.2006.01.006>
36. Servadio, P., Marsili, A., Belfiore, N.P.: Analysis of driving seat vibrations in high forward speed tractors. *Biosys. Eng.* **97**, 171–180 (2007). <https://doi.org/10.1016/j.biosystemseng.2007.03.004>
37. Vergara, M., Sancho, J., Rodríguez, P., Pérez-González, A.: Hand-transmitted vibration in power tools: accomplishment of standards and users' perception. *Int. J. Indust. Ergon.* **38**, 652–660 (2008). <https://doi.org/10.1016/j.ergon.2007.10.014>

Thermogravimetric Analysis for the Evaluation of Coffee Grounds in Combustion and Gasification Processes



Colantoni Andrea, Leonardo Bianchini, Enrico Paris, Monica Carnevale,
Beatrice Vincenti, Adriano Palma, and Francesco Gallucci

Abstract Fossil fuels are still widely used, and this generates a lot of environmental pollution. There are many resources and technologies to progressively replace the use of these sources. Among these, agro-industrial residues are of interest. Instead of treating them as waste, they could be recovered to produce energy. Thermochemical conversion processes such as combustion, gasification and pyrolysis are promising technologies for the use of renewable energy resources. Spent coffee grounds represent a high proportion of agro-industrial residues, so that scientific and industrial interest in this raw material is growing.

In this work, after a detailed chemical-physical characterization, combustion and gasification spent coffee grounds pellets and a variant of combustion coffee pellets to which olive pomace oil was added in the palletization process were tested. The tests were carried out using thermogravimetric analysis (TGA) to check the process and the reaction of the biomass at varying temperatures in terms of weight and energy output.

The results provide important information on the properties of coffee grounds on energy production. Spent coffee grounds in combustion are exhausted at 550 °C and in gasification at about 675 °C, while pellets mixed with pomace oil have not yet exhausted their mass at 800 °C. The largest amount of power is provided by the pellets with olive pomace oil with a peak of 247.63 mW, followed by the pellets in combustion 205.64 mW and the pellets in gasification 61.47 mW. Non-parametric tests were applied and significant differences between the factors were observed.

This represents preliminary work within a larger project that will involve the analysis and comparison of many types of biomass used in thermochemical processes. The data obtained are important for using biomass in the most appropriate technology and optimizing the process.

C. Andrea · L. Bianchini (✉)

Department of Agriculture and Forestry Science (UNITUS-DAFNE), Tuscia University, 01100 Viterbo, Italy
e-mail: l.bianchini@unitus.it

E. Paris · M. Carnevale · B. Vincenti · A. Palma · F. Gallucci

Council for Agricultural Research and Economics Research, Engineering and Agro-Food Processing (CREA-IT), Monterotondo, 00015 Rome, Italy

Keywords TGA · Spent Coffee Ground · Biomass · Waste · Circular economy

1 Introduction

In recent years, the search for renewable energy sources has been gaining momentum, with public awareness and research focusing on environmental and energy security issues. Examples of renewable energy sources include: solar, wind, geothermal and marine energy, biomass, biofuels; the use of biomass produces energy in a sustainable way to replace fossil fuel [1]. Today's economic models and the resulting supply chains lead to large quantities of materials being treated as waste, without considering that many of them can be recovered and used as raw materials for various applications [2]. In the energy field, the use of non-renewable resources poses considerable difficulties in the fight against climate change and many residues from the agro-industrial sector, for example, could be recovered and used to produce energy [2]. In this scenario, it is essential to sift through the residues and check whether they can be used in the energy field without having an environmental impact [3]. European Union policies and strategies encourage the use of renewable energy [4, 5]. Biomass provides 14% of the world's energy needs and ranks fourth as an energy resource [6]. In this context, it is a key renewable resource, given the increasing CO₂ emissions associated with electricity production. There are different types of agro-industrial residues such as olive pomace, residues from the processing of rice, grapes or citrus fruits, etc. [7–11]. In this context, large quantities of coffee grounds are produced, being the most consumed beverage in the world and the most marketed product in the world after oil [12]. These residues often have great potential for different uses, but if handled incorrectly they can represent a major source of environmental pollution [13]. Indeed, given the presence of many harmful components such as caffeine, tannins and polyphenols, large concentrations of waste can damage the environment [14]. Moreover, due to these characteristics it can only be used as a compound to a limited extent [15]. In 2018, 9.58 million tonnes of coffee were produced and one tonne of coffee generates about 650 kg of SCG [16, 17]. Coffee grounds are interesting because they have a wide distribution, in fact they can be found very easily on a territory and are not influenced by seasonality like other biomasses, they are always available throughout the year. Interest in this resource is constantly growing, so much so that many researches are trying to find suitable uses, for example the production of biodiesel has been evaluated, or it has been evaluated as a precursor for the creation of activated carbon, or as a sorbent for the removal of metals [18–21].

In addition to coffee grounds, olive oil production is a major source of waste. Olive oil extraction generates huge amounts of waste that can have a strong impact on terrestrial and aquatic environments due to its high cytotoxicity. Several studies have demonstrated the negative effects of these wastes on the microbial component of the soil, on aquatic ecosystems and even in the atmosphere [22–24]. Olive pomace oil (OPO) along with olive mill solid waste, olive mill wastewater and leaf wood are four by-products of the olive oil extraction process [25].

The paste that remains after centrifugation is still rich in oil (about 12–15% of the total oil), which is extracted through a second centrifugation process. This oil, together with that obtained by extraction with hexane from the by-product corresponds to crude olive pomace oil. Crude Olive pomace oils require chemical refining to remove compounds responsible for undesirable colors and flavors and compounds that affect the stability of the oil. Refined olive pomace oil is mixed with an appropriate amount of virgin olive oil (normally about 10%), resulting in a crude olive oil that is more stable. The refined olive pomace oil is blended with an appropriate amount of virgin olive oil (normally about 10%), resulting in commercially available olive pomace oil [26]. Over time, many possibilities have opened up and are opening up for the use of olive pomace, which was previously considered waste and represented a cost for mills [27]. For example, olive pomace oil, extracted from pomace, is a raw material that can be used for the production of biodiesel [23, 26].

This work aimed to characterize coffee grounds and pomace oil from a chemical-physical point of view and to assess their behavior through thermogravimetric analysis against the different thermochemical processes, in the presence and absence of air, to form pellets also of the two resources.

2 Materials and Methods

The chemical characterisation of spent coffee grounds (SCG) and olive pomace oil (OPO) was carried out at the Laboratory of Experimental Activities - Renewable Energies from Biomass (LASER-B) of CREA-IT in Monterotondo.

For the analysis of the moisture content, reference was made to the UNI EN ISO 18134-1:2015 standard with Stove Memmert UFP800. The biomass sample was dried in an oven at 105 ± 2 °C for 24 h. The moisture content was calculated from the weight loss of the sample before and after drying. For the analysis of ash content, reference was made to UNI EN ISO 18122:2016 with Muffle furnace Lenton EF/11 8B. The biomass sample was first heated up to 250 °C with a ramp of 6.5 °C/min and then up to 550 °C with a ramp of 10 °C/min. For the analysis of the heating value, reference was made to UNI EN ISO 18125:2018 with Calorimeter Parr 6400. The biomass sample was placed in a crucible inside the calorimetry bomb from which the high heating value (HHV) was determined. From this it was possible to derive the lower heating value (LHV) given by the hydrogen content. For the analysis of carbon, hydrogen and nitrogen (C, H, N) reference was made to the UNI EN ISO 16948:2015 standard with Costech ECS 4010 elemental analyser. For the analysis of inorganic micropollutants the (experimental) procedure that was adopted is shown below. For sample preparation, an aliquot of each sample (approximately 500 mg) was transferred into Teflon containers and subjected to acid attack using a microwave digester (Start D, Milestone, Italy). The attack mixture used consisted of 4 ml HNO₃ and 2 ml H₂O₂. All the solutions obtained were brought to a final volume of 100 ml with the addition of ultrapure water and analysed. The Agilent 7700 series ICP-MS spectrometer was used for the determination of the elements.

After the chemical-physical characterisation, pelletising tests were carried out with a Master 380 C Bianco-Line pelletizer, in order to verify the best system to thicken the grounds and obtain the fuel, with SCG plus a mixture of 50% SCG and 50% OPO. 2% maize starch was used as pellet binder with only SCG.

The instrument used for the tests is a TGA-DSC thermogravimetric analyser (TGA/DSC 1 STARe System - Mettler Toledo), the rate used was 30°C per minute to 800 °C, and the tests were carried out as follows:

1. SCG-air;
2. SCG-nitrogen;
3. SCG-OPO-air.

Biomass characterisation and pellet tests were performed using three samples as independent replicates. A cubic spline smoother with $\lambda = 0.05$ was applied to the TGA curves, with standardised x-values and 95% confidence interval. Before proceeding, normality and homogeneity of variance were checked using the Shapiro–Wilk test and Levene’s test, respectively ($P = 0.05$ for both). Failing both characteristics, the data were analysed using the non-parametric Kruskal–Wallis test. Significance between pairs was determined using Wilcoxon’s post hoc test for multiple comparisons at the 95% family confidence level ($P = 0.05$). All Statistical analyses were performed using JMP PRO 15 (Trial version ©SAS Institute Inc.).

3 Results and Discussion

Characterization allowed the biomass characteristics to be defined, averaging coffee grounds: C:52.83%, H:16.7%, N:2.36%. Olive pomace oil shows C:11.71%, H:0.83% and N:0.14%. Sulphur was also analysed but in each case it was below the level of quantification SCG has a higher hydrogen content than OPO and other waste biomass such as olive, vine or stone prunings, as also found in other works on coffee grounds [3, 28].

The heating value for SCG is high, 21.17 MJ kg⁻¹, better than other vegetal biomasses, however OPO presents higher and much better values than SCG and especially higher than olive pomace 37.35 MJ kg⁻¹ (Table 1) [27]. In any case, both residues are excellent fuels in this respect. The heating value is high despite the fact that nitrogen negatively affects the latter, on the one hand by reducing the percentage of C, H, O, and on the other hand by the bond that is created with other elements that are then found in the ashes [7, 29, 30]. The elemental analysis values were consistent with other biomass.

ICP-MS analysis allowed characterization of the SGC and OPO matrices respect to metals present (Table 2). Macro elements such as Mg, K, Ca, and Na are present in high concentrations. These elements are the characteristic metals of biomass, while the others were detected in trace amounts [31]. Titanium shows a higher level in OPO and this could be due to certain materials used in the extraction machinery [32].

Table 1 Results of characterization of SCG and OPO. Data are presented as mean

	Moisture %	Ash %	C %	H %	N %	HHV MJ kg ⁻¹	LHV MJ kg ⁻¹
SCG	42.31	0.90	52.83	16.7	2.36	21.17	17.73
OPO	-	-	11.71	0.83	0.14	37.34	37.17

Table 2 Results of metal analysis of SCG and OPO. Data are presented as an average in mg kg⁻¹

Metals mg kg ⁻¹	OPO	SCG
Li	<LOQ	0,53
Be	<LOQ	<LOQ
B	<LOQ	10,6
Na	141,57	37,15
Mg	2710,67	1981,71
Al	72,32	21,44
K	37,133,32	1684,12
Ca	603,99	250,09
Ti	1837,47	37,03
V	<LOQ	<LOQ
Cr	<LOQ	<LOQ
Mn	53,53	10,52
Fe	437,69	9,87
Co	<LOQ	<LOQ
Ni	10,89	1,23
Cu	74,04	9,82
Zn	54,54	3,57
Ga	9,01	0,27
As	<LOQ	<LOQ
Se	2,91	0,3
Rb	49,02	12,07
Sr	18,06	10,51
Mo	0,38	0,31
Ag	<LOQ	<LOQ
Cd	<LOQ	<LOQ
Sn	<LOQ	<LOQ
Ba	6,69	3,17
Tl	<LOQ	<LOQ
Pb	<LOQ	<LOQ

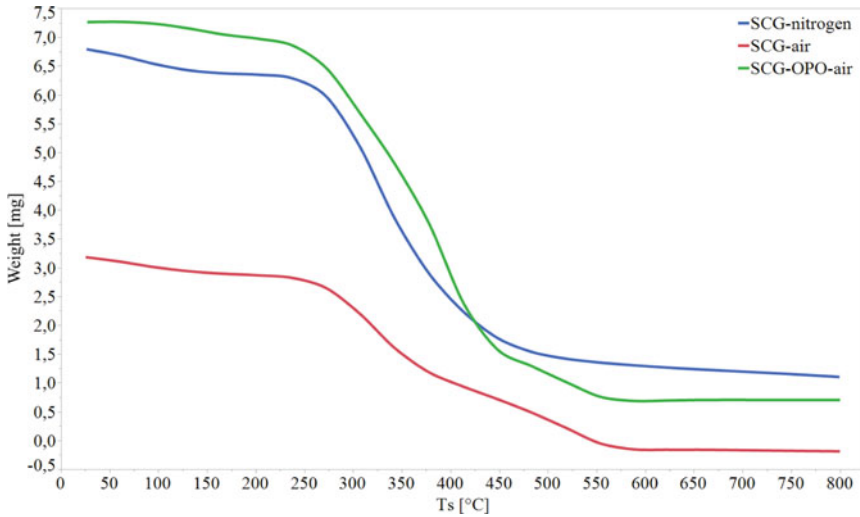


Fig. 1 DTA curves of tests. Spent Coffee Ground with nitrogen (SCG-nitrogen, blue); Spent Coffee Ground with air (SCG-air, red); Spent Coffee Ground mixture with Olive Pomace Oil with air (SCG-OPO-air, green)

Thermogravimetric analysis showed a mass loss of 5,6%, 3,8%, and 0,6% at about 100 °C, respectively for tests SCG-air, SCG-nitrogen, SCG-OPO-air.

The greatest variation is observed between approximately 250 and 500 °C for all three tests where there is a weight loss of 75,9% 76,8% 70,0% respectively for SCG-air, SCG-OPO-air and SCG-nitrogen (Fig. 1). Other authors also report biomass decomposition with temperature ranges of 100–300, 300–400, and 400–600 °C in their constituent parts of hemicellulose, cellulose, and lignin [31, 33].

As seen above, the mass loss of about 2% around corresponds to a loss of moisture. While what takes place between 300 and 350 °C is the beginning of biomass volatilization which corresponds to the decomposition of the three above mentioned constituents and represents the phase where the energy release is increasing. Normally this reaches up to 600 °C and at this temperature there is the peak of energy release (Fig. 2). As the temperature increases above 600 °C there is a stabilization of the weight loss and an oxidation of the carbon. In this case the peak energy for the SCG-air test we get 540 °C with 205 mW. The nitrogen test has a peculiar trend with little energy emission and no real peak with a maximum of 61.47 mW at 557 °C, probably indicating that processes in the absence of oxygen may not be suitable for this type of resource. The test with with SCG-OPO-air, on the other hand, shows two peaks. One at 414 °C with 247 mW and the other at 525 °C with 224 mW.

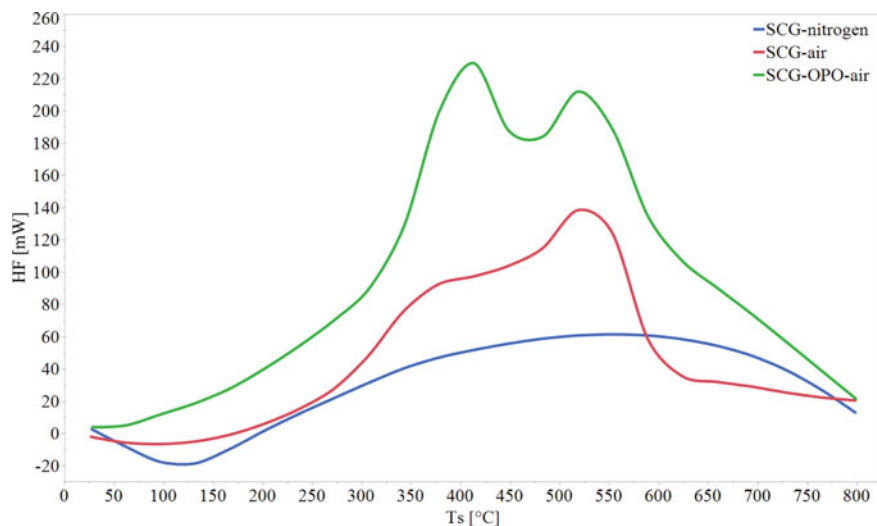


Fig. 2 DTA curves of tests. Spent Coffee Ground with the nitrogen (SCG-nitrogen, blue); Spent Coffee Ground with air (SCG-air, red); Spent Coffee Ground mixture with Olive Pomace Oil with air (SCG-OPO-air, green)

Table 3 Results of statistical analysis of the thermogravimetric tests. Values represent mean ± standard deviation

	SCG air	SCG nitrogen	SCG-OPO-air	p value
Weight [mg]	1.26 ± 47.75	3.44 ± 2.32	4.85 ± 83.64	<0.0001
HF [mW]	47.27 ± 1.33	31.08 ± 27.36	105.31 ± 2.49	<0.0001

This could indicate the two peaks in the emission of the two basic pellet materials olive pomace oil and coffee grounds, and the former seems to have an earlier and higher peak than the latter.

The data from the thermogravimetric analysis were compared using a nonparametric statistical test to check for any differences. Significant differences emerged in both weight and energy (Table 3). In both cases, all three tests were statistically significant (Fig. 3,4).

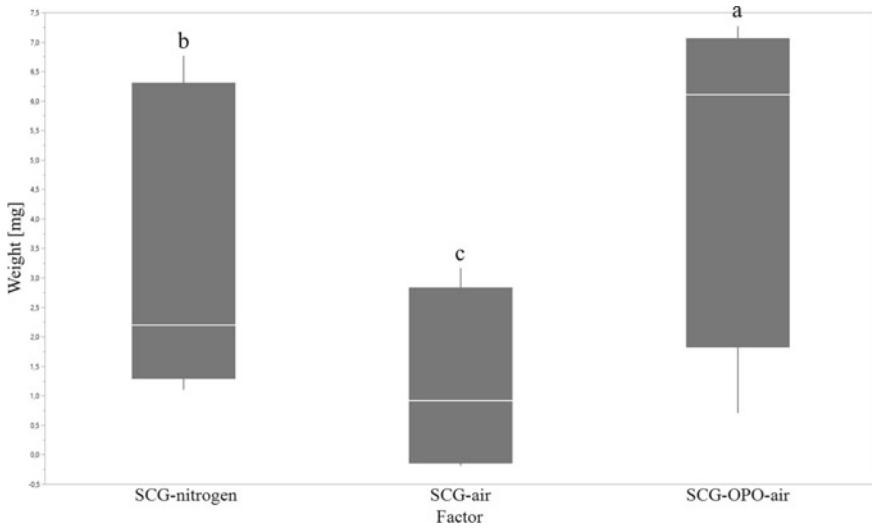


Fig. 3 Comparison of different test from thermogravimetric analysis. Different letters indicate a significant difference for $\alpha = 0.05$

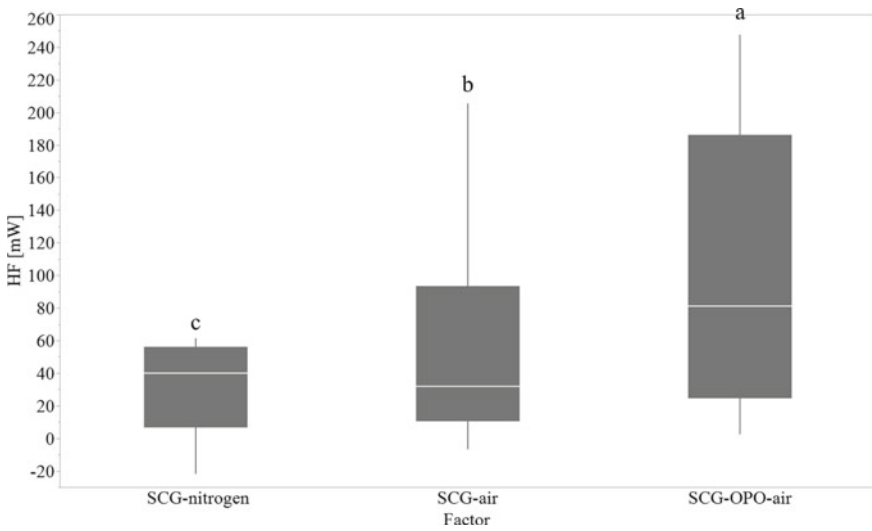


Fig. 4 Comparison of the different test from thermogravimetric analysis. Different letters indicate a significant difference for $\alpha = 0.05$.

4 Conclusion

The results of this work show the excellent energy characteristics of the two residues SCG and OPO. Thermogravimetric analysis has allowed to highlight the energy emission and weight variation of the different test conditions allowing to observe their behavior in the presence and absence of oxygen for SCG and the coffee-oil blend. The different test showed significant differences with the highest energy output for the pellet blend SCG-OPO.

These types of analyses allow for more in-depth fundamental biomass information by being able to work on a small scale.

The excellent energetic results allow to consider these mixtures valid resources for thermochemical conversion processes. Although the percentage ratio between SCG and OPO should be enhanced to improve mechanical properties. This represents ground-breaking work as for the first time a coffee pellet is made using not just one waste, but two by adding olive pomace oil and there are no examples of this in the literature.

References

1. Algieri, A., Andiloro, S., Tamburino, V., Zema, D.A.: The potential of agricultural residues for energy production in Calabria (Southern Italy). *Renew. Sustain. Energy Rev.* **104**, 1–14 (2019). <https://doi.org/10.1016/j.rser.2019.01.001>
2. Marcantonio, V., Bocci, E., Monarca, D.: Development of a chemical quasi-equilibrium model of biomass waste gasification in a fluidized-bed reactor by using Aspen plus. *Energies* **13** (2019). <https://doi.org/10.3390/en13010053>.
3. Bianchini, L., Costa, P., Dell'omo, P.P., Colantoni, A., Cecchini, M., Monarca, D.: An industrial scale, mechanical process for improving pellet quality and biogas production from Hazelnut and Olive pruning. *Energies* **14**, 1–13 (2021). <https://doi.org/10.3390/en14061600>
4. Carlini, M., Mosconi, E., Castellucci, S., Villarini, M., Colantoni, A.: An economical evaluation of anaerobic digestion plants fed with organic agro-industrial waste. *Energies* **10**, 1165 (2017). <https://doi.org/10.3390/en10081165>
5. Monarca, D., Cecchini, M., Guerrieri, M., Santi, M., Colopardi, F.: The evolution of the hazelnut harvesting technique. *Acta Hort.* **845**, 353–358 (2009). <https://doi.org/10.17660/ActaHortic.2009.845.54>
6. Marucci, A., Zambon, I., Colantoni, A., Monarca, D.: A combination of agricultural and energy purposes: evaluation of a prototype of photovoltaic greenhouse tunnel. *Renew. Sustain. Energy Rev.* **82**, 1178–1186 (2018)
7. Colantoni, A., et al.: Spent coffee ground characterization, pelletization test and emissions assessment in the combustion process. *Sci. Rep.* **11**, 1–14 (2021). <https://doi.org/10.1038/s41598-021-84772-y>
8. Colantoni, A., et al.: Different pellet mixtures obtained from spent coffee grounds: energetic characterization. In: *Proceedings of the 28th European Biomass Conference and Exhibition* (2020)
9. Palma, A., Colantoni, A., Vincenti, B., Bianchini, L., Carnevale, M., Paris, E., Gallucci, F.: Comparison between coffee and common lignocellulosic biomass for energetic potential prediction. *Environ. Eng. Manag. J.* **20**, 1619–1627 (2021). <https://doi.org/10.30638/eemj.2021.150>

10. Paris, E., et al.: Residues from harvesting of tree nuts: an appraisal of energy value of walnut and almond husks. In: Proceedings of the 27th European Biomass Conference and Exhibition (2019)
11. Paris, E., et al.: Characterization of emissions from combustion of agricultural waste: wheat straw and rice straw. In: Proceedings of the 27th European Biomass Conference and Exhibition (2019)
12. Park, S., Kim, S.J., Oh, K.C., Cho, L., Kim, M.J., Jeong, I.S., Lee, C.G., Kim, D.H.: Investigation of agro-byproduct pellet properties and improvement in pellet quality through mixing. *Energy* **190**, 116380 (2020). <https://doi.org/10.1016/j.energy.2019.116380>
13. Feroso, J., Mašek, O.: Thermochemical decomposition of coffee ground residues by TG-MS: a kinetic study. *J. Anal. Appl. Pyrolysis* **130**, 249–255 (2018). <https://doi.org/10.1016/j.jaap.2017.12.007>
14. Rajabi Hamedani, S., Colantoni, A., Bianchini, L., Carnevale, M., Paris, E., Villarini, M., Gallucci, F.: Environmental life cycle assessment of spent coffee ground pellet. *Energy Rep.* **8**, 6976–6986 (2022). <https://doi.org/10.1016/j.egy.2022.05.031>
15. McNutt, J., He, Q.: (Sophia) Spent coffee grounds: a review on current utilization. *J. Ind. Eng. Chem.* **71**, 78–88 (2019). <https://doi.org/10.1016/j.jiec.2018.11.054>
16. Tsai, W.T., Liu, S.C., Hsieh, C.H.: Preparation and fuel properties of biochars from the pyrolysis of exhausted coffee residue. *J. Anal. Appl. Pyrolysis* **93**, 63–67 (2012). <https://doi.org/10.1016/j.jaap.2011.09.010>
17. International Coffee Organization (ICO) Coffee Market Report (2018)
18. Caetano, N., Silva ac, V.F., Mata, T.M.: Valorization of coffee grounds for biodiesel production. In: 5th International Conference on Safety and Environment in the Process, vol. 26 (2012)
19. Kante, K., Nieto-Delgado, C., Rangel-Mendez, J.R., Bandosz, T.J.: Spent coffee-based activated carbon: Specific surface features and their importance for H₂S separation process. *J. Hazard. Mater.* **201–202**, 141–147 (2012). <https://doi.org/10.1016/j.jhazmat.2011.11.053>
20. Oliveira, W.E., Franca, A.S., Oliveira, L.S., Rocha, S.D.: Untreated coffee husks as biosorbents for the removal of heavy metals from aqueous solutions. *J. Hazard. Mater.* **152**, 1073–1081 (2008). <https://doi.org/10.1016/j.jhazmat.2007.07.085>
21. Pappa, P., Pelleri, F., Gidarakos, E.: Characterization of biochar produced from spent coffee waste. In: 3rd International Conference of Industrial and Hazardous Waste Management, CRETE 2012, Chania, Crete, Greece (2012)
22. DellaGreca, M., Monaco, P., Pinto, G., Pollio, A., Previtiera, L., Temussi, F.: Phytotoxicity of low-molecular-weight phenols from olive mill waste waters. *Bull. Environ. Contam. Toxicol.* **67**, 352–359 (2001). <https://doi.org/10.1007/S001280132>
23. Paredes, M.J., Moreno, E., Ramos-Cormenzana, A., Martinez, J.: Characteristics of soil after pollution with waste waters from olive oil extraction plants. *Chemosphere* **16**, 1557–1564 (1987). [https://doi.org/10.1016/0045-6535\(87\)90096-8](https://doi.org/10.1016/0045-6535(87)90096-8)
24. Rana, G., Rinaldi, M., Introna, M.: Volatilisation of substances after spreading olive oil waste water on the soil in a Mediterranean environment. *Agric. Ecosyst. Environ.* **96**, 49–58 (2003). [https://doi.org/10.1016/S0167-8809\(03\)00013-6](https://doi.org/10.1016/S0167-8809(03)00013-6)
25. Buttol, P., et al.: Uso efficiente delle risorse nelle imprese olivicole olearie - ENEA (2018). ISBN: 9788882863685
26. Mateos, R., Sarria, B., Bravo, L.: Nutritional and other health properties of olive pomace oil. *Crit. Rev. Food Sci. Nutr.* **60**, 3506–3521 (2019). <https://doi.org/10.1080/10408398.2019.1698005>
27. Miranda, T., Arranz, J.I., Montero, I., Román, S., Rojas, C.V., Nogales, S.: Characterization and combustion of olive pomace and forest residue pellets. *Fuel Process. Technol.* **103**, 91–96 (2012). <https://doi.org/10.1016/j.FUPROC.2011.10.016>
28. Carnevale, M., et al.: Characterization of agricultural residues: physical and chemical analysis for energy transformations. *European Biomass Conference on Exhibition Proceedings*, pp. 27–30 (2019)
29. Brunerová, A., Roubík, H., Brožek, M., Haryanto, A., Hasanudin, U., Iryani, D.A., Herák, D.: Valorization of bio-briquette fuel by using spent coffee ground as an external additive. *Energies* **13**, 1–15 (2019). <https://doi.org/10.3390/en13010054>

30. Limousy, L., Jeguirim, M., Dutournié, P., Kraiem, N., Lajili, M., Said, R.: Gaseous products and particulate matter emissions of biomass residential boiler fired with spent coffee grounds pellets. *Fuel* **107**, 323–329 (2013). <https://doi.org/10.1016/j.fuel.2012.10.019>
31. Yang, H.: Characteristics of hemicellulose, cellulose and lignin pyrolysis. *Fuels* **86**, 1781–1788 (2007). <https://doi.org/10.1016/j.fuel.2006.12.013>
32. Beltrán, M., Sánchez-Astudillo, M., Aparicio, R., García-González, D.L.: Geographical traceability of virgin olive oils from south-western Spain by their multi-elemental composition. *Food Chem.* **169**, 350–357 (2015). <https://doi.org/10.1016/j.foodchem.2014.07.104>
33. Zapata, B., Balmaseda, J., Fregoso-Israel, E., Torres-García, E.: Thermo-kinetics study of orange peel in air. *J. Therm. Anal. Calorim.* **98**, 309–315 (2009). <https://doi.org/10.1007/S10973-009-0146-9>

Convolutional Neural Network Based Detection of Chestnut Burrs in UAV Aerial Imagery



Lorenzo Comba , Alessandro Biglia , Alessandro Sopegno , Marco Grella , Emilio Dicembrini , Davide Ricauda Aimonino , and Paolo Gay 

Abstract Uncrewed Aerial Vehicles (UAVs) based remote sensing proved to be a valuable tool to acquire extensive data of crops, which are essential for feeding innovative decision support systems aimed at improving growers' farm management. In this context, the capability to automatically assess chestnut fields production by UAV has been considered a valuable service by sector stakeholders to properly plan the harvesting tasks and the pricing.

In this work, an innovative image processing method to automatically detect pixels representing chestnut burrs in aerial multispectral imagery is presented, which is based on U-Net Convolutional Neural Network (CNN). The method was tested on the imagery of a case study chestnut field located in Dronero (Italy). The aerial imagery was acquired on September 2021 at noon, using an airborne MAIA RGB-NIR camera. The flight altitude was 20 m from the terrain, obtaining a ground sample distance of 10 mm. The Matlab Image Segmenter was used to manually classify pixels (burr, canopy, ground) and obtain datasets for CNN training. Sixteen trees were selected from the map, and, for each tree, the results of the CNN segmentation were compared with those manually obtained. The accuracy in the automatic burrs detection was assessed by defining a confusion matrix, which refers to properly detected or missed burrs, and regions of the image wrongly classified as burrs. The obtained results show the feasibility of the CNN with an accuracy in correct detection of 92.3%. The image processing here presented enables the development of new decision support system specifically conceived for chestnut growers, with a focus on the production and harvesting phases.

Keywords Remote sensing · UAV · Image processing · Image clustering · Machine learning

L. Comba (✉) · A. Biglia · A. Sopegno · M. Grella · E. Dicembrini · D. Ricauda Aimonino · P. Gay
Department of Agricultural, Forest and Food Sciences (DiSAFA), Università Degli Studi di Torino, Largo Paolo Braccini 2, 10095 Grugliasco, TO, Italy
e-mail: lorenzo.comba@unito.it

© The Author(s), under exclusive license to Springer Nature Switzerland AG 2023
V. Ferro et al. (eds.), *AIIA 2022: Biosystems Engineering Towards the Green Deal*,
Lecture Notes in Civil Engineering 337,
https://doi.org/10.1007/978-3-031-30329-6_51

501

1 Introduction

In the last decade, the role of Uncrewed Aerial Vehicles (UAVs) in agriculture is becoming more and more relevant, thanks to their capability of performing monitoring missions, or in field operations, in an autonomous and time effective way [1]. Indeed, precision agriculture approaches have been boosted by autonomous vehicles, which can nowadays acquire huge amount of data related to crops status [2], even in a cooperative way [3]. Sensors available on the market, which have increased resolution capabilities and reduced weight with respect to the past, allow to extend the flight autonomy of UAVs, with e.g. benefits in terms of covered surface with a single mission [4]. Compared with satellite and/or aircrafts, UAVs have several advantages: flexible time and altitude of the flight, very high spatial resolution when low altitude is adopted, and continuous and reliable multi-temporal analysis [5]. For mapping purposes, the huge amount of acquired aerial raw images have to be geometrically corrected and merged, in order to obtain a single orthomosaic of the entire analysed field. For the optimal results of this task, images should have at least 80–90% frontal and 70–80% side overlapping rate [6].

The characteristic of images acquired by UAVs airborne cameras, which can have thus a millimetric Ground Sample Distance (GSD), enable analysis at several level of detail, e.g. at field scale [7], plant scale [8] or even its subpart, such as trunk, branches, fruits etc. [9]. However, the raw dataset acquired by sensors are only a representation of the region of interest, so that a semantic interpretation of each element of the dataset is essential, in order to detect the desired targets [10]. This procedure, applied to an orthomosaic, provides a labelled imagery where each pixel is assigned to the proper class, which is essential to extract valuable information about the crop from imagery data [11].

In this work, a semantic interpretation method to detect burr within multispectral imagery of chestnut orchard is presented, which is based on a machine learning approach. In particular, the algorithm is able to automatically detect pixels of the map which represent the burrs, together with ones of crop canopy and inter row paths. Results has been compared with ones obtained by using standard clustering methods, such as Otsu's one [12]. The burr detection within aerial images enables the assessment of crop yield by remote sensing techniques, allowing farmers to obtain valuable information in advance with respect to the subsequent harvesting phase.

2 Materials and Methods

2.1 Case Study

A chestnut orchard, located in Dronero ($44^{\circ}27'51''$ N - $7^{\circ}24'51''$ E, North-west Italy), was selected as case study for this work. The field has an extension of 0.4 ha. Chestnut trees are planted at 3 m distance each other and the inter row path, which is partially

covered by grass, is 3.5 m wide. In the considered orchard, two variety of chestnut are cultivated, which are Bouche and Volos.

The UAV flight was conducted on September 2021, the 15th, at noon during a sunny day, in order to acquire images with the highest available illumination intensity and to reduce as much as possible the presence of shadow in the field of view, which resulted to be almost null. The height of the UAV flight was maintained close to 20 m with respect to the terrain by using a set of waypoints, which were defined in the UgCS Pro mission planning software [12]. The UAV path planning was performed in order to guarantee a forward and side overlapping rate between adjacent images greater than 80%, in accordance with the good practices described in literature [6].

2.2 Instrumentation

The sensor adopted to acquire multispectral imagery was a MAIA S2 multispectral camera [13], which features 9 sensors with 1.2 Megapixel resolution with a frame rate up to 5 Hz. The provided spectral coverage ranges from 390 to 950 nm, with average spectral resolution of 37 nm. The camera has been equipped on a DJI Matrice 300 quadcopter, with a support that allow a nadiral view of the sensor (Fig. 1). With this configuration, and with a flight altitude of 20 m, the acquired images were characterised by a ground sample distance (GSD) of 10 mm pixel⁻¹ and the obtained field of view (FOV) was 13.4 × 10 m. The 9 shutters of the MAIA camera were set to open simultaneously, so that the multiband measurements resulted to be synchronous. In addition, the shutters short exposure time ($\ll 0.01$ s), together with the low velocity of the UAV flight, assured the absence of blurring within the aerial images. Acquired data were corrected in relation to light changes during the flight by exploiting information provided by an incident light sensor (ILS), that was mounted on the top of the drone. Indeed, ILS measures the ambient light level for each shot in each band during the UAV flight.

The pre-processing phase of raw images involved geometric correction, coregistration (or stitching) and radiometric correction, using the MultiCam Stitcher Pro software. Finally, a georeferenced ortho-mosaics of the chestnut orchard (Fig. 2) was obtained processing aerial images with Agisoft Metashape [14] software, which performs photogrammetric procedure to generate a GeoTIFF file in the WGS84 EPSG:4326 reference system. Proper georeferencing task was assured by placing six markers as ground control points (GCP), the position of which was acquired with the Stonex S900A differential GNSS (accuracy of about 2 cm).

2.3 Semantic Clustering

The proposed method to detect pixels representing burrs within 9 channels multispectral imagery is based on a U-Net, a symmetric convolutional neural network

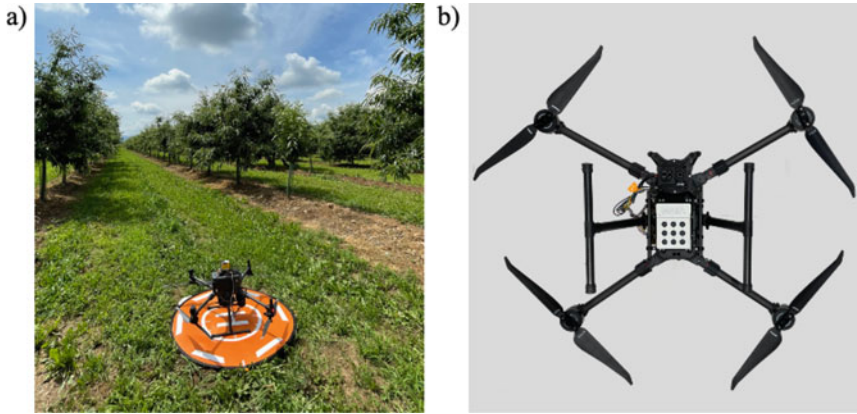


Fig. 1 DJI Matrice 300 UAV equipped with MAIA 9-band multispectral camera, a) before the acquisition in Dronero chestnut and b) in laboratory, with a bottom view

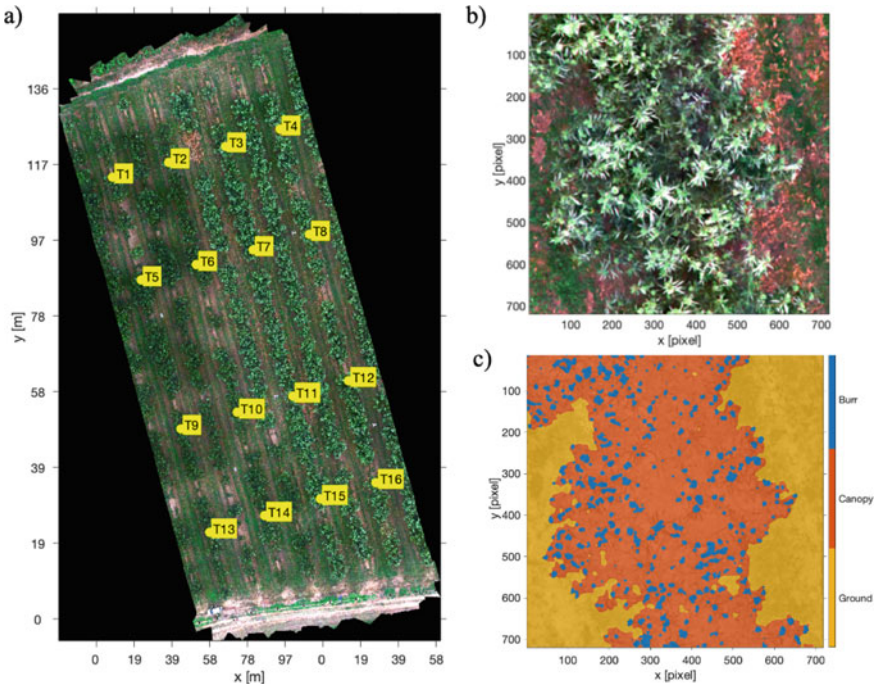


Fig. 2 a) RGB visualisation of the multispectral orthophoto of the considered case study chestnut, with considered chestnut trees location (yellow dots) and code (yellow labels). b) Enlargement of the chestnut tree T9 used as training subset for the U-net. c) Manually labelled pixels mask of T9 chestnut tree used as training reference of the U-net.

(CNN) specifically improved to be trained by a reduced amount of data with respect to traditional ones [15]. The method performs a semantic interpretation of the aerial map, and provided a categorical map where pixels were classified into three categories: (1) burrs, (2) canopy and (3) inter-row paths. The selection of three classes, instead of only two (burrs and not burrs pixels) was adopted to reduce the difference among cardinality of different considered sets of pixels. Indeed, this approach improves U-Net performances.

The GeoTIFF ortho-mosaic was processed to select 16 portions of map representing a set of chestnut trees (named T1 to T16), the positions of which was selected on a regular grid and was acquired with the DGNSS receiver (Fig. 2a). Each selected subset of the map results to have 712×712 pixel size. The selected set of trees was then divided to be used as training, validation, and test data of the U-Net. Please note that only a single tree imagery (representing chestnut T9) was used to train the CNN (Fig. 2b), which was finely labelled into the three selected classes using Image Segmenter tool by Matlab [15] (Fig. 2c). The cardinality of the training subset was less than 6% of the entire dataset (more than 8 million pixels); this emphasises that the adopted U-net is a powerful tool to automatically classify a large dataset using few a priori information.

The architecture of the adopted U-net is composed of an encoder subnetwork and a corresponding decoder subnetwork that are connected by a bridge section. The encoder and decoder subnetworks consist of 56 stages of downsample and upsample the input image (called batch, with the size $16 \times 16 \times 9$ [pixels, pixels, bands]) according to the EncoderDepth factor. The stages within the U-Net encoder subnetwork are two sets of convolutional and ReLU layers (bridge section), followed by a 2-by-2 max pooling layer. The bias term of all convolutional layers was initialised to zero.

2.4 U-Net Accuracy Assessment

The accuracy of the proposed method to semantically segment multispectral imagery to detect pixels representing burrs was investigated by defining three quality indices: (i) good detection I_G , (ii) under detection I_U and (iii) over detection I_O . The good detection index was defined as

$$I_G = \frac{\text{card}(A_B \cap M_B)}{\text{card}(M_B)} \quad (1)$$

where A_B is the set of pixels representing burrs automatically detected by the trained U-Net, and M_B manually ones. The under detection index, which represents the false negative, was defined as

$$I_U = \frac{\text{card}(M_B - (A_B \cap M_B))}{\text{card}(M_B)} \quad (2)$$

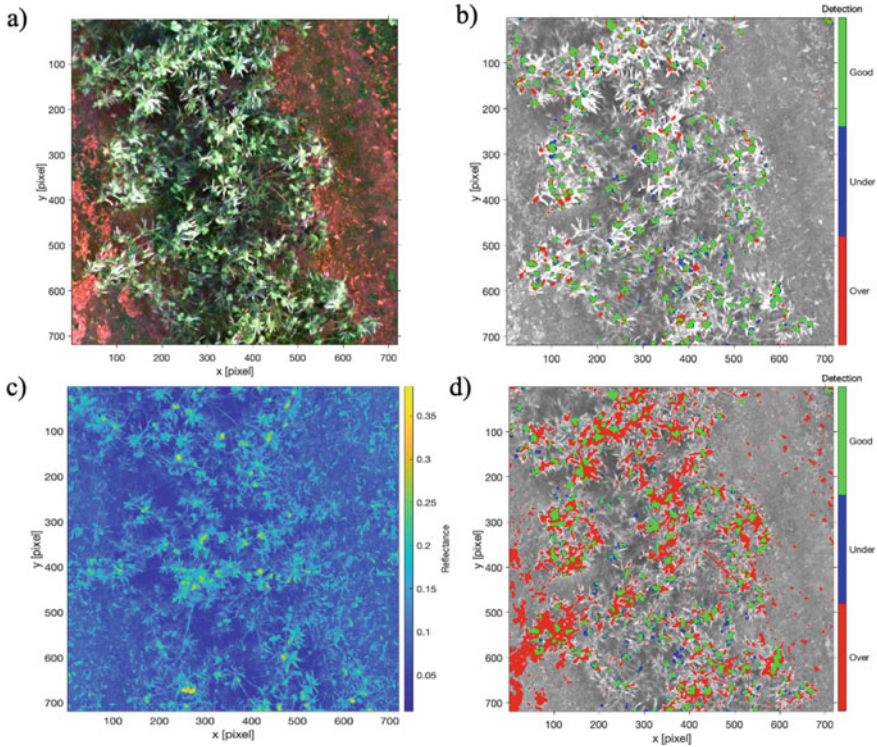


Fig. 3 a) RGB visualisation of the sample imagery of chestnut T11 and b) results of clustering using U-Net. c) Red-edge band false colour visualisation and d) results of clustering using Otsu's methods.

and finally the over detection (false positive) as

$$I_U = \frac{\text{card}(A_B - (A_B \cap M_B))}{\text{card}(M_B)} \tag{3}$$

3 Results and Discussion

During U-Net training, the convergence of the accuracy and loss was achieved with a single epoch, with a computing time lower than 1 h running on a 5000 TFLOPS GPU machine. The trained U-Net was then used to process the imagery of 15 trees for clustering pixels to detect ones representing burrs. Results in terms of average value and standard deviation of the defined accuracy indices are reported in Table 1. A graphical representation of classes of pixels used to compute the accuracy indices, obtained on the sample imagery of chestnut T11 (Fig. 3a), is reported in Fig. 3b. The

Table 1 Results of burr detection accuracy

Detection scores	U-Net on Multispectral Map		Otsu's on Red-Edge Map	
	Mean	Standard deviation	Mean	Standard deviation
Good I_G	92.3%	3.1%	86.4%	3.7%
Under I_U	13.1%	7.0%	11.5%	7.6%
Over I_O	4.3%	3.9%	182.2%	54.3%

U-Net was found to be able to correctly detect more than 92% of pixels representing burrs, with low error rate, mainly related to false negative detection. Low values of standard deviation obtained by indices for U-Net confirmed the reliability of the proposed method. A standard clustering method based on Otsu's clustering was used as comparison, and results of its application on the most performing spectral band (Red-Edge) are reported in Table 1. This method, which results to be less computing demanding (average 0.2 s for processing one tree imagery instead of 1.1 s required by the U-Net), showed lower accuracy in the burr detection. In particular, the over estimation was its main limit.

4 Conclusions

The method to semantically interpret multispectral imagery of chestnut orchard presented in this work, based on the U-Net machine learning approach, was proved to be effective and reliable. In particular, the algorithm was able to automatically detect, with high accuracy, pixels of the map which represent the chestnut burrs. Exploiting the whole spectral content of the imagery, the U-Net based method showed higher accuracy with respect to standard Otsu's one. In the considered case study, the method was found to be robust to different chestnut variety. The image processing here presented enables the development of new decision support system specifically conceived for chestnut growers, with a focus on the production and harvesting phases.

Funding This research was partially funded by the Italian Ministry of University and Research (MIUR), PRIN 2020 project “*DATA-BUS - Digital Agriculture Technology to Achieve Data to Build User-friendly Sustainability Indicators*” (Prot. 2020SCNF4L), and PON 2020 “*VALTIFRU 4.0: Enhancement of the supply chains of nuts and fresh fruits with high added value*” (Prot. ARS01_01060).

Declaration of Competing Interest The authors declare that they have no known competing financial interests or personal relationships that could have appeared to influence the work reported in this paper.

References

1. Biglia, A., Grella, M., Bloise, N., Comba, L., Mozzanini, E., Sopegno, A., et al.: UAV-spray application in vineyards: flight modes and spray system adjustment effects on canopy deposit, coverage, and off-target losses. *Sci. Total Environ.* **845**, 157292 (2022). <https://doi.org/10.1016/j.scitotenv.2022.157292>
2. Comba, L., Biglia, A., Ricauda Aimonino, D., Barge, P., Tortia, C., Gay, P.: 2D and 3D data fusion for crop monitoring in precision agriculture. In: IEEE International Workshop on Metrology for Agriculture and Forestry, pp. 62–67 (2019). <https://doi.org/10.1109/MetroAgriFor.2019.8909219>
3. Mammarella, M., Comba, L., Biglia, A., Dabbene, F., Gay, P.: Cooperative agricultural operations of aerial and ground unmanned vehicles. In: IEEE International Workshop on Metrology for Agriculture and Forestry, pp. 224–229 (2020). <https://doi.org/10.1109/MetroAgriFor50201.2020.9277573>
4. Feng, A., Zhou, J., Vories, E.D., Sudduth, K.A., Zhang, M.: Yield estimation in cotton using UAV-based multi-sensor imagery. *Biosys. Eng.* **193**, 101–114 (2020). <https://doi.org/10.1016/j.biosystemseng.2020.02.014>
5. Mammarella, M., Comba, L., Biglia, A., Dabbene, F., Gay, P.: Cooperation of unmanned systems for agricultural applications: a case study in a vineyard. *Biosyst. Eng.* **223**(B), 81–102 (2021). <https://doi.org/10.1016/j.biosystemseng.2021.12.010>
6. Vong, A., Matos-Carvalho, J.P., Toffanin, P., Pedro, D., Azevedo, F., Moutinho, F., et al.: How to build a 2D and 3D aerial multispectral map? All steps deeply explained. *Remote Sens.* **13**, 3227 (2021). <https://doi.org/10.3390/rs13163227>
7. Kerkech, M., Hafiane, A., Canals, R.: Vine disease detection in UAV multispectral images using optimized image registration and deep learning segmentation approach. *Comput. Electron. Agric.* **174**, 105446 (2020). <https://doi.org/10.1016/j.compag.2020.105446>
8. Mammarella, M., Comba, L., Biglia, A., Dabbene, F., Gay, P.: Cooperation of unmanned systems for agricultural applications: a theoretical framework. *Biosyst. Eng.* **223**(B), 61–80 (2022). <https://doi.org/10.1016/j.biosystemseng.2021.11.008>
9. Jurado, J.M., Pádua, L., Feito, F.R., Sousa, J.J.: Automatic grapevine trunk detection on UAV-based point cloud. *Remote Sens.* **12**, 3043 (2020). <https://doi.org/10.3390/rs12183043>
10. Comba, L., Zaman, S., Biglia, A., Ricauda Aimonino, D., Dabbene, F., Gay, P.: Semantic interpretation and complexity reduction of 3D point clouds of vineyards. *Biosys. Eng.* **197**, 216–230 (2020). <https://doi.org/10.1016/j.biosystemseng.2020.05.013>
11. Biglia, A., Zaman, S., Gay, P., Ricauda Aimonino, D., Comba, L.: 3D point cloud density-based segmentation for vine rows detection and localisation. *Comput. Electron. Agric.* **199**, 107166 (2022). <https://doi.org/10.1016/j.compag.2022.107166>
12. Comba, L., Biglia, A., Ricauda Aimonino, D., Barge, P., Tortia, C., Gay, P.: Semantic interpretation of multispectral maps for precision agriculture: a machine learning approach. *Precis. Agric.* **21**, 291–297 (2021). https://doi.org/10.3920/978-90-8686-916-9_34
13. SPH Engineering, Latvia. <https://www.ugcs.com>
14. EOPTIS srl 2020 Trento (TN) 38121, Italy. <https://www.eoptis.com/it/home>
15. Agisoft Metashape. Agisoft LLC, St. Petersburg, Russia, 191144 (2020). <https://www.agisoft.com/>
16. Mathworks Matlab R2021a. <https://it.mathworks.com/help/vision/ref/unetlayers.html>

Evaluation of Precision Sprayer Technologies Practical Application



Maurizio Cutini , Elio Romano , Alberto Assirelli , Carlo Bisaglia ,
and Massimo Brambilla 

Abstract Misappreciating the benefits of precision agriculture (PA) is among the main reasons for its present low adoption rate. Concerning crop spraying, the present study focuses on analyzing the economic and ergonomic advantages of adopting precision spraying technology and the approach a farmer must perform for precision spraying tasks.

The study starts with describing the necessary technical requirements for annual crops considering, afterwards, the tractor-implement coupling to manage specific PA sprayers, i.e., auto-guidance, a virtual terminal and ISOBUS implements were considered. RTK receiver was preferred for this operation as well. The experiment compared crop spraying with a conventional 79 kW tractor coupled with a sprayer and a 65 kW PA tractor coupled with an ISOBUS sprayer. The ISOBUS sprayer worked with variable sections at fixed rates, not using prescription maps. The operators carried out a whole working day, and the work rate and the applied dose were the parameters evaluated. Operating with PA machinery resulted in a work rate of 43% higher and a product saving of about 9%. The reasons for this difference were analyzed in detail and reported in the paper.

Literature reports mean reduction of 20–30% of product and time; however, these data must be fitted to the specific kind of performed operation.

The test method adopted with the PA machines also requires attention, and the reasons are given in the paper. Results highlighted that the tractor's technological level is a key factor to achieve the viable PA rank.

Keywords Tractor · agriculture · variable rate · auto-guidance · operator comfort

M. Cutini · E. Romano (✉) · A. Assirelli · C. Bisaglia · M. Brambilla
CREA Research Centre for Engineering and Agro-Food Processing, Council for Agricultural Research and Economics, Via Milano, 43 24047 Treviso (BG), Italy
e-mail: elio.romano@crea.gov.it

1 Introduction

Precision agriculture (PA) relies on managing plot variability allowing each homogeneous area of a farm to express its maximum sustainable production. Farming 4.0 was coined to characterize this information-based farming [1] that requires farmers to process challenging extensive datasets. Many studies report low adoption levels of PA. There is a general low digitalization adoption in agribusiness firms where mainly young farmers managing larger farms are optimistic about adopting PA because of their awareness of the costs and benefits of precision farming [2]. Concerning farm size, studies have shown that working on small farms reduces the adoption rate of PA [3]. Small farm owners are normally unable to keep up with the new technologies because of a lack of investment capital or knowledge, which creates a significant digital divide between them and large farm owners. A study on maize crops' land and water efficiency concluded that PA could automate and simplify information collection and analysis resulting in more prompt decisions and implemented management zones within the fields [4].

Tractor guidance alone was widely used because its operation did not require additional skills, and its advantages were appreciable in the short term. With tractor guidance, farmers could have taken care of their fields without work area overlap, leading to a 20–30% decrease in the related inputs. The relationship between the adoption of precision farming technology and some parameters of farms or farmers was examined with a cross-table analysis. It turned out that the quantity of the cultivated land and the age of the farmers were the leading factors on which the adoption of precision farming technology depended. More in detail, farms with more than three hundred hectares of cultivated land and farmers younger than 40 years of age were those adopting precision farming technology for the most part. However, the slower-than-expected advance of PA adoption reveals the need for a more profound knowledge of the farmers' reluctance in PA investment [5, 6].

Developments in agricultural machinery technology include navigation systems and ISOBUS tractor-implement connection (i.e., tractor guidance, steering control systems, implement operation and path planning systems) to enable the precise positioning of the tractor in the field (or relative to the crop) with minimal driver interaction. As a result, it reduces driver fatigue, frees him to better monitor implement and machine operations, and fosters the adoption of more advanced agronomic techniques following enhanced position accuracy.

This work aims to investigate and quantify what the first approach to agriculture automation technologies (adoption of navigation system and ISOBUS tractor-implement connection) entails in the frame of the PA and its advantages for a farmer. Therefore, considering sprayer application as a reference, the research compares the introduction of PA technology, considering two kinds of tractor-implement couplings that underwent technical comparison in an experimental trial of crop protection with a sprayer. The hypothesis is to verify the advantages of PA technologies and to understand in detail their origin.

2 Materials and Methods

One experimental pre-emergency crop protection with sprayers trial was carried out using a traditional tractor and implement (T1) compared to another tractor equipped for PA and ISOBUS implement (T2).

2.1 *The Farm*

A commercial farm located in North Italy cultivated with corn for livestock feeding was used for the trial. Experienced staff, but not specialized in PA machinery was hired together with experienced PA research personnel.

2.2 *The Tractors*

Two tractor types were adopted for the trials; the tractor without PA technologies was a 4WD, 79 kW, 4 gears and 4 ranges (T1); the tractor with PA technologies (ISOBUS, GNSS, and auto-guidance systems) was a 2WD, 65 kW, 5 gears and 3 ranges (T2).

2.3 *The Sprayers*

The conventional sprayer was a 15 m bar boom and 1100 L tank; the ISOBUS sprayer was a 12 m bar boom and 1000 L tank, 5 sections, 25 nozzles.

2.4 *The PA Technologies Options*

The variables considered were the following:

- level of precision: RTK precision GNSS (2 cm);
- virtual terminal: high level (for RTK and the possibility of managing the tractor and the implement on the same screen);
- implement: ISOBUS, variable sections and VRT (Variable Rate Technology, but in this experimental trial the rate was constant);
- auto-guidance system: auto-guidance at the steering wheel, not available for turning.

2.5 The Trials: Methodology

For the evaluation of the advantages and costs potentially resulting from the adoption of PA technologies, the experimental trial method resulted as follows:

- T1 and T2 had to work 9 h on the same day starting together;
- T1 and T2 had to distribute at the same target speed of 5 km h^{-1} ;
- the fields with the less regular shape were assigned to T2. This could appear penalising for T2, but it was retained a priority not to give it preference;
- the tractors had to come back to the farm to fill the tank;
- the experimental fields were all in the same area (Fig. 1, the fields worked by T2);
- the farm was barycentric with respect to the adopted fields;
- the dose per hectare (250 L ha^{-1}) was the same for all the fields, it resulted 0.7 L of herbicide diluted in 250 L of water;
- T2 worked with variable section technology without following prescription maps (constant rate).

The measured variables were: worked surface and the distributed herbicide.

When adopting precision systems, the coordinates of the field boundaries must be determined first. However, this operation was not considered during the experimental test given the maps already present in the T2 tractor. In any case, this operation needs to be done only once.

Fig. 1 Global layout of the fields worked by T2



Table 1 The main results of the experimental test of weeding carried out

Setting code	C1	C2
Total working time (h)	9:00	9:00
Worked area (ha)	28.5	40.9
The error of distributed herbicide (%)	+10	+1.1

3 Results

3.1 Sprayer Application

The main advantages reported by users already equipped with PA technologies on agricultural machines are improved work management and operator comfort. Unfortunately, such considerations are not straightforwardly measurable, while there is a growing feeling that PA provides several benefits that are not uniquely determinable or measurable. However, the detailed analysis of one implement (i.e. the sprayer machine) helps overcome such difficulty.

The results of the experimental test carried out with the two tractors and sprayers are reported in Table 1.

The results are favorable for the PA tractor and ISOBUS sprayer combination. The extra 43% of working rate is not immediate to explain, considering that one hypothesis was that 20% could be expected from the literature. The dose distributed per hectare without PA technologies resulted in 10% more than the target; this last result is close to what literature reports.

However, it is not enough to consider system precision or the overlap hypothesis to evaluate and appreciate this data. Even when considering these factors, the 43% more field capacity of T2 could not be made clear. Perhaps, that latter could explain the advantages of PA technology. This issue is usually attributed to the overlap or the borders. However, it is better to explain what this means in practice for the operator. In fact, the following considerations can be made only thanks to an experience involving the whole working day and not working only on one experiment plot.

The conventional operator (T1) gave more herbicide than the target because:

- T1 was worried to leave untreated skips;
- every time the tractor pauses, T1 continues distributing and has to be stopped manually, whereas F2 stops automatically; same discussion is before starting forwarding;
- T1 and T2 follow different paths; generally, T2 follows first the borders and then the S path in the middle (Fig. 2) and, thanks to the automatic closing section and geopositioning technology, in doesn't overlap during turning; whereas for T1, this would mean losing product, he does just the S path and, than, the borders with an overlapping;
- after some hours becomes difficult for T1 counting the corn rows to turn at the correct place, some error (always as overlapping in the doubt) could be taken into account;



Fig. 2 Example of map of the dose (different colours represent the doses in $L\ ha^{-1}$) distributed by the T2 operator (from the MyJohnDeere® management system)

- in case T1 arrived at the end of the field and the dose distributed was less (by looking in the implement tank), he had to pass again on the same field, losing time and precision;
- T2 cares automatically for precision close to the borders or to country roads;
- T2 minimizes the overlap automatically.

To explain the 43% more hectares worked and, consequently, fuel and operator working hours saving, it has to be clear that this is above all because T2 has forwarded less distance. As the target forward speed was the same and the bar length similar, it must be considered the following:

- if T1, in some fields or parts thereof, cannot go forward at $5\ km\ h^{-1}$, i.e., 4, he must work at the minimum allowable speed for that whole part and calibrate the implement accordingly; for T2, this is not a problem because the ISOBUS implement changes automatically the dose distribution based on the speed;
- T1 does not fill the tank but loads the quantity necessary for the target field ($hectares * kg * hectares^{-1} = no. of\ liters$) in order to have a reference to verify that the distributed dose is correct; T2 loads all the product possible because it is not important where the tank becomes empty;
- when T1's tank gets empty without covering the targeted surface, he had to turn and go back to the farmhouse, fill the container again and return to the same field, thus losing time and covering more distance;
- if the field's dimensions require several full containers, C1 shall divide the fields into smaller surfaces to check the distributed dose. This situation does not occur with the PA implement because the herbicide distribution is corrected continuously (load cell and flow rate) so that the dose is adapted constantly to the target. As a result, the target soil surface is correct when the tank is empty.

The described advantages are evident when looking at the distributed dose map of one of the experimental fields (Fig. 2).

Apart from the general precision shown in the figure, it is possible to notice the path followed by the operator without overlapping, the effect of the automatic closing of the sections and the management of a particularly demanding field.

Moreover, we can consider that using a sprayer presents some difficulties in operation management that also affect the working time. The traditional operator brings the maps of the different terrains to verify the field that follows, to check the relative dose to be distributed and the amounts of distributed product. Such operator effort is time-consuming and also has two practical consequences:

- the T1 operator is concentrated to check the correct borders, the liquid in the tank and the fields. The T2 operator can check the correct performance of the work, the herbicide distribution, and the proper functioning of the nozzles;
- the T1 operator cannot change the operational plan of that day, and it would not be able to change the sequence of the field, change work if required or interrupt in case of emergency on the farm. T2 work can be completely flexible in this way.

It is fundamental to underline that the advantages reported here require the adoption of both the PA tractor and the PA implement. It is not possible to suppose such results only with auto-guidance or only with an ISOBUS implement.

4 Discussion

The discrepancy between an ordinary use of ICT in everyday life and a still low adoption rate in agricultural business stresses the importance of identifying the possible reasons for this. However, the apparent difference in the investment costs required for reaching higher PA technologies levels discourages farmers from furthering the discussion. This study presents an overview of the main advantages of adopting two different crop spray technologies to evaluate the practical benefits of the “technology transition”.

An experimental test with a traditional and an ISOBUS sprayer was carried out to compare their performance during a working day.

This methodology approach of considering an entire working day (9 h), instead of a sample area of soil or working time, resulted fundamental for the study because several advantages have been found thanks to this choice. The experimental test results allowed achieving considerable field capacities (+43% with PA) and herbicide savings (−9% with PA). These data could also be adopted in a cost dataset focused on weeding operations.

The experience carried out using an ISOBUS sprayer confirms that some technologies are already set to be adopted, especially when considering the environmental and economic advantages of lower agronomic inputs.

Environmentally, results confirmed what the literature reports: it is possible to reduce the chemical input by about 10–20% (depending on the operation) than

conventional technologies maintaining the agronomic target. Or, another interesting approach, it is possible to maintain the dose per hectare differentiating the doses according to the crop's needs. Furthermore, the saving of fuel and energy both for the distribution and to produce chemical substances allows a further advantage in terms of the environmental sustainability of the crop production phase.

Another important consideration is the method for assessing the field capacity of the implement. With this work, we have demonstrated that such an assessment required an entire working day and that, probably, PA introduces new parameters for assessing mechanized work phases in agriculture. It is important to emphasize that the experiment involved both the auto-guidance system and the ISOBUS operator unit.

This paper has been focused on weeding, in the hypothesis that it is one of the operations that could benefit the most from the PA technology. Although this hypothesis has been confirmed with results that extending them to other implements is impossible.

Acknowledgements The authors wish to thank Ivan Carminati, Gianluigi Rozzoni, Alex Filisetti and Elia Premoli for their valuable help in carrying out the experimental trials and the Pallavicina Farm in Treviglio, Bergamo, Italy for hosting the trials.

Funding This research was funded by the Italian Ministry of Agriculture (MiPAAF) under the AGROENER project (DD n. 26329, 1 April 2016) - <http://agroener.crea.gov.it/> and the AgriDigit Programme, DDL n. 2111-B/2015.

References

1. Clasen, M.: Farming 4.0 und andere Anwendungen des internet der Dinge. In Ruckelshausen, A., et al. (eds.) Proceedings of GIL Annual Meeting. Informatik in der Land-, Forst- und Ernährungswirtschaft. Bonn, pp. 15–18 (2016)
2. Roland, K.R., et al.: Adoption of site-specific information and variable-rate technologies in cotton precision farming. *J. Agric. Appl. Econ.* **36**(1), 143–158 (2004). <https://doi.org/10.1017/S107407080002191X>
3. Caffaro, F., Cavallo, E.: The effects of individual variables, farming system characteristics and perceived barriers on actual use of smart farming technologies: evidence from the Piedmont Region. *Northwestern Italy Agric.* **9**, 111 (2019). <https://doi.org/10.3390/agriculture9050111>
4. El Nahry, A.H., Ali, R.R., El Baroudy, A.A.: An approach for precision farming under pivot irrigation system using a remote sensing and GIS techniques. *Agric. Water Manag.* **98**, 517–531 (2011). <https://doi.org/10.1016/j.agwat.2010.09.012>
5. Zhang, N., Wang, M., Wang, N.: Precision agriculture – a worldwide overview. *Comput. Electron. Agric.* **36**, 113–132 (2002)
6. Paustian, M., Theuvsen, L.: Adoption of precision agriculture technologies by German crop farmers. *Precision Agric.* **18**, 701–716 (2017). <https://doi.org/10.1007/s11119-016-9482-5>

New Technologies and Safety in Agriculture: SAFETY AR



Valerio Di Stefano, Leonardo Bianchini, Riccardo Alemanno, and Andrea Colantoni

Abstract New technologies, such as augmented reality or artificial intelligence, are able to offer contributions to delicate sectors of our society, such as the world of safety at work.

Suffice it to say that in 2021 in Italy accidents at work increased significantly and fatal cases were 1,270, 181 more than the 1,089 in 2019 (+16.6%). Against a reduction in deaths of about 30.1%, those occurring at work have in fact increased by over a third (+34.9%). Important numbers that make us reflect on the importance of correct training and information on safety at work as required by the European directives implemented by Legislative Decree 81/2008 in Italy.

One of the main problems in the world of agriculture appears to be the total negligence of employers in respecting the training and information obligations towards workers. For this reason, the University of Tuscia has developed, at the end of intense research, an augmented reality system called Safety AR, through which workers and also employers, pursuant to the very recent d.l. taxation and safety (146/2021), can train and inform themselves about the risks present in the workplace and avoid injuries or, in the most serious cases, white deaths.

Safety AR is an innovative multifunctional tool, which identifies the real needs of every single production process with an interactive and functional approach. Safety AR is accessible thanks to one of the most innovative technologies of the moment, recognized by the national development plan among the enabling tools of industry 4.0 because it increases real-world interactions without replacing it.

The Safety AR allows you to reproduce the safety pictograms on “markers”, that is aluminum signs, which once framed by the workers through a phone / tablet and an application, will be animated in augmented reality explaining the meaning of the pictogram and the various risks and dangers. The data extracted from the Safety AR will be treated with the utmost respect for the confidentiality of the worker. Through this system, an important decrease in accidents at work is estimated.

V. Di Stefano (✉) · L. Bianchini · R. Alemanno · A. Colantoni
Department of Agricultural and Forestry Sciences, University of Tuscia, Viterbo,
Via San Camillo de Lellis, snc, 01100 Viterbo, Italy
e-mail: v.distefano@unitus.it

Keywords safety at work · technologies · augmented reality · normative compliance · agriculture

1 Introduction

Each employer has the obligation to invest in safety at work, which in addition to reducing the risk of accidents at work, brings a tangible improvement to the working environment and company climate. Designing, drafting and implementing an effective safety plan allows you to increase the well-being of those who work and to enhance the company's reputation towards all stakeholders, employees, partners, suppliers and customers. A workplace that complies with all safety standards supports the prevention of risks and accidents, guarantees employees a peaceful environment in which to work, improving the sense of belonging and motivation; in this way, production efficiency is increased, and last but not least, the employer protects himself from possible sanctions for not having had adequate attention to the health and safety of their workers.

It is now established that in a work environment in which strict safety standards are adopted, the level and quality of production is improved, and all this also passes into concrete savings, because systematic compliance with safety standards minimizes accidents and occupational diseases, also reducing the social costs that this entail.

The protection of health and safety in the workplace is a subject in continuous evolution, which is no longer willing to tolerate white deaths and injuries, which are decreasing but in any case, above the European average, which can be incurred by those who are doing his duty. Over time, starting from the 1950s, the legislation has been adapted to the vicissitudes that arose, making it increasingly severe, up to now with the Consolidated Law on health and safety at work, more commonly called TUSL, changing the approach of employers and workers who are now called to dialogue and collaborate to adopt precautions, precautions and innovative technologies, aimed at preventing accidents at work.

Among the main forms of precaution we find, continuous training, which is the key in these circumstances. The improvement and advancement of new technologies, such as virtual reality VR and augmented reality AR could contribute to the training, information and training of workers by involving them in the learning process in order to raise awareness and pay greater attention to their health. and encourage a reduction in accidents and deaths in the workplace.

The agricultural and forestry sector is undoubtedly one of the most affected by accidents and deaths at work and for this reason applying new technologies such as augmented reality to occupational safety in this sector is equivalent to greatly reducing the number of injuries and white deaths.

2 Definition of Augmented Reality

A rather shared definition of augmented reality was provided by the Canadian Paul Milgram of the Department of Industrial Engineering - University of Toronto and the Japanese Fumio Kishino of the Department of Electronic, Information Systems and Energy Engineering - Osaka University, who conceived it as the 'set of circumstances in which a real environment is "augmented" by virtual objects. They describe it in a continuum between real context and pure virtual environment where the variable values of virtuality and reality are placed in the middle, according to the representation below.

AR promises to bridge the gap between the digital and physical world, reducing the "cognitive distance" and minimizing the "cognitive load". The first represents the gap between the form in which the information is presented and the context in which it is applied.

The second is related to the mental effort required to process a given type of information and depends on the cognitive distance.

3 Safety AR

Safety AR was created with the aim of ensuring safety in companies by informing and educating internal and external staff on the meaning of safety signs. It is an innovative multifunctional tool, which identifies the real needs of each individual production process with an interactive and functional approach.

The Safety AR system is accessible thanks to one of the most innovative technologies of the moment, recognized by the national development plan as one of the enabling tools of industry 4.0 because it increases interactions with the real world without replacing it. The experiential approach, thanks to its interactive capacity linked to the surrounding reality, increases the conceptual memorization by the end user because it relates the physical object and its digital content in the same environment in which it is located.

The services produced, the thematic areas, the safety pictograms, the company equipment will be accompanied by an info point active 24 h a day and 7 days a week, always accessible from the furnishing devices supplied.

In this way, companies will be able to create an economic asset, for example virtual ad hoc with targeted, specific, and personalized content to facilitate the assimilation of experiential notions, contextualized in the workplace, for workers.

All operators interconnected with Safety AR will be able to transfer their objective skills, creating Augmented Reality content available to the entire corporate community.

To verify and monitor the quality and updating of work activities by crossing data and statistics and pursuing the maintenance of safety standards, collaboration, creation and knowledge of business processes are necessary.

The Safety AR system, with the help of Augmented Reality and a web platform dedicated to it, will make available the data processed in the company on a digitized support. Marker cards printed on aluminium, on Totem, on paper or on adhesive ready to be placed in the workplace.

The visualization of process data or information content will be activated by framing with the camera of the enabled mobile devices the markers inserted on pre-established guide paths, or company areas in common use to enrich the company work environment with multimedia content (consult a maintenance sheet or view a 3D graph containing data or audio video explaining the information and terms of the requested service will no longer be a problem).

Safety AR will manage all AR content from a web platform that will process the data by updating the databases in the cloud.



4 Conclusions

In conclusion, AR technology applied to the field of workplace safety allows workers to be provided with adequate training and information and to monitor, as already mentioned, the views and training hours through a system connected to the network. Furthermore, the augmented reality system integrated with workplace safety allows the Prevention and Protection Service Manager to carefully monitor the basic training hours (4 h according to Legislative Decree 81/200) for each operator.

Therefore, alongside an integrated system that significantly improves information and training for workers, there is a control system. This significantly facilitates the tasks of the RSPP, allowing them to complete their duties more quickly and efficiently.

AR is more than a coaching tool for OSH innovation; it also helps motivate workers, encourages interactive learning, and develops critical thinking and decision-making skills.

AR models can also directly help train workers better, significantly reducing workplace accidents and fatalities, allowing workers to directly examine risks and potential dangers. This will ensure greater protection for the employer, as he will be partially exempt from civil and criminal liability deriving from the accident.

References

1. Arduini, G.: La realtà aumentata e nuove prospettive educative, *Education Sciences and Society*. saggi ONLINE 2/2012.indd 209 (2012)
2. Azuma, R.: A survey of augmented reality presence: *Teleoperat. Virtual Environ.* **6**(4), 355–385 (1997)
3. Bagassi, S., De Crescenzo, F., Masotti, N.: Augmented reality in the control tower: a rendering pipeline for multiple head-tracked head-up displays. In: *International Conference on Augmented Reality, Virtual Reality and Computer Graphics*, Springer, Cham (2010). https://doi.org/10.1007/978-3-319-40621-3_23
4. Banbury, S., Hollands, J.G., Wickens, C.D., Parasuraman, R.: *Engineering Psychology and Human Performance*. Psychology Press (2015)
5. Banzi, A., Bonacini, E., Capriotti, G., Montella, M.: Il Capitale culturale: studies on the value of cultural heritage, *J. Depart. Cult. Herit.* **9** (2014)
6. Bianchini, L., Colantoni, A., Di Stefano, V., Egidi, G.: Health and safety on workplace between augmented reality and regulatory compliance: safety AR. *Int. J. Entrepreneur.* **26**(special issue 2), 1–5 (2022)
7. Bimber, O., Raskar, R.: *Spatial Augmented Reality: Merging Real and Virtual Worlds*. A. K. Peters, Ltd., Natick (2015)
8. Buffolano, C., Nacciarone, L., Solombrino, M.: *Compendio di Sicurezza sul lavoro – II Edizione* (2020)
9. Caligiana, G., Carricato, M., De Crescenzo, F., Piastra, S.: *Interfacce di realtà aumentata per applicazioni efficienti e sicure nell'industria e nei servizi. Progettazione industriale, costruzioni meccaniche e metallurgia - Università di Bologna* (2021)
10. Caudell, T.P., Mizell, D.W.: *Augmented reality: An application of head-up display technology to manual manufacturing processes*. Boeing Computer Services, Research and Technology (1992)
11. Cawood, S.: *Augmented Reality. A Practical Guide*, Pragmatic Bookshelf, Raleigh (2007)

12. Dallasega, P., Linder, C., Rauch, E.: Anthropocentric perspective of production before and within Industry 4.0. *Comput. Indust. Eng.* **139**, 1–15 (2019)
13. De Kerckhove, D.: Realtà aumentata: Grande Mutazione di oggi, in *Media Duemila*, n. **270**, 13–15 (2010)
14. Gerosa, M., Moioli, G.: *Brera academy virtual lab. Un viaggio dai mondi virtuali alla realtà aumentata nel segno dell'Open source*, Milano (2010)
15. Harvard Business Review. *A Manager's Guide to Augmented Reality* (2010)
16. Ilze, S., Merlino, M.: The augmented supply chain. *Procedia Eng.* **178**, 308–318 (2017)
17. Kishino, F., Milgram, P.: A taxonomy of mixed reality visual displays. *IEICE Trans. Inf. Syst.* **77**(12) 1321–1329 (1994)
18. Lanzotti, A., Minopoli, V., Tarallo, A., Vanacore, A.: Interactive tools for safety 4.0: virtual ergonomics and serious games in real working contexts. In: *Ergonomics. Per collegarsi a questo articolo* (2019): <https://doi.org/10.1080/00140139.2019.1683603>
19. Lemieux, A., Mekni, M.: *Augmented Reality: Applications, Challenges and Future Trends* (2014)
20. Nee, A.Y., Ong, S.K.: *Virtual Reality and Augmented Reality Applications in Manufacturing*. Springer Verlag, London (2004). <https://doi.org/10.1007/978-1-4471-3873-0>
21. Peddie, J.: *Augmented Reality: Where We Will All Live*. Springer, Cham (2017)
22. Peterson, S., Pinska, E.: Human performance with simulated collimation in transparent projection screens. In: *Proceedings of the Second International Conference on Research in Air Transportation (ICRAT)* (2016)
23. Poelman, R., Van Krevelen, D.: A survey of augmented reality technologies, applications and limitations. *Int. J. Virtual Real.* **9**(2), 1 (2010)
24. Sheridan, T.B.: *Humans and Automation: System Design and Research Issues*. Human Factors and Ergonomics Society (2002)
25. Imbrenda, V., Coluzzi, R., Di Stefano, V., Egidi, G., Salvati, L., Samela, C., . . . Lanfredi, M.: Modeling spatio-temporal divergence in land vulnerability to desertification with local regressions. *Sustainability (Switzerland)* **14**(17) (2022). <https://doi.org/10.3390/su141710906>

Waste Heat from District Heating Plants for Forage Drying in the Camonica Valley



Marco Fiala, Luca Nonini, and Leonardo Colnago

Abstract The aim of the work was to evaluate the possibility of using the waste heat generated by District Heating Plants (DHP) for drying baled forage in a mountainous area (Camonica Valley, Lombardy Region, Italy) where dairy cattle farming is widespread. In this condition, the natural forage drying is quite difficult because of the altitude, fields slope, and climatic conditions. Furthermore, during the hay season, the thermal demand to DHPs, compared to winter months, is lower, and the plants usually have some waste heat. The study was performed in 2019 and concerns the DHP located at Ponte di Legno municipality, which was the most interesting to investigate due to its particular location and technical characteristics: 2 woodchips burners for heat production (10.4 MW), 1 woodchips burner (4.0 MW) linked to an Organic Rankine Cycle unit (ORC) for combined heat and electricity generation (2.95 MW heat; 0.73 MW electricity), and 1 diesel-oil burner (back-up unit). The waste heat over the spring–summer time was computed as the difference between the total heat generated by the plant, the one sold to the users, and the one lost through the distribution grid. During the three two-months periods, the total DHP waste heat amounted to: 514 MWh in May–Jun (power: 351 kW, assuming a continuous operation), 314 MWh in Jul–Aug (211 kW) and 229 MWh in Sep–Oct (156 kW). Currently, in 8 cattle farms near the DHP, the forage is collected in round bales, partly as “haylage” (moisture content: $U_{Bhl} = 65\%$) and partly as “hay” ($U_{Bh} = 13\%$). Assuming that all the fodder could be baled as “semi-dry” ($U_{Bsd} = 45\%$; 324 kg) and transported to a central bales-dryer (located inside the DHP), the masses to be dried were: May–Jun: 834 t; Jul–Aug: 486 t; Sep–Oct: 97 t. The technical characteristics of the bales-dryer were chosen according to the maximum waste heat available from the DHP (May–Jun, during which also the forage production reaches its maximum),

M. Fiala (✉) · L. Nonini

Department of Agricultural and Environmental Sciences. Production, Landscape, Agroenergy (DiSAA), University of Milan, Via G. Celoria 2, 20133 Milan, Italy
e-mail: marco.fiala@unimi.it

L. Nonini

e-mail: luca.nonini@unimi.it

L. Colnago

Mountain University (UNIMONT), Via A. Morino 8, 25048 Edolo, BS, Italy

assuming to achieve the rated thermal power of the dryer increasing the DHP woodchips consumption during Jul-Aug and Sep-Oct. Switching the current haymaking techniques into the two-stages one (2SH), a dryer for 20 bales/cycle: (i) allows to dry the whole amount of fodder currently needed from farms, and (ii) increasing the woodchips consumption of 276 t to operate at full capacity from May to October, ensures a considerable increase of round bales available for the territory.

Keywords Circular economy · District Heating Plant · Forage drying · Waste heat

1 Introduction

The well-known process of drying consists in evaporating water from a biomass to avoid the proliferation of microorganism which can cause its degradation. Drying method - by sun energy supply - is the most used conservation technique for forage; artificial drying can also be applied by evaporating the water by heated air blown into the fodder using a fan [1].

The “two stages haymaking technique (2SH)” consists of cutting fresh-grass, reach a moisture content of $U = 40\text{--}50\%$ by natural drying, collect (bulk or in round-bales) the “semi-dried” forage and finally dry it in a forage-dryer (up to $U = 15\text{--}18\%$) [2]. The 2SH requires heat generation for the drying air but is very interesting because it allows the production of high-quality forage even in situations for which climatic conditions are not particularly suitable for cereals cultivation and haymaking (such as in mountainous areas) and, therefore, the possibility to support animal breeding (cattle and goats, mainly). If the second drying is carried out with hot air produced from fossil energy sources, the process is very expensive and usually unsustainable; on the contrary, if the thermal source is renewable (or some waste heat is available), the process can be economically attractive and cost-effective (circular economy) [1].

In the Camonica Valley (Lombardy Region, Italy), nine District Heating Plants (DHP) are operating and generating thermal energy (ET) mainly addressed for space-heating (Autumn–Winter, particularly), as well as for sanitary hot-water production (all the year). In Spring–Summer time, the heat demand is lower and therefore DHPs have thermal energy that could be used in other processes, such as the drying of semi-dried fodder harvested using 2SH technique. The aim of the work was to evaluate the possibility of using the waste heat generated by a District Heating Plants (DHP) in a round-bales dryer for drying forage of the Camonica Valley, where dairy cattle farming is widespread.

2 Materials and Methods

2.1 DHP Located in Ponte di Legno Municipality

In this plant – powered by woodchips partially coming (40% of the total annual consumption) from local forests – the heat distribution grid extends for 33.8 km (13.9 and 19.9 km in Temù and Ponte di Legno municipalities, respectively); users are: 1060 residential, 96 tertiary sector, 3 industrial.

The plant consists of 3 thermal generators fed by woodchips and 1 rescue/integration generator, powered by diesel oil. The third generator (G_3 , rated power: 4.0 MW. Year 2019: operating time 8121 h/year) supplies an Organic Rankine Cycle unit (ORC) that combines heat generation (2.9 MW. Year 2019: 19,421 MWh into the district heating grid) and electricity (0.7 MW. Year 2019: 4800 MWh, into the electricity grid). The remaining two biomass generators (G_1 and G_2 , rated power: 5.8 and 4.6 MW, respectively) serve the district heating network only (year 2019: 16,010 MWh; operating time 2975 and 4991 h/year, respectively). The interest in Ponte di Legno plant for this study was due to:

- proximity of 8 cattle farms in which natural drying of fodder is particularly difficult, due to the local conditions and the long time (compared with the valley bottom) required for the hay-making process. The distance of farms from DHP ranges between 3.7 km and 15.0 km (average: 8.7 km). These values are, however, related to the farm center, whereas fields from which the agricultural vehicles depart for forage delivering to the DHP plant can be located even at longer distances;
- peripheral position in the town, with available of spaces close to the heat generators (to locate the bales-dryer, which requires a lot of open area, both for transport/unloading means (delivered bales) and for short storage (dried bales);
- availability of accurate technical and management information, provided by the DHP management company.

This information allowed to calculate the waste heat in the Spring–Summer period (ET_{WS} ; MWh), as the difference between the energy produced and fed into the distribution grid (ET_{PRt} ; MWh), the one sold and used by the users (ET_{VD} ; MWh), as well as the heat lost through the distribution grid (ET_{DS} ; MWh) (Table 1, Fig. 1).

$$ET_{WS} = ET_{PRt} - (ET_{VD} + ET_{DS}) \quad (1)$$

According to [4], ET_{WS} was calculated – on a monthly basis, separately for supply and return pipes – according to: (i) resistance to heat exchange of piping materials (R_p ; $m \cdot ^\circ C/W$); (ii) temperature difference between the heat transfer fluid and the environment (ΔT ; $^\circ C$); (iii) pipes diameter (\varnothing_p ; mm) and (iv) proximity between supply and return pipes (Db ; mm). The percentage of heat dissipation along the distribution grid (average: 27%) was higher in the summer time (Jul-Aug: 50%) than in the winter one (Nov-Dec: 20%).

Table 1 Ponte di Legno DHP: operating parameters (year 2019)

Bimester	Wood-chips (G1, G2)	Wood-chips (G3)	Wood-chips (total for DHP)	Heat (grates cooling)	Heat (burner exchangers)	Total generated heat	Spec. consumpt.	Lost heat (grid dissip.)	Heat sold (by grid)	Waste heat (available)	
	mCH1	mCH2	mCH3	ETPR1	ETPR2	ETPRt	cs	ETDs	ETVD	ETWs	
	t	t	t	MWh	MWh	MWh	kg/kWh	MWh	%	MWh	
Jan-Feb	3359	3057	6416	347	9784	10131	0.633	2091	21%	8015	24
Mar-Apr	1219	2662	3881	369	6278	6647	0.584	1998	30%	4449	200
May-Jun	449	1651	2100	244	3658	3902	0.538	1616	41%	1772	514
Jul-Aug	0	1614	1614	270	2812	3082	0.524	1537	50%	1230	314
Sep-Ott	45	2053	2099	336	3220	3556	0.590	1759	49%	1568	229
Nov-Dic	3555	2379	5934	278	9680	9958	0.596	2027	20%	7205	726
TOTAL	8626	13417	22043	1844	35431	37275	0.591	11029	30%	24239	2008

Note: in 2019, the diesel-oil back-up unit never worked.

Fig. 1 Ponte di Legno DHP: heat balance (year 2019)

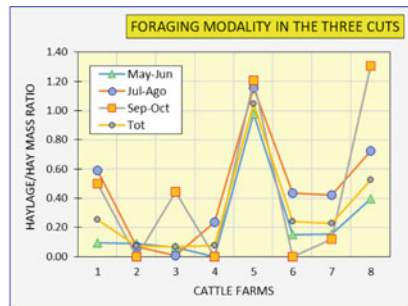
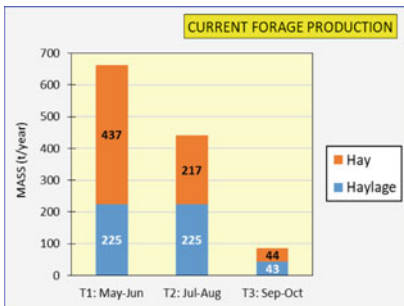
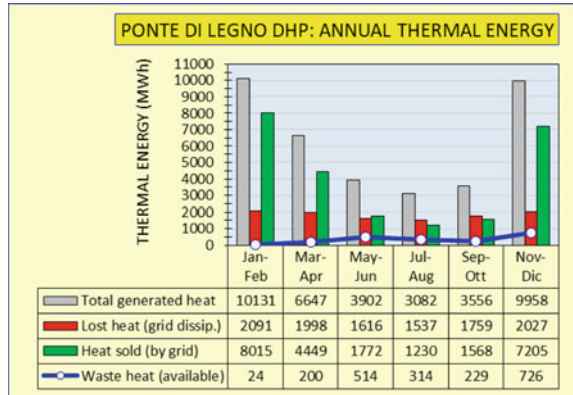


Fig. 2 8 cattle-farms: haylage and hay production (left) and ratio for the three cuts (right) (year 2019).

Overall, in 2019, the DHP burned 22,043 t of woodchips, entering the thermal network with $ET_{\text{PRT}} = 37,275$ MWh of heat (including 1844 MWh from the combustion grates cooling system) and the electrical grid with $EE_{\text{PRT}} = 4800$ MWh of electricity. The thermal energy sold and used – detected bimonthly – was $ET_{\text{VD}} = 24,239$ MWh.

Assuming a continuous (24/24 h) and a constant operation of the thermal generators, the average power associated with the waste heat was $PT_{\text{WS}} = 351, 211, 156$ kW in May-Jun, Jul-Aug, and Sep-Oct, respectively.

2.2 Cattle Farms Close to DHP and Current Forage Production

In the upper part of the Camonica Valley, 12 farms for cattle are operating: 3 for milk & meat and 5 for milk only. 8 of these farms are located close (range: 4–15 km; average: 8.7 km) to the Ponte di Legno DHP (3 milk & meat, 5 milk only, 673 cattle, including rebound), at 1000–1600 m asl, covering a total area of 1899 ha, 463 of which (24.4%) used for fodder production.

Half of the 8 farms operates only two cuts per year, while the remaining four farms perform three cuts, but only in plots located at lower altitude.

The fodder is mainly packed in round bales, and it was quantified by a detailed “Questionnaire” aimed at farmers. The survey showed that:

- in the three two-months of 2019 the produced fodder was: (i) hay: $m_h = 698$ t, packed in 3404 round bales (average mass $m_{\text{Bh}} = 205$ kg; moisture $U_{\text{Bh}} = 13.0\%$); (ii) haylage: $m_{\text{hl}} = 493$ t, packed in 967 round bales (average mass $m_{\text{Bhl}} \cong 509$ kg; moisture $U_{\text{Bhl}} = 65.0\%$) (Fig. 2, left);
- to obtain: (i) hay by natural drying 49, 63 and 66 h, on average, were needed, (ii) haylage 27, 39 and 48 h on average were needed, for 1st, 2nd and 3rd cut, respectively.

More than half (56%) of forage is produced during May-Jun, 37% in Jul-Aug and the remaining 7% in Sep-Oct, when climate conditions make difficult the natural drying of the cut grass (Table 2).

The ratio (in dry mass) haylage/hay in the three cuts (Fig. 2, right) was rather constant for some farms (Az_5, Az_7) and variable for others (Az_3, Az_8), it ranged between 0.07 (Az_2, Az_3, Az_4) and 1.05 (Az_5), with average of 0.28.

Table 2. Studied farms: main characteristics and forage production (year 2019)

Farm	Area		Dist.	T1: May-Jun		T2: Jul-Aug		T3: Sep-Oct		TOTAL		
	Total	Forage		Haylage	Hay	Haylage	Hay	Haylage	Hay	Haylage	Hay	Total
	ha	ha		%	t	t	t	t	t	t	t	t
Az_1	200	80	40%	9.6	11.3	49.1	20.5	14.0	16.2	13.0	76.1	124.1
Az_2	400	100	25%	9.7	10.4	47.6	4.1	24.9	4.4	7.5	80.0	94.5
Az_3	300	70	23%	6.6	1.7	10.7	0.4	23.6	4.0	4.0	38.3	44.8
Az_4	400	10	3%	15.0	0.0	45.0	12.6	21.4	0.0	0.0	66.4	79.0
Az_5	140	33	24%	8.1	76.5	31.5	43.0	15.0	12.0	4.0	50.5	182.0
Az_6	220	90	41%	3.7	39.0	104.0	51.0	47.0	0.0	0.0	151.0	241.0
Az_7	94	25	27%	8.7	38.0	100.0	48.0	46.0	4.0	13.5	159.5	249.5
Az_8	145	55	38%	7.9	48.0	49.0	45.0	25.0	6.5	2.0	76.0	175.5
Mass	t/year	1899	463	24%	8.7	225	437	217	43	44	698	1190
	%				662	56%	442	37%	87	7%	59%	100%
Round-bales	-				441	2131	441	1058	85	215	3404	4371

Table 3 Studied farms: a possible new fodder production system

Farm	T1: May-Jun		T2: Jul-Aug		T3: Sep-Oct		TOTAL		Total	
	ex-Haylage	ex-Hay	ex-Haylage	ex-Hay	ex-Haylage	ex-Hay	ex-Haylage	ex-Hay		
	t	t	t	t	t	t	t	t		
Az_1	7.2	77.7	13.0	22.1	10.3	20.6	31	120	151	
Az_2	6.6	75.3	2.6	39.4	0.0	11.9	9	127	136	
Az_3	1.1	16.9	0.3	37.3	2.8	6.3	4	61	65	
Az_4	0.0	71.2	8.0	33.9	0.0	0.0	8	105	113	
Az_5	48.7	49.8	27.4	23.7	7.6	6.3	84	80	164	
Az_6	24.8	164.5	32.5	74.3	0.0	0.0	57	239	296	
Az_7	24.2	158.2	30.5	72.8	2.5	21.4	57	252	310	
Az_8	30.5	77.5	28.6	39.5	4.1	3.2	63	120	184	
Mass	t/year	143	691	143	343	27	70	313	1104	1417
	%	834	59%	486	34%	97	7%			
Round-bales		2573		1499		299		4371		

2.3 Two Stages Haymaking: a Possible New Fodder Production System

A different approach to the forage supply for the 8 farms showed that the whole production of hay and haylage baled fodder could be collected – using the existing machinery fleet – in round-bales of semi-dried forage (moisture $U_{Bsd} = 45\%$), with further drying (down to $U_{BH} = 13\%$) in a central bales-dryer, located inside the DHP and using – from May to October – the waste heat (Table 3).

The masses of hay and hay-silo produced in the year 2019 were equal to semi-dried forage for: May-Jun: 834 t; Jul-Aug: 486 t; Sep-Oct: 97 t. As the mass of a single semi-dried round-bale reached $m_{Bsd} \cong 324$ kg, the number of bales to dry amounted to: May-Jun: 2573 ($n_{Bday*} = 42$); Jul-Aug: 1499 ($n_{Bday*} = 24$); Sep-Oct: 299 ($n_{Bday*} = 4$), for a total of $n_{Btot} = 4371$ (in 184 days).

2.4 The Dryer for Round-Bales

The market offers different solutions of fixed round-bales dryers in terms of size and operating parameters (mainly: heat output, air flow rate, drying cycle duration and productivity). In this case – given the characteristics of the ambient air (temperature, moisture content and average density in the three two-month periods) – the dryer was chosen considering its rated thermal power (in order to have $PT_{ESS} \cong PT_{WS}$), and verifying that the bimonthly thermal gap (ΔT ; °C) was achieved with an air flow consistent with the nominal air flow of the fan-dryer (Q_{ESS} ; m³/h). Considering PT_{WS} (May-Jun) = 351 kW, the technical characteristics of the dryer are shown in Table

4.

Table 4 Round-bales dryer with a thermal power of $PT_{ESS} = 349$ kW (source: Clim.Air)

Bales number	Air pressure	Air flow	Thermal power	Drying temp	Drying capacity	Cycle time
n_B	P_{AMB}	Q_{AMB}	PT_{ESS}	T_{ESS}	Q_{H_2O}	t_{ESS}
-	mmH ₂ O	m ³ /h	kW	°C	kg/day	h
20	120	40,000	349	27	286	11

Then: (i) heat of evaporation: $H_{EV} = PT_{ESS}/Q_{H_2O} = 1.22$ kW/kg; (ii) drying process efficiency¹: $h_{ESS} = H_{EV_H_2O}/H_{EV} = 51\%$; (iii) daily drying cycles: $n_{ESS} = 24/T_{ESS} = 2$ (no-stop operation); (iv) daily dried bales: $n_{Bday} = n_B \cdot n_{ESS} = 40$; (v) daily mass of semi-dried: $m_{sd} = n_{Bday} \cdot m_{Bsd} = 12971$ kg were computed.

3 Results and Discussion

Considering that in two bimonths (Jul-Aug and Sep-Oct) the waste heat from the DHP was correlated with a lower thermal power ($PT_{WS} = 211$ and 156 kW, respectively), to reach the nominal thermal power of the dryer (PT_{ESS} , thus ensuring its full and correct functioning), it is necessary to increase the woodchips flow (Δc_{hCH} ; kg/h) that feeds the DHP thermal generators. Knowing the average specific bi-monthly consumption of woodchips (cs; kg/kWh):

$$\Delta c_{hCH} = \Delta PT/c_s = (PT_{ESS(May-Jun)} - PT_{WS})/c_s \quad (2)$$

$\Delta c_{hCH} = 265$ and 328 kg/h for Jul-Aug and Sep-Oct, respectively, were obtained. This corresponded to a yearly increase of woodchips equal to $\Delta m_{CH} = 276$ t.

It was therefore possible to check, for each of the three bimonths, whether the round-bales dryer – with its work output – covers the demand for drying semi-dried bales (Δn_B) coming from the 8 cattle farms: $\Delta n_B = n_{Bday} - n_{Bday*} = -2$ (in May-June), $+16$ (in Jul-Aug), $+36$ (in Sep-Oct). With a slight increase ($+1.2\%$) of the current annual woodchip consumption, the forage dryer with the abovementioned technical characteristics, working at full power from May to October, can satisfy the whole production of forage of the farms, for a total of 707 t (also allowing a significant improvement in the baled fodder quality). This extra-forage can be used to increase the number of bred cows or sold on the local market. The solution, however, requires a strong coordination between the cattle farms, in order to organize their cuts (in May–June, especially), and to generate a constant daily flow of semi-dried round-bales to the dryer. This logistic problem could be solved by drawing up among the farms a “hay cutting plan”, scheduling the forage cuts according to the plant drying capacity, avoiding the accumulation of semi-dried bales. The farm-to-drying plant

¹ By using $H_{EV_H_2O} = 0.628$ kWh/kg as average heat of evaporation of water at atmospheric pressure.

distance is a crucial factor: the higher the distance, the higher the direct transport costs.

The present study focused on the general feasibility to use the waste heat of a District Heating Plant in a forage dryer; certainly, a more complete analysis will be necessary. It must include the evaluation of investments (structures and machinery), operating and environmental costs of the possible solutions as well, with the goal to develop animal husbandry in the Camonica Valley.

4 Conclusions

The exploitation of the waste heat of the Ponte di Legno DHP in a commercially available centralized round-bales dryer would allow to dry the whole amount of fodder currently used by the 8 cattle farms located near the DHP, if existing haymaking techniques were modified into the two 2SH. The production of haylage is rather complex and expensive; the adoption of 2SH – against the investment for the dryer and more transportation costs – allows to greatly improve the quality of the fodder for cows, with production costs particularly low because of the use of waste heat. The proposed organizational model is an excellent example of circular economy, with high and immediate benefits for the territory.

References

1. Aschauer, C., et al.: Direttive per la ventilazione del fieno in catasta. *Agroscopttransfer* **38** (2014)
2. De Zanche, C., et al.: Essiccazione e conservazione dei prodotti agricoli. ENEA – Ente per le Nuove Tecnologie, Roma (1990)
3. Degli Atti, F., Sellerio, U.: L'essiccazione dei prodotti agro-alimentari. In: Angeli, F. (ed.) *Per un uso razionale dell'energia*, Milano (1991)
4. Scanagatta, F.: Analisi energetica di reti di teleriscaldamento: controllo per mezzo di approccio qualitativo e quantitativo. Master's Theses Università degli Studi di Padova, Department of Industrial Engineering (2015)

Remote Sensing Imagery for Mapping and Monitoring High Nature Value Farmland Area (HNVF)



Costanza Fiorentino , Angelo R. Donvito, Paola D'Antonio ,
Domenico Conte, Vincenzo Scalcione, and Francesco Toscano 

Abstract The definition of High Nature Value Farmland Area (HNVF) was provided by Andersen in 2003: “HNVF comprises those areas in Europe where agriculture is the major (usually the dominant) land use and where that agriculture supports or is associated with either a high species and habitats diversity, or the presence of species of European conservation concern or both”. The study area was located in the Basilicata region, in southern Italy. The map of HN VF area was elaborated at municipal level (spatial resolution) in 2012. The objective is to develop a GIS prototype service for the identification and characterization of HN VF adaptable to different scales (local, regional, national). The proposed methodology is based on the statistical and farm systems approach. The developed procedure uses MODIS satellite images to improve the number and the accuracy of the land cover classes of the Corine Land Cover map and to calculate indicators aimed at monitoring soil and vegetation properties. A good agreement was found between our HN VF map and the results of literature works, although the analysis approaches were different. The developed algorithm provides the possibility to vary the spatial resolution of the HN VF map from the national to farm level. The main advantage of the proposed methodology is that the inputs are free data, accessible from the public authority data-base.

Keywords biodiversity conservation · natural value · MODIS · GIS · bioeconomic · Big-Data

C. Fiorentino · P. D'Antonio (✉) · V. Scalcione · F. Toscano
University of Basilicata, Potenza, Italy
e-mail: paola.dantonio@unibas.it

C. Fiorentino · A. R. Donvito · D. Conte
Digimat SPA - Research and Development, Matera, Italy

© The Author(s), under exclusive license to Springer Nature Switzerland AG 2023
V. Ferro et al. (eds.), *AIIA 2022: Biosystems Engineering Towards the Green Deal*,
Lecture Notes in Civil Engineering 337,
https://doi.org/10.1007/978-3-031-30329-6_55

1 Introduction

In agriculture, generally, a higher level of biodiversity is found in those areas where agricultural production systems make use of fewer inputs of fertilizers, pesticides and machinery, or in semi-natural areas with extensive agriculture or, again, in agricultural areas which have preserved particular structural elements such as hedges, grassy strips, rows of trees, patches of spontaneous vegetation [9, 18]. Crop diversity alone, if not associated with low input intensity management, is not an indication of agricultural areas with high naturalistic value [10]. The term “High Nature Value Farming” (HNVF) was first introduced in the early 1990s by [2, 3, 5]. The issue of HNVF was addressed by the European Commission with the agro-environmental indicators (COM (2000) 20) and, even more, becoming one of the main themes of the Pan-European Ministerial Conference ‘Environment for Europe’ of Kiev in 2003 (UN/ECE 2003) and of the European Conference on Biodiversity in 2004. The definition of High Nature Value Farmland Area (HNVF) was provided by Andersen in 2003: “HNVF comprises those areas in Europe where agriculture is the major (usually the dominant) land use and where that agriculture supports or is associated with either a high species and habitats diversity, or the presence of species of European conservation concern or both” [13] p. 12). Since the first studies, starting with Andersen [1], three types of HNVF area have been defined:

- Type 1: Agricultural land with high coverage of semi-natural vegetation;
- Type 2: Agricultural lands dominated by low-intensity agriculture or by a mosaic of semi-natural and cultivated territories;
- Type 3: Agricultural land with rare species or a high proportion of animal and/or plant species of conservation interest at European or world level.

As described in [4], HNVs are agricultural areas characterized by low intensity soil management, low animal density and the presence of semi-natural vegetation. Martino [15] pointed out that low-intensity agricultural systems often have labor-intensive production cycles, low chemical inputs and are in general ecologically sustainable. Particular habitats, such as semi-natural grasslands, steppes and small mosaic areas with numerous landscape elements constitute these areas; HNVFs are also abundantly present in mountain areas. In Italy, these agricultural systems can be mainly associated with semi-natural pastures, permanent meadows, traditional orchards and arable crops [6, 28]. The last ISPRA report (May 2021) on biodiversity in Italy shows the updated conservation status of animal and plant species and habitats (protected at EU level) present in our country in both the marine and terrestrial areas. The situation that emerges is critical for the species and habitats that populate our country: although protected for decades, 54% of the flora and 53% of the terrestrial fauna, 22% of the marine and marine species are in an unfavorable state of conservation. 89% of terrestrial habitats, while marine habitats show favorable status in 63% of cases and unknown in the remaining 37%. The results highlight the urgent need for greater commitment to the conservation and management of species and habitats in Italy, also with reference to the objectives of the new European Biodiversity Strategy

for 2030. Further improvements of a more local nature can be adopted, for instance, [27] found that an increase of measures aimed at improving food availability (e.g., reduced pesticide applications) enhanced diversity of farmland birds at field scales, whereas balanced food and shelter measures (e.g. delaying harvest) enhanced bird abundance. HNMF support biodiversity conservation, but they are also increasingly recognized for delivering valuable ecosystem services to wider society, contributing to both sustainability and resilience in the Europe [21]. HNMF will have a key role in future CAP. However, the level of definition of HNMF, in scientific terms, as well as in relation to their spatial distribution is still rather limited, on both a European scale and, even more, a national and regional scale [7, 15]. The objectives of the present work are:

1. define the indicators to elaborate the HNMF map by using the Big Data available (free of charge) in the valuable repository of information of the public authority database;
2. to assess a GIS prototype (QGIS software) service for the identification and characterization of HNMF area adaptable to different scales (local, regional, national).

The proposed methodology has the advantage of using free input data, accessible from the local, national and international public data-base (e.g., the regional orthophotos, the national and regional statistical information, the maps of Corine Land Cover (CLC), Remote sensing images, etc.).

2 Material and Methods

2.1 Study Site

The study area was the entire Basilicata region at municipal level spatial resolution. The developed algorithm provides the possibility, having adequate data available, to vary the spatial resolution of the HNMF map from the national to the corporate level. The year of study is 2012. In order to produce a map of the HNMF area, the following data were used to compute the HNMF indicators. The training data consists of three categories of data, that were uploaded in a GIS project (QGIS):

1. Landscape conformation and structure: DEM/DTM computed from remote sensing SAR images (<http://rsdi.regione.basilicata.it/>); Topographic maps (<http://rsdi.regione.basilicata.it/>); Map of coastal areas and dunes covered by vegetation.
2. Land Use: Corine Land Cover map (CLC); Modis Satellite Images; Orthophoto 2012 (<http://rsdi.regione.basilicata.it/>); Map of protected area: National and Regional Parks, SPAs, SIC and Habitat map; Map of DOP, IGP and organic crops; Vulnerability maps (<http://rsdi.regione.basilicata.it/>); Zoning map (2007–2013 RDPs) divides the Basilicata territory into 3 homogeneous zone. This layer

provides information on the degree of agricultural specialization and indirectly on the intensity of external inputs.

3. Statistical data: Data from the 6th agricultural census (ISTAT, <http://www.istat.it/it/censimentoagricoltura/>); FDAN Farm accountancy data network; RICA Structural data and economic indicators network (Italian CREA).

The test data were the HNMF maps found in the literature (reported in the previous paragraph) on the study area and processed in the same period to which our study refers.

2.2 *Experimental Design*

The methodology proposed in this paper is based on the statistical and farm systems approach. The developed procedure uses MODIS satellite images to improve the number and the accuracy of the land cover classes of the Corine Land Cover map and to calculate indicators aimed at monitoring soil and vegetation properties. The methodology for identifying HNMF is based on the integration of three components that are summarized in a single index that characterizes the areas of interest:

1. Crop Diversity (CD Index);
2. Extensive practices (EP Index);
3. Presence of natural elements (Index Ne).

The criterion for defining the belonging of a municipality to the HNMF area is as follows:

$$\text{Index HNMF} = (\text{CD} + \text{EP} + \text{Ne}) > \text{Threshold}$$

The threshold value, according to the literature [14, 19, 20, 22, 23], should oscillate between the 15th and 30th percentile. The detailed calculation of the indicators is shown in Table 1 in Appendix A, the indicators refer to the Utilized Agricultural Area (UAA). The UAA was calculated by excluding from the total municipal area the woods, the man-made areas, the stretches of water (including rivers and canals) and the coastal areas of dunes covered by vegetation. The formulas of the indicators in Table 1 were applied to each of the 131 municipality of the Basilicata region.

3 **Result and Discussion**

The HNMF area was identified according to the criterion: HNMF Index > Threshold. In the specific case of Basilicata, the range of variability of the threshold goes from the minimum value corresponding to the 30th percentile of the value of the HNMF Index equal to 18.34 to the maximum value corresponding to the 15th percentile

equal to 19.27. Using the maps of protected areas as training data, the threshold at the 30th percentile seemed the most appropriate to adopt. 39 municipalities were found to respond to the characteristics of agricultural areas with a high naturalistic value, showed in green in Fig. 1. These areas have greater crop diversity and a greater presence of natural elements that favor biodiversity. As far as extensive practices are concerned, in these areas there is a lower coverage of extensive crops, but this is linked to the greater crop diversity. The average value relating to the presence of extensive meadows and pastures is much lower in the areas classified as non-HNVF. The soil moisture index is on average higher for HNVF area, while the nitrogen supplied to crops but not used is lower in these areas. A further subdivision of these two macro-areas into sub-areas, characterizing their properties in detail, would be interesting, especially for non-HNVF, in order to identify the critical factors on which to intervene. Figure 1 shows the map of HNVF municipalities, highlighting the municipalities that have a HNVF index value closest to that of the municipalities classified as HNVF (in green). In particular, the municipalities that fall between the 30th and 40th percentile, equal to 13 municipalities, were examined. The closest to the HNVF area by value of the total index (differs from the minimum HNVF value of 0.001) is the municipality of Salandra, this is characterized by a lower CD index value than to the average value of the HNVF class, a value of the EP index comparable to the average value of the HNVF class and a value of the Ne index slightly lower than the average value of the HNVF class.

Analyzing the sub-indices that make up the EP index, it can be seen that the municipality of Salandra has a greater coverage dedicated to extensive crops than the average of the HNVF class, as well as a better value than the index relating to extensive farms, but the presence of natural meadows is practically comparable with the average index value of the non-HNVF class. Therefore, the municipality of Salandra should increase crop diversity and/or increase the area of extensive meadows and pastures in order to re-enter the HNVF area, but only 4% of the UAA is intended for non-extensive meadows and pastures. Another aspect not to be overlooked is that uncultivated crops also contribute to the EMC index associated with the presence of extensive crops, which in 2010 for the municipality of Salandra represented 35% of the total UAA, compared to 35% of the UAA intended for agricultural crops, of which extensive crops accounted for 15%. In conclusion, the municipality of Salandra should maintain and increase the agricultural area dedicated to extensive crops in order to be able to return to the HNVF area. Many factors contribute to maintaining biodiversity and improving soil conservation. For example, the regulations on organic farming set limits on the application of synthetic chemicals but do not guarantee high levels of biodiversity and ecosystem services. The benefits of the absence of chemicals can be offset by the negative effects of increased mechanical processing or irrigation to increase production [8, 26]. The organically grown area cannot be considered dedicated to biodiversity conservation unless direct evidence of net positive effects is provided [25]. Monitoring, evaluating multiple aspects by calculating multiple indicators, would help assess the impacts of these practices on biodiversity and soil. In this way it would be possible to identify and intervene in a targeted manner to introduce, if possible, virtuous practices.

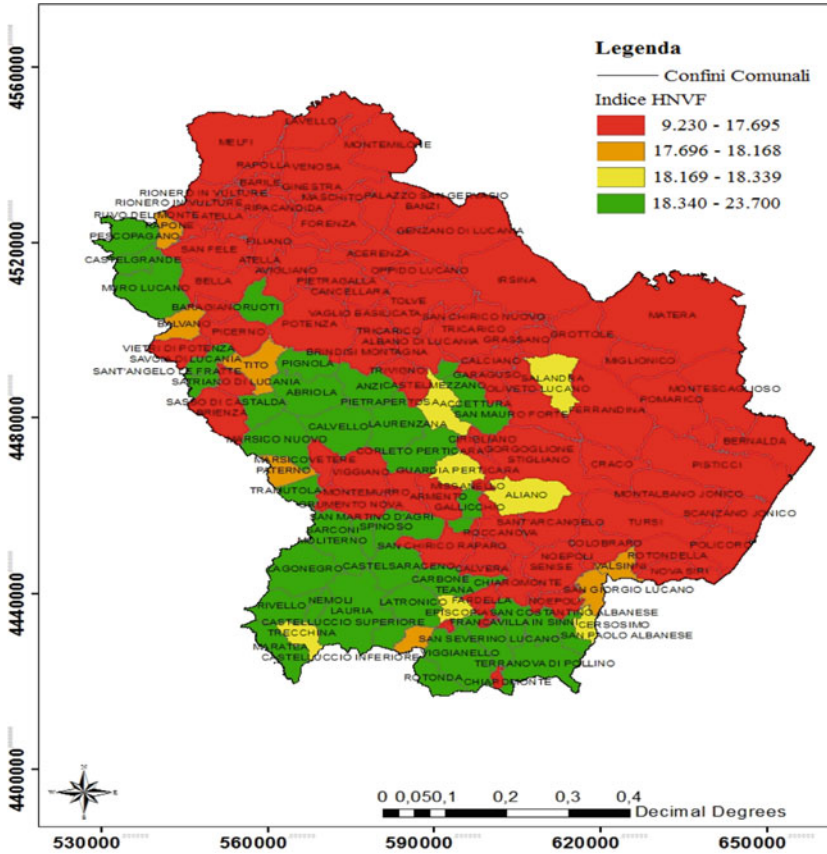


Fig. 1 Map of the HNVF Index. The municipalities classified HNVF (at the 30th percentile) are displayed in green. The municipalities that fall between the 65th and 70th percentile are shown in yellow, while those that fall between the 60th and 65th percentile are displayed in orange

4 Conclusions

HNVF index, elaborated with the statistical approach, was integrated by the processing of medium resolution satellite images. The GIS allows to visualize the individual sub-indices selecting some of them in order to focus on specific problems. The proposed approach is very versatile both because it allows to manage multiple geo-referenced information layers and because it is applicable to different spatial scales (local, regional, national). The HNVF map was validated and it was found a good agreement with the results of literature works, although the analysis approaches were different. Our future research will be oriented towards the study of a wide range of social, economic, biodiversity and ecosystem services indicators, because to advance HNV farmland management change needs to be seen as an opportunity rather than as a constraint.

Acknowledgements This research was carried out in the framework of the project ‘Smart Basilicata’ (2012–2018) which was approved by the Italian Ministry of Education, University and Research (Notice MIUR n.84/Ric 2012, PON 2007-2013 of 2 March 2012) and was funded with the Cohesion Fund 2007–2013 of the Basilicata Regional authority.

Appendix A

Table 1 Indicators for the calculation of HNVF with the statistical approach

Index	Sub-Index	Calculation Procedure
Cultural Diversity (CD)	-	$CD = 10 + (1 - (CI/UAA * 10)) + (1 - (C2/UAA * 10))$ <i>CI is the crop area > 10% of the UAA In addition to temporary and permanent forage areas</i> $1 \leq CD \leq 10$
Extensive practices (EP)	2.1. Extensive Managed Crops (EMC) (Weight = 2) 2.2. Soil Moisture Index (SMI) (Weight = 2) 2.3. Extensive Breeding (EB) (Weight = 2) 2.4. Extensive Managed Pastures (EMP) (Weight = 2) 2.5. Nitrogen Surplus (Ns) (Weight = 2)	$EMC = (Extensive\ crops + Fallow)(ha)/UAA(ha)$ $SMI = \text{derived from Surface Temperature and NDVI (MODIS images)}$ $EB = 1 - \Sigma(\text{Number of livestock units} * LSU Grazing)/UAA(ha)$ $EMP = \text{Permanent Grassland}(ha)/UAA(ha)$ $Ns = \Sigma(Nfc - Nrc * Rc) * Ac(i);$ $c = \text{crop}$ $Nf = \text{Suggested fertilization}$ $Nr = \text{nutrient content per unit of biomass of the crop}$ $R = \text{Yield of the crop}$ $Ac(ha) = \text{area occupied by crop } c \text{ in cluster } i$ <i>(The value of each indicator is between 0 and 1)</i>
Presence of natural elements (Ne)	3.1 Hedges and stone wall Length (LSM) (Weight = 2) 3.2 Canals and Streams Length (LC) (Weight = 2) 3.3 Lagoons, wetlands, and ponds (SPLS) (Weight = 2) 3.4 Numbers of Lakes (N) (Weight = 2) 3.5 Number of isolated Trees (Nt) (Weight = 2)	$LSM = \text{Hedges and dry-stone wall Length}(mt)/UAA(ha)$ <i>(if $0 < LSM < 50\ mt/ha$) $LSM = LSM/50$</i> <i>(if $LSM > 50\ Mt/ha$) $LSM = 1$</i> $LC = \text{Canals and Streams Length}(mt)/UAA(ha)$ <i>(if $0 < LC < 0.1\ mt/ha$) $LC = LC/0.1$</i> <i>(if $LC > 0.1\ mt/ha$) $LC = 1$</i> $SPLS = \text{Lagoons, wetland and ponds surface}(ha)/UAA(ha)$ <i>(if $0 < SPLS < 0.001\ mt/ha$) $SPLS = SPLS/0.001$</i> <i>(if $SPLS > 0.001\ mt/ha$) $SPLS = 1$</i> $L = \text{Number of lakes}/UAA(ha)$ <i>(if $0 < L < 0.003\ mt/ha$) $L = L/0.003$</i> <i>(if $SPLS > 0.003\ mt/ha$) $L = 1$</i> $Nt = \text{Number of isolated trees}/UAA(ha)$ <i>(if $Nt > 1$) $Nt = 1$</i> <i>(The value of each indicator is between 0 and 1)</i>

References

1. Andersen, E., et al.: Developing a high nature value farming area indicator. Report for the European Environment Agency, European Environment Agency, Copenhagen (2003)
2. Baldock, D., Beaufoy, G., Bennett, G., Clark, J.: Nature Conservation a New Directions in the Common Agricultural Policy. IEEP, London (1993)
3. Beaufoy, G., Baldock, D., Clark, J.: The Nature of Farming: Low Intensity Farming Systems in Nine European Countries. Institute for European Environmental Policy, London (1994)
4. Beaufoy, G., Cooper, T.: Guidance Document to the Member States on the Application of the HNV Impact Indicator. BE: European Evaluation Network for Rural Development (EENRD), Brussels (2008)
5. Bignal, E.M., McCracken, D.I.: Low-Intensity farming systems in the conservation of the countryside. *J. Appl. Ecol.* **33**(3), 413–424 (1996). <https://doi.org/10.2307/2404973>
6. Bozzo, F., Fucilli, V., Petrontino, A., Girone, S.: Identification of high nature value farmland: a methodological proposal. *Italian Rev. Agric. Econ.* **74**(3), 29–41 (2019). <https://doi.org/10.13128/rea-11210>
7. Campedelli, T., Calvi, G., Rossi, P., Trisorio, A., Florenzano, G.T.: The role of biodiversity data in High Nature Value Farmland areas identification process: a case study in Mediterranean agrosystems. *J. Nat. Conserv.* **2018**(46), 66–78 (2018). <https://doi.org/10.1016/j.jnc.2018.09.002>
8. Clark, S.: Organic farming and climate change: the need for innovation. *Sustainability* **12**, 7012 (2020)
9. De Lucia, S.: Approccio all'identificazione delle Aree ad Alto Valore Naturale. ISPRA (2003)
10. European Evaluation Network for Rural Development. Guidance Document to the Member States on the Application of the HNV Impact Indicator (2008)
11. European Commission. Farming for Natura 2000. Guidance on how to support Natura 2000 farming systems to achieve conservation objectives, based on Member States good practice experiences. EU, Luxembourg (2008). <https://ec.europa.eu/environment/nature/natura2000/management/docs/ES.pdf>
12. European Commission. A Farm to Fork Strategy for a Fair, Healthy and Environmentally-friendly Food System (2008). COM (2020) 381 final
13. ISPRA. Aree Agricole ad alto valore naturale: dall'individuazione alla gestione. Manuali e linee guida: 62/2010 (2010)
14. Lazzerini, G., Dibari, C., Merante, P., Pacini, G.C., Moschini, V., Migliorini, P., Vazzana, C.: Identification and mapping the high nature value farmland by the comparison of a combined and species approaches in Tuscany Italy. *Italian J. Agron.* **10**(3), 132–143 (2015). <https://doi.org/10.4081/ija.2015.676>
15. Madureira, L., Santos, J.L., Ferreira, A., Guimaraes H.: Feasibility study on the valuation of public goods and externalities in EU agriculture. JRC scientific and policy reports. Publications Office of the European Union, Luxembourg (2013)
16. Martino, S., Muenzel, D.: The economic value of high nature value farming and the importance of the Common Agricultural Policy in sustaining income: The case study of the Natura 2000 Zarandul de Est (Romania). *J. Rural Stud.* **60**, 176–187 (2018). <https://doi.org/10.1016/j.jrurstud.2018.04.002>.
17. Moderate Resolution Imaging Spectroradiometer (MODIS) <https://modis.gsfc.nasa.gov/data/>
18. Morelli, F., Jerzak, L., Tryjanowski, P.: Birds as useful indicators of high nature value (HNV) farmland in Central Italy. *Ecol. Ind.* **38**(2014), 236–242 (2014)
19. Paracchini, M.L., Terres, J.M., Petersen, J.E., Hoogeveen, Y.: Background document on the methodology for mapping High Nature Value farmland in EU27, EU JRC (2006)
20. Paracchini, M.L., Petersen, J., Hoogeveen, Y., Bamps, C., Burfield, I., Van Swaay, C.: High nature value Farmland in Europe - an estimate of the distribution patterns on the basis of land cover and biodiversity data. EUR 23480 EN – Joint Research Centre – Institute for Environment and Sustainability Office for Official Publications of the European Communities, Luxembourg (2008)

21. Plieninger, T., Torralba, M., Hartel, T., Fagerholm, N.: Perceived ecosystem services synergies, trade-offs, and bundles in European high nature value farming landscapes. *Landsc. Ecol.* **2019**(34), 1565–1581 (2019)
22. Pointereau, P.M. L. Paracchini, J.-M. Terres, F. Jiguet, Y. Bas, Biala, K.: Identification of high nature value farmland in France through statistical information and farm practice surveys. Office for Official Publications of the European Communities. EUR 22786 EN, Luxembourg (2007)
23. Pointereau, P., Doxa, A., Coulon, F., Jiguet, F., Paracchini, M.L.: Analysis of spatial and temporal variations of High Nature Value farmland and links with changes in bird populations: a study on France. Office for Official Publications of the European Communities. EUR 24299 EN, Luxembourg (2010)
24. QGIS. <https://qgis.org/en/site/forusers/download.html>
25. Schneider, M.K., Lüscher, G., Jeanneret, P., Arndorfer, M., Ammari, Y., Bailey, D., et al.: Gains to species diversity in organically farmed fields are not propagated at the farm level. *Nat. Commun.* **5**, 1–9 (2014)
26. Schmitz, M.F., Arnaiz-Schmitz, C., Sarmiento-Mateos, P.: High nature value farming systems and protected areas: conservation opportunities or land abandonment? A study case in the Madrid Region (2021)
27. Tarjuelo, R., Concepción, E.D., Guerrero, I., Carricondo, A., Cortés, Y., Díaz, M.: Agri-environment scheme prescriptions and landscape features affect taxonomic and functional diversity of farmland birds. *Agric. Ecosyst. Environ.* **315** (2021), 107444 (2021). <https://doi.org/10.1016/j.agee.2021.107444>
28. Trisorio, A., De Natale F., Pignatti, G.: Le aree agricole ad alto valore naturale in Italia: una stima a livello regionale. *Agrirregionieuropa* **33**. www.agrirregionieuropa.it

Design of a System for the Mechanization of Subsoil Compost Tea Distribution



Ester Foppa Pedretti, Alessio Ilari, Riccardo Scuppa,
Carmine De Francesco, and Daniele Duca

Abstract Compost tea is an aqueous mixture of organic and inorganic compounds generated by compost. Although several authors have highlighted how these extracts have a positive effect on the control of pathogens and as a promoter of plant growth, the biological mechanism underlying the effects found is still unclear. Similarly, there is no mechanised agricultural system or machine designed for distribution. The application of compost tea is currently carried out on soil or leaves, generally on small surfaces. Interest in these extracts is growing from both researchers and farmers. Regarding soil distribution, this should be subsurface to avoid stress to the compost tea microbiota, while for foliar distribution, this occurs through sprayers. The pressure and the formation of organic films represent the two critical factors in distribution. The study aims to design the mechanics of a machine for soil processing using mathematical models. The designed machine is a 5-shank ripper with a tow hitch with a hydraulic tilt piston, the main frame, and a rear trolley (500/50 R17 wheels) built in C40 steel. The anchors have been sized on forces of 30kN applied to the edge of the tips and lateral face. The processing elements are arranged in two rows (48 cm apart). The anchors have a thickness of 35 mm. In aisi440 stainless steel, the distribution system includes two 300 l tanks coupled to a 6-element membrane pump and 5 distribution tubes (40 mm). The distribution system has been designed to house various monitoring sensors.

Keywords Compost tea · Ripper · Localized distribution · Mechanical model

1 Introduction

Compost tea is the natural evolution of the practical application of the soil food web concepts developed by Dr Elaine Ingham. In her studies [1], Dr Ingham highlighted

E. Foppa Pedretti · A. Ilari (✉) · R. Scuppa · C. De Francesco · D. Duca
Dipartimento di Scienze Agrarie, Alimentari ed Ambientali, Università Politecnica delle Marche,
Via Breccie Bianche 10, 60131 Ancona, Italy
e-mail: a.ilari@univpm.it

how the analysis and management of microbial and non-soil flora and fauna together with conservative and organic agriculture is the key to emulating natural systems even in disturbed soil conditions [1] (as for agricultural soils) and thus favour control of nutrients cycle temporary stored in plants tissues [2, 3]. This control would guarantee a constant and modulated flow of nutrients and, therefore, greater resilience to the crop. Other authors highlighted that whole micro-biodiversity has a key role in determining and maintaining the ecosystem functions of the soil [4, 5]. More generally, the effects of the soil microbiota are an increase in Organic Matter content, decrease in pH, increase in salinity, and decrease in CaCO_3 , decrease in soil bulk density, increase in NPK absorption capacity [6]. Compost tea is an aqueous mixture of organic and inorganic compounds generated by compost itself and subsequently fermented with possible air blowing [7]. The production of tea compost follows two distinct procedures that generate different products (Fig. 1). The discontinuous system (defined in batches) considers anaerobic treatment conditions on basically consistent volumes for long infusion times (even up to 1 week). The aerated system exploits an aerobic environment for the treatment, which could also be carried out continuously. Generally, this system produces lower volumes than the previous one (due to the need to aerate the system) but has a reduced infusion time (maximum 1 day).

Being rich in minerals in solution, organic substances and microorganisms, Compost tea is considered a soil improver with good fertilising capacities [8, 9]. The chemical-physical characteristics of compost tea can be very variable in relation to the production conditions and intended use. However, generally, they have a neutral-alkaline pH (7–8); a high ammonium concentration (400–600 ppm) on a nitrogen concentration of around 1%; high levels of humification and bacterial and fungal counts in some cases more than double that of the starting compost [10]. The

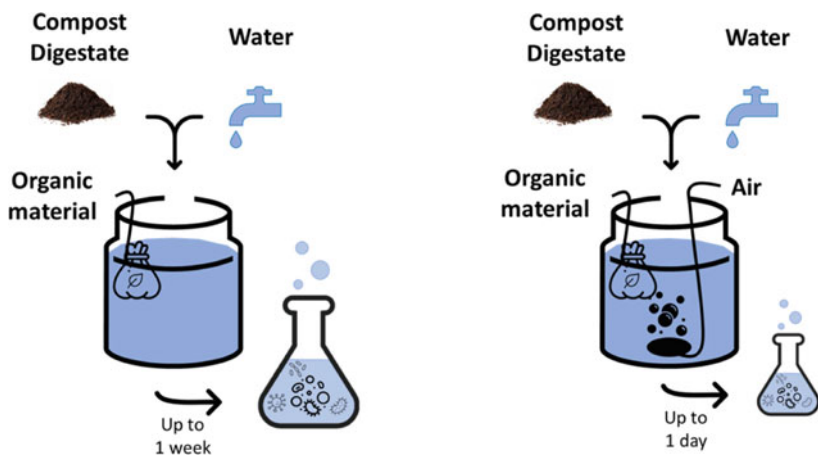


Fig. 1 Compost-tea production options, on the left, the anaerobic system and on the right, the aerated system

same microorganisms actively free soil fertility and counter plant pathogenic organisms [11]. Regarding the above functions concerning the desired effect, compost tea can be applied to the soil or directly on the crop. For each of these two application typologies, the respect of certain parameters is needed. Indeed, it is necessary to preserve the microbial flora and simultaneously overcome the problems related to the tendency of compost tea to create films that can occlude distribution systems (nozzles and small holes). In most of the studies in the literature, the application is carried out with manual systems and on relatively small portions of plant or soil such as not to cause a problem for the distribution itself [7, 12]. Currently, there are no known designed ad hoc and dedicated systems for distributing these extracts. The only recordable exception is an individual initiative on a small scale and with an empirical approach (refer to the case of Tree Yo educational program, a permaculture and conservation agriculture training company). The objective of this study is to design a ripper for the distribution of compost tea in the different layers of the soil at the same time as the primary tillage and to size the working elements according to a physical and mathematical approach based on the angle of soil failure plane, soil friction cutting coefficient, soil overburden cutting coefficient, soil cohesion cutting coefficient, soil adhesion cutting coefficient and soil resistance force. This design is necessary considering the sensitivity of the compost tea to different distribution parameters (e.g., distribution pressure) for which existing machines are not suitable.

2 Materials and Methods

The sizing of the ripper elements intended for compost tea distribution starts from a specific assumption. The compost tea application is considered useful both in the superficial layers (rhizosphere) and deeper, where the flora of the compost tea should favour the deconstruction of hard or not very fertile layers (limestone horizons or processing soles). Useful sizing parameters are shown in Table 1.

Tine working dept (d) was selected as 0.6 m for two main reasons: the first concerns the possibility of working at greater depths compared to normal ploughing to eliminate any hardpan layer or hard horizons such as calcareous ones; the second concerns the possibility of offering wide flexibility on the distribution depth of the compost tea (through the lengthening or shortening of the inlet pipes). Tine width

Table 1 Parameters used for ripper sizing. Data are typical of hard soils and have been chosen to apply the greatest possible and plausible effort to the machine

Parameter	Symbol	Value	Unit
Tine working dept	d	0.4–0.6	metre
Tine width	w	0.035 – 0.065	metre
Tool rake angle	α	45	degree
Soil failure plane angle	β	47.14 - 47.2	degree
External soil friction angle	δ	29	degree

(w) is mainly influenced by the standard dimensions of the steel profiles and by the maximum tensile stress they can withstand without deforming or breaking (this last aspect is also linked to the depth of the profile of which the tine and the anchors are made). Tool rake angle (α) represents the insertion angle of the working element with respect to the vertical plane, in this case, a relatively high angle has been chosen, which allows a greater disintegration of the clods and a rise of the ground along the tine. The soil failure angle has been calculated using the formulae reported below (Eq. 1).

$$\beta = \cot^{-1} \left\{ \frac{\alpha + \delta + \varphi + \frac{w}{d} \sqrt{\left(\frac{d}{w} \cot \alpha\right)^2 + 1 - \cot \alpha}}{2} \right\} \quad (1)$$

In this formula, d and w must be considered as operational depth and width, specifically, w can be considered as constant (equal to 0.035 m), and d can vary between 0 and 0.6 m (in this case, 0.4 m to 0.6 m). The internal friction angle (sometimes shear angle) is a characteristic of soils. It is a function of friction, cohesion and the shape of the granules that form the soil. The external friction angle instead defines the friction interactions between the soil particles and external elements (e.g. ripper working elements). The values used are specific for clay soil and vary between 20° and 55° (wet and dry clay soil, respectively). To define the soil resistance force starting from the defined parameters, it is necessary to determine different dimensionless parameters, such as the soil friction cutting coefficient (N_γ), defined below (Eq. 2).

$$N_\gamma = \frac{\left\{ 0.5(\cot \alpha + \cot \beta) \left(1 + \frac{2d}{3w} \sqrt{\cot^2 \alpha + 2\cot \alpha \cot \beta} \sin(\beta + \varphi) \right) \right\}}{\sin(\alpha + \beta + \delta + \varphi)} \quad (2)$$

soil overburden cutting coefficient (N_q) defined as follows (Eq. 3)

$$N_q = \frac{(\cot \alpha + \cot \beta) \left(1 + \frac{d}{w} \sqrt{\cot^2 \alpha + 2\cot \alpha \cot \beta} \right) \sin(\beta + \varphi)}{\sin(\alpha + \beta + \delta + \varphi)} \quad (3)$$

soil cohesion cutting coefficient (N_c) defined as follows (Eq. 4)

$$N_c = \frac{\cos \varphi \left(1 + \frac{d}{w} \sqrt{\cot^2 \alpha + 2\cot \alpha \cot \beta} \right)}{\sin(\alpha + \beta + \delta + \varphi)} \quad (4)$$

soil adhesion cutting coefficient ($N_{c\alpha}$) defined as follows (Eq. 5)

$$N_{c\alpha} = \frac{-\cos(\alpha + \beta + \varphi)}{\sin \alpha \sin(\alpha + \beta + \delta + \varphi)} \quad (5)$$

Soil resistance force F_s (kN) defined as the force applied on the working element under the soil tillage conditions outlined above can be calculated using the following formula (Eq. 6)

$$F_s = (p_d g d^2 N_y + C d N_c + C_\alpha d N_{c_\alpha}) w \quad (6)$$

where;

p_d is the soil bulk density (g/cm^3); g is the gravity acceleration (m/s^2); C is the soil cohesion (kPa); C_α is the soil adhesion (kPa). For this formula the information used are: $p_d = 1.02 \text{ g/cm}^3$; $C = 10 \text{ kPa}$; $C_\alpha = 1.47 \text{ kPa}$. To define the tractor power required P (kW) Eq. 7 can be applied using operating speed (S) values between 4 and 8 km/h.

$$P = \frac{F_s * S}{3.67} \quad (7)$$

3 Results and Discussions

3.1 Sizing

This section shows the results of force sizing that will affect the ripper working elements and will be used as a limit value for the applied loads on which any breakage will occur. The results relative to β , N_y , N_q , N_c and N_{c_α} are shown in Table 2.

In Table 3 are reported the values calculated for F_s , P and P_t (this last is relative to the total power necessary for a total of 5 tines).

From what is reported in Table 3, the stress related to the breaking of the soil that is discharged on the tine varies between 7.6 kN and about 19.8 kN (65 and 152% average increase) in relation to the working depth, these efforts were used to size the anchors and to test their strength at specific points. The variation in the width of the tine is much less evident (an increase of less than 5%). To indicate the power that a coupled tractor should express to use the designed machine by applying a vehicle forward speed of 4 km/h, the power required is between 41 and 107 kW, equivalent to a specific power absorption that varies between 8.3 and 21.6 kW for each single tine. Although the greater stresses are useful for sizing the machine, the stress values at lower depths are useful for evaluating the possible effects of breakage on the pipes for distributing the compost tea.

Table 2 Results of applying Eqs. 1–5 based on the data reported in Table 1

	B (°)			Ny (°)			Nq (°)			Nc (°)			Nca (°)		
	0.4	0.5	0.6	0.4	0.5	0.6	0.4	0.5	0.6	0.4	0.5	0.6	0.4	0.5	0.6
d/w	47.17	47.19	47.20	29.59	36.46	43.33	86.64	107.24	127.85	38.16	47.25	56.34	1.76	1.76	1.76
0.035	47.15	47.18	47.20	26.16	32.17	38.18	76.33	94.37	112.40	33.61	41.57	49.52	1.76	1.76	1.76
0.04	47.13	47.17	47.19	23.48	28.83	34.17	68.32	84.35	100.38	30.07	37.15	44.22	1.76	1.76	1.76
0.045	47.11	47.15	47.18	21.34	26.16	30.96	61.90	76.33	90.76	27.23	33.61	39.98	1.75	1.76	1.76
0.05	47.09	47.14	47.17	19.59	23.97	28.34	56.65	69.77	82.89	24.91	30.71	36.50	1.75	1.76	1.76
0.055	47.06	47.12	47.15	18.14	22.15	26.16	52.28	64.31	76.33	22.98	28.30	33.61	1.75	1.75	1.76
0.06	47.17	47.19	47.20	29.59	36.46	43.33	86.64	107.24	127.85	38.16	47.25	56.34	1.76	1.76	1.76

Table 3 Results of applying Eqs. 6 and 7 and total power required

	Fs (kN)			P (kW)			Pt (kW)		
	0.4	0.5	0.6	0.4	0.5	0.6	0.4	0.5	0.6
d/w	7.57	12.54	19.11	8.25	13.66	20.83	41.26	68.32	104.16
0.035	7.63	12.62	19.23	8.32	13.76	20.95	41.61	68.79	104.77
0.04	7.70	12.71	19.34	8.39	13.85	21.08	41.95	69.26	105.38
0.045	7.76	12.79	19.45	8.46	13.95	21.20	42.28	69.73	105.99
0.05	7.82	12.88	19.56	8.52	14.04	21.32	42.62	70.19	106.60
0.055	7.88	12.96	19.67	8.59	14.13	21.44	42.95	70.65	107.20
0.06	7.94	13.05	19.78	8.66	14.22	21.56	43.28	71.11	107.80

3.2 Design Drawing

The machine for distributing and burying liquid bio-stimulants was designed using as a model a subsoiler with a working width of 230 cm and a maximum overall dimension of 250 cm (Fig. 2).

The frame is modular and comprises fully bolted tubular structures in C40 steel. This contrivance allows to carry out fewer welds in the assembly and construction phase. Furthermore, since the various components are separate, it is possible to carry

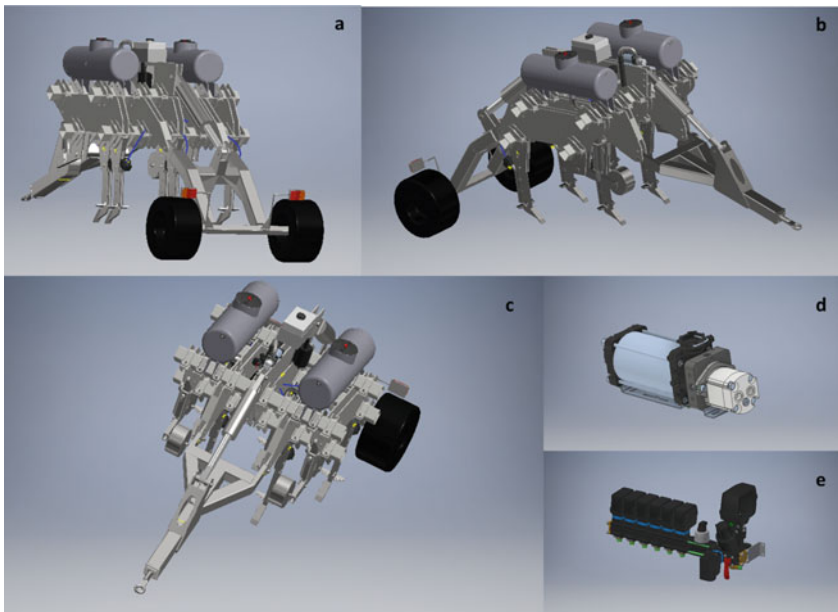


Fig. 2 Non-quoted project of the machine and details. Rear left view (a), right anterior view (b), top view (c), pump (d), valve group (e)

out any post-processing heat treatments more easily. The machine was also designed with a three-point hitch on which the pivot and the rear trolley were assembled, making this machine a trailed implement. In this way, the machine's weight does not weigh on the tractor, and it will be possible to have a flexible tool for any farm based on farmers' different needs. The various components and the anchors are fixed to the frame with a system of corner clamps to limit the stresses on the fixing bolts, thus limiting their breakage. The machine has been designed with 5 straight anchors to decompact the soil and obtains an environment suitable for the survival of the compost tea microorganisms. The anchors and tines have been designed in Hardox 440 steel with dimensions of 800×200 mm with a thickness of 35 mm. In the terminal part of the anchors, there is a 100 mm long share screwed onto the main body (Fig. 3). The anchors have a double curvature at 90° and 45° . This is because the deeper part having a lower angle of 45° , will have a lower resistance to horizontal advancement and, therefore, will give the possibility to use a greater number of working parts with the same absorbed power. The most superficial part of the anchors has an angle of attack of 90° to prevent the soil from rising to the surface and avoid the formation of surface clods. A bolt mechanical safety system (easily replaceable) has been installed on each anchor, which breaks when an obstacle occurs (maximum effort 19.8 kN), thus safeguarding the structure of the machine. The frame has also been designed to house a NO-STOP hydropneumatics safety system consisting of a nitrogen accumulator with regulating valve and a series of cylinders, each mounted on each anchor, allowing the anchors to absorb shocks and stresses with a gradual return avoiding damage to the frame structure. Side wings were then applied to the anchors also to perform horizontal soil working, and the installation of stainless steel pipes for the distribution of the bio-stimulant was arranged behind the anchor.

For the distribution of the bio-stimulant, two easily washable AISI 440C stainless steel tanks were installed to prevent problems related to the formation of biofilm. The tanks are 300 L each, placed above and at the edge of the machine. To distribute the product, a low-pressure multistage pump was chosen (ARAG mp), to avoid excessive stress on the biotic flora that would occur with high pressures. A 5-section

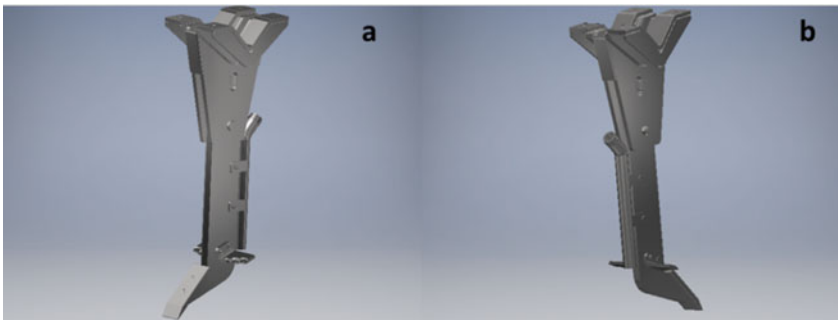


Fig. 3 Detail of the working element (a) with the tube for the distribution of compost tea housed in the rear part (b)

valve group has also been included, in the designed prototype, with the addition of a proportional valve for varying the distribution flow rate, these connected to an ISOBUS system and a satellite guidance system with prescription maps will allow for variable rate distribution. A magnetic flow meter has been placed between the valve group and the pipes on the anchors to control the flow rate and any occlusions. For correct distribution at certain depths, it was decided to install pressure switches on the hydraulic circuit of the cylinders of the depth wheels, which, through a control unit, can act on the rudder and the trolley cylinders always to keep the tool at the working depth. Given the various problems that could occur in compost tea, a nephelometer, “TurbSense” by PI (Process Instruments (UK) Ltd.), was installed at the outlet of each tank, with which during the experimental and testing of the agricultural tool, it will be possible to monitor the behaviour of the suspended solids and possibly record the effects that could cause the different turbidity of the liquid to be distributed.

Regarding the control of biofilm formation, sensors such as PI’s “Biosense” were envisaged. This last is to monitor the formation of biofilm and where the formation of biofilm could damage the various components. The “Biosense” sensors will be installed upstream of the pump, the valve group, the flow meter and inside the tanks. These sensors will interact with the tank valve to clean the system when necessary. No filter has been included considering that the compost tea is filtered at the end of the production phase and never too much to avoid retaining microorganisms. The machine has been designed for variable rate distribution not only to allow the application of precision farming principles but also because the distribution of the compost tea is variable in space (in relation to the specific needs of each area of the field) and in time (doses vary from the first year of application in the same areas) and objectives (reduction of working soles, increase in soil properties, fertilisation, etc.). For this reason, defining a specific dose is impossible, considering that there is no precise indication of this in the literature.

In summary, the pros and cons of the designed system are compared below. Among the positives is that the project itself is seemingly unavailable yet; the system is then able to distribute the tea compost not only in the superficial but also deep layers; the applied models are intuitive and quick to apply, making the sizing part not excessively time-consuming. Negative factors certainly include the cost of manufacturing the machine, estimated at €45,000 (pump, valves and sensors €5,000; isobus system with trimble satellite €6,000; stainless steel tanks €1,000; plastic tank €200; pressure switches for depth wheels €300; Chassis, anchors, trolley, rudder, lift pistons, depth wheel pistons, depth wheels, labour €32,500) and the cost of use of approximately €78/ha (average agricultural diesel price €1.45/l, 54 l/ha consumption for ripping). Concerning the mathematical models used in sizing, these must be validated practically, possibly evaluating the actual efforts under different conditions of use in specific experimental tests.

4 Conclusions

The project was proposed in view of the growth in fertiliser prices linked to the increase in energy and raw material costs. The use of compost tea could be a valid alternative for replacing synthetic nitrogenous substances. Using compost tea would also favour the creation of microbial flora and fauna of the soil capable of supporting its biological functions, reducing the need for fertilisers and processing interventions. The inclusion of sensors and systems for variable distribution is justified by the high variability of the quantities distributed in space and time. Compost tea is a living product whose administration depends on pre-existing objectives and conditions (e.g., doses for conversion of production systems vs maintenance doses) Given the slow action of microorganisms, the designed machine may not have frequent use in a company, but given its flexibility, it can also be used for other purposes. Although the models used in this study are based on peer-reviewed documents, their actual validity should also be tested in the field after realising the prototype designed in this study.

References

1. Rygiewicz, P.T., Monleon, V.J., Ingham, E.R., Martin, K.J., Johnson, M.G.: Soil life in reconstructed ecosystems: Initial soil food web responses after rebuilding a forest soil profile for a climate change experiment. *Appl. Soil Ecol.* **45**, 26–38 (2010). <https://doi.org/10.1016/j.apsoil.2010.01.006>
2. Ingam, E.: Dr Elaine's Soil Foodweb School. <https://www.soilfoodweb.com/>. Accessed 5 July 2022
3. Feng, J., He, K., Zhang, Q., Han, M., Zhu, B.: Changes in plant inputs alter soil carbon and microbial communities in forest ecosystems. *Glob. Chang. Biol.* **28**, 3426–3440 (2022). <https://doi.org/10.1111/gcb.16107>
4. Gibbons, S.M., Caporaso, J.G., Pirrung, M., Field, D., Knight, R., Gilbert, J.A.: Evidence for a persistent microbial seed bank throughout the global ocean. *Proc. Natl. Acad. Sci. U. S. A.* **110**, 4651–4655 (2013). <https://doi.org/10.1073/pnas.1217767110>
5. Lynch, M.D.J., Neufeld, J.D.: Ecology and exploration of the rare biosphere. *Nat. Rev. Microbiol.* **13**, 217–229 (2015). <https://doi.org/10.1038/nrmicro3400>
6. El-Shaieny, A.H.A.H., Farrag, H.M., Bakr, A.A.A., Abdelrasheed, K.G.: Combined use of compost, compost tea, and vermicompost tea improves soil properties, and growth, yield, and quality of (*Allium cepa* L.). *Not. Bot. Horti Agrobot. Cluj-Napoca* **50** (2022). <https://doi.org/10.15835/nbha50112565>
7. González-Hernández, A.I., Pérez-Sánchez, R., Plaza, J., Morales-Corts, M.R.: Compost tea as a sustainable alternative to promote plant growth and resistance against *Rhizoctonia solani* in potato plants. *Sci. Hortic. (Amsterdam)* **300** (2022). <https://doi.org/10.1016/j.scienta.2022.111090>
8. De Corato, U.: Agricultural waste recycling in horticultural intensive farming systems by on-farm composting and compost-based tea application improves soil quality and plant health: a review under the perspective of a circular economy. *Sci. Total Environ.* **738**, 139840 (2020). <https://doi.org/10.1016/j.scitotenv.2020.139840>
9. Zaccardelli, M., Sorrentino, R., Caputo, M., Scotti, R., De Falco, E., Pane, C.: Stepwise-selected *Bacillus amyloliquefaciens* and *B. Subtilis* strains from composted aromatic plant waste able to control soil-borne diseases. *Agric.* **10** (2021). <https://doi.org/10.3390/agriculture10020030>

10. Nour, M., Sarhan, E., Wadi, M.: Suppressive effect of compost /pomegranate peel tea combination against *Fusarium oxysporum* f. sp. lupini, and *Rhizoctonia solani* as an alternative synthetic fungicide. *Egypt. J. Exp. Biol.* **1** (2020), <https://doi.org/10.5455/egyjebb.20191208124236>
11. Ilangumaran, G., Smith, D.L.: Plant growth promoting rhizobacteria in amelioration of salinity stress: a systems biology perspective. *Front. Plant Sci.* **8**, 1–14 (2017). <https://doi.org/10.3389/fpls.2017.01768>
12. Pant, A.P., Radovich, T.J.K., Hue, N.V., Paull, R.E.: Biochemical properties of compost tea associated with compost quality and effects on pak choi growth. *Sci. Hortic. (Amsterdam)* **148**, 138–146 (2012). <https://doi.org/10.1016/j.scienta.2012.09.019>

Environmental Impact of Real Gaseous Pollutants Emission of Agricultural Tractors



L. E. Galli , D. Facchinetti , M. Gibin, and D. Pessina 

Abstract The gaseous pollutants produced by the internal combustion engines fitted on vehicles powered with fossil fuels are considered one of the main sources causing the global warming and consequently the climate change. In this scenario, the agricultural self-propelled machinery, in particular tractors, are believed to have a significant role, due to the generalized fitting of diesel engines. Trying to improve the situation, from 1996 for non road vehicles (therefore also for self-propelled agricultural machinery) some Standards were issued, based on steps referred to the time, defining progressively stringent emission limits, from Stage I to Stage V (in Europe), roughly correspondent to Tier 1 to Tier 5 in USA. The compliance of an engine to a given step is referred to dedicated homologation tests, on the basis of a series of defined running conditions.

At present, no subsequent tests are provided to check the conformity of the engine along its service life. Consequently, there is no assurance that the engine is respecting the emission limits provided by its homologation step, especially in case it is heavily used and/or is not submitted to a diligent periodical maintenance.

To ascertain the real pollutants gaseous emission of used tractors, a model equipped with an engine compliant to the Stage IIIA level was tested, using PEMS (Portable Emission Measurement System), measuring NO_x, CO, HC and PM emissions, in comparison with the limits established by its homologation stage.

Keywords Agricultural tractors · Environment · Gaseous pollutants · PEMS

1 Foreword

The main pollutants found in gaseous emission of internal combustion engines powered with fossil fuels are carbon monoxide (CO), unburned hydrocarbon (HC),

L. E. Galli · D. Facchinetti · M. Gibin · D. Pessina (✉)

Department of Agricultural and Environmental Sciences, Università Degli Studi di Milano,

Via Celoria 2, 20133 Milan, Italy

e-mail: domenico.pessina@unimi.it

nitrogen monoxide and dioxide (NO and NO₂, combined in NO_x) and particulate matter (PM). In this scenario, the agricultural self-propelled machinery, in particular tractors, are believed to have a significant role, due to the generalized fitting of diesel engines, producing important amounts especially of NO_x and PM.

The studies on these pollutants, regarding the so-called off-road machines (thus including also the agricultural machinery) have been carried out from the beginning of the '90 of the last century, both in Europe in 1990 [1] and in the USA [2].

Therefore, both the EU Commission and US Environmental Protection Agency (EPA), issued standards to regulate the exhaust emission coming from off-road vehicles [3, 4], based on steps referred to the time, defining progressively stringent emission limits. More in detail, the European legislation refers to emission Stages (from I to V for tractors) while in the US legislation they correspond to Tier (from 1 to 5). Then, the manufacturers of the engines were compelled to respect the restrictions, applying several both known and new technologies. The most popular of them were the Exhaust Gas Recirculation (EGR), the Selective Catalytic Reduction (SCR), the Diesel Oxidation Catalyst (DOC) and the Diesel Particulate Filtration (DPF) [5], at a first time fitted alone and later also in combination.

More in detail, the diesel combustion is usually producing a remarkable amount of nitrogen monoxide and dioxide (NO_x) and particulate matter (PM), while the pollution of carbon monoxide (CO) and unburned hydrocarbon (HC) is normally less significant. On the contrary, the gasoline combustion is generating more CO and HC in respect to NO_x and PM. As a consequence, due to the generalized adoption of diesel engines on non-road machinery, the various device used in this case were devoted especially to reduce the emission of NO_x (the EGR and SCR) and/or the PM (the DPF and partially the DOC). More recently the dramatic restrictions imposed lead to the adoption of a combination of these devices, finalized to the maximum reduction of all the pollutants.

Starting approx from the new millennium, the studies and researches in this topic, focused on agricultural self-propelled machinery emissions, increased remarkably, so confirming a keen interest on the scientific point of view. The pollutant ascertainment was approached in different ways, measuring the gaseous emissions in some well-defined engine conditions, sometime in accordance to the running cycles stated by the dedicated standards (e.g., torque at rated speed, max torque, etc.) [6–12], but also quantifying the pollution in real field working conditions [13–18].

The European Directive 97/68/EC (and the following amendments) established the limits, in terms of their amount in mass referred to the energy produced (g/kWh), for gaseous pollutants emission produced by engines of rated power in the range 37–560 kW, divided in some classes (Fig. 1). The engine has to be tested in accordance to a steady-state cycle consisting of 8 different modes, referring to its rated speed and torque loads (Table 1). The gaseous emissions are measured in each individual mode, and properly weighted according given factors based on usage time, to calculate a comprehensive value for each pollutant and then compared to the prescribed limits provided for the relevant homologation Stage (Table 2).

No subsequent tests are provided to check the conformity of the engine along its service life. Consequently, there is no assurance that the engine is respecting the

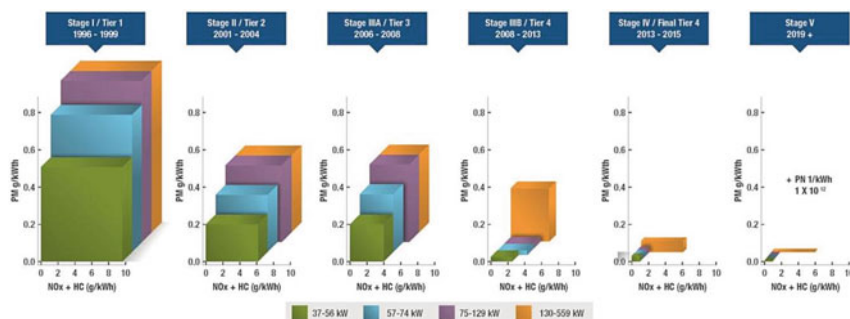


Fig. 1 Limits of emissions of gaseous pollutants established by the European Directive 97/68/EC (and following amendments) for non-road machinery, regarding PM (Particulate Matter) and NOx (nitrogen mono and dioxide)

Table 1 Load and weighting factors for evaluating the pollutants gaseous emission of engines fitted on non-road machines, according to ISO 8178-4 standard (C1 cycle) [19]

Mode no	1	2	3	4	5	6	7	8
	Torque at rated speed				Max torque			Low idle
	100%	75%	50%	10%	100%	75%	50%	0%
Weighting factor	0.15	0.15	0.15	0.10	0.10	0.10	0.10	0.15

Table 2 Pollutants limits (in g/kWh) and timetable for their coming in force established for the most recent emission EU Stages, for engines fitted on non-road machinery

Power [kW]	2006	2007	2008	2009	2010	2011	2012	2013	2014	2015	2016	2017	2018	2019	2020	2021	2022
0 < P < 8																Stage V CO 0.80 / HC+NOx 7.80 / PM 0.47 / PM ₁₀	
8 ≤ P < 19																Stage V CO 0.80 / HC+NOx 7.80 / PM 0.43 / PM ₁₀	
19 ≤ P < 37			Stage III A CO 5.3 / HC+NOx 7.7 / PM 0.8												Stage V CO 0.80 / HC+NOx 4.70 / PM 0.35 / PM ₁₀ (BANK)		
37 ≤ P < 56			Stage III A CO 5.3 / HC+NOx 4.7 / PM 0.8					Stage III B CO 5.0 / HC+NOx 4.7 / PM 0.35							Stage V CO 0.80 / HC+NOx 4.70 / PM 0.35 / PM ₁₀ (BANK)		
56 ≤ P < 75			Stage III A CO 5.3 / HC+NOx 4.7 / PM 0.8				Stage III B CO 5.0 / HC 0.18 / NOx 3.3 / PM 0.35		Stage IV (01.10.2013) CO 5.0 / HC 0.18 / NOx 3.4 / PM 0.35						Stage V CO 0.80 / HC 0.18 / NOx 3.40 / PM 0.35 / PM ₁₀ (BANK)		
75 ≤ P < 130			Stage III A CO 5.3 / HC+NOx 4.8 / PM 0.8				Stage III B CO 5.0 / HC 0.18 / NOx 3.3 / PM 0.35		Stage IV (01.10.2014) CO 5.0 / HC 0.18 / NOx 3.4 / PM 0.35						Stage V CO 0.80 / HC 0.18 / NOx 3.40 / PM 0.35 / PM ₁₀ (BANK)		

emission limits provided by its homologation stage, especially in case it is heavily used and/or is not submitted to a diligent periodical maintenance.

This paper shows the pollutants gaseous emission of the engine fitted on a used tractor, by using a dedicated instrumentation chain (PEMS, Portable Emissions Measuring System) [20], to verify if, and in case to what extent, the limits of gaseous pollutants established for the homologation emission stage of the engine are exceeding the reference values.

2 Materials and Method

2.1 *The PEMS*

PEMS measure emissions from combustion engines as the vehicle or the equipment is being used, which allows real-world in-use testing, offering an innovative counterpart to check the impact of emissions from combustion engines upon the environment. The PEMS provide a complete and very accurate real-time monitoring of the main pollutants emitted by the engines (HC, CO, CO₂, NO_x [or NO + NO₂], PM, etc.).

For the tests of this survey, the following instrumentation chain was used:

1. a portable flue gas analyser for professional flue gas analysis, Testo 350 (Testo SE & Co KGaA, Titisee Neustadt - Germany), consisting in a control unit, for displaying readings, and a measuring box, controlled via Bluetooth. Among several tasks, the analyser is specifically designed also for the emission control and inspection of compliance with emission guidelines. To make possible the comparison with the limits established by the correspondent EU Directive, for the purposes of the present survey the parameters analyzed were the concentration (in terms of mg/m³) of NO, NO₂, NO_x, HC and CO. Also the exhaust gases temperature was monitored, at the level of the testing probe, just to obtain information about the engine running conditions;
2. a portable hand-held smoke tester, Testo 338 (Testo SE & Co KGaA, Titisee Neustadt - Germany), for measuring the degree of blackening in the diesel engines in terms of soot concentration (mg/m³). The smoke tester working principle is based on a LED white light reflectance on to a blackening mark, consisting in a filter paper on which the soot is deposited in a given time;
3. a flow meter, Trotec TA 400 (Trotec GmbH, Heinsberg - Germany), to measure the volumetric flow in gases duct (of known shape and dimensions), in terms of m³/h.

2.2 *The Tested Tractor and Other Device Used*

The agricultural tractor tested was a 4WD, medium powered model, Deutz-Fahr Agrofarm 430, equipped with the Deutz-Fahr engine TCD2012 L04 of nominal 80 kW (109 CV), complying the EU Stage IIIA level for the pollutants gaseous emission. Although manufactured in 2011, the tested tractor has been working for approx. 1400 h only.

To reproduce properly the running steady-state cycle established by the EU emission Directive, the tractor was coupled through its standard 540 rpm PTO to the electromagnetic dynamometer Eggers-dynamometer PT 301 MES (KL-Maschinenbau GmbH Rendsburg - Germany). Starting from the power recorded at the PTO, the effective engine power was calculated taking into account the mechanical transmission efficiency, previously ascertained.



Fig. 2 Experimental arrangement of the tested tractor. Left: general view; top right: the gas probe; bottom right: the flow meter

The gases coming from the tractor exhaust were conveyed into a duct, where the probes of the measuring instruments were conveniently placed (Fig. 2).

3 Results and Discussion

To define the 8 running points provided for the measurement of the gaseous emissions, the engine torque and power curves at full delivery have been previously obtained (Fig. 3).

To compare the amount of any pollutant produced by the tractor with the limit established by the correspondent homologation EU Stage, the data coming from the instrumentation were managed in accordance the following formula:

$$P_a = \frac{(P_c \times Q)}{P}$$

where:

- Pa = pollutant amount (g/kWh)
- Pc = pollutant concentration (g/m³)
- Q = gas flow (m³/h)
- P = engine power (kW)

In Table 3 the results for each pollutant and for all the running conditions are shown, while in Table 4 the overall results are compared with the limits established by the corresponding homologation emissive Stage.

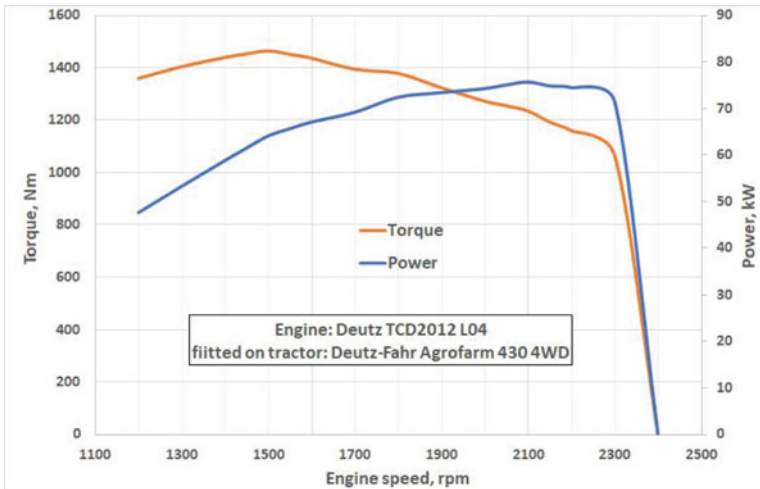


Fig. 3 Torque and power curves at full delivery of the engine fitted on the tested tractor

Table 3 Concentration values of the pollutants measured for all the running conditions considered (g/m³)

Mode no	1	2	3	4	5	6	7	8
	Torque at rated speed				Max torque			Low idle
	100%	75%	50%	10%	100%	75%	50%	~ 0%
NOx	8.75	9.04	11.62	34.12	8.08	8.96	10.53	35.40
CO	1.44	1.92	2.76	20.70	1.14	1.68	2.14	8.46
HC	6.62	9.36	14.10	23.20	3.94	8.16	11.78	29.45
PM	0.13	0.14	0.19	0.35	0.09	0.14	0.16	0.05
Temp.(°C)	413	372	315	244	416	397	350	157

Table 4 Overall amount for each pollutants compared to the homologation emission Stage (III A) limits for the engine fitted on the tested tractor

Pollutant	Limit (Stage III A)	Measured
	(g/kWh)	
NOx + HC	4.00	29.53
CO	5.00	4.15
PM	0.30	0.15

To reduce the gaseous pollutant emission, the engine of the tested tractor (compliant to Stage III A) was equipped only with external cooled Exhaust Gas Recirculation (EGR), managed electronically. In general, the trend of the pollutants amount is strictly related to the power produced by the engine, as well as the smoke temperature. More in detail, they increases when the power (but also the

torque) decrease. As expected, when a low power is produced by the engine, all the pollutants highlighted a dramatic increase, due to a poor fuel combustion. Because the overall values are coming from the weighted average of those measured in the different running conditions, the low power running (10% of the torque recorded at the max power speed) as well as the low idle conditions affected remarkably the final outcome.

In particular, the CO and PM overall values were inside the provided limits, while the combination NO_x + HC showed a value exceeding more than 7 times the limit. With reference to the tested tractor, this represents a quite important outcome of the research, also taking into account that the tested engine worked for only 1400 h, a much shorter time than that considered as the normal lifecycle of a modern diesel engine fitted on agricultural machinery, established generally in 4–5000 h before submitting it to a general maintenance service. Moreover, the heavy overcome of the NO_x (and HC) limits, recorded in this case with the only application of the EGR, lead in recent years to the addition of the Selective Catalytic Reduction (SCR) to meet the subsequent more stringent homologation stages. SCR is in fact a post-treatment solution, to reduce in particular the NO_x production, applied without any modification of the combustion efficiency, that shows its maximum according with high working temperature.

4 Conclusions

While CO and PM were found below the limits, the tests carried out highlighted a dramatic overshoot of the NO_x + HC limit for the investigated engine. This outcome confirms the need to check along the entire tractor service life the pollutants produced. In this view, a certain increase of measured amounts could be admitted, taking into account the natural worsening of the engine running conditions (made even more burdensome in case of neglected maintenance).

The periodical inspection of agricultural tractors, including the gaseous pollutants check is not yet in force in Italy. On the other hand, the regulatory proposal in preparation are providing only the check of the PM, but its extension to other pollutants, and primarily the NO_x, would contribute to an effective reduction of the environmental impact.

References

1. Samaras, Z., Zierock, K.H.: Off-road vehicles: a comparison of emissions with those from road transport. *Sci. Total Environ.* **169**, 249–255 (1995). [https://doi.org/10.1016/0048-9697\(95\)98123-Z](https://doi.org/10.1016/0048-9697(95)98123-Z)
2. Kean, A., Sawyer, R., Harley, R.: A fuel-based assessment of off-road diesel engine emissions. *Air Waste Manag. Assoc.* **50**, 1929–1939 (2000). <https://doi.org/10.1080/10473289.2000.10464233>

3. Pouliot, G., Pierce, T., Denier van der Gon, H., Schaap, M., Moran, M., Nopmongcol, U.: Comparing emission inventories and model-ready emission datasets between Europe and North America for the AQMEII project. *Atmos. Environ.* **53**, 4–14 (2011). <https://doi.org/10.1016/j.atmosenv.2011.12.041>
4. Lovarelli, D., Bacenetti, J.: Exhaust gases emissions from agricultural tractors: State of the art and future perspectives for machinery operators. *Biosyst. Eng.* **186**, 204–213 (2019). <https://doi.org/10.1016/j.biosystemseng.2019.07.011>
5. Cavallo, E., Pampuro, N., Facello, A.: Consumption of diesel exhaust fluid (DEF) of agricultural tractor engines using selective catalytic reduction (SCR) system. In: 69th International Conference on Agricultural Engineering: Solutions for Intelligent and Sustainable Farming. Hannover, Germany, vol. 2124, pp. 259–264 (2011)
6. Bacenetti, J., Lovarelli, D., Facchinetti, D., Pessina, D.: An environmental comparison of techniques to reduce pollutants emissions related to agricultural tractors. *Biosyst. Eng.* **171**, 30–40 (2018). <https://doi.org/10.1016/j.biosystemseng.2018.04.014>
7. Janulevicius, A., Juostas, A., Pupinis, G.: Engine performance during tractor operational period. *Energy Conv. Manag.* **68**, 11–19 (2013). <https://doi.org/10.1016/j.enconman.2013.01.001>
8. Lindgren, M., Larsson, G., Hansson, P.-A.: Evaluation of factors influencing emissions from tractors and construction equipment during realistic work operations using diesel fuel and bio-fuels as substitute. *Biosyst. Eng.* **107**, 123–130 (2010). <https://doi.org/10.1016/j.biosystemeng.2010.07.010>
9. Janulevicius, A., Juostas, A., Cipliene, A.: Nitrogen-oxide emissions from diesel-engine farm tractors during real-life cycles and their correlation with the not-to-exceed operating zones. *Biosyst. Eng.* **161**, 93–105 (2017). <https://doi.org/10.1016/j.biosystemseng.2017.06.022>
10. Ai, Y., et al.: Quantifying air pollutant emission from agricultural machinery using surveys—a case study in Anhui, China. *Atmosphere* **12**, 440 (2021). <https://doi.org/10.3390/atmos12040440>
11. Li, R., et al.: A comprehensive inventory of agricultural atmospheric particulate matters (PM10 and PM2.5) and gaseous pollutants (VOCs, SO₂, NH₃, CO, NO_x and HC) emissions in China. *Ecol. Indicat.* **107**, 105609 (2019). ISSN:1470-160X. <https://doi.org/10.1016/j.ecolind.2019.105609>
12. Shao, Z.: An emissions inventory for agricultural tractors and construction equipment in India. International Council on Clean Transportation (2016). pp. 1–15. https://theicct.org/wp-content/uploads/2021/06/India-Non-road-Emissions-Inventory-Working-Paper_vF.pdf
13. Juostas, A., Janulevičius, A.: Tractor's engine efficiency and exhaust emissions' research in drilling work. *J. Environ. Eng. Landsc. Manag.* **22**(2), 141–150 (2014). <https://doi.org/10.3846/16486897.2013.852556>
14. Janulevicius, A., Juostas, A., Cipliene, A.: Nitrogen-oxide emissions from diesel-engine farm tractors during real-life cycles and their correlation with the not-to-exceed operating zones. *Biosyst. Eng.* **161**, 93–105 (2017). <https://doi.org/10.1016/j.jclepro.2018.07.078>
15. Ge, Y., Liu, H., Ding, Y., Yin, H., Fu, M., Li, J.: Experimental study on characteristics of emissions and fuel consumption for combines. *Trans. Chin. Soc. Agric. Eng.* **29**(19), 41–47 (2013)
16. Mingliang, F., Yan, D., Zhe, J., Yunshan, G., Bin, L.: Characteristics of agricultural tractors emissions under real-world operating cycle. *Nongye Gongcheng Xuebao/Trans. Chin. Soc. Agric. Eng.* **29**(6), 42–48 (2013)
17. Hou, X., Tian, J., Song, C., Wang, J., Zhao J., Zhang, X.: Emission inventory research of typical agricultural machinery in Beijing, China. *Atmos. Environ.* **216**, 116903 (2019). ISSN:1352-2310. <https://doi.org/10.1016/j.atmosenv.2019.116903>
18. Lovarelli, D., Fiala, M., Larsson, G.: Fuel consumption and exhaust emissions during on-field tractor activity: a possible improving strategy for the environmental load of agricultural mechanisation. *Comput. Electr. Agric.* **151**, 238–248 (2018). <https://doi.org/10.1016/j.compag.2018.06.018>
19. ISO 8178-4:2020. Reciprocating internal combustion engines — Exhaust emission measurement — Part 4: Steady-state and transient test cycles for different engine applications

20. EU Science hub. Portable Emission Measurements Systems (PEMS).https://joint-research-centre.ec.europa.eu/scientific-tools-and-databases/portable-emissions-measurement-systems-pems_en

A Method for Energy Efficiency Rating of Low-Power Tractors Based also on Intensity of Use



L. E. Galli , D. Facchinetti , and D. Pessina

Abstract The efficiency of the so-called “low-power” tractors is affected not only by the evolution of their engine and transmission design, but also by the usage modes adopted. Especially in specialized crops, such as vineyards and orchards, many tasks do not require high engine power and/or traction pull, being the power of the tractor used by the hydraulic system. A customizable method to analyze and evaluate the real efficiency of narrow tractors (N-TRE) have been developed in 2019, taking into account some tractor models working in different scenarios. These scenarios have been characterized in given working activity and usage intensity, along the growing season. The working conditions and the power requirement of the main operations carried out in viticulture were simulated in a stationary mode by means of an electromagnetic dynamometer, integrated with devices for measuring the fuel consumption. The basic output has been a series of engine performance curves (power, torque and Specific Fuel Consumption, SFC), both at full and partial loads. On these curves, some characteristic working points were identified, simulating the typical tractor running conditions in vineyard. The aim of this study is to validate the N-TRE model by testing its robustness with a given number of tractors, to build a suitable database. The database will be finalized to classify the machines in some efficiency classes, identified with letters from A to G, similarly to what happens for example in several electric and electronic household appliances. Furthermore, the classes A to G were associated to a colour tag, adopting the traffic light criterion (green/yellow/red). These codes could immediately and easily show the tractor global efficiency in different working scenarios, to offer at a glance to farmers a comprehensive machine evaluation.

Keywords Narrow tractors · Vineyard · Efficiency · Specific fuel consumption

L. E. Galli (✉) · D. Facchinetti · D. Pessina

Department of Agricultural and Environmental Sciences, Università Degli Studi di Milano, Via Celoria 2, 20133 Milan, Italy

e-mail: lavinia.galli@unimi.it

1 Foreword

The maximum efficiency of agricultural tractor use is obtained primarily with its best coupling with the implements. Moreover, the most correct tractor setting, above all in terms of engine speed and fuel delivery, assures the best exploitation of energy potential of the diesel fuel. Along their entire lifecycle, most of the tractors are working at engine partial loads [1–6]. In these conditions, the tractor should be conveniently work at reduced engine speed, because at high speed the friction and heat losses are higher, and moreover due to the rise of the temperature, the cooling system engages more power to work properly, till to 10% of the max engine power [7].

The efficiency of an internal combustion engine is strictly linked with an inverse relationship to the Specific Fuel Consumption (SFC), i.e. the amount of the fuel (diesel, e.g. expressed in g) burned to produce a given energy (e.g. expressed in kWh). As a consequence, the SFC is usually measured in g/kWh.

For a given engine, the SFC will vary over the range of operating speeds and loads. To better understand its performance, manufacturers, dealers, and end users sometimes construct engine performance maps. More in detail, engine manufacturers generally supply some curves to ascertain the performance over the range of operating speeds, for some percentages of the maximum load (partial loads) [8].

On the other hand, the use of biofuels is offering more options to users at the progressive scarcity of oil based fuels. Among the various alternatives for diesel engines, e.g. the use of biodiesel and/or ethanol, besides reducing dependence on fossil fuel, would help to reduce emissions of some greenhouse gases [9–11], but change the performance of the diesel engine cycle, causing variations in the power and SFC. More in detail, the addition of ethanol in diesel fuel lead to a decrease of the power and the engine torque and an increase of fuel consumption, as a consequence of lower calorific value, cetane number, and delay in the injection point of ethanol. Several studies have been carried out in the last decades on the performance and efficiency of agricultural tractors. In this view, the most popular test procedures are the OECD Code 2 [12] and, more recently, the PowerMix settled out by DLG (Deutsche Landwirtschafts-Gesellschaft, Germany). PowerMix in particular is a procedure finalized to evaluate the performance of agricultural tractors normally used in open field, by measuring the engine power required at the PTO, at the drawbar and by the hydraulic system [13, 14]. These tests are basically carried out thanks to a dynamometer wagon travelling on tracks, trying to simulate the tractor real working conditions in the field. The data obtained, mainly in terms of Specific Fuel Consumption (SFC) values, allow an overall calculation of the performance and therefore the efficiency index of the tested machine. The tractor efficiency based on SFC values has been recently considered also by many other organizations/laboratories. Some country, as USA [15, 16], Spain [17], Turkey [18] and Korea [19], defined test protocols adopting SFC criteria to evaluate the tractors efficiency.

Anyway, although several protocols are available for the assessment of the energy efficiency of agricultural tractors, they do not usually classify the models into different

categories, based on the architecture (e.g. open field, utility, narrow-track, tracked, etc. tractors) and/or the power class. Moreover, these protocols do not generally take into account the real usage intensity of the tractors neither the most frequently operations carried out by them.

1.1 The Narrow-Track Tractors

Tractors used in orchards and vineyards (but also in the green maintenance sector) are usually included in the low-power category: for these models, the engine power ranges between 35 and 90 kW, being the major part of the models included in the interval 50–75 kW. Due to the typical tasks carried out, the drawbar power request is frequently very low, while the power needed at the PTO and for the hydraulic system is often remarkable.

These models are defined “narrow track” because their reduced overall width, suitable to travel smoothly into the crop rows. As a consequence, the tractor-implement mass distribution on the two axles is a quite important feature to be taken into account, because it is affecting the stability, and so the roll-over risk. In these cases, to reach a satisfactory stability condition, the use of an over-sized tractor (in terms of mass and so power) is practically due, even if the implement power demand is very frequently low or negligible. This is fatally affecting negatively the engine efficiency.

Also the time of operation is likewise influencing the overall machine efficiency: for example, in specialized cultivations the pruning (including also the topping) is usually executed twice in a year (before and in the middle of the growing season), while on the contrary pesticide treatments are much more frequently carried out, up to 15–20 times/year.

To consider properly all these parameters, an efficiency model, named N-TRE (Narrow Tractors Real Efficiency) specifically dedicated to the tractors used in orchards and vineyards was then created, taking into account their usage characteristics, both for power demand and the working time.

The aim of this paper is to apply the N-TRE model to two narrow-track tractors, considering two usage scenarios, different for number and frequency of the operations carried out. Moreover, the two tractor models examined were equipped with engines having a slight different max power and also compliant to different anti-pollution emission stages, to point out the overall efficiency and the expected benefits, mainly in terms of fuel saving.

2 Materials and Method

The main technical characteristics of the two tractors examined are shown in Table 1.

Table 1 Main technical characteristics of the two tractors investigated in the survey

Tractor	Type	Mass, kg	Wheel- base, mm	Engine					
				Cylinder, no.	Displace- ment, cm ³	Max power, kW (CV)	Rated speed, rpm	Emis- sive Stage	Devices for emission reduction
A	4WD, isodiametric	2275	1550	3	2227	60 (82)	2600	III B	EGR+DOC +DPF
B	4 WD, traditional	3420	2250	4	3769	71 (97)	2300	IV	SCR+DPF

The usage scenarios involved the operations carried out in two typical wineries located in Northern Italy: the first has a cultivated extension of 3.5 ha with slight slope terrain, while the UA of the second is 10 ha, completely flat. More in detail, the first scenario includes 6 tasks: only 15% of the total working time is referred to an operation performed in the inter-row, while 75% of them have been carried out on the canopy or in the row. The remaining 10% regards the grape transport. In the second scenario, 10 tasks have been considered: 20% of the time was engaged for operations in the inter-rows and the remaining 80% regards activity on the canopy or in the row. Obviously, these working times were defined taking into account the repetitions of a given operation along the entire growing season (Table 2).

Thanks to dedicated interviews of the users of the two tractors, the running conditions of the engines were ascertained, in terms of nominal engine speed at zero load (i.e. at the starting of each task) and subsequent speed reduction due to the increase of the load (i.e. the engine speed under load). For example, for the grass shredding, a nominal engine speed of 2000 rpm and a working speed under load of 1900 rpm were considered for tractor A in scenario 1. This protocol made easy the subsequent

Table 2 Operations and relative time of usage for the two scenarios taken into account

No.	Scenario 1	Time, % of the total	Scenario 2	Time, % of the total
1	grass shredding	15	pre-pruning	5
2	pruning shredding	10	pruning shredding	5
3	pneumatic spraying	50	grass shredding	10
4	chemical weeding	10	shoot pruning	5
5	topping	5	topping	5
6	grape transport	10	defoliation	5
7	--		spreading	10
8	--		chemical weeding	10
9	--		pneumatic spraying	35
10	--		mechanical harvesting	10

simulation of the work cycles, through the electromagnetic dynamometer connected to the tractor PTO. To make possible a suitable data elaboration, for the execution of each task a constant running speed of the engine was considered, so not taking into account the usual load variation caused by the correspondent resistance produced by the implement work.

To get information about the SFC values in the defined working conditions, a series of power curves at partial load of the engine were obtained (Fig. 1), connecting the PTO of the two tractors investigated to the wheeled electromagnetic dynamometer Eggers-Dynamometer PT 301 MES (KL-Maschinenbau GmbH Rendsburg - Germany), integrated with its dedicated fuel consumption meter (Fig. 2) and its dedicated software.

All the working conditions previously defined were then fixed on the correspondent power curve, ascertaining the relative value of SFC (in g/kWh), to obtain the so-called “Typical Running Points” (TRP). In Fig. 3 an example of this type of data elaboration is shown.

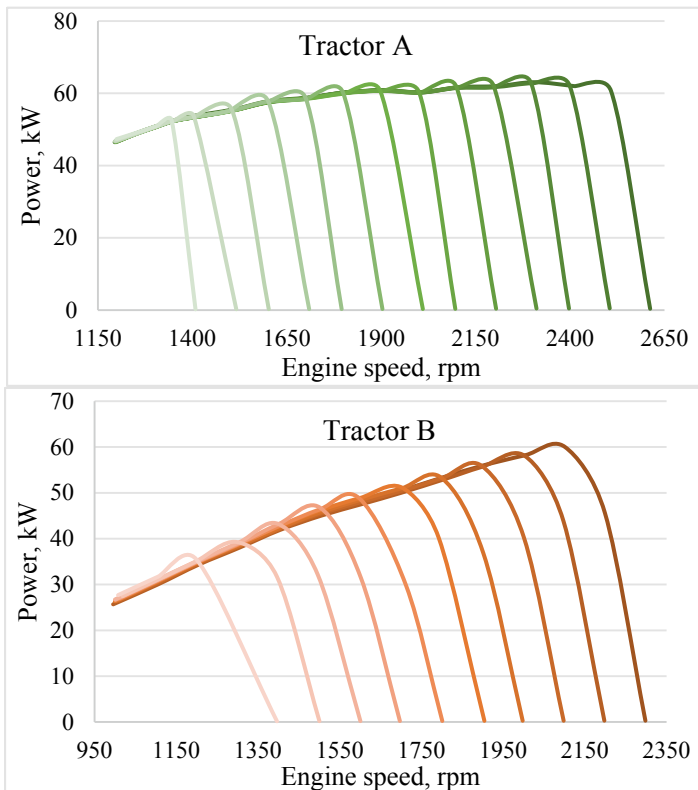


Fig. 1 Power curves at partial load of the investigated tractors A and B



Fig. 2 Left: the wheeled electromagnetic dynamometer Eggers-Dynamometer PT 301 MES (KL-Maschinenbau GmbH Rendsburg - Germany). Right: the control panel located on the device (top) and the screen of the control through the computer, via Bluetooth (bottom)

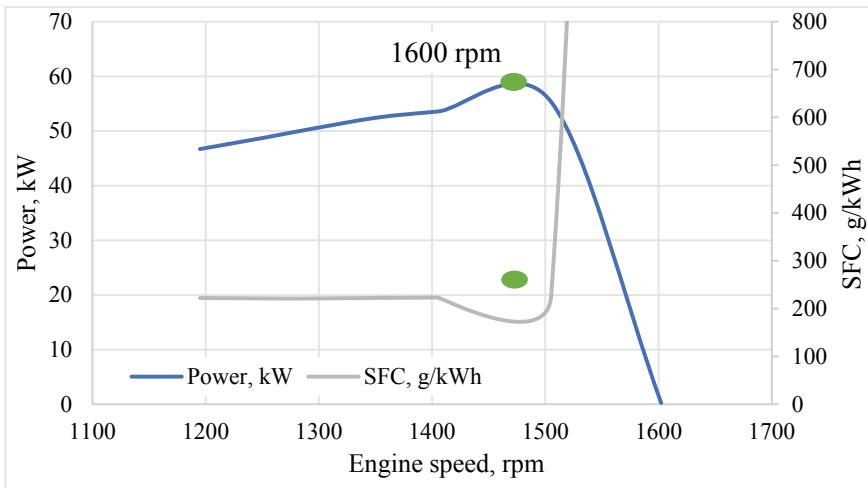


Fig. 3 An example of “Typical Running Points” (TRP), identifying a given working conditions previously defined

All the TRPs were then divided into some classes, as a function of the correspondent SFC value. Similarly to what established in other several production fields (e.g. buildings, household appliances, etc.) each SFC value, i.e. the energy efficiency, was classified into 7 classes, identified with letters, from A (the best) to G (the worst), matching to those a colour tag, adopting the “traffic light” criterion (green/yellow/red). All the data were managed with the MS Excel software, thanks to predefined sheets. The addition of the colour tag makes easy an immediate identification of the energy efficiency level. For this survey, the SFC classes have been established with reference to the values measured in the tests (Table 3).

Table 3 Classification of the measured SFC values into energy efficiency classes and colour tags

Tag	SFC, g/kWh	Colour tag
A	220-229	Green
B	230-239	
C	240-249	Yellow
D	250-259	
E	260-269	Red
F	270-279	
G	280-289	

Matching the time dedicated to the various tasks considered and the SFC values attributed to each TRP, some weighted average SFC were then calculated, for both tractors A and B in the two scenarios examined. Also in these cases the results were classified in classes and colour tags.

3 Results and Discussion

In Tables 4 and 5 each operation was classified, as well as the weighted average for the two tractors and the two scenarios.

For tractor A in the first scenario, the average SFC (250 g/kWh) was noticeably influenced by the SFC assigned to the pneumatic spraying (249 g/kWh), because this operation is very frequently executed along the growing season, and so weights for 50% of the total working time. At the opposite, tasks as chemical weeding and grape transport evidenced low SFC values (221 and 222 g/kWh respectively), but they were carried out for limited time. Always for tractor A, in the second scenario the SFC values were similar for all the operations, ranging from 222 to 229 g/kWh. Therefore, the average value is included in this range, not being affected by the different time dedicated to the various tasks.

Tractor B showed in general SFC values higher of approx. 8–9% than tractor A. In the first scenario, the SFC values for the various tasks are similar, ranging from 249 to 253 g/kWh. As a consequence, in this case the remarkable time for pneumatic spraying is not affecting the average SFC. In scenario 2, the grass shredding evidenced an SFC of 265 g/kWh, the highest measured. This is due to the high power request to the engine to carry out this heavy task. Nevertheless, this operation is executed only for 10% of the total time, not affecting significantly the average SFC. In this second scenario, the pneumatic spraying is weighting for 35% of the whole working time, and consequently the relevant SFC value is less influencing the average value.

Referring to the tags assigned to the single and the average SFC values, the most evident difference between the two tractors is the dominance of green (classes A and B) for tractor A and yellow (class D) for tractor B. More in detail, tractor B shows an increase in the average SFC of 5.5% in scenario 1, and 11.6% in scenario 2, with a

Table 4 SFC values and classification of each operation for tractor A and both scenarios

Tractor A					
	Nominal engine speed, rpm	Working engine speed, rpm	Power, kW	SFC, g/kWh	Time of usage, %
Scenario 1					
Grass shredding	2000	1900	60,5	245	15
Pruning shredding	2100	1900	60,7	245	10
Pneumatic spraying	2000	1800	57,4	240	50
Chemical weeding	1500	1300	50,8	221	10
Topping	1600	1500	55,3	226	5
Grape transport	1400	1300	51,0	222	10
Class/average				B	236.9
Scenario 2					
Pre-pruning	1400	1200	47,3	222	5
Pruning shredding	1800	1600	57,7	228	5
Grass shredding	1700	1600	57,7	229	10
Shoot pruning	1500	1400	53,6	224	5
Topping	1600	1500	55,3	226	5
Defoliation	1500	1400	53,6	224	5
Spreading	1400	1350	52,5	222	10
Chemical weeding	1400	1350	52,5	222	10
Pneumatic spraying	1800	1500	55,2	226	35
Mechanical harvesting	1700	1500	55,0	226	10
Class/average				A	225.2

resulting colour and class change. This is justified observing the partial load curves of the engine fitted on the two tractors (Fig. 1): tractor A showed a power curve more “constant” over the speed in respect of that of tractor B, very probably due to a different working setting, managed electronically. In this case, because the power remain high for a wide range of rotation speed, the SFC values remain likewise low in the same range.

4 Conclusions

Although based on the efficiency evaluation of only two tractors, the advanced N-TRE model highlighted promising features to build specific usage scenarios, on which evaluate the performance of different tractor models.

Moreover, similarly to other production sectors, the classes and colour tags assignment was confirmed as being an immediate and easy solution to recognize the efficiency of a given tractor.

Table 5 SFC values and classification of each operation for tractor B and both scenarios

Tractor B					
	Nominal engine speed, rpm	Working engine speed, rpm	Power, kW	SFC, g/kWh	Time of usage, %
Scenario 1					
Grass shredding	2000	1800	53	249	15
Pruning shredding	2100	1900	56	252	10
Pneumatic spraying	2000	1800	53	249	50
Chemical weeding	1500	1300	39	251	10
Topping	1600	1500	32	250	5
Grape transport	1400	1200	35	253	10
Class/average				D	250.0
Scenario 2					
Pre-pruning	1400	1200	35	253	5
Pruning shredding	1800	1600	49	246	5
Grass shredding	1700	1600	31	265	10
Shoot pruning	1500	1400	32	252	5
Topping	1600	1300	39	252	5
Defoliation	1500	1400	32	252	5
Spreading	1400	1100	32	256	10
Chemical weeding	1400	1200	35	253	10
Pneumatic spraying	1800	1500	46	247	35
Mechanical harvesting	1700	1500	47	247	10
Class/average				D	251.3

The model described could be easily adapted to other agricultural tractor segments (e.g. utility, open field, high power, etc.) by building appropriate scenarios, considering suitable tasks and time durations. The most important goal is in fact to offer a useful instrument for farmers' evaluation, to identify the most efficient tractor for their needs. A future step could be the building of a robust database of tractors and scenarios, to find the best machine for any working situation.

Finally, the model could find fruitful application in the public administration sector, to select the most efficient tractor models, in view of an assignment of dedicated financial supports for farmers purchasing.

References

1. Juostas, A., Janulevicius, A.: Evaluating working quality of tractors by their harmful impact on the environment. *J. Environ. Eng. Landsc. Manage.* **17**(2), 106–113 (2009). <https://doi.org/10.3846/1648-6897.2009.17.106-113>
2. Hansson, P.A., Noren O., Bohm M.: Effects of specific operational weighting factors on standardized measurements of tractor engine emissions. *J. Agric. Eng. Res.* **74**(4), 347–353 (1999). <https://doi.org/10.1006/jaer.1999.0471>

3. Janulevičius, A., Juostas, A., Pupinis, G.: Engine working modes during tractors operational period. *Mechanika* **3**(83), 58–63 (2010). <https://mechanika.ktu.lt/index.php/Mech/article/view/15537>
4. Zoz, F.M., Grisso, R.D.: Traction and tractor performance. ASAE Distinguished Lecture Series 27; ASAE Publication Number 913C0403. 48 p (2003). https://www.researchgate.net/publication/237106038_Traction_and_Tractor_Performance
5. De Farias, M.S., Schlosser, J.F., Linares, P., Bertollo, G.M., Martini, A.T.: Reduction of fuel consumption using driving strategy in agricultural tractor, *Rev. Bras. Eng. Agric. Ambient.* **23**(2) (2019). <https://doi.org/10.1590/1807-1929/agriambi.v23n2p144-149>
6. Galli, L.E., Facchinetti, D., Pessina, D.: N-TRE: a model for the evaluation of the narrow tractors real efficiency. In: Coppola, A., Di Renzo, G., Altieri, G., D'Antonio, P. (eds.) *Innovative Biosystems Engineering for Sustainable Agriculture, Forestry and Food Production. MID-TERM AIIA 2019, LNCE*, vol. 67, pp. 389–398. Springer, Cham (2020). https://doi.org/10.1007/978-3-030-39299-4_44
7. Janulevičius, A., Juostas A., Pupinis G.: Engine performance during tractor operational period, *Energy Conv. Manag.* **68**1, 1–19 (2013). ISSN:0196-8904, <https://doi.org/10.1016/j.enconman.2013.01.001>
8. Keller, J.K., Kranz, W.K., Hoy, R.M., Martin, D.L.: Applying data from the Nebraska Tractor Test Laboratory to Predict BareDiesel engine performance. *Appl. Eng. Agric.* **31**(1), 33–42 (2015), <https://doi.org/10.13031/aea.31.10283>
9. Rahimi, H., Ghobadian, B., Yusaf, T.; Najafi, G.; Khatamifar, M.: Diesterol: an environment-friendly IC engine fuel. *Renew. Energy* **34**(1), 335–342 (2009). <https://doi.org/10.1016/j.renene.2008.04.031>
10. Estrada, J.S., Schlosser, J.F., De Farias, M.S., Rodrigues, F.A., Martini, A. T.; Dos Santo, G.O.: Performance of an agricultural engine using blends of diesel and ethanol. *Rural Eng. Cienc. Rural* **46**(7) (2016). <https://doi.org/10.1590/0103-8478cr2015046>
11. Emaish, H., Abualnaja, K.M., Kandil, E.E., Abdelsalam, N.R.: Evaluation of the performance and gas emissions of a tractor diesel engine using blended fuel diesel and biodiesel to determine the best loading stages. *Sci. Rep.* **11**, 9811 (2021). <https://doi.org/10.1038/s41598-021-89287-0>
12. OECD. OECD Standard Code for the official Testing of Agricultural and Forestry Tractor Performance, Paris (2022). <https://www.oecd.org/agriculture/tractors/codes/02-oecd-tractor-codes-code-02.pdf>
13. DLG-PowerMix. DLG, Gross Umstadt, Germany (2022). <https://www.dlg.org/en/agriculture/tests/dlg-powermix>
14. Pieke, C., Stark, W., Pfister, F., Schyr, C.: DLG powermix on the dynamometer. *ATZoffhighway worldwide* **10**(2), 26–3 (2017). <https://doi.org/10.1007/s41321-017-0018-3>
15. Grisso, R.: Predicting tractor diesel fuel consumption. In: Virginia Cooperative Extension, pp. 442–073, 1–10 (2010). <https://vtechworks.lib.vt.edu/bitstream/handle/10919/98875/BSE-328.pdf?sequence=1>
16. Howard, C.N. Kocher, M.F., Hoy, R.M., Blankenship, E.E.: Testing fuel efficiency of tractors with both continuously variable and standard geared transmissions. In: ASABE Annual International Meeting, Louisville, Kentucky (2011). <https://digitalcommons.unl.edu/biosysengpre/s/56>
17. Ortiz-Cañavate, J., Gil-Sierra, J., Casanova-Kindelán, J., Gil-Quirós, V.: Classification of agricultural tractors according to the energy efficiencies of the engine and the transmission based on OECD tests, *Appl. Eng. Agric.* **25**(4), 475–480 (2009). <https://doi.org/10.13031/2013.27464>
18. Turker, U., Ergul, I., Cumhuri Eroglu, M.: Energy efficiency classification of agricultural tractors in Turkey based on OECD tests. *Energy Educ. Sci. Technol.* **28**(2), 917–924 (2012). <https://avesis.ankara.edu.tr/yayin/a3399ae2-779a-4622-a944-1bd1068e56a9/energy-efficiency-classification-of-agricultural-tractors-in-turkey-based-on-oecd-tests>.
19. Shin, C.S., Kim, K.U., Kim, K.W.: Energy efficiency classification of agricultural tractors in Korea *J. Biosyst. Eng.* **37**(4), 215–224 (2012), <https://doi.org/10.5307/JBE.2012.37.4.215>

Design, Setup and Virtual Test of a Three-Section Foldable Rear Rollbar for a Low-Power Tractor



D. Gattamelata , V. Laurendi, L. Vita , L. E. Galli , and D. Pessina 

Abstract In Italy, vineyards are cultivated mainly on slope terrain, using typically low-power, narrow-track tractors, showing a lower stability than the traditional models. This leads to a high probability of overturning, made often worse also for the coupling with heavy implements and/or wrong maneuvers. The most effective measure, recognized from decades worldwide, to protect the driver in case of overturning is to fit a roll-over protective structure combined with the diligent use of the safety belt. On the narrow-track tractors, a two-pillars front mounted tiltable rollbar is frequently fitted. Sometime, as an alternative, they are equipped also with two-pillars rear mounted partially folding rollbar. In any case, the tilting/folding function is normally used when travelling among the vineyard rows, to avoid damaging of the canopy and in particular the grapes, due the unexpected contacts with the rollbar, and to enter in sheds or garages with low height doors. In all the other working situations it should be in vertical (protection) position. The transition between the rest and the protection positions is normally carried out by hand, but this task is very often neglected, because generally considered tiring and time consuming. Therefore, the rollbar remains in rest position at any time, so assuring absolutely no protection in case of overturning. This occurrence was recorded as being the main reason of tens of fatal accidents of tractor overturning happened every year in Italy. The introduction of automatic or semi-automatic systems to manage the rollbar position could solve the problem.

For this purpose, a new 3-sections folding rear rollbar was dimensioned, designed and virtually tested on a tractor model of 3200 kg of reference mass. The movements of the rollbar are driven thank to a four-bar linkage solution, and are based on the management of the locking/unlocking system. Particular attention was devoted to

D. Gattamelata · V. Laurendi · L. Vita

INAIL - National Insurance Institute for Occupational Accidents -P.Le Pastore 6, 00144 Roma, Italy

L. E. Galli · D. Pessina (✉)

Department of Agricultural and Environmental Sciences, Università Degli Studi di Milano, Via Celoria 2, 20133 Milan, Italy

e-mail: domenico.pessina@unimi.it

the devices executing the various movements of the 3 rollbar sections, to assure the highest robustness in case of overturning and the best reliability over time.

Keywords Low-power tractors · vineyard · ROPS · 3-section foldable rollbar · Virtual and real tests

1 Foreword

The mechanization of agricultural crops carried out on sloping terrain creates often stability problems for the machinery used. In Italy, these situations occur frequently in vineyards, where low-power, narrow-track tractors are normally used, so making critical the overall stability, made furtherly worse also for the coupling with heavy implements and/or wrong maneuvers. A poor stability involves a high risk of overturning, causing for a long time and worldwide a remarkable number of accidents, resulted fatal or with very serious injuries suffered by the drivers.

In Italy, about 160 fatal accidents per year have occurred recently in agriculture, most of them for tractor overturning. More in detail, an independent survey carried out on the web in the period 2008–2019 revealed a total of 1414 fatal accidents, corresponding to an average of about 118 fatal events per year, with a minimum of 102 in 2017 and a maximum of 145 in 2011 [1].

The most effective measure, worldwide recognized from decades to protect the driver in case of overturning, is to fit a Roll-Over Protective Structure (ROPS) combined with the diligent use of a safety belt. Among the various ROPS types fitted on tractors, on narrow-track models a two-pillars front mounted tiltable rollbar is frequently fitted. Sometime, as an alternative, they are equipped also with a two-pillars rear mounted partially folding rollbar. Both are profitably used in low clearance situations, such as the travelling inside rows with low canopy without damaging branches and shoots and/or entering in garages having low height doors. But an improper use of the tilting/folding ROPS contributes to fatalities in overturning events: theoretically, only in the temporary described conditions the rollbar could not be in protection configuration.

Most fatal accidents involving tractors with tiltable/foldable ROPS have occurred because, at the moment of the overturn, the ROPS was at the lowered position, so assuring no protection [2]. This critical situation was detected in several countries: for example in Italy in 19.4% of the fatal overturning recorded in the period 2008–2019 the tractor involved were fitted with a tiltable front two-post roll-bar fixed in a horizontal position, so ensuring no protection [1]. This is substantially due to negligence or carelessness of the drivers, who do not consider properly the ROPS safety role, and/or to other actual difficulties in tilting/folding the protective structure, because of poor design or inconsistencies with human anthropometrics requiring awkward position or movements [3]. To solve this problem, along the last three decades some researchers worldwide were engaged to point out automatic or

semi-automatic systems to manage the rollbar position depending on the working conditions, such as slope, travelling speed, steering angle, etc.

1.1 Deployment Systems

Based initially in the '90 of the last century, the rollbar deployment systems were applied firstly in the automotive sector, in particular on some roadster models, by using an integrated rollbar normally located in retracted position between the rear seats and the soft-top recess, raised via a spring/damper mechanism and locked into position in case of imminent rollover [4]. After this application, the deployment systems were diffused also in other sectors, included that of agricultural tractors, on two-pillars ROPS, adopting different solutions, such as spring-type, chemically and hydraulically deploying systems.

The chemically deploying system was considered and tested from 2000 in USA by NIOSH (National Institute for Occupational Safety and Health), to activate the deployment system of a telescopic rollbar (named AutoROPS), consisting into two parts: the first is a retractable ROPS that is normally latched in its lowered position for day-to-day use. The second is a subsystem that monitors the inclination angle of the tractor. If a potential rollover condition is detected by the sensor, the retracted ROPS will deploy thanks to the intervention of a pyrotechnic squib and lock in the full upright position before ground contact [5]. The device is a spring-action, telescoping structure that releases on signal to pyrotechnic squibs that actuate release pins. Upper post motion begins when the release pins clear an internal piston. The structure extends until the piston impacts an elastomeric ring and latches at the top position. In lab tests, the two-post structure consistently deployed in less than 0.3 s and latched securely [6]. Of course, the motion features of this kind of ROPS must not affect its safety requirements. For this reason, the structure of AutoROPS was later tested according to the correspondent standards adopted worldwide, following the static procedure [7, 8].

The chemically deploying solution using pyrotechnic squib was also studied in Turkey, where was applied to an anchor mechanism to increase the driver's clearance zone on narrow-track wheeled agricultural tractors [9, 10]. In this case, the anchor mechanism is represented by two side bars extending horizontally at the top of the two-post front mounted rollbar. The deployment of the anchors and their latching by the pins is completed before the rollbar touches the ground. In laboratory tests, the two anchors consistently deployed in less than 0.160 s and latched securely. The system behaviour was determined by means of simulations and field upset tests. The tests were performed with a radio-controlled full-size tractor and video technology was used to validate the deployment time and overturning speeds. To determine the strength of the system, a static side-loading test and field test were performed to the anchor mechanism. In the field test, strain gauges were installed to determine the forces affecting the anchor mechanism. The tractor rolled over up to 119°, while the total time of overturning was 720 ms [11].

In more recent years, in Spain the pyrotechnic squib solution was resumed similarly to deploy the ROPS till to the protection position. This technique is similar to that used for airbag inflators, so assuring a proved excellent longterm reliability, because they are expected to perform properly over the lifetime of the vehicle in which they are installed. Under the safety structure point of view, the Spanish solution is able to increase at the same time the height and the upper overall width of the ROPS, in order to reduce the continuous rolling risk, and increasing the safety zone in the lateral direction [12]. The same research group developed later the project, arranging three automatically deployable ROPS (AD-ROPS) to find the best option for airbag inflators and deploying time, being also tested for ascertain their strength features according to OECD Code 6 [13].

Always in Spain, also the hydraulic solution was investigated. An automatically deployable ROPS (HydraROPS) was designed, manufactured and tested. The prototype established two assistance levels for the managing of the tilting ROPS. The first level is represented by the driver on board manual intervention to change the ROPS position; the second in represented by an automatic change towards the protection position in situations of impending rollover, while at the same time a mobile phone message with the GPS location of the machine is produced, to contact emergency personnel. The tractor hydraulic power was used to manage the protective structure. In order to increase the deployment speed of ROPS, a pressure accumulator was added to the hydraulic system, so reaching a deployment time of 0.743 s [14].

On the other hand, the mechanical systems assisted by electric devices were not yet deeply investigated in the described research field, probably due to the unavailability in the past of proper solutions. The recent development of many devices electrically driven, also favoured by the diffusion of suitable energy sources (e.g. Li-ion battery packs of suitable capacity) made feasible to design and manufacture new opportunities in managing tilttable and foldable ROPS.

This paper shows a new 3-sections two-post folding rear rollbar, to be fitted on narrow-track tractor models. The movements of the rollbar sections are driven mechanically, using a four-bar linkage solution, and are based on the release of the unlocking system, the lifting step (i.e. the activation of the actuator) and the locking step (engagement of the locking system) when the roll-bar is in its final protection position. For the transition from protection and rest positions the same steps are provided, of course in opposite order. To assure a suitable strength in case of overturning, the rollbar was conveniently sized. The prototype was subjected to a virtual strength test, using Abaqus software for structural and dynamic analysis following the requirements of the corresponding OECD Code.

2 Materials and Method

This study consisted of the following main steps:1) mechanism synthesis of the foldable rear mounted ROPS, (in the following named “QROPS”); 2) design of the

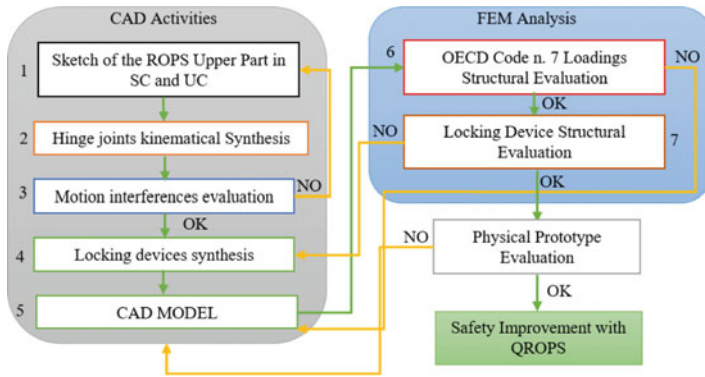


Fig. 1 Flow chart of the iterative virtual prototyping

locking devices; 3) virtual analysis of the whole system and actuators, to test their features and strength.

Such phases were involved in an iterative process hereinafter described. More in detail, the methodology adopted to design the 3-section foldable rear rollbar was based on a sequence of virtual prototyping activities, then connected to an iterative procedure. The two main design activities were based on CAD and FEM analysis softwares.

Figure 1 shows an overview of the design process. The CAD use is based on 5 steps, being the first two relevant to the kinematical. In particular, the use of combining the four-bars synthesis method of applied mechanics with the sketching features of SolidWorks allows the drawing and quick adaptation of the hinge joints position. Then, with the use of SolidWorks, the 2-D structure motion was simulated with reference to the vertical longitudinal median plane of the tractor, modifying accordingly the elements shape and hinge joint positions at an early stage of the design process. This solution allowed to save time and to test easily multiple solutions.

Inside the CAD activity two structural dimensioning checks are provided, involving the entire ROPS structure and the locking device. A negative outcome of at least one of the FEM analysis steps leads back to the modification of the entire CAD model and/or the locking device. Once the design iterative process is complete, the CAD model is transferred into manufacturing drawings to manufacture the physical prototype.

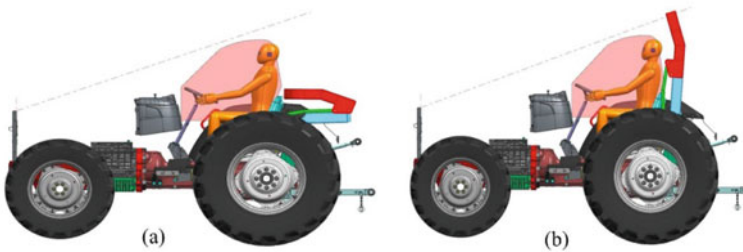


Fig. 2 QROPS configurations: rest (a) and protection (b)

3 Results and Discussion

3.1 Mechanism Synthesis of the QROPS

To arrange a completely deployable ROPS through just one mechanism for the lowering and raising steps, some hinge joints were introduced in a two-post rear mounted structure, to be managed thanks to a four-bar linkage having only one degree of freedom, controlled by a linear or circular actuator. Through a suitable CAD software (SolidWORKS - DassaultSystem), the parametric sketch blocks were used to draw the 2-D profile of the upper part of the ROPS and the hinge joints position. The mechanism ensures the motion between the Rest Configuration (RC), when the QROPS is completely folded down, and the Protection Configuration (PC), where it is raised up (Fig. 2). The application of 4-bar inverse synthesis method of applied mechanics science made possible to determine the best location of the hinge joints, to obtain a RC where the upper part of the QROPS is very closed to the top part of the tractor rear fenders. For safe operation, the QROPS has to not interfere with any part of the tractor, and of course nor with the driver, seated in his/her normal position. More in detail, the foldable parts of the QROPS shall not hit any tractor component along their entire trajectories, and of course nor enter the driver's safety zone.

In Fig. 3 a geometrical comparison between the original rollbar and the new 3-sections foldable rollbar is shown in the side view, considering the trajectory of the upper and most advanced QROPS point in comparison with the driver location.

3.2 Design of the Locking Device

To avoid a dangerous misuse of the QROPS, a proper locking device was settled up, to link automatically the sections. This need led to the adoption of a mechanical system, consisting of the use of a pawl of suitable dimensions locking the structure at the end of the extension movement towards the PC. The sections movement and the

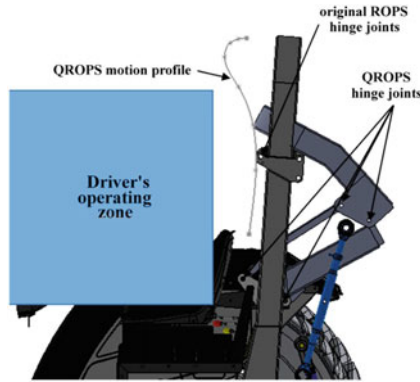


Fig. 3 Comparison between the original ROPS and the QROPS motion profile

consequent contacts were simulated via a numerical multibody analysis. In detail, the locking device assumes two configurations: compressed, when it is pulled back, and engaged, when it is extended. At the raising, the pawl is engaged, and it is pulled back by contact with the QROPS upper part. Viceversa, at the end of the movement, the pawl is pushed into the slot because of the spring action, so locking the entire structure (Fig. 4).

As well as all the other QROPS part, also the locking device shall withstand the OECD Code 7 loading requirements; its dimensioning has been included in the Virtual Analysis step.

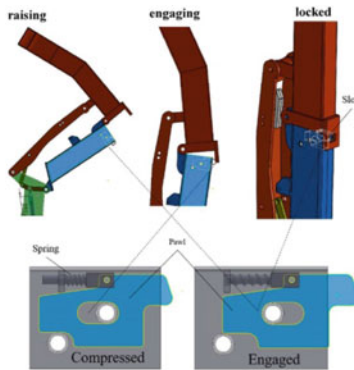


Fig. 4 Locking device operation and configurations

3.3 Virtual Analysis

The entire system, including both the mechanical joints and the locking device, was modeled virtually to test its features and strength. The dynamic analysis of the rigid bodies was useful to verify if the motion (lowering/raising) of the structure and its engagement through the automatic locking device were correct. On the other hand, the structural analysis allows the ascertainment of the correct dimensioning of the locking device and the kinematical joints, taking into account the requirements of OECD code 7 in terms of expected loads. More in detail, the entire structure including the locking device was modeled applying the Finite Elements Method (FEM) using the software Abaqus from Simulia (Fig. 5). With reference to a tractor having a reference mass of 3200 kg, in Table 1 the test sequence, the force and the energy values required are shown.

The results of the simulation are shown in Fig. 6, where the Von Mises stress contour plot and the clearance zone provided by OECD code 7 are shown. The study of the stress distribution and the overall deflections lead to a reinforcement of the

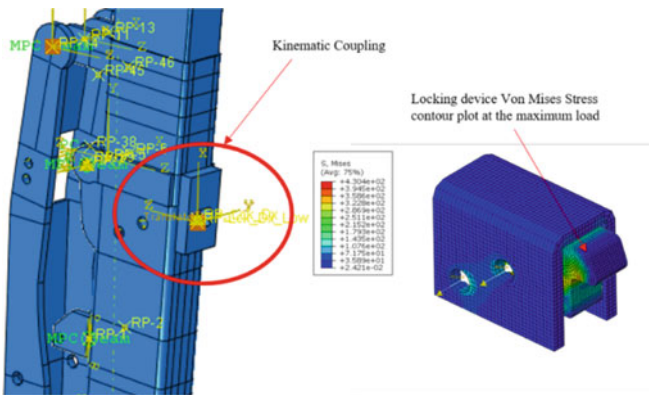


Fig. 5 Locking device simulation: kinematic coupling (left) and structural behaviour under load (right)

Table 1 FEM simulation of the energy absorption and force application with reference to the OECD Code 7 requirements, for the tractor taken into account

Test order	Loading	Energy		Force	
		required, kJ	absorbed, kJ	required, kN	Applied, kN
1	Longitudinal from the rear	2.1	2.6	- -	49.9
2	1 st vertical	- -	- -	64.0	64.7
3	Longitudinal from the front	2.1	2.6	- -	51.8
4	Lateral	5.6	5.8	- -	45.8
5	2 nd vertical	- -	- -	64.0	64.7

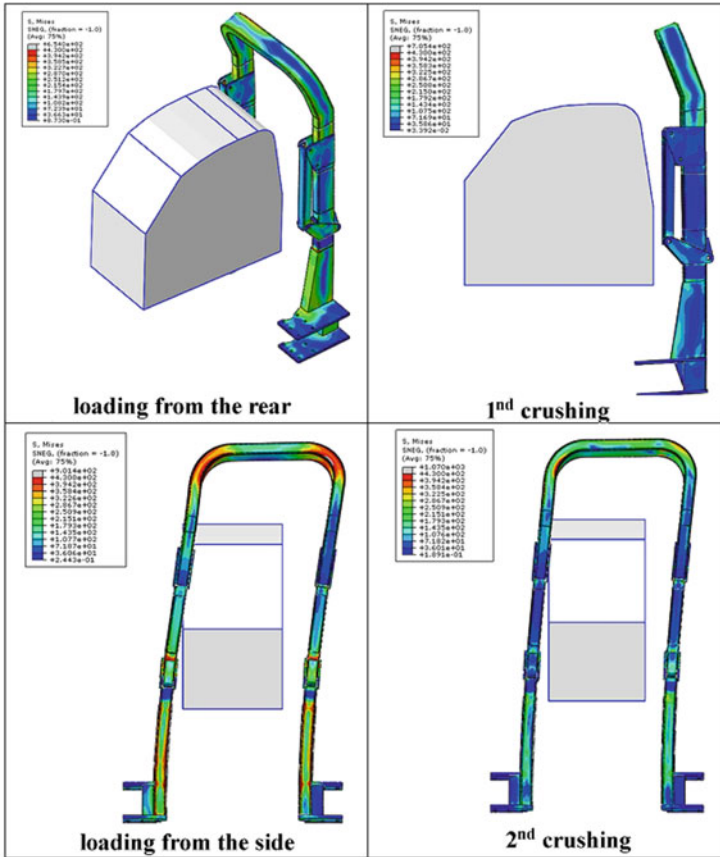


Fig. 6 Contour plots of Von Mises stress for the test loadings

structure, increasing where necessary the thickness of the most stressed elements and carrying out again the FEM analysis until all of them were able to satisfy the minimum requirements. The ultimate version of the structure is in full accordance with the provided loading tests, applying the force and absorbing the energy shown in Table 1. After this fundamental step, an actuator system has been designed; in view of reducing the overall cost and consider a reliable solution, a steel spring and two more elements was selected and then designed. In detail, the spring is compressed in the UC, viceversa it is reaching an extension close to its maximum in the SC; the mover element is connected to the spring, acting on the follower element to raise the QROPS. Depending on the time required for raising the structure, the spring element can assume different wire diameter values.

In accordance to the dynamic simulation, applying on each structure sides two springs with 18 coils, a free length of 254 mm and a wire diameter of about 9 mm

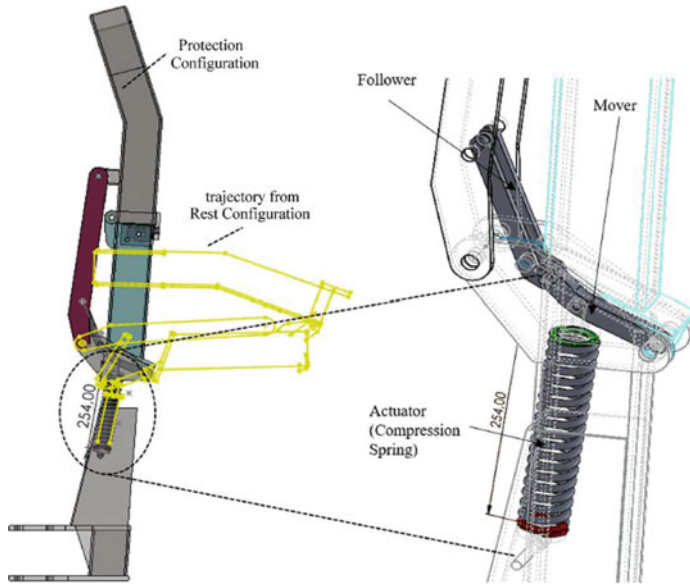


Fig. 7 The actuator system, consisting of a spring and two more connecting elements

(Fig. 7), the QROPS should rise completely in 0.65 s, a time admissible for an effective protection, comparable to the findings of other similar studies [11, 14].

4 Conclusions

In this study, the 3-section foldable rear rollbar was designed to be fitted on a narrow-track tractor having a reference mass of 3200 kg. In respect to the pyrotechnic squib and hydraulic solutions, the mechanical solution is cheap and flexible. In fact, in the locking device is possible to correlate the spring dimensions, and so its strength, to the time of ROPS raising, to obtain acceptable performance. On the other hand the spring is made of steel, and over time this component could suffer corrosion, thereby reducing its original strength and/or creating difficulty in its extension/compression motion.

To overcome this problem an alternative could be represented by the use of one (or two) cylinder(s) fed by the main hydraulic circuit of the tractor, but this solution should be complex and expensive, also considering the need to provide a series of valves, pipes, nitrogen accumulators, etc. An other interesting opportunity, both cheap and simple, could be to consider an electric linear actuator of suitable technical characteristics. In fact, many models showing good performance are actually available on the market, both in terms of working displacement and actuating strength.

Moreover, the virtual prototyping procedure described could be usefully applied to develop a design methodology to replace fixed or partially foldable ROPS with a completely foldable structure, maintaining unchanged the level of safety.

References

1. Facchinetti, D., Santoro, S., Galli, L.E., Pessina, D.: Agricultural tractor roll-over related fatalities in Italy: results from a 12 years analysis. *Sustainability* **13**, 4536 (2021). <https://doi.org/10.3390/su13084536>
2. Ballesteros, T., Arana, I., Perez Ezcurdia, A., Alfaro, J.R.: E2D-ROPS: development and tests of an automatically deployable, in height and width, front-mounted ROPS for narrow-track tractors. *Biosyst. Eng.* **116**, 1–14 (2013). <https://doi.org/10.1016/J.BIOSYSTEMSENG.2013.05.009>
3. Cremasco, M.M., Caffaro, F., Giustetto, A., Vigoroso, L., Paletto, G., Cavallo, E.: Tractor rollover protection: is the incorrect use of foldable rollover protective structures due to human or to technical issues? *Hum. Factors J. Hum. Factors Ergon. Soc.* **62**, 64–76 (2019). <https://doi.org/10.1177/0018720819848201>
4. Baumann, K., Wünsche, M.: The Raisable Roll-Over Bar of the New Mercedes-Benz Roadster. SAE Technical Paper 901124 (1990). <https://doi.org/10.4271/901124>
5. Power J.R., et al.: Preventing tractor rollover fatalities: performance of the NIOSH autoROPS. *Int. J. Prev. (Suppl 1)*, i54–58 (2001). https://doi.org/10.1136/ip.7.suppl_1.i54
6. Etherton, J.R., Cutlip, R.G., Harris, J.R., Ronaghi M., Means, K.H., Howard, S.: Dynamic performance of the mechanism of an automatically deployable ROPS. *J. Agric. Saf. Health* **8**(1), 113–118 (2002). <https://doi.org/10.13031/2013.7222>
7. Etherton, J.R., Cutlip, R.G., Harris, J.R., Ronaghi, M., Means, K.H., Gillispie A.: Static load test performance of a telescoping structure for an automatically deployable ROPS. *J. Agric. Saf. Health* **8**(1), 119–26 (2002). <https://doi.org/10.13031/2013.7223>
8. Alkhaleedi, H., Means, K., McKenzie, E., Smith, J.: Reducing occupational fatalities by using NIOSH 3rd generation automatically deployable rollover protective structure, *Saf. Sci.* **51**(1), 427–443 (2013). <https://doi.org/10.1016/j.ssci.2012.08.004>
9. Silleli, H.: Research on applying an anchor mechanism to orchard and vineyard tractors produced in Turkey. *Turkish J. Agric. Forestry* **31**(6), 5. <https://journals.tubitak.gov.tr/agriculture/vol31/iss6/5>
10. Silleli, H.: Anchor mechanism to increase the operator clearance zone on narrow-track wheeled agricultural tractors: prototype and first tests. *Biosyst. Eng.* **97**(2), 153–161 (2007). <https://doi.org/10.1016/j.biosystemseng.2007.02.016>
11. Silleli, H.: Anchor mechanism to increase the operator clearance zone on narrow-track wheeled agricultural tractors: static and field upset test results, *Biosyst. Eng.* **99**(2), 196–204 (2008). <https://doi.org/10.1016/j.biosystemseng.2007.10.014>
12. Ballesteros, T., Arana, I., Pérez Ezcurdia A., Alfaro, J.R.: E2D-ROPS: development and tests of an automatically deployable, in height and width, front-mounted ROPS for narrow-track tractors. *Biosyst. Eng.* **116**(1) (2013). <https://doi.org/10.1016/j.biosystemseng.2013.05.009>
13. Ballesteros, T., Arana, J.I., Pérez de Ezcurdia A., Alfaro, J.R.: Development and validation of automatically deployable ROPS based on airbag inflator technology. *Biosyst. Eng.* **130**, 92–105 (2015). <https://doi.org/10.1016/j.biosystemseng.2014.12.007>
14. Ojados Gonzalez, D., Martín-Gorriç, B., Ibarra Berrocal, I., Miguel Hernandez B., Caro Garcia, F.: Morales Sanchez, P.: Development of an automatically deployable roll over protective structure for agricultural tractors based on hydraulic power: prototype and first tests. *Comput. Electron. Agric.* **124**, 46–54 (2016), <https://doi.org/10.1016/j.compag.2016.03.027>

Microclimatic Conditions at the Interior of Small-Sized Insect-Proof Nethouses with Tomato Cultivation



Anastasios Giannoulis, Nikoleta-Georgia Papardaki, Antonis Mistriotis, and Demetres Briassoulis

Abstract Insect-proof nethouses are low-cost structures that can provide efficient protection against harmful insects and environmental hazards, and a favorable microclimate for the protected cultivation during the summer period. In this study, a full-scale experiment of two neighboring low-rise insect-proof nethouses with tomato cultivation was employed for the estimation of the indoor wind velocities, temperature, relative humidity, and solar radiation. The impact of these parameters on the cultivation growth and production quality and quantity was investigated. Two different types of insect-proof nets were used as covering materials, namely the 3353BT Biorete Airplus 50 mesh and the Optinet 50 mesh. Open-field tomato cultivation was used as reference. Results showed that temperature and relative humidity inside the nethouses were similar to the corresponding ambient values due to the structures' small size and the small number of the protected tomato plants. The total radiation entering the two nethouses was found to be reduced by 40% (Optinet) and 11% (Airplus) compared to the incoming solar radiation. The shading effect and the reduced indoor air velocity affected the evapotranspiration mechanism of the protected cultivation, resulting in a significantly faster plant growth inside the nethouses with the final height of the tomato plants being almost double the ones in the open-field cultivation. In addition, during the harvesting period the total yield was higher from the nethouses than from the open-field (peak harvesting day weight increase: 76%, Airplus; 159%, Optinet). The quantity of fruits collected was also higher for the nethouses (peak harvesting day number of fruits increase: 56%, Airplus; 71%, Optinet).

Keywords Nethouse · Insect-proof · Tomato cultivation · Microclimate · Agricultural nets

A. Giannoulis (✉) · N.-G. Papardaki · A. Mistriotis · D. Briassoulis
Department of Agricultural Engineering, Agricultural University of Athens,
11855 Athens, Greece
e-mail: agian@aua.gr

© The Author(s), under exclusive license to Springer Nature Switzerland AG 2023
V. Ferro et al. (eds.), *AIIA 2022: Biosystems Engineering Towards the Green Deal*,
Lecture Notes in Civil Engineering 337,
https://doi.org/10.1007/978-3-031-30329-6_60

587

1 Introduction

In hot regions or during the summer period, extreme climatic conditions and enemy insects can be catastrophic for the open-field cultivations. Insect-proof nethouses can be an alternative. They offer protection from the harmful insects, reduce wind velocities in their interior, while they also regulate the internal microclimate by reducing the incoming solar radiation. Thus, they allow for the improvement of the cultivation production quality and quantity through an environmentally friendly approach by reducing the irrigation and insecticides inputs.

The published research work in the international literature regarding nethouses is relatively limited. Most of the studies analyzed the airflow around such structures or the microclimate in their interior through full-scale experiments or CFD models [3, 5, 6]. It has been reported, that the use of insect-proof nets as cladding materials, may reduce the air exchange rate with the environment, resulting in a microclimate unfavorable for the protected cultivation (e.g., higher temperature/humidity during the summer period) [2, 4]. Further research work and appropriate design modifications could allow for the optimization of the microclimatic conditions of nethouses.

This research work presents a full-scale experiment regarding two neighboring low-rise nethouse structures with tomato cultivation. The air velocities around and inside the nethouses were measured to estimate their air exchange performance. Microclimatic parameters such as temperature, relative humidity, and irradiance were also recorded inside the nethouses and compared to the open-field conditions. The tomato plants growth and fruit production have also been evaluated through comparisons to an open-field cultivation.

2 Materials and Methods

2.1 Setup of the Full-Scale Experiment

The full-scale experiments took place in the experimental field of the Agricultural University of Athens, located in Spata, Attiki, Greece. The nethouses were low-rise semi-circular steel frame structures (tunnels) with a ridge height of 2 m, span width of 4 m and length of 8 m. OptiNet 50 mesh (Ginagar, Israel; optical exclusion technology; porosity: 38.7%; OptiNet) and the 3353BT Biorete 50 Mesh AirPlus (Arrigoni, Italy; enhanced ventilation technology; porosity: 53.4%; AirPlus) were selected as the insect-proof cladding materials. The OptiNet was installed at the northern nethouse structure (OptiNet Nethouse), while the southern nethouse was covered with the AirPlus insect-proof net (AirPlus Nethouse) (Fig. 1, left). The nethouses were parallel to each other, oriented almost perpendicular to the N-S direction, with a small deviation of 4° to the NNE-SSW direction.

Regarding the cultivation, a climber tomato variation named Bellfort F1 was selected. Two rows of tomatoes were planted in each tested case (open field; Airplus

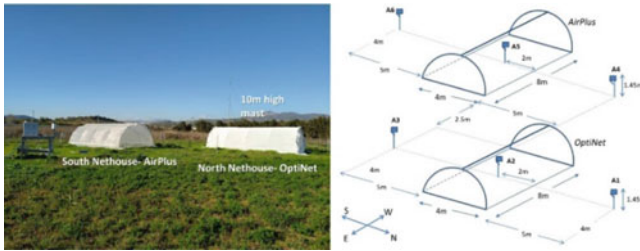


Fig. 1 The insect-proof nethouses at the field (left); Detailed geometrical configuration of the locations of the rotary cup anemometers around and inside the nethouses (right)

and Optinet nethouse). The space between the rows was 1.5 m while the distance between the plants rows was 0.5 m. Each row had 14 plants (28 total for each case) with an initial height of approximately 10 cm.

2.2 Equipment – Data Acquisition

8 rotary cup anemometers (Vector Instruments, A100K, accuracy: 0.1 m s^{-1}) were used for the estimation of the airflow at discrete points windward, leeward and inside the nethouses. Two of them were located on a 10 m high mast at 10 m and 4 m (M10 and M4 correspondingly). The remaining six anemometers (A1–A6) were located along the centerline of each nethouse (three anemometers at each nethouse, Fig. 1, right).

The anemometers inside the nethouses were located at the mid-point of the interior area of the structure, while the outside anemometers were placed 5 m away from the nethouses sides. All were at the height of 1.45 m. The anemometer on the mast at 10 m height, served as the reference anemometer so that the rest of the anemometers were correlated to it. Wind velocity data were recorded and analyzed only for South wind direction, which was perpendicular to the sides of the nethouses. A potentiometer wind vane was set at 4 m high to constantly monitor the wind direction (Vector Instruments, W200P, accuracy: $\pm 2^\circ$). The range of the wind vane rotation was 360° (North wind: 0° and 360° ; South wind: 180°). Analysis of the data was carried out only for winds normal to the nethouse structures sides.

The solar radiation (W m^{-2}) was measured with pyranometers (Kipp & Zonen, CMP6b) that could monitor the full solar spectrum range (285 nm to 2800 nm). The sensor accuracy was less than 4%. Two pyranometers were available; one was constantly at the experimental field for the solar radiation measurements; the second was placed in turns at the interior of each nethouse. Data from the anemometers, the wind vane and the pyranometers were recorded every 15 s and averaged over a 2-min period.

The temperature and relative humidity were also monitored (Meter Group, ATMOS 14). The accuracy of the instrument was $\pm 2\%$ for the relative humidity

and ± 0.2 °C for the temperature. Each sensor was protected by a radiation shield to prevent direct sunlight to heat the sensor. Three sensors were used. Two of them were inside each of the nethouse structures and the third monitored the field temperature and relative humidity. Recordings were 5-min averages for both the temperature and the relative humidity.

Insect traps (black chromatropic sticky panels; two at each plants' row) were placed inside the nethouses and at the open-field in order to confirm the insect-proof ability of the nethouses. The trapped insects were identified in the laboratory stereoscope.

The tomato cultivation growth was recorded from June to September 2021. In each testing case (open field/nethouses) the plants' height was measured. Simultaneously, the captured insect population was also observed. For the harvesting period (i.e. August) the quantity of the collected fruits was recorded approximately every week.

3 Results

3.1 Air Velocity Results

Recordings were carried out for a ten (10) day period (1–10 February 2021) when south wind was dominant. The 6 anemometers at the nethouses level were correlated to the data recorded for the reference anemometer M10. Table 1 presents the correlation between the reference anemometer (M10) and the most windward anemometer (A6) with the anemometers around and inside both nethouses.

The incoming wind initially interacts with the windward insect-proof nethouse and its windward anemometer (A6, $A6/M10 = 0.59$). A minor increase for the wind velocity was measured for the windward anemometer of the leeward/Optinet nethouse ($A3/A6 = 1.08$) when compared to the windward anemometer A6 of the AirPlus nethouse. As the airflow impinges on the windward nethouse (AirPlus), the wind that does not penetrate the net covering, slightly accelerates towards the A3 anemometer. A substantial velocity drop was recorded for both the nethouses interior ($A5/A6 = 0.58$, $A2/A6 = 0.41$). Results showed lower wind velocity drop for the AirPlus insect-proof nethouse (enhanced aerodynamic behaviour).

The wind velocity further decreases as the wind passes through the leeward side of the AirPlus nethouse ($A4/A6 = 0.31$), as expected. For the Optinet nethouse

Table 1 Ratio of the anemometers at the nethouse level with the reference anemometer M10 and the most windward anemometer for South wind (A6)

Nethouse level Anemometers	Ratios					
	A1	A2	A3	A4	A5	A6
(M10)/reference	0.26	0.24	0.64	0.18	0.34	0.59
A6/ most windward	0.44	0.41	1.08	0.31	0.58	1.00

leeward anemometer ($A1/A6 = 0.44$) the air velocity ratio was like the ratio of the anemometer inside the nethouse ($A2/A6 = 0.41$). The interaction of the wind with two insect-proof nethouses close to each other could result in airflows of highly complex pattern (eddy formation at nethouses wake).

3.2 Temperature and Relative Humidity Results

Recordings for a 12-days period (8th to 20th of August 2021) are presented in Fig. 3. For this period the cultivation inside the nethouses was at its full growth. Figure 2 presents the average daytime (07.00 am to 20.00 pm) temperature variations and temperature difference variations (comparison between the field and the nethouses temperature and the difference between the two nethouses). It appears that the average temperatures were similar inside and outside the nethouses. For high wind velocity days (12th–16th of August, velocity: 5.5–7.5 m s⁻¹) the average temperature differences are practically zero. However, for low wind velocity days (e.g., 8th–11th of August, velocity: 1.8–3.2 m s⁻¹) higher average temperatures were observed at the interior of the nethouses. The highest average temperature was recorded equal to 36.85 °C (10th of August) inside the Optinet nethouse. The 11th of August was the day with the highest temperature differences, that was 1.14 °C (Optinet-field) and 0.9 °C (Airplus-field). The average temperature differences between the two nethouses were also small, with the highest being 0.54 °C (higher inside the Optinet nethouse). For high wind velocities the airflow convection becomes dominant and the air mass flow from the environment through the small-sized nethouses is constant and rapid. For low wind velocities, the corresponding low air exchange rates favor the rise of the temperature inside the nethouses.

Figure 3 shows the daytime RH averages for the period of 12 days that the measurements took place. The average daytime RH (%) graphs appear to be very similar for all the cases (nethouses and field). This is also verified by the average daytime RH (%) differences, since for all cases they were insignificant (Fig. 3, right). The highest RH (%) difference was equal to 2% (Optinet-Field) while in almost all cases the RH (%) differences did not exceed 1%.

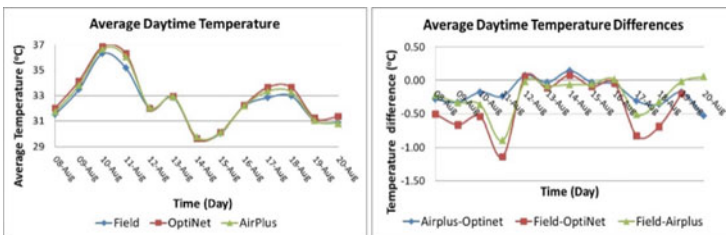


Fig. 2 Daytime average temperature variation at the field and inside the nethouses (left); daytime average temperature difference variation between the nethouses and the field temperature (right)

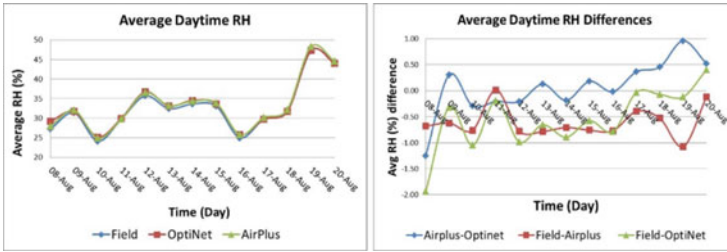


Fig. 3 Relative Humidity (%) variation for the nethouses and the field; average daytime (left); average daytime differences (right)

3.3 Insects Attacks

No important attacks by insects were recorded in the open-field cultivation, except for a small-scale presence of the *Empoasca spp* insect, a leafhopper species considered to be a very destructive pest. These insects could damage the leaves causing their premature drop or the tomato fruits or they could be potential vectors of virus diseases. No insect attacks were recorded inside the nethouses confirming the physical exclusion of insects and the associated benefits for the cultivations protected by nethouses.

3.4 Solar Radiation Results

For the OptiNet nethouse measurements have been carried out for the period 29 January–6 February 2021, while for the AirPlus nethouse for the period 26 February–3 March 2021. Figure 4 presents the intensity of solar radiation for both pyranometers, inside and outside the OptiNet and the AirPlus nethouse.

For all the days except the 1st of February 2021 (cloudy day, Fig. 4, left), the field irradiance ($W m^{-2}$) had an average value of $624.73W m^{-2}$ while for the OptiNet

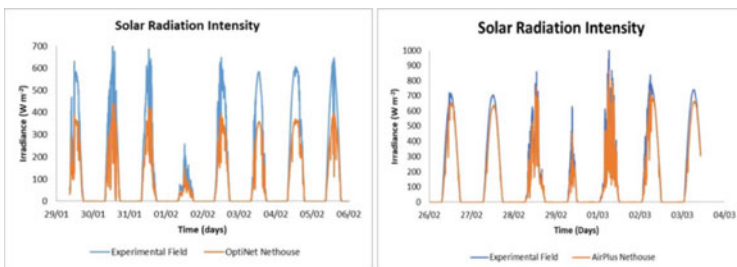


Fig. 4 Solar radiation measurements at the experimental field as compared to the interior of the: OptiNet nethouse (left); AirPlus nethouse (right)

nethouse this value was equal to 375.94 W m^{-2} . The ratio of the two averages provided the radiation transmission at the interior of the OptiNet nethouse: 0.601 or 60.1%; shading factor: 0.399 or 39.9%.

For the second period the solar average irradiance value was 810.50 W m^{-2} , while for the Airplus nethouse it was equal to 719.63 W m^{-2} (except the cloudy 29th of February 2021). The transmission of the solar radiation regarding the AirPlus nethouse was calculated was equal to 0.889 or 88.9% (shading factor: 11.1%). The optical properties of the insect-proof nets were previously tested through laboratory experiments (shading factor: Optinet = 43.25%; Airplus = 7.81%; [1]. Field experiment results were in very good agreement.

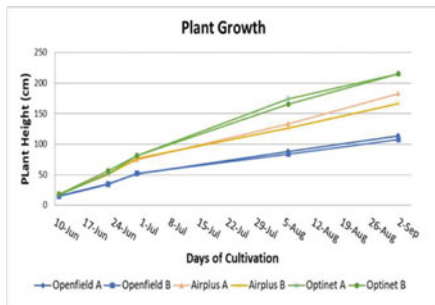
3.5 Cultivation Production

Data related to the tomato plants cultivation at the interior of the insect-proof nethouses were monitored from the 8th of June to the 8th of September 2022. The height of the plants, the quantity and the size of the fruits were recorded and compared to the open field cultivation. Figure 5 presents the average height of each plant row (A, B represent the rows) inside the nethouses and for the open field cultivation.

For the first month, the tomato plants inside the nethouses had a similar average height of 80 cm. For the second and third month the Optinet nethouse tomato plants were the highest (2nd month plants height: 170 cm, Optinet; 130 cm, Airplus; 3rd month plants height: 215 cm, Optinet; 180 cm, Airplus). At the end of the third month the tomato plants of the Optinet nethouse exceeded the nethouse maximum height (215 cm). Regarding the open field cultivation, tomato plants appeared to be significantly underdeveloped for the entire duration of the experiment (Open field plants height: 50 cm, 1st month; 85 cm, 2nd month; 110 cm, 3rd month).

Figure 6 presents the quantity (total weight (kg)) of fruits and the amount (number of fruits) correspondingly, each time they were collected during the harvesting period (9th of August–2nd of September 2021). For the two weeks period from the 13th to the 26th of August, the total weight and the number of tomato fruits collected was significantly higher for the nethouses. The 13th of August was the day that tomato

Fig. 5 Average plant height for the two rows of each case (field, Optinet and Airplus nethouse)



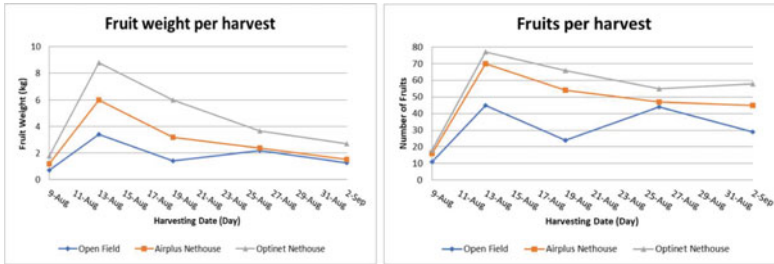


Fig. 6 Weight and number of fruits per harvest

fruits harvesting was at its peak (Total weight, Optinet nethouse: Open field: 3.4 kg; Airplus: 6.0 kg, increase 76%; Optinet: 8.8 kg, increase 159% – Number of fruits, Open field: 45; Airplus nethouse: 70, increase 56%; Optinet nethouse: 77, increase 71%). After the 26th of August the differences in the tomato fruits production between the nethouses and the open field were smaller.

4 Conclusions

A full-scale experiment on the microclimatic conditions of two low-rise tunnel-type insect-proof nethouses covered with different nets with tomato cultivation has been carried out. The more permeable AirPlus nethouse allowed for higher air velocities at its interior and thus better air exchange. However, this result did not significantly affect the temperatures and humidity recordings especially for high wind velocity days. For days with low wind velocities small temperature increase has been detected inside the nethouses. The nethouses allowed for reduced incoming solar radiation (mostly the Optinet nethouse), that along with the reduced airflow velocities in their interior led to the reduction of the plants' evapotranspiration and the alleviation of radiation stress. Additionally, no harmful insects were detected inside the nethouses. As a result, the plants growth and fruit yield were significantly higher inside the nethouses than at the open-field.

Acknowledgements This research was implemented within the framework of the research project «SmartNethouse» (code: 865) supported by the Hellenic Foundation of Research and Innovation (HFRI) of the General Secretariat of Research and Technology (GSRT).









References

1. Giannoulis, A., Briassoulis, D., Papadaki, N.G., Mistriotis, A.: Evaluation of insect-proof agricultural nets with enhanced functionality. *Biosys. Eng.* **208**, 98–112 (2021)

2. Mahmood, A., Hu, Y., Tanny, J., Asante, E.A.: Effects of shading and insect-proof screens on crop microclimate and production: a review of recent advances. *Sci. Hortic.* **241**, 241–251 (2018)
3. Mistriotis, A., Castellano, S.: Airflow through net covered tunnel structures at high wind speeds. *Biosys. Eng.* **113**, 308–317 (2012)
4. Tanny, J., Cohen, S., Teitel, M.: Screenhouse microclimate and ventilation: an experimental study. *Biosys. Eng.* **84**, 331–341 (2003)
5. Tanny, J., Haijun, L., Cohen, S.: Airflow characteristics, energy balance and eddy covariance measurements in a banana screenhouses. *Agric. For. Meteorol.* **139**, 105–118 (2006)
6. Teitel, M., Ozer, S., Mendelovich, V.: Airflow temperature and humidity patterns in a screenhouse with a flat insect-proof screen roof and impermeable sloping walls - computational fluid dynamics (CFD) results. *Biosys. Eng.* **214**, 165–176 (2022)

The Effect of Adjuvants in Reducing Potential Spray Drift



Marco Grella , Paolo Marucco , Marco Resecco , Claudio Bozzer ,
Alessandro Biglia , Lorenzo Comba , Paolo Balsari ,
and Fabrizio Gioelli 

Abstract Drift containment during plant protection products spray application is essential to achieve sustainable crop protection. Adjuvants are designed to perform specific functions during the mixing and application of pesticides, but they can also reduce evaporation, foaming, volatilization, and spray drift. Laboratory trials aimed to measure the capability of different adjuvants to reduce potential spray drift were performed. Two adjuvant formulations were tested separately at two dosages. Three types of nozzles were considered: conventional hollow-cone and flat fan, and air-inclusion flat fan nozzles. The effect of adjuvants on the obtained droplet size spectra were measured using a laser diffraction system. Furthermore, adjuvants effect on potential spray drift was evaluated measuring the distortion of single nozzles spray patterns, using an ad hoc designed “wind-tunnel horizontal patternator”. Pure water was used as a spray liquid reference for the evaluation of (i) changes in droplet size spectra and (ii) the potential spray drift reduction attributable to the adjuvants. Both tested adjuvants increased the droplet size spectra of the three types of tested nozzles to a different extent, in the range of 2–60% for the Volume Median Diameter. The variation of droplet size spectra was reflected in the reduction of potential spray drift, which ranged between 9 and 62%. Different reductions were observed according to the nozzle types. Significant differences between the two tested adjuvants were detected for their capability to reduce potential spray drift. Finally, the adjuvants dosage generally did not affect either the droplet size or the drift reduction figures.

Keywords Droplet Size Spectra · Nozzles · Spray patterns · Wind tunnel measurements · Spray drift

M. Grella (✉) · P. Marucco · C. Bozzer · A. Biglia · L. Comba · P. Balsari · F. Gioelli
Department of Agricultural, Forest and Food Sciences (DiSAFA), University of Turin (UNITO),
Largo P. Braccini, 2, 10095 Grugliasco, TO, Italy
e-mail: marco.grella@unito.it

M. Resecco
National Interuniversity Consortium of Materials Science and Technology (INSTM), Via G.
Giusti, 9, 50121 Firenze, Italy

1 Introduction

Drift containment during spray application of plant protection products (PPP) is essential to achieve sustainable crop protection accomplishing the EU directives and strategies. Indeed, during spray applications with conventional sprayers, only a limited fraction of the total amount of PPP is deposited on the intended target. Therefore, part of the applied PPP can be transported as spray drift outside the sprayed area by the action of air currents during the application process.

Among the different factors influencing spray drift, wind speed and direction are the main ones [1]. The higher the wind speed, the higher carrying effect it will have for droplets; therefore, the spray drift risk increases. The main solution to minimize spray drift is to act on technical factors through a proper adjustment of the spraying equipment [2]. Droplet size has proven to be the most effective factor in reducing spray drift by means of drift reducing nozzles [3, 4]. The bigger the droplet size, the higher the weight and, therefore, the lower the drift, as the carrying effect of wind will be lower with heavier drops. This was the way followed to develop drift-reducing hydraulic nozzles decades ago. These nozzles produce coarser droplets than the conventional ones do. Recently different studies have been focused to demonstrate that drift reducing nozzles generate important drift reduction while keeping the necessary spray deposition to ensure the biological efficacy of treatments [5]. Nevertheless, some farmers still prefer conventional nozzles as small size drops generate higher coverage on the leaf surface, even if studies demonstrated the success of drift reducing nozzle to control pest and diseases.

In this context, the use of adjuvants able to increase the droplet size spectra could be a possible solution to reduce spray drift also when using conventional nozzles or even enhance the capability in reducing spray drift for drift reducing nozzles [6]. In Europe, up to now, the adjuvants have been more used to perform specific functions involving the mixing and application of pesticides maximizing the biological efficacy of treatments [7] (i.e. buffering, dispersing, emulsifying, spreading, sticking, and wetting), but they can also reduce evaporation, foaming, volatilization, and spray drift. In the last years, several chemical companies are introducing new adjuvants which are specific for drift mitigation purposes [8]. This type of adjuvants is already spread in Northern America [9], where the market of adjuvants is much more developed than in Europe. To date interest in using adjuvants as an additional tool to increase the spray application efficiency, by concurrently increasing the spray deposition and reducing the spray drift risk, is on the rise in Europe also because of the European Green Deal that, within the Farm to Fork strategy, strives to reduce by 50% the overall use of agrochemicals within 2030.

In this context, laboratory trials aimed to measure the capability of two adjuvant formulations to increase the droplet size spectra and therefore reduce potential spray drift under different wind speed conditions were carried out.

2 Materials and Methods

Two commercial adjuvants were tested under laboratory conditions for their potential effect in drift reducing. The first one, from this point on “adjuvant A”, was a product mainly composed by soy lecithin to be used in the dosage range of 3.0 and 4.5 g l⁻¹. The second one, from this point on “adjuvant B”, was a liquid fertilizer based on yeast extract and containing brown algae to be used in the dosage range of 2.0 and 3.0 ml l⁻¹.

Two series of trials were carried out i) to measure the effect of adjuvants on the droplet size spectra generated during spray application and ii) to determine the potential spray drift reduction achievable with the use of adjuvants.

For these purposes all trials were carried out using conventional flat fan nozzles XR 110 03 VS (TeeJet, Spraying Systems Co., Wheaton, Illinois USA) at 0.3 MPa spray pressure, air induction flat fan nozzles AI 110 03 VS (TeeJet) at 0.3 MPa spray pressure and conventional hollow cone nozzles ATR 80 lilac (Albuz® CoorsTek, Evreux, France) at 0.7 MPa spray pressure. The different spray pressure adopted testing the flat fan and the hollow cone nozzles was inferred from their practical use. Flat fan nozzles are generally used for the arable crop spray application with horizontal boom sprayers at low pressure, meanwhile hollow cone nozzles are used for bush/tree crop spray application with airblast sprayers at higher pressure.

For both adjuvants, the minimum and maximum dosages mentioned before and reported in the product labels were tested combined with the three nozzle types. Concurrently, trials using pure water (spray liquid reference) were always carried out and data obtained were used as reference for the comparison of droplet size spectra and for the calculation of potential spray drift reduction achieved by using adjuvants.

2.1 Droplet Size Spectra Measurements

The droplet size spectra were measured with a Malvern Spraytec® laser diffraction system STP5342 (Malvern Instruments Ltd., Worcestershire, UK). The instrument has a maximum measurement frequency of 10 kHz and a measurement range of 0 to 2,000 μm when equipped with 750 mm lens. In all the tests, the nozzle tip was positioned at 50 cm distance from the laser beam and targeting the laser beam towards the center of the spray jet emitted by the nozzle. The droplet diameter corresponding to 10th (D[v,0.1]), 50th or Volume Median Diameter (VMD) (D[v,0.5]), and 90th (D[v,0.9]) percentiles of spray liquid volume was determined for each combination nozzle/dosage and for the pure water. Additionally, the % of spray liquid volume generated with droplet diameters smaller than 100 μm was calculated as V₁₀₀ for its relationship with droplet driftability [3].

2.2 Potential Spray Drift Reduction Measurements

To calculate the potential spray drift reduction attributable to the use of adjuvants, firstly the distortion of single nozzle spray pattern due to the cross-air flow effect was evaluated. For this purpose, an ad hoc designed “wind-tunnel horizontal patterator” was used. The device consists in a horizontal patterator complying with ISO 5682–1 and equipped with 60 grooves (50 mm width each) collecting the liquid sprayed in 60 tubes [10]. The patterator characterized by 3.0 m total length was placed inside a wind tunnel having a square section of 1.45×1.45 m above it. On the left side of the wind tunnel cage an electrical driven axial fan 1,200 mm in diameter, equipped with a special downstream air conveyor able to guarantee the uniformity of the air flow generated, was installed. The axial fan provides a variable air stream, between 1.7 and 3.8 m s^{-1} , which invested the nozzle spray jet. The nozzle was placed at 0.95 m from the left edge of patterator (aligned with the center of 19th groove – 0 m from spray source) and above it at 0.5 m height.

The three selected nozzles were tested in combination with the minimum and maximum dosages defined for the two tested adjuvants. For all combination two air flow speeds (1.7 and 2.8 m s^{-1} at the nozzle position) were tested.

Once obtained the horizontal spray pattern, the Drift Index (I_d) was calculated according to Eq. (1):

$$d = \sum_{i=1}^{60} \left(\frac{L_i}{\sum_{j=1}^{60} L_j} * d_i \right) \quad (1)$$

where L_i is the amount of liquid collected by each patterator groove (ml); d_i is the distance of the grooves (m) where 0 m correspond to the 19th groove (the one aligned with the nozzle), -0.9 m correspond to the 1st groove (the one nearest to the axial fan) and 2.05 m correspond to the 60th groove (the one farthest to the axial fan); i and j are the number of patterator grooves from the 1st to the 60th.

Based on the Drift Index (I_d) the potential drift reduction ($I_{d_{red}} - \%$) was calculated separately for the adjuvants and for each air flow speed, according to Eq. (2):

$$I_{d_{red}} = 100 - \left(\frac{I_{d_{cand}} * 100}{I_{d_{ref}}} \right) \quad (2)$$

where $I_{d_{cand}}$ is the Drift Index achieved by the candidate configuration (combination of nozzle type and adjuvant dosage) and $I_{d_{ref}}$ is the Drift Index measured for the reference configurations (combination of nozzle type and adjuvants dosage tested at the same air flow speed conditions of candidate configuration).

Finally, to detect the effect of adjuvants (A and B) and dosages (minimum and maximum) and their interactions on the potential drift reduction ($I_{d_{red}}$) a two-way ANOVA was carried out using IBM SPSS Statistics (Version 28) predictive analytics software for Windows. The significance threshold was set to 0.05.

3 Results and Discussion

The droplet size spectra generated by the three tested nozzles when spraying adjuvants at different dosages are displayed in Table 1. The adjuvants allowed in all cases to increase the $D [v,0.1]$, $D [v,0.5]$ and $D [v,0.9]$ to different extent depending on the adjuvant type and nozzle type used. The volume median diameter (VMD) increased of 61.7, 25.5 and 1.5% using adjuvants A and of 27.4, 11.4 and 11.2% using adjuvant B when conventional and air induction flat fan, and hollow cone nozzles were tested combined with the minimum dosage, respectively. Concurrently, increasing the dosage the droplet size increase was null or very limited. Interestingly, for both adjuvants the V_{100} parameter decrease in all cases in the range of 13.7 and 55.6% using the conventional flat fan, as well as conventional hollow cone nozzles showed a less pronounced reduction between 3.8 and 15.1%. This latter was due to the higher spray pressure used for the tests. Very limited V_{100} reduction was achieved using air induction flat fan nozzles.

In Fig. 1 the spray profiles obtained testing the adjuvant A and B, respectively are displayed. Profiles are presented in separate boxes per nozzles and cross-air flow speed to visually catch the spray profile distortion testing the minimum, maximum and the reference spray liquid (pure water). Irrespective of the adjuvant and dosage, the ATR80 lilac at 7 bar was affected by higher distortion of the profile (ratio of

Table 1 Droplet size spectra generated by the tested nozzles spraying the two adjuvants and two dosages. Pure water was tested as reference spray liquid

Adjuvant	Dosage	Nozzle model	Pressure (Mpa)	$D [v,0.1]^a$ (μm)	$D [v,0.5]^a$ (μm)	$D [v,0.9]^a$ (μm)	V_{100}^b (%)
–	Water	XR11003VS	0.3	73	149	332	27
–	Water	AI11003VS	0.3	139	425	866	6
–	Water	ATR80 lilac	0.7	47	96	177	54
A	Min	XR11003VS	0.3	110	241	438	13
A	Max	XR11003VS	0.3	107	240	437	12
A	Min	AI11003VS	0.3	277	534	945	5
A	Max	AI11003VS	0.3	272	533	943	4
A	Min	ATR80 lilac	0.7	55	97	256	49
A	Max	ATR80 lilac	0.7	55	99	262	51
B	Min	XR11003VS	0.3	90	190	382	17
B	Max	XR11003VS	0.3	91	188	375	17
B	Min	AI11003VS	0.3	213	474	879	3
B	Max	AI11003VS	0.3	210	474	876	3
B	Min	ATR80 lilac	0.7	54	106	232	52
B	Max	ATR80 lilac	0.7	60	115	223	46

a 10% of the spray liquid volume fraction is made up of droplets smaller than $D[v,0.1]$; $D[v,0.5]$ is the volume median diameter; 90% of the spray liquid volume is made up of droplets smaller than $D[v,0.9]$.
 b V_{100} : spray liquid fraction generated with droplets smaller than 100 μm

sprayed liquid collected on the left and right side of the reference red dashed line) as it generated smaller droplets compared to the other nozzles; furthermore, the hollow cone spray pattern is the more affected by the cross-air flow as more surface of projected spray pattern is invested by the air flow in the test bench. Contrarily, the flat fan nozzles spray pattern has very limited surface invested by the cross-air flow thus resulting in less distortion of spray profile compared to the hollow cone nozzle. It must be considered that the lower pressure used (0.3 MPa) testing the conventional flat fan nozzles XR11003VS also contribute to lowering the distortion. Nearly no distortion was noticed using the air induction nozzles as their generated very/extra coarse droplet size spectra that are well known to be less affected by air flow and therefore recommended as spray drift reducing technology (SDRT).

From the spray profiles the Drift Index (I_d) were calculated for the different combination of tested parameters. The potential drift reduction ($I_{d,red}$ - %) obtained is showed in Fig. 2 for the two tested adjuvants and the minimum and maximum

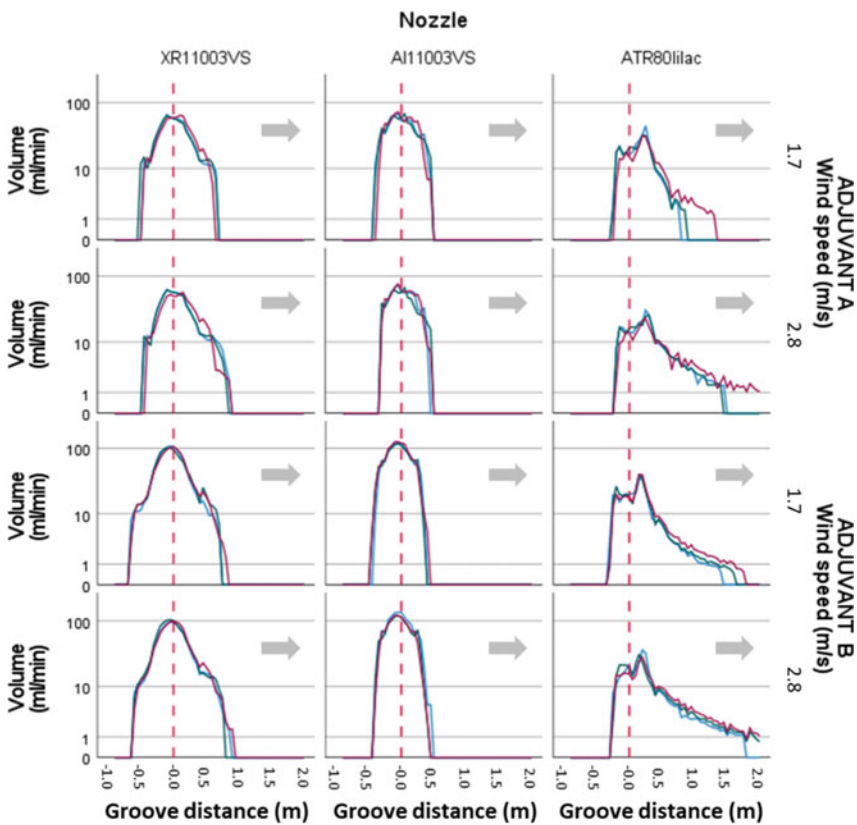


Fig. 1 Horizontal spray patterns obtained testing three nozzle types with the adjuvant A and B at two dosages (● minimum, ● maximum) and using pure water (●). Dashed line represents the nozzle position and grey arrow represents the cross-air flow direction

dosages per nozzle types and per air flow speed are compared. In general, the adjuvants allowed in all cases to obtain a certain potential drift reduction. Significant difference between the two adjuvants were detected [$F(1,68) = 98.810, p < 0.001$] with adjuvants A reaching the best performances, with values comprised between 62 and 30% irrespective the nozzle type. Meanwhile the adjuvants B reached potential drift reduction in the range of 26 and 9%. Interestingly the dosage did not significantly affect the potential drift reduction [$F(1,68) = 0.850, p = 0.360$], thus increasing the dosage from the minimum to the maximum prescribed by the label no significant further benefits can be achievable using both adjuvants. No significant interaction was detected between adjuvant and dosage [$F(1,68) = 0.036, p = 0.849$]. Finally, in all cases, lower potential drift reduction was achieved when the higher cross-air flow was used, meaning that the effects of adjuvant were not enhanced by the worst wind speed conditions as happen when air induction nozzles (SDRT) is compared to the conventional one. As final remarks, the reduction achieved by conventional nozzle is much more interesting and important than those achieved by air induction nozzles. Indeed, comparing the spray profiles in Figs. 1 and 2 it is clear that combining adjuvants with conventional nozzles the travelling distance of small droplets spray fraction, blown away by the air currents, can be strongly reduced.

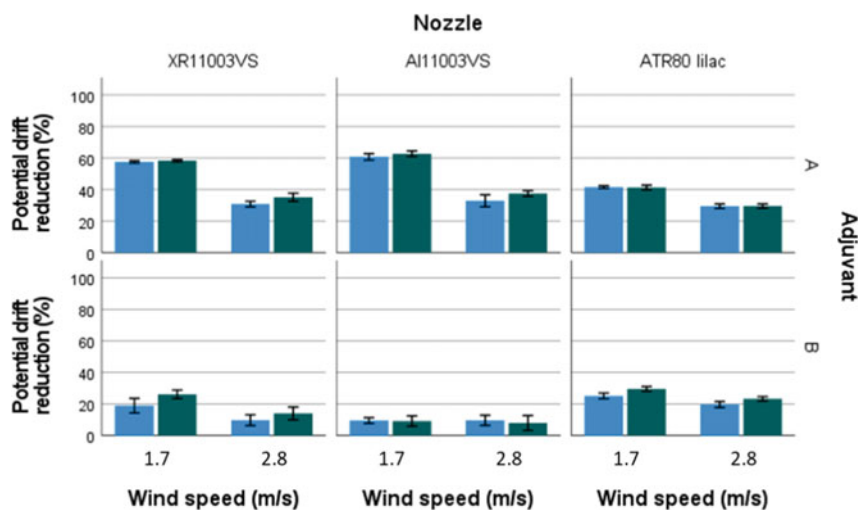


Fig. 2 Potential spray drift reduction (%) achieved by the three nozzle types using the two formulations (A and B) at minimum (●) and maximum (●) dosage under two different wind speed conditions

4 Conclusion

Adjuvants can be considered an interesting option to reduce the spray drift during spray application. However, testing their capability to reduce potential spray drift case by case is essential as different formulation can lead to completely different capability to reduce spray drift. Even if in combination with air induction nozzles they can further contribute to reduce spray drift, the most interesting usage is when combined with conventional (both flat fan and hollow cone) nozzles generally used with boom sprayers for arable crops and airblast sprayers for bush/tree crops, respectively.

References

1. Grella, M., Gallart, M., Marucco, P., Balsari, P., Gil, E.: Ground deposition and airborne spray drift assessment in vineyard and orchard: the influence of environmental variables and sprayer settings. *Sustainability* **9**(5), 728 (2017)
2. Grella, M., Marucco, P., Zwertvaegher, I., Gioelli, F., Bozzer, C., Biglia, A., Manzone, M., Caffini, A., Fountas, S., Nuyttens, D., Balsari, P.: The effect of fan setting, air-conveyor orientation and nozzle configuration on airblast sprayer efficiency: insights relevant to trellised vineyards. *Crop Prot.* **155**, 105921 (2022)
3. Van de Zande, J.C., Holterman, H.J., Wenneker, M.: Nozzle classification for drift reduction in orchard spraying: identification of drift reduction class threshold nozzles. *Agric. Eng. Int. CIGR Ejournal* **10**, 1–12 (2008)
4. Grella, M., Miranda- Fuentes, A., Marucco, P., Balsari, P., Gioelli, F.: Development of drift-reducing spouts for vineyard pneumatic sprayers: measurement of droplet size spectra generated and their classification. *Appl. Sci.* **10**(21), 7826 (2020)
5. Garcerá, C., et al.: Comparison between standard and drift reducing nozzles for pesticide application in citrus: Part II. Effects on canopy spray distribution, control efficacy of *Aonidiella aurantii* (Maskell), beneficial parasitoids and pesticide residues on fruit. *Crop. Protect.* **94**, 83–96 (2017)
6. Hilz, E., Vermeer, A.W.P.: Spray drift review: the extent to which a formulation can contribute to spray drift reduction. *Crop Prot.* **44**, 75–83 (2013)
7. Auweter, H., et al.: New approaches to optimize spray efficacy and foliar uptake. In: *Proceedings of 16th International Reinhardtsbrunn Symposium*, pp. 317–324. DPG Selbstverlag, Braunschweig (2011)
8. Oliveira, R.B., Antuniassi, U.R., Gandolfo, M.A.: Spray adjuvant characteristics affecting agricultural spraying drift. *Engenharia Agrícola* **35**(1), 109–116 (2015)
9. Lan, Y., Hoffmann, W.C., Fritz, B.K., Martin, D.E., Lopez, J.D.: Spray drift mitigation with spray mix adjuvants. *Appl. Eng. Agric.* **24**(1), 5–10 (2008)
10. International Standard Organization: ISO5682–1:2017 - Equipment for crop protection - Spraying equipment - Part 1: Test methods for sprayer nozzles. International Organization for Standardization: Geneva, Switzerland, pp. 1–35 (2017)

Whole-Body Vibration for Tractor Drivers



Rino Gubiani, Nicola Zucchiatti, and Ugo Da Broi

Abstract Among the main health risks for operators in the agricultural sector, exposure to mechanical vibrations is certainly one of the most difficult factors to quantify, in relation to the continuous and heterogeneous use of agricultural machinery during the agricultural year. According to data provided by the European Agency for Safety and Health at Work (EU-OSHA), 24% of workers in the European Union are exposed to mechanical vibration. Italian workers result to be exposed to the risk of this physical agents with frequencies around 21%. In reason of this data and in order to avoid the consequences of exposure to vibrations on workers' health, it is therefore necessary to carry out a risk analysis in the workplace and, where necessary, to take appropriate preventive measures. The aim of our research was, therefore, to measure vibration exposure and disturbances that can be transmitted while driving agricultural tractors. In particular, the vibrations transmitted, through the seat, at the lumbar spine, lumbosacral spine and cervical-dorsal junction were assessed.

The results showed that the vibrations were evenly distributed over the entire spinal column without statistically significant differences depending on the areas sampled. In some cases, higher accelerations were observed in the cervical-dorsal area, probably due to the vibrations transmitted by the steering wheel. The analysis of whole-body vibration transmission in relation to the different fat mass (BMI) of the operators involved in the tests showed no significant differences moment.

Keywords Body index · effect vibration on health · tractor driver vibrations · vibration

R. Gubiani (✉) · N. Zucchiatti · U. Da Broi
Department of Agricultural, Food, Environmental and Animal Sciences (D4IA), University of Udine, Via delle Scienze 208, 33100 Udine, Italy
e-mail: rino.gubiani@uniud.it

© The Author(s), under exclusive license to Springer Nature Switzerland AG 2023
V. Ferro et al. (eds.), *AIIA 2022: Biosystems Engineering Towards the Green Deal*,
Lecture Notes in Civil Engineering 337,
https://doi.org/10.1007/978-3-031-30329-6_62

605

1 Introduction

The vibrations of agricultural tractors are high and the relationships between this amount of vibration and the effects on the human body are still not well studied, and it has been estimated that in tractor drivers the energy load of acceleration is even higher than in other categories such as excavators, wheel loaders and tram drivers [1, 2]. This is due both to the intrinsic characteristics of our agriculture [3] and to the technical obsolescence of the machines, which in 75% of the tractors in circulation is more than 25 years old. Vibrations, on the other hand, are a complex event and not easily perceived by everyone, both because of the physical phenomenon itself and because the effects manifest themselves over the long term.

This is why much research has been conducted in recent years [4, 5] finding high levels of exposure during transfers and in the use of old tractors. From the point of view of the pathologies that can be manifested, vibrations transmitted to the whole body involve risks such as lumbago and traumatism to the spinal column. In fact, the vibration spectra measured on tractor seats show maximum accelerations between 2.5 and 6 Hz [6, 7]. Biodynamic studies have shown that the lumbar spine of a seated driver subjected to vibrations has a resonance frequency precisely between 2 and 6 Hz and the vibrations transmitted by tractors are located precisely on these frequencies and the vertebrae most affected are L4-L5 where the maximum compressive force is also developed during all tractor driving operations. Another important factor positively correlated with vibration exposure levels is the increase in forward speed [8, 9]) and this phenomenon is more evident on dirt road than on asphalt and at the expense of the x-axes and z-axes.

The soil, where the machine operates, influences the vibration level, wet or soft the vibrations decrease hard increase [10] as the particles that make up the soil affect the behaviour of the tyre. On the soil-vibration interaction, many studies have been carried out and it has also been noted that slightly moist soil conducts less vibration to the operator in comparison to dry soil and that the driver with the highest body fat mass reduces these vibration phenomena even more [11].

The most important variable, however, is the seat, as it can dampen vibrations and thus provide greater comfort [12]. In fact, testing a seat with polyurethane as a shock absorber dampened the vibrations transmitted by the tractor. Other parameters were measured on the seat such as the seat plane, the curvature of the backrest and its angle of inclination [13]. Further tests were carried out by comparing a wheeled tractor with a crawler tractor when performing some work with varying ground inclinations [14], however, the slope did not seem to have an effect on the vibration level. The effect of the age in hours of the tractor related to its wear and tear was also studied and it was found that up to 3000 h worked, the risk is low, between 3000 and 6000 h, the risk is medium and above 6000 h, the risk becomes high [15]. From the point of view of human physiology, the weight of the drivers, who were 63, 69 and 78 kg respectively, was taken into consideration and it was observed that the person with a greater body mass suffered less vibration disturbance [16]. The latest research with the study of vibrational patterns on the human body [17] and on sitting in the seat

goes in this direction. Research shows that leaning fully back in the seat has the greatest effect of vibrations on the body [18].

The low-frequency vibration generated by the wheels in contact with the ground is similar to the natural frequency of human organs. And to study this, an experiment was conducted to collect human physiological indicators relevant to vibration fatigue such as surface electromyography, skin electricity, skin temperature and photoplethysmography signal while subjects were subjected to vibration on a seat. The results of the test showed that with increasing human fatigue, the overall physiological parameters show the following trends: the median frequency of the surface electromyography of the human body and the slope of the skin surface temperature decrease, the value of the skin conductivity and the mean value of the photoplethysmography signal increase [19].

On the basis of the state of the art that is being addressed on the human factor and the effects of vibrations on the human body, the University of Udine undertook a study aimed at investigating the vibrational phenomenon related to the BMI (body mass index) of operators at different seats and treatments.

2 Material and Methods

To evaluate the effect of vibrations on the human body, a new, non-standardised methodology was tried out by placing the sensor not only on the seat but also on the driver's body. For this purpose, several tests were conducted between 2021 and 2022.

The first series of tests took place in September and October 2021 and were carried out at the "Antonio Servadei" didactic-experimental university farm of the University of Udine as follows:

- 2 drivers (1 and 2 in Table 1) with different BMI;
- 2 different tractors (Table 2)
- 2 speeds;
- 3 different positions of sensor (seat, lumbar, cervical)
- 2 replicates for each factor ($2 \text{ BMI} \times 2 \text{ tractors} \times 2 \text{ speed} \times 3 \text{ position}$), 48 tests.

The measurements were carried out with standard tyre pressures while driving on a dirt road. The speeds used for the field tests, which were similar but not perfectly equal due to the different gearbox configurations for both tractors, were.

Table 1 Characteristic of drivers enter in the test

Driver	1	2	3
Age (years)	58	54	60
Tall (cm)	185	168	182
BMI	46.3	24.8	27.2

Table 2 Characteristic of the tractors

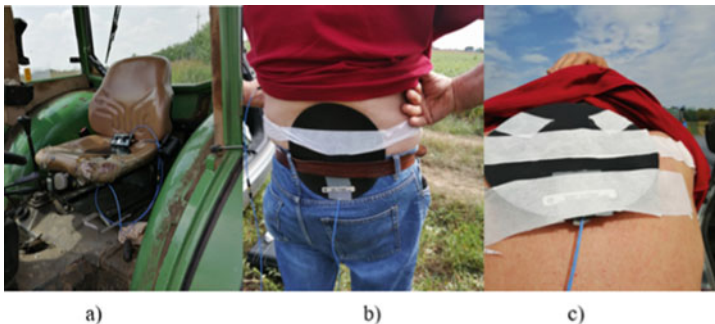
Tractor	1	2
Brand	FIAT 680	New Holland T4
Wheeled	2WD	FAWD
Engine (kW)	51	44
Age (years)	35	9
Hours	11,545	1725
Seat suspension	Mechanic with spring	Mechanic with bellow
Cab suspension	Silent block	Silent block

-for the Fiat 680 tractor, the V1 (low) speed was 10.9 km/h obtained using 1st fast gear at an engine speed of 1500 rpm, while the V2 (high) speed was 15.9 km/h with the gearbox positioned in 4th fast and an engine speed of 1600 rpm;

- for the New Holland T4/F tractor, the V1 speed was 10.6 km/h obtained in 1st gear and 1500 rpm engine speed, while the V2 speed was 16.1 km/h with gearbox in 4th gear and engine speed of 1600 rpm.

The measurement of the vibrational levels was performed with a triaxial accelerometer, Larson & Davis HVM 200, with pillow support (Fi. 1), fixed respectively to the seat for the lumbo-sacral measurements, to the back (at level L10–L12) and neck of the operator for the verification of the vibrational impact at the lumbo-sacral spine (LS) points around mid-back (LL) cervical-dorsal junction (CD). Measurements are taken every second (Fig. 1).

The field test was carried out by operating the agricultural machines on a dirt road of approximately 500 m with a duration of therefore 160 s at the lowest speed and 110 s at the highest speed. The aim of this procedure was to have sufficient bearing capacity so that the ground would have stable and non-deformable characteristics as a result of repeated stresses transmitted by the tractors during repeated passages.

**Fig. 1** Position of sensors: **a** seat; **b** lumbosacral spine (LS); **c** cervical-dorsal junction (CD)

A second test, carried out in November 2021, was carried out with only one operator (number 3 Table 1) again using the two tractors (Table 2) from the first test only with the lower speed of 10.6 and 10.9 km/h along the same track as the first test in order to obtain further answers on the transmissibility of vibrations on the body.

Finally, a third series of tests was carried out in August 2022. In this case only the tractor was used, again the FIAT 680 with the same triaxial accelerometer and the same driver 3 of the 2021 tests and the same speed, for the FIAT 680 tractor the V1 (low) speed was 10.9 km/h obtained using 1st gear at 1500 rpm engine speed, but with a different position on the seat so as to decouple the contribution of the hands from the steering wheel. So the tractor was driven using the steering wheel and without using the steering wheel to highlight the contribution of vibrations attributed to the steering wheel. In this case, the route, again about 500 m long on grassland, was almost linear so that the test could be carried out without excessive difficulty.

3 Results

The results of the first test showed that BMI has no effect on vibration transmission. The hypothesis that vibrations could be dampened by a higher BMI was not significant (Table 3). The table shows that there is a correlation between vibration and sensor position on the body and vibration and sensor axes with greater significance for the vertical (z) axis.

In Figs. 2 and 3 we see the different behaviour of the seats of the two tractors. Although the two machines are technologically different and have different ages and

Table 3 Correlations in the first test

	MBI	speed	vibration	position	sensor
MBI Pearson Corr	1	0	0.069	0	0
Sig.(2-tailed)	72	1	0.564	1	1
N	72	72	72	72	72
Speed Pearson Corr	0	1	0.132	0	0
Sig.(2-tailed)	1	72	0.270	1	1
N	72	72	72	72	72
vibrtion Pearson Corr	0.069	0.132	1	0.317*	0.668*
Sig.(2-tailed)	0.564	0.270	72	0.007	0
N	72	72	72	72	72
position Pearson Corr	0	0	0.317*	1	0
Sig.(2-tailed)	1	1	0.007	72	1
N	72	72	72	72	72
sensor Pearson Corr	0	0	0.668*	0	1
Sig.(2-tailed)	1	1	0	1	72
N	72	72	72	72	72

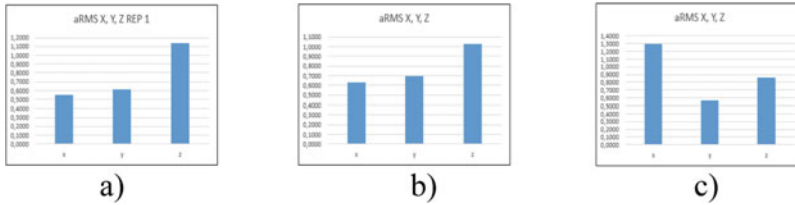


Fig. 2 Whole body vibration on FIAT 680 at 10.6 speed: **a** seat; **b** lumbo-sacral; **c** cervical position of sensor

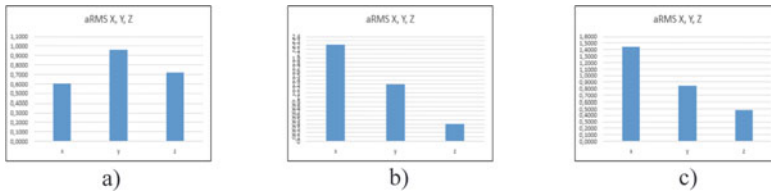


Fig. 3 Whole body vibration on NH T4 at 10.9 speed: **a** seat; **b** lumbo-sacral; **c** cervical position of sensor

seats, there is little difference in terms of vibration, understood as the sum of the three horizontal and vertical components, but if we look at the seat of the tractor NH T4, vibrations are dampened on the vertical axis, while they increase on the Y and X axes, a phenomenon that is evident while driving, as the meandering is much more evident on this seat than on the seat of the tractor FIAT 680.

With regard to the effect of speed on the phenomenon of vibration propagation, a positive correlation is noted between increased speed and vibrations, especially in the z-axis, while a lesser effect is noted in the y-axis, a phenomenon already observed by other authors (Table 4).

This meandering effect decreases the acceleration on the Z-axis, but remains evident at the level of the sensor placed at cervical level on both tractors and on all drivers because the head, which weighs about 7% of the body weight, is very heavy and undergoes this acceleration, which is borne by the cervical vertebrae.

Figure 4 shows the averages of the frequencies on the three axes. We can immediately see that the frequencies with the greatest impact are on the Z-axis with frequencies between 2 and 4 Hz. We must remember that vibrations around 2 Hz are the most dangerous because at 2 Hz the resonance of the head occurs due to longitudinal vibrations while sitting and between 2 and 6 the resonance of the whole body while sitting, which is also the resonance for the thoracic-abdominal organs that can then cause problems for the respiratory system while problems for the visual field due to the movement of the head.

In the second series of tests, the effect of the two tractors on the same driver was observed. From Table 5 it can be seen that there is no effect between the two tractors in terms of overall vibration.

Table 4 Correlation in the test with two tractors and two driver.

	MBI	possensor	speed	x	y	z
MBI Pearson Corr	1	0	0	0.323	0.160	-0.406
Sig.(2-tailed)	12	1	1	0.306	0.619	0.191
N		12	12	12	12	12
Possensor Pearson Corr	1	1	0	-0.363	0.268	0.003
Sig.(2-tailed)	12	12	1	0.247	0.401	0.992
N1			12	12	12	12
Speed Pearson Corr	0	0	1	0.546	0.655*	0.710*
Sig.(2-tailed)	1	1	0	0.066	0.210	0.100
N	12	12	12	12	12	12
x Pearson Corr	0.323	-0.363	0.546	1	0.640	0.180
Sig.(2-tailed)	0.306	0.247	0.066	12	0.843	0.575
N	12	12	12		12	12
y Pearson Corr	0.160	0.268	0.655*	0.640	1	0.594*
Sig.(2-tailed)	0.619	0.401	0.210	0.843	12	0.420
N	12	12	12	12		12
z Pearson Corr	-0.406	0.003	0.710*	0.180	0.594*	1
Sig.(2-tailed)	0.191	0.992	0.100	0.575	0.420	12
N	12	12	12	12	12	

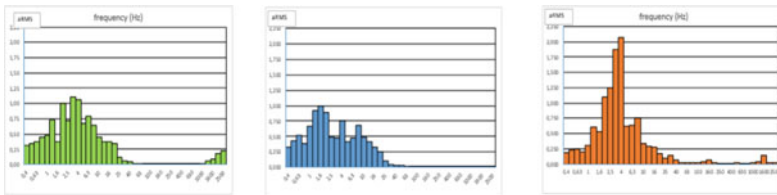


Fig. 4 Frequency of vibration during the first test

Table 6 shows the test with hands on the steering wheel and without. As can be seen, there is no correlation, but in spite of this, if we go to analyse the average of the 4 repetitions, it must be noted, however, that the vibrations are always higher than the legal limit of 8 h (1.06 x; 0.61 y; 0.92 z).

4 Conclusions

This first series of tests is the result of a collaboration between the Agricultural Engineering and Medical Engineering groups in order to verify the effects of vibrations on the human body and transmission through bone structures and organs. During the

Table 5 Correlation in the test with two tractors and one driver

	possens	speed	x	y	z
Possens Pearson Corr	1	0	0.671	-0.476	-0.670
Sig.(2-tailed)	6	1	0.144	0.340	0.154
N1	6	6	6	6	6
Speed Pearson Corr	0	1	-0.160	0.547	-0.115
Sig.(2-tailed)	1	6	0.977	0.261	0.828
N	6	6	6	6	6
x Pearson Corr	0.671	-0.160	1	0.100	-0.236
Sig.(2-tailed)	0.144	0.977	6	0.851	0.653
N	6	6	6	6	6
y Pearson Corr	-0.476	0.547	0.100	1	0.277
Sig.(2-tailed)	0.340	0.261	0.851	6	0.595
N	6	6	6	6	6
z Pearson Corr	-0.670	-0.115	-0.236	0.277	1
Sig.(2-tailed)	0.154	0.828	0.653	0.595	6
N	6	6	6	6	6

Table 6 Correlation to drive with hand on wheel and not

	hands	x	y	z
hands Pearson Corr	1	0.857	0.116	-0.503
Sig.(2-tailed)	4	0.143	0.884	0.497
N	4	4	4	4
x Pearson Corr	0.857	1	0.566	0.010
Sig.(2-tailed)	0.143	4	0.434	0.990
N	4	4	4	4
y Pearson Corr	0.116	0.566	1	0.768
Sig.(2-tailed)	0.884	0.434	4	0.232
N	4	4	4	4
z Pearson Corr	-0.503	0.010	0.768	1
Sig.(2-tailed)	0.497	0.990	0.232	4
N	4	4	4	4

research, an attempt was made to construct a new methodology to correlate vibrations on agricultural machinery with the effects on the human body. This was only a first series of tests that provided some results such as the independence of BMI with the vibrations transmitted by tractors while verifying that there is a positive correlation between increased tractor speed and increased vibrations. Another important result is that with the current seats, which are normally mounted on tractors, vibrations are reduced very little and, above all, those very dangerous to human health, which are between 2 and 4 Hz, are not reduced.

References

1. Gores, B., Ellegast, R., Hermanns, I., Raffler, N., Rissler, J.: Assessing combined exposures of whole body vibration and awkward posture – further results from application of a simultaneous field measurement methodology. *Ind. Health* **48**, 638–644 (2010)
2. Peretti, A., Carletti, E., Pedrielli, F., Jacopo, G.: Vibration tests on an agricultural tractor equipped with advanced vibration control systems for different configurations. *Atti di convegno (in stampa)*. Società italiana di Acustica (2019)
3. Peretti, A.: Analisi delle vibrazioni su trattori agricoli in normali condizioni di lavoro e in condizioni predefinite. In: *Rivista Italiana di Acustica* **39**(3), 90–103 (2015)
4. Scarlett, A.J., Price, J.S., Stayner, R.M.: Whole-body vibration: evaluation of emission and exposure levels arising from agricultural tractors. *J. Terramechanics* **44**(1), 65–73 (2007)
5. Pessina D., Bonalume V.: Esposizione a vibrazioni nella filiera viticola. *Convegno AIIA, Ischia*, 12–16 settembre (2009)
6. Bovenzi, M., Betta, A.: Low-back disorders in agricultural tractor drivers exposed to whole-body vibration and postural stress. *Appl. Ergon.* **25**(4), 231–241 (1994)
7. Bonomini, F., et al.: Analisi delle vibrazioni su trattori agricoli in normali condizioni di lavoro e in condizioni predefinite. *Rivista Italiana di Acustica* **39**(3), 1 (2015)
8. Mohan, D.M., Adarsh, K., Indra, M.: Whole body vibration on drivers seat and fender with fully loaded. *J. AgriSearch* **8**(2), 149–154 (2021). ISSN: 2348–8808 (Print), 2348–8867 (Online)
9. Pessina, D.: Valutazione delle vibrazioni sul sedile di guida di un trattore convenzionale equipaggiato con differenti pneumatici radiali. *Atti del convegno nazionale AIGR Il ruolo dell'ingegneria per l'agricoltura* **2000**, 429–440 (1993)
10. Laib, L.: Analysis of the vibration-excitation effect caused by deformable soil surfaces. *J. Terramechanics* **32**(3), 151–163 (1995)
11. AL-Mafrachi, A. A. A. H., et al.: Whole body, arm-hand vibration and performance drivers tractors during conservation tillage under different velocity and soils. *Int. J. Adv. Eng. Manag. Sci. (IJAEMS)* **2**(1), 239362 (2016)
12. Mehta, C.R., Tewari, V.K.: Damping characteristics of seat cushion materials for tractor ride comfort. *J. Terramechanics* **47**(6), 401–406 (2010)
13. Tewari, V.K., Prasad, N.: Optimum seat pan and back-rest parameters for a comfortable tractor seat. *Ergonomics* **43**(2), 167–186 (2000)
14. Catania, P., Vallone, M.: Whole body vibrations during field operations in the vineyard. *J. Agric. Eng.* **44**(s2), e143, 710–714 (2013)
15. Vallone, M., Bono, F.: Risk exposure to vibrations and noise in the use of agricultural track-laying tractors. *Ann. Agric. Environ. Med.* **23**(4), 591–597 (2016)
16. AL-Mafrachi, A.A.A.H.: Whole body, arm-hand vibration and performance drivers tractors during conservation tillage under different velocity and soils. *Int. J. Adv. Eng. Manag. Sci. (IJAEMS)* **2**(1), 239362 (2016). ISSN: 2454–1311.
17. Singh, A., Singh, I., Kalsi, S.: Transmissibility evaluation of whole-body vibration using three-layer human CAD Model. *J. Inst. Eng. India Ser. C* **101**(3), 595–602 (2020). <https://doi.org/10.1007/s40032-020-00559-6>.
18. Adam, S.A., Jalil, N.A., Rezali, K.M., Ng, Y.G.: The effect of posture and vibration magnitude on the vertical vibration transmissibility of tractor suspension system. *Int. J. Ind. Ergon.* (2020) <http://www.elsevier.com/locate/ergon>.
19. Gao, R., Yan, H., Yang, Z.: Evaluation of tractor driving vibration fatigue based on multiple physiological parameters. (2021). <https://doi.org/10.1371/journal.pone.0254636>.

A Facilitating Machine for Silkworm Rearing



Rino Gubiani and Nicola Zucchiatti

Abstract The Silkworm breeding is an activity that was formerly practiced in China and began in Friuli Venezia Giulia (Italy) between 1400 and 1500 AD. In the Friuli countryside declining after 1950 and all attempts to revive this industry have subsequently failed for various reasons, not least the lack of adequate technology. The problem of producing silk today is in fact linked to the design and construction of machinery to facilitate silkworm rearing so as to make it attractive to farms in terms of both working conditions and production. The SILK project financed by the Friuli Venezia Giulia region was conceived within this framework with the aim of relaunching silk production. The agricultural mechanization research group of DI4A of the University of Udine took charge of the design and construction of a prototype of a facilitating machine for the first larval ages of the silkworm.

The objectives conceived for the prototype machine were to allow the silkworm rearer to easily and relatively quickly manage the cleaning of the bedding with the aid of stainless steel trays fitted with mesh or perforated paper. To have also the possibility of keeping the silkworms on stackable shelves so as to rationally exploit the surface area of the available rooms.

The design phase was done in CAD and then the machine was built, assembled and brought to a silkworm farmer where the first tests were carried out to check the advantages compared to the manual operations adopted up to that moment.

Keywords silk · silk machinery · machine design · silkworm breeding

1 Introduction

Silk is produced by silkworm (*Bombyx mori*) for spinning its cocoon and it is a fibrous protein, which is light in weight, soft to touch, has high durability, natural sheen and

R. Gubiani (✉) · N. Zucchiatti
Department of Agricultural, Food, Environmental and Animal Sciences (D4IA), University of Udine, Via Delle Scienze 208, 33100 Udine, Italy
e-mail: rino.gubiani@uniud.it

integral affinity for dyes. The process of mass scale rearing of silkworms to obtain silk is called “sericulture”. Asia contributes to more than 95% of the total global silk output and therefore is considered as the main silk producer globally. China, are the main bulk producer of the world (Table 1) However, the widespread availability of synthetic fibers at low cost caused a decline in interest in silk. Sericulture began in Friuli and Veneto between 1400 and 1500 AD when the Venetian Republic began producing, weaving and exporting the silk produced by rearing silkworms. As is well known, the silkworm can only feed on the leaves of plants of the genus *Morus* (family Moraceae), in particular *Morus alba* (white or common mulberry) and *Morus nigra* (black mulberry), and so there was a massive and rapid propagation of the cultivation of this tree species, which has come to characterise the Friuli-Veneto landscape to this day. Sericulture set up by the Serenissima began to change towards the end of the eighteenth century after the Friulian economist, Antonio Zanon, became convinced that a potentially profitable market lay in the possibility of having small family businesses produce cocoons and in the 1800s, following this increased awareness, silkworm breeding expanded rapidly in the Friulian and Veneto countryside, and it is on this tradition of businesses that we want to leverage to relaunch sericulture.

An initial setback to silkworm breeding in Friuli and Veneto was brought about by the autarchy laws of the Mussolini government, as silk was almost exclusively exported abroad, which led to a drastic reduction in income. In the post-war period, Italian sericulture experienced a progressive decline due to competition from the eastern market. It is worth remembering that in 1924, 57,000 tonnes were produced in Italy, which dropped to 13,000 in 1950, 7,000 in 1959 and almost disappeared around 1970. The 1990s saw the failure of the attempt to bring sericulture back to our territory and the causes were to be found in the spread of a phytosanitary product (*fenoxycarb*) for the defence of apple, peach trees, etc. against *tortrix* beetles, but which, when deposited on mulberry trees, caused harmful effects on silkworms but since 2012 this plant protection product is no longer authorised (Table 2).

On the other hand, China’s silk production is also declining, especially as regards the quality product, as a result of the increase in the labour force, while, as far as the

Table 1 World silk production in the world (in t)

Country	2014	2018	2020
China	146,000	120,000	53,359
India	28,708	35,261	33,770
Uzbekistan	1,100	1,800	2,037
Vietnam	420	680	969
Thailand	692	680	520
Brazil	560	650	377
North Korea	320	350	370
Japan	30	20	16
Turkey	32	32	5
Italy	3.5	2.8	2

Table 2 Country by Import and export fabrics of silk in 2020

Country	Import (t)	Country	Export fabric (millions \$)
India	3,263	China	276
EU	1,563	Italy	137
Romania	1,224	India	44.2
Italy	639	Japan	40.7
Vietnam	566	France	38
Japan	292	Uzbekistan	20.2

organisation of work is concerned, it has remained the same as in the last century. These conditions, therefore, could pave the way for a new development in sericulture, bearing in mind that the problem of the increasingly invasive presence of nano- and microplastics is also growing. In this regard, it is necessary to remember that in our society, plastics are a ubiquitous component of everyday life and are found in household goods, furnishings, clothes, packaging, cars and the most technological items. Plastics are light, versatile, inexpensive, and durable. This is why they have replaced conventional materials such as metals, glass, paper and even silk in many uses. Synthetic fibres in clothing account for 60% of the total consumption of plastics such as polyester, polyamide, acryl, etc., to name the best known [1]. Mechanical degradation is particularly important for synthetic fibres, and the domestic washing machine is the major source of microplastics due to the action of the internal water current, abrasions and impacts during washing [2], while it has been found that the wear and tear of garments can release microplastic fibres directly into the air [3].

In all countries, however, the issue of new silk development is need increase research conducted in this sector about [4]:

- mulberry farming and mechanisation of leaf collection;
- facilities in silkworm rearing with suitable environments and equipment.

As can be seen from Table 1, production is declining almost everywhere because, as previously mentioned, the rearing technique is still traditional and therefore there is a need to design and build machines to facilitate the work of silkworm rearing so as to make it attractive to farms from the point of view of both working conditions and production. Even in Indian publications, these are still rearing stands made of wood or bamboo [5]. In China, where the drop in production has been very conspicuous in recent years, attempts have been made to mechanise part of the breeding management and new methods are being tried out to improve frame cleaning [6]. The rearing devices were an assembly one equipped with wheels, and its weight was reduced so that the convenience was improved. In the budget of labour hour, the devised collecting equipment have reduced the labour of traditional handy work to 65% and the productivity of labour (kg/hour) was increased to 55%. The cost of production was also decreased to 35.9% [7].

Another problem is the reduction of space, which in traditional flat structures is usually very large.

Within this framework, the “SILK” project financed in 2018 by the Friuli Venezia Giulia region under the 2014–2020 RDP was conceived with the aim of relaunching silk production. The project not only envisages a structuring of silk into “silk districts”, where alongside the study of new machines to facilitate silkworm breeding, it also envisages relaunching mulberry cultivation, first through the study of the existing plant heritage, then to possibly plant new mulberry groves; finally, to look for new uses for silk (cosmetics) in addition to the traditional use of thread.

As part of this project, the Biosystem Engineering research group of the DI4A of the University of Udine took charge of the design and construction of a prototype of a facilitating machine for the first larval ages of the silkworm.

2 Material and Methods

The project’s objectives were to design a prototype in relation to rearing the first three larval ages, which are the most difficult to manage. The idea, in fact, is that in a silk district, a company rears the first three ages where it is necessary to feed more precisely with finely cut mulberry leaves and often clean the litter from vegetation residues, excrement and dead larvae: at the end of the third age, the worms are handed over to other companies to continue with the ground rearing, which is much more practical and needs less attention.

The project demands can be summarised as follows:

1. - facilitating machine that allows operation with one or two people standing or seated in an ergonomic position avoiding displacements;
2. - handle at least 3 frames (20,000 eggs per frame) (Table 3);
3. - facilitate litter cleaning and reduce working time;
4. - easy feeding of worms;
5. - easy temperature and humidity management;
6. - compliance with workplace safety regulations.

Table 3 Standard parameters for a polyhybrid silkworm farm (20,000 eggs) [8]

Stage	Spacing of each age (m ²). At beginning at the end		Mulberry leafs (kg)	T (C°)	Humidity (%) Start-Moulting	Durations (days) + moulting
1 st Instar	0.4	0.8	1.5–2.0	27	90–65	4–5 + 1
2 st Instar	1.0	1.8–2.0	3.0–4.0	26	85–65	3 + 1
3 st Instar	2.0	3.6–4.0	15–20	25	80–65	4 + 1
4 st Instar	4.0–4.5	8.0–10.0	65–70	25	75–60	5 + 1
5 st Instar	10	15–20	300–340	24	70	7–8
Total	–	–	385–436	–	–	27–29

The following solutions were chosen to answer the 5 questions posed during the prototype design phase:

- 1 - for the first objective, we opted for a wheel equipped with trays on stackable shelves to rationally exploit the surface area of the available rooms. In fact, by rotating the frames, this allows an employee to do all the operations while remaining in an almost fixed position without moving masses or moving considerably from the initial workstation. The trays can be locked either to allow an operator to work standing with the tray stopped at 1000–1200 mm in height or locked so that he can work seated with the tray stopped 700–800 mm from the ground;
- 2 - for the second objective, by calculating the surface area required at the third age, it was seen that at least 8 trays of 1.5 m² were needed for a total of 12 m² (Table 3);
- 3 - in order to facilitate the cleaning of the trays, AISI 304 stainless steel was chosen as the material, attached to a 2,500 mm × 600 mm frame. The trays were fitted with four small wheels at one end so as to facilitate their extraction either for complete tilting to discharge the dirt onto a container underneath or for partial extraction and cleaning with a Hoover. In the frame supporting the tray, small threaded bars (ø 5 mm × 50 mm in height) have been placed every 200 mm along the top of the frame so that a fibreglass construction reinforcing mesh with a mesh size of 11.0 × 10.0 mm or 5 × 5 mm can be attached, depending on the size of the larvae. On these threaded rods, metal spacers (washers) can be fitted to vary the distance of the net from the bottom of the tray and thus depending on the age of the larvae. In fact, at the beginning the larvae are placed on a sheet of paper on top of the tray and the net is placed a few mm above it so that the larvae can come up to feed. At the next feeding, the tray is cleaned and then the larvae are moved from above the netting to the newly replaced paper on top of the tray and the netting is put back on top and then this operation is repeated each time. During this phase, sorting must then be carried out in order to eliminate sick or weak larvae and those that have not moulted at the same time as the others (laggards). During this operation, the area occupied by the larvae must also be enlarged easily and quickly;
- 4 - the larvae of the first three ages should be fed with crushed mulberry leaves so the operation to be carried out is to feed over the net so that the larvae can climb up and eat. In this case, if the basket with the leaves is placed near the prototype, an attendant feeds in a few seconds and then proceeds to move another tray;
- 5 - humidity and temperature are essential to obtain good results for larvae growth, so the prototype was designed to have a certain distance between the trays for good ventilation and without an excessive excursion in height as in a room the temperature and humidity can be different between the lowest and highest points (Table 3);
- 6 - since it is a wheel that turns on a support frame to prevent random momentum during cleaning, control and feeding operations on the trays, the prototype is equipped with three safety systems: two wheel brakes on the frame, two pins for

additional safety in addition to the two brakes; a third pin to prevent the trays from swinging. An electric motor was not used to rotate the system, although the possibility of installing it in an eventual upgrade was envisaged, as this would have increased the design and safety systems costs and exceeded the planned budget.

The design of the prototype began in the spring of 2018 with some hand-made sketches on sheets of paper and then moved onto the AUTOCAD platform adapting the dimensions of the prototype to the environment in which it would be housed, 2.75 m high, 6 m long and 3 m wide. For this purpose, the prototype was designed in pieces to be able to pass even with a door opening of 2×2 m and then be assembled on site.

Once the design was finished on AUTOCAD, the design was taken to a metal carpentry company where it was constructed with some adaptations to the available commercial parts.

The prototype was then taken to a company in Aquileia (Friuli Venezia Giulia Region, Italy), where silkworm cultivation is practised, assembled and tested on half a canvas of silkworms (10,000 eggs), then in a reduced size, due to the lack of mulberry leaves, in autumn 2021 and spring 2022.

3 Results

The prototype was then taken to a company in Aquileia (Friuli Venezia Giulia Region, Italy), where silkworm cultivation is practised, assembled and tested on half a canvas of silkworms (10,000 eggs), then in a reduced size, due to the lack of mulberry leaves, in autumn 2021 and spring. The construction of the prototype was based on the design made with AUTOCAD (Fig. 1).

The wheel supports eight trays with a size of $2,500 \times 600$ mm and rotates on a shaft on a steel support frame like all parts of the machine. The trays are made of stainless steel and are supported by a support frame that allows the trays to be pulled out, drawer-style, with four castors for easy sliding. Threaded rods are placed on the edges of the trays so that the net and paper on which the worms are to be placed are hooked in such a way that they are raised off the bottom of the tray. The distance from the bottom can be varied by placing shims on the threaded bars (Fig. 2).

Two safety systems were then installed on the finished machine to prevent any risk of crushing hands during rotation. For the same purpose, an electric motor was

Fig. 1 Design of prototype

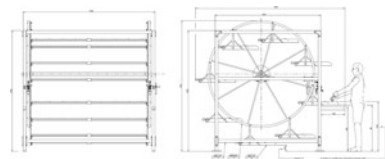


Fig. 2 Design of stainless steel box

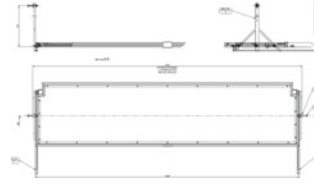
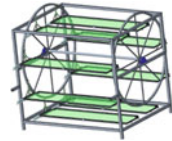


Fig. 3 3D visual of prototype



avoided to facilitate rotation, as the complexity of the safety systems would have increased considerably (Fig. 3).

In Fig. 4, painted in red, one can see the two brakes on the two wheels and a wheel spoke lock to safely block rotation when working on the drawers. On the drawers you can see the two hinges to lock the bottom of the drawer in the closed position.

Detail of the three locking systems: brake on the wheel; fork for fixing the wheel on the quadrangular element; wheel spoke lock (Figs. 5 and 6).

Tests of the prototype's functionality with bred worms yielded good results. From the measured times, the times are significantly reduced. Due to the difficulties on

Fig. 4 Safety system mounted on prototype



Fig. 5 Detail of the hinge for securing the bottom of the stainless steel drawer fitted with castors

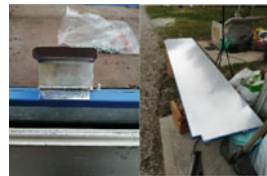
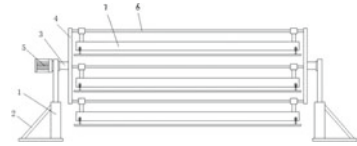


Fig. 6 First test with half standards eggs (10,000) of silkworm of first-generation



Fig. 7 Chinese patented prototype



the farm where the prototype was tested, caused by the problem of finding mulberry leaves, a comprehensive test could not be carried out. However, according to the operator, fatigue is much less and the ergonomic position was very good compared to the previous work. The analysis carried out to patent the prototype showed that a similar machine was patented [9] in China in 2020 (with coverage of China only) while the project (with first design of the prototype) on the Friuli Venezia Giulia RDP was in 2018 (Fig. 7).

4 Conclusions

Silk production has considerable potential in pharmaceuticals, beauty and textiles, especially in Italy, where fine garments are world-class. For silk production to become relevant again in Italy, equipment is needed to improve the ergonomics of work and its productivity. The prototype realised for the first three larval ages has proven that it can work properly and go in the direction of reducing costs, improving work ergonomics and can be installed in small companies. This, on the other hand, should only be the first in a series of equipment, such as, for example, the detaching of leaves from mulberry branches, and the extraction of the peel from cocoons, in order to provide farms with the appropriate facilitating machines and make sericulture viable and profitable again.

References

1. Cesa Flavia Salvador, Turra Alexander, Baruque-Ramos Julia. Synthetic fibers as microplastics in the marine environment: A review from textile perspective with a focus on domestic washings. *Science of The Total Environment*, Volumes 603–604, 15 December 2017, Pages 836.
2. Cesa Flavia Salvador, Turra Alexander, Leonardi, Baruque-Ramos Julia. Laundering and textile parameters influence fibers release in household washings. *Environmental pollution*, Volume 257, February 2020, 113553. <https://doi.org/10.1016/j.envpol.2019.113553>.
3. De Falco Francesca Cocca Mariacristina Avella Maurizio Thompson Richard C. Microfiber Release to Water, Via Laundering, and to Air, via Everyday Use: A Comparison between Polyester Clothing with Differing Textile Parameters. *Environ. Sci. Technol.* 2020, 54, 6, 3288.
4. Singh T., Nigam A., Kapila R., 2021. Innovations in silkworm rearing and importance: recent advances. *Journal of the textile association* 82/2 (87–90) (Jul-Aug).
5. Hatibaruah D., Borah D., Saikia N. Constraints Perceived By Farmers In Adoption Of Sericulture Production Technologies In Jorhat District Of Assam. *International Journal of*

6. Agricultural Science and Research (IJASR). ISSN (P): 2250–0057; ISSN (E): 2321–0087. Vol. 11, Issue 2, Dec 2021, 175–182.
7. Wenchu Li, Yangsheng Zhong, Fangyan Chen, Yeyuan Wang, Yangjin Zhong, Jianrong Lin (2017). Focus on Economic Benefits and the Most Appropriate Strategy of Sericulture in Yuexi Area of Guangdong, China. *Journal of Investment and Management* 2017;
8. Jung, I-Yeon; Kang, Pil-Don; Kim, Kee-Young; Lee, Sang-Uk; Kim, Mi-Ja Ryu, Kang-Sun,.; Development of Collecting System of Silkworm Excreta Using a Devised Equipment. *Journal of Sericultural and Entomological Science* **48**(1), 28–31 (2006).
9. Cappelozza Silvia (2010). Manuale di buona pratica agricola per la bachicoltura. CRA-APV, https://www.politicheagricole.it/flex/files/8/7/c/D.60d46250dbc0314586d7/manuale_pratica_bach.pdf.
10. Men Lei (2020). Patented number: CN210470715U U. Novel silkworm breeding frame facilitating silkworm feeding.

Intermittent Drying of Walnuts: Evaluations of Warm Air Consumption on a Thin Layer



Lorenzo Guerrini, Andrea Pezzuolo, Giovanni Ferrari, Giovanni Pippa, and Francesco Marinello

Abstract Walnuts trade standards require a maximum humidity of the 8% (w/w) to protect the commercialized fruits during their shelf-life. To achieve the target humidity, walnuts must be dried. During drying, the water migrates slowly from the inner to the outer parts of the fruits before its transfer to the warm air. However, the water migration is slow and the efficiency in the use of the drying heat is poor. The intermittent drying alternates periods when warm air is driven to fruits, with tempering periods allowing the water to diffuse on fruit surface. The aim of the work is to test if the intermittency in walnuts drying could provide advantages in the use of warm air and quantify them.

Two trials were carried out at laboratory scale to test the effect of the intermittent drying at different frequency and on shelled and in shell walnuts.

In the walnuts continuously dried were always the faster to complete the process. However, intermittent drying allowed to decrease the use of heated air roughly of the 30% at 30 min^{-1} and of the 25% at 60 min^{-1} . Considering shelled walnuts intermittent drying saved the 36% of time using heat air.

In conclusion, intermittency in walnuts drying could decrease the use of heat air of the process of roughly the 30–35%, and consequently it could improve process sustainability. Further improvement in the process sustainability could be achieved through the optimization of the intermittency conditions.

Keywords Drying · Heat use efficiency · In-shell walnuts · Shelled walnuts · Sustainability

1 Introduction

Nowadays, one of the main aims of several researchers is the improvement of processes sustainability. This goal is pursued either trying to produce clean energy

L. Guerrini (✉) · A. Pezzuolo · G. Ferrari · G. Pippa · F. Marinello
TESAF, Università Degli Studi Di Padova, Via Dell'Università 16, 35020 Legnaro, PD, Italy
e-mail: lorenzo.guerrini@unipd.it

© The Author(s), under exclusive license to Springer Nature Switzerland AG 2023
V. Ferro et al. (eds.), *AIIA 2022: Biosystems Engineering Towards the Green Deal*,
Lecture Notes in Civil Engineering 337,
https://doi.org/10.1007/978-3-031-30329-6_64

625

from by-products of the process [1, 2] and trying to save energy and materials during the processing [3].

Drying is a necessary operation to store walnuts. Moreover, fresh walnuts were harvested at humidity of roughly the 30% (wet basis – w.b), while commercial standards required a maximum humidity of the 8% w.b. [4]. Natural drying is often slow, labor-consuming, and, in certain areas climatic conditions do not allow to achieve the commercial humidity. Moreover, in the “Delta del Po” area, where the present study was conducted, natural drying allow to obtain minimum humidity of 15–16% w.b. Thus, in these cases, the use of forced drying is mandatory.

Different kinds of dryers are used for walnuts. The most spread in the study area were silo dryers with or without internal cochlea, and single/multiple layers dryers. Common control parameters in these dryers are the temperature, the air speed, and the amount of air recirculation [5]. The process temperatures are low, usually chosen between 32 °C and 40 °C to maintain the kernel quality, and consequently the drying times are high [6].

The traditional drying method uses air entering the system with constant temperature and speed. However, during drying, water evaporates from the surface of the product at a faster rate than that of movement within the sample [7]. Consequently, during the final stages of drying the same amount of energy is provided but there is not enough water to remove from the dry surface of the product.

Conversely, intermittent drying changes temperature or air flow during the process to obtain intervals of heating and resting (tempering) of the products. During the tempering phase the internal humidity of the product migrates by diffusion up to its surface, while warm air is not provided with the aim of reducing energy wastes. Moreover, by decreasing the actual drying time and the use of air, energy consumption is reduced [8]. The aim of this work is to test if intermittent drying is suitable for walnuts, and to quantify the operative effects.

2 Materials and Methods

2.1 Trial 1

The fresh walnuts used in Trial 1 were collected at Azienda Agricola Bellombra (Adria, Rovigo, Italy). Two different worldwide spread cultivars were tested, namely of *Chandler* (CP) and *Lara* (LP).

Walnuts underwent to different drying treatments. Treatments were:

- a continuous drying in a ventilated oven set at 38 °C;
- an intermittent drying, with cycles of 30 min at 38 °C in the same ventilated oven followed by 30 min at environmental temperature;
- an intermittent drying, with cycles of 60 min at 38 °C followed by 60 min at environmental temperature;
- a natural drying at environmental temperature.

Hence, from each walnut batch (LP and CP) 6 samples of roughly 1 kg weight were collected. One sample was assigned to the continuous drying, 2 samples to intermittent 30 min drying, 2 samples to the intermittent 60 min drying and 1 sample to the natural drying.

Fresh walnuts were initially characterized for humidity as follow; the initial weight was recorded, by placing a 100 g sample in oven at 105 °C Humidity was determined through weight difference until constant weight was reached. On a sample of 15 fruits, walnuts were also characterized for maximum length, weight of the whole walnut, kernel weight, and shell weight.

The drying kinetics were followed through the weight loss. Samples were periodically weighted until the target humidity of 8% (w.b.) was reached. Then, walnuts humidity was determined again to verify the end of process.

Temperature and air humidity were monitored by placing dataloggers (EL-USB2 RH/TEMP datalogger, Lascar Electronics, UK) in the environment, in the oven and directly in contact with on the walnuts of the different treatments.

2.2 Trial 2

In trial 2 only *Lara* cultivar was considered. The fresh walnuts were collected at Azienda Agricola Bellombra (Adria, Rovigo, Italy – LP2), and at Azienda Tenuta La Spiga (Eraclea, Venezia, Italy - LG). Trial 2 considered both in-shell and shelled walnuts. The shelled walnuts were obtained by manually removing the shells. The treatments tested in trial 2 were:

- a continuous drying in a ventilated oven set at 38 °C;
- an intermittent drying, with cycles of 30 min at 38 °C in the same ventilated oven followed by 30 min at environmental temperature;
- a natural drying at environmental temperature.

Walnuts were characterized for initial and final humidity, weight of the whole walnut, kernel and shell weights with the same methods described for trial 1.

3 Results and Discussion

Fresh *Lara* walnut had 40.59 ± 1.46 mm caliber, 21.84 ± 2.07 g total weight divided in 9.23 ± 1.38 g of kernel, and 12.60 ± 1.62 g of shell. Fresh *Chandler* walnut had 35.66 ± 2.17 mm caliber, and the weights of the whole fruit, kernel and shell were 16.42 ± 3.26 g, 6.03 ± 1.47 g, and 10.37 ± 2.12 g respectively. The walnuts dryings were modelled as first order kinetics according to the literature [9]. The resulting equation of the changing of walnuts humidity during drying was:

$$X_t = X_0 e^{-kt} \quad (1)$$

Table 1 Estimated model coefficients of each walnut drying trial 1. X_0 represents the initial moisture, and k the drying rate coefficient. The time required to reach the moisture required by the commercial standards is reported in the last column

Drying method	Batch	X_0	k (min^{-1})	R2	Time to $Y = 0.08$ (min)
Continuous	LP	0.36	$7.4 \cdot 10^{-4}$	0.999	1913
Intermittent (30')	LP	0.35	$6.3 \cdot 10^{-4}$	0.995	2215
Intermittent (30')	LP	0.35	$6.1 \cdot 10^{-4}$	0.996	2250
Intermittent (60')	LP	0.37	$5.1 \cdot 10^{-4}$	0.993	2825
Intermittent (60')	LP	0.36	$5.7 \cdot 10^{-4}$	0.999	2503
Continuous	CP	0.41	$8.3 \cdot 10^{-4}$	0.996	1861
Intermittent (30')	CP	0.45	$5.3 \cdot 10^{-4}$	0.986	3061
Intermittent (30')	CP	0.45	$5.3 \cdot 10^{-4}$	0.994	3085
Intermittent (60')	CP	0.46	$5.0 \cdot 10^{-4}$	0.987	3324
Intermittent (60')	CP	0.42	$5.9 \cdot 10^{-4}$	0.994	2687

where X_t is the walnut humidity on dry basis at time t , X_0 is the initial walnut humidity, k is the drying rate and t is the time (min).

Results are shown in Table 1.

First order kinetics were able to well describe the walnuts drying, being the lower R^2 among the models 0.993. The walnuts continuously dried were the faster to reach the humidity required by the commercial standards (i.e., 0.08 on wet basis, corresponding to 0.087 on dry basis). However, in the 2 intermittent drying methods the heated air was used the 50% of the time, halving the effective drying time. The comparison among the effective heating time required is shown in Fig. 1.

Intermittent drying allowed to decrease the use of heating for both the walnuts cultivars. In Lara walnuts the more pronounced decrease was found in 30' intermittent drying, allowing to reduce the heating time of the 41.6% on the average, while a reduction of the walnuts heating time of the 30.4% was found for 60' intermittent drying. The advantage provided by intermittent drying was less pronounced in Chandler walnuts, reducing the heating time on the average of the 18.3% without significant differences between the frequencies of intermittence.

Data allow to calculate to easily calculate the water flow rate from walnuts in each interval of the drying curve (G_{ev} [$\text{g}_{\text{water}}/\text{min}$]), as in Eq. (2):

$$G_{ev} = (X_t - X_{(t+1)})/TI \quad (2)$$

where X_t is the humidity measured at time t [$\text{g}_{\text{water}}/\text{g}_{\text{dm}}$], X_{t+1} is the humidity in the subsequent measurement time [$\text{g}_{\text{water}}/\text{g}_{\text{dm}}$] and TI is the length of the time interval [min]. Consistently to the above presented results, the G_{ev} decreased during drying. Differences could be easily noticed in Fig. 2. The G_{ev} during time could be successfully regressed as a line with a negative slope for continuous drying. Conversely, in the intermittent drying, 2 G_{ev} s could be seen, and 2 separate regressions have to be

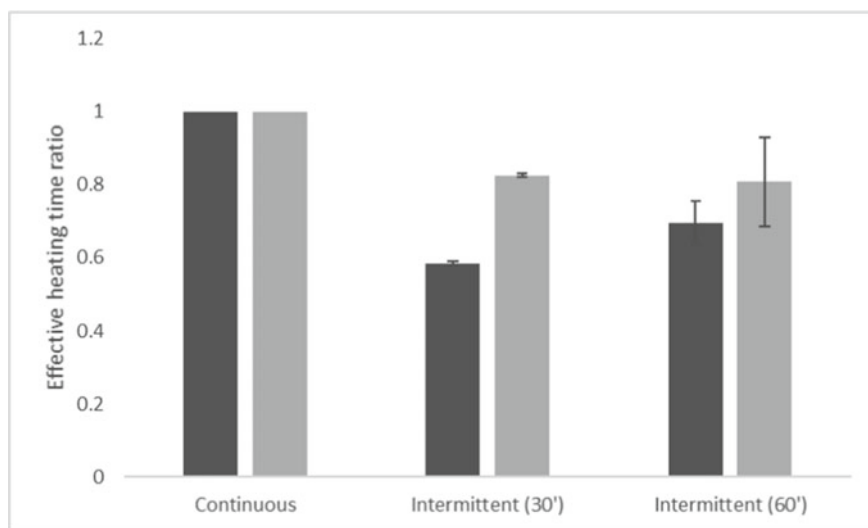


Fig. 1 Effective heating time ratio of the drying methods in trial 1. Dark grey bars represent the LP walnuts, while light grey bars the CP walnuts. Error bars represent the standard deviations

performed to describe data. A higher G_{ev} was observed for the portion of time when the walnuts were heated, and a lower in tempering periods.

In trial 2 in shell walnuts results were consistent with those obtained in trial 1. Moreover, first order kinetic was able to well describe the walnuts drying, being 0.957 the worst R^2 coefficient (Table 2).

The continuously heated walnut batches were the faster to reach the commercial humidity, but the 2 different batches of Lara walnuts processed with 30' intermittent drying allowed to save the 34.4% and the 30.1% of heating time (i.e., batches grown in Pippa and Gaggia fields, respectively – Fig. 3).

The drying coefficients obtained in trials 1 and 2 were comparable. Moreover, the k for the continuous drying were between $7.4 \cdot 10^{-4}$ and $8.3 \cdot 10^{-4} \text{ min}^{-1}$ in trial 1 and between $6.6 \cdot 10^{-4}$ and $7.4 \cdot 10^{-4} \text{ min}^{-1}$ in trial 2. Despite the similarity of the order of magnitude of the k coefficient, the observed differences resulted in different drying time. Being different the initial humidity of the batches (i.e., X_0), the times to dry walnuts between 0.25 (i.e., the initial humidity of the driest batch) and 0.086 (i.e., the humidity required by the trade standards) were calculated. The required drying times were between 1606 min (LP2, $k = 6.6 \cdot 10^{-4} \text{ min}^{-1}$) and 1281 min (CP, $k = 8.3 \cdot 10^{-4} \text{ min}^{-1}$). Thus, applying the same settings to the dryer, to reach the same final humidity starting from the same initial humidity, in different batches of walnuts produced 5 h and 25 min of difference in optimal drying time.

A large uncertainty in drying time could be very problematic for walnuts producers since a too low drying results in excessive humidity and risks of microbial spoilages during storage, while too long drying results in less incoming (e.g., walnuts are sold by weight), in higher processing costs (e.g., labour, energy and plant productivity).

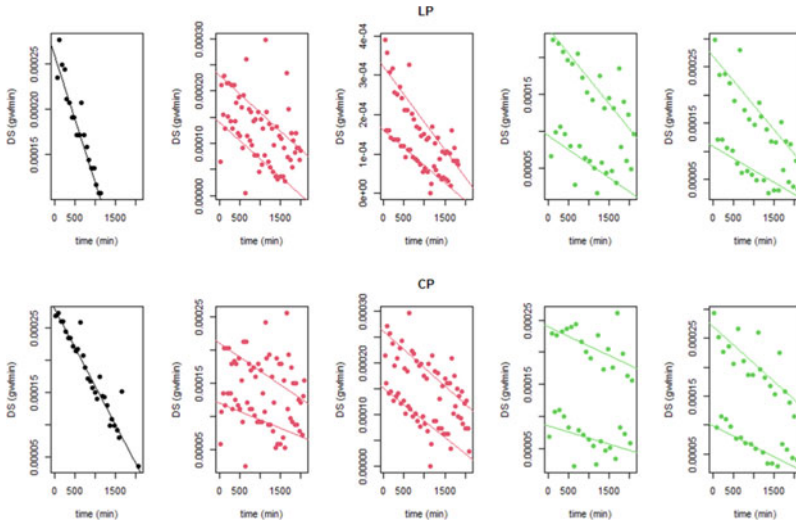


Fig. 2 Changes of the drying speed during the drying length. The upper graphs are referred to the LP batch, while the lower graphs to the CP. Trend lines represent the found statistically significant linear models. Black points refer to the continuous drying, red points to 30' intermittency, and green points to 60' intermittency

Table 2 Estimated model coefficients of in-shell walnuts in trial 2. X_0 represents the initial moisture, and k the drying rate coefficient. The time required to reach the moisture required by the commercial standards is reported in the last column

Drying method	Batch	X_0	k (min^{-1})	R2	Time to $Y = 0.08$ (min)
Continuous	LP2	0.25	$6.6 \cdot 10^{-4}$	0.999	1606
Intermittent (30')	LP2	0.25	$5.1 \cdot 10^{-4}$	0.996	2040
Intermittent (30')	LP2	0.25	$4.8 \cdot 10^{-4}$	0.957	2176
Continuous	LG	0.30	$7.4 \cdot 10^{-4}$	0.987	1678
Intermittent (30')	LG	0.38	$6.2 \cdot 10^{-4}$	0.998	2382
Intermittent (30')	LG	0.33	$5.7 \cdot 10^{-4}$	0.999	2310

Furthermore, the incorrect choice of drying time always results in higher environmental impacts (i.e., product losses or energy consumption) and in a decrease of product quality (i.e., microbial spoilage or product oxidation). The drying time is difficult to be controlled since it is difficult to measure real time the humidity of in shell walnuts at industrial scale. Moreover, the humidity sensors commercially available measured the shell of the walnuts, while for drying purposes the measurement of interest is those of the whole fruit. Conversely, the determination of humidity drying the walnut until constant weight is reached is not fast enough to be used as process control. Hence, efforts to improve the process control of drying and consequently

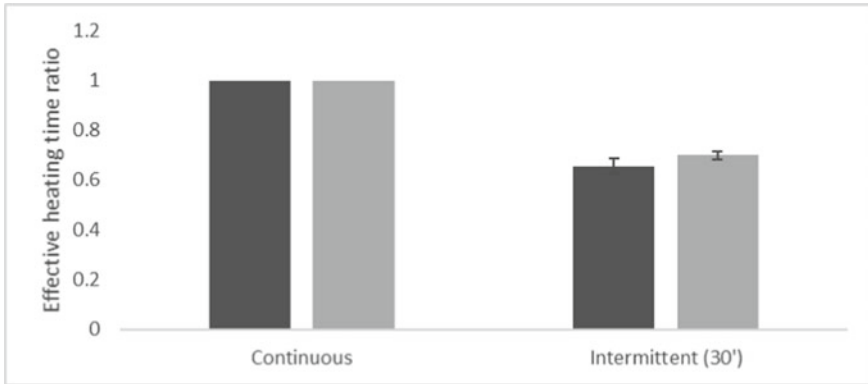


Fig. 3 Effective heating time ratio of the drying methods in trial 2. Dark grey bars represent the LP walnuts, while light grey bars the LG walnuts. Error bars represent the standard deviations

Table 3 Estimated model coefficients of shelled walnuts in trial 2. X_0 represents the initial moisture, and k the drying rate coefficient. The time required to reach the moisture required by the commercial standards is reported in the last column

Drying method	Batch	X_0	k (min^{-1})	R2	Time to $Y = 0.08$ (min)
Continuous	LP	0.21	1.4×10^{-3}	0.977	628
Intermittent (30')	LP	0.20	1.1×10^{-3}	0.990	749
Intermittent (30')	LP	0.22	9.7×10^{-4}	0.992	958
Continuous	LG	0.28	1.3×10^{-3}	0.964	895
Intermittent (30')	LG	0.29	1.4×10^{-3}	0.986	848
Intermittent (30')	LG	0.28	8.8×10^{-4}	0.990	1329

the accuracy in the determination of the drying time should be done. The improvement of process control could be considered as a suitable method to improve process efficiency, product quality, and producer income.

Shelled walnuts showed the same behavior of in-shell fruits. Moreover, their loss of humidity during drying could be modeled as a first order kinetic (Table 3).

In this case, the intermittent drying allowed to save the 36% of warm air use. This value is consistent with the save measured for in-shell walnuts. The considerations done for in-shell walnuts could be extended to shelled fruits.

4 Conclusions

Walnuts drying is a not avoidable operation to enhance the fruits storage time. Drying is an energy consuming process, usually performed with heated air. However, the

efficiency of use of heat air is poor. Intermittent drying allows to improve that efficiency, by lowering the consumption of heated air of roughly the 30–35% in both shelled and in-shell walnuts. Moreover, the loss of moisture from the walnuts could be successfully modeled as a first order kinetic, allowing theoretically to roughly predict the drying time after few hours of drying. However, the development of suitable devices for on-line humidity determination in walnuts seems to be very important for the improvement of the operative, qualitative and environmental performance of the process.

References

1. Parenti, A., Masella, P., Guerrini, L., Guiso, A., Spugnoli, P.: Energetic and economic viability of olive stone recovery as a renewable energy source: a Southern Italy case study. *J. Agric. Eng.* **45**(2), 60–63 (2014)
2. Ferrari, G., Ai, P., Alengebawy, A., Marinello, F., Pezzuolo, A.: An assessment of nitrogen loading and biogas production from Italian 2 spatial analysis. *J. Clean Prod.* **317**, 128388 (2021)
3. Ferrari, G., Ai, P., Marinello, F., Pezzuolo, A.: Where and how? A comprehensive review of multicriteria approaches for bioenergy plant siting. *J. Clean. Prod.* **346**, 131238 (2022)
4. UNECE standard DDP-01 Concerning the marketing and commercial quality control of Inshell Walnuts. United Nations, New York and Geneva (2014)
5. Amirante, P.: *Macchine e impianti per la coltivazione delle noci e per l'industria dei derivati* (2018)
6. Hassan-Beygi, S.R., Aghbashlo, M., Kianmehr, M.H., Massah, J.: Drying characteristics of walnut [*Juglans regia* L.] during convection drying. *Int. Agrophys.* **23**(2), 129–135 (2009)
7. Chen, C., Venkatasamy, C., Zhang, W., Deng, L., Meng, X., Pan, Z.: Effect of step-down temperature drying on energy consumption and product quality of walnuts. *J. Food Eng.* **285**, 110105 (2020)
8. Kumar, C., Karim, M.A., Joardder, M.U.H.: Intermittent drying of food products: a critical review. *J. Food Eng.* **121**, 48–57 (2013)
9. Friso, D.: *Ingegneria dell'industria agroalimentare*, volume II, ed. Cleup (2018)

Open Field Geometric Primitives' Representation by a 2D Low-Cost LIDAR for Vineyard Sprayer Application Under Different Conditions



Alessio Ilari, Fabrizio Favi, Francesco Zingaretti, Luana Centorame, and Ester Foppa Pedretti

Abstract Light Detection and Ranging (LIDAR) is the application of Laser to objects distance measurement. A pulsed light or a continuous wave defines distance through two different principles: Time of Flight (TOF) and Phase-Shift (PS). Recently, 2D and 3D TOF LIDARs found application in the agricultural field for vegetation analysis and distribution of agricultural input, intending to optimize the quantity of distributed active principle. The most used devices are TLS (Terrestrial Laser Scanner), particularly the MTLs (Mobile TLS). LIDAR is potentially more accurate in point distance definition and more suitable to determine small objects or vegetation gaps with respect to Sonar. The present study aims to test a 2D low-cost LIDAR-based real-time sprayer for vineyards by positioning specific targets and their subsequent recognition in the point cloud analysis. The test was conducted in open field with different light conditions and speeds. Field tests were conducted in Ancona and Arcevia municipalities, Marche region, Italy. Field trial consists of recognizing circular (10 to 100 cm of diameter) and square (10 to 30 cm side) targets. The targets are divided into 28 white (to ensure maximum laser reflectance) and 28 green (to simulate the leaves color). The outward and return speeds varied between 2.5 and 8 km/h. In addition, the same device was used to define two-dimensional and three-dimensional structures in comparison. The results show that the system can identify objects or gaps in vegetation, even on small surfaces, and with speeds comparable to those used to apply pesticides.

Keywords Variable rate sprayer · Verdicchio · Mobile laser scanner

A. Ilari (✉) · L. Centorame · E. Foppa Pedretti
Dipartimento di Scienze Agrarie, Alimentari ed Ambientali, Università Politecnica delle Marche,
Via Breccie Bianche 10, 60131 Ancona, Italy
e-mail: a.ilari@univpm.it

F. Favi · F. Zingaretti
ISELQUI Technology Srl, Via Sandro Totti 12/A, 60131 Ancona, Italy

© The Author(s), under exclusive license to Springer Nature Switzerland AG 2023
V. Ferro et al. (eds.), *AIIA 2022: Biosystems Engineering Towards the Green Deal*,
Lecture Notes in Civil Engineering 337,
https://doi.org/10.1007/978-3-031-30329-6_65

1 Introduction

LIDAR, Light Detection and Ranging, is the application of Laser to the specific use of object distance measure. A Pulsed light or a continuous wave is used to define distance throughout two different principles: Time of Flight (TOF) and Phase-Shift (PS) [1]. Although PS is more accurate than TOF, this last one has more application potential due to the longer detectable distance [2]. LIDAR devices are typically divided into two groups based on support on which they are brought: (i) ALS (airborne laser scanner) concerns devices installed on aircrafts or UAVs and (ii) TLS (terrestrial laser scanner) refers to two different subclasses, static TLS (STLS) and mobile TLS (MTLS). Another classification is based on type of data generated and the body rotation: 3D LIDARS have double axis rotation/oscillation and can determine distance and both vertical/horizontal angle; meanwhile, 2D LIDARS have a single axis rotation and can determine points on a plane. As well described in a recent review, TLS applications depends on their characteristics: 3D TLS are often characterized by high resolution thanks to a dense point cloud generated and commonly used for environmental mapping, automotive applications, vegetation analysis, architectural representation, and diagnostics [2]. 2D TLS are characterized by a lower resolution but a larger detection angle (270–360 degrees) and they are largely used for industrial automation of transport in warehouses. Moreover, 2D TLS are also less expensive than 3D ones. Recently 2D and 3D LIDARS found application in agricultural field for vegetation analysis and for distribution of agricultural input [3–5]. This application aims to optimize the quantity of active ingredient distributed [14], which in fixed dose distribution systems generates losses between 30 and 50% due to drift or deposition on non-target areas [4]. LIDAR can be considered a direct upgrade of other field sprayer equipped with ultrasounds for distance and object recognition [3, 6–11]. LIDAR with respect to Sonar (ultrasounds) uses light generated by a laser in infrared spectra. The laser beam is monochromatic with a low divergence. These characteristics allow LIDAR to be potentially more accurate in point distance definition and more suitable to determine small objects or vegetation gaps [9]. The LIDAR application to variable rate pesticide distribution can work in two ways: the first consists in the use of LIDAR point cloud to generate a canopy 3D model from which then extract useful information and/or to generate prescription maps [9, 12]; the second consists in a real-time spraying [5], an alternative use is for pesticide drift assessment [13]. Both the first two approaches have pros and cons: in the first case, point cloud post processing can take several days and the information generated could be not representative of the actual crop phytosanitary state, but the potential accuracy of the data can be very high. In the second case, the distribution of plant products is immediate but the amount of data to be processed often requires an excessive degree of simplification or a slowdown in the tractor's forward speed. The present study aims to test a 2D low-cost LIDAR based real-time sprayer for vineyard through the positioning of specific targets and their subsequent recognition in the analysis of the point cloud.

2 Materials and Methods

Field tests have been conducted in Ancona on a road surface and in the presence of low background noise on 3rd February 2020, field location is in Arcevia municipality, Marche region, Italy (43.517325, 12.966688 – coordinates system WGS84). In this last case the area has a typically sub-Mediterranean climate with average monthly temperatures ranging between 3.5 °C and 22.51 °C. Average annual rainfall is 11571 mm. Vineyard is espalier trained with a row spacing of 2.8 m. The variety grown in the test area is Verdicchio around 10–12 years old. The system used is composed of 4 different devices interconnected (Fig. 1).

LIDAR used is produced by SLAMTEC (RPLIDAR A3). The device is a 360-degree 2D LIDAR for indoor and outdoor application, the maximum range radius is 25 m and the maximum sampling frequency is 16 kHz (indoor) and 10 kHz (outdoor). GPS receiver employed is an Ag Leader GPS 1500. Inertial measurement unit (IMU) used is a WIT MPU6050 3-Axis, needed to correct inclination errors due to soil roughness and vibrations. A single board computer (Raspberry PI model B +) has been used to manage all the devices. The controller is essential to communicate basically the time of GPS internal clock, used as a reference to combine the individual measurements of each device and to store csv files generated. As shown in Fig. 1, the devices that constitute the prototype are installed on an aluminum grooved profile that allows the GPS to be raised above the crop and the position of the Lidar to be adjusted. The profile is held by metal brackets on the front of the sprayer chassis.

The field sprayer used is a SAE Turbomatic model Defender MK2 91DP firstly implemented with ultrasounds sensors. The sprayer is equipped with a 1500 l polyethylene tank and a fan (910 mm diameter) with front air intake. The distribution nozzles (14) are mounted on a rectangular parallelepiped turret (7 for each side). The range of inter-row width that the machine can handle varies between 2.8 and 6 m with a plant maximum height of 5–6 m. In the basic model, the only possible settings are the choice of the fan speed (2 settings foreseen), the closure of a section of the turret (7 nozzles) and the orientation and positioning of the nozzles. The model equipped with ultrasound can automatically exclude a section of the turret when the sensor does not detect an obstacle in the range 1–6 m (adjustable). In practical terms, the ultrasound machine is only able to close the sections during the turning at the end of the rows.

The field trial consists in verifying the functionality of the LIDAR system in three different conditions: (i) low disturbance on road surfaces and using a fence to support the targets and varying the speed on three levels (Fig. 2); (ii) in total absence of vegetation directly in the vineyard to reduce the noise on targets (Fig. 3); (iii) on road surfaces for the recognition of three-dimensional elements (Fig. 4). Target shape selected are round and square, colors selected instead are white and light green, the range selected is reported in Table 1 together with 3D targets.

Squared shape has been selected because easier to be approximated even with reduced laser impacts. Round targets have been selected because is the regular geometric shape that best approximates the shape of any vegetation gap. The target

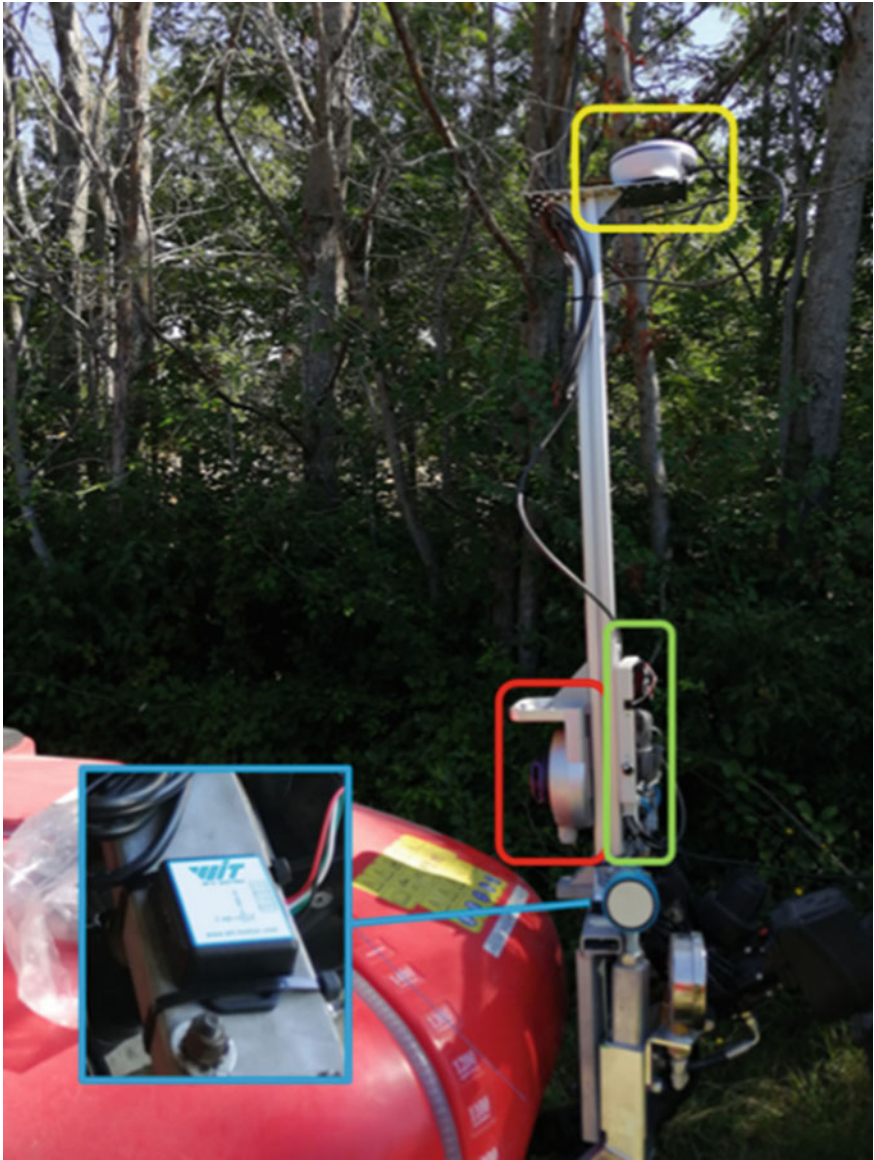


Fig. 1 Overview of LIDAR system: in red square RP LIDAR A3; in green square Raspberry PI B + with wirings; in yellow square GPS receiver; in light blue a detail of IMU



Fig. 2 Bidimensional targets positioning in the first road test (low noise-low speeds)



Fig. 3 North-West **a** and South-East **b** sides of vineyard used for field trial



Fig. 4 3D targets of the third road field test

Table 1 number of targets by shape and colors used for field trial.

Target shape	Dimensions (cm)	White	Green
Square	L x L		
	10 x 10	7	7
	20 x 20	6	6
	30 x 30	3	3
Round	Diameter		
	10	5	5
	20	3	3
	30	2	2
	60	1	1
	100	1	1
Conical 3D	Base diameter (cm)	Height (cm)	
	24	50	
	33.5 (2)	60 (2)	
	39.5	75	
	45.5	100	

dimensions selected instead follows the consideration that LIDAR can detect gaps even smaller than 10 cm diameter but the pesticide distribution system is not capable to avoid distribution in such confined spaces even admitting the independence of each individual nozzle. Another justification relating to the size of the targets derives from the characteristics of both LIDAR and vineyard. At the speeds set in the test, the LIDAR manages within a second to generate around 10 k points arranged in a surface varying between 7.3 and 19.5 m². However, the useful surface for the registration of the points from LIDAR is that corresponding to the two espaliers which varies between 2 and 5.3 m² (height of the front of vegetation 1.2 m) this involves about 2700 impacts for the affected area. Considering the angular resolution range of the instrument, on the vertical plane each point would be spaced about 4–7 cm. Considering these values it was decided to use targets with dimensions starting from

Table 2 characteristics of different field trip (G = Go, B = Back).

Field trip	Time (time zone UTC + 2)	Tractor speed km/h
1-2 (G & B)	10.53-10.57	3.5
3-4 (G & B)	10.59-11.02	5
5-6 (G & B)	11.04-11.06	6
7-8 (G & B)	11.18-11.21	7
9-10 (G & B)	11.22-11.25	8
11-12 (G & B)	11.30-11.32	7.5
13-14 (G & B)	11.34-11.37	3

10 cm. Therefore, for the first and second trials, the size of the targets serves on the one hand to verify the detection capabilities of the LIDAR on small objects and on the other to verify the ability to recognize exactly the shape of larger objects. Other variables considered in the study are tractor speed set from 2.5 and 4.5 km/h (first trial), 3 km/h to 8 km/h (second trial) in roundtrip as reported in Table 2. The last test, purely exploratory, was conducted at an approximate speed of 3 km/h. For the second trial, roundtrip also allowed to record data in different light conditions. In fact, the rows are oriented in a NE-SW direction, so the SE surface is exposed to the sun and the opposite one in the shade at the time of the tests. In these conditions the LIDAR optics was directly irradiated by the sun's rays while recording the points of the surfaces exposed to NW.

3 Results and Discussions

Figure 5 shows the results of the first test while Table 3 shows the numerical results of the determination of the target surfaces with respect to the real dimensions for the three speeds.

From Table 3 it is possible to note how the reduction in the surface of the targets corresponds to an increase in the estimation error. The same error (quantifiable in about 0.5-1 cm) is repeated almost unchanged for round or square targets. The measurements were determined as the average of the target limit values over points in the x and z axis corresponding to width and height. Considering these values separately, it is possible to define the estimation error along the horizontal and vertical axis. In the first case it is much higher (11-750% for round targets, 42-380% for squared ones) in the second case contained between (1-74% for round targets, 18-36% for squared ones). This phenomenon is easily explained by considering the orientation of the 2D lidar which carries out measurements on the vertical axis determining point clouds that estimate the size of the targets very well while on the horizontal axis the resolution is dependent on the forward speed which determines the distance between single point clouds.

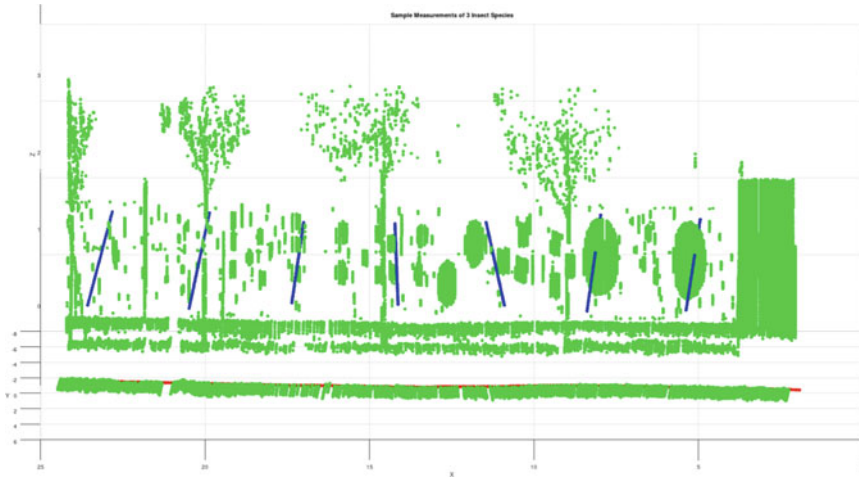


Fig. 5 Graphic representation of the first registration test, it is possible to distinguish the shape of the targets represented by the green dots. The red points represent the path of the system while the blue points represent the direction orthogonal to the path

Table 3 Surface calculated and relative difference to reference for targets of different shape and dimensions Sq(square), Ro(round), (10 cm targets not reported because not graphically detectable; positive values indicate estimated surface increases compared to the standard, negative values lower surfaces)

Target	Surface reference	Surface calculated 2.5 km/h	Difference %	Surface calculated 3.5 km/h	Difference %	Surface calculated 4.2 km/h	Difference %
Sq 20 × 20	0.04	0.033	-17.42%	0.044	9.32%	0.046	13.82%
Sq 30 × 30	0.09	0.097	7.55%	0.084	-6.13%	0.100	10.80%
Ro 20	0.031	0.025	-21.90%	0.019	-39.45%	0.021	-33.30%
Ro 30	0.071	0.084	19.31%	0.075	5.59%	0.039	-44.96%
Ro 60	0.283	0.268	-5.18%	0.242	-14.39%	0.211	-25.53%
Ro 100	0.785	0.807	2.76%	0.705	-10.24%	0.739	-5.88%

The vineyard trials (Fig. 6) showed much less defined point clouds where only the largest targets can be distinguished. Comparing the different speeds, it is possible to notice a reduction in the density of the points and an increase in the disturbance caused by the roughness of the ground. Despite this, the difference between targets exposed to light or shade is not appreciable. In the test on conical targets, the system was able to recognize the three-dimensionality as can be seen in Fig. 7, it should be emphasized that this test is also characterized by low soil disturbance.

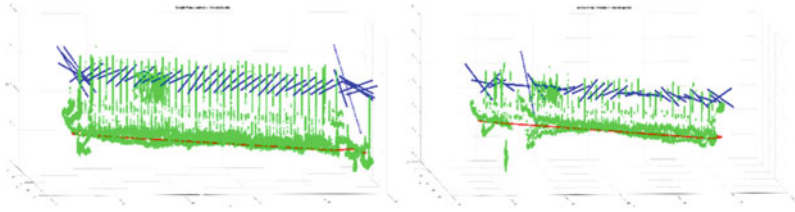


Fig. 6 Graphic representation of vineyard trial, on the left 3 km/h points cloud on the right 8 km/h points cloud

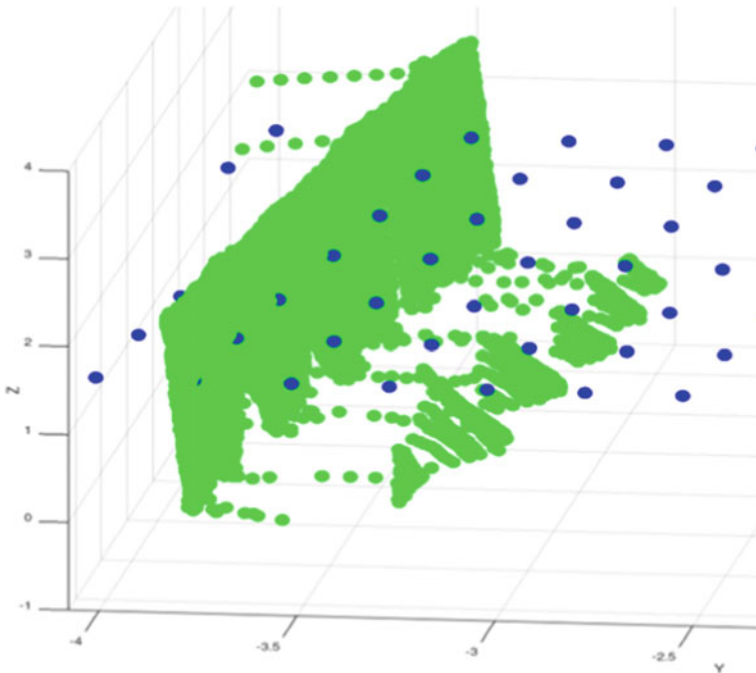


Fig. 7 Graphic representation of 3D target trial

4 Conclusions

The system can recognize characteristic elements and two-dimensional geometric primitives. With low forward speeds and little disturbed environments, elements up to 20 cm side/diameter can be graphically recognized with variable errors in the surface estimation. In open field, the maximum achievable detail seems to be about 1 m. This suggests that the system can regulate the distribution of vegetation on relevant gaps as in the case of missing plants. The system can also recognize three-dimensional structures however for the intended use this capability would be superfluous and too

expensive in terms of processor calculation. In the applications of the same machine (already current today) it would be desirable to determine in greater detail the limits of the acquisition and evaluate the goodness of the distribution regulation, for example using devices that record the dispersion of pesticide mixture. Future developments of the prototype, already planned, will concern the installation of solenoid valves for the independent control of each nozzle, consequently reprogramming the processor through a pixelization of the lidar data in accordance with what emerged in the present study. Considering that the investigated system (with on/off type control) cannot be considered a VRD (variable rate distribution) it could still be modified for this purpose. For the VRD application, however, the fine-tuning of the performance of the lidar, the GPS and the processor will be crucial, which will necessarily have to be able to process large amounts of data, conditions that are not always easy to satisfy.

References

1. Grotti, M., Calders, K., Origo, N., Puletti, N., Alivernini, A., Ferrara, C., et al.: An intensity, image-based method to estimate gap fraction, canopy openness and effective leaf area index from phase-shift terrestrial laser scanning. *Agric. Meteorol.* **280**, 107766 (2020). <https://doi.org/10.1016/j.agrformet.2019.107766>
2. Xia, S., Chen, D., Wang, R., Li, J., Zhang, X.: Geometric primitives in LiDAR point clouds: a review. *IEEE J. Sel. Top Appl. Earth Obs. Remote Sens.* **13**, 685–707 (2020). <https://doi.org/10.1109/JSTARS.2020.2969119>
3. Colaço, A.F., Molin, J.P., Rosell-Polo, J.R., Escolà, A.: Application of light detection and ranging and ultrasonic sensors to high-throughput phenotyping and precision horticulture: current status and challenges. *Hortic. Res.* **5** (2018). <https://doi.org/10.1038/s41438-018-0043-0>
4. Wandkar, S.V., Bhatt, Y.C., Jain, H.K., Nalawade, S.M., Pawar, S.G.: Real-time variable rate spraying in orchards and vineyards: a review. *J. Inst. Eng. Ser. A* **99**, 385–390 (2018). <https://doi.org/10.1007/s40030-018-0289-4>
5. Chen, Y., Zhu, H., Ozkan, H.E.: Development of a variable-rate sprayer with laser scanning sensor to synchronize spray outputs to tree structures. *Trans. ASABE* **55**, 773–781 (2012)
6. Balsari, P., Doruchowski, G., Marucco, P., Tamagnone, M., Van de Zande, J.C., Wenneker, M.: A System for adjusting the spray application to the target characteristics. *Agric. Eng. Int. CIGR Ejournal* **8**, 11 (2008)
7. Gil, E., Llorens, J., Llop, J., Fàbregas, X., Escolà, A., Rosell-Polo, J.R.: Variable rate sprayer. Part 2 - Vineyard prototype: design, implementation, and validation. *Comput. Electron. Agric.* **95**, 136–50 (2013). <https://doi.org/10.1016/j.compag.2013.02.010>
8. Doruchowski, G., Balsari, P., Van De Zande, J.: Development of a crop adapted spray application system for sustainable plant protection in fruit growing. *Acta Hortic.* **824**, 251–260 (2009). <https://doi.org/10.17660/ActaHortic.2009.824.29>
9. Llorens, J., Gil, E., Llop, J., Escolà, A.: Ultrasonic and LIDAR sensors for electronic canopy characterization in vineyards: advances to improve pesticide application methods. *Sensors* **11**, 2177–2194 (2011). <https://doi.org/10.3390/s110202177>
10. Escolà, A., Rosell-Polo, J.R., Planas, S., Gil, E., Pomar, J., Camp, F., et al.: Variable rate sprayer. Part 1 - Orchard prototype: design, implementation and validation. *Comput. Electron. Agric.* **95**, 122–35 (2013). <https://doi.org/10.1016/j.compag.2013.02.004>
11. Escolà, A., Planas, S., Rosell, J.R., Pomar, J., Camp, F., Solanelles, F., et al.: Performance of an ultrasonic ranging sensor in apple tree canopies. *Sensors* **11**, 2459–2477 (2011). <https://doi.org/10.3390/s110302459>

12. Sanz-Cortiella, R., Llorens-Calveras, J., Escolà, A., Arnó-Satorra, J., Ribes-Dasi, M., Masip-Vilalta, J., et al.: Innovative LIDAR 3D dynamic measurement system to estimate fruit-tree leaf area. *Sensors* **11**, 5769–5791 (2011). <https://doi.org/10.3390/s110605769>
13. Torrent, X., Gregorio, E., Rosell-Polo, J.R., Arnó, J., Peris, M., van de Zande, J.C., et al.: Determination of spray drift and buffer zones in 3D crops using the ISO standard and new LiDAR methodologies. *Sci. Total Environ.* **714** (2020). <https://doi.org/10.1016/j.scitotenv.2020.136666>
14. Gregorio, E., Torrent, X., Planas, S., Rosell-Polo, J.R.: Assessment of spray drift potential reduction for hollow-cone nozzles: part 2. LiDAR Tech. *Sci. Total Environ.* **687**, 967–977 (2019). <https://doi.org/10.1016/j.scitotenv.2019.06.151>

Valorizing Agro-Industry Residues to Improve the Environmental Sustainability of Frozen Products



Ilari Alessio, Boakye-Yiadom Kofi Armah, Duca Daniele, and Foppa Pedretti Ester

Abstract Considering the paradigm shift towards renewable energy due to the high ecological impacts associated with fossil fuels, generating biogas energy from agricultural residue for electricity is a smart use. However, the sustainability of biogas production can be limited by several factors along its production. Thus, this study evaluated the environmental sustainability of electricity generation from a biogas plant fed with maize silage, animal manure, and agri-food residue at Osimo (Marche region) in Italy. The plant produces, on average 12,000 Nm³ of biogas and 23 MWh of electricity daily with slight variations due to the addition of different quantities and types of agri-food residues. We conducted the study using the life cycle assessment methodology (ISO 14040/14044). The selected functional unit (FU) was 1 MWh of electricity produced from the biogas, and the impact assessment was carried out based on the ReCiPe method (2016). The global warming score obtained was 429 kg CO₂ eq./FU, with maize cultivation contributing more than 90% to the total impact. Substituting maize silage with more agri-industrial residue can significantly improve the overall environmental sustainability of the biogas plant.

Keywords Biogas · Renewable energy · Life cycle assessment (LCA) · Anaerobic digestion · Digestate · Electricity

1 Introduction

Biomass is one of the renewable energy sources with the potential to reduce the carbon footprint per unit of electricity generated and provide energy for domestic use and transportation [1–3]. Generally, biomass is the biodegradable fraction of products, wastes, and residues from agriculture, forestry, and related industries [4]. It is a versatile source that can generate heat, electricity, and liquid biofuels [5].

I. Alessio · B.-Y. K. Armah (✉) · D. Daniele · F. P. Ester
Department of Agricultural, Food and Environmental Sciences, Università Politecnica delle Marche, Via Brecce Bianche 10, 60131 Ancona, Italy
e-mail: k.boakye-yiadom@pm.univpm.it

Biogas is produced by the anaerobic digestion of biomass via the breakdown of complex organic matter by various anaerobic microorganisms during fermentation [6]. As a result of the challenges associated with organic waste management, biogas generation represents a means of valorizing agri-food residues, which is in line with the circular economy concept. Compared to other waste treatment technologies, such as landfilling and incineration, anaerobic digestion of biowaste is deemed more cost-effective [7, 8]. Biogas has average methane and carbon dioxide content of 60% and 40%, respectively, making it suitable for combustion to generate heat and electricity and as a transportation fuel [9]. The remaining digestate also finds application in agricultural production as organic fertilizer, plant-growing media, and soil amendment [10]. However, to advocate for extensive biogas use as an energy source, it is crucial to assess the ecological impacts of the operation of a biogas plant, considering the source of biomass, energy use, the efficiency of the plant, and related emissions.

Environmental sustainability assessment is mainly conducted using the life cycle assessment (LCA), which provides a holistic approach to evaluating a product's or service's ecological burdens [11]. LCA is an internationally recognized tool based on the ISO 14040 and 14,044 standards, which helps quantify the environmental aspects of materials, energy, and emissions associated with a product or service [12]. Recently, the LCA approach has been widely applied to analyze biogas production's pros and cons in the surrounding environment, especially in Europe [13]. Despite being considered a sustainable energy source, biogas production, especially from organic waste, may be threatened by environmental concerns such as biomass cultivation, transportation, digestate treatment, and combustion emissions [6]. Therefore, these LCA studies were conducted primarily to assess biogas production's ecological sustainability and to identify hotspots along the production process for improvement [10, 14]. The sustainability assessment of energy performance in terms of energy balance (production and consumption) has also been well studied [15]. Recycling organic waste for biogas production also confers economic advantages when feedstock includes a significant amount of waste, such as animal manure, agri-food waste, and municipal solid waste. Thus, several LCA studies have included the economic aspects of operating a biogas plant as part of the study's goals [6, 16].

The environmental performance of biogas production is affected by several factors, such as the quality of biomass raw materials, cultivation system (energy crops), transportation of biomass, pre-treatment processes, purification of biogas gas, the efficiency of the technology employed, digestate and waste treatment, and related greenhouse gas emissions [6, 13]. In Europe, maize silage is the most predominantly used feedstock for anaerobic digestion due to its high bioenergy content, with an estimated biogas yield of up to 0.35 m³CH₄ per kg VS (after silaging) [17]. Biogas production using dedicated bioenergy crops has raised environmental, social, and economic concerns due to the competition for soil use between food and non-food products. Overexploitation of bioenergy crops such as maize silage can pose a significant threat to the environment by encouraging the creation of mono-crops to meet the energy demand [18–20]. To mitigate this challenge, agriculture and food industry residues are replacing these energy crops that have been criticized for their environmental impact. Commercial energy crops are often mixed with lower energy

biowaste, such as animal manure (cattle, pig, and poultry) and agri-food waste, to decrease over-dependence on bioenergy crops. However, this can also affect the biogas yield and quality and the overall sustainability of biogas production. Therefore, this study aimed to assess the environmental and energy performance of a biogas production system belonging to a big agro-industrial producer, considering including different horticultural residues from a life cycle assessment perspective.

2 Methodology

We used the life cycle assessment (LCA) to calculate the impacts of a 1 MW biogas power plant, following the ISO 14040/14044 standards [21, 22]. The standard LCA has four interrelated phases: goal and scope definition, life cycle inventory analysis (LCI), life cycle impact assessment (LCIA), and interpretation of results. Further details are provided in the sub-sections below.

2.1 Goal and Scope Definition

This LCA study aims to evaluate the environmental performance of an agricultural biogas plant that produces biogas from anaerobic co-digestion of maize silage, animal manure, and agri-industrial residues for power generation. We assess the energy performance using agri-industrial waste typologies from frozen horticulture production chains to generate biogas. The study's results aim to provide a preliminary overview of the current environmental sustainability of electricity production from this biogas plant and identify hotspots to improve the company's overall environmental footprint.

The biogas plant is in Osimo, Marche region in Italy, and was set up due to the government's financial incentivization to encourage renewable energy production. However, due to the environmental concerns associated with using bioenergy crops, biogas plants have to reduce the use of bioenergy crops like maize silage to continue benefitting from the profitable tariff. Thus, there has been a need for collaboration between the biogas plant and agri-food processing companies to obtain a reliable source of residual organic material as a substitute for maize silage.

The selected functional unit was 1 MWh of electricity produced from biogas combustion considering the plant's primary function is to produce electricity. The entire system encompasses both the agri-food and bioenergy production systems. Due to the complexities of allocation, while assessing both systems simultaneously, the ISO standards recommend splitting the different phases and evaluating them individually. For this reason, this study focuses on the part related to the bioenergy production system though linked to the valorization of the residues from the agri-food production chain. Therefore, the system boundary includes upstream activities like maize cultivation, feedstock collection and transportation to the biogas plant.

Core activities included the mixing feedstock, anaerobic digestion of feedstock and combustion of biogas. Downstream operations also include digestate separation and spreading. Due to the lack of economic exploitation for the heat produced, all impacts are attributed to electricity production and no allocation is required.

2.2 System Description and Inventory

The system model is based on a biogas plant with an average daily capacity of 23.5 MWh of electricity for 2021 from the co-digestion of 60-ton daily feedstock. The modelling of the different lifecycle stages was based on primary plant data from the plant, supplemented where necessary by secondary data. Figure 1 shows the study's system boundary with the biogas production's flowchart.

The maize silage is obtained from cultivated fields close to the biogas plant and other regional commercial fields. Chicken manure is obtained from commercial poultry producers within 15–30 km of the biogas plant, while the agro-industrial residue comes from a large horticultural consortium (55 km away). Anaerobic digestion of the feedstock takes place in three special reactors between 70–90 days, mainly to reduce the volume of the feedstock. The biogas obtained is purified and filtered to remove residual sulfates using iron compounds. The combined heat and power (CHP) internal combustion engine generates electricity and heat from the biogas. About 5% of the electricity is consumed internally for conveying and mixing feedstock, while part of the heat is used to maintain the temperature of the digestors. The remaining electricity is exported to the main grid to provide households and small-scale industries with electricity. After digestion, the digestate (estimated 20,000 tons) is separated with a mechanical screw press into a solid/dry fraction and a liquid fraction. Both digestate undergo further storage in a vast tank (liquid fraction) and a

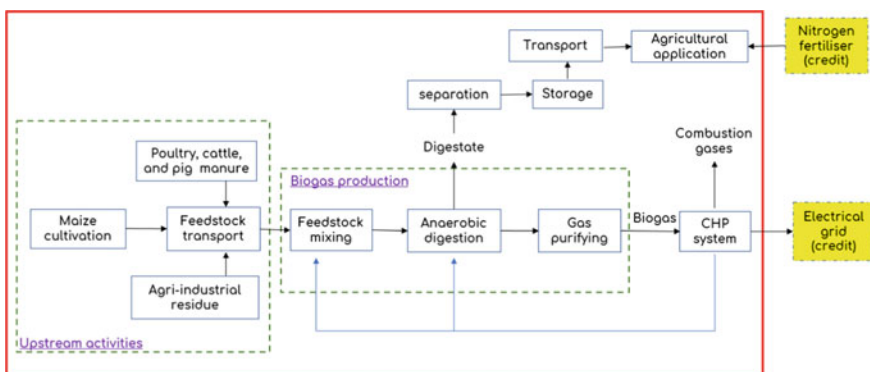


Fig. 1 A simplified schematic representation of the anaerobic digestion system considered in the study. Substituted products are highlighted in the yellow boxes.

Table 1 Inventory data for bioenergy production per 1 MWh of electricity via anaerobic digestion of the studied biogas plant

Input	Quantity	Data Source
Maize silage	2.01 t wb	Secondary
Poultry manure	0.21 t wb	Primary
Pig slurry	0.15 t wb	Primary
Cattle manure	0.06 t wb	Primary
Agri-food residue	0.25 t wb	Primary
Electricity	0.05 MWh	Primary
Output		
Electricity	1.00 MWh	Primary
Digestate	2.44 t	Primary
<i>Emissions to air</i>		
Methane	3.03 g	Primary
Carbon monoxide	1.10 g	Primary
Nitrogen oxides	1.33 g	Primary
NM VOC	0.20 g	Primary

pit (solid fraction). The digestate is transported and spread directly on the fields as organic fertilizer and soil amendment.

Regarding the data quality for the life cycle inventory (LCI), primary data on the feedstock quality and quantity, biogas produced, electricity generated, direct emissions (NO_x, CO, TOC, CH₄, and NMHC) from gas combustion, and digestate volume were obtained directly from the company through questionnaires, official documents, interviews, and results of the analysis conducted to meet regulatory mandates. Where the data were unavailable, we relied on secondary data obtained from the Ecoinvent databases v3.9 (APOS), which were used to model the maize silage cultivation, digestate intended for fertilizer, and background processes (material and energy production). The efficiency of electricity generation from the CHP system is 41%. The inventory data is summarized in Table 1.

2.3 Impact Assessment

The life cycle impact assessment (LCIA) results were modelled using the ReCiPe method 2016 (H) with the SimaPro software version 9.4 to determine the environmental impacts. The study focused mainly on midpoint impact categories directly affected by airborne emissions for the sake of brevity: global warming (GW), stratospheric ozone depletion (OD), terrestrial acidification (TA), marine eutrophication (ME), ozone formation, human health (OF), and fine particulate matter formation (PMF).

3 Results and Discussion

The results obtained show that both the biogas produced and electricity generated were constant throughout the year with little variations (as shown in Fig. 2). The slight variation is due to the inclusion of different agri-food residues as and when they become available. Between January and March, the biogas produced included bioenergy from residual processed tomatoes added as feedstock three months prior. April to June contains bioenergy and biogas from spinach and other leafy vegetable residues. Biogas from pea residues between July and August, and fresh tomatoes between September and December. It is worth noting that the biogas produced is also due to the quantity of the agri-food residue added, which affects the overall ratio of the co-digested feedstock. The similar electricity output from the co-digestion of different feedstock suggests that the biogas plant is well managed.

The midpoint characterization results per 1 MWh of electricity produced in the biogas plant show a climate change score of 429 kg CO₂ eq. Other midpoint results are shown in Table 2. More than 85% of all the impacts for the various impact categories assessed were associated with maize cultivation. Anaerobic digestion and the CHP system contributed less than 2% across all impact categories. This is also due to the low direct emissions (NO_x, CH₄, CO, and NMVOC) generated by the CHP unit and the avoided impact from the auto-consumption of electricity generated by the biogas. Feedstock transport contributed less than 5% across the impact categories due to the relatively short distance and the efficiency of the transport means. Credit was also awarded for using digestate as a substitute for urea in maize cultivation and the surplus used in other crop production systems based on the estimated total nitrogen content of the solid (6% d.m.) and liquid (14% d.m.) digestate.

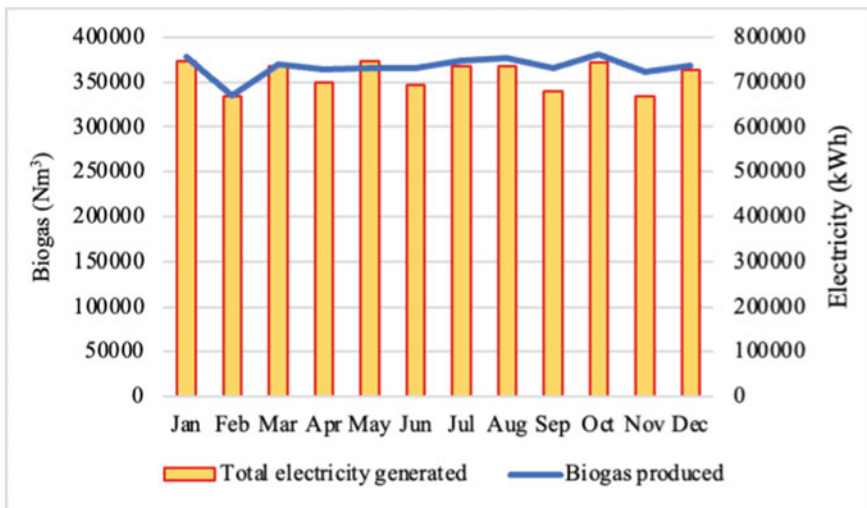


Fig. 2 Monthly biogas produced vs electricity generated by the biogas plant

Table 2 The midpoint characterization results per MWh of electricity produced

Impact category	Total	Maize cultivation	Feedstock transport	Bioenergy production	Electricity (credit)	Urea (credit)
GW (kg CO ₂ eq.)	429	465	3.8	0.1	-20.2	-19.4
OD (kg CFC-11 eq.)	9.72×10^{-3}	9.74×10^{-5}	8.58×10^{-7}	0.0	-1.64×10^{-5}	-7.13×10^{-6}
TA (kg SO ₂ eq.)	12.05	12.2	0.02	0.0	-0.07	-0.06
ME (kg N eq.)	0.36	0.36	0.001	0.0	-0.0006	-0.0008
OF (kg NO _x eq.)	2.61	2.65	0.03	0.0	-0.04	-0.03
PMF (kg PM _{2.5} eq.)	2.04	2.08	0.004	0.0	-0.02	-0.02

The contribution analysis of maize cultivation shows that direct nitrogen emissions in the digestate were the main contributor (54%) to climate change. Chopping/harvesting of the silage was also a significant contributor across all impact categories except marine eutrophication. The planting material contributed over 80% to ME. The highest credit from avoided urea was obtained for OD (26%) and CC (19%). Figure 3 shows the relative contribution of maize cultivation for the various impact categories assessed.

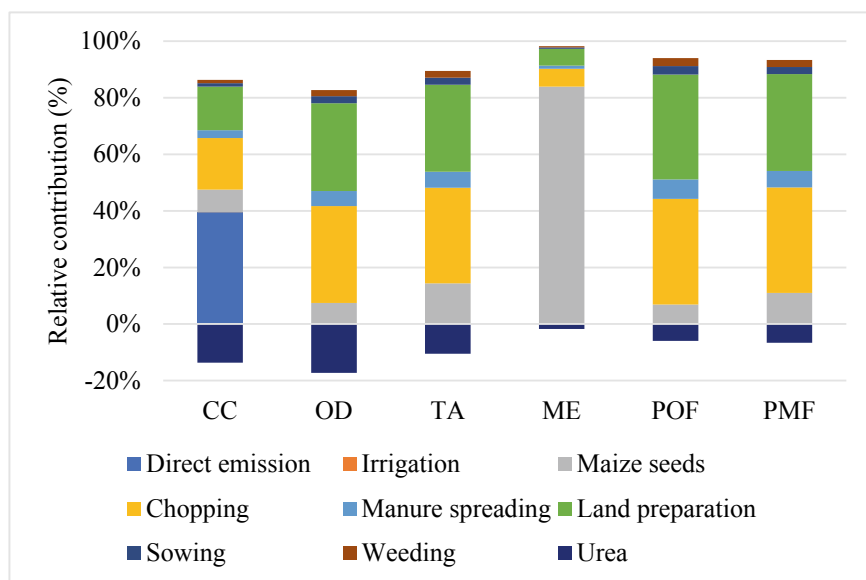


Fig. 3 Relative contribution for maize cultivation

Although it is challenging to compare LCA results due to possibly wide variations in phases included in the system boundary, allocations, assumptions, and temporal and geographical differences, our climate change result was comparable to some of the LCA results reported for other biogas plants in Italy. Table 3 summarizes the selected LCA studies on biogas production in Italy. Most of the studies were carried out in the Lombardy region, which has more than 40% of all biogas plants in Italy [23]. This is due to the large flat area in Po Valley, which is a hub for agricultural activities with a higher maize cultivation yield per hectare (over 70 tons/ha) than in the Marche region (50–55 tons/ha). Some studies reported feedstock production and transport, especially bioenergy crops, as a major contributor to global warming potential (GWP) [23, 24], while others reported bioenergy production as the most impacting [25, 26]. Other studies also considered digestate management and reported considerable contributions from direct emissions in open storage systems, typical of large plants [23, 25, 27]. However, due to the unavailability of primary data, we excluded digestate management.

Table 3 GWP scores per MWh of electricity produced from some agricultural biogas plants in Italy

Author (s)	Year	Results (kgCO ₂ eq.)	Feedstock	Number of plants	Region
This study	2022	429	Maize silage, poultry manure, cattle manure, pig slurry, agri-food residue	1	Marche
Mistretta et al. [28]	2022	394–566	Maize, triticale, sorghum, bovine manure	2	Piedmont and Lombardy
Cusenza et al. [24]	2021	1223	Olive pomace, whey, chicken manure, bovine manure, sulla, citrus residue	1	Sicily
Lijo et al. [26]	2017	194–286	Maize silage, triticale, chicken manure, pig slurry, food waste, municipal solid waste	2	Lombardy
Lijo et al. [23]	2017	152–619	Energy crops and residues	15	Lombardy
Fusi et al. [27]	2016	37–408	Maize silage, cow slurry, pig slurry, agri-food waste	4	Lombardy

4 Conclusion

We evaluated the environmental impacts of electricity generation from a biogas plant fed with maize silage, animal manure, and agri-food residue. The results show that the selected feedstock type and origin were critical to biogas production's sustainability. Maize cultivation was the most impacting phase, accounting for more than 90% of the total impacts across all categories. Thus, substituting maize silage with more agri-food residue like horticultural residue, livestock manure, and other organic waste from the locality will significantly improve the efficiency and sustainability of electricity production, depending on the energy potential of these residues. However, the right balance of feedstock is essential to ensuring a good biogas yield. Improved sustainable maize silage production through valorizing biogas digestate as an inorganic fertilizer substitute can also be environmentally and economically beneficial. In addition, valorizing the excess heat produced by the CHP unit, such as for heating greenhouses and district heating, can also reduce the overall impacts associated with biogas production. Horticultural value chains can also be made more sustainable by incorporating agri-residue treatment strategies, such as mushroom rearing and insect biowaste treatment, to obtain other valuable products.

References

1. Kimming, M., Sundberg, C., Nordberg, Å., Baky, A., Bernesson, S., Norén, O., et al.: Biomass from agriculture in small-scale combined heat and power plants - a comparative life cycle assessment. *Biomass Bioenerg.* **35**, 1572–1581 (2011). <https://doi.org/10.1016/j.biombioe.2010.12.027>
2. Beagle, E., Belmont, E.: Comparative life cycle assessment of biomass utilization for electricity generation in the European union and the United States. *Energy Policy* **128**, 267–275 (2019). <https://doi.org/10.1016/j.enpol.2019.01.006>
3. Uusitalo, V., Havukainen, J., Manninen, K., Höhn, J., Lehtonen, E., Rasi, S., et al.: Carbon footprint of selected biomass to biogas production chains and GHG reduction potential in transportation use. *Renew Energy* **66**, 90–98 (2014). <https://doi.org/10.1016/j.renene.2013.12.004>
4. Schöpe, M.: Renewable energy directive. *Eur Wind Energy Conf Exhib* **2008**(1), 32–38 (2008)
5. Lam, H.L., Varbanov, P., Klemeš, J.: Minimising carbon footprint of regional biomass supply chains. *Resour. Conserv. Recycl.* **54**, 303–309 (2010). <https://doi.org/10.1016/j.resconrec.2009.03.009>
6. Aziz, N.I.H.A., Hanafiah, M.M., Gheewala, S.H.: A review on life cycle assessment of biogas production: challenges and future perspectives in Malaysia. *Biomass Bioenerg.* **122**, 361–374 (2019). <https://doi.org/10.1016/j.biombioe.2019.01.047>
7. Fodor, Z., Klemeš, J.J.: Waste as alternative fuel - minimizing emissions and effluents by advanced design. *Process Saf. Environ. Prot.* **90**, 263–284 (2012). <https://doi.org/10.1016/j.psep.2011.09.004>
8. Jingura, R.M., Matengaifa, R.: Optimization of biogas production by anaerobic digestion for sustainable energy development in Zimbabwe. *Renew. Sustain. Energy Rev.* **13**, 1116–1120 (2009). <https://doi.org/10.1016/j.rser.2007.06.015>

9. Aziz, N., Hanafiah, M.M., Gheewala, S.H., Ismail, H.: Bioenergy for a cleaner future: a case study of sustainable biogas supply chain in the Malaysian energy sector. *Sustain* **12** (2020). <https://doi.org/10.3390/SU12083213>
10. Iordan, C., Lausset, C., Cherubini, F.: Life-cycle assessment of a biogas power plant with application of different climate metrics and inclusion of near-term climate forcers. *J. Environ. Manage.* **184**, 517–527 (2016). <https://doi.org/10.1016/j.jenvman.2016.10.030>
11. Finnveden, G., Hauschild, M.Z., Ekvall, T., Guinée, J., Heijungs, R., Hellweg, S., et al.: Recent developments in life cycle assessment. *J. Environ. Manage.* **91**, 1–21 (2009). <https://doi.org/10.1016/j.jenvman.2009.06.018>
12. Curran, M.A.: *Life Cycle Assessment Handbook: A Guide for Environmentally Sustainable Products*. Wiley, Hoboken (2012)
13. Achparaki, M., Thessalonikeos, E., Tsoukali, H., Mastrogianni, O., Zaggelidou, E., Chatzinikolaou, F., et al.: Biogas power energy production from a life cycle thinking. In: *Intech*, vol. 13 (2019).
14. Vu, T.K.V., Vu, D.Q., Jensen, L.S., Sommer, S.G., Bruun, S.: Life cycle assessment of biogas production in small-scale household digesters in Vietnam. *Asian-Australasian J. Anim. Sci.* **28**, 716–729 (2015). <https://doi.org/10.5713/ajas.14.0683>
15. Chen, S., Chen, B., Song, D.: Life-cycle energy production and emissions mitigation by comprehensive biogas-digestate utilization. *Bioresour Technol.* **114**, 357–364 (2012). <https://doi.org/10.1016/j.biortech.2012.03.084>
16. Chen, B., Chen, S.: Life cycle assessment of coupling household biogas production to agricultural industry: a case study of biogas-linked persimmon cultivation and processing system. *Energy Policy* **62**, 707–716 (2013). <https://doi.org/10.1016/j.enpol.2013.07.084>
17. Battista, F., Frison, N., Bolzonella, D.: Energy and nutrients' recovery in anaerobic digestion of agricultural biomass: an Italian perspective for future applications. *Energies* **12** (2019). <https://doi.org/10.3390/en12173287>
18. Wu, Y., Zhao, F., Liu, S., Wang, L., Qiu, L., Alexandrov, G., et al.: Bioenergy production and environmental impacts. *Geosci. Lett.* **5** (2018). <https://doi.org/10.1186/s40562-018-0114-y>
19. Tamburini, E., Gaglio, M., Castaldelli, G., Fano, E.A.: Is bioenergy truly sustainable when land-use-change (LUC) emissions are accounted for? The case-study of biogas from agricultural biomass in emilia-romagna region, Italy. *Sustain* **12** (2020). <https://doi.org/10.3390/SU12083260>
20. Peter, C., Fiore, A., Hagemann, U., Nendel, C., Xiloyannis, C.: Improving the accounting of field emissions in the carbon footprint of agricultural products: a comparison of default IPCC methods with readily available medium-effort modeling approaches. *Int. J. Life Cycle Assess* **21**, 791–805 (2016). <https://doi.org/10.1007/s11367-016-1056-2>
21. ISO. 14040: Environmental management — Life cycle assessment—Principles and framework. *Int Organ Stand* 2006 (2006)
22. ISO. 14044: environmental management — life cycle assessment — Requirements and guidelines. *Int Organ Stand* **46**, 14044, (2006).
23. Lijó, L., Lorenzo-Toja, Y., González-García, S., Bacenetti, J., Negri, M., Moreira, M.T.: Eco-efficiency assessment of farm-scaled biogas plants. *Bioresour. Technol.* **237**, 146–155 (2017). <https://doi.org/10.1016/j.biortech.2017.01.055>
24. Cusenza, M.A., Longo, S., Guarino, F., Cellura, M.: Energy and environmental assessment of residual bio-wastes management strategies. *J Clean Prod* **285**, 124815 (2021). <https://doi.org/10.1016/j.jclepro.2020.124815>
25. Blengini, G.A., Brizio, E., Cibrario, M., Genon, G.: LCA of bioenergy chains in Piedmont (Italy): a case study to support public decision makers towards sustainability. *Resour. Conserv. Recycl.* **57**, 36–47 (2011). <https://doi.org/10.1016/j.resconrec.2011.10.003>
26. Lijó, L., González-García, S., Bacenetti, J., Moreira, M.T.: The environmental effect of substituting energy crops for food waste as feedstock for biogas production. *Energy* **137**, 1130–1143 (2017). <https://doi.org/10.1016/j.energy.2017.04.137>
27. Fusi, A., Bacenetti, J., Fiala, M., Azapagic, A.: Life cycle environmental impacts of electricity from biogas produced by anaerobic digestion. *Front Bioeng. Biotechnol.* **4** (2016). <https://doi.org/10.3389/fbioe.2016.00026>

28. Mistretta, M., Gulotta, T.M., Caputo, P., Cellura, M.: Bioenergy from anaerobic digestion plants: energy and environmental assessment of a wide sample of Italian plants. *Sci. Total Environ.* **843** (2022). <https://doi.org/10.1016/j.scitotenv.2022.157012>

Requirements and Challenges in the Design and Potential of Smart and Efficient Winch Assisted Forestry Machinery



S. Leitner, M. Perez, G. Carabin, M. Renzi, R. Vidoni, and F. Mazzetto

Abstract Recent regulations on greenhouse emissions and pollutants are forcing forestry machinery companies to target new solutions for limiting emissions while maintaining performance through electrification or hybridization. Moreover, thanks to the availability of new and affordable mechatronic and IoT technologies, concepts such as sustainable, smart, and precision forestry are gaining credit. In this work, the activities on winch assisted forestry machinery carried out at the FiRST and AFI labs of the unibz are reported. These are firstly revised in terms of requirements and constraints. Then, with electrification being still in its infancy in this sector, design challenges for electrification/hybridization are discussed. Finally, mechatronic solutions for making them ready for smart and precision forestry are presented and discussed.

Keywords Forestry-mechatronics · Smart forestry · Electrification and hybridization · Precision forestry

1 Introduction and State of the Art

Forests play a critical role as water reservoirs, absorbers of carbon dioxide, protectors from landslides and avalanches, and as habitats for animals and humans. To

S. Leitner (✉) · M. Perez · G. Carabin · M. Renzi · R. Vidoni (✉) · F. Mazzetto
Faculty of Science and Technology, Free University of Bozen-Bolzano (Unibz), Bolzano, Italy
e-mail: stefan.leitner@natec.unibz.it

R. Vidoni
e-mail: renato.vidoni@unibz.it

S. Leitner
Leitalpin LTD, Piazza Fiera 1, Bolzano, Italy

R. Vidoni · F. Mazzetto
Competence Center for Plant Health, Free University of Bozen-Bolzano (Unibz), Bolzano, Italy

allow them to fulfill these roles it is essential to ensure sustainable forest management. Natural disasters such as storm Vaia in 2018 and global warming connected to more frequent drought periods have weakened alpine forests. These circumstances provide optimal conditions for the rapid and widespread infestation of the bark-beetle in Europe's forests, with far reaching consequences for decades [1]. Fighting this infestation requires the immediate removal of infested trees before the beetle breeds out and infests neighboring trees. Removal of individual trees, especially in remote terrain far off any access roads, often fails due to unsustainable costs and the lack of qualified personnel. Due to the oversupply of (storm-damaged) timber, high fuel, and equipment costs, harvesting timber in difficult terrain is often uneconomical. To counteract this trend, it is of utmost importance to develop high performance and low operating cost logging equipment.

In the absence of a dense road structure into the forest, in the European Alps cable logging is often the only viable harvesting solution. In a typical setup, a skyline is installed under several tons of tension between two anchor points, usually a number of trees, logging equipment or other artificial fixation points. A cable-car (carriage) moves along the skyline, to transport the timber from the felling site to an unloading point. Extraction distances range from about 60 m up to 3 km. The carriage can be self-propelled or be powered from a stationary winch system. Traditionally, mechanical sled winches were predominant. Later, hydraulic sled winches gained more traction due to their good controllability regarding limiting maximum force, which is key to ensure the safety of the operation. The drawback of sled winches is that they require a dedicated operator, and usually must be transported to the upper end of the cableway, requiring significant effort for cableway installation. Tower yarders (TY) don't have these limitations and have thus become omnipresent within the industry today. A TY is an all-in-one solution mounted on a trailer, independent tracked vehicle, tractor, or truck.

Self-propelled carriages are a more recent technology, which became available with advancements in drivetrain technology and industrial electronics. The entire hydraulic drivetrain is integrated into the carriage, in the most compact and lightweight way possible. Depending on the type of traction system, the carriage may propel itself forward by acting directly on the skyline or via a separate fixed mainline. These carriages have thus far not been able to gain widespread acceptance among the logging firms, likely due to their low power to weight ratio.

Of the three main types of logging equipment, so far only TYs appear to be close to or in commercialization of hybrid models. Koller (Koller Forsttechnik GmbH, Schwoich, Austria) presented the hybrid yarder K507e-H in 2017 [2] and commercialized it by 2022. Hybridization and electrification are further ahead in not self-propelled carriages, carriages mostly employed in combination with TYs. The first models of electrified slack pullers were available by 2015 [2]. Other carriage types, including dropline carriages, still rely on conventional Diesel-hydraulic drivetrains. The introduction of hybrid-electric systems unlocks opportunities for datalogging, remote control and digitalization, and thus has positive attributes beyond an efficiency gain or increased performance.

2 Carriage Hybridization and Electrification

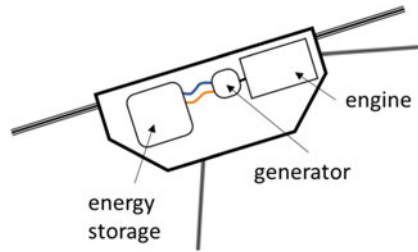
Hybridization and electrification have proven to be effective means to reduce the fuel consumption and emissions in on- and off-road agro-forestry applications [3–7]. Modern electric drives, often based on field-oriented vector control of permanent magnet motors are very power dense. They far outperform the dynamics of mechanical and hydraulic drivetrains, such that their integration does not usually pose a particular challenge. The greatest difficulty when designing electrified equipment is usually associated with the supply of energy. Stationary machinery and mobile equipment bound to a small area can often be grid supplied. This is not an option for forestry equipment. Ground based forestry equipment such as skidders and tower yarders can work with quite bulky energy storage systems based on advanced battery technology or supercapacitors, combined with an engine-generator set in series hybrid setup. This, since space and weight are not very critical. Carriages for cable logging on the other hand don't have this advantage. There are extreme space, but especially weight constraints in such equipment. At the same time carriages need to be very robust since they are prone to mechanical damage from falls or colliding with obstacles along the cableway.

Conventionally, all automated carriage types (slack pullers, dropline carriages and self-propelled carriages) have been powered via Diesel-hydraulic drivetrains. Non automated models with clamping mechanisms worked with hydraulic energy storage units internal to the carriage. Membrane accumulators were charged while moving along the skyline, providing sufficient storage to power only the clamping mechanism, a linear hydraulic actuator.

The far superior energy density of electric energy storage with respect to hydraulic storage units opens an array of new possibilities in how to guarantee energy supply to the carriage. Self-propelled carriages must power the traction drive and the winch system, and must compete with small to medium TYs in terms of their productivity to be commercially viable. This implies that energy must be available at a rate of several tens of kilowatts RMS, with a cycle energy need of several kWh [8]. The only viable option thus seems to be high power energy storage within the carriage, making maximum use of energy to be recovered when moving downhill or lowering the load. Energy which cannot be provided by recuperation must be supplied via an internal engine-generator set. The startup Leitalpin (Leitalpin GmbH, Bolzano, Italy) pursues a concept in this direction [9].

Dropline carriage's movement along the skyline is powered by an external stationary winch system. Thus, energy need and RMS power within the carriage reduce drastically when compared to self-propelled carriages. Lateral yarding only accounts for about 18.2%–22.3% of total cycle time [10, 11]. For the sake of lower fuel consumption, it is therefore likely acceptable, if the carriage achieves significantly smaller performance than conventional dropline carriages. With slack pullers, both the carriage's movement along the skyline and the winch system are powered from an external winch system. Slack pulling thus requires even smaller power and energy.

Fig. 1 Charging via engine - series hybrid concept



Arguably the most obvious approach to supply electrified dropline carriages and slack pullers with energy is the hybridization of their Diesel-hydraulic drivetrains (see Fig. 1). Replacing hydraulic parts with an electric drivetrain leads to fuel savings based on more efficient energy delivery and energy recuperation when lowering the load. Since weight is of utmost concern, avoiding the need of an onboard engine may however be key. This also eliminates the need of frequent refueling. Once installed a sufficiently large energy storage system to cover a complete operation cycle, only average net energy consumption must be guaranteed via some external means of energy supply. This opens an array of new possible technical solutions, discussed as follows.

Both dropline carriages and slack pullers could be supplied by recovering energy while moving along the cableway. Ladstätter (Gebrüder Ladstätter KG, Sankt Jakob in Deferegggen, Austria) presented a new concept in this direction very recently at the international wood fair Klagenfurt 2022. The concept works with an additional, specifically introduced cable (denoted as charging cable) as the fixed reference point (see Fig. 2). The charging cable is wrapped around a pulley in the carriage to create traction for energy recovery. Alternatively, the skyline itself could be used as a fixed reference point to extract energy from while moving along the cableway. Pulleys coupled to generators and pressed from below onto the skyline could create the traction necessary to spin the generators (see Fig. 3). Both concepts would charge a battery system in the carriage when moving downhill, whose energy would later be used for lateral yarding. If controlled properly, otherwise wasted energy can be harvested, effectively improving overall logging efficiency.

Fig. 2 Charging from charging cable while moving downhill

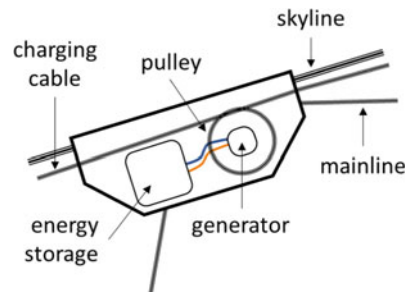


Fig. 3 Charging from skyline while moving downhill

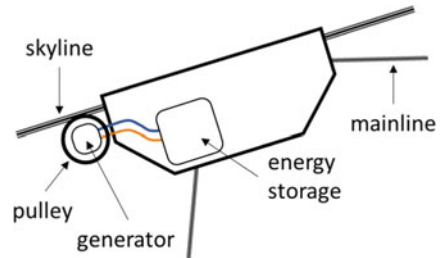
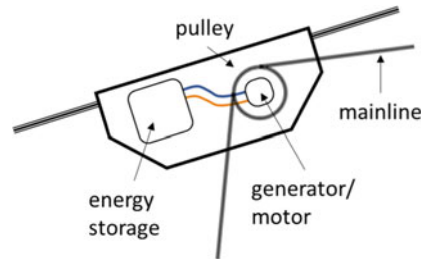


Fig. 4 Charging during lateral yarding



Electrified slack pullers can harvest energy during lateral yarding (see Fig. 4). The external winch system, usually a TY, must power the yarding process and the recharging of the slack puller. While this is a way to fully electrify the carriage, it is not an energy efficient approach. Energy for slack pulling is supplied by a low efficiency TY mechanically by means of a cable, subjected to substantial additional losses, as found by [8]. This approach is, however, very straightforward and robust and has in the meantime been pursued by most of the leading manufacturers. Of all mentioned concepts, only this setup has so far been commercialized.

Both dropline carriages and slack pullers require at least two cables for operation. That is, the skyline and the mainline. This may open the possibility to supply electric energy to the carriage from a stationary power unit (see Fig. 5). A prerequisite is electric isolation between skyline and mainline. While this could be quite easily accomplished at the carriage, the TY would have to be specifically redesigned as well. For safety purposes and based on the general product safety directive (2001/95/EC), 75 V DC would not have to be exceeded. 800 m of 11 mm mainline cable has a resistance of about 1 Ω . This can be computed from the specific resistance and density of steel (0.1 $\mu\Omega\text{m}$, 7850 kg/m³) respectively and the specific weight of the cable (0.63 kg/m) [11]. Accepting a 10% energy loss across the mainline cable (6 A) would thus allow for a transfer of 360 W of power at 60 V. With an average cycle duration of approximately 360 s and 86 Wh–287 Wh of energy need per lateral yarding cycle [12], this could only supply about 12.5–41.9% of the energy need of dropline carriages and would thus not be feasible. Electrified slack pullers provide a force of about 1000 N for about 80 m of slack pulling distance, constituting 80 kW_s of energy, not considering losses. Assuming losses as large as 35%, sufficient energy could still be supplied via the cables.

Fig. 5 Charging via power supply between skyline and mainline

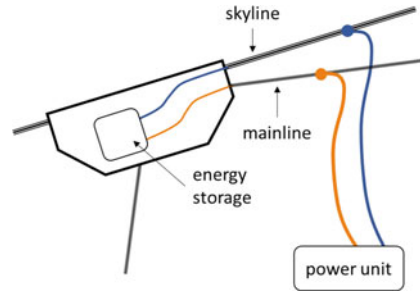
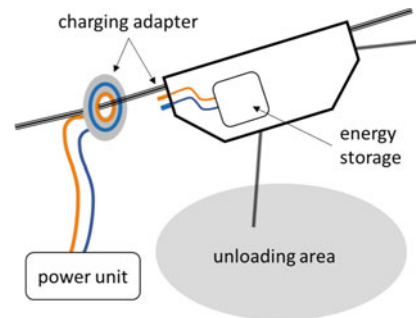


Fig. 6 Charging via power adapter on the skyline



The unloading point for the payload is usually fixed, and accessible via road vehicles. There it may be possible to recharge the carriage via an adapter on the skyline, connecting via cables to a stationary power unit (see Fig. 6). The voltage level could be brought up to the common EV levels of 350 V or 700 V, and a charging power of at least 50 kW can be envisioned. Charging a dropline carriage would then only last about 20 s [12]. A slack-puller could be charged with lower power in even less time, not impacting the productivity of the logging system. Such high charging power would also be feasible for a supercapacitor pack providing enough energy for the demanded operation.

3 Mechatronic Solutions for Smart Carriages

In recent years as technology has advanced, it has enabled a major revolution in the industrial world, i.e., Industry 4.0: large amounts of data are collected from various process activities, organized, and interpreted to obtain usable information about the state, the productivity, the efficiency and the estimation of input and output. This smart approach principle is slowly expanding into other sectors and the agro-forestry one is not exempt.

Data collection therefore becomes a key point of this approach. The amount of timber cut, the characteristics of the logs in terms of diameter, length, wood,

and crown characteristics, as well as the felling position are all part of the useful information set for the operational monitoring of the forestry activity. Advanced forestry machines are nowadays equipped with integrated Information Technology (IT) systems that automatically perform this task. However, the forestry sector is very variable, ranging from large companies equipped with such kind of machines, to small ones with few forestry tractors and where felling and rigging is carried out directly by operators with chainsaws. In this latter case, the collection of data can rely only on the filling in of reports/tables by the operators themselves. Time, however, is often lacking and the field activity registers are filled in at the weekend or at the end of the entire operation, leading to uncertainties and missing information due to forgetfulness [13].

Focusing on the activity of cable logging, while its practice is well established, productivity is dependent on many stand and terrain variables. Being able to continuously monitor a cable yarder operation would provide the opportunity not only to manage and improve the system, but also to study the effect on operations in different conditions. Usually, cable logging is characterized by a low level of integrated IT systems. However, operational monitoring could be implemented at different levels through the integration of proper sensors, independent of the system itself, to make operational monitoring possible. Indeed, a multisensory system can be added to the carriage [14] or, in future, can be embedded in the hybrid-electric machine. Thanks to a Global Navigation Satellite System (GNSS) module placed on the carriage (see Fig. 7), it is possible to carry out an automatic time study by recognizing all the elemental phases (i.e., outhaul, hook, inhaul, and unhook) as well. Meanwhile, an automatic and fast estimation of the hauled weights without the need of any manual measurement for the operator during the hooking phases could be implemented. On this regard, a load-cell, mounted between the hook and the chokers, to measure the pulling force applied by the carriage as well as an Inertial Measurement Unit (IMU) integrated into the hook to detect the rope orientation and therefore to correct the weight result in case of skidding/dragging operations are appropriate additional sensors to be considered.

Fig. 7 Carriage operational monitoring

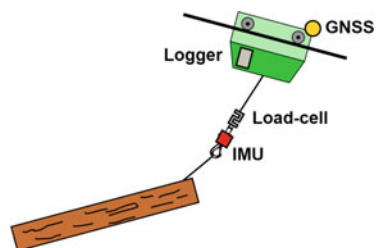


Table 1 Overview carriage energy supply concepts with respect to their technical complexity, overall logging efficiency and applicability

Energy supply concept	Technical complexity	Overall system efficiency	Possibility of lack of energy	Applicability		
				SPC	DC	SP
Series hybrid	●●●	●●●	NO	✓	●	●
Charging cable	●●	●●●	YES		✓	●
Skyline pulley	●●	●●●	YES		●	●
Lateral yarding	●	●	YES			✓
Skyline and mainline	●●●	●	NO			●
Power adapter	●●	●●	YES	●	●	●

4 Discussion

Table 1 gives an overview of all carriage energy supply techniques discussed in Sect. 2, including their technical complexity, overall logging efficiency and applicability in self-propelled carriages (SPC), dropline carriages (DC) and slack pullers (SP). In the columns labelled as “Applicability”, “✓” indicates that a carriage employing this concept is being developed or already commercialized. “●” indicates that the concept appears technologically feasible for the application but hasn’t been explored yet in practice. It does, however, not automatically imply that the concept is attractive for the given application.

To the author’s knowledge, non-automated carriages continue to rely on conventional hydraulic energy storage. This is likely because this is a well-tested, robust, and straightforward solution, satisfying all requirements for this particular application solely based on linear hydraulic actuators.

The availability of sensors such as the GNSS, load-cell or IMU allows the implementation of a control system that manages collected data and carries out the first data processing. Data can today be synchronized and stored in a buffer memory or in a mini-SD and then be downloaded to feed a Database Management System. In the next future, also thanks to the availability of hybrid-electric systems with embedded sensors and computational power, real-time processing and elaboration can be envisioned to support forestry operations and operators’ work and safety.

5 Conclusion and Future Work

Most equipment for cable yarding, including carriages, still relies on conventional Diesel-hydraulic drivetrains. Only electrified slack pullers are already on the market, but electrified dropline carriages and self-propelled carriages are under development (Ladstätter and Leitlpin, respectively). This work presented the activities on winch assisted forestry machinery carried out at the FiRST and AFI labs of the unibz.

An overview of the different ways in which electrified carriages could be supplied with energy as well as a discussion on the opportunities of digitalization for their operational monitoring is presented. While not all concepts fit all carriage types, a few design ideas appear promising and should be further explored. The objective of future work is to perform practical tests with electrified carriages and mechatronic devices for operational monitoring to validate the concepts and quantify their potential benefits.

Acknowledgements This study was carried out within the Agritech National Research Center and received funding from the European Union Next-GenerationEU (PIANO NAZIONALE DI RIPRESA E RESILIENZA (PNRR) – MISSIONE 4 COMPONENTE 2, INVESTIMENTO 1.4 – D.D. 1032 17/06/2022, CN00000022). This manuscript reflects only the authors' views and opinions, neither the European Union nor the European Commission can be considered responsible for them.

References

1. Jaime, L., Batllori, E., Ferretti, M., Lloret, F.: Climatic and stand drivers of forest resistance to recent bark beetle disturbance in European coniferous forests. *Global Change Biol.* **28**(8), 2830–2841 (2022)
2. Visser, R.: Harvesting technology watch - new cable yarding technology from Europe - Koller hybrid tower Yarder (2015). <https://fgr.nz/documents/download/3763> Accessed 09 Dec 2022
3. Mergl, V., Pandur, Z., Klepárník, J., Kopešek, H., Bačič, M., Sušnjar, M.: Technical solutions of forest machine hybridization. *Energies* **14**(10), 2793 (2021)
4. Pandur, Z., Sušnjar, M., Bačič, M.: Battery technology – use in forestry. *Croatian J. Forest Eng.* **42**(1), 135–148 (2021)
5. Karlušić, J., et al.: Simulation models of skidder conventional and hybrid drive. *Forests* **11**(9), 921 (2020)
6. Rong-Feng, S., Xiaozhen, Z., Chengjun, Z.: Study on drive system of hybrid tree harvester. *Sci. World J.* **2017**, 1–7 (2017).
7. Prochazka, P., Pazdera, I., Cipin, R.: Hybrid tree harvester machine with battery powered hydro-electric drive. *ECS Trans.* **95**, 349–354 (2019). Chap. 1
8. Leitner, S., Perez Estevez, M.A., Renzi, M., Vidoni, R.: Tower yarder energy efficiency study in logging operations: hydraulic vs. hybridized drivetrain. In: 10th International Conference on Sustainable Energy Engineering and Application, ICSEEA 2022; Research Organization for Energy and Manufacture; November 22–23, 2022, Puspiptek, Serpong, Tangerang Selatan, Indonesia (2022)
9. Leitalpin Ltd., What. <https://www.leitalpin.com/en/Projects/>. Accessed 16 Sep 2022
10. Varch, T., Erber, G., Spinelli, R., Magagnotti, N., Stampfer, K.: Productivity, fuel consumption and cost in whole tree cable yarding: conventional diesel carriage versus electrical energy-recuperating carriage. *Int. J. Forest Eng.* **32**, 20–30 (2021)
11. Spinelli, R., et al.: The effect of carriage type on yarding productivity and cost. *Int. J. Forest Eng.* **28**, 34–41 (2017)
12. Teufelberger Homepage. <https://www.teufelberger.com/en/f20.html>. Accessed 12 Sep 2022
13. Cadei, A., et al.: Energy efficiency of a hybrid cable yarding system: a case study in the North-Eastern Italian Alps under real working conditions. *J. Agric. Eng.* **52** (2021)

14. Gallo, R., Carabin, G., Vidoni, R., Sacco, P., Mazzetto, F.: Solutions for the automation of operational monitoring activities for agricultural and forestry tasks. *Die Bodenkultur: J. Land Manag. Food Environ.* **69**(3), 131–140 (2018). <https://doi.org/10.2478/boku-2018-0012>
15. Gallo, R., Visser, R., Mazzetto, F.: Developing an automated monitoring system for cable yarding systems. *Croatian J. Forest Eng.* **42**(2), 213–225 (2021). <https://doi.org/10.5552/crojfe.2021.768>

Feasibility of Two MEMS-NIR Spectrophotometers for Characterizing Different Biofuel Origin



Elena Leoni, Manuela Mancini, Alberto Assirelli, Sara di Stefano, and Giuseppe Toscano

Abstract The EU common effort to reduce fossil fuel consumption paves the way to enhancing interest towards renewable resources, as solid biofuel. Its properties and origin are fundamental issues affecting energy conversion efficiency and supply chain sustainability. Laboratory conventional analyses are time consuming and require huge economic efforts, so it is essential to obtain rapid and real-time quality information along all the supply chain. Near Infrared Spectroscopy (NIRS) is able to satisfy these requirements, minimizing the time delay and promoting on site analysis along the whole process. The aim of the present work is to evaluate the performance of two different portable MEMS (Micro Electro Mechanical System) NIR spectrophotometers for identifying the raw biomass of which pellet is made. Thus, samples of different categories have been collected, particularly Italian softwood and hardwood species, wood processing industry residues and bioenergy crops. Ten replicates for each sample have been performed and different spectral pretreatments have been tested to reduce noise and scattering effects. Principal Component Analysis (PCA) has been used to investigate the spectral variability and look for groupings among the categories. According to the spectral range, the C12 and C13 spectrophotometers revealed different performance in groups separation due to the detection of different chemical bonds, for example glue presence. More interesting results could be obtained by widening the biomass samples to manage stronger dataset for chemometrics analysis. Nevertheless, results of the research aim at introducing NIR sensor, coupled with chemometrics, onboard pellet combustion devices to improve process efficiency and environmental performance.

Keywords Precision bioenergy · NIRS · PCA · Quality · Pellet

E. Leoni (✉) · M. Mancini · S. di Stefano · G. Toscano
Department of Agricultural, Food and Environmental Science, Università Politecnica delle Marche, 60131 Ancona, Italy
e-mail: e.leoni@pm.univpm.it

A. Assirelli
CREA-IT, Via delle Pascolare 16, 00016 Monterotondo, Roma, Italy

© The Author(s), under exclusive license to Springer Nature Switzerland AG 2023
V. Ferro et al. (eds.), *AIIA 2022: Biosystems Engineering Towards the Green Deal*,
Lecture Notes in Civil Engineering 337,
https://doi.org/10.1007/978-3-031-30329-6_68

1 Introduction

The current economic and political situation and the EU effort to reduce fossil fuel consumption paves the way to enhancing interest towards renewable resources. Solid biofuels play a key role, but their physical properties and origin are fundamental issues affecting energy conversion efficiency and supply chain sustainability [1]. Specific standards regulate the quality parameters and the analysis procedures of solid biofuels, ensuring the acquisition of comparable data. Specifically, solid biofuel characterization is regulated by EN ISO 17225, which, in addition, defines the standard assigned to the analytic procedure of each parameter. But laboratory conventional analyses are time consuming and require important economic efforts, therefore it is crucial to obtain rapid and real-time quality control method along all the supply chain [2]. Near Infrared Spectroscopy (NIRS), coupled with chemometrics, proves to be able to satisfy these requirements, minimizing the time delay of the laboratory analyses and promoting on-site monitoring along the whole process [3]. According to the guidelines of NIRS application provided by the UNI/TS 11,765:2019 and according to standard reference applications, moisture content, ash content, and gross calorific value are considered key quality indicators. Furthermore, the origin of the biofuel (Table 1 of EN ISO 17225–1) is a crucial parameter which affects biomass characteristics.

The main aim of the present work is to evaluate the performance of two different portable MEMS (Micro Electro- Mechanical System) NIR spectrophotometers for identifying and detecting the raw inner components of different pellet source. In this

Table 1 Class division of considered biomass samples

Aim	Biomass origin	Number of samples
<i>Softwood/Hardwood</i>	Pine tree (<i>Pinus</i>)	15
	Fir wood (<i>Abies alba</i>)	19
	Oak (<i>Quercus petraea</i>)	9
	Chestnut (<i>Castanea sativa</i>)	4
	Beech (<i>Fagus sylvatica</i>)	25
<i>Treated wood</i>	Oriented Strand Board (OSB)	12
	Chipboard (CB)	29
	Plywood (PW)	2
	Multilayer (MLT)	3
<i>Herbaceous</i>	Straw ¹	15
	Sorghum (<i>Sorghum vulgare</i>)	15
	Sorghum stalk (<i>Sorghum vulgare</i>)	15
	Corn stalk (<i>Zea mays</i>)	15

1: *Triticum durum*, *Triticum aestivum*, *Hordeum vulgare*

way, three categories are investigated to evaluate three groups separation: i) soft-wood and hardwood species, ii) wood processing industry residues and iii) bioenergy crops. The multivariate analysis of PCA, thanks to the chemometric approach related to NIRS application, has been developed for each comparative group. Two spectrophotometers with different spectral range have been considered to evaluate differences in chemical components detection.

2 Material and Method

2.1 Biomass Material

To start the investigation, a total of 178 sample have been considered. According to the different classification analyses, different biomass typologies have been collected for each category, as shown in Table 1.

Each sample, after stabilization process, has been milled to 1 mm of particle size using a cutting mill (mod.SM 2000, RETSCH), then each sample has been stored in hermetically closed plastic vial to maintain physical characteristics unaltered.

2.2 NIRS Analysis

NIR spectral acquisitions were performed using two compact and portable spectrophotometers MEMS (Micro Electro-Mechanical System, HAMAMATSU) operating on different spectral range: i) C15712 model (C12): 1350–1650 nm (7407–6061 cm^{-1}), spectral resolution of 18 nm, and ii) C15713 model (C13): 1550–1850 nm (6452–5405 cm^{-1}), spectral resolution of 20 nm. These modules have built-in light source (tungsten lamp) and MEMS-FPI spectrum sensor (InGaAs photodiode), using Fabry–Perot Interferometer. Their compact size and weight (32 × 74 × 16 and 80 gr) make them handy and suitable for on-field application.

The acquisitions were carried out in reflectance mode. The reference, shading (light on) and background spectrum (light off) were acquired every hour during the analysis. Ten replicates were performed for each sample, following pyramidal scheme around the little heap poured from the plastic vial on a flat surface.

2.3 Chemometric Elaboration

Chemometrics turned out to be fundamental to multivariate analyses performances to extract relevant information from spectral data about the material origin, according to chemical differences between biomass sources. PCA method was computed for

each material classification using Matlab (ver. 9.7.0, 2019) to group sample among different categories. Spectra were pretreated to reduce noise and scattering effect, coming from external lights interference. PCA analysis were developed on mean-centered data of the replicates and performances have been checked using score plot. Then spectra interpretation has been carried out in the loading plot to main relevant peaks assessment, considering Principal Components (PCs) investigation to identify main discriminative chemical components.

3 Results

3.1 Softwood/Hardwood

A total of 72 virgin wood samples have been considered to discriminate softwood from hardwood. According to the spectral range, C13 spectrophotometer has shown to provide a better separation between hardwood and softwood species than C12 due to C-H bonds detection related to wood components. The best performance has been obtained with second derivative pre-treatment (second polynomial order, 21 smoothing points with Savitzky-Golay) on the entire spectral range and each sample was averaged across its ten replicates.

The spatial distribution for the first and second PC has been provided in the score plot (Fig. 1). The clear separation between groups and the higher scattering distribution of hardwood samples could be due to their higher inner variability [4].

The most relevant wavenumbers, related to the negative peaks according to the derivative pretreatment (second derivative), have been provided in the loading plot

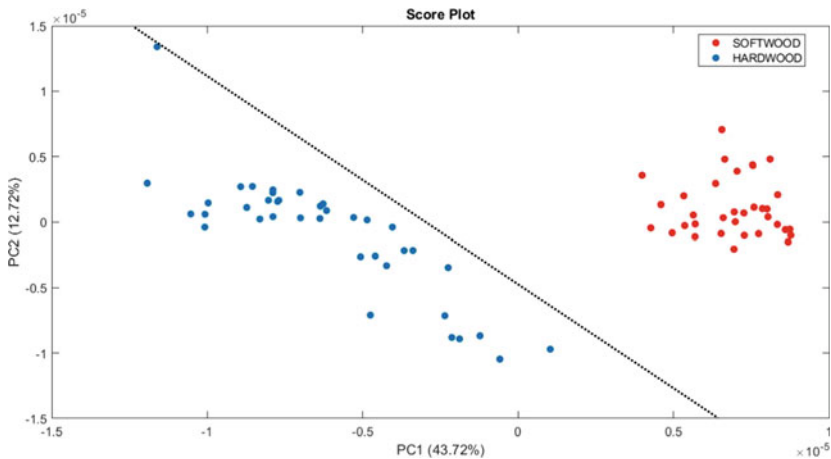


Fig. 1 Score plot of the two PCs for the virgin wood separation (softwood/hardwood). The dash line shows the evident separation between groups

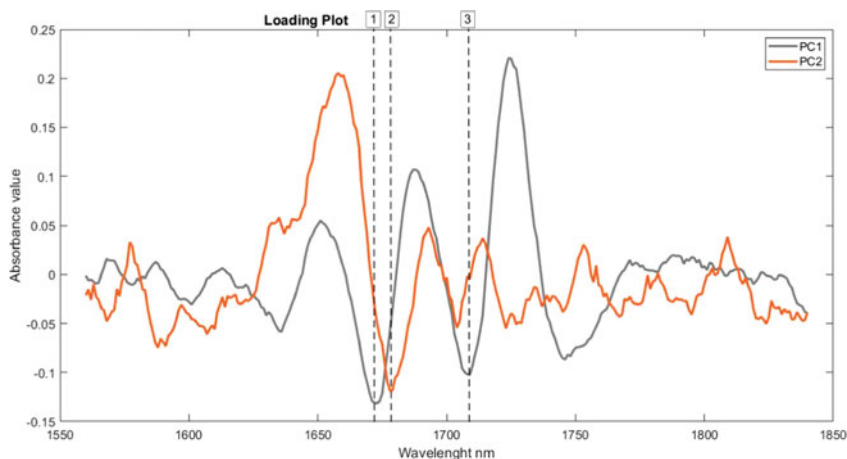


Fig. 2 Loading plot of spectra with second derivative (second polynomial order, 21 smoothing points with Savitzky Golay) related to softwood/hardwood separation. Dash lines and respective number refer to the main negative peaks revealed

(Fig. 2). Dash line and corresponding number have been used to identify the main negative peaks both related to the first and second PCs. In particular: 1) peak at 1672 nm is related to aromatic groups of lignin, while 2) peak at 1679 nm and 3) peak at 1709 nm are related to hemicellulose (C-H stretching bonds) [5].

3.2 Virgin Wood/Herbaceous

A total of 72 virgin wood and 60 herbaceous samples have been considered to discriminate between different biomaterials. According to the spectral range, C13 spectrophotometer has again shown a slight better separation between typologies than C12, related to wood components. The best performance has been obtained with second derivative pre-treatment (second polynomial order, 21 smoothing points with Savitzky-Golay) on the entire spectral range and each sample was averaged across its ten replicates.

The spatial distribution for the first and second PC has been provided in the score plot (Fig. 3). The clear separation between hardwood and softwood is confirmed, as well as the separation with herbaceous material, where samples show a less scattering because of the reduced heterogeneity.

The most relevant wavenumbers, related to the negative peaks according to the derivative pretreatment (second derivative), have been provided in the loading plot (Fig. 4). Even in this case, dash line and corresponding number have been used to identify the main negative peaks both related to the first and second PCs. Detected

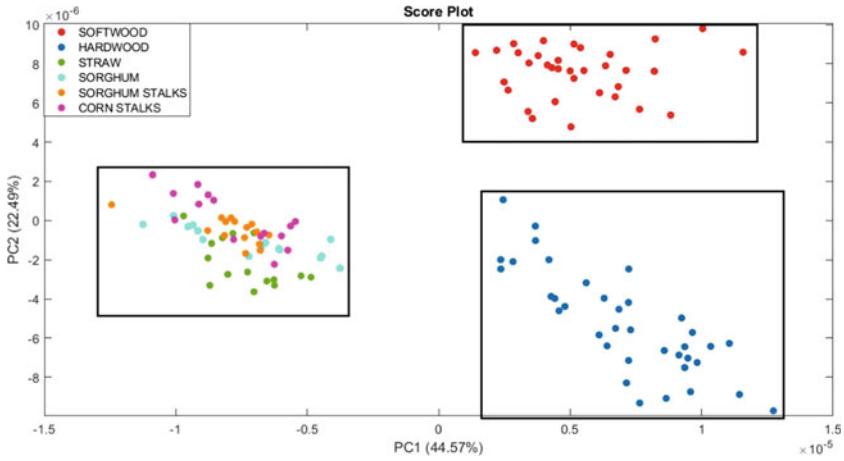


Fig. 3 Score plot of the two PCs for the virgin wood-herbaceous separation. The rectangular blocks help to better shaping the separation

peaks comply with the previous detection for the virgin material separation, in particular: 1) peak at 1670 nm is related to aromatic groups of lignin, while 2) peak at 1705 nm is related to hemicellulose; 3) peak at 1725 nm corresponded to C-H stretching bonds [5].

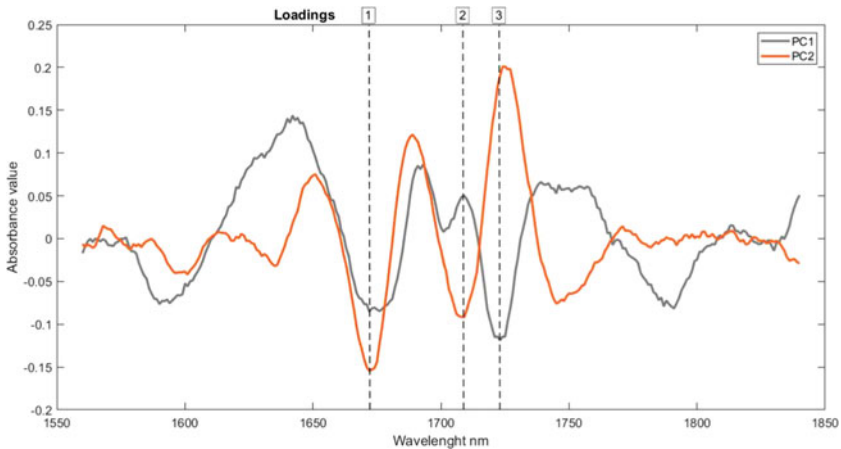


Fig. 4 Loading plot of spectra with second derivative (second polynomial order, 21 smoothing points with Savitzky Golay) related to virgin wood/herbaceous samples separation. Dash lines and respective number refer to the main negative peaks revealed

3.3 Virgin Wood/Treated Wood

A total of 72 virgin wood and 46 treated wood samples have been considered to discriminate the treatment degree of wood. According to the spectral range, C12 spectrophotometer has shown better performance than C13 in grouping related to wood additives and components. The best performance has been obtained with first derivative pre-treatment (second polynomial order, 21 smoothing points with Savitzky-Golay) on the entire spectral range and each sample was averaged across its ten replicates.

The spatial distribution for the first and second PC has been provided in the score plot (Fig. 5). The limited separation between virgin and treated wood is more evident along both PC1 and PC2 directions. In particular, virgin wood main fitting the positive PC1 and negative PC2, whereas the opposite has been confirmed for treated wood. The closeness between softwood and treated wood reflects the use of fir wood residues in industrial wood treatment, in particular for OSB and plywood [6], while hardwood is confirmed more heterogenous than other groups [4].

The most relevant wavenumbers, related to the positive peaks according to the first derivative pre-treatment, have been provide in the loading plot (Fig. 6). Even in this case, dash line and corresponding number have been used to identify the main positive peaks both related to the first and second PCs. Although detected peaks shown to be less significant, they are more concentrated in different wavenumbers than previous separations, in particular: 1) peak at 1405 nm, related to lignin and extractives and 2) peak at 1480 nm, related to cellulose and to O-H stretching bonds. This shifting is probably related to specific glue bonds detection [7].

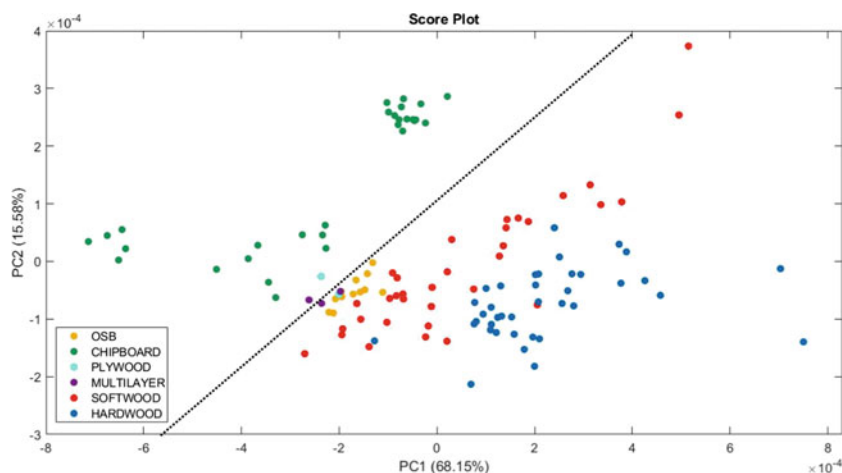


Fig. 5 Score plot of the two PCs for the virgin wood-treated wood separation. The dash line shows the slight and not marked separation between groups

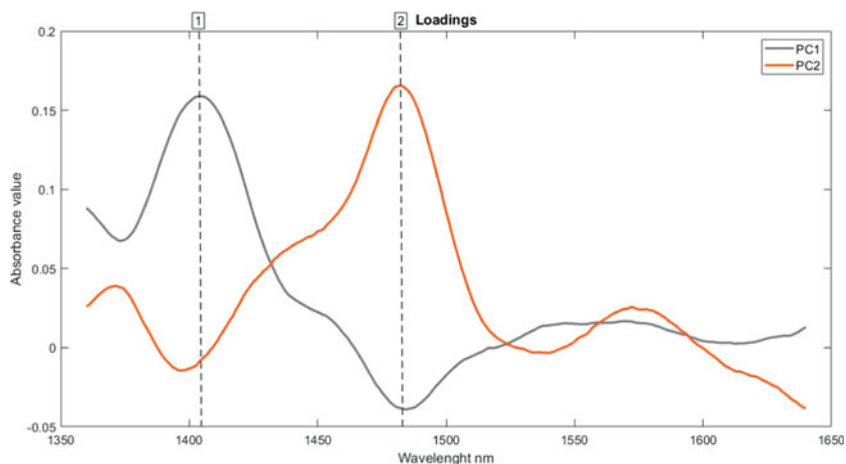


Fig. 6 Loading plot of spectra with first derivative related to virgin wood/treated wood samples separation. Dash lines and respective number refer to the main positive peaks revealed

4 Conclusion

Results demonstrate the reliability of the performances of NIR application to discriminate origin and biomass chemical components. More useful results could be obtained by widening the biomass samples to manage stronger dataset for chemometrics analysis. Nevertheless, NIRS can be considered a smart, rapid and cost-effective tool to characterize biofuel quality and to improve the effectiveness of biomass placing and utilization as a renewable resource. Furthermore, the use of portable NIRS instruments, coupled with chemometrics, could enhance the monitoring performance, onboard combustion devices and along conveyor belts, to control environmental impact.

References

1. Toscano, G., Leoni, E., Feliciangeli, G., Duca, D., Mancini, M.: Application of ISO standards on sampling and effects on the quality assessment of solid biofuel employed in a real power plant. *Fuel* **278**, 118142 (2020). <https://doi.org/10.1016/j.fuel.2020.118142>
2. Mancini, M., Duca, D., Toscano, G.: Laboratory customized online measurements for the prediction of the key-parameters of biomass quality control. *J. Near Infrared Spectrosc.* **27**(1), 15–25 (2019). <https://doi.org/10.1177/0967033518825341>
3. Pasquini, C.: Near infrared spectroscopy: a mature analytical technique with new perspectives – a review. *Anal. Chim. Acta* **1026**, 8–36 (2018). <https://doi.org/10.1016/j.aca.2018.04.004>
4. Duca, D., et al.: Soft independent modelling of class analogy applied to infrared spectroscopy for rapid discrimination between hardwood and softwood **117** (2016). <https://doi.org/10.1016/j.energy.2016.10.092>.

5. Schwanninger, M., Rodrigues, J.C., Fackler, K.: A review of band assignments in near infrared spectra of wood and wood components. *J. Near Infrared Spectrosc.* **19**, 287–308 (2011). <https://doi.org/10.1255/jnirs.955>
6. Mancini, M., et al.: Near infrared spectroscopy for the discrimination between different residues of the wood processing industry in the pellet sector. *Fuel* **217**, 650–655 (2018). <https://doi.org/10.1016/j.fuel.2018.01.008>
7. Mancini, M., Rinnan, Å., Pizzi, A., Toscano, G.: Use of fourier transform near infrared spectroscopy for the detection of residues from wood processing industry in the pellet sector. In: *Proceedings of the 18th International Conference on Near Infrared Spectroscopy*, pp. 77–84 (2019). <https://doi.org/10.1255/nir2017.077>

A Prototype of Photovoltaic Dryer for Nutraceutical and Aromatic Plants



Michele Massimo Mammano, Antonio Comparetti, Salvatore Ciulla, Carlo Greco, and Santo Orlando

Abstract In the past, the interest in nutraceutical and aromatic plants mainly concerned the derivatives and ingredients industries, while nowadays their growing use occurs in different sectors, such as functional food (nutraceuticals), infusion drinks (herbal teas) and bio-ecological cosmetics. The microbiological quality of nutraceutical and aromatic plants is an important criterion for buyers. In order to reduce the bacterial load of these plants, Italian producers impose specific hygiene rules, that mainly concern the operations carried out between harvest and packaging, i.e. the drying process. The drying process takes place at low or high temperatures, from 20 to 50 °C. This type of drying can be obtained by means of a device equipped with a heat pump: drying is obtained by applying very dry air (having a humidity of 5%) to the dehumidified products and heating them up to the desired temperature. This process allows to rapidly dry food, by preserving its colour, aroma and chemical composition, thereby obtaining high quality products. This work describes a prototype of dryer powered by a photovoltaic Renewable Energy Source (RES) for nutraceutical and aromatic species produced in Sicily. The aim of this work is to satisfy the yearly consumption of the dryer through the energy produced by the photovoltaic generator, mounted on the roof and one of the facades of the dryer structure (on-site exchange and self-consumption of electrical energy).

The yearly potential production of the photovoltaic generator is 8383 kWh. A total electrical energy consumption of 190 kWh is estimated for each drying cycle. Thus, the dryer can be used for up to 44 drying cycles a year using the energy produced by the photovoltaic generator.

M. M. Mammano · C. Greco (✉)

Council for Agricultural Research and Economics (CREA), Research Centre Protection and Certification, 90011 Bagheria, Palermo, Italy
e-mail: carlo.greco@crea.gov.it

A. Comparetti · S. Orlando

Department of Agricultural, Food and Forest Sciences, University of Palermo, Viale Delle Scienze, Building 4, 90128 Palermo, Italy

S. Ciulla

Association of Producers SiciliaBio, Via Vittorio Emanuele, 100, 92026 Favara, Agrigento, Italy

The prototype of the photovoltaic dryer will allow to monitor and control the drying process, in order to identify any critical points during it, as well as the failures occurring inside the drying chamber.

Keywords Nutraceutical species · Aromatic species · Drying process · Renewable Energy Sources (RES) · Photovoltaic generator · Energy efficiency

1 Introduction

1.1 Nutraceutical and Aromatic Plants

In the past, the interest in nutraceutical and aromatic plants mainly concerned the derivatives and ingredients industries, while nowadays their growing use occurs in different sectors, such as functional food (nutraceuticals), infusion drinks (herbal teas) and bio-ecological cosmetics [1].

In the last few years, the interest of consumers towards nutraceutical and aromatic herbs recorded a growing trend, both in terms of product types and consumption [1, 2].

There is a growing interest in nutraceutical and aromatic plants worldwide. These species are used for food, flavourings, cosmetics and medicinal purposes. Dr. Stephen L. De Felice coined the term “nutraceutical”, derived from the words “nutrition” and “pharmaceutical”. In 1989, he stated: “a nutraceutical is any substance that is a food or a part of a food and provides medical or health benefits, including the prevention and treatment of disease. Such products may range from isolated nutrients, dietary supplements and specific diets to genetically engineered designer foods, herbal products, and processed foods such as cereals, soups, and beverages” [2].

In Sicily, *Origanum vulgare* L., *Lavandula angustifolia* L., *Salvia officinalis* L., *Rosmarinus officinalis* L., *Laurus nobilis* L. and other similar aromatic plant species could be used for nutraceutical purposes [3–8].

Special attention is paid to superfood plants, such as *Moringa oleifera* Lam., an evergreen shrub native to the sub-Himalayan belt, characterised by rapid growth and high resistance to drought, as well as widespread in different world areas. All the components of this plant (leaves, flowers, pods, fruits, bark and roots) can be used, as they are particularly rich in nutrients, vitamins, aminoacids and antioxidants. These characteristics allow it to be used for human and livestock nutrition, for obtaining food supplements and, last but not least, for producing compounds biostimulating cultivated plants [1, 6].

1.2 Drying Process

The microbiological quality of nutraceutical and aromatic plants is an important criterion for buyers. In order to reduce the bacterial load of these plants, Italian producers impose specific hygiene rules, that mainly concern the operations carried out between harvest and packaging, i.e. the drying process.

The drying process takes place at low or high temperatures, from 20 to 50 °C. This type of drying can be obtained by means of a device equipped with a heat pump: drying is obtained by applying very dry air (having a humidity of 5%) to the dehumidified products and heating them up to the desired temperature.

Drying is a process aimed at rapidly reducing the water content in plant materials below a limit where the activity of microbes and decomposing enzymes deteriorates the quality of nutraceutical and aromatic plants.

Drying is one of the key steps in the processing of aromatic plants. It is essential to perform it in the best way possible, to preserve the organoleptic qualities (i.e. colour, aroma and contents of essential oils and active ingredients) of the final product.

Research performed on some food products, e.g. ginger, mint, onion, chilli and bay leaves, show that an appropriate selection of treatment conditions, i.e. temperature and time, can reduce appearance alterations, such as global colour change and degradation of molecules of nutritional interest, e.g. ascorbic acid and gingerol [5].

A freshly harvested plant contains up to 80% of water. This content (expressed as a percentage) is computed from the ratio between the total mass of water contained in the plant and the initial total mass.

Drying is essential to preserve the product in optimal conditions and must be carried out immediately after harvesting. The simple working principle of this process consists in extracting the water contained in the plant by evaporation in the air. Evaporation occurs due to a gradient between the water content on the plant surface and the water vapour in the air. Therefore, a stable dried plant has a water content between 5 and 13%, depending on the species [9].

A product is dried when it is stabilised in the air and has no longer risk degradation, which is mainly due to mould development.

Yet, as the plants are hygroscopic, i.e. they can absorb water from the environment, a dried plant material, even considered stable, can absorb water and, therefore, degrade, if it is not correctly stored.

Therefore, to avoid product degradation, it is needed to pay attention to the storage conditions, packaging and environmental parameters, i.e. air temperature and humidity.

This work describes a prototype of a dryer powered by a photovoltaic Renewable Energy Source (RES) for nutraceutical and aromatic species [10–12] produced in Sicily.

1.3 Dimensioning the Photovoltaic Dryer

A prefabricated iron structure consisting of a standard container, type 20 feet (width 2.43 m × length 6.05 m × height 2.56 m), was suitably modified to house the dryer (Fig. 1). A photovoltaic generator, appropriately sized to generate the energy needed to perform 44 drying cycles at full load, was mounted on the roof and one of the two facades of this structure.

In order to be able to use the whole potentiality of a such dimensioned photovoltaic generator, a wet mass of 140 kg, having a water content (WC) of 80%, must be fed into the dryer. The drying cycle ends when the product has a final residual water content of 10%.

Therefore, the quantity of water to be removed from the product during each drying cycle can be calculated according to the block diagram shown in Fig. 2.

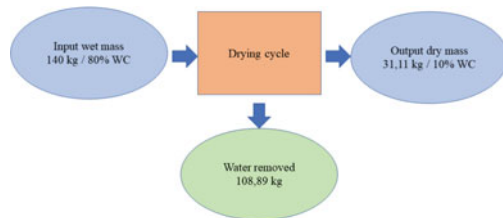
During each drying cycle at full load, approximately 109 l of water can be removed from the wet product fed in the dryer. An absorption machine is sized on this quantity. This machine has a dehumidification power of 52.8 kg 24 h⁻¹, in the standard conditions of suction air, i.e. temperature of 20 °C and humidity of 60%.

Therefore, each drying cycle lasts for 49.5 h, just more than two days. However, the drying cycle time can be variable, depending on the nutraceutical or aromatic species to be dried, the drying season and the desired quantity of final wet product. In addition to the absorption machine, to keep the temperature within a range between 10 and 30 °C, the drying chamber can be equipped with a reversible compression heat pump having a power of 9000 BTU. The dehumidification contribution given by the



Fig. 1 Structure of a photovoltaic dryer for nutraceutical and aromatic plants

Fig. 2 Calculation the quantity of water to be removed from the product during each drying cycle



air conditioner, operating in the winter period for increasing the room temperature, is conservatively neglected in sizing the photovoltaic dryer.

The aim of this work is to satisfy the yearly consumption of the dryer through the energy produced by the photovoltaic generator, mounted on the roof and one of the facades of the dryer structure, as well as constituted by two strings.

In fact, it is possible to mount six photovoltaic modules, each having a power of 500 W, on the roof of this structure, with an azimuth of 0° South and an inclination of 30° with respect to the horizontal plane, and other six photovoltaic modules of 500 W, on the South elevation of the container, with an azimuth of 0° South and an inclination of 60°, with respect to the horizontal plane.

The yearly potential production of the photovoltaic generator is 8383 kWh, being the sum of the production of photovoltaic strings 1 and 2, i.e. 4407 and 3976 kWh, respectively.

Then, based on the yearly potential production of the photovoltaic generator, it is possible to compute the maximum number of drying cycles which can be performed at full load during a year, so that the total electrical energy consumption does not exceed the renewable energy produced by the photovoltaic generator itself.

The nominal power of the absorption machine is 3.0 kW, while the nominal electrical power of the 9000 BTU heat pump is 0.78 kW.

Therefore, assuming that both the absorption machine and the heat pump work at their nominal power in a constant manner, the total electrical energy consumption during each drying cycle is 187.11 kWh.

Considering the energy required to power the temperature and humidity sensors, the PLC (Programmable Logic Controller) and the LED light, a total electrical energy consumption of 190 kWh is estimated for each drying cycle.

Thus, the dryer can be used for up to 44 drying cycles a year using the energy produced by the photovoltaic generator.

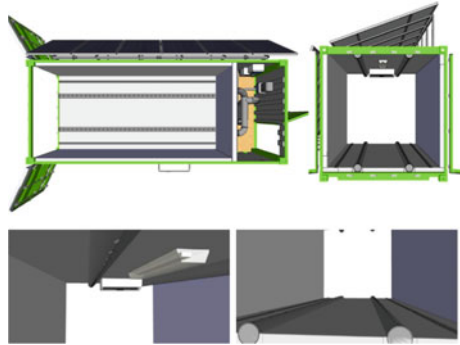
2 Description of the Dryer

2.1 Drying Chamber

The dryer consists of two compartments, i.e. drying chamber and the technical compartment.

The drying chamber (Fig. 3) has the following net dimensions: width 2.18 m × length 4.65 m × height 2.20 m, for a net volume of 22.30 m³. The walls, the ceiling and the floor are insulated from the external environment through an internal lining with an 80 mm multilayer panel having a thermal conductivity of 0.025 W mK⁻¹. This insulation allows the chamber to reduce thermal fluctuations due to the environmental temperature and/or external irradiation.

Two suitably perforated PVC pipes are mounted on the insulated floor of the drying chamber, to remove the process air (humid air becomes dried). Other PVC

Fig. 3 Drying chamber

pipes are symmetrically mounted on the ceiling of this chamber, to introduce the dry air coming from the absorption machine into the drying chamber itself.

The drying cycle can be regulated by a hygrometric probe, placed inside the drying chamber and directly connected to the absorption machine.

In order to keep the drying temperature constant within the 10–30 °C range, the drying chamber can be equipped with a 9000 BTU reversible compression heat pump, having a power of 2.9 kW ca. for heating (Coefficient Of Performance - COP - higher or equal to 3.71), and 2.7 kW for cooling (COP higher or equal to 3.52). In addition, to keep the temperature within the above operating range, this heat pump will further reduce the drying cycle time.

The drying chamber is equipped with an IP65 LED ceiling light, to allow loading/unloading and maintenance of the chamber itself.

The access to the drying chamber can be assured through the opening of two hinged doors, placed on the side opposite the technical compartment, to allow an easy loading/unloading of the chamber itself.

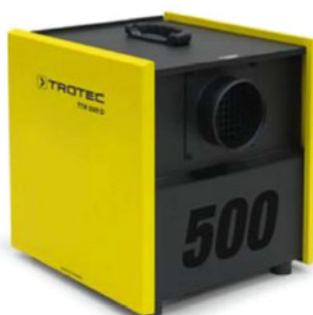
The nutraceutical or aromatic herbs to be dried can be placed inside two drying trolleys in stainless steel (Fig. 4). The trolleys, having dimensions width 1.90 m × length 2.15 m × height 1.90 m, can house up nine removable shelves in stainless steel and aluminium, having width 1.83 m × length 2.15 m. The removable shelves are constituted by a mesh in stainless steel, on which the nutraceutical or aromatic herbs can be placed for drying.

For dimensioning the photovoltaic dryer, it has been estimated that each square metre of shelf can contain up to 2 kg of wet product to be dried. The drying chamber can house 18 removable shelves, arranged on two trolleys, for a total of 70 m² ca. of useful drying surface. Thus, the fully loaded drying chamber can contain up to 140 kg of wet product to be dried.

Fig. 4 Drying trolleys in stainless steel



Fig. 5 Absorption machine TROTEC TTR 500 D



2.2 Absorption Machine

The absorption machine can be the TROTEC TTR 500 D (Fig. 5) or equivalent, sized for a drying cycle duration of approximately two days.

This machine works with two separate air cycles. The first cycle is that of the process air and has two inlet/outlet sockets to be connected to the drying chamber through flexible pipes having a diameter of 6 mm. The second cycle is that of generation air to be connected through flexible pipes, for transporting the air outside the dryer.

2.3 Photovoltaic Generator

The photovoltaic generator, having a power of 6 kW, can be mounted on the roof and the South facade of the container.

The legislative framework allows three different possibilities for exploiting the produced energy: 1) sale of all the produced energy (sale contract - total transfer);

2) transfer of the energy exceeding its self-consumption to the grid (partial transfer), 3) consumption of all the produced energy, according to an on-site exchange and self-consumption contract.

Among the above three types of energy exploitation, the photovoltaic generator can be connected to 230 V low voltage network of Enel Distribuzione spa (grid-connected) for on-site exchange and self-consumption.

The photovoltaic generator is aimed at producing electrical energy from RES, i.e. solar energy, which does not involve any type of polluting emissions. The production of electrical energy from a photovoltaic source allows an environmental gain: for each kWh of electrical energy supplied to the user 0.25 kg of fuel oil is saved and the emission of 0.53 kg of CO₂ into the environment is avoided.

Six photovoltaic modules of 500 W can be mounted on the roof of the container, with an azimuth of 0° South and an inclination of 30° with respect to the horizontal plane, while other six photovoltaic modules of 500 W can be installed on the South elevation of the container itself, with an azimuth of 0° South and an inclination of 60° with respect to the horizontal plane.

Therefore, the photovoltaic generator consists of 12 photovoltaic modules of 500 W, constituting two strings with a total absorption surface of 29 m² ca. The photovoltaic generator can be placed on the container with the aid of a module-holder structure, having triangular brackets in hot-dip galvanised iron or aluminium.

2.4 PLC and Sensors for Remote Control

The dryer can be equipped with a PLC for the remote control of the working parameters of the drying chamber, i.e. temperature and humidity.

The PLC is connected to temperature and humidity sensors, to control, through a counter, the operation of the absorption machine, even remotely through a GSM data connection.

The PLC can autonomously manage the drying cycle and generate alarm or error messages, as well as messages on the progress of the drying cycle itself.

3 Conclusions

The prototype of the photovoltaic dryer described in this work will allow to monitor and control of the drying process, to identify any critical points during it, as well as the failures occurring inside the drying chamber.

Moreover, this dryer will allow focusing also on the microbial loads of the nutraceutical and aromatic herbs after drying.

Finally, by using the above-described drying method, it will be possible to study the microbial stability and, consequently, the shelf life of the examined species.

References

1. Greco, C., Comparetti, A., Mammano, M., Orlando, S.: Sustainable, circular and innovative value chains using growing substrata alternative to peat for the cultivation of nutraceutical species. In: Raupelienè, A. (ed), Proceedings of the International Scientific Conference: Rural Development Research and Innovation for Bioeconomy, pp. 13–20. Vytutas Magnus University, Agriculture Academy (2019). <https://doi.org/10.15544/RD.2019.040>
2. Brower, V.: Nutraceuticals: poised for a healthy slice of the healthcare market? *Nat Biotechnol.* **16**, 728–731 (1998)
3. Greco, C., Comparetti, A., Febo, P., La Placa, G., Mammano, M.M., Orlando, S.: Sustainable valorisation of biowaste for soilless cultivation of *salvia officinalis* in a circular bioeconomy. *Agronomy* **10**(8), 1158 (2020). <https://doi.org/10.3390/agronomy10081158>
4. Comparetti, A., Greco, C., Orlando, S., Ciulla, S., Mammano, M.M.: Comparison of mechanical, assisted and manual harvest of *origanum vulgare* L. *Sustainability* **14**(5), 2562 (2022). <https://doi.org/10.3390/su14052562>
5. Catania, P., Gaglio, R., Orlando, S., Settanni, L., Vallone, M.: Design and implementation of a smart system to control aromatic herb dehydration process. *Agriculture* **10**, 332 (2020). <https://doi.org/10.3390/agriculture10080332>
6. Pr.e.va.n.i.a (Eco-friendly products with high nutritional value) project report
7. Hadjibagher Kandi, M.N., Sefidkon, F.: The influence of drying methods on essential oil content and composition of *Laurus nobilis* L. *J. Essent. Oil Bear. Plant* **14**, 302–308 (2011)
8. Sadowska, U., Kopeć, A., Kourimska, L., Zarubova, L., Kloucek, P.: The effect of drying methods on the concentration of compounds in sage and thyme. *J. Food Process. Pres.* **41**, e13286 (2017)
9. Kudra, T.: Energy aspects in drying. *Dry. Technol.* **22**, 917–932 (2004)
10. Sarsavadia, P.N.: Development of a solar-assisted dryer and evaluation of energy requirement for the drying of onion. *Renew. Energy* **32**, 2529–2547 (2007)
11. Chakraborty, R., Tilotama, D.: Drying protocols for traditional medicinal herbs: a critical review. *Int. J. Eng. Technol.* **4**, 1–8 (2016)
12. Müller, J., Reisinger, G., Kisgeci, J., Kotta, E., Tesic, M., Mühlbauer, W.: Development of a greenhouse-type solar dryer for medicinal plants and herbs. *Solar Wind Technol.* **6**, 523–530 (1989)

A Model of Sicilian Environmentally Friendly Multifunctional Farm for Soil Protection



Michele Massimo Mammano, Antonio Comparetti, Carlo Greco, and Santo Orlando

Abstract Roccaforte farm is an example of the implementation of environmentally friendly best practices in inland Sicily. A model of environmentally friendly cultivation of wild asparagus, i.e. *Asparagus acutifolius* L. and *Asparagus albus* L., intercropping with walnut in a multifunctional farm, is described in this work: the methods for the propagation, cultivation and transformation of wild asparagus, as well as the best practices of conservation soil tillage, aimed at reducing soil degradation, i.e. compaction and erosion, are explained. These best practices can reduce fuel consumption, keep the active topsoil layer and soil organic matter, increase the water retention capacity and carbon sequestration in the soil and, therefore, reduce the emission of Greenhouse Gases (GHGs), i.e. CO₂, into the atmosphere.

Wild asparagus is used for the preparation of preserves in the form of tops or sauces and as an ingredient in soups, creams, risottos, puddings and omelettes. The bioactive compounds contained in *Asparagus* species have beneficial effects on human health, for their antitumoral and antioxidant activities.

The cultivation of wild asparagus, above all intercropping with tree plants, could represent an interesting entrepreneurial opportunity, by promoting crop diversification or expanding the offer of agritourism. In fact, despite the low crop yield (1.3 t ha⁻¹), it can be assumed that the current high price of the product (€ 10–20 kg⁻¹), combined with a low working capacity of harvest (3.8 kg h⁻¹ without cutting vegetation), allows economically viable cultivation.

Thus, from the results of this work, it is possible to deduce that the production of wild asparagus and walnut can be combined with environmental protection, to enhance the marginal areas of the Sicilian Region.

M. M. Mammano · C. Greco (✉)

Council for Agricultural Research and Economics (CREA), Research Centre Protection and Certification, 90011 Bagheria, Palermo, Italy
e-mail: carlo.greco@crea.gov.it

A. Comparetti · S. Orlando

Department of Agricultural, Food and Forest Sciences, University of Palermo, Viale Delle Scienze, Building 4, 90128 Palermo, Italy

Keywords Wild asparagus · Walnut · Intercropping · Agricultural mechanisation · Environmental protection

1 Introduction

1.1 *Example of Environmentally Friendly Best Practices in Inland Sicily*

The farm “Roccaforte Giovanni” is located in San Biagio Platani (Agrigento, Sicily, Italy) and has an area of 8 ha ca., of which 2 ha ca. are cultivated with wild asparagus (*Asparagus acutifolius* L). This farm aims at enhancing a typical Sicilian product, through the integration of the supply chain, from cultivation to processing to rural catering.

In this farm the best mechanisation practices are performed, i.e. conservation soil tillage such as contour ploughing with upstream soil slice rotation or minimum tillage using a subsoiler. These best practices of conservation soil tillage can reduce soil degradation, i.e. compaction and erosion, as well as fuel consumption. Thus, the farmer knows the best mechanised agricultural practices for soil conservation, i.e. minimum and zero soil tillage [1], to avoid some human activities, which are not suitable for certain sites can cause hydrogeological instability.

Nowadays it is needed to make the field manager aware of his paramount role of being responsible to implement sustainable soil use. The field manager must select the appropriate agricultural implements and machines needed for performing the best mechanisation practices [1].

Moreover, the above best mechanisation practices can keep the active topsoil layer and soil organic matter, increase the water retention capacity and carbon sequestration in the soil and, therefore, reduce the emission of Greenhouse Gases (GHGs), i.e. CO₂, into the atmosphere.

In this perspective, Roccaforte farm is an example of the implementation of environmentally friendly best practices in inland Sicily.

1.2 *Multifunctional Farm*

This farm represents a virtuous example of multifunctionality: it starts from the propagation of wild asparagus (*Asparagus acutifolius* L.) seedlings in shaded greenhouses, with the self-production of propagation materials (seeds) aimed also at enhancing local genetic resources. The sustainable cultivation of asparagus plants follows, from transplanting to harvesting and selling the shoots. Finally, it is possible to produce preserved asparagus products based on the Sicilian tradition (e.g. preserves and

asparagus-based sauces), to enhance and rediscover typical Sicilian dishes in rural catering (agritourism) as a marketing channel for both fresh and processed products.

1.3 Wild *Asparagus*

Wild asparagus, meaning various spontaneous species of *Asparagus* is particularly appreciated for its well-known health properties and organoleptic qualities in Mediterranean countries, e.g. Italy, Tunisia, Turkey, Spain and Portugal, being also an indispensable component in many regional culinary traditions (e.g. omelettes, risottos and sauces).

The two most representative species of wild asparagus in the Sicilian territory, i.e. *Asparagus acutifolius* L. and *Asparagus albus* L. (Fig. 2), are cultivated in Roccaforte multifunctional farm [2, 3] (Fig. 1).



Fig. 1 Plants of *Asparagus acutifolius* L. (left) and *Asparagus albus* L. (right)

Fig. 2 Plants of wild asparagus (*Asparagus acutifolius* L.) cultivated in a shaded greenhouse in Roccaforte farm



Fig. 3 Intercropping between *Asparagus albus* L. and walnut



2 Cultivation as Sustainable Soil Use

2.1 Intercropping and Soil Protection

The cultivation of wild asparagus is very different from that of *Asparagus officinalis* L., which is commonly cultivated, as *Asparagus acutifolius* L. and *Asparagus albus* L. have ecological needs and yield different from those of the former one [3–7]. The two above species of wild asparagus are very rugged and easy to adapt to different soil and climate conditions, so they are suitable for a multi-year crop rotation together with other vegetable species and reach full production after three or four years. Its extensive cultivation can also contribute to enhancing marginal areas, offering a valuable income and alternative to grazing or land abandonment, while allowing the consolidation of sloping soils, due to their strong roots. Asparagus is also suitable for intercropping with fruit tree species, such as walnut and olive tree, with which it often shares the same habitat (Fig. 3). The intercropping between olive or walnut and asparagus is possible and advantageous, from both economic and environmental points of view, as suggested by several studies [7]. The intercropping between asparagus and walnut represents a high economic added value, in terms of yield and production diversification, as well as it is strongly linked with the territory.

2.2 Soil Tillage and Fertilisation

In order to cultivate wild asparagus, the optimal soil conditions are pH between 6.5 and 7.5; high permeability; arable layer depth higher or equal to 80 cm; groundwater depth higher or equal to 100 cm.

Soil tillage is very important concerning the life cycle of asparagus and the depth of its roots: their most absorption activity is performed at a depth higher or equal to

40 cm. Therefore, in different autumn months, digging must be carried out, leaving the soil in place. In February, organic fertilisation must be performed, by using well-mature manure. Then, mineral fertilisation must be carried out, by applying 20 g m^{-2} ca. (equal to 200 kg ha^{-1} ca.) of phosphorus (P_2O_5) and potassium (K_2O) [7].

Generally, the amount of organic matter to be used is $30\text{--}50 \text{ t ha}^{-1}$ of mature manure or $2\text{--}2,5 \text{ t ha}^{-1}$ of organic fertiliser in the form of pellets.

The most common field operations are soil tillage between the rows in May and shredding (Fig. 4) in October, to plan the gradual harvest. After shredding it is possible to see a selection of weeds, above all *Oxalis cernua* Thunb., that contributes to reducing soil erosion (Fig. 5).

Fig. 4 Shredding of wild asparagus



Fig. 5 *Asparagus albus* L. and walnut together with *Oxalis cernua* Thunb., able to reduce soil erosion



2.3 *Transplanting Seedlings*

The 4–5-year-old seedlings, cultivated inside alveolar containers, must be transplanted between the end of April and the end of May [7].

Transplanting is generally manually performed, even if a semi-automatic transplanter, where the distributors are filled in by operators, has been recently developed.

The asparagus seedlings can be transplanted by covering the rhizome with a layer of thin soil of 2–3 cm ca. The planting distances (Fig. 4) must be 0.4–0.5 or 0.8 m along the row and 2–2.5 m between the rows, to obtain a density of 10,000–12,000 plants ha⁻¹. The distances between the rows can also be changed in order to allow mechanised field operations [7–10].

2.4 *Weed Control and Harvest*

After transplanting the seedlings, weed control must be carried out and, then, in autumn and spring, the soil must be slightly compacted along the row. Weed control is performed using a sprayer between the rows, while it is manually carried out along the rows.

Generally, in autumn and spring, asparagus is gradually harvested, as the shoots exceeding the height of 10–12 cm from the ground are cut a few centimetres above the ground, by means of a small knife or a special tool (Fig. 6).

Manual harvest is usually carried out between late winter and early spring (March–April), although a low amount of shoots may rise in autumn (September–October). The average working capacity of harvest is variable between 3.8 kg h⁻¹, without cutting the vegetation, and 7.2 kg h⁻¹, by cutting the vegetation. Each plant has an average production of 0.5 kg, up to a maximum of 1 kg, until the temperature

Fig. 6 Harvested shoots of *Asparagus albus* L



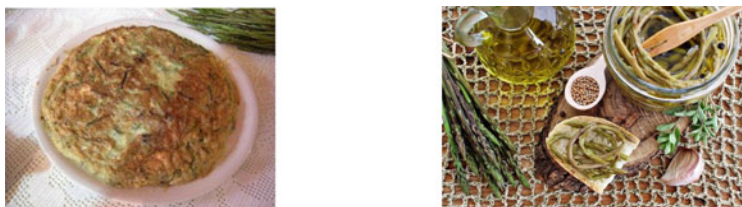


Fig. 7 Omelette and preserves of wild asparagus

decreases below 6 °C [10–13]. As part of the enhancement of species of nutraceutical interest, the harvesting of asparagus using facilitating machines is currently being tested [14].

2.5 Valorisation of Wild Asparagus

Wild asparagus is used for the preparation of preserves in the form of tops or sauces and as an ingredient in soups, creams, risottos, puddings and omelettes (Fig. 7).

The bioactive compounds contained in *Asparagus* species have beneficial effects on human health, for their antitumoral and antioxidant activities. The most important bioactive compounds are rutin (bioflavonoid) and protodioscin (steroid saponin), whose concentration can be variable inside each shoot: protodioscin is mostly located in the basal part of the shoot, which, however, is discarded in food preparations. Therefore, the recovery of these parts could be useful for the development of new nutritional products [11–13, 15–18].

3 Conclusions

The field management of wild asparagus must be improved, from both the plant protection and nutritional (crop needs for nutrients and water) points of view. Wild asparagus must be periodically monitored during spring and autumn because disease problems can occur, due, above all, to insects belonging to *Altica* and *Cryocera* species, which affect the young shoots and other parts of the plant, thereby compromising the product for the excessive presence of larvae.

The cultivation of wild asparagus, above all intercropping with tree plants, could represent an interesting entrepreneurial opportunity, also contributing to enhancing marginal areas, by promoting crop diversification or expanding the offer of agritourism. In fact, despite the low crop yield (1.3 t ha⁻¹), it can be assumed that the current high price of the product (€ 10–20 kg⁻¹), combined with a low working capacity of harvest (3.8 kg h⁻¹ without cutting vegetation), allows economically viable cultivation.

Thus, from the results of this work, it is possible to deduce that the production of wild asparagus and walnut can be combined with environmental protection, to enhance the marginal areas of the Sicilian Region.









References

1. Puccio, D., Comparetti, A., Greco, C., Raimondi, S.: Proposal of a nomenclature for hydrogeological instability risks and case studies of conservative soil tillage for environmental protection. *Land* **11**, 108 (2022). <https://doi.org/10.3390/land11010108>
2. Mammano, M.M., Fiore, M.C., Abbate, L., Airò, M., Falavigna, A.: Studio morfologico e genetico dell'asparago selvatico: esistono due distinte specie di asparago spontaneo in Sicilia comunemente note come asparago nero? In: Atti X° Convegno Nazionale sulla Biodiversità, Roma, 3–5 settembre 2014, [ITA, ita], pp. 219–224 (2014)
3. La Mantia, A., Sortino, S., Guarino, L., Spatà, G.: Caratterizzazione ecologica di alcune popolazioni siciliane di asparago selvatico (*Asparagus Acutifolius e A. Albus*). In: VII Convegno nazionale sulla biodiversità, Catania 30 marzo–2 aprile (2005)
4. Aliotta, G., et al.: Natural history, cultivation and biodiversity assessment of *Asparagus*. In: Research Advance in Agriculture and Food Chemistry, vol. 5, pp. 1–12. Ed. Global Research Network (2004)
5. Rosati, A., Pepe, R., Senatore, A., Perrone, D., Falavigna, A.: Produttività dell'asparago selvatico. *L'Informatore Agrario* **8**, 75–77 (2005)
6. Sicilian Region and CRA: Razionale tecnica di coltivazione dell'asparago in Sicilia. Le conoscenze tecnico-scientifiche e l'attività di ricerca condotta nel PROM al servizio del produttore agricolo. Progetto di Ricerca per potenziare la competitività di Orticole in aree Meridionali. Delibere CIPE 17/2003 e 83/2003 (2009)
7. Rosati, A., Castellini, C., Dal Bosco, A., Mugnai, C., Paoletti, A.: Manuale per la coltivazione consociata Olivo Asparago selvatico Pollo rustico, Edizioni 3a-PTA (2012). ISBN: 88-88417-06-0
8. Fiori, P.P., Giola, M., Ledda, M.G., Tedde, M.: Valorizzazione dell'asparago selvatico. *Informatore Agrario* **50**(57), 47 (2001)
9. Benincasa, P., Tei, F., Rosati, A.: Plant density and genotype effects on wild asparagus (*Asparagus acutifolius* L.) spear yield and quality. *HortScience* **42**, 1046–1311 (2007)
10. Conversa, G., Elia, A.: Effect of seed age, stratification, and soaking on germination of wild asparagus (*Asparagus acutifolius* L.). *Scietia Horticulturæ* **119**, 241–245 (2008)
11. Falavigna, A., Palumbo, A.D.: La coltura dell'asparago. Calderini Edagricole, Agricole Bologna (2001)
12. Venezia, A., Soressi, G.P., Falavigna, A.: Aspetti relativi alla valorizzazione di specie di asparago spontanee in Italia. *Agricoltura Ricerca* **141**, 41–48 (1993)
13. Rosati, A.: Un possibile futuro per l'asparago selvatico. *L'Informatore Agrario* **7**(2001), 89–92 (2001)
14. Comparetti, A., Greco, C., Orlando, S., Ciulla, S., Mammano, M.M.: Comparison of mechanical, assisted and manual harvest of *origanum vulgare* L. *Sustainability* **14**, 2562 (2022). <https://doi.org/10.3390/su14052562>
15. Wang, M., Tadmo, Y., Wu, Q., Chin, C., Garrison, S.A., Simon, J.E.: Quantification of protodioscin and rutin in asparagus shoots by LC/MS and HPLC methods. *J. Agric. Food Chem.* **51**(21), 6132–6136 (2003)
16. Salvatore, S., et al.: Antioxidant characterization of some sicilian edible wild greens. *J. Agric. Food Chem.* **53**(24), 9465–9471 (2005)

17. Fuentes Alventosa, J.M., Moreno Rojas, J.M.: Chapter 13 - Processing and Impact on Active Components in Food. In: Processing and Impact on Active Components in Food, pp. 103–110. Press Academy (2015)
18. Chin, C.K., Garrison, S.: Functional elements in asparagus for human health. *Acta Horticulturae ISHS* **776**, 234 (2008)

LLL Strategies for New Educational Approaches in Smart Agriculture from an Agricultural Engineering Perspective in Italy



Andreas Mandler , Giovanni Carabin , Lorenzo Becce , Sandro Liberatori, Heinz Bernhardt , Maximilian Treiber , Christina Paulus, Andreas Gronauer , Anders Herlin , and Fabrizio Mazzetto 

Abstract Lifelong learning (LLL) is increasingly important due to current technological and social changes. Against the background of constantly advancing agricultural production and processing, the continuous training and qualification of people working for the agricultural sector is becoming increasingly relevant. This applies in particular to the opportunities offered by smart agriculture.

The project USAGE set out to develop LLL initiatives in the realm of agricultural engineering and smart agriculture throughout Europe. The project examines the opportunities for universities and the requirements of particular parts of the agricultural sector. Based on a survey with 70 participants in Germany, Austria and South Tyrol, the demand for LLL courses in the field of smart farming was analyzed. It shows a corresponding interest in offers at universities.

The paper refers to the potentials of new educational approaches. It elaborates the role of universities in LLL education and concludes with an overview of preliminary experiences of LLL offers on smart agriculture in South Tyrol.

A. Mandler (✉) · G. Carabin · F. Mazzetto
Faculty of Science and Technology, Free University of Bozen-Bolzano, Piazza Università 5,
39100 Bolzano, Italy
e-mail: andreas.mandler@unibz.it

L. Becce
Competence Center for Plant Health of the Free University of Bozen-Bolzano, Bolzano, Italy

S. Liberatori
ENAMA Service Srl, Roma, Italy

H. Bernhardt · M. Treiber
Technical University of Munich, Freising, Germany

C. Paulus · A. Gronauer
University of Natural Resources and Life Sciences, Vienna, Austria

A. Herlin
Swedish University of Agricultural Sciences, Alnarp, Sweden

Keywords Lifelong learning · Smart farming · Agricultural engineering · Hybrid learning · Industry 4.0

1 Introduction

The term lifelong learning (LLL) designates an approach to further and permanent education for either personal or professional reasons, which has become important also in the agricultural sector. LLL is particularly relevant for farm machinery industry, users and service providers who need to adapt to a rapidly changing technological environment [1, 2].

Like other economic sectors, agriculture and agricultural machinery industry are affected by massive changes. Changes in agriculture derive from general environmental and social transformations, but are also linked to Industry 4.0 and IoT. These latter terms intended to describe current industrial evolutionary processes in the context of digitization and automatization. In the agricultural sector, these processes are summarized as smart agriculture [3], which shares with Industry 4.0 the methodological and cognitive approaches of knowledge management 4.0 [4]. KM4.0. is about the independent interaction of different technological systems into a self-organizing overall system, through intensive and integrated applications of electronic devices, ICT, interconnected and cloud architectures and machine learning approaches [5]. It is assumed that this will bring about similar structural and social changes as previous industrial revolutions.

In this transformation process, the role of work and thus of humans involved in the system is deeply changing. As these processes are taking place quickly, the qualification of workers and professionals cannot take place in the cycle of generational change, but requires the current workforce to continuously qualify and adapt. Further education and LLL are therefore central to the development of smart farming solutions on any farm business.

Agriculture has a particular weakness in this situation. While the phase of Industry 3.0 [6] represented for the industrial sector the advent of the IT revolution, for the agricultural sector this phase has been largely skipped for economic, financial and cultural reasons. Despite technological progress between 1970 and 2020 that introduced many mechanical and electronic innovations and led to the high level of automation of many solutions in precision farming [7], however this period failed to bring about the maturation of a solid IT culture in farm management processes in Europe and elsewhere [8, 9]. This gap of IT capacities, the lack of adequately trained professionals, is the cause of many of the delays in the diffusion of smart agriculture practices.

LLL opportunities can help to overcome this void. Universities have excellent preconditions to become important providers of LLL activities in the field of smart agriculture. This article describes new educational initiatives and approaches in this regard. It discusses the role of universities and elaborates first experiences of LLL opportunities in smart agriculture focusing on South Tyrol, Italy.

Smart agriculture is an evolution from previous concepts such as precision agriculture. “In addition to precision and efficiency, the optimization of processes and anticipatory planning are key aspects of Smart Farming” [10, p. 112]. Smart agriculture solutions enhance the management quality of decision making processes in agriculture as they allow to make decisions based on targeted information previously collected through monitoring of production processes [6].

In a general view, the term smart agriculture combines technologies and procedures that relate to digital processes in agriculture [9]. Developing and running smart farming solutions is a transversal process that requires action from various actors: Farmers, farm managers, agronomists and agrarian engineers. As industry and institutional partners confirm, at present time professionals that can drive the digital transformation in rural areas are in short supply [7, 9].

2 USAGE – Upskilling Agricultural Engineering in Europe

The project USAGE¹, supported by the Erasmus + program of the European Union, focused on the upskilling of agricultural engineers in Europe. It set out to address the shortage of adequately skilled persons to bring forward smart agricultural solutions.

The project is carried out jointly by the University of Natural Resources and Life Sciences (**BOKU**)/Austria, the Free University of Bolzano/Italy (**UNIBZ**), the Swedish University of Agricultural Sciences/Sweden (**SLU**) and the Technical University of Munich/Germany (**TUM**).

The main objective of USAGE is to enable smart, sustainable and inclusive growth through up-skilling, innovative pedagogic approaches and access to experience. Therefore the implementation of different modules regarding digital transformation as well as development of an innovative LLL strategy is at the center of the project. Experts from universities, industries and leading farms worked together to ensure a broad offer of high-level education as well as stronger cooperation between universities and companies. The immediate objectives of the USAGE project are:

- Increase the number of skilled staff in digital agriculture necessary for filling the gaps regarding digital transformation
- Train new experts able to analyze and evaluate newly developed methods, machinery, equipment and constructions for various areas of applications (FMIS, ISOBUS, digitized logistics and telemetry systems to name a few)
- Increase the learning mobility between countries and disciplines – inspiring more engineers to choose a career within smart farming, and more agronomists to further specialize in technological subjects.

The immediate outcomes of USAGE are several LLL courses in the realm of agricultural engineering and smart agriculture, offered in new online learning formats.

¹ The Erasmus + project USAGE runs from 2019 to 2022. Website: <https://usage.projects.unibz.it/>.

The following LLL courses of 3 to 15 ECTS were already held or are currently underway:

- Smart Farming and IoT in Agriculture (TUM)
- Advanced Technologies in Crop Farming (BOKU together with UNIBZ)
- Introduction to Smart Agriculture (UNIBZ)
- Precision livestock farming for sustainable production (SLU).

Three of the above courses were held already several times. This underlines the sustained request for training and learning opportunities in this field, too.

Need Analysis. To understand better the characteristics of the demand, USAGE started with the implementation of a needs analysis among professionals from industry, academia, public institutions and practitioners in the realm of smart farming. Seventy potentially interested parties from the agricultural engineering industry, associations and organizations from Germany, Austria and South Tyrol were interviewed using a standardized questionnaire [11].

The results of this analysis show the significant demand for innovative LLL learning opportunities on smart agricultural engineering in all target groups and partner countries.

The questionnaire posed the question which format potential LLL offers should have. Interviewed people reacted positively to the flexible model of attending single thematic modules. In terms of content, the proposed learning program was divided into eight topics, of which “GIS&FIMS”, “Logistics”, “Environmental Sustainability” and “Crop Production” received the highest priority among respondents, as can be seen in Fig. 1.

It became apparent that especially small and medium-sized companies in the agricultural engineering sector are interested in the topic of LLL Smart Farming. Here, the individual employees have to cover many topics as generalists and always need new expertise. This finding resonates with the smallholder agricultural structures found in South Tyrol, while large engineering companies often have established learning opportunities for their employees, and hence are less interested [11, p. 3].

3 New Educational Approaches

LLL opportunities are central to train workers and employees throughout the agricultural sector. Lifelong learning, as laid out in the EU ET2020 program,² is inclusive to many different people as it lowers the barriers to participation by reducing the importance of formal educational degrees [12]. At the same time, its offers come in new educational formats that allow many different types of stakeholders to benefit from learning opportunities [13].

² <https://lllplatform.eu/policy-areas/participatory-democracy/et2020/> last accessed 2022/09/11.

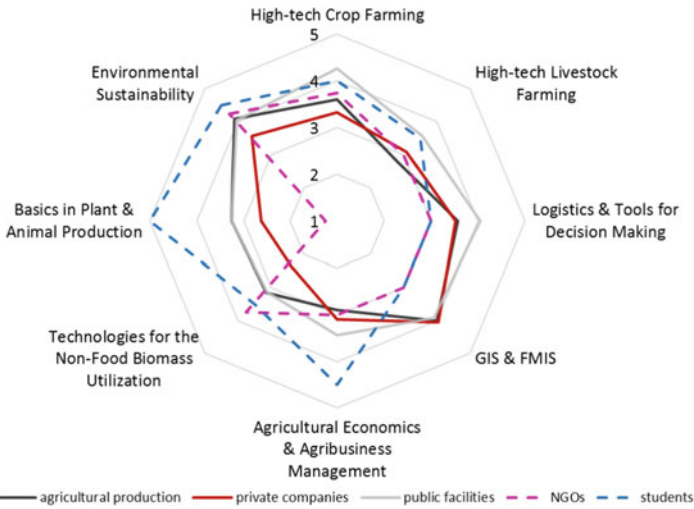


Fig. 1 Level of interest in topics by organization type, measured in mean values (n = 70) (from Bernhardt et al. 2022)

A central concern of the USAGE project was to develop guidelines on validation of non-formal and informal education. This is particularly relevant in the agricultural sector, where the labor force often has a high level of practical knowledge without respective degrees.

New Formats and Methods. One advantage of the LLL approach is the flexibility to react to educational needs and to establish and try out new learning formats and methods. This flexibility is particularly relevant to attract learners into technical fields as agricultural engineering. Smart agriculture has many different aspects so that highly specialized learning formats of limited size can address previously identified needs.

LLL formats allow for meaningful learning opportunities with regard to the right timing of lectures, learning volume, pedagogical approach and implementation. LLL courses and seminars are usually held in the evenings or during weekends, so as to avoid clashes with the usual schedule of participants. LLL allows for many different formats of learning sessions, e.g. online, in-presence, synchronous and asynchronous lectures or hybrid courses. These formats are highly diverse and can be adjusted to immediate needs. The structure may range from completely asynchronous to 1:1 synchronous online sessions. Ideally, the pedagogic concept of the course in terms of language, timing, technologies and others is tailored to the intended participants.

Moreover, LLL courses rely on stable online backup, where course sessions and learning materials are stored. The availability of these materials is standard and enhances the learning effect. Beside Massive Open Online Courses (MOOC), access to LLL courses is paid, therefore participants expect the structured availability of course materials and services.

Role of Universities. Universities have an important stake in the transition of current agriculture towards smart farming technologies. Research and the education of future agricultural engineers are fundamental to develop and implement future smart agriculture solutions. University studies contribute to the advancement of IT formation in agrarian studies. Future agricultural engineers are equipped with the necessary skills to realize smart agricultural solutions. The tertiary educational sector has therefore the resources and facilities to offer high level learning activities in many different formats. From learning in presence, through hybrid formats or experimental laboratories that enable new practical experiences. Such practical exercises are especially relevant for agricultural engineering.

Agricultural engineering is the driving force of smart agricultural solutions and therefore central to the foreseen transition of the agricultural sector. The project USAGE was designed to increase the visibility of agricultural engineering. Accordingly, the four participating academic institutions, developed a curriculum for a LLL online master study in smart agriculture to reach out to more students.

Universities possess the knowledge, experiences and capacities to offer the required engineering education. Universities are prone to participate in the growing and expanding LLL market. However, to meet the demands of the professional LLL market, regarding service quality and educational support, universities are required to create specialized supporting structures.

4 Experiences in South Tyrol, Italy

The Free University of Bozen-Bolzano brought to the USAGE project the Italian and South Tyrolian perspective. Although not all activities of the project have been terminated so far, some considerations on LLL strategies for new educational approaches in smart agriculture are preliminarily concluded.

A) There is wide interest in LLL opportunities on smart agriculture in South Tyrol

Throughout agricultural networks in South Tirol as advisory services, producer associations and professional groups, great interest in LLL courses on smart farming was generated. Due to small-structured situation in South Tirol, many of the small and medium-sized companies sense the demand to upgrade working procedures and technologies.

Two courses are offered in the South Tyrolian region and with explicit reference to local agricultural production. One course is offered at low costs by the *studium generale* program of the UNIBZ. The second course is jointly organized from BOKU and UNIBZ and is on payment.

B) Topics requested

Content of the courses orients on typical challenges that farmers in South Tirol face: Calculating machine use in mountain areas, smart farming solutions in fruit and vine production (e.g. efficient spraying technologies), farm management information systems. Agricultural structures in South Tyrol are comparably small, therefore participants get introduction on how to plan and modify

smart applications to realize individual solutions tailored to the horticulture and vine sector. Both LLL courses foresee hands-on exercises at the AgroForestry Innovation Lab (AFI-Lab) at NOI Techpark in Bozen.

C) First Experiences

LLL courses on smart agriculture have not started yet, thus we cannot give the full account of experiences. The course in the framework of *studium generale* at UNIBZ is mainly booked by university students. The joint BOKU-UNIBZ course has attracted working professionals from small agricultural enterprises, producer associations or advisory services.

D) Strategies which work

Preliminary we can say that the blended format of the courses with online and seminars in presence is attractive to the participants. The timing of the seminars and lectures is scheduled in such a way that the events can be attended alongside daily professional commitments. Most of the lectures are held online in late afternoon. Two practical exercises are scheduled for each course which take place at AFI-Lab in Bozen at the end of the week.

In a multilingual region as South Tyrol seminars and content must be provided in various languages in order to reach the intended audience. The above courses are offered in German and English. An Italian/English course is planned for the near future.

5 Results

Without anticipating the final results of the project, it can be said that LLL is a necessary and useful approach in building a future resilient smart agriculture and closing technical gaps in the contemporary agricultural sector. New educational approaches as LLL are efficient ways to train and upskill both, engineers and the agricultural workforce. Such approaches help to closing the gap of IT skills in agriculture.

Thanks to its flexible structure, LLL courses are timely, represent the state of the art and are open to many different stakeholders in the agricultural sector.

Due to its capacities and experiences, universities are ideal providers of advanced LLL opportunities. Such LLL offers cannot be managed by the current teaching staff alone, but must be supported by adequate pedagogic and service structures.

References

1. Carnoy, M., Luschei, T.F.: Skill acquisition in 'high tech' export agriculture: a case study of lifelong learning in Peru's asparagus industry. *J. Educ. Work* **21**(1), 1–23 (2008)
2. Atchoarena, D., Holmes, K.: The role of agricultural colleges and universities in rural development and lifelong learning in Asia. *Asian J. Agric. Dev.* **2**(1362–2016–107652), 15–24 (2005)

3. Mazzetto, F., Gallo, R., Sacco, P.: Reflections and methodological proposals to treat the concept of “information precision” in smart agriculture practices. *Sensors* **20**(10), 2847 (2020)
4. Ansari, F.: Knowledge management 4.0: theoretical and practical considerations in cyber physical production systems. *IFAC-PapersOnLine* **52**(13), 1597–1602 (2019)
5. Mazzetto, F., Gallo, R., Riedl, M., Sacco, P.: Proposal of an ontological approach to design and analyse farm information systems to support Precision agriculture techniques. *IOP Conf. Ser. Earth Environ. Sci.* **275**(1), 012008 (2019)
6. Mazzetto, F., Riedl, M., Sacco, P.: Sistemi informativi aziendali ed agricoltura di precisione. In: Casa, R. (ed.) *Agricoltura di precisione, metodi e tecnologie per migliorare lefficienza e la sostenibilit dei sistemi culturali*. Edagricole-Edizioni Agricole di New Business Media Srl, Milano, pp. 9–42 (2016)
7. Bernhardt, H., et al.: Challenges for agriculture through industry 4.0. *Agronomy* **11**(10) (2021). <https://doi.org/10.3390/agronomy11101935>
8. FAO and ITU: Digital excellence in agriculture in Europe and Central Asia. <https://policycommons.net/artifacts/1860967/digital-excellence-in-agriculture-in-europe-and-central-asia/2609051/>. Accessed 22 Sept 2022
9. ITU and FAO: Status of Digital Agriculture in 18 countries of Europe and Central Asia (2020)
10. Schönfeld, M.v., Heil, R., Bittner, L.: Big data on a farm—smart farming. *Big Data Context*, 109–120 (2018)
11. Bernhardt, H., et al.: Development of a life long learning concept for smart farming, St. Joseph, MI, p. 1 (2022). <https://doi.org/10.13031/aim.202200130>
12. European Commission, Directorate-General for Employment Social Affairs and Inclusion, and Sienkiewicz, Ł.: Future skills, career guidance and lifelong learning in PES: thematic paper. Publications Office of the European Union (2022). <https://doi.org/10.2767/640074>.
13. Council of the European Union: Council Recommendation on a European approach to micro-credentials for lifelong learning and employability, Brussels, 9790/22 (2022)

First Results of Digestate Spreading Trials in Mediterranean Crops



Giuseppe Manetto, Emanuele Cerruto, Rita Papa, and Roberta Selvaggi

Abstract Biogas production by Anaerobic Digestion (AD) is more and more widespread due on the one hand to the large quantity of biodegradable residues and by-products produced by livestock and agro-industrial activities and on the other to the growing interest in alternative energy sources. The by-product of the AD, the digestate, allows closing the production cycle: in fact, it is a stabilized bio-fertilizer with an amount of nutrients depending on feedstock features, which can be used as an organic soil improver and can contribute to organic soil matter turnover. In this paper the first results of digestate spreading trials are discussed. The digestate came from an anaerobic digestion plant of 600 kW (electric), which processes agri-food industry by-products. The digestate was separated into the two fractions, liquid and solid, by means of a mechanical separator. The solid fraction was spread in a vineyard and a citrus orchard under effective field conditions, using implements provided by a local agricultural subcontractor and with spreader settings and operating parameters usually adopted by him. The liquid fraction was microfiltered at the digestion plant, and the microfiltered fraction, after dilution and a further microfiltration, was spread in three other citrus orchards by means of drip fertigation plants. First results suggest the need to improve the uniformity of application of the solid fraction and to carefully adjust the parameters of the final microfiltration of the microfiltered fraction so to reduce water consumption and the overall economic costs.

Keywords Solid fraction · Liquid fraction · Fertigation · Circular economy

1 Introduction

Energy supply is a problem that attracts the attention of all nations, because human welfare is closely related to the amount and quality of energy used. At present, energy

G. Manetto · E. Cerruto (✉) · R. Papa · R. Selvaggi
Department of Agriculture, Food and Environment, University of Catania - Via Santa Sofia, 100,
95123 Catania, Italy
e-mail: emanuele.cerruto@unict.it

© The Author(s), under exclusive license to Springer Nature Switzerland AG 2023
V. Ferro et al. (eds.), *AIIA 2022: Biosystems Engineering Towards the Green Deal*,
Lecture Notes in Civil Engineering 337,
https://doi.org/10.1007/978-3-031-30329-6_72

705

demand is mainly covered by fossil fuels, but their impact on the environment in terms of greenhouse gas emissions, global warming and climate change is no longer sustainable. So, a growing interest in alternative and renewable energy sources has emerged. In the context of renewable energy sources, probably biomass used in anaerobic digestion plants for biogas production, represents a perfect example of circular economy [8, 9, 13], especially when it operates on a local scale, collecting organic products from farms in its agricultural area and distributing digestate in the same area. In fact, anaerobic digestion on the one hand allows reusing the large quantity of biodegradable residues and by-products coming from livestock and agro-industrial activities for biogas production and on the other hand completes the production cycle with the redistribution in field of the digestate [1, 5, 6, 17, 27].

The digestate is a stabilized bio-fertilizer with an amount of nutrients, both macro and microelements, depending on feedstock features, that can be considered a soil-improver with positive effects on soil fertility, organic soil matter, organic carbon soil content, erosion reduction, water retention, humification process, physical structure of the soil, and reduction in using fossil fuels and mineral fertilizers [3, 14, 18, 21, 24, 29].

Digestate spreading rate is generally regulated on the basis of its nitrogen content, so not to exceed the legislation limits [25]. Moreover, it should be spread at the most suitable time for the best plant uptake, minimizing losses to the atmosphere, ground and water, which are affected by climatic and soil characteristics and by spreading techniques [2, 26]. To optimize digestate management, it is very often separated into two fractions: a solid palatable fraction and a clarified liquid one [11]. The solid fraction has mainly amending properties, with nutrient concentration depending on the biogas feedstock, whereas the liquid fraction has a high rate of readily available nitrogen. After separation, the solid fraction could be further processed, often being used in composting [4, 7, 28], second drying [16] and pelletization [12].

Generally, slurry and manure spreaders have been widely used for spreading the liquid and solid fraction of digestate, respectively [30]. A microfiltered fraction obtained by the liquid fraction may be also spread by means of drip fertigation plants [10]. This study is focused on the Mediterranean area (Sicily), where, despite the great availability of biomass, there are few digesters and the use of digestate is still very limited [15, 23], so new markets for digestate could be opened up and farmers' incomes could be improved [19]. Some preliminary tests were carried out in citrus orchards and in a vineyard to evaluate the quality of spreading of solid and microfiltered fraction of digestate.

2 The Digestate Distribution Systems

Spreading trials regarded the solid and microfiltered liquid fractions of the digestate produced by a 600-kW electrical anaerobic digestion plant processing agri-food industry by-products, mainly citrus pulp and olive pomace, located in the south-eastern part of Sicily, in the province of Ragusa, Italy (36°57'22.39" N, 14°33'43.56"

E). The digestate is normally treated at the digestion plant by means of a mechanical separator, whose outputs, solid and liquid, are piled up and stored in a large concrete tank, respectively. For this research, the liquid fraction was further micro-filtered with an experimental innovative microfilter (SEPCOM MFT Micro-filter by WAMGROUP) equipped with $40\ \mu\text{m}$ screens, also installed at the digestion plant.

The solid fraction was spread in a citrus orchard and in a vineyard of the same farm located about 15 km from the anaerobic digestion plant ($36^{\circ}58'30.54''\ \text{N}$, $14^{\circ}26'56.86''\ \text{E}$). The digestate was transported from the digestion plant by means of a $20\ \text{m}^3$ trailer and discharged in heap near the citrus orchard. The spreading was carried out by using different implements provided by a local agricultural subcontractor: in the citrus orchard, a broadcast manure spreader (Mutti Amos, model SLM 18) with a $2.1\ \text{m}^3$ hopper equipped with two counter-rotating rear vertical rollers (Fig. 1-left); in the vineyard, two spreaders equipped with cylindrical-shaped hopper. One (Gamberini, model SCD 600, with a $0.6\ \text{m}^3$ hopper) was used in its standard configuration (centrifugal broadcast spreading in the inter-row by means of a distribution disc, Fig. 1-centre) whereas the second, equipped with a $0.7\ \text{m}^3$ hopper, had been built by its owner in such a way to spread the digestate in a localized manner (two lines near the vine rows, Fig. 1-right). All spreading tests were carried out under effective field conditions, keeping the operating parameters usually adopted by the contractor (Table 1).

The microfiltered fraction was distributed, after proper dilution, in three citrus groves of three different farms by means of drip fertigation plants. The first citrus grove was adjacent to the anaerobic digestion plant, so no transport was necessary: the microfiltered digestate was accumulated in a tanker before its distribution. The second and third citrus groves were located in the province of Enna ($37^{\circ}25'32.68''$



Fig. 1 Machines used to spread the solid fraction of digestate: the broadcast manure spreader used in the citrus orchard (left), the centrifugal broadcast spreader (center) and the localized spreader (right) used in the vineyard

Table 1 Average field conditions during the spreading of the solid fraction of the digestate

Crop	Layout (m × m)	Implement	Speed (m s^{-1})	PTO rotation speed (rad s^{-1})
Citrus	6.0×4.0	Broadcast spreader (Mutti Amos)	1.52	56
Vineyard	2.4×1.0	Broadcast spreader (Gamberini)	0.66	56
Vineyard	2.4×1.0	Localized spreader (self-made)	1.05	56

N, 14°37'32.83" E) and Syracuse (37°17'16.51" N, 15°5'42.47" E) respectively, both about 80 km far from the digestion plant. The microfiltered digestate was transported in these two orchards by means of a tanker with a capacity of about 30 m³ and then stored in three plastic tanks with a capacity of 10 m³ each.

In all the three citrus groves the digestate was sucked from the tanks by a centrifugal pump, diluted with the irrigation water and then injected in the drip fertigation plant of the farm; the digestate flow rate was manually adjusted through valves (Fig. 2). To prevent the emitters from clogging up in the drip tape, the mixture of microfiltered digestate and water was filtered again by means of a self-cleaning 130 µm hydraulic filter (Spin Klin™ Disc Filter, Arkal), inserted immediately after the injection point. The cleaning procedure of the filter could be set on a time basis (for example every 30 min) or made automatic when the pressure drop between the inlet and the outlet section reached a prefixed value (for example 100 kPa). During the cleaning phase, a three-way valve, controlled by the filter control unit, recirculated the digestate in one of the tanks (Fig. 2). The washing water was accumulated in a tank and successively released in the citrus grove.

The filtering surface consisted in a disk series packed inside a filter pod, where the liquid passes through the spaces existing between two adjacent disks. In two plants filters with two filter pods and in the third a filter with three filter pods were installed (Fig. 3).

The average field conditions during the trials are summarized in Table 2. The amounts of digestate to be distributed over the three citrus plots were established based upon its chemical content and considering the nitrogen requirements of field crops (according to age, species, and crop form): about 45 m³ in farm A (corresponding to about 21.2 m³ ha⁻¹), 15 m³ in farm B (corresponding to about 15.0 m³ ha⁻¹), and 40 m³ in farm C (corresponding to about 25.0 m³ ha⁻¹). In addition, the ordinary fertilization plan adopted by the farms at which the tests were conducted was considered in determining the amount of digestate to be fed.

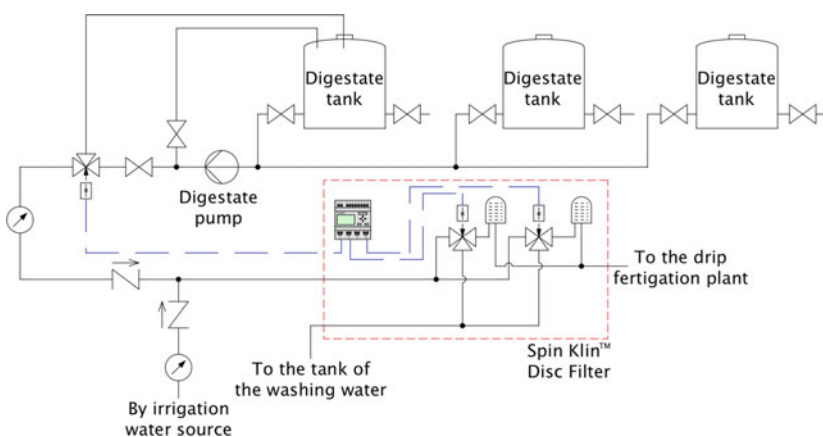


Fig. 2 Scheme of the distribution plant of the microfiltered fraction of the digestate

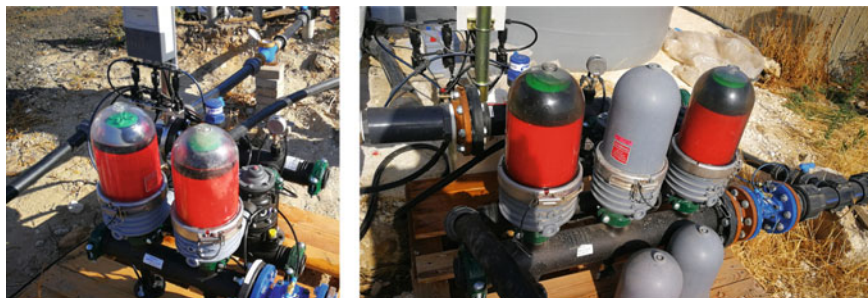


Fig. 3 Final filtering of the mixture of microfiltered digestate and water with self-cleaning disk filters equipped with two (left) or three (right) filter pods

Table 2 Main features of fertigation and irrigation plants in the test sites

Farm	Layout (m × m)	Surface plot (ha)	Dripline			Irrigation plant	
			Flow rate (L h ⁻¹)	Spacing (m)	Total length (m)	Pressure (MPa)	Flow rate (L min ⁻¹)
A	6.0 × 5.0	2.12	2.3	0.80	7070	0.29	305
B	5.0 × 5.0	1.00	2.3	0.50	3000	0.25	201
C	5.0 × 3.5	1.60	2.3	0.60	5719	0.29	371

3 Data Analysis

The solid fraction of the digestate was characterized in terms of total solid content (TS). Three samples of about 2.3 kg each were taken from the heap just after the digestate had been discharged and other three samples of about 2.0 kg each were taken from the product spread in the field after the last spreading. TS content was assessed by drying the samples in a laboratory oven at 105 °C until a steady mass was obtained.

In this first study, the research was mainly focused on assessing the uniformity of spreading. Assuming that the digestate had characteristics similar to those of other digestates of the same origin reported in the literature [22], the amount of nitrogen distributed remained within the limits fixed by the current regulation and in line with the directives on integrated production in Sicily both for citrus orchards and vineyards [20].

Uniformity of spreading was assessed by weighing, immediately after the spreading, the quantities of digestate collected by means of 2 m × 2 m plastic sheets spread out on the ground in three inter-rows. Sampling was carried out both in longitudinal (three sampling points along the inter-rows) and transversal direction (left, middle, and right in the citrus grove and left and right in the vineyard with respect to the travel direction).

The microfiltered fraction of the digestate was also characterized in terms of total solid content, volatile solid content (VS), and N, P, K content. Analyses were carried out on samples of microfiltered digestate after the microfiltration at the digestion plant, before feeding into the fertigation system. During its distribution in field all the operating parameters were monitored (number and duration of the fertigation interventions, pressure and flow rate of the irrigation water, flow rate of the digestate, amount of water and digestate distributed, frequency of cleaning of the filters, amount of water discharged during the cleaning). All data were used to draw the first indications about the sustainability, both economic and environmental, of the use of microfiltered digestate in fertigation plants.

4 Results and Discussion

4.1 Solid Fraction

Total solid content of the digestate sampled from the heap after its discharging was $42.7\% \pm 0.5\%$ (mean \pm standard deviation), whereas that of the digestate sampled in field after the last spreading was $63.9\% \pm 3.9\%$. The increase was due to water loss due to the sun exposure during the day.

Spreading trials on citrus orchard showed that the effective work time was about 28% of total field time (sum of times for spreading, refilling, regulation, and preparation) and that the real work capacity was about 0.96 ha h^{-1} . The average quantity of digestate distributed was 1.57 kg m^{-2} , corresponding to around 6.7 t ha^{-1} of dry matter, assuming a solid content of 42.7%. The comparison between the sampling points left, middle and right of the inter-row always showed a greater amount of digestate in the middle of the inter-rows, due to the direction of rotation of the rotors (Fig. 4). On average, the amount of digestate in the center part of the inter-rows was 3.9 times that in the lateral ones: 3.12 kg m^{-2} vs 0.80 kg m^{-2} . Variability between inter-rows had a coefficient of variation equal to 2.7% and that within inter-rows equal to 31.4% due to changes in instantaneous speed of the tractor and to the progressive emptying of the hopper.

In the vineyard, spreading speed was on average 0.66 m s^{-1} for broadcast distribution and 1.05 m s^{-1} for localized distribution; the corresponding real work capacities were about 0.16 ha h^{-1} and 0.26 ha h^{-1} . On average, the amount of digestate spread in the inter-rows was $1.09 \pm 0.54 \text{ kg m}^{-2}$ for broadcast spreading and $1.61 \pm 0.49 \text{ kg m}^{-2}$ for localized spreading; the corresponding dry matter quantities were around 6.9 and 7.1 t ha^{-1} . Transverse uniformity of spreading (difference between left and right) was better in localized distribution (left = 1.67 kg m^{-2} and right = 1.55 kg m^{-2} , difference not statistically significant) and worse in broadcast distribution (0.80 vs 1.39 kg m^{-2} , difference statistically significant), due to the direction

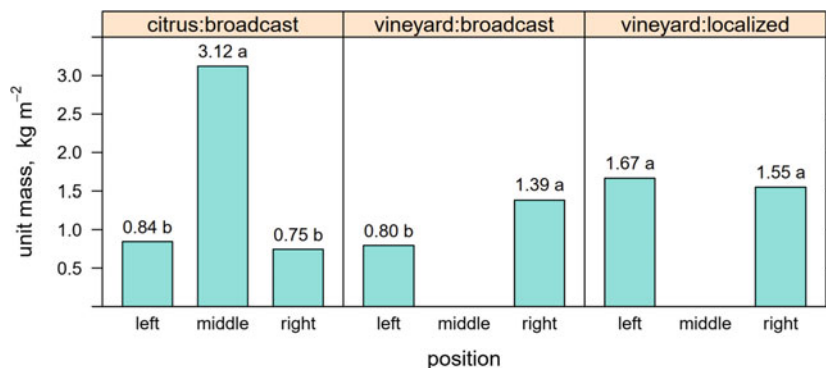


Fig. 4 Unit masses of digestate solid fraction spread on citrus and vineyard

Table 3 Main chemical and physical parameters of the microfiltered liquid fraction of the digestate*

TS (g kg ⁻¹)	VS (g kg ⁻¹)	NTK (mg kg ⁻¹)	N-NH ₄ ⁺ (mg kg ⁻¹)	TP (mg kg ⁻¹)	TK (mg kg ⁻¹)
53.7	27.6	6266	4219	846	4542

(* TS = total solid; VS = volatile solid; NTK = Total Nitrogen (Kjeldahl method); N-NH₄⁺ = total ammoniacal nitrogen; TP = total phosphorous; TK = total potassium

of rotation of the distributor disc (Fig. 4). Even in this case, variability within inter-rows was greater than that between inter-rows (coefficient of variation equal 15.1 and 33.3%, respectively), attributable to the progressive emptying of the hopper.

4.2 Microfiltered Liquid Fraction

Table 3 reports the main chemical and physical parameters of the microfiltered liquid fraction of the digestate. Values are similar to those reported in the literature when inputs at the digestion plant are energetic crops and agro-industrial by-products [22].

The average results obtained during field experiments are summarized in Table 4. In Farm A about 37.8 m³ of microfiltered digestate were distributed, subdivided into three interventions. The average dilution factor, computed as ratio between digestate and water flow rate, was 11.5%. In Farm B about 13.9 m³ of digestate were distributed, subdivided into three interventions; the average dilution factor was 6.6%. Finally, in Farm C about 42.0 m³ of digestate were distributed, subdivided into two interventions, with average dilution factor of 13.3%.

The cleaning procedure of the filter disks required 20 s per filter pod. So, the amount of water required per each cleaning intervention was about 203 L in Farm A, where the filter was equipped with two filter pods, about 134 L in Farm B, where the filter was also equipped with two filter pods, and about 371 L in Farm C, where

Table 4 Average field conditions during the spreading of the digestate liquid fraction

Farm	Water flow rate (m ³ h ⁻¹)	Digestate flow rate (m ³ h ⁻¹)	Total flow rate (m ³ h ⁻¹)	Nominal dripline flow rate (m ³ h ⁻¹)	Dilution factor (%)
A	18.3	2.1	20.4	20.3	11.5
B	12.1	0.8	12.9	13.8	6.6
C	22.3	3.0	25.3	21.9	13.3

the filter was equipped with three filter pods. The cleaning frequency was of about 10 min or less using filters with two pods and 30–45 min with three pods. Being the amount of washing water and the time need to complete the distribution of the digestate increasing with the number of the cleaning cycles, it is fundamental that the cleaning interval is greater than 30 min.

5 Conclusions

The field distribution of digestate, by-product of the anaerobic digestion process carried out with local agricultural and agro-industrial biomasses, constitutes the final phase of a cycle that begins and ends in the field. Therefore, the entire process of biogas production can be considered an example of circular economy. In this paper are reported the results of the first tests of distribution of both solid and liquid fraction of digestate in tree crops. The results, despite other experimental tests being necessary, helped us to draw the following conclusions:

- The spreaders used to distribute the solid fraction of digestate, even if designated to the distribution of other products, were found to be suitable to this purpose, but they require some adjustments in order to keep the flow rate constant during emptying of the hopper.
- The transverse uniformity is influenced by the distribution system. In fact, in the citrus orchard, the digestate was mainly spread in the middle of the inter-row (66%), and in the vineyard, with the centrifugal distributor, in the right side (64%), while was quite uniform between the left and the right side (52 vs 48%) with the localized distributor.
- The distribution of the liquid fraction of the digestate with the drip fertigation plants requires its dilution in the irrigation water that cannot exceed the percentage of 10–15% to avoid the increase in both water and time consumption due to the high frequency of self-cleaning of the final hydraulic filter.
- Considering the flow rate of the irrigation water usually adopted, filters with three filter pods should be used to reach intervals of self-cleaning procedure more than 30–45 min.

Further studies could usefully investigate the suitability of other spreaders, possibly with the support of precision agriculture equipment to control real time spreading uniformity. In addition, an automatic system should be implemented to maintain the dilution percentage of the liquid fraction of the digestate in the irrigation water constant.

Acknowledgements This research was carried out in line with the project titled FERTIMED “Sustainable and innovative soil improvers for Mediterranean crops” funded by the Mis. 16.1 of the Sicilian PSR 2014–2020 (CUP G54I20000560009).

References

1. Albuquerque, J.A., de la Fuente, C., Ferrer-Costa, A., Carrasco, L., Cegarra, J., Abad, M., Bernal, M.P.: Assessment of the fertiliser potential of digestates from farm and agroindustrial residues. *Biomass Bioenergy* **40**, 181–189 (2012). <https://doi.org/10.1016/j.biombioe.2012.02.018>
2. Bacenetti, J., Lovarelli, D., Fiala, M.: Mechanisation of organic fertiliser spreading, choice of fertiliser and crop residue management as solutions for maize environmental impact mitigation. *Eur. J. Agron.* **79**, 107–118 (2016). <https://doi.org/10.1016/j.eja.2016.05.015>
3. Barlóg, P., Hlisnikovský, L., Kunzová, E.: Effect of digestate on soil organic carbon and plant-available nutrient content compared to cattle slurry and mineral fertilization. *Agronomy* **10**, 379 (2020). <https://doi.org/10.3390/agronomy10030379>
4. Bustamante, M.A., Restrepo, A.P., Albuquerque, J.A., Perez-Murcia, M.D., Paredes, C., Moral, R., Bernal, M.P.: Recycling of anaerobic digestates by composting: effect of the bulking agent used. *J. Clean. Prod.* **47**, 61–69 (2013). <https://doi.org/10.1016/j.jclepro.2012.07.018>
5. Cerruto, E., Selvaggi, R., Papa, R.: Potential biogas production from by-products of citrus industry in Sicily. *Qual. Access Success* **17**(S1), 251–258 (2016)
6. Comparetti, A., Febo, P., Greco, C., Orlando, S., Navickas, K., Venslauskas, K.: Sicilian potential biogas production. *Journal of Agricultural Engineering* **44**(s2), 522–525, e103 (2013). <https://doi.org/10.4081/jae.2013.s2.e103>
7. Czekala, W., Dach, J., Dong, R., Janczak, D., Malinska, K., Józwiakowski, K., Smurzyńska, A., Cieślík, M.: Composting potential of the solid fraction of digested pulp produced by a biogas plant. *Biosys. Eng.* **160**, 25–29 (2017). <https://doi.org/10.1016/j.biosystemseng.2017.05.003>
8. Di Maria, F., Sisani, F.: A sustainability assessment for use on land or wastewater treatment of the digestate from bio-waste. *Waste Manage.* **87**, 741–750 (2019). <https://doi.org/10.1016/j.wasman.2019.03.015>
9. Garrido, S., Sequeira, T., Santos, M.: Renewable energy and sustainability from the supply side: A critical review and analysis. *Appl. Sci.* **10**, 5755 (2020). <https://doi.org/10.3390/app10175755>
10. Guido, V., Finzi, A., Ferrari, O., Riva, E., Quílez, D., Herrero, E., Provolo, G.: Fertilization of maize with digestate using drip irrigation and pivot systems. *Agronomy* **10**, 1453 (2020). <https://doi.org/10.3390/agronomy10101453>
11. Guilayna, F., Jimenez, J., Rouez, M., Crest, M., Patureau, D.: Digestate mechanical separation: Efficiency profiles based on anaerobic digestion feedstock and equipment choice. *Biores. Technol.* **274**, 180–189 (2019). <https://doi.org/10.1016/j.biortech.2018.11.090>
12. Kratzeisen, M., Starcevic, N., Martinov, M., Maurer, C., Müller, J.: Applicability of biogas digestate as solid fuel. *Fuel* **89**, 2544–2548 (2010). <https://doi.org/10.1016/j.fuel.2010.02.008>

13. Longhurst, P.J., Tompkins, D., Pollard, S.J.T., Hough, R.L., Chambers, B., Gale, P., Tyrrel, S., Villa, R., Taylor, M., Wu, S., Sakrabani, R., Litterick, A., Snary, E., Leinster, P., Sweet, N.: Risk assessments for quality-assured, source-segregated composts and anaerobic digestates for a circular bioeconomy in the UK. *Environ. Int.* **127**, 253–266 (2019). <https://doi.org/10.1016/j.envint.2019.03.044>
14. Makadi, M., Tomocsik, A., Orosz, V.: Digestate: A new nutrient source - Review. In: Sunil Kumar, Dr. (Ed.), *Biogas*. InTech, 295–310 (2012). Available from, <http://www.intechopen.com/books/biogas/digestate-a-new-nutrient-source-review>
15. Manetto, G., Cerruto, E., Papa, R., Selvaggi, R., Pecorino, B.: Performance evaluation of digestate spreading machines in vineyards and citrus orchards: preliminary trials. *Heliyon* **6**(6), e04257 (2020). <https://doi.org/10.1016/j.heliyon.2020.e04257>
16. Maurer, C., Müller, J.: Drying characteristics of biogas digestate in a hybrid waste-heat/solar dryer. *Energies* **12**, 1294 (2019). <https://doi.org/10.3390/en12071294>
17. Nayal, F.S., Mammadov, A., Ciliz, N.: Environmental assessment of energy generation from agricultural and farm waste through anaerobic digestion. *J. Environ. Manage.* **184**, 389–399 (2016). <https://doi.org/10.1016/j.jenvman.2016.09.058>
18. Nkoa, R.: Agricultural benefits and environmental risks of soil fertilization with anaerobic digestates: a review. *Agronomy for Sustainable Development*, Springer Verlag/EDP Sciences/INRA **34**(2), 473–492 (2014). <https://doi.org/10.1007/s13593-013-0196-z>
19. Pappalardo, G., Selvaggi, R., Bracco, S., Chinnici, G., Pecorino, B.: Factors affecting purchasing process of digestate: evidence from an economic experiment on Sicilian farmers' willingness to pay. *Agricultural and Food Economics* **6**(16), 1–12 (2018). <https://doi.org/10.1186/s40100-018-0111-7>
20. Regione Siciliana: Assessorato regionale dell'agricoltura, dello sviluppo rurale e della pesca mediterranea - Dipartimento regionale dell'agricoltura. *Disciplinare regionale produzione integrata. Norme tecniche agronomiche*. Allegato A 61, 159 (2019)
21. Riva, C., Orzi, V., Carozzi, M., Acutis, M., Boccasile, G., Lonati, S., Tambone, F., D'Impranzano, G., Adani, F.: Short-term experiments in using digestate products as substitutes for mineral (N) fertilizer: Agronomic performance, odours, and ammonia emission impacts. *Sci. Total Environ.* **547**, 206–214 (2016). <https://doi.org/10.1016/j.scitotenv.2015.12.156>
22. Rossi, L., Mantovi, P.: Digestato, un utile sottoprodotto del biogas. *Conoscere per Competere*, 4. CRPA, Emilia Romagna (2012)
23. Selvaggi, R., Pappalardo, G., Pecorino, B., Vecchio, R.: Factors influencing farmers' decision to enter digestate market. *J. Clean. Prod.* **321**, 128961 (2021). <https://doi.org/10.1016/j.jclepro.2021.128961>
24. Slepetiene, A., Volungevicius, J., Jurgutis, L., Liaudanskiene, I., Amaleviciute-Volunge, K., Slepetyus, J., Ceseviciene, J.: The potential of digestate as a biofertilizer in eroded soils of Lithuania. *Waste Manage.* **102**, 441–451 (2020). <https://doi.org/10.1016/j.wasman.2019.11.008>
25. Stürmer, B., Pfundtner, E., Kirchmeyer, F., Uschnig, S.: Legal requirements for digestate as fertilizer in Austria and the European Union compared to actual technical parameters. *J. Environ. Manage.* **253**, 109756 (2020). <https://doi.org/10.1016/j.jenvman.2019.109756>
26. Tambone, F., Scaglia, B., D'Impranzano, G., Schievano, A., Orzi, V., Salati, S., Adani, F.: Assessing amendment and fertilizing properties of digestates from anaerobic digestion through a comparative study with digested sludge and compost. *Chemosphere* **81**, 577–583 (2010). <https://doi.org/10.1016/j.chemosphere.2010.08.034>
27. Valenti, F., Porto, S.M.C., Selvaggi, R., Pecorino, B.: Evaluation of biomethane potential from by-products and agricultural residues co-digestion in southern Italy. *J. Environ. Manage.* **223**, 834–840 (2018). <https://doi.org/10.1016/j.jenvman.2018.06.098>
28. Valentinuzzi, F., Cavani, L., Porfido, C., Terzano, R., Pii, Y., Cesco, S., Marzadori, C., Mimmo, T.: The fertilising potential of manure-based biogas fermentation residues: pelleted vs. liquid digestate. *Heliyon* **6**, e03325 (2020). <https://doi.org/10.1016/j.heliyon.2020.e03325>

29. Vašínka, M., Badalíková, B.: Changes in soil properties due to application of digestate. *Mechanization in agriculture & Conserving of the resources* **65**(4), 129–131 (2019)
30. Vilanova Plana, P., Noche, B.: A review of the current digestate distribution models: storage and transport. *Proceedings of the 8th International Conference on Waste Management and The Environment, WIT Transactions on Ecology and The Environment* 202, 345–357 (2016). <https://doi.org/10.2495/WM160311>

Preliminary Trials to Investigate the Effect of Sprayer Setting for Ozonated Water Spray Applications to Improve Plants Disease Control Efficacy



Marco Sozzi, Alessandro Zanchin, Franco Gasparini, Francesco Marinello, and Luigi Sartori

Abstract The environmental and socioeconomic constraints force the agricultural sector to find alternative plant protection solutions. As a result, several alternative plant protection products (PPP) have been developed in the last decades. Ozonated water sprayed on the vegetation proved to be a partial alternative to agricultural chemical PPP for plant diseases. The ozonated water efficacy is related to the production of reactive oxygen species (ROS). At the same time, ozonated water showed no significant phytotoxicity when the spraying was carried out under well-ventilated conditions. In the present study, a corona discharge ozonating water tool was installed on a commercial mist-blower axial sprayer then the redox potential was measured to assess the sanitizing effects on plants due to ROS concentration. First, the redox potential (ORP) was measured inside the tank, after the pump, at the nozzle level, and on a test bench that simulated the vertical wall of the plant. Next, the redox growth rate was measured at each point to assess the system's latency. Then, different nozzle types were used to measure the effect of varying droplet sizes on redox potential. The result shows potential redox decreases by 7%, 12%, and 29% after the pump, at the nozzle, and at the test bench, respectively. These losses are affected by the droplet size, and they increase in the case of a smaller droplet. Significant differences were found among different nozzle types.

Keywords Integrated Pest Management · Ozone · Spray Droplet Size · Air Speed

1 Introduction

Plant protection products (PPPs) consumption has increased since the spreading of the grapevine downy mildew (*Plasmopora viticola*) and the grapevine powdery mildew (*Erysiphe necator*), which have been causing severe yield losses on *Vitis*

M. Sozzi (✉) · A. Zanchin · F. Gasparini · F. Marinello · L. Sartori
Department of Land Environment Agriculture and Forestry, University of Padova, Padua, Italy
e-mail: marco.sozzi@unipd.it

© The Author(s), under exclusive license to Springer Nature Switzerland AG 2023
V. Ferro et al. (eds.), *AIIA 2022: Biosystems Engineering Towards the Green Deal*,
Lecture Notes in Civil Engineering 337,
https://doi.org/10.1007/978-3-031-30329-6_73

717

vinifera [1]. Nowadays, viticulture represents the first sector for fungicide consumption in Europe. In 2020, the total consumption of fungicide at the EU-27 level has remained almost unchanged from the 2011 level (+0.52, [2]). Since the introduction of the directive 2009/128/EC, the European Commission has asked farmers the reduction of PPPs, banning the most toxic substance for humans and the environment. Recently, the Farm to Fork strategy foresees to reduce by 50% the chemical inputs in agriculture [3]. For years researchers and farmers improved the treatment applications reducing PPPs consumption. Moreover, they have looked for less hazardous alternative active ingredients than common PPPs.

Ozone (O₃) represents an affordable product widely used against several fungal and bacterial pathogens. The lethality of ozone against pathogens and insects was proved by several laboratory studies [4, 5]. Moreover, ozone can be used as odour management tool in biogas plants and stable [6] to increase animals' comfort [7]. The applicability of ozonated water (OW) has been verified by bubbling ozone gas into a water tank since ozone gas can negatively affect vegetation and environment [8]. In grapevine, a high ozone concentration reduces yield and the must quality of [9].

On the other hand, OW does not cause direct damage to both vegetables and grapevine [10]–[12]. When ozone is bubbled into the water, the reaction produces reactive oxygen substances (ROS), increasing the solution's oxidation–reduction potential (ORP). After this process, OW is toxic for pathogens, but not enough to damage the plants' tissues. OW is much more toxic against fungi than other microorganisms [13]. Besides, it has been proved that at least two positive effects of OW for irrigations and plant treatments. First, OW has been verified as a suitable alternative for synthetic fungicides concerning vegetables. Also, OW can promote the yield and quality of fruits [14, 15]. Second, it has been proved crucial in activating the plant defence strategy acting as a fungi elicitor. The defence-promoting activity has been verified against powdery mildew in grapevine [14].

OW must be produced onsite since ozone is an unstable compound with a relatively short half-life. According to this, it might be produced by mounting an ozone generator on an irrigation system or a sprayer. Ozone is usually generated by corona discharge method: O₂ flows between two electrodes with a different voltage; the electrical discharge breaks the oxygen molecule and forms two oxygen radicals, which combine with oxygen molecules to form ozone. This ozone is then bubbled into a water tank to produce OW. Since OW is moved away from the generator, ORP is destined to decrease due to the ROS' instability. Therefore, an accurate evaluation of the working parameters should be done before treating a crop with OW. Droplet size and target distance are two of the crucial patterns affecting an OW treatment efficacy [16].

The present study aims to determine the ORP of OW falling in a sprayer prototype designed for vineyard uses. For this research, an ozone generator tool was installed on a commercial mist-blower axial sprayer designed for vineyard treatments. First, the ORP was measured repeatedly along all the paths inside the hydraulic pipeline and outside of the nozzles. Then, different nozzle types and fan speeds were tested to evaluate the effect of different droplet sizes and airflow on the final redox potential.

Table 1 Technical features of OW generator

Ozone generator features	Value	Units
Maximum ozone production	20	g/h
Optimal ozone concentration	70	g/m ³
Supply voltage	12	V
Power	250	W
Weight	35	kg
Dimensions	800 × 420 × 250	mm

2 Materials and Methods

2.1 Ozone Generator

The ozone generator was mounted on an axial mist-blower sprayer (ELK 88, Europiave, Cimadolmo -TV, Italy). This sprayer was composed of a 400 L tank, a 4-diaphragm pump, a filter, a hydraulic control system, a pressure gauge, and 12 nozzles divided into two sections. For these trials, only ten nozzles were used (5 per section). All the trials were performed stationary by operating the sprayer with the power take-off of a tractor (Tigre, Antonio Carraro, Campodarsego -PD, Italy). Tests were carried out at the mechanical workshop of the TeSAF department of the University of Padova (Legnaro -PD, Italy) from 07/02/2022 to 18/02/2022.

The ozone generator used a corona discharge system (Airone G2000, Ecofarm Storti, Belfiore -VR, Italy), whose features are shown in Table 1. The generator consists of a current transformer, air-cooled borosilicate dielectric, an activated alumina O₂ concentrator, an activated carbon filter, a membrane dryer, an O₂ tank, an ORP measurement tool with a probe inside the tank, a programmable logic controller (PLC), and a bubbler mounted inside the sprayer tank. The OW production is managed by a tablet which communicates with the PLC via Bluetooth. According to the producer, the antifungal effect is assumed to be effective at 850 mV (ORP value in the tank). Since the action of OW is by contact, a high volume of products must be sprayed (800–1000 L/ha).

2.2 ORP Measurement and Tests

ORP was measured by the embedded ORP probe of the ozone generator (inside the sprayer tank) and a portable ORP platinum probe (ORP60, Apera Instruments, Wuppertal, Germany). Before the tests, both probes were calibrated with a 222 mV solution (Apera Instruments).

The first test was carried out inside the sprayer tank by monitoring the ORP with the embedded probe, aiming to estimate the time required to produce OW.



Fig. 1 (A) Mist-blower sprayer equipped with the ozone generator and linked to the tractor used for the trials. On the right of the ozone generator the Apera probe is visible; (B) OW sprayer during the test with the vertical test bench

The second test was performed by measuring the ORP right after the control system (Fig. 1A) to assess the influence of the diaphragm pump on the OW. The ORP was measured simultaneously in the tank and close to the control system. The Apera probe was installed in an always-full cup in line with the sprayer pipeline.

Finally, the ORP was measured right after the nozzles by collecting the OW with a nozzle adapter and tube and on a vertical test bench (Patternator with discs, Salvarani, Poggioleone -RE, Italy). The vertical test bench was mounted to reach a height of three meters to simulate the vegetation (Fig. 1B). The ORP measurement on the vertical test bench was used to estimate the effects of the interaction of the OW with the atmosphere. In addition, different nozzle types were tested to evaluate the impact of different drop sizes on OW ORP.

Three different nozzles were used according to ISO 10625 colour coding: Green, Yellow, and Red (Table 2). Since high-volume spraying was required, the pressure was varied to reach 1000 L/ha with a simulated speed suitable for professional users. Such a high volume was required by the manufacturer, since the ephemeral action of OW on vegetation.

All measurements were carried by filling the tank by 75% (300 L) every time with tap water (average temperature of 14.6 °C, and pH of 7.66). The ORP measurement range was 30 s for 15 min.

Table 2 Pressure, speed, and estimated drop size of the nozzle used

ISO 10625 Colour coding	Pressure 10^5 Pa (Bar)	Speed km/h	Drop size
Green	15	3.5	VF (60–145 μ m)
Yellow	10	4.0	VF (60–145 μ m)
Red	5	5.5	F (145–225 μ m)

ORP measurements with different nozzle types were statistically compared with one-way ANOVA and Tukey’s range tests. Statistical analysis was carried out within R software (R CRAN, Vienna, Austria).

The statistical distribution obtained by this selected dataset were statistically compared with ANOVA test and Tukey’s range test. According to the statistical analysis, all the differences were statistically significant (p-value < 0.001).

3 Results and Discussion

The ORP dynamics obtained by the measurement performed in the three tests in the four measurement locations (Tank, Panel, Nozzles, and Bench) are showed in Fig. 2. Data are showed as average value with a confidence interval of 95% obtained from the different replicas performed.

All the ORP curves showed a similar evolution over time. In the initial stages, the ORP showed exponential growth up to an inflexion point. After that, the value of ORP rises considerably slower till it reaches a horizontal asymptote. The horizontal asymptote was reached after 250 s by approximating slight differences. On the other hand, these latter asymptote values significantly differ in the four measurement locations. The ORP decreased by 7%, 12%, and 29% after the pump, at the nozzles, and the test bench, respectively, compared with the value in the tank. This decline may be caused by the need to reach an electrochemical balance in each part of the sprayer (tubes, rings, pump), which has a different redox potential from the OW.

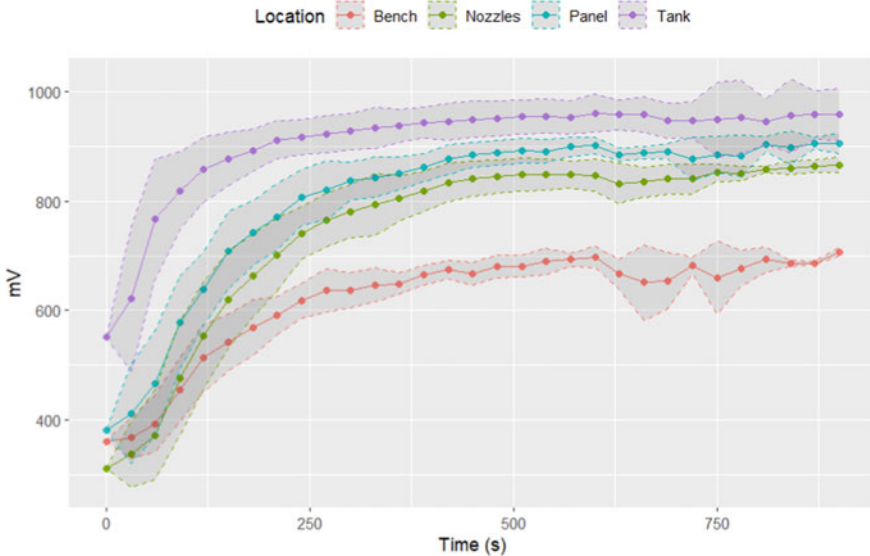


Fig. 2 ORP dynamics in four measurement locations (confidence interval of 95%)

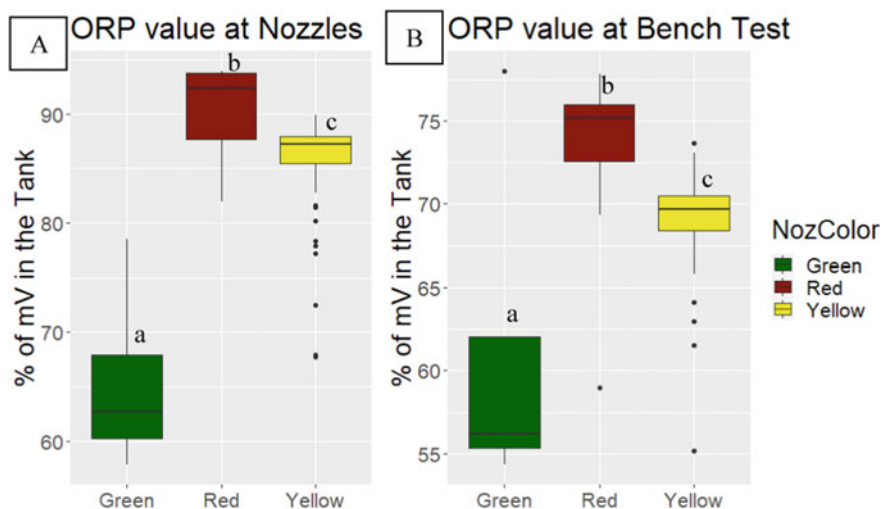


Fig. 3 (A) Distribution of ORP with different nozzles at nozzle measurement location (B) Distribution of ORP with different nozzles at test bench measurement location. Letters refers to Tukey's range test (p -value < 0.001)

The significant drop of the ORP at the bench test may be caused by the interaction with the atmosphere. According to this, different nozzles and pressure were tested. ORP values were normalized on the tank values, to remove the effects of dynamics. In addition, only values measured after 250 s were used. The statistical distribution obtained by this selected dataset was statistically compared with the ANOVA test and Tukey's range test. Although data did not show normal distribution (according to the Shapiro–Wilk test), the violation of the normality assumption was not considered according to the large sample size (95 observations).

On the other hand, Levene's test confirmed homoscedasticity. According to the statistical analysis, all the differences were statistically significant (p -value < 0.001). The distribution of the ORP using different nozzles is shown in Fig. 3.

4 Conclusions

This study aimed to provide relevant information on the behaviour of OW sprayed with an axial mist-blower sprayer. Since ROS dissolved in the water have a relatively low half-life, it is crucial to set the correct parameters of the sprayer to optimize the plant disease control efficacy. According to the tests presented in this study, the redox potential of the OW inside the sprayer components is affected by a lag time to achieve an electrochemical balance. The time required by the sprayer used for this experiment was 250 s (6 min), which represents a suitable time for the farmer since it is comparable to or even lower than the time required for chemical plant protection

products preparation. On the other hand, this time is considered spraying time since nozzles must be open to achieve the electrochemical balance.

Different types of nozzles and working pressure were tested in this study. Statistical differences found in the redox potential of OW at nozzles and on the test bench suggest that the drop size affects the redox drop after the spraying, with a more critical decline in case of a finer drop, due to a higher surface in contact with the atmosphere. This latter consideration confirms the founding of Fujiwara & Fuji by measuring dissolved ozone concentration [16].

References

1. Schröder, S., Telle, S., Nick, P., Thines, M.: Cryptic diversity of *Plasmopara viticola* (Oomycota, Peronosporaceae) in North America. *Org. Divers Evol.* **11**(1), 3–7 (2011). <https://doi.org/10.1007/s13127-010-0035-x>
2. Eurostat: Pesticide sales in EU. Eurostat (2021). https://ec.europa.eu/eurostat/databrowser/view/aei_fm_salpest09/default/table?lang=en. Accessed 17 Aug 2022
3. European Commission: A Farm to Fork Strategy for a fair, healthy and environmentally-friendly food system. Brussels (2020). https://agridata.ec.europa.eu/Qlik_Downloads/Jobs-Growth-sources.htm. Accessed 03 Jan 2023
4. Guo, Z., Wang, Z., Li, Y., Wang, Q.: Effect of different concentrations of ozone on in vitro plant pathogens development, tomato yield and quality, photosynthetic activity and enzymatic activities. *Ozone Sci. Eng.* **41**(6), 531–540 (2019). <https://doi.org/10.1080/01919512.2019.1591268>
5. Savage, B.A., Masten, S., Chung, H., Grieshop, M.: Exploring the insecticidal potential of gaseous and aqueous ozone to control spotted-wing *Drosophila*, *Drosophila Suzukii* (Diptera: Drosophilidae). *J. Econ. Entomol.* **115**(4), 1203–1212 (2022). <https://doi.org/10.1093/jee/toac091>
6. Ferrari, G., Ioverno, F., Sozzi, M., Marinello, F., Pezzuolo, A.: Land-use change and bioenergy production: soil consumption and characterization of anaerobic digestion plants (2021). <https://doi.org/10.3390/en14134001>
7. Sozzi, M., et al.: Measuring comfort behaviours in laying hens using deep-learning tools. *Animals* **13**(1), 33 (2022). <https://doi.org/10.3390/ani13010033>
8. Tiwari, S., Agrawal, M.: Effect of ozone on physiological and biochemical processes of plants. In: Tiwari, S., Agrawal, M. (eds.) *Tropospheric Ozone and its Impacts on Crop Plants*, pp. 65–113. Springer, Cham (2018). https://doi.org/10.1007/978-3-319-71873-6_3
9. Fumagalli, I., Cieslik, S., De Marco, A., Proietti, C., Paoletti, E.: Grapevine and ozone: uptake and effects. *Climate* **7**(12), 140 (2019). <https://doi.org/10.3390/CL17120140>
10. Modesti, M., et al.: Effects of treatments with ozonated water in the vineyard (cv Vermentino) on microbial population and fruit quality parameters. *BIO Web Conf.* **13**, 04011 (2019). <https://doi.org/10.1051/BIOCONF/20191304011>
11. Campayo, A., de la Hoz, K.S., García-Martínez, M.M., Salinas, M.R., Alonso, G.L.: Spraying ozonated water on Bobal grapevines: effect on wine quality. *Biomolecules* **10**(2), 213 (2020). <https://doi.org/10.3390/BIOM10020213>
12. Guo, Z., Wang, Q.: Efficacy of ozonated water against *Erwinia carotovora* subsp. *carotovora* in *Brassica campestris* ssp. *Chinensis* **39**(2), 127–136 (2017). <https://doi.org/10.1080/01919512.2016.1270744>
13. Raio, A., Feliciani, A., Ferri, V., Carboni, C.: Integrated vineyard management trials using ozonated and electrolyzed water. *Integr. Vineyard Manag. Trials Ozonated Electrolyzed Water* **6**(2) (2016)

14. Risoli, S., Lauria, G.: Ozonated water application as an innovative tool for elicitation of plant defense response: a minireview. *Curr. Opin. Environ. Sci. Health* **28**, 100375 (2022). <https://doi.org/10.1016/J.COESH.2022.100375>
15. Peykanpour, E., Ghehsareh, A.M., Fallahzade, J., Najarian, M.: Interactive effects of salinity and ozonated water on yield components of cucumber. *Plant Soil Environ.* **62**(8), 361–366 (2016). <https://doi.org/10.17221/170/2016-PSE>
16. Fujiwara, K., Fujii, T.: Research note: effects of ozonated water spray droplet size and distance on the dissolved ozone concentration at the spray target **26**(5), 511–516 (2010). <https://doi.org/10.1080/01919510490507892>

Evaluation of Potential Fuel Saving of Tractor Electrification Layouts Using Real-World Data



Michele Mattetti, Giovanni Molari, and Massimiliano Varani

Abstract In 2020, the European Commission (EC) presented the European Green Deal which is an ambitious package of measures aiming to transform Europe into the first climate-neutral continent. Agricultural mechanisation is responsible for around 70 million tons of CO₂ of yearly emissions. To significantly reduce CO₂ emissions, hybrid powertrains are under investigation by industry and researchers. This paper aims to investigate a few hybrid powertrain architectures and to report the advantages of such solutions based on real-world data to obtain the potential benefits perceived by farmers. Real-world data were collected with a CANBUS data logger on a row-crop tractor rated at approximately 190 kW. In this tractor, engine and transmission operating parameters were recorded for approximately 2500 h of field use. Data were firstly classified into tasks, and then a series of metrics permitting to outline the usage of tractors were calculated. This permitted us to highlight the operational inefficiency of each type of task. Two different hybrid architectures were studied and evaluated with the load-point shifting principles. The studied architectures are engine start-stop and PTO-electrification. The most inefficient operations are idling and transportation since the engine operates at a low load which is an operation where the specific fuel consumption is below the optimum. The tractor was run on idle for 25% of the entire and cutting down idling with an idling stop system would permit to achieve a potential fuel saving of 1.7%. On the other hand, PTO-electrification would permit to achieve a potential fuel saving ranging from 2% for high demanding operations up to 16% for low demanding ones.

Keywords Fuel saving · electrification · tractors · real-world data

M. Mattetti (✉) · G. Molari · M. Varani

Department of Agricultural and Food Sciences (DISTAL), Alma Mater Studiorum - University of Bologna, Bologna, Italy

e-mail: michele.mattetti@unibo.it

1 Introduction

According to the European Environment Agency, agricultural mechanisation is responsible for around 70 million tons of CO₂ of yearly emissions. With the approval of the European Green Deal, the ambition of the European Commission is to transform Europe into the first climate-neutral continent. Researchers and machinery manufacturers have been studying novel solutions for reducing GHG emissions of agricultural machinery and powertrain electrification is considered a feasible solution in this regard since it permits overcoming a few downsides of internal combustion engines (ICE) [1]. In particular, ICEs can achieve their optimal fuel efficiency (i.e., specific fuel consumption) only when they operate within high engine loads [2]. However, agricultural tractors operate for a significant amount of time in low-demanding operations [3] leading to inefficient operating conditions especially if ICEs are not properly sized. Powertrain electrifications permit to avoid that ICEs operate at those inefficient operating conditions permitting to increase ICE efficiency. Generally, farmers should down-speed the engine to a certain extent. For drawn-implement, farmers can easily adopt this principle by adjusting the gearbox and applying the “gear-up and throttle down” approach [4]. However, for implements driven by the power take-off (PTO), farmers are forced to overspeed the ICE since PTO must operate at its nominal speeds occurring only at a certain engine speed due to the mechanical gearbox between the engine and the PTO shaft. Another operational inefficiency is caused by idling and tractors are exposed to prolonged idling [5], which is an operating status in which the ICE is running without any substantial load. Idling can be a consequence of farming operations such as implement hitching but it can also be the consequence of farmers’ negligence [6]. In such conditions, a system permitting to automatically turning off the ICE on unnecessary idling stops would be beneficial. This study aimed to develop a method for outlining the use of a tractor and to estimate the potential fuel savings of innovative electrified solutions.

2 Materials and Methods

The analysis was applied to a New Holland T7 tractor (CNH Industrial N.V., Amsterdam, NL) (Fig. 1) whose specifications are reported in Table 1. This was chosen because tractors of this class are rich in terms of embedded sensors allowing for comprehensive monitoring of the embedded subsystems (i.e., ICE, gearbox, PTO, and three-point linkage).

One unit of that tractor was in use in the Agricultural Farm of the University of Bologna for three years and it was monitored with a stand-alone CAN-BUS data logger equipped with a GNSS receiver. During that time, the tractor was dedicated to transportation, and primary and secondary tillage tasks by 5 drivers. In the That data logger was set-up to automatically record all the CANBUS data anytime the tractor was turned on. The data logger recorded all the operating parameters related to the



Fig. 1 Tractor monitored during the study

Table 1 Main specifications of the tractor used in this study retrieved from the datasheet

Parameter	Value
Engine displacement [m^3]	6728
Number of cylinders	6
Engine tier	4 A
Engine rated power with PTO disengaged [$kW@rpm$]	158@2200
Engine rated power with PTO engaged [$kW@rpm$]	181@2200
Maximum engine torque with PTO engaged [$Nm@rpm$]	995@1500
Maximum engine torque with PTO engaged [$Nm@rpm$]	1120@1500
Transmission	Full powershift with 19 forward and 6 rearward gears
Engine speed at PTO 540/540E/1000/1000E speed [rpm]	1931/1598/1912/1583

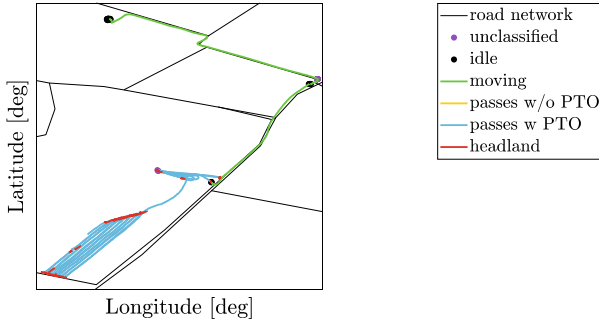


Fig. 2 Example of the auto-tagging algorithm

engine, transmission, and vehicle. In particular, the following signals were used for the analysis:

- Engine torque (T_e);
- Engine speed (n_e);
- Engine power (P_e);
- Engine fuel rate;
- Engine specific fuel consumption (\dot{f}_{sc});
- Position of the three-point linkage;
- Speed of the PTO;
- Vehicle speed;
- Tractor position.

All the signals were tagged with an auto-tagging algorithm developed by Mattetti et al. [8]. The defined tags were idling, headland turns, passes without PTO, passes with PTO, moving, and unclassified (Fig. 2).

A continuous portion of signals where the tag type did not change was considered as a task and for each task, the average value of the recorded signals was calculated to characterise the use of the tractor and to evaluate the room of improvements by removing the mechanical constraints which impose to the ICE to operate with a certain operational inefficiency.

3 Results

During the monitoring period, the tractor accumulated more than 2500 h. In Table 2, the contribution in terms of time, and fuel of each work state are reported together with their mean values of n_e , P_e , and \dot{f}_{sc} .

The passes and moving tags were the ones with the greatest time contribution since they account for approximately 78% together. On the other hand, passes states were the tags with the largest fuel contribution due to the great power delivered by

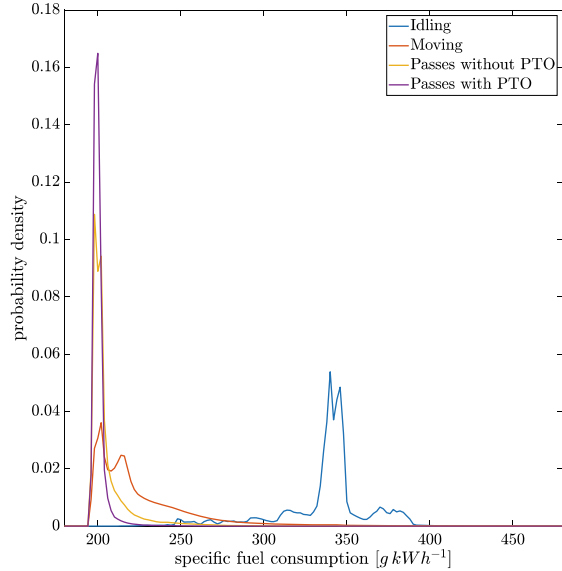
Table 2 Summary of the tractor use. In the brackets, the deviation standard were reported

Tractor classification	Time [%]	Fuel [%]	P_e [kW]	n_e [rpm]	\dot{f}_{sc} [g kWh ⁻¹]
Idle	25	3.6	6 (2.1)	862 (53.2)	338 (36.7)
Moving	38	36.1	43 (33.0)	1410 (330.7)	229 (35.0)
Passes without PTO	16	24.0	100 (37.8)	1701 (220.9)	201 (20.5)
Passes with PTO	14	32.0	156 (32.4)	1911 (131.1)	199 (21.0)
Headland turns	7	4.3	36 (15.4)	1593 (274.8)	237 (20.3)

the ICE in these tags. Indeed, the mean value of P_e for passes states was up to 76% greater than that of moving state. P_e for passes with PTO state was 56% greater than that of passed without PTO state. This is probably caused by the specific use of the tractor, and by the fact that with the PTO engaged, the engine peak power is increased by the electronic control unit of the ICE. The mean value of n_e on passes when the PTO was engaged was that which permitted running the PTO shaft at its nominal speed in the standard mode (Table 1). On the other hand, n_e on passes when the PTO was not engaged was between the engine speeds where maximum torque and power occur to maximise engine drivability. The highest value of \dot{f}_{sc} was observed for the idling state due to the fact is the tractor tag where the engine load is the lowest.

In Fig. 3, the probability density distribution of \dot{f}_{sc} is reported. One can note that for the two passes tags, the distributions are quite narrow, and they are placed in the low range of \dot{f}_{sc} . On the other hand, when the tractor was in the moving tag, \dot{f}_{sc} ranged from 200 up to 300 g kWh⁻¹ and the distribution does not show any significant peak. The distribution of \dot{f}_{sc} for the idling tag was quite wide but mostly concentrated at a high value (approximately 350 g kWh⁻¹). Those distributions showed that there is a certain room of improvement especially for idling, moving, and passes with PTO states. It will be convenient to completely skip the engine operating points when the ICE idles since \dot{f}_{sc} is very low and to optimise the other points such as when the tractor operates in passes with PTO tags. For a former it was evaluated the potential fuel savings by installing an idling stop which automatically stopped the tractor anytime the tractor was on unnecessary idling stops [9] and in that case, the potential fuel saving was estimated to be 1.7%. Instead, when the tractor operated with the PTO, it was assumed that in the tractor an electric CVT transmission was installed which permitting to down speed the ICE to the speed where the minimum specific fuel consumption occurs. This solution permitted us to obtain potential fuel savings that ranged from 2% in high-demanding operations up to 16% on low-demanding ones.

Fig. 3 Probability density distribution of the specific fuel consumption (f_{sc}) for each type of tag



4 Conclusions

Fuel consumption reduction is a key target of modern tractor's development and drivetrain electrification is probably a promising solution for this goal. Effective electrified drivetrains should permit to avoid operational inefficiencies which were identified by using real-world data and permitted to outline a few electrified drivetrain layouts. For each proposed layout, the potential fuel savings were identified. Those were estimated using simple modelling and deviations from those results could be estimated especially during transient engine operations. Fuel savings could also change in the function of the tractor mission profile and how and how long the engine, transmission, and PTO are used. For example, PTO electrification might be very beneficial for tractors used for long on low demanding operations with the PTO. This is also confirmed by Varani et al. [7], who tested a hybrid prototype which resulted in a reduction of fuel consumed per hectare by up to 30% compared to a conventional powertrain. On the other hand, the idling stop solution is effective on tractors that operate for long on idling and low demanding non-idling operations. The solutions reported in this study will permit to pave the way towards solutions which permit to reduce of GHG emissions in the future and help to defossilise agriculture.

References

1. Scolaro, E., Beligoj, M., Estevez, M.P., Alberti, L., Renzi, M., Mattetti, M.: Electrification of agricultural machinery: a review. *IEEE Access* **9**, 164520–164541 (2021). <https://doi.org/10.1109/ACCESS.2021.3135037>
2. Mattarelli, E., et al.: Potential of electrification applied to non-road diesel engines. *SAE Technical papers*, vol. 2019-24–0202, September 2019. <https://doi.org/10.4271/2019-24-0202>
3. Mattetti, M., Medici, M., Canavari, M., Varani, M.: CANBUS-enabled activity-based costing for leveraging farm management. *Comput. Electron. Agric.* **194**, 106792 (Mar.2022). <https://doi.org/10.1016/j.compag.2022.106792>
4. Grisso, R.D., Pitman, R.M.: Gear up and throttle down—saving fuel. *Va. Coop. Ext.*, 442–450 (2001)
5. Perozzi, D., Mattetti, M., Molari, G., Sereni, E.: Methodology to analyse farm tractor idling time. *Biosys. Eng.* **148**, 81–89 (2016). <https://doi.org/10.1016/j.biosystemseng.2016.05.007>
6. Mattetti, M., et al.: Start and stop systems on agricultural tractors as solution for saving fuel and emissions. *Biosyst. Eng.* **216**, 108–120 (2022). <https://doi.org/10.1016/j.biosystemseng.2022.02.006>
7. Varani, M., Mattetti, M., Molari, G.: Performance evaluation of electrically driven agricultural implements powered by an external generator. *Agronomy* **11**(8), Article no. 8 (2021). <https://doi.org/10.3390/agronomy11081447>
8. Mattetti, M., Maraldi, M., Lenzini, N., Fiorati, S., Sereni, E., Molari, G.: Outlining the mission profile of agricultural tractors through CAN-BUS data analytics. *Comput. Electron. Agric.* (submitted 2021)
9. Molari, G., Mattetti, M., Lenzini, N., Fiorati, S.: An updated methodology to analyse the idling of agricultural tractors. *Biosys. Eng.* **187**, 160–170 (2019). <https://doi.org/10.1016/j.biosystemeng.2019.09.001>

Technological Solutions for Implementing Sustainable Cereal-Based Value-Chains in High Mountain Areas



Fabrizio Mazzetto , Giovanni Carabin , Lorenzo Becce ,
Andreas Mandler , and Pasqualina Sacco 

Abstract The project Brotweg (“The Bread path for/in mountain areas”) aimed to develop radical innovations for cereal cultivation in extreme mountain contexts, on land with very high slopes (even more than 80%) where cereal cultivation has so far been precluded to any form of mechanisation, resulting in abandonment due to high labour demands. The need to identify new development models for mountain agriculture, complementary to the currently prevailing zootechnical ones, has brought back the alternative of the “cereal chain” (cereal-flour-bread), compared to the “forage chain” (hay-milk-cheese) for the considerable advantages that the former entails in terms of reduced workload, investments and environmental impact. However, the implementation of the cereal chain requires clearing the main obstacles in the way of the adoption of suitable technological solutions for field mechanisation and conservation/management in small farms. The Brotweg project therefore envisages the development of prototypes to be used for (a) cereal cultivation, developing new machines for sowing and harvesting suitable for steep slopes; (b) post-harvest handling and storage of the grain directly at the farm; (c) grain processing with micro-bakery lines. The project was based on integrated evaluations capable of taking into account the economic and operational performance, safety conditions for operators, control of erosive phenomena and landscape protection, and levels of sustainability of the entire chain. The results of the project show the viability of new models of mountain agriculture, complementary to zootechnical production, and creates opportunities for new mountain livelihoods.

F. Mazzetto (✉) · G. Carabin · A. Mandler
Faculty of Science and Technology, Free University of Bozen-Bolzano, Piazza Università 5,
39100 Bolzano, Italy
e-mail: fabrizio.mazzetto@unibz.it

L. Becce
Competence Center for Plant Health, Free University of Bozen-Bolzano, Piazza Università 5,
39100 Bolzano, Italy

P. Sacco
Fraunhofer Italia, Innovation Engineering Center, Via Alessandro Volta 13a, 39100 Bolzano, Italy

Keywords Mountain agriculture · Minimum tillage · Stripper header · Cable traction · Value chains · Mountain livelihoods

1 Introduction

The Brotweg project (“The Bread path in mountain areas”) aimed to develop radical innovations for cereal cultivation in extreme mountain contexts, on land with very high slopes (even more than 80%) where cereal cultivation has so far been precluded to any form of mechanisation, resulting in abandonment due to high labour demands [1, 2]. The need to identify new development models for mountain agriculture, complementary to the currently prevailing livelihoods based on zootechnical production, has brought the alternative of the “cereal chain” (cereal-flour-bread) back to the forefront [3], compared to the “forage chain” (hay-milk-cheese) for the considerable advantages that the former entails in terms of reduced labour and annual workload, investments and environmental impact as shown in Fig. 1.

The implementation of the cereal chain requires the prior resolution of the main obstacles to the adoption of appropriate technological solutions for field mechanization [4, 5] and conservation/management in small farms. The project Brotweg therefore envisaged the development of prototypes to be used for the following tasks: a) cultivation, with new machines suitable for the steep slopes in the most critical operations (sowing and harvesting); b) post-harvesting and storage of the grain directly at the farm; c) processing, with micro-bakery lines. The research was based on integrated evaluations capable of taking into account economic and operational performance, safety conditions for operators, control of erosive phenomena and protection of the landscape, and levels of sustainability of the entire chain.

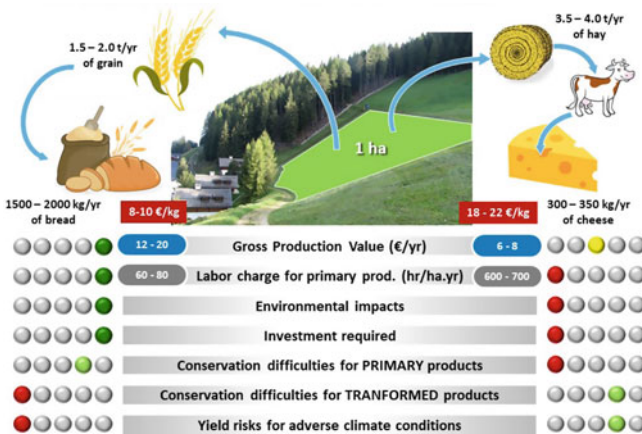


Fig. 1 Comparison of the cereal-flour-bread value-chain with the hay-milk-cheese value-chain

This paper specifically describes the technologies that have been adopted and/or developed in order to guarantee a mechanized approach to the problem. In addition, the results of the agronomic and operational performance achieved with the prototype set up in two production seasons 2020 and 2021 are reported.

2 Materials and Methods

The initial project activities focused on the development of new machines for the integral mechanisation of field operations, especially for minimum tillage, sowing and harvesting. These implements are based on a tool-carrying tractor (TLY-85, Geier s.r.l., Marling (BZ)) which integrates a cable traction system to allow transit and workability even in the most extreme conditions.

Moreover, the project focused on the post-harvest and conservation line that was entirely adapted into existing buildings to avoid the negative visual impact of external industrial equipment.

2.1 Sod-Seeding Drill

Conventional tillage practices place great risks of erosion, as [6] describes, so a minimum tillage approach was chosen to limit the competition from the existing vegetation, without completely eradicating it and hence conserving the traditional landscape (Fig. 2).

The selected solutions were a rotary harrow and a custom seed drill for hard ground capable of injecting seeds together with organic fertilizer. As shown in and Fig. 3, this mounted implement consists of four sections: (a) soil etching and seed deposition system (8 modules) with pneumatically assisted feeding mechanism; (b) two tanks, for seed and organic fertilizer (granular or pelleted), respectively, which are

Fig. 2 CAD view of the seeder subsystem





Fig. 3 The seeder in action with traditional farm buildings in the background

independent and hermetically sealed to prevent product spillage on extreme slopes; (c) pneumatic system, with centrifugal fan connected by independent pipes (one for each deposition element) to both tanks; the pneumatic distribution helps to control product losses on high slopes, while at the same time guaranteeing greater distribution regularity; d) support frame for coupling with the tool-carrying tractor; the working height of the distribution apparatus can be adjusted by a hydraulically-actuated device. Each deposition module also includes: 1) an incision wheel (disc blade, diameter 32 cm), connected to the support frame through a spring device, capable of exerting an adequate penetration force of the blades into the soil; 2) a furrow-covering disc, slightly inclined with respect to the direction of advancement and designed to drag some topsoil into the open furrow after seed deposition.

2.2 *Stripper Harvester*

To conduct harvesting operations, a mounted implement with a stripper header [7] was developed, to allow easier management of the biomass on steep terrain and in the subsequent transport phases. In particular, all the components are partially housed on the platform of the tool-carrying tractor, which realizes a device for “tear-off” harvesting of grain, that is, removing only the ear. The operational principles behind this idea include: (a) the inaccessibility of mountainous areas by conventional harvesters, due to excessive bulk, risks of excessive losses at the cutting bar, the straw cleaning system and the storage tank even in self-levelling machines; the need to (b) limit biomass pickup, to simplify the logistics and the transit on slopes; (c) manage frequent situations of bedded crops; (d) limit the use of labor in harvesting, possibly avoiding the need to manually handle individual sheaves (e.g. reaper-binders); e) the ambition to mechanize harvesting operations on extreme slopes, even above 100%. Based on these requirements, the developed prototype, to be seen in Fig. 4 coupled



Fig. 4 The tractor Geier TLY-85 with stripper header

to the tractor, comprises the following working parts: 1) harvesting header, which in turn includes: (a) “nose” for approaching the crop, (b) rotor with eight rows of “stripper” combs for the removal of apical ears/inflorescences; (c) adduction auger; (d) protection and containment casing; (2) loading system (bucket lifting device, hooked to a rotating chain); (3) collection tank, made of metal sheet and hydraulically tipping for unloading operations; (4) coupling and transmission organs.

2.3 Post-Harvest Facility

Post-harvest operations concern the treatment of the grain and its storage until milling. They require a whole set of machines, including: 1) a fixed-point thresher for separating the grain from the ears and chaff; 2) a cleaning system for dehulling the coarser parts covering the caryopses of some crops (such as spelt); 3) a continuous-belt dryer, with a heat exchanger heating system, for low-temperature operation (preferably $<45^{\circ}\text{C}$); 4) three vertical silos, dedicated to long-term storage of the product and equipped with an aeration system to ensure optimal sanitary conditions.

One of the conditions of the project Brotweg was to set up the entire system inside the old/traditional structures of the existing barn, so as to: i) leave nothing exposed outside the building so as not to alter the pre-existing architectural features, as well as to avoid a negative impact on the landscape; ii) share the interior spaces with the farm’s hay storage and related machinery (a crane with mobile arm suspended from the ceiling). The design arranged the system on three wooden floors, as shown in Fig. 5, seamlessly joining all components (Fig. 6). The harvested material is delivered to the upper floor, where the thresher and cleaning system are housed; all subsequent movements are set up facilitating paths by gravity, through a system of

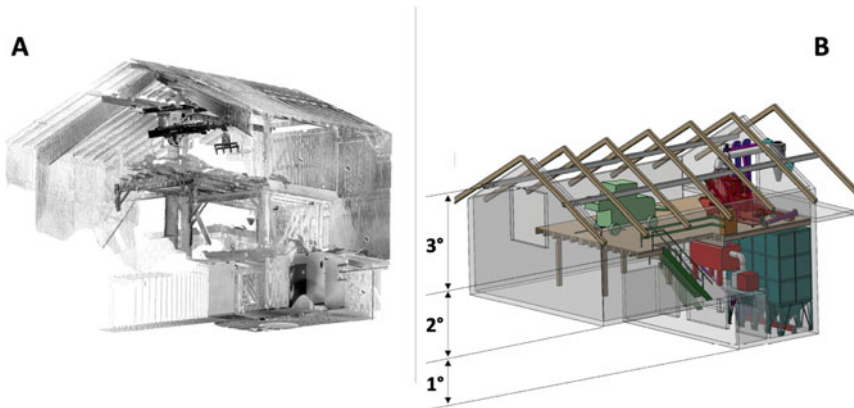


Fig. 5 Before proceeding to the design of the post-harvest line, the interior spaces of the available barn were scanned to ensure an accurate allocation of all components (A). A structure with the plant line spread over three floors was finally designed (B)

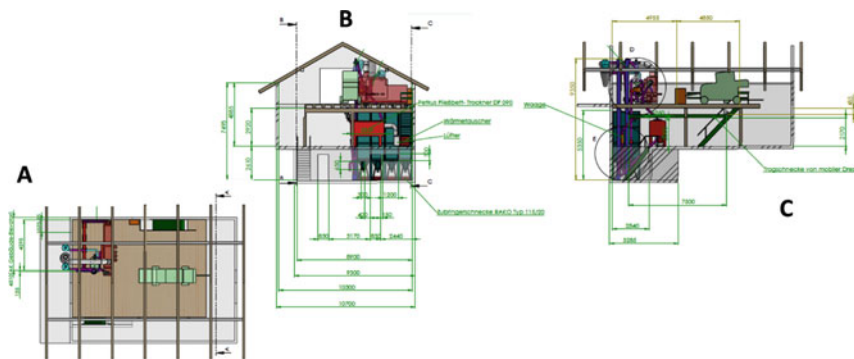


Fig. 6. Construction details (with sections) of the post-harvest barn: map (A), front view (B), side view (C)

trapdoors and ducting that keep all components connected to each other allowing quick reconfiguration of the operation sequences if needed (e.g. kilning of already clean grain, recovery of cleaned grain for storage elsewhere, etc.).

3 Results

During the experimental field trials, conducted in two production seasons 2020 and 2021, the performance of the developed/assembled devices was verified. The field tests envisioned: the measurement of several parameters (1) working times and paths, by a GNSS datalogger with 1 s resolution, installed on the tractor, (2)

fuel consumption, (3) pre-harvest productivity, with direct sampling of biomass (then split into weeds, straw and grain) on sample areoles; (4) crop monitoring via drone multispectral surveys, for the analysis of the status of the biomass present; (5) sampling of stripper header losses and unharvested product, during harvesting operations. The measurements in (1) and (2) are obviously common to the tests at both planting/herbiculture and harvesting stages. The results obtained are overall more than satisfactory, considering the followings.

- (a) For the seed drill, the best performance—in terms of germination efficiency and final yields—was obtained by associating the operation with a prior minimum tillage operation by a simple rotary harrow. This, in fact, allows better control over the herbaceous vegetation present (typically consisting of forage/grazing grasses), which is potentially harmful both in the vegetative phase and during harvesting due to flooding phenomena that risk increasing grain losses in the final fixed-point threshing phase. A possible future evolution of the seeder, therefore, could foresee the combination of arrowing and seeding in a unique implement.
- (b) In terms of theoretical productivity (pre-harvest grain) there were the expected reductions in yields, although with values not always dramatically lower—except for particularly extreme conditions—than those found in intensive lowland crops; the greatest reductions were observed on barley and spelt (with 2.22 and 2.35 t/ha of grain, respectively, equal to reductions of 70 and 51%), while on oats and rye the differences were even less marked (with 3.20 and 4.13 t/ha of grain, respectively, equal to reductions of 27 and 32%). Most critical situations were observed on the most sloping and uneven soils, with variabilities highlighted through drone monitoring, thanks to which a negative correlation between yield reduction and relevance of areas with lodged product could also be observed.
- (c) Header losses varied from 7 to 25%, with the highest values still corresponding to harvest under particularly critical conditions (lodging, relevant infestation of pre-existing grasses). Less problematic were the losses due to non-harvesting (always less than 6%); as a reference, the overall losses observed in the plains with conventional machines varied from 6 to 12%.
- (d) At operational level, field efficiency indices (i.e., the incidence of actual work time on total operational time) averaged 70%, 43%, and 35% for harrowing, seeding, and harvesting operations, respectively. Here the need for no-till return always affects, with times between 20 and 40% of the total, depending on the slope. In case of harvesting, moreover, hopper unloading times at field edges affect 45% of the time; operational working capacities range between 0.10 and 0.15 ha/h;.
- (e) Fuel consumption was always high on average, varying from 62 *l/ha* in harrowing to 98 *l/ha* in harvesting; this depends on many factors, but especially on slopes and field lengths, taking into account that cable traction—necessary and indispensable on steep mountain terrains—always requires a no-till return maneuver, with related consequences on time and consumption.

All the experimental results, together with the technical-operational performance also noted on the remaining parts of the processing chain (post-harvest and bread-making), finally allowed comparative evaluations to be conducted between possible alternative supply chains, while simultaneously taking into consideration a multiplicity of aspects through the methodology of multicriteria analysis [8]. In detail, evaluations compared the cereal-bread supply chain with the following alternative supply chains: a) forage-cow cheese; b) forage-goat cheese; and c) cereal-beer. For the comparative scenarios, ad hoc surveys were conducted based on direct interviews, literature references, and modeling approaches. All scenarios referred to the same production context, which was assimilated to the reality of the Taser Alm (farmstead at altitudes around 1200–1300 m; individual plots <1 ha; average fragmentation of plots; slopes between 20 and 70%). The assessments were conducted by involving 7 decision makers (including entrepreneurs) with different decision-making profiles. Accordingly, the supply chains that received a higher level of approval were those based on cereal cultivation, with a slight preference in favor of the “bread” supply chain due to its lower investment and operational loads compared to the beer supply chain. Livestock supply chains are seen as the best solution only by assigning great weight to the risk of crop loss due to weather/climate adversity. Weather shocks may cause significant loss of production, a risk that is particularly high in cereal cultivation in mountainous areas.

4 Conclusions

The starting hypothesis of radical innovations to enable mechanized cereal cultivation in mountain areas was confirmed. The data that could be collected thanks to the technologies developed in the project showed that new models of mountain agriculture, complementary to the currently prevailing zootechnical production, are viable.

The cereal supply chain—although with objective limitations—proves to be a viable alternative model for improving agricultural sustainability and adding value to agricultural livelihoods even in the most critical mountainous areas.

References

1. Bätzing, W.: *Die Alpen. Das Verschwinden einer Kulturlandschaft*. Darmstadt: Wissenschaftliche Buchgesellschaft/Theiss-Verlag, Darmstadt (2021)
2. Mann, S.: *The Future of Mountain Agriculture*. Springer, Heidelberg (2013)
3. Pramsohler, M., Peratoner, G.: *Südtiroler Getreideanbau im Regiokorn-Projekt*, Bolzano (2021). https://brotweg.projects.unibz.it/?page_id=497
4. Franco, W., Barbera, F., Bartolucci, L., Felizia, T., Focanti, F.: Developing intermediate machines for high-land agriculture. *Dev. Eng.* **5**, 100050–100050 (2020). <https://doi.org/10.1016/J.DEVENG.2020.100050>

5. ARGE RoKPOb: Mini combine harvester (2020). <https://www.sortengarten.ch/arge-rokpob/>
6. Cavalchini, A.G., Rognoni, G.L., Tangorra, F.M., Costa, A.: Experimental tests on winter cereal: sod seeding compared to minimum tillage and traditional plowing. *J. Agric. Eng.* **44**(2s) (2013). <https://doi.org/10.4081/jae.2013.s2.e79>
7. Klinner, W.E., Neale, M.A., Arnold, R.E., Geikie, A.A., Hobson, R.N.: A new concept in combine harvester headers. *J. Agric. Eng. Res.* **38**(1), 37–45 (1987). [https://doi.org/10.1016/0021-8634\(87\)90137-5](https://doi.org/10.1016/0021-8634(87)90137-5)
8. Sacco, P.: Il Progetto Brotweg: valutazioni integrate di filiera e benefici attesi, Bolzano (2021). https://brotweg.projects.unibz.it/?page_id=497

Energy Valorization of Fruit Shells and Stones Deriving from the Food Industry



Alessio Mencarelli , Raffaele Cavalli , Gina Marano, Marco Povolo, and Rosa Greco 

Abstract Shells and stones are the main residues deriving from nuts and fresh fruit processing, representing a cost for food industries due to their disposal. This study investigated the main physical and chemical characteristics of twenty fruit shells and stones deriving from Italian food companies, for their use for energy purposes in biomass boilers. For each sample the moisture content, heating value, ash content, bulk density, ash fusibility and analysis of micro and macro elements were determined. Low ash contents (<1.5%) and high higher heating values (19.5–23.6 MJ/kg) and bulk density (>270 kg/m³st) were found. The latter two are higher than forest wood chips. Low concentrations of S and Cl were detected, avoiding the risk of emissions corrosive agents emissions. Walnut shells and peach stones have N concentrations greater than 1.0%, causing possible risks of air pollutants release. High values of Na, K and P were found in the biomasses, increasing the ash fusibility. Shells have low melting points (<900 °C) while the fruit stones have higher values (>1100 °C). Overall, fruit shells and stones have suitable characteristics for being used for energy purposes. It would be advisable to use them in medium-large size power plants due to the presence of low melting ash and the possible risk of NO_x emissions. The combine use of shells and stones with woody biomass, such as wood chips, could guarantee a reduction of the problem of ash fusibility and at the same time fill the lack of material that could occur during the year.

Keywords Fruit shells · Fruit stones · Bioenergy · Ash fusibility · By-products · Food industry

A. Mencarelli · R. Cavalli · G. Marano · M. Povolo · R. Greco (✉)
Department of Land, Environment, Agriculture and Forestry, University of Padova, Legnaro (PD), Italy

e-mail: rosa.greco@unipd.it

A. Mencarelli

e-mail: alessio.mencarelli@unipd.it

R. Cavalli

e-mail: raffaele.cavalli@unipd.it

1 Introduction

Italy is one of the major European producers and importers of nuts, stone fruit and dried fruit [1, 2]. The fruit is distributed and sold in large-scale distribution or used in the agro-food industry to produce jams, marmalade, juices and fruit syrups. In the food industry, for the realization of these products, the fruit is subjected to a series of processes, producing large amounts of waste and by-products. Shells and stones are in many cases an additional cost for food companies due to their disposal. However, considering their composition, low cost and ease of supply, they could be valorized for energy production [3], obtaining both environmental and economic benefits. Few studies have investigated the combustion properties of fruit shells and stones [3, 4]. Before being used, it is necessary to assess if their characteristics are suitable for energy production. The aim of this work was to investigate the main physical and chemical characteristics of fruit shells and stones of different varieties and origins deriving from Italian industries. This in order to use the shells and stones in medium-scale plants present in the food industries for the production of thermal and electric energy. For twenty samples the moisture content, the ash content, the heating value, the bulk density, the ash fusibility, the analysis of micro and macro elements were determined.

2 Material and Methods

2.1 Samples

A total of twenty samples of fruit stones and shells, provided directly by Italian companies in the agro-food industry, were analyzed. The samples were grouped into two groups, respectively fruit shells and fruit stones (Table 1). Each sample was different in terms of fruit variety and origin.

Table 1 Type of fruit and region of production of the analyzed fruit shells and stones

Biomass	Fruits	Samples number	Samples ID	Regions of production
Shells	Almond	3	AL01, AL02, AL03	Sicily, Campania
	Hazelnut	9	HN01, HN02, HN03, HN04, HN05, HN06, HN07, HN08, HN09	Campania, Lazio, Piedmont
	Walnut	2	WN01, WN02	Veneto
	Pistachio	2	PN01, PN02	Sicily
Stones	Peach	1	PC01	Emilia-Romagna
	Apricot	3	AP01, AP02, AP03	Emilia-Romagna

Table 2 Physical analyses conducted and relative reference standards

Parameter	Unit of measurement	Reference standard
Moisture content	% in mass as received	EN ISO 18134-1:2015 [6]
Ash content	% in dry mass	EN ISO 18122:2016 [7]
Higher heating value on dry basis (HHV ₀)	MJ/kg	EN ISO 18125:2018 [8]
Lower heating value as received (LHV _{as})	MJ/kg	EN ISO 18125:2018 [8]
Bulk density	kg/m ³ st as received	EN ISO 17828:2015 [9]
Ash fusibility	°C	EN ISO 21404:2020 [10]

2.2 Physical Analysis

Table 2 shows the physical analyses conducted (EN ISO 17225-1:2021 standard [5]).

2.3 Ultimate Analysis and Determination of Major and Minor Elements

The determination of Sulfur (S) and Chlorine (Cl) was conducted according to the EN ISO 16994:2016 standard [11]. Cl was determined using ion chromatography (IC). S was detected through the analytical technique of inductively coupled plasma optical emission spectrometry (ICP-OES). This technique was also used for the analysis of the major elements and minor elements, in accordance with the respective standards, the EN ISO 16967:2015 [12] and EN ISO 16968:2015 [13]. For the determination of Carbon (C), Hydrogen (H) and Nitrogen (N) an Elementar® Vario MICRO Cube analyzer was used (EN ISO 16948:2015 standard [14]). Equation (1) was used for calculating the oxygen percentage.

$$O(\%) = 100 - C_d(\%) - H_d(\%) - N_d(\%) - S_d(\%) - A_d(\%) \quad (1)$$

where Cd is the carbon percentage, Hd is the hydrogen percentage, Nd is the nitrogen percentage, Sd is sulfur percentage and As the ash content. All element concentrations were expressed in dry basis.

2.4 Statistical Analysis

The data collected from the physical analyses were statistically analyzed using a one-way analysis of variance (ANOVA), with a 95% confidence level. Using Tukey's honestly significant difference (HSD) test, the groups with no statistically significant differences were identified. The software used were Statgraphics® Centurion 19 and Microsoft® Excel.

3 Results and Discussion

3.1 Physical Analyses

Table 3 shows the results of the physical tests conducted. The ash content, representing the solid residue resulting from the combustion, causes management problems to the power plants and decreases the heating value of the material [15]. The values observed are included in a range between 0.5% and 2.0%. As regard the fruit shells, walnut (1.6%), almond (1.3%) and hazelnut (1.3%) have values higher than 1.0% while pistachio shells (0.7%) lower than this threshold. The values obtained are slightly higher than what observed by Gorshkov et. al [16]. The differences could be do to the use of different fruit varieties. Peach (0.6%) and apricot (0.9%) stones have lower values than shells. Regarding the heating value,

HHV0 varies between 19.5–23.6 MJ/kg while LHVas between 16.3–19.6 MJ/kg. The highest heating values, both in terms of HHV0 and LHV0, were found in walnut shells (23.5 MJ/kg and 19.6 MJ/kg) and in peach stones (23.6 MJ/kg and 19.6 MJ/kg). The lowest values were found in pistachio shells (19.5 MJ/kg and 16.4 MJ/kg). Overall, the heating values of shells and stones were similar to the heating values of forest woodchips (HHV0 = 19–20 MJ/Kg, LHVas = 15–16 MJ/kg) [17]. The fruit stones tend to have slightly higher values than shells. This could be link to the higher concentrations of oil, included unsaturated fatty acids [18]. Fruit stones also have higher bulk density values than shells. In the latter, the lowest values were found in walnut shells (270 kg/m³st). This is due to the conformation of the shells which, in addition to having a low weight, have numerous empty spaces lowering the bulk density. Shredding the material could reduce the voids, improving its space occupation. Increasing the bulk density, benefits will be obtained in terms of energy density and reduction of transport and storage costs of the material. On the contrary, peach (460 kg/m³st) and apricot (500 kg/m³st) stones have the highest bulk density. The bulk density of shells and stones is higher than wood chips (150–250 kg/m³st) [17]. Overall, having characteristics similar to wood chips, fruit shells and stones have good physical characteristics to be used for the energy production in medium-sized plants (35–500 kW).

Table 3. Physical characteristics of fruit shells and fruit stones

Samples ID	Ash (%)	HHV ₀ (MJ/kg)	LHV ₀ (MJ/kg)	Bulk density (kg/m ³ st)
AL01	1.7 g	20.1 b	16.9 b, c	410 i
AL02	0.8 b, c	20.1 b	17.0 b, c	450 l
AL03	1.5 g	20.8 c	16.7 b	340 g
HN01	1.2 e, f	21.5 f	17.5 f	330 d, e, f
HN02	1.3 f	21.5 e, f	17.5 f	400 h, i
HN03	1.3 f	21.1 d, e, f	17.7 g	330 e, f
HN04	1.6 g	21.3 d, e	17.4 f	340 f, g
HN05	1.1 d, e	20.9 c	17.1 d, e	310 c
HN06	1.2 e, f	21.0 c	17.1 d, e	400 h, i
HN07	1.1 e, f	21.5 e,f	17.3 f	400 h
HN08	1.2 f	21.2 d	17.3 f	320 c, d, e, f
HN09	1.3 c, d	21.4 d, e, f	17.3 e, f	320 c, d, e
WN01	2.0 h	23.5 i	19.6 h	270 a
WN02	1.3 e, f	21.9 g	18.8 h	290 b
PN01	0.6 a	19.5 a	16.4 a	330 e, f
PN02	0.9 b	18.2 a	16.3 a	310 c, d
PC01	0.6 a	21.4 d, e, f	17.7 g	460 l, m
AP01	1.3 e, f	22.8 h	19.4 h	500 n
AP02	1.0 b, c	24.3 i	19.6 h	520 o
AP03	0.5 a	20.8 c	16.9 c	470 m

a, b, c, d, e, f, g, h, i, l, m, n, o Values having the same letter are not significantly different (HSD Tukey multiple-range test)

3.2 Ultimate Analysis

Table 4 shows the results of the ultimate analysis. C, H, O represent the elements most present within solid biofuels [19]. The oxidation of the first two elements involves the formation of H₂O and CO₂ and they positively affect the higher heating value while oxygen reduce it [19]. The average C content is 51.5%, ranging from 48.2% to 56.2%. Because fruit stones have C values higher than fruit shells they have slightly higher heating values [20]. Regarding the H content, the range of values observed are included between 5.4% to 7.0%. Oxygen present greater variability, with values ranging from 33.2% to 45.0%, presenting an average value of 41.0%. The percentage of the three elements were similar to the elemental composition of wood [21]. The N content plays a key role in terms of air pollution, involving the release of NO_x, NO and NO₂ [22]. An increase in N concentration in the fuel cause higher NO_x emissions [22]. According to Obernberger [19], a concentration of N greater than 0.6% is linked to emissions problems into the atmosphere. Most of the biomasses analyzed are below this threshold. However, walnut shells (1.4%) and apricot stones

Table 4 Ultimate analysis of fruit shells and stones

Samples ID	C (%)	H (%)	N (%)	O (%)	S (%)	Cl (%)
AL01	49.6	5.7	0.2	42.9	0.01	0.02
AL02	49.9	5.7	0.1	43.6	0.01	0.02
AL03	50.0	5.7	0.1	42.7	0.01	0.02
HN01	51.2	5.6	0.3	41.5	0.02	0.03
HN02	51.4	5.6	0.3	41.3	0.02	0.03
HN03	50.9	5.8	0.5	41.5	0.02	0.02
HN04	51.8	5.5	0.2	40.9	0.02	0.03
HN05	51.4	5.6	0.3	41.6	0.01	0.02
HN06	51.7	5.4	0.4	41.2	0.02	0.03
HN07	51.6	5.6	0.2	41.4	0.02	0.03
HN08	51.6	5.6	0.2	41.4	0.02	0.03
HN09	51.4	5.5	0.2	41.5	0.02	0.03
WN01	53.8	6.3	1.9	35.9	0.04	0.07
WN02	54.2	6.5	0.9	37.1	0.03	0.06
PN01	48.4	5.7	0.1	45.3	0.01	0.01
PN02	48.2	5.7	0.2	45.0	0.01	0.02
PC01	52.7	5.7	0.3	40.7	0.02	0.01
AP01	56.2	7.0	2.2	33.2	0.04	0.01
AP02	53.8	6.2	1.3	37.6	0.03	0.01
AP03	51.0	5.6	0.1	42.9	0.01	0.01

(1.2%) have high nitrogen values, resulting in risks of release of pollutants (NO_x) during their combustion. For this reason, these materials should not be used in small-scale plants where the necessary NO_x abatement systems are often lacking, due to the high costs, present instead in larger-sized plants [20]. S and Cl are responsible for the formation of fly ashes, SO_x, Cl₂, sulphates and corrosive molecules for the combustion chamber (e.g., HCl) [21]. Corrosion and emissions problems occur when the S and Cl contents are above 0.2% and 0.1% respectively [19]. Both fruit shells and fruit stones analyzed have values lower than this threshold.

3.3 Major and Minor Elements and Ash Fusibility

Table 5 reports the results of the analysis of the major and minor elements and the ash deformation temperature (DT). Only the elements present with concentrations above the detection limit of the instrument was reported. The elemental composition of the biomass influences its behavior during its use causing problems related to the ash fusibility. This can lead to the formation of slag, agglomeration and corrosion inside the combustion chamber of boilers, reducing its heat transfer and efficiency [20, 23, 24]. Their formation is linked to various factors, mainly the combustion temperature and the residence times of the biomass in the chamber [25]. An increase in the

concentration of K, Na, P, Si and Cl causes the ash melting, with consequent greater risks of agglomeration [20, 26, 27]. The ash fusibility tests of fruit shells showed lower fusibility temperature than fruit stones, due to a higher concentration of Cl, K, Na and Si than stones. Except for sample HN03, the ash fusibility temperatures are all below 900 °C. Almond shells have the lowest fusibility values (790°C), followed by walnut (835 °C), hazelnut (820 °C) and pistachio shells (905 °C). Values above 1000 °C were observed for peach (1400 °C) and apricot (1120 °C) stones. Usually, biomass is burned in boilers where temperatures reach values between 800–1000 °C. At these temperatures, the ashes of the shells will melt, causing slagging and corrosion processes inside the combustion chamber reducing the energy efficiency of the plant [24]. The combined use of shells and stones with high quality virgin wood chips (A1 or A2) could help to reduce the onset of these problems, increasing the ash melting point. Traces of heavy metals such as Cu and Zn were found in the biomasses. Their presence determines repercussions on the ash composition quality and in the particulate matter emissions [23]. High concentrations of heavy metals, in particular Zn, could contribute to the formation of low-melting chlorides, increasing the corrosive processes [24]. However, the found concentrations of these metals are low. The maximum Cu value observed is 7 mg/kg while the highest Zn concentration were found in the apricot stones samples (AP01 and AP02).

Table 5. Major and minor elements and ash deformation temperature of fruit shells and stones

Samples ID	Major elements									Minor elements			Ash
	Al	Ca	Fe	K	Mg	Na	P	Si	Ti	Cu	Mn	Zn	DT
	mg/kg	mg/kg	mg/kg	mg/kg	mg/kg	mg/kg	mg/kg	mg/kg	mg/kg	mg/kg	mg/kg	mg/kg	(°C)
AL01	32	1195	71	4123	208	82	173	30	4	3	4	3	780
AL02	0	857	26	2190	110	68	105	14	4	2	2	0	760
AL03	28	1171	45	4705	194	57	206	29	3	3	3	0	830
HN01	68	1481	111	2978	242	0	177	51	2	4	18	2	760
HN02	89	1569	104	3073	256	34	181	59	2	4	19	0	780
HN03	118	1555	136	2760	360	0	276	82	3	4	23	4	1080
HN04	53	1367	57	3099	188	54	114	42	2	4	7	0	810
HN05	0	1194	26	2423	176	33	112	17	0	3	5	0	810
HN06	57	1298	67	2637	215	0	170	46	3	3	17	2	760
HN07	35	1211	43	2528	194	0	144	34	2	3	15	0	790
HN08	48	1328	53	2692	208	0	158	46	2	4	14	4	800
HN09	65	1477	75	2817	231	0	174	59	2	4	18	5	770
WN01	0	1172	32	5216	556	51	893	11	3	7	4	9	730
WN02	0	1686	25	3514	446	26	647	13	0	5	5	7	940
PN01	0	283	26	1922	102	0	90	12	0	1	0	0	900
PN02	0	355	27	2440	124	0	151	12	0	1	0	0	910
PC01	0	336	22	1589	375	0	461	4	4	3	3	4	1400
AP01	0	683	37	2839	676	0	1173	3	2	6	6	18	1260
AP02	0	572	19	2214	547	29	944	5	2	5	4	13	1095
AP03	0	444	25	1089	156	0	159	12	4	3	2	3	1010

4 Conclusions

The results obtained in this work show how fruit shells and stones deriving from the food industry have good qualitative characteristics for being burned in biomass boilers for energy purposes. This would guarantee both environmental benefits and economic advantages for companies, avoiding disposal costs and at the same time producing energy. However, due to the presence of low melting ashes and high N concentrations, which in some materials exceed 1.0%, it would be advisable to use fruit shells and stones in medium-scale plants (35–500 kW), equipped with NO_x abatement systems. The combined use with wood chips would help to reduce the corrosion and slagging problems deriving from the ashes melting by increasing their melting point (>1000 °C). Finally, it is necessary to investigate the real quantity of fruit shells and stones available in companies to feed the boilers. The combined use with wood chips could also reduce the problems related to their scarce availability, particularly in certain periods of the year.

References

1. Eurostat. Agriculture, forestry and fishery statistics - 2020 edition (2020)
2. FAO, Value of Agricultural Production - Apricots, peaches and nectarines. <https://www.fao.org/faostat/en/#data/QV>. Accessed 30 June 2022
3. Chen, P., Cheng, Y., Deng, S., Lin, X., Huang, G., Ruan, R.: Utilization of almond residues. *Int. J. Agric. Biol. Eng.* **3**(4), 1–18 (2010)
4. Bryś, A., Zielińska, J., Głowacki, S., Tulej, W., Bryś, J. Analysis of possibilities of using biomass from cherry and morello cherry stones for energy purposes. In: Jewiarz, 6th International Conference – Renewable Energy Sources, vol. 154, p. 01005 (2020)
5. EN ISO 17225–1:2021 Solid biofuels - Fuel specifications and classes - Part 1: General requirements
6. EN ISO 18134–1:2015 Solid biofuels - Determination of moisture content - Oven dry method - Part 1: Total moisture
7. EN ISO 18122:2015 Solid biofuels - Determination of ash content
8. EN ISO 18125:2017 Solid biofuels - Determination of calorific value
9. EN ISO 17828:2015 Solid biofuels - Determination of bulk density
10. EN ISO 21404:2020 Solid biofuels - Determination of ash melting behaviour
11. EN ISO 16994:2016 Solid biofuels - Determination of total content of sulphur and chlorine
12. EN ISO 16967:2015 Solid biofuels - Determination of major elements. Al, Ca, Fe, Mg, P, K, Si, Na and Ti
13. EN ISO 16968:2015 Solid biofuels - Determination of minor elements
14. EN ISO 16948:2015 Solid biofuels - Determination of total content of carbon, hydrogen and nitrogen
15. Demirbas, A.: Relationships between heating value and lignin, moisture, ash and extractive contents of biomass fuels. *Energy Explor. Exploit.* **20**(1), 105–111 (2002)
16. Gorshkov, A., et al.: Analysis of the physicochemical characteristics of biochar obtained by slow pyrolysis of nut shells in a nitrogen atmosphere. *Energies* **14**(23), 8075 (2021).
17. Hellrigl, B. Elementi di xiloenergetica. (Elements of xyloenergetics), AIEL, Legnaro (Pd) (2006)
18. Kamel, B.S., Kakuda, Y.: Characterization of the seed oil and meal from apricot, cherry, nectarine, peach and plum. *J. Am. Oil Chem. Soc.* **69**(5), 492–494 (1992)

19. Obernberger, I., Brunner, T., Bärthaler, G.: Chemical properties of solid biofuels-significance and impact. *Biomass Bioenerg.* **30**(11), 973–982 (2006)
20. van Loo, S., Koppejan, J.: *The Handbook of Biomass Combustion and Co-firing*. Earthscan (2008)
21. Rowell, R.M., Pettersen, R., Tshabalala, M.A.: Cell Wall Chemistry. In *Handbook of Wood Chemistry and Wood Composites*, 2nd edn., CRC Press (2012)
22. Ozgen, S., Cernuschi, S., Caserini, S. An overview of nitrogen oxides emissions from biomass combustion for domestic heat production. *Renew. Sustain. Energy Rev.* **135**, 110113 (2021)
23. Obernberger, I., Thek, G.: Physical characterisation and chemical composition of densified biomass fuels with regard to their combustion behaviour. *Biomass Bioenerg.* **27**(6), 653–669 (2004)
24. Niu, Y., Tan, H., Hui, S.: Ash-related issues during biomass combustion: Alkali-induced slagging, silicate melt-induced slagging (ash fusion), agglomeration, corrosion, ash utilization, and related countermeasures. *Prog. Energy Combust. Sci.* **52**, 1–61 (2016)
25. Mlonka-Mędrala, Magdziarz, A., Gajek, M., Nowińska, K., Nowak, W.: Alkali metals association in biomass and their impact on ash melting behaviour. *Fuel* **261**, 116421 (2020)
26. Hiltunen, M, Barišić, V., Coda Zabetta, E. Combustion of different types of biomass in CFB boilers. In: *16th European Biomass Conference*, pp. 2–6. Valencia, Spain (2008)
27. Obernberger, I.: Reached developments of biomass combustion technologies and future outlook. In: *17th European Biomass Conference*, pp. 20–37. Hamburg, Germany (2009)

Improving Combine Harvester Management Through CANBUS Data Analyses



Michielan Enrico, Mattetti Michele, and Molari Giovanni

Abstract In a global market, where the prices of agricultural commodities are so volatile and the prices of the inputs increase, farmers and agricultural contractors struggle to obtain at the end of the agricultural season a consolidated profit. The aim of this study is to evaluate the operational efficiency and energy performance of two selected combine harvesters, operating in real-world scenarios. With that knowledge is possible to provide to farmers and contractors information that help them to make operational and economically informed decisions regarding optimal fleet management during harvesting time, in order to reduce the harvesting costs and sustain overall profit. The data for the study was acquired from two New Holland harvester combines, operating in real world condition, during harvesting season 2020. The results show that the harvesters spent about 10% of their time in the idle on-field state, the 2% of their time in the idle on-farm, about 63% of the time on actual harvesting and about 13% of their time on headland turn, the 3% of the time on in-field transport, the 7% of the time for road transport, about 1% of time on unloading and less than 1% of the time on harvesting and unloading contemporarily. The large amount of time spent in the idle state, potentially depend on inadequate work planning, especially the planning of the transport logistics, which forced the combines to halt operation several times. The sum of these forced breaks, inevitably impact the overall cost of harvesting and on the operational capability, and this causes increased harvesting costs and a reduction of the end-of-year revenues for farmers and contractors.

Keywords CANBUS · Task classification · Real-world data · Combine harvester

M. Enrico (✉) · M. Michele · M. Giovanni
Department of Agricultural and Food Sciences, Alma Mater Studiorum, University of Bologna,
Viale G. Fanin 50, 40127 Bologna, Italy
e-mail: enrico.michielan@unibo.it

M. Michele
e-mail: michele.mattetti@unibo.it

M. Giovanni
e-mail: giovanni.molari@unibo.it

1 Introduction

Harvesting is the last and most expensive task in crops growing, and it influences the overall in-field machinery costs for almost 30% [1, 2]. To perform this task, farmers and agricultural contractors use combine harvesters, which represent the highest expenditure on many arable farms [3], for this reason planning their use during harvesting time is crucial. To increase the efficiency of the use of combine harvesters is mandatory to take into account that the purchase price of a new combine harvester has been constantly rising due to the technological advances, inflation, competition among manufacturers, etc. [4]. In the last decades, manufacturers have developed combines with increasing engine thrust [5] and higher capability to clean and reduce the damages to the harvested crops. This was possible also thanks to the advent of electronics especially with the launch of the Controller Area Network (CANBUS) that helps the operators in the workflow management during the critical function. In addition maintenance costs are important because, they contribute from 10 up to 15% of the total costs of agricultural machinery; however this share increases with the age of machinery [6, 7]. These costs are strictly related to the effective working hours of the machine and such correlation helps farmers and agricultural contractors to estimate the right moment to replace a machine. Moreover, the prices of raw materials (i.e., crude oil, methane, etc.) should be considered since their costs change monthly and in turn, they influence the volatility of crop prices and the revenue at the end of the agricultural seasons [8]. Under this scenario, seems that nowadays is not easy for farmers and agricultural contractors obtain at the end of the season good revenues because there are many costs to consider during the planning process. If agricultural manager may forget to consider one of these costs, revenues reduction or losses will occur. The aim of the study is to recognize each different activities performed by the combine harvesters, in order to be able to identify the most time-consuming activities. This aim is carried out by analysing the CANBUS data of two combine harvesters to compute the harvesting efficiency.

2 Materials and Methods

For the purpose of this analysis, a search was undertaken among farms and agricultural contractors that doing business in the Bologna's Province and with the requirements of using combine harvesters equipped with the CANBUS network. In this study the choice fell on an agricultural contractor that managed almost 1000 ha, this company owns two CR 7.90 New Holland combine harvester (CNH Industrial N.V., Amsterdam, NL) whose specifications are reported in Table 1. These combine harvesters were in use between June and October 2020 by different operators with more than twenty years of experience. On the two combines was mounted a stand-alone data-loggers optimized by CNH Industrial. The CANBUS data-logger

is equipped of two CANBUS channels, and of a GNSS receiver, with no differential correction and a claimed accuracy of 2.5 m to monitor the position. These data loggers were set to automatically acquire all CANBUS messages whenever the combine engine was turned on, so as not to interfere with the harvesting procedure and not to require any operator training phase for their use.

For the purpose of this study, only the signals used for the analysis are reported:

- Engine Reference Torque: that reports the torque as a percent of Engine Reference Torque, and it is denoted as T_{er} .
- Actual Engine Percent Torque: that reports the torque as a percent of T_{er} and it is denoted as T_{ae} .
- Nominal Friction-Percent Torque: that reports the frictional and thermodynamic loss of the engine itself, pumping torque loss and the losses of fuel, oil and cooling pumps as a percent of T_{er} , and it is denoted as T_{nf} .
- Engine Speed: that reports the revolution speed of the engine crankshaft, and it is denoted as n_e .
- Engine Fuel Rate: that reports the fuel consumption of the engine, and it is denoted as \dot{F}_r .
- Header Down: that reports the position of the combine header it is a logical signal and is 0 when the header is up and 1 when the header is down. It is denoted as Hdr_{Dn} .
- Crop Flow: that reports the amount of crops harvested by the combine per unit of time expressed in $L h^{-1}$, and it is denoted as C_f .
- Unload Engine Auger: that reports if the auger's engine status, it was 0 when it was turn off and it was 1 when it was turn on, and it is denoted as U_{EA} .
- Navigation Bases Vehicle Speed: that reports the speed of the vehicle expressed in $km h^{-1}$, and it is denoted as V .
- Compass Bearing: that reports the direction of the movement of the vehicle expressed in deg, and it is denoted as C_b .

For data analysis, the MATLAB R2022a programming environment (The Math-Works Inc., Natick, Massachusetts, USA) was used. All the signals acquired were resampled at 10 Hz. The data analysis was divided into three tasks:

- Autonomous task identification
- Autonomous harvested field identification
- Combine harvester's parameters analysis

2.1 Autonomous Task Identification

The way to identify the different tasks, in which the combine harvesters are involved during harvesting season, it was to set precise rules based on the perfect knowledge of what appends inside the combine during harvesting. First, the data were classified due to the position in three different categories by using the information provided by the GNSS receiver:

Table 1 Specifications of the combine harvesters used in this study

Maximum engine power	(kW)	338
Engine displacement	(cm ³)	8700
Number of cylinders	(–)	4
Engine emissions	(–)	4B
Weight	kg	18,000
Cutting bar width	(m)	7.62
Reel diameter	(m)	1.07

- **Farm**, anytime the combine harvesters were inside the boundary of any farm unit.
- **Road**, anytime the combine harvesters were closed than 3 m to any section of the roads.
- **Field**, anytime the combine harvesters were inside the boundary of any field.

To allow the classification of the combine's position, three shapefiles containing the road network and boundaries of field plots, and the boundaries of the farm units were created. To generate the first three shapefiles, data were downloaded from the website of the Emilia Romagna's region geoportal [9]. The combine harvesters operating states were classified into five categories: idle, transport, work, unload and work during unload. The idling condition occurred when the combines were standing, and the n_e was at 900–1000 rpm and no other operation were made like i.e. unloading, threshing, etc.. The transport condition was defined when V was greater than 0 km h^{-1} and the combine was not harvesting, i.e., C_f was 0 g s^{-1} ; while the work condition was defined when the header was lowered, C_f was greater than 0 g s^{-1} and V was between 0 and 7 km h^{-1} . Rules used for the unload condition was defined as the state where the combines was unloading the tank, the threshing system was turned off, V was 0 km h^{-1} and the header was up. The work during unload condition was defined when the combines were in the work and unload condition at the same time.

The operating status of the combines were classified according to a combination of combines position and operating activity (Table 2).

2.2 Autonomous Harvested Field Identification

This task was performed by using the data that comes from the embedded GNSS receiver in the data-logger. The GNSS data were firstly cleaned with the Savitzky-Golay filtering formula by using the MATLAB function "sgolayfilt". As reported by Heiß et al. [10] to perform this task, it has been chosen to set a polynomial order of the filter to 1 because it fit the chronological sequence of the recorded track, and a frame length with a value of 25 was considered to give a smoothing that represent the track. After filtering the GNSS data, expressed in latitude and longitude coordinates, converted in Cartesian coordinates by using the MATLAB function

Table 2 Rules used for the identification of the operative states of combine harvesters

Operating status	Combine position	Boolean operator	Classified combine harvester operating activity
Idle on farm	Farm	AND	Idle
Idle on field	NOT(Road)	AND	Idle
Transport on road	Road	AND	Moving
Transport on field	NOT(Road)	AND	Moving
Harvesting	Field	AND	Header down, Crop Flow > 0
Unload	Field	AND	Engine auger ON, Stop, Header up
Unload work	Field	AND	Engine auger ON, Moving, Header down

“lonlat2local” and were selected only the coordinates where the combines were in harvesting activities. The coordinates obtained were clustered by using the MATLAB function “dbscan”, the choice fell on this function because, it allows to perform a density-based spatial clustering of the GNSS data by setting the neighborhood search radius and the minimum number of points per each cluster. To perform this task these parameters were set respectively at 19 and at 9. The results of dbscan clustering were compared with those found through a visual inspection by using the free program QGIS [11].

2.3 Combine Harvester’s Parameters Analysis

Thanks to the autonomous harvested field identification, it was possible to analyse the combine harvester’s parameters like for i.e., the harvested area, the time spent by the combine harvester during harvesting, the total yield and the yield per hectare per each field identified. For the purposes of calculate the harvesting area and the perimeter, after the clustering of the fields, the MATLAB function “alphaShape” was used to create a MATLAB object containing all the 2D surfaces created with the GNSS points of each cluster. From this object were calculated, the area (A_f) and the perimeter (P_f) of each field harvested by the combines, by using the MATLAB function “Area” and “Perimeter” respectively. Instead to calculate the time spent by the combine in the harvesting task the time was summed. The crop harvested per each field (C_f) was calculated as in Eq. 1:

$$C_t = \int_{t_1}^{t_2} C_f dt \tag{1}$$

where t_1 and t_2 the starting and finishing time per each harvested field. While the yield per each field was calculated as in Eq. 2:

$$C_y = \frac{C_t}{A_f} \quad (2)$$

3 Results and Discussion

3.1 *Autonomous Task Identification*

The two combine harvesters have worked respectively for approximately 92 and almost 211 h per a total of 303 h during the 2020 harvesting season. The combines have spent 63% of time in harvesting, 12% of time in idle activities and respectively 10% on field and 2% on farm, 13% of time in headland turn, 10% of time in transport, 1% in unload activities. As stated by Hunt and Wilson [12], the amount of time spent in on work activities is around 60–70%. The idle activities occurred at farm and on field:

- **On farm:** mostly occurred at the beginning of the harvesting season for each harvested crops, for planned or unplanned maintenance;
- **On field:** occurred more often than the other, mostly for driver turn over, attached/detached of the cutting bar, failures, etc.

Headlands turns contributed for the 14% of the entire harvesting activity, this parameter is higher than the idle on field because it is strictly related to the shape of the field and it can change also in the field due to the fact that could be some obstacles on field that requires more attention by the operator.

3.2 *Autonomous Harvested Field Identification*

In this case study the fields harvested by the two combines were 54, they were visually identified by using the free suite QGIS (Fig. 1), and the number of fields identified by the clustering algorithm were 39, this introduces a percentage difference of 27% compared with the total number of the fields recognized with QGIS. The errors in the clustering operations occur especially in field very close one to each other, because the distance of the GNSS points of one field and the GNSS points of another is very low. By the way if the distance between two fields is around 6 m this misclassification did not happened (Fig. 2).

Fig. 1 Field identification by using QGIS

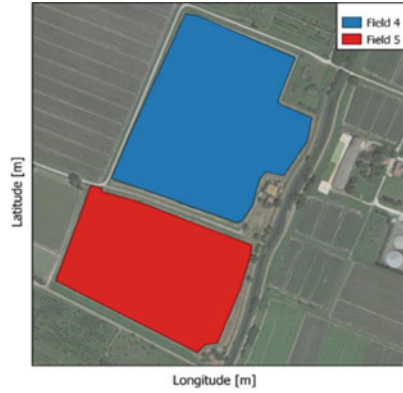
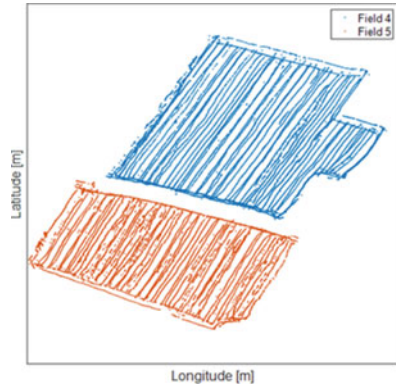


Fig. 2 Field identification by using MATLAB



3.3 *Combine Harvester's Parameters Analysis*

The field and the tasks identification have allowed to obtain information about the operational parameters of the combines such as harvested area, duration of the harvesting for each field, the total yield for each field and the crop yield. The mean area of the harvested fields is around 8.60 ha, this parameter is a slightly greater than the national average (i.e., 8.40 ha) calculated from the Italian Institute of National Statistics [13]. The 41% and 43% of the harvested fields show an area less than 6 ha and 12 ha, less than 10% of the fields have an area between 12 and 18 ha, less than the 2% and the 3% of the field have respectively an area between 18 and 24 ha and between 24 and 30 ha and only the 2% present an area between 32 and 38 ha.

4 Conclusions

Obtaining information about the usage of combine harvesters in real world conditions and monitoring their operational parameters are not easy since most of the farmers and agricultural contractors rely on handwritten logbook data. This trend probably in few years will change thanks to the European Program called Farm2Fork, that helps European farmers to reduce the input and the GHG emissions required for the food production and at the same time increase food safety and traceability. Thanks also to the presented data acquisition systems, CANBUS data was easily collected and georeferenced through the GNSS receiver permitting to estimate the operational states of combines. Thus, a synthetic view on the usage of the combines in real world conditions during harvesting season could be obtained. Thanks to the information provided by the model, a large part of the data required by national governmental organizations can be obtained and then sent to comply with regulatory obligations, or alternatively it can be provided to the agronomist or the client who managing the farm in order to give them a more complete picture of the farm situation. In addition the proposed methodology should help researchers to easily have access to a large amount of data and perform better analysis on combine harvesters. This analysis wants to open up to further development of the proposed algorithm in order to be able to find new solutions to increase the efficiency of these so relevant agricultural machinery.

References

1. de Toro, A., Gunnarsson, C., Lundin, G., Jonsson, N.: Cereal harvesting – strategies and costs under variable weather conditions. *Biosyst. Eng.* **111**, 429–439 (2012). <https://doi.org/10.1016/j.biosystemseng.2012.01.010>
2. Sørensen, C.: Workability and machinery sizing for combine harvesting. *Agric. Eng. Int. CIGR E-J.* (2003)
3. Phillips, P.R., O’Callaghan, J.R. Cereal harvesting - a mathematical model. *J. Agric.Eng. Res.* **19**(4), 415–433 (1974)
4. Mimra, M., Kavka, M.: Risk analysis regarding a minimum annual utilization of combine harvesters in agricultural companies. 469.4Kb (2017). <https://doi.org/10.15159/AR.17.022>.
5. Hilliard, S.B.: The dynamics of power: recent trends in mechanization on the American farm. *Technol. Cult.* **13**, 1–24 (1972). <https://doi.org/10.2307/3102653>
6. Calcante, A., Fontanini, L., Mazzetto, F.: Repair and maintenance costs of 4WD tractors and self propelled combine harvesters in Italy. *J. Agric. Eng.* **44** (2013). <https://doi.org/10.4081/jae.2013.312>.
7. Lips, M., Burose, F.: Repair and maintenance costs for agricultural machines. *Int. J. Agric. Manag.* **1**, 7 (2012)
8. Huchet-Bourdon, M.: *Agricultural Commodity Price Volatility: An Overview*. OECD, Paris (2011)
9. Dati Preconfezionati. <https://geoportale.regione.emilia-romagna.it/download/dati-e-prodotti-cartografici-preconfezionati/pianificazione-e-catasto/uso-del-suolo/2017-coperture-vettoriali-uso-del-suolo-di-dettaglio-edizione-2020/dati-preconfezionati>. Accessed 9 Oct 2022

10. Heiß, A., Paraforos, D., Griepentrog, H.: Determination of cultivated area, field boundary and overlapping for a plowing operation using ISO 11783 communication and D-GNSS position data. *Agriculture* **9**, 38 (2019). <https://doi.org/10.3390/agriculture9020038>
11. QGIS, D.T.: QGIS Geographic Information System
12. Hunt, D., Wilson, D.: *Farm Power and Machinery Management: Eleventh Edition*; Waveland Press (2015). ISBN 978-1-4786-3177-4
13. Censimento Istat: meno aziende agricole, ma più grandi e sempre familiari Available online: <https://www.cia.it/news/notizie/censimento-istat-meno-aziende-agricole-ma-piu-grandi-e-sempre-familiari/>. Accessed 10 Jan 2023

Hazelnut Harvesting Machines: Recent Advances and New Trends



Danilo Monarca, Riccardo Alemanno, Gianmarco Rigon, and Pierluigi Rossi

Abstract In the last decade, world hazelnut production has increased by about 25%. Italy is the world's second largest hazelnut producer after Turkey, the total area invested in our country is just over 92,000 hectares, marking an increase of over 20,000 hectares in the last ten years. The coriliculture production remains very concentrated, with 80% of the invested area located in only three regions, Piemonte (29%), Lazio (28%) and Campania (24%) and 19% in four regions, including Sicilia. There is, however, an important growth phenomenon also in other regions: among these, Toscana and Veneto stand out.

In order to meet a growing demand from the market, the development of newer harvesting machines in the hazelnut sector became mandatory. Italy is one of the principal producers of hazelnut harvesting machinery. The need to adapt to different production areas and conditions has resulted in a large market which currently offers diversified solutions for any business, both inside and outside the country. The leading companies in the hazelnut harvesting mechanization sector have been therefore identified and their main products have been examined.

The purpose of the paper is to describe the innovations and technological advances implemented on these machines in recent years. All these improvements mainly aimed to increase their productivity and to improve safety and comfort for the operators.

Consequently, a taxonomy of the systems adopted for the hazelnut harvesting operations is presented, differentiated according to the type of machines used (tractor mounted mechanical harvesters, trailed vacuum harvesters, self-propelled vacuum and mechanical harvesters). The research also aims to present early applications of agriculture 4.0 technologies in hazelnut mechanized harvesting, with a specific focus on possible applications of precision agriculture technologies.

Keywords Agricultural machinery · Hazelnut · Harvester · Agriculture 4.0

D. Monarca · R. Alemanno · G. Rigon (✉) · P. Rossi
DAFNE Department, Tuscia University, Viterbo, Italy
e-mail: gianmarco.rigon@unitus.it

1 Introduction

1.1 *Hazelnut Production and Development of Coriliculture*

According to FAO data, world production of in-shell hazelnuts was around 1.1 million tonnes in 2020. Worldwide, in 2010–11, production was in fact around 800 thousand tonnes, so the current value shows a growth of more than 37%. If we consider data from the last two years available, in order to mitigate fluctuations in production values, Turkey is the first producer, with around 720 thousand tonnes of in-shell hazelnuts. Italy is the second largest producer, with about 120 thousand tonnes, and accounts for 11% of the total production.

If we analyze the Italian production situation, between 2010 and 2021, the total area under hazelnut cultivation in Italy increased from 70,000 to 92,000 hectares, with an overall increase of 28%.

The rapid development of the Italian hazelnut sector is related to the growing demand for the product from the processing industry, in particular the confectionery one.

An important characteristic of the hazelnut production potential is its concentration for 96% in four regions: Piemonte (29%), Lazio (28%), Campania (24%), and Sicilia (15%). There is, however, an important growth phenomenon also in other regions: among these, Tuscany and Veneto stand out.

On a provincial level, the top four provinces cover 68% of the national total: Viterbo (26%), Cuneo (18%), Messina (14%) and Avellino (10%).

1.2 *Main Manufacturers in Italy*

To meet the growing demand for hazelnuts in the market, the need to develop new harvesting machines has been mandatory. Italy is the main producer of harvesting machines.

Therefore, the leading companies in the hazelnut harvest mechanization sector have been identified and their main products listed in Table 1, have been examined. It should be noted that the best-known manufacturers are located where the production is more concentrated in Italy.

In fact, in Lazio, precisely in the province of Viterbo, where the Monti Cimini production area is located, we find companies like FACMA, GF Costruzioni, SAMAC, Giampi and Souto, while in Piemonte, in the province of Cuneo, we find Monchiero and Chianchia.

Table 1 Main harvesters produced by Italian companies

	Mechanical		Vacuum	
	Mounted/pulled	Self-propelled	Mounted/pulled	Self-propelled
FACMA Lazio Viterbo	Mek 1800	Semek 1000	Cimina 120 T	Cimina 180S
	Mek 1600		Cimina 200 T	Cimina 200S
			Cimina 300 T	Cimina 300S
			Cimina 380 T	Cimina 380S
GF Lazio Viterbo	Jolly 1500	Super Jolly Conveyor belt		
	Jolly 1800	Super Jolly Corvello		
	Jolly 2500			
	Jolly 2800			
GIAMPI Lazio Viterbo	Star 1600	Futura 100	Star 111	
	Star 1800		Star 211	
	Star 2000		Star 311	
	Star super + 1400			
	Star super + 1800			
SAMAC Lazio Viterbo		S1/100		
		S2/70		
SOUTO Lazio Viterbo	Supernova			
MONCHIERO Piemonte Cuneo		2075		
		2095		
		20,115		
		20,125		
		20,145		
		20,240		
CHIANCHIA Piemonte Cuneo	K1800		EU 1000	
			EU 2000	
			KF-501	
			KF-601	

2 Hazelut Harvesters

Currently, harvesters can be equipped with autonomous propulsion system (self-propelled), or rely their functioning on a tractor (pulled, mounted). A further classification can be made by considering the physical principle of picking the product up from the ground: some harvesters use a fan to vacuum up the product from the ground (vacuum harvesters), while others mechanically pick up the product from the ground

by means of rotating devices (mechanical harvesters). Combining the listed categories, we obtain the commercial solutions available today: pulled and self-propelled vacuum harvesters, mounted and self-propelled mechanical harvesters.

In the following paragraphs, the two types of self-propelled machines, both vacuum and mechanical, will be analyzed.

These harvesters allow to drastically increase the harvesting capacity and simplify the harvesting process, reducing the amount of labour.

For these reasons self-propelled machines are becoming widespread, and represent the type of machines characterized by a greater technological development.

2.1 *Self-propelled Vacuum Harvesters*

The principle of suctioning the product from the ground allows these machines (Fig. 1) to work on irregular grounds, even on steeper slopes than mechanical harvesters. With optimal working conditions, harvesting times can be reduced to under 2 h/ha. Although the harvesting capacity tends to be lower than mechanical self-propelled machines, a higher degree of cleaning of the harvested product is achieved. To significantly increase this type of performances, a mechanical picker device can be installed frontally on the machine (Fig. 1). The installed power on such machines reaches values up to 55 kW. The operating costs analysis [7], combined with the harvesting performance, make the use of such machines profitable for farms with area of more than 15 ha.

Harvested Product Path. The fruit, lying on the ground, is conveyed towards the harvesting system through counter-rotating brushes made of radial rubber paddles.



Fig. 1 FACMA Cimina 300S self-propelled vacuum harvester, with RM210 and driver's cab

Using a centrifugal fan, hazelnuts are sucked in a flexible duct and conveyed into the vacuum chamber. At the bottom of this chamber a dosing valve seals and gradually discharges the heavier material (hazelnuts, stones and twigs). At the valve outlet, an airflow, generated by a tangential fan, allows the lighter waste material to be expelled (leaves and empty shells). The product is conveyed though an auger into the double rotating sieve. The latter is a rotary screen, consisting of more coaxial cylinders made of perforated sheet metal, which by means of a sheet metal helix conveys the fruit in an axial direction and separates it from the remaining coarser and finer waste material, like dirt, stones and woods. Finally, the product is pneumatically conveyed by a second centrifugal fan into sacks or, more frequently, pulled trailers. The air, leaving the vacuum chamber, sucked by the first-mentioned fan passes through one or more dust-abatement devices, made of two dust-removing cyclones.

2.2 Mechanical Harvesters

These machines (Fig. 2) are employed on overall flat terrain and, although they typically deliver a less clean harvested product than vacuum harvesters, are characterized by a greater harvesting capacity, that, with optimal working conditions, can be about 1,5 h/ha. Nowadays, these machines have power ratings between 55 and 75 kW. Again, the operating costs, combined with the harvesting performance, make it convenient to use these machines on cultivated areas of more than 15 ha.

Harvested Product Path. The fruit, lying on the ground, is conveyed to the harvesting system by means of counter-rotating rubber brushes or plastic rakes with transverse motion. Subsequently, the product is lifted by blades or rakes fixed on a horizontal rotating shaft. Some machines are equipped, in the harvesting header, with augers and/or rollers, which perform an initial removal of the fine waste material (soil and leaves respectively). The product is then carried on a grid-structured conveyor belt, that elevates it and enables spontaneous removal of finer waste material. Then the falling nuts, unloaded from the belt, are separated from the leaves and lighter



Fig. 2 GF Super Jolly 4 × 4 self-propelled mechanical harvester with driver's cab

impurities (including leaves and empty shells) by a tangential fan. The nuts then fall onto a grid that permits other fine rejects to be removed. Alternatively, there is an auger that transports the product to a rotating sieve, performing another sorting (removing stones, twigs and remaining fine waste material) according to the size of the elements, as described in 2.1. The hazelnuts discharged from the sieve, or falling from the grid, are pushed by blown air, generated by a centrifugal fan, into a duct that conveys them to the bagging device or directly to the trailer pulled by the self-propelled vehicle.

2.3 Construction Features Analysis of Self-propelled Machines

An analysis of technical construction features of the main self-propelled vehicles produced by companies in the province of Viterbo was conducted. The results of this analysis, shown in Table 2, lead to a series of considerations.

The FACMA company produces both vacuum and mechanical self-propelled harvester models, while the other manufacturers only provide mechanical harvester models.

Analyzed self-propelled vehicles have masses ranging from 3000 to 4000 kg and power ratings of 55 or 74 kW.

The overall dimensions of the vehicles analyzed are more developed in length, which can exceed 5 m, while the heights are contained within 2.3 m. Typically the front-end collecting devices ensure harvesting widths of more than 3 m.

The harvesters produced by FACMA and SAMAC have 3-wheel drive with a single steering wheel. The model produced by Giampi, with 4-wheel drive, provides steering capabilities to the 2 rear wheels. In order to reduce the turning radius that a 4-wheel drive system implies, GF allows all 4 wheels to steer, enabling both all-wheel and crab steering thanks to an electro-hydraulic control.

The common practice and the most suitable solution for transmitting motion to the wheels in self-propelled harvesters is to use hydrostatic transmissions. The Jolly and Futura harvesters adopt differential axles, placed after the hydraulic motors. The hydrostatic transmission permits a continuous and precise modulation of working speed in the 0 to 10 km/h range. A gearbox is installed on each harvester after the hydraulic motors, to enable higher road speeds, up to 35 km/h. The Jolly also features a variable-displacement hydraulic motor in order to provide two additional gear ratios.

It can be noted that two different solutions are adopted to rake and gather the product on the ground: a frontal collector device with radial counter-rotating brushes, and a transverse collector device with rakes.

The table also shows, indicatively, the cleaning stages of the harvested fruit that take place inside the harvesters. The devices used for sorting the product include: rollers, augers, fans, conveyor belts, and double rotary screens, called rotating sieves.

Table 2 Technical specifications of main self-propelled harvesters, produced in the province of Viterbo

	FACMA Cimina 300S	FACMA Semek 1000	GF Super Jolly	Giampi Futura 100	SAMAC S1/100
Type	Vacuum	Mechanical	Mechanical	Mechanical	Mechanical
Length [m]	5,9	5,8	4,89	4,46	4,3
Width [m]	1,77	2,3	2,17	2,15	2,3
Height [m]	1,72	2,3	2,17	1,52	1,8
Working length [m]	2,5–3,5	3–3,7	2,7–3,7	2,2–5	3
Mass [kg]	3100	3800	2900	3200	3800
Engine	Deuz	Deuz	Kubota	Kubota	Iveco
Power [kW]	55	55	74	55	74
Drive	3WD	3WD	4WD	4WD	3WD
Steering wheels	1	1	4	2	1
Transmission	Hydraulic	Hydraulic	Hydraulic	Hydraulic	Hydraulic
			Front axle	Rear axle	
			Rear axle		
N. of speeds	2	2	4	2	2
Type of raking	Brushes	Brushes	Brushes	Rakes	Rakes
Cleaning stages	Grid and Augers	Augers	Rollers	Conveyor belt	Conveyor belt
	Dust removing cyclon	Conveyor belt	Augers	Ventilation	Ventilation
	Ventilation	Ventilation	Conveyor belt	Grid	Grid
	Rotating sieve	Rotating sieve	Ventilation		
			Rotating sieve		
Max speed [km/h]	8–30	10–30	36	8–35	8–25
Harvesting capacity [h/ha]	1 ÷ 3	0,8 ÷ 2	0,8 ÷ 2	0,8 ÷ 2	0,8 ÷ 2
Driver's cab	Yes	Yes	Yes	No	Yes
Agriculture 4.0	Yes	Yes	Yes	No	No

Listed in the table we see also the typical harvesting capacities of vacuum and mechanical harvesters, which data are extrapolated from recent studies [3] in accordance with the statements of farmers and manufacturers. It is important to emphasize that the harvesting speeds and efficiency depend on several factors: the soil conditions, in terms of irregularity and slope, moisture and vegetative state, the user's driving skills, the density of the crop on the ground, and hence the crop's productive capacity.

3 Latest Innovations and Recent Developments

3.1 Performance Improvements

Among the innovations affecting the productivity and efficiency of harvesting machines, the RM210 mechanical picker, installed on self-propelled vacuum machines, deserves to be mentioned. This is a device driven by a hydraulic motor and chain drive installed on the front of the self-propelled machine, between the brush collection system and the suction pipe.

A shaft equipped with rubber blades, rotating in opposite direction to the wheels, lifts the fruit up from the ground. The brush is housed in a cylindrical wire mesh casing. Fine waste, such as soil, passes through the grid and is then discharged to the ground through an auger from the side of the mechanical picker. The material lifted by the brushes is thrown towards a cylindrical chamber containing two augers with different helix direction, which have the task of driving the fruit towards the centre of the head, where a flexible suction pipe is located.

Compared to the conventional machine, equipped only with rotating brushes, it has been shown that the prototype is able to reduce the airborne dust generated by the harvester [6].

This device also makes possible to achieve higher harvesting speeds during the process and then substantially raise the harvesting capacity of the self-propelled vacuum machine to values compatible with mechanical ones.

The last obvious advantage is the improved cleanliness of the harvested product, thanks to the addition of the sorting processes that the picker provides. This therefore preserves the other parts of the harvester from wear and tear.

3.2 Improvements of Safety and Comfort

The increasing importance of safety in agricultural activities has characterizing this sector both from the equipment manufacturers' and from users' points of view since the use of tractors is recognized as the main cause of fatalities. In fact, tractor overturn associated with the absence or the improper use of the roll-over protective structure

(ROPS) represents the main cause of this phenomenon [4]. With reference to the Italian context, the obligation to install ROPS on agricultural and forestry tractors entered into force on January 1st 1974 for new tractors; then, in 1981 the obligation was extended to all tractors, including those put on the market before 1974.

The task of the ROPS is to protect the operator from the vehicle overturning by providing the driver with access to a suitable living space. In this case, the reference standard refers to this safety volume as clearance zone [2].

The same function of safety and protection of the driver from the hazards associated with overturning agricultural vehicles is nowadays performed by modern driver's cabs (Fig. 3), which have also found widespread use on self-propelled nut harvesters.

Driving cabs also insulate the driver from external agents, whether atmospheric or of a different nature, and they especially reduce the risk of exposure to airborne dusts generated during the harvesting process.

The concentration of such dusts can reach values between about 8 mg/m³ and about 21.5 mg/m³, depending on the types of machinery used and the condition of the soil [5]. These values are well above the TLV-TWA defined by the ACGIH.

In addition, the driver's cab significantly mitigates the noise to which the driver is subjected during harvesting operations. A study has shown that, in the presence of the most common harvesting machines, the sound pressure levels detected near the ear of workers often exceed 90 dB(A) [5].

Fig. 3 External and internal view of the FACMA Cimina 300S new driver's cab



As a final benefit, cabin air conditioning provides optimal thermal comfort conditions for the driver.

3.3 Deployment of Electronics and Agriculture 4.0

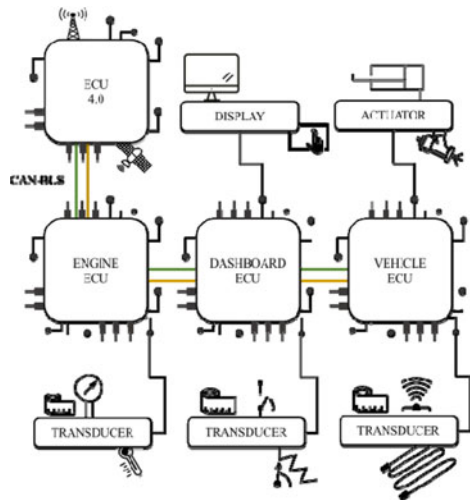
Speaking of innovations that go beyond the concept of Agriculture 4.0, which are however related to the spread of electronic equipment in agricultural vehicles, self-propelled hazelnut harvesters are now equipped with tools and devices to support the user both in driving and harvesting operations.

For instance, it is now common practice to install cameras on different locations of the vehicle. Some cameras permit to extend the peripheral view of the vehicle. Other cameras, mounted near the rotating sieve or near other cleaning sorting devices, allow to monitor the correct functioning of the machine and the state of cleanliness of the harvested product. Finally, it is possible to mount cameras that, having a view of harvester area, keep track of fruits left on the ground and thus of harvesting efficiency.

Among the electronic technologies of Agriculture 4.0 used in agricultural machinery today, it is worth mentioning: GNSS or GPS satellite navigation systems, data processing technologies such as ECUs, transducers and measurement sensors, assisted, semi-automatic and automatic guidance systems, CAN-BUS technologies with ISOBUS communication protocol, telemetry and wireless communication systems, communication and data processing technologies based on big data, IoT.

Some of these technologies are now also being applied on board hazelnut harvesters. Figure 4 schematizes the main devices that constitute data acquisition systems of these self-propelled vehicles.

Fig. 4 Data acquisition system scheme of a hazelnut self-propelled harvester



This data acquisition system now makes it possible to remotely control the self-propelled harvesters in several aspects: position, routes, worked areas, remote diagnostics, warning indicators, engine hours, switching on and off and other operating parameters.

4 Future Developments and Conclusions

Although the machines have achieved excellent performances, in terms of efficiency, productivity and ease of use, it can be said that the sector of mechanization in coriliculture is still undergoing strong development.

Among the aspects and systems of harvesting machines that are likely to undergo changes and improvements in the years to come are data acquisition systems for precision farming and agriculture 4.0.

First of all, remote monitoring systems need to be improved enabling the control in further aspects such as power, fuel consumption, emissions, and the operating parameters of all machine devices out of the engine, such as working speed and efficiency of sorting processes.

Production mapping systems need to be introduced on hazelnut harvesters, to determine the harvesting performance of the machines and the production yields of hazelnut orchards.

What is most important, however, is an adequate data processing system and user-friendly devices that can translate the Big Data collected by machinery into accessible and easy-to-interpret information for the farmer, which can support him in agronomic decisions and crop monitoring.

References

1. Casa, R.: *Agricoltura di precisione*. Edagricole Ed (2016)
2. Rigon, G.: *Progettazione e verifica di una cabina per semovente agricola*, Università di Modena e Reggio Emilia, Tesi Magistrale in Ingegneria Mechanical (2021)
3. Assettati, L.: *Recenti evoluzioni nella meccanizzazione della raccolta del nocciolo*, Università degli studi della Tuscia, Tesi Triennale in Scienze Agrarie e Ambientali (2020)
4. Davide, G., Daniele, P., Leonardo, V., Fagnoli, M., Lombardi, M.: *Retrofitting Agricultural Tractors with Aftermarket Weather Cabins: Safety Issues for Manufacturers and Users* (2021)
5. Monarca, D., Cecchini, M., Guerrieri, M., Santi, M., Bedini, R., Colantoni, A.: *Safety and health of workers: exposure to dust, noise and vibrations*. In: VII International Congress on Hazelnut, pp. 437–442 (2008)
6. Pagano, M., et al.: *Dust emissions with a new hazelnut mechanical harvesting prototype*. In: Proceedings of International Conference Ragusa SHWA Safety Health and Welfare in Agriculture Agro-food and Forestry Systems, Lodi, Italy, pp. 8–11 (2015)
7. Franco, S., Monarca, D.: *Technical and economic aspects of hazelnut mechanical harvesting*. In: V International Congress on Hazelnut 556, pp. 445–452 (2000)

CANBUS Data for Site-Specific Tractor Performance Analysis and Prediction



Danilo Monarca, Riccardo Alemanno, Pierluigi Rossi, Gianmarco Rigon, Leonardo Bianchini, and Massimo Cecchini

Abstract Tractors' working performances can be affected by many environmental variables such as terrain slope, ambient temperature, terrain conditions. Such aspects interact with other performance parameters which are determined by agricultural activities, like power take-offs (PTOs) utilization, torque, and drive system. Since these parameters can be used to define the type of activities carried out on the field, determine machinery efficiency, and can also be employed to define machinery impact on operating costs and business outcomes, understanding the relationship among them can be a reliable source of information for performance analyses and fleet management systems (FMS).

This paper provides a solution for tractor performance analysis based on real-time machinery data that can be collected from tractors' CANBUS and on external data sources such GPS and Digital Elevation Models (DEM) which help to better define the operating conditions of every activity that is being carried out in a vineyard during an entire year.

The result of data analysis generated a dataset containing information that allowed, with the use of clustering and machine-learning algorithms, to understand which agricultural activities have been carried out for the entire yearly dataset. From that point, comparisons could thus be made on tractor's field capacity, fuel consumptions, torque at different moments on the same field, or at the same external conditions on close fields. Such information can be of great help for farming businesses, allowing finer cost analyses and the definition of the most suitable working set-ups for their agricultural machinery based on site-specific environmental and soil conditions.

Keywords Big data · Artificial intelligence · Machine learning · Agriculture

D. Monarca · R. Alemanno · P. Rossi (✉) · G. Rigon · L. Bianchini · M. Cecchini
DAFNE Department, Tuscia University, Viterbo, Italy
e-mail: pierlugi.rossi@unitus.it

© The Author(s), under exclusive license to Springer Nature Switzerland AG 2023
V. Ferro et al. (eds.), *AIIA 2022: Biosystems Engineering Towards the Green Deal*,
Lecture Notes in Civil Engineering 337,
https://doi.org/10.1007/978-3-031-30329-6_79

775

1 Introduction

Modern tractors often gather lots of useful data during agricultural activities and they elaborate it to provide information to the driver: for instance, onboard sensors can keep track of parameters such as wheel speed, torque, utilization of power take-offs (PTOs), temperature (ambient, coolant, oil) and expected fuel consumption. These data are used to let the driver understand how the tractor and its equipment are working and notify any possible anomaly if present. Their goal, although, ends there while the information could be further useful for a better farm fleet management. There consequently is the need to store such sensor data and eventually combine them with other external data coming from sensors or from any other available sources in order to generate proper information to the users and farming businesses: environmental and soil information, tractor's GPS position, elevation of the GPS coordinates, terrain slope and many other data collected on field through sensors or obtained from monitoring systems and can help farmers to keep track of important parameters such as actual fuel consumption and exact field capacity; it could also be possible to determine if the vehicles are undersized or oversized for the requested activities, or to develop a preventive maintenance system based on engine parameters.

The goal of this paper is thus to show how it can be possible to exploit available data to analyze tractor performance through artificial intelligence [1], specifically Random Forest machine learning algorithms and similar [2, 3], and transform it into valuable information about the vehicle itself, the specific characteristics of equipment under every condition and help farming business to determine whether agricultural vehicles are good enough for their needs. The fulfillment of those purposes might also lead to better quantification of operating costs, emissions and provide a good basis for preventive maintenance tools and monitoring systems on tractors [4].

2 Materials and Methods

2.1 Context and Data Availability

The study involved 6 orchard tractors with 75 kW of engine power and 408 Nm maximum torque, that have performed every activity that is required in a 1-year time span (01 May 2021- 30 April 2022) in a vineyard in Tuscany, Italy. Such vehicles have been enhanced with a real-time data monitoring system which added GPS information and provided internet connection to upload CANBUS data to a fleet management server. Machinery data regarding engine performance and vehicle itself like speed, temperatures and PTO has been collected from tractors right as they carry out their daily activities by intervals of one minute, gathering up to 60 entries per working hour. Such dataset relies only on CANBUS information from tractor's electronic control unit (ECU) which report data from various on-board sensors (wheel speed, temperatures, etc.) and engine parameters (PTO speed, engine speed, oil and coolant

Table 1 Data gathered from tractor and from external sources

Data source	Data type	Variable
Engine	Real-time	Relative Engine Torque (%), Actual Engine Torque (%), engine speed (rpm), fuel consumption (L/h)
Onboard sensors	Real-time	GPS coordinates, date and time, temperatures, PTO speed
External sensors	Big data	Digital Elevation Model (DEM)

temperatures, torque, etc.). A list of valuable data that can be stored and uploaded to the server from tractors is shown in Table 1, as well as the dataset that can be acquired from external sources, such as the Digital Elevation Model (DEM) provided by the European Union’s Earth Observation Programme called “Copernicus” which allowed to integrate existing datasets with additional information.

2.2 Data Processing

Data from Table 1 need to be elaborated and joined together to provide more precise information and help to determine vital information regarding the activity type, terrain conditions and tractor performance parameters. A flow-chart has been defined to identify what can be obtained from existing real-time data and other big data available from remote sensing, earth monitoring and other sources. As a result, activity types performed on the vineyard can be predicted and consequently tractor and equipment performances can be evaluated, as shown in Fig. 1.

The processed data defined in the central blocks (2nd column) of Fig. 1 are shown in detail in Table 2, in which dependencies from Table 1 and unit measures are

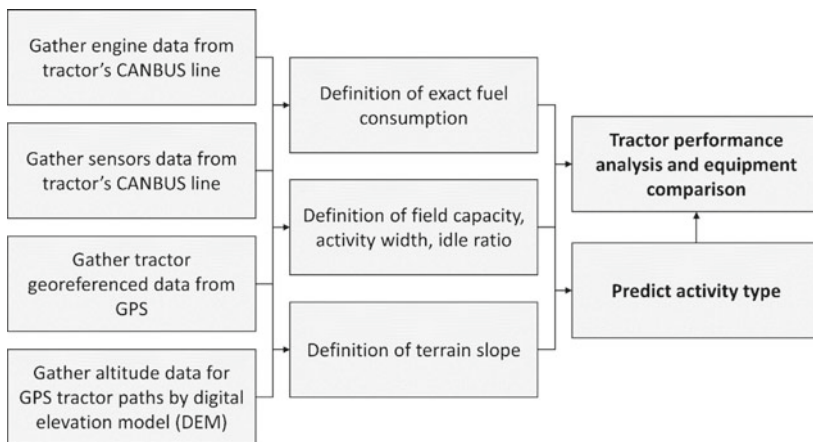


Fig. 1 Flow chart of the data processing

Table 2 Post-elaboration data and information

Information	Data dependency	Elaborated data
Engine performance	Slope, Fuel tank gap	Exact fuel consumption (L/h)
Terrain characteristics	DEM big-data, GPS data	Altitude (m), slope (%), travelled distance (m), tractor path, area (ha)
Activity performance	Elapsed time, travelled distance, covered area, tractor path	Overall idle time (%), work width (m), field capacity (ha/h)
Activity identification	Date, time, field ID, travelled distance, PTO speed, work width, field capacity	Type of activity, activity statistics

Table 3 Dataset details

Dataset type	Columns	Rows
Tractor no. 1	25	42.525
Tractor no. 2	25	17.693
Tractor no. 3	25	55.978
Tractor no. 4	25	60.418
Tractor no. 5	25	49.562
Tractor no. 6	25	64.714
Operations logbook	26	4.006

reported. These variables have been utterly subdivided into different group to highlight the type of information that they can provide; authors have hence identified information categories regarding tractor engine performance, terrain characteristics, activity identification and activity performance (Table 3).

The information generated by post-elaboration data shown in Table 2 helps to understand how machines are working and define the type of activity they carried out in a specific time and day. Having such kind of information, it could be possible to understand their operating costs and assess if they're ineffective, fit or overqualified to carry specific tasks that could be better performed by other tractors or equipment.

2.3 Data Cluster Analysis

Post-processed data, together with data collected from CANBUS, generated 6 dataset containing available and post-processed data for each tractor, covering an entire year of activities in the vineyard starting from the 1st of May 2021 and ending the 30th of April 2022. Every row of the datasets indicates an operation that has been carried out for a minute, values from the tractors must be considered as instantaneous and not averages over the minute-long period. A total of 290.890 rows have been collected, hence indicating 4848 h of tractor hours; 25 variables have been stored for every row, totaling 7.272.250 values. It must be said that some of the rows report a repetition

of the same GPS coordinates and no speed, indicating that the involved tractor was idle. To further investigate those data and provide additional information regarding the specific field in which they have been carried out and a summary of the operation, authors merged the tractor-specific datasets into a single dataset, summarized it and generated a newer and smaller dataset in which every row is associated with one specific activity carried out by one of the six tractors in a specific period of the year, for a total of 4006 operations. Short activities, such as those that lasted less than 10 min, as well as abnormal values (like activities carried outside of the vineyard's borders) have been discarded since they would be of no interest for the purpose of this research. That dataset has then been utterly filtered to make the dataset suitable for machine-learning algorithms.

The "operations logbook" dataset, being a summary of every activity performed in the vineyard, can be considered as a meaningful source of analysis to predict the type of activity that could be associated with every row. A preliminary evaluation procedure involved cluster analysis, with the aim of understanding the entropy of the dataset: to do so, a k-means supervised algorithm has been implemented and tuned to define 7 clusters as the 7 main activities that have been identified on the yearly operations carried out in the vineyard, namely: grass management, treatments, pruning, green pruning, harvesting, suckering, and tilling.

Figure 2 shows the resulting plot from k-means clustering with $k = 7$ clusters, which is the number of the different kinds of vineyard's activities. It is evident that cluster 2 overlaps with several other clusters (almost entirely with cluster 5, then partially cluster 6, cluster 3 and 4), showing that such hypothetical and yet unknown activity can be easily mistaken for up to 4 different activities. Such condition shows why artificial intelligence cannot be easily implemented to solve agronomic problems since the datasets must first be processed in order to eliminate possible sources of misunderstanding: this can be done by precise evaluation by experts that can discriminate activities simply by looking at additional information that is not ready to use in the dataset or by determining domains (seasons, weather conditions, soil conditions, etc.) in which an activity can be carried out or not.

This procedure is highly recommended since the dataset must be prepared and filtered in order to diminish its complexity and variability: for instance, certain operations can be carried out only during specific seasons and there would be no reason for any algorithm to check the entire dataset for assessing any row that is not referred to the month of September for vineyard harvesting, since it is the only month in which such activity happens in Tuscany. As a result, if the identification of harvesting activities could be identified as they are by date, the number of unknown clusters would diminish to 6.

3 Results

Given the nature of the starting dataset and the presence of two overlapping clusters, information has been further improved by changing date format to percentage over

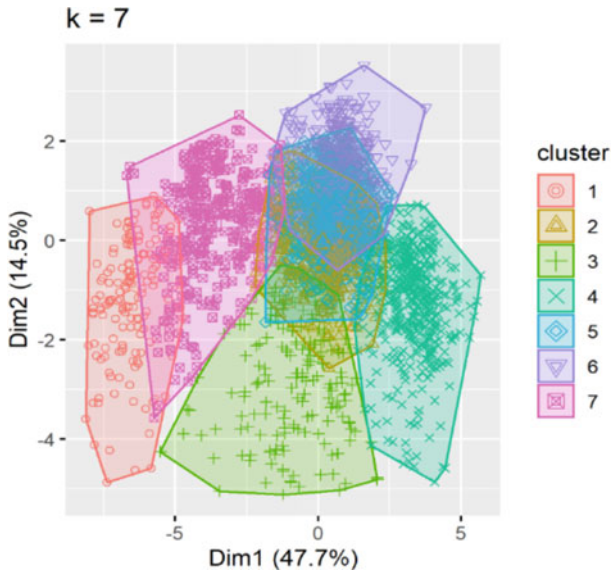


Fig. 2 K-means clustering for the operations' dataset given $k = 7$ clusters

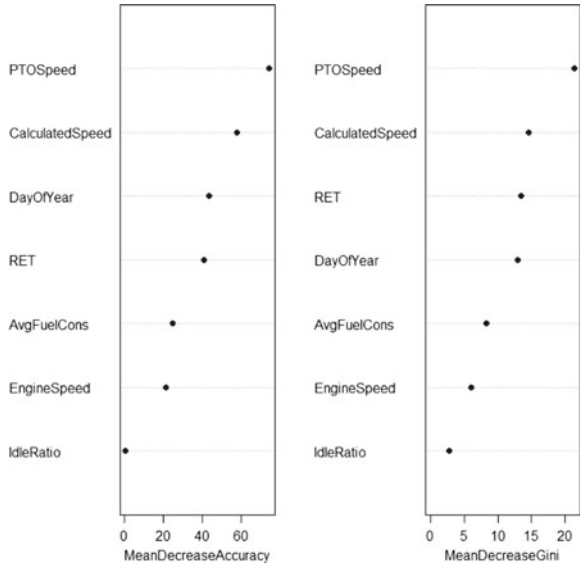
365 days in a year (i.e., July 1st would be showed as 0,5 while December 31st would be 0.999). To provide better classification, the dataset has been reduced to information concerning only one of the 40 fields included in it (approx. 140 rows) which have been labelled manually by experts: this way, every row would have its expected classification of activity (label) and a supervised machine-learning (ML) algorithm could be used, like Random Forests (RF) [5, 6]. Activity labels have been summarized as follows:

- Fertilization (Label 1);
- Phytosanitary treatments (Label 2);
- Soil Tillage – pruning shredder (Label 3);
- Soil Tillage – inter-row (Label 4);
- Soil Tillage – disc harrow or chisel (Label 5);
- Pruners (Label 6);
- Grape harvester (Label 7);
- Trailer for grape transportation (Label 8).

The dataset has been passed to the RF algorithm made of 1000 trees and 3 variables taken each time (out of 8 columns I the dataset). This fine tuning allowed to perform a fast training over 70% of the rows, leaving the remaining 30% as test dataset to verify the predictive algorithm. As a result, an Out Of Bag (OOB) estimate of error rate of 15.62% has been achieved and an importance plot of the variables has been generated.

In a Random Forest Algorithm, values such as Mean Decrease Accuracy and Mean Decrease Gini's impurity measures show the importance of the dataset's features for

Fig. 3 Importance of variables in the dataset



label classification, and higher results represent a higher importance of a specific variable inside the dataset. These parameters can hence be used to understand which “features” in the dataset are the most responsible for final label classification, given the higher gain of information during the process.

Given the previously stated meaning of Mean Decrease Gini and Mean Decrease Accuracy, data shown in Fig. 3 proves how Power Take Off Speed (PTOSpeed), Speed calculated over GPS data (CalculatedSpeed), season (DayOfYear) and Relative Engine Torque (RET) has been the most important variables in the dataset.

Despite it could be predictably reasonable to consider such parameters as the most characteristics parameters to classify a vineyard’s mechanised activities, the degree of importance adds up extra information regarding their weights in the algorithm. Having saved part of the dataset as testing ground, predictions have been therefore performed on it to verify the reliability of the predictive algorithm. Such information is shown in the following Table 4, in which the known activities from the test dataset and the predicted activities according to the Random Forest algorithm are listed and highlighted to indicate right predictions (green) and wrong predictions (red).

Table 4 represents the activities (rows) and their classifications (columns). Only 2 out of 43 rows in the test dataset have been mis-predicted by the activity classifier algorithm (4,65% error rate), which are shown in red. Other predictions, highlighted in green and by their number in the test dataset, have been proven right.

Table 4 Activity classifier algorithm, test dataset results. Wrong predictions in red background)

Activity / Prediction	F	P.T.	S.T.S.	S.T.I.	S.T.D.	P	G.H.	T
Fertilization (F)	2							
Phytosanitary tr. (P.T.)		7						
Soil tillage shedder (S.T.S.)			4			2		
Soil tillage interrow (S.T.I.)				7				
Soil tillage disk (S.T.D.)					8			
Pruners (P)						7		
Grape harvester (G.H.)							5	
Trailer (T)								1

4 Conclusions

Given a prediction efficiency of 95,35% the authors agree that the algorithm can be considered as a valuable tool to monitor vineyard activities through CANBUS data and big data, allowing to generate farming businesses' logbook and, consequently, to better predict operating costs and machinery performances according to every single activity. The perspectives of such a promising result can also include further studies for the estimation environmental impacts and provide interoperability for Life Cycle Assessments (LCA).

References

1. Ceja, E.G.: Behavior Analysis with Machine Learning Using R (1st ed.). Chapman and Hall/CRC (2021). <https://doi.org/10.1201/9781003203469>
2. Breiman, L.: Random forests. *Mach. Learn.* **45**(1), 5–32 (2001). <https://doi.org/10.1023/A:1010933404324>
3. Elith, J., Leathwick, J.R., Hastie, T.: A working guide to boosted regression trees. *J. Anim. Ecol.* **77**(4), 802–813 (2008). <https://doi.org/10.1111/j.1365-2656.2008.01390.x>
4. Cecchini, M., Piccioni, F., Ferri, S., Coltrinari, G., Bianchini, L., Colantoni, A.: Preliminary investigation on systems for the preventive diagnosis of faults of agricultural operating machines. *Sensors* **21**, 1547 (2021). <https://doi.org/10.3390/s21041547>
5. Fernández-Delgado, M., Cernadas, E., Barro, S., Amorim, D.: Do we need hundreds of classifiers to solve real world classification problems. *J. Mach. Learn. Res.* **15**, 3133–3181 (2014)
6. Zhou, Z.-H.: Ensemble methods: foundations and algorithms. *Ensemble Methods Found. Algorithms* 1–218 (2012). <https://doi.org/10.1201/b12207>

A Deep Learning Artichoke Plants Identification Approach for Site-Specific UAV Spraying



Jacopo Motta, Alberto Sassu, Alessandro Deidda, Luca Ghiani, Alberto Carlevaro, Giovanni Garibotto, and Filippo Gambella

Abstract Deep Learning techniques combined with Unmanned Aerial Vehicles (UAVs) are leading to significant improvements in agricultural systems practices management for input optimization and environmental impact reduction. The study aims at identifying and georeferencing individual artichoke plants as a first step to develop an on-the-fly UAVs aerial agrochemical spray system and to monitor spatial and temporal crop development. The images were acquired by an UAV RGB sensor within an artichoke field in Sardinia (Italy) in different growing stages during the 2021–2022 season. Each orthophoto was labeled to train a Single Shot Detector (SSD) object detector developed from a Feature Pyramid Network structure capable of identifying artichoke plants inside the field. The experimental results showed a high detection level with an average F1 score of around 0.9. Plants growing index confirmed a stronger process in October, reaching the maximum at the beginning of December. The results highlight how the proposed approach will contribute to execute reliable site-specific real-time UAV spraying distribution, and design prescription maps for a precise identification of critical zones.

Keywords Single shot detector · Multi-target object detection · Multi-temporal tracking · Site-specific management · Precision agriculture

J. Motta · A. Carlevaro · G. Garibotto

Funded Research Department, Aitek SpA, Via Della Crocetta 15, 16122 Genova, Italy

A. Sassu · A. Deidda · L. Ghiani · F. Gambella (✉)

Department of Agricultural Sciences, University of Sassari, Viale Italia 39 a, 07100 Sassari, Italy

e-mail: gambella@uniss.it

A. Carlevaro

DITEN Department, University of Genoa, Via All'Opera Pia, 11a, 16145 Genova, Italy

1 Introduction

Food sustainability and consumer protection are relevant issues today, as shown by the growing consumer interest in how vegetables are produced and distributed on the market [1]. The health concern regards the increasing use of pesticides, applied worldwide to destroy, or control insects and pests and often misapplied with considerable health risks for consumers [2]. Conventional spraying mechanization, deployed by ground machinery, is essential to reduce human and environmental harm and labor intensity, but more effective and efficient application techniques are required to reduce the environmental impact of pesticides [3]. Unmanned Aerial Vehicles (UAVs) have recently gained attention for pesticide spraying operations and they are the best candidates to replace conventional aerial vehicles, despite regulations and restrictions allow aerial agrochemicals spraying only in few countries [4]. The globe artichoke *Cynara cardunculus* L. var. *scolymus* Fiori, also known as Spinoso Sardo, is a Mediterranean native crop diffused in Sardinian Island (Italy) that strongly contributes to the agricultural economy of the country [5]. Artichoke plants are attacked by several insects and pests like which require pesticide application, easily deployable through UAVs.

A fast and real-time approach to optimize UAV spraying operations, reduce the overall operation time, and execute accurate distributions over target plants is required. In this scenario, the Deep Learning (DL) approach represents a valid and effective solution for real-time recognition and the consequent task execution [6]. The Feature Pyramid network used in the present work for the detection of artichoke plants is a particular type of Single Shot Detector (SSD) [7], characterized by working in a single forward pass of the network, locating, and classifying objects at the same time. The basic concept of these networks is the use of a grid that divides the image into cells responsible for detecting objects and the use of priors, predefined boxes responsible for detecting objects of specific sizes and shapes within a grid cell. In the Feature Pyramid networks the main structure of the architecture is composed by a bottom-up pathway for the feature extraction and by a top-down pathway for position detection on the image. The combination of these two phases allows the network to detect objects of different scales with a good level of location precision in rapid training times. Deep learning approaches not only allow plant detection from UAV images but also allow the deployment of multitemporal analysis for crop features analysis. The incorporation of multi-temporal UAV imagery could significantly boost the accuracy and compensate the low spectral resolution of RGB imagery [8]. Such approach could be applied to different crops for plant counting, crop health monitoring, yield estimation, and to plan optimized fertilizer, pesticide, and other input distribution within farm management.

The work aims at developing a deep learning approach for artichoke plant identification intended for real-time spraying applications from UAV and an automatic multitemporal tracking procedure for artichoke plants monitoring.

Table 1 Performance measure of the FPN Detection at each individual date and phenological phase of the test

Date	BBCH ¹	TP	FP	FN	precision	recall	F ₁
7 Sept	14	474	11	72	0.977	0.868	0.919
14 Sept	16	533	22	53	0.960	0.910	0.934
1 Oct	35	541	39	66	0.933	0.891	0.912
15 Oct	47	544	18	57	0.968	0.905	0.936
9 Nov	51	460	32	141	0.935	0.765	0.842
3 Dec	55	450	73	125	0.860	0.783	0.820
23 Dec	59	509	71	95	0.878	0.843	0.860

¹BBCH stages derived by [11]

2 Materials and Methods

2.1 Images Acquisition Campaign and UAV Platform

Experiments took place on a 3000 m² surface Artichoke cultivation. (cv. Spinoso sardo) in Uri, North-west Sardinia, Italy (Long. 8.472029, Lat. 40.623619; WGS84, EPSG 4326) at 125 m above sea level. The surveys were performed following the phenological development of the culture for a total of 7 days (see Table 1). To get the higher resolution possible and reduce the distortion effect flights were performed at 15 m height Above Ground Level (AGL) by a DJI Phantom 4 Pro UAV equipped with RGB CMOS 1” sensor. An RTK GNSS Reach RS + (Emlid) connected to a NTRIP correction system was used to record the geographic coordinates of 12 Ground Control Points (GCPs), for orthomosaics orthorectification and to plants geolocation in the object detection process.

2.2 Deep Learning Plant Detection

In UAV spraying application scenario, characterized by different flight heights, the choice of a network able to detect objects at different scales was crucial. This is the reason why Feature Pyramid networks was implemented for. The organization of the implementation of the object detector were made according to the following subsections.

Data Preprocessing. The image dataset was extracted from seven UAV orthomosaics in the months between September 2021 and February 2022 generated by using OpenDroneMap and used for the network training. After an initial phase of manual labeling performed using the VGG Image Annotator (VIA) software for ground truth estimation, the dataset generation was performed by randomly cropping orthomosaics at different heights and performing data-augmentation. The resulting dataset

was then divided into training, validation and test sets and provided as input to the detection network.

Network Building. The network implementation input parameters regarded the Grid Sizes px^2 (4×4 , 8×8 , 16×16), Priors Size px^2 (1×1), Input Size px^2 (512×512) and Total params (2.8 M), where px refers to 1 pixel size of 0.5 cm. 3.10.5 opencv-python 3.4.11.43, NumPy 1.21.2, SciPy 1.21.2, and matplotlib 3.4.3 were used.

Network Training. The detector was trained on the datasets constructed in the preprocessing phase, dividing them into training and testing sets with a proportion of 70% and 30% respectively. The test set was used to get initial feedback on the network detection performance before applying the model for offline detection. Generally, each dataset was trained for about 72–80 h to obtain satisfactory results. The training inputs were the Loss Function (Boxiness loss + Location loss), IoU (50%), Batch Size (8), Learning Rate ($1e-4$), and Optimizer (Adam).

Network Testing and Performance Evaluation. Before applying the model for offline detection, a test was performed for each training phase to evaluate the network performance and to maximize network's detection capabilities. The 30% of the datasets were used to test the network, extracting the measures of recall, precision and F_1 score that are the usual metrics adopted for the evaluation of a machine learning model.

Offline Detection. The step prior to the future real-time scenario model application is the evaluation of its offline behavior. The quality of detection in the offline phase should be almost the same in the real-time application, since what the network processes are always videos and images, whether they have been collected and stored beforehand or transmitted directly from a camera. In fact, the Nvidia Jetson Nano board was selected, a small and powerful computer for embedded and AI IoT applications, to check the feasibility of running the trained and tested network on it.

2.3 Multi-temporal Analysis

The first step of the multi-temporal approach is a spatial registration of the consecutive pairs of orthomosaics. 12 physical markers were placed on the ground by recording their georeferenced position according to WGS84 (EPSG 4326) geographic projection model. As such, all the centers of gravity of the DL detected boxes can be always remapped in world coordinates with an affine transformation in real-time crop operations. The adopted solution for orthomosaics registration at different recording times is an automatic registration process, based on the information provided by the box-plants detected by the Neural Network process [9]. Such automatic registration is implemented in two following steps:

- search for the overall translation (dx, dy) that maximizes the IoU (Intersection over Union) between the boxes detected in the two consecutive orthomosaics images.
- selection of the boxes with IoU above a predetermined threshold (>50%) and computation of the relative homographic transform between the centers of mass.

The automatic registration allows to perform a spatial prediction between the coordinates of the orthomosaic at time t0 (past) with those at time t1 (next) and vice versa [10]. It represents the basis of the time tracking process, which, in turn, is implemented in 2 phases:

- tracking forward: for each box detected at time t0, the best match is searched (in terms of max IoU) among all the boxes detected at time t1; if an acceptable match is not found (IoU threshold), a new hypothesis (prediction) is generated and added to the list of the boxes available at time t1, thus ensuring the propagation and continuity of the current track.
- tracking backward: when the last available orthomosaics data has been reached, the process is repeated in reverse, generating backward predictions for all the boxes that do not have yet connections with the previous stages of the crop.

The result of this tracking process is a series of complete traces, from the first orthomosaic image recorded, up to the last available, for all the box-plants that have been detected by the Neural Network.

3 Results

3.1 Deep Learning Plant Detection

The evaluation phase of the FPN was conducted testing the network on the portion of the dataset not used for training (Table 1). Table 2 shows performance measures of the FPN network after multi-temporal tracking.

Table 2 Performance measures of the FPN network after multi-temporal tracking

Date	BBCH	TP	FP	FN	precision	recall	F ₁
7 Sept	14	487	146	59	0.769	0.892	0.826
14 Sept	16	531	95	55	0.848	0.906	0.876
1 Oct	35	555	102	52	0.845	0.914	0.878
15 Oct	47	550	82	51	0.870	0.915	0.892
9 Nov	51	517	124	84	0.807	0.860	0.833
3 Dec	55	499	121	76	0.805	0.868	0.835
23 Dec	59	519	106	85	0.830	0.859	0.845

Table 1 shows the performances of the network in the detection of the artichoke plants. TP is the number of the boxes correctly identified by the network, with an overlap measure IoU of more than 50% over the ground truth boxes that were selected during the manual annotation process. FP is the number of boxes detected by the network which do not correspond to ground truth boxes, or the IoU is lower than the 50% threshold. FN is the number of ground truth boxes (in the annotation list) that have been missed by the detection network. Recall (sometimes called sensitivity) is a measure of the detection efficiency of the network to minimize the number of missed objects. Precision is a measure of the network accuracy to achieve the minimum number of detection error. F1-score is the weighted average of Recall and Precision including both false positives and false negatives. In this case the DL SSD network has been designed to achieve the minimum number of detection errors (maximum precision), which adversely affects the detection rate (lower value of recall). Table 2 shows the results after multi-temporal tracking, which are more “balanced”, with a significant improvement of the detection rate (recall), greater than 90% most of the time. Conversely, in a real-time application, on-board of the UAV, to drive the direction of the sprayer towards the actual position of the plants, the best network configuration should exhibit a high recall rate, to minimize the number of missed targets; some additional detection errors (lower precision) will be acceptable in this case.

3.2 Multi-temporal Analysis

The Growing Index showed in Fig. 1a is computed as the ratio between the average size (width and height) of the bounding box of the plants detected at the different times of the experiment. The figure shows the range of variations on a differential scale (between consecutive maps) as well as the cumulative value during time. As we

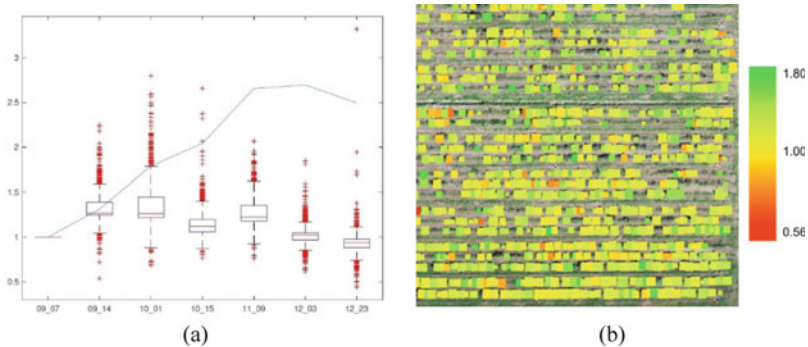


Fig. 1 **a** The evolution of the Growing Index (GI) for the Feature Pyramid network. **b** A detail of the heat-map of the growing index (from Oct. 1st to Oct 15 of the dataset). The color scale (from red to green) shows the range values (from a minimum of 0.55 to a maximum of 1.8)

could expect the growing process is stronger during the month of October, reaching its maximum values at the beginning of December. To address the issue of the uniformity or uneven distribution of the growing rate, it is possible to display a heat-map (Fig. 1b) where the spatial distribution of the growing index value for each tracked plant, is shown (color scale) over the full crop field.

4 Discussion

The obtained dataset results (Table 1 and 2) show that the network performs satisfactorily on artichoke plants detection irrespectively of the date of the test. It is worth reminding that the same trained network was used for the whole experimental season, without any optimization for the individual datasets. This time independence is crucial for an industrial application in precision agriculture scenarios because it can be applied to different scenarios in a small amount of time for different crops. In general, the detection rate (recall) is higher in the early period of the crop (when the plants are smaller and more isolated) and is lower in the late period of the year. This behavior highlights the increasing difficulties to detect and distinguish plants in the last phases due to the mutual overlap of the bigger plants within the rows. A similar trend is also visible for the measure of precision which is over 90% in the early dates. Missing plants tend to decrease during the experimental dates, except on November 09 2021. Different weather conditions, the related diverse illumination condition, and the presence of *Oxalis pes-caprae*, one of the most abundant alien species in artichoke fields during the last days of winter, could have given a higher contrast, helping the detection system to distinguish artichoke plants more easily from weeds or other elements in the latest survey dates.

Significant improvements were obtained thanks to the multi-temporal analysis, with the aggregation of information from all stages of the crop. It was possible to compensate for a possible lack of detection on a certain date, thanks to the availability of new detection data, as well as to manage the partial overlaps of neighboring plants, and correct some evident errors of localization and size. From the availability of the complete temporal traces of each plant it is possible to obtain useful indicators on the evolution of the crop and get a complete history of the evolution of the plant starting from the first observation. This information can be used by expert agronomists to properly plan irrigation and fertilization interventions, improving plant productivity and health. In addition to the overall estimates on the evolution of the crop (vegetative mass, growth indices), averaged over the entire observed field, some detailed spatial maps can also be provided to highlight any anomalies or non-uniformities in the different areas of the field. The automatic process will easily allow the operator to monitor the entire field and evaluate the condition of each plant, specifically for those that show different conditions respect to the rest of the field. Figure 1a reports the trend of the Growing Index as the datasets vary, calculated as the ratio of the average size (width and height) of the plant at different times of the experiment. It is in line

with what might be expected from plant growth, i.e., that the GI tends to decrease as the crop matures.

Once the net is trained to detect a specific crop, intermediate monitoring flights should be performed to check eventual missing plants and plants' growth, adapting flight parameters and the required agrochemical amount to distribute.

Real-time approaches, even if characterized by a preliminary hard and long process of data processing and training, are required to optimize UAV agrochemicals spraying. UAVs application in precision agriculture scenarios relies on the optimization of site-specific input application, path planning and quick results obtainment.

5 Conclusion

The deep learning artichoke plant identification approach based on Feature Pyramid Network showed satisfactory detection performances during the offline phase executed on the Nvidia Jetson Nano board, opening to future UAV real-time agrochemicals spraying applications. The proposed automatic multitemporal analysis allowed significant improvements compensating detection lacks, correcting localization and size estimation errors, and improving detection reliability. It allowed the development of an automatic crop monitoring procedure over the entire season, showing crucial results related to the growing field heterogeneity. It also showed the possibility of developing a UAV path planning procedure for flight optimization, essential for accurate and precise pesticide application and reduce operations' timing and cost. Next steps will regard the Jetson Nano board implementation on the UAV to perform real-time spraying application, giving a significant scope to this work.

References

1. Kriflik, L.S., Yeatman, H.: Food scares and sustainability: a consumer perspective. *Health Risk Soc.* **7**(1), 11–24 (2005). <https://doi.org/10.1080/13698570500042439>
2. Chavarri, M.J., Herrera, A., Arino, A.: Pesticide residues in field-sprayed and processed fruits and vegetables. *J. Sci. Food Agric.* **84**, 1253–1259 (2004). <https://doi.org/10.1002/jsfa.1791>
3. Popp, J., Pető, K., Nagy, J.: Pesticide productivity and food security: a review. *Agron. Sustain. Dev.* **33**, 243–255 (2013). <https://doi.org/10.1007/s13593-012-0105-x>
4. Chen, H.B., Lan, Y.B., Fritz, B.K., Hoffmann, W.C., Liu, S.B.: Review of agricultural spraying technologies for plant protection using unmanned aerial vehicle (UAV). *Int. J. Agric. Biol. Eng.* **14**(1), 38–49 (2021)
5. Spanu., E., Deligios, P.A., Azara, E., Delogu, G., Ledda, L.: Effects of alternative cropping systems on globe artichoke qualitative traits. *J. Sci. Food Agric.* **98**(3), 1079–1087 (2018). <https://doi.org/10.1002/jsfa.8558>
6. Kamilaris, A., Prenafeta-Boldú, X.F.: Deep learning in agriculture: a survey. *Comput. Electron. Agric.* **147**, 70–90 (2018). <https://doi.org/10.1016/j.compag.2018.02.016>

7. Liu, W., Anguelov, D., Erhan, D., Szegedy, C., Reed, S., Fu, C.Y., Berg, A.C.: SSD: single shot multibox detector. *Comput. Vis.* **9905**, 21–37 (2016). https://doi.org/10.1007/978-3-319-46448-0_2
8. Feng, Q., et al.: Multi-temporal unmanned aerial vehicle remote sensing for vegetable mapping using an attention-based recurrent convolutional neural network. *Remote Sens.* **12**, 1668 <https://doi.org/10.3390/rs12101668>
9. Hartley, R.I., Zisserman, A.: *Multiple View Geometry in Computer Vision*, 2nd edn. Cambridge University Press, Cambridge (2004)
10. Kalal, Z., Mikolajczyk, K., Matas, J.: Forward-backward error: automatic detection of tracking failures. In: *Proceedings of the 2010 20th International Conference on Pattern Recognition*, pp. 2756–2759. USA (2010). <https://doi.org/10.1109/ICPR.2010.675>
11. Archontoulis, S.V., Struik, P.C., Vos, J., Danalatos, N.G.: Phenological growth stages of *cynara cardunculus*: codification and description according to the BBCH scale. *Ann. Appl. Biol.* **156**, 253–270 (2010). <https://doi.org/10.1111/j.1744-7348.2009.00384.x>

Forestry Machinery Chain Productivity in Stands Hit by the Vaia Storm: First Results for the Camonica Valley



Luca Nonini and Marco Fiala

Abstract The aim of the work was to compute the working productivity of a forestry machinery chain (FMC) applied for wood recovery in a mountainous stand of *Picea Abies* L. of the Camonica Valley (Lombardy Region, Italy), damaged by the Vaia storm (October 2018). The FMC was made up of the following operations (OP): (OP1) biomass extraction to the landing (“Full-Tree” method using a cable crane with mobile drive station); (OP2) wood positioning (from the landing to the delimiting and sectioning point) and stacking (roundwood and logging residues are separately accumulated) using an earthmoving machine equipped with hydraulic clamp; (OP3) delimiting and sectioning into commercial assortments using a chainsaw. Three field tests (October 2021) were carried out (total time of monitoring: 22 h) to collect data about: (i) duration of working times (h) and (ii) extracted volume of roundwood (m^3) and residues (stacked cubic meters; stcm). The working times were detected according to the Comité International d’Organisation Scientifique du Travail en Agriculture (C.I.O.S.T.A.) definitions, specifically adapted for forestry operations. For each OP, the working productivity was then computed for both roundwood and residues, and expressed as both volume basis ($\text{m}^3 \cdot \text{h}^{-1}$ and $\text{stcm} \cdot \text{h}^{-1}$ for roundwood and residues, respectively) and mass basis ($\text{t} \cdot \text{h}^{-1}$ of fresh matter; $\text{t} \cdot \text{h}^{-1}$ of dry matter). The results of the study can be useful for rationalizing the work and understanding the machinery chains performances under complex and dangerous working conditions, and can be used as a starting point for economic cost quantification.

Keywords Forestry operations · Machinery chain productivity · Salvage logging · Working times

L. Nonini (✉) · M. Fiala

Department of Agricultural and Environmental Sciences. Production, Landscape, Agroenergy (DiSAA), University of Milan, Via G. Celoria 2, 20133 Milan, Italy

e-mail: luca.nonini@unimi.it

M. Fiala

e-mail: marco.fiala@unimi.it

Mountain University (UNIMONT), Via A. Morino 8, 25048 Edolo, BS, Italy

1 Introduction

The role of EU forests in providing ecosystem services can be seriously compromised by natural disturbances, which, in the last decade, considerably increased in terms of frequency, severity and extent (Gardiner et al. 2013; [7]. This made forests even more susceptible to fungi and insect outbreaks attacks. Under these conditions, salvage logging (i.e., the widespread removal of damaged trees from the forest floor as consequence of harmful events) is an essential management practice, as wood should be recovered as fast as possible to prevent biological diseases, the reduction of timber quality and its economic values, and to promote an active post-disturbance forest restoration [5]. To this aim, having information on the working productivity of forest operation (OP) is an essential step.

In the mountainous area of Valle Camonica (Lombardy Region, Italy) the Vaia storm (26th–30th October 2018) caused a loss of 8×10^2 ha of forest lands and 3×10^5 m³ of merchantable volume, approximately. In that area, salvage logging is generally based on the “Full-Tree” method (i.e., extraction of stems, branches, and tops - in case of coniferous - to the landing) using a cable crane, and in the further wood processing at the landing using earthmoving machines and chainsaws.

The aim of the study was to compute the working productivity of a forestry machinery chain (FMC) applied for wood recovery in a forest stand of the Camonica Valley damaged by the Vaia storm, from wood extraction to the processing at the landing. The obtained results can be used by logging companies, forestry consortia, managers and planners, and local decision-makers as a basis for: (i) understanding the machinery chains performances under complex and dangerous working conditions; (ii) rationalizing the work and improving the organization of the activities; (iii) selecting machines and equipment to remove wood quickly while preventing, at the same time, damages to the ecosystem and (iv) calculating the economic cost of wood recovery (Bodaghi et al. 2018). This last aspect could be quite important for setting public subsidies and proper operations tariffs.

2 Materials and Methods

2.1 Case Study Area and Machinery Chain Organization

The research was carried out in October 2021 in a public forest stand (i.e., managed through a Forest Management Plan) owned by the municipality of Saviore dell’Adamello and managed by the Forestry Consortia of the “Upper” Camonica Valley (Consorzio Forestale Alta Valle Camonica). The stand has an altitude between 1400 and 1600 asl and was composed of uneven-aged trees of *Picea abies* L. The FMC was made up of the following OPs (Fig. 1, Table 1): (OP1) wood extraction to the landing (“Full-Tree” method; distance: 500 m); (OP2) wood positioning (from the landing to the delimiting and sectioning point) and subsequent stacking (roundwood



Fig. 1 Typology of used machines. Left: cable crane with mobile drive station; center: earthmoving machine equipped with hydraulic clamp; right: chainsaw

Table 1 Organization of the FMC: operations, machines, and number of employees

Operation	Typology of machine	Manufacturer	Model	Max engine power (kW)	N. of employees
Extraction	Cable crane with mobile drive station	Konrad	KMR4000U	265.0 ^a	4
Positioning and stacking	Earthmoving machine equipped with hydraulic clamp	Volvo	ECR88PLUS	40.0	1
Sectioning and delimiting	Chainsaw	Stihl	MS 462	4.4	1

^a It includes the power of the carriage (55 kW)

and logging residues are separately accumulated); this was considered as a single OP as it was carried out using the same machine; (OP3) delimiting and sectioning into commercial assortments. Before the tests, preliminary inspections were carried out to evaluate the site characteristics: all the trees were already detached from the stump (either due to the windstorm and because—for few trees—the cut was carried out some months before the tests to better prepare the area for wood recovery operations). In any case, the Forestry Consortia declared that the stem cutting was very slight, almost negligible in terms of required time.

2.2 *Experimental Data Collection and Productivity Calculation*

Three field tests (T; T1, T2, T3) were carried out (total time of monitoring: 22 h) to collect data about: (i) duration of working times and (ii) volume of extracted wood. First of all, each OP was subdivided into several phases, each of which corresponded to a specific working time (t_i ; h). The phases were defined according to the Comité

International d'Organisation Scientifique du Travail en Agriculture (C.I.O.S.T.A.) [6] – widely used for on field agricultural operations – and here specifically adapted for forestry conditions. In each T, the time of beginning and ending of each phase related to each OP was detected through a clock as “hours: minutes: seconds” (hh:mm:ss) at the landing by 2 operators: the first one to monitor OP1, and the second one to monitor OP2 and OP3. In addition, the time of beginning and ending of each T as a whole was separately collected.

Some of the detected times were specific for each OP, whereas others were in common. In this work, the C.I.O.S.T.A. methodology was used as an effort to standardize the terminologies used for agricultural and forestry mechanical operations (Forest Work Study Nomenclature of the International Union of Forestry Research Organizations, IUFRO; [1], making possible the comparison. Some of the times were simply differently named, whereas others were further split (due to the very detailed experimental measures that were carried out) but can be easily aggregated (Table 2).

Overall, the number of working times monitored during the tests amounted to: (i) 12 for OP1, (ii) 17 for OP2 and (iii) 8 for OP3.

The volume of the extracted wood was calculated for both roundwood (V_R ; m^3) and residues (V_L ; stacked cubic meters; stcm). For this, the following data were measured in each T: (i) diameter (in the center of the stem portion; cm) and length (m) of each sectioned stem portion suitable for commercial purpose, and (ii) dimensions (m) of the residues stack. The diameter and the length were measured every time wood was sectioned and delimbed, using a volume calliper and a tape measure, respectively. The dimensions of the residues stack were measured at the end of each T using a tape measure, and assuming that the stack had a trapezoidal prism shape. Then, in each T, for each OP and for the whole FMC, the productivity was quantified for both roundwood and residues as both volume basis ($m^3 \cdot h^{-1}$ and $stcm \cdot h^{-1}$ for roundwood and residues, respectively) and mass basis ($t \cdot h^{-1}$ of fresh mass, FM; $t \cdot h^{-1}$ of dry mass, DM). The calculation on mass basis was done by applying two different methods, based on: (i) bulk density (MV, i.e., ratio between wood FM and wood fresh volume, $t \cdot FM \cdot m^{-3}$) and (ii) wood basic density (DB, i.e., ratio between wood DM and wood fresh volume, i.e. the volume at the saturation point of the fibers, with water content equal or higher than 30%; $t \cdot DM \cdot m^{-3}$). The MV method was applied assuming a MV value of the dry matter equal to $0.4 \cdot t \cdot DM \cdot m^{-3}$ DM and a water content of the wood equal to 30%; the DB method was applied using a value of $0.38 \cdot t \cdot DM \cdot m^{-3}$ [2]. For residues, the productivity on mass basis was calculated assuming a volume coefficient between residues and roundwood equal to 6 [3]. This was a simplification that was introduced because, on the one hand, data relating to the bulk density of the residues were not made available (the range of variation is considerably higher than that of woodchips, as it strongly depends on how the stack is set up and on the mass distribution of branches and tops), and, on the other hand, it was not possible to monitor the chipping operation, through which it would have been possible to calculate the volume of woodchips and therefore the mass more accurately.

Table 2 OPs working times and IUFRO classification (S = Start time; E = End time)

	Working time	Description	IUFRO classification
OP1	1 – Travel unloaded	S: at the end of the machine on-field preparation or after unloading the wood at the landing E: carriage stops on the cable crane line	Main Work Time
	2 – Wood loading	S: carriage stops on the cable crane line E: rope is below the carriage with wood	
	3 – Travel loaded	S: rope is below the carriage with wood E: carriage stops on the cable crane line	
	4 – Rope descent	S: carriage stops on the cable crane line E: rope reaches the ground with the loaded wood	
	5 – Wood release	S: rope is on the ground with the loaded wood E: wood is released from the rope	
	6 – Rope ascent	S: wood is released from the rope E: rope is below the carriage to start a new travel	
OP2	1 – Waiting (wood extraction)	S: at the end of the machine on-field preparation or after waiting the wood to be extracted E: rope is below the carriage to start a new travel	Interference Time
	2 – Approaching to wood	S: machine approaches to the wood E: machines is ready to grasp the wood	Main Work Time

(continued)

Table 2 (continued)

	Working time	Description	IUFRO classification
	3 – Wood grasping	S: machines starts to grasp the wood E: all the wood is grasped	Main Work Time
	4 – Wood displacement	S: all the wood is grasped E: machine reaches the point of sectioning/delimiting	Main Work Time
	5 – Wood deposit	S: machine reaches the point of sectioning/delimiting E: wood is placed for further processing	Main Work Time
	6 – Waiting (wood cutting)	S: wood starts to be cut E: all the wood is cut	Interference Time
	7 – Roundwood stacking	S: roundwood is grasped E: all the roundwood is stacked	Main Work Time
	8 – Residues stacking	S: residues are grasped E: all the residues are stacked	Main Work Time
	9 – Unavoidable delay times related to residues	See point 7	Interference Time
	10 – Unavoidable delay times related to roundwood	See point 8	Interference Time
	11 – Return to wood extraction point	S: wood (roundwood/residues) stacking ends E: machine waits for wood extraction	Complementary Work Time
OP3	1 – Waiting (wood extraction/positioning)	S: end of the machine on-field preparation or when the employee waits for wood deposit E: time n. 5 of OP2 ends	Interference Time
	2 – Wood cutting	S: wood started to be sectioned and delimited E: all the wood is processed	Main Work Time

(continued)

Table 2 (continued)

	Working time	Description	IUFRO classification
OP1 OP2 OP3	1 – Machine on-field preparation	S: at the beginning of the work E: machine is ready for the OP	Operational Preparatory Time
	2 – Machine on-field maintenance	S: machine stops the OP E: maintenance ends	Maintenance time
	3 – Machine filling	S: machine stops the OP E: filling ends	Refuel Time
	4 – Employee rest	S: employees stop to do the OP E: employees finished the break	Rest and Personal Time
	5 – Avoidable delay	S: the OP could not continue due to idleness, bad organization of the work, gathering information, or visitors E: this condition is solved	Disturbance time
	6 – Unavoidable delay	S: the OP could not continue due to operators personal needs (for OP2, see point 9 and 10) E: personal needs are completed (for OP2, see point 9 and 10)	Rest and Personal Time (for OP2, see points 9 and 10)

3 Results and Discussion

For OP1 the working times and volume of extracted wood are shown in Table 3.

Table 3 OP1 – Working times and volume of extracted wood (R: repetitions)

Test	R	Time		Total volume	
		Total	Average	Roundwood	Residues
–	–	h	h	m ³	stcm
T1	20	5.56	0.28 ± 0.06	10.6	116.0
T2	40	7.95	0.20 ± 0.06	7.3	301.4
T3	33	7.35	0.22 ± 0.09	22.7	370.9

Table 4 OP2 – Working times for roundwood and residues (R: repetitions)

Test	Roundwood			Residues		
	R	Time		R	Time	
		Total	Average		Total	Average
–	–	h	h	–	h	h
T1	12	3.23	0.27 ± 0.11	20	5.85	0.29 ± 0.11
T2	13	6.47	0.18 ± 0.06	40	8.17	0.20 ± 0.09
T3	24	2.29	0.27 ± 0.14	33	7.92	0.24 ± 0.13

Table 5 OP3 – Working times (R: repetitions)

Test	R	Time	
		Total	Average
–	–	h	h
T1	20	6.01	0.30 ± 0.08
T2	39	8.13	0.21 ± 0.08
T3	40	7.08	0.24 ± 0.12

For OP2 the working times were related to both the roundwood only (if both roundwood and residues were extracted within the same repetition) and to the residues (there could be the case in which both roundwood and residues were extracted, or only residues). This subdivision was done to compute the productivity of roundwood and residues separately. The results are shown in Table 4.

For OP3 the results are shown in Table 5.

Regarding the productivity, for roundwood, the following weighted average values (T1, T2, T3) were obtained:

1. stem detachment from stumps: 0.00 m³/h (0.00 t/h DM MV; 0.00 t/h DM DB) (operation non monitored);
2. extraction: 2.39 m³/h (0.95 t/h DM MV; 0.91 t/h DM DB), ranging from 0.92 m³/h (0.36 t/h DM MV; 0.35 t/h DM DB) to 3.10 m³/h (1.23 t/h DM MV; 1.18 t/h DM DB);
3. positioning and stacking: 3.39 m³/h (1.34 t/h DM MV; 1.29 t/h DM DB), ranging from 3.18 m³/h (1.26 t/h DM MV; 1.21 t/h DM DB) to 3.51 m³/h (1.39 t/h DM MV; 1.33 t/h DM DB);
4. sectioning and delimiting: 2.42 m³/h (0.96 t/h DM MV; 0.92 t/h DM DB), ranging from 0.90 m³/h (0.36 t/h DM MV; 0.34 t/h DM DB) to 3.21 m³/h (1.27 t/h DM MV; 1.22 t/h DM DB);
5. FMC: 2.25 m³/h (0.89 t/h DM MV; 0.86 t/h DM DB), ranging from 0.89 m³/h (0.35 t/h DM MV; 0.34 t/h DM DB) to 2.90 m³/h (1.15 t/h DM MV; 1.10 t/h DM DB).

Figure 2 shows the weighted average productivities for roundwood, expressed as volume (m³/h) and dry mass (t/h DM).

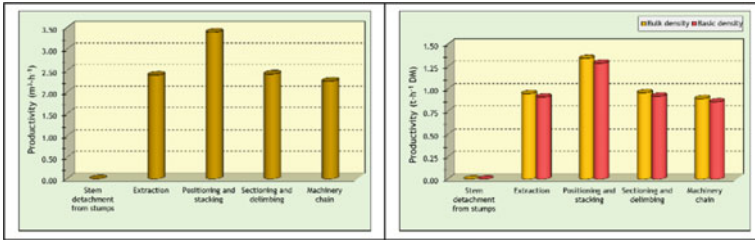


Fig. 2 Weighted average productivities for roundwood: volume basis (left) and dry mass basis (right)

For residues, the following weighted average productivities (T1, T2, T3) were obtained:

1. stem detachment from stumps: 0.00 stcm (0.00 t/h DM MV; 0.00 t/h DM DB) (operation non monitored);
2. extraction: 41.31 stcm/h (2.73 t/h DM MV; 2.62 t/h DM DB), ranging from 20.84 stcm/h (1.38 t/h DM MV; 1.32 t/h DM DB) 50.49 stcm/h (3.33 t/h DM MV; 3.20 t/h DM DB);
3. positioning and stacking: 39.05 stcm/h (2.58 t/h DM MV; 2.47 t/h DM DB), ranging from 19.82 stcm/h (1.31 t/h DM MV; 1.26 t/h DM DB) to 46.81 stcm/h (3.09 t/h DM MV; 2.96 t/h DM DB);
4. sectioning and delimiting: 41.68 stcm/h (2.75 t/h DM MV; 2.64 t/h DM DB), ranging from 19.31 stcm/h (1.27 t/h DM MV; 1.22 t/h DM DB) to 52.41 stcm/h (3.46 t/h DM MV; 3.32 t/h DM DB);
5. FMC: 39.28 stcm/h (2.59 t/h DM MV; 2.49 t/h DM DB), ranging from 19.82 stcm/h (1.31 t/h DM MV; 1.26 t/h DM DB) to 47.24 stcm/h (3.12 t/h DM MV; 2.99 t/h DM DB).

Figure 3 shows the weighted average productivities for residues, expressed as volume (stcm/h) and dry mass (t/h DM).

For both roundwood and residues, the use of bulk density rather than basic density caused a variation of 4.2% of the dry mass value. The dry mass of the residues was from 1.8 to 6.9 times higher than the dry mass of the roundwood, whereas the productivity of the residues in terms of dry mass was from 1.9 to 2.9 times higher than the

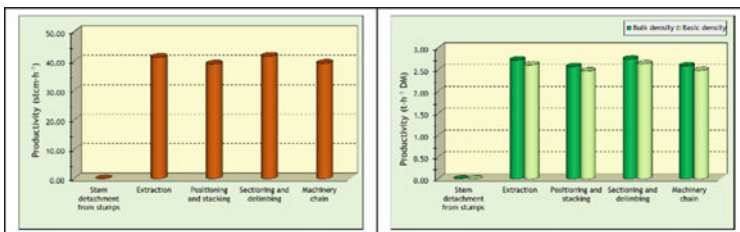


Fig. 3 Weighted average productivities for residues: volume basis (left) and dry mass basis (right)

productivity of the roundwood. As it generally occurs in salvage logging interventions, most of the extracted wood is of poor quality (branches, tops, rotten, broken and irregularly shaped stems), and can be valorized only through energy conversion processes, whereas roundwood suitable for industrial purposes is a small fraction of the total recovered mass. Therefore, the values of the productivity here computed should not be compared to those related to “standard” FMCs applied for ordinary silvicultural treatments in regularly managed stands, where roundwood is the main output. Moreover, the analyzed FMC was performed for the “cleaning of the end-of-line”, during which all the residues were extracted to the landing to avoid the risk of fires, parasitic attacks, as well as trees regeneration problems [8]. On the one hand, this promote a further availability of biomass for energy purposes but, on the other hand, the extraction of all the residues causes the removal of deadwood, which has several ecological functions, such as biodiversity enrichment, carbon sequestration, nutrient release to the soil, reduction of soil erosion and water runoff. Because of this, the post-disturbance wood to be removed should always be evaluated case by case.

The comparison of productivity values across areas/region/countries, where contrasting working and environmental conditions occur is quite difficult, even if the used machines can be similar. In this study, working time and productivity of salvage logging operations were investigated, but the particular conditions of the area as well as the lack of similar tests based on cable crane for salvage logging, did not allow for a complete comparison of the results. In addition, similar studies usually take into consideration roundwood only; indeed, in this paper, also the logging residues are computed, being this a remarkable aspect of the study.

As mentioned before, stem detachment from stumps is a key aspect in the recovery of storm damaged timber. The exclusion of this preliminary operation was certainly an important limiting factor that could invalidate the completeness of the study, and must certainly be considered for future research.

4 Conclusions

This study investigated working times and productivity of a FMC applied in a forest stand of an Italian alpine area damaged by the Vaia storm in October 2018. The OPs that made up the FMC were: (OP1) extraction; (OP2) positioning and stacking; (OP3) sectioning and delimiting. The total time of each OP was computed by summing up different working times, each of them corresponding to a specific working phase. This allowed the identification of the main factors which influence time variation and FMC organization. Even if the productivity was here calculated as both volume, fresh and dry mass basis, this latter should always be preferred, as it expresses the real mass of wood that a machine can process within a specific unit of time. This is important when comparing the productivity of operations performed under different environmental conditions and/or in different period of time, for which the water content of the wood can be different. The results of this study demonstrated that

the productivity values expressed as dry mass bases varied according to the method applied for the calculation. Future research is needed on other damaged stands for results comparison, also including the preliminary operation of stem detachment from stumps, and the operations of: (i) woodchips production and (ii) roundwood and woodchips transport.

References

1. Björheden, R., Apel, K., Shiba, M., Thompson, M.A.: IUFRO forest work study nomenclature 1995. Department of Operational Efficiency, Swedish University of Agricultural Science, Garpenberg, p. 22 (1995)
2. Federici, S., Vitullo, M., Tulipano, S., De Lauretis, R., Seufert, G.: An approach to estimate carbon stocks change in forest carbon pools under the UNFCCC: the Italian case. *iForest Biogeosci. For.* **1**, 86–95 (2008)
3. Fiala: Energy from agricultural biomass. Production and use. With application examples. Maggioli Edition, p. 430 (2012)
4. Gardiner, B., Andreas, S., Schelhaas, M.-J., Orazio, C., Blennow, K., Nicoll, B.: Living with Storm Damage to Forests; European Forestry Institute: Joensuu, Finland, vol. 3 (2013)
5. Müller, J., Noss, R.F., Thorn, S., Bässler, C., Leverkus, A.B., Lindenmayer, D.: Increasing disturbance demands new policies to conserve intact forest. *Conserv. Lett.* **12**, e12449 (2019)
6. Reboul, C.: Temps de travaux et jours disponibles en agriculture. *Économie rurale* **61**, 55–80 (1964)
7. Seidl, R., Schelhaas, M.-J., Rammer, W., Verkerk, P.J.: Increasing forest disturbances in Europe and their impact on carbon storage. *Nat. Clim. Change* **4**, 806–810 (2014)
8. Spinelli, R., Nati, C., Magagnotti, N.: Recovering logging residue: experiences from the Italian Eastern Alps. *Croat. J. For. Eng.* **28**(1), 1–9 (2007)

Can a Variable-Rate Sprayer Be Efficient and Economic? Testing and Economic Analysis in Viticulture



Andrea Pagliai, Daniele Sarri, Carolina Perna, and Marco Vieri

Abstract The European Union has set ambitious goals in terms of reducing pesticides in agriculture. These goals could be achieved in different ways e.g. by Variable-Rate Application (VRA) technologies. This work aims to assess the spraying performance of a VRA sprayer and its economic sustainability. To evaluate operational performance, three trials (BBCH 65, BBCH 73, BBCH 83) were performed in a vineyard following a profile sampling strategy (BS ISO 22522:2007). A randomized complete block design was performed with three replications for each application mode (Uniform and Variable - UA and VRA). Variables (normalized deposition and spray coverage) were extracted from artificial targets using spectrophotometry and image analysis techniques, respectively. Moreover, the economic performance of the VRA sprayer compared to the UA sprayer was performed for an entire vegetative season in two plots. Normalized deposit results showed differences between detection heights (H1, H2, H3, H4) rather than between modes (VRA vs UA). Therefore, VRA and UA efficacy was confirmed, given the similar values of deposit. The same trend was evident in the spray coverage results, even though the UA spray coverages were higher than VRA, usually exceeding the overspray threshold. The economic performance highlighted an average volume saving of 35% for VRA, ranging from 76% in the first session to 10% in the last. The resulting economic saving was €2,599.50, consisting of: €2,502.5 in pesticides, €52.14 in water and €44.86 in fuel. Overall, the VRA system showed good spray performances reducing the spray volume significantly and enhancing economic sustainability.

Keywords VRA · Spraying optimization · Pesticide · Ultrasonic sensor · Vineyard · Environmental sustainability

The original version of this chapter was revised: The first and last names of the chapter authors were interchanged. The correction to this chapter is available at https://doi.org/10.1007/978-3-031-30329-6_131

A. Pagliai (✉) · D. Sarri · C. Perna · M. Vieri
DAGRI, University of Florence, Piazzale Delle Cascine 15, 50144 Firenze, Italy
e-mail: andrea.pagliai@unifi.it

© The Author(s), under exclusive license to Springer Nature Switzerland AG 2023, 805
corrected publication 2023
V. Ferro et al. (eds.), *AIIA 2022: Biosystems Engineering Towards the Green Deal*,
Lecture Notes in Civil Engineering 337,
https://doi.org/10.1007/978-3-031-30329-6_82

1 Introduction

The economic sustainability of farms has always been the main aspect to consider in order to maintain a stable business. In recent years, environmental sustainability has been complemented by economic sustainability [1]. Particularly in viticulture, some field activities such as crop protection have a heavy environmental and economic footprint [2]. Recently, the war between Russia and Ukraine, the post-pandemic situation and ongoing inflation are hitting all sectors hard. The price of raw materials as fertilizers, fuel, pesticides and energy is increasing, pushing farms in a difficult position [3]. At the same time, the attention of public decision-makers is focused on green policies. Recently, the European Commission, through the documents «From Farm to Fork», has set ambitious goals to reach a healthy and sustainable food system [4]. To achieve these targets, farmers must reduce the number of chemical inputs as PPP (plant protection products), fertilizers and antimicrobials products.

In particular, many techniques and tools exist in viticulture to achieve these goals for example decision support systems, development of less dangerous PPP, low volume applications, anti-drift nozzles and variable-rate applications [5].

The latter is one of the most interesting tools for adapting plant protection products to the canopy characteristics, thus reducing their consumption [6]. In general, the new VRA sprayers are very expensive compared to conventional ones. This fact leads farmers not to buy them, even if VRA sprayers can improve spray performance, reduce the consumption of pesticides and, in general, enhance economic and environmental sustainability [7].

Within this context, the present work aims to develop a low-cost modification kit to convert the existent sprayer into an innovative VRA in order to reduce pesticides consumption and enhance environmental and economic sustainability without affecting operational performance. Therefore, the purpose of this research is to test and assess the spraying and economic performance of this kit, for conventional sprayers, able to perform variable rate spraying according to canopy size. The study can be split in two different parts. In the first part, three trials were conducted at different phenological stages to evaluate the spraying performance of the sprayer in VRA compared to UA mode. In the second, the same sprayer was used to perform an entire season of spraying in VRA mode, with the aim of assessing its economic performance in relation to UA one.

2 Materials and Methods

A vineyard in the Chianti Classico area has been the place of experimentation. In particular, the vineyard was located in Gretole (4,813,930.984 N; 680,511.290 E), Castellina in Chianti, Siena, Italy (Fig. 1). The vineyard had a density of 5000 vines ha^{-1} , with a planting distance of 2.50×0.80 m, and the cultivar was the *Vitis vinifera*

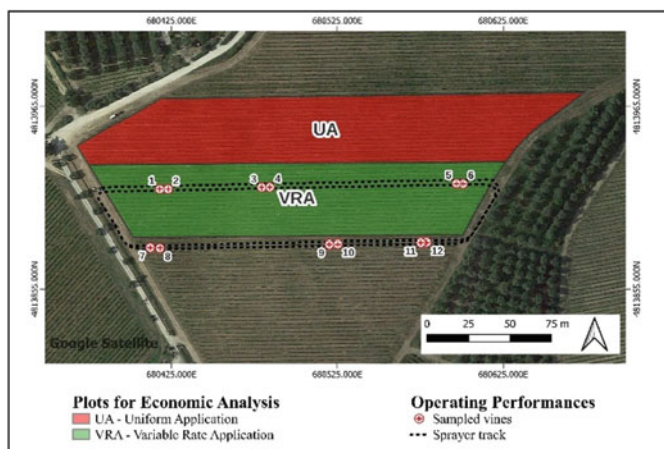


Fig. 1 Experimental site for operating and economic performances of VRA sprayer

L. cv. ‘Sangiovese’. The vines were 16-years old and trained with a horizontal spur-cordon. This vineyard was used for both operational and economic performance tests.

During the trials, a tractor-drawn, PTO-powered, pneumatic sprayer (Martignani M612 Whirlwind, Ravenna, Italy) was used. The sprayer was equipped with a 1000 L polyethylene tank, a centrifugal fan, a centrifugal pump (120 l/min, 150 kPa), and 6 nozzles per side (\varnothing 4 mm). Air was expelled by two radial fans at 90° to the direction of the travel, with a homogeneous air flow around $26,000 \text{ m}^3 \text{ h}^{-1}$. The sprayer was customized to be able to apply pesticides at variable rate (VRA) according to the canopy size. A new generation of ultrasonic sensors has been installed at the forepart of the sprayer to perform the VRA (NORAC Topcon, Tokyo, Japan). These sensors can analyse the canopy in terms of thickness, foliar layers and density. These data were used to adjust the spray volumes to the size of the canopy. The spraying components were also customised. In fact, the original valves have been replaced by electronic ones. In particular, in the rear of the sprayer, there were eight electro-valves, four for the left side and four for the right side. These valves control the flow rate of spray volume, thanks to their switching on/off. The combination of opening and closing of electro-valves and the variation of pressure from 1 to 2 bars permits to apply pesticides at variable rate. The flow rates for each electro-valves are shown in Table 1, at 1.5 bar of pressure.

Table 1 Flow rates for each electro-valves (EV – Electro-Valve; L or R – Left or Right; A, B, C, D – correspond to different electro-valves)

1.5 bar	EV _{LA}	EV _{LB}	EV _{LC}	EV _{LD}	EV _{RD}	EV _{RC}	EV _{RB}	EV _{RA}
Flow rate (1 m^{-1})	0.56	0.86	1.46	2.26	2.26	1.46	0.86	0.56

All the instrumentations were controlled by X25 Topcon console, mounted on the cabin of the tractor and connected with a D-GNSS antenna (Differential Global Navigation Satellite Systems). From this monitor, all working parameters can be controlled, managed and recorded.

2.1 Operating Performances

The operating performances of VRA consist of evaluating the quality and quantity of the application against the uniform application (UA). Both of them followed the British Standard ISO 22522/2007. In particular, the profile sampling strategy was used. During the growing season, three trials were carried out in three different phenological phases (BBCH 65, BBCH 73, BBCH 83) and, in each one, twelve vines were sampled [8]. Before each trial, the sprayer was calibrated correctly. During each test, air temperature, air humidity, wind speed and direction were monitored at a height of 2 m, using a 2900ET Watchdog Weather Station (Spectrum Technologies Inc., Illinois, USA). Figure 2 shows the sampling strategy within the vines and in the different tests. To guarantee a good sampling strategy, following the BS ISO, a randomized complete block design was performed with three repetitions for each application mode (UA vs. VRA) and both sides of the canopy were sampled.

Concerning the spray volume applied in the trials, the farm protocol for the UA mode was followed. Instead, a calibration curve between the canopy size, spray volumes and sensor readings was developed and applied for the VRA mode. During trials, the forward speed of tractor was of 5 km h⁻¹. Table 2 shows the whole spray settings in the three trials.

Fig. 2 Sampling strategy in different phases (L or R—Left or Right; H1, H2, H3, H4—Different heights of sampling; ●—collectors; ■—plastic collector; ■—water sensitive paper)

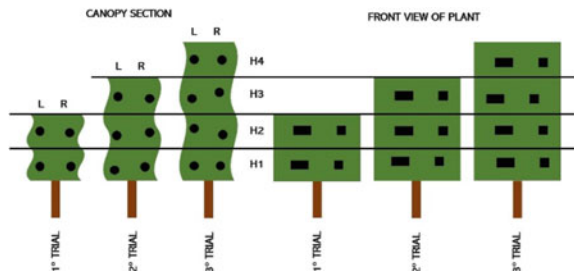


Table 2 Application parameters during the field trials

Trial	Phenological stage	UA mode	<i>sd</i>	VRA mode	<i>sd</i>	
1° trial	BBCH 65	200	±0.5	0 (48 - 198)	±4.5	1 ha ⁻¹
2° trial	BBCH 73	250	±1.9	0 (109 - 299)	±1.6	1 ha ⁻¹
3° trial	BBCH 83	300	±0.5	0 (131 - 344)	±0.8	1 ha ⁻¹

Regarding the samples, water-sensitive papers (WSP, 26×76 mm, Syngenta, Switzerland) and plastic collectors (50×90 mm, SEFAR NITEX) were arranged to evaluate the quality and the quantity of spraying, respectively [9, 10]. In laboratory, the WSPs were scanned at a resolution of 600 dpi using a Kyocera TASKalfa 3554ci KX scanner-printer and then, were analysed by the software ImageJ (v. 1.38x) to extract the spray coverage parameter (%). The amount of application was instead evaluated through the use of tartrazine, plastic collectors and spectrophotometry methodology. In particular, E-102 yellow Tartrazine (Andrea Gallo S.r.l., Genova, Italy) were added to the sprayer's tank at a concentration of 8 g l^{-1} [11]. The tartrazine concentration on plastic collectors was quantified by using a spectrophotometer UV-1200 (ChromTech, Bad Camberg, Germany), after having washed collectors with 20 ml of distilled water. Before obtaining the absorbance values of the samples, the blank values were subtracted from the samples to obtain the real absorbance. Then, the absorbance values were converted to deposits (d_i) using a calibration curve, obtained by dilutions of the tank liquid, and the below formula:

$$d_i = \frac{(A_r - A_b)}{\alpha} \times V_{dil} \text{ mg cm}^{-2} \quad (1)$$

where: d_i is the spray deposit expressed in mg cm^{-2} ; A_r is the absorbance value of the sample; A_b is the absorbance of the blank sample; α is the calibration curve coefficient; V_{dil} is the washing solution of collectors; S_{ps} is the area of plastic collectors.

In order to avoid influences of different rate of application and tracer concentration, values of deposit (d_i) were converted to normalized deposits (d_n) values through the below formula (Eq. 2).

$$d_n = \frac{d_i \times 100}{A_{vol} \times c_{tar}} \text{ mg cm}^{-2} \quad (2)$$

where: d_n is the spray normalized deposit expressed in mg cm^{-2} ; d_i is the spray deposit expressed in mg cm^{-2} ; A_{vol} is the application volume of sprayer expressed in l ha^{-1} ; c_{tar} is the concentration of tartrazine (8 g l^{-1}).

2.2 Economic Performances

The economic performance analysis was conducted on an entire season of crop protection in two neighbouring plots of around 1 ha each (Fig. 1). In the first plot, the sprayer was used in UA mode, i.d. the same spray volume was applied within the plot for each individual crop protection phase. In the other plot, the sprayer was operated in VRA mode, i.d. the ultrasonic sensor varied the spray volume according to the size of the canopy.

Concerning the crop protection protocol (spray volumes, pesticides and schedule), the farm protocol was followed for the UA mode while, only the spray volumes were modified for the VRA mode. In particular, a calibration curve between the canopy size, application volume and sensor readings was developed and applied at every crop protection phase. Table 3 shows the spray settings during the entire crop protection season.

To perform a costs/benefits analysis, spraying volumes, pesticides, equipment and raw materials were monitored. Specifically, the reports for each phase of crop protection were downloaded from the monitor's storage memory and analysed to extract the values of spraying volumes for both modes (UA, VRA). Finally, the accounting of pesticides, equipment and raw materials (water, fuel) was evaluated in terms of quantity and costs using the farm's fields-book and the national/regional quotation.

2.3 Statistical Analysis

The variables of operating performance ($\%$, d_n) were analysed using the open-source software R (R Core Team, 2021). First, the variables were analysed for reliability and accuracy in relation to the linear model assumption, the normal distribution of errors was then checked using the Shapiro–Wilk test ($p < 0.05$) and visual analysis (frequencies histogram, normal Q-Q plots). Furthermore, the respect of homoscedasticity was checked using the Levene's test. Afterward, a two-ways Analysis of Variance (ANOVA) was used with a p-value of 0.05. ANOVA was performed within each phenological phase, verifying the effect of the independent variables, i.e. application mode (UA, VRA) and sampling heights (H1, H2, H3, H4), on the dependent variables, i.e. spray coverage ($\%$) and normalized deposits (d_n). Finally, significant differences of means were tested using Tukey's HSD test ($p < 0.05$), while the variables of economic analysis were evaluated with analytics accounting and managed with Excel and QGIS software (Office 365 pack, Microsoft Corporation, 2021; QGIS 3.22.1, QGIS.org, 2022).

3 Results and Discussion

3.1 Operative Performances

The results of the spraying performance were shown in Fig. 3a and b. The three phenological phases, were reported in each graph. According to the plant growth, the sampling heights increase in the different trials (BBCH 65, BBCH 73, BBCH 83).

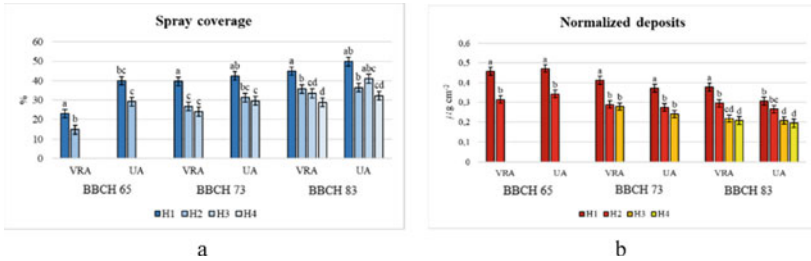


Fig. 3 Results of the two-way ANOVA for the spray coverage (%) and the normalized deposits ($\mu\text{g cm}^{-2}$). Statistical significance: $p < 0.05$ (Tukey’s HSD post-hoc test)

Considering the spraying coverage graph (Fig. 3a), it was found that statistically significant differences were found between heights and application mode (VRA, UA) in all these and trials, with the exception of H3 in BBCH 73 and H2 in BBCH 83 among the application mode, and for H2 and H3 within VRA in BBCH 73 phase. However, the overall spraying coverage trend highlighted quite constant rates of coverage between phenological phases, with the first stage in VRA mode, which was significantly lower than the other theses. In relation to the UA mode, it could mean that the farm protocol was correct because it ensured the same rate of coverage in different canopy volumes. However, the values of coverage are too high in relation to the overspray threshold widely agreed upon by other authors [12]. Regarding the graph in Fig. 3b, it was found that statistically significant differences were only found between different sampling heights and in the BBCH 83 phase between the application modes in H1, H2 and H3. In all these cases, deposits were higher in VRA in VRA than UA. Generally, the common trend between analysed variables ($\%$, d_n) is the decreasing of values between the H1 detection height and subsequent ones. This aspect was highlighted in both the VRA and UA and was probably due to the construction characteristics of the sprayer. In fact, the sprayer had two fans located below the cordon and they sprayed the entire canopy with a radial spraying. Therefore, the vertical profile of canopy was not at the same distance as the fans, causing scalar values in both deposits and coverage. This aspect was also highlighted by Matthews et al. (2014) [13].

Reading the overall values of the three trials, the minimum values for good pesticide efficacy were respected in all cases [11, 14, 15]. In general, uniform application provides higher values in the coverage parameter, especially for the sampling zone near the cordon., these values often exceed the maximum value for good coverage.

3.2 Economic Performances

The results of economic performance were shown in Table 3. In particular, two main aspects were shown in the table. The first one is called technical analysis, where

important parameters such as the number of crop protection phases, volumes of mixture applied in UA and VRA modes, the number of tank refills and the number of days to complete a work activity were reported. These values were recorded or calculated from reports provided by the tractor console and the spatial layout of the farm's vineyards, which affected the downtime of refills. The second aspect concerns the costs of pesticides, water and fuel. Here, the economic performance of the UA and VRA modes were reported for each phase.

Regarding the technical analysis, the wine farm protected the vineyards with nine phytosanitary treatments during the season for both spraying modes. During this period, there was a saving in spray volume ranging from 76% in the first stage to 10% in the last. This decreasing trend in spray volume savings between the first and the last stage is a normal consequence of modern training systems. This is due to the closing and compactness of the canopy during the growing season [16]. The average saving was 35%. Similar savings were found in other studies as reported by Gil et al. (2007), Ježič et al. (2011) and Tona et al. (2018) [12, 17, 18]. As far as work performance is concerned, an increase in efficiency in VRA mode compared to UA one can be shown. This is due to fewer refills of the sprayer tank because of less spray volume consumption. This increased the work performance of VRA in terms of days to complete a crop protection stage in a 22 ha field. The wine farm size was set at around 22 ha because Tona et al. (2018) stated this value is the limit to perform crop protection with a single sprayer ("sharp cost edges" effect) [18].

With regard to the costs analysis, the type and quantity of pesticides and their costs were monitored at each stage using the field book of the wine farm. Then, the unit cost per litre was calculated and multiplied by the volume sprayed in both application modes for each stage thus obtaining the cost of each treatment. The same was done for water costs. In this case, the local water cost per cubic metre was used. The increase in the fuel cost in UA mode, on the other hand, is due to the need for more refills due to the higher consumption of spray volume. This leads to the farmer going to the farm centre several times to refill the sprayer tank, especially in the early stages, causing considerable fuel consumption. The accounting of cost fuel was carried out following the methodology of Sarri et al. (2020) and analysing the wine farm arrangement of vineyards [2].

In terms of pesticide cost savings, the farm was able to save € 113.75 per year, and € 2,502.50 for a 22 ha farm by using VRA. The savings in terms of water use was smaller. In fact, the farm was able to save € 52.14 per a 22 ha-farm. This is due to the cheaper price for water use. In terms of fuel cost, the farmer was able to save € 44.86 over an entire season and for 22 ha thanks to VRA mode. Overall, the cost saving in VRA mode was € 2,599.50. Regarding savings on raw materials, the farm can reduce its consumption of pesticides by around 262.67 kg, water by around 18.00 m³ and fuel by around 35.00 l.

The costs for customising the sprayer amounted to approximately € 20,000.00. These costs mainly regarded sensors, electro-valves, console, cables and working customisation time. Taking this and the VRA savings into account, it was possible to perform a break-even analysis, as shown in Fig. 4. This analysis highlighted that the profitability of this technology will be within the 8th year of customization. However,

Table 3 Summary table of main parameters and their costs in a whole crop protection season both in UA and VRA mode.

Crop protection stages	Technical parameters						Pesticides cost				
	UA	VRA	Diff. %	Refill UA	Refill VRA	n° days to end UA	n° days to end VRA	Unit price	UA price	VRA price	Price diff. UA_VRA
n°	l ha ⁻¹	l ha ⁻¹	%	n° day ⁻¹	n° day ⁻¹	n° days 22ha ⁻¹	n° days 22ha ⁻¹	€ l ⁻¹	€ ha ⁻¹	€ ha ⁻¹	€ ha ⁻¹
1	200	49	76	2	1	2.62	2.29	0.10	20.00	4.90	15.10
2	200	56	72	2	1	2.62	2.29	0.22	44.00	12.32	31.68
3	200	69	66	2	1	2.62	2.29	0.11	22.00	7.59	14.41
4	200	80	60	2	1	2.62	2.29	0.14	28.00	11.20	16.80
5	250	155	38	3	2	2.75	2.62	0.23	57.50	35.65	21.85
6	250	212	15	3	2	2.75	2.62	0.15	37.50	31.80	5.70
7	330	285	14	3	3	2.82	2.82	0.09	29.70	25.65	4.05
8	330	289	12	3	3	2.82	2.82	0.06	19.80	17.34	2.46
9	330	296	10	3	3	2.82	2.82	0.05	16.50	14.80	1.70
Values referred to year								€	275.00	161.25	113.75
Values referred to 22 ha								€	6,050.00	3,547.50	2,502.50

Water cost			Fuel cost		
UA price	VRA price	Price diff. UA_VRA	UA price	VRA price	Price diff. UA_VRA
€ ha ⁻¹	€ ha ⁻¹	€ ha ⁻¹	€ 22ha ⁻¹	€ 22ha ⁻¹	€ 22ha ⁻¹
0.60	0.15	0.45	13.20	5.78	7.42
0.60	0.17	0.43	13.20	5.78	7.42
0.60	0.21	0.39	13.20	5.78	7.42
0.60	0.24	0.36	13.20	5.78	7.42
0.75	0.47	0.28	20.79	13.20	7.59
0.75	0.64	0.11	20.79	13.20	7.59
0.99	0.86	0.13	21.32	21.32	-
0.99	0.87	0.12	21.32	21.32	-
0.99	0.89	0.10	21.32	21.32	-
6.87	4.50	2.37			
151.14	99.00	52.14	158.34	113.48	44.86

customisation costs were considered as actual costs and therefore overestimated due to prototyping actions. Considering that, it is estimated that customization costs can be reduced by around 50%. For this reason, the break-even point was set at year^{4th}.

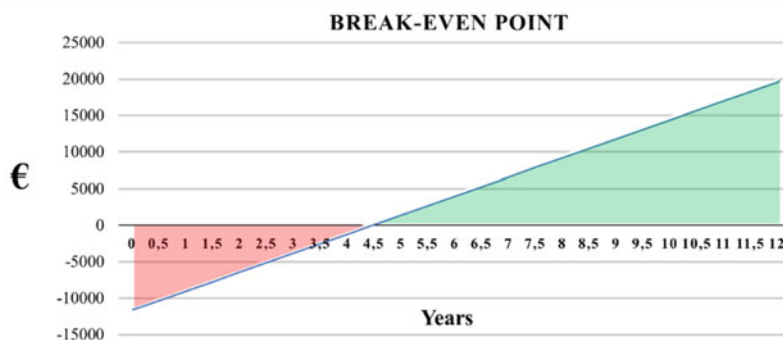


Fig. 4 Results of costs/benefits analysis in terms of break-even point

4 Conclusion

In order to achieve the EU goals in terms of reducing pesticide use and effectively introducing new technologies on farms, the technological innovation must be both environmentally and economically sustainable. In particular, spatial variability in vineyards is one of the most important aspects to take into account to reduce the environmental footprint of crop protection. This variability can be managed with new variable rate sprayers that can adapt the spray volume to the size of the canopy. However, to keep costs under control, an economic modification kit was presented in this paper. This kit is able to convert conventional sprayers into innovative VRA sprayers to reduce pesticide consumption and enhance environmental and economic sustainability without affecting operational performance. The results obtained are promising. In fact, the differences reported in the results section mainly reflect the architectural design of the sprayer rather than the mode of application (UA & VRA). However, all parameters examined (normalized deposit and spray coverage) in the trials ensure good quality and quantity distribution of pesticides. Moreover, the variable-rate application reduces application volumes while ensuring excellent performance in terms of normalized deposit and spray coverage. Nonetheless, economic analysis has demonstrated that variable-rate technology enhances the economic and environmental sustainability of crop protection.

References

1. Recchia, L., Sarri, D., Rimediotti, M., Boncinelli, P., Cini, E., Vieri, M.: Towards the environmental sustainability assessment for the viticulture. *J. Agric. Eng.* **49**, 19–28 (2018). <https://doi.org/10.4081/jae.2018.586>
2. Sarri, D., Lombardo, S., Pagliai, A., Zammarchi, L., Lisci, R., Vieri, M.: A technical-economic analysis of telemetry as a monitoring tool for crop protection in viticulture. *J. Agric. Eng.* **51**, 91–99 (2020). <https://doi.org/10.4081/jae.2020.1029>

3. Nayak, J., Mishra, M., Naik, B., Swapnarekha, H., Cengiz, K., Shanmuganathan, V.: An impact study of COVID-19 on six different industries: automobile, energy and power, agriculture, education, travel and tourism and consumer electronics (2022)
4. European Commission: A Farm to Fork Strategy for a fair, healthy and environmentally-friendly food system (2020)
5. Pagliai, A., et al.: Comparison of aerial and ground 3D point clouds for canopy size assessment in precision viticulture. *Remote Sens.* **14** (2022). <https://doi.org/10.3390/rs14051145>
6. Gil, E., Llorens, J., Llop, J., Fàbregas, X., Escolà, A., Rosell-Polo, J.R.: Variable rate sprayer. Part 2 - Vineyard prototype: design, implementation, and validation. *Comput. Electron. Agric.* **95**, 136–150 (2013). <https://doi.org/10.1016/j.compag.2013.02.010>
7. Sarri, D., et al.: Smart farming introduction in wine farms: a systematic review and a new proposal. *Sustainability* **12** (2020). <https://doi.org/10.3390/su12177191>
8. Lorenz, D., Eichhorn, K., Bleiholder, H., Klose, R., Meier, U., Weber, E.: Growth stages of the grapevine: phenological growth stages of the grapevine (*Vitis vinifera* L. ssp. *vinifera*)—codes and descriptions according to the extended BBCH scale. *Aust. J. Grape Wine Res.* **1**, 100–103 (1995). <https://doi.org/10.1111/j.1755-0238.1995.tb00085.x>
9. Salyani, M.: Methodologies for assessment of spray deposition in orchard applications. In: 2000 ASAE Annual International Meeting. American Society of Agricultural Engineers, Milwaukee, Wisconsin, USA, p. 11 (2000)
10. BS ISO: BS ISO 22522-2007 - Crop protection equipment-Field measurement of spray distribution in tree and bush crops (2007)
11. Miranda-Fuentes, A., Rodríguez-Lizana, A., Gil, E., Agüera-Vega, J., Gil-Ribes, J.A.: Influence of liquid-volume and airflow rates on spray application quality and homogeneity in super-intensive olive tree canopies. *Sci. Total Environ.* **537**, 250–259 (2015). <https://doi.org/10.1016/j.scitotenv.2015.08.012>
12. Gil, E., Escolà, A., Rosell, J.R., Planas, S., Val, L.: Variable rate application of plant protection products in vineyard using ultrasonic sensors. *Crop Prot.* **26**, 1287–1297 (2007). <https://doi.org/10.1016/j.cropro.2006.11.003>
13. Matthews, G.A.: Air-assisted sprayers. In: *Pesticide Application Methods*, 4th edn., pp 215–244. Wiley, Hoboken (2014)
14. Salcedo, R., Zhu, H., Zhang, Z., Wei, Z., Chen, L., Ozkan, E., Falchieri, D.: Foliar deposition and coverage on young apple trees with PWM-controlled spray systems. *Comput. Electron. Agric.* **178**, 105794 (2020). <https://doi.org/10.1016/j.compag.2020.105794>
15. Grella, M., et al.: Field assessment of a pulse width modulation (PWM) spray system applying different spray volumes: duty cycle and forward speed effects on vines spray coverage (2021)
16. Zhang, Z., Wang, X., Lai, Q., Zhang, Z.: Review of variable-rate sprayer applications based on real-time sensor technologies. In: *Automation in Agriculture - Securing Food Supplies for Future Generations*, p 13 (2018)
17. Jecic, V., et al.: Design and testing of an ultrasound system for targeted spraying in orchards. *J. Mech. Eng.* **57**, 587–598 (2011). <https://doi.org/10.5545/sv-jme.2011.015>
18. Tona, E., Calcante, A., Oberti, R.: The profitability of precision spraying on specialty crops: a technical–economic analysis of protection equipment at increasing technological levels. *Precis Agric.* **19**, 606–629 (2018). <https://doi.org/10.1007/s11119-017-9543-4>

Performance Analysis of a Harrowing Implement of New Concept



Simone Pascuzzi, Volodymyr Bulgakov, Iaroslav Gadzalo,
and Volodymyr Nadykto

Abstract One of the fallows soils problems in dry conditions is the lack of technical implements that ensure moisture availability in the soil when sowing winter crops. The peculiarity of a new harrow, which has been developed by the authors, is the use of flat-cut working tools, which allows loosening the upper (5–6 cm) layer of soil without significantly removing its wet part to the field's daytime surface. Experimental research has been carried to evaluate the operative performance of the following implement-tractor unit: a universal tractor with traction force 14 kN and the new harrowing implement. This machine-tractor unit has been compared with a conventional one for similar purposes. It included a general-purpose wheeled tractor with traction force 30 kN and a mounted behind cultivator of KPS-8 type. The experimental studies have established that using the new machine-tractor unit for fallow tillage in the lack of soil moisture conditions productivity is increased by at least 8%. The probability that the new harrow unit maintains the tolerance of fluctuations in the cultivation depth of the fallow field at the level of ± 1 cm is 78%.

Keywords Tractor · Harrow section · Tine · Productivity · Turning · Fuel consumption

S. Pascuzzi (✉)

Department of Soil, Plant and Food Science, University of Bari Aldo Moro, Bari, Italy
e-mail: simone.pascuzzi@uniba.it

V. Bulgakov

National University of Life and Environmental Sciences of Ukraine, Kyiv, Ukraine

I. Gadzalo

National Academy of Agrarian Sciences of Ukraine, Kyiv, Ukraine

V. Nadykto

Dmytro Motornyi, Tavria State Agrotechnological University, Melitopol, Ukraine

1 Introduction

In many Countries of the world with agricultural production it is generally accepted that the best precursor for winter wheat is fallow [1–3]. Proper fallow field maintenance helps to conserve, store moisture, and kill weeds in the soil by the time winter wheat is sown [4, 5]. According to some scientists, the fallow tillage strategy is based on four mechanisms: 1) lifting roots or rhizomes of perennial weeds to the soil surface to dry them out; 2) conducting tillage at a time when the mass of dry matter of roots is minimal; 3) cutting weed roots into pieces and burying them deep in the soil; 4) lifting roots to the soil surface and removing them [6, 7].

Analysis of this strategy shows that it is mainly aimed at weed control rather than moisture conservation/accumulation. At the same time it is noted [8], that the technical means to implement the mechanisms mentioned above are very difficult to produce [9–11]. One of the most promising areas of fallow cultivation in conditions of soil moisture shortage is a systematic shallow (5–6 cm) loosening it without bringing it to the day surface of the field [12–15]. For practical implementation of this direction can be used a harrow conceived and built by the authors, which is appropriate for fallow land tillage.

The purpose of this article is to present the results of field tests carried out for assessing the operational and technological performance of this harrow for fallow tillage of new construction compared to the one pertinent to a conventional harrow implements.

2 Materials and Methods

The harrow of new concept was built by linking 9 modular harrow sections. Each module section of the harrow was composed by a steel frame on which 20 tines were assembled in compliance to a zig-zag pattern (Fig. 1a). Linking rods allowed to connect each modular section of the harrow to a transversal common beam. This beam was in turn linked to a MTZ-892 tractor with dual 16.9R38 tires (Fig. 1b).

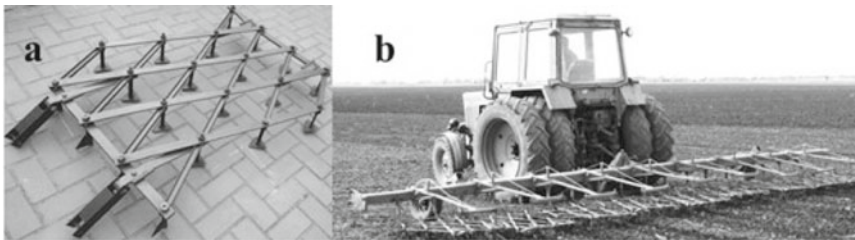


Fig. 1. a. Harrow of new concept; b. Tractor-harrow of new concept for fallow tillage



Fig. 2 Conventional machine-tractor unit for fallow treatment

The performance of the new harrow implement has been compared with that of the aggregate formed by HTZ-17221 tractor and KPS-8 (Ukraine) mounted cultivator with 9 sections (Fig. 2). Each section of this conventional cultivator was equipped with lancet tines.

Experimental studies were carried out under field conditions characterized by such geographic data (46°5 0′56″ north latitude, 35°2 1′55″ east longitude, altitude: 37 m) and soil type – dark chestnut chernozem. The granulometric composition of the soil was heavy loamy since the content of physical clay is 46–48%. The humus content is in the range of 2.8–3.6%, and the reaction of the soil solution was close to neutral.

Before conducting the field studies, we measured soil density and moisture in the 0–15 cm layer. Both parameters were determined along the field diagonal with a step of 1 m and the number of measurements not less than 30.

The longitudinal profile of the field was measured with a special profile measurer developed by authors (Fig. 3). It was mounted on a 4 m long rod placed parallel to the field surface. The lever of the device contacted the field profile with one end, and the other end is pivotally fixed on the axis connected to the SP-3A variable resistance. When the instrument was moved along the rail, the lever makes oscillating movements in the longitudinal-vertical plane, thus changing the SP-3A resistance value.

The generated electrical signal was fed to the analog input of the Arduino Uno (Italy), and then to the computer with its subsequent conversion for processing in Microsoft Excel.

The oscillations of the longitudinal field profile were recorded on a 100 m section. For this purpose, 25 permutations of the profiler were made. The rate of instrument movement along the rail was approximately 0.05 m s^{-1} . The periodicity of recording an electric signal at the Arduino input was 1 s. This made it possible to obtain at least 80 values of the field profile ordinates on each installation of the profiler. There were at least 2000 such measurements on a 100 m section. The error of measuring the oscillations of the field profile by this device does not exceed $\pm 0.5 \text{ cm}$.

The depth of tillage by both compared machine-tractor units was measured along the diagonal of the plot in twofold replications. The step of measurement of this



Fig. 3 Instrument for measuring longitudinal field profile

parameter was 0.2 m, and the number of measurements in each repetition was not less than 300. To measure the depth of tillage we used an ad hoc device, created by authors based on HC-SR04 ultrasonic sensor (China) and Arduino UNO board (Italy). The error of measuring the depth of tillage with this device does not exceed ± 0.5 cm.

For the obtained values of tillage depth of the fallow field, in addition to the mean, mean square values and the normalized correlation function, we determined two other performance indicators: i) the probability (P , %) of maintaining the technological tolerance for variations in the soil loosening depth; ii) the frequency of deviation (N , m^{-1}) of the actual value of the soil tillage depth from the specified tolerance.

The first of these indicators (P) has been calculated by the formula [16]:

$$P = 2 \cdot F \cdot \left(\frac{\Delta}{\sigma} \right) \quad (1)$$

where F is the tabulated Laplace function; Δ is the tolerance for fluctuations in the depth of steam field treatment, \pm cm; σ is the root mean square deviation of the depth of fallow field treatment, \pm cm.

To calculate the second indicator (N), we have used the following relationship [16]:

$$N = \left[\frac{2}{n} \sum_{i=0}^n (\tau_{i+1} - \tau_i) \right]^{-1} \cdot e^{\left(-\frac{\Delta^2}{2\sigma^2} \right)} \quad (2)$$

where n is the number of points where the normalized correlation function crosses the abscissa axis; τ_i and τ_{i+1} are the consecutive abscissa values at the points where the normalized correlation function takes zero values.

During the field study, both units were monitored for 3 working days of at least 8 h each. In the process of observations, using a stopwatch FS-8200 (China), we recorded the time spent by each unit for: i) performance of basic work; ii) turns; iii) technological maintenance; iv) elimination of technological failures; v) technical

maintenance; vi) elimination of technical failures; and vii) moving the unit from the place of basic parking to the field and vice versa.

Working width and driving speed of each machine were determined by the methodology described in [17, 18].

To eliminate the influence of the subjective factor, the same machine operator alternately worked on both tillage units (conventional and new).

To ensure the reliability of experimental data, the arrays of measured parameters (tillage depth, field profile ordinates, etc.) were checked for the presence of doubtful values. For this purpose, the well-known K_I criterion was used [19]. Its value has been calculated by the following expression:

$$K_I = \frac{Y_n - Y_{n-1}}{\sigma} \quad (3)$$

where Y_n is the questionable experimental version of the measured parameter; Y_{n-1} is the closest thing to a questionable option; σ is the standard deviation of the measured parameter.

The calculated values through Eq. (3) were compared with the table values accepted for the statistical significance level of 0.05. In case of violation of condition (3), the doubtful variant of the measured parameter was excluded from the data set [19].

3 Results and Discussion

The data analysis showed (Table 1) that the new harrowing machine-tractor unit was 11.4% more productive. This advantage is practical due to the greater working width of the new tractor-machine unit.

The utilization coefficients of the working and operating time in both units were almost identical. Even at the statistical significance level of 0.01 (confidence level of 99%), the obtained difference in the values of these coefficients was purely random, and therefore the null-hypothesis of their equality was not rejected.

For such a technological process as fallow treatment, agronomic requirements for the tolerance of fluctuations in the depth of tillage are not officially formulated. Considering this for further analysis, we assumed that the value should not exceed ± 1 cm to ensure minimum moisture loss while harrowing. This is half as much as the commonly known equivalent value set for ploughing.

Because for the research harrowing machine-tractor unit $\sigma = \pm 0.8$ cm (see Table 1), the ratio $\Delta \bullet \sigma^{-1} = 1 \bullet 0.8^{-1} = 1.25$. As follows from common reference table data [15], the Laplace function for this value is 0.39. Given the above formula for the value P , it turns out that the probability of preserving the new harrow and tractor unit of fluctuations in the depth of the fallow field cultivation at the level of ± 1 cm is 78%.

Table 1 Operational and technological performance of tested tillage machines and tractors

Indicator	Harrowing implement-tractor unit	
	Conventional	New
Unit composition:		
tractor implement	HTZ-17221 KPS-8	MTZ-892 BP-9
Operating mode:		
– working width, m	7.9	8.7
– speed movement, km h ⁻¹	8.9	9.0
– depth of cultivation, cm	12	6
Performance, ha h ⁻¹ :		
– main time	7.0	7.8
– variable time	6.2	6.9
– operating time	6.1	6.8
Coefficients:		
– use of working time	0.89	0.88
– use of operating time	0.87	0.87
– reliability of the technological process	0.99	0.99
– use of working strokes	0.90	0.93
Agrotechnical indicators:		
– average value of the tillage depth, cm	12.3	5.8
– tillage depth stability, \pm cm	1.8	0.8

As mentioned above, the frequency of deviation of the actual value of tillage depth (h) from the specified tolerance was estimated using the normalized correlation function of this process and Eq. (2). Analysis of this function shows that fluctuations of the parameter h have some hidden periodic component (Fig. 4). The correlation length in this case is 1 m. This is the value of the abscissa at which the first intersection of the correlation function with the zero line takes place.

As a result, the calculations based on Eq. (2) show that the value of the parameter N is 0.66 m⁻¹. It means that for every 1.5 m of the tillage unit path, one deviation case of the fallow field treatment depth oscillating from the tolerance within ± 1 cm is possible. This result is acceptable.

For comparison: the probability of keeping the conventional cultivator unit tolerance $\Delta = \pm 1$ cm at $\sigma = 1.8$ cm (see Table 1) is 44%, i.e. almost half as much. In this case, the parameter N is 1.23 m⁻¹. It means that for each 0.81 m, there can be one case of the processing depth deviation of the fallow field from the accepted tolerance within limits ± 1 cm.

And this result is quite logical because the uniformity of the tillage depth with a new harrowing unit is significantly higher than the conventional harrowing machine-tractor unit (Fig. 5).

Fig. 4 Normalized correlation function of the furrow depth for measuring tillage depth

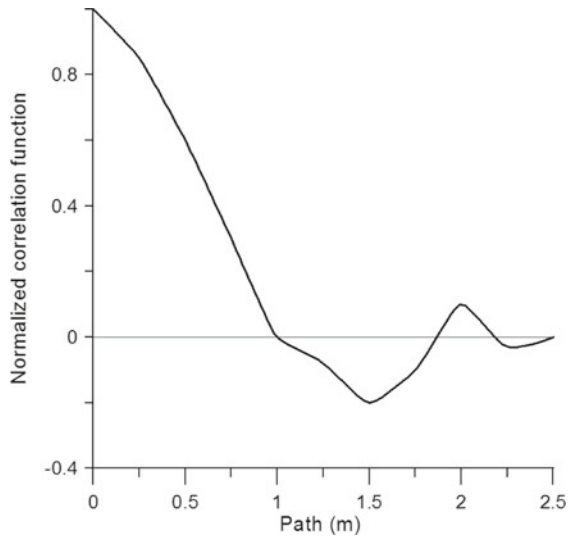
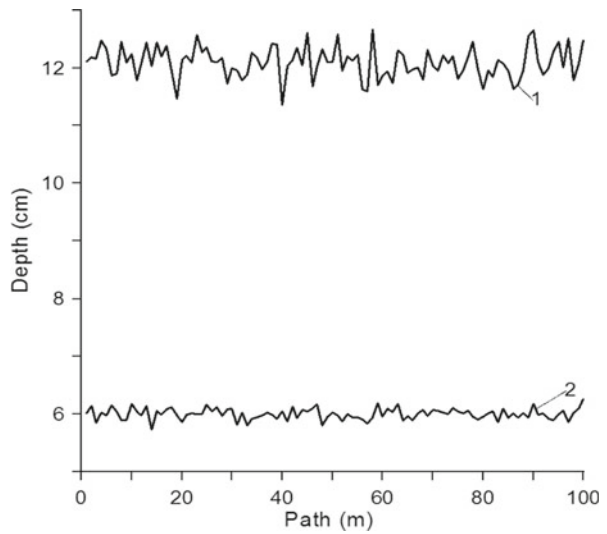


Fig. 5 Longitudinal profile of the field after the pass of conventional (1) and new (2) harrowing units



Analyzing this figure, we see that the depth of the conventional machine-tractor unit cultivation (curve 1 in Fig. 5) ranged from 11 to 13 cm. At the same time, after the passage of the new harrowing unit, the profile of the treated field (curve 2 in Fig. 5) changed in a twice narrower range: from 5.5 to 6.5 cm.

Comparing the variances of this parameter (3.24 cm^2 and 0.64 cm^2) by Fisher's F-criterion, we can say that the null hypothesis of their equality at almost any statistical significance level is rejected.

Thus, the obtained results indicate the significant advantages of our new harrow unit based on a new harrow tool designed for soil fallow cultivation in arid conditions, i.e. with the existing soil moisture deficit. And this unequivocally indicates that the uniformity of the depth of tillage by the new harrow unit is naturally higher than the conventional cultivator machine and tractor unit.

4 Conclusions

Using a new machine-tractor unit equipped with a new harrowing tool for fallow treatment in conditions of lack of soil moisture compared to the conventional machine-tractor unit of similar purpose increases productivity by at least 11%.

With a probability of 95%, there is every reason to believe that the uniformity of the depth of tillage harrowing machine-tractor unit equipped with a harrow of a new design is higher than the conventional cultivator unit for similar purposes.

Acknowledgements The Authors equally contributed to the present study.

References

1. Ghimire, R., Ghimire, B., Mesbah, A.O., Sainju, U.M., Idowu, O.J.: Soil health response of cover crops in winter wheat-fallow system. *Agron. J.* **111**, 2108–2115 (2019). <https://doi.org/10.2134/agronj2018.08.0492>
2. Schillinger, W.F., Papendick, R.I.: Tillage mulch depth effects during fallow on wheat production and wind erosion control factors. *Soil Sci. Soc. Am. J.* **61**, 871–876 (1997)
3. Smith, E.G., Peters, T.L., Blackshaw, R.E., Lindwall, C.W., Lamey, F.J.: Economics of reduced tillage fallow-crop systems in the dark brown soil zone of Alberta. *Can. J. soil Sci.* **76**, 411–416 (1996). <https://doi.org/10.4141/cjss96-049>
4. Riar, D.S., Ball, D.A., Yenish, J.P., Wuest, S.B., Corp, M.K.: Comparison of fallow tillage methods in the intermediate rainfall inland Pacific Northwest. *Agron. J.* **102**, 1664–1673 (2010). <https://doi.org/10.2134/agronj2010.0054>
5. Donaldson, E., Schilinger, W.F., Dofing, S.M.: Straw production and grain yield relationships in winter wheat. *Crop Sci.* **41**, 100–106 (2001)
6. Lötjönen, T.; Salonen, J.: Intensifying bare fallow strategies to control *Elymus repens* in organic soils. *Agric. Food Sci.* **25**, 153–163 (2016). <https://doi.org/10.23986/afsci.55533>
7. Melander, B.; Nørremark, M.; Kristensen, E.F.: Combining mechanical rhizome removal and cover crops for *Elytrigia repens* control in organic barley systems. *Weed Res.* **53**, 461–469 (2013). <https://doi.org/10.1111/wre.12042>
8. Kristensen, E.F., Melander, B., Nørremark, M.: New optimized technique for mechanical control of *Elymus repens*. In: International Conference on Agricultural Engineering, Clermont Ferrand, France, pp. 1–8 (2010)
9. Bulgakov, V., Pascuzzi, S., Adamchuk, V., Kuvachov, V., Nozdrovicky, L.: Theoretical study of transverse offsets of wide span tractor working implements and their influence on damage to row crops. *Agriculture* **9**, 144 (2019). <https://doi.org/10.3390/agriculture9070144>
10. Bulgakov, V., Pascuzzi, S., Ivanovs, S., Nadykto, V., Nowak, J.: Kinematic discrepancy between driving wheels evaluated for a modular traction device. *Biosyst. Eng.* **196**, 88–96 (2020). <https://doi.org/10.1016/j.biosystemseng.2020.05.017>

11. Bulgakov, V., Ivanovs, S., Nadykto, V., Kaminskiy, V., Shymko, L., Kaletnik, H.: Movement stability of a section of the machine for black fallow cultivation in a longitudinal-verticale plane. *INMATEH Agric. Eng.* **62**, 99–106 (2020). <https://doi.org/10.35633/inmateh-62-10>
12. Adamchuk, V.; Bulgakov, V.; Nadykto, V.; Ivanovs, S. Investigation of tillage depth of black fallow impact upon moisture evaporation intensity, in: *Engineering for Rural Development 2020*, 377–383. <https://doi.org/10.22616/ERDev2020.19.TF090>
13. Bulgakov, V., Nadykto, V., Kaminskiy, V., Ruzhylo, Z., Volskyi, V., Olt, J.: Experimental research into the effect of harrowing unit's operating speed on uniformity of cultivation depth during tillage in fallow field. *Agron. Res.* **18**, 1962–1972 (2020). <https://doi.org/10.15159/AR.20.200>
14. Drew, J.L., Baltensperger, D.D., Blumenthal, J.M., Burgener, P., Harveson, R.M.: Eliminating summer fallow reduces winter wheat yields, but not necessarily system profitability. *Crop Sci.* **44**, 855–860 (2004)
15. Bulgakov, V., Pascuzzi, S., Ivanovs, S., Santoro, F., Anifantis, A.S., Ihnatiev, I.: Performance assessment of front-mounted beet topper machine for biomass harvesting. *Energies* **13**, 3524 (2020). <https://doi.org/10.3390/en13143524>
16. Jeff Wu, C.F.; Hamada, M.S.: *Experiments: Planning, Analysis, and Optimization*. Wiley, Hoboken (2011)
17. Nadykto, V., Kyurchev, V., Bulgakov, V., Findura, P., Karaiev, O.: Influence of the plough with tekron moldboards and landsides on ploughing parameters. *Acta Technol. Agric.* **1**, 40–45 (2020). <https://doi.org/10.2478/ata-2020-0007>
18. Pascuzzi, S., Anifantis, A.S., Santoro, F.: The concept of a compact profile agricultural tractor suitable for use on specialised tree crops. *Agriculture* **10**, 123 (2020). <https://doi.org/10.3390/agriculture10040123>
19. Irwin, J.O.: On a criterion for the rejection of outlying observations. *Biometrika* **17**, 238–250 (1925). <https://doi.org/10.2307/2332079>

Concept of a Foldable Transmission Chain Used Inside Tobacco Leaves Harvesting Machine



Simone Pascuzzi, Katarzyna Łyp-Wrońska, Francesco Santoro, and Francesco Vicino

Abstract Italy is the first tobacco producing Country in the European Union with high quality standards of the product. A foldable facilitating arm suitable for the black tobacco “Kentucky” leaves harvesting has been studied in this paper together with the articulated chain placed inside. This chain underwent to a patented modification to make it consistent with the characteristics of the foldable facilitating arm. Experimental tests during a tobacco leaves harvesting campaign were carried out to evaluate both the performance of the modified articulated roller chain and the harvesting chain as a whole, which consisted of the aforesaid facilitating arm made connected to a four-wheel drive tractor and to a trailer, which supported a steel structure suitable to arrange the harvested leaves. Throughout the work phases, the forward speed of the tractor was $V_a = 0.46 \text{ m s}^{-1}$ (1.66 km h^{-1}), whereas the running velocity of the chain $V_c = 0.45 \text{ m s}^{-1}$. In these operative conditions the work capacity of the harvesting chain employed was 0.48 ha h^{-1} and its harvesting capacity $765 \text{ leaves h}^{-1}$. During the tests carried out, the articulated chain inside the facilitating arm operated constantly without discrepancy.

Keywords Joint · Roller shackles · Motion efficiency · Foliage picking

1 Introduction

In 2021, the total area dedicated to tobacco cultivation in Italy has been 12,857 ha with a harvested production of 41,012 ton. Italy is the first tobacco producing Country in the European Union, but it faces competition from various realities such as India, Brazil, Southern Africa, where production and labor costs as well quality standards of the product, with reference to its traceability, are lower than the Italian ones [1, 2].

S. Pascuzzi (✉) · F. Santoro · F. Vicino
Department of Soil, Plant and Food Science, University of Bari Aldo Moro, Bari, Italy
e-mail: simone.pascuzzi@uniba.it

K. Łyp-Wrońska
AGH University of Science and Technology, Cracow, Poland

© The Author(s), under exclusive license to Springer Nature Switzerland AG 2023
V. Ferro et al. (eds.), *AIIA 2022: Biosystems Engineering Towards the Green Deal*,
Lecture Notes in Civil Engineering 337,
https://doi.org/10.1007/978-3-031-30329-6_84

The Italian Region most suited to tobacco cultivation is Umbria, with cultivated area of 35% and harvested production of 31% respectively, of the Italian ones [1]. Virginia Bright and Kentucky tobaccos are mainly produced in Umbria, as well as in Tuscany for the production of the famous Tuscan cigars. Currently, many tobacco farmers in Umbria and Tuscany harvest leaves manually aided by facilitating machines, which are self-propelled or mounted to agricultural tractors [3, 4]. Generally, the self-propelled machines are equipped with hydrostatic traction and during harvesting, seated operators manually detach the leaves from the plants and unload them in a basket [5, 6]. Conversely, the mounted machines mainly consist of a conveyor belt of about 12–15 m in length that hydraulically can be folded [7]. During the harvesting operations, the conveyor belt is placed transversely with respect to the tractor forward direction at an height of 1.0 to 1.70 m above the soil. To collect the leaves, the machine is followed at the rear by workers on foot that manually detach the leaves from the plants and place them on the conveyor belt. The leaves are then unloaded at one of the two ends on a trailer pulled by a tractor that moves on the side road that flanks the fields [8].

In this regard, the Pulcinelli Giovan Battista Ltd. manufacturer, located in S. Leo di Anghiari (Arezzo province, Italy), designed and developed an agricultural implement, suitable for the harvesting of black tobacco “Kentucky” leaves devoted to cigars production. This machine was equipped with a foldable arm supporting an articulated roller chain at its inside [9, 10]. The articulated roller chain, in turn, which worked as a conveyor belt for the detached leaves, underwent to a patented modification to make it suitable for the motion transmission and simultaneously consistent with the possibility to fold the arm. This paper reports the main characteristics of the modified roller chain and the evaluation of its performance inside the facilitating arm during the tobacco leaves harvesting operations.

2 Materials and Methods

2.1 *The Agricultural Implement for Facilitating the Tobacco Leave Harvesting*

The agricultural implement designed and developed by “Pulcinelli Giovan Battista Ltd.” manufacturer mainly consists of a steel box profiles support frame, which has to be connected to the rear 3-point hitch of an agricultural tractor (“fully mounted coupling”) (1 in Fig. 1). A facilitating arm built with two steel truss beams, each long about 6 m and jointed each other was linked to this support frame by a cylindrical joint. The beam directly connected to the support frame (2 in Fig. 1) can only rotate around a vertical axis [11, 12]. Therefore, it can be positioned transversely to the tractor forward direction during the leaf harvesting operations or be arranged parallel to the tractor forward direction in order to allow the transportation of the agricultural implement on public roads (Fig. 1). The other end of this steel truss beam is linked

Fig. 1 Kentucky Black tobacco leaves facilitating arm manufactured by Pulcinelli Giovan Battista Ltd.: 1. support frame linked to the rear 3-point hitch of the tractor; 2. folded truss beam arranged parallel to the tractor forward direction



to a second steel truss beam, through another cylindrical joint can rotate with respect to the first one in a vertical plane by way of a hydraulically operated mechanism. Therefore, it can be positioned horizontally aligned with the other beam for the harvesting operations or be positioned overturned so to reduce the overall size of the arm (Fig. 1). The mutual rotation of the two truss beams in the vertical plane is an effective solution because it allows to considerably reduce the sizes of the agricultural implement for the transport phases [13].

The truss beams horizontally aligned arranged support a conveyor belt, which is mainly composed of an articulated roller transmission chain connecting two toothed wheels located at the opposite ends of both the truss beams [14]. A hydraulic motor, which is connected through a control unit to the hydraulic linkage of the tractor, gives the motion to the drive toothed wheel, mounted near the support frame. Conversely, the idler toothed wheel is positioned at the far end of the second beam [14].

2.2 Alteration Applied to the Articulated Roller

The use of the roller chain for the transmission of motion between toothed wheels requires a suitable coupling between the teeth of the wheels and the empty spaces between the links of the chain itself [15, 16]. Due to their structure, the main limitation of the articulated chains is that they can undergo pleats, allowed by the reciprocal rotations between the individual links, only in their operational plan [17]. Conversely, bendings or complete folds are not possible in any plane other than the operational one.

Inside the agricultural implement made by Pulcinelli Giovan Battista Ltd., the articulated roller chain fulfils the entire path between the toothed wheels in the horizontal operative plane, involving both beams horizontally aligned arranged. Obviously, this occurs throughout the working conditions of the machine. On the other hand, the arm was built using two truss beams hinged to each other at one end, so as to overturn one beam on the other one. But this overturning of the beam would

not be allowed according to the characteristics of the roller chain. To overcome this mismatch, it has been necessary to study a mechanical solution that would permit also to the chain to bend in correspondence of the joint connecting the beams.

The solution consisted in replacing two portions of equal length L_n , arranged symmetrically on opposite sides of the roller chain with corresponding portions of ring chains having lengths that did not change the original overall length L of the articulated roller chain (Fig. 2).

Therefore, on each of the opposite sides of the roller chain, N links corresponding to 4 teeth in succession of the toothed wheels, were replaced by two sections of ring chain. Figure 3 shows the detail of the roller chain highlighting the removal of 4 consecutive links replaced by two sections of chain with rings. The two ring chains sections are connected, by means of solid pins, on the external sides of the disconnected links, so as to leave a free space consistent with the thickness of the wheels. The teeth of the wheel corresponding to the missing section of the roller chain then can enter between the two sections of the ring chain, without hindering the motion (Fig. 3).

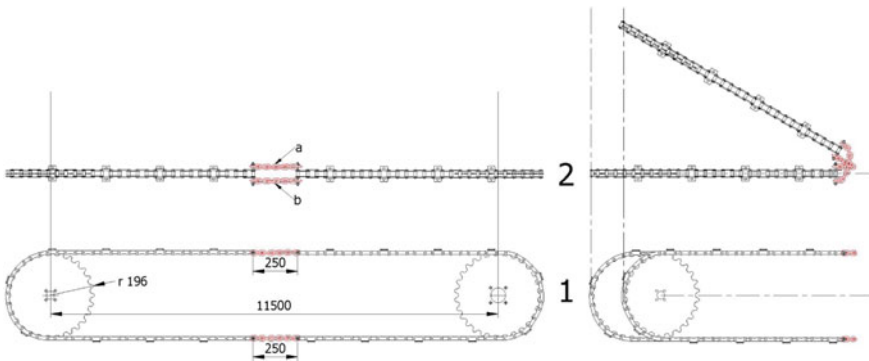


Fig. 2 Roller chain coupled with the toothed wheels, with the portions on opposite sides replaced by ring chain portions. 1. Front view. 2. Side view. Not folded chain at the left, folded chain at the right

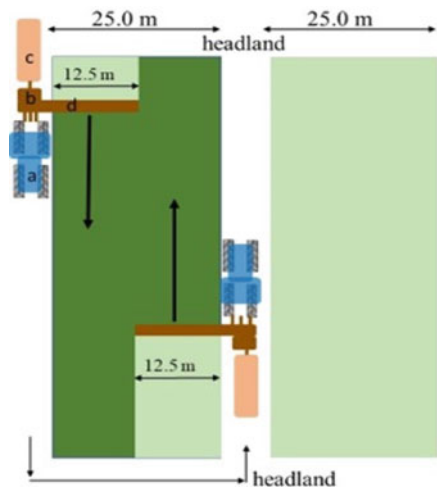


Fig. 3 Teeth of the wheel entered between the two sections of the ring chain

2.3 Field Tests

In the 31st week of 2021, experimental tests of tobacco leaves harvesting were carried out in a black tobacco “Kentucky” plantation devoted to Tuscan cigars production, located on a farm in the territory of Anghiari (Arezzo Province, Tuscany, Italy). The tobacco plants were placed on a flat cultivable land with controlled growth weed and irrigation with a layout of 1.0 m × 1.0 m, giving a density of about 10,000 plant ha⁻¹. Furthermore, the cultivation was arranged on soil bands having width 25.0 m. Each band was separated from the adjacent one by a lane having width of about 2.5 m for the machines transits (Fig. 4). The harvesting chain consisted of the agricultural implement built by Pulcinelli Giovan Battista Ltd., linked to the rear 3-point hitch of a four-wheel drive tractor and by a drawbar to a trailer equipped with a steel frame suitable to arrange the harvested leaves. The length of the facilitating arm, i.e. its working front, was 12.5 m and then the tractor first advanced in a direction laterally outside along the tobacco band. Subsequently, at the headland, the tractor with the aggregates rotated and transited the other lane adjacent to the same band in the opposite direction. In this way, the entire tobacco plants bandwidth was undergone to the harvesting operations (Fig. 4). During the tests, the tractor forward speed V_a and the running velocity of the chain V_c were kept constant and chosen according to the owner farmer’s experience. These two parameters, very important for evaluating the implement work capacity, were closely related both to the amount of leaves to be harvested, in turn linked to the phenological state of the tobacco cultivation, and to the available labour at the time of harvesting. Furthermore, the functioning of the modification made to the articulated chain inside the facilitating arm was evaluated from a qualitative point of view.

Fig. 4 Scheme of the tobacco leaves harvesting operations with sizes of the crop and of the implement working front. a. tractor; b. support frame; c. facilitating arm; d. trailer for the harvested tobacco leaves storage



3 Results and Discussion

Throughout the work phases, the tractor slowly advanced laterally outside the tobacco field and 3 workers followed on foot the facilitating arm among the tobacco plants, choosing, harvesting, and hanging the leaves on hooks, in turn strictly linked to the articulated roller chain (Fig. 5a). Conversely, other 2 workers, which were on the support frame, detached the leaves from the hooks of the chain and placed them on special iron bars about 1.70 m long (Fig. 5b). Each bar was filled with about 20–24 leaves in a time of 50 s and then another worker hauled it on the frame mounted on the trailer (Fig. 5c). The forward speed of the tractor was $V_a = 0.46 \text{ m s}^{-1}$ (1.66 km h^{-1}), whereas the running velocity of the chain $V_c = 0.45 \text{ m s}^{-1}$. In these operative conditions the work capacity of the harvesting chain employed was 0.48 ha h^{-1} and the harvesting capacity was $765 \text{ leaves h}^{-1}$. The harvested leaves, arranged on the frame placed on the trailer, were then ready for the subsequent drying process, required to give the valuable final characteristics to the tobacco. At the end of the harvesting operations the arm was folded and arranged for its transport on the road.

Finally, throughout the tobacco leaves collection operations carried out, the articulated chain inside the facilitating arm worked continuously without jamming problems. The ring chain sections inserted along the articulated roller chain did not create any mismatches in the coupling with the teeth of the wheels and the transmission of motion between the toothed wheels took place with evenness.

Fig. 5 Tobacco leaves harvestings



4 Conclusions

An articulated joint suitable for installation in roller chains has been studied, engineered, and patented in Italy, making it possible to fold the widespread and widely used roller chains on planes other than the operational one. The good performance of the facilitating arm for the harvester of tobacco leaves, in which the roller chain fitted with the created articulated joint has been mounted, did not show any deterioration in terms of productivity, strength and reliability, and therefore highlighted the correct behavior of the device.

Other tests are planned to evaluate the efficiency of the described alteration made on articulated roller chain when used to transmit the motion between toothed wheels, which involve torques and speeds higher than those ones required by the tested facilitating arm.

Acknowledgements The Authors equally contributed to the present study.

References

1. ISTAT (Italian Central Statistics Institute) (2022). <http://dati.istat.it/Index.aspx?QueryId=33707>. Accessed 14 Sept 2022
2. FAO 2018: Food and Agriculture Organization of the United Nations. <https://www.fao.org/fao-stat/en/#data/QCL>. Accessed 14 Sept 2022
3. Masanotti, G.M., Abbafati, E., Petrella, E., Vinciguerra, S., Stracci, F.: Intensive tobacco cultivations, a possible public health risk? *Environ. Sci. Pollut. Res.* **26**, 12616–12621 (2019)
4. Bulgakov, V., Pascuzzi, S., Ivanovs, S., Santoro, F., Anifantis, A.S., Ihnatiev, I.: Performance assessment of front-mounted beet topper machine for biomass harvesting. *Energies* **13**, 3524 (2020). <https://doi.org/10.3390/en13143524>
5. Schmitt, N.M., Schmitt, J., Kouimintzis, D.J., Kirch, W.: Health risks in tobacco farm workers: a review of the literature. *J. Public Health* **15**, 255–264 (2007)
6. Bulgakov, V., Pascuzzi, S., Ivanovs, S., Nadykto, V., Nowak, J.: Kinematic discrepancy between driving wheels evaluated for a modular traction device. *Biosyst. Eng.* **196**, 88–96 (2020). <https://doi.org/10.1016/j.biosystemseng.2020.05.017>
7. Lecours, N., Almeida, G.E.G., Abdallah, J.M., Novotny, T.E.: Environmental health impacts of tobacco farming: a review of the literature. *Tob. Control* **21**, 191–196 (2012). <https://doi.org/10.1136/tobaccocontrol-2011-050318>
8. Damalas, C.A., Georgiou, E.B., Theodorou, M.G.: Pesticide use and safety practices among Greek tobacco farmers: a survey. *Int. J. Environ. Health Res.* **16**, 339–348 (2006)
9. Kanehira, M., Otani, T., Yoshikawa, M., Takahashi, T.: *The Complete Guide to Chain*. U.S. Tsubaki, Inc. Wheeling Illinois (1997)
10. Pascuzzi, S., Anifantis, A.S., Santoro, F.: The concept of a compact profile agricultural tractor suitable for use on specialised tree crops. *Agriculture* **10**, 123 (2020). <https://doi.org/10.3390/agriculture10040123>
11. Bulgakov, V., Pascuzzi, S., Adamchuk, V., Ivanovs, S., Pylypaka, S.: A theoretical study of the limit path of the movement of a layer of soil along the plough mouldboard. *Soil Tillage Res.* **195**, 104406 (2019)
12. Bulgakov, V., Pascuzzi, S., Anifantis, A.S., Santoro, F.: Oscillations analysis of front-mounted beet topper machine for biomass harvesting. *Energies* **12**(14), 2774 (2019). <https://doi.org/10.3390/en12142774>

13. Bulgakov, V., Pascuzzi, S., Adamchuk, V., Kuvachov, V., Nozdrovicky, L.: Theoretical study of transverse offsets of wide span tractor working implements and their influence on damage to row crops. *Agriculture* **9**, 144 (2019)
14. Lodge, C.J., Burgess, S.C.: A model of the tension and transmission efficiency of a bush roller chain. *J. Mech. Eng. Sci.* **216**(4), 385–394 (2002)
15. Tsubakimoto Chain Company: *The Complete Guide to Chain - Reference Handbook*. Sachio Shimura, Osaka Japan (2006)
16. Hollingworth, N., Hills, D.A.: Forces in a heavy duty drive chain during articulation. *J. Mech. Eng. Sci.* **200**(5), 367–374 (1986)
17. Naji, M.R., Marshek, K.M.: Experimental determination of the roller chain load distribution. *J. Mech. Transm. Autom. Des.* **105**, 331–338 (1983)

Assessment of Soil and Vegetation Index Variability in a Traditional Olive Grove: A Case Study



C. Perna, D. Sarri, A. Pagliai, S. Priori, and M. Vieri

Abstract Precision Agriculture (PA) is nowadays one of the most feasible solutions to reduce input and pollution in agriculture [1]. One of PA's most important techniques is identifying in-field spatial variability. Multiple techniques can be used to identify the variability: soil analysis and vegetation index identification are two of the most applied. In this study, the variability of an olive grove was assessed to evaluate the best option for creating variability maps and assessing the relationship between soil and vegetative variability in the case study. The study was carried out in two olive orchards, with a 6×4 m planting layout; the mean plants' height was 3 m. To assess soil variability an EMI (Electromagnetic Induction) analysis was performed. The field was completely mapped at 0–50, 100 cm deep. After the evaluation of the electric resistivity, maps were created. The proximal OptRx Crop Sensor (Ag Leader, Iowa, USA) was used to assess the plant vegetation index. This sensor was mounted on a tractor and positioned at a height of 2 m from the ground to assure the acquisition of the vegetation index for all the assessed plants. NDVI and NDRE indexes were measured. To georeferenced all the acquisitions, a GNSS system was installed on the tractor (Ag Leader GPS6500 GNSS receiver, Ag Leader, Iowa, USA). Through this method, site-specific olive canopy NDVI NDRE data gathering was performed. Soil characterization maps revealed significant in-field differences in electric resistivity for all the evaluated depths, through this analysis a homogeneous resistivity-value map was created. The data points of every sampling were interpolated within the whole plots by ordinary kriging through the GIS software QGIS (GNU General Public License). NDVI and NDRE predictive maps were developed using ordinary kriging fitting the best variogram. An exploratory correlation analysis was performed between NDVI, soil proximal sensing (EMI 0.5, EMI 1, RP), and soil strength,

C. Perna (✉) · D. Sarri · A. Pagliai · M. Vieri
Department of Agriculture, Food, Environment and Forestry (DAGRI), University of Florence,
Piazzale Delle Cascine 15, 50144 Florence, Italy
e-mail: carolina.perna@unifi.it

S. Priori
Department of Agrarian and Forestry Sciences (DAFNE), University of Tuscia, Via San Camillo
de Lellis, 01100 Viterbo, Italy
Princeton University, Princeton, USA

to highlight the statistical relationships between the main parameters used for this study. Collected data were analysed and interpolated by k-means clustering to make thematic maps.

Keywords Precision agriculture · Data collection · Olivegrowing · Innovation

1 Introduction

Nowadays Precision Agriculture is widely recognized as one of the most practical ways to reduce input and pollution in agriculture in general [1] and in olive production specifically [2]. Studies also demonstrate how PA can be a valid instrument to estimate the potential yield and quality of olive production, allowing at the same time to reduce climatic impact by lowering emissions [2–5]. To apply PA techniques, the fundamental is data gathering, particularly regarding soil and plant vigour variability: the multi-dimensional approach to data gathering and every data collected can lead to an added value for farm management and production [6]. As a matter of fact, by studying variability, it is possible to assess the correct management of various in-field operations (i.e. fertilization, tillage, cover crop seeding). Plant vigour indexes (NDVI, NDRE, NDWI) are already well established as a practical way to obtain data about spatial variability in olive growing, but the used sensor to acquire that information may vary: it is considered more viable to use remote sensing instead that proximal sensing [7], even if the latter can provide more specific and precise information.

Electromagnetic Induction sensors are the most reliable solution to assess soil variability, even if studies demonstrate that soil resistance to penetration can also be a valid source of data for precision agriculture purposes [8, 9].

The objectives of this case study are to assess the variability in soil characteristics and plant vigour in an olive orchard and to verify the reliability of vegetation index proximal sensors and soil resistance to penetration sensors, by creating variability maps and assessing the relationship between soil and vegetative variability. The final purpose is to evaluate the critical issue of proximal sensing instruments in olive cultivation.

2 Materials and Methods

The experimentation was carried out in an olive orchard in Montalcino (Tuscany, Italy) at 42.99771619654586, and 11.458105541925473. This area is classified as Warm-summer Mediterranean climate (Csb) in the Köppen Climate Classification; characterised by dry and warm summers. The soil is typical of the Anti-Appennine chains of Tuscany and characterised by Cambisol, Luvisol and Leptosol soils, expressed as Reference Soil Group of World Reference Base of Soil resources

[10]. The experimentation site was 0.2 ha, the olive grove had a planting layout of 6×4 m, and the plants had an average height of 3.5 m, with traditional canopy management. The soil management included tillage in the first part of summer, allowing the soil to be bare of weeds. The tillage was performed in the first cm of the soil and didn't compromise the structure of its deeper layers.

In this experiment, three different kinds of sensors were used: a dynamometric knife, a vegetation vigour sensor, and an EMI (Electromagnetic Induction) sensor. The dynamometric knife was composed mainly of a steel pivoted knife connected to a load cell. The measurement principle was based on a first-order lever. This allows for achieving the load force (N) necessary to perform a cut at specific deep and to obtain a measure of the soil resistance to penetration (RP). Then, the collected data was related to the contact surface between the knife and soil to get the specific pressure (MPa). The instrument was coupled with a standard three-hitch point and is adjustable for acquiring data at a depth ranging from 0 to 0.4 m. The data acquisition was performed through a signal sensor processor, i.e. a CM-2T load cell.

The software allowed the collection of the force required to cut the soil at the pre-established depth, and the relative geographical position in real-time [11]. The dynamometric knife was combined with a Kubota B2420 tractor mounted with a GPS6500 GNSS receiver (AgLeader Technology, Ames, IO, USA) on the rear part. Data acquisition was performed by creating a grid throughout the experimentation site, following the tractor path. The pre-established depth was 25 cm, this depth was chosen as it represents the most susceptible soil fraction to compaction.

The vegetation vigour sensor used was the OptRx® Crop Sensors (AgLeader Technology, Ames, IO, USA). This sensor was mounted in the central part of the tractor, on the right side of the Roll-Over Protective Structure (ROPS). The OptRx sensor was placed and coupled with the hardware and the rough book for data collection and storing and arranged parallel to the vertical canopy axis, to avoid any noises of soil and grass. It was positioned at 1,8 m, as it is assumable a good olive canopy vegetation density at this height. The OptRx measures the reflectance in the 630–685 nm (red), 695–750 nm (red edge) and 760–850 nm (NIR—Near InfraRed) wavebands, which were used to process the NDVI and NDRE indexes. The data was collected by creating a grid through the orchard to obtain vegetation index data for all the olive canopies.

The EMI sensor used in the experimentation was the EM38-Mk2 electromagnetic induction sensor (Geonics Ltd., Ontario, Canada), EM38-Mk2 measures the soil's apparent electrical conductivity (ECa) across two depth ranges of 0–75 (ECa1) and 0–150 cm (ECa2), approximately [12].

The collected data had to be processed and to do so, two software were used. RStudio (RStudio, PBC) statistical software was used to process the statistical analysis. Three RStudio's packages were used in the statistical analysis, namely: DescTools, rcompanion and caret. To analyse the data with geostatistical methods, QGIS software (QGIS.org, 2022. GNU General Public License) was used. The data were cleaned, specifically by removing wrong data (i.e. negative values) and out-layer (i.e. values outside the threshold of the vegetative indexes). After the cleaning, with the QGIS software, the data were processed to obtain a 2×2 m point grid; this

was necessary for obtaining uniform, analysable data. At each point was attributed a value of every variable of interest (NDVI, NDRE, Resistance to Penetration, and soil resistivity) was through the nearest neighbour value attribution function. Based on the new data grid, statistical analysis was performed.

R-squared and correlation between the variables were performed to evaluate the degree of dependence. Some data transformations were required and performed through logarithmic transformation and Turkey transformation.

A K-mean analysis was performed to comprehend in-field variability and variation between and within data. Three clusters were created based on the values of the variable, with a maximum of 25 random centroids and 10 iterations. Basic statistical analyses were performed on each cluster.

To assess and visualize the spatial variability of the variables, thematic maps for every variable was also created.

To create the maps, Inverse Distance Weighting (IDW) interpolation was performed on the point values for each variable. This allowed us to create the first raster. Then, on the created raster, the K-mean algorithm was performed. The algorithm was settled through the Combined Minimum Distance method, with a maximum reiteration of 10 times. This allowed us to create maps with 3 different clusters. Subsequently, the cluster raster was elaborated through a Gaussian filter, a smoothing operator, to highlight significative patterns.

3 Results and Discussion

For the data, verification of assumptions for the linear regression was performed, allowing us to identify the necessity of some data collection. In particular, EMI data and NDRE data didn't follow the normal distribution. EMI data have been transformed with logarithmic transformation, instead, NDRE data required Turkey transformation. After those transformations, linear regression and correlation were performed.

The analysis highlighted the lack of statistically significative interaction between almost all the studied variables, except in some cases. The first case regards the correlation between soil force shear and ECa1 deep, which resulted in a weak negative correlation (Pearson coefficient = -0.1 , p-value = 0.05). The second case is the linear regression between the resistance to penetration (RP) and the ECa1, which registered a positive R^2 ($R^2 = 0.012$, p-value = 0.05). The last case is the linear regression between NDVI and ECa1 with an $R^2 = 0.015$ and p-value = 0.027 . Even if the results in those cases were positive, it is evident that both the correlation that the linear regression implies a lack of relationship between the variables. This leads us to conclude that, for this case study, all those variables must be treated as separate in-field characteristics and their studies have to be persecuted separately.

To evaluate the spatial variation and statistical differences, the K-means algorithm was performed, allowing to obtain for each variable three clusters classified according to the values; the mean and standard deviation for each cluster were also calculated.

Table 1 Cluster analysis in R. Size states the number of values for each cluster. The Centre represent the mean values of that cluster. The standard deviation (SD) was obtained from the sum of the squared deviations from each observation and the cluster centroid

		Size	Centre (μ) \pm SD (σ)
NDVI	Cluster 1	78	0.31 \pm 0.73
	Cluster 2	162	0.55 \pm 0.71
	Cluster 3	74	0.74 \pm 0.69
NDRE	Cluster 1	237	0.19 \pm 0.70
	Cluster 2	54	0.40 \pm 0.55
	Cluster 3	23	0.77 \pm 0.48
RP	Cluster 1	43	218.6 \pm 818.63
	Cluster 2	155	595.5 \pm 1132.2
	Cluster 3	116	883.1 \pm 1253.8
ECa1	Cluster 1	267	7.3 \pm 14.83
	Cluster 2	40	13.4 \pm 4.72
	Cluster 3	7	20.6 \pm 2.41
ECa2	Cluster 1	205	15.7 \pm 12.65
	Cluster 2	102	18.4 \pm 13.93
	Cluster 3	7	37.4 \pm 8.38

The results of the k-mean algorithm and the statistical analysis are summarized in Table 1.

The table shows for each cluster the corresponding number of observations, mean (centre of the cluster) and standard deviation. Regarding the size, the number of observations for each cluster in NDRE and ECa1 is more uneven compared to the other variables. The first cluster, containing the lowest values, is more represented, with differences of more than 200 units in some cases. In the NDRE case, this is a critical condition, as the majority of the data are in the cluster between 0 and 0.2, index values that identify senescent or weak vegetation. It may be due to the porosity of the canopy that does not allows us to be certain of the quality of the collected data. Regarding mean and standard deviation, EMIs values registered low dispersion from the mean, meaning that between the cluster the mean is well representative of the data, and the clusters themselves classifies the data in a statistically significant way. Instead, the RP standard deviation state a high dispersion from the mean, suggesting that a three-cluster K-mean algorithm may not be enough for this kind of data. Regarding NDVI and NDRE data, standard deviation show the highest dispersion around the mean in the first cluster, the one with lower values. The difference between NDVI data and NDRE data (as also shown graphically in the next paragraph) may be due to the different sensibility of the two indices to canopy structure and biomass, as the NDRE, by using the red-edge region, can create a more accurate evaluation compared to NDVI [13, 14]. The differences can be also reconducted to the porosity of the canopy; theoretically, the reading of the nearest part of the canopy can be instead the reading of the internal and furthestmost part of it, if higher porosity is present (Fig. 1).

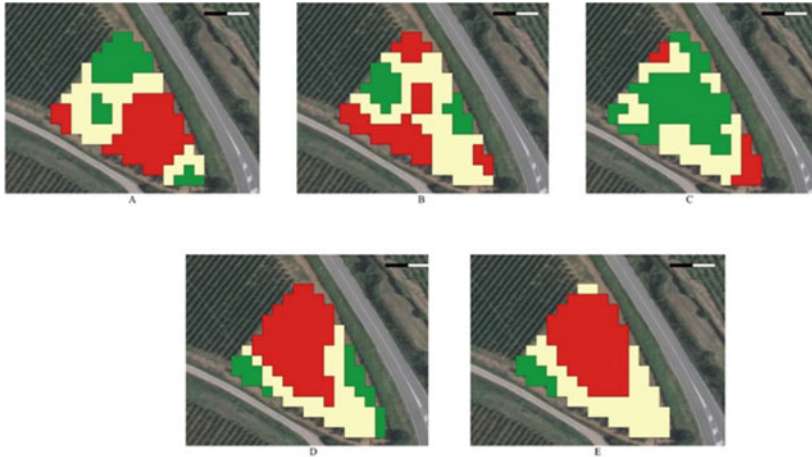


Fig. 1 Thematic maps: (A) NDVI map, (B) NDRE map, (C) Soil RP map, (D) ECa1 map, (E) ECa2 map. The clusters follow a colouration where the red clusters contain the lowest values and, instead, the green clusters contain the highest

The thematic maps allow us to visualize more clearly the differences in the spatial distribution of the variable. The creation of the maps had as an objective the evaluation of the collected data as a viable option to create prescription maps for field operation, specifically variable rate fertilization, cover crop seeding, and variable tillage.

The maps show a clear pattern in the distribution of the variables, but some issues are presented: the first noticeable element is the difference in values distribution between the soil RP map and the EMIs maps: there is a negative trend between the two variables, and the zone in which the values are higher for the RP, is the zone with the lowest values for the EMI. This can be attributed to the presence of rock and stone in the soil, a condition that results in lower EMI values but enhances soil resistance to penetration. This is a critical element to be considered in creating the prescription maps, especially when considering cover crop seeding.

There is also a consistent difference between NDVI and NDRE maps, which can be reconducted to the differences in the efficacy of the two indexes, as stated before. This difference can be problematic in the creation of fertilization prescription maps, and result in the necessity of evaluating the best index for the olive plant.

4 Conclusion

In the present case study, various kinds of sensors were applied in an olive orchard to evaluate and assess the significance of the use of those instruments in olive production and the critical issues in doing so. Electromagnetic Induction, soil Resistance to Penetration and olives' plant vegetation index (NDVI and NDRE) were studied.

Through statistical analysis it was discovered the absence of a relationship between the variables, indicates the necessity of evaluating and treating those variables in in-field management in separate ways. The study of the k-means classification cluster highlights some critical issues in data collection with proximal sensing in the olive orchard, suggesting the necessity for further studies. The thematic maps allowed us to evaluate the possibility of using the information collected to create prescription maps for field management and highlighted some issues in converging different types of information to create clear and univocal prescription maps.

The objectives of the case study were satisfied, allowing us to assess the critical issues in the proximal sensing use in olive production and to evaluate a workflow for further investigations. In this regard, studies are in process in Ente Terre Regionali Toscana farm, in Cesa (Ar) to evaluate the proximal sensing methodology, to assess the most suitable for olive plants.

References

1. European Commission: New CAP: 2023–27 (2021). https://agriculture.ec.europa.eu/common-agricultural-policy/cap-overview/new-cap-2023-27_en. Accessed 8 Aug 2022
2. van Evert, F.K., Gaitán-Cremaschi, D., Fountas, S., Kempenaar, C.: Can precision agriculture increase the profitability and sustainability of the production of potatoes and olives? Sustainability (2017). <https://doi.org/10.3390/su9101863>
3. Brilli, L., et al.: Simulation of olive grove gross primary production by the combination of ground and multi-sensor satellite data. *Int. J. Appl. Earth Obs. Geoinf.* **23**, 29–36 (2013)
4. Manna, P., Bonfante, A., Colandrea, M., et al.: A geospatial decision support system to assist olive growing at the landscape scale. *Comput. Electron. Agric.* **168**, 105143 (2020)
5. Recchia, L., Boncinelli, P., Cini, E., Vieri, M., Pegna, F.G., Sarri, D.: Olive oil production chain. In: Recchia, L., Boncinelli, P., Cini, E., Vieri, M., Pegna, F.G., Sarri, D. (eds.) *Multicriteria Analysis and LCA Techniques*. Green Energy and Technology, pp. 99–128. Springer, London (2011). https://doi.org/10.1007/978-0-85729-704-4_5
6. Sarri, D., et al.: Smart farming introduction in wine farms: A systematic review and a new proposal. Sustainability (2020). <https://doi.org/10.3390/su12177191>
7. Roma, E., Catania, P.: Precision oliviculture: research topics, challenges, and opportunities—a review. *Remote Sens.* (2022). <https://doi.org/10.3390/rs14071668>
8. Cortez, J.W., Cavassini, V.H., Motomiya, A.V.d.A., Orlando, R.C., Valente, I.Q.M.: Spatialization of soil resistance to penetration for localized management by precision agriculture tools. *Eng. Agric.* **38**, 690–696 (2018)
9. Sirjacobs, D., Hanquet, B., Lebeau, F., Destain, M.F.: On-line soil mechanical resistance mapping and correlation with soil physical properties for precision agriculture **64**, 231–242 (2002)
10. Costantini, E.A.C., Dazzi, C.: The Soils of Italy (2013). <https://doi.org/10.1007/978-94-007-5642-7>
11. Sarri, D., Martelloni, L., Priori, S., Lisci, R., Rimediotti, M., Lombardo, S.V.M.: Design and preliminary evaluation of a soil resistance sensor for soil compaction sensing in viticulture. In: *Interv. Present. al convegno Biosyst. Eng. addressing Hum. challenges 21st century tenutosi a Bari nel 5–8 Luglio 2017*. Press Office, University of Bari ©Università degli studi di Bari Aldo Moro, pp. 42–47 (2017)

12. Priori, S.: Mapping soil spatial variability at high detail by proximal sensors for a vineyard planning. *EQA Int. J. Environ. Qual.* **30**, 9–15 (2018)
13. Morlin Carneiro, F., Angeli Furlani, C.E., Zerbato, C., Candida de Menezes, P., da Silva Gírio, L.A., Freire de Oliveira, M.: Comparison between vegetation indices for detecting spatial and temporal variabilities in soybean crop using canopy sensors. *Precis. Agric.* **21**, 979–1007 (2020)
14. Miller, J.J., et al.: Characterizing soybean vigour and productivity using multiple crop canopy sensor readings. *Field Crops Res.* **216**, 22–31 (2018)

Microclimatic Monitoring and Analysis in a Hydroponic Greenhouse



Claudio Perone, Michela Orsino, Pasquale Catalano, Biagio Bianchi, Ferruccio Giametta, and Giovanna La Fianza

Abstract In the last decades, the increasing reduction of per capita arable land and the increasing demand for food requires the development of advanced solutions like soilless cultivations. Hydroponics represents an interesting and efficient response for sustainable cultivations, in particular its evolution hydroponic greenhouse that uses water instead of soil and, so, characterized by different management. In particular, it is important to well manage not only the cultivation area but also: the structural characteristics of greenhouse, the microclimate management, and the nutrients management. To maximize resources efficiency and quality food production, it is fundamental to characterize the microclimatic parameters and their distribution inside greenhouses.

This work provides a preliminary study to measure and analyze the main microclimatic parameters in a hydroponic greenhouse without a microclimatic controlling system, located in Vinchiaturò (Italy), with a set of sensors that acquire data continuously.

After the installation of sensors to monitor the temperature, humidity, and light intensity, a supervision system was installed to manage and historicize all the measured data.

From the data analysis, appropriate management of the hydroponic greenhouse was identified allowing reduced expenses and improved efficiency.

Keywords Microclimate monitoring · Hydroponic greenhouses · Sensors · Soilless culture

C. Perone · B. Bianchi

University of Bari Aldo Moro, Department of Agricultural and Environmental Science (DISAAT), Via Amendola 165/A-, 70126 Bari, Italy

M. Orsino · P. Catalano · F. Giametta (✉) · G. La Fianza

University of Molise, Department of Agricultural, Environmental and Food Sciences, Via Francesco De Sanctis -, 86100 Campobasso, Italy

e-mail: ferruccio.giametta@unimol.it

1 Introduction

The lack of per capita arable land and the growing demand for food over the last decades is now a serious problem [1] and the greenhouse is becoming the most widespread cultivation method guaranteeing the increment of food production and the reduction of climate change damages [2].

In addition, the greenhouse can be used in places that are not suitable for cultivation thanks to its controlled environment and the sustainable management of resources [3]. To this purpose, the development of an indoor cultivation environment is fundamental, especially in farming practices and technologies.

The most promising technology is the soilless cultivation inside greenhouse and hydroponics systems, in which soil is replaced by water-based mineral nutrient solutions in aqueous solvents, are now very common and efficient [2]. The management of this type of greenhouse takes into account not only the cultivation area, but it involves also other factors, for example, the greenhouse structural characteristic, the microclimate, and nutrients management [4–7]. Thus, to optimize the management of resources efficiency and quality food production is needful the local evaluation of the main microclimatic parameters [8, 9].

The aim of this work is the preliminary study of the main microclimatic parameters in a hydroponic greenhouse, located in Vinchiaturò (Italy), comparing the case study without a microclimatic controlling system and with a ventilation system. For this purpose, a set of temperature, humidity, and light intensity sensors were installed to continuously acquire data near the cultivation bed. Sensors were managed by a supervision system that allowed also to historicize all measured data. From the analyzed data, an appropriate management of the hydroponic greenhouse was identified to reduce expenses and improve efficiency.

2 Materials and Methods

In this work, microclimatic parameters were acquired in an operating hydroponic greenhouse of 500 m² (10 × 50 m) (Width x Depth). This greenhouse (Fig. 1a, b) is located in Vinchiaturò, Molise (Italy) at 850 m above sealevel.

The greenhouse structure is made of metal and polycarbonate with side openings and anti-aphid meshes. The greenhouse has two separate cultivation tanks in deep water culture hydroponic system; water inside the tanks circulates continuously. There are two entrances at opposite ends of the building and two cultivation tanks along the sides. Above these tanks, a system of nozzles is mounted to moisturize canopies. This hydroponic greenhouse is not equipped with artificial lamps or LEDs to enhance crop growth. The main crops cultivated in this hydroponic greenhouse were some lettuce varieties, a few aromatic herbs, and edible flowers. These crops were raised in polystyrene rafts and were pushed from the bottom to the main entrance as Fig. 2 shows.



Fig. 1 Hydroponic greenhouse structure pictures; **a.** external environment; **b.** indoor cultivation environment

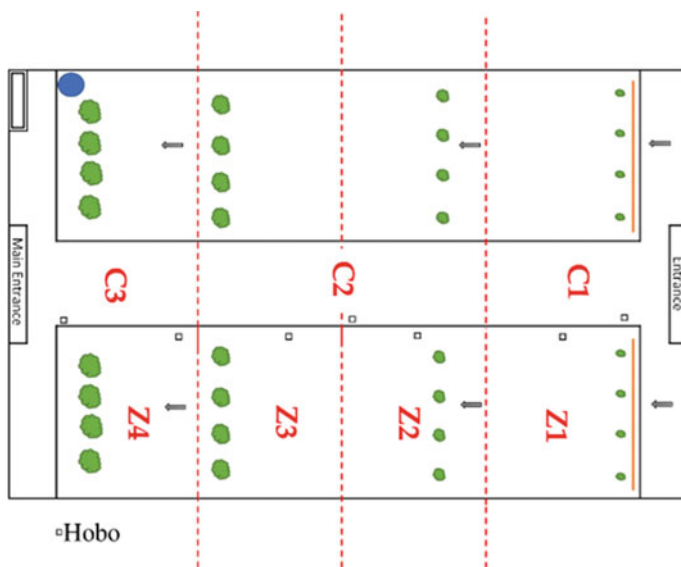


Fig. 2 Schematic view of indoor cultivation environment, where the blue circle represents the water source tank, the green shapes the crops, the arrow the direction of the path followed by the plant; Z1, Z2, Z3, and Z4 indicate the four stages of the cultivation tank; C1, C2, and C3 are the area of the central aisle close to the entrance, in the middle, and close to the other entrance

Measurements were carried out on two productive cycles of Salanova® lettuce (28th March-27th April 2022; 14th July- 13th August 2022), following two complete crop growth cycles and monitoring two targeted floating rafts with 4 crops each.

Tests have been made without modifying the ongoing management of the greenhouse; in fact, the first monitored cycle was characterized by the absence of a mechanical ventilation system, while the second cycle of measurements with a mechanical fan installed in May 2022 and without any automatic control for the on / off cycles.

First of all, tests were carried out by dividing the inner environment into different zones both on the aisle and on the selected cultivation side tank. The cultivation tank was divided into four zones (Z1, Z2, Z3, Z4) to identify different growth stages; the central aisle in three sections (C1, C2, C3) (Fig. 2).

Seven HOBO sensors for Temperature, Relative Humidity, and Light monitoring (Table 1) were placed close to the main openings of the greenhouse and close to the selected leafy crops for their growing phase monitoring (Fig. 3).

In particular, four of them were evenly distributed at a distance in height of 30 cm from the cultivation bed and another three sensors in the central aisle at a height of 1.80 m.

Salanova® lettuce and Parsley (*Petroselinum crispum*) growing cycles were followed during the experimental monitoring using HOBOWare Pro supervision system that measured and historicized data for 30 days (day-night cycle) with a sampling time per parameter of 6 min.

Table 1 Sensors’ characteristics used for the experimental tests

Measurements	Accuracy
<p>Temperature Measurement range: -20° to 70 C (-4° to 158°F) Response time: 6 min (to 90% in airflow of 1 m/s)</p>	<p>± 0.35 C from 0° to 50 C (0.63°F from 32° to 122°F)</p>
<p>Relative Humidity (RH) Measurement range: 5% to 95% RH Response time: 1 min (to 90% in airflow of 1 m/s) Light Intensity Range: 1 to 3000 footcandles (lumens/ft²) typical 0–32,300 lumens/m² [0–3,000 footcandles (lumens/ft²)]</p>	<p>± 2.5% typical, 3.5% maximum, from 10 to 90% RH</p>
<p>External Input External sensors for temperature, AC current, AC voltage, CO₂, 4–20 mA, 0–10 VDC Input range: 0 to 2.5 VDC Output power: 2.5 VDC at 2 mA, active only during measurements</p>	<p>± 2 mV, ± 2.5% of absolute reading</p>

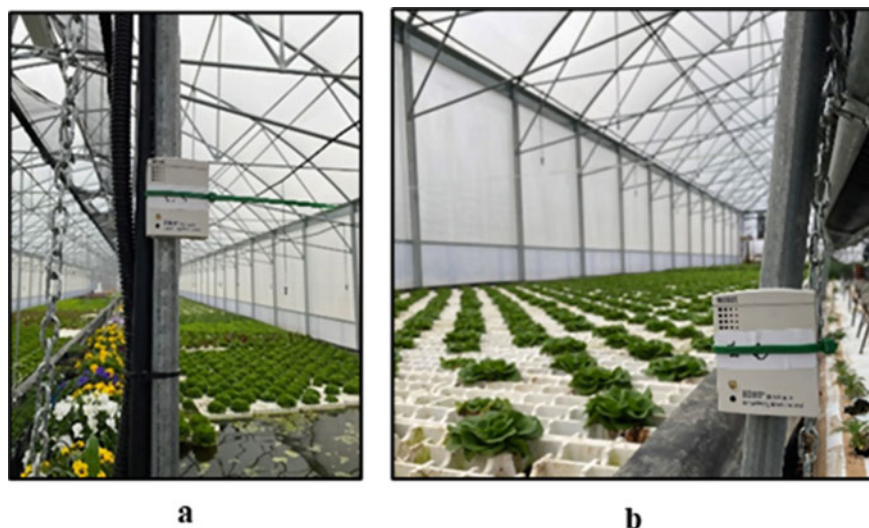


Fig. 3 Picture of HOBO sensors located in C3 (a) and near the leafy crops (b)

3 Results and Discussions

The acquired data were elaborated to evaluate the trend of the microclimatic parameters inside the hydroponic greenhouse and to identify the best optimization asset. The first monitoring test of the cultivation cycle was carried out from March 28th to April 27th, characterized by unfavorable weather conditions for this cultivation system. The trend of the temperature, relative humidity, and light intensity shows no substantial differences between the different areas, both for Z and C. The results of these measurements are shown in Fig. 4a, b, and c.

In particular, the first cycle was cold and rainy, explaining the thermal excursion of 22.33 °C with a standard deviation of 6.63 °C. This happened also because the absence of mechanical ventilation and not proper insulation of the structure that affected the internal cultivation environment.

Also, the relative humidity was strongly affected by the bad weather: the daily variation average of the relative humidity was 57.63%, with a standard deviation of 15.91%. The light intensity (measured in lux) was representative of the external weather conditions and was almost similar in all the zones; the average of maximum values achieved was 30,000 lx, optimal value for plants growing (the optimal range is 20000–50,000 lx).

The strong variability of temperature and humidity can be better understood by analyzing data in a short period time, showed in Fig. 5.

In fact, during the rainy days like April 10th, very clear and strong fluctuations of temperature and relative humidity were evident and strictly related to the outdoor environment. For example, the indoor day temperature had an average value of 15.83

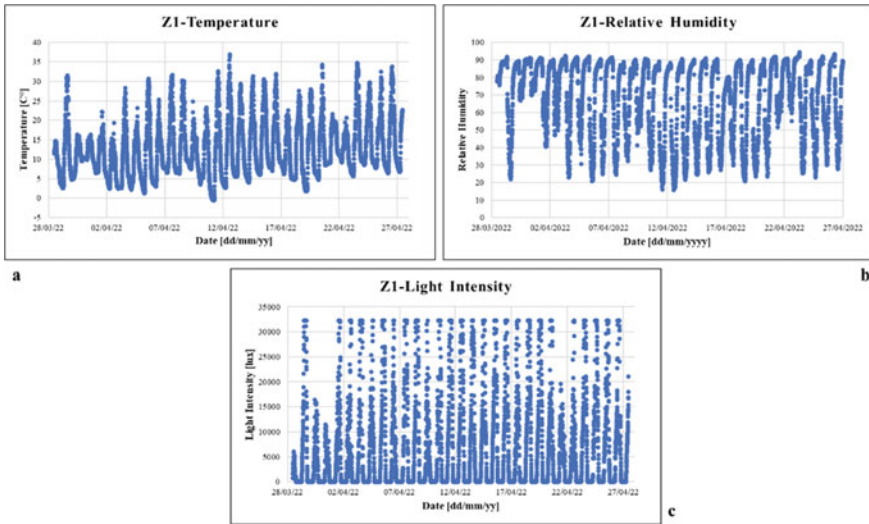


Fig. 4 Growing cycle in Z1 (March 28th - April 27th, 2022) temperature a., relative humidity b. and light intensity c. trend

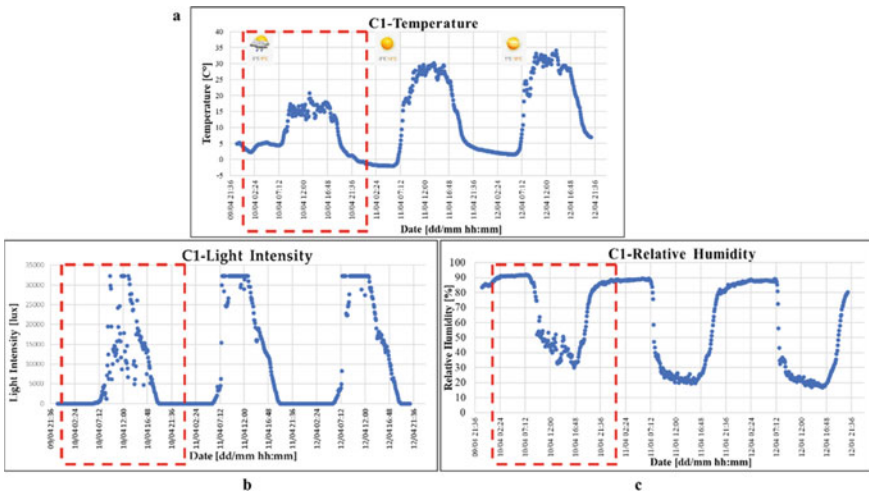


Fig. 5 Few day data (April 10th - April 12th, 2022) of total cultivation growing cycle in C1, C2, C3 (March 28th - April 27th, 2022): a. Temperature trend; b. Relative Humidity trend; c. Light Intensity trend

°C on April 10th, while on April 11th and 12th it was 26.95 °C and 30.11 °C. Thereby, on April 10th relative humidity increased by 20% and the light intensity decreased by 20.49% compared to the following days. This behavior did not slow down the crops' growth but caused physiopathies, especially rots such as *Sclerotinia sclerotium*. It is evident the need for a ventilation system automatically controlled to reduce the temperature difference and of a well-insulated structure.

The second monitoring test of the cultivation cycle was carried out from July 14th to August 13th, 2022. During the monitoring test, a mechanical fan was daily managed. Despite maximum temperature values achieved throughout the greenhouse of 34 °C, with an average of 22 °C, the average daily temperature in the side cultivation zones and the central aisle decreased by about 15% compared to the first test; in the central aisle decreased by about 6%. The variation in average daily temperature from first test to the second decreased of about 3 °C in both cultivation and central parts (from 21.88 °C to 19.07 °C in Z areas and from 23.17 °C to 20.16 °C in C areas).

Regarding the relative humidity, it decreased by 11.86% above the side cultivation bed (Z) and by 12.56% in the central aisle (C) compared to the first test. The variation in average daily relative humidity decreased from 57.05% to 51.00% in the Z areas and from 58.54% to 52.01% in C areas; thus, is evident uniformity in the decreasing of the relative humidity compared to the Z areas. Although there was a strong temperature and relative humidity range in both tests, in the last case there were no physiopathies, thanks not only to the higher temperature but also to the less amount of fluctuations through the fan.

From this analysis, it is clear that, to reduce the day-night excursion and increase the production efficiency, this hydroponics greenhouse management will improve by consistently implementing a ventilation system controlled by a set of permanent probes. Taking into account the vegetative growth of the cultivated crops, the fan activation is recommended after a continuous period of time above a set-point of 27 °C and if the relative humidity exceeds 80%. During rainy days and in the winter/spring season, this timely action would allow not to have too low temperatures (also in the case of the not well-insulated structure of the greenhouse).

4 Conclusions

For this work, two microclimatic monitoring tests were carried out in a hydroponic greenhouse placed in Vinchiatturo (Italy), at a height of 850 m. Tests were conducted on Salanova® lettuce and parsley, differentiating two areas (Z and C). In the first monitoring test, corresponding to the Spring season, issues related to high humidity levels were relevant, especially on rainy days. In the second monitoring test, during the Summer season, the indoor humidity conditions improved not only for higher temperatures but also for the use of the mechanical fan with a reduction of 12% and of 30% respectively on the cultivation side and in the central aisle. This impacted positively on the plant pathology side, avoiding the onset of diseases. Regarding the temperature, even if maximum temperature values achieved about 34 °C throughout

the greenhouse, the average daily temperature in the side cultivation zones and the central aisle decreased by about 15% compared to the first test. This proved that the fan was effective.

Based on the results of these two microclimatic tests is clear the need to improve the structure, because it is not completely closed and insulated (day/night temperature range), and the need of an automatic mechanical ventilation system to control temperature and humidity to reduce the fluctuations controlled by the set of sensors used for this work.

References

1. Fedoroff, N.V.: Food in a future of 10 billion. *Agri. Food Secur.* **4**(1), 1–10 (2015)
2. Khan, F.A.: A review on hydroponic greenhouse cultivation for sustainable agriculture. *Int. J. Agri. Environ. Food Sci.* **2**(2), 59–66 (2018)
3. Sardare, M.D., Admane, S.V.: A review on plant without soil-hydroponics. *Int. J. Res. Eng. Technol.* **2**(3), 299–304 (2013)
4. Singh, M.C., Singh, J.P., Pandey, S.K., Cutting, N.G., Sharma, P., Shrivastav, V., Sharma, P.: A review of three commonly used techniques of controlling greenhouse microclimate. *Int. J. Curr. Microbiol. App. Sci* **7**(1), 3491–3505 (2018)
5. Bugbee, B.: Nutrient management in recirculating hydroponic culture. In: *South Pacific Soilless Culture Conference-SPSCC 648*, pp. 99–112 (2003)
6. Orsino, M., Perone, C., La Fianza, G., Brunetti, L., Giametta, F., Catalano, P.: Microclimatic control in confined agricultural environment for plants cultivation. *Chem. Eng. Trans.* **87**, 229–234 (2021)
7. Perone, C., Orsino, M., La Fianza, G., Giametta, F., Catalano, P.: Study of a mechanical ventilation system with heat recovery to control temperature in a monitored agricultural environment under summer conditions. *J. Build. Eng.* **43**, 102745 (2021)
8. Erfianto, B., Rakhmatsyah, A., Ariyanto, E.: Micro-climate control for hydroponics in greenhouses. In: *2020 8th International Conference on Information and Communication Technology (ICoICT)*, pp. 1–6. IEEE (2020)
9. Singh, M.C., Yousuf, A., Singh, J.P.: Greenhouse microclimate modeling under cropped conditions-a review. *Res. Environ. Life Sci.* **9**, 1552–1557 (2016)

Optimization of a New Knife Crusher to Increase Olive Oil Quality



Claudio Perone, Antonia Tamborrino, Antonio Berardi,
Roberto Romaniello, and Alessandro Leone

Abstract Olive crushing has the purpose of breaking the olives, creating a paste made up of all the vegetable parts, suitable for subsequent processing. The crushers hit the drupe violently, transferring part of their kinetic energy. However, the shape, geometry and speed of the crusher tool can also produce a different way of breaking up plant tissues due to the different combination of compressive, shear and friction forces and different temperature of the olive paste. To increase the performance of this stage, a new knife crusher was studied. Specifically, a new knife rotor was studied to replace the hammer rotor and implemented in a traditional crusher. The aim was that of a preliminary optimization of the specific energy based on a new configuration of the blades to crush the olives, so to avoid an excess of temperature increasing into the grid. As a reference the results obtained were compared with those of a traditional hammer crusher. Test results reported an increase in the phenolic content of the olive oil when knife rotor was used, while about the olive oil extractability of the no significative difference was found between the two crushers compared.

Keywords Hammer crusher · Knife crusher · Phenolic compounds · Olive paste temperature · Impact energy

1 Introduction

A well-designed extraction process is essential to improve both high quality extra virgin olive oil (EVOO) and its extractability. This task is carried out through the continuous improvement of the main machines involved in the process. In recent

C. Perone (✉) · A. Tamborrino · A. Berardi · A. Leone
Department of Soil, Plant and Food Science (DISSPA), University of Bari Aldo Moro, Via Amendola 165/a, 70126 Bari, Italy
e-mail: claudioperone@gmail.com

R. Romaniello
Department of Agriculture, Food, Natural Resources and Engineering (DAFNE), University of Foggia, Via Napoli 25, 71122 Foggia, Italy

decades, several important developments in the technology of the extraction line have been made, in order to optimize each stage of the process [1–13] and olive oil storage [14]. Among the main phases involved in the EVOO production, crushing is essential to obtain a well-prepared olive paste, that is a semifluid paste made of solid phase (pit fragment, skin and pulp) and liquid phase (oil and water emulsion) [15].

To date, the most used crusher machines are hammer crusher and disc crusher. In recent years also total destoner and partial destoner machines are also becoming increasingly popular [16–19]. The main differences are in how energy is transferred from the tool to the product [19]. For what has been said so far, the way in which the forces exerted by the crusher are transferred is of great importance in terms of both extractability and quality of the olive oil produced.

In this study, we analyzed the effects of a new knife crusher rotor on quantitative and qualitative parameters of the olive oil, by using as reference case a hammer rotor. This was possible thanks to a new modular crusher machine. The aim is to understand the main modes of action of the tools on the product as a function of the energy transferred, and thus also their thermal effects.

2 Materials and Methods

2.1 Modular Crusher and Experimental Design

The modular crusher consists of a standard crusher frame in which it was possible to exchange two different types of rotor: hammer (HC) and knife (KC). The hammer rotor has three spokes at the end each is mounted a parallelepiped-shaped tool made of mild steel. The knife rotor has 10 radial knives made of mild steel. The knives are positioned in three rows and spaced 45° from each other. Two pairs of knives are double. The basic frame has an inner grid with external holes of 6 mm. The machine was installed in a 2-phase extraction line with mass flow rate of 5 t h^{-1} , without water process added (Amenduni Nicola s.p.a., Bari, Italy). Olive fruits (*Olea europaea L.*) from Coratina variety were used for the experimental tests. Each performed test was repeated 8 times using homogeneous 3500 kg batches of olives. The malaxation was performed for 40 min at $25 \pm 1 \text{ }^\circ\text{C}$, and the plant mass flow rate was 5 t h^{-1} , without the addition of process water. During each test the olives were sampled and the quantity of oil extracted was measured in order to calculate the extractability of the plant. In addition, for each test the extracted olive oil was sampled in order to determine the quality parameters. Finally, particle size distribution was analyzed on the olive paste samples.

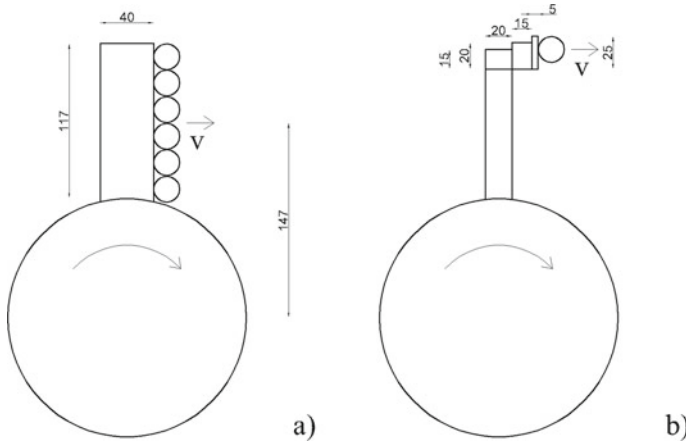


Fig. 1 Schematic representation and geometric dimensions of **a** knife tool and **b** hammer tool during the impact with olives

2.2 Particle Size Measurements

During the comparative tests, for each type of crusher used (HC and KC), aliquots of crushed olive paste were taken at regular intervals, up to a final sample of 5 kg. Subsequently, the pulp samples were treated to recover only the crushed pits (Fig. 1), removing the remaining solid and liquid parts by washing with water. The samples were then sieved using a series of sieves with diameters between 600 and 5500 μm to obtain 14 size classes according to Doane’s equation [17] and frequency distributions was obtained. Mean, mode, median, standard deviation, skewness (Fisher’s moment coefficient) and kurtosis (Persons’s moment coefficient), were calculated.

The significant difference was detected using the two-tailed t-test hypothesis test ($p < 0.05$).

2.3 Specific Energy Estimation: Energy Conservation and Comminution Theory

The energy of impact was estimate whit two method: energy conservation and comminution theory.

As for the energy conservation we assumed: 1) tool mass is greater than mass of impacted olives; 2) before impact, linear velocity of the tool is greater than the particle velocity of fruits, and thus, kinetic energy of olives is negligible.

With these assumptions the energy released is represented by the kinetic energy of the crusher tool, as reported in [20]. By considering non-elastic collision and the conservation of linear momentum:

$$E_c = \frac{1}{2} M_c v^2 \quad (1)$$

where E is the kinetic energy of the crusher tool ($c = H, K$ for hammer and knife), M and v its mass and velocity respectively. The geometric parameters of the two tools are shown in Fig. 1. To obtain the specific energy e_c , the kinetic energy must be divided by the mass of the amount of impacted olives M_{oc} :

$$e_c = \frac{E_c}{M_{oc}} \quad (2)$$

$$M_{oc} = M_o \frac{H_c}{d_o} \frac{D_c}{d_o} \quad (3)$$

where M_o is the mass of one olive, d_o its diameter and D_c the depth of the tool.

As for the comminution theory it can be used the Bond equation [21]:

$$e_c = K_B \left[\left(\frac{D_r}{D_2} \right)^{0.5} - \left(\frac{D_r}{D_1} \right)^{0.5} \right] \quad (4)$$

where D_r is the reference diameter, D_1 is the initial diameter of the pit, D_2 is the final diameter of the pit (mean value), and K_B is an empirical constant related to the resistance offered by the product. However, the second term of Eq. 10 can be neglected since the diameter of the pit is much higher than that referenced.

Once the specific energy released in the impact is known, it is possible to calculate the average temperature increase T_{mc} of the olive paste by operating a thermal balance, as indicated in [21]:

$$T_{mc} = T_e + \frac{M_p}{M_o} \frac{e_c Q_o}{hS} \quad (5)$$

where T_e is the environmental temperature, M_p is the mass of the pit, Q_o is the average flow rate through the crusher, and h and S are the heat transfer coefficient and external surface of the crusher, respectively.

2.4 Plant Extractability and Olive Oil Qualitative

To evaluate the quantitative performance of the olive oil extraction plant, extractability parameter, calculated as reported in [8], was used.

Moisture and oil content in olives and pomace were evaluated as reported in [6]. Legal extra virgin olive oil quality parameters and phenolic compounds were evaluated as reported in [10].

3 Results and Discussion

3.1 Particle Size Distribution

The analysis of the average size distribution of the pit fractions by the two different crushers can be seen in Figs. 2a and 2b, while the distributions parameters are shown in Table 1.

In the figures, the least-square fitting is drawn to show the profile of the distribution across the size classes. The mechanical action of the two types of crushers was substantially different based on the size of the pits produced. Comparing the values in Table 1, the average particle size produced by the HC crusher is significantly lower than that of the KC crusher, as well as for the median value and the modal value. Both distribution curves show moderate negative asymmetry with the tail on the left side of the distribution. The kurtosis value is negative for the HC distribution curve and positive for the KC distribution curve. This indicates that the distribution curve of the pit fragments is platykurtic for HC, with frequencies better distributed between

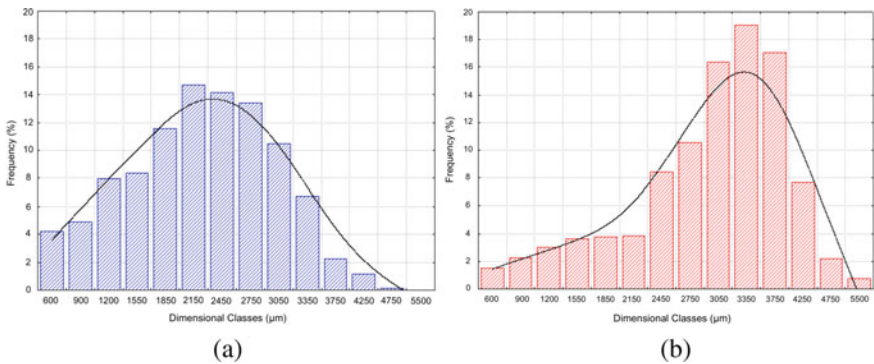


Fig. 2 Frequency distribution of pits from Hammer **a** and Knives **b** Crusher

Table 1 Frequency distribution parameters of pits fragments for HC and KC

	HC	KC
Mean [μm]	2224.3 \pm 52.2 <i>a</i>	3017.9 \pm 25.2 <i>b</i>
Mode [μm]	2225.5 \pm 54.0 <i>b</i>	3371.4 \pm 26.3 <i>a</i>
Mode frequency [%]	14.9 \pm 1.4 <i>b</i>	18.1 \pm 1.4 <i>a</i>
Median [μm]	2265.6 \pm 14.7 <i>a</i>	3140.0 \pm 22.6 <i>b</i>
Standard deviation [μm]	796.4 \pm 33.5 <i>b</i>	940.3 \pm 55.3 <i>a</i>
Kurtosis	-0.04	-0.64
Skewness	-0.34	0.36

Different letters in rows denotes significant statistical differences (t-test, $p < 0.05$).

the classes and leptokurtic for KC, where a higher frequency concentration around the modal value is highlighted. This means that KC generate a higher percentage of large fragments than the HC.

3.2 Specific Energy and Temperature Comparison

The specific energy comparison provided by the hammer rotor and knife rotor was made through energy conservation and comminution theory. As for the kinetic energy conservation we must consider the geometric parameters reported in Fig. 1 and Eqs. (1), (2) and (3). The relationship between the main parameters of the two rotors are reported in Table 2.

It can be seen that, by assuming the same material of the tool, and thus the same density, the mass of the hammer is two times that of a knife. The whole mass of the tool is considered in its center of gravity, that is 34% higher in the case of hammer. Since the angular velocity was the same in each test and for both rotors, also the velocity of the tool is 36% higher in the case of hammer respect to the knife. As a result, the kinetic energy of the hammer is 3.70 times that of knife, due to the quadratic dependence on velocity. To calculate the specific energy (related to the unit of product) it is essential to evaluate the amount of impacted mass (Eq. (3)). Since the depth of the hammer tool was 155 mm and that of knife 12 mm, the mass of impacted olives is 2.76 times in the case of hammer. This means that the specific energy of the hammer tool was 34% higher that that of knife.

As for the specific energy evaluated by comminution theory, we must refer to Fig. 2a and 2b and Table 1, where it is where it is possible to consider a measure of central tendency. It is easy to note that HC tool provided a higher impact energy, since the mean, mode and median values were higher than that of KC one. Table 3 shows the specific energy deduced by comminution theory by referring to mean and mode values (the median values lead to the same conclusions as the mean ones). Table 3 also reports the average increase of temperature due to the energy released has heat in the product. Since in Eq. 5 the only variable is the specific energy, the mean temperature increasing is 15–34% higher in the case of hammer.

Table 2 Table captions should be placed above the tables

Parameters	Comparison	Equation
Tool mass (M)	$M_H = 2.00 M_K$	$M_C = \rho V_C$
Radius of center of gravity (R)	$R_H = 1.36 R_K$	–
velocity (v)	$v_H = 1.36 v_K$	$V_C = \omega R_C$
Kinetic energy (E)	$E_H = 3.70 E_K$	Equation (1)
Mass of olives per tool (M)	$M_{OH} = 2.76 M_{OK}$	Equation (3)
Specific energy (e)	$e_H = 1.34 e_K$	Equation (2)

Table 3 Table captions should be placed above the tables

Parameters	Comparison	Equation
Specific energy (mean/median values)	$e_H = 1.15 e_K$	Equation (4)
Specific energy (mode values)	$e_H = 1.22 e_K$	Equation (4)
Mean temperature of the paste	$T_{mH} = 1.15-1.34 T_{mK}$	Equation (5)

The theoretical analysis carried out in this study certainly represents a simplification of the problem, but it is essential to hypothesize the main modes of transmission of stresses by the tools. Both theories lead to the conclusion that the energy released by the impact of the hammer is greater than that of the knife. Thus, it is reasonable to imagine that the knife mainly provides shear stresses, due to its thin thickness, while the hammer provides normal stresses, due to its large cross-sectional area. This leads to a lower dissipation as heat in the product in the case of the new knife tool, ensuring a higher quality of the final product, as better discussed in the next section.

3.3 *Quantitative and Qualitative Results*

In all the comparative tests carried out both with the use of the hammer crusher and with knives, the extractability of the plant was about 90% without significant difference between the two theses compared. This means that the breaking capacity of the vegetable tissues, although lower in the knife crusher than in the hammers, is still sufficient to effectively break the cell vacuoles avoiding oil losses in the pomace. No significant differences were found for the olive oil legal parameters as free acidity, peroxide value and UV spectrophotometric indices (K232, K270 and ΔK). When the knife crusher was used it was found an increase in the total phenol content of the oil compared to the hammer crusher, of about 30%. The increase was mainly found for the oleurope in derivatives.

4 Conclusions

The results demonstrated that as for the hammer tool, it produces mainly impulsive and compressive stress, while the knife crusher transfers mainly shear stress. The specific energy transferred by a single tool on the unit of product was 25–34% higher in the case of hammer. As a result also the increase of temperature is higher of the same magnitude. This information was correlated with results concerning oil quality and the extraction efficiency of the plant. Quality results demonstrated that, when compared to the hammer mill, the new knife rotor used in the crushing

phase led to an improvement in VOO quality, mainly in terms of an improvement in phenolic compounds. The increase of phenols content was mainly found for the oleuropein derivatives. No significant difference was found regarding the olive oil legal parameters and extractability.

References

1. Tamborrino, A., et al.: Assessment of the olive oil extraction plant layout implementing a high-power ultrasound machine. *Ultrason. Sonochem.* **73**, 105505 (2021)
2. Tamborrino, A., et al.: Development of an innovative rotating spiral heat exchanger with integrated microwave module for the olive oil industry. *LWT* **147**, 111622 (2021)
3. Perone, C., Romaniello, R., Leone, A., Catalano, P., Tamborrino, A.: CFD analysis of a tubular heat exchanger for the conditioning of olive paste. *Appl. Sci.* **11**(4), 1858 (2021)
4. Tamborrino, A., Perone, C., Catalano, F., Squeo, G., Caponio, F., Bianchi, B.: Modelling energy consumption and energy-saving in high-quality olive oil decanter centrifuge: numerical study and experimental validation. *Energies* **12**(13), 2592 (2019)
5. Perone, C., Romaniello, R., Leone, A., Berardi, A., Catalano, P., Tamborrino, A.: CFD analysis of a tube-in-tube heat exchanger to pre-heat olive pastes. *Chem. Eng. Trans.* **87**, 253–258 (2021)
6. Tamborrino, A., et al.: Combined continuous machine to condition olive paste: Rheological characterization of olive paste. *Chem. Eng. Trans.* **87**, 283–288 (2021)
7. Tamborrino, A., Urbani, S., Servili, M., Romaniello, R., Perone, C., Leone, A.: Pulsed electric fields for the treatment of olive pastes in the oil extraction process. *Appl. Sci.* **10**(1), 114 (2019)
8. Leone, A., Tamborrino, A., Esposto, S., Berardi, A., Servili, M.: Investigation on the effects of a pulsed electric field (PEF) continuous system implemented in an industrial olive oil plant. *Foods*, **11**(18), 2758 (2022)
9. Tamborrino, A., et al.: Assessment of the olive oil extraction plant layout implementing a high-power ultrasound machine. *Ultrasonics Sonochem.* **73**, 105505 (2021)
10. Servili, M., Veneziani, G., Taticchi, A., Romaniello, R., Tamborrino, A., Leone, A.: Low-frequency, high-power ultrasound treatment at different pressures for olive paste: effects on olive oil yield and quality. *Ultrasonics Sonochem.* **59**, 104747 (2019)
11. Perone, C., Romaniello, R., Leone, A., Berardi, A., Tamborrino, A.: Towards energy efficient scheduling in the olive oil extraction industry: comparative assessment of energy consumption in two management models. *Energy Convers. Manag.* **16**, 100287 (2022)
12. Squeo, G., et al.: Assessment of the influence of the decanter set-up during continuous processing of olives at different pigmentation index. *Food Bioprocess Technol.* **10** (3), 592–602 (2017)
13. Tamborrino, A., Leone, A., Romaniello, R., Catalano, P., Bianchi, B.: Comparative experiments to assess the performance of an innovative horizontal centrifuge working in a continuous olive oil plant. *Biosys. Eng.* **129**, 160–168 (2015)
14. Leone, A., Romaniello, R., Tamborrino, A.: Development of a prototype for extra-virgin olive oil storage with online control of injected nitrogen. *Trans. ASABE* **56**(3), 1017–1024 (2013)
15. Olive Milling and Pitting the Extra-Virgin Olive Oil Handbook, pp. 117–126 (2014)
16. Leone, A., Romaniello, R., Peri, G., Tamborrino, A.: Development of a new model of olives de-stoner machine: evaluation of electric consumption and kernel characterization. *Biomass Bioenerg.* **81**, 108–116 (2015)
17. Romaniello, R., Leone, A., Tamborrino, A.: Specification of a new de-stoner machine: evaluation of machining effects on olive paste's rheology and olive oil yield and quality. *J. Sci. Food Agric.* **97**(1), 115–121 (2017)
18. Tamborrino, A., Servili, M., Leone, A., Romaniello, R., Perone, C., Veneziani, G.: Partial de-stoning of olive paste to increase olive oil quality, yield, and sustainability of the olive oil extraction process. *Eur. J. Lipid Sci. Technol.* **122**(11), 2000129 (2020)

19. Leone, A., Romaniello, R., Zagaria, R., Sabella, E., De Bellis, L., Tamborrino, A.: Machining effects of different mechanical crushers on pit particle size and oil drop distribution in olive paste. *Eur. J. Lipid Sci. Technol.* **117**, 1271–1279 (2015)
20. Nikolov, S.: Modelling and simulation of particle breakage in impact crushers. *Int. J. Miner. Process.* **74**, S219–S225 (2004)
21. Caponio, F., Catalane, P.: Hammer crushers vs disk crushers: the influence of working temperature on the quality and preservation of virgin olive oil. *Eur. Food Res. Technol.* **213**, 219–224 (2001)

Effect of Image Binarization on Drop Diameters Measurement



Salvatore Privitera, Emanuele Cerruto, Domenico Longo,
and Giuseppe Manetto

Abstract With reference to agricultural nozzles for pesticide applications, droplet size affects biological efficacy of a phytosanitary treatment, environmental pollution, and operator's safety. Measuring droplet size spectrum of nozzles is a very complex task which has been addressed in multiple ways over the years. Measurement methods based upon image analysis have to solve the problem of recognizing the droplets and separating them from the background. This is accomplished by means of "binarization" or "segmentation" of the image, and it requires setting a threshold value to separate specific pixel intensities from each other. In this research the effects of the choice of the threshold value on computed volumetric diameters were analyzed. The study was carried out considering images of droplets of an air induction hollow cone nozzle TVI 8002 at the pressure of 1.0 MPa, obtained by applying the liquid immersion method in a custom test bench. A starting threshold value was selected based on the average gray level of the image and then variations of ± 5 units were considered. The results showed that the corresponding variations in volumetric diameters were less than 1%. This means that, once the image acquisition system is established, the binarization process may be made automatic and operator independent, with variations in results fully compatible with the precision of the whole measurement system.

Keywords Droplet pulverization · Image analysis · Threshold · ImageJ

1 Introduction

Over the years, the need to increase food quality and production and, simultaneously, prevent or control pests, diseases, weeds, and other plant pathogens, has led to consider the application of Plant Protection Products (PPPs) as one of the essential means of crop protection. When used appropriately, PPPs play an important role

S. Privitera · E. Cerruto (✉) · D. Longo · G. Manetto
Department of Agriculture, Food and Environment, University of Catania - Via Santa Sofia, 100,
95123 Catania, Italy
e-mail: emanuele.cerruto@unict.it

in agricultural activities because they can reduce the losses of agricultural products and improve food quality in a more sustainable way [18, 19, 26]. The potentially adverse consequences deriving from the use of PPPs have led to the issuing of specific regulations from European Authorities. For instance, the European Directive 2009/128/EC [6] recognizes that the correct use of pesticides plays a major role in safeguarding human health and the environment from the undesirable effects of these products [7, 8, 14]. In general terms, population's exposure, environmental effects, and biological efficacy are affected by several factors related to, but not only, amount of mixture to be sprayed, Personal Protective Equipment (PPE) used by farmers, sprayer settings, types of nozzles and their status. Among all these aspects, the droplet size spectrum has proven to be of great importance because it affects the biological efficacy of a treatment, the environmental contamination and the operator's safety [5, 11, 12, 24, 27].

According to the International Standard ISO 25358:2018 [10], the assessment of the droplet size distribution can be carried out following any non-intrusive method, but intrusive methods such as the use of Water Sensitive Papers (WSP) and the liquid immersion method are also adopted due to their easy to use and low cost [15]. Regardless of the method used, both have a strong influence on the droplet size spectrum measurement. When image analysis methodologies are used, further problems may occur due to the digitization process [16]. The "binarization" or "segmentation" of an image is a basic issue in digital image processing applications, when the objects of interest (the droplets) are separated from the background in such a way to be sufficiently distinct, so producing a binary image with only two colors: black (the droplets) and white (the background) pixels (or vice versa). Segmentation is usually carried out by applying threshold methods, where, starting from an 8-bit gray scale image, droplets are extracted by setting appropriate threshold values, mostly based on the operator's experience [21, 3]. In general terms, to obtain an informative binary image, the "reference" threshold value must be correlated with some features of the image (average, median, mode gray level), exploited by the several algorithms available in the literature (Otsu, isoData, Huang, etc.). This enables to automate the thresholding process, minimizing the worker's subjectivity and the margin of error in the measurement during binarization [22, 25, 28].

The primary aim of this research was to analyze how variations in threshold levels used to segment droplet images affect volumetric diameter measurements. The final goal is to develop a fully automatic procedure able to segment images and provide all spray droplet parameters. The study was carried out on droplet images of an air induction hollow cone nozzle TVI 8002 at the pressure of 1.0 MPa, obtained by applying the liquid immersion method.

2 The Droplet Image Acquisition System

The measurement of the spray parameters was based on the liquid immersion method, following the guidelines reported in the ISO 5682-1:1996 [9] standard. The droplets

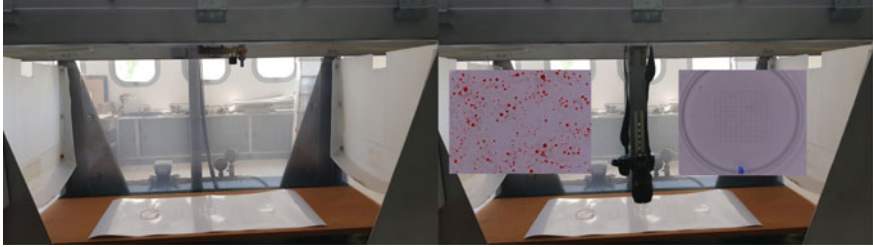


Fig. 1 The target plane with the three Petri dishes and the nozzle during the spraying tests (left) and the acquisition system (DSLR camera, pattern to calibrate the images and example of image) (right)

produced by the nozzle under test (an air induction hollow cone nozzle TVI 8002, Albus, France, at the pressure of 1.0 MPa) were captured in three Petri dishes containing silicone oil and then immediately photographed using a high-resolution (6000×4000 pixel) DSLR camera (Nikon D5500) equipped with a macro lens (Nikon Micro Nikkor AF-S 60 mm f/2.8 G ED) and an electronic flash. The spraying procedure was repeated three times, so nine images were acquired. To better identify the droplets, a solution of clean water and soluble coloring agent Ponceau Red at the concentration of 2 g L^{-1} was sprayed. Images were calibrated by photographing a 10×10 mm grid pattern engraved on a glass disc and an average calibration factor C_f was calculated equal to $5.25 \mu\text{m pixel}^{-1}$ (Fig. 1). The tests were carried out by means of a test bench developed and built at the Section of Mechanics and Mechanization of the Di3A [4, 13], which allows testing nozzles with hydraulic pulverization in real field conditions.

3 Image Analysis

At first, a preliminary analysis of the images was aimed at finding an “optimal” threshold value (OTV) based on the operator’s judgment. This value was then correlated to the average gray level (AGL) of the image, ranging from 0 (black pixel) to 255 (white pixel) for 8-bit gray level images, and the correlation was well described by the Eq. (1):

$$TV^* = 1.045 \times AGL - 24.48 \quad (1)$$

where TV^* is the threshold value predicted by the linear model. Since the determination coefficient R^2 (0.922) was highly significant ($p\text{-level} < 0.001$), an optimal threshold value, according to the judge of one expert and for the image acquisition system used in this study, is then strictly related to the average gray level of the image. Therefore, the regression equation was used to predict the threshold value to

be used for the image segmentation according to the average gray level of the image and make the process as objective as possible.

Subsequently, to study more in depth the effects of the threshold values on the spray droplet size distribution measurement, each image was reanalyzed 11 times with 11 different thresholds: TV^* and its variations of ± 5 units with step of 1 unit. To compare the effect of the threshold variation in all repetitions, the threshold values were normalized to the TV^* value chosen in each repetition. The volumetric diameters $D_{v0.1}$, $D_{v0.5}$ and $D_{v0.9}$, usually adopted to describe the pulverization capability of a nozzle, were calculated in correspondence of each threshold value. The results were then compared to those obtained when the optimal threshold value OTV was used.

Image analysis was carried out by means of the image processing software ImageJ [1]. Original color JPEG images were initially converted into 8-bit gray level images, segmented by applying the chosen threshold value and processed with the “watershed” binary filter to separate some touching particles. Subsequently, all the images were carefully inspected at a suitable zoom factor to manually remove some foreign particles arising from the segmentation process or to separate some particles not separated by the watershed filter. Finally, all particles present in the images were extracted and for each particle the following features were considered (all data in pixel): area, primary and secondary axis of the best fitting ellipse, aspect ratio (ratio between primary and secondary axis), maximum and minimum calliper (Feret’s diameters). Particles touching the edges of the images were discharged, as well as those up to four contiguous pixels, considered as digital noise. In addition, particles with aspect ratio or ratio between maximum and minimum calliper greater than 1.50 were also excluded, because deviating excessively from the circular shape. Starting from the particle area A'_i (pixel), the corresponding particle diameter D'_i (pixel) was computed according to Eq. (2):

$$D'_i = \sqrt{\frac{4A'_i}{\pi}} \quad (2)$$

Real-world diameter was obtained by applying the measured calibration factor:

$$D_i = C_f \times D'_i (\mu\text{m}) \quad (3)$$

Finally, knowing the diameter of each particle (droplet), volumetric diameters $D_{v0.1}$, $D_{v0.5}$ and $D_{v0.9}$ were computed by using suitable R functions expressly written [20].

4 Results and Discussion

Table 1 reports the OTV values (chosen by the expert) and those (TV^*) predicted by Eq. (1) for each analyzed image. They were almost always coincident (8 out of 9)

Table 1 Threshold values chosen by an expert (OTV) and predicted by Eq. 1 (TV^*)

Replicate/Petri dish	OTV			TV^*		
	PD1	PD2	PD3	PD1	PD2	PD3
R1	108	108	107	108	108	107
R2	107	108	106	107	108	106
R3	106	107	108	106	107	107

and then the model described by the Eq. (1) can be considered a good starting point for selecting the threshold value to be used in the image segmentation process.

Table 2 reports the volumetric diameters $D_{v0.1}$, $D_{v0.5}$ and $D_{v0.9}$, calculated considering the threshold value established by the expert (OTV). In order to calculate the volumetric diameters on a representative sample of droplets (greater than 2000, as recommended by ISO 5682–1 [9]), droplets contained in the three Petri dishes were merged for each replicate.

Figure 2 shows the effects on the three volumetric diameters $D_{v0.1}$, $D_{v0.5}$ and $D_{v0.9}$ due to changes in threshold values. Points represent average values of the three repetitions.

Table 2 Volumetric diameters (μm) calculated considering the threshold values OTV

Replicate	$D_{v0.1}$	$D_{v0.5}$	$D_{v0.9}$	Droplet number
R1	219	455	697	2801
R2	210	455	745	2702
R3	209	459	792	2835
mean	213	456	745	2779

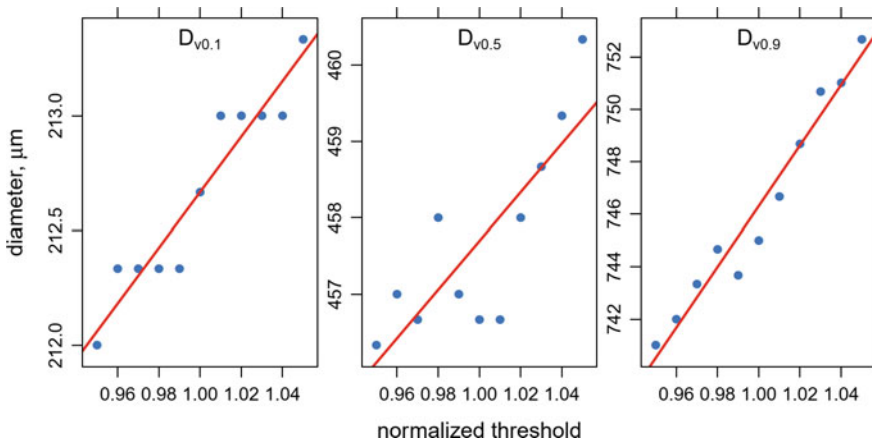


Fig. 2 Variations on measured volumetric diameters as affected by threshold values

From the Fig. 2 emerges that an increase in the threshold value produced an increase in the calculated droplet diameters, well described by linear trends. The regression lines were characterized by determination coefficients R^2 equal to 0.909 ($D_{v0.1}$), 0.627 ($D_{v0.5}$) and 0.956 ($D_{v0.9}$), all statistically significant. This result confirms the importance of carefully choosing the threshold value to be used in the segmentation process. However, from a practical point of view, the effect on volumetric diameters was negligible: in fact, according to the regression lines, when the threshold value changed from 0.95 to 1.05 (normalized with respect to TV^*), $D_{v0.1}$ varied from 212.1 to 213.3 μm , $D_{v0.5}$ from 456.1 to 459.3 μm , and $D_{v0.9}$ from 740.5 to 752.1 μm . With respect to the reference values obtained on the base of the operator's experience (Table 2), differences ranged from -0.19% to 0.38% ($D_{v0.1}$), from -0.04% to 0.65% ($D_{v0.5}$) and from -0.55% to 1.01% ($D_{v0.9}$). Then, when the segmented images were visually inspected to eliminate some foreign particles arising from the segmentation process, variations in threshold values of ± 5 units with respect to the value predicted by Eq. (1), produced changes in volumetric diameters lower than $\pm 1\%$. This result can be considered very promising, because it allows to make the process less subjective and to keep deviations from reference values very limited and in agreement with the precision of the whole measuring system. On the other hand, results discussed in the literature [17, 23] report that different measurement techniques produce different results, and variations in results may be much higher than those obtained in this study due to the threshold choice, in absolute terms always lower than 1%.

Trying to make the process full-operator-independent, a final comparison was carried out between the average volumetric diameters obtained considering the threshold values OTV and TV^* followed by a visual inspection of the segmented images and TV^* without any image inspection (Table 3).

The automatic method produced a slight increase in the three volumetric diameters with respect to the manual method with threshold value OTV, even if differences in results can be neglected: in fact, $D_{v0.1}$ did not change with the three methods (213 μm), $D_{v0.5}$ increased by 0.2% only (from 456 to 457 μm), and $D_{v0.9}$ increased by 0.4% (from 745 to 748 μm). The number of particles used to compute the diameters decreased by 1.00% (from 2779 to 2754). This reduction was due to the lack of manual separation of some particles not separated by the watershed filter, which also explained the slight increase in volumetric diameters.

Table 3 Volumetric diameters (μm) calculated considering the three image processing approaches

Threshold value and image inspection	$D_{v0.1}$	$D_{v0.5}$	$D_{v0.9}$	Droplet number
OTV (expert, with image inspection)	213	456	745	2779
TV^* (Eq. 1, with image inspection)	213	457	745	2778
TV^* (Eq. 1, without image inspection)	213	457	748	2754

5 Conclusions

Using a measurement method based on image analysis, the present paper analyzes the issue of how much the calculated volumetric diameters of a spray were affected by the choice of the threshold value adopted for the image segmentation. The study was limited to an air induction nozzle TVI 8002 at the pressure of 1.0 MPa, but may be extended to other nozzle types and other working pressures. Standard segmentation algorithms such as Otsu or mean proved to be unsatisfactory for the image acquisition system used in this study, so a reference threshold calculated on the base of the average gray level of the image and the researcher judgment was used as starting point. The main results allowed drawing the following conclusions:

- An increase in the threshold value produced an increase in the calculated volumetric diameters, well described by statistically significant linear trends, confirming the importance of accurately choosing the threshold value to be used in the segmentation process.
- Variations in volumetric diameters, however, were almost negligible from a practical point of view: in fact, with respect to the reference values obtained on the base of the operator's judgment, differences ranged from -0.19% to 0.38% for $D_{v0.1}$, from -0.04% to 0.65% for $D_{v0.5}$, and from -0.55% to 1.01% for $D_{v0.9}$. These differences may be considered in agreement with the precision of the measuring system adopted and they are much lower than those found in the literature between different laboratories that use different measuring principles.
- A first approach aimed at making the process full-operator-independent, based on the choice of the threshold value in function of the average gray level of the image and without any visual inspection of the image after segmentation, produced results very promising. In fact, it was observed a slight increase in the volumetric diameters (lower than 0.4% for $D_{v0.9}$ and increasing when the fraction α in the volumetric diameter $D_{v\alpha}$ increased). However, a more accurate study must be carried out, also considering images with different light conditions and/or different gray levels.

Acknowledgements This research was funded by the University of Catania with the research projects "Sostenibilità ed innovazioni della ricerca in agricoltura, alimentazione e ambiente - WP 6: Monitoraggio ambientale, Meccanica e Meccanizzazione Sostenibile nell'Agricoltura Mediterranea", premialità Linea 2 PIACERI and "Safe and Smart Farming with Artificial Intelligence and Robotics" (S2FAIR) - Programma Ricerca di Ateneo UNICT 2020-22 linea 2 PIACERI.

References


1. Abramoff, M.D., Magelhaes, P.J., Ram, S.J.: Image processing with image. J. Biophotonics Int. **11**(7), 36–42 (2004)

2. Albuz: Spray nozzles catalog. http://www.albuz.pl/wp-content/uploads/2016/03/cat_UK_23_03_16.pdf. Accessed 24 May 2022
3. Bhargavi, K., Jyothi, S.: A survey on threshold based segmentation technique in image processing. *Int. J. Innov. Res. Dev.* **3**, 234–239 (2014)
4. Cerruto, E., Manetto, G., Longo, D., Failla, S., Schillaci, G.: A laboratory system for nozzle spray analysis. *CET* **58**, 751–756 (2017). <https://doi.org/10.3303/CET1758126>
5. Damalas, C.A., Eleftherohorinos, I.G.: Pesticide exposure, safety issues, and risk assessment indicators. *Int. J. Environ. Res. Public Health* **8**(5), 1402–1419 (2011). <https://doi.org/10.3390/ijerph8051402>
6. European Union: Directive 2009/128/EC of the European Parliament and of the Council establishing a framework for Community action to achieve the sustainable use of pesticides. Retrieved from European Union: <https://leap.unep.org>. Accessed 24 May 2022
7. Figueiredo, V.O., Miranda, J.A.T., Colares, L.G.T., de Carvalho, J.L.V., Castro, I.M., de Carvalho, L.M.J.: Organophosphorus pesticides residues in cooked capsicum annum. *CET* **44**, 241–246 (2015). <https://doi.org/10.3303/CET1544041>
8. Finizio, A., Villa, S.: Environmental risk assessment for pesticides: a tool for decision making. *Environ. Impact Assess. Rev.* **22**, 235–248 (2002). [https://doi.org/10.1016/S0195-9255\(02\)00002-1](https://doi.org/10.1016/S0195-9255(02)00002-1)
9. ISO (International Organization for Standardization): ISO 5682–1, Equipment for crop protection - Spraying equipment - Part 1: Test methods for sprayer nozzles. Geneva, Switzerland. (1996). <https://www.iso.org/standard/60053.html>. Accessed 14 Mar 2022
10. ISO (International Organization for Standardization): ISO 25358, Crop protection equipment - Droplet-size spectra from atomizers - Measurement and classification. Geneva, Switzerland. (2018). <https://www.iso.org/standard/66412.html>. Accessed 22 Mar 2022
11. Lambert, M., Richardson, J., Grimbuhler, S.: Pesticide Exposure and Sprayer’s Task Goals: Comparison Between Vineyards and Greenhouses. IOS Press, pp. 4994–5002 (2012). <https://doi.org/10.3233/WOR-2012-0045-4995>
12. Lodwik, D., Pietrzyk, J., Malesa, W.: Analysis of volume distribution and evaluation of the spraying spectrum in terms of spraying quality. *Appl. Sci.* **10**, 2395 (2020). <https://doi.org/10.3390/app10072395>
13. Longo, D., Manetto, G., Papa, R., Cerruto, E.: Design and construction of a low-cost test bench for testing agricultural spray nozzles. *Appl. Sci.* **10**, 5221 (2020). <https://doi.org/10.3390/app10155221>
14. Marucco, P., Balsari, P., Roettele, M.: Prevention of water contamination from pesticides: the TOPPS project BMP dissemination in Italy. *CET* **58**, 781–786 (2017). <https://doi.org/10.3303/CET1758131>
15. Pascuzzi, S., Manetto, G., Santoro, F., Cerruto, E.: A brief review of nozzle spray drop size measurement techniques. In: 2021 IEEE International Workshop on Metrology for Agriculture and Forestry (MetroAgriFor) (2021). <https://doi.org/10.1109/MetroAgriFor52389.2021.9628757>
16. Manetto, G., Cerruto, E., Longo, D., Papa, R.: Error on drop size measurement due to image analysis digitisation. *LNCE* **252**, 365–374 (2022). https://doi.org/10.1007/978-3-030-98092-4_37
17. Nuyttens, D., Baetens, K., De Schamphelleire, M., Sonck, B.: Effect of nozzle type, size and pressure on spray droplet characteristics. *Biosyst. Eng.* **97**, 333–345 (2007). <https://doi.org/10.1016/j.biosystemseng.2007.03.001>
18. Pertot, I., Caffi, T., Rossi, V., Mugnai, L., Hoffmann, C., Grando, M.S., Gary, C., Lafond, D., Duso, C., Thiery, D., Mazzoni, V., Anfora, G.: A critical review of plant protection tools for reducing pesticide use on grapevine and new perspectives for the implementation of IPM in viticulture. *Crop Prot.* **97**, 70–84 (2017). <https://doi.org/10.1016/j.cropro.2016.11.025>
19. Pogăcean, M.O., Gavrilescu, M.: Plant protection products and their sustainable and environmentally friendly use. *Environ. Eng. Manag. J.* **8**(3), 607–627 (2009)
20. R Core Team: R: A language and environment for statistical computing. R Foundation for Statistical Computing, Vienna, Austria (2021). www.R-project.org/. Accessed 15 Mar 2022

21. Saleh Alamri, S., Kalyankar, N., Khamitkar, S.: Image segmentation by using threshold techniques. *J. Comput.* **2**, 83–86 (2010)
22. Sánchez–Hermosilla, J., Medina, R.: Adaptive threshold for droplet spot analysis using water-sensitive papers. *Appl. Eng. Agric.* **20**(5), 547–551 (2004). <https://doi.org/10.13031/2013.17454>
23. Sijts, R., Kooij, S., Holterman, H.J., van de Zande, J., Bonn, D.: Drop size measurement techniques for sprays: comparison of image analysis, phase doppler particle analysis, and laser diffraction. *AIP Adv.* **11**, 015315 (2021). <https://doi.org/10.1063/5.0018667>
24. Sookhtanlou, M., Allahyari, M.S.: Farmers' health risk and the use of personal protective equipment (PPE) during pesticide application. *Environ. Sci. Pollut. Res.* **28**, 28168–28178 (2021). <https://doi.org/10.1007/s11356-021-12502-y>
25. Surovy, P., Dinis, C., Marusak, R., Ribeiro, N.: Importance of automatic threshold for image segmentation for accurate measurement of fine roots of woody plants. *Lesn. Cas. For. J.* **60**, 244–249 (2014)
26. Tudi, M., Ruan, H.D., Wang, L., Lyu, J., Sadler, R., Connell, D., Chu, C., Phung, D.T.: Agriculture development, pesticide application and its impact on the environment. *Int. J. Environ. Res. Public Health* **18**, 1112 (2021). <https://doi.org/10.3390/ijerph18031112>
27. Wong, H.L., Garthwaite, D.G., Ramwell, C.T., Brown, C.D.: Assessment of exposure of professional agricultural operators to pesticides. *Sci. Total Environ.* **619–620**, 874–882 (2018). <https://doi.org/10.1016/j.scitotenv.2017.11.127>
28. Zhu, S., Xia, X., Zhang, Q., Belloulata, K.: An image segmentation algorithm in image processing based on threshold segmentation. In: *IEEE Conference*, pp. 673–678 (2008). <https://doi.org/10.1109/SITIS.2007.116>

Application of Spectral Indices for the Evaluation of Conservative Techniques in Crops Management



Elio Romano , Federico Calcagno, Carlo Bisaglia , Nicola Furnitto ,
Giampaolo Schillaci , and Sabina Failla 

Abstract Soil conservative practices, including no-tillage and sod-seeding, reduce energy inputs and prevent organic matter from exposure to oxidation and hinder losses of moisture; for these reasons, they could represent a solution for crop cultivation not only in water stress conditions.

The satellite image acquisition technology allows to access databases of satellite maps with different spectral indices. Some of these, based on spectrum bands with wavelengths in the near and far infrared zone, are dedicated to the surface water content of crops or soils.

The purpose of the study was to compare durum wheat yield in conservative agricultural practices compared to conventional one in a Mediterranean climate conditions, by analysing data collected from the Sentinel2 satellite; to study the effects of automatic driving versus manual one on crop production and on the spectral indices NDVI (Normalized Difference Vegetation Index), NDWI (Normalized Difference Water Index) and NMDI (Normalized Multi-band Drought *Index*); and to find a correlation between the indices considered and the yields of the current crop.

The results indicated the possibility of the spectral indices to understand the effect of the tillage practices on soil moisture. The use of these indices - available free of charge from ESA (European Space Agency) dataset - allows to have a high-frequency information tool for evaluating the effect of agricultural practices, dynamics of crops

E. Romano (✉) · C. Bisaglia

Consiglio Per la Ricerca in Agricoltura e L'analisi Dell'economia Agraria (Council for Agricultural Research and Economics), CREA Research Centre for Engineering and Agro-Food Processing, Via Milano, 43 - 24047 Treviglio, (BG), Italy
e-mail: elio.romano@crea.gov.it

N. Furnitto · G. Schillaci · S. Failla · S. Failla

Department of Agriculture, Food and Environment (Di3A), Section of Mechanics and Mechanisation, University of Catania, Via Santa Sofia 100, 95123 Catania, Italy

F. Calcagno

Consiglio Per la Ricerca in Agricoltura e L'analisi Dell'economia Agraria (Council for Agricultural Research and Economics), Centro Di Ricerca Viticoltura Ed Enologia, CREA Research Centre for Engineering and Agro-Food Processing, (CREA-VE), Via Casamassima, 148 - 70010 Turi, (BA), Italy

and characteristics of the soil; moreover, it could provide a greater awareness on the application of management choices dedicated to sustainability.

Keywords No tillage · NDVI · NMDI · NDWI · Satellites image · Precision agriculture

1 Introduction

Conservation tillage practices improves water availability for wheat crops by increasing soil water absorption capacity and reducing water losses for evapotranspiration [1–3]. Peng et al. [2] showed that no tillage practices significantly increased soil water potential compared to tillage system at the seedling and jointing phenological phases of wheat. Sowing on minimum or no tilled soil can ensure a more efficient use of the water resources and a suitable productivity of the crop [4–6].

Several multispectral indices have been used to analyze crop variability and soil moisture content. The most used are NDVI (Normalized Difference Vegetation Index), NDWI (Normalized Difference Water Index) and NMDI (Normalized Multi-band Drought Index). The NDVI spectral index is dedicated to the evaluation of vegetative vigor and to the estimation of the variability in the vegetation cover and it is studied throughout the cultivation season. The NMDI, is dedicated to the evaluation of bare soil and the NDWI is used both on crops and soil. Both decode the surface moisture [7, 8]. Pezzuolo et al. [9] studied the evolution of NDVI in relation to soil tillage techniques management on soft wheat. They showed there was an increase of NDVI from conventional tillage to minimum tillage, and no-tillage. Varghese et al. [10] reported that they used Sentinel-2 to investigate the plant responses to different soil moisture conditions and variations in canopy water level at regional and field levels. Sentinel-2 outperformed Landsat-8 and showed a significant correlation with soil moisture (<30 cm depth) [11].

The purpose of this study was to evaluate the trend of the spectral indices on an experimental site, cultivated with durum wheat under no-tillage practices. A further objective was to examine the effects of automatic driving of tractor versus non-automatic driving in cultivation practices, on production yields and on the indices considered.

2 Material and Methods

2.1 *Experimental Site and Agricultural Machines*

The study was carried out in a parcel cultivated with durum wheat in Sicily (Italy), Enna province, 1.47 ha size, in a typical Mediterranean climate area. According to the



Fig. 1 The seeder

USDA classification [12] the soil of the site could be classified as Sandy Clay Loam. The experimental field consists of 4 plots, two of 17×200 m each on flat ground (A1, A2) and two of 17×150 m each on land with a slope of 4% (B1, B2). These plots are cultivated under no tillage practices and sod seeding techniques. Another plot of 17×200 m was taken as control test (CT) and it is managed according to minimum tillage practices for seedbed preparation. In the plots A1, A2 and B1, B2 a pre-sowing weeding, sod-seeding, fertilisation, spring weeding with a non-selective herbicide based on glyphosate and harvesting were carried out. In the CT plot, a minimum tillage was carried out with a cultivator at a depth of about 20 cm. Weeding was carried out twice using a mechanical pulverisation sprayer of 15 m. The sowing of the DW Antalis cultivar (195 kg ha^{-1}) was carried out on January 19th, 2022, according to the no-till seeding practice, using a row seeder with pneumatic distribution, 4.2 m wide with 20 furrows and wheelbase of 21 cm (Fig. 1) The seeder was connected to a NewHolland T6.180 4WD tractor (year of manufacture 2019), 116 kW nominal power and 5.46 t total mass. The automatic guide, in plot A1 and B1, to be compared with the manual one, in plot A2 and B2, was activated both in the flat parcel and in the sloping one. On July 7th, 2022, the harvesting was carried out for a single test thesis with a New Holland model CX7.90 combine harvester, 275 kW having a monitor, installed in the cab, able to display and control all functions and parameters of the machine (Fig. 2).

2.2 Image Analysis

The map files of reflectance values of the selected bands from the Sentinel-2 satellite databases were processed using R software.



Fig. 2 The harvester

In total 45 images were downloaded from January to August 2022 and of these 20 cloudless images were chosen and processed to obtain the three spectral indices (NDVI - NMDI - NDWI) chosen.

The indices were studied through images relating to the plots under study according to the formulas shown below:

$$NDVI = \frac{R_{842nm} - R_{665nm}}{R_{842nm} + R_{665nm}} \quad (1)$$

$$NDWI = \frac{R_{560nm} - R_{842nm}}{R_{560nm} + R_{842nm}} \quad (2)$$

$$NMDI = \frac{R_{865nm} - (R_{1610nm} - R_{2190nm})}{R_{865nm} + (R_{1610nm} - R_{2190nm})} \quad (3)$$

Then, ANOVA was carried out to study the significance between the averages of the compared tests. Moreover, post-hoc tests were applied for analysing significant differences between the tests.

To verify differences between crop phenological stages and soil water content in the different tests, the NDVI and NDWI were studied in the period from January to June (just before harvest). The NMDI index, dedicated to the observation of soil water content, was studied after the wheat harvesting.

3 Results and Discussion

The NDWI and NDVI spectral indices showed similar trends over time. Very low values were recorded until March and subsequently rose until early May.

From May to June the values decreased due to maturation which naturally involves a reduction in photosynthetic activity (Fig. 3 and 4).

In all observed dates, both indices showed significantly different values (p -value < 0.001) between the control test (CT) and other tests cultivated with manual guidance (A2 and B2).

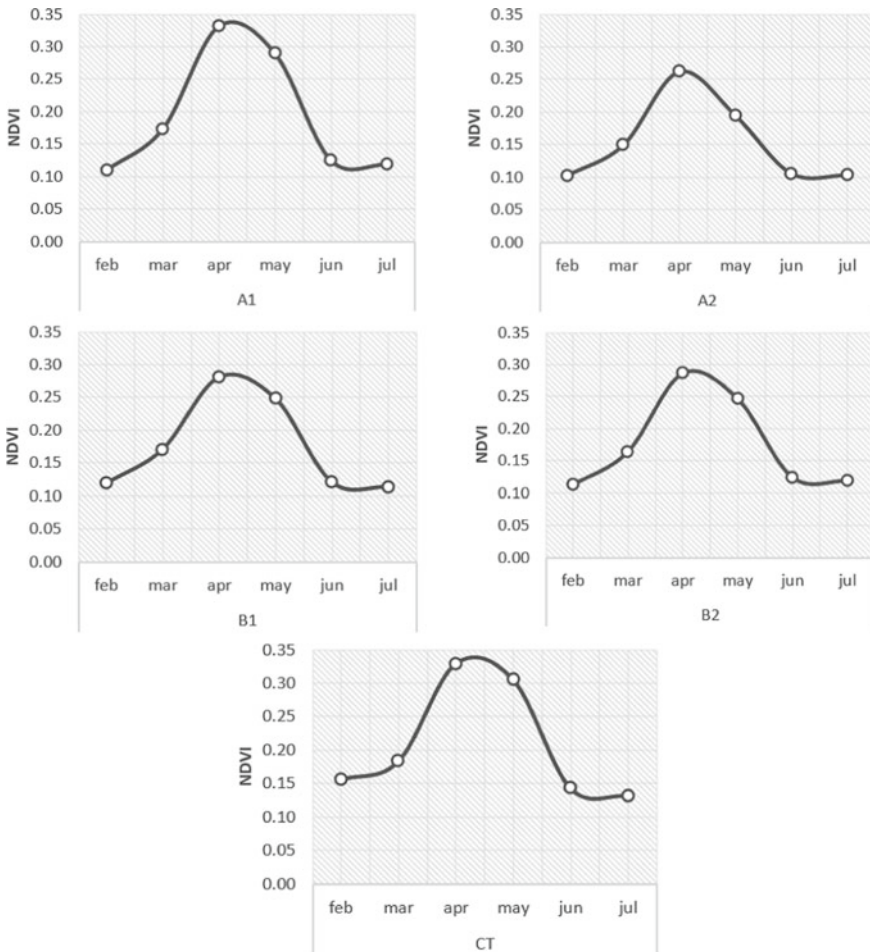


Fig. 3 NDVI trend during the crop in the five conditions

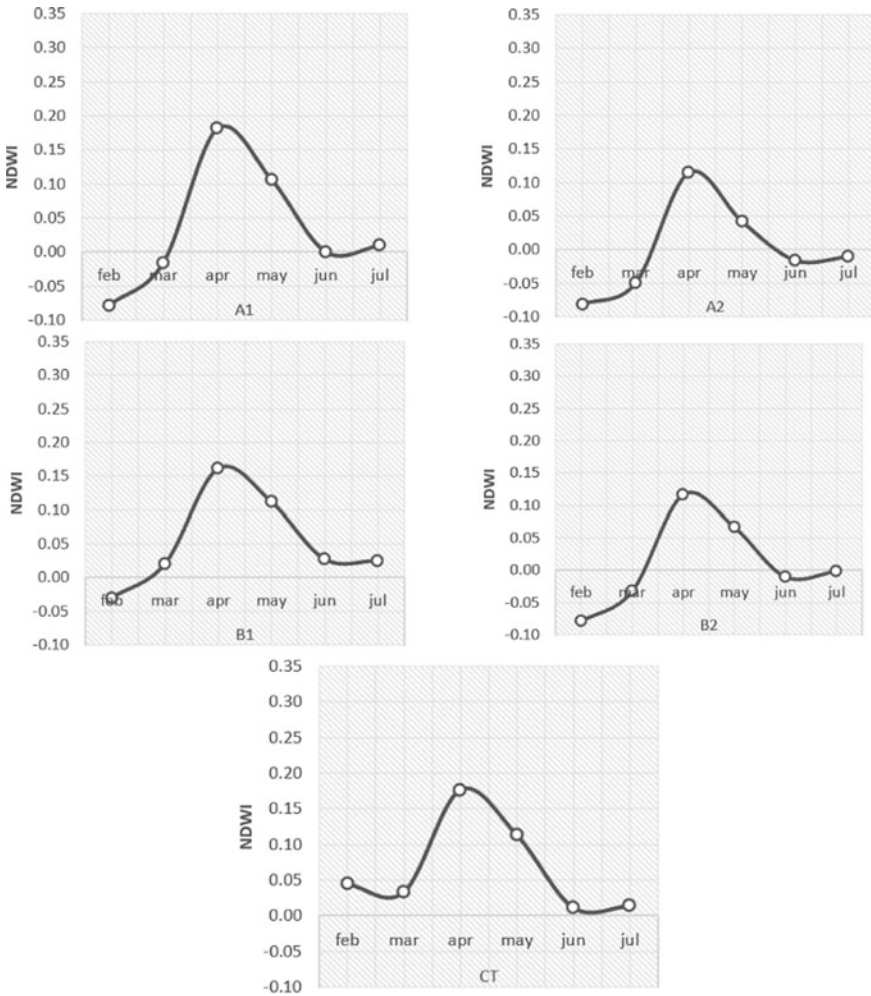


Fig. 4 NDWI trend during the crop in the five conditions

On the other hand, there is no difference between the values of the CT and the values recorded in other tests cultivated with automatic driving, both in the flat and in sloping plots (Fig. 5 and 6).

The NMDI index was observed in the months after harvest, and it showed that the tests maintained a condition of soil moisture with most values below 0.7. Manual driving in flat slope showed less humidity (Fig. 7).

Moreover, the intrinsic variability of the soil generates, in these types of experimental tests, a dispersion of the values of the response variable. In fact, a variability is observed, in the graph highlighted by the dispersion of the points outside the boxplot, measured by the standard deviation which in the average of the NMDI was equal to

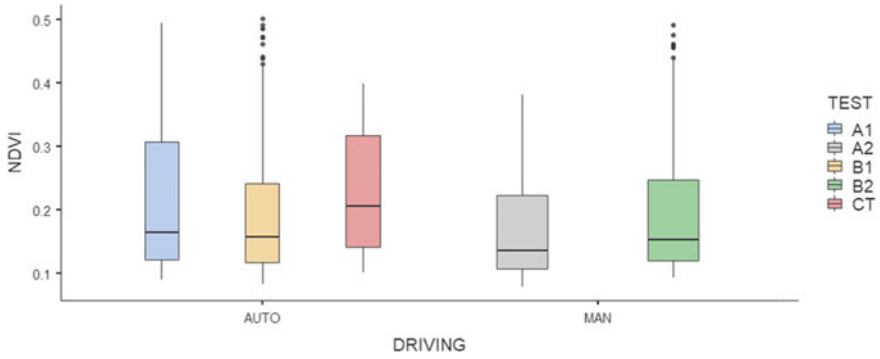


Fig. 5 NDVI in the tests.

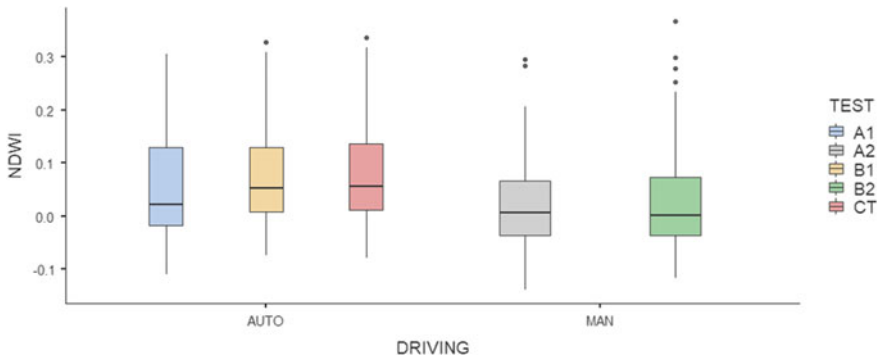


Fig. 6 NDWI in the tests

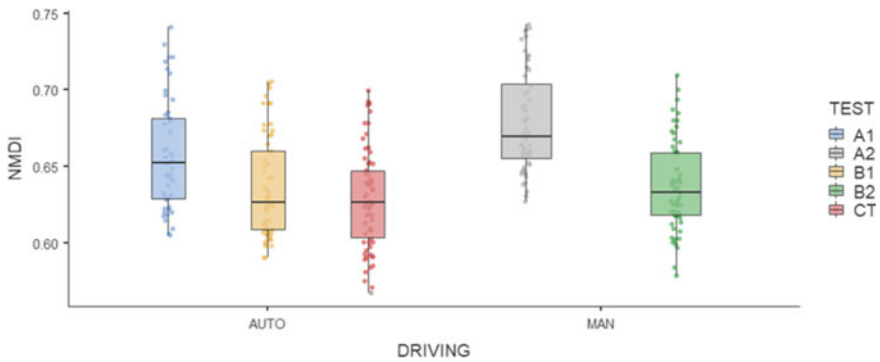
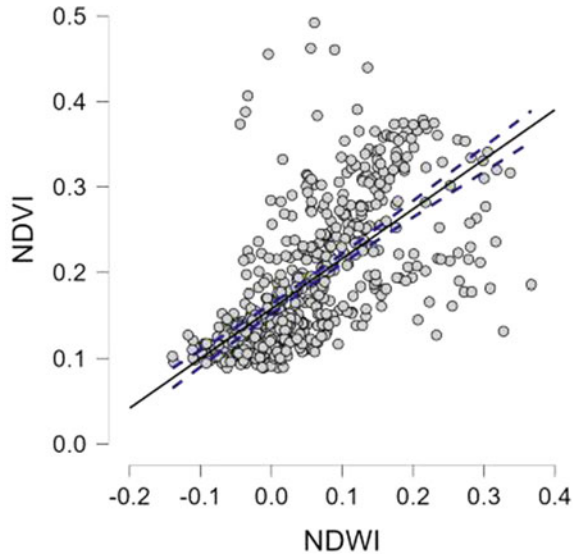


Fig. 7 NMDI after the harvest

Fig. 8 Correlation between NDVI and NDWI



0.037, almost 5% of the average value detected in the whole experimentation, with a range between 4.57% in condition B2 and 5.54% in condition A1.

Furthermore, the correlation between NDVI and NDWI (Fig. 8) in the entire observation period showed a Pearson coefficient of 0.646, with p -value < 0.001 .

4 Conclusions

The analysis of the spectral indices observed in the experimental plots showed a high correspondence between the variations in the recorded values and the tests compared. In a similar way, the NDWI and NDVI indices were found to be very suitable for reading the differences between the plots that were cultivated with automatic guidance compared to those conducted with manual guidance and their correlation was found to be significant. The plots sown with manual guidance showed a distribution of the lowest values, in the two indices NDVI and NDWI. This could be explained by the increased likelihood of uncovered surfaces with manual guidance. As indicated by Wang and Qu [13], NMDI is well suited to monitor dry soil status. In fact, the NMDI index observed in the months after the harvest showed how the plots retained moisture in the soil.

The possibility of using satellite information, which is available free of charge and with high frequencies, represents a precious resource for the management of land and its characteristics such as water in different cultivation conditions. Further in-depth studies will be aimed at comparing the satellite data with those collected in the field in a multi-year experimentation.

Acknowledgements This study was supported by the Italian P.O.N. “RICERCA E INNOVAZIONE” 2014 – 2020, Azione II – Obiettivo Specifico 1b – Progetto “Miglioramento delle produzioni agroalimentari mediterranee in condizioni di carenza di risorse idriche–WATER4AGRIFOOD”. The authors are very grateful to Dr Marco Frasson for giving hospitality to the experimental tests in his agricultural farm; and for providing agricultural machineries to perform the experimental campaign and for his valuable support during the experimental tests.

References

1. Zheng, C.Y., Yu, Z.W., Shi, Y., Cui, S.M., Wang, D., Zhang, Y.L., Zhao, J.Y.: Effects of tillage practices on water consumption, water use efficiency and grain yield in wheat field. *J. Integr. Agric.* **13**, 2378–2388 (2014)
2. Peng, Z., Wang, L., Xie, J., Li, L., Coulter, J.A., Zhang, R., Luo, Z., Kholova, J., Choudhary, S.: Conservation tillage increases water use efficiency of spring wheat by optimizing water transfer in a semi-arid environment. *Agronomy* **9**, 583 (2019)
3. Jakab, G., Madarász, B., Szabó, J.A., Tóth, A., Zacháry, D., Szalai, Z., Kertész, Á., Dyson, J.: Infiltration and soil loss changes during the growing season under ploughing and conservation tillage. *Sustainability* **9**, 1726 (2017)
4. Pittelkow, C.M., Liang, X., Linguist, B.A., van Groenigen, K.J., Lee, J., Lundy, M.E., van Gestel, N., Six, J., Venterea, R.T., van Kessel, C.: Productivity limits and potentials of the principles of conservation agriculture. *Nature* **514**, 365–368 (2015)
5. Gonzalez-Sanchez, E.J., Veroz-Gonzalez, O., Blanco-Roldan, G.L., Marquez-Garcia, F., Carbonell-Bojollo, R.: A renewed view of conservation agriculture and its evolution over the last decade in Spain. *Soil Tillage Res.* **146**, 204–212 (2019)
6. Failla, S., Pirchio, M., Sportelli, M., Frascioni, C., Fontanelli, M., Raffaelli, M., Peruzzi, A.: Evolution of smart strategies and machines used for conservative management of herbaceous and horticultural crops in the mediterranean basin: a review. *Agronomy* **11**(1), 106 (2021)
7. Casamitjana, M., Torres-Madroño, M.C., Bernal-Riobo, J., Varga, D.: Soil moisture analysis by means of multispectral images according to land use and spatial resolution on andosols in the colombian andes. *Appl. Sci.* **10**, 5540 (2020)
8. Jackson, T., Chen, D., Cosh, M., Li, F., Anderson, M., Walthall, C., Doriaswamy, P., Hunt, E.: Vegetation water content mapping using Landsat data derived normalized difference water index for corn and soybeans. *Remote Sens. Environ.* **92**, 475–482 (2004)
9. Pezzuolo, A., Cillis, D., Marinello, F., Sartori L.: relationship between satellite-derived NDVI and soil electrical resistivity: a case study. In: 6 th International Conference on Trends in Agricultural Engineering, pp. 7–9, Prague, Czech Republic (2016)
10. Varghese, D., Radulović, M., Stojković, S., Crnojević, V.: Reviewing the potential of sentinel-2 in assessing the drought. *Remote Sens.* **13**(17), 3355 (2021)
11. West, H., Quinn, N., Horswell, M., White, P.: Assessing vegetation response to soil moisture fluctuation under extreme drought using sentinel-2. *Water* **10**, 838 (2018)
12. USDA Natural Resources Conservation Service Soil. https://www.nrcs.usda.gov/wps/portal/nrcs/detail/soils/survey/?cid=nrcs142p2_054167
13. Wang, L., Qu, J.J.: NMDI: a normalized multi-band drought index for monitoring soil and vegetation moisture with satellite remote sensing. *Geophys. Res. Lett.* **34**, L20405 (2007)

Big Data for Farm Machines: An Algorithm for Estimating Tractors' Operating Costs



Pierluigi Rossi, Gianmarco Rigon, Riccardo Alemanno, Leonardo Bianchini, Massimo Cecchini, and Danilo Monarca

Abstract Estimating the operating costs of agricultural tractors is key to the decision-making process of any farm, helping to assess the feasibility of investments in machinery and thus the impact on agricultural profitability.

However, the variation of several parameters over the years, such as environmental conditions, technological innovations, field capacity and the performance of agricultural machinery, have now led to a different impact on these indicators.

The aim is to provide new tools for the precise estimation of tractor operating costs, based on the information gathered from machines via CANBUS interfaces and geospatial data processing. To this end, GPS data from the machines were collected and combined with the European Copernicus digital elevation models (DEM) in order to supplement the dataset with information on altitude, distance and average speed.

As a result, after data aggregation, the algorithm was able to determine working times, fuel consumption and areas worked for the open field operations examined. All information could be reproduced on geographic information systems (GIS) as well as terrestrial browsers.

These parameters might provide a detailed estimate of the operating costs of any farm. Further developments may include maintenance alerts, analysis of equipment performance and even an additional classification of other agricultural activities (ploughing, mowing, pesticide distribution, fertilisation, etc.).

Keywords Tractor operating costs · Big data · Artificial intelligence · Agriculture · Precision farming

P. Rossi · G. Rigon · R. Alemanno (✉) · L. Bianchini · M. Cecchini · D. Monarca
DAFNE Department, Tuscia University, Viterbo, Italy
e-mail: riccardo.alemanno@unitus.it

© The Author(s), under exclusive license to Springer Nature Switzerland AG 2023
V. Ferro et al. (eds.), *AIIA 2022: Biosystems Engineering Towards the Green Deal*,
Lecture Notes in Civil Engineering 337,
https://doi.org/10.1007/978-3-031-30329-6_90

881

1 Introduction

One of the pivotal points in agriculture, especially Italian agriculture, is cost reduction. Italian agriculture, like every other productive sector, is currently suffering a deep crisis linked to the rising costs of energy: diesel fuel and electricity costs among others. In particular, the price of agricultural diesel fuel has been rapidly increasing in Italy from January 2022, and then reached an all-time high as shown in Fig. 1 [1].

In addition, normal business organisation inevitably leads to downtime, which is a hidden cost for the farm. Correct planning of work sites allows a reduction in costs and working time. Being able to make diesel fuel consumption more efficient, avoiding inefficiencies in the use of vehicles allows for a not inconsiderable optimisation of production processes.

Modern agriculture increasingly makes use of means that have been enhanced with a great deal of technology over the past two decades. This has made it possible to obtain precise information on the use and operation of vehicles, which was previously only available on an experimental level and to a certain degree of approximation. The tractors that are normally used, equipped with CANBUS interfaces, make it possible to obtain huge amounts of information, which is all the more precise and numerous, thanks to the sensors that are present on-board. In an era in which data collection is all the rage, and agriculture is not excluded from this phenomenon either [2], it is essential to be able to acquire the telemetry data produced by agricultural tractors, analyse it and be able to interpret it.

All this raw data, independently generated, just needs to be interpreted to make it fundamental for the preparation of the farm's balance sheet and for the profit and loss account. A perfect understanding of the parameters, in the case of agricultural mechanisation, allows in fact for a is more in line with reality and less approximate construction of the balance sheet and profit and loss account. The large variety of available information regarding fuel consumption and maintenance information from fleet management services provides greater data accuracy, in a future that might

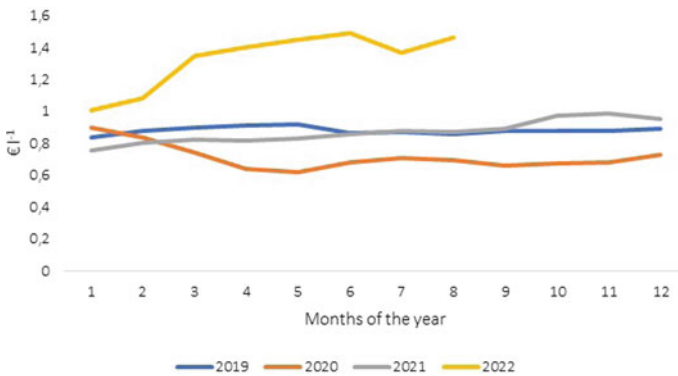


Fig. 1 Agricultural diesel fuel cost trend in Italy

even involve satellite – based systems for live monitoring [3]. It is well known that consumption and labour impact on mechanisation costs by more than 60% of the total cost per hectare [4].

The aim of this article is to highlight, albeit in a preliminary way, how current technologies, present on agricultural vehicles, allow for very important information to be obtained from the CANBUS interface. This information naturally has a positive impact on the farm's balance sheet, at least being able to know the real disbursements that an Italian wine-growing farm in central Italy may have to face in the use of its tractor and operating machines during the year.

2 Materials and Methods

Six orchard tractors with a unit power of 75 kW and 408 Nm of maximum torque were employed in the present study, which carried out all the machining tasks of a vineyard in Tuscany, Italy, over a one-year period (01 May 2021 – 30 April 2022). These vehicles were enhanced with a real-time data monitoring system that added GPS information and provided an Internet connection to upload CANBUS data to a fleet management server. Data on the performance of the engine and the vehicle itself, such as speed, temperatures and PTO, were collected from the tractors as they went about their daily activities at one-minute intervals, collecting up to 60 entries per working hour. This data set is based solely on CANBUS information from the tractor's electronic control unit (ECU), which reports data from various on-board sensors (wheel speeds, temperatures, etc.) and engine parameters (PTO speed, engine speed, oil and coolant temperatures, torque, etc.).

In addition to all of this data, it was possible to process other information and to acquire a range of information from external sources, such as the Digital Elevation Model (DEM) provided by the European Union's Earth observation programme called 'Copernicus', which made it possible to supplement the existing datasets with additional information.

In order to be able to provide concrete, precise information and allow their interpretation relative to the type of activity, the data were processed and subsequently merged to form clusters. In detail, the raw data was clustered, opting for an arbitrary choice, namely that of grouping all those activities that presented a continuity of at least 5 min, i.e., without interruptions due to inactivity on the part of the machine, and stripped of the first 10 readings that were generally those most affected by telemetric fluctuations. In addition, all those activities that fell spatially within the perimeter of the vineyard under study were considered. The latter were used to proceed with the determination of the activities carried out by the various vehicles during the year, as there was no automatic recording of the coupling of driving and operating machines.

The determination of activities, on a singular plot with a surface area of around 7 ha, followed a discrimination process that was initially based on what typical activities are carried out in a vineyard in central Italy over the course of an entire year. After which it was further noted what the farm's real equipment was in terms

of operating machinery; finding a complete equipment that allows all for all the activities of nutrition, defence, soil working, pruning and harvesting in the vineyard to be carried out. Finally, this information, before being used, was implemented and improved through a comparison with the farm management itself.

Regarding the methods used in this research, a Gantt chart has been created to match every activity with its period and highlight any overlapping phase. Figure 2 shows the Gantt chart summarising the 11 planned agricultural activities, carried out with the aid of the tractor-machine coupling, during the various months of the year.

In the same Fig. 2, those tasks performed by machines that do not require power via the tractor’s Power Take Off (PTO) are also specified.

At this point, it was possible to examine the data and assign the various tasks, using the discriminating logic shown in Table 1 as the order of assignment.

The criterion, which was followed, and which led to the assignment of a process to one set of data rather than another, basically followed the combination of what is shown in Fig. 2 with the order of the various telemetry parameters in Table 1. It therefore began with the observation of which day of the month the data referred to and to which machine. This initial identification made it possible to assume the continuity of a single operation. After that, one went on to look for a positive match in all the other data, thus being able to organise a classification that was constantly updated, becoming more and more adherent as one proceeded with the allocation of

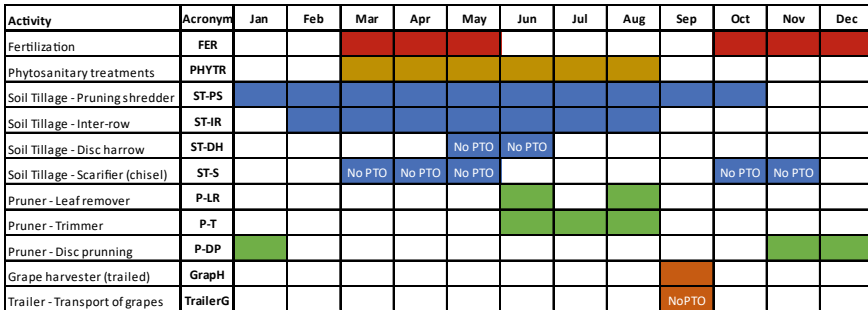


Fig. 2 Gantt chart of viticultural processing in central Italy in one year

Table 1 Parameters used in the assignment process and their order

Order	Parameter
1	Month and Day
2	Tractor serial number
3	Power Take Off (PTO)
4	Engine torque output
5	Forward speed
6	Fuel consumption
7	Slope change

the entire year. Of course, the activity or non-activity of the PTO was fundamental for a rapid discrimination of the only three possible processes that did not require its use (working the soil with a disc harrow and/or scarifying and transporting the grapes with a trailer).

To complete this activity, it was possible to examine the characterising data of the various processes carried out in the vineyard, in terms of: time spent expressed in h; average consumption expressed in $l\ h^{-1}$ and finally average torque required by the engine expressed in Nm.

3 Results and Discussion

In the interpretation of the results presented below, a small premise must be made. Following the previously described methodology, one can note the presence of some months of the year in which as many as 6 operations could be carried out at the same time: for example, in May or June, as shown in the Gantt diagram in Fig. 2. This meant that by increasing the variables, the uncertainty of activity attribution was also greater. It was precisely in these instances that the score, attributed to the identified work, was lower than that of the case with less possible work in that particular month. In fact, on average, the certainty in the attribution of one operation over the others, in these cases, was reduced to values around just 60%.

Data were recorded, in which PTO utilisation was reported, in months where theoretically it should not have been. Of course, these were in any case inscribed in those activities involving the use of idle equipment (mainly soil working) that are closest in time to those in the working calendar proposed in Fig. 2. The main explanation, which has been formulated, is that these activities have been conditioned and therefore postponed due to adverse weather, such as rain that prevented the normal access to vehicles in the field to carry out those specific workings.

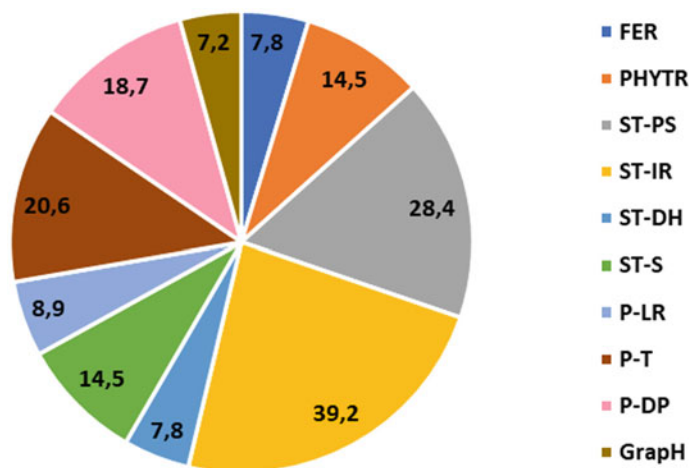
The partial variability of the data, in addition to the uncertainty of attribution of the processes, could also be sought in the different pedoclimatic conditions that alternated over the course of the year. In addition, grape transport never seems to occur in the field object of this study. This can be explained by the fact that in the September data, there were no significant activities with deactivated PTO; thus, there were no clusters reporting activities with deactivated PTO. For the same reason, no activity was found in the December period.

Of the primary analyses conducted, the time required to perform the various tasks in the various months was highlighted. Table 2 shows the sum of the times expressed in hours (h), for the individual processing and in the individual month.

Adding up all the working hours, the result is 172.4 h. This is the annual utilisation, in terms of hourly employment, of mechanisation on a single plot cultivated as a vineyard. As explained above, without considering additional downtime. To better understand the numerical information in Table 2, a pie chart was chosen, shown in Fig. 3.

Table 2 Cumulative occupation in terms of hours (h) of each work in the vineyard in the various months

Time of Work (h)	FER	PHYTR	ST-PS	ST-IR	ST-DH	ST-S	P-LR	P-T	P-DP	GrapH
January			11,2			4,0			5,7	
February						4,9				
March						4,0				
April	0,8		6,9	3,7						
May		4,4	1,4	5,6	1,1					
June		5,5		5,5			5,3			
July		4,6		9,7	6,7			16,9		
August			1,9	14,7			3,5	3,6		
September										7,2
October	7,1		7,1			6,7				
November									13	

**Fig. 3** Time (%) used for the various processes as a percentage of the total

With the help of the aerogram in Fig. 3, we can see the weight in terms of hours that each tillage has on the total amount of hours. It is worth noting the clear dominance of the soil working activities, with particular detail on the work carried out in the inter-row (ST-IR) (39.2% of the occupation) and that of shredding (ST-PS) of pruning residues and control of the turf (28.4% of the occupation). This was followed by topping (P-T) and pre-pruning (P-DP) activities, respectively 20.6% and 18.7% of the total time employed. Using the same procedure, the average data shown in Table 3 was obtained, relating to the diesel fuel consumption of tractors when used in

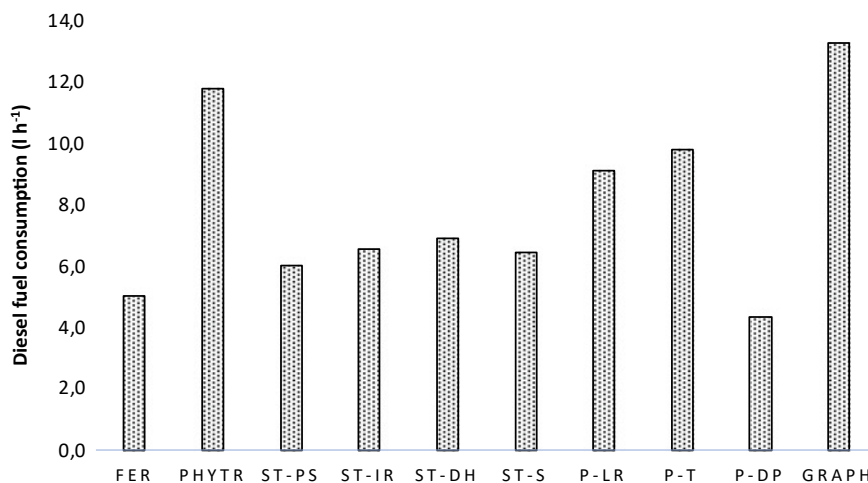


Fig. 4 Average hourly consumption ($l\ h^{-1}$) of vineyard work

combination with the various equipment to carry out the activities described above (Table 4).

As it can be seen, the average estimates tend to have rather small standard deviation values. Although this is only a preliminary analysis, it can be said that there is a certain consistency in the average consumption of individual activities over the various months.

With the bar graph shown in Fig. 4, it can be seen that on average, the processes with the highest specific diesel fuel consumption are grape harvesting (GRAPH)

Table 3 Average hourly diesel fuel consumption $l\ h^{-1}$ (\pm standard deviation) of each vineyard operation in the various months

	Jan	Feb	Mar	Apr	May	Jun	Jul	Aug	Sep	Oct	Nov
FER				4,59 \pm 1,12						5,45 \pm 0,39	
PHYTR					11,30 \pm 1,06	12,27 \pm 0,70	11,71 \pm 0,34				
ST-PS	7,00 \pm 0,49			7,90 \pm 1,21	4,12 \pm -			5,83 \pm -		5,15 \pm 0,60	
ST-IR				5,64 \pm 0,42	8,72 \pm 2,91	6,39 \pm 1,64	6,79 \pm 0,39	5,18 \pm 0,24			
ST-DH					7,78 \pm 3,94		5,97 \pm 1,17				
ST-S	6,24 \pm 1,13	6,23 \pm 0,78	6,93 \pm 1,14							6,29 \pm 0,93	
P-LR						6,68 \pm 1,62		11,49 \pm 0,75			
P-T							7,95 \pm 2,80	11,60 \pm 1,47			
P-DP	4,27 \pm 0,27										4,37 \pm -
Graph									13,26 \pm 0,96		

Table 4 Average engine torque Nm (\pm standard deviation) absorbed for each work in the vineyard in the various months

	Jan	Feb	Mar	Apr	May	Jun	Jul	Aug	Sep	Oct	Nov
FER				172,21 \pm 19,66						177,52 \pm 5,80	
PHYTR					269,92 \pm 17,07	284,78 \pm 28,06	277,56 \pm 6,74				
ST-PS	214,31 \pm 8,37			189,36 \pm 6,69	154,00 \pm -			198,70 \pm -		171,16 \pm 11,52	
ST-IR				186,33 \pm 6,84	208,19 \pm 66,02	182,28 \pm 12,95	170,27 \pm 4,35	177,64 \pm 8,55			
ST-DH					205,56 \pm 62,54		221,64 \pm 41,52				
ST-S	176,41 \pm 18,72	213,89 \pm 14,88	215,25 \pm 16,90							195,56 \pm 26,95	
P-LR						184,43 \pm 2,83		249,42 \pm 3,21			
P-T							222,70 \pm 21,74	251,42 \pm 15,32			
P-DP	136,05 \pm 3,80										125,12 \pm -
Graph									289,75 \pm 6,03		

and phytosanitary treatments, 13.3 and 11.8 l h⁻¹ respectively. This is followed by pruning (P-T and P-LR) with values above 9 l h⁻¹. All the others remain at values of average specific consumption close to 6 l h⁻¹.

At this point, we move on to the use of tractors, then to the preliminary verification of the sizing of the machinery and equipment fleet in the case study. It is again reported that the data refer to six orchard tractors, each capable of generating a maximum torque of 408 Nm.

In Table 4 of the following data, it can be seen that the actual torque used in the various machining operations is in most cases less than 50% (on average 47%–193 Nm) of the torque that is available under those conditions.

Only the two working operations involving the use of machinery for phytosanitary treatments (PHYTR - sprayer) and for grape harvesting (trailed grape harvester) required, on average, 68% (–277 Nm) and 71% (–290 Nm) respectively of the maximum torque generated by the tractor.

This last, primary and partial piece of information is very important and, if associated to the employment of the machines over a period of time, it allows us to guess that, in the present case of study, machines that are tendentially oversized are used. A simple inferable consideration is that it might be advisable to use differentiated means in terms of power for the various tasks. In this specific case: for all those activities that on average recorded that it was employed less than 50% of the maximum available engine torque under those operating conditions, it could be advisable to

use vehicles that generate 20–30% less torque. This would allow a direct economic saving on the purchase, which would also be reflected in lower annual depreciation costs and various allowances.

4 Conclusions

The information generated by the post-processing data reported in this study helps to understand how the machines are working and to define the type of tasks they performed at any given time and day. By having this type of information, it is possible to understand their operating costs and assess whether they are inefficient, unsuitable or overqualified to perform specific tasks that may be better performed by other tractors or equipment.

This methodology is certainly implementable and easily translatable to the entire farm, and also to other types of farms, thus granting full awareness of the direct costs associated with the amount of diesel fuel used throughout the year and the time spent working. It could also allow for inefficiencies on the various plots to be detected in real time and for corrective systems to be implemented.

Such parameters could provide a detailed estimate of operating costs for any farm. Future developments may include maintenance alerts, analysis of equipment performance, and even an additional classification of other farming activities.

All this is aimed at enabling farmers to make more informed decisions about their investments in machinery and innovations in operation management.

References

1. TESEO by CLAL; Agricultural Diesel Price. https://teseo.clal.it/?section=gasolio_agricolo
2. Cravero, A., Pardo, S., Sepúlveda, S., Muñoz, L.: Challenges to use machine learning in agricultural big data: a systematic literature review. *Agronomy* **12**(3), 748 (2022). <https://doi.org/10.3390/agronomy12030748>
3. Centenaro, M., Costa, C.E., Granelli, F., Sacchi, C., Vangelista, L.: A survey on technologies, standards and open challenges in satellite IoT. *IEEE Commun. Surv. Tutorials* **23**(3), 1693–1720 (2021). <https://doi.org/10.1109/COMST.2021.3078433>
4. Mattetti, M., Medici, M., Canavari, M., Varani, M.: CANBUS-enabled activity-based costing for leveraging farm management. *Comput. Electron. Agric.* **194**, 106792 (2022). <https://doi.org/10.1016/j.compag.2022.106792>

Obstacle Avoidance Safety System for Agricultural Tractors and Autonomous Vehicles Based on Bluetooth and Passive RFID



Pierluigi Rossi, Filippo Cossio, Massimo Cecchini, and Danilo Monarca

Abstract Proper interaction of workers on foot and machines is a key aspect for safety analysis of agricultural and forestry operations. Autonomous vehicles might utterly increase accident probability and severity, meaning that such vehicles must rely on inherently safe designs and that better safety devices for workers should be developed.

An attempt to address these challenges for safer working contexts in future is represented by the “SMARTGRID” project, funded by the Italian National Institute for Insurance against Accidents at Work (INAIL), which designed a brand-new wireless safety network based on Bluetooth Low Energy (BLE) devices and passive Radio Frequency IDentification (RFID) tags. The whole point of its design is to rely on a multilayer infrastructure made of two wireless networks with very different performance levels, where the strengths of a system can fill the gaps of the other and vice versa.

SMARTGRID involves antennas placed on every vehicle in order to scan for the presence of nearby RFIDs attached on workers’ personal protective equipment. To complete the system, BLE beaconing systems are also placed on vehicles: such systems will both deliver alerts to nearby workers as they enter a higher-risk area and notify all the occurrences to a backend server to store statistical data for safety purposes.

System’s range of detection spans within 8 and 12 m, but it may vary depending on tractor’s height and field conditions. Further test programs are underway in an experimental farm and will provide additional results by the end of 2022.

Keywords Agriculture · Smart farming · Work safety · Obstacle avoidance · Tractor

P. Rossi (✉) · F. Cossio · M. Cecchini · D. Monarca
DAFNE Department, Tuscia University, Viterbo, Italy
e-mail: pierluigi.rossi@unitus.it

© The Author(s), under exclusive license to Springer Nature Switzerland AG 2023
V. Ferro et al. (eds.), *AIIA 2022: Biosystems Engineering Towards the Green Deal*,
Lecture Notes in Civil Engineering 337,
https://doi.org/10.1007/978-3-031-30329-6_91

891

1 Introduction

Agriculture is a very hazardous working sector given the large number of mechanical equipment and activities that can lead to fatal accidents. Despite a fast growth of smart devices for farming automation, agricultural safety still needs to be fully explored and enhancements are needed to allow the safe use of autonomous vehicles: with the increasing usage of remotely controlled vehicles and automated equipment, previous research has already shown that safety plays a key role even at design stage [1] and its management needs to be embedded with quality in every agricultural practice [2]. Given the high number of fatalities which involved agricultural machineries during the last decade in Italy [3, 4] the lack of compliance to health and safety legislation [5] and the need to protect nearby bystanders or children as well which are consistently involved in farm-related injuries [6, 7], the “Smart system for managing the safety of operators in work environments with remote-controlled operating machines” (SMARTGRID) project described in this paper aims to mix passive radio-frequency (RFID) devices and Bluetooth low energy (BLE) devices into an integrated system to detect nearby obstacles and workers on foot. Previous attempts regarding smart devices for safety purposes in agriculture involved wearable transponders made of near-field electronic components [8] and laser-based obstacle detection devices [9] but they can be employed for short detection distances and may become costly, making them unfeasible for the purpose of the project. Other solutions involving cameras and artificial intelligence applied to video analysis have also been discarded since the working environment might affect the possibility of acquiring live images [10].

Financed by the Italian National Institute for Insurance against Accidents at Work (INAIL), SMARTGRID involved the installation of RFID antennas on board of an agricultural tractor to scan for batteryless RFIDs placed on obstacles and on worker’s personal protective equipment (PPE) and inform the workers in case of danger through alerts on their mobile phones delivered by BLE beaconing systems placed on the tractor.

2 Materials and Methods

The first step required to build the SMARTGRID’s safety system has been the definition of a detection and alert notification system [11, 12]. In order to set what kind of notifications are needed and when they must be produced, distance thresholds have been introduced to define which alerts shall be sent to the involved workers’ mobile phones; on the other hand, since events must be logged, notifications must be sent to a backend server to keep track of every dangerous event. Risk-based zones can be defined accordingly to risk evaluation and accident history: for instance, acceptable risk (safe) areas if no other RFID tags are found nearby the vehicle, which means that no fixed obstacles or workers are too close to the tractor. If instead RFIDs can be

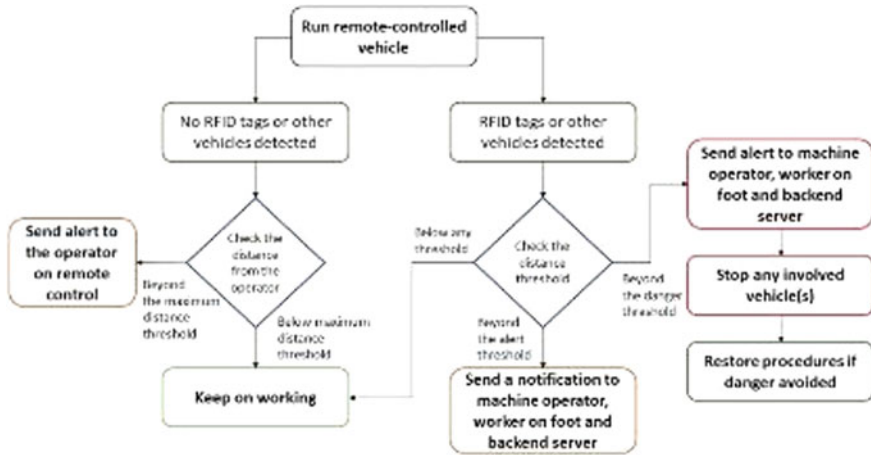


Fig. 1 Flowchart of the safety system

found around the vehicle, notification can be sent to the operator and if the distance too short danger alerts might even stop any machine in the danger area. The whole system relies on PPEs since RFID tags are placed on them and antennas wouldn't spot any worker on foot if they don't wear them; to avoid this issue, additional checks are done at the entrance of the working area by scanning RFIDs in dedicated gates, where every worker is required to stop by in order to verify the presence of PPEs. It must be highlighted that, this way, it can be automatically checked statistics on PPE usage among workers on foot (Fig. 1).

The need to place a “beaconing” system and X-Ray antennas capable of detecting the presence of obstacles or workers on the ground using passive RFIDs has led to the preparation of a system for fixing the components on the FIAT 55–66 tractor available in the Experimental Farm of the University of Viterbo. The tractor, equipped with a cab, already presented on its chassis a series of potential threaded supports that could be used for attaching the antennas: however, the need to tilt the antennas at a certain angle required the creation of additional supports for Vesa 200 × 200 brackets that have been identified as a solid way to support their weight (approximately 8 kg) (Fig. 2).

The structure of the cabin, as shown in the following image, has several points in which to potentially hook the supporting structures of the antennas or, at least, fasten their supports by a series of bolts to threaded holes already present on the tractor's cabin. Given the need to anchor 40 × 20 cm or 40 × 40 cm antennas weighing 3.6 or 8 kg each to the supporting structure, three different anchoring points were proposed respectively at the height of the rear-view mirror, at the top of the central pillar of the cabin of the tractor and finally on the rear pillar of the tractor cab.

The three solutions have a height from the ground of over 2 m and are separated by a distance of about 70 cm from each other, in order to avoid interferences which might reduce their RFID detection range. The identification of these three possible

Fig. 2 FIAT 55–66 tractor



anchorage points has been performed by keeping in mind that they must not obstruct the view of the operator on board, that they have to avoid any damage to the components due to the vibrations of the vehicle during the maneuvering phases in the field and finally that there must be enough space to allow an easy wiring of the antennas without interfering with moving parts, heat sources or other electrical wiring already present on the tractor’s cab (Fig. 3).

Figure 4 also shows CAD drawings of the supports for the antennas, made with 4 mm thick and 3 cm wide steel bars fixed on M6 or M8 threaded holes already present on the structure of the vehicle cabin. VESA 200 × 200 support has been integrated on the steel brackets, adjustable both in inclination and in lateral orientation. The adaptation of the components and of the assembly on agricultural fields has then been tested in the experimental farm to check their stability during various field operations.



Fig. 3 Support distances

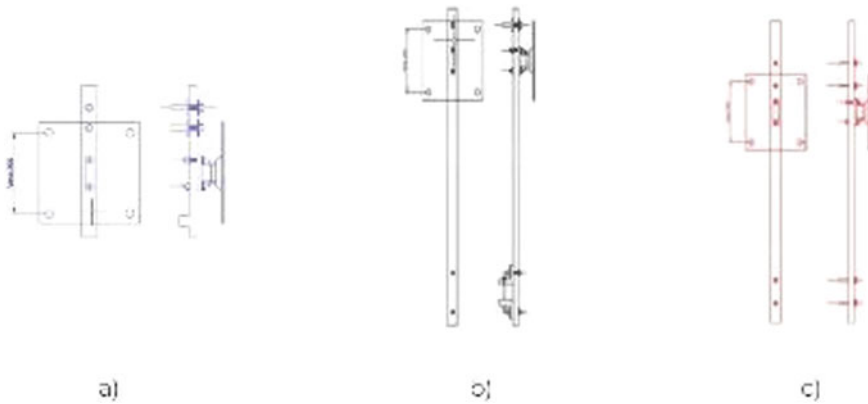


Fig. 4 Computer Aided Drawings (CAD) of the three anchorage solutions: **a** front pillar, **b** middle pillar, **c** rear pillar of the tractor's cabin

Figure 4 shows 3 different designs for antenna anchoring on the tractor's cab: front (a), middle (b) and rear (c). Of these three proposals, two were to be picked. The chosen setups had been identified in a) and c), discarding the central bracket on the tractor cab. This choice was motivated by the need to maintain at least one meter distance between the antennas and to be able to orient them correctly for a correct localization of obstacles and workers on foot. The VESA supports, anchored on the vertical steel bars, were put very close to the cabin structure to minimize vibrations. The anchoring to the cabin has been ensured in 4 distinct points using the threaded holes already present on it by default.

Sufficient distance between the two brackets must also be guaranteed to minimize the encumbrance of any other components for the identification of passive RFIDs in the vicinity.

The x-array antenna for passive RFID scanning can be seen in Fig. 5 fixed to the Vesa bracket and anchored to the support. The distance from the ground, the distance between the antennas and their angles of inclination are symmetrical to the central pillar of the tractor's cabin and this facilitates the configuration of the layout on the data acquisition software.

The 24 V power supply of the antennas is supplied by two power banks positioned on board the tractor, together with a Wi-Fi router to which antennas are connected via ethernet cables.

3 Results

Field tests have been performed to check the structural reliability of the system and define beaconing range and maximum detection for passive RFIDs in the experimental farm of Tuscia University. The tests simulated the presence of workers and



Fig. 5 VESA support on the rear pillar's anchorage

obstacles alongside a tractor's path: antennas placed on the tractor scanned for the presence of workers on foot and other machines, as shown in Fig. 6.

A pair of RFID antenna arrays can be seen tracking nearby RFID tags in Fig. 6. The antennas work by extracting Angle of Arrival (AoA) of RFID tags through the acquisition of signal strength, available from RSSI (Received Signal Strength Indicator) output parameter. AoA measurements have then been combined to estimate RFID tag coordinates, while tractor's trajectory was also tested to verify the distance from the operator's wearable RFIDs by tracking it with Ultra-Wide Band systems (UWB).

The result of this last measurement is shown in Fig. 7, in which green markers indicate the antennas, results from RFID scanning are reported in red while output from UWBs is shown in blue.



Fig. 6 Tractor during field tests. Antennas are visible on the tractor and passive RFIDs have been placed on obstacles all around the working area

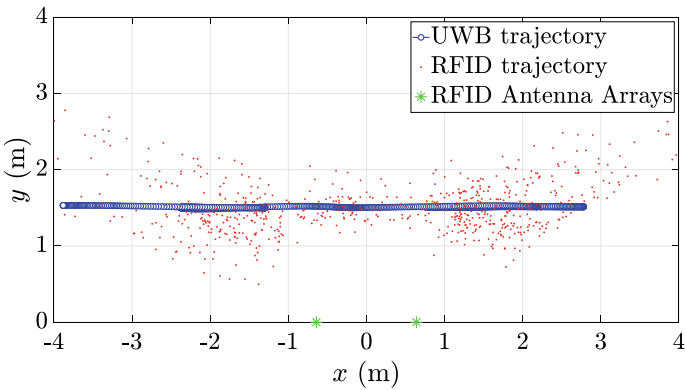


Fig. 7 Tractor trajectory relative to an operator equipped with passive RFID tags measured with UWB (blue) and RFID system (red dots)

In Fig. 7, by comparing UWB output and RFID output, is possible to see evidence of a good correlation among the estimated path of the tractor and the actual one. This localization system was validated through field acquisition campaign, which showed a good correlation in a range of 8–12 m, a detection range which is what authors expected from known limits of passive RFID systems.

4 Conclusions

The expectations on maximum detection capabilities of the passive RFID-based SMARTGRID system have been confirmed by the detection range measured on testing field, which spans from 8 to 12 m. The presence of multiple RFIDs on all sides of PPEs proved to be enough to avoid erroneous localization of workers on foot. The research showed the possibility of using passive RFID tags as low-cost and reliable safety device if combined to PPEs, showing even a good potential in estimating workers' position nearby agricultural machinery. The promising results confirm that smart solutions and wireless devices can greatly enhance safety in agriculture and forestry and, in addition, improve the detection of misuse or absence of PPEs. Limits of the system can be identified as being unable to detect workers that do not wear RFID-enhanced PPEs and being hard to deploy on vehicles that operate outside of their perimeter, such as telescopic handlers.

References

1. Bruzzone, A.G., et al.: Autonomous systems & safety issues: the roadmap to enable new advances in industrial applications. In: 29th European Modeling and Simulation Symposium, EMSS 2017, Held International Multidisciplinary Modeling and Simulation Multiconference, I3M 2017, March 2018, pp. 565–571 (2017)
2. Pirozzi, M., Di Donato, L., Tomassini, L., Ferraro, A.: Possible innovative technical measures for risk prevention during the use of mobile machines with remote guide/control. *Procedia Manuf.* **42**, 457–461 (2020). <https://doi.org/10.1016/j.promfg.2020.02.049>
3. Facchinetti, D., Santoro, S., Galli, L.E., Pessina, D.: Agricultural tractor roll-over related fatalities in Italy: results from a 12 years analysis. *Sustainability* **13**(8) (2021). <https://doi.org/10.3390/su13084536>
4. Fargnoli, M., Lombardi, M., Haber, N., Puri, D.: The impact of human error in the use of agricultural tractors: a case study research in vineyard cultivation in Italy. *Agriculture* **8**(6) (2018). <https://doi.org/10.3390/agriculture8060082>
5. Cecchini, M., Colantoni, A., Monarca, D., Cossio, F., Riccioni, S.: Survey on the status of enforcement of european directives on health and safety at work in some farms of central Italy. *Chem. Eng. Trans.* **58**, 103–108 (2017). <https://doi.org/10.3303/CET1758018>
6. Adams, J., Kennedy, A., Cotton, J.: Child farm-related injury in Australia : a review of the literature, pp. 1–16 (2021)
7. Becot, F., Bendixsen, C., Barnes, K., Rudolphi, J.: Broadening our understanding of farm children's risk exposure by considering their parents' farming background, pp. 18–21 (2021)
8. Quendler, E., et al.: Child safety driver assistant system and its acceptance. *J. Agromed.* **14**(2), 82–89 (2009). <https://doi.org/10.1080/10599240902779394>
9. Kise, M., Zhang, Q., Noguchi, N.: An obstacle identification algorithm for a laser range finder-based obstacle detector. *Trans. Am. Soc. Agric. Eng.* **48**(3), 1269–1278 (2005). <https://doi.org/10.5916/jkosme.2013.37.7.737>
10. Rossi, P., Mangiavacchi, P.L., Monarca, D., Cecchini, M.: Smart machinery and devices for reducing risks from human-machine interference in agriculture: a review. In: Biocca, M., Cavallo, E., Cecchini, M., Failla, S., Romano, E. (eds) SHWA 2020. LNCE, vol. 252, pp. 195–204. Springer, Cham (2022). https://doi.org/10.1007/978-3-030-98092-4_21

11. Montanaro, T., et al.: An IoT-aware smart system exploiting the electromagnetic behavior of UHF-RFID tags to improve worker safety in outdoor environments. *Electronics* **11**, 717 (2022)
12. Monarca, D., et al.: Autonomous vehicles management in agriculture with bluetooth low energy (BLE) and passive radio frequency identification (RFID) for obstacle avoidance. *Sustainability* **14**, 9393 (2022). <https://doi.org/10.3390/su14159393>

Sustainability Performance of Mountain Food Value Chains



P. Sacco, D. Don, L. Becce, G. Carabin, A. Mandler, and F. Mazzetto

Abstract In the framework of the Brotweg project (“The bread route for mountain areas”), the performance of alternative food value chains was evaluated. Geomorphological considerations on the territory, namely the high slopes and highly uneven terrain, meant that the chosen sites are suitable for the cultivation and processing of different types of cereals and for animal husbandry. Four alternative supply chains were considered: (1) rye-bread, (2) barley-beer, (3) cow’s milk-cheese, (4) goat’s milk-cheese. Regarding the cereal cases, the innovative cultivation and post-harvest methods developed during the Brotweg project were considered. For the dairy farming ones, the haymaking phase was also included. Two methodologies were used to assess the performance of the supply chains: Lifecycle Analysis (LCA) and Multi-Criteria Analysis (MCA). Both approaches present pros and cons, hence affecting their applicability depending on the context and decision-making processes that they must support. The article introduces the preliminary results of the supply chain analysis and the resulting considerations. In particular: (a) for both approaches there is a need for consistent knowledge of the performance of different alternative supply chains, (b) for territories such as the studied ones, a further assessment of short supply chains (all on-farm) and cooperative models (e.g., sharing of plants and machinery) is necessary and needs to be integrated with logistics considerations, and (c) the short cereal-bread chain is an interesting alternative, but very much linked to the climatic risk—e.g. loss of primary production. On the contrary, alternative systems linked to animal husbandry are less risky.

Keywords Mountain agriculture · LCA · Multi-criteria analysis · Sustainability

P. Sacco (✉) · D. Don
Fraunhofer Italia Scarl, Bozen-Bolzano, Via Volta 13 A, 39100 Bolzano, Italy
e-mail: pqlsacco@gmail.com

L. Becce
Competence Center for Plant Health of the Free University of Bozen-Bolzano, Bolzano, Italy

G. Carabin · A. Mandler · F. Mazzetto
Faculty of Science and Technology, Free University of Bozen-Bolzano, Bolzano, Italy

1 Introduction

Food security, while still being one of the foundational needs of society, saw a shift in its concept formulation [12]. Nowadays, ensuring the quantity and quality of food is no longer enough. It is also necessary to rethink agricultural and livestock production systems in order to be sustainable, while at the same time reducing waste and ensuring food security [2, 8, 9]. In addition to this, the challenges of climate change and the abandonment of marginal agricultural land, especially for mountainous areas, must also be considered. Looking more specifically at the requirements to ensure a sustainable food production, the climate and geomorphological properties of the site become also relevant factors. In the mountain area, like the context of the South Tyrolean region where the European Regional Development Fund (ERDF) project: “Brotweg—The bread route for mountain areas” (FESR 1089, Operative Program: ERDF, Autonomus Province of Bozen/Bolzano Investment for economic growth and occupation—FESR 2014—2020), was developed, the climate limits the number of possible cultivation choices and the morphology further constrains such variety and requires the adoption of specific techniques and equipments for the actual agricultural activity, like for the cereal cases, where the innovative cultivation and post-harvest methods developed during the Brotweg project were considered. In that sense, selecting the best land use enables to assess which is the most sustainable choice and for that reason four food supply chains were investigated using both Life-Cycle Analysis (LCA) and Multi-Criteria Analysis (MCA), namely: (1) rye-bread, (2) barley-beer, (3) cow’s milk-cheese, (4) goat’s milk-cheese. The considered steps in each supply chain are: cultivation and dairy, intermediate product, final product.

2 Materials and Methods

The assessment followed the conventional steps foreseen for an LCA as described by ISO 14040 and ISO 14044 [5, 6] and for an MCA [11]. In line with the data quality hierarchy principle, precedence has been given to directly collected data on each step of the process, average data specific for the context of South Tyrol and then secondary data derived from literature and LCA Databases (in this case Agribalyse v3.0.1). All data have been referred to a functional unit of 1 hectare of cultivated land in order to favour comparability between the different production systems from a perspective of land management. The chosen analysis approach follows the “Cradle-to-Gate” approach, as the scope of analysis begins with the cultivation of the first raw feedstock and ends at the farm itself (both for selling or direct reuse in farmhouse activities). The scheme below in Fig. 1 describes the steps within the system boundaries and the considered flows.

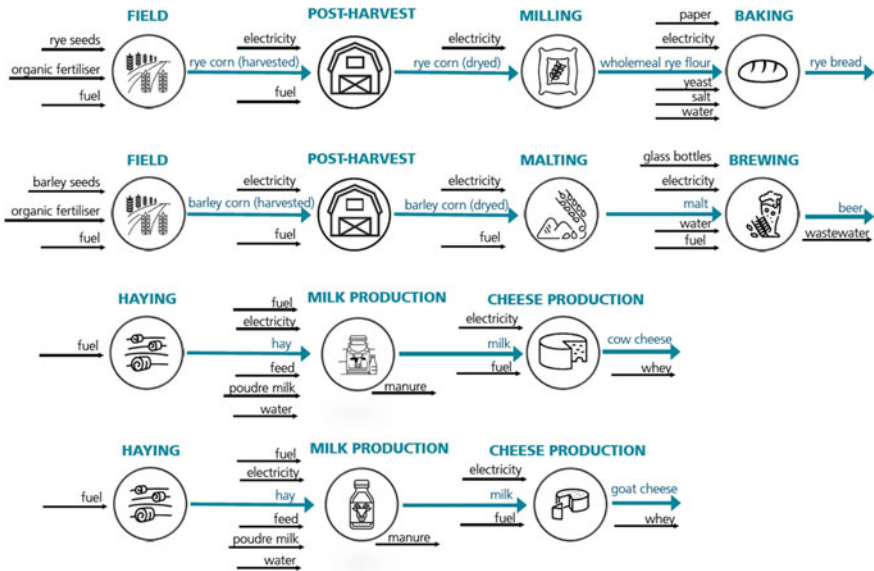


Fig. 1 Steps within the system boundaries and the considered flows

The Life-cycle Impact Assessment method chosen for this work is ReCiPe Endpoint (H) without considering the longterm effects as the temporal frame considered is the Hierarchical one “H” which considers 100 years. Following the endpoint method, the data were aggregated into the three macro impact categories: Ecosystem quality, Resources depletion and Human health. Nevertheless, the results of these impacts are built on the elaboration of the midpoint categories, therefore the most representative of them for the observed system were also investigated.

Another relevant aspect of this research work is the use of a MCA in parallel to the more conventional LCA. The latter, in fact, can be seen as a specific method of analysis in the context of Multicriteria Decision Aids (MCDAs). MCAs go beyond the pure environmental perspective as in LCAs and enables to consider and balance different points of view by introducing evaluation criteria and relying on a multi-actor approach. This is a quite relevant difference as LCA provide a snapshot of the environmental impacts linked to a life cycle without giving any indication as to which is preponderant, while MCAs can partly overcome this problem of interpretation and give recommendations based on what the analysis has found [3]. The same four alternatives stetted up for LCA were used also for the MCA. The criteria were selected to consider all the relevant economical, operational, social and environmental aspects. The multi-actor approach is reached by assigning weights to the different criteria. Most of the multi-criteria decision support tools stop at the assessment matrix, but the approach proposed in this work aims also to cluster criteria into groups and perform a sensitivity analysis to understand which are the most relevant while still being reflective of the different points of view [7]. Being the normalisation of the

criteria embedded in the MCA approach, the clustering works even by grouping qualitative (based on a value scale defined by the practitioner e.g. Likert scale) and quantitative criteria. The tool adopted in this project, WeQual AMC [4], enables to perform this grouping and to present the results on a graphical form and where the priorities of a specific decision-maker would fall in the graph. The method used for the MCA is Electre with the introduction of a syntetic index and the three clusters are named: ECO, representing the economic perspective (income, investment, loss risk, AMB, which expresses the ecological perspective embodying aspects of the social one (effluent risk, energy consumption, landscape, mountain garrison; OPE, which stands for operational and includes the technological aspects as well (risk primary production, risk final production, work primary production, work primary transformation, work final product).

3 Results and Discussion

The section below presents the results of the analysis work and compares the findings of the LCA analysis with those from the MCA.

The following graphs (Fig. 2a–c) show the comparison of four supply chains according to the three endpoint impact categories. From the left its' possible to see the performance of the rye bread chain, the barley beer one, and then cow and goat cheese. The graphs (Fig. 2) show how the animal-based chains have the lowest

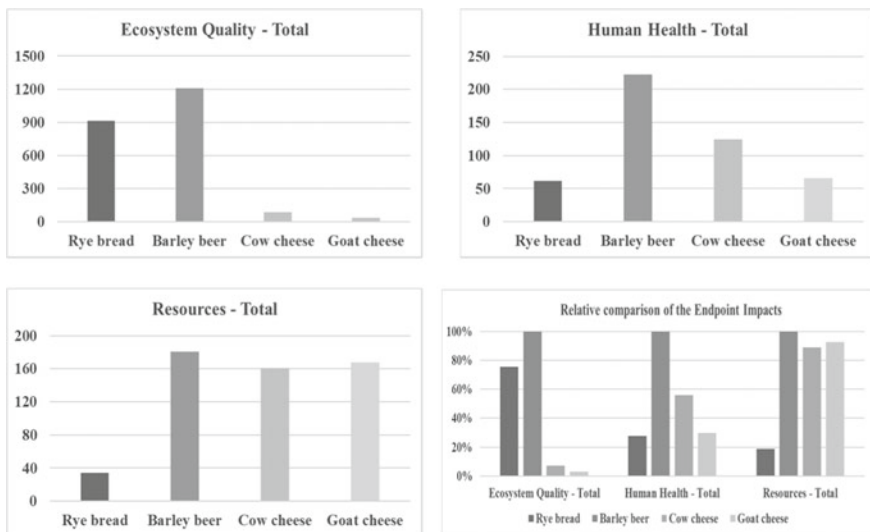


Fig. 2 Comparison of the endpoint environmental impacts: ecosystem quality (a), human health (b) and resources depletion (c), and comparison of the impacts on the endpoint categories as percentage of the maximum impact value (d)

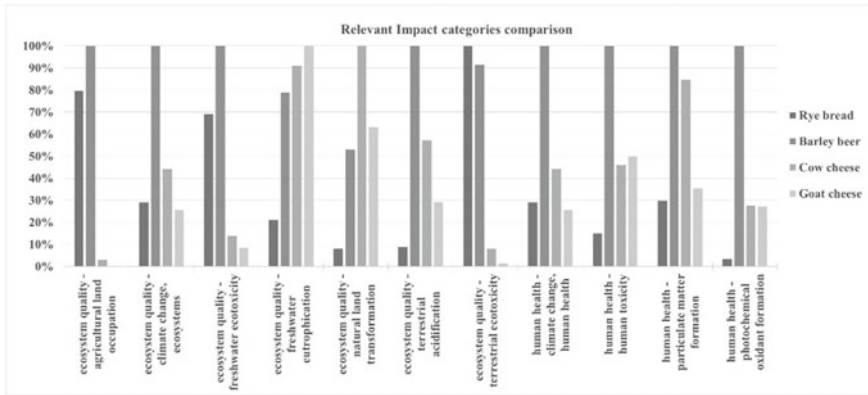


Fig. 3 Comparison of normalised midpoint impact categories with reference to related endpoint

impact on the quality of the ecosystem due to the fact that no pesticides and fertilizers are used for hay cultivation but have quite high resources depletion as there is the need fuel and considerable quantities of hay to feed the animals and then processing the milk. The barley beer chain is the one presenting the highest impacts but it is important to stress out that a considerable component of those impacts is due to the production of the glass bottle for packaging as it will be further investigated in the next part of this research work. The graph below compares the performances of several relevant midpoint impact categories and how they affect the above clustered values into the endpoint ones. It is important to note that all analysis methods that have both midpoint and endpoint impact categories rely on conversion factors to pass from one to the other and it isn't just the sum of contributes. The impact of the goat cheese supply chain on land occupation is very low but existent (0.21% of the maximum value) and it is the supply chain with the highest impact in terms of freshwater eutrophication. In that same impact category, the second highest is the cow cheese production, which probably considers the environmental effect of animal wastewaters and their nutrients content. Cow cheese production is the one with the highest "natural land transformation" impact. To present the comparison between different performances and impact categories, a normalisation of the results has been performed by dividing each impact entry for the maximum value of the same group. This way each chain is expressed as the relative performance to the one with the highest score and different impacts can be compared (Fig. 3).



Fig. 4 Appraisal matrix of the four supply chain by considering the relevance for the various stakeholders

The results of the MCA go beyond a comparison of the environmental impacts of the four agricultural system options and shows which is the best one considering the perspective of the different actors in the chain (Fig. 4). The 6 scenarios are based on different actors' priorities: (I) Balanced, (II) Environmental community, (III) Traditional policy-makers, (IV) Innovation-oriented policy makers, (V) Farmer income-oriented, (VI) Farmer low-risk oriented. In general, the best choice is the cultivation of rye for bread production, even though not being the most indicated in terms of revenue from that land occupation choice and being identified as the worst option when trying to minimise or avoid entirely risks. Considering that the second least favourable option is barley beer production, a possible explanation of these results can be found in the fact that they are both very sensitive and dependent on the climate and its instability. On the contrary, the supply chains relying on animal husbandry have poorer performances but appear as safer options in case of low-to-no risk income options.

The sensitivity analysis on different scenarios supports such considerations by showing where the different scenarios sit when observed against the criteria clustering (Fig. 5).

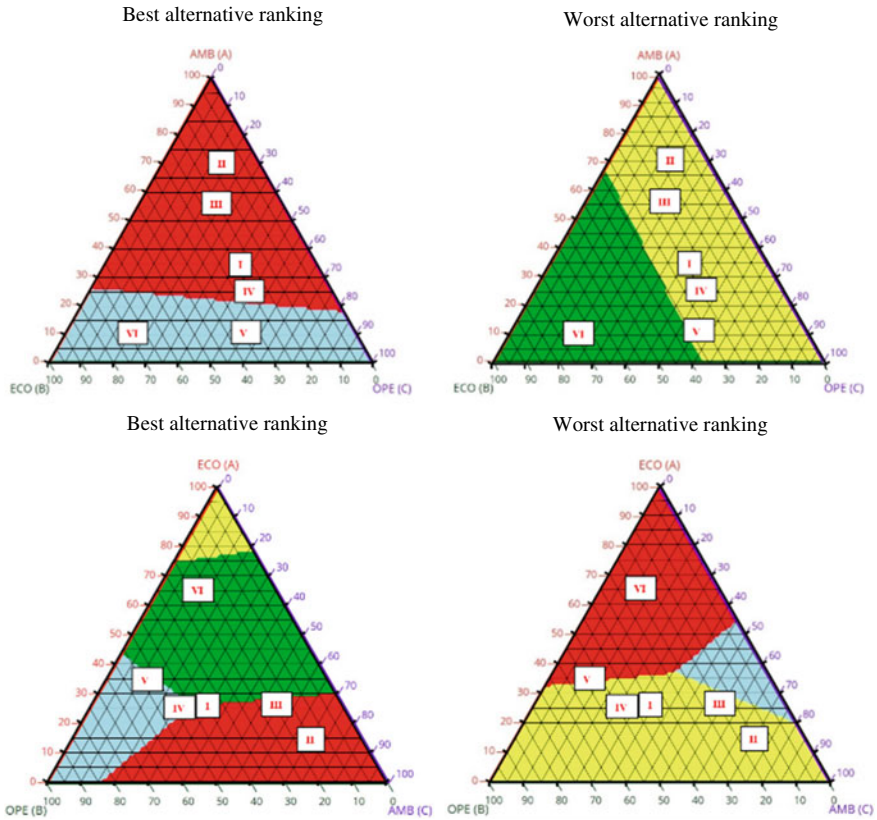


Fig. 5 Sensitivity analysis on different scenarios: balanced priorities (upper), prudential with respect to crop losses risk (lower). Alternatives: bier (light blue), goat cheese (yellow), cow cheese (green), bread (red)

4 Conclusions

The comparison of the four agricultural production systems in the context of the Brotweg project enabled to highlight several interesting aspects. Regarding the pure analytical key takeaways, for very specific situations, standard analysis methodologies can provide guidelines and insight, and the more primary data (based on actual in-field processes) is used, the more reliable are the considerations taken from the analysis results. In the case of a LCA performed on a product, favouring the use of directly acquired data from processes can be useful for product standardisation and labelling such as the Environmental Product Declarations (EPD) or Ecolabels. The results of the MCA also showed the strong dependency on the detail of information available in the impact matrix and the need for homogeneous knowledge of the performance of the different alternative supply chains. Regarding the findings from

comparing the supply chains, the short cereal-bread chain showed to be an interesting land use choice, even though very much dependent on climate risks—i.e. loss of primary production. On the contrary, the animal husbandry alternatives, while having overall high environmental impacts, seemed to be more cautious. Further steps for this work are the assessment on the performance of short supply chain (e.g. all on-farm production) and cooperative models (e.g. sharing of plant and machinery, marketing), being particularly mindful of considerations on the logistic aspects.

References

1. Benoit, V., Rousseaux, P.: Aid for aggregating the impacts in life cycle assessment. *Int. J. Life Cycle Assess.* **8**, 74 (2003). <https://doi.org/10.1007/BF02978430>
2. Buller, H., Morris, C.: Growing goods: the market, the state, and sustainable food production | enhanced reader. *Environ. Plan. A Econ. Space* **36**, 1065–1084 (2004). <https://doi.org/10.1068/a35282>
3. Finnveden, G.: On the limitations of life cycle assessment and environmental systems analysis tools in general. *Int. J. Life Cycle Assess.* **5**, 229 (2000). <https://doi.org/10.1007/BF02979365>
4. Gallo, R., et al.: Assessment of riparian environments through semi-automated procedures for the computation of eco-morphological indicators: preliminary results of the WEQUAL project. *Bodenkultur* **70**(3), 131–145 (2019). <https://doi.org/10.2478/boku-2019-0012>
5. International Standardisation Organisation (ISO): ISO 14040 - environmental management - life cycle assessment - principles and framework. *Int. Stand. Organ.* (2006a)
6. International Standardisation Organisation (ISO): ISO 14044:2006 - environmental management - life cycle assessment - requirements and guidelines (2006b)
7. Mazzetto, F., Bonera, R.: MEACROS: a tool for multi-criteria evaluation of alternative cropping systems. *Eur. J. Agron.* **18**(3–4), 379–387 (2003). [https://doi.org/10.1016/S1161-0301\(02\)00127-2](https://doi.org/10.1016/S1161-0301(02)00127-2)
8. McKenzie, F.C., Williams, J.: Sustainable food production: constraints, challenges and choices by 2050. *Food Secur.* **7**, 221–233 (2015). <https://doi.org/10.1007/s12571-015-0441-1>
9. Pawlak, K., Kołodziejczak, M.: The role of agriculture in ensuring food security in developing countries: considerations in the context of the problem of sustainable food production. *Sustainability* (2020). <https://doi.org/10.3390/su12135488>
10. Piclet, J.: *Dépasser L'évaluation Environnementale - Procédure d'étude et insertion dans la décision globale*, 1st Editio. ed. Jacques Piclet (1996)
11. Recchia, L., Boncinelli, P., Cini, E., Vieri, M., Garbati Pegna, F., Sarri, D.: *Multicriteria Analysis and LCA Techniques - With Applications to Agro-Engineering Problems*, 1st edn. Springer, London (2011). <https://doi.org/10.1007/978-0-85729-704-4>
12. Sánchez Cantillo, M.V., Rosero Moncayo, J., Holleman, C.: Food security and nutrition in the world repurposing food and healthy diets more affordable (2022)

Combining Smart Glasses and Thermal Imaging as a Tool for Water Stress Detection in Greenhouses: A Preliminary Study



Gabriele Sara, Giuseppe Todde, Daniele Pinna, and Maria Caria

Abstract The aim of the study was to combine low-cost thermal imaging camera with smart glasses to evaluate the feasibility of augmented reality system for monitoring water stress under protected conditions. The tests were performed in a greenhouse on 208 Petunia hybrid ‘Surfinia’ plants. All the plants were irrigated to reach field capacity, while 15 of them did not receive irrigation water for seven days before the trials. Three qualified operators had to identify the plants in water stress condition, using 3 operative modes: naked eyes (NE); thermal imaging camera (Thermal Compact Pro, Seek, USA) associated with a smartphone (TSP); thermal imaging camera associated with smart glasses (TSG, M400, Vuzix, USA). The results showed a general low rate of water stressed plants identification in the three operative modes considered. On the other hand, the unsuccessful detection of the plants in water deficit made by the operators was reduced about 40% when adopting the TSG as compared to NE operative mode.

Keywords Augmented reality · AR headset · Digital farming · Precision agriculture · Protected cultivations · Wearable device

1 Introduction

All plants need an adequate water supply to growth. Limited soil water availability results in decreases plant growth, plant size, plant quality and reduction in crop production time. The methods of irrigation adopted be determined mainly by the crop, soil type, cultural practices, farm management and farm sustainability.

In greenhouses different methods can be implemented to provide irrigation water to the crops. Drip irrigation system is widely used because of numerous advantages over other methods (e.g., furrow irrigation) [1–3]. This system works by delivering

G. Sara · G. Todde · D. Pinna · M. Caria (✉)

Department of Agricultural Sciences, University of Sassari, Viale Italia 39/A, 07100 Sassari, Italy
e-mail: mariac@uniss.it

water slowly and directly to the plant and/or pot, following the irrigation plan established by the company or implementing a sensor-based automated irrigation control. However, common problems found with this irrigation system occur when plugging of drip hoses or when the emitters and risers break. For these reasons, it is needed to adopt a systematic way to perform a simple distribution uniformity evaluation checking flows and pressures at the pump and in the field to monitor system performance. Therefore, the irrigation maintenance routine plays an effective role to optimize all characteristics of cropping and crop quality.

Assessment of regular irrigation status is often done manually. This activity is, therefore, a process that requires considerable manual and labor carried out by qualified operators.

Thermal imaging cameras are widely used in crop water stress assessment and in detection of malfunctions in irrigation systems [4, 5]. Moreover, given the development of infrared thermal technologies in recent years, thermal camera with high resolution has become more affordable, which increases the opportunities to employ this device for crop water stress detection. Over the past decades, agricultural farms have adopted innovative technologies to improve their productivity and profit [6–8]. Smart glasses for augmented reality can be considered as one of the most pioneering technologies, that can be implemented with different sensors. In the agricultural sector, some authors investigated the potentiality of Smart Glasses (SG) to support and improve farmer activities [9–12].

Specifically, an important aspect regarding the use of SG in agriculture is related to farmer operations, which requires the use of both hands. Therefore, using a hands-free system information on plants, soil, animals, and machineries can be obtained while working [13, 14].

The aim of the study was to combine low-cost thermal imaging camera with SG to evaluate the feasibility of augmented reality system for monitoring water stress under protected conditions.

2 Materials and Methods

Trials were carried out in the greenhouse facilities of the Florgarden company, in Olmedo, Italy. For the experiments, a plot of 208 plants of *Petunia* hybrid “Surfinia” grown in pot, divided into 4 rows, was selected. The plot was managed following the irrigation plan established by the farm. Additional water with a volume of 100 ml per pot was supplied before the tests to ensure standard irrigation conditions of watered plants. The irrigation system was surface drip, by means of applying water to the media surface of the pots through drip tubes. A total of 15 plants were introduced to three different water-stress levels (5 plants remained without water for 7 days, 5 plants for 4 days and 5 plants for 2 days) by withholding water through dripper removal from the pot. The day of the test, these plants were randomly placed within the plot, just before the start of the trials.

Table 1 Seek infrared camera specification

Thermal resolution (pixel)	Temperature range (°C)	Frame rate (Hz)	Field of view	Spectral range (μm)	Sensor
206 × 156	−40 to 330	<9	36°	7.5–14	Microbolometer

Table 2 Smart Glasses and Smartphone specification

	Vuzix M400	Samsung S5 Neo
CPU	Qualcomm XR1 (8 core 2.52 Ghz)	Exynos 7580 (8 core 1.6 Ghz)
RAM (GByte)	6	2
ROM (GByte)	64	16
Display type and resolution	Video Oled, 640 × 360 pixel	Super AMOLED, 1080 × 1920
Operative system	Android 8.0	Android 6.0.1
Camera (MP)	12.8	16
Battery capacity (mAh)	135 + 1000	2800
Weight (g)	180	145

2.1 Data Acquisition and Analysis

The tests were conducted by three experienced operators, on a cloudy day of February 2022 at 10 a.m. The days before the tests were also cloudy and the temperatures were low (6–16 °C). During the tests, operators were asked to identify water-stressed plants within the plot using three modalities: the naked eye (NE); using a thermal imaging camera associated with a smartphone (TSP); and using a thermal imaging camera combined with smart glasses (TSG). Camera, smartphone, and smart glasses specifications are shown in Tables 1 and 2.

The day before the test, a brief training was given to the operators to explain to them the features and operation mode of the technology used. The data recorded for each operator were: task completion time (i.e., water-stressed plant detection); the number of plants detected for each level of water stress (stress 1: two days without water; stress 2: four days; stress 3: seven days); and the number of errors made by each operator. Specifically, errors were classified into two types as follows: “weighed plants” i.e., plants that were detected and weighed (the plant was lifted by the operator to feel the weight and assess the level of water content) and then placed in the plot; “detected plants” i.e., plants that were detected, weighed, and wrongly indicated as plants in water-stress.

During the trials, each operator completed the task following specific order: first NE, then TSP, and finally TSG.

3 Results

Operators’ response to detect water-stressed Surfinia plants was observed during specific tests carried out in a greenhouse. Differences were found among the three modalities of water-stress detection, both for task completion time and number of errors. Even though the presence of well-irrigated plants was important as a reference point to discriminate the water-stressed plants, the results showed a low rate of plants correctly detected (Table 3). In general, operators had difficulty in identifying water-stressed plants, both with “naked eye” and with the support of the devices tested (thermal camera plus smartphone and smart glasses). In fact, the plants identified were overall 5 to NE, 1 with TSP and 2 with TSG out of 15. Nevertheless, the total number of errors done by the operators attempting to identify plants water-stressed was higher without the use of a device associated to the thermal camera. The device with the lowest number of errors was the smart glasses, with a reduction of about 59% compared to the “naked eye” modality. Whereas the use of the thermal camera associated with the smartphone resulted similar to the NE method, showing a slight decrease of about 6%. When considering the results obtained for each operator, the number of plants correctly detected was similar for each testing modalities, despite the three water-stress levels considered for the plants. Regarding the number of errors, the results highlighted a difference among the operators. Specifically, one of them weighed a large number of plants to assess the level of water content (25 times out of 37). Anyhow, for all operators, the lowest number of errors was recorded with the TSG (0, 1 and 6 errors per operator).

Table 3 Task completion time (TCT), number of water-stressed plants detected (WS) and number of errors for each of the different detection modalities adopted

Operator	Detection modality	TCT (min: seconds)	Plants detected (N)			Wp ^a (N)	Ip ^b (N)	Total ^c errors (N)
			WS 2 day	WS 4 day	WS 7 day			
1	NE	01:49	2	0	0	2	1	3
	TSP	04:36	0	0	0	0	0	0
	TSG	03:10	0	0	1	0	0	0
2	NE	01:30	0	0	1	5	0	5
	TSP	02:56	0	0	0	4	1	5
	TSG	01:30	1	0	0	1	0	1
3	NE	02:15	1	1	0	8	1	9
	TSP	06:15	0	0	1	11	0	11
	TSG	03:15	0	0	0	6	0	6

^a Number of pots weighted (error): number of plants weighted to evaluate the water status of the plant and then placed to the plot

^b Number of plants indicated (error): number of plants weighted and wrongly recognized in water-stress

^c Total errors: Number of pots weighted + Number of plants indicated

The completion time of the “naked-eye” water-stressed monitoring activity averaged 111 s per operator. In contrast, the use of the thermal imaging camera associated with the smartphone and smart glasses averaged 276 and 158 s respectively. The smart glasses are a wearable device that allows operators to view contents superimposed on the real environment hands-free. For this reason, the operators completed the task faster when using TSG rather than TSP, although the number of water-stressed plants detected was low. Overall, the task completion times recorded during the trials suggest that adequate training is needed to train the operator on how to be supported by the thermal images (i.e., specifically on how to interpret the displayed images) and, in general, by innovative devices.

4 Discussion

Water-stressed plants of “Surfinia” were detected with comparable results using three different operative modalities, “naked eyes”, thermal imaging camera associated with a smartphone and thermal imaging camera associated with smart glasses. The number of water-stressed plants detected was low. The time of day and the period when the tests were carried out may affected the recognition of plants by operators when using the devices (TSP and TSG). In fact, the cloudy days and the low temperatures that occurred during the three days before the tests, influenced the evapotranspiration of the plants, regulating the leaf surface temperature. In this way, the thermal images of plants in water deficit did not show clear color differences from those properly watered. Nevertheless, the strength of the systems tested is that the operator can detect plants water-stressed just by comparing the colors of plants shown in the thermal image displayed in the device. Despite smart glasses and smartphone solutions showing a comparable number of water-stressed plant detection, the activity completion time resulted on average 40% higher when the thermal imaging camera was associated with the smartphone. The reasons could be related to different technical and ergonomic factors of both devices. Using smartphone, the operator’s focus shifted between the display and the surround (Fig. 1a). In contrast, smart glasses offered the advantage of a direct line of sight through the lens display with a more intuitive, hands-free user experience [15]. Moreover, smart glasses are wearable devices that follow the movement of the head and thus what the operator wants to see (Fig. 1b). This improves the operator’s performance and takes less time when manually weighing plants to determine their water status. However, no operators reported symptoms of cybersickness which could be associated with immersive technology [16, 17].

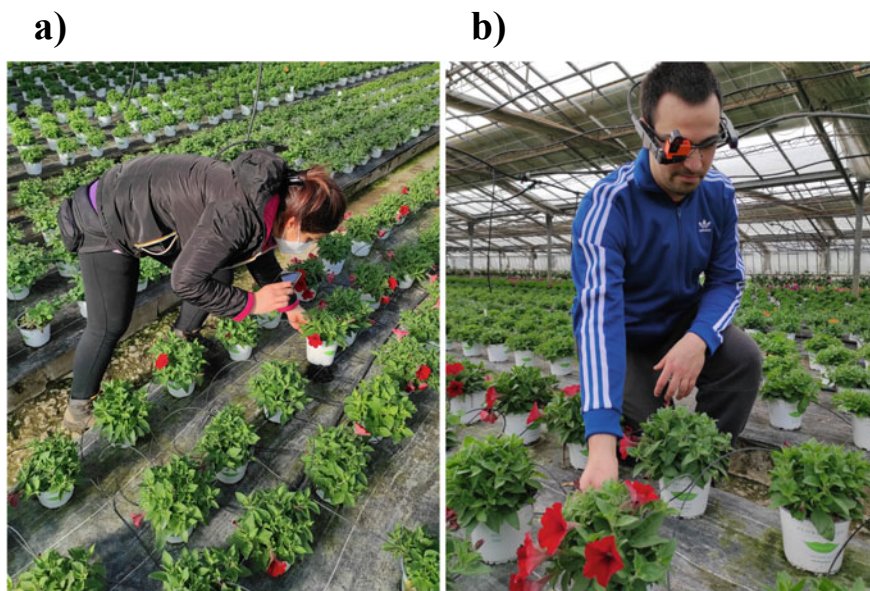


Fig. 1 Operators detecting a water-stressed plant with thermal imaging camera: handling a smartphone **a** and wearing smart glasses **b**

5 Limitations and Future Studies

The findings of this study have to be seen in the light of some limitations. These limitations are mainly related to the low number of operators and the short-time training made on the new technologies tested. Anyway, another aspect that influenced the results obtained was the period when the tests has been carried out. In fact, although the thermal camera could be considered a device to support the operator all year long, warm periods are critical for the management of the plants. During this period, the problem of plant desiccation could be higher if irrigation failures occur during the day. Moreover, in warm periods, color differences between stressed and unstressed plants are highlighted by the thermal camera in a more pronounced way. For these reasons, it would be convenient to schedule a second experimental trial in the April–May period, following the methodology already adopted in previous tests. Leading additional trials in periods where a great number of irrigation cycles are needed and monitoring operators with familiarity with the technology tested, would provide further insights into the adoption of thermal imaging camera systems in greenhouse contexts. In addition, future tests should consider a higher number of operators, considering the gender balance, in order to gain more accurate results on productivity. Finally, researchers should include questionnaires to measure the workload, acceptability, and usability to draw additional conclusions on operator experience.

6 Conclusions

The present research is a preliminary study concerning the implementation of augmented reality smart glasses in the protected crops management. Therefore, it is considered important to continue with other trials to evaluate the use of the thermal camera associated with smart glasses in different climatic conditions, highlighting the limitations and opportunities of this technology. The results showed the possibility to use emerging technologies to support operators in on-field activities. Although has been demonstrated the real implementation of smart glasses with a thermal imaging camera, additional steps are needed to miniaturize the entire system, in order to improve human comfort and replace traditional methods.

Acknowledgements The authors thank the Florgarden floriculture company for their availability and collaboration and Dr. Marco Polese for his valuable help during data collection.

Funding This work was supported by: ATLANTIDE project (Advanced Thecnologies for LANds management and Tools for Innovative Development of an Ecosustainable agriculture), Progetti di Ricerca e Sviluppo della Regione Autonoma della Sardegna.

References

1. Hanson, B.R., Schwankl, L.J., Schulbach, K.F., Pettygrove, G.S.: A comparison of furrow, surface drip and subsurface drip irrigation on lettuce yield and applied water. *Agric. Water Manag.* **33**, 139–157 (1997)
2. Fekadu, Y., Teshome, T.: Effect of drip and furrow irrigation and plant spacing on yield of tomato at Dire Dawa, Ethiopia. *Agric. Water Manag.* **35**, 201–207 (1998)
3. Ertek, A., Kanber, R.: Effects of different irrigation programs on the growth of cotton under drip irrigation. *Turk. J. Agric. For.* **2**, 415–425 (1999)
4. Zhou, Z., Majeed, Y., Naranjo, G.D., Gambacorta, E.M.: Assessment for crop water stress with infrared thermal imagery in precision agriculture: a review and future prospects for deep learning applications. *Comput. Electron. Agric.* **182**, 106019 (2021)
5. Dag, A., et al.: Automated detection of malfunctions in drip-irrigation systems using thermal remote sensing in vineyards and olive orchards. In: *Proceedings of 10th European Conference on Precision Agriculture Volcani Center, Israel 12–16 July 2015*, pp. 519–525 (2015)
6. Montes de Oca Munguia, O., Pannell, D.J., Llewellyn, R.: Understanding the adoption of innovations in agriculture: a review of selected conceptual models. *Agronomy* **11**(1), 139 (2021)
7. Ogundari, K., Bolarinwa, O.D.: Impact of agricultural innovation adoption: a meta-analysis. *Aust. J. Agric. Resour. Econ.* **62**(2), 217–236 (2018)
8. Todde, G., Murgia, L., Caria, M., Pazzona, A.: A multivariate statistical analysis to characterize mechanization, structural and energy profile in Italian dairy farms. *Energy Rep.* **2**, 129–134 (2016)
9. Sara, G., Todde, G., Caria, M.: Assessment of video see-through smart glasses for augmented reality to support technicians during milking machine maintenance. *Sci. Rep.* **12**(1) (2022)
10. Caria, M., Todde, G., Sara, G., Piras, M., Pazzona, A.: Performance and usability of smartglasses for augmented reality in precision livestock farming operations. *Appl. Sci.* **10**, 2318 (2020)
11. Huuskonen, J., Oksanen, T.: Soil sampling with drones and augmented reality in precision agriculture. *Comput. Electron. Agric.* **154**, 25–35 (2018)

12. Santana-Fernández, J., Gómez-Gil, J., Del-Pozo-San-Cirilo, L.: Design and implementation of a GPS guidance system for agriculture tractors using augmented reality technology. *Sensors* **10**, 10435–10447 (2010)
13. Caria, M., Sara, G., Todde, G., Polese, M., Pazzona, A.: Exploring smart glasses for augmented reality: a valuable and integrative tool in the precision livestock farming. *Animals* **9**, 903 (2019)
14. Okayama, T., Miyawaki, K.: The “smart garden” using augmented reality. *IFAC Proc.* **46**, 307–310 (2013)
15. Pratt, P., Ives, M., Lawton, G., Simmons, J., Radev, N., Spyropoulou, L., et al.: Through the HoloLens looking glass: augmented reality for extremity reconstruction surgery using 3D vascular models with perforating vessels. *Eur. Radiol. Exp.* **2**(1), 2 (2018)
16. Vovk, A., Wild, F., Guest, W., Kuula, T.: Simulator sickness in augmented reality training using the Microsoft HoloLens. In: *Conference on Human Factors in Computing Systems*, Montreal, Canada, New York, NY United States. Association for Computing Machinery, New York (2018)
17. Rebenitsch, L., Owen, C.: Review on cybersickness in applications and visual displays. *Virtual Real.* **20**(2), 101–135 (2016)

A Smart Automation System for the Management and Control of a Medium Scale Digester Plant



Luigi Scarcello, Souraya Benalia, Giuseppe Zimbalatti, Antonio Fazari, and Bruno Bernardi

Abstract The paper describes the implementation of the control logic for the management of a medium-scale digester plant through a smart automation system. Such a digester was developed to produce biogas and biomethane subsequently to anaerobic digestion of agri-food wastes, with a particular interest in olive mill by-products. Temperature and pH are the main parameters that control prototype running and automatism. The plant is fed with two matrices having respectively acid (in the case of olive mill wastewater) and alkaline pH (i.e. livestock manure), thanks to which, substrate pH value is set. The temperature control is ensured by a couple of armoured heater elements, while cooling can occur thanks to a water main directly connected to the digester. The control logic is implemented for maintaining the temperature and pH values within a certain range to guarantee the optimal process parameters. The smart automation system consists of three PLC units, which manage the sensors to acquire temperature and pH data for process control, and pressure and flow sensors to determine biogas production. A remote control interface was designed to allow manual or automatic control of the plant. The interface enables to navigate between four different windows: manual control, automatic control, parameter setting and trends, which shows the real-time measurements provided by the sensors. Furthermore, the interface allows for setting process parameters, controlling process progress and saving data history.

Keywords Automation system · Biogas plant · By-product smart use · ICT · Sensors

L. Scarcello
ICAR-CNR, Via P. Bucci 8/9C, 87036 Rende (CS), Italy

S. Benalia (✉) · G. Zimbalatti · A. Fazari · B. Bernardi
Department of Agriculture, University Mediterranea of Reggio Calabria, Località Feo Di Vito, Snc, 89122 Reggio Calabria (RC), Italy
e-mail: soraya.benalia@unirc.it

1 Introduction

The war in Ukraine is speeding Europe's pivot toward renewable energies. In this context, biomass anaerobic digestion for biogas and biomethane becomes an attractive energy production source because of its environmental advantages [1, 2], which led the European Commission to propose ramping up biomethane production to 35 billion cubic metres by 2030.

In anaerobic digestion process, various types of biomass and organic wastes are converted into biogas using several types of plants. However, the process instabilities in the reactors, because of biomass properties, limit the expansion of facilities to high loading rates. The irregularities in the process can be addressed directly by altering the feedstock characteristics if a robust, and sensitive monitoring device is available [3]. Several offline methods were proposed to monitor anaerobic digestion process, from gas chromatography to mid-infrared spectroscopy, but they are expensive and time-consuming [4, 5]. Bio-electrochemical systems are an alternative for the online monitoring of these processes [6], but still, need improvements. On the other hand, among the online monitoring systems, Cruz et al. [7] constructed an automated system capable of monitoring some indicators of the anaerobic digestion process using the platform Arduino; while Bernardi et al. [8] developed a medium-scale plant based on a programmable logic controllers (PLC), which is more efficient to use in industrial processes. This latter was realised with the scope to improve methane production starting from the combination of olive mill wastewater (matrix A) and livestock manure (matrix B). To allow optimal production conditions, a control logic is implemented to maintain the temperature and pH of the global mixture, obtained from the union of matrices A and B, within a certain operating range. This research reports how logic and interface controllers, for the acquisition and management of several inputs and outputs, were developed.

2 Medium-Scale Digester Plant Controllers

2.1 *Smart Automation System*

The automation system consists of several ABB PLC, particularly, one unit AC500-ETH, one unit DC562 and two units AX561, which manage actuators and sensors according to process parameters, i.e., substrate temperature and pH. In addition, they enable to acquire, thanks to appropriate sensors, biogas properties in terms of temperature, pressure and flow, permitting therefore to quantify biogas production. Automation Builder 2.2.5 software was used as programming domain. The first step was to declare all the PLC units and then define the interface of communication. In our case, we used COM1 and ETH1 interfaces; this latter allows us to interact with the automation system by using a proper web server. Figure 1 shows the device window of the AC500-ETH unit.

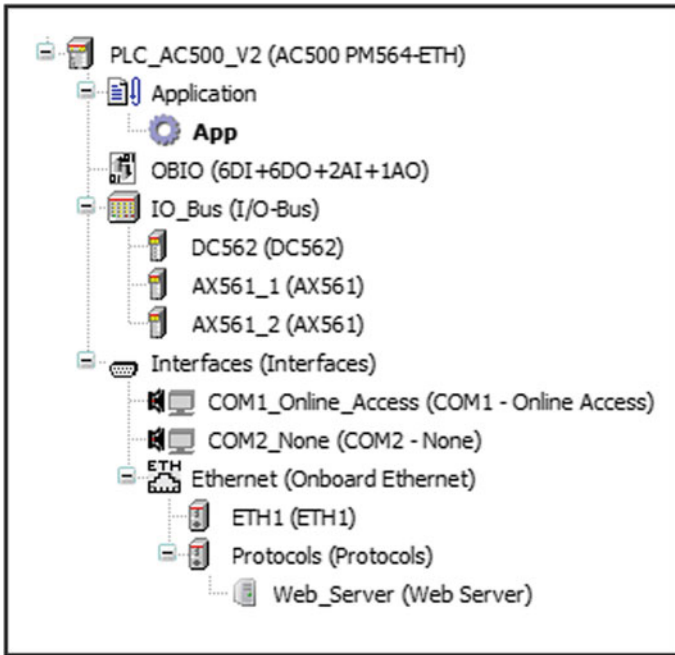


Fig. 1 Device window of the AC500-ETH unit

Communication with PLC units takes place physically via RJ45 Ethernet cable, which connects the automation system to the notebook used to run the programming software. The use of the Ethernet protocol allows opening the control interface linked to the PLC through any client connected to the same LAN. In particular, the web server provided by the PLC that contains the control interface is invoked using a specific link.

The prototype running and automatism depend on the following sensors: a temperature probe (placed inside the digester to measure the whole substrate temperature); a pH-meter (placed inside the digester to measure the pH of the whole substrate); a pressure meter (placed at the outlet of the digester to measure the pressure of the biogas); and two flow meters (placed at the exit of the digester to measure the flow rate of biogas). While, actuators concern a suction pump (to feed the digester); a mixer (placed inside the digester to mix and favour substrate homogeneity); three solenoid valves (to control the matrices flows and water flow in case of cooling needs); two electrical resistors (to heat the substrate).

2.2 Control Logic

The implemented control logic is based on the acquisition and control of the following input and output signals, which can be analogical or digital. Table 1 reports the variables associated with the analogical/digital signals received or emitted by the automation system (the terminals correspond to the physical ports present on the AC500 and AX561 PLCs).

The programming language required by the automation system is based on the use of functional blocks, through which the system allows the acquisition of the analogical signals provided by the temperature, pH, pressure and flow sensors and properly manages the corresponding actuators (Fig. 2). The flowchart of the control strategy is shown in Table 1.

The plant is fed, using an electric pump, with two matrices having respectively acid (in the case of olive mill wastewater) and alkaline pH (i.e. livestock manure), until reaching the optimum pH value (around 7). The temperature control is ensured by a couple of armoured heater elements, while cooling, can occur thanks to a water main directly connected to the digester, when temperature goes beyond T_{max} . The water flow rate is controlled by a solenoid valve.

Table 1 Input and output signals

Variable name	Type of signal	Type	Terminal
pH _{in}	Analog input AI0	INT	8
Temperature _{in}	Analog input AI1	INT	9
Pump _{out}	Digital output DO0/NO0	BOOL	13
Mixer _{out}	Digital output DO1/NO1	BOOL	14
Resistors _{out}	Digital output DO2/NO2	BOOL	15
MatrixA _{out}	Digital output DO3/NO3	BOOL	16
MatrixB _{out}	Digital output DO4/NO4	BOOL	17
HeatingWater _{out}	Digital output DO5/NO5	BOOL	18
GasFlowRate1 _{in}	Analog input I0+	INT	2
GasFlowRate2 _{in}	Analog input I1+	INT	5
GasPressure _{in}	Analog input I2+	INT	8

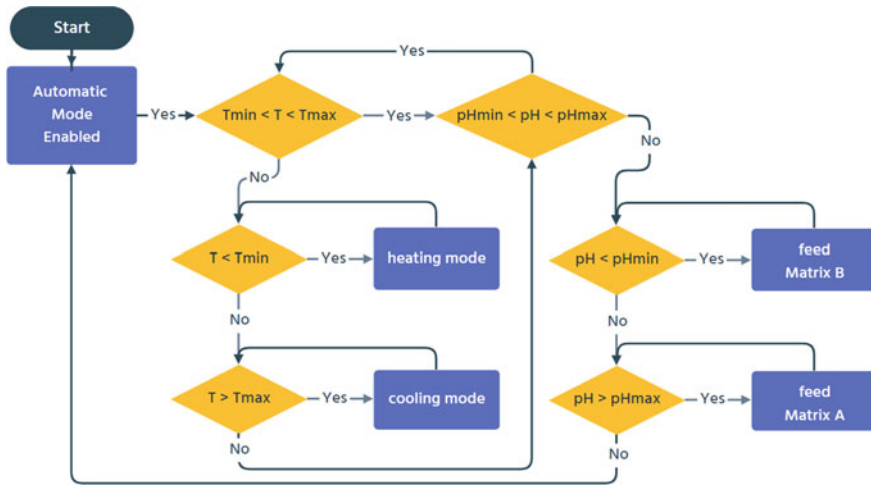


Fig. 2 Flowchart of the control strategy

2.3 Graphical Control Interface

The control interface, based on a smart interface, was designed to allow the user to control both manually and automatically the actuators, i.e. feed aspiration through an electric pump and respective solenoid valves, the mixer, the solenoid valve for the aspiration of cooling water and the two armoured heater elements.

Furthermore, it allows setting process parameters, controlling process progress, and saving data history. The interface enables to navigate between four different windows: manual control, automatic control, parameter setting and trends, which shows the progress of the measurements provided by the sensors in real-time.

Manual Control Mode

Figure 3 shows the manual control window. The display reports the biogas pressure and the gas flow rates measured by the two flow switches (left side), allowing to start and reset a timer for counting the days, hours, minutes, and seconds. The temperature and the pH of the substrate are displayed on the right side. Some lights (high and low) come on if the previous values exceed the maximum values or fall below the minimum values. By clicking on the grey buttons, certain actions are performed (after the activation, the active button changes colour).

For example, by clicking on the “CARICA A” button, matrix A is loaded. The operation is performed at a time interval of 10 s. This range can be changed by dragging the corresponding selection bar. At the bottom, status lights are displayed to provide the real-time status of the actuators (red colour indicates off, green colour indicates on). It is possible to change the window and choose the working mode by clicking on the type control buttons placed at the bottom of the control interface.

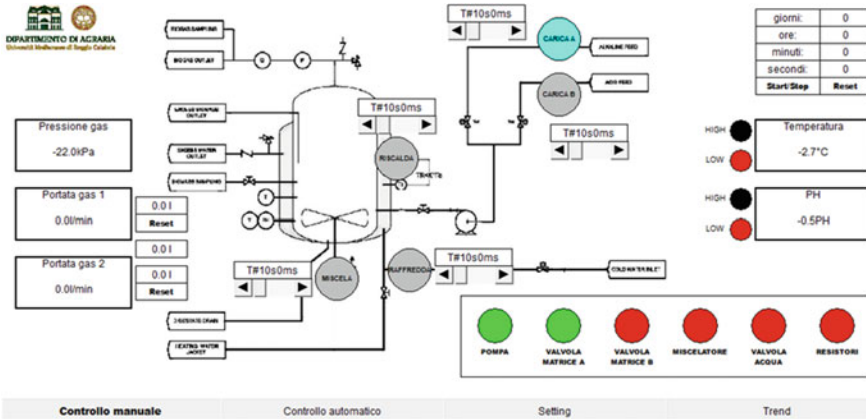


Fig. 3 Manual control window and loading activation of matrix A

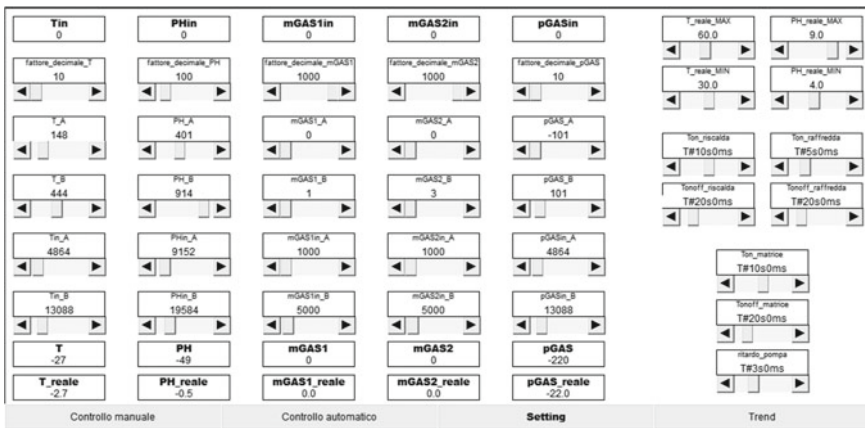


Fig. 4 Setting window

Automatic Control Mode

In this configuration, the control of the individual actuators is not allowed but it is only possible to start or stop (by clicking on the START button) the operation of the digester. In this mode, the PLC will automatically intervene on resistors, electric pump and solenoid valves whenever a correction of the temperature and pH values is required.

The Graphical Interface also provides a “Setting” window, shown in Fig. 4, which supplies the tools to tune and modify the variables that affect the control logic, that is:

- T_reale_MAX = maximum temperature value;
- T_reale_MIN = minimum temperature value;

- PH_reale_MAX = maximum PH value;
- PH_reale_MIN = minimum PH value.

The heating and cooling of the substrate occur cyclically. That is, the resistor heats the substrate intermittently through the succession of on and off phases. This solution has been chosen because it allows the management of the thermal inertia of the system. The intermittent heating and cooling phases provide the system with the time necessary to reach the preferential temperature conditions, avoiding excessive overheating or under-cooling. From the setting window, it is possible to modify the intermittence intervals.

The loading phase of matrices A and B also occurs cyclically. That is, the pump supplies matrix A or B intermittently through the succession of on and off phases. The intermittent loading phase provides the system with the time necessary to reach the preferential pH conditions, avoiding making the global matrix too acidic or too basic (due, even in this case, to the inertia of the system). From the setting window, it is possible to modify the intermittence intervals. The loading phase of matrices A and B takes place in two steps: in the first step, the solenoid valve related to the matrix to be loaded (A or B) is activated; then the electric pump with the task to pump the corresponding matrix is activated. This delay is necessary to be sure that the solenoid valve has performed a complete rotation.

On the right side of the “Setting” window, the necessary variables to calibrate the measurement of the temperature, pH, flow and pressure sensors are shown. In detail, for each measurement, a proportionality coefficient was applied between the analogical signal and the measurement itself.

Finally, a “Trend” window (Fig. 5) shows the real-time trends of the measurements acquired by the sensors and supplies information on:

- substrate temperature;

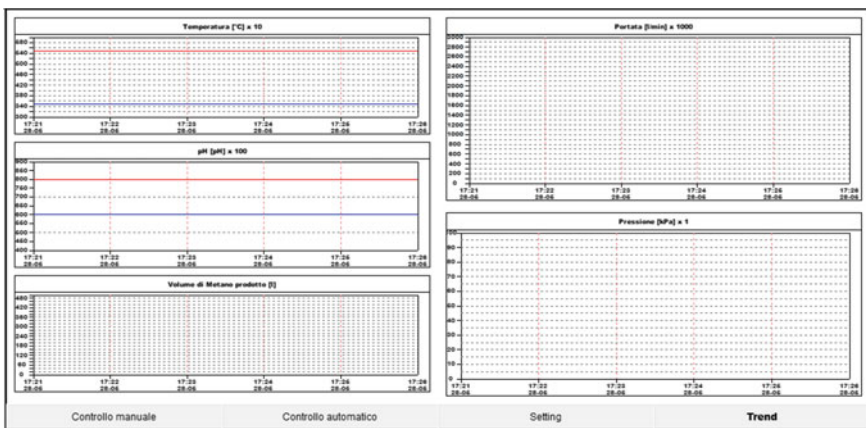


Fig. 5 Trend window

- pH of the substrate;
- flow rate, pressure, and cumulative volume of the produced biogas.

The performed measurements displayed in the Setting window are also saved in text files. The data history stores not only the pH values, flow rate, pressure, and temperature but also the operating status of the actuators. A history file is automatically created and saved in the notebook.

3 Conclusions

The control logic presented in this paper, and developed for the management of a medium-scale digester plant through a smart automation system, is characterized by flexibility and operating easiness. Such an equipment represents a useful solution, particularly if used in small and medium olive oil mills, as it allows to manage sustainably olive mill by-products and recover them into renewable energy, which can be used *in situ* according to a multifunctional approach considering both economic and environmental aspects [9, 10].

Acknowledgements This research was funded by the National Operative Project PON01_01545 OLIOPIU⁺ and AGER 2 Project Sustainability of the Olive-oil System S.O.S. (grant no. 2016-0105).

References

1. Benalia, S., Falcone, G., Stillitano, T., De Luca, A.I., Strano, A., Gulisano, G., Zimbalatti, G., Bernardi, B.: Increasing the content of olive mill wastewater in biogas reactors for a sustainable recovery: methane productivity and life cycle analyses of the process. *Foods* **10**, 1029 (2021). <https://doi.org/10.3390/foods10051029>
2. Zema, D.A., Zappia, G., Benalia, S., Zimbalatti, G., Perri, E., Urso, E., Tamburino, V., Bernardi, B.: Limiting factors for anaerobic digestion of olive mill wastewater blends under mesophilic and thermophilic conditions. *J. Agric. Eng.* **49**(2), 130–137 (2018). <https://doi.org/10.4081/jae.2018.792>
3. Singh, A., Kumar, V.: Recent developments in monitoring technology for anaerobic digesters: a focus on bio-electrochemical systems. *Bioresour. Technol.* **329**, 124937 (2021). ISSN 0960-8524. <https://doi.org/10.1016/j.biortech.2021.124937>
4. Ward, A.J., Bruni, E., Lykkegaard, M.K., Feilberg, A., Adamsen, A.P.S., Jensen, A.P., Poulsen, A.K.: Real time monitoring of a biogas digester with gas chromatography, near-infrared spectroscopy, and membrane-inlet mass spectrometry. *Bioresour. Technol.* **102**(5), 4098e4103 (2011).
5. Falk, H.M., Reichling, P., Andersen, C., Benz, R.: Online monitoring of concentration and dynamics of volatile fatty acids in anaerobic digestion processes with mid-infrared spectroscopy. *Bioprocess Biosyst. Eng.* **38**(2), 237e249 (2015)
6. Jin, X., Li, X., Zhao, N., Angelidaki, I., Zhang, Y.: Bio-electrolytic sensor for rapid monitoring of volatile fatty acids in anaerobic digestion process. *Water Res.* **111**, 74e80 (2017)

7. Cruz, I.A., de Melo, L., Leite, A.N., Melquiades Sátiro, J.V., Santos Andrade, L.R., Torres, N.H., Cabrera Padilla, R.Y., Bharagava, R. N., Tavares, R. F., Romanholo Ferreira, L. F.: A new approach using an open-source low cost system for monitoring and controlling biogas production from dairy wastewater. *J. Clean. Prod.* **241**, 118284 (2019). ISSN 0959-6526. <https://doi.org/10.1016/j.jclepro.2019.118284>
8. Bernardi, B., Benalia, S., Zema, D.A., Tamburino, V., Zimbalatti, G.: An automated medium scale prototype for anaerobic co-digestion of olive mill wastewater. *Inf. Process. Agric.* **4**(4), 316–320 (2017). <https://doi.org/10.1016/j.inpa.2017.06.004>
9. Stillitano, T., De Luca, A.I., Falcone, G., Spada, E., Gulisano, G., Strano, A.: Economic profitability assessment of Mediterranean olive growing systems. *Bulgarian J. Agr. Sci.* **22**(4), 517–526 (2016)
10. Bernardi, B., Falcone, G., Stillitano, T., Benalia, S., Bacenetti, J., De Luca, A.I.: Harvesting system sustainability in Mediterranean olive cultivation: other principal cultivar. *Sci. Total Environ.* **766**, 142508 (2021). <https://doi.org/10.1016/j.scitotenv.2020.142508>

Using Multiple Correspondence Analysis to Evaluate Milking Parlour Performance



Francesco M. Tangorra  and Annamaria Costa 

Abstract Modern milking parlours allow the automated collection of many data for each cow being milked that can potentially be used to monitor the overall performance of milking process. A group of 24 dairy farms located in Lombardy (Northern Italy) with RFID technology for electronic identification of cows, milk meters to measure individual milk yield and the same milking machine settings (42 kPa system vacuum, 60 cycles/min pulsator rate, and 60% pulsator ratio) were involved in the study. Cows milked/stall per hour [n], milk yield/stall per hour [kg], milking efficiency [%] were downloaded by the herd management software and combined with additional information such as number of milking stalls, stalls/milker, type of exit from milking parlour (rapid or conventional), and type of milking routine (full or partial). Relationships among variables were evaluated through a multiple correspondence analysis (MCA) that identified three main groups of related parameters. Large parlours (>32 milking stalls) were associated with a high number of stalls/milker (>15), low number of cows milked/stall per hour (<2.5), low milking efficiency (<31%), low milk yield/stall per hour (<39 kg). On the contrary, small parlours (<16 milking stalls) were associated with a low ratio stall/milker (<8), high performance in terms of cows milked and milk yield per stall per hour (>3.5 and > 52 kg) and milking efficiency (>39%). Parlours of medium size (16–32 milking stalls) were associated with intermediate performance. Results suggest that MCA can potentially be used to evaluate milking parlours performance.

Keywords Multiple Correspondence Analysis · Milking Parlour Performance · Milking Efficiency

F. M. Tangorra (✉) · A. Costa
Department of Veterinary Medicine and Animal Sciences, Università Degli Studi Di Milano,
Milan, Italy
e-mail: francesco.tangorra@unimi.it

© The Author(s), under exclusive license to Springer Nature Switzerland AG 2023
V. Ferro et al. (eds.), *AIIA 2022: Biosystems Engineering Towards the Green Deal*,
Lecture Notes in Civil Engineering 337,
https://doi.org/10.1007/978-3-031-30329-6_95

927

1 Introduction

After the removal of milk production quotas imposed by the European Union the average herd size in dairy cattle production system has been increasing, as expected [1]. In Lombardy Region (Northern Italy), since quota abolition to date, dairy cattle farms with more than 500 heads increased over 54% from 330 to 510 [2] and farm intensity in term of milk yield/cow per year increased by about 11% from 9,333 kg to 10,357 kg [3].

Milking the cows is likely the most time consuming task on dairy farm, requiring significant labour inputs over the year [4]. As herds sizes expand, milking parlour needs to be remodelled selecting the appropriate number of milking units and the adequate technological level to limit the number of rows and time required to milking the herd [5]. Milking parlour performance can be assessed using data extracted from electronic milk meters. For example, first and last cluster-attachment times, number of cows milked and milk yield can be used to calculate benchmarks such as cow throughput, milking and operators' efficiency. Nevertheless, these values are affected by the number of milking units in the parlour, work routine time of the operator, individual cow milking duration, making difficult comparisons between parlours [5]. Multiple correspondence analysis (MCA), a multivariate descriptive data analytic technique, could be used to overcome this problem. Although MCA is mainly used as an exploratory technique, it is particularly powerful as it uncovers groupings of variable categories in the dimensional spaces, providing key insights on relationships between categories. The use of MCA is particularly relevant in studies where a large amount of qualitative data is collected in pair with quantitative data [6].

The current study aimed to test if MCA can potentially be used to assess milking parlours performance.

2 Materials and methods

A group of 24 dairy farms located in Lombardy (Northern Italy) was visited to collect the following data from the herd management software (AfiFarm v. 3.07, Afimilk) over one-year experimental period: cows milked/stall per hour [n]; milk yield/stall per hour [kg]; milking efficiency [%]. Additional collected information were number of milking stalls, stalls to milker ratio, exit from milking parlour (rapid or conventional), and type of milking routine (full or partial).

Common conditions to all the systems investigated were the electronic identification of cows using Radio Frequency Identification (RFID) technology, the use of milk meters to measure milk yield for individual cows, the adoption of the same herd management software, and the milking machine settings (42 kPa system vacuum, 60 cycles/min pulsator rate, and 60% pulsator ratio).

Quantitative variables were transformed into three classes, using their quantile position with respect to the mean. This provided the frequencies of observations that were within the quantiles < 25%, between 25 and 75%, and > 75% of the mean value for a chosen variable. Relationships among variables were evaluated through a multiple correspondence analysis (MCA). Significant differences ($P < 0.05$) between classes means were tested by a one-way ANOVA with Tukey–Kramer mean comparison (JMP Pro 16.1, SAS Institute).

3 Results and discussion

MCA identified three main groups of related parameters (Fig. 1): in the first group large parlours (>32 milking stalls) were associated with a high number of stalls/milker (>15), low number of cows milked/stall per hour (<2.5), low milking efficiency (<31%), low milk yield/stall per hour (<39 kg). On the contrary, small parlours (<16 milking stalls) were associated with a low stall to milker ratio (<8), high performance in terms of cows milked and milk yield per stall per hour (>3.5 and > 52 kg) and milking efficiency (>39%). Parlours of medium size (16–32 milking stalls) were associated with intermediate performance.

Small and medium size milking parlours usually applied a full milking routine (predipping, forestripping, teats drying before milking cluster attachment) while in large parlours teats were only wiped or stripped before milking unit attachment.

Rapid exit characterized all large parlours. Small milking parlours showed significant ($P < 0.05$) higher performance in terms of cows milked/stall per hour (+24% and

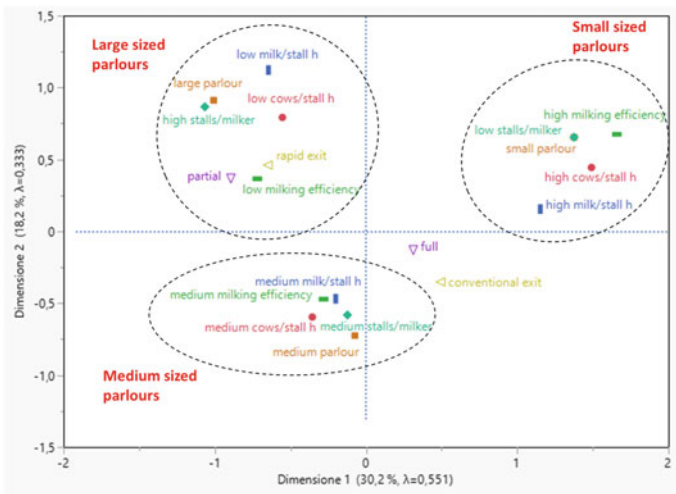


Fig. 1 Biplot of the first two axes of the multiple correspondence analysis (MCA) illustrating the relationships among parameters considered to evaluate milking parlours performance

Table 1 Milking parlours performance according to their size (means \pm SD)

Parameters	Milking parlour size		
	Small	Medium	Large
Cows/stall per h (n)	3.63 \pm 0.28 ^a	2.92 \pm 0.03 ^b	2.57 \pm 0.14 ^b
Milk yield/stall per h (kg)	48.58 \pm 4.84	46.4 \pm 3.26	40.44 \pm 4.84
Milking efficiency (%)	41.0 \pm 3.0 ^a	33.6 \pm 6.0 ^b	31.5 \pm 3.0
Stalls/milker (n)	6.2 \pm 0.8 ^A	10.4 \pm 2.2 ^B	18.8 \pm 3.8 ^C

^{a,b} Values in the same row with different superscripts differ significantly ($P < 0.05$)

^{A,B} Values in the same row with different superscripts differ significantly ($P < 0.01$)

+ 28%) and milking efficiency (+22% and + 30%) if compared respectively with medium and large parlours (Table 1). Long row parlours increase working routine time for entering and exiting cows, especially in milking parlours with one operator [7], affecting the number of cows/stall per hour.

No significant differences were observed in terms of milk yield/stall per hour between parlours of different size (Table 1), milk yield not being affected by milking unit number or parlour size at either peak or late lactation [8].

Significant differences were found about the number of stalls/milker (Table 1), confirming that in large parlours milking procedures can have a dramatic impact on the number of units one operator can handle. When a full milking procedure is used, the number of units a milker can operate reduces up to 40% compared to using minimal milking procedures [9].

4 Conclusions

Results suggest that MCA can potentially be used to evaluate milking parlours performance, allowing farm advisors to identify customer needs and to plan a possible intervention adaptively for a larger pool of farms instead of following each one individually.

References

1. O'Donnell, S., Horan, B., Butler, A.M., Shalloo, L.: A survey of the factors affecting the future intentions of Irish dairy farmers. *J. Agric. Sci.* **149**, 647–654 (2011). <https://doi.org/10.1017/S0021859611000037>

2. Sistema Informativo Veterinario – Statistiche, Homapage, https://www.vetinfo.it/j6_statistiche/index.html/, last accessed 2022/09/11.
3. Associazione Italiana Allevatori, Bollettino On Line, Controlli sulla produttività del latte, <http://bollettino.aia.it/#>, last accessed 2022/09/11.
4. O'Donovan, K., O'Brien, B., Ruane, D.J., Kinsella, J., Gleeson, D.: Labour input on Irish dairy farms and the effect of scale and seasonality. *J. Farm Manag.* **13**, 327–342 (2008).
5. Edwards, J.P., O'Brien, B., Lopez-Villalobos, N., Jago, J.G.: Milking efficiency of swingover herringbone parlours in pasture-based dairy systems. *J. Dairy Res.* **80**, 467–474 (2013). <https://doi.org/10.1017/S0022029913000393>
6. Costa P.S., Santos N.C., Cunha P., Cotter J., Sousa N.: The use of multiple correspondence analysis to explore associations between categories of qualitative variables in healthy ageing. *Journal of Aging Research*, e302163. <https://doi.org/10.1155/2013/302163> (2013).
7. Bickert, W.G., Speicher, J.A., Armstrong, D.V.: Milking systems for large herds. *J. Dairy Sci.* **57**, 369 (1974).
8. Stewart S.C., Eicker S.W., Reid D.A., Mein G.: Using computerized data to find time for milk quality. Proc. of the 52nd Annual Meeting of the National Mastitis Council, San Diego (CA), January 27–29, 2013. 85–94 (1999).
9. Smith, J.F., Harner III J.P., Brouch M.L., Armstrong D.V., Gamroth M.J., Meyer M.J. Relocation and Expansion Planning. In proceedings of Western Herd Management Conference, Las Vegas, NV, 73–85 (1999).

Effect of Automatic Feeding System (AFS) on Dairy Cows Feeding Activity



Francesco M. Tangorra  and Aldo Calcante 

Abstract Supplying a total mixed ration (TMR) to dairy cows with a higher frequency is a key factor to have more distributed visits to the feeding fence over 24 h and longer feeding times. All this optimizes dry matter ingestion and stabilize the ruminal pH with positive effects on cows' health and milk production. A CMOS monochromatic camera was used to monitor the effect of TMR distribution and push-up operated by an AFS on dairy cows' attendance of feeding alleys. The study was carried out in a dairy farm of Lombardy (Northern Italy) with 121 lactating cows divided into two groups (A and B) and milked by two milking robots. Groups A and B consisted respectively of 58 and 63 animals with respectively 63 and 69 feeding places (feeding alleys 1 and 2). The camera was conveniently placed to frame the two feeding alleys and a software tool written in Matlab controlled its settings (interval shooting, exposure time, gain). Images were acquired at 5 min interval from 6 a.m. to 6 p.m. for ten consecutive days in January 2019 and the feeding place index (FPI), obtained by comparing the feeding cows to the feeding places, was calculated at the same interval. Significant differences between FPI means calculated at each TMR distribution and push-up were tested by analysing the variances. Results showed that TMR distributions determine significant higher ($P < 0.01$) FPI compared to TMR push-up (0.46 vs. 0.26). FPI increased up to 0.54 and 0.51 respectively after 15 and 30 min TMR distributions, even if the differences were not significant. On the contrary, FPI reduced significantly ($P < 0.01$) to 0.19 after 30 min TMR push-up. These results confirm the feeding activity of dairy cows may be influenced by TMR distributions and push-up operated by AFS.

Keywords Automatic feeding system · Feeding activity · Total mixed ration · Feeding place index

F. M. Tangorra (✉)

Department of Veterinary Medicine and Animal Sciences, Università degli Studi di Milano, Milan, Italy
e-mail: francesco.tangorra@unimi.it

A. Calcante

Department of Agricultural and Environmental Sciences, Università degli Studi di Milano, Milan, Italy

1 Introduction

Recently automatic feeding systems (AFS) have been successfully introduced on the market and currently more than 1250 feeding robots are used worldwide [1, 2]. Feeding the herds, with 16% of total labour requirement, represents the third-largest labour input in dairy farming after milking and rearing of calves and young stock [3].

Running up to 16 total mixed ration (TMR) distributions • day⁻¹, AFS allow meeting the herd's nutritional needs without depending on human labour and incurring additional labour costs. Under the aspects of saving working time, easing workload and bringing more flexibility, AFS are becoming more and more popular among dairy cattle farmers [1, 2, 4–6].

Increasing the feeding frequency results in more distributed visits to the feeding fence over 24 h and longer feeding times leading to a greater dry matter ingestion by cows and a higher stability of ruminal pH with positive effects on cows' health and milk production [7–10].

The aim of the study reported here is to assess the effect of AFS on dairy cows feeding activity measured through the feeding place index (FPI), obtained by comparing the number of feeding cows to the available places along the feeding alley thanks an automatic monitoring carried out through a CMOS monochromatic camera.

2 Materials and Methods

The present study was carried out over a period of ten days, from the 16th to 25th of January 2019, in a dairy farm of Lombardy Region (Northern Italy) with 121 Holstein Friesian lactating cows divided into two groups (A and B) and milked by two milking robots (Astronaut A4, Lely Holding, Maassluis, the Netherlands). Group A consisted of 58 animals and had available 63 feeding places (Feeding alley 1), while group B consisted of 63 cows with 69 feeding places (Feeding alley 2).

From 2018, an AFS (Vector system, Lely Holding, Maassluis, the Netherlands) was introduced in the farm to feed the lactating and dry cows. The TMR distributed to lactating cows was composed by corn silage, ryegrass hay, alfalfa hay, concentrate and cottonseed. In dry cows, ryegrass silage and straw substituted ryegrass hay and cottonseed. Lactating cows received individual feed portions of their concentrate ration, according to their lactation period and milk yield, from the relative automatic dispenser in the AMS during milking.

2.1 The Automatic Feeding System

The AFS installed at the farm consists of three main parts: (i) a feed kitchen, an enclosed area where blocks of roughage are stored; (ii) a feed grabber with a bridge crane to grab roughage and loads it into the mixing bin of a mixing and feeding robot (MFR); (iii) a MFR capable of automatically distribute a self-mixed ration to the animals along the feeding alleys. The MFR is a self-contained battery-operated vehicle, with a mixer bin of 2.0 cubic meter capacity.

All the roughages (silage blocks, shredded hay, and cottonseed) used to prepare the TMR are stored in the feed kitchen in specific storage locations according to a chessboard logic, while concentrates are stored in vertical silos. The feed kitchen is filled on average every three days with corn silage and cottonseed, and once a day with the shredded hay using a telescopic handle.

The loading sequence of the MFR follows the same logic as for the conventional TMR wagon: first hay followed by concentrate and last silage. After all feed types are loaded, the mixing continues for a set time and when the mixing is completed, the MFR drives from the feed loading point to the feeding alley in the barn. While it is on the route it measures the height of the TMR previously distributed and pushes it toward the fence of all locations with animals. The MFR stops when it arrives at the location on the feed fence of the animals that need to be fed and starts to dose the TMR measuring its height and pushing it toward the fence. When the mixing bin is empty, the MFR drives away from the feed fence and comes back to the charger waiting for a new TMR distribution cycle. Measuring continuously the height of the residual TMR on the feed alley means to provide feed only when strictly necessary.

2.2 Assessing of the Dairy Cows Feeding Activity

A CMOS monochromatic camera (Lumenera LU125M, Lumenera Corporation, Canada) was used to monitor the effect of TMR distribution and push-up operated by the MFR on dairy cows' attendance of feeding alleys.

The camera was conveniently placed to frame the two feeding alleys and its settings (interval shooting, exposure time, gain) were controlled by a software tool written in Matlab v.R2017B (MathWorks Inc., Massachusetts, USA). Images were acquired at 5 min interval approximately from 6 a.m. to 6 p.m. during the experimental period (ten days). The poor lighting conditions of the barn did not allow acquiring neither images nor calculating feeding place index (FPI) for the evening and night hours.

The dairy cows' attendance of feeding alleys was assessed by using the FPI, calculated at the same time interval of image acquisition, at each TMR distribution and push-up, and at +15 min and +30 min after TMR distribution and push-up with the following Eq. (1):

$$FPI = \frac{\text{feeding cows}}{\text{feeding places}} \tag{1}$$

FPI was analyzed for TMR distribution and push up at time t_0 , $t_{15 \text{ min}}$ and $t_{30 \text{ min}}$. The Shapiro–Wilk test was used to assess the normality of the measured variables.

A 2×3 ANOVA was applied to evaluate the effects of type of action (TMR distribution or push-up), time after TMR distribution or push-up (t_0 , $t_{15 \text{ min}}$ and $t_{30 \text{ min}}$) and the interaction between these two factors on FPI. The Tukey–Kramer post hoc test was used to compare each mean between them. Results were reported as least square means \pm SEM, significance was declared at $P < 0.05$.

3 Results and Discussion

Figures 1 and 2 show the FPI calculated at 5 min interval during the experimental period (16–25 January) for the feeding alleys 1 and 2. Unfortunately, data of January 21st are missing due to a problem encountered with the images acquisition managed by the Matlab tool.

The presence of cows at the feeding alleys varied dynamically each day following the delivery of fresh feed and subsequent push-up (Fig. 3). As reported by [7] and [11] the delivery of fresh feed can be considered an important exogenous factor stimulating dairy cows to feed. The logic of distribution of the MFR, based on providing feed only when necessary by measuring continuously the height of the residual TMR in the feeding alley, determines day-by-day different feeding activity patterns (Figs. 1 and 2).

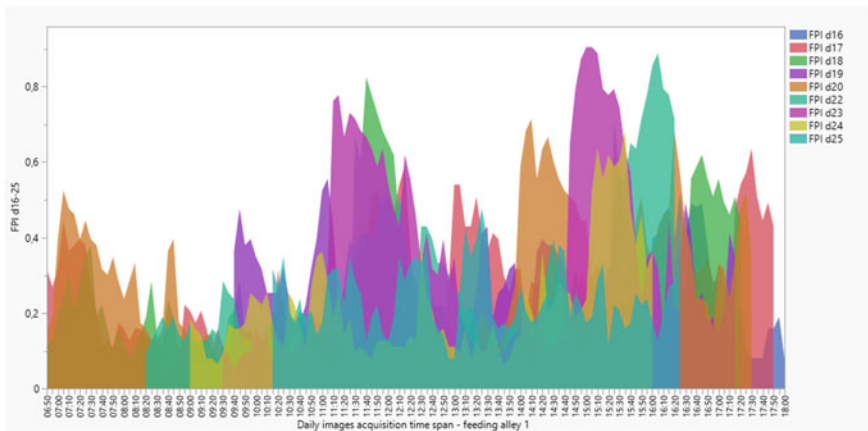


Fig. 1 Feeding place index (FPI) calculated at 5 min interval for the feeding alley 1 over the experimental period (days 16–25, 6:50–18:00)

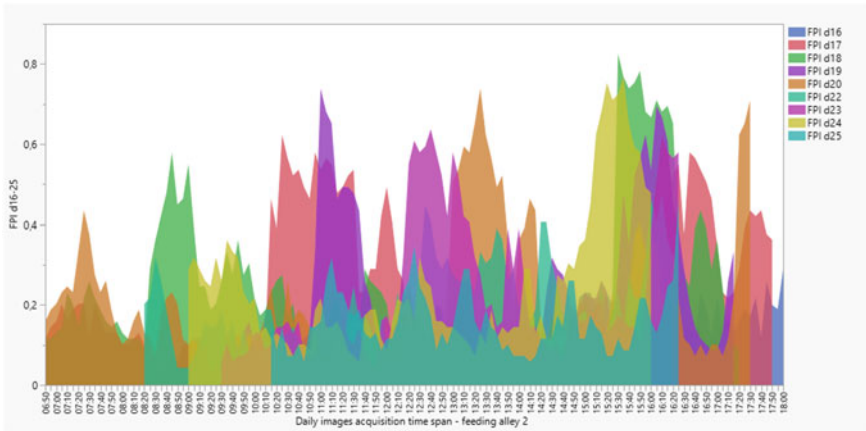


Fig. 2 Feeding place index (FPI) calculated at 5 min interval for the feeding alley 2 over the experimental period (days 16–25, 6:50–18:00)

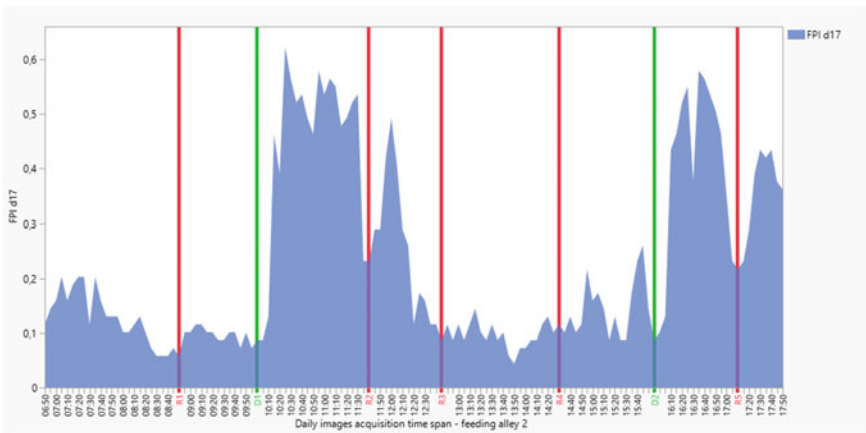


Fig. 3 Feeding place index (FPI) and TMR distribution (green line) and push up (red line) for the feeding alley 2 at the day 17 (6:50–17:50)

Results highlighted a statistically ($P < 0.01$) higher FPI for TMR distribution compared to push up (0.50 ± 0.02 vs. 0.23 ± 0.01), while time after TMR distribution and push-up not influenced the FPI values. A significant ($P < 0.01$) time-by-type of action interaction was observed for FPI from t_0 to t_{30min} as reported in Table 1. The greatest number of cows attending the feeding alley was seen after the delivery of fresh feed compared to feed push-ups as observed in a previous study by [12], confirming the lower influence of feed push-up on behavioral patterns of dairy cows [13].

Table 1 Time-by-type of action for Feeding place index (FPI). Values reported as $\text{I means} \pm \text{SEM}$

	Type of action	Time ^a		
		t ₀	t _{15min}	t _{30min}
FPI	TMR distribution	0.46 ± 0.03 ^a	0.54 ± 0.03 ^b	0.51 ± 0.03 ^b
	TMR push up	0.26 ± 0.02 ^b	0.25 ± 0.02 ^c	0.19 ± 0.02 ^c

^aAfter TMR distribution or push up

^{b,c} Values in the same column with different superscripts differ significantly ($P < 0.01$)

4 Conclusions

The diurnal pattern of feeding alley attendance varied dynamically being influenced by the logic of distribution of the MFR that provides feed only when necessary by measuring the height of the residual TMR in the feeding alley. Moreover, the delivery of fresh feed showed greater effect on the diurnal pattern of feeding alley attendance than feed push-ups.

References

1. Belle, Z., André, G., Pompe, J.: Effect of automatic feeding of total mixed rations on the diurnal visiting pattern of dairy cows to an automatic milking system. *Biosyst. Eng.* **111**(1), 33–39 (2012)
2. Oberschätzl-Kopp, R., Haidn, B., Peis, R., Reiter, K., Bernhardt, H.: Effects of an automatic feeding system with dynamic feed delivery times on the behaviour of dairy cows. In: *Proceedings of CIGR-AgEng Conference, Aarhus, Denmark*, pp.1–8 (2016)
3. Macuhova, J., Haidn, B.: Labour input on Bavarian dairy farms with conventional or automatic milking. In: *Proceedings of International Conference of Agricultural Engineering – CIGR-AgEng, Valencia, Spain*, p. 1617 (2012)
4. Bisaglia, C., Belle, Z., Van den Berg, G., Pompe, J.C.A.M.: Automatic vs. conventional feeding systems in robotic milking dairy farms: a survey in The Netherlands. In: *Proceedings of International Conference of Agricultural Engineering CIGR-AgEng 2012, Valencia, Spain*, pp. 100–104 (2012)
5. Pezzuolo, A., Chiumenti, A., Sartori, L., Da Borso, F.: Automatic feeding system: evaluation of energy consumption and labour requirement in North-East Italy dairy farm. In: *Proceedings of Engineering for Rural Development, Jelgava, Latvia*, 15, pp. 882–887 (2016)
6. Tangorra, F.M., Calcante, A.: Energy consumption and technical-economic analysis of an automatic feeding system for dairy farms: results from a field test. *J. Agric. Eng.* **49**(4), 228–232 (2018)
7. DeVries, T.J., von Keyserlingk, M.A.G., Beauchemin, K.A.: Frequency of feed delivery affects the behavior of lactating dairy cows. *J. Dairy Sci.* **88**(10), 3553–3562 (2005)
8. Mantysaari, P., Khalili, H., Sariola, J.: Effect of feeding frequency of a total mixed ration on the performance of highyielding dairy cows. *J. Dairy Sci.* **89**(11), 4312–4320 (2006)
9. Mattachini, G., Riva, E., Pompe, J.C.A.M., Provolo, G.: Automatic monitoring of cow behaviour to assess the effects of variations in feeding delivery frequency. In: *Proceedings of 7th Precision Livestock Farming CPLF 2015, Milan, Italy*, pp. 473–481 (2015)

10. Sloth, K.H., et al.: Effects of frequent feed pushes of mixed feed on feeding behaviour, feed intake, and milk production in an AMS herd. In: Proceedings of 8th European Conference on Precision Livestock Farming ECPLF 2017, Nantes, France, pp.459–466 (2017)
11. Melin, M., Svennersten-Sjaunja, K., Wiktorsson, H.: Feeding patterns and performance of cows in controlled cow traffic in automatic milking systems. *J. Dairy Sci.* **88**(11), 3913–3922 (2005)
12. DeVries, T.J., von Keyserlingk, M.A.G., Beauchemin, K.: Short communication: diurnal feeding pattern of lactating dairy cows. *J. Dairy Sci.* **86**(12), 4079–4082 (2003)
13. Miller-Cushon, E.K., DeVries, T.J.: Short communication: associations between feed push-up frequency, feeding and lying behavior, and milk yield and composition of dairy cows. *J. Dairy Sci.* **100**(3), 2213–2218 (2017)

Use of Heavy Metals Contaminated Industrial Hemp (*Cannabis Sativa* L.) for Bioenergy Production



Giuseppe Todde, Gianluca Carboni, Serena Marras, Maria Caria, and Costantino Sirca

Abstract Worldwide human-related activities have caused the heavy metals contamination of large areas. Nowadays, different soil remediation activities are undertaken to ameliorate contaminated soils. Among the various soil reclamation technologies, phytoremediation is considered one of the most cost-effective and eco-friendly practices, where the use of industrial hemp (*Cannabis sativa* L.) has shown promising remediation potential. However, the proper management, disposal or valorization of the contaminated biomass represents a key point for the sustainability of the entire remediation process. This study aims to assess and evaluate the energy and environmental burdens of using heavy metals contaminated industrial hemp for bioenergy production. Specifically, the cumulative energy demand and climate change impact categories were selected from the life cycle assessment methodology. The data sample comes from real heavy metals contaminated sites, located in Sardinia (Italy), which have been subjected to soil reclamation by growing industrial hemp. The energy and environmental impacts of using the contaminated biomass as an energy resource were then modeled from a “field to wire” approach. The designed scenario analyzed the processes associated with field level, transportation, combustion of the contaminated biomass in a power plant and ash disposal. The results obtained underlined that the field level represents the main impacting process, while the electricity produced from the contaminated biomass allowed to save about 32 GJ ha⁻¹ of primary energy while avoiding emissions of 642 kg CO₂e per phytoremediated hectare. The study highlights that the use of heavy metals contaminated biomass for bioenergy production, improved the sustainability of soil reclamation activities turning unproductive lands into productive areas.

G. Todde (✉) · S. Marras · M. Caria · C. Sirca
Department of Agricultural Sciences, University of Sassari, Viale Italia 39a, 07100 Sassari, Italy
e-mail: gtodde@uniss.it

G. Carboni · S. Marras · C. Sirca
Agris Sardegna, Viale Trieste 111, 09123 Cagliari, Italy

S. Marras · C. Sirca
Centro Euro-Mediterraneo Sui Cambiamenti Climatici (CMCC Foundation), IAFES Division, Via De Nicola 9, 07100 Sassari, Italy

Keywords Contaminated biomass · Renewable electricity · Soil remediation · Phytoremediation · Sustainability

1 Introduction

Worldwide human-related activities have caused the heavy metals (HM) contamination of large areas [1]. HM have non-biodegradable and persistent characteristics which may cause water and soil contamination and can pose a risk to human health [2]. According to the EEA [3] and JRC [4], in Europe, potentially polluting activities have taken place at an estimated 2.8 million sites, where only 24% of these sites have been investigated for determining if soil remediation is required. The soil remediation technologies indicate activities that are undertaken to limit the extent of contaminated soils and to prevent exposure to harmful chemicals to living beings [5]. Nowadays, different soil remediation technologies are undertaken to ameliorate contaminated soils. Among the various soil reclamation options, phytoremediation is considered one of the most cost-effective and eco-friendly practices, where the use of industrial hemp (*Cannabis sativa* L.) has shown promising remediation potentials [6–10]. In fact, metal hyperaccumulator plants can accumulate large amounts of HM in their biomass and remain healthy, which makes them suitable for the phytoremediation of HM contaminated areas [11]. Linger et al. [12] found that industrial hemp accumulates HM in all of its plant parts and especially in the leaves. This outcome highlights the importance of contaminated biomass management, treatment and disposal in order to avoid secondary pollution. In fact, the proper disposal or valorization of the contaminated biomass represents a key point for the sustainability of the entire remediation chain. Nevertheless, the phytoremediation of HM contaminated soils is perceived as an eco-friendly technique, it might cause considerable environmental impacts, mostly due to the cultivation activities, transportation, treatment and disposal of the biomass. In order to assess the environmental loads of phytoremediation technologies, the life cycle assessment (LCA) is considered one of the most valuable approaches to analyze the in-depth impacts [13]. Recent studies applied the LCA methodology for evaluating the impacts of phytoremediation technique, where the results underlined that the combination of soil remediation and biomass valorization could be more beneficial for the environment rather than other remediation technologies [14–18]. Although the technical issues and suitability of industrial hemp for phytoremediation have been deeply analyzed, less attention has been given to the energy and environmental aspects of the entire bioenergy supply chain, especially when the contaminated biomass has been used as an energy resource. This study aims to assess and evaluate the energy and environmental burdens of using heavy metals contaminated industrial hemp (*Cannabis sativa* L.) for bioenergy production along the overall supply chain.

2 Materials and Methods

The on-field data used in this study were collected by Agris Sardegna at two experimental sites located in the southwest of Sardinia (Italy). The fields were characterized by HM-contaminated soils with Pb, Zn, and Cd concentrations above the contamination threshold established by the Ministerial Decree 46/2019 [19]. The “Futura 75” industrial hemp cultivar was used for phytoremediation purposes and it was sown at a 40 kg ha^{-1} rate. Nitrogen fertilization was applied at a 60 kg ha^{-1} rate, while water supplementation was distributed following thermopluviometric trends with an approximate rate of $4,500 \text{ m}^3 \text{ ha}^{-1}$. Other input–output data were obtained from the Ecoinvent database [20] and the scientific literature. The system boundaries of the study were set from cradle to grave following the “field-to-wire” approach, including all the activities carried out for on-field cultivation, harvesting, transport of the products, biomass conversion and ash disposal (Fig. 1). The functional units consisted of 1 ha of HM contaminated soil and 1 MWh of electricity produced.

The scenario developed includes the overall activities carried out at field level, where a specific dataset was acquired from on-site measurements and including overall inputs and outputs of the system. Specifically, the on-field tasks conducted were soil preparation, crop management, harvesting of the industrial hemp by mowing dried whole plants and baling activities. Consequently, the bales were

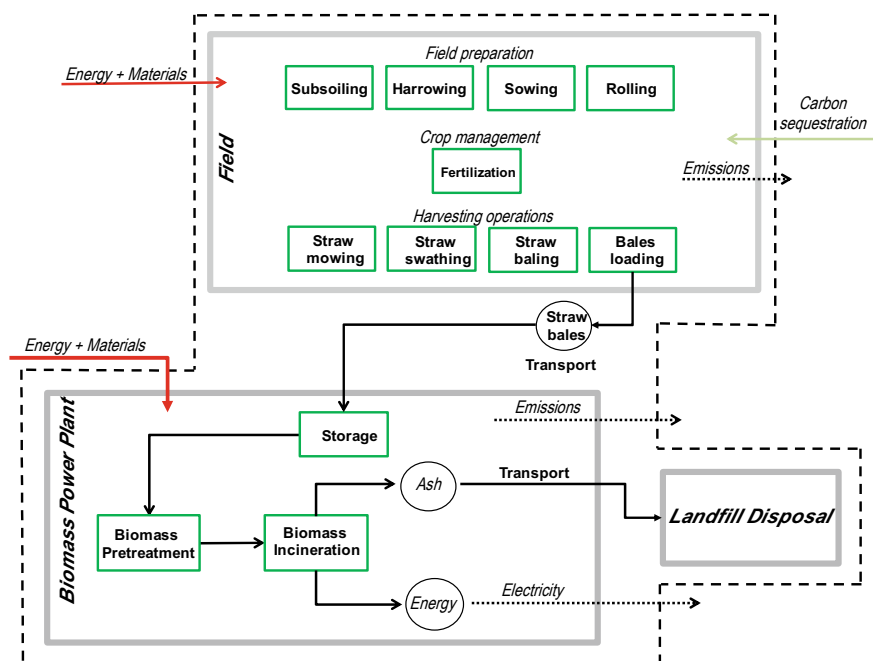


Fig. 1 System boundaries of HM contaminated industrial hemp supply chain “field to wire”

loaded into lorry trucks (16–32-t Euro 5) for road transportation (50 km) from field to Biomass Power Plant (BPP). The contaminated industrial hemp bales were stocked at the BPP where mechanical pretreatment before incineration was assumed with an energy expenditure of 12 kWh t^{-1} of biomass. The life span of the BPP was assumed to be 20 years, while the electrical generation efficiency was 24%. The electricity generated from the combustion of the contaminated feedstock was injected into the grid and replaced the national electricity assuming 9.21 MJ kWh^{-1} [21] as energy equivalent and $0.288 \text{ kg CO}_2\text{e kWh}^{-1}$ [22] as emission factor. The utilization of the waste heat that originated from the BPP was not included in this analysis since the limited availability of district heating structures. The contaminated ashes were transported (30 km) to a landfill site for underground deposit.

The impact categories considered to quantify and analyze the energy and environmental aspects of producing bioenergy from HM contaminated industrial hemp were the cumulative energy demand (CED) and climate change (CC). The first impact category is largely used to analyze the primary energy requirements, expressed in MJ, of a given system, while the second category measures the greenhouse gasses emitted by the studied system (CO_2e). Moreover, the Monte Carlo simulation (1,000 runs analysis) was performed to address uncertainty analysis of the parameters investigated and to test the robustness of the Life Cycle Impact Assessment.

3 Results and Discussion

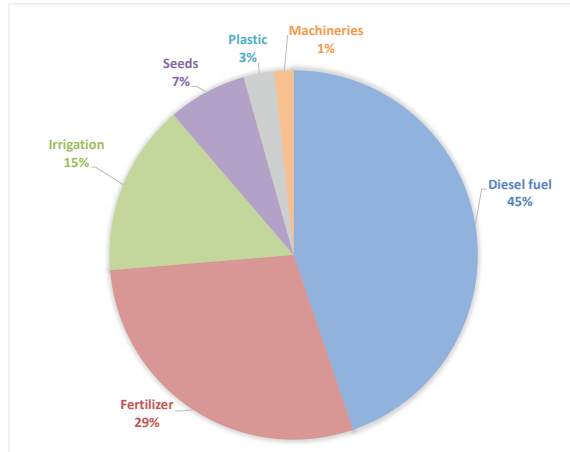
The data collected through the bioenergy supply chain allowed us to quantify the amount of inputs and outputs that were employed and obtained for industrial hemp cultivation, harvest, transportation, conversion of the contaminated biomass and ash disposal. Specifically, for the on-field activities, the total diesel fuel requirements accounted for 97 kg ha^{-1} , where soil preparation and harvesting operations were the most demanding activities. The average rated power employed at field level was 67 kW ha^{-1} and a total working time of 7.8 h ha^{-1} . The harvested product consisted of dried whole industrial hemp with production yields of $4,988 \text{ kg}_{\text{DM}} \text{ ha}^{-1}$, with an average dry matter content of 83%.

Among the inputs utilized for field cultivation and harvesting (Fig. 2), the diesel fuel was the most impacting one with a share of 45%, followed by the use of fertilizers (29%) and irrigation (15%).

After biomass combustion, the contaminated ashes were assumed to be disposed of in an underground deposit at a landfill site. The amount of contaminated ashes accounted for about 100 kg per hectare and the energy requirement for disposal corresponded to 1.2 GJ ha^{-1} and emitting about $52 \text{ kgCO}_2\text{e ha}^{-1}$.

Transport activities were involved in the transportation of the contaminated biomass, from field to BPP, and for the transportation of the contaminated ashes from BPP to landfill site. Total impacts of lorry transport activities accounted for 834 MJ ha^{-1} of primary energy and the emission of $51 \text{ kgCO}_2\text{e ha}^{-1}$.

Fig. 2 Impacts (climate change) distribution of the inputs employed at the field



The overall cumulative energy demand and climate change impacts of the contaminated biomass supply chain were shown in Fig. 3, and accounted for a total of 15.1 GJ ha⁻¹ and 842 kgCO₂e ha⁻¹, respectively. The on-field activities represent the most energy and environmental impacting subsystem, accounting for 77% and 81% of the total impacts, respectively. A minor share of the impacts were found for the BPP, ash disposal and transportation activities (approximately 6–10%).

The energy and environmental benefits that were obtained from the exploitation of the contaminated industrial hemp were considerable. The energy valorization of

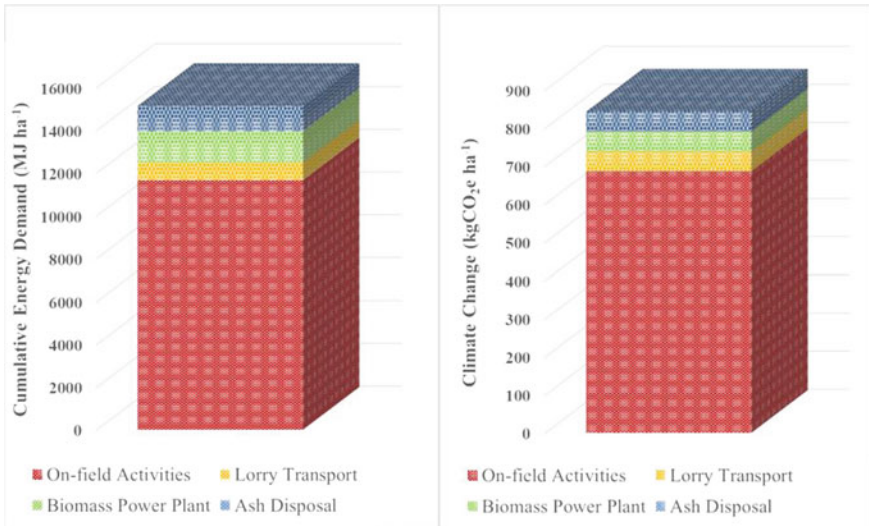


Fig. 3 Distribution of CED and CC impacts among the contaminated industrial hemp supply chain

the feedstocks allowed the generation of 5,144 kWh of electricity per hectare. The bioenergy produced from the combustion of the biomass was assumed to replace the national electricity mix, avoiding the exploitation of 47.5 GJ ha⁻¹ of primary energy and the emission of 1,484 kgCO₂e ha⁻¹. The outcomes of the Monte Carlo analysis (Fig. 4) for the designed biomass supply chain scenarios, demonstrated that the results were robust and highlighted the energy and environmental benefits of using contaminated industrial hemp as an energy resource. In fact, the benefits obtained through the conversion of the contaminated biomass (electricity) were significantly higher than the impacts of the whole supply chain. The energy generated from the studied system was found to be 3.1 times greater than the primary energy spent in the whole supply chain (from field to wire). Similar results were also observed for the emissions analysis, where the avoided emissions were found to be 1.8 times greater than CO₂e emitted from field to wire.

For the results of the input–output of the study, the cumulative energy demand was found to be 2,936 MJ MWh⁻¹, while the emission rate corresponded to 165 kgCO₂e MWh⁻¹, both considering field to wire boundaries.

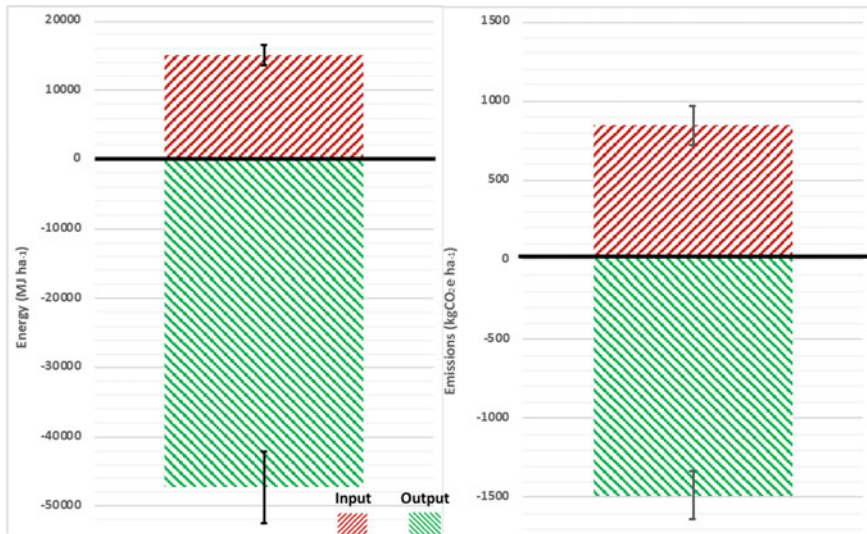


Fig. 4 Uncertainty analysis results from the Monte Carlo simulation for the contaminated industrial hemp supply chain. Total inputs of the system are shown as positive values (red diagonal stripes), while the outputs from the bioenergy production are shown as negative values (green diagonal stripes)

4 Conclusions

In this study a life cycle assessment approach was adopted to evaluate energy and environmental loads of using HM contaminated industrial hemp for bioenergy production. The outcomes of this research highlights the high value of using contaminated biomass as an energy resource for bioenergy generation. Specifically, the study found that the on-field cultivation activities (especially the use of diesel fuel) represents the most impacting energy and environmental stage, reaching up to 80% of the overall supply chain impacts. On the other hand, the valorization of the HM contaminated biomass enabled the generation of about 5,000 kWh ha⁻¹. The energy generated from the studied system was found to be 3.1 times greater than the primary energy spent from field to wire. Similarly, the avoided emissions were found to be 1.8 times greater than CO_{2e} emitted from the supply chain. Finally, the combination of phytoremediation technologies and the energy valorization of the contaminated biomass has been found promising to support the exploitation of unmanaged and unproductive areas.

Acknowledgements This work was supported by Legge Regionale 9 marzo 2015, n 5 Disposizioni per la formazione del bilancio annuali e pluriennale della Regione Sardegna. Art 27 Progetto sperimentale di bonifica terreni agricoli. Title of the project: Canapa: opportunità ambientali ed economiche in Sardegna (CANOPAES).

References

1. FAO, 2018. Food and Agriculture Organization of the United Nations. Outcome Document of the Global Symposium on Soil Pollution, 2–4 May 2018 Rome, Italy.
2. Saxena, G., Purchase, D., Mulla, S.I., Saratale, G.D., Bharagava, R.N.: Phytoremediation of heavy metal- contaminated sites: eco-environmental concerns, field studies, sustainability issues, and future prospects. *Rev Environ Contam T* **234**, 71–131 (2020)
3. EEA, 2020. European Environment Agency. The European Environment – State and Outlook 2020, Knowledge for Transition to a Sustainable Europe.
4. JRC, Joint Research Centre, Status of Local Soil Contamination in Europe. Revision of the indicator ‘Progress in the management contaminated sites in Europe (2018)
5. Dhaliwal, S.S., Singh, J., Taneja, P.K., Mandal, A.: Remediation techniques for removal of heavy metals from the soil contaminated through different sources: a review. *Environ Sci Pollut Res* **27**, 1319–1333 (2020)
6. Ali, H., Khan, E., Sajad, M.A.: Phytoremediation of heavy metals—concepts and applications. *Chemosphere* **91**(7), 869–881 (2013)
7. Patra, D.K., Pradhan, C., Patra, H.K.: Toxic metal decontamination by phytoremediation approach: concept, challenges, opportunities and future perspectives. *Environ Technol Inno* **18**, 100672 (2020)
8. Canu, M., Mulè, P., Spanu, E., Fanni, S., Marrone, A., Carboni, G.: Hemp Cultivation in Soils Polluted by Cd, Pb and Zn in the Mediterranean Area: Sites Characterization and Phytoremediation in Real Scale Settlement. *Appl Sci.*, 3548 (2022)
9. Stonehouse, G.C., McCarron, B.J., Guignardi, Z.S., El Mehdawi, A.F., Lima, L.W., Fakra, S.C.: Selenium Metabolism in Hemp (*Cannabis sativa* L.) Potential for Phytoremediation and Biofortification. *Environ Sci Technol.*, 54:4221–30 (2020)

10. Asquer, C., Melis, E., Scano, E.A., Carboni G.: Opportunities for green energy through emerging crops: biogas valorization of *Cannabis sativa* L. residues. *Climate* 2019; 7:142 (2019)
11. Awa, S.H., Hadibarata, T.: Removal of heavy metals in contaminated soil by phytoremediation mechanism: a review. *Water Air Soil Pollut* **231**, 47 (2020)
12. Linger P, Müssig J, Fischer H, Kobert J. Industrial hemp (*Cannabis sativa* L.) growing on heavy metal contaminated soil: fibre quality and phytoremediation potential. *Ind. Crop. Prod.*, 16:33–42.(2002)
13. Chandra, R., Kumar, V., Tripathi, S., Sharma, P.: Phytoremediation of industrial pollutants and life cycle assessment. In *Phytoremediation of Environmental Pollutants*. CRC Press. 441–470 (2018)
14. Witters, N., Mendelsohn, R.O., Van Slycken, S., Weyens, N., Schreurs, E, Meers, E.: Phytoremediation, a sustainable remediation technology? Conclusions from a case study. I: Energy production and carbon dioxide abatement. *Biomass Bioenergy*, 39:454–69 (2012)
15. Vigil, M., Marey-Perez, M.F., Martinez Huerta, G., Cabal V.A.: Is phytoremediation without biomass valorization sustainable? — Comparative LCA of landfilling vs. anaerobic co-digestion. *Sci Tot Environ*, 505:844–50 (2015)
16. Voccianti, M., Caretta, A., Bua, L., Bagatin, R., Franchi, E., Petruzzelli, G., et al.: Enhancements in phytoremediation technology: Environmental assessment including different options of biomass disposal and comparison with a consolidated approach. *J Environ Manage* **237**, 560–568 (2019)
17. Espada, J.J., Rodríguez, R., Gari, V., Salcedo-Abraira, P., Bautista L.F.: Coupling phytoremediation of Pb-contaminated soil and biomass energy production: A comparative Life Cycle Assessment. *Sci Tot Environ.*, 156675–840 (2022)
18. Todde, G., Carboni, G., Marras, S., Caria, M., Sirca, C.: Industrial Hemp (*Cannabis sativa* L.) for Phytoremediation: Energy and Environmental Life Cycle Assessment of Using Contaminated Biomass as an Energy Resource. *Sustainable Energy Technol. Assess* 52 10208 (2022) <https://doi.org/10.1016/j.seta.2022.102081>
19. Marzo, D.M.: 2019, n.46.Regolamentorelativoagliinterventidi bonifica, di ripristino ambientale e di messa in sicurezza, d'emergenza, operativa e permanente, delle aree destinate alla produzione agricola e all'allevamento, ai sensi dell'articolo 241 del decreto legislativo 152. (19G00052) (GU Serie Generale n.132 del 07–06–2019) (2006)
20. Wernet, G., Bauer, C., Steubing, B., Reinhard, J., Moreno-Ruiz, E., Weidema, B.: The ecoinvent database version 3 (part I): overview and methodology. *Int. J. Life Cycle Assess.* **21**(9), 1218–1230 (2016)
21. MISE (Ministero Dello Sviluppo Economico). 2019. Direzione generale per la sicurezza dell'approvvigionamento e le infrastrutture energetiche. La situazione energetica nazionale nel 2018. Giugno (2019)
22. ISPRA, Istituto Superiore per la Protezione e Ricerca Ambientale. Fattori di Semissione per la produzione ed il consumo di energia elettrica in Italia. (2020) Link: <http://www.sinanet.isprambiente.it/it/sia-ispra/serie-storiche-emissioni/fattori-di-emissione-per-la-produzione-ed-il-consumo-di-energia-elettrica-in-italia/> view.

Smart Glove: Development and Testing of a Wearable RFID Reader Connected to Mixed Reality Smart Glasses



Giuseppe Todde, Gabriele Sara, Daniele Pinna, Valentino Artizzu, Lucio Davide Spano, and Maria Caria

Abstract The evolution of Precision livestock farming has given the possibility to the farmer to obtain a large amount of information. However, to access the database, the operator often is forced to use PC or mobile devices, losing time during on-fields activities. In this context, the use of mixed reality smart glasses (MRSG), such as HoloLens (Microsoft, USA), represents an interesting tool to consult the information in real-time leaving the operator hands-free. The aim of the study was to decrease the technological gap between the animal's electronic identification to all the information linked to a specific animal. Specifically, the research focused on developing a smart wearable system composed of a prototype, called SmartGlove (SG), capable to link the RFID tag and MRSG, via Bluetooth connection. The MRSG displays all the information related to the animal stored in an online or offline database thanks to the development of a dedicated software. The use of the SG system allows the operator to visualize, monitor, and modify the information related to the animal during on-field activities. From the preliminary experiments, the system shows promising in reducing the required workforce and improving productivity in farm management. The SmartGlove system allow farmers to activate both ear tags and rumen bolus at a distance up to 5 cm, and to visualize animal data in a variable timeframe of 4.3 s for ear tag and 3.8 s for the rumen bolus. Future works will aim to improve the reading capability of the SmartGlove, improving the antenna performances, expand the battery life, and to upgrade the MRSG software.

Keywords Augmented Reality Smart Glasses · HoloLens · RFID · Animal identification · Digital Farming

G. Todde (✉) · G. Sara · D. Pinna · M. Caria
Department of Agricultural Sciences, University of Sassari, Viale Italia 39/A, 07100 Sassari, Italy
e-mail: gtodde@uniss.it

V. Artizzu · L. D. Spano
Department of Mathematics and Computer Science, University of Cagliari, Via Ospedale 72,
09124 Cagliari, Italy

© The Author(s), under exclusive license to Springer Nature Switzerland AG 2023
V. Ferro et al. (eds.), *AIIA 2022: Biosystems Engineering Towards the Green Deal*,
Lecture Notes in Civil Engineering 337,
https://doi.org/10.1007/978-3-031-30329-6_98

949

1 Introduction

The advance in technology made possible the miniaturization of powerful computer units, and the consequent development of smartphones, tablets, and smart glasses. This device can be considered a portable computer that can be worn like a pair of glasses [1]. Smart glasses have been mainly developed to implement augmented reality (AR) technology, which allows seeing the real world supplemented with virtual information without occluding the vision of reality. The Mixed Reality (MR) technology is an extension of AR, where the virtual overlay contents are interactable by the user's hands that are recognized by the MR smart glasses (MRSg) [2]. MR devices are now considered a useful tool in a large variety of sectors such as construction, manufacturing [3, 4], automotive [5, 6], education [7, 8], and psychology [9, 10]. In the agricultural sector, the enhancement of precision livestock farming (PLF) technologies enabled the farmers to collect a large variety of data, which may help operators in the decision-making process and automatic farm management [11]. Moreover, Caria et al. [12] and Sara et al. [13] underline the capabilities of AR technologies to be integrated, with a PLF approach, into a farming environment to support operators in the field. However, consultation and rational use of these data remain a difficult and time-consuming task [14]. In addition, electronic animal identification is a technology that enables the implementation of many PLF applications in livestock farms. This is based on radio frequency identification (RFID) which is widely used for the identification of many livestock animals and is mandatory in several European countries for sheep, goats, and cattle identification. RFID consists in a transceiver (fixed or portable) that reads a transponder (ear tag, rumen bolus, subcutaneous glass tags) with the animal identification number encoded. Moreover, the RFID systems for livestock identification are regulated by ISO 11784 and ISO 11785 standards [15]. As RFID enables the implementation of many PLF technologies it could be used to connect animal information displayed in MR. Moreover, MRSg may allow operators to visualize animal data directly on-farm helping to optimize timely decisions during farm activities [16]. To bridge the gap between livestock farming identification and real-time data access, this study aimed to develop and test a wearable RFID reader capable to connect MRSg, to visualize animal data directly on the farm.

2 Materials and Methods

2.1 *The developed system framework*

The SmartGlove (SG; Fig. 1) is a prototype, currently in TRL3 (Technology Readiness Level). The hardware is composed of an Arduino Control Unit connected to a RFID reader chip and a 125 kHz copper antenna. All the components powered by a 3.7 V Lithium-Polymer battery, with a capacity of 2000 mAh, are enclosed in a 3D



Fig. 1 The SmartGlove hardware developed

printed plastic case. The device used as a glove, with the antenna extended in the back of the hand, leaving the user to continue working while wearing it.

The SG can be connected, via Bluetooth, to the MRSG (Microsoft HoloLens 2) which shows all the information related to the specific ID number of the livestock animal. For the connection between the SG and MRSG a specific application was developed in Visual Studio 2022 (Microsoft, New York). All the characteristics of HoloLens 2 were listed in Table 1.

2.2 *Software and user interface development*

In this section, we discuss the implementation of the mixed reality interface for interacting with the SG data. The solution consists of different modules: a C# application for the HoloLens 2, and MicroPython module for the running of the SG. When the MRSG interface receives a new identifier from the SG, it displays the complete information about the animal in the database. The database consists in a Google Sheets spreadsheet with a quite simple structure that can be freely modified by the farmer to adapt to their specific needs. The only assumption in the structure is having the RFID identifier as the first column in the spreadsheet, which acts as the primary

Table 1 Microsoft HoloLens 2 main features and components

Item	Features
Processor	Qualcomm Snapdragon 850
Flash memory	4 GB LPDDR4x
Operating System	Windows Holographic
Display	See-through Holographic Lenses (2 K resolution 3:2)
Field of View	52°
Sensors	4 visible light cameras, 2 IR cameras, 1MP ToF sensor, Accelerometer, gyroscope, magnetometer
Connectivity	GPS, WiFi, Bluetooth, USB-C
Camera	8MP
Battery	Lithium polymer
Battery duration	2.5 h
Controller input	Hand and Voice recognition
Weight	566 g

key. A copy of the shared spreadsheet can be uploaded in the MRSG as a Comma Separated Values (CSV) for offline working and synchronize the changes back when the network is available. At the startup, the application shows the interface (Fig. 2), giving the possibility to connect the SG to the headset with “Connect” button. At the connection the devices exchange the information required by the GATT protocol for the Bluetooth Low Energy devices. When the SG reads an RFID tag the application checks the code against all saved entries in the database and, if it finds a match displays all the related data. An error message is showed if there was any error during the scanning process or if the tag is not present in the database. By pressing the button “Parameters” the operator can choose which columns visualize or hide. If modified in offline mode, the database can be updated with the “Update Database” button.

2.3 Laboratories tests

To evaluate the operating performances of the systems, laboratory tests were carried out. First, the transponders activation distance was measured, both for the SG and for a conventional RFID reader as control. Moreover, the time needed for all the process of reading tag and data visualization in the SG were measured. In the test, two types of transponders were used i.e., FDX ear tag and FDX rumen bolus.

Concerning the activation distance, the transponder activation distance with both the SG and conventional RFID reader was measured by performing laboratory tests. The transponders were left for 3 s at determined distance (10 cm, 5 cm, 4 cm, 3 cm, 2 cm, and 1 cm). For each distance were carried out 20 reading process recording the positive or negative response of the devices. The SG positive response signal

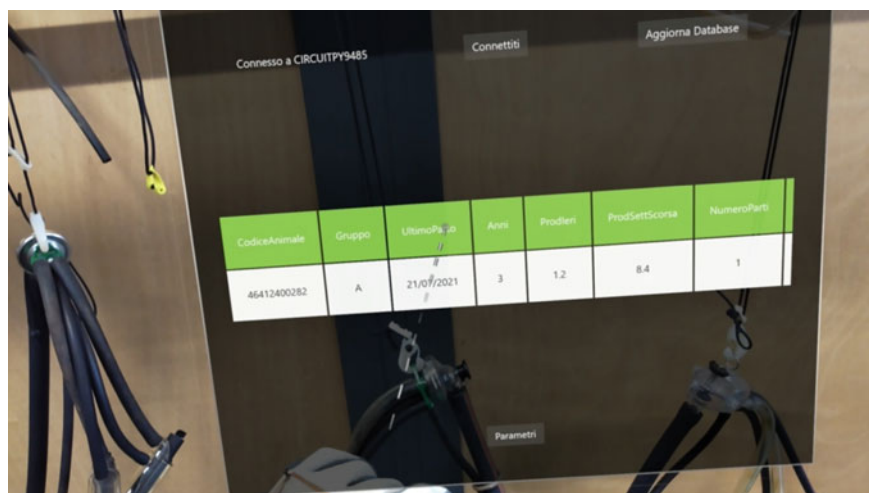


Fig. 2 User Interface of the developed application showing the animal information associated with the transponder identification number (first column)

consists in a vibration of the device, whereas an acoustic signal was emitted by the conventional reader.

Concerning the second test, the time needed for reading the tags and the visualization data in mixed reality was measured. The time frame was measured starting from the positioning of the transponder at 2 cm until the visualization of animal data in the MRSG display.

3 Results and Discussion

Table 2 reports the results of the comparison for activation distance among SG reader and conventional RFID reader. The maximum activation distance was observed for both system and both type of tags at 5 cm but with different level of success rate. An acceptable distance between antennas and tags was observed at 3 cm for the SG with ear tags and rumen bolus (70% and 60% respectively), while for the conventional reader settle at 5 cm with both types of tags (95% for ear tags and 65% for rumen bolus). This result shows no significant difference between the SG and a conventional reader, even if an improvement of the SG's antenna is desirable. However, this distance range allows a normal reading of both ear tags and rumen bolus in on-farm conditions. The difference in the success rate of reading between rumen bolus and ear tag can be due to the calibration of the RFID antenna module on the SmartGlove.

Table 3 shows the results of the reading process time evaluation. For both type of tags an average time of 4.3 s and 3.8 s were observed. For rumen bolus a higher maximum time was founded due to a worse capability of reading of the SG. Anyway,

Table 2 Comparative results of success rate of transponder activation in relation to the distance between transreceiver and transponder. N = 480

Distance (cm)	Success rate (%)			
	SmartGlove		Conventional RFID reader	
	Ear Tag	Rumen bolus	Ear Tag	Rumen bolus
10	0.0	0.0	0.0	0.0
5	5.0	25.0	95.0	65.0
4	10.0	15.0	100.0	65.0
3	70.0	60.0	100.0	65.0
2	100.0	100.0	100.0	100.0
1	100.0	100.0	100.0	100.0

Table 3 Average times of transponder reading and data visualization in mixed reality smart glasses' display. SD = standard deviation. N = 100

	Reading process time (s)	
	Ear Tag	Rumen bolus
Mean	4.3	3.8
SD	2.0	2.1
min	2.2	2.2
max	8.6	10.1

the difference in the time of reading between the two types of transponders can be considered irrelevant, as there is no statistical difference. Therefore, the responding time of the system measured in the tests is an acceptable timeframe considering normal duration of farm activities. For example, this system could be used for the instant identification of most productive subjects or to isolate animals with health problems directly in the field.

4 Conclusions

The paper describes the development of a prototype wearable RFID reader capable to bridge the technological gap between electronic identification of livestock animals and real-time access of data in Mixed reality. The devices showed promising results considering its level of readiness and would allow farmers to have an instant access to all animal data and information directly on-farm, improving time efficiency of operators work. The possibility to visualize data superimposed to the specific animal could help to minimize errors during farm operations and to improve farmer decision process. Anyway, further improvement will be focused on upgrading Smart-Glove antenna to improve the distance and time of reading, especially with rumen bolus. Future activities will be dedicated to the adoption of this technology in large-scale, optimizing hardware and software components with a miniaturization of the

SmartGlove and upgrading the user interface of SG application. Finally, this device represents a preliminary step in the development of an automated digital system to manage all animal information in livestock farms, that will help to reduce required workforce while improving farm productivity.

Acknowledgements This work was supported by:

SmartGlove Project Starting Grant finalizzati al raggiungimento del Technology Readiness Level 3. L.R. 7 Agosto 2007, N 7, Regione Sardegna;

ATLANTIDE project (Advanced Technologies for LANds management and Tools for Innovative Development of an Ecosustainable agriculture), Progetti di Ricerca e Sviluppo della Regione Autonoma della Sardegna.

References

1. Syberfeldt, A., Danielsson, O., Gustavsson, P.: Augmented reality smart glasses in the smart factory: Product evaluation guidelines and review of available products. *Ieee Access* **5**, 9118–9130 (2017)
2. Holz, T., Campbell, A. G., O’Hare, G. M., Stafford, J. W., Martin, A., Dragone, M. Mira—mixed reality agents. *Int. J. Hum. Comput. Stud.*, 69(4), 251–268. (2011).
3. Rodriguez, L., Quint, F., Gorecky, D., Romero, D., Siller, H.R.: Developing a mixed reality assistance system based on projection mapping technology for manual operations at assembly workstations. *Procedia computer science* **75**, 327–333 (2015)
4. Büttner, S., et al.: The design space of augmented and virtual reality applications for assistive environments in manufacturing: a visual approach. In: *Proceedings of the 10th International Conference on Pervasive Technologies Related to Assistive Environments*, pp. 433–440 (2017).
5. Bordegoni, M., Caruso, G.: Mixed reality distributed platform for collaborative design review of automotive interiors: This paper presents how mixed reality technologies allow a closer collaboration among designers, final users and engineers and hence reduce the time for reviewing and validating car interior designs. *Virtual and Physical Prototyping* **7**(4), 243–259 (2012)
6. Regenbrecht, H., Baratoff, G., Wilke, W.: Augmented reality projects in the automotive and aerospace industries. *IEEE Comput. Graphics Appl.* **25**(6), 48–56 (2005)
7. Pan, Z., Cheok, A.D., Yang, H., Zhu, J., Shi, J.: Virtual reality and mixed reality for virtual learning environments. *Comput. Graph.* **30**(1), 20–28 (2006)
8. Cheng, K.H., Tsai, C.C.: Affordances of augmented reality in science learning: Suggestions for future research. *J. Sci. Educ. Technol.* **22**(4), 449–462 (2013)
9. Jun, H., Bailenson, J.: Effects of behavioral and anthropomorphic realism on social influence with virtual humans in AR. In *2020 IEEE International Symposium on Mixed and Augmented Reality Adjunct (ISMAR-Adjunct)*, pp. 41–44 (2020).
10. Pellencin, E., Paladino, M.P., Herbelin, B., Serino, A.: Social perception of others shapes one’s own multisensory peripersonal space. *Cortex* **104**, 163–179 (2018)
11. Tedeschi, L.O., Greenwood, P.L., Halachmi, I.: Advancements in sensor technology and decision support intelligent tools to assist smart livestock farming. *J. Anim. Sci.* **99**(2), skab038. (2021).
12. Caria, M., Sara, G., Todde, G., Polese, M., Pazzona, A.: Exploring smart glasses for augmented reality: A valuable and integrative tool in precision livestock farming. *Anim.* **9**(11), 903 (2019)
13. Sara, G., Todde, G., Caria, M. Assessment of video see-through smart glasses for augmented reality to support technicians during milking machine maintenance. *Sci. Rep.* **12**(1), (2022).
14. Van Hertem, T., Rooijakkers, L., Berckmans, D., Fernández, A.P., Norton, T., Vranken, E.: Appropriate data visualisation is key to Precision Livestock Farming acceptance. *Comput. Electron. Agric.* **138**, 1–10 (2017)

15. Brown-Brandl, T.M., Adrion, F., Maselyne, J., Kapun, A., Hessel, E.F., Saeys, W., Gallmann, E.: A review of passive radio frequency identification systems for animal monitoring in livestock facilities. *Appl. Eng. Agric.* **35**(4), 579–591 (2019)
16. Caria, M., Todde, G., Sara, G., Piras, M., Pazzona, A.: Performance and usability of smartglasses for augmented reality in precision livestock farming operations. *Appl. Sci.* **10**(7), 2318 (2020)

Experimental Analysis of Chainsaw Emissions in Chestnut Wood Operations



Francesco Toscano , Paola D'Antonio , Carmen D'Antonio, Nicolino De Iorio, Felice Modugno, and Costanza Fiorentino 

Abstract In Italy, the orography of the territory, the medium-small size of the farms and the composition of the wooded capital (prevalence of hardwoods governed by coppice) make it easier to use chainsaws for in field operations of Felling (FE), Delimiting (DE) and Bucking (BU). With the spread of chainsaws, there is an increase in the incidence of injuries and illnesses caused by exposure to physical (noise, dust and vibrations) and chemical (volatile compounds of various kinds) agents. The legislation on occupational health and safety in Italy has followed various phases, first of all the approval of the U.T. 81/2008.

In the present work, the concentration of pollutants contained in the chainsaw exhaust gases (CO, VOC and C₆H₆) is evaluated with respect to the limits set by current legislation during interventions on a chestnut coppice. The correlation between the type of work performed (FE, DE, BU) and the ratio between the maximum and average values of CO and VOC was analysed. In particular, similar levels of maximum VOC emissions were recorded in the FE and BU phases, however in the same phases the average emission values were particularly different, suggesting a greater production of VOC in condition of the engine running but not operating at cut-off. The greatest emissions occurred in the FE phase (CO = 135 ppm, VOC = 17.28 ppm and C₆H₆ = 2.13 ppm).

Secondly, the noise emitted by the chainsaw during the exploitation of the chestnut coppice was analysed. It was found that the legal limits were exceeded during all chainsaw operations, with peaks of over 110 dB. The analysis revealed that the legal limits were respected only during the delimiting operation.

Keywords Injuries · Chainsaw · Forest utilizations · Occupational health · Noise

F. Toscano · P. D'Antonio (✉) · C. D'Antonio · N. De Iorio · F. Modugno · C. Fiorentino
University of Basilicata, Potenza, Italy
e-mail: paola.dantonio@unibas.it

© The Author(s), under exclusive license to Springer Nature Switzerland AG 2023
V. Ferro et al. (eds.), *AIIA 2022: Biosystems Engineering Towards the Green Deal*,
Lecture Notes in Civil Engineering 337,
https://doi.org/10.1007/978-3-031-30329-6_99

957

1 Introduction

The increase in portable equipment for urban green care and maintenance and for hobbies has generated serious problems in terms of operator safety and ergonomics [3, 4, 6]. Often these are tools purchased online and without any training before use. Moreover, in the forestry sector, even after the advent of state-of-the-art machines and systems, the chainsaw is still undoubtedly the main machine with which to carry out felling operations, delimiting logs, and bucking timber into various assortments. The reason for this is the complex orography of the Italian territory. In fact, this is characterised by a significant steepness, which is even more accentuated in wooded areas, since lowland and hillside forests have long since given way to agricultural land. Secondly, Italian forestry companies are mostly medium or small, and therefore very often unable to bear the costs of purchasing, depreciating and managing state-of-the-art machinery. Another determining factor in determining inadequate machinery [10] fleets is the nature of the organisational structure and the composition of the wood capital of forestry companies. According to data from the RAF Italy 2017–2018, at the national level about 66% of forests are privately owned, while the remaining 34% are publicly owned. As far as private enterprises are concerned, there is also an extreme fragmentation of extensions, which, together with the prevalence of broadleaf forests, often coppice-governed, makes the application of Harvester and similar methods rather difficult. Moreover, Italian silviculture is mainly focused on the production of low-value timber or, even worse, as biomass for energy purposes [3, 4, 6]. Therefore, the material that can be harvested from most Italian forests is not very profitable and far from the application of management models based on advanced mechanisation. The chainsaw, actually, is still the most widely used machine in the sector. Investigations conducted systematically since the 1960s have revealed several critical issues related to the constant and perpetual use of such portable equipment. In particular, continuous and repeated exposure to physical agents such as noise and vibration [20] are at the root of the aetiology of many occupational diseases. In fact, several studies have shown that the amount of noise emitted by chainsaws can exceed 90 dB (A) [2], putting the operator at serious risk of hearing loss [13]. The vibrations that are discharged onto the hand-arm system, in turn, cause irreversible damage to the peripheral circulatory system of the hands (rupture of capillaries), with the onset of Raynaud's syndrome or 'white fingers' disease [14]. There are few works in the literature referring the critical issues related to the emissions of airborne pollutants [19] associated with continuous long-term exposure to machines such as chainsaws. Both temporary and chronic damage resulting from the inhalation of exhaust gases from chainsaws and brush-cutters has so far only been considered in very general terms, or worse, compared to that found in other contests involving the use of hand-guided power tools (lawn mowers, motor-hoes, etc.). The peculiar characteristics of the work carried out with such equipment have not been taken into account, which, for example, favouring considerable operator fatigue [12], increasing the heartbeat and, consequently, accelerating breathing, which can lead to a respiratory rate greater than 60 L per minute. This further aggravates the operator's exposition to airborne

pollutants, which composition is characterised both by the gases produced during combustion, and by the fraction of non-combusted mixture expelled with the latter's residues (approximately 30% of the mixture initially used in two-stroke engines). To address these critical issues, in recent decades, a series of national and EU laws have been enacted to regulate tolerable exposure levels and the prevention tools to be used according to them. Among the most important and up-to-date laws in the sector in Italy is Legislative Decree No. 81 of 9 April 2008 on the 'Consolidation Act on health and safety in the workplace', an extremely innovative and constantly updated provision aimed at reorganising and integrating all the relevant regulations.

The objectives of the present work are:

1. To assess whether the concentration of pollutants contained in chainsaw exhaust gases complies with the limits set by current legislation during operations in a chestnut coppice;
2. To assess the noise emitted by the chainsaw during the utilisation activities of a chestnut coppice.

2 Material and Methods

2.1 Study Site

The experimental trials were carried out between 13 and 20 December 2013 in a chestnut coppice managed with clear-cuts. The experimental area is located in the municipality of Sassano (SA), precisely in the locality of "Gravola", at an altitude of approximately 900–1000 m above sea level. The silvicultural operations surveyed were as follows: Felling (FE), Delimiting (DE) and Bucking (BU).

All tests were carried out under clear sky, weak wind conditions and a temperature of 9 ± 3 °C.

2.2 Chainsaw

Today, the market offers a wide range of chainsaw solutions and models with different power ratings and features. For the experimental tests, a Husqvarna 357xp chainsaw was used, the main technical data of which are shown in the table (Table 1).

A 5% mixture of petrol and synthetic oil was prepared for the experimental tests.

Table 1 Technical data
Husqvarna 357 XP chainsaw

Technical data: Husqvarna 357 XP chainsaw	
Sound power level dB (A)	100 dB (A)
Sound pressure level dB (A)	112 dB (A)
Vibration values (handle ant/post m/s ²)	3.9/4.2 m/s ²
Engine displacement (cm ³)	56.5 cm ³
Power (KW/HP)	3.2 kW
Weight (Kg)	5.5 kg
Maximum rotation speed	9600 rpm
Recommended bar length (min–max)	40 cm

2.3 Dosimeter

For the evaluation of the overall sensation resulting from the perception of a complex sound or noise, a Noise sensor TES 1355 dosimeter is used to simulate the response of the human ear. This instrument, which goes by the name of sound pressure level meter (dosimeter), is capable of transforming sound pressure into decibels. A TES 1355 dosimeter consisting of a microphone, preamplifier, frequency-weighting circuit, third octave, RMS circuit, analogue output, integrator circuit and a display system was used for the experimental tests.

2.4 Gas sensor

A MultiRAE PGM-50 plus professional gas detector was used to assess personnel exposure to airborne pollutants in the exhaust gases emitted by the chainsaw. It is a programmable multi-gas monitor that allows continuous real-time monitoring of toxic, oxygen and combustible gases. The instrument detects and records in the data logger the instantaneous concentration of gases in real time in parts per million (ppm) for toxic gases, in volume percentage (%vol) for oxygen and in volume percentage referred to the lower explosive limit (%vol of LEL) for combustible gases.

2.5 Experimental Design and Data Analysis

Noise measurements were carried out during FE, DE, BU operations on a sample of 30 trees. 140 observations were made for each silvicultural operation, making a total of 420 observations. Each silvicultural operation also involved individuals with different diametrical classes, in order to have data relating to the different situations to which the operator is subjected. The dosimeter was mounted directly on the operator during chainsaw cutting operations in order to obtain a good simulation of the stresses

to which the hearing apparatus is subjected. Exhaust gas, i.e. CO, VOC and C₆H₆, sampling was carried out by applying the instrumentation on the operator's belt, using special clips. This method gives acceptable results, since during the movements of the operator, the basic condition required by the standards, i.e. the proximity of the analyser to the worker's mouth, is constant. The instantaneous measurements of the three variables relating to the gas emission were acquired at sampling time of 15-min intervals during each processing phase (FE, DE, BU). Therefore, 8 sets of measurements were carried out for each type of operation. The descriptive statistics for each data set were calculated: maximum values (V_{max}), minimum (V_{min}), average (μ) and standard deviations (σ) relating to each time interval and each work process. In particular, to estimate the variability of the parameters acquired, the coefficient of variation was:

$$CV (\%) = \frac{\sigma}{|\mu|} \times 100 \quad (1)$$

3 Result and Discussion

The 420 observations made using the TES 1355 sound level meter showed that the limit established by current Italian legislation, set at 85 dB (A), is far exceeded in every silvicultural operation carried out with a chainsaw. The situation becomes particularly critical in the case of large diameters, especially during felling operations, where the highest average values and peaks are recorded. The table below shows the comparison between the data obtained from the analysis of variance for each operation (Table 2).

Figures 1 a, b and c, graphically show the respective average values of CO, VOC and C₆H₆ detected in each of the 8 times intervals and for each process, using the MultiRAE PGM-50 plus professional gas detector. Each figure also shows the emission limits established by law. The graphs show considerable asymmetries especially

Table 2 Average noise for different operations

		Mean	Variance
Felling	Diameter 5 cm	86,393	159,118
	Diameter 7 cm	88,379	162,097
	Diameter 9 cm	90,576	169,589
Delimiting	Diameter 12 cm	90,796	187,655
	Diameter 16 cm	92,256	190,733
	Diameter 18 cm	94,932	196,136
Bucking	Diameter 10 cm	90,735	154,147
	Diameter 15 cm	94,344	177,325
	Diameter 20 cm	101,541	204,845

for the emissions in the FE phase. Table 3 shows the mean values of the maxima detected in each of the 8 repeated measurements and the mean values of the same measurements, with the relative standard deviations and relative CVs. To evaluate the data variability, the average of the maximum values, although more subject to the presence of momentary peaks, is more reliable, since during the 15 min of constant detection by the instrumentation the chainsaw condition often occurs with engine running but not working. In accordance with what has just been highlighted, the comparison between the coefficients of variation revealed relatively low values for the coefficients of variation calculated on the maximum values and high values for those calculated on average values, as shown in the table below. However, the table shows a greater variability of the coefficient of variation for delimiting operations compared to the other two cases. This can be correlated to the great diameter variability that can be found between the branches of the same tree. Analyzing the coefficients of variation calculated on the average values, they are generally higher, with the particular exception of CO emissions during BU operations (CV = 7%).

Subsequently, a comparison was made between the average values recorded and the limits established by international legislation (Table 4). From the investigation it is possible to state that these limits are always disregarded in relation to the maximum

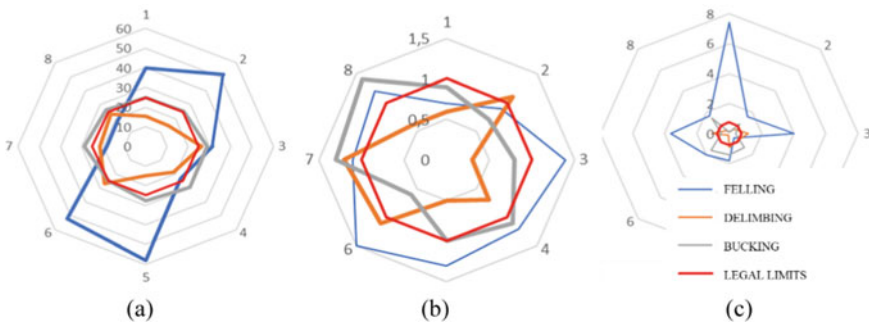


Fig. 1 Average CO (a), VOC (b) and C₆H₆ (c) emission in each reference interval and for each machining operation

Table 3 Data on gaseous emissions during wood processing

	Felling – FE (ppm)			Delimiting – DE (ppm)			Bucking – BU (ppm)		
	CO	VOC	C6 H6	CO	VOC	C6 H6	CO	VOC	C6 H6
MED (Max)	135.96	17.28	2.51	33.09	2.65	1.13	76.26	15.24	1.73
SD (Max)	25.75	4.63	0.48	11.15	1.07	0.21	11.31	4.12	0.55
CV (Max)	0.19	0.27	0.19	0.34	0.40	0.18	0.15	0.27	0.32
MED(Vm)	36.66	2.81	1.16	20.21	0.60	0.76	27.08	0.96	0.98
SD (Vm)	16.09	2.18	0.26	5.02	0.44	0.33	1.92	0.57	0.28
CV (Vm)	0.44	0.78	0.22	0.25	0.73	0.43	0.07	0.59	0.29

Table 4 Comparison between gaseous emissions measured in the field during wood processing and the limits permitted by law

	Felling – FE (ppm)			Delimiting – DE (ppm)			Bucking – BU (ppm)		
	CO	VOC	C6 H6	CO	VOC	C6 H6	CO	VOC	C6 H6
Leg_Lim	25	0.75	1	25	0.75	1	25	0.75	1
$\frac{MED(Max)}{Leg_Lim}$	5.44	23.03	2.51	1.32	3.53	1.13	3.05	20.3	1.73
$\frac{MED(Vm)}{Leg_Lim}$	1.47	3.75	1.16	0.81	0.8	0.76	1.08	1.28	0.98

values recorded during the three different operations. However, based on the average values recorded, the situation appears less critical. This data is particularly encouraging, considering that during the various operations the maximum values are reached infrequently. In particular, the BU operations emit below-threshold values on average, the BU operations settle in values slightly higher than the threshold while the FE operations are the most critical, determining values well beyond the threshold, above all with reference to the VOC. What has been stated suggests the use of PPE for the protection of the respiratory system especially in this phase, which can be considered particularly risky for the health and safety of the operators. In Table 4, from the comparison between the average of the maximum values and the average values acquired during the operations in the field, it is notable the presence of high peaks of VOC emissions during the three operations. The data becomes even more alarming for the FE operations, where the maximum values recorded are almost 16 times higher than the average values. From the analysis of the graphs in Fig. 1 and the comparison between the averages of the measured values and the maximum values, it follows that:

1. The three operations, in accordance with what was found by Neri et al. [19] and Bernini [1], from the point of view of the effort required of the gear, can be characterized differently according to the CO and C₆H₆ emissions:
 - a. **Felling:** during this operation the chainsaw is called upon to make great efforts, this can be correlated with the high emissions of CO and C₆H₆, however important time intervals are recorded within the same operation, also to make the operator catch his breath more susceptible to fatigue;
 - b. **Cutting:** during this operation the chainsaw is called to express medium efforts, this can be correlated with sufficiently high emissions of CO and C₆H₆, however the time intervals in which the tool is on but not operating at cutting in the measurement range of 15 min are less than what happens in the blast chilling phase.
 - c. **Delimiting:** during this operation the tool is called upon to exert small efforts, releasing moderate doses of CO and C₆H₆ into the environment, moreover the intervals in which the engine is running but not operating in the 15 min of detection are extremely reduced if compared to the operations pre-teeth.

2. The chainsaw, in accordance with Gallo [11] and Kovac [15] produces high VOC emissions when it is switched on but not operating at the cut. By examining what happens during logging operations, it can be stated that:
 - a. The maximum emissions recorded during the two operations are similar (17.28 ppm for abatement and 15.24 ppm for bucking), being 1.3 times higher in the abatement phase;
 - b. The average emissions recorded during the two operations are particularly different (2.81 ppm for abatement and 0.96 ppm for bucking), being 2.9 times higher in the abatement phase;
 - c. The high risk of exposure occurs in the abatement phase, when VOC emissions are particularly higher than the legal limits;
 - d. The least risk situation, on the other hand, occurs during demilling operations when, as the chainsaw's non-working intervals are minimal, low VOC emissions are recorded, both considering the maximum (2.65 ppm) and average (0.60 ppm) values.

4 Conclusions

The analysis of the noise level of silvicultural operations highlights a high risk for operators in the sector and the constant exceeding of the limits envisaged by the regulations in force. However, the risk factors can be easily controlled through the use of PPE. The risk assessment of worker exposure to airborne pollutants is alarming. After calculating personal exposure on the basis of the measurements taken during the samplings, it appears that, according to current regulations, only 7 out of 25 construction sites present a risk that can be described as moderate for CO emissions. In all other samplings, the chemical risk from inhaling CO, VOCs and benzene was found to be non-moderate. As far as carbon monoxide emissions are concerned, the activity that presents the greatest problems is FE. Statistical analysis of VOC and C₆H₆ highlighted more critical issues, in fact high VOC emissions were detected in the case of chainsaws not in operation and high C₆H₆ when the machinery is working intensely. This criticality is being investigated through further measurements in different contexts. Finally, the introduction also at professional level of electric battery power chainsaw will reduce and probably solve in few years most of the problems which have been highlighted by the study.

References

1. Bernini, M.: Valutazione dell'esposizione agli inquinanti aerodispersi, durante l'uso delle attrezzature portatili. Tesi di dottorato di ricerca. 19. Ciclo. Università degli studi della Tuscia – Viterbo (2008)

2. Cavalli, R., Miola, P., Sartori, L.: Diffusione del rumore prodotto dalla motosega in boschi con differenti forme di governo. *L'Italia Forestale e Montana* **59**(5), 375–390 (2004)
3. D'Antonio, P., Scalcione, V.N., D'Antonio, C.: Experimental tests of ventilation on biomasses to be used for energy purpose. *Sch. J. Agric. Vet. Sci.* (2020). ISSN 2348-1854. <https://doi.org/10.36347/sjavs.2020.v07i06.001>
4. D'Antonio, P., Scalcione, V.N., D'Antonio, C.: Innovative systems in the production and organization of forest biomass and urban green areas. *J. Adv. Res. Food Agric. Environ. Sci.* (2020). ISSN: 2208-2417. <https://doi.org/10.53555/ar.v6i5.3621>
5. D'Antonio, P., Scalcione, V.N., Evangelista, C., Daddato, V.: The assessment of the sawmill noise. *J. Agric. Eng.* **44**(s2) (2013)
6. D'Antonio, P., Scalcione, V.N., D'Antonio, C.: Sustainable urban green management systems: battery powered machines and equipment. *IJA Food Sci.* (2020). ISSN: 2208-2719. <https://doi.org/10.53555/gafs.v6i3.1242>
7. Davis, G.: Noise and vibration hazards in chainsaw operations: a review. *Aust. For.* **41**(3), 153–159 (1978)
8. Vasiliki, D.: Apostolos Kantartzis Chrisovalantis Malesios mmanouil Kasampalis “Research of exhaust emissions by chainsaws with the use of a portable emission measurement system.” *Int. J. For. Eng.* **30**(3), 228–239 (2019)
9. Falcone, P.M., Sica, F.: Assessing the opportunities and challenges of green finance in Italy: an analysis of the biomass production sector. *Sustainability* **11**(2), 517 (2019)
10. Fiorentino, C., Crimaldi, M., Libergolo, P., D'Antonio, P., Scalcione, V.: Farm management information systems: digital register of farm management in Southern Italy. In: *International Conference on Safety, Health and Welfare in Agriculture and Agro-food Systems*. Springer, Cham (2020)
11. Gallo, P.: Particolato aerodisperso da attività agroforestali e sistemi di contenimento (2014). Tesi di dottorato di ricerca. 19. Ciclo. Università degli studi della Tuscia - Viterbo
12. Hinze, A., König, J.L., Bowen, J.: Worker-fatigue contributing to workplace incidents in New Zealand Forestry. *J. Saf. Res.* **79** (2021)
13. Iftime, M.D., Dumitrascu, A.-E.: Chainsaw operators' exposure to occupational risk factors and incidence of professional diseases specific to the forestry field. *Int. J. Occup. Saf. Ergon.* **28**(1), 8–19 (2022)
14. Jesus, A.T., Fiedler, N.C., de Assis do Carmo, F.C., Juvanhol, R.S.: Exposure of operators to chainsaw vibration in forest harvesting. *Floresta* **50**(3), 1653–1659 (2020)
15. Kováč, J., Krilek, J., Dado, M., Beno, P., Beno, P.: Investigating the influence of design factors on noise and vibrations in the case of chainsaws for forestry work. *FME Trans.* **46**(4), 513–519 (2018)
16. Häggström, C., Öhman, M., Burström, L., Nordfjell, T.: Vibration exposure in forwarder work: effects of work element and grapple type. *Croat. J. For. Eng.* (2016)
17. Muhdi, M., et al.: Intensità del rumore e suo impatto sulla percezione e sul livello di concentrazione tra i lavoratori della raccolta forestale nelle piantagioni forestali industriali, Sumatra settentrionale, Indonesia. *F1000Ricerca* **11**(627), 627 (2022)
18. Neri, F., Piegai, F.: Uso di motoseghe a batteria rispetto a quelle a benzina nella silvicoltura: confronto delle prestazioni sui tempi di taglio. *Foreste* **13**(5), 683 (2022)
19. Neri, F., et al.: Determining exhaust fumes exposure in chainsaw operations. *Environ. Pollut.* **218**, 1162–1169 (2016)
20. Rukat, W., Barczewski, R., Jakubek, B., Wróbel, M.: The comparison of vibro-acoustic impact of chainsaws with electric and combustion drives. In: *Proceedings of the 17th International Conference Diagnostics of Machines and Vehicles, MATEC Web of Conferences*, Bydgoszcz, Poland, 30 July 2018, p. 02020 (2018). <https://doi.org/10.1051/mateconf/201818202020>

Quantity and Type of Logging Residues Following Cut-to-Length and Full-Tree Salvage Logging Systems in Damaged Mountain Forests



Alberto Udali, Lorenzo Garollo, Raffaele Cavalli, and Stefano Grigolato

Abstract Salvage logging operations usually leave behind a considerable mass of residues or deadwood, fundamental for the ecosystem to maintain soil fertility and facilitate the establishment of regeneration and the reconstitution of new forest. This study aims to estimate the amount of deadwood released after the operations characterized by two different logging systems: Cut-to-length (CTL) and Full-Tree system (FT). Moreover, also the carbon and nutrient content of the deadwood was investigated and their interaction with the soil organic layer.

Deadwood in the areas logged was sampled using linear transects. The collected data were divided into diameter class and the quantity of residues was estimated using the Brown method for fine wood debris (FWD) and the Van Wagner method for coarse wood debris (CWD). A higher amount of FWD was observed in the yards cleared with the FT system and a higher quantity of CWD in the yards logged with the CTL system. The chemical analysis of the carbon and nutrient components of the soil and deadwood samples revealed a higher amount of carbon stored in 10 cm of soil (up to 85 Mg C/ha), compared to deadwood (up to 29 Mg C/ha).

Keywords Forest mechanization · Carbon cycle · Impact · Management

1 Introduction

In last decades, European forests have become increasingly more vulnerable to extreme events, in particular to wildfires and windstorms [1], occurring mainly in the Mediterranean region [2] and in Northern and Central-Eastern Europe with increasing incidence [3], respectively. In recent years, however, storms are becoming a relevant problem even in Southern Europe like the Vaia storm in 2018 [4, 5].

A. Udali (✉) · L. Garollo · R. Cavalli · S. Grigolato
Department of Land, Environment, Agriculture and Forestry, University of Padova, Viale dell'Università 16, 35020 Padua, Legnaro, Italy
e-mail: alberto.udali@phd.unipd.it

© The Author(s), under exclusive license to Springer Nature Switzerland AG 2023
V. Ferro et al. (eds.), *AIIA 2022: Biosystems Engineering Towards the Green Deal*,
Lecture Notes in Civil Engineering 337,
https://doi.org/10.1007/978-3-031-30329-6_100

967

Forests are characterized by multifunctionality, especially in the alpine environment where they serve not only as production but also for protection and recreation functions. One of the most valuable functions of forests is the ability to capture and store carbon: almost half of the total organic carbon in terrestrial ecosystems in the world is stored in forest soils [6]. Nowadays, the living biomass in the European forests represents around 36% of the total carbon stock in the world and have sequestered one tenth of carbon dioxide emission for each year since 1990. Moreover, between 2010 and 2020 the average annual sequestration of carbon in forest biomass reached above 155 Mt [7]. The carbon stored in this way gets stocked in the trees and in the surrounding soil, where it helps to build up nutrients for the trees to grow [8]. However this important function is jeopardized due to climate change and the increasing incidence of extreme events [9]. New alternative strategies are proposed to allow forests to preserve this function and to also fight climate change induced events, according to different locations and needs [10–15].

Consequently to the increased incidence and magnitude of extreme events, the increment of forest damaged areas is leading to an increment of salvage logging operations which generally are fully or highly mechanized. Salvage logging is the practice of extracting timber from disturbed forest areas in order to minimize the loss of commercial timber [1]. This level of mechanization is highly recommended to reduce the risk of accidents to the operators and to maintain a high efficiency in terms of productivity and reduction of logging cost [16, 17]. The salvage logging operations usually have high environmental impacts in comparison to ordinary operations, amplifying the risks of impact on damaged forest areas in terms of soil exposure and risk of erosion [18, 19], as well as the risk of soil degradation, due to loss of nutrients and carbon and therefore loss of fertility [20]. Salvage logging is also affecting the residues left after the operations, such as branches, tops and stumps, causing variation in the residues' regime. The quantity and quality of residues left (fine or coarse woody debris) depend on the harvesting methods adopted (Fig. 1a and Fig. 1b) [21, 22]: in salvage logging operations the two most common harvesting systems adopted are: i) Cut-to-Length (CTL) and ii) Full-Tree (FT) extraction systems.

CTL is often associated, when terrain is gentle, to fully mechanized systems with the combined use of a harvester and a forwarder. In the case of full-mechanized CTL, the tree is processed at stump site by the harvester machine and consequently most of the logging residues are left on the ground homogeneously distributed or piled in heaps. When terrain gets steeper, FT is the preferred system favoring the higher mechanization level of cable yarder system [23]. In the case of FT, the tree is extracted with branches and top and thus most of the logging residues are accumulated at roadside in the same area in which the trees are processed by the processor head. Therefore, these systems represent two opposite ways of logging in terms of residues generation and removal from the forest [21, 22].

Forest residues, along with deadwood, are major sources of nutrients and carbon [24, 25]. Variations in quantity and quality of residues are impacting the soil fertility [6], and therefore jeopardizing the establishment and correct growth of future forests [8, 26–28]. These variations can also impact forest biodiversity and alter disturbances regime such forest fire and bark beetle outbreaks [29–31]. Moreover they create

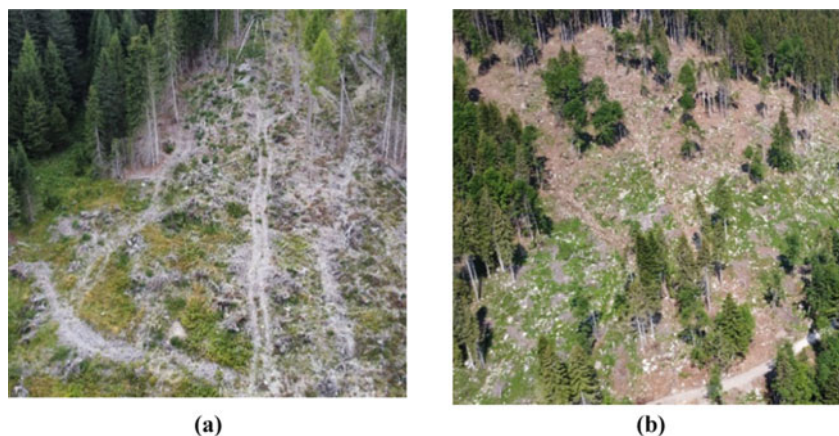


Fig. 1 Effect of a salvage logging operation based on **a** CTL system with full mechanized harvesting system with the integration of harvester and forwarder machines, and **b** based on FT system with semi-mechanized felling, cable yarder extraction and tree processing at roadside

uncertainty in the quantification of carbon stock since fine residues stand ignored in the estimations [32].

Specifically for the two systems, cable yarding is considered a more environmentally friendly compared to ground-based mechanized system [33]. In fact, cable-yarding extraction has a lower impact on soil, if compared to ground-based system (e.g. harvest-forwarder or tractor and winch system) and, at the same time, in terms of costs [17]. However, in terms of residues left in the forest (e.g. branches, top and stump), conventional FT harvesting has a substantially higher amount of nutrients removed from harvest sites than in CTL harvesting due to the extraction of nutrient-rich branches and foliage [21].

The aim of this study is thus verify if there is a difference in terms of logging residue type and quantity according to the harvesting system adopted.

2 Materials and Methods

2.1 Study Area

The mountain forests considered are located in the Province of Trento, Northeastern Italy, and belong to the Autonomous Province of Trento: these are the forests of Cadino, Paneveggio and S. Martino di C. (Fig. 2). The forests here consist into a typical Spruce mountain forest, composed mainly by Norway spruce (*Picea abies* (L.) H. Karst) and Larch (*Larix decidua* Mill.), with an average altitude above sea level between 1550–1670 m, and average growing stock of 425 m³/ha. Two sites from each forest were selected with similar characteristics: large and cleared surfaces, with

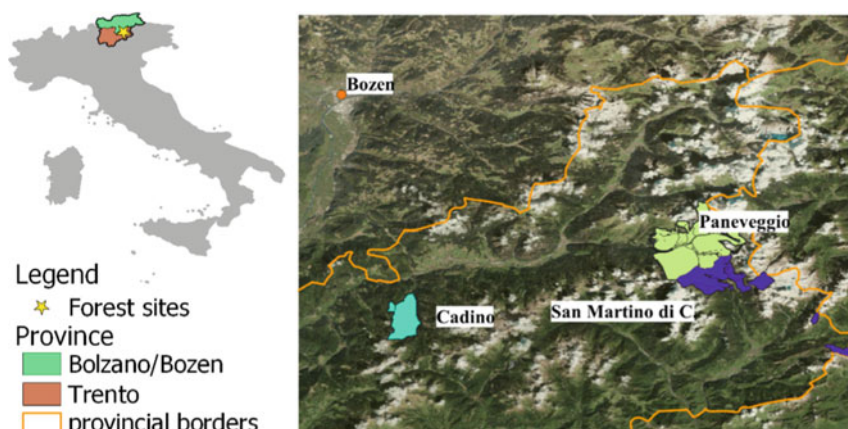


Fig. 2 Study areas locations

Table 1 Summary of data related to the study sites selected

Site	Paneveggio		S. Martino di C		Cadino	
	PAN1	PAN2	SMC1	SMC2	CAD1	CAD2
Average altitude	1650	1550	1570	1670	1660	1640
Aspect	S	SE	SE	S	E	NW
Surface (ha)	24.28	18.38	14.48	19.92	16.88	20.12
Damaged surface (%)	69.7	63.5	92.5	27.5	96.3	19.1
Salvage logging	HF 2019	CC 2020	CC 2019	CC 2021	HF 2020	HF 2021

the possibility to find machine tracks and with comparable forest types. The two sites from Cadino have slopes facing east and north-west, but all the other four sites are facing south. The sites have been all subjected to salvage logging operations in the years following the Vaia storm, with the use of both CTL systems, with harvester and forwarder (HF), and FT systems, using cable crane (CC). The field sampling over the area was performed in the summer of 2021. Table 1 summarize the main data related to the study sites selected.

2.2 Field Sampling and Residue Quantity Estimation

Field sampling of residues was performed by adopting a line intercept sampling (LIS) method, which indirectly measures fuel quantities [34, 35]. The LIS technique assumes that the pieces of residues to be sampled are oriented at random, horizontal, circular in shape, and that there is a normal distribution within diameter classes. For this study, the sampling method was adapted from Rizzolo [36], registering the

Table 2 Diameter classes distribution and criteria for forest residues

Class	D min	D max	Category
A	0	6 mm	FWD
B	6 mm	25 mm	
C	25 mm	76 mm	
D	76 mm	203 mm	CWD
E	>203 mm		

diameter of each woody debris under a 20 m line and dividing them in classes as shown in Table 2: material finer than 76 mm in diameter belongs to fine woody debris (FWD) and larger material to coarse woody debris (CWD). For CWD larger than 203 mm both the diameters have been recorded as well as the length of the debris. Each transect is composed of three blocks, one central where the machine or the carriage was passing and two on the side. The central one has been modified into a series of four sub transects orthogonal to the extraction line to better account for the variability of residues and the machine effect. The distance between the central block and the lateral ones is 10 m for HF and 15 m for CC. Moreover, in order to minimize the road influence, the starting points had to be at least 20–25 m for both HF and CC blocks.

Residues quantity estimation (Mg/ha) was performed for both categories of residues: Brown's formulas [34] are applied for elements smaller than 203 mm, so Eq. (1) describes the estimation for FWD and Eq. (2) for CWD. For bigger elements, instead, the estimator is described by Eq. (3) using the Van Wagner formula [37].

$$\hat{Y}_{FWD} = \left(\frac{1.234 \cdot n \cdot \bar{d}^2 \cdot SG \cdot c \cdot a}{\sum L} \right) \cdot k_{decay} \cdot 10.000 \quad (1)$$

$$\hat{Y}_{CWD} = \left(\frac{1.234 \cdot n \cdot \bar{d}^2 \cdot c}{\sum L} \right) \cdot k_{decay} \cdot 10.000 \quad (2)$$

$$\hat{Y}_{CWD(E)} = \frac{\pi^2 \sum d^2}{8L} \quad (3)$$

where: 1.234 is a conversion constant derived from the literature; n is the number of elements for each class; \bar{d}^2 is the average squared diameter for the class; SG is the specific gravity for the wood species considered; c is the corrected slope; a is the correction coefficient for the position of the elements and equal to 1,13 for FWD and equal to 1 for CWD; L is the length of the sampling line(s); k_{decay} is the decay coefficient as described by Woodall et al. [35]; 10,000 are the square meters in 1 ha. The corrected slope is calculated as described in Eq. (4).

$$c = \sqrt{1 + \left(\frac{Slope_{\%}}{100} \right)^2} \quad (4)$$

The residues estimations of the same year, but performed with different harvesting system, were also statistically compared looking for any significant differences using the Mann–Whitney U-test. The confidence level was established at $\alpha = 0.05$ with H_0 as “there is no significant difference due to the extraction system” and H_a as “there is a significant difference due to the extraction system”.

2.3 Soil and Residues Chemical Analysis

For each forest, soil and residues, sites have also been sampled for chemical analysis. Soil samples have been taken randomly over the sites for a total of 800 g on 8 different locations and mixed together before the analysis. For the residue analysis, a sample for each diameter class was collected randomly on each site and then mixed together obtaining four samples for the three forests combined. For every forest, then, the carbon stock was computed [38] as well as the soil density derived from the total organic carbon available, as showed in Eq. (5) where ρ is the soil density (g/m^3) and $TOC\%$ is the concentration in percentage of organic C [39].

$$\rho = -0.00745 \cdot TOC\% + 0.593 \quad (5)$$

3 Results and discussion

3.1 Residues Estimators and Statistical Analysis

Table 3 reports the results for the residues estimations. To get the result, an average specific gravity of spruce equal to 0.44 was used to calculate the content (Mg/ha), due to the characteristics of the material.

Table 3 Forest residues content estimations for each diameter class (Mg/ha)

	FWD			CWD	
	A	B	C	D	E
HF 2019	1.79	9.77	19.33	13.01	10.79
HF 2020	2.49	10.04	14.74	8.61	14.24
HF 2021	1.93	7.68	10.64	9.66	22.43
CC 2019	2.74	7.19	13.45	15.16	5.92
CC 2020	2.97	10.72	14.01	11.72	12.51
CC 2021	6.69	15.73	16.37	21.68	9.61

In the sites cleaned with harvester and forwarder, it emerges that, despite the A class with fairly similar values, there is a tendency for the contents in the other classes to generally decrease with the years. Still the higher estimation remains for the material of the third class (C). This could be a random effect or due to the characteristics of the species in the area. For the crane sites, the emerging trend is different: for each year, the highest estimators belong to the D class, except for 2020 that is the C. Moreover, compared to HF areas, CWD values for CC are higher for all the years considered. For the coarser material (E), HF areas deliver higher estimators for all the years considered compared to CC areas.

The amount of material present following salvage logging operations in 2019, when there was almost no degradation in the plant materials, is less and therefore comparable to ordinary operations conducted with the FT method. This technique involves the almost total removal of the residues from the forest. In the following years, with the drying up of the trees and their degradation, it is possible to observe an increase in biomass in the forest, and that can be perceived to some extent for both HF and CC. The increase in the amount of material is due to the greater susceptibility to breakage of dry branches compared to green ones due to the loss of elasticity due to desiccation. Therefore, the collisions due to dragging in the phases of concentration and removal of the material cause the loss of branches and twigs. For the coarser material (E) the reasons for higher values are slightly different but are still due to the machine behavior: during the preparation phase with the harvester, the operator cuts the logs in order to retrieve only the quality timber. On the contrary, with cable logging, the operator hooks the whole plant, therefore even the parts with defects or low value. This difference can therefore be variable depending on the quantity of trees cut down rather than with the stumps uprooted.

For each year, the estimators for each class were then statistically compared using the Mann–Whitney U-test. Table 4 shows a summary of the p-value computed with the test divided by year and classes. For the years 2019 and 2020, all the values derived from the test are greater than the threshold of 0.05, therefore there is no significant difference between the two harvesting systems. The values for year 2021, on the other hand, show a different result: the p-value calculated for 3 out of 5 estimators are lower than alpha, pointing out that there are significant differences and those are related to the harvesting system.

Table 4 P-values calculated with the Mann–Whitney U-test between CC and HF for each year

	FWD			CWD	
	A	B	C	D	E
2019	0.0503	0.1903	0.1135	0.4236	0.8100
2020	0.6048	0.9314	0.3401	0.2805	0.7967
2021	0.0012	0.0056	0.1135	0.0106	0.1455

3.2 Soil and Residues Chemical Analysis

The soil analysis, as presented in Table 5, shows several differences between the forests, in particular between the Cadino forest and the other two: all elements, with the exception of P are lower in Cadino. Same goes for the carbon stock. Whereas the differences between Paneveggio and San Martino are not large, but despite the closer geographic location, there is a higher concentration of Ca, Mg and Mn in the first one, and higher concentration of N, C, Fe, K and P in the second one.

The same analysis was repeated on the residues samples (Table 6). The general tendency for all the elements is to maintain a higher concentration on the finer residues and decreasing as the size of material increases.

Table 5 Soil analysis for the three forests

Element	Unit	Paneveggio	San Martino di C	Cadino
N	g/kg d.m	7,35	9,41	5,20
C organic	g/kg d.m	127,47	186,99	86,51
Ca	mg/kg d.m	3577,62	2054,58	1299,39
Fe	mg/kg d.m	20,637,05	22,152,22	15,272,03
K	mg/kg d.m	4677,20	4794,01	3349,72
Mg	mg/kg d.m	4294,74	3821,68	1991,27
Mn	mg/kg d.m	455,77	267,18	201,66
P	mg/kg d.m	395,21	576,63	384,75
Carbon stock	Mg/ha	63	85	45

Table 6 Average nutrients values for each residue diameter class across the three forests

Element	Unit	A	B	C	D/E
N	g/kg d.m	10,86	4,05	3,92	4,30
C organic	g/kg d.m	559,76	533,15	530,75	518,51
Ca	mg/kg d.m	6566,98	3197,47	3525,09	1227,86
Fe	mg/kg d.m	300,73	81,71	24,21	46,23
K	mg/kg d.m	1306,38	332,58	512,07	365,57
Mg	mg/kg d.m	616,37	325,67	207,80	123,72
Mn	mg/kg d.m	310,38	163,82	128,02	64,28
P	mg/kg d.m	666,34	108,56	84,60	50,79

4 Conclusions

The aim of the study was to verify the presence of differences in terms of logging residue type and quantity according to the harvesting system adopted in the case of a salvage logging scenario.

From the results obtained it was possible to observe that in the full mechanized Cut-to length (HF) sites there are on average lower volumes of dead wood, generally Fine Wood Debris (FWD). In the Full-Tree cable yarder extraction sites (CC) the values of these classes are higher on average. The difference relating to the first two classes is attributable to the greater interference that the passage of forest machine (harvester and forwarder) has inside the forest compared to the cable crane. In fact, the transit of vehicles causes a mixing of the soil that can incorporate dead wood of the smaller classes, preventing it from being correctly counted in the sampling. As for the remaining two classes, the values are similar for the third, while for the coarser material (E) there is on average the double of the material estimated for HF than CC. This difference is presumed to be caused by the selection process in the sorting, debarking and delimiting operations of the material by the harvester operator (CTL) – which is performed on the cutting site and therefore leaving more material on the ground – and by the ground crew or the processing head (FT), performed at roadside thus extracting the whole tree from the forest and leaving very few residues on site. Statistically, the amount of dead wood following salvage logging operations is not influenced by the logging system, but by other factors maybe related to the characteristics of the stand.

Based on this study outcomes, further investigations should address the residues spatial distribution after logging operations, and the possible effects on nutrients and soil.

References

1. Seidl, R., et al.: Forest Disturbances under Climate Change. *Nat. Clim. Chang.* **7**, 395–402 (2017)
2. Verkerk, P.J., Martinez de Arano, I., Palahí, M.: The bio-economy as an opportunity to tackle wildfires in mediterranean forest ecosystems. *Forest Policy Econ.* **86**, 1–3 (2018)
3. European Environment Agency Forest Dynamics in Europe and Their Ecological Consequences. *Biodiversity* **16**, 1–7 (2018).
4. Chirici, G., et al. Forest Damage Inventory after the “Vaia” Storm in Italy. *Forest@ - Rivista di Selvicoltura ed Ecologia Forestale* **16**, 3–9 (2019). <https://doi.org/10.3832/efor3070-016>
5. Motta, R., Ascoli, D., Corona, P., Marchetti, M., Vacchiano, G.: Silviculture and Wind Damages. The Storm “Vaia.” *Forest@ - Rivista di Selvicoltura ed Ecologia Forestale* **15**, 94–98 (2018). <https://doi.org/10.3832/efor2990-015>.
6. Mayer, M., et al.: Influence of forest management activities on soil organic carbon stocks: a knowledge synthesis. *Forest Ecol. Manage.* **466** (2020)
7. FOREST EUROPE State of Europe’s Forests 2020, vol. 394 (2020)
8. Bauer, G.A., et al.: Linking Plant Nutrition and Ecosystem Processes. In: Schulze, ED. (eds) Carbon and Nitrogen Cycling in European Forest Ecosystems. *ECOLSTUD*, vol. 142. Springer, Berlin, Heidelberg (2000). https://doi.org/10.1007/978-3-642-57219-7_4

9. Lindner, M., et al.: Climate change impacts, adaptive capacity, and vulnerability of european forest ecosystems. *For. Ecol. Manage.* **259**, 698–709 (2010). <https://doi.org/10.1016/j.foreco.2009.09.023>
10. Irauschek, F., Rammer, W., Lexer, M.J.: Can current management maintain forest landscape multifunctionality in the eastern alps in Austria under climate change? *Reg. Environ. Change* **17**, 33–48 (2017). <https://doi.org/10.1007/s10113-015-0908-9>
11. Kramer, K., Brang, P., Bachofen, H., Bugmann, H., Wohlgemuth, T.: Site factors are more important than salvage logging for tree regeneration after wind disturbance in central european forests. *For. Ecol. Manage.* **331**, 116–128 (2014). <https://doi.org/10.1016/j.foreco.2014.08.002>
12. Mina, M., Bugmann, H., Klopčič, M., Cailleret, M.: Accurate modeling of harvesting is key for projecting future forest dynamics: a case study in the slovenian mountains. *Reg. Environ. Change* **17**, 49–64 (2017). <https://doi.org/10.1007/s10113-015-0902-2>
13. Pilli, R., Vizzarri, M., Chirici, G.: Combined effects of natural disturbances and management on forest carbon sequestration: the case of vaia storm in Italy. *Ann. For. Sci.* **78**, 46 (2021). <https://doi.org/10.1007/s13595-021-01043-6>
14. Priewasser, K., Brang, P., Bachofen, H., Bugmann, H., Wohlgemuth, T.: Impacts of salvage-logging on the status of deadwood after windthrow in Swiss forests. *Eur. J. Forest Res.* **132**, 231–240 (2013). <https://doi.org/10.1007/s10342-012-0670-1>
15. Wohlgemuth, T., Schwitter, R., Bebi, P., Sutter, F., Brang, P.: Post-windthrow management in protection forests of the Swiss Alps. *Eur. J. Forest Res.* **136**, 1029–1040 (2017). <https://doi.org/10.1007/s10342-017-1031-x>
16. Bodaghi, A.I., et al.: Ground-based extraction on salvage logging in two high forests: a productivity and cost analysis. *Forests* **9**, 729 (2018). <https://doi.org/10.3390/f9120729>
17. Heinimann, H.R., Stampfer, K., Loschek, J., Caminada, L.: Perspectives on central european cable yarding systems. *Austrian J. Forest Sci.* **123**, 121–139 (2006)
18. Prats, S.A., Malvar, M.C., Wagenbrenner, J.W.: Compaction and cover effects on runoff and erosion in post-fire salvage logged areas in the valley fire, California. *Hydrol. Processes* **35** (2021). <https://doi.org/10.1002/hyp.13997>
19. Robichaud, P.R., Lewis, S.A., Brown, R.E., Bone, E.D., Brooks, E.S.: Evaluating post-wildfire logging-slash cover treatment to reduce hillslope erosion after salvage logging using ground measurements and remote sensing. *Hydrol. Process.* **34**, 4431–4445 (2020). <https://doi.org/10.1002/hyp.13882>
20. Valipour, M., et al.: Simulation of the effects of forest harvesting under changing climate to inform long-term sustainable forest management using a biogeochemical model. *Sci. Total Environ.* 767 (2021). <https://doi.org/10.1016/j.scitotenv.2020.144881>
21. Huber, C., Kastner, M., Hochbichler, E., Stampfer, K.: Effect of topping trees on biomass and nitrogen removal in the thinning of norway spruce stands. *Sustainability (Switzerland)* **9**, 1–14 (2017). <https://doi.org/10.3390/su9101856>
22. Tamminen, P., Saarsalmi, A., Smolander, A., Kukkola, M., Helmisaari, H.S.: Effects of logging residue harvest in thinnings on amounts of soil carbon and nutrients in scots pine and Norway spruce stands. *For. Ecol. Manage.* **263**, 31–38 (2012). <https://doi.org/10.1016/j.foreco.2011.09.015>
23. Visser, R., Stampfer, K.: Expanding Ground-Based Harvesting onto Steep Terrain: A Review, vol. 36 (2015)
24. Janowiak, M.K., Webster, C.R.: Promoting ecological sustainability in woody biomass harvesting. *J. Forest.* **108**, 16–23 (2010). <https://doi.org/10.1093/jof/108.1.16>
25. Palviainen, M., Finér, L., Laiho, R., Shorohova, E., Kapitsa, E., Vanha-Majamaa, I.: Carbon and nitrogen release from decomposing scots pine, Norway spruce and silver birch stumps. *For. Ecol. Manage.* **259**, 390–398 (2010). <https://doi.org/10.1016/j.foreco.2009.10.034>
26. Bače, R., Svoboda, M., Pouska, V., Janda, P., Červenka, J.: Natural regeneration in central-european subalpine spruce forests: which logs are suitable for seedling recruitment? *For. Ecol. Manage.* **266**, 254–262 (2012). <https://doi.org/10.1016/j.foreco.2011.11.025>
27. Motta, R., Berretti, R., Lingua, E., Piussi, P.: Coarse woody debris, forest structure and regeneration in the Valbona Forest Reserve, Paneveggio, Italian Alps. *Forest Ecol. Manage.* **235**, 155–163 (2006). <https://doi.org/10.1016/j.foreco.2006.08.007>

28. Zielonka, T., Niklasson, M.: Dynamics of dead wood and regeneration pattern in natural spruce forest in the Tatra mountains, Poland. *Ecol. Bull.* 159–163 (2001)
29. Carlson, A.R., Sibold, J.S., Assal, T.J., Negrón, J.F.: Evidence of compounded disturbance effects on vegetation recovery following high-severity wildfire and spruce beetle outbreak. *PLoS ONE* **12** (2017). <https://doi.org/10.1371/journal.pone.0181778>.
30. Mattson, L.R., Coop, J.D., Battaglia, M.A., Cheng, A.S., Sibold, J.S., Viner, S.: Post-spruce beetle timber salvage drives short-term surface fuel increases and understory vegetation shifts. *For. Ecol. Manage.* **437**, 348–359 (2019). <https://doi.org/10.1016/J.FORECO.2019.01.048>
31. Sullivan, T.P., Sullivan, D.S., Klenner, W.: Fate of Postharvestwoody debris, mammal habitat, and alternative management of forest residues on clearcuts: a synthesis. *Forests* **12** (2021). <https://doi.org/10.3390/f12050551>.
32. Maas, G.C.B., Sanquetta, C.R., Marques, R., Machado, S.D.A., Sanquetta, M.N.I.: Quantification of carbon in forest necromass: state of the art. *Cerne* **26**, 98–108 (2020). <https://doi.org/10.1590/01047760202026012661>
33. Mologni, O., Grigolato, S., Cavalli, R.: Harvesting systems for steep terrain in the Italian Alps: state of the art and future prospects. *Contemp. Eng. Sci.* **9**, 1229–1242 (2016). <https://doi.org/10.12988/ces.2016.68137>
34. Brown, J.K.: Handbook for inventorying downed woody material. *USDA For. Serv. Gen. Tech. Rep.* **24** (1974)
35. Woodall, C.W., Monleon, V.J.: Sampling protocol, estimation, and analysis procedures for the down woody materials indicator of the FIA program. *Gen. Tech. Rep. NRS-22* **68** (2008)
36. Rizzolo, R.: Fuel Models Development to Support Spatially-Explicit Forest Fire Modelling in Eastern Italian Alps **156** (2016)
37. van Wagner, C.E.: The line intersect method in forest fuel sampling. *Forest Sci.* **14**, 20–26 (1968). <https://doi.org/10.1093/FORRESTSCIENCE/14.1.20>
38. Papais, E., Gallo, A., Bini, C.: Valutazione Dello Stock Di Carbonio Di Suoli Forestali Del Friuli Vg (Ne Italia). In: Proceedings of the Proceedings of the Second International Congress of Silviculture; Florence (2014)
39. Hollis, J.M., Woods, S.M.: The Measurement and Estimation of Saturated Soil Hydraulic Conductivity. SSLRC report to MAFF, Soil Survey and Land Research Centre (1989)

Concerning the Relationship Between Tilled Soil Aggregates Dimension and Power Harrow Energy Requirements



Massimiliano Varani, Michele Mattetti, Alessandro Biglia, Lorenzo Comba, and Giovanni Molari

Abstract The literature reports energy requirements for several instruments based on different operating conditions and soil properties. However, tillage cannot be evaluated only by its energy consumption alone. Improvements in soil structure and consequent agricultural benefits must also be examined. The number of tine revolutions per meter (called C) is controlled by both the angular speed of the tine rotors and the machine's ground speed, which together allow power harrows to alter the soil's cloddiness. This study seeks to identify relationships between the seedbed quality and the energy needed to operate a power harrow in various configurations. A tractor with a 107 kW rated engine power and a power harrow with a 3 m operating width were tested in the field at the University of Bologna's experimental farm. Tractor metrics such as speed, engine power, fuel rate consumption, draught, and power take-off (PTO) speed and torque were recorded with a datalogger. Field tests were conducted by adjusting C from 2.3 rev rev m^{-1} to 12.57 rev m^{-1} , following harrowing soil samples were sieved, and important granulometric parameters were computed and correlated with information obtained from the tractor-power harrow system. The findings indicate that high values of implement-soil impact speed are necessary to achieve the best seedbed conditions.

Keywords Power harrow · Tillage operations · soil aggregates · energy consumption

M. Varani (✉) · M. Mattetti · L. Comba · G. Molari
Department of Agricultural and Food Sciences – Alma Mater Sudiorum (DISTAL), University of Bologna, Bologna, Italy
e-mail: massimiliano.varani@unibo.it

A. Biglia
Department of Agricultural, Forest and Food Sciences (DiSAFA), Università degli Studi di Torino, Turin, Italy

1 Introduction

The greatest energy-consuming agricultural practice is tillage, which is used in primary production. 92% of the energy used for tillage comes from fossil fuels and makes up around one-fourth of the overall energy input for crop production [1]. Several studies have extensively characterized the energy consumption of the tractor-implement system under various operating parameters (i.e., working depth and speed), as well as various soil types and moisture levels [2, 3]. However, the benefits for soil structure and other agronomic factors (such as crop yield) must also be taken into account when evaluating tillage operations. The size, shape, and arrangement of soil particles and pores are referred to as soil structure; it is essential for plant germination and growth as well as for controlling soil water content. It is generally accepted that an aggregate size of 1 to 8 mm is necessary for a good seedbed [4], but deviations from this general rule should be adopted according to the crop, weather, rainfall, and type of soil. Finer soil aggregates typically result in higher field emergence and crop yield. Secondary tillage operations are carried out to achieve the required size of soil aggregates in the topsoil utilizing traditional tillage management. Because it only needs a little amount of tractor draught, ensures little loss from wheel-slip and rolling resistance, and creates a viable seedbed even in challenging conditions, the power harrow is an extensively used secondary tillage tool in Europe. With power harrows, the angular speed of the tine rotors and the machine's ground speed, which both regulate the number of tine revolutions per meter, can be used to modify the soil's cloddiness [5, 6]. Increasing the rotational speed of the tines while maintaining the same machine ground speed can result in an up to 40% increase in specific energy (i.e., the energy per unit area or volume), according to research by Balsari et al. [2]. There aren't many studies looking at the ideal power harrow operation conditions in terms of energy consumption and soil structure. With the use of several power harrow setups, this study intends to get a greater understanding of regulating soil structure and discover a correlation between the energy needs of the machinery and the resulting soil structure.

2 Materials and Methods

A 3 m working width (b) power harrow with a packer roller (Frudent Eternum R303-19, Frudent Group Srl, Italy) was used for the testing. The power harrow that was chosen had a gearbox that could be utilized to alter the transmission ratio (τ_{ph}) between the PTO and the tine rotors. The power harrow was pulled by a four-wheel-drive row crop tractor; Table 1 presents power harrow and tractor main specifications. The following tractor parameters were acquired through the tractor's controller area network (CAN) SAE J1939 diagnostic port and recorded with a Kvaser Memorator 2 datalogger (Kvaser Inc., Mission Viejo, CA, USA): Engine speed (n_e), power take off (PTO) rotational speed (n_{PTO}), engine fuel rate (\dot{f}). Then, a GNSS

Table 1 Power harrow and tractor specifications

Parameter	Value
Power Harrow	
Working width (b) [m]	3
Number of rotors	12
Rotor radius (R_{ph}) [m]	0.1
Mass (harrow + roller) [kg]	1323
Tractor	
Manufacturer	CNH Industrial N.V. (Amsterdam, Netherlands)
Model	Case IH Maxxum 115
Unladen mass [kg]	4890
Rated engine speed [rpm]	2000
Maximum engine power at rated engine speed [kW]	107
Transmission	Partial-powershift, 16 forward and 16 reverse speeds

receiver (IPESpeed, Ipetronik GmbH & Co. KG, Baden-Baden, Germany) was used to measure the tractor's ground speed (V_t). The datalogger was directly attached to the GNSS receiver's output signal, which was already in the CAN bus protocol. To measure the draught force (D), a three-point hitch coupler with three biaxial load pins mounted at the three-point linkage's hitch points was installed between the tractor and the power harrow.

The biaxial load pins (N.B.C. Elettronica Group Srl, Italy) had a load capacity of 10 kN in each direction and could withstand forces along two orthogonal axes. A torque meter (NTCE 7000 series, NTCE AG, Germany) with a full scale of 5000 Nm was used to measure the torque delivered at the PTO of the tractor (M_{PTO}). Because the Kvaser datalogger only complies with the CAN bus protocol and the signals from the load pins and torque meter were in voltage output, a conversion module was employed to convert their outputs from analogue to the CAN bus protocol (ADMM 8 pro, CSM GmbH, Filderstadt, Germany).

The research was conducted in autumn 2021 at the experimental farm of the University of Bologna located in Cadriano. The field used for the test was 200 m long and 50 m wide, and it was classified as silty clay loam soil according to the USDA textural soil classification [7]. The liquid limit (LL) and the plastic limit (PL) of the soil are 31% and 21%, respectively. A plasticity index (PI) of 10% permits the soil to be classified as low-plasticity clay. The mean value and the standard deviation of the soil moisture content (based on the dry mass) were 20.7% and 1.6%, respectively.

Equation 1 was used to determine the rotational speed of the tines (n_{ph}) as a function of the rear PTO output shaft speed and the gearbox transmission ratio.

Table 2 Trial target configurations

Trial name	n_e [rpm]	V_t [km h ⁻¹]	PTO mode	τ_{ph}	n_{ph} [rpm]	C [rev m ⁻¹]
T1	2000	6.6	540E	1.24	256	2.33
T2	2000	6.6	540E	0.81	398	3.64
T3	2000	4.0	540E	1.24	256	3.75
T4	2000	2.5	540	1.24	184	4.41
T5	2000	3.8	1000	1.24	340	5.37
T6	2000	2.1	1000	0.97	440	12.57

$$n_{ph} = n_{PTO} \tau_{ph} \tag{1}$$

The number of revolutions per linear metre that the tines traveled (C), which was calculated using Eq. 2, represents the combined impact of V_t and n_{ph} on the tractor performance and the soil granulometry

$$C = 0.06 \frac{n_{ph}}{V_t} \tag{2}$$

n_{ph} and V_t are represented in rev min⁻¹ and km h⁻¹, respectively.

As shown in Table 2, there were six different field operation configurations tested, each with a different C ranging from a practicable minimum of 2.33 rev m⁻¹ to a maximum of 12.57 rev m⁻¹. Lower or higher values were too challenging to obtain; these boundary values were set by the physical properties of the tractor and power harrow employed for the experiments. These parameters were chosen in accordance with the outcomes of an initial field test since specific C values can be produced with various combinations of n_{ph} and V_t . The selected configurations matched the soil properties, tractor gearbox ratios, and maximum engine power requirements the best.

In order to perform four replicates of each configuration, the field mentioned above was divided into 24 parcels, each measuring 4 m in width and 100 m in length. To reduce the reliance of the results on differences in soil properties, the repetitions were randomly distributed around the field. For all test condition, the working depth of the implement (δ) was held constant at 15 cm.

Equation 3 was used to get the maximum implement-soil impact speed (V_{is}).

$$V_{is} = n_{ph} \frac{2\pi}{60} R_{ph} + V_t \tag{3}$$

Equation 4 was used to determine the torque delivered to the power harrow rotors.

$$M_{ph} = \frac{M_{PTO}}{\tau_{ph}} \tag{4}$$

Since it remained constant throughout all of the configurations examined, the efficiency of the power harrow transmission was not taken into account.

The power required to tow the implement (P_D) (Eq. 5) and the power used to drive the power harrow rotors through the PTO (P_{PTO}) (Eq. 6) were added to determine the total power absorbed by the power harrow (P_{ph}), as illustrated in Eq. 7:

$$P_D = DV_t \quad (5)$$

$$P_{PTO} = M_{ph} n_{ph} \frac{2\pi}{60} \quad (6)$$

$$P_{ph} = P_D + P_{PTO} \quad (7)$$

Using Eq. 8, the amount of energy needed to process 1 m³ of tilled soil (E) was estimated.

$$E = \frac{P_{ph}}{V_t b \delta} \quad (8)$$

Using signal differentiation to calculate the rate of change of P_{ph} , the passes and headland turns were separated. Then, about 8 kg of dry tilled soil were collected from each parcel following ASTM D2488 [8] methods after harrowing in order to gauge the aggregate size distribution. Then, five sieves with nominal hole diameters (d_i) of 2, 4, 8, 16, and 31.5 mm were used to sift soil samples. For each parcel, Eqs. 7 and 8 were used to derive the aggregates Mean Weighted Diameter (MWD) and Geometric Mean Diameter (GMD).

$$MWD = \sum_{i=1}^{n_s} d_i W_{i,j}^{r\%} \quad (9)$$

$$GMD = \exp\left[\sum_{i=1}^{n_s} \ln(d_i) W_{i,j}^{r\%}\right] \quad (10)$$

where is the percentage of soil mass retained ($W_{i,j}^{r\%}$) in the i^{th} sieve collected in the j^{th} parcel.

The mean values and standard deviations of the considered parameters during the passes were determined for each configuration in order to find any possible correlation between each other. Moreover, from an economic perspective, choosing V_t is especially crucial because it is closely related to the field capacity, which determines the operation's length, and the fuel consumption per hectare, which determines its expenses. To emphasize any notable changes in their energy and soil fragmentation markers, the experiments carried out at the same V_t with varied n_{ph} (and, subsequently, different C and V_{is}) were grouped. So, the Low Speed (LS) group is composed by the trials T4 and T6, the Medium Speed (MS) group by T3 and T5 and the High Speed (HS) group by the T1 and T2. Then, One way ANOVA tests

were performed to remark any significative difference between the trials in the same group.

3 Results

Between E and C a strong linear association was discovered, as showed in Fig. 1.

From values around 85 kJ m^{-3} at around 2 rev m^{-1} to 200 kJ m^{-3} at over 12 rev m^{-1} , the value of E rises linearly with C . On silt loam and clay loam soil Balsari [2] and Daraghmeh [9] found results with comparable magnitudes and behaviors. Indeed, high values of C indicate longer tine travel distances, which in turn means more energy is needed to till a given volume of soil. One can note that the behavior of the fuel consumption per hectare is strictly linked to E , as the energy needed to till the soil increases, more fuel will be consumed. Surprisingly, the values of C and E do not appear to be directly associated to the soil aggregate dimensions MWD and GMD.

However, as seen in Fig. 2, both MWD and GMD demonstrated a monotonic decline with rising V_{is} . This outcome can be explained by the fact that as the relative speed between the soil and rotors increases due to the inertial force, the soil disaggregates more and more, increasing the overall soil response force (McKyes 1985), Due to the variability of soil engineering properties, such as soil bulk density, soil cohesion, internal friction angle, soil moisture content, and soil shear strength [12, 13], the variability of the operational conditions, such as tool working speed, and the fact that manually sieving the soil implies a certain variability, both regressions showed relatively low R^2 values.

The findings of the ANOVA test indicated that, at similar V_t values, the considerable differences in n_{ph} between the configurations led to significant differences in the mean values between the pairs of configurations (Fig. 3).

Particularly, T4 has a MWD value that is 16% greater than T6, whereas T4 has an E value that is 52% lower than T6. Despite the obtained soil particle size being

Fig. 1 Linear regression of E as a function of C , $R^2 = 0.95$

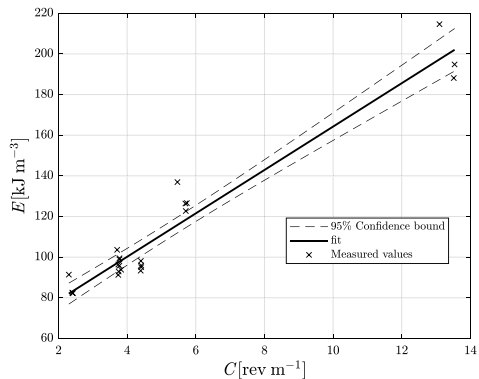


Fig. 2 Linear regression of MWD and GMD as a function of C , $R^2 = 0.57(\text{MWD}), 0.46$

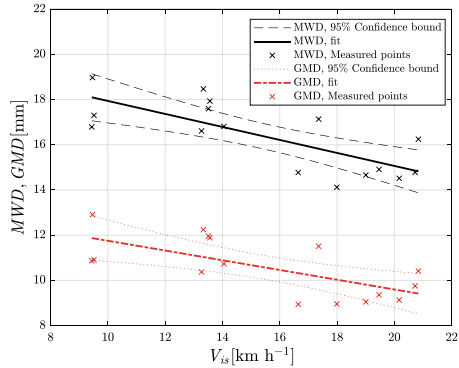
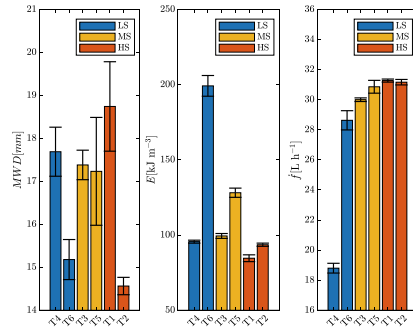


Fig. 3 MWD, E and f values for the low speed (LS), medium speed (MS), and high speed (HS) tertiles. The error bars represent the standard deviations



suitable for seeding, the energy requirements that were recorded in T6, which has an extraordinarily high C value, are economically and environmentally unsustainable. The obtained soil particle size was similar in the two configurations for the MS group since there was no discernible variation in terms of MWD. But because T3 has a lower C value than T2, it uses 22% less energy to till the same amount of soil. Due to the two distinct C values, the ANOVA test conducted on the HS group revealed a significant difference in MWD and E . While E in T1 was 10% lower than in T2, the mean MWD value in T1 was 28% higher than in T2. This leads to the conclusion that T2 was the overall best configuration, simultaneously ensuring the best soil disaggregation and a low energy consumption.

4 Conclusions

This report describes the findings of a thorough in-field experimental campaign where several tractor-power harrow system indicators and seedbed quality indicators were tracked under various working situations. Six distinct field operating configurations were tested in order to produce variable C , with values ranging from a theoretical

minimum of 2.33 rev m⁻¹ to a theoretical maximum of 12.57 rev m⁻¹. Additionally, it was discovered that the amount of energy needed to process 1 m³ of tilled soil increased linearly with the number of tine spins per linear meter, with a difference of around 115 kJ m⁻³ between the mean values of the two most severe examined configurations. However, there was no relationship between the value of *C* and the indices of soil fragmentation. Instead, they were linked to the impact speed of the implement on the soil. Indeed, the size of the soil aggregate is decreased by high implement-soil impact speeds. In conclusion, the ideal circumstances to guarantee a high-quality seedbed are produced with high implement-soil impact speeds and the lowest *C* values to minimize fuel consumption. Extremely low *C* values should be avoided because the power harrow would then function almost passively, creating the potential to overstress the rotor bearings. The findings in this research will be helpful for the creation of new variable-rate tillage implements, a current area of intense attention.

References

1. Borin, M., Menini, C., Sartori, L.: Effects of tillage systems on energy and carbon balance in north-eastern Italy. *Soil and Tillage Res.* **40**(3), 209–226 (1997). [https://doi.org/10.1016/S0167-1987\(96\)01057-4](https://doi.org/10.1016/S0167-1987(96)01057-4)
2. Balsari, P., et al.: Performance analysis of a tractor - power harrow system under different working conditions. *Biosys. Eng.* **202**, 28–41 (2021). <https://doi.org/10.1016/j.biosystemseng.2020.11.009>
3. Mattetti, M., Varani, M., Molari, G., Morelli, F.: Influence of the speed on soil-pressure over a plough. *Biosys. Eng.* **156**, 136–147 (2017). <https://doi.org/10.1016/j.biosystemseng.2017.01.009>
4. Braunack, M.V., Dexter, A.R.: Soil aggregation in the seedbed: A review. I. Properties of aggregates and beds of aggregates. *Soil and Tillage Res.* **14**(3), 259–279 (1989). [https://doi.org/10.1016/0167-1987\(89\)90013-5](https://doi.org/10.1016/0167-1987(89)90013-5)
5. Celik, A., Altikat, S.: The effect of power harrow on the wheat residue cover and residue incorporation into the tilled soil layer. *Soil and Tillage Res.* **215**, 105202 (2022). <https://doi.org/10.1016/j.still.2021.105202>
6. Raparelli, T., Eula, G., Ivanov, A., Pepe, G.: Kinematic analysis of rotary harrows. *J. Agric. Eng.* **51**(1), 1 (2020). <https://doi.org/10.4081/jae.2019.976>
7. USDA. Soil Mechanics Level I', U.S. Department of Agriculture (1987)
8. ASTM, 'D2488 - Practice for Description and Identification of Soils (Visual-Manual Procedure)', ASTM International (2009)
9. Daraghmeh, O.A., et al.: Impact of tillage intensity on clay loam soil structure. *Soil Use Manag.* **35**(3), 388–399 (2019). <https://doi.org/10.1111/sum.12501>
10. Kshetri, S., Steward, B.L., Tekeste, M.Z.: Modeling soil forces on a rotary tine tool in artificial soil. *Trans. ASABE* **64**(5), 1693–1704 (2021). <https://doi.org/10.13031/trans.14336>
11. McKyes, E.: *Soil Cutting and Tillage*. Elsevier (1985)
12. Abo Al-kheer, A., et al.: Theoretical analysis of the spatial variability in tillage forces for fatigue analysis of tillage machines. *J. Terramech.* **48**(4), 285–295 (2011). <https://doi.org/10.1016/j.jterra.2011.05.002>
13. Abo Al-kheer, A., El-Hami, A., Kharmanda, M.G., Mouazen, A.M.: Reliability-based design for soil tillage machines. *J. Terramech.* **48**(1), 57–64 (2011). <https://doi.org/10.1016/j.jterra.2010.06.001>

“Green” Investments in Sustainable Farming Systems: A Survey Among Italian Enterprises



Lucia Vigoroso , Giorgia Bagagiolo , Giulia De Paolis,
Niccolò Pampuro , Eugenio Cavallo , and Federica Caffaro 

Abstract In the context of climate change mitigation and/or adaptation, the present study investigated the diffusion of sustainable agricultural practices and technologies among Italian farm enterprises. An online questionnaire was administered to a sample of 456 farm managers and contractors. Participants were asked to evaluate their rate of adoption, intention to adopt and willingness to invest in sustainable practices and technologies aimed at limiting the environmental and climate impacts of their farming activities. Results showed that the majority of the participants have already adopted practices and technologies aimed at reducing agro-chemical inputs, whereas practices and technologies aimed at reducing emissions and generating renewable energies from agricultural biomass had a more limited and recent diffusion. However, 59% and 47% of participants, respectively, expressed the intention to adopt them in the short/medium term, probably due to the positive pressure exerted by the ambitious targets of the European Green New Deal. Only 7.4% of the respondents were prone to invest more than 100 k€ in “green” practices, whereas more than half of the enterprises (54%) would be willing to invest a maximum of 10 k€. This willingness to invest may vary according to the farm operation and farm size. The present study allowed us to glimpse future lines of investments and to identify intervention measures aimed at fostering the “green” transition within the Italian agricultural sector.

Keywords Green Deal · water resources · emissions · renewable energies · sustainable practices

L. Vigoroso · G. Bagagiolo (✉) · N. Pampuro · E. Cavallo
Institute of Sciences and Technologies for Sustainable Energy and Mobility (STEMS), National Research Council of Italy (CNR), Strada Delle Cacce 73, 10135 Torino, Italy
e-mail: giorgia.bagagiolo@stems.cnr.it

G. De Paolis · F. Caffaro
Department of Education, University of Roma Tre, Via del Castro Pretorio 20, 00185 Rome, Italy

1 Introduction

Agriculture is one of the economic sectors most affected by the impact of climate change [1], as evidenced by the rising temperatures and the increasing frequency of extreme weather events such as drought and heavy rainfalls [2]. On the other hand, agricultural activities represent a significant source of greenhouse gas (GHG) emissions and one of the major causes of natural resource depletion [1, 3]. At the European level, the agricultural sector is responsible for the production of about 12% of total GHG emissions [4], and the use of more than 50% of water resources [5, 6]. Furthermore, at least a quarter of the agricultural soil in Europe is affected by degradation (i.e., erosion, compaction, desertification, [7]). Under the framework of Common Agricultural Policy (CAP), in the next years, the European agricultural sector will have to comply with a set of policies aimed at reaching climate neutrality by 2050, implementing strategic plans aimed at “contributing to climate change mitigation and adaptation” and promoting sustainable development and the efficient management of natural resources such as water, soil and air [8].

In this context, the spreading of sustainable agricultural practices and technological innovations in the agricultural sector has been crucial to address the impacts of climate change. Several strategies have been developed and implemented in different agricultural branches to ensure lower resource consumption, reduce waste, limit the use of inputs such as fertilizers and pesticides, reduce GHG emissions and promote the adoption of renewable energies [9]. Examples of the agricultural practices and technologies for sustainable agriculture include those aimed to protect soil from degradation (e.g., reduced or no tillage, cover crops), saving water (e.g., micro-irrigation systems, controlled deficit irrigation), precision farming and decision support systems, based on parameters measured in the field or through remote sensing [10, 11]. Furthermore, proper management of livestock waste (e.g., storage tanks coverage and slurry acidification) allows to limit the production of GHGs and ammonia and to improve soil nutrient and organic matter content [12, 13]. Mitigation of GHG emissions can also be pursued through the use of tractors and machinery powered by alternative fuels (e.g., biomethane) or the use of tractors equipped with emission reduction systems and the use of electrically powered robots, machinery and equipment [3]. However, according to previous studies, the difficulties to disseminate sustainable practices and innovations related to precision agriculture and digital agriculture (also known as Agriculture 4.0) are particularly noteworthy in many European countries, including Italy [14, 15]. Based on this, it is important to understand what is the actual diffusion of such practices and to point out which are the farmers’ characteristics, needs and perceived barriers affecting the adoption of sustainable innovations.

2 Materials and Methods

2.1 *Participants and Instrument*

Four hundred and fifty-six participants (90.8% men, 9.2% women), including farm managers and contractors, took part in the study. The sample consisted mainly of farm managers (92.8% of the sample, contractors 7.2%), with an average education of 13 years (high school) and a mean age of 49.87 years ($SD = 13.8$), which is in line with the national statistics [16]. Participants were administered an online questionnaire disseminated through the agricultural magazine “*Informatore Agrario*”. The different sections and items of the questionnaire were designed based on previous instruments [15]. The overall questionnaire included seven sections investigating the most important barriers and motivating factors for the adoption of innovative practices and technologies belonging to a sustainable agriculture model, namely agricultural practices and advanced technologies typical of precision agriculture and Agriculture 4.0, aimed at efficiently managing natural resources and mitigating environmental impacts. For the aims of this contribution, not all the variables included in the questionnaire were analyzed, but only those regarding the adoption (“for more than 5 years”, “for less than 5 years”), intention to adopt (“will adopt shortly”, “will adopt in the future”, “will not adopt”) and willingness to invest in sustainable practices and technologies aimed to limit the environmental impact of agricultural activities (8 points scale from less than 5 k€ to more than 100 k€). In detail, the investigated practices and technologies were clustered into 4 groups: saving water (4 items), reducing agro-chemical inputs (4 items), reducing emissions (5 items) and producing renewable energies (2 items) (Table 1).

2.2 *Data Analysis*

Descriptive statistics were computed for all the variables of interest. Then, contingency tables and non-parametric Chi-squared tests were performed to test whether some characteristics of the farm (turnover, size and production orientation) or personal characteristics of the entrepreneur (age and level of education) could significantly affect the “willingness to invest”. The p-value for statistical significance was set at $p < 0.05$ and all the analyses were conducted using IBM SPSS Statistics 26.0 (IBM, Armonk, NY, USA).

3 Results and Discussions

Results showed that most of the responses came from farms settled in northern regions of Italy (61.4%), followed by southern regions (16.4%), central regions (15.6%) and

Table 1 Items considered in the present study

Category	Items
Saving water	<ol style="list-style-type: none"> 1. Soil management and tillage techniques 2. Micro-irrigation systems 3. “Controlled deficit” irrigation 4. Recovery / recycling of waste water for irrigation
Reducing agro-chemical inputs	<ol style="list-style-type: none"> 5. Monitoring of agri-environmental parameters and DSS 6. Organic fertilization, green manure, planting of crop residues 7. Agronomic practices aimed at reducing the use of synthetic products 8. Use of precision farming systems for localized fertilization and weeding
Reducing emissions	<ol style="list-style-type: none"> 9. Management of livestock waste and/or reducing emissions from fertilizers 10. Tractors and machines powered by alternative fuels 11. Tractors equipped with emission reduction engines 12. Electrically powered robots, machines and equipment 13. Controlled traffic farming (CTF)
Producing renewable energy	<ol style="list-style-type: none"> 14. Biomass boilers 15. Anaerobic digestion plants

lastly islands (6.6%). The predominant line of production of the sample was cereal farming (45.4%), followed by viticulture (16.9%), fruit and olive growing (13.4%). Most of the farms were medium-large size, indeed 54.4% had an extension of more than 20 ha, 32.4% had a size from 20 to 5 ha, and the remaining part included small farms with less than 5 ha. More than half of the farms investigated (61.8%) had an annual turnover of less than 100 k€.

3.1 Adoption

Regarding the current adoption of sustainable measures, the results showed that most respondents had already adopted practices and technologies for the conservation of natural resources like water (39.5%) and practices to reduce the use of agrochemical inputs (54.8%). Most farms have been applying these types of practices for at least 5 years, as they mainly consist of well-established and widely used soil management techniques or agronomic practices recently supported by technology and digitalization [17]. Based on the present survey, it appears that, so far, farms have pursued sustainability mainly focusing on the conservation of natural resources and the reduction of chemicals, probably driven by economic profits and production efficiency. Conversely, practices and technologies aimed to reduce GHGs' emissions and producing renewable energy from agricultural biomasses have been adopted more recently and to a lesser extent (16.0 and 12.2%, respectively) (Fig. 1). With particular

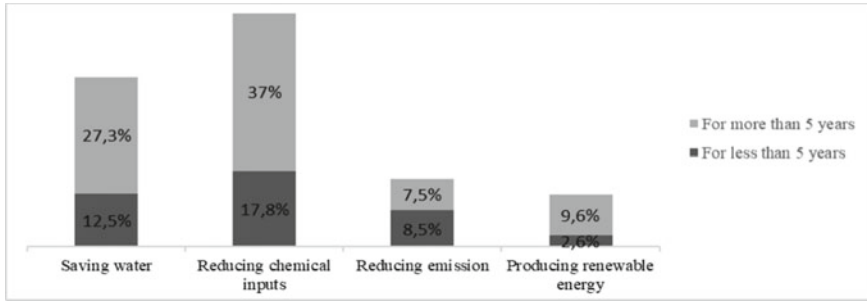


Fig. 1 Current adoption of sustainable practices and technologies aimed at limiting the environmental impact of agricultural activities

reference to on-farm energy production, the latest economic figures [18] report that production grew by 0.8% (in terms of volume and value), exceeding 2.2 billion euros. This trend may be driven by a growing interest, even within the agricultural sector, for solid biomasses in substitution of conventional fuels, as observed by Bibbiani and colleagues [19], in their study on greenhouse heating in Italy, being one of the European countries most vulnerable to the impacts of high energy costs. On the other hand, as reported by Story and Forsyth [20], farmers seem to be more likely to protect the environment when they are aware of environmental problems and more conscious of their actions. Moreover, according to Shaffer and Duvelmeyer [21], the successful implementation of on-farm energy production relates to both farm and farmers’ characteristics such as farm type and size, or farmers’ age and level of education and local and regional determinants, such as regional transformation ability, agricultural structure or neighborhood effects. Based on these considerations and the results of the present study, further investigations should examine more in depth which factors are able to push Italian farms to produce sustainable energies.

3.2 Intention to Adopt

Regarding the intention to adopt sustainable technologies and innovations in the near future, 58.6% of the respondents expressed the intention to adopt agricultural machinery powered by alternative fuels (such as biomethane) or by electric battery in the short to medium term to limit pollutants emission, followed by 47% of respondents who expressed their interest in producing renewable energy (Fig. 2).

In detail, the participants that expressed the greatest interest in limiting pollutant emission and producing renewable energy belonged to livestock (64.7 and 59.6% respectively), cereal crops (56.1 and 48.8% respectively) and horticulture farms (68.2 and 63.6% respectively), which represent the sectors most involved in energy production through anaerobic digestion of crops. The present results are promising, since, according to Niles et al. [22], farmers who have adopted one type of practice will be

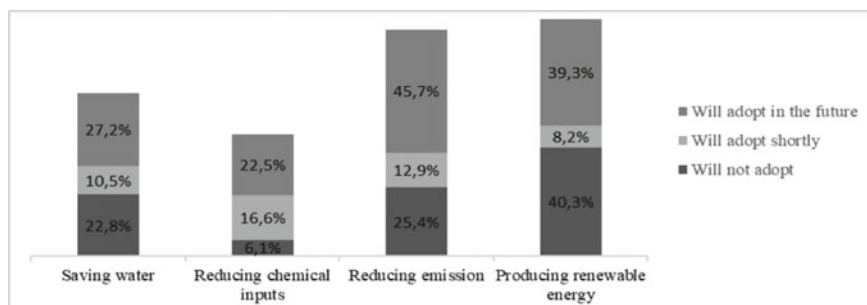


Fig. 2 Intention to adopt sustainable practices and technologies aimed at limiting the environmental impact of agricultural activities

more likely to adopt other practices in the future. However, the increased interest in the future implementation of emission reduction and renewable energy production may be due to a general change in perspective dictated by the ambitious goals of the European Green Deal, which will certainly require the sector's commitment [23].

3.3 Willingness to Invest

With regard to the willingness to invest in sustainable practices and technologies, slightly more than half of the respondents (54%) would be willing to invest in "green" practices, up to a maximum of 10 k€, whereas the remaining part (46%) would be willing to invest higher amounts. Among these, as much as 7.4% of the respondents were willing to invest more than 100 k€ (Fig. 3). Thus, despite the adoption of any new technologies implies costs, the willingness of farm enterprises to invest in them is promising [24]. The results showed that the willingness to invest is related to the size of enterprises and their production orientation. In detail, 74% of the farms that were willing to spend more than 50 k€ were medium-large sized farms (more than 20 ha).

These results were confirmed by the Pearson Chi-Square test pointing out that willingness to invest was significantly affected by the farm's turnover ($\chi^2(42) = 172.965$, $p = 0.000$) and the farm size ($\chi^2(24) = 67.614$, $p = 0.000$). Despite these results, as remarked by [24], if the expected returns are sufficient and the risk of failure is low, also small-scale farmers, with limited access to capital are prepared to invest. Therefore, it is important to develop educational information actions that highlight these issues, helping even small-scale farmers to clarify their doubts and incentivizing them to invest.

When considering the type of farm, results highlighted that the willingness to invest in sustainable practices and technologies was higher in those sectors that are particularly affected by the problem of emissions and pollution, such as the livestock sector (19.1% of livestock farms willing to spend more than 50 k€), or in those

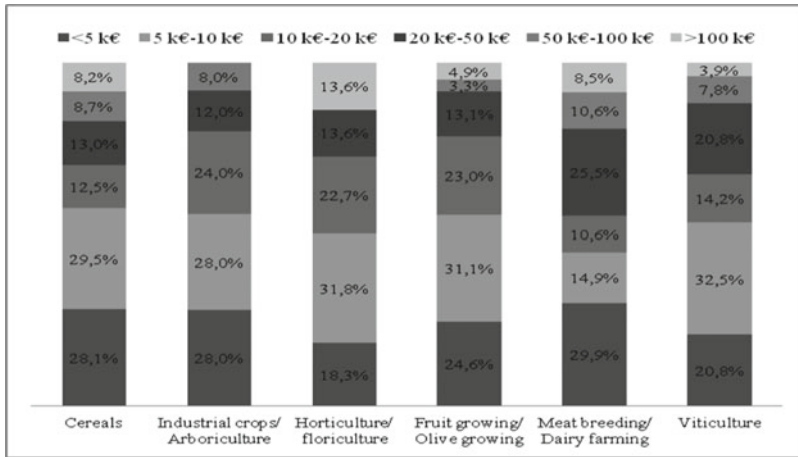


Fig. 3 Farms’ willingness to invest in the near future in sustainable technologies and innovations

sectors, as in the case of the horticultural one, in which the implementation of sustainable initiatives may improve the value of products and the farm’s reputation among consumers (13.7% of horticulture farms reporting a spending threshold of more than 100 k€). Nevertheless, the Pearson Chi-Square test did not show any significant associations between willingness to invest and either production orientation or the personal characteristics of the entrepreneur (age and level of education).

4 Conclusions

The present study allowed glimpsing future lines of investments and identifying intervention measures aimed to foster the “green” transition within the Italian agricultural sector. In particular, some of the investigated and most promising sustainable practices include the conversion of farm machinery fleets to solutions powered by alternative fuels, the construction of new plants for the production of renewable energy or the improvement of the existing ones. The interventions planned at the European level for the coming years seem to favor this transition and support the agricultural sector, facilitating the availability of capital and increasing the investment capacity. Indeed, our results revealed that, at present, most of the farms willing to invest are medium-large ones. Based on this, future studies should further investigate “the specific interplay between farm characteristics, market, local regulation and the CAP in the adoption of energy-related technologies” [25].

References

1. International Panel on Climate Change (IPCC): Special Report. In: Delmotte, V. et al. (eds.) Global warming of 1.5°C. Masson-IPCC, Geneva (2018). <http://www.ipcc.ch/report/sr15/>. Accessed 17 Sept 2022
2. Niles, M.T., Brown, M., Dynes, R.: Farmer's intended and actual adoption of climate change mitigation and adaptation strategies. *Clim. Change* **135**, 277–295 (2016)
3. Gołasa, P., et al. : Sources of greenhouse gas emissions in agriculture, with particular emphasis on emissions from energy used. *Energies* **14**(13), 3784 (2021)
4. Eurostat. Quarterly greenhouse gas emissions in the EU. (2022). https://ec.europa.eu/eurostat/statistics-explained/index.php?title=Quarterly_greenhouse_gas_emissions_in_the_EU#:~:text=Greenhouse%20gas%20emissions%20in%20the%20fourth%20quarter%20of%202021%20increased,by%20the%20COVID%2D19%20crisis. Accessed 17 Sept 2022
5. European Commission. How is water used within the EU agricultural sector? Study provides new analysis. 18th January 2021 (555). https://ec.europa.eu/environment/integration/research/newsalert/pdf/555na1_en_how-is-water-used-within-eu-agriculture-sector.pdf. Accessed 17 Sept 2022
6. Zhang, S., Wang, X., Zhou, L.A.: Review on water-saving agriculture in Europe. *J. Water Resour. Prot.* **14**(4), 305–317 (2022)
7. Soil4Life. L'essenziale è invisibile agli occhi. Soil Degradation. <https://soil4life.eu/en/degrado-del-suolo/>. Accessed 17 Sept 2022
8. European Parliament. The Green Deal and the CAP: policy implications to adapt farming practices and to preserve the EU's natural resources. (2020) [https://www.europarl.europa.eu/RegData/etudes/STUD/2020/629214/IPOL_STU\(2020\)629214_EN.pdf](https://www.europarl.europa.eu/RegData/etudes/STUD/2020/629214/IPOL_STU(2020)629214_EN.pdf). Accessed 17 Sept 2022
9. Anderson, R., Bayer, P.E., Edwards, D.: Climate change and the need for agricultural adaptation. *Curr. Opin. Plant Biol.* **56**, 197–202 (2020)
10. Bagagiolo, G., Biddoccu, M., Rabino, D., Cavallo, E.: Effects of rows arrangement, soil management, and rainfall characteristics on water and soil losses in Italian sloping vineyards. *Environ. Res.* **166**, 690–704 (2018)
11. Liao, Y., Zhang, B., Kong, X., Wen, L., Yao, D., Dang, Y., Chen, W.A.: Cooperative-dominated model of conservation tillage to mitigate soil degradation on cultivated land and its effectiveness evaluation. *Land* **11**(8), 1223 (2022)
12. Eihe, P., et al. : The effect of acidification of pig slurry digestate applied on winter rapeseed on the ammonia emission reduction. In : IOP Conference Series: Earth and Environmental Science, vol. 390, issue 1, 012043. IOP Publishing (2019)
13. Tullo, E., Finzi, A., Guarino, M.: Environmental impact of livestock farming and Precision Livestock Farming as a mitigation strategy. *Sci. Total Environ.* **650**, 2751–2760 (2019)
14. Cullen, R., Forbes, S.L., Grout, R.: Non-adoption of environmental innovations in wine growing. *N. Z. J. Crop. Hortic. Sci.* **41**(1), 41–48 (2013)
15. Caffaro, F., Cremasco, M.M., Roccato, M., Cavallo, E.: Drivers of farmers' intention to adopt technological innovations in Italy: the role of information sources, perceived usefulness, and perceived ease of use. *J. Rural. Stud.* **76**, 264–271 (2020)
16. Istituto Nazionale di Previdenza Sociale (INPS). Statistiche in breve. Mondo Agricolo (2021). <https://www.inps.it/osservatoristatistici/api/getAllegato/?idAllegato=1003>. Accessed 17 Sept 2022
17. Hrustek, L.: Sustainability Driven by Agriculture through Digital Transformation. Sustainability, pp. 1–17 (2020)
18. Istituto Nazionale di Statistica (ISTAT). Andamento dell'economia Agricola, Anno 2020. www.istat.it/it/files/2021/05/REPORT-ANDAMENTO-ECONOMIA-AGRICOLA_2020.pdf. Accessed 17 Sept 2022
19. Bibbiani, C., Fantozzi, F., Gargari, C., Campiotti, C.A., Schettini, E., Vox, G.: Wood biomass as sustainable energy for greenhouses heating in Italy. *Agric. Sci. Procedia* **8**, 637–645 (2016)
20. Story, P.A., Forsyth, D.R.: Watershed conservation and preservation: environmental engagement as helping behavior. *J. Environ. Psychol.* **28**, 305–317 (2008)

21. Schaffer, A., Düvelmeyer, C.: Regional drivers of on-farm energy production in Bavaria. *Energy Policy* **95**, 361–369 (2016)
22. Niles, M.T., Brown, M., Dynes, R.: Farmer’s intended and actual adoption of climate change mitigation and adaptation strategies. *Clim. Change* **135**(2), 277–295 (2016)
23. Bartolini, F., Viaggi, D.: An analysis of policy scenario effects on the adoption of energy production on the farm: a case study in Emilia-Romagna (Italy). *Energy Policy* **51**, 454–464 (2012)
24. Wall, P.C.: Tailoring conservation agriculture to the needs of small farmers in developing countries: an analysis of issues. *J. Crop Improv.* **19**(1–2), 137–155 (2007)
25. Giannoccaro, G., Bartolini, F., Raggi, M., Viaggi, D.: Assessing the CAP influence on European farmers’ preferences towards the adoption of renewable energy production (No. 1052-2016-85909) (2013)

Characterization of a Multispectral Camera for Abiotic and Biotic Stress Detection in Greenhouse



Alessandro Zanchin, Marco Sozzi, Tiziano Valentini, Leonardo Placentino, Francesco Marinello, Alberto Pozzebon, and Carlo Duso

Abstract Nowadays, multispectral sensors are not commonly used in protected crops due to structural features and the presence of an artificial light. This study describes the application of RGB-NIR multispectral camera for greenhouse applications. Different light conditions were evaluated for their influence on the vegetation index on *Rosa rugosa*. Images were acquired in a darkroom at natural, and light-emitting diodes. The abiotic stress identify was evaluated on a randomized block (5×5) trial on 250 plants of *Pelargonium spp.* LAI and VARI indexes showed to be suitable to highlight the growth stages of plants. Finally, the spreading of an infection was evaluated on *Mandevilla spp.* The highest correlation was found using image analysis indexes. According to these results, RGB-NIR cameras can be profitably used in the greenhouse environment by I) correcting the incident light, II) combining pixel classification.

A. Zanchin (✉) · M. Sozzi · F. Marinello
Department of Land Environment Agriculture and Forestry, University of Padova, 35020 Legnaro, Italy

e-mail: alessandro.zanchin@phd.unipd.it

M. Sozzi

e-mail: marco.sozzi@unipd.it

F. Marinello

e-mail: francesco.marinello@unipd.it

T. Valentini · A. Pozzebon · C. Duso

Department of Agronomy, Food, Natural Resources, Animals and Environment, University of Padova, 35020 Legnaro, Italy

e-mail: tiziano.valentini@phd.unipd.it

A. Pozzebon

e-mail: alberto.pozzebon@unipd.it

C. Duso

e-mail: carlo.duso@unipd.it

L. Placentino

Phoenix - Ricerca E Tecnologie Ottiche S.R.L., 35127 Padova, Italy

e-mail: phoenix@phoenix-rto.it

Keywords Integrated Pest Management · Image Analysis · Precision Agriculture · Light Conditions

1 Introduction

Greenhouses and protected cultivations are widespread in many Italian regions. However, horticulture and floriculture are the primary agricultural sectors that exploited greenhouse structures more. Greenhouses can have many shapes, they can be made of plastic materials or glass, but all of them have the same function to control the ambient inside the structure. Greenhouses work to create an optimum environment for plant growth, preserving temperature, humidity, and light intensity management. Achieving optimum plant growth means increasing crop yield and the whole production process efficiency [1, 2].

Much manual labor is needed for seeding, plant maintenance operations, gathering and packaging. Due to labor costs increasing and lacking skilled labor, many operations have been replaced by machines and automation systems [3]. Irrigation and environmental control are the two operations most automatized [4].

Other authors explored the field of plant disease detection and fruit counting by image analysis [5, 6]. RGB cameras and multispectral sensors are proven devices to check plant growth and detect plant diseases in greenhouses. While RGB cameras retrieve a colored picture of the target, multispectral sensors can give additional information about the lights reflected by plants.

The Raspberry Pi cameras are cheap but affordable devices for plant and crop monitoring. Raspberry Pi exploits a multichannel camera capturing light from the visible to the infrared range of the light. Raspberry Pi boards have been used in agriculture for a wide range of scopes, in particular, to control tools and storage sensors measurement [7, 10]. Researchers used the Raspberry board and camera to detect weeds among the crop to optimize the herbicide spraying. to monitor plant development and stress due to water deficiency [9, 11, 12]. In addition, the sensor channel can be modified applying specific light filters on the camera [13].

This study aims to implement a robust and cheap monitoring system suitable for greenhouses conditions based on image and spectral analysis. Based on the above-mentioned successful experiences, the proposed module consists of a sensor, a master device, and a router access point. The sensor can work under extreme temperature, humidity, and dust conditions. Trials take part in laboratory conditions and greenhouses to test the implementation affordable and identify issues and any possible improvements. More in detail, one trial took place in a laboratory to detect the influence of natural and artificial light on plant reflectance. Two trials took place in greenhouses to monitor both young and adult plants. Two analysis techniques were compared, spectroscopy and image analysis.

2 Materials and Methods

Monitoring Unit. The sensor was composed of a Raspberry Pi board, and three multi-channel cameras compatible with Raspberry boards. The board had an individual supplying cable and a WI-FI antenna. The master device consists of a Raspberry Pi board working with the Linux-based operating system Raspbian Buster. The master device has an interface designed in Python programming language that allows to store data and manage the primary sensor's settings. Each camera module captures and sends the photos to the master device thanks to the Wi-Fi network provided by a router. Each one of the three cameras were assigned to capture some specific wavelength as resumed in Table 1.

Monitoring Techniques. The analysis followed both spectroscopy and image segmentation techniques. Thanks to the multispectral sensor the reflectance of red (R), blue (B), green (G), and near-infrared radiation (NIR) were available in each photo. Many vegetation indexes (VI) are available to compare the band's reflectance, Table 2. The RGB images were useful to extract additional features such as texture, shape, colour, and boundary from the colour of the pixel following the considerations evidenced by [14, 15]. Image segmentation allows computing the area covered by specific features for example healthy leaves, background, and dead leaves.

Table 1 Camera's specifications

Camera name	Light	Wavelength (nm)	Resolution
Camera RGB	Whole visible spectrum	400 ÷ 1000	3280 × 2464 pixels
Camera red	Red	600 ÷ 650	3280 × 2464 pixels
Camera NIR	NIR	850 ÷ 1000	3280 × 2464 pixels

Table 2 The Table lists the VI computed in the present study. The letter means the absorbance value of red (R), blue (B), green (G), and near-infrared (N) bands. LAI and DLI are two indexes computed from the image analysis

Name	Abbreviation	Formula
Normalized Vegetation Index	NDVI	$(N-R)/(N+R)$
Enhanced Normalized Vegetation Index	ENDVI	$(N+G-2B)/(N+G+2B)$
Enhanced Vegetation Index	EVI	$(N-R)/(N+6R-7.5B+1000)$
Visual atmospheric resistance Index	VARI	$(G-R)/(G+R-B)$
Ratio vegetation Index	RVI	R/N
Green Normalized Difference Vegetation Index	GCVI	$(N/G)-1$
Leaf Area Index	LAI	Green leaves/Total pixels
Dead Leaf Index	DLI	Dry leaves/Total pixels

Trials. Three trials took part in 2020 and 2021 in the northeast of Italy, the Veneto region.

Rose. 75 young plants of *Rosa rugosa* were bred into a laboratory of the University of Padua and they have been monitored for 14 days taking photos every day. The sensor and a LED light strip were mounted upon a dark box. Each day a white cotton target and a black one was laid on the plants and captured too. Vegetation, white, and black targets were captured at natural light (N), LED light (L) closing the dark box, and natural light with LED (N + L) with the LED lighting and dark box open. The dataset was split into cloudy and sunny days according to the natural light conditions. Spectroscopy analysis was carried out on R and NIR. Image J (National Institutes of Health) is the software used to extract each band's reflectance from the photos. Then, the percentage difference of R, NIR, and NDVI of L with N and L with L + N was computed for every photo. In addition, the R and NIR ratio (R/N) was computed at each light condition. Finally, multifactorial analysis of the percentage differences was carried out to find differences according to the light sources. Because the trial occurred in winter, rose plants did not grow up, and the sampling dates were considered as repetitions.

Mandeville. "Mandeville" took place at Soc. Agr. Vergerio on ready-to-sell adult plants of *Mandevilla spp.* During this trial, the sensor was mounted on the irrigation boom exploiting the automatic movement of the boom. Mandeville plants were distributed on 9 Tables measuring 15.5 m in total length. The distance between Mandeville's canopy and the camera was about 1.10 m. Considering the camera's field of view was 1.2 m wide, 40 plants per Table were monitored for a total of 360 plants. Plants were monitored every 3 days for 35 days. The Plants were classified according to a disease scale for assessing a bacterial infection spreading. The rating scale was ranged from 0 to 4 split based on the percentage of yellow/brown leaves. In each survey, the average disease score was computed per Table. The irrigation boom forward speed was 0.07 m/s and the camera took a photo every 2 s ensuring 88% overlapping between consecutive photos. It has been decided to ensure at least the 80% of overlapping, due to the high concentration of objects and particulars. The whole orthophoto of the monitored area was built thanks to the software Agisoft Metashape (Agisoft LLC). The orthophotos were elaborated in ArcGIS Pro, applying a mask to cut each of the nine Tables. The spectroscopy analysis was carried out in ArcGIS Pro (Esri), R, G, B and NIR were extracted from each feature to compute the VI. Finally, the orthophoto was analyzed on Food Color Inspector (Cofilab) for the pixel classification in healthy and dead leaves. A principal component analysis (PCA) and a longitudinal ANOVA were carried out on RStudio (version 1.2.1335 © 2009–2019 RStudio) to detect the best indexes for the sick plants recognition.

Geranium. "Geranium" took place at Gruppo Padana Ortofloricoltura S.S. on young plants of *Pelargonium spp.* The trial aimed to monitor the growth of geranium after their transplanting of two stems cutting per plot. Five box rows were arranged 30 m along with the greenhouse. Each box contained ten plots. Five blocks were chosen every six rows, and some artificial damages were carried out as resumed in Fig. 1. While double irrigation occurred at each irrigation time, the artificial damages were repeated every two weeks. The camera was mounted on the irrigation boom

Block 1	Block 2	Block 3	Block 4	Block 5
5 Control	4 Irrigation x2	3 Stem -1	1 Bites	2 Defoliating
4 Irrigation x2	3 Stem -1	1 Bites	2 Defoliating	5 Control
2 Defoliating	1 Bites	4 Irrigation x2	5 Control	3 Stem -1
1 Bites	5 Control	2 Defoliating	3 Stem -1	4 Irrigation x2
3 Stem -1	2 Defoliating	5 Control	4 Irrigation x2	1 Bites

Fig. 1 Experimental design for the Geranium trial. A randomized block design was chosen. Five treatments are indicated with different colour, number and name. All treatments were repeated in five blocks

and the distance between the camera and the canopies was 1.20 m. Photos were taken each 3 s because the boom forward speed was 0.29 m/s. Monitoring followed the same methods for the Mandevilla trial. The growing trend of each treatment was investigated on a longitudinal ANOVA.

3 Results

Rose. The main results of the multifactorial analysis are resumed in the charts in Figs. 2 and 3. There has never been a difference between light sources in white targets and vegetation at high natural light intensity. On the contrary, significant differences between light sources have been found in cloudy days on NDVI in the white target and vegetation. Large differences were found between the absorbance intensity on R/N of the white target in L + N and L, while the average R/N appeared more smoothed on the vegetation. The black target was the less affected by all the other light conditions. Looking at the mean standard errors, L showed the most stable measures, while N data are very scattered. L + N is always ranged between L and N.

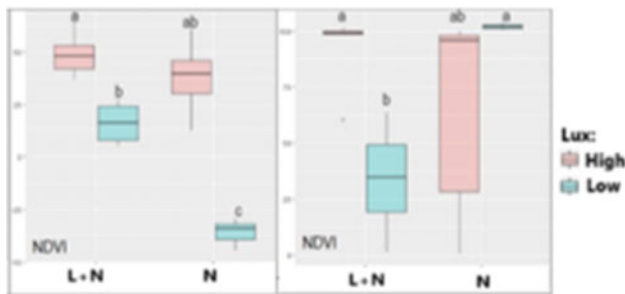


Fig. 2 The box plots display the percentage difference of reflectance bands between L with L + N, and L with N. left chart is referred to white target, while the right one is referred to vegetation. Lux means the natural light intensity

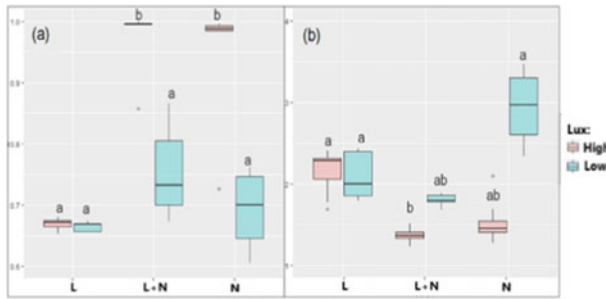


Fig. 3 The box plots display the R/N in L, L + N, and N. Chart **a** is referred to the white target, while chart **b** is referred to vegetation

Table 3 Multifactorial analysis outputs. “***” means a p-value < 0.001, “**” means a p-value < 0.01, “*” means a p-value < 0.05, while “N.S.” means not significance

Factor	LAI	DLI	NDVI	ENDVI	EVI	GCVI	VARI	RVI
Disease	***	***	N.S	***	N.S	***	*	N.S
Date	***	**	**	***	***	***	***	*
Interaction	N.S	N.S	N.S	*	N.S	N.S	N.S	N.S

Mandeville. The outputs of multifactorial analysis between the disease score and the sampling date are resumed in Table 3. Apart from NDVI, EVI, and RVI, the other indexes strongly differ between disease classes. According to the PCA, ENDVI DLI and LAI are the most correlated with plant disease severity. ENDVI is the only VI from spectroscopy highly correlated with plant disease severity. The charts in Fig. 4 display the regression line between the indexes and the disease rating. The average reduced the classes range from 0 to 2. While the disease classes are well separated in DLI and LAI, classes are smoothed in ENDVI and NDVI.

Geranium. The slope of the regression line between the index and the time was investigated in every box. Thus, the regression line comparison of each thesis was based on the Fisher Z-Transformation. The main results suggest that LAI and VARI are the most robust indexes to detect different plant growth trends, particularly in the first 30 days. As shown in the charts (a) in Fig. 5, box 2 and 3 have a lower slope than 5 and 1. Box 4 has got the highest slope. In VARI (a), boxes 2 and 3 have a lower slope than 5 and 1, while only box 2 is lower than box 4. Box 2 shows the lowest slope while box 4 shows the highest slope of the regression line for LAI in 30 days period. Compared to LAI, VARI lost much more precision because in 30 days only box 2 showed a regression line slope lower than the others. After 30 days, it was impossible to find differences between any boxes and VI.

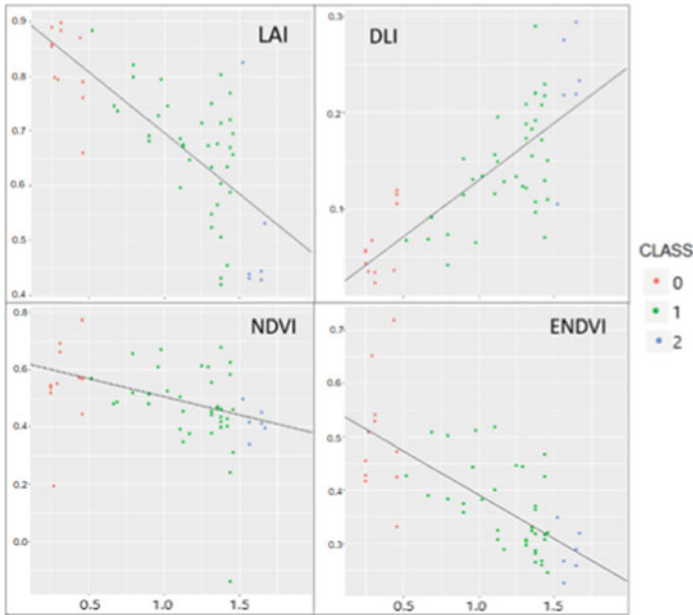


Fig. 4 The scatter plots represent the sample distribution among disease ratings on the horizontal axis and the measured index on the vertical axis. Different colour indicates the disease severity class. The black lines describe the regression lines between the disease rating and the index values

4 Discussion

Rose. The Rose trial focused on the need to measure and take note of the light intensity. NIR reflectance and NDVI of vegetation are affected by natural light. Also, R and NIR reflectance of white objects and NIR of black are strongly affected. Black and white object are important as vegetation because they could represent the background effects. Artificial light reduces the scattering measures due to the natural light intensity.

Mandeville. For this trial purpose, the image indexes DLI and LAI are the most powerful to monitor the bacterial infection spreading among plants. In particular, the DLI better represents the health status trend of each Table with Mandeville. Consequently, the detection of specific pixels could be a more precise technique than spectroscopy analysis for the sick plant detection.

Geranium. All the regression lines have a positive slope due to plant growth and biomass increasing. LAI and VARI are the most accurate indicators for monitoring young geranium plant growth. Moreover, LAI distinguished many more issues than VARI. However, it has been verified only for the first 30 days period. After that, any indexes could detect differences among boxes growing. Maybe, it was due to the significant biomass increase, and the overlapping of many leaves layer could saturate the monitoring area.

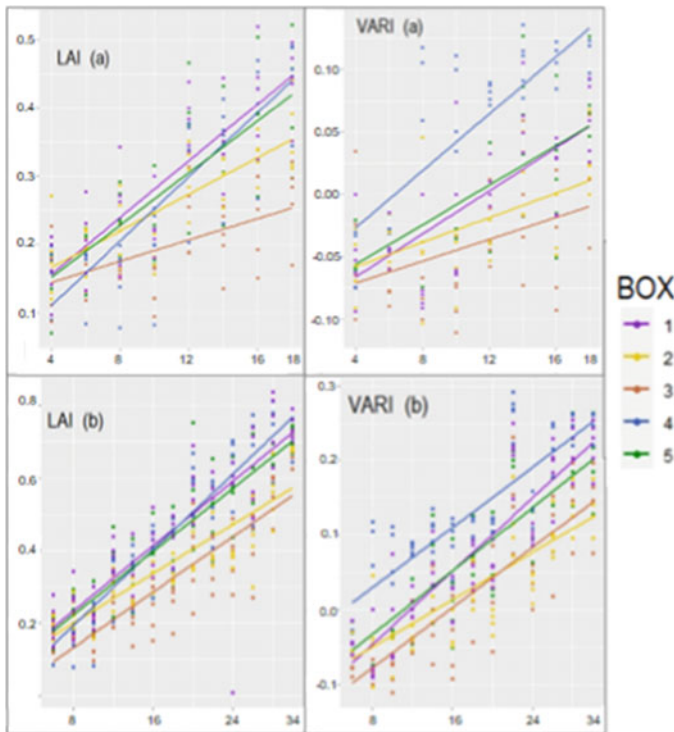


Fig. 5 The scatter plots represent the sample distribution among sampling dates on the horizontal axis and the measured index on the vertical axis. Different colours indicate the boxes. Each line figures the regression line between the sampling date and the index values

5 Conclusions

The presented study investigated the crucial issues in greenhouses crop monitoring using a multispectral camera. The natural light intensity can affect R and NIR proportion of the reflected light from both vegetation and the background. Using an artificial light source can reduce the disturbing effects of natural light. Image segmentation techniques seem to be the most precise method to monitor adult plant health. Among the studied indexes, LAI and VARI are the best indexes for young plants' development monitoring and detection of boxes affected by biotic and abiotic issues, or wrong farming practices. Finally, the greenhouses trials proved the availability of embedding a multispectral camera to the irrigation boom for crops monitoring while the boom moves.

Acknowledgements The authors would like to acknowledge all the partners of the project "FLORORTO". The project was financed by the PSR Veneto 2014-2020, Misura 1.1.1/16.1.1/16.2.1-DGR 736-2018.

References

1. Reddy, P.P.: Sustainable crop protection under protected cultivation. In: Sustainable Crop Protection under Protected Cultivation, pp. 1–434, January 2016. <https://doi.org/10.1007/978-981-287-952-3>.
2. Cillis, D., Pezzuolo, A., Marinello, F., Sartori, L.: Field-scale electrical resistivity profiling mapping for delineating soil condition in a nitrate vulnerable zone. *Appl. Soil Ecol.* **123**, 780–786 (2018)
3. Ghosh, C., Biswas, P.: Horticulture Mechanization-stepping towards increased farm income. *SATSA mukhapatra* **25**, 129–137 (2021). [Online]. <https://www.researchgate.net/publication/357899837>. Accessed 2 May 2022
4. Posadas, B.C.: Socioeconomic determinants of the level of mechanization of nurseries and greenhouses in the southern United States. *AIMS Agric. Food.* **3** (2018). <https://doi.org/10.3934/agrfood.2018.3.229>.
5. Schor, N., Berman, S., Dombrovsky, A., Elad, Y., Ignat, T., Bechar, A.: A robotic monitoring system for diseases of pepper in greenhouse. In: Precision Agriculture 2015 - Papers Presented at the 10th European Conference on Precision Agriculture, ECPA 2015, pp. 627–634 (2015). https://doi.org/10.3920/978-90-8686-814-8_78
6. M. Sozzi, S. Cantalamessa, A. Cogato, A. Kayad, and F. Marinello.: Automatic bunch detection in white grape varieties using YOLOv3, YOLOv4, and YOLOv5 deep learning algorithms. *Agronomy* **12**(2), 319 (2022). <https://doi.org/10.3390/AGRONOMY12020319>.
7. U. Shafi, R. Mumtaz, J. García-Nieto, S. A. Hassan, S. A. R. Zaidi, and N. Iqbal, “Precision agriculture techniques and practices: from considerations to applications. *Sensors* **19** (17), 3796 (2019). <https://doi.org/10.3390/S19173796>
8. Ardiansah, I., Bafdal, N., Suryadi, E., Bono, A.: Greenhouse monitoring and automation using Arduino: a review on precision farming and Internet of Things (IoT). *Adv. Sci. Eng. Inf. Technol.* **10**(2), 704–709 (2020). <https://doi.org/10.18517/ijaseit.10.2.10249>
9. Ramos-Giraldo, P., *et al.*: Low-cost smart camera system for water stress detection in crops; low-cost smart camera system for water stress detection in crops (2020). doi: <https://doi.org/10.1109/SENSORS47125.2020.9278744>.
10. B. Patil, H. Panchal, S. Yadav, A. Singh, and D. Patil, “Plant monitoring using image processing, raspberRY PI & IOT. *Int. Res. J. Eng. Technol.* **4**(10), 1337–1342 (2017). [Online]. www.irj.et.net. Accessed 24 Jan 2022
11. R. Aravind, M. Daman, and S. Kariyappa, B, Design and development of automatic weed detection and smart herbicide sprayer robot; Design and development of automatic weed detection and smart herbicide sprayer robot (2015). <https://doi.org/10.1109/RAICS.2015.7488424>.
12. Valle, B., *et al.*: PYM: a new, affordable, image-based method using a Raspberry Pi to phenotype plant leaf area in a wide diversity of environments. *Plant Methods* **13**(1) (2017). <https://doi.org/10.1186/s13007-017-0248-5>
13. Daroya, R., Ramos, M.: NDVI image extraction of an agricultural land using an autonomous quadcopter with a filter-modified camera. In: 7th IEEE International Conference on Control System, Computing and Engineering, pp. 110–114 (2017)
14. Marinello, F., Bariani, P., de Chiffre, L., Hansen, H.N.: Development and analysis of a software tool for stitching three-dimensional surface topography data sets. *Meas. Sci. Technol.* **18**(5), 1404–1412 (2007). <https://doi.org/10.1088/0957-0233/18/5/028>
15. Marinello, F., *et al.*: Increase of maximum detectable slope with optical profilers, through controlled tilting and image processing. *Meas. Sci. Technol.* **18**(2), 384 (2007). <https://doi.org/10.1088/0957-0233/18/2/S09>.

Low Dose Precision Distribution with Micro-Granules Fertilizer Using Different Spreader Machines



N. Zucchiatti and R. Gubiani

Abstract Field fertilisation trials were conducted in the province of Udine to test a new organic biostimulant for agriculture produced from amino acids and peptides by the SICIT Group's research and development centre in Vicenza.

The fertiliser under test was in the form of both micro-granules with a size of around 0.5 mm and cylindrical tablets (pills) with sizes ranging from 3 to 5 mm.

The aim of the trial was to test the fertiliser at low-dosage fertiliser with quantities distributed across the field that ranged from 5 to 20 kg/ha. Tests were carried out using two types of fertiliser spreader with a micro-granulator distribution system for row crops and a centrifugal fertiliser spreader for full-field fertilisation. The results obtained showed a good regularity and uniformity of distribution considering the low dose of fertiliser per hectare distributed.

Keywords Fertiliser · Low-dosage fertiliser · Micro-granules · Spreader

1 Introduction

In any agricultural and horticultural crop, the rapid development of a strong root system is a fundamental condition for expressing the full production potential; this is due to better exploration by the roots of the soil and the formation of more vigorous reproductive structures. The distribution of trace elements and a targeted amount of nitrogen are an important factor in this process. Nitrogenous fertilisers also play a key role in plant development and growth. Their importance is significant because nitrogen is a basic component in the formation of plant tissue cells. It also influences plant metabolism, entering into the formation of substances such as amino acids and enzymes, as well as a large number of hormones and vitamins.

At the same time, the use of chemical fertilisers in excess of actual needs can give rise to environmental problems [1]. This latter aspect, in the light of a highly

N. Zucchiatti (✉) · R. Gubiani

Department of Agri-Food, Environmental and Animal Sciences, Udine, Italy

e-mail: nicola.zucchiatti@uniud.it

articulated regulatory framework and an increasing attention to environmental issues, is of growing interest today.

There are numerous techniques for distributing farmyard fertilisers, recycled fertilisers and mineral fertilisers. Over the years, the significant technical advances applied to distribution methods have made it possible to increase the precision of doses and the homogeneity of spreading, guaranteeing the plants a supply of fertilisers suited to their needs [2]. With reference to mineral fertilisation, this can be carried out with fertiliser spreaders with localised distribution on the row using pneumatic systems and machines with a release system for fertilisers in the form of micro-granules or by scattering using, among the numerous types on the market, centrifugal driven machines for open field crops [7].

For precise distribution of mineral elements, even at doses varying between 5 and 20 kg/ha, both pneumatic or micro-granulator-type spreaders and centrifugal-type spreaders can generally be used. The pneumatic fertiliser spreader has the advantage over the centrifugal type of spreader in that it does not require overlapping passages for better product delivery, since the homogeneity of spreading is guaranteed by the technical and construction solutions. The pneumatic fertiliser spreader can be used for fertilisers in the form of micro-granules or possibly reduced to powder, while it cannot be used at all for crystals and pelleted fertilisers. The Micro-granulator system equipped the seeding machine and mounted worm screw systems that can be operated either mechanically, with an electric motor or hydraulically, ensuring high precision in fertiliser distribution. The centrifugal fertiliser spreaders are the machines currently most widely used for the distribution of mineral fertilisers, appreciated by users for their simple construction and low cost. Carried type machines are equipped with hoppers with a capacity of between 0.4 and 2 m³, while trailed ones can reach up to 10 m³. They are able to achieve high working capacities, and at the same time, especially in the double-disc models, ensure good distribution uniformity by achieving positive coefficients of variation. Centrifugal spreaders are based on the action of one or two gravity-fed turntables with hopper with adjustable discharge lights and rotating agitator and they can have a variable working width from 6 to 24 m and more. The performance of the distribution system depends on the correct working configuration of the spreader, particularly in terms of height, longitudinal and transverse inclination, while the working width depends mainly on the size of the fertiliser granules and the setting of the discs. In this respect, the physical-mechanical properties of the fertilisers are an important key to ensuring exact and precise distribution. These properties, which often vary depending on the production process of the fertiliser itself, are collectively represented by the following items: density; shape, diameter, harness, fluidity [6].

The aim of the experimental trial was to analyse the field distribution (with varying fertiliser dosages from 5 to 20 kg/ha) of a starter fertiliser that comes in two different production types - micro-granules and cylindrical tablets (Fig. 1).

Fig. 1 The two types of fertiliser used in the field trial



2 Materials and Methods

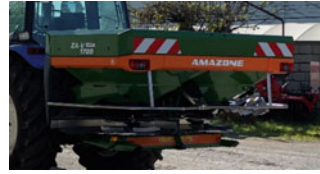
Three types of fertiliser spreaders were used for this purpose. A precision fertiliser spreader, equipped with a micro-granulator, from Kverneland and two centrifugal spreaders from Kverneland and Amazone respectively.

- 1) The first machine is a Kverneland precision pneumatic seeder of the Optima HD e-drive type used on maize, sunflower, etc. (Fig. 2). The precision seed drill, an eight-row, semi-mounted type with a 75 cm row spacing, consists of a frame with a fixed, load-bearing structure, a three-point hitch and a pair of wheels with a support function. Equipped with a telescopic frame, the elements are inserted in maintenance-free plastic slides and positioned on the square frame. With a working width of 8 m and a 900 l central hopper, it is combined with a 1200 l front fertiliser tank with an internal partition. The fertiliser distributors, one for every two seeding units, are of the volumetric type and consist of a honeycomb wheel with centralised manual adjustment and chain drive. The drive unit, moved by a rubber wheel in contact with one of the two support wheels, is connected to the distributor via a direct-drive chain system (comprising interchangeable toothed gears). The fertiliser coulter, consisting of a double disc with a straight profile and toothed edge, is connected to the frame via a spring-loaded elastic support.
- 2) The second fertiliser spreader, a centrifugal type, used for the field trial was an Amazone model ZA-V 1700 (Fig. 3). The machine is equipped with a weighing system and proportional spreading (DPA), the electronic management of the

Fig. 2 Kverneland Optima seed drill with microgranulators



Fig. 3 Amazone ZA-V fertiliser spreader used for the second field test



opening of the fertiliser lowering bulkheads, as well as the adjustment of the electric border device and the management of the working sections, are controlled by a Trimble XCN 1050 monitor. The system can adjust the maximum spreading width and spreading profile by adjusting the length of the spreading vanes and the position of the fertiliser drop point on the vanes. In other models, hydraulically driven, it is also possible to act on the rotation speed of the discs. Communication is managed according to ISOBUS protocols and the Trimble terminal is connected to the GPS antenna receiving EGNOS signals (± 20 cm). The tank has a capacity of 1700 l.

The machine can work with an effective width of between 10 and 21 m, which is adjusted by moving the spreading vanes on the two discs according to the indications provided by the special tables. The rotational motion of the discs is transmitted via the tractor's power take-off. The spreader is driven by a New Holland T5.120 Auto Command tractor (88 kW).

- 3) The third machine used is Kverneland's Exacta CL Geospread model fertiliser spreader with centrifugal operation (Fig. 4) [3]. With a working width ranging from 10 to 33 m, it has a hopper capacity of 2000 L and is equipped with automatic control of the spreading sections and rate, guaranteeing exact fertiliser coverage in a single pass.

The weighing system ensures even extreme distribution in irregular fields or on hilly slopes, thanks to a 4-cell load cell weighing system with reference sensor and automatic calibration system. Centrifugal spreading is ensured by uniform initial acceleration of the fertiliser, which prevents fragmentation of the granules when they impact on the blades. The adjustable discharge point also allows the settings of the main fertiliser properties to be adjusted. The fertiliser is spread by two centrifugal discs, each equipped with eight blades, which ensure a variable spreading width from 9 to 36 m, guaranteeing a continuous fertilisation flow in the field.

With this machines we carried out 3 test:

Fig. 4 Kverneland Exacta CL Geospread used for the third field test





Fig. 5 Plastic boxes used for field trials **a** and **b**

- 1) First field tests were carried out on July 2021 in Buttrio (UD) with Kverneland's centrifugal spreader model Exacta CL Geospread connected to a Deutz Fahr DX 3.60 tractor. The working height of the spreader was set at 90 cm above the vegetation line and the forward speed set at 7 km/h. Subsequently, 13 plastic boxes measuring $55.5 \times 39.0 \times 28.5$ cm were placed on the ground and placed at a distance of 1.5 m from each other for a total width of 18 m [4, 5]. A rough silicone mat was placed inside each box to prevent bouncing (Fig. 5). The weight of 10 cylindrical tablets (tabs) of mineral fertiliser was also calculated, which was equivalent to 0.3 g. For the field test, the centrifugal spreader was adjusted to distribute 10 and 20 kg/ha of mineral fertiliser respectively. Four passes were made for each dosage. After each pass, the pelleted granules were counted for each container and subsequently weighed using a Gibertini precision balance (sensitivity 0.01 g).
- 2) The second test was carried out with Kverneland's 7-row variable-width seed drill model Optima HD and driven by a Deutz-Fahr 6160.4 TTV tractor.

The fertilisation test was carried out by covering a stretch of land of approximately 100 m in order to operate the micro-granulator distribution system. Four repetitions were carried out. The calculated average of fertiliser actually distributed was 6.56 kg/ha.
- 3) Third test with Amazone model ZA-V 1700 centrifugal fertiliser spreader was used. The working height of the spreader was set at 90 cm above the vegetation line and the forward speed set at 7 km/h. A New Holland T5.120 AutoCommand tractor (88 kW) was used for the fertilisation test.

The following materials were used for the fertilisation test: 13 polyethylene boxes measuring $555 \times 390 \times 285$ mm positioned 1.5 m apart for a width of 18 m; wrinkled silicone mats positioned inside the boxes to prevent rebound of the captured fertilizer;

AccuWeight precision scales with a maximum capacity of 300 g and 0.01 g sensitivity; metric string. The boxes were placed at a distance of 1.5 m from each other and perpendicular to the direction of travel of the tractor, with the long side in the direction of travel. The boxes were positioned within the roadway. The distribution uniformity was measured in both directions to simulate a classic distribution under normal conditions. The spreader was placed at a height of 0.90 cm above the ground and the speed was 7 km/h.

A graph showing the distribution curves was subsequently created for all test using Microsoft Excel software.

3 Results

In the first test no significant differences emerged between the distribution diagrams in the four replications carried out ($P > 0.05$) and therefore the average values are shown below. The distribution diagrams obtained show a triangular shape typical of two-disc centrifugal spreaders (Fig. 6 and 7).

In the second trial, Figs. 8 and 9 show the distribution diagram with the distribution dose set at 20 kg/ha and calculation of distribution variability.

As can be seen from the graphs, the distribution obtained, using the two doses of pelleted fertiliser (10 and 20 kg/ha), are comparable to the theoretical distribution curves for centrifugal spreaders with the same technical characteristics and reduced dosages.

Third test with fertiliser spreader equipped with micro-granulator distribution system and the average amount of fertiliser distributed was 6.56 kg/ha a result very

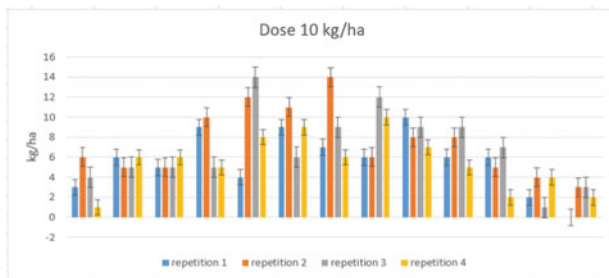


Fig. 6 Spreading fertilizer at 10 kg/ha

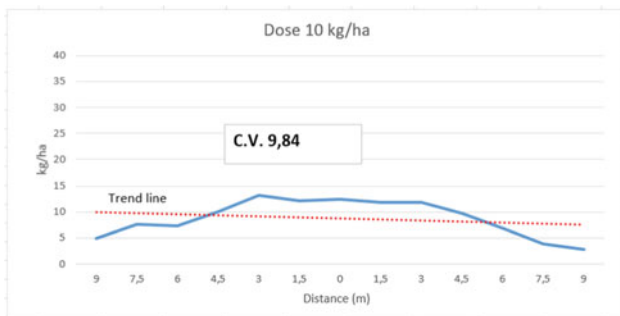


Fig. 7 Average distribution obtained with 4 replication with a distributed dose of 10 kg/ha

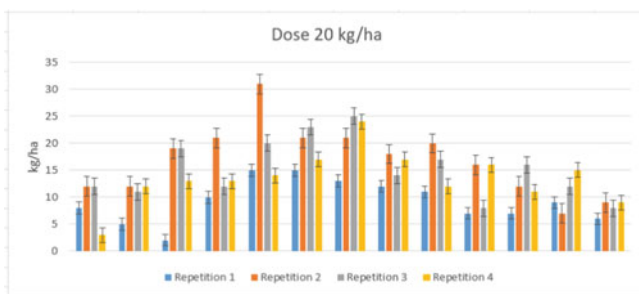


Fig. 8 Spreading fertiliser at 20 kg/ha



Fig. 9 Average distribution obtained with 4 replications with distributed dose of 20 kg/ha

similar to the use of a granular nematicide insecticide such as Counter. The trials therefore showed how, with Kverneland’s, precise fertiliser distributions in the form of micro granules were obtained.

The fertilisation trial conducted using the Amazone spreader showed that fertiliser doses close to 5 kg/ha could be distributed. Fertiliser distribution as well as distribution uniformity was good with a reduced C.V. of less than 10%. The result was similar to the first trial conducted in July 2021.

This indicates that the pelleted fertiliser in blue SICIT tablets can be easily and precisely distributed with the centrifugal type machines currently used on almost all farms of a certain level and certainly those that do precision farming and consequently agriculture 4.0 (Fig. 10).

Test with micro-granulator Kverneland seed drill (Fig. 11) using fertiliser in the form of pelleted micro-granules to avoid the problem of hygroscopicity that we had encountered during the July 2021 test. For the test, the fertiliser spreader, adjusted to three different positions, guarantee a distribution of kg/ha of 3.16, 2.2 and 4.21 without any problems with the outflow.

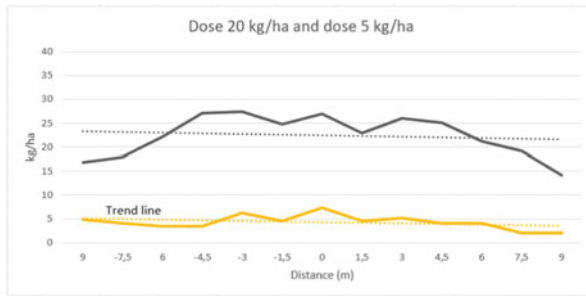


Fig. 10 Distribution diagram with 5 and 20 kg/ha with Amazone ZA-V 1700 spreader

Fig. 11 Kverneland seed drill with microgranulators for localised distribution in the row



4 Conclusions

The main objective of fertilisation is to obtain as even a distribution of fertiliser as possible over a plot, using specific machines. This allows homogenous fertilisation throughout the field, avoiding deficiency phenomena or excesses and thus guaranteeing a good yield in production.

To achieve this objective, certain precautions must be taken depending on the soil, the crop and the state of the field being treated.

To avoid errors, the main quantities to be taken into account when spreading are.

- dose: the quantity of product distributed per unit area (kg/ha);
- flow: the quantity spread per unit of time, expressed in kg/min;
- working width: the distance between two neighbouring passes of the spreader. It is also the distance between the passages;
- spreading width, or projection: is the distance of the spreading layer in a direction perpendicular to the travel of the medium;
- coverage width: the difference between the spreading width and the working width.

Given these factors, the objective is therefore to obtain a regular distribution, which depends on the uniformity of the fertiliser exiting the spreading disc and the working coverage between the two passes, outward and return.

Tests carried out in the open field, at farm in Buttrio (UD), and at the farm in Castions di Strada (UD), showed good regularity and uniformity of distribution, considering the low dose of fertiliser per hectare distributed (5–10–20 kg/ha).

The distribution curves and the coefficient of variability obtained are, in fact, technically comparable with the main types of centrifugal fertiliser spreaders on the market equipped with double distribution discs.

The distribution test performed with the precision seed drill equipped with a micro-granulator device confirmed the good quality and precision of distribution. The only drawback noted was the high degree of hygroscopicity of the mineral fertiliser in the form of micro-granules, which led to clogging of the distribution system at the end of the distribution operation. This problem was overcome by using pelleted micro-granules in the second trial.

In conclusion, both types of fertiliser, pelleted and micro-granules, can be distributed either open-field or localised on the row. In the latter case, doses can be as low as 1–5 kg/ha.

References

1. Hofstee, J.W.: Handling and spreading of fertilizers: part 2, physical properties of fertilizer, measuring methods and data. *J. Agric. Eng. Res.* **53**, 141–162 (1992)
2. Balsari, P., Airoidi, G., Casa, R.: Trattamenti fitosanitari in agricoltura di precisione. In: Casa, R. (ed.) *Agricoltura di precisione*, Edagricole, pp. 301–328 (2016)
3. Cavalli, R.: Analisi della distribuzione di una miscela di fertilizzanti solidi mediante spandiconcime di tipo centrifugo. *Macchine e Motori Agricoli* **10**, 13–20 (1984)
4. EN 13739-1, Agricultural machinery – Solid fertilizer broadcasters and full width distributors – Environmental protection – Part 1: Requirements, European Standard (2003)
5. EN 13739-2, Agricultural machinery – Solid fertilizer broadcasters and full width distributors – Environmental protection – Part 2: Test methods, European Standard (2003)
6. Fiala, M., Oberti, R.: Prove di un DPPE per il controllo della distribuzione su uno spandiconcime ad azione centrifuga. In: *Atti del VI Convegno Nazionale di Ingegneria Agraria*, Ancona, pp. 557–565 (1997)
7. Hofstee, J.W., Huisman, W.: Handling and spreading of fertilizers Part 1: physical properties of fertilizer in relation to particle motion. *J. Agric. Eng. Res.* **47**, 213–234 (1990)

**Part III: Smart Engineering Techniques,
Design and Planning of Resilient Land
and Built Systems**

Local Community's Perception of Agrobiodiversity as Cultural Heritage and the Role of *Ceratonia Siliqua* L. in Characterizing the Rural Landscape Identity of Modica and Rosolini (Sicily-Italy)



Abbate Rosaria, Menconi Maria Elena, and Grohmann David

Abstract This paper develops a proposal to valorize the *Ceratonia siliqua* L. (carob) in two Sicilian municipalities (Rosolini and Modica, Italy). The carob tree in this area is a crucial resource for understanding the identity of the rural local landscape since the first descriptions of the island's flora. Furthermore, it has a significant productive value, representing the municipalities with the highest numbers of carob trees of the Free Municipal Consortiums of Ragusa and Syracuse, covering 98% of the Italian production. Carob's production in Italy follows only the production of Portugal at the international level, covering 14.36% of world production. At the same time, the carob trees often are located in marginal agricultural areas, and the local communities do not recognize their value.

For this reason, the method uses a multi-stakeholder approach to involve the elderly living in the municipalities, the farmers producing the carobs, and the local product storage and processing companies. The method develops a network to activate cooperation between stakeholders producing a collaborative GIS map dedicated to the carob as the main result. This map highlighted the rural dimension of Modica and Rosolini and allowed sharing of memories, practices, recipes, and moments between local communities and companies. Furthermore, the map can be used for the tourist promotion of carob plants by sharing it online using standard devices (smartphones, tablets). The paper also develops two tourist paths dedicated to *Ceratonia siliqua* L., its products, its traditional and actual uses, and the rural landscape.

Keywords Rural landscape · Agrobiodiversity · Collaborative maps · Participatory process · Carob supply chain

A. Rosaria (✉) · M. M. Elena · G. David
University of Perugia, 06122 Perugia, Italy
e-mail: rosaria.abbate@outlook.it

M. M. Elena
e-mail: mariaelena.menconi@unipg.it

G. David
e-mail: david.grohmann@unipg.it

1 Introduction

The improvement of agrobiodiversity is pivotal for the provisioning of ecosystem services in rural areas [5]. Thanks to the complexity of the relationships it hosts, it can influence agricultural production and enhance resilience, well-being, quality of life, and rural landscape. Worldwide, farmers substituted many local crops to achieve higher yields and follow mechanical and standardized cultivation practices [4]. These choices increase earnings quickly, but the food system becomes more vulnerable to shocks [3]. There is a need for more research to develop participatory processes to improve local communities' awareness of the value of agrobiodiversity [11].

1.1 Aim of the Paper

This paper aims to develop a participatory method to valorize *Ceratonia Siliqua* L. in a Sicilian area, improving local stakeholders' awareness of the supply chain's versatility, landscaping value, and contribution to agrobiodiversity.

Section 2 of the paper highlights the value and versatility of this tree in an international context. Section 3 sketches the developed method and reports the main results.

2 *Ceratonia Siliqua* L.

2.1 Description and Uses of *Ceratonia Siliqua* L.

Ceratonia siliqua L., the carob tree, is a typical legume of xerophytic environments and lives well with temperatures until 50 °C and rainfall between 200 and 300 mm per year. It has a slow growth reaching huge dimensions. It's a dioecious specie; therefore, in nature, we find trees bearing female inflorescences, reddish racemes with greenish carobs, and trees bearing male inflorescences. The leaves are green and covered with wax that limits transpiration. It is an evergreen tree. The fruit is a pod initially green and dark brown when ripe. The mature legume comprises a complex and woody brown epicarp, a paler mesocarp rich in sugar, while the epicarp is clear and bright, set in lodges that will house the seeds, which are also called carats (Fig. 1).



Fig. 1 Photo of an ancient carob tree located in Modica (Italy, Sicily region) with some botanical elements

The different parts of the tree have various and significant uses. The traditional and best-known use of its fruit is the zotechnical one, as feed [8]. Over time, scholars found various uses for this tree showing its versatility. The branches and the trunk supply a natural additive to polypropylene filler, capable of increasing its resistance to traction and bending [1], and the foliage supplies a component of biofuels [12]. Carob trees' seeds can be transformed into E-410, an additive and an emulsifier for textiles, cosmetics, food, and pharmaceutical uses [2]. Finally, the pulp of the fruit, which has a high sugar content, is used to produce carob flour, sweets, and bitters.

2.2 *Production of Carobs*

As demonstrated by the FAOSTAT data (Fig. 2), the cultivation of the carob tree in the world has slowly decreased in the last 20 years. The figure report data until the year 2017, because there are not available data for these last few years for European countries. After a slight decrease around 2000, we notice a certain constancy in the area covered with carob trees, associated with alternation of production, linked to the coexistence of fruits and flowers during the harvest and to the price volatility. Indeed, farmers do not collect them when the price is too low.

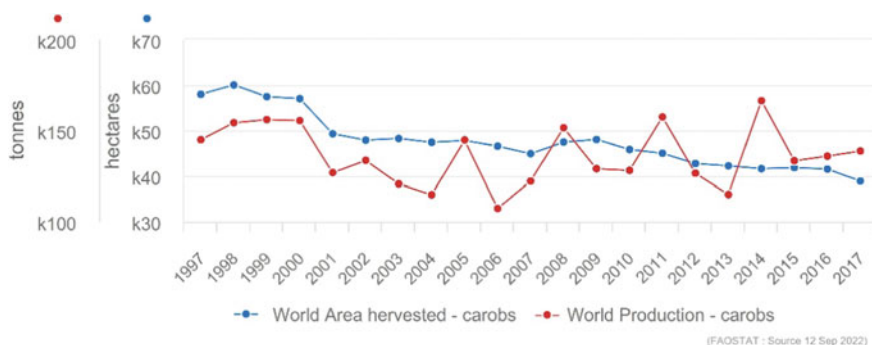


Fig. 2 Production/yield quantities of Carobs in World 1997–2017 (FAOSTAT, 2022)

Table 1 World area harvested in carob tree, year 2017. (FAOSTAT, 2022)

Country	Area [ha] 2017	%
Portugal	13,240	34.11
Morocco	10,234	26.36
Italy	5576	14.36
Spain	2368	6.10
Greece	1757	4.53
Israel	1730	4.46
Cyprus	982	2.53
Algeria	827	2.13
Turkey	674	1.74
Croatia	513	1.32
Lebanon	413	1.06
Tunisia	402	1.04
Ukraine	101	0.26
Total	38,817	100.00

This tree's cultivation characterizes environments in the Mediterranean climate. Indeed, the last evaluation by FAO shows that many Mediterranean countries invest in the production of carob. Table 1 reports area harvested in carob trees. The first producer is Portugal, followed by Morocco and Italy. This podium varies if we refer to the production expressed in tons (Fig. 3), for which Portugal remains the first producer, followed by Italy and later by Morocco. Therefore, it's noteworthy that although Italy dedicates half of the hectares of Morocco to carob trees, it surpasses it in production. Despite Italy being the second producer of carobs worldwide, only eight provinces of three Italian regions cultivate the carob tree. They are Latina (Lazio region), the provinces of Foggia, Bari, Brindisi, and BAT, of the Apulia region, and the provinces of Agrigento, Syracuse, and Ragusa of Sicily. The free consortium

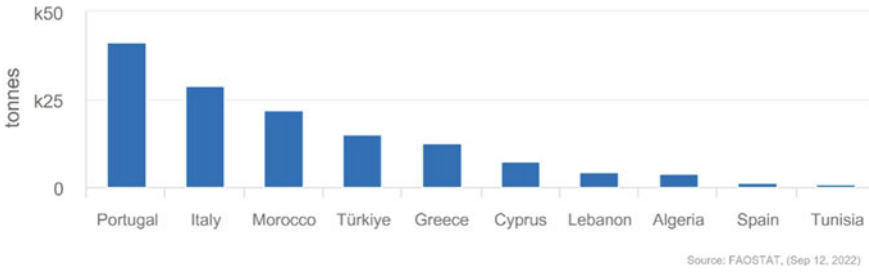
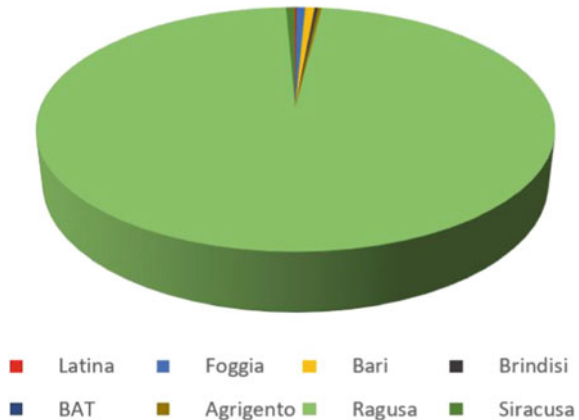


Fig. 3 Top 10 producers of carobs, year 2017 (FAOSTAT 2022)

Fig. 4 Italian provinces producing carobs (ISTAT 2020)



of Ragusa has the most considerable hectares cultivated with carob trees (about the 97%) and produces approximately 98% of the Italian carob beans (Fig. 4).

3 Developing a Collaborative Map to Enhance Sicilian Carob Trees

3.1 Study Area

The study area consists of two neighboring Sicilian municipalities, Rosolini and Modica (belonging to the Free consortiums or Ragusa and Syracuse, respectively). Carob trees have been crucial for understanding the identity of their rural local landscapes since the first descriptions of the island's flora [13]. In the study area, dedicated surfaces and promiscuous cultures consociated with carobs currently cover 52% of Rosolini municipality and 68.7% of Modica municipality. Furthermore, carobs in the study area have a significant production value. Indeed, this area has the highest

number of carob trees of the Free Municipal Consortiums of Ragusa and Syracuse, which covers 98% of Italian production (ISTAT 2020). Despite these considerations, carob trees are in areas cultivated despite their presence, considering them a marginal production. Local communities do not recognize their value and too often neglect them.

3.2 Materials and Method

The participatory process involved inhabitants and local stakeholders belonging to the carob supply chain. As the first step, we interviewed elder inhabitants (over 65 years), developing a survey in Italian and Sicilian to evaluate their sense of belonging to carob trees, asking for memories, traditional practices, and recipes. The second step involved local stakeholders belonging to the carob supply chain. We have created different surveys for producers, storage, and processing companies, with a first section dedicated to memories and a second section to economic aspects and proposals of valorization. Finally, the method develops a network to activate cooperation between stakeholders producing a collaborative GIS map dedicated to the carob. The GIS software are Qgis and Mymaps.

3.3 Results and Discussion

We involved 140 elders living in the study area and all the local companies of the carob supply chain (one producer, one storage, and four processing companies).

93% of the inhabitants identify carob as a characterizing element of the rural territory of Modica and Rosolini. 60% of them listed this tree as representative of their childhood with olive and almond trees. However, all elders evaluated the carob tree as the most important specie for local rural landscape recognizability. We have also asked how they think the significance of the carob tree on the landscape has changed. 6% affirmed not changes, while 74% affirmed that it decreased and 20% increased, due to price changes. From this survey, we can say that, despite the carob tree being a characteristic resource of the local rural landscapes, the attachment of the producers is strongly linked to its value inside the carob chain varying according to the price.

Only one farm has carob trees as the main crop. The name of the farm is “Antico carrubo”. Other farms have carob trees, but they represent a marginal crop and harvest the fruit based on the yearly price. There is only one storage company, “La Valle del sole,” that sells carobs to a processing company producing the additive E-410 outside the study area. However, the study area has four interesting processing companies producing feed and different food for humans as snacks, flour, syrups, pasta, spirits, candies, and flavors.

During the participatory process, we sketched with the involved stakeholders some actions for a mutual enhancement between the local carob supply chain and the whole rural landscape of the two municipalities.

The involved stakeholders affirm that the local rural landscape represents an identity resource able to define a clear brand for the carob supply.

The main result is a collaborative online map on MyMaps (Fig. 5), called “in the shadow of the carob tree,” where the companies share their contact, introduce themselves and offer differentiated activities for building collaborations between them, such as new products, strategies for selling, and activities dedicated to inhabitants and tourists, such as agronomic training or disseminating traditional recipes related to the carob tree. The companies also report their eCommerce site, description, carobs' origin, and participation in national and non-national fairs. The map also shows the cropland of the study area detailing crops consociated with carob trees, the locations that stakeholders defined as characterized by carob trees, and the monumental carob trees surveyed by Mipaaf.

Furthermore, local widespread carob trees and the linked companies could represent interesting attractions able to recall tourists from the crowded Sicilian beaches.

The map suggests two routes dedicated to tourism to achieve this goal. The paths connect the inhabited centers of the two municipalities, the main arrival points on the island for tourists, and all the resources linked to the carob trees resulting from this participatory process. The routes are designed based on the carob chain, so we start from the monumental trees. We move on to the producing companies, then to the storage one, and finally to the producers where tourists can participate in laboratories

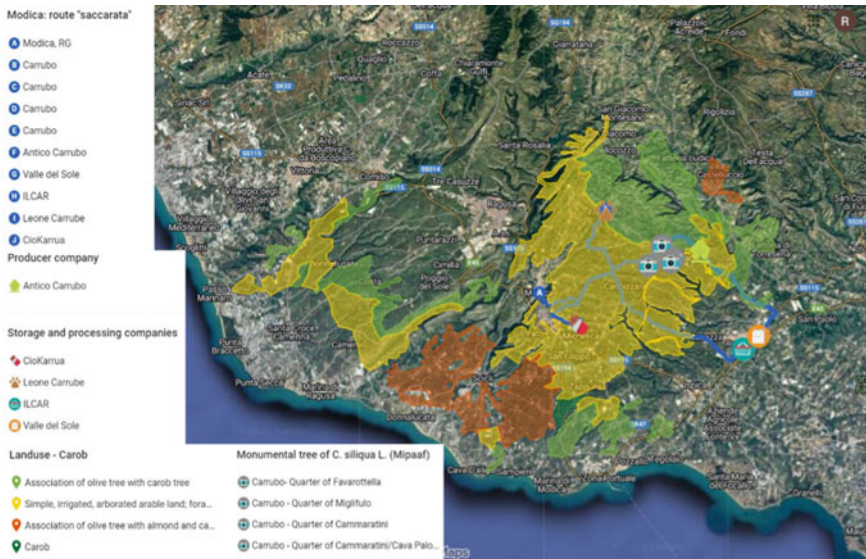


Fig. 5 Screenshot of the resulting main layers of the online map

or buy products derived from the carob. The name of the two paths derive from two of the main cultivars widespread in the area, namely *Racemosa* and *Saccarata*.

4 Conclusion

The research showed the central role that vegetation, especially tree species, plays in defining a landscape's character [9]. Moreover, the participatory process confirmed the great potentialities that such an approach could provide in community building dynamics, with particular reference to rural areas where stakeholders can reach a critical mass and represent a crucial asset in strengthening local, sustainable development [10].

[5] demonstrated that the first motivation of micro firms to invest in building company networks to promote rural tourism is the possibility of a better income. At the same time, the logic of the market, oriented only to economic gain, is not capable of increasing long-lasting slow tourism [7]. This paper highlights how collaborative maps could bolster shared promotion strategies between local stakeholders. Furthermore, the participatory process helped build trust among the participants, addressing one of the main weaknesses in developing systematic and shared methods of rural identity valorization [10]. This research showed that collaborative maps are interesting tools for developing local networks to promote thematic strategies of rural landscape valorization. Furthermore, this research confirmed the underestimation of the value of carob trees for the case study and the potentiality of the whole municipalities' enhancement linked to the valorization of their local chain. Local Institutions and planners need to develop strategies to sensitize rural communities to the value of agrobiodiversity and traditional local crops.

The research has been carried out within the LO-FI Project (Developing Key Competencies for Local traditional knOwledge on Food ProcessIng in High School Education), co-funded by the Erasmus + Programme of the European Union. Project Number: 2021-1-ES01-KA220-SCH-000024513. The European Commission's support for the production of this publication does not constitute an endorsement of the contents, which reflect the views only of the authors, and the Commission cannot be held responsible for any use which may be made of the information contained therein.

References

1. Atagur, M., et al.: Evaluating of reinforcing effect of *Ceratonia Siliqua* for polypropylene: tensile, flexural and other properties. *Polym. Testing* **89**, 106607 (2020)
2. Ayache, S.B., et al.: Chemical characterization of carob seeds (*Ceratonia siliqua* L.) and use of different extraction techniques to promote its bioactivity. *Food Chem.* **351**, 129263 (2021)
3. FAO, et al.: *The State of Food Security and Nutrition in the World 2020. Transforming food systems for affordable healthy diets.* Rome, FAO (2020)

4. Galli, A., et al.: Mediterranean countries' food consumption and sourcing patterns: an ecological footprint viewpoint. *Sci. Total Environ.* **578**, 383–391 (2017)
5. Haines-Young, R., et al.: Revision of the Common International Classification for Ecosystem Services (CICES V5.1): a policy brief. *One Ecosyst* **3**, e27108 (2018)
6. Kelliher, F., Reinl, L., Johnson, T.G., Joppe, M.: The role of trust in building rural tourism micro firm network engagement: a multi case study. *Tour. Manage.* **68**, 1–12 (2018)
7. Manthiou, A., Klaus, P., Luong, V.H.: Slow tourism: conceptualization and interpretation – a travel vloggers' perspective. *Tour. Manage.* **93**, 104570 (2022)
8. Maymone, B., Battaglini, A.: Ricerche sulla digeribilità e sul valore nutritivo della carruba (*Ceratonia siliqua* L.). *Ann. Sperim. Agraria* **5**(4), 721–744 (1951) [in Italian]
9. Menconi, M.E., Artemi, S., Borghi, P., Grohmann, D.: Role of local action groups in improving the sense of belonging of local communities with their territories. *Sustainability* **10**(12), 4681 (2018)
10. Menconi, M.E., Grohmann, D., Mancinelli, C.: European farmers and participatory rural appraisal: a systematic literature review on experiences to optimize rural development. *Land Use Policy* **60**, 1–11 (2017)
11. Menconi, M.E., Stella, G., Grohmann, D.: Revisiting global food production and consumption patterns by developing resilient food systems for local communities. *Land Use Policy* **119**, 106210 (2022)
12. Sánchez, S., Lozano, L.J., Godínez, C., Juan, D., Pérez, A., Hernández, F.J.: Carob pod as a feedstock for the production of bioethanol in Mediterranean areas. *Appl. Energy* **87**, 3417–3424 (2010)
13. Tornabene, F.: *Flora sicula viva et exsiccata* (rist. anast. Catania, 1887) Arnaldo Forni Editore: Sala Bolognese, Italy. ISBN-13: 9788827111406 (1974)

Spatial Variability of Microclimatic Parameters in a Closed Compost-Bedded Pack Barn for Dairy Cows with Tunnel Ventilation



Rafaella Resende Andrade , Ilda de Fátima Ferreira Tinôco ,
Gabriel Araújo e Silva Ferraz , Valentina Becciolini , Giuseppe Rossi ,
and Matteo Barbari 

Abstract The aim of this study was to evaluate the spatial distribution of microclimatic conditions inside a closed Compost-Bedded Pack Barn (CBP), equipped with a negative ventilation system in tunnel mode, associated with an evaporative cooling system (EC), through geostatistical analysis. The research was conducted during the summer in a CBP placed in the area of Zona da Mata, Minas Gerais, Brazil. In different periods of the day, microclimatic parameters were measured inside the building, such as air temperature and relative humidity. Temperature and Humidity Index was subsequently calculated. The results showed the predominance of strong spatial dependence, as well as variability of attributes within the CBP, with heat stress zones occurring. It was verified that the most critical conditions were mainly found from the central part of the CBP towards the northwest face, close to the exhaust fans. On summer afternoons, the entire area of the CBP was in a situation of discomfort.

V. Becciolini · G. Rossi · M. Barbari (✉)

Department of Agriculture, Food, Environment and Forestry, University of Florence, Via San Bonaventura, 13, 50145 Firenze, Italy
e-mail: matteo.barbari@unifi.it

V. Becciolini

e-mail: valentina.becciolini@unifi.it

G. Rossi

e-mail: giuseppe.rossi@unifi.it

I. de Fátima Ferreira Tinôco

Department of Agricultural Engineering, Federal University of Viçosa, Av. Peter Henry Rolfs, Viçosa, Minas Gerais BR 36570-900, Brazil
e-mail: iftinoco@ufv.br

G. A. S. Ferraz

Department of Engineering, Federal University of Lavras, Lavras, Minas Gerais BR 37200-000, Brazil
e-mail: gabriel.ferraz@ufla.br

R. R. Andrade (✉)

Biosystems Engineering Department, Federal University of Goiás, Campus Samambaia - UFG, Goiânia 74690900, Brazil
e-mail: rafaella.andrade@ufg.br

As a result, it is possible to affirm that an increase in the ventilation flow inside the building could allow to reach more favourable conditions for the thermal comfort of the animals. It was observed that the EC can help to improve the internal thermal conditions of the barn. However, probably due to the lack of thermal insulation of the enclosures, it does not allow to reach a spatial thermal uniformity and to create comfortable conditions for dairy cows.

Keywords Animal welfare · Compost barn · Dairy cattle · Geostatistics · Heat stress

1 Introduction

The development of breeding systems contributing to improve animal welfare and to increase productivity and milk quality, with a sustainable use of resources, is one of the main challenges of modern dairy farming. In Brazil, the dairy activity has undergone major transformations, with high records of production and consumption. Milk is among the most important products in the Brazilian agricultural sector, with a significant participation in job creation [1].

However, productivity in Brazil is still low compared to the levels of the world's largest producers, since cattle with high dairy aptitude are mainly from temperate countries and, when inserted in tropical and subtropical regions, find it difficult to express their maximum productivity [2]. Thus, to raise production levels of Brazilian dairy cattle, production systems that prioritize maximum animal comfort have to be adopted, in order to overcome the numerous challenges arising mainly from the country's climatic conditions. Simultaneously, there is a search for breeding systems that provide the reduction of emissions, the reuse of waste and efficiency in the return on invested capital [3].

According to these considerations, the confinement of dairy cattle in compost-bedded pack barn (CBP) systems has shown promise for dairy farming [4, 5]. In Brazil, most CBP are open on the sides and can be naturally ventilated or using mechanical ventilation by positive pressure. However, recently, some closed CBP facilities have been implemented in the country. In this case they are obligatorily equipped with negative pressure mechanical ventilation systems [6].

The adoption of the closed CBP system associated with negative ventilation in tunnel mode is relatively new for the Brazilian dairy industry. The pioneering closed CBP facility was built in the state of Minas Gerais, in 2015, and, since then, it has been spreading in several regions of the country [7]. The system seeks to ensure more uniform ventilation that provides better comfort conditions inside animal buildings, especially during the hottest periods of the day and year. However, as we observe the increase of this CBP technology in milk production systems in Brazil, questions have also been intensified by producers regarding the real applicability of totally closed facilities for the constructive typology and climatic conditions. present in the country [6]. The aim of this study was to evaluate the spatial distribution of microclimatic

conditions inside a closed CBP, equipped with a negative ventilation system in tunnel mode, through geostatistical analysis.

2 Material and Methods

2.1 Description of the Compost-Bedded Pack Barn

The data were collected in a closed compost-bedded pack barn (CBP) for the confinement of dairy cows in the lactation phase, during summer; and during different periods of the day. The CBP is provided with negative pressure ventilation in tunnel mode, associated with the evaporative cooling system (EC), with porous plates use. The studied CBP is located in the Zona da Mata region, Minas Gerais, Brazil (670 m altitude, coordinates 20° 46' 41" S, and 42° 48' 57" W). The local climate, according to the Köppen classification, is of the Cwa-type, with cold, dry winter and hot and humid summer [8].

The CBP, built in May 2017, has a northwest-southeast orientation, total dimensions of 55.0 m long × 26.4 m wide, a gable roof, corrugated metal roof tiles, a height of 5 m, and eaves of 0.8 m. The internal spatial distribution of the CBP is composed of: a) drive-through alley with a concrete floor with an area of 220 m² (containing a single trough 55 m long), being the region where the tractor circulates for food distribution; b) feeding alley with concrete floor with an area of 220 m², with four drinking fountains in this region; c) 880 m² bedding area; d) management corridor with concrete floor and an area of 132 m². The facility roof lining and the lateral closure material are made of polypropylene without insulation. Five deflectors were installed across the facility to direct and increase the animals' airflow. The deflectors extended over the bed area and feeding alley.

On the southeast side of the CBP, a series of five porous cellulose panels was used in the EC composition. A sensor positioned inside the CBP monitored environmental conditions and was programmed to be activated when the air temperature was equal to or higher than 21 °C and relative humidity below 75%. Thus, the plates were moistened by dripping to allow the adiabatic cooling of the external air that passed through the same suction path (negative pressure). At the opposite end (northwest side) of the facility five large exhaust fans were placed (BigFan®, HVLS, 3.5 m in diameter, six propellers, an air volume of 150,000 m³ h⁻¹, and power of 1491.4 W). The five exhaust fans remained on continuously (24 h day⁻¹).

The CBP had a bed made up of a mixture of wood shavings and coffee husks. Following the management already practiced on the farm, lactating cows (total of 80 cows) were distributed in two batches inside the CBP, according to the animals' milk production. The animals with the highest production rates (average of 31.0 ± 5.1 kg milk day⁻¹) were housed in Batch 1 (bed area 38.5 m × 16.0 m), located close to the evaporative plates. Batch 2 (bed area 16.5 m × 16.0 m), with the lower production animals (average of 19.1 ± 6.8 kg milk day⁻¹) was located close to the exhaust fans.

2.2 Environmental Instruments and Measurements

The microclimatic data collection occurred uninterruptedly, 24 h day⁻¹, at 5-min intervals, for fifteen days continuously in summer. The air dry-bulb temperature (t_{db} , °C) and air relative humidity (RH, %) data were recorded using 54 low-cost sensors (DHT22, model AM2302) distributed over the region of the bed and the feeding alley, defining a total measurement area of 55 m × 20 m. The internal area of the CBP was divided into a regular mesh of 5.5 × 3.5 m, totaling 54 points sensors uniformly spaced throughout the facility. Each sensor was positioned at a measurement point. The sensors were installed at a height of 2.0 m.

The data collected by the sensors were sent every 5 min to the main station for processing and storing the data in a micro-SD. This station consisted of the Arduino Mega 2560 board, capable of receiving t_{db} and RH data from the air, from 54 DHT22 sensors. To assess the external environmental conditions, a meteorological shelter was used, in which two t_{db} and RH recorders were placed inside. The data were collected every 5 min, 24 h a day⁻¹. These data were used for the climatic characterization of the region where the CBP was located.

To identify the most critical environmental periods inside the CBP, the average daily values of t_{db} and RH of the air obtained during each experimental period were divided into four periods. Dawn period (00:00 a.m. to 5:59 a.m.), morning (6:00 a.m. to 11:59 a.m.), afternoon (12:00 p.m. to 5:59 p.m.), and night (6:00 p.m. to 11:59 p.m.). Subsequently, in possession of the collected microclimate data and to assess possible conditions of heat stress and the spatial variability of the attributes, the average of Temperature-Humidity Index (THI) was calculated for the four periods of the day investigated, using Eq. (1) corrected and modified by Mader et al. [9].

$$THI = 0.8.t_{db} + RH.\left(\frac{t_{db} - 14.4}{100}\right) + 46.4 \quad (1)$$

where: t_{db} = air dry-bulb temperature (°C); RH = air relative humidity (%).

2.3 Statistical Analysis

The geostatistics technique was used to verify the spatial distribution of the microclimate within the CBP and the dependence between the collection points. The spatial dependence of environmental variables (THI) was analyzed using semivariogram adjustments and ordinary kriging interpolation. This method was used to predict the levels of the variables in places not sampled inside the CBP. To estimate the semi-variogram, the Matheron estimator [10] was used according to Eq. (2), to quantify the spatial dependence of the variables within the facility.

$$\hat{\gamma}(h) = \frac{1}{2N(h)} \sum_{i=1}^{N(h)} [Z(X_i) - Z(X_i + h)]^2 \quad (2)$$

where: $N(h)$ is the number of observation pairs $Z(X_i)$ e $Z(X_i + h)$ separated by a distance h .

From the adjustment of a mathematical model $\hat{\gamma}(h)$, the coefficients of the theoretical model were obtained for the semivariogram, called nugget effect (C_0), contribution (C_1), sill ($C_0 + C_1$), and range (a). The spatial dependence index (SDI) was used to analyze the spatial dependence and calculated from the ratio between the nugget effect (C_0) and the sill ($C_0 + C_1$). To analyze the SDI of the attributes under study, the classification by Cambardella et al. [11], in which a strong dependence is considered in semivariograms with $SDI \leq 0.25$; moderate dependence on semivariograms with $0.25 < SDI \leq 0.75$ and weak dependence on semivariograms with $SDI > 0.75$. The semivariogram was adjusted by the Method of Restricted Maximum Likelihood (REML), as suggested by Marchant & Lark [12]. The models tested for the adjustment of the experimental semivariogram were spherical, exponential, and Gaussian, according to Vieira et al. [13], and through the software R DEVELOPMENT CORE TEAM (2016).

Subsequently, once the semivariogram of the variables was known and spatial dependence occurred, the levels of spatial distribution maps of the microclimatic variables were made using the ordinary data kriging technique. This method allows the visualization of data spatialization, through the interpolation of values, without trend and with minimal variance [13]. From the interpolated data, maps of the response surface were generated using the Surfer® software, version 13.4.

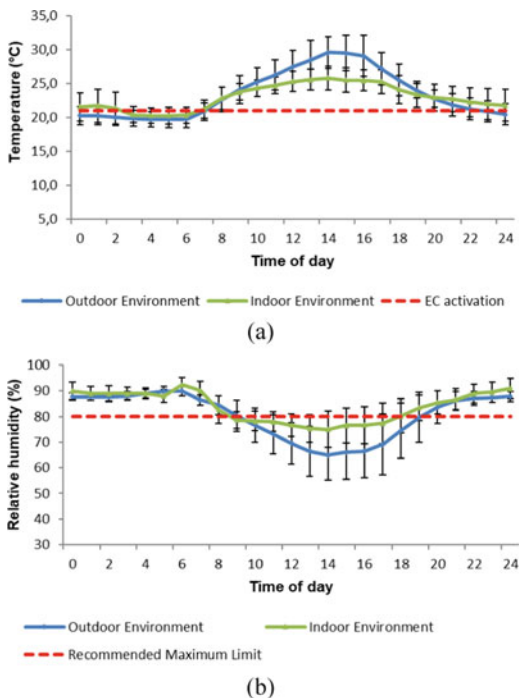
3 Results and Discussion

3.1 Analysis of Microclimate Variables

The profile of the hourly average values of temperature and relative humidity inside the CBP and in the external environment (weather shelter) is shown in Fig. 1. The average air temperature inside the CBP during summer was similar to the outdoor environment until the moment when the internal temperature of the air reached 21.0 °C. After that, the automatic spraying of the porous material occurred to promote the evaporative cooling of the incoming air.

Before the activation of the EC (indoor air temperatures below 21.0 °C), although following similar behavior curves, it was found that the air temperature values inside the CBP were slightly higher than those observed for external temperatures. This can be attributed to the heat produced by the cows and the equipment, the heat generated in the bed composting process, and the heat energy from the short-wave solar radiation that passed through roofs and sides walls and was retained temporarily inside the CBP.

Fig. 1 Average variation and standard deviation of the hourly mean values of a air temperature, in °C, and b relative humidity, in %, of the air inside the closed CBP, equipped with the EC - Adiabatic Evaporative Cooling System



After the activation of the EC, there was an inversion of the temperature curves, with a reduction in the internal temperatures of the housing, compared to those of the outdoor environment. Those variations in the internal and external average temperatures (Fig. 1a) show, therefore, that the use of the EC was able to reduce the t_{db} of the air inside the CBP, during the most critical periods of the day, with an average of 4.0 °C below the outdoor environment. It was found that, during the afternoon, in summer, the averages of t_{db} remained above the thermoneutrality zone, that is, above the value of 25 °C cited by Roenfeldt [14] as being comfortable for dairy cattle.

Concerning the variable RH, it can be observed, based on Fig. 1b, similar behaviors of average hourly values of the indoor air relative humidity over time when compared to the values measured in the outdoor environment. However, in the case of periods with higher temperatures, it was necessary to use the EC in the hottest hours of the day (temperatures above 21 °C), requiring the activation of the sprinklers on the porous plate, generating an increase in the relative humidity value of the air inside the CBP. The mean RH values observed were high inside the CBP facility (predominance of mean RH values above 70%).

Based on the results of the geostatistical analysis (Table 1), it appears that the variable THI showed spatial dependence.

The variables THI showed high spatial dependence. The larger the SDI, the less the nugget effect contributes to the variability of the data and, therefore, kriging is better

Table 1 Model and estimated parameters of the experimental semivariogram for the mean values of each period for the variables Temperature-Humidity Index (THI)

Variable	Model	C ₀	C ₁	C ₀ + C ₁	a	SDI
THI _{Dawn}	Gaussian	0.010	0.760	0.011	19.488	0.026
THI _{Morning}	Gaussian	0.026	0.713	0.010	20.629	0.051
THI _{Afternoon}	Spherical	0.012	0.624	0.008	46.371	0.021
THI _{Night}	Gaussian	0.090	0.577	0.008	38.744	0.160

C₀ nugget effect; C₁ contribution; C₀ + C₁ sill; a range; e SDI spatial dependence index.

[15]. When analyzing the range, concerning the spatial extent to which the data are correlated, for all periods in which the data were sampled, the points were associated with other points at considerable distances. The highest range values for the THI were in the afternoon (46.371 m) in the summer. From the semivariogram adjustments for the THI indexes under study, the values of these variables were estimated using ordinary kriging. Therefore, it was possible to build spatial distribution maps for the THI during each study period (Fig. 2). The THI thresholds that characterize a situation of comfort or discomfort differ among authors. In general, the proposed limits for dairy cattle are $THI \leq 74$ - thermal comfort condition; $74 < THI < 79$ - alert condition for producers; $79 \leq THI < 84$ - danger condition and safety measures must be taken to avoid losses to the squad; and $THI \geq 84$ - emergency situation [9]. From the data collected in the summer (Fig. 2, a, b, c, d), it was observed that, even with the presence of artificial ventilation, the THI values remained above the limits ($THI > 74$) characterized as comfort situations for animals, except during the early morning. However, there were no conditions of intense thermal stress ($THI \geq 84$) during the analyzed periods. The highest value determined for the THI (78) was verified in the afternoon, considered an alert condition for producers, a fact that occurred due to the combination of high values of t_{db} and RH verified for this region.

The THI values increased sharply over the last 25 m of the CBP, closer to the exhaust fans, reaching the value of 74, during the morning and night (Fig. 2, b, d). Those results indicate that, during the morning and night, the animals in Batch 2 were in heat stress condition. During the summer afternoon, the THI values increased sharply over the last 35 m closest to the exhaust fans, reaching a value of 78 (Fig. 2c), close to the same ones (northwest face). During that period, the animals in Batch 1 and Batch 2 were in a heat stress condition. This THI behavior profile indicates critical points where the distribution of this variable represented a certain degree of discomfort for the animals. Based on the above arguments, it appears that the low insulation of the side closure (curtains) and the roof did not guarantee the thermal inertia of the CBP, negatively affecting the thermal uniformity of the facility.

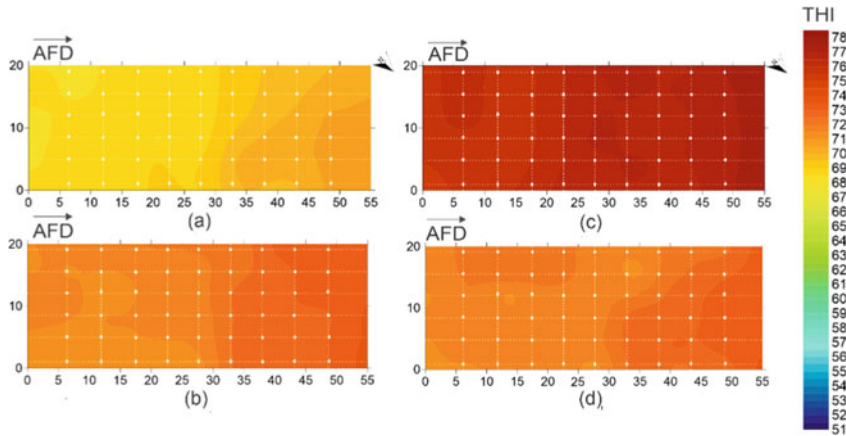


Fig. 2 Spatial distribution of the Temperature and Humidity Index (THI) during the dawn a, morning b, afternoon c and night d, inside the CBP. AFD - Air Flow Direction

4 Conclusions

The study allowed us to observe, from the kriging maps, that the most critical housing conditions were found, mainly, from the central part of the CBP, towards the north-west face, close to the exhaust fans. During summer afternoons, the entire CBP region was in a situation of discomfort for lactating cows.

Acknowledgements This work was carried out with the support of CNPq, National Council for Scientific and Technological Development - Brazil, FAPEMIG and CAPES.

References

1. EMBRAPA Empresa Brasileira de Pesquisa Agropecuária. <https://www.embrapa.br>. Accessed 22 Aug 2022
2. Ricci, G.D., Orsi, A.M., Domingues, P.F.: Estresse calórico e suas interferências no ciclo de produção de vacas de leite: revisão. *Veterinária e Zootecnia* **20**(3), 9–18 (2013)
3. Galama, P.J., Ouweltjes, W., Endres, M.I., Klopčič, M.: Symposium review: future of housing for dairy cattle. *J. Dairy Sci.* **103**(6), 5759–5772 (2020)
4. Leso, L., Barbari, M., Lopes, M.A., Kuipers, A.: Invited review: compost-bedded pack barns for dairy cows. *J. Dairy Sci.* **103**(2), 1072–1099 (2020)
5. Bewley, J.M., Robertson, L.M., Eckelkamp, E.A.: A 100-year review: lactating dairy cattle housing management. *J. Dairy Sci.* **100**(12), 10418–10431 (2017)
6. Andrade, R.R., et al.: Spatial distribution of bed variables, animal welfare indicators, and milk production in a closed compost-bedded pack barn with a negative tunnel ventilation system. *J. Therm. Biol* **105**, 103111 (2021)
7. Damasceno, F.A.: *Compost Barn como alternativa para a pecuária leiteira*. Ied. Adelante, Divinópolis, Brazil (2020)

8. Alvares, C.A., Stape, J.L., Sentelhas, P.C., Moraes, J.L.D.G., Sparovek, G.: Köppen's climate classification map for Brazil. *Meteorol. Z.* **22**, 711–728 (2013)
9. Mader, T.L., Davis, M.S., BrownBrandl, T.: Environmental factors influencing heat stress in feedlot cattle. *J. Anim. Sci.* **84**, 712–719 (2006)
10. Matheron, G.: *Treaty of applied geostatistics, vol. I: Mémoires du Bureau de Recherches Géologiques et Minières, n. 14*, Editions Technip, Paris (1962)
11. Cambardella, C.A., et al.: Field-scale variability of soil properties in central Iowa soils. *Soil Sci. Soc. Am. J.* **58**, 1501–1511 (1994)
12. Marchant, B.P., Lark, R.M.: Robust estimation of the variogram by residual maximum likelihood. *Geoderma* **140**, 62–72 (2007)
13. Vieira, S.R.: Geostatística em estudos de variabilidade espacial do solo. *Tópicos em ciência do solo, Viçosa: Sociedade Brasileira de Ciência do Solo* **1**, 1–53 (2000)
14. Roenfeldt, S.: You can't afford to ignore heat stress. *Dairy Manage* **35**, 6–12 (1998)
15. Curi, T.M.R.C., et al.: Positioning of sensors for control of ventilation systems in broiler houses: a case study. *Sci. Agricola* **74**, 101–109 (2017)

Landscape Valorization and Rural Tourism Development: A Mobile Application for the Promotion of the Lauretana Way in Tuscany Region (Italy)



Gianluca Bambi , Giuseppe Rossi , Matteo Barbari ,
Lorenza Gasparella , and Serena Savelli

Abstract Europe has in its walkable landscape a pillar of its cultural identity (Steiner et al., 2006) Italy, where the way to Santiago and the way to Jerusalem connect by the via Francigena, assumes a barycentric role in this footprint geography. The Belpaese has a network of 44 routes (Cammini) recognized by the Ministry of Cultural Heritage and Activities and Tourism (MiBACT, 2016) for their historical-cultural interest. Whilst following, in most cases, ancient pilgrimage routes, these itineraries are not strictly related only to religious tourism that has its main motivation in visiting religious sites—that have often great artistic and historic value. Similarly, those traditional agricultural and rural landscapes that the routes often intercept are of great value. They can be the main driving force behind the sustainable socio-economic and cultural development of many rural areas. (Makuc, N.: Fostering socio-economic development of rural areas through cultural and religious tourism: innovative solutions for involvement of private sector. Firenze, 4–6 Dicembre 2014. Firenze University Press (2015)). The rural tourism, fostering the discovery of wine and food, agriculture, and typical handicraft, becomes a great potential for a wide range economic development and represents that form of “experiential tourism”. The Iter App provides a tool for reading and gaining experiential knowledge of the landscape of cultural routes, aimed at fostering their landscape valorisation and economic promotion. The case study presented is the Tuscan segment of the ancient Via Lauretana that mainly goes through the Siena countryside. The main output is an application for smartphones and tablets designed to narrate the landscape as well as to provide the practical and experiential exploration of the territory. The app

G. Bambi (✉) · G. Rossi · M. Barbari
Department of Agriculture, Food, Environment and Forestry (DAGRI), University of Florence,
Via San Bonaventura 13, Florence, Italy
e-mail: gianluca.bambi@unifi.it

L. Gasparella
Department of Architecture and Arts, University of Venice, Santa Croce 191, Venice, Italy

S. Savelli
Member of the Landscape Local Commission of the Municipality of Asciano, Siena, Italy

intends to connect insiders and outsiders, architects/actors and users/spectators of the landscape, inhabitants and pilgrims. In this way the experience of the cultural roads could be transformed, for travellers, in an opportunity for a cultural growth and for residents in an economic chance.

Keywords Rural tourism · Agricultural landscape · Heritage route · Mobile application

1 Introduction

1.1 *Cultural Itineraries and Landscape, a Synergy with High Potentiality*

The ICOMOS Charter on Cultural Routes states that “the Cultural Route is closely linked to its setting and forms an inseparable part of it [...] The territorial setting, whether natural or cultural (urban or rural), provides the framework of the Cultural Route, gives it its particular atmosphere, characterized by elements and values of both physical and intangible nature, and is fundamental for the comprehension, conservation and enjoyment of the route” [6]. The same document also expressly refers to the landscape realising that “Cultural Routes and their setting are related to their different landscapes, natural or cultural [...] The different landscapes contribute to characterize the diverse sections of the Route as a whole, enriching it with their diversity” [6]. In the UNESCO Report on Routes as a Part of our Cultural Heritage, the relationship between routes and landscape is expressed as an identity. In fact, “a heritage route may be considered as a specific, dynamic type of cultural landscape” (UNESCO, 2011). Council of Europe Resolutions on Cultural Routes (CM/Res(2007)12, CM/Res(2010)52) identify them as sites of experimentation for European Chartes, first of all the European Landscape Convention [3]. Europe has in its walkable landscape a pillar of its cultural identity (Steiner et al., 2006) Italy, where the way to Santiago and the way to Jerusalem connect by the via Francigena, assumes a barycentric role in this footprint geography. The Belpaese has a network of 44 routes (Cammini) recognized by the Ministry of Cultural Heritage and Activities and Tourism (MiBACT, 2016) for their historical-cultural interest. The rural tourism, fostering the discovery of wine and food, agriculture and typical handicraft, becomes a great potential for a wide range economic development and represents that form of tourism that today takes the name of “experiential tourism”.

1.2 Cultural Itineraries as Tools for Reading and Preserve the Landscape, to Promote by a Mobile Application

Walkin involves a physical participation imposed by moving on foot, but also sentimental, intellectual and socializing. Walking allows to live and look at the landscape from inside, halfway between insiders and outsiders [10] especially in the case of traditional cultural landscapes. These concepts are similar and often overlapping. Both are characterized by the permanence, in the same place and for many centuries, of land use systems, crop systems, crops and cultivars, forms of breeding, settlement and infrastructural systems unaltered or slightly altered until today [1]. According to the more recent definitions, traditional cultural landscapes must be present in a territory for a long time, stabilized or in slowly evolution, showing characteristics of resilience, connection and complexity both environmental and economic than social. They must have preserved not only forms but also functions during a local and site-specific coevolution between agricultural practices of the rural community, ecological conditions of land, floristic associations of the spontaneous vegetation and native agrarian cultivars [3, 8, 9]. Thus, the traditional cultural landscapes carry more and better the substantial global identity underlying the local differences, that underpin the idea of Europe (Steiner et al., 2006), assuming the role of important references for the local identity. For these reasons they have to be preserved as real hybrid nature-culture monuments. Itineraries can be the best mean for preserving and enhancing the territory and especially its traditional cultural landscape in sustainable ways, contributing to the socio-economic subsistence of rural areas, enhancing agro-food typical product, contributing to the dissemination of cultural identity and intergenerational exchange, recovering the historical heritage of the ancient streets and the annexed structures, favoring the sustainable development of tourism, encouraging healthy lifestyles and historical-cultural and educational activities.

The dynamic growth of mobile communications technology is creating opportunities for economic growth and grassroots innovation in developing rural areas. For both agricultural supply and demand, mobile phones can reduce waste, make delivery more efficient, and forge closer links between farmers and consumers.

2 Materials and Methods

2.1 The ITer Concept

According to the purposes of this work, the enhancement is defined under two analytical and operational perspectives. The first one considers the path as a powerful medium for landscape narration and, consequently, as an effective instrument for the indirect valorization of the landscape itself (Savelli, 2017b). The second one accounts

itinerary as vector of tourism and, therefore, as catalyst of the economic valorization of traditional agricultural practices. One of the fast-emerging sectors of small business is small tourism business in rural settlements (so-called “rural tourism”) which is well represented in such many EU countries including Italy. Noteworthy is the fact that in the EU countries 10–20% of the income from tourism industry falls to the rural tourism [9], mostly in those areas where many farms offer on-farm tourism experiences and/or the direct sale of their products. According to a study of the Tuscany Region done in 2015–2016 along the Via Francigena in Tuscany, from a questionnaire filled by 1000 pilgrims/walkers it appears that the enjoyment, the experiential knowledge and the understanding of the crossed landscape are their higher expectations [2]. Starting from these assumptions an innovative application, that will be a useful tool for navigating the territory and a delightful medium of knowing the landscape, is developing. The structure of the application reflects a research approach aimed at enhancing the high potential of historical rural landscapes and traditional agricultural landscapes connected to cultural itineraries. The application follows a concept expressed by the naming ITer. “I” refers to the high customization of the app designed to adapt the itinerary experience on the characteristics and aspirations of each walker. “IT” refers to Italy because the project can be replicable and declined for all religious and lay paths on the national, and even European, territory. “Ter” refers to territory and landscape, the perceived part of territory, the place within which the experience happens. “ITer”, in latin, is route, itinerary, but above all as path of knowledge to indicate a journey, configured not only as a trekking or a food and wine experience, but as a formative and cultural process for reading and understanding the landscape in its crossover sections and its staging points.

2.2 *The ITer Structure*

The aims of the App consists in the valorization of the landscape experience, especially the rural landscape, facilitating the permanence within it. Today the fixed stages travel approach is increasingly disappearing. Designing a path viable by different types of travellers (hikers, pilgrims, tourists) in different ways (on foot, by bicycle or on horseback), mainly requires a diversified offer of accommodation facilities, staging points where you can sleep and have other services. A network of host is at the base of the project. In this way hospitality points can be distributed along all the path in order to ensure the stages adaptation also according to contingent needs related to fatigue, weather conditions, but, above all, the inspiration of the moment and the suggestion given by the places, now really very limited on the paths of Italy. Agricultural producers can present a spontaneous candidacy for joining the network and obtaining a label related to the itinerary for their products. It will be facilitated by the technical operators who carry out the mapping survey and promoted in collaboration with the local administrations and the trade associations. The description of experiences of accommodation and/or short stay offered by the farms can be consulted in a specific section and can also appear by push notifications when you

Fig. 1 The ITer App interface



approach a potential stop point. A reservation function allows travellers to book not only overnight stays at the farms, but also food and wine tastings, visits, horse hire, local guides and story-telling experiences (Fig. 1).

The ITer App also provides travelers a brief description of the different traits composing different landscapes such as geomorphology, vegetation, agronomic features, settlements, urban planning background, anthropological aspects, historical and artistic references. These descriptions are available both in multi-lingual (italian and english) texts and as audio-guide, read by inhabitants and experts who produced them. Always consultable in the specific section of the application, they can appear as push notifications when you approach a noticeable point or you enter a certain area or landscape unit. Moreover, in the ITer App navigation interface the path is not represented as a simple line, loaded on a map or an aerial photo, but within its visual basin limits that represents the walkscape (Savelli, 2017a) clearly distinguishing the ITer App from the other apps for outdoor activities and slow tourism.

2.3 The Via Lauretana Senese ITer App

The ITer App is designed to introduce a new way to experience the landscape, to indulge the evolving needs, wishes of walkers and to trigger their curiosity ongoing being free hem from predetermined stages, daily mileage and predetermined stops as much as possible. The Via Lautetana Senese is a perfect pilot case to testing out this approach. High quality agricultural landscapes are widespread and farms are relatively small, likewise the average size of the Italian farms. Thus it is possible to offer intermediate staging points every 5 km maximum, and accommodation and place to have dinner or to make a multi-day experience every 10 km (Fig. 2).



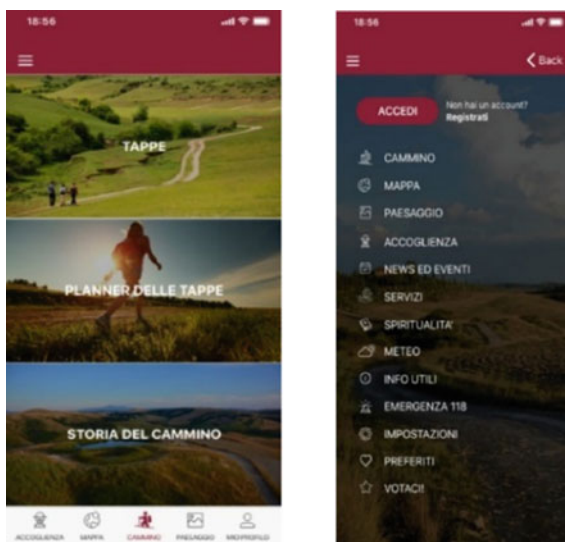
Fig. 2 The Lauretana Senese Way

We defined seven walkscapes. Hiking through the territory the history and geography of places arise. Traces of previous glances can be retraced. Memories, that subtly unfolds over time, can reaches us, from one text to another, from one painting to another, feeding our real knowledge as well as our imaginary. Contemporary travelers pass through places full of voices and echoes of the past and where history is well hidden, imaginary may has well been preserved. Art and literature tell the places as they were, bringing us back to the many legacies on which we built our journey through space and time between past and future [4]. For this reason each walkscape description is introduced by a sentence that previous travellers have jotted down in their diaries, thus attempting to identify the invariants, “icomemi” [11] the elements and signs that can still be recognised and interpreted as effects of the reciprocal relationships between geomorphology, climate, economic actions, political choices and cultural projections, condensed into what is called landscape.

2.4 The Via Lauretana Senese ITer App: Technical Details

The application has been realized for iOS and Android devices and is to be developed using the open source platform called Cordova. Cordova allows you to develop the package of a single codebase in a native executable. The application groups HTML, CSS and JavaScript into a client-side package. Thus, the software executes and returns the customized code within a native WebView. By wrapping the Web code in a native Cordova package, Cordova can provide access to the API native. This allows the application to communicate directly with the phone hardware and have access to the camera, to the GPS, and to the sensors present in the device. The application can use the mobile connection to communicate with a webservice for

Fig. 3 - Home Page and Menu



data exchange or operate in an offline mode to allow users to access information even in the absence of coverage. The application will be able to connect to a push messaging management system, to allow the user to be updated on events or other types of communication. The push notification is a type of instant messaging with which the message reaches the recipient without it having to perform a download operation (pull mode). This mode is typically used by applications such as WhatsApp, or operating system services such as Android or as numerous applications derived from websites (for example, the classic weather service or news service). For the application interface will be used Framework7, an application framework (based on Vue.js) and a series of ready interface elements that allow to simulate native interfaces. This tool recreates Google's standard iOS designs and Material Design models to replicate the "native" look that mobile device users have come to expect. Framework7 also allows effective intervention on interface customization (Fig. 3).

3 Discussion of the Results

In addition to give a practical support to the travelers, the aim of the ITer App is to reveal the intrinsic characteristics of cultural and increase walking as an aesthetic and analytical practice [5]. Forced and often exhausting pace imposed by fixed stages can thus be reformulated expanding the permanence of the users as well as the travel time increasing the number and type of places to eat and sleep stops into farms. The ITer approach also intends to promote alternatives, even radical, to usual services, like a brief work experience in a farm, sleeping on a hammock between olive trees or on a bale of hay offered as an open-air mattress, in a tent or in a

temporary modular hut. Finally, it allows to build networks of people and landscapes, travelers and inhabitants, users, producers and products. Applied at the moment of the pilot case of the Via Lauretana, this innovative tool for the enhancement of the landscape and in particular of the agricultural lands, could be replicable on all cultural itineraries. Unlike the other applications available for the navigation of cultural itineraries, ITer focuses on the narration of the landscape considered the medium between the viator and the knowledge of the territory and the application precisely serves to implement this intrinsic vocation. Therefore, in addition to the canonical subdivision into stages (both fixed and customizable) ITer offers a narration of the route organized by landscape chapters. These are the different sections into which the landscape along the path can be divided, which are called walksapes. In the particular case of the Via Lautetana Senese, the correspondence between the municipal limits and landscape units is marked in terms of physical homogeneity, land use and historical evolution. The convenience of considering municipal limits to structure the narrative of the walkscape is twofold. On the one side there is an operational convenience because the municipality is the administrative unit that will be an active part in the management of the cultural itinerary as well as of the app itself. On the other side, there is an affirmed methodological convenience because the municipality is the minimum organic cell for a territorial study based on certain and knowable data [11].

4 Conclusions

Finally thanks with this App, tourists can experience a new way of seeing the landscape and to do tourism. All cultural itineraries, but especially itineraries that follow ancient pilgrim routes, by their nature, can narrate their landscapes. The landscape unfolds itself along its typical routes, which have a typical way of driving within the landscape, telling its story.

In many cases, the road gave the primitive imprinting [10] to a territory and cities and villages were generated from it. The route is the driving force that has shaped the sequence of the crossed places, shaping economic, territorial and landscape structures on a trans-regional scale. Walking from stage to stage, is equivalent to carrying out a diachronic study of the landscape palimpsest, its evolutionary events and its territorial structures. Walking gives the rhythm of crossing, the sweetness of a perception all around. Developing not so much the itinerary, but rather the landscape of the itinerary can bring a new wide-spread awareness. Inhabitants can know that a cultural itinerary is a structural part of their daily life landscape. For farmers, craftspeople and others productive structures this mobile application created for the Via Lauretana can be a valuable economic opportunity through which territories can preserve their identity and develop themselves in a sustainable way.

References

1. Agnoletti, M.: Rural landscape, nature conservation and culture: some notes on research trends and management approaches from a (southern) European perspective. *Landsc. Urban Plan.* **126**, 66–73 (2014)
2. Bambi, G., Iacobelli, S.: Study and monitoring of itinerant tourism along the Francigena route, by camera trapping system. *Almatourism J. Special Issue*, **8**(6) (2014)
3. Barbera, G., Biasi, R., Marino, D.: *I paesaggi agrari tradizionali, un percorso per la conoscenza*. Franco Angeli, Milano (2017)
4. Berti, E., Mariotti, A.: The landscape dimension along Cultural Routes: common ground. *Cultural Routes management: from theory to practice. Step-by-step guide to the Council of Europe Cultural Routes*, 42 (2015)
5. Bonadei, R.: I luoghi nel mosaico degli sguardi. In: Bonadei R., Volli U. (a cura di), *Lo sguardo del turista e il racconto dei luoghi*, pp. 11–28. Franco Angeli, Milano (2006)
6. Careri, F.: *Walkscapes, camminare come pratica estetica*. Einaudi, Torino (2004)
7. CIIC International Scientific Committee on Cultural Routes (CIIC) of ICOMOS. *ICOMOS Charter on Cultural Routes*, Québec, Canada (2008)
8. Cullotta, S., Barbera, G.: Mapping traditional cultural landscapes in the Mediterranean area using a combined multidisciplinary approach: method and application to Mount Etna (Sicily; Italy). *Landsc. Urban Plan.* **100**(1–2), 98–108 (2011)
9. Marino, D., Nofroni, L., Savelli, S.: *Le greenways come fattore di resilienza dei Paesaggi agrari tradizionali in ambiente periurbano*. Atti del convegno “Architettura e Natura” 16–20 dicembre 2014, San Venanzo. Milano: Franco Angeli (2015)
10. Paresishvili, O., Kvaratskhelia, L., Mirzaeva, V.: Rural tourism as a promising trend of small business in Georgia: Topicality, capabilities, peculiarities. *Ann. Agrar. Sci.* **15**(3). 344–348 (2017). ISSN 1512–1887
11. Turri, E.: *Il paesaggio come Teatro*. Marsilio, Venezia (1998)
12. Turri, E.: *La conoscenza del territorio. Metodologia per un’analisi storico-geografica*. Marsilio, Venezia (2002)

Real-Time Measurements of Gaseous and Particulate Emissions from Livestock Buildings and Manure Stores with Novel UAV-Based System



V. Becciolini , L. Conti , G. Rossi , D. Bedin Marin , M. Merlini, G. Coletti, U. Rossi, and M. Barbari 

Abstract In the framework of the European environmental policies towards a green transition, the adoption of strategies to improve the sustainability of the agricultural system is a key element. In a perspective of adaptive farm management where a continuous monitoring process is implemented to meet the goal of environmental and economic sustainability of food productions, new tools need to be developed to provide cost-effective and real time measurements. In this context, a novel system based on Unmanned Aerial Vehicles (UAVs) and on prototypical measurement units (MU) equipped with low-cost sensors was designed and developed. The system is based on a flexible architecture, which can be adapted to a variety of operational fields. The MU is provided with a multisensor board to monitor environmental conditions, gaseous pollutants (CO_2 , CH_4 , NH_3) and particulate matter. A prototype version of the system was tested in a commercial dairy farm to assess its technical feasibility. In-flight and ground-based measurements were performed and cross-referenced with data collected by commercial dataloggers and colorimetric tubes. The test showed that a system integrating ground and in-flight measurements of air pollutants is feasible and could be implemented at farm level. Despite the accuracy of measurements could be improved, the test proved that average measurements of carbon dioxide over a 10 min time span can be considered as a reliable indicator of the actual CO_2 levels.

Keywords greenhouse gases · sustainable livestock farming · drones · dairy farming

V. Becciolini · L. Conti · G. Rossi (✉) · D. B. Marin · M. Merlini
Department of Agriculture, Food, Environment and Forestry (DAGRI), University of Florence,
50145 Florence, Italy
e-mail: giuseppe.rossi@unifi.it

G. Coletti · U. Rossi · M. Barbari
Project & Design S.r.l.s, 50142 Florence, Italy

© The Author(s), under exclusive license to Springer Nature Switzerland AG 2023
V. Ferro et al. (eds.), *AIIA 2022: Biosystems Engineering Towards the Green Deal*,
Lecture Notes in Civil Engineering 337,
https://doi.org/10.1007/978-3-031-30329-6_108

1049

1 Introduction

Pursuing sustainable and smart agricultural systems is the trending strategy to face the upcoming challenges regarding food chain safety and integrity of ecosystems in a scenario where, by 2050, global population will grow by 22% [1] and global greenhouse gases (GHGs) emissions from the agricultural sector will be increased between 26 and 54% [2]. The European environmental policies are targeting a reduction of 55% of GHGs emissions by 2030 and aim to ensure food security in the face of climate change and biodiversity loss. Smart agriculture, in the context of Industry 4.0, is able to provide farmers a variety of tools to address food production challenges associated with farm productivity, environmental impact, food security, crop losses and sustainability [3] as well as to monitor and analyze a wide series of environmental factors. Among the most used Industry 4.0 technologies for the digitalization of agriculture are Internet of Things (IoT), wireless sensor networks, cloud computing and autonomous robotic systems as drones [3]. Their integration in agricultural and farming activities is intended to provide farmers with up-to-date decision support tools towards an improvement of the enterprise efficiency and sustainability. In particular, drones equipped with chemical sensing payloads are becoming the new frontier of real-time monitoring in a variety of fields [4]. Rotary (RW) or fixed-wing (FW) drones were employed in atmospheric chemistry research, for experimental measurements of atmospheric constituents, as CH₄, CO₂, NO_x and O₃, and of thermodynamic variables (temperature, humidity, atmospheric pressure, wind), or to investigate vertical and horizontal variations in GHGs in the atmospheric boundary layer. Additional relevant applications are related to in-flight emission monitoring in industrial activities. The monitoring of fugitive emissions in industrial sites specifically targets combustion gases (SO₂, NO_x, CO), VOCs, acid gases (HCl, HF, NH₃) or GHGs as in the case of refineries (CH₄) and waste treatment sites (CH₄, CO₂, N₂O). The use of sensing drones in precision agriculture, conversely, is still pioneering. This technology was tested in different plant production systems, to study environmental conditions in greenhouses [5] or to assess fruit maturity in orchards [6]. When coming to the applications in the field of livestock farming, knowledge and experiences are still lacking. One attempt was made to evaluate the use of methane sensing UAVs for emission quantification in a dairy farm [7]. In all cases, the restrictions in payload capacity of small drones needs lightweight and low-power sensing technologies. A current limitation to the implementation of small and low-cost UAV-based gas monitoring systems is the availability of sensors on the market with appropriate limits of detection and accuracy. Among the wide array of gas sensors, the most popular for drone-based measurements are represented by amperometric gas sensors (cheap, quite selective for some gases but slow response and recover time), metal oxide semiconductor sensors (small, less selective, faster response, durable), non-dispersive infrared sensors (less accuracy, more power consumption, more expensive), and photoionization detectors (high cost, low specificity). In this framework, the aim of this research is to develop an integrated system for ground and in-flight gas and particulate matter (PM) measurement in livestock farms, providing real-time

data from low-cost sensors that could be integrated in a decision-support system helping farmers, researchers and public authorities to achieve the goals of sustainable production systems.

2 Materials and Methods

2.1 Description of the System

A system integrating ground and in-flight assessment of air pollutants by means of prototype measurement units (MU) was developed. The unit is designed to transmit data in real-time in a cloud environment and to provide their graphical representation on a web-application (Fig. 1a). The MU was developed with limited size ($120 \times 100 \times 67$ mm) and weight (0.75 kg) in order to be used both for ground measurements and to be installed as payload to medium-size drones (Fig. 1b).

The system was organized into four levels, concerning: 1) the set of commercial low-cost sensors embedded in the MU; 2) the data transmission system of the MU; 3) the cloud environment for data storage; 4) the digital dashboard for real-time data visualization.

The MU embedded in total 7 sensors selected to monitor air quality and assess environmental conditions (Table 1). Three sensors were devoted to gas sensing, specifically CO_2 (Non-Dispersive InfraRed sensor), CH_4 and NH_3 (electrochemical sensors); one sensor recorded the air concentration of particulate matter ($\text{PM}_{2.5}$, PM_{10} ; optical sensor); three sensors were inserted to monitor environmental conditions: air temperature ($^{\circ}\text{C}$), relative humidity (%) and atmospheric pressure (hPa). The MU was provided with a fan ensuring an adequate airflow inside the device.

The system for data collection, processing and transmission was composed by a Raspberry Pi® and an ESP32® board. Air quality and environmental variables measurements were both stored on board and transmitted real-time to a cloud platform

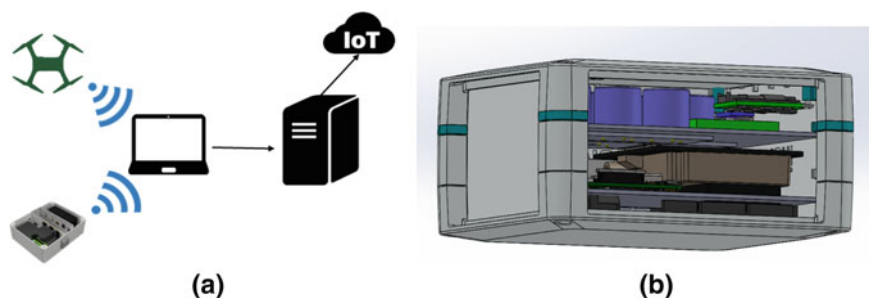


Fig. 1 1a, 1b: 1a: graphical representation of the system. 1b: 3D design of the prototype MU

Table 1 Sensors embedded in the prototype MU: type, measurement range and accuracy (declared by manufacturer)

Measurement	Sensor type	Measurement range	Accuracy
PM _{2.5} ,PM ₁₀	Optical	0 to 999.9 $\mu\text{g}/\text{m}^3$	$\pm 10 \mu\text{g}/\text{m}^3$
NH ₃	Electrochemical	0 to 100 ppm	$\pm 3 \text{ ppm}$
CH ₄	Electrochemical	0 to 10,000 ppm	$\pm 100 \text{ ppm}$
CO ₂	Non-dispersive infrared	400 to 10,000 ppm	$\pm 30 \text{ ppm}$
Atmospheric pressure	–	300 to 1100 hPa	$\pm 1 \text{ hPa}$
Temperature	–	–40 to 70 °C	$\pm 0.1 \text{ °C}$
RH	–	0 to 100%	$\pm 0.1\% \text{ RH}$

where they could be accessed and downloaded in spreadsheet format or graphically visualized as time series plots.

2.2 Description of the Field Test

A technical test of the prototype system was carried out in a commercial dairy farm located in Borgo San Lorenzo, Florence, Central Italy. The dairy cattle herd was composed in total by 135 heads, with 65 lactating cows. The farm also hosted donkeys ($N = 4$), beef cattle ($N = 12$), and poultry. Lactating cows were housed in a cubicle pen inside the main building, while the other cows and youngstock were allocated in pens with deep straw bedding. Slurry was mechanically separated after being removed from the barn; the solid fraction was stored in an uncovered outdoor area while the liquid fraction was stored in an uncovered concrete tank.

The test was carried out during one day. The prototype measurement unit was deployed in 2 locations: outdoor, at an external side of the cattle barn in proximity to the uncovered slurry tank and to the solid manure storage, and inside the building in the feeding corridor (Fig. 2a). Recordings were performed for 12 min at each location, at a sampling rate of 1 record every 5 s. In total, 276 measurements were collected. In order to cross-reference measurements, simultaneous recordings of CO₂ concentration (ppm), temperature (°C) and relative humidity (%) were collected using a commercial data logger equipped with an infrared sensor (HD31 handheld data logger; HD31.B3 probe for CO₂. DeltaOhm s.r.l.). NH₃ concentration (ppm) was determined using Dräger tubes (outdoor: ammonia 0.25/a, range 0.2–3 ppm; indoor: ammonia 2/a range 2–30 ppm) coupled with Dräger-Tube pump Accuro.

The MU was then deployed as payload to a quadcopter drone (DJI® Matrice 300), with RTK positioning system, as in Fig. 2b. The unit was placed in the upper side of the UAV, to avoid the downwash in the bottom part of the drone and to minimize airflow turbulences generated by the rotors.

Measurements were recorded during a flight over the cattle barn and manure storages at an average height of 30 m a.g.l., with a total duration of 8.5 min. During

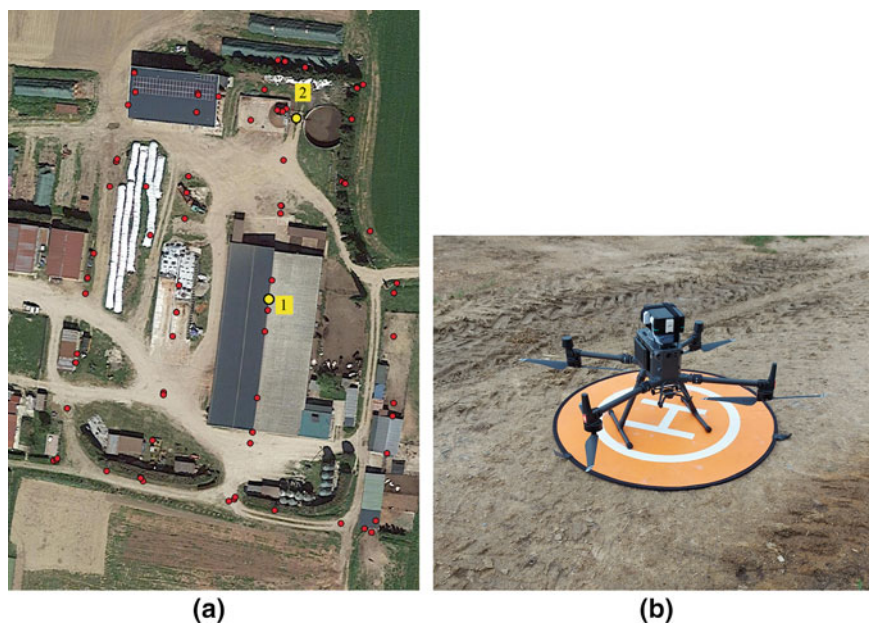


Fig. 2 2a, 2b.2a: Satellite image of the study farm with location of the ground MU (1: indoor, 2: outdoor) and of the UAV sampling points. 2b: quadcopter UAV equipped with the prototype MU

the flight, the drone stopped at predefined coordinates (i.e. waypoints) and recorded air quality and environmental data. Overall, 77 recordings were collected.

Data were downloaded in a spreadsheet format. Descriptive statistics of the collected measurements were computed. Moreover, the correlation with data recorded by the commercial data logger was evaluated with Pearson correlation coefficient.

3 Results and Discussion

The technical test carried out with the prototype MU assessed the feasibility of ground and in-flight measurements. Among the whole set of sensors, 5 provided measurements in the expected range. The NH_3 sensor was not able to yield concentration measurements, since gas concentrations were under the detection limit of the sensor (1 ppm). Indeed, simultaneous measurement carried out with the tubes indicated an ammonia concentration of 0.75 ppm for indoor environment and 0 ppm for outdoor environment. The NH_3 sensor however, tested under laboratory conditions (data not published), showed good response to ammonia variations at low, medium and high concentrations. The CH_4 electrochemical sensor yielded values that were

Table 2 Descriptive statistics of indoor ground measurements (N = 141)

	Min–Max	Ave \pm S.D
Temperature ($^{\circ}$ C)	28.89–30.40	29.66 \pm 0.42
Relative humidity (%)	57.04–60.66	58.86 \pm 0.79
Atmospheric pressure (hPa)	980.24–980.41	980.35 \pm 0.04
PM ₁₀ (μ g/m ³)	7.60–19.70	10.61 \pm 2.24
PM _{2.5} (μ g/m ³)	2.90–5.80	3.73 \pm 0.61
CO ₂ (ppm)	553.00–809.00	632.73 \pm 56.59
NH ₃ (ppm)	below limit of detection	

Table 3 Descriptive statistics of outdoor ground measurements (N = 135)

	Min - Max	Ave \pm S.D
Temperature ($^{\circ}$ C)	32.02–35.83	34.24 \pm 1.24
Relative humidity (%)	46.11–55.24	50.32 \pm 2.22
Atmospheric pressure (hPa)	979.79–980.05	979.91 \pm 0.06
PM ₁₀ (μ g/m ³)	5.2–11.6	7.8 \pm 1.13
PM _{2.5} (μ g/m ³)	2.3– 3.2	2.71 \pm 0.22
CO ₂ (ppm)	420–439	427.8 \pm 4.31
NH ₃ (ppm)	below limit of detection	

not consistent with expected concentrations in a farming environment, thus results of the recordings were not shown.

Results obtained from ground and in-flight measures are reported in Table 2, Table 3 and Table 4.

Ground measures of environmental parameters (temperature, relative humidity) were comparable to those recorded by the commercial data logger (DL). MU measurements for temperature inside the barn ranged from 28.89 to 30.40 $^{\circ}$ C, with an average of 29.66 \pm 0.42 $^{\circ}$ C (Table 2). Simultaneous DL measures ranged from 24.41 to 25.29 $^{\circ}$ C, with an average value of 24.74 \pm 0.25 $^{\circ}$ C. Despite the bias in MU recordings, the two sets of measurements resulted highly correlated ($r_p = 0.923$). The

Table 4 Descriptive statistics of in-flight measurements with UAV (N = 77)

	Min - Max	Ave \pm S.D
Temperature ($^{\circ}$ C)	27.53–28.74	28.06 \pm 0.26
Relative humidity (%)	57.98–61.30	59.90 \pm 0.82
Atmospheric pressure (hPa)	976.83–980.29	977.18 \pm 0.75
PM ₁₀ (μ g/m ³)	5.90–9. 80	8.12 \pm 0.85
PM _{2.5} (μ g/m ³)	3.00–4.40	3.75 \pm 0.31
CO ₂ (ppm)	389.00–469.00	421.57 \pm 14.87
NH ₃ (ppm)	below limit of detection	

relationship also was linear, suggesting that, in indoor conditions, appropriate corrections could ensure an adequate accuracy for this parameter. In the outdoor recording session, however, correlation between MU and DL data was poor ($r_p = 0.430$). As in indoor conditions, the average measurements from MU (34.24 ± 1.24 °C) were higher respect to DL (30.74 ± 1.19 °C), the latter displaying a wider range (28.94 – 33.17 °C). Despite the absence of wind and direct sunlight at the time of the outdoor test, it appears that measures in external conditions may be affected by greater bias. When considering RH, an inverse tendency in measures bias appeared respect to temperature in indoor conditions. On average, MU tended to underestimate humidity (MU: $58.86 \pm 0.79\%$; DL: $70.35 \pm 0.94\%$), however correlation among the two sets of measures was relevant ($r_p = 0.740$). Conversely, in outdoor conditions, correlation was poor ($r_p = 0.350$), but average values resulted similar (MU: $50.32 \pm 2.22\%$; DL: $49.32 \pm 3.07\%$). Average carbon dioxide values inside the barn resulted comparable when measured with MU (632.73 ± 56.59 ppm) and DL (639.98 ± 36.08 ppm). However, range of measures for MU was wider than the range provided by DL (572 – 727 ppm). Accordingly, correlation between the two sets of measures, was poor ($r_p = 0.593$). Similarly, in outdoor conditions MU (427.8 ± 4.31 ppm) and DL (428.9 ± 7.47 ppm) provided very similar average values, but data were not correlated ($r_p = -0.06$). When examining the range of measurements in outdoor conditions, DL resulted wider (414 – 445 ppm).

Recordings of particulate matter showed moderate concentrations, with slightly higher values inside the barn. Feed (total mixed ration) was distributed 1 h prior the time of measurements, thus cows were feeding while the test was carried out. As expected, PM_{10} recordings showed higher values than $PM_{2.5}$, since the latter represents the fraction of PM_{10} with smaller aerodynamic diameter. As to environmental variables measured during the flight (UAV-based measurements), recordings and their variability (range, S.D.) of temperature and RH resulted similar to those collected inside the cattle building (Table 4). In addition, as expected, measurements of CO_2 concentrations highlighted lower values than those collected outside the building. Finally, fine particulate ($PM_{2.5}$) measurements displayed consistent yet slightly higher concentrations than those provided by ground measures, while the opposite occurred for PM_{10} measures. Given that surveying height is able to affect the representativeness and reliability of measurements [4], modeling gas and particulate dispersion under different wind speed and direction conditions would represent a necessary preliminary tool to assess the optimal height for UAV-based measurements.

4 Conclusions

The test carried out at the livestock farming facilities showed that a system integrating ground and in-flight measurements of air pollutants and environmental variables is feasible and could be implemented at farm level. However, the accuracy of measurements (temperature, RH, CO_2) should be improved and further tests in laboratory and field conditions are required. Nevertheless, regarding gaseous concentrations, CO_2

values provided by the MU reflected the expected values under indoor and outdoor conditions. Thus, with the current setup of the prototype MU, average measurements of carbon dioxide over a 10 min time span can be considered as a reliable indicator of the actual CO₂ levels. For ammonia and methane sensors, however, further investigation is required.

Measuring gaseous and particulate air concentrations, both at fixed points at ground and at different heights using UAVs, opens new perspectives towards their implementation within air quality dispersion models as tools to simulate the dispersion of pollutants in the bottom atmospheric boundary layer or to estimate gas emission fluxes from sources using reverse modeling.

References

1. UN DESA (United Nations Department of Economic and Social Affairs). World population prospects: The 2017 revision. (2017)
2. Sands, R.D., Suttles, S.A.: World agricultural baseline scenarios through 2050. *Appl. Econ. Perspect. Policy* **44**, 1–15 (2022)
3. Abbasi, R., Martinez, P., Ahmad, R.: The digitization of agricultural industry—a systematic literature review on agriculture 4.0. *Smart Agricultural Technology* (2), 100042. (2022).
4. Burgués, J., Marco, S.: Environmental chemical sensing using small drones: a review. *Sci. Total Environ.* **748**, 141172 (2020)
5. Roldán, J.J., Joossen, G., Sanz, D., del Cerro, J., Barrientos, A.: Mini-UAV based sensory system for measuring environmental variables in greenhouses. *Sensors* **15**, 3334–3350 (2015)
6. Valente, J., Almeida, R., Kooistra, L.: A comprehensive study of the potential application of flying ethylene-sensitive sensors for ripeness detection in apple orchards. *Sensors* **19**, 372 (2019)
7. Vinković, K., et al.: Evaluating the use of an unmanned aerial vehicle (UAV)-based active AirCore system to quantify methane emissions from dairy cows. *Sci. Total Environ.* **831**, 154898 (2022)

Detecting Coffee Leaf Nitrogen with UAV-Based Vegetation Indexes and Machine Learning



Diego Bedin Marin , Gabriel Araújo e Silva Ferraz , Matteo Barbari , Giuseppe Rossi , and Leonardo Conti 

Abstract This study evaluated the potential of vegetation indexes (VI) based on Unmanned Aerial Vehicle (UAV) and machine learning to estimate nitrogen content (N) in coffee leaves. The study was carried out in a coffee plantation located in Santo Antônio do Amparo, MG, Brazil. In this crop, 10 sampling points were demarcated, consisting of 5 plants. The sampling points were classified as N deficient (<2.5%), N critical (2.5 to 3.0%) and N adequate (3.0 to 3.5%). The images were captured using a commercial UAV 3DR Solo, equipped with a Parrot Sequoia multispectral camera. Chemical analyses of N in coffee leaves and VI values at sampling points were used as input parameters for image training and its classification by Random Forest (RF). The RF performance was evaluated using the metrics global accuracy and kappa coefficient. In general, the classification showed a good performance in evaluating N in the coffee leaves, with global accuracy and kappa coefficient values ranging from 0.64 to 0.78 and 0.52 to 0.73, respectively. Among the evaluated indexes, the Green Normalized Difference Vegetation Index (GNDVI) presented the best results, while the Normalized Difference Red Edge Index (NDRE) was the worst. In addition, it was possible to estimate the spatial distribution of N classes throughout the crop. The GNDVI also presented the best class definitions, demonstrating that 24% of the crop had N deficiency, 49% critical N and 27% sufficient N. The model proposed in this study can offer a promising approach to mapping and quantifying N in a coffee crop.

Keywords Random Forest · Remotely Pilot Aircraft · Nitrogen Management · Coffee Crop

D. B. Marin (✉) · M. Barbari · G. Rossi · L. Conti

Department of Agriculture, Food, Environment and Forestry, University of Florence, Via San Bonaventura 13, 50145 Florence, Italy

e-mail: db.marin@hotmail.com

G. A. S. Ferraz

Agricultural Engineering Department, Federal University of Lavras, Lavras 37200-000, Brazil

1 Introduction

Coffee plants require a high level of fertility and an intensive fertilizer program is a prerequisite for successful coffee production [3]. Despite the importance of Nitrogen (N) for the coffee crop, its proper management is still a challenging task for most producers, as the incorrect diagnosis of N can be a problem from an economic and environmental point of view (Wang et al. 2017). The application of N in excess can cause intoxication in plants and the environment through the processes of leaching and volatilization of the non-absorbed part [1]. On the other hand, doses of N lower than those required by plants can cause reduced leaf production and plant growth, reduced fruit filling, reduced leaf area, and reduced photosynthesis, resulting in gradual chlorosis of older leaves and greater disease susceptibility [11].

To achieve satisfactory levels of N in the coffee tree, producers apply nitrogen fertilizers on a calendar basis, or samples occasionally collected from soil and leaves for laboratory analysis [2, 15]. These traditional methods require a lot of human resources, materials, sample collection, and laboratory tests and are impractical in large areas [18]. Therefore, as an alternative to traditional methods, UAV-based vegetation indexes (VI) are often used to monitor N in plants [13, 19]. However, due to the amount of generated data, analyzing VI based on UAVs requires a robust technique, such as machine learning methods [12]. When applied to agriculture, these methodologies achieve advantages such as solving non-linear problems using datasets from multiple sources [4, 9] and discovering hidden information in the data [16]. In this context, this study evaluated the potential of vegetation indexes (VI) based on UAV and machine learning to estimate N content in coffee leaves.

2 Material and Methods

2.1 Study Site

The study was carried out on a commercial farm on the Bom Jardim farm, located in Santo Antonio do Amparo, Minas Gerais, Brazil, with an average altitude of 935 m. The total area is approximately 1.5 ha, cultivated with coffee (*Coffea arabica* L.), cultivar Catuai 99, with 5 years of the initial planting, with a spacing of 3.5 m between rows and 0.5 m between plants, totaling 5,700 plants ha⁻¹.

2.2 UAV Image Acquisition and Preprocessing

Images were obtained using a commercial UAV 3DR Solo (3D Robotics, Berkeley, CA, USA) equipped with a Parrot Sequoia multispectral camera. This camera has an RGB sensor with a resolution of 16 megapixels (4608 × 3456) and four extra

Table 1 Vegetation indexes from multispectral images obtained with Unmanned Aerial Vehicle (UAV)

Vegetation indexes	Equation	Reference
GNDVI (Green Normalized Difference Vegetation Index)	$\frac{\rho_{nir} - \rho_{green}}{\rho_{nir} + \rho_{green}}$	[6]
NDVI (Normalized Difference Vegetation Index)	$\frac{\rho_{nir} - \rho_{red}}{\rho_{nir} + \rho_{red}}$	Rouse et al. [17]
NDRE (Normalized Difference Red Edge)	$\frac{\rho_{nir} - \rho_{edge}}{\rho_{nir} + \rho_{edge}}$	[7]

ρ_{green} : reflectance in the green band; ρ_{red} : reflectance in the red band; ρ_{nir} : reflectance in the near-infrared band; ρ_{edge} : reflectance in the red-edge band

sensors with a resolution of 1.5 megapixels (1280 × 960) in the spectral bands of green (550 nm BP 40), red (660 nm BP40), red-edge (735 nm BP 10) and near-infrared (790 nm BP 40). Image processing was performed using Agisoft PhotoScan® Professional software, version 1.2.4 (Agisoft LLC, Saint Petersburg, Russia). After image processing, the orthomosaics of the individual spectral bands (green, red, red-edge and near-infrared) were used to calculate the vegetation indexes. Vegetation indexes (Table 1) were chosen based on their ability to determine nitrogen content in coffee crops from remote sensing data [2, 14].

2.3 Leaf Nitrogen Analysis

The N analysis was carried out in 10 sample points defined with the aid of the RGB orthomosaic. For this, regions were visually identified in the crop considered to be nitrogen deficient (<2.5%), critical (2.5 to 3.0%) and sufficient (3.0 to 3.5%). The identification of these regions was based on the number of yellow leaves on the coffee plants since yellow leaves are a sign of nitrogen deficiency. Each sampling point consisted of 5 plants, 1 central plant and 2 plants oriented north–south of the central plant. From each plant, 3 leaves were collected from both sides of the planting line at three different canopy heights, totaling 30 leaves for each sampling point. After collection, the leaves were sent to the foliar analysis laboratory at the University of Lavras to quantify the nitrogen content using the Kjeldahl method.

2.4 Random Forest (RF) Classification

To classify the N content in coffee leaves from the VI, the Random Forest (RF) machine learning method was used. The modeling was created in R (R Core Team), using the R Random Forest package [10]. For the algorithm’s training, the values of the vegetation indexes in the pixels referring to each of the 5 plants of each sampling point were used with the chemical analysis of the N content in the leaves

of the coffee tree samples. Classification performance was evaluated based on standard statistical measures [5] derived from the confusion matrix. Statistical measures selected included overall accuracy (Eq. (1)) and kappa coefficient (Eq. (2)).

$$\text{OverallAccuracy} = \frac{\sum_{i=1}^q n_{ii}}{n} \times 100\% \quad (1)$$

$$\text{Kappa Coefficient} = \frac{n \sum_{i=1}^q n_{ii} - \sum_{i=1}^q n_{i+} n_{+i}}{n^2 - \sum_{i=1}^q n_{i+} n_{+i}} \times 100\% \quad (2)$$

where q is the number of classes, n represents the total number of considered pixels, n_{ii} are the diagonal elements of the confusion matrix, n_{i+} represents the marginal sum of the rows in the confusion matrix, and n_{+i} is the marginal sum of the columns in the confusion matrix.

3 Results and Discussions

3.1 Accuracy Assessment

In general, the classification of images by RF from VI showed a good performance in evaluating the nitrogen content of leaves in coffee plants. The overall accuracy and kappa coefficient values ranged from 0.64 to 0.78 and 0.52 to 0.73, respectively (Fig. 1).

It was possible to observe that the vegetation index GNDVI presented the best results, while the NDRE index the worst results. The better performance for GNDVI may be related to the greater number of plants with sufficient N content in the crop and, consequently, higher chlorophyll content in the leaves. The reflectance in the green band is greatly affected by variations in the chlorophyll content, when compared to the reflectance in the red band [8], explaining the small difference in the results between the GNDVI and NDVI. Regarding the NDRE, the poor performance may be related to the bandwidth of the Parrot Sequoia camera. This camera has a bandwidth 4 times smaller for Red Edge when compared to green and red, making the NDRE less sensitive to variations in chlorophyll content in coffee leaves. This relationship was also evidenced by [2].

3.2 Classification Maps of the Spatial Distribution of N in the Field

The classification maps of the spatial distribution of N in the crop based on RF and IV can be seen in Fig. 2.

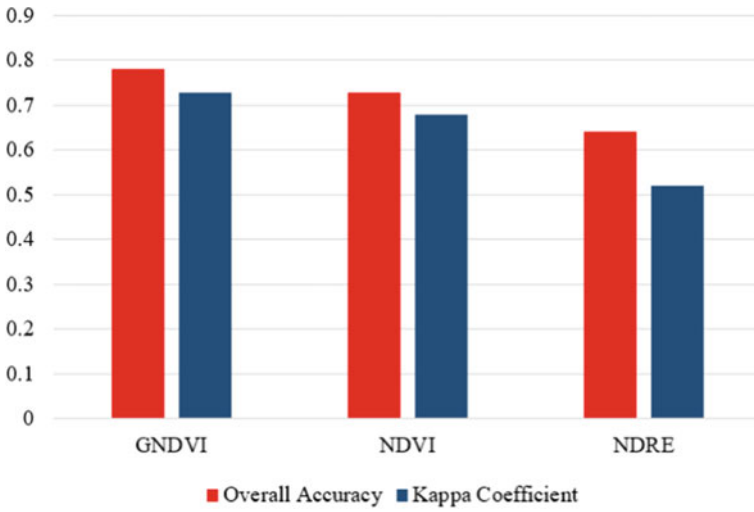


Fig. 1 Overall Accuracy and Kappa Coefficient for image classification through Random Forest (RF) from vegetation indexes (VI)

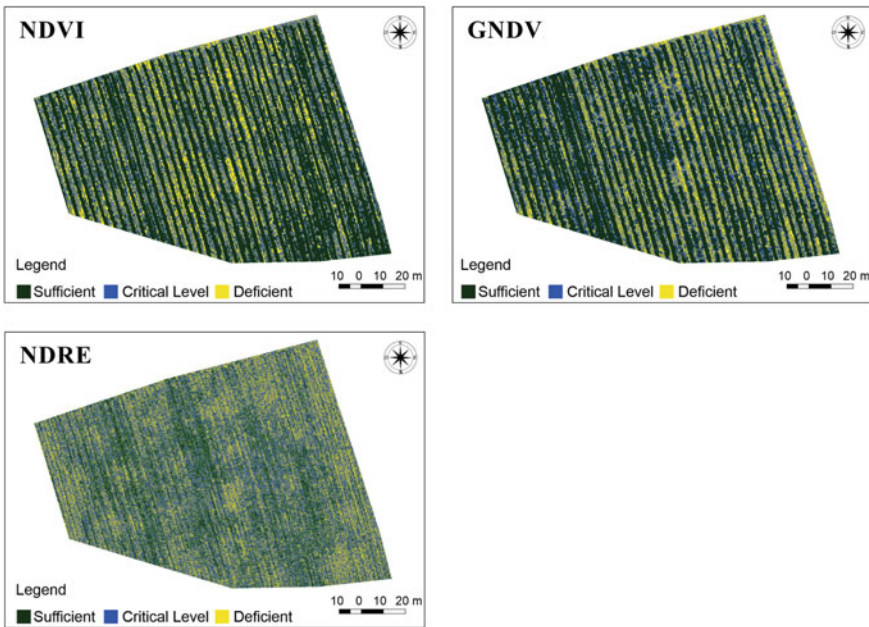


Fig. 2 Predictive maps of the N content spatial distribution in coffee leaves, obtained from the classification of images using RF from vegetation indexes

Table 2 Percentage (%) of areas in the coffee plantation that had N content sufficient, critical, and deficient, according to the appraisal maps of the N content spatial distribution in coffee leaves

Vegetation Indexes	Area (%)		
	Sufficient	Critical	Deficient
GNDVI	49	27	24
NDVI	53	23	24
NDRE	21	40	39

It was possible to observe that the maps of the vegetation indexes GNDVI and NDVI showed good class definitions. The NDVI showed the highest number of plants with N deficiency in the central region of the crop. In the GNDVI map, the plants with deficiency extended from the central region to the eastern region of the crop. Regarding the NDRE, the map did not present a good class definition, making it difficult to identify crop regions with N deficiency.

3.3 Quantification of N in the Crop

The quantification of N content in plants across the field based on classification maps are shown in Table 2.

The GNDVI and NDVI indexes showed the same percentage of the area of plants with nitrogen deficiency (24%). However, the NDVI overestimated the area with sufficient N and overestimated the area with critical N when compared to the GNDVI. In relation to the NDRE, this index showed a high percentage of the area of plants with deficient N, in contrast to a low percentage of area for plants with sufficient N.

The results of the classification and quantification maps of N in the whole crop showed the possibility of applying N in a localized and varied way. For example, for the GNDVI and NDVI, only 24% of the area was deficient in N. Thus, an application of N based on these maps could promote a reduction of up to 76% in the application of nitrogen fertilizers. However, it is worth mentioning that further studies are recommended to validate the proposed methodology. For example, to improve classification performance, as well as accurately quantify the percentage of crop area with deficient, critical, and sufficient N levels, a pre-classification can be applied to remove vegetation between planting rows. Thus, the classification and quantification of N in the crop will be performed only for coffee plants.

4 Conclusions

The detection of nitrogen in coffee leaves with vegetation indexes based on UAV and machine learning can offer the producer a very promising methodology to monitor and quantify the N content in coffee crops. The application of this methodology can contribute to a more sustainable coffee production with the reduction of the

environmental impacts caused by the application of N in excess, as well as economic gains with the reduction in the consumption of fertilizers.

References

1. Ciampitti, I.A., Salvagiotti, F.: New insights into soybean biological nitrogen fixation. *Agron. J.* **110**, 1185–1196 (2018)
2. Chemura, A., Mutanga, O., Odindi, J., Kutuywayo, D.: Mapping spatial variability of foliar nitrogen in coffee (*Coffea arabica* L.) plantations with multispectral Sentinel-2 MSI data. *ISPRS J. Photogrammetry Remote Sens.* **138**, 1–11 (2018)
3. Chemura, A.: Modelling spatial variability of coffee (*Coffea Arabica* L.) crop condition with multispectral remote sensing data. Ph.D. Thesis, University of KwaZulu-Natal, Pietermaritzburg, South Africa (2017)
4. Chlingaryan, A., Sukkarieh, S., Whelan, B.: Machine learning approaches for crop yield prediction and nitrogen status estimation in precision agriculture: a review. *Comput. Electron. Agric.* **151**, 61–69 (2018)
5. Foody, G.M.: Status of land cover classification accuracy assessment. *Remote Sens. Environ.* **80**, 185–201 (2002)
6. Gitelson, A.A., Kaufman, Y.J., Merzlyak, M.N.: Use of a green channel in remote sensing of global vegetation from EOS-MODIS. *Remote Sens. Environ.* **58**, 289–298 (1996)
7. Gitelson, A., Merzlyak, M.N.: Quantitative estimation of chlorophyll-a using reflectance spectra: Experiments with autumn chestnut and maple leaves. *J. Photochem. Photobiol. B* **22**, 247–252 (1994)
8. Hunt, E.R., Doraiswamy, P.C., McMurtrey, J.E., Daughtry, C.S.T., Perry, E.M., Akhmedov, B.: A visible band index for remote sensing leaf chlorophyll content at the canopy scale. *Int. J. Appl. Earth Obs. Geoinf.* **21**, 103–112 (2013)
9. Liakos, K.G., Busato, P., Moshou, D., Pearson, S., Bochtis, D.: Machine learning in agriculture: a review. *Sensors* **18**, 2674 (2018)
10. Liaw, A., Wiener, M., Breiman, L., Cutler, A.: Package “randomForest”. (2018) <https://cran.r-project.org/web/packages/randomForest/randomForest.pdf>. Accessed 10 July 2020
11. Mengel, K.; Kirkby, E.A. *Principios de nutrición vegetal*. International Potash Institute, Basel (2001)
12. Osco, L.P., et al.: Predicting canopy nitrogen content in citrus-trees using random forest algorithm associated to spectral vegetation indices from UAV-imagery. *Remote Sens.* **11**(24), 2925 (2019)
13. Osco, L.P., et al.: Leaf nitrogen concentration and plant height prediction for maize using UAV-based multispectral imagery and machine learning techniques. *Remote Sens.* **12**(19), 3237 (2020)
14. Putra, W.B.T., Soni, P.: Enhanced broadband greenness in assessing chlorophyll a and b, carotenoid, and nitrogen in Robusta coffee plantations using a digital camera. *Precision Agric.* **19**, 238–256 (2018)
15. Putra, B.T.W., Soni, P., Morimoto, E., Pujiyanto, P.: Estimating biophysical properties of coffee (*Coffea canephora*) plants with above-canopy field measurements, using CropSpec. *Int. Agrophys.* **32**, 183–191 (2018)
16. Qiu, J., Wu, Q., Ding, G., Xu, Y., Feng, S.: A survey of machine learning for big data processing. *EURASIP J. Adv. Sig. Process.* **67**, 1–16 (2016)
17. Rouse, J.W., Haas, R.H., Deering, D.W., Schell, J.A., Harlan, J.C.: Monitoring the vernal advancement and retrogradation (Green Wave Effect) of natural vegetation; Type III Final Report; NASA/GSFC: Greenbelt, MD, USA (1974)

18. Ye, X., Abe, S., Zhang, S.: Estimation and mapping of nitrogen content in apple trees at leaf and canopy levels using hyperspectral imaging. *Precision Agric.* **21**, 198–225 (2020)
19. Zheng, H., et al.: Evaluation of RGB, color-infrared and multispectral images acquired from unmanned aerial systems for the estimation of nitrogen accumulation in rice. *Remote Sens.* **10**, 824 (2018)

Mapping and Disposal of Irrigation Pipes for a Sustainable Management of Agricultural Plastic Waste



Ileana Blanco, Giuliano Vox, Fabiana Convertino, and Evelia Schettini

Abstract Plastic materials are largely used in agricultural activities. Plastic products are commonly employed as covering in greenhouses and tunnels, for soil mulching, silage, pots, and containers and for irrigation and drainage pipes. The use of plastic products provides several benefits for agricultural production. However, the downside is represented by the large amount of generated agricultural plastic waste (APW). There is a need of a conscious and sustainable management of APW from an environmental and economic point of view. APW should be considered as a resource, in the optic of a circular economy. To this end, the definition of a rigorous approach for agricultural plastic detection, mapping, collection, and disposal is required. In this study, the attention was focused on the irrigation pipes. An agricultural area, characterized by a variety of crops, in Apulia region (Southern Italy) was considered as case study. The paper proposes a territorial analysis, performed using a Geographical Information System (G.I.S), for mapping areas of use of irrigation pipes and of waste production from these. As a result, a georeferenced database and the quantification of the potential waste were obtained. This allows identifying critical areas for plastic waste production due to irrigation pipes and can be used as tool for planning a proper collection and disposal strategy.

Keywords Sustainability · G.I.S. · Land Use · Plastic Detection · Agricultural Plastic Waste · Waste Valorization

I. Blanco

Department of Biological and Environmental Sciences and Technologies (DiSTeBA), University of Salento, S.P. 6 Lecce - Monteroni, 73100 Lecce, Italy

G. Vox · F. Convertino (✉) · E. Schettini

Department of Agricultural and Environmental Science (DISAAT), University of Bari "Aldo Moro", Via Amendola 165/A, 70126 Bari, Italy

e-mail: fabiana.convertino@uniba.it

1 Introduction

In 2020, the 3.2% of the total European demand for plastic products, equal to 49.1 million tons, came from the agriculture sector. In the same year, more than 29 million tons of plastic post-consumer waste was collected in Europe, 23% of which still sent to landfill [1]. The large use of plastic in agriculture is mainly due to the spread of intensive and semi-intensive agricultural practices [2, 3]. Plastic products are used due to their peculiar characteristics, such as: lightness and good mechanical properties, versatility of applications, ease of installation, use and management, and low cost. Plastics can be processed in many ways to obtain different shapes and due to their characteristics, they have significantly replaced other traditional materials. In agriculture, plastics are used both in open field and in protected cultivation. Agricultural plastics can be classified based on their application into covering and shading, mulching, solarization and direct covering, irrigation pipes (IPs), pots, bags and various containers, packaging, sacks and strings and materials for transport, storage, and sale agricultural products.

The use of plastic products in agriculture has simplified many activities and brought a positive contribution to the production. Most of the plastic materials used in agriculture are made of synthetic petrochemical polymers. Base polymer, additives, physical characteristics, and thickness differ in the various products [4].

As the plastic products are so largely used in agriculture, these are also one of the main sources of waste. Much of the agricultural plastic waste (APW) in Mediterranean area is made of after-use covering and mulching films, IPs, and nets [5–7]. Given their chemical composition, plastic products at the end of their useful life need to be properly collected, disposed of, and possibly recycled. Moreover, these products are often dirty of soil or organic matter and contaminated by chemicals. This represents a serious environmental issue, requiring proper efficient disposing solutions, often expensive. However, APW is very often managed in improper ways. Abandonment in field, open field burning, burying in soil, and disposing in landfills are very widespread practices. Serious environmental and economic consequences, as ecosystems degradation, soil, water and food contamination, release of dangerous pollutants, arise from such wrong practices [3, 4].

APW can be managed in an economical and environmentally friendly way, in an optic of circular economy [8]. APWs, if appropriately collected, can be recycled, and used to produce other plastic materials. Thus, valorizing APW can lead to a double benefit: the reduction of waste generated, and the limitation of plastics produced with non-renewable materials [2, 9]. For any non-recyclable fractions, the energy recovery could be considered [4].

APW are generated all year round, but the accumulation of specific plastic waste products is linked to the season and the geographic area [3]. The issue related to APW location is well known [10]. A correct management of APW implies minimization, collection, sorting, treatment, and disposal [11].

The lack or the inefficiency of the existing management systems for APW is often the main reason of the dangerous and illegal practices carried out by many farmers

in European countries. Related issues are the lack of standard methods for APW types classification and quantification and for sites and flows identification within an agricultural area. Such tools could be useful to create a georeferenced database to be used for APW management. An efficient and sustainable APW management plan could be developed knowing the amount of APW generated in an area and where there is the highest APW concentration.

A georeferenced database for mapping and continuously updating information on APW can be realized by using geographical information systems (GISs) [7, 12–14]. GISs allow storing, georeferencing, analyzing and displaying large amount of data. Using a GIS can be precious to make territorial analyses, to identify APW generation sites and relative quantities, to select disposal sites by considering infrastructure, landscape constraints, social and economic factors.

The aim of this paper is to apply the approach based on GIS to quantify the APW due to IPs, with reference to the different crop types (CTs), in a South Italy rural area. This was made by applying specific plastic waste indices (PWIs). In this way, a georeferenced database of APW generated by IPs use was created. Such database can be easily managed and used as a tool by Authorities and Stakeholders for APW production monitoring and APW flows managing. This tool, continuously upgradeable, can support the sustainable development and planning of the rural territory and landscape.

2 Materials and Methods

The municipality of Noicattaro (Bari, Apulia Region, Southern Italy) was chosen as case study. The territory of Noicattaro has an extension of about 4080 ha and about 25,000 inhabitants. The area is particularly devoted to vineyards cultivation and partially to olive groves. Thus, the agricultural area is responsible for an intense production of APW due to the local crops production.

In this study, the attention was focused on APW generated by IPs use. A GIS database was created, APW generated by IPs was georeferenced on the land.

The free software QGIS [15] was used. This allowed the elaboration of land use map starting from data provided by the territorial information system of the Apulia Region [16]. Land use map was used for selecting and highlighting the different crop production that imply IPs use and in turn APW generation. Before quantifying the APW due to IPs, crop classification was verified by photointerpretation using Google satellite images. The different crop areas were manually adjusted in QGIS and checked for correspondence with the CT. To quantify the APW from IPs, PWIs, as defined by Blanco et al. [7], were adopted. PWIs are available for the different plastic applications and for the CTs. The ones concerning IPs are shown in Table 1.

The PWIs, each to the relative CT, were attributed to the land use map features. The APW was quantified and georeferenced and the APW map of Noicattaro was produced. Then, the suitable location for the collection centre was identified. The position of the collection centre was defined by considering the centroids for the

Table 1 Plastic Waste Index (PWI) for irrigation pipes and different crop types

Crop type	Pipe length [m ha ⁻¹] PL ₂₅ ^a	PL ₁₀₀ ^b	Life [month]	PWI [kg ha ⁻¹ yr ⁻¹]
Vineyards	4001.33	200.13	215.36	83.33
Olive groves	1600.00	200.00	216.80	50.00
Orchards	2500.00	200.13	217.28	62.50
Vegetables	3000.00	200.40	216.16	69.44
Greenhouses	4500.00	300.00	216.00	104.17

^a: length of pipes with diameter of 25 mm, ^b: length of pipes with diameter of 100 mm

different CTs areas, appropriately weighted. The presence of territorial constraints, as defined by the Regional Territorial Landscape Plan of the Apulia Region (PPTR), was considered too.

Concerning IPs, these are made of header tubes of HDPE, having a diameter of 100 mm, and secondary tubes of HDPE, with a diameter of 25 mm [7]. Thus, the PWI [kg ha⁻¹ yr⁻¹] of IPs for all the crops was obtained as [7]:

$$PWI = (PL_{25} \cdot PW_{25} + PL_{100} \cdot PW_{100}) \cdot life^{-1} \cdot U_{cvp} \quad (1)$$

where: PL_{25} and PL_{100} [m ha⁻¹] are the lengths of pipes with diameter of 25 mm and 100 mm, respectively; PW_{25} and PW_{100} [kg m⁻¹] are the weights of pipes with diameter of 25 mm (0.25 kg m⁻¹) and 100 mm (2.5 kg m⁻¹), respectively; $life$ [months] is the plastic useful lifetime; U_{cvp} (12 months yr⁻¹) is the pipes unit factor for converting the results in kg ha⁻¹ yr⁻¹ unit.

The base map materials used consisted of the Google satellite images, the municipality boundaries and the Land Use (LUS) Map of the Apulia Region. These were freely provided and derived from the 2006 orthophotos, with 50 cm pixel resolution, updated in 2011. The map legend complies with the European CORINE Land Cover Changes Database with an extension to the fourth level. The maps elaborated with QGIS were placed in the WGS 84 / UTM zone 33N reference system. The Apulia LUS map containing the data on the CTs distribution consists of several shapefiles related to the analysed area. These shapefiles were merged in QGIS to create one, that was clipped according to the municipality boundaries, to limit the information to the study area.

Only crops associated with APW due to IPs were selected on the LUS map. After checking the CT features by photointerpretation, the database of the LUS map was extended by adding in the attribute table new fields about the area of each feature (S_i , m²) and the PWI for IPs for each CT (PWI_{CT}). Finally, the amount of APW for CT (APW_{CT} , kg yr⁻¹) was obtained by:

$$APW_{CT} = S_i \cdot PWI_{CT} \quad (2)$$

The sum of the amount of APW of the different CTs provided the total quantity of APW due to IPs in the territory of Noicattaro.

The GIS information was used to identify a suitable location for the first collection centre. The QGIS centroid tool for localizing the geometric centre of the features allowed to locate the collection centre.

3 Results and Discussion

The crop distribution in the study area obtained by the selection on the LUS map was showed in Fig. 1 together with the map modified after the photointerpretation. The corrected map suggested that vegetables and vineyards were overestimated in the unmodified map, while orchards and olive groves underestimated.

The predominant CT are the vineyards (80.37%), followed by olive groves and negligible percentage of orchards and vegetable/greenhouses (Fig. 2).

The application of the PWIs on the LUS map allowed to identify the spatial distribution of APW due to IPs in Noicattaro. The density of waste due to pipes was shown in Fig. 3. The most diffuse areas (vineyards) are characterized by a high PWI. As highlighted in Fig. 3, the APW due to IPs in Noicattaro is mainly generated in vineyards cultivation (166.42 t yr^{-1}). This accounts for about the 87% of all the APW from IPs in the study area.

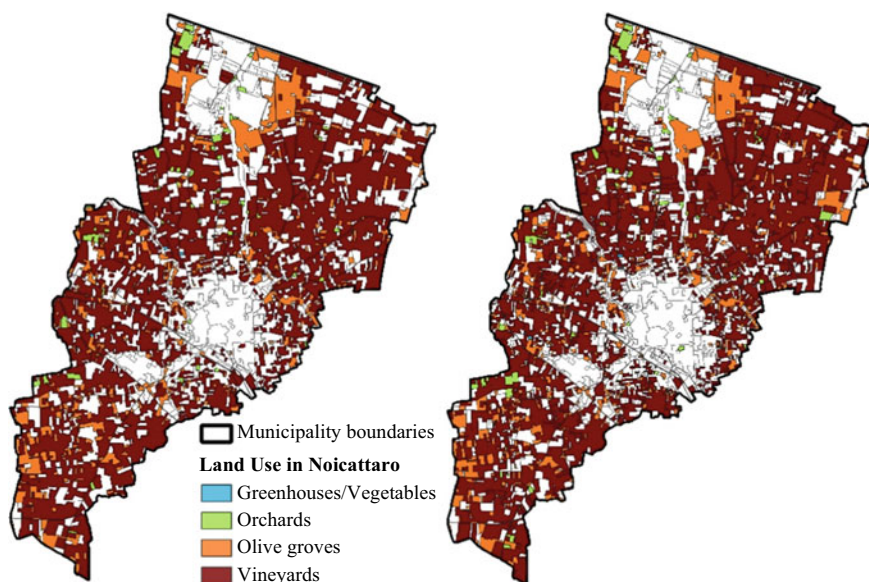


Fig. 1 Land use in Noicattaro: map as taken from database (on the left) and corrected through photointerpretation (on the right)

Fig. 2 Percentage distribution of land uses in Noicattaro

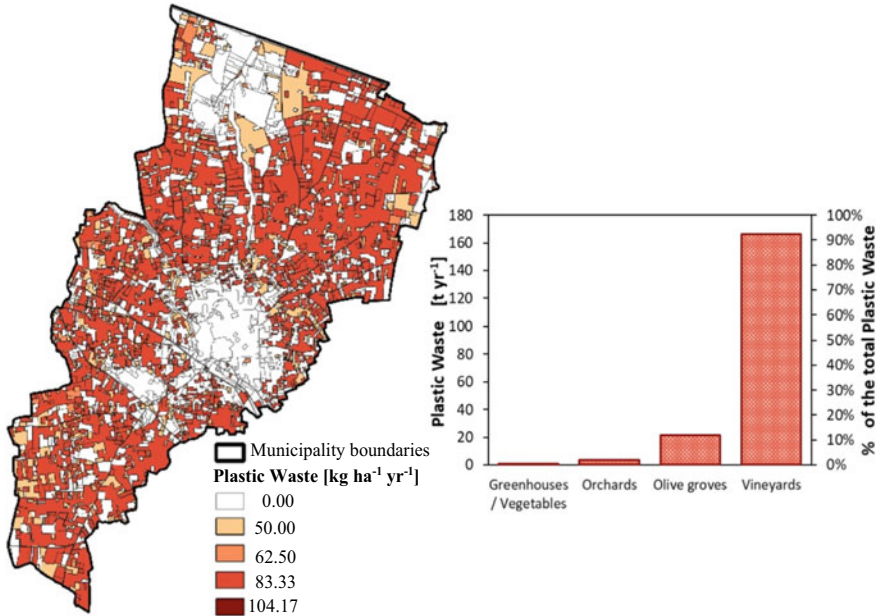
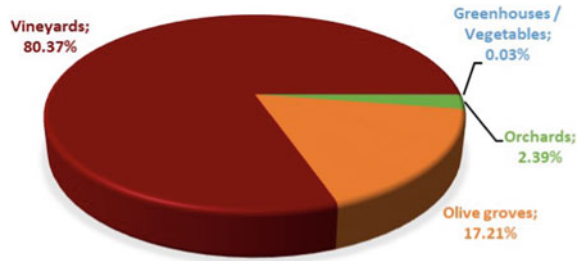


Fig. 3 APW in Noicattaro: distribution of APW density (on the left) and total amount of APW per year and crop type (on the right)

Finally, the most suitable location for the collection centre for APW made of IPs was defined considering the quantities and the distribution on the land (Fig. 4). The collection centre position was defined with a buffer zone of radius equal to 500 m.

The suitable position was defined considering the sensitive areas indicated in the Apulia PPTR (Fig. 4). It was taken care that the collection centre was not in the areas with landscape restrictions. Because the centroid of the features fell in the landscape constraint area around “Lama San Giorgio” and “Torrente Chiancarello”, it was moved just outside this area to avoid conflict with this sensitive area. This map can be a useful tool for making a first selection of suitable area for a collection centre.

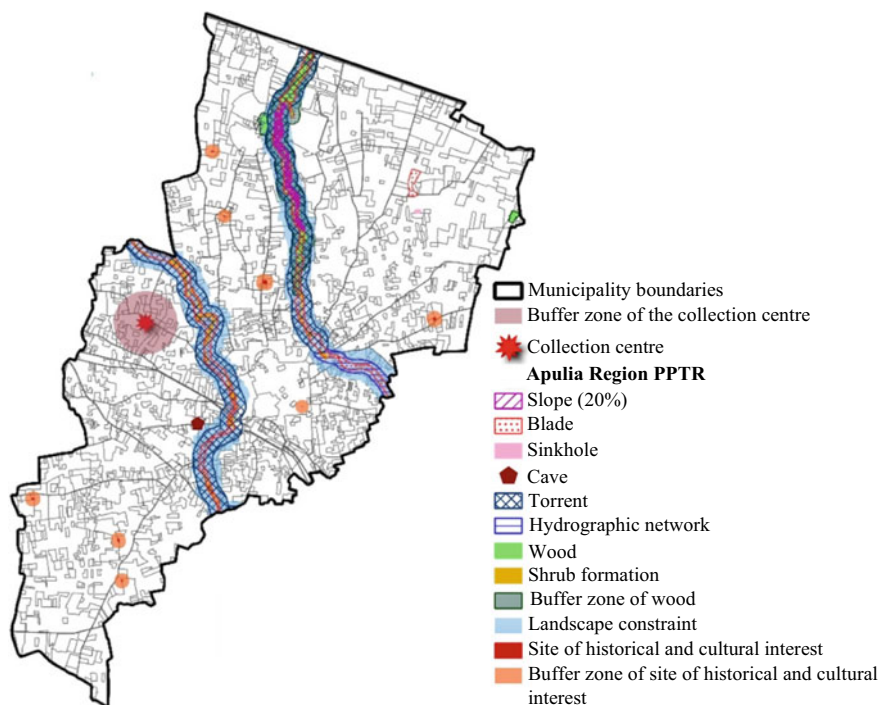


Fig. 4 Suitable location of the collection centre

The collection centre location was defined within the municipality boundaries of Noicattaro. The proposed methodology can be extended to include some surrounding municipalities for defining a common collection centre. This would be useful considering that the APW management could be implemented more efficiently on an intermunicipal scale.

4 Conclusions

The spread of intensive and semi-intensive agricultural practices implies the use of huge quantities of plastic products. This means also that large amounts of plastic waste are generated and that these need to be disposed of in the most proper way to limit the negative impact on the ecosystem. An efficient management system is necessary. The Apulia Region, in Italy, is characterized by a relevant consumption of plastic products for agricultural activities. One of the most produced agricultural plastic wastes is due to irrigation pipes used for several crop productions.

In the municipality of Noicattaro, the highest production of plastic waste made of pipes is generated in vineyards cultivation. A territorial analysis based on the

use of a GIS was proposed. It allowed to update the available land use map, adding information related to the plastic products use and waste generation. The result is a georeferenced database, continuously upgradeable through land use and plastic waste changes monitoring.

This can be a precious tool for decision makers and planners to quantify and localize agricultural plastic waste generation, to identify the most suitable areas for collection centres and to analyze possible development scenarios for rural areas.

Acknowledgements The contribution to programming and conducting this research was equally shared between the Authors.

This research was carried out as a part of the Project “Plastic in Agricultural Production: Impacts, Lifecycles and Long-term sustainability—PAPILLONS”, financed by the European Union—Topic: SFS-21-2020 Emerging challenges for soil management—Sub-Topic B [2020]: Emerging challenges for soil management: use of plastic in agriculture (RIA)—Grant agreement ID: 101000210.

References

1. Plastics Europe: Plastics - the Facts 2021: An analysis of European plastics production, demand and waste data (2021)
2. Picuno, P.: Innovative material and improved technical design for a sustainable exploitation of agricultural plastic film. *Polym-Plast Tech. Mat.* **53**, 1000–1011 (2014). <https://doi.org/10.1080/03602559.2014.886056>
3. Briassoulis, D., Babou, E., Hiskakis, M., Scarascia, G., Picuno, P., Guarde, D., Dejean, C.: Review, mapping and analysis of the agricultural plastic waste generation and consolidation in Europe. *Waste Manag. Res.* **31**, 1262–1278 (2013). <https://doi.org/10.1177/0734242X13507968>
4. Scarascia Mugnozza, G., Sica, C., Russo, G.: Plastic materials in European agriculture: actual use and perspectives. *J. Ag. Eng.* **3**, 15–28 (2011). <https://doi.org/10.4081/jae.2011.3.15>
5. Briassoulis, D., Hiskakis, M., Babou, E., Antiohos, S.K., Papadi, C.: Experimental investigation of the quality characteristics of agricultural plastic wastes regarding their recycling and energy recovery potential. *Waste Manag.* **32**, 1075–1090 (2012). <https://doi.org/10.1016/J.WASMAN.2012.01.018>
6. Lanorte, A., De Santis, F., Nolè, G., Blanco, I., Loisi, R.V., Schettini, E., Vox, G.: Agricultural plastic waste spatial estimation by landsat 8 satellite images. *Comput. Electron. Agric.* **141**, 35–45 (2017). <https://doi.org/10.1016/J.COMPAG.2017.07.003>
7. Blanco, I., Loisi, R.V., Sica, C., Schettini, E., Vox, G.: Agricultural plastic waste mapping using GIS. A case study in Italy. *Resour. Conserv. Recycl.* **137**, 229–242 (2018). <https://doi.org/10.1016/J.RESCONREC.2018.06.008>
8. Plastics Europe: the circular economy for plastics: a European overview (2022)
9. González-Sánchez, C., Martínez-Aguirre, A., Pérez-García, B., Martínez-Urreaga, J., De La Orden, M.U., Fonseca-Valero, C.: Use of residual agricultural plastics and cellulose fibers for obtaining sustainable eco-composites prevents waste generation. *J. Clean. Prod.* **83**, 228–237 (2014). <https://doi.org/10.1016/J.JCLEPRO.2014.07.061>
10. De Lucia, C., Paziienza, P.: Market-based tools for a plastic waste reduction policy in agriculture: a case study in the south of Italy. *J. Environ. Manag.* **250** (2019). <https://doi.org/10.1016/j.jenvman.2019.109468>

11. Horodytska, O., Valdés, F.J., Fullana, A.: Plastic flexible films waste management – a state of art review. *Waste Manag.* **77**, 413–425 (2018). <https://doi.org/10.1016/J.WASMAN.2018.04.023>
12. Schettini, E., Scarascia Mugnozza, G., Blanco, I., Convertino, F., Vox, G.: Agricultural plastic waste. In: Colangelo, F., Cioffi, R., Farina, I. (eds.) *Handbook of Sustainable Concrete and Industrial Waste Management*, pp. 255–268 (2022)
13. Jiménez-Lao, R., Aguilar, F.J., Nemmaoui, A., Aguilar, M.A.: Remote sensing of agricultural greenhouses and plastic-mulched farmland: an analysis of worldwide research. *Remote Sens.* **12**, 2649 (2020). <https://doi.org/10.3390/RS12162649>
14. Vox, G., Loisi, R.V., Blanco, I., Scarascia Mugnozza, G., Schettini, E.: Mapping of agriculture plastic waste. *Agric. Agric. Sci. Procedia.* **8**, 583–591 (2016). <https://doi.org/10.1016/j.aaspro.2016.02.080>
15. QGIS <https://www.qgis.org>
16. SIT Puglia <http://www.sit.puglia.it>

Buildings for Citrus Juices and Essential Oil Manufacturing: The Floor Design



Giuseppe Davide Cardinali and Francesco Barreca

Abstract It is essential to pay equal attention in the agroindustry buildings design to all systems and components, but the floor design is very often neglected. The hot oils, greases and chemicals used in processing invariably end up on the floor and corrode the surface. Thermal shock from hot water wash downs crack and disintegrate weak surfaces and frequent impacts from heavy machinery, foot and vehicle traffic dent, damage and destroy unprepared floors. In particular, within the processing area of citrus juices and essential oil, floors can be subject to spillages of water, essential oil, citric acid, natural chemical substances contained into citrus products, generating both a slip and hygiene risk. These substances can generate safety problems related not only to slipping and cleanability but also wear, and deterioration, which they put down to a choice of the wrong floor material. The essential oils on the market are mainly obtained from vegetable substances and in particular from citrus fruits, using low-value materials such as rind, pulp and seeds, remaining parts of the production activities. The fruits of all citrus species constitute a potential source of essential oils and are of commercial interest, such as lemon, orange, grapefruit and other more particular ones such as bergamot, a typical citrus fruit of the south Italy, whose essences are used in the food, cosmetic and pharmaceutical industries. Essential oils are composed of a volatile and a non-volatile part, the latter consisting of numerous substances such as: fatty acids, waxes, coumarins, psoralens, flavonoids, etc. A study was carried out on the right solutions design of the floor in the buildings for citrus juices and essential oil manufacturing. Were analysed the floor main performances, in respect to workers safety, hygiene risk and management in use, to choice the more suitable floor material. Were evaluated the effects that a spillage of citrus essential oils and juice has on the surface characteristics of flooring from more traditional ones, such as ceramic ones to the most innovative ones such as resins. The test were carried out in accord to international standard or national rule as the Italian Ministerial Decree 236/89 to evaluate the dynamic friction coefficient for slip risk, measured with the Tortus tribometer, or specific tests, to assess the level of cleanability and wear resistance of the flooring.

G. D. Cardinali (✉) · F. Barreca
Mediterranean University, 89100 Reggio Calabria, Italy
e-mail: gcardinali@unirc.it

© The Author(s), under exclusive license to Springer Nature Switzerland AG 2023
V. Ferro et al. (eds.), *AIIA 2022: Biosystems Engineering Towards the Green Deal*,
Lecture Notes in Civil Engineering 337,
https://doi.org/10.1007/978-3-031-30329-6_111

1075

Keywords Essential oil · safety slipperiness · floor materials · wear safety · agri-food industry

1 Introduction

The modern food processing buildings have to adhere to stricter performance criteria than respect in the past. In particular, employee safety, food hygiene and environmental sustainability are pillars of the new design concepts. However, these criteria should not limit innovation or the range of products offered to the customer. The unique features of the raw materials of the food processing industries, such as the seasonality and perishability required for processing to maintain high quality standards, necessitates special attention towards the building and the design of the components. Great care must be taken to achieve high levels of product quality and preserve product integrity, and these aims can only be obtained by having an appropriate design. To achieve these aims the European Parliament and the Council of the European Union, over the past few years, have adopted different regulations and directives on food safety throughout the food chain, starting with the primary production and the food processing plants. Many of the elements of the building design are the same for food facilities as they are for other agro-industrial processing buildings, particularly for those processing citrus essence. However, there are a few significant differences, particularly in the working and storage products area design. The differences occur due to the following:

- The storage life of foods is relatively limited and strongly affected by temperature, pH, water activity, maturity, prior history, and initial microbial contamination levels.
- The foods are highly susceptible to microbial attack and insect and rodent infestation, for these reasons very high and verifiable levels of process safety and sterility have to be provided.
- The citrus essence is strongly affected by temperature, and has a low inflammable point.
- Food packaging in small containers is often used or required; and strong-package-product interactions exist. Segregation often causes problems in the packaging of powdered foods. Aseptic packaging is starting to be widely used.
- The citrus essence is transported to the processing and storage area using tanks by means of forklift trucks.
- Citrus essence is highly corrosive on the materials which it comes into contact with.
- In the food process usually a large amount of water is used, which often spreads surrounding environment.

For the above mentioned reasons an appropriate layout and building solution should be designed for each different type of processing building.

Not only is the production quality the only aim of a correct design, but also the safety of employees should be considered. It is very important to guarantee a better working environment, the safety of employees and a reduction in the health hazards. Slips, trips and falls are the main causes of accidents in the food and beverage industry. Slip injuries in particular happen more often in this industry than in most other industries, mostly due to wet or contaminated and greasy floors (e.g. with juice) [1] In this production sector is very important to adopt preventative measures. Slip prevention can be managed very effectively and can cut serious injuries by 50% or more, significantly reducing costs and lost time [2, 3].

Preventing spillages through equipment design and adequate maintenance, keeping walking and working surfaces clean and dry, and providing workers with anti slip footwear where still necessary often is not sufficient to prevent slips, trips and falls [4]. The floor materials and rough surfaces play an important role in preventing slipping [5]. In this study a slip resistance analysis was conducted for five floor surfaces commonly used in buildings food processing to evaluate their suitability in the buildings for citrus juices and essential oil manufacturing. Italy is the third largest producer of citrus fruit in Europe, with 2.8 million tons per year, after both Spain and Turkey [6]. Almost all of the national fruit production is located in the south Italy [7] where oranges, lemons, tangerines, clementine and bergamots are marketed as fresh products or processed. The main area of bergamots production is the ionic coastline of Reggio Calabria, the most southern town on the Italian peninsula [5]. In this area there are a lot of juice processing plants, but the characteristics of this essence tend to damage floors and make them more slippery than other citrus fruits.

2 Materials and Method

Nowadays, the most common solution in the food industry is the concrete floor. This floor type offers more durability than wood and tile, but it must have a food-safe resin coating. The resins provide a durable protective coating for flooring that can withstand the daily activity of a food processing plant, ensuring the facility maintains the appropriate levels of sanitation. The resin is usually used as a coating, or combined with mineral aggregates to form a resin screed. Applied as an in situ floor finish, the resin floor screeds and coatings show very low water absorption and forms a continuous surface. It is possible to obtain high standards of hygiene, with a good level of durability under severe conditions with this resin coating [8]. Sometimes the resin is used to bond the aggregate to the floor and in this form the resin component is known as the binder. The durable hygienic properties in-service of the resin coating are essential for the food and drink industries and their ability to carry out repairs or to accommodate changes to processing equipment while limiting the risk of taint [9]. Another vital characteristic of the resin coating is the ability to cover a large surface area in a short period of time. The cure time is reduced, typically to five hours or less, from installation to walk-on. There are several types of resin coating on the market, they differ in materials, number of layers and setting methods.

Table 1 Technical performance of the floor covering analysed

Technical Performance	A	B	C	D	E
Bonding strenght [N/mm ²] (DIN ISO 4624)	>1.5	>1.5	>1.5	>1.5	>1.5
Abrasion resistance [mg] (EN ISO 5470-1)	665	2,150	85	55	90
Compressive strenght [N/mm ²] (EN 196)	50	59	85	85	87
Flexural strength [N/mm ²] (EN 196)	15	13	35	45	30
Service Temperature [°C]	-20/ + 70	-40/ + 70	-20/ + 60	-20/ + 60	-20/ + 60

Five resin coating systems, widely used in food processing plants, were analysed in this study (Table 1):

- A. self-levelling polyurethane/cement-based (Mapefloor CPU/MF);
- B. high-strength polyurethane/cement-based mortar (Mapefloor CPU-HD);
- C. multi-layered vapour-permeable epoxy system (Mapefloor System 52);
- D. multi-layered solvent-free low thickness epoxy system (Mapefloor System 32);
- E. multi-layered high thickness epoxy system for floor renovation (Mapefloor System 91).

2.1 Roughness Measure

A sample of 80 × 80 cm for each floor covering system was prepared. A survey of sample's surface roughness was carried out by means DeltaPix a digital optical measurement system, this method differs from the mechanic stylus-type measuring instruments, as it does not damage the surface and is not influenced by the hardness of the surface sample.

For each floor sample was conducted 10 measures of roughness on casual but diffuse points on area. The average value of main surface roughness parameters are reported in Table 2.

Table 2 Value of roughness parameters

Sample	R _p [μm]	R _v [μm]	R _z [μm]	R _q [μm]	R _{sk} [μm]	R _{ku} [μm]	R _a [μm]
A	398.6 ± 33.5	-366.6 ± 20.1	765.6 ± 24.7	136.8 ± 2.9	-0.51 ± 0.17	3.33 ± 0.29	105.9 ± 5.9
B	520.2 ± 31.7	-436.4 ± 30.5	956.8 ± 10.5	195.4 ± 20.6	-0.43 ± 0.08	2.39 ± 0.40	166.2 ± 22.0
C	610.6 ± 37.2	-377.4 ± 41.9	986.4 ± 13.5	237.8 ± 19.9	0.19 ± 0.09	2.03 ± 0.10	205.6 ± 18.9
D	730.0 ± 50.3	-278.0 ± 53.1	1,008.0 ± 0.0	233.4 ± 32.2	0.85 ± 0.32	3.83 ± 0.87	191.8 ± 33.8
E	348.6 ± 35.5	-427.8 ± 9.4	776.8 ± 29.4	150.8 ± 13.4	-0.69 ± 0.25	3.11 ± 0.15	121.6 ± 10.3

Where:

R_p is the maximum peak height of the roughness profile within one sampling length

R_v is the maximum valley depth of the roughness profile within one sampling length. Previously, the parameter symbol R_m was used in place of R_v

R_z is the arithmetic mean value of the single roughness depth R_{zi} of consecutive sampling lengths. Single roughness depth R_{zi} is the vertical distance between the highest peak and the deepest valley within a sampling length

R_q is the root mean square for the local slope dz/dx within the sampling length.

R_{sk} is the mean depth of the valleys protruding from the roughness core profile

R_{ku} is the quotient of the mean quadratic value of $Z(x)$ and the fourth power of R_q within a sampling length

R_a is the arithmetic mean of the absolute values of the roughness profile ordinate

2.2 Slip Resistance Measure

The coefficient of friction (COF) and slipperiness for the analysed floor covering systems was conducted by means of the Tortus method, developed by Malkin and Harrison at the British Ceramic Research Association and based on the measurement of the sliding friction value of a slipping element [10]. The measurement was conducted in accordance with D.M. 236/89 Decreto del Ministro dei Lavori Pubblici 14 June 1989 - n. 236 [11] using the Floor Slide Control FSC2011, which is a computerised system that detects the dynamic friction coefficient of installed floors in real conditions of use, both wet (with a rubber 4S slider) and dry (with a leather slider).

Real conditions were simulated to measure the COF (Fig. 1). To simulate the wet condition the floor samples were contaminated, in different phases with: 40 cc of distilled water, 40 cc of cloudy bergamot juice and with 40 cc of citrus essence oil (Table 3) spread on floor sample surface. The choice of bergamot cultivar for the production of essence oil and for juice contaminants was the Castagnaro cultivar. The physicochemical properties of the bergamot juice and the chemical composition of citrus essential oil for the slip resistance measure are reported in Table 4 [12] and Table 5 respectively.

2.3 Wear Measurement

The cleanability of floor surfaces effect environmental hygiene and food safety. In addition to factors associated with hardness and friction, floorings should withstand strong chemical and mechanical stresses associated with cleaning and use of the flooring. Usually the floors of juice processing plants are cleaned every day at the end of the day using a manual procedure aiming to dry the floor where the juice or the citrus oil essence has fallen. Only once a week is a floor cleaning machine

Fig. 1 COF values for different samples and conditions of use

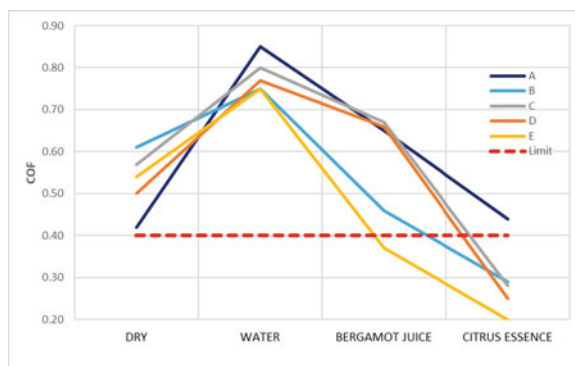


Table 3 Values of the measured COF

Sample	Dry	Water	Bergamot juice	Citrus essence
A	0.42 ± 0.06	0.85 ± 0.09	0.65 ± 0.07	0.44 ± 0.06
B	0.61 ± 0.06	0.75 ± 0.07	0.46 ± 0.09	0.29 ± 0.04
C	0.57 ± 0.07	0.80 ± 0.10	0.67 ± 0.05	0.28 ± 0.05
D	0.50 ± 0.08	0.77 ± 0.05	0.66 ± 0.07	0.25 ± 0.03
E	0.54 ± 0.05	0.75 ± 0.06	0.37 ± 0.05	0.20 ± 0.04

Table 4 Physicochemical properties of the bergamot juice

Brix [°]	H [°]	Pulp [%]	Turbidity [%]	Acidity [%]	Vitamin C [mg/L]	Formol number
8.79	2.58	9.83	38.22	45.54	568.00	19.40

Table 5 chemical composition of citrus essential oil

Compound	Percentage	Kovats Indice HP-1	Kovats Indice HP-Innowax
Limonene	59.21	1,029	1,214
Linalyl acetate	16.83	1,244	1,559
Linalool	9.51	1,087	1,542
β -Pinene	4.38	973	1,118
Myrcene	1.23	981	1,163
α -Terpineol	1.09	1,173	1,691
Sabinene	0.73	966	1,126

Table 6 Value of the roughness parameters for the wear surfaces

Sample	R _p [μm]	R _v [μm]	R _z [μm]	R _q [μm]	R _{sk} [μm]	R _{ku} [μm]	R _a [μm]
A	482.0 ± 53.2	-257.4 ± 41.1	740.2 ± 18.1	112.4 ± 8.3	0.22 ± 0.37	3.50 ± 0.30	86.8 ± 5.9
B	516.7 ± 47.4	-393.7 ± 32.7	910.7 ± 19.5	186.5 ± 11.6	0.98 ± 0.77	2.32 ± 0.41	156.5 ± 11.2
C	531.4 ± 77.0	-94.6 ± 13.0	622.6 ± 77.3	90.2 ± 18.3	1.23 ± 0.23	5.84 ± 1.37	72.6 ± 14.6
D	702.8 ± 31.4	-275.4 ± 21.2	978.6 ± 16.9	177.0 ± 2.8	0.39 ± 0.07	2.48 ± 0.07	148.6 ± 3.0
E	614.4 ± 14.7	-100.8 ± 19.6	715.4 ± 21.8	70.1 ± 3.5	2.56 ± 0.41	17.82 ± 3.01	49.9 ± 2.7

Table 7 Values of the COF for the wear surfaces

Sample	Dry	Citrus essence
A	0.73 ± 0.08	0.39 ± 0.05
B	0.48 ± 0.06	0.33 ± 0.06
C	0.78 ± 0.09	0.36 ± 0.04
D	–	0.33 ± 0.04
E	0.07 ± 0.05	0.22 ± 0.02

provided during the cleaning procedure. A experimental test was conducted to evaluate the cleaning effects on the roughness and on the COF of the floor surface. An apparatus prototype was made to correctly simulate the actions performed during manual cleaning, to evaluate the wear and tear on the floor caused by cleaning. It is composed of a 100-cm-long and 50-cm-wide rectangular aluminium frame on which guides were fixed to drive a 13 × 42 cm sliding block supporting a cleaning cloth. The sliding block was driven by an electric engine powered by an Arduino programmable board. For the test the Scotch-Brite™ General Purpose Scouring Pads 96 cleaning of 158 mm × 224 mm was utilised, with a total sliding block weight of 1 kg, each floor sample was contaminated with 30 cc of citrus essence oil and ten rubbing cycles were carried out with a velocity of 5 cm/sec. After the clean simulation were measured the roughness parameters (Table 6) and the COF in dry and citrus essence condition, of the wear surfaces (Table 7).

3 Results

An analysis of the variance (ANOVA) was performed with a statistical level of significance of 95% using the value of COFs for each contaminant used in the test (Table 8). Table 8 shows the ANOVA of the measured COF obtained in different conditions of use, in particular the test allows us to evaluate the influence of the contaminant on the risk of slipping. The P-value is used in the hypothesis test to support or reject the null hypothesis. The smaller the p value the greater the differences between the averages of some groups. In this test the p-value is less than 0.05 (confidence level

Table 8 ANOVA of the COF

Source	DF	Sum of Square	Mean Square	F Statistic	P-value
Groups	3	0.608	0.202	23.722	0.393×10^{-5}
Error	16	0.136	0.008		
Total	19	0.745	0.039		

>95%) for all parameters. It is possible to state that for the tested floor covering system surfaces, there is a strong correlation between all the evaluated parameters (P-value = $0.393 \cdot 10^{-5}$) in which the influence of the surface condition (dry or wet) on the COF results is demonstrated.

The parameter R_z was correlated with the COF (Fig. 2). R_z was chosen because, according to Bowman [13], it is a parameter that presents specific value ranges related to slip resistance. It was evident that floor covering A, with the lowest R_z value (765 μm) (surface very smooth), showed the higher COF when it was contaminated with water (COF = 0.85) or citrus essence (COF = 0.44).

Conversely the floor covering E with a high R_z value ($R_z = 975 \mu\text{m}$) showed the lowest COF values when it was contaminated with bergamot juice (COF = 0.37) or citrus essence (COF = 0.20), which represents a serious risk of slipping in the buildings where citrus juice and essential oil is manufactured.

Following the cleaning of the floor with a prototype apparatus, the scenario changed after wear was simulated. In fact the floor covering A showed an increment of the COF (Fig. 3) in dry condition (COF = 0.73) probably due to the increase of R_p roughness parameter (Fig. 4), but at the same time a decrease of the COF with the presence of citrus essence (COF = 0.39), however, this was very close to the

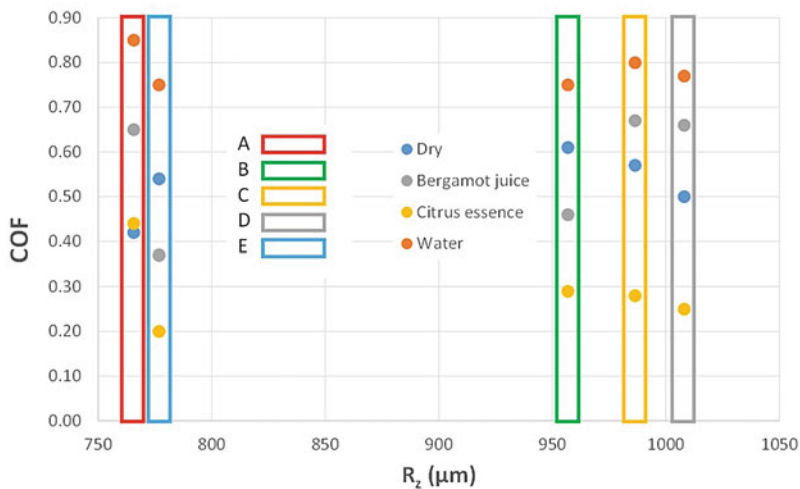


Fig. 2 COF values for the R_z roughness parameters

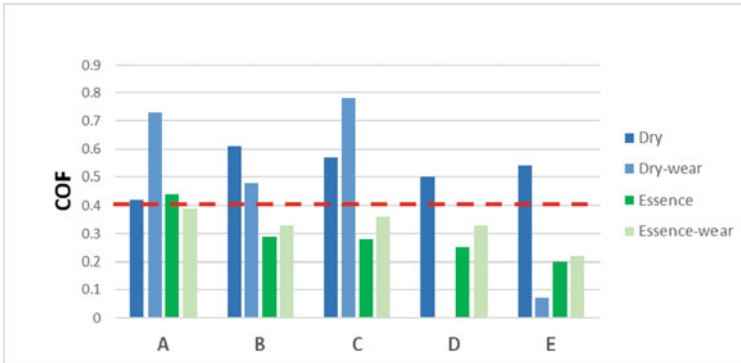


Fig. 3 Variance of the COF after simulation cleaning

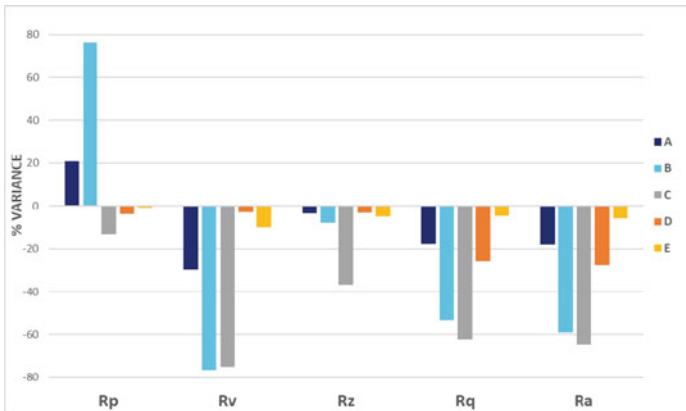


Fig. 4 Variance of the roughness parameters after simulation cleaning

limit allowed by law. It is important to report that the floor covering D increased very much such as the Tortus equipment did not able to finish the slippery test. The floor covering E highlighted, after the wearing simulation, the lowest level of COF in all condition use, therefore it is unable for citrus processing plant use.

4 Conclusion

In this paper five floor resin covering systems were analysed. These systems are widely used in food processing plants to improve food hygiene and safety, and moreover and moreover, due to their lower costs and time saving. Nowadays, the market offers a lot of floor resin covering systems specifically oriented to the food industry, but not all of these are adequate for all food production sectors. The results of this

study highlighted the differences in performance of the floor resin coverings analysed. The COF does not strictly depend on the roughness (R_z) but more directly on the conditions of use (dry or wet). The epoxy resin and the polyurethane/cement-based covering showed a comparable COF variable in dry conditions, between 0.44 and 0.61, both values are higher than the limits in Italian law (0.40), even the polyurethane/cement-based coverings have a low level of roughness. The covering system A showed the best slippery resistance performance in wet and contaminated conditions (with bergamot juice or citrus essence), in particular when citrus essence was spread on the floor. Only the value of the COF of the covering system A was higher than the Italian law limit i.e. 0.4. Barreca et al. [14] reported the high level of performance of this floor covering system when also used with the olive oil contamination. In effect the citrus essence is characterised by the significant presence of volatile oil (Linalool, α -Terpineol, etc.). The good anti-slip resistance of this floor covering system is combined with a low level of roughness which leads to easier cleanability. The good performance of the in real use condition of this floor covering system make this solution the best floor covering system for the citrus processing plants. Particular attention is to pay to the vehicular traffic such as that of the lift trucks because the Compressive strength (50 N/mm^2) is lesser than analysed solutions. The future of the work will be to study the single roughness parameters effects on the slipping resistance.

References

1. Books, H.S.E.: A recipe for safety - occupational health and safety in food and drink manufacture. **252**, 1–57 (2015)
2. Barreca, F., Cardinali, G., Fichera, C.R., Lamberto, L., Modica, G.: A fuzzy-based model to implement the global safety buildings index assessment for agri-food buildings. *J. Agric. Eng.* **45** (2014). <https://doi.org/10.4081/jae.2014.227>
3. Barreca, F., Praticò, P.: Post-occupancy evaluation of buildings for sustainable agri-food production—a method applied to an olive oil mill. *Buildings* **8**, 83 (2018). <https://doi.org/10.3390/buildings8070083>
4. European Agency for Safety and Health at Work (EU-OSHA), Safe Maintenance – Food and Drink Manufacturing 12 (2015)
5. Liu, L., Li, K.W., Lee, Y.-H., Chen, C.C., Chen, C.-Y.: Friction measurements on “anti-slip” floors under shoe sole, contamination, and inclination conditions. *Saf. Sci.* **48**, 1321–1326 (2010). <https://doi.org/10.1016/j.ssci.2010.04.014>
6. Schmid, D.: Volume of citrus fruit production in Europe in 2018. In: STATISTA (2019). <https://www.statista.com/statistics/578387/citrus-fruits-production-volume-europe/>. Accessed 8 Sep 2022
7. ISTAT (2021) Coltivazioni legnose fruttifere. <http://dati.istat.it/Index.aspx?QueryId=33705>. Accessed 8 Sep 2022
8. Barreca, F., Cardinali, G.D., Borgese, E., Russo, M.: Development of a method for evaluating floor dry-cleanability from wheat flour in the food industry. *J. Food Sci.* (2017). <https://doi.org/10.1111/1750-3841.13659>
9. Barreca, F., Cardinali, G., Borgese, E., Russo, M.: Influence of the roughness of floor tiles on the cleanability from wheat flour residues in agri-food buildings. *J. Food Agric. Environ.* **15**, 3–6 (2017). <https://doi.org/10.1234/4.2017.5455>

10. Powers, C.M., Brault, J.R., Stefanou, M.A., Tsai, Y-J., Flynn, J., Siegmund, G.P.: Assessment of walkway tribometer readings in evaluating slip resistance: a gait-based approach. *J. Forensic Sci.* **52**, 400–4005 (2007). <https://doi.org/10.1111/j.1556-4029.2007.00386.x>
11. Ministero dei Lavori Pubblici, Decreto Ministero Lavori Pubblici 14 giugno 1989, n.236. Italy (1989)
12. Giuffrè, M.A., Nobile, R.: Citrus bergamia, Risso: the peel, the juice and the seed oil of the bergamot fruit of Reggio Calabria (South Italy). *Emirates J. Food Agric.* **32**, 522–532 (2020). <https://doi.org/10.9755/ejfa.2020.v32.i7.2128>
13. Bowman, R.: Cerámica y Vidrio Slip resistance testing - Zones of uncertainty. *Boletín de la Sociedad Española de Cerámica y Vidrio* **49**, 227–238 (2010)
14. Barreca, F., Cardinali, G., Fichera, C.R.: Assessment of flooring slipperiness for food industry buildings. *Agric. Eng. Int. CIGR J* **17**, 23–30 (2015)

Evaluation of the Efficacy of a Radial Flow Settler for Aquaculture Wastewater Treatment



Bibbiani Carlo, Guidi Christian, and Rossi Lorenzo

Abstract Aquaculture effluents contains solids, such as uneaten feed and feces, that need to be removed as earlier as possible to avoid water quality depletion. The aim of this study was to evaluate the efficacy of a customized device layout of the radial flow settler (RFS).

The prototype was designed according to the existent literature and commercially available products. The experimental phase lasted four months starting from June 2020 and was conducted in a land-based aquaculture farm in Orbetello (Grosseto, Italy). The RFS received a part of the outlet flow from one of the rearing ponds of the farm. The inlet flow was set at 2 L s^{-1} . Samples of inlet and outlet water and sediments were collected on a monthly basis to evaluate the suspended solids content through gravimetric and filtration methods and the concentration of phosphorous, nitrogen, ammonium, nitrite, and nitrate.

The results suggest that the designed device complied with the intended use. Moreover, the functioning of the RFS required a modest hydraulic load (15–20 cm) and therefore low energy requirement. However, a cover on the device to prevent algal blooming is necessary. The gravimetric methods used did not allow a correct evaluation of the amount of sediments as a difference between inlet and outlet, since the error of the method exceeded the difference between the solids content in the inlet and outlet water. However, a sedimentation efficiency of 15–30% was observed through the filtration of the sedimented material, together with a reduction of the P and N contents.

Keywords Aquaculture · Wastewater treatment · Radial flow settler · Land-based aquaculture

B. Carlo (✉) · R. Lorenzo
Department of Veterinary Sciences, University of Pisa, Viale delle Piagge 2, Pisa, Italy
e-mail: carlo.bibbiani@unipi.it

G. Christian
Il Vigneto - Soc. Agricola a r.l., Strada Comunale di Ansedonia 4, 58015 Orbetello, GR, Italy

© The Author(s), under exclusive license to Springer Nature Switzerland AG 2023
V. Ferro et al. (eds.), *AIIA 2022: Biosystems Engineering Towards the Green Deal*,
Lecture Notes in Civil Engineering 337,
https://doi.org/10.1007/978-3-031-30329-6_112

1087

1 Introduction

Metabolic processes in fish generate by-products and waste products that potentially have a polluting impact on river or marine systems [1]. Aquaculture solid waste are mostly represented by uneaten feed, feces, and other particles (e.g., algae and biofouling). This is by no means exceptional; all human activities, and certainly all forms of intensive farming, generate waste products. The simplest waste removal process from water is gravitational sedimentation. The difference in density between the particles and the fluid allows the particles to go down when they are immersed in a still or very slow-moving body of water by effect of gravity force. The sedimentation rate depends on the characteristics of the material to be sedimented (including their size), and on the speed and turbulence of the water in which the particles are suspended. Inorganic particles such as sand have a high specific weight and therefore settle more quickly. On the contrary, the density of aquaculture waste is close to that of water (1–1.2) and, therefore, they settle at a low rate [2]. A large part of the uneaten feed and feces can be separated from the water stream by sedimentation. The sedimentation of suspended solids is made more difficult by the breakdown of feed and feces within the system. The turbulence of the water, created by the speed of the flow and the swimming action of the fish, keeps the feces in suspension and this is the cause of the progressive destruction and division into smaller particles. Also, the passage throughout pumps and other equipment contribute to this process. As a consequence, very small particles become “non-sedimentable”. The permanence of these fine particles in the water is responsible for nutrients leaching into water. The project for the wastewater treatment system of a fish farming plant should therefore have the aim of capturing and removing suspended solids as soon as possible after their release into the water to reduce this degradation process. Moreover, the concentrations of pollutants are, in particular, very low in the wastewater of open circuit systems. Generally, untreated waste contains between 5 and 80 mg L⁻¹ of SS. Therefore, the search for an adequate technological solution for the treatment of wastewater, characterized by high flows and low concentrations of pollutants, represents one of the most important challenges of modern engineering. Currently, there are two methods for reducing suspended solids in aquaculture wastewater: 1) sedimentation, that uses gravitational compaction systems of varying complexity, and 2) mechanical filtration, that uses energy and filters with mesh sized to trap solids.

The aim of this study was to evaluate the efficacy of a customized device layout of a radial flow settler designed and installed at “Il Vigneto - soc. agricola a.r.l.” aquafarm located in Orbetello (GR) within the Project FLAG Code 2019”, approved as part of the ‘Costa d’Argento Local Development Strategy - Measure 2.47’, named “Study aimed at mitigating the environmental impact of farm plant waste and improving the health and hygiene conditions of farmed fish”.

2 Materials and Methods

The experimentation was started by analyzing the types of Radial Flow Settlers (RFS) available on the market in the aquaculture sector. The research concerning the possibility of separating suspended solids has been directed towards the experimentation of a recent type of radial settler expressly built for the wastewater of fish farms [3].

Unlike cyclone separators, which are effective in applications where the particles (sand) to be removed have a specific gravity >2.0 , radial flow settlers are used in wastewater treatments and in aquaculture where particles they have a low specific weight (in any case >1.0). This makes the RFS ideal for recirculating aquaculture systems (RAS) and effluent treatment applications. In RAS applications and in water collection, the RFS can be placed upstream of the drum filter to reduce the total Suspended Solids (SS) or downstream receiving the washing water from the drum filters themselves, to ‘thicken’ the concentration of solids for further treatment. Within the pilot project it was decided to withdraw and treat only a percentage of the wastewater, in order to be able to proceed with an evaluation of the separation efficiency of the SS. A commercial type of a new radial settler produced by the company WMT-Innovasea-Boston, MA 02,210 USA, and in particular the RFS model with a diameter of 48" (around 1200 mm) was identified (<https://www.innovasea.com/wp-content/uploads/2022/02/Innovasea-radial-flow-settler-product-overview-0122.pdf>).

Due to COVID-19 restrictions, it was decided to build the aforementioned equipment in the aquafarm facility. After a careful market survey, the Lamar Udine company was identified for the supply of the sedimentation tank (<http://www.lamarudine.com/lamar-udine/acquacoltura/>).

The RFS consisted of a fiberglass cylindrical tank 1500 mm diameter and 2020 mm height with a conical bottom of 60° . A ‘Thompson weir’ was proven to be effective, so the height of the ‘V-shaped tooth’ was design accordingly. The V-notch weir diameter was 1350 mm with V-notch height of 20 mm, the diameter and height of stilling cylinder were 400 and 500 mm, respectively, the surface-loading rate of $2.1 \text{ L s}^{-1} \text{ m}^{-2}$, and the inlet and outlet pipes diameter of 50 mm.

The parameters and technical drawings of the executive project of the radial flow settler are fully equivalent to, or higher than the original RFS48" of the WMT Company. The location and view of the installed settler at “Il Vigneto - soc. agricola a r.l.”, are shown in Fig. 1.

The flow rate out of the breeding tank (named ‘2B’), in the test-period was about 14 L s^{-1} ; only during in a single day it underwent a slight variation from 14 to 16.5 L s^{-1} .

The inlet flow rate to the settler was set, to evaluate its performance, equal to 2.0 L s^{-1} corresponding to a load equal to $2/3$ of the maximum design flow rate of the radial settler.

On field measurements were made to evaluate the sedimentation efficiency of the SS of the incoming and outgoing waters of the radial settler, avoiding as much as possible the dissolution of the suspended solids into very fine particles and therefore

impossible to settle down by the aforementioned means. This analysis was conducted by gravimetric determination. The efficiency was calculated by Eq. (1):

$$\text{Efficiency (\%)} = (SS_{\text{inlet}} - SS_{\text{outlet}}) / SS_{\text{inlet}} \times 100 \quad (1)$$

Samples were collected on a monthly basis for four consecutive months. The analytical methods followed the APAT CNR IRSA 2090B Man 29–2003 standards.

3 Results

The Fig. 2 shows the analyzes performed by filtering the samples taken from the inlet and outlet of the radial settler.

The largest part of the solids accumulated in water is less than 50 μm diameter (approx. 54 and 58% for inlet and outlet water, respectively) was retained in 0.7–20 μm filters.

The analysis of the sedimented spill out are shown in Fig. 3, for the period August–November 2020.

The SS concentration of the water discharged varied around 30 mg L^{-1} (Fig. 2), while total SS accumulated in sediments spillout accounted for 300 mg L^{-1} (Fig. 3a). The removal efficiency calculated on the total SS retained by the filters 0.7 μm (Eq. 1) at the end of the experimentation period, was between 15 and 30% (Fig. 3b).

According to the construction details of the RFS, and the maximum flow rate (3 L s^{-1}) is it possible to calculate the minimum residence-time (time elapsed towards



Fig. 1 Location of the ‘Test site’ at ‘Il Vigneto - soc. agricola a r.l.’, Orbetello (GR) and details of the weir and the pumping system



Fig. 1 (continued)

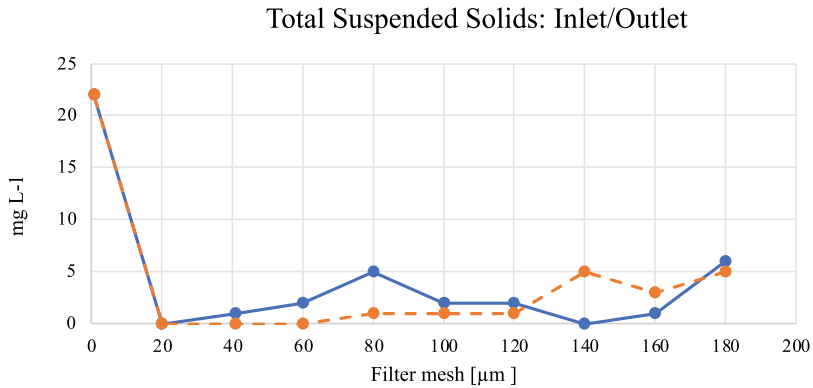


Fig. 2 Distribution chart of the retained by each filter mesh-size (Inlet = Blue color; Outlet = Dashed line -Orange color) during one of the sampling time

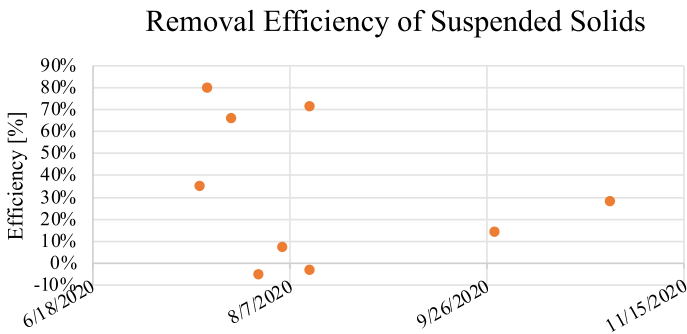
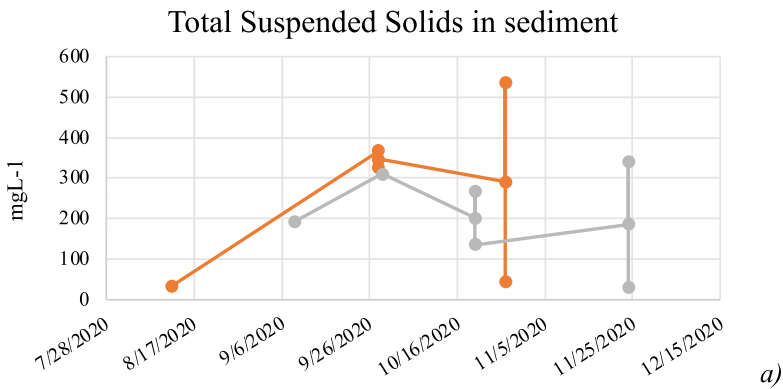


Fig. 3 a Graph of the concentration of sedimented spillout (1st Laboratory = Gray color; 2nd Laboratory = Orange color). The values on the vertical bars refer to split spill out volumes of 600 L: also the average value is reported at half height of the bar). **b** Removal efficiency of suspended solids, values are calculated according to Eq. (1)

the weir), given the average speed of water rising in the settler which is equal to 2.1 mm s^{-1} . The average residence-time turns out to be around 240 s. The residence time was calculated as ratio between mean water flux and water flow area.

4 Discussion

From a laboratory analysis performed on three samples of wastewater from the breeding tank, the data of the percentages SS sedimented were obtained as a function of the expected time for a known depth. It can be deduced that in correspondence to sedimentation speed higher than or equal to 3.3 mm s^{-1} , the percentage of sedimented SS is higher than 50%. Therefore, since the average speed of the rising water in the settler set in the project is 2.1 mm s^{-1} , the aforementioned particles will be able to settle due to their falling speed $> = 3.3 \text{ mms}^{-1}$.

Following the chronology of the results, after a very promising first start, with efficiencies between 35 and 70% (Fig. 3), an algal 'blooming' phenomenon occurred also due to the absence of an opaque cover on the RFS (Fig. 4). In addition, the sampling procedure provided for sampling on Monday and sending on Tuesday morning, without having discharged the sediment accumulated in the previous days have led to the accumulation in the cone of a large mass of sedimentation which was subsequently removed together with a part of algae grown in the channel of the circular spillway. The two contributions therefore recorded negative returns (withdrawals on 29 July and 5 August), obviously not logical except from this point of view. Consequently, it was decided in August both to modify the sampling procedure by inserting a sampling well for the outgoing waters (therefore waters with less contents of Suspended Solids) using a 24-h sampler with hourly sampling, and to purge the sedimentation cone daily and collect the volume of 'mud' in two tanks with a capacity of 600 L each.

As showed in Fig. 3, the low removal efficiency of the total SS, at the end of the experimental period should be further investigated in order to better understand the reasons for its variability. One possible reason could be linked to biological phenomena established in the sedimented mass due to non-continuous removal, i.e. every 24 h.

Furthermore, given the geometric configuration of the device (water inlet and outlet pipes, channel of the Thomson weir), the hydraulic load necessary for the hydraulic operation of the settler is very modest: in the present case it shows a value between 100 and 150 mm of water column (calculations not reported).



Fig. 4 Algal bloom within the weir and radial settler view without cover cap

5 Conclusions

At the end of the experimentation and the analysis of the results of the sampling carried out on the incoming and outgoing waters, as well as on the sedimented part, of the radial settler object of this report, the following observations were noted:

The settler was built and operated continuously. The design parameters proved to be compliant with the initially chosen device. The operation of the settler requires a very modest hydraulic load (about 150 mm water column), and therefore requires little energy for its operation. It was necessary to cover the settler tank to limit the development of algae inside it which would affect its functioning, in particular during summer months. The applied analytical methodologies for the determination of the total Suspended Solids, did not allowed to calculate the sedimented quantity accounting the difference between Inlet and Outlet. The sedimentation efficiency of the Suspended Solids, measured by filtration, was variable, in the last phase of the experimentation, between 15 and 30%. The causes of this variability, also linked to the daily and not continuous feeding routine, would require further investigation. The thickening of the SS can be estimated to be around one order of magnitude, i.e. the concentration of the Suspended Solids passes from a value of around 30 mgL^{-1} to an average value of 300 mg L^{-1} .

References

1. van Rijn, J.: Waste treatment in recirculating aquaculture systems. *Aquacult. Eng.* **53**, 49–56 (2013). <https://doi.org/10.1016/j.aquaeng.2012.11.010>
2. Lekang, O.I.: *Aquaculture Engineering* (2nd edn). Wiley-Blackwell (2007). <https://doi.org/10.1002/9780470995945>
3. Davidson, J., Summerfelt, S.T.: Solids removal from a coldwater recirculating system - comparison of a swirl separator and a radial-flow settler. *Aquacult. Eng.* **33**(1), 47–61 (2005). <https://doi.org/10.1016/j.aquaeng.2004.11.002>

IoT Technologies for Herd Management



Giulia Castagnolo, Dominga Mancuso, Francesca Valenti,
Simona M. C. Porto, and Giovanni Cascone

Abstract Recently, the scientific community has shown increasing interest in the adoption of wearable sensors in intensive livestock systems for monitoring animals and, more generally, to improve the quality of production. In extensive livestock farming, the use of wearable sensors can be significantly useful, since in this type of breeding system there is an infrequent farmer-to-animal contact. Furthermore, extensive livestock systems generate various environmental impacts, among which the most significant concern greenhouse gas emissions and soil degradation. However, it is not easy to quantify and model the environmental impact of the extensive breeding systems, unlike intensive ones, as it is not possible continuous long-distance monitoring of the herd. A valid solution to the above reported issues could be provided by IoT technologies, which recently are becoming increasingly efficient and reliable. Cow location and tracking are crucial information to study environmental impacts of grazing cows. By analysing such data in a Geographical Information System (GIS), it is possible to have very useful information about the activities of animals around the grazing areas, the spatial heterogeneity of the areas occupied by the animals, the pasture utilization, and soil degradation. The aims of the present study were: to investigate, in an extensive livestock farm-ing, the feasibility of a locating and tracking system based on space–time data provided by a prototype of an IoT-based low-power

G. Castagnolo

Department of Electrical, Electronics and Computer Engineering (DIEEI) University of Catania,
Viale Andrea Doria, 6, 95125 Catania, Italy
e-mail: giulia.castagnolo@phd.unict.it

D. Mancuso · F. Valenti · S. M. C. Porto (✉) · G. Cascone

Department of Agriculture, Food and Environment (Di3A), University of Catania, Via Santa
Sofia, 100, 95123 Catania, Italy
e-mail: simona.porto@unict.it

D. Mancuso

e-mail: dominga.mancuso@phd.unict.it

F. Valenti

e-mail: francesca.valenti@unict.it

G. Cascone

e-mail: gcascone@unict.it

global positioning system (LP-GPS); to test the battery life of the LP-GPS prototype and the signal coverage of the low-power network in rural locations; and to analyse the activities of animals around the considered grazing area by using GIS tool.

Keywords grazing cows · IoT · cow behavior · GIS · spatial analysis

1 Introduction

With the advent of precision livestock farming (PLF) [1], wearable sensors have played a crucial role in improving animal welfare and, more generally, farm management in intensive livestock systems. Nowadays, with the development of increasingly efficient IoT systems it has been possible to use sensor networks even in extensive livestock systems located in rural areas which are often lacking in electricity and internet networks. Animal tracking and location are of crucial importance for farmers because they could reduce the probability of theft, guard animal trespassing and, moreover, recover animals when they are injured and no longer able to move.

In extensive livestock systems one of the most studied sensors is the Global Position System (GPS) [2] used to monitor the position of animals. However, the context of extensive pastures requires the use of technologies with specific requirements such as reliable telecommunication networks and long-life battery for IoT sensors functionality. These factors are crucial because in rural areas it is not always possible to have access to the electric and internet network [3], so the short duration of the batteries would impose to farmers high labour costs for attaching and detaching the devices from animal body for their recharge and/or replacement. These issues influenced the use of GPS-based technology in extensive farms [4, 5], despite the technological advances achieved recently [4–6].

In terms of energy consumption, one of the most important factors is certainly represented by the telecommunications network used for data transmission: technologies based on the use of GSM networks are inefficient in energy saving terms for applications in extensive livestock systems [7]. Moreover, as also highlighted by Tomkiewicz et al. [8], in rural areas GSM coverage may not be stable and constant, and the reliability of the locating and tracking system could not be guaranteed. To overcome these problems, several low-power wide-area networks (LPWAN) could be adopted [9], such as SigFox and LoRa [10] and they are recently being considered for developing Internet of Things (IoT) technologies also in the field of precision livestock farming (PLF) [11]. LPWAN adopted techniques are mostly a trade-off, which is between cost, data rate and deployment cost [12].

The GPS sensor can be embedded in a device and attached to the animal body by using a collar and, therefore, it is not invasive. Moreover, considering that each device is uniquely identified over the telecommunications network, it is possible to identify each animal of the herd. Identification is important because by knowing the position over time it is possible to monitor the movement of each individual animal, which is a relevant parameter for a first remote screening of animal well-being.

The main objectives of this paper were: to investigate, in an extensive livestock farming of the cow-calf line located in south Italy in an area not covered by LPWAN networks, the feasibility of a locating and tracking system based on space–time data provided by a prototype of a low power position system (LP-GPS) based on SigFox network; to test the battery life of the LP-GPS and the signal coverage after the installation of a SigFox repeater in the grazing area; and to analyse the activities of animals around the considered grazing area by using Kernel Density Estimation (KDE) method in GIS tool. In this context, IoT-based solutions could help researchers for long-distance monitoring of herd position for modelling the environmental impacts of extensive livestock systems.

2 Materials and Method

2.1 Experimental Trial

The experimental trial was carried out in an extensive pasture situated in centre of Sicily (Italy), in Aidone in province of Enna (Fig. 1a). This area is positioned at an altitude of about 800 m a.s.l. and is characterized by a typical Mediterranean climate, with mild, humid winters and hot, dry summers. The farm covers about 300 hectares of surface and has an irregular conformation. The pasture can be defined as artificial: the farmers carry out the sowing operations by using seeds belonging to different species such as *Trifolium alexandrinum*, *Vicia sativa*, *Avena sativa*, *Triticum aestivum* and *Hordeum vulgare*.

Through direct surveys and visual inspections carried out in the study area, it was possible to investigate the floristic composition of the field, which appears to be homogeneous in all areas of the pasture. The area was subdivided in three different areas (Fig. 1b): area 1 is characterized by olive trees and spontaneous meadow, area 2 is characterized by *Trifolium alexandrinum* and area 3 which is composed of by *Triticum* stubble, *Vicia faba*, *Vicia sativa* and weeds such as *Lolium L*, *Hedysarum coronarium L*, *Avena fatua L*, *Sinapis arvensis* and *Papaver rhoeas*.



Fig. 1 (a) Localisation of the grazing area. (b) Grazing area subdivisions after visual inspection

For the experiment, the breeder selected 6 female animals from a group of 130 cows of the cow-calf line. The animals were selected considering their age, breed, good physical condition and above all docility. All the selected cows were in the fertile period. The grazing area was delimited by an electrified fence for avoiding cattle's trespassing.

The experimental activity was carried out between July and August 2021 and the air temperature ranged between 22 °C and 42 °C. The area 1 (Fig. 1b) was the most comfortable regarding air temperature, as it was equipped with trees, which protected cows from solar radiation. Therefore, from 6 AM to 5 PM the herd generally stayed in the area 1 (Fig. 1b) where they can access to a manger filled with hay and they can drink from a special watering tank. During the cooler hours of the day, from 5 PM to 6 AM, the herd is moved in areas 2 and 3 (Fig. 1b) where cows were free of grazing.

2.2 Data Collections System

The developed prototype of a low power position system based on Sig-Fox network (LP-GPS) allows the collection of cows' positions (i.e., latitude and longitude) by receiving information from up to three global navigation satellites systems (GPS, Galileo, GLONAS). The prototype is composed of a wearable electronic device, a cloud server for the information storage, a WebApp for data managing and visualization and a Sigfox repeater to increase the signal power and coverage. The wearable electronic device is equipped with an omnidirectional GPS antenna and receiver with -167 dBm sensitivity and 72 channels, an ultra-low power microcontroller, a SigFox radio module 868 MHz, 14 dBm E.R.P., an omnidirectional SigFox antenna, powered by Li-SOCL2 batteries (ExtraCell 3.6 V C ER – 2×6500 mAh).

The electronic device was put into a commercial case of small dimension $119 \times 66 \times 43$ mm, having IP68 protection, so it was dust and water resistant. One device was attached to the collar of each selected cows. The collars were made by using a very resistant plastic material but able to model itself based on the required shape, in such a way as not to cause stress to the animal.

The acquisition period started on July 2021 and finished on August 2021; the data analysed through KDE are referred to 38 days (about 6 weeks) of observations acquired at time-intervals of 10 min.

For each position detection, in addition to the longitude and latitude coordinates, the following data are also stored: date and time of the detection and the distance traveled with respect to the previous detection of the position.

2.3 Data Analysis

Data acquired during the observation period were imported in QGIS tool for further elaborations through both statistical and geo-spatial analyses. In detail, spatial analysis was carried out by using the QGIS software tool (v.3.10.11), a free software provided by Open-Source Geo-Spatial Foundation (Chicago, USA), which allows data elaboration and visualization at territorial level to deeply understand the link between livestock and environment.

Statistical analysis on the position of each animal considered in this test was conducted by using Kernel Density Estimation (KDE). The Kernel Density Estimation is a mathematic process of finding an estimate probability density function of a random variable, so with KDE it was possible to calculate the home range of the species, that is the area of the land where a species lives and provide a density estimation of the use of the territory. The results produced applying KDE analysis are maps that represent, for each animal, the area of the agricultural land most frequently used. Therefore, through these maps it was possible to understand the area preferred by each considered animal. Knowing the latter and the distribution of the type of forage in the various areas of the land, it was also possible to make assessments about of the forage most ingested by each animal during the grazing period.

3 Results and Discussion

By applying KDE algorithm to the dataset acquired through the LP-GPS prototype, 6 thematic maps were obtained by using QGIS software. Each map, one for each cow considered, reports in blue the perimeter of the whole grazing areas, in yellow the most frequented area and in red all the positions occupied during the observation period. In Table 2 the distance travelled per day and per week by each cow during the grazing timeslot are reported. By analysing the maps (Fig. 2) emerged that all the cows considered remain for long time into area 2, i.e., the area where the forage is *Trifolium alexandrinum*, maybe because this kind of forage is considered by cows more palatable than others. Observing the maps, it emerged that, different from the others, cow 2 and cow 6 spent long time not only in area 2 but also in area 3.

Comparing the distance travelled per day by each cow (Table 2), it emerged that the maximum distance was reached by cow 6 (6.2 km), while the minimum by cow 4 (3.8 km).

It is interesting to note that cow 5 and cow 6 have travelled a greater distance than the others, this is probably due to their young age as reported in Table 1. Cow 4 is the same age as cow 6, however it travelled less distance as it was affected by lameness at the time of the experiment. By analysing the data related to the distance travelled per week in Table 2, it emerged that during the 3rd week the cows have increased the distance travelled of about 1.5–2 km per day. After, gradually the distance covered is decreased during 5th – 6th week, returning at the level of 1st–2nd week. This variation

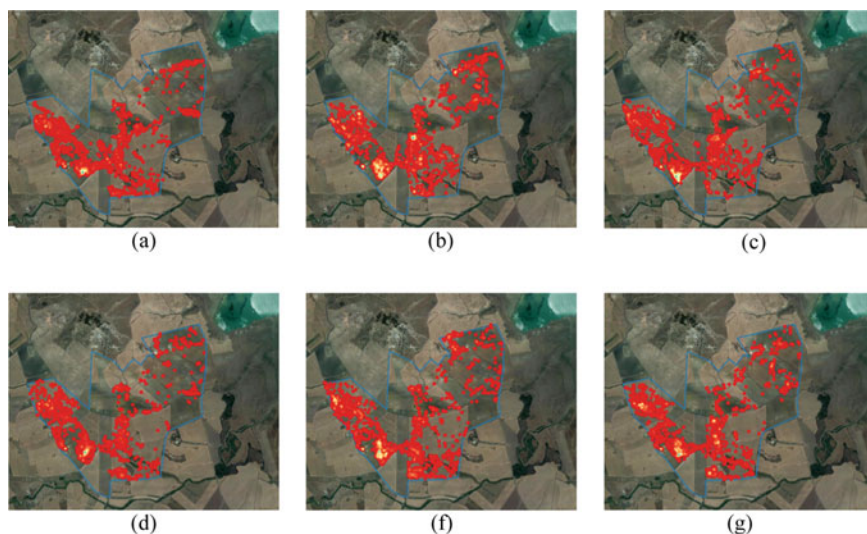


Fig. 2 Heatmaps of the six cows. (a) Cow 1. (b) Cow 2. (c) Cow 3. (d) Cow 4. (e) Cow 5. (f) Cow 6.

in the travelled distance was explained by the breeder, who pushed cows towards zone 3 to make the ingested forage more varied.

As described in the Sect. 2, a SigFox repeater had to be installed in this area, to guarantee a better signal quality. It made it possible to receive data in a consistent

Table 1 Age and breeds of the considered cows

	Cow 1	Cow 2	Cow 3	Cow 4	Cow 5	Cow 6
Age	6 yr	6 yr	9 yr	2 yr	3 yr	2 yr
Breeds	Italian Pezzata Rossa	Limousine	Limousine	Limousine x Pezzata Rossa	Limousine	Limousine

Table 2 Average distance (in km) per day travelled by each cow

Cow	Mean distance per day	Average 1 st week	Average 2 nd week	Average 3 rd week	Average 4 th week	Average 5 th week	Average 6 th week
1	4.0	3.8	3.8	5.7	4.3	3.2	3.0
2	4.5	3.5	4.2	5.5	4.8	3.8	3.6
3	4.8	3.5	3.9	5.8	4.7	3.2	3.6
4	3.8	2.8	3.0	4.5	4.7	3.5	3.5
5	4.9	3.6	4.1	5.4	4.9	4.1	4.1
6	6.2	5.3	5.7	7.0	6.5	5.6	5.3

manner and the number of lost positions acquired is significantly lower than the experiment reported in Porto et al. (2021, 2022) [13, 14]. To compute the heatmaps 6 weeks of data were used. However, to test the battery life more data were acquired for further time. The battery life of the LP-GPS prototype, in this experiment reached 4 months. It is important to highlight that this battery life was reached by using a 10-min data monitoring. In this regard, as reported in [15], due to the limited battery life of the devices, in some research studies, the animal's position was detected only one time per hour (or a little bit more) with the result that by reducing the number of detections it is impossible to achieve efficient monitoring of grazing animals.

By processing the acquired data, it was possible to identify the areas where the cows spent the most time, also understanding what type of forage they ingested. To obtain more information regarding the behaviour of the cows during the grazing period as well as to be able to make further assessments aimed at the validation of the system, it will be necessary to revise the hardware of the LP-GPS prototype by integrating an accelerometer, and to develop a software for behaviour detection [16, 17].

4 Conclusions

As previously mentioned, through the data acquired using LP-GPS it was possible to highlight the areas where each cow spent most of its time and consequently the ingested forage. Furthermore, it was possible to understand the distance travelled by each individual animal and to identify variations during the monitoring days.

Therefore, the heatmaps carried out by elaborating the data acquired by the LP-GPS prototype, could represent a fundamental aspect for the livestock management since farmers can have feedback on the type of forage ingested as well as on the soil conditions of the grazing areas.

Potential applications of the proposed LP-GPS prototype may be of interest also for stakeholders, local authorities, and regional environmental protection agencies. The GPS data, as shown, were very useful, however the current limit in LP-GPS is the lack of an accelerometer, which could be useful for monitoring the behaviour and therefore understanding the habits of the animals. In future the LP-GPS prototype will be integrated with accelerometer and a behaviour detection software and, also, the validation of the acquired data will be performed using a UAV system.

Acknowledgements The research study was funded by PRIN 2017 “Smart dairy farming: innovative solutions to improve herd productivity” (ID: E64I18002270001) and P.O. FESR SICILIA 234 2014/2020 - “*Innovazioni tecnologiche negli allevamenti per bovine da latte: sviluppo del prototipo di un sistema automatico di monitoraggio del comportamento delle bovine per il miglioramento del benessere e delle prestazioni produttive e riproduttive (CowTech)*” (ID: G69J18001020007) both coordinated by Prof. Simona M.C. Porto.

The authors are grateful to Massimo Pollino and Paolo Vasta of Trecastagni s.r.l., developers of the Low Power GPS devices and the WebAPP.

References

1. Berckmans, D.: General introduction to precision livestock farming. *Anim. Front.* **7**, 6–11 (2017)
2. Aquilani, C., Confessore, A., Bozzi, R., Sirtori, F., Pugliese, C.: Review: precision livestock farming technologies in pasture-based livestock systems *animal* **16**(1), 100429 (2022)
3. Rivero, M.J., Grau-Campanario, P., Mullan, S.: Factors affecting site use preference of grazing cattle studied from 2000 to 2020 through GPS tracking: a review. *Sensors* **21**, 2696 (2021)
4. Evans, J.C., Dall, S.R.X., Bolton, M., Owen, E., Votier, S.C.: Social foraging European shags: GPS tracking reveals birds from neighbouring colonies have shared foraging grounds. *J. Ornithol.* **157**, 23–32 (2016)
5. Nóbrega, L., Tavares, A., Cardoso, A., Gonçalves, P.: Animal monitoring based on IoT technologies. In: *Proceedings of the IoT Vertical and Topical Summit for Agriculture*, Tuscany, Italy, 8–9 May 2018
6. Davis, J.D., Darr, M.J., Xin, H., Harmon, J.D., Russell, J.R.: Development of a GPS herd activity and well-being kit (GPS HAWK) to monitor cattle behavior and the effect of sample interval on travel distance. *Appl. Eng. Agric.* **27**, 143–150 (2011)
7. Zeadally, S., Shaikh, F.K., Talpur, A., Sheng, Q.Z.: Design architectures for energy harvesting in the internet of things. *Renew. Sustain. Energy Rev.* **128** (2020)
8. Tomkiewicz, S.M., Fuller, M.R., Kie, J.G., Bates, K.K.: Global positioning system and associated technologies in animal behaviour and ecological research. *Philos. Trans. Roy. Soc. B* **365**, 2163–2176 (2010)
9. Buurman, B., Kamruzzaman, J., Karmakar, G., Islam, S.: Low-power wide-area networks: design goals, architecture, suitability to use cases and research challenges. *IEEE Access* **8**, 17179–17220 (2020). <https://doi.org/10.1109/ACCESS.2020.2968057>
10. Peruzzi, G., Pozzebon, A.: A review of energy harvesting techniques for low power wide area networks (LPWANs). *Energies* **13**(13), 3433 (2020)
11. Mengjie, Z., Xuepei, W., Huanhuan, F., Qiuyi, H., Xinqing, X., Xiaoshuan, Z.: Wearable internet of things enabled precision livestock farming in smart farms: a review of technical solutions for precise perception, biocompatibility, and sustainability monitoring. *J. Clean. Prod.* **312**, 127712 (2021)
12. Bembe, M., Abu-Mahfouz, A., Masonta, M., et al.: A survey on low-power wide area networks for IoT applications. *Telecommun. Syst.* **71**, 249–274 (2019)
13. Porto, S.M.C., Valenti, F., Castagnolo, G., Cascone, G.: A Low Power GPS-based device to develop KDE analyses for managing herd in extensive livestock systems. In: *2021 IEEE International Workshop on Metrology for Agriculture and Forestry (MetroAgriFor)*, pp. 243–247 (2021)
14. Porto, S.M.C., Castagnolo, G., Valenti, F., Cascone, G.: Kernel density estimation analyses based on a low power-global positioning system for monitoring environmental issues of grazing cattle. *J. Agric. Eng.* **53**, 1323 (2022)
15. Raizman, E.A., Barner, R.H., King, L.E., Ihwagi, F.W., Douglas-Hamilton, I.: Feasibility study on the spatial and temporal movement of Samburu's cattle and wildlife in Kenya using GPS radio-tracking, remote sensing and GIS. *Prev. Vet. Med.* **111**, 76–80 (2013)

16. Porto, S.M.C., Castagnolo, G., Mancino, M., Mancuso, D., Cascone, G.: On the determination of acceleration thresholds for the automatic detection of cow behavioural activities in extensive livestock systems. In: Biocca, M., Cavallo, E., Cecchini, M., Failla, S., Romano, E. (eds.) *Safety, Health and Welfare in Agriculture and Agro-food Systems. SHWA 2020. LNCE*, vol. 252, pp. 106–114. Springer, Cham (2022). https://doi.org/10.1007/978-3-030-98092-4_12
17. Castagnolo, G., Mancuso, D., Palazzo, S., Spampinato, C., Porto, S.M.C.: Cow behavioural activities classification by convolutional neural networks. In: *Proceedings of the 10th European Conference on Precision Livestock Farming (ECPLF)*, Vienna, pp. 48–55 (2022)

Assessing Application Potential of Species Distribution Models to the Case Study of Citrus in Eastern Sicily



G. A. Catalano, F. Maci, F. Valenti, P. R. D'Urso, and C. Arcidiacono

Abstract Climate changes are responsible for considerable effects on agriculture due to the variation of temperatures and weather patterns. Governments are implementing different actions for a transition towards sustainable food and agriculture reducing the impacts on the environment. Environmental monitoring is of utmost importance in the identification of these actions as it allows resources protection, impacts mitigation, by ensuring a sustainable use of natural resources. Advanced technologies such as remote sensing and geographical information system, coupled with statistical tools, are helpful in determining the variation in the land cover due to climate changes. Based on the literature, the geostatistical tool Software for Assisted Habitat Modeling Package (SAHM) is a promising tool for environmental monitoring. On this basis, this study aimed at assessing SAHM for monitoring suitability and potential distribution of a specific vegetation in a territory. In the case study, the main objective was to predict the potential citrus coverage distribution in Eastern Sicily by the application of different geospatial models available in the SAHM environment. Based on the bioclimatic data acquired from open-source databases, species probabilities of occurrence were investigated in the territorial area belonging to the province of Syracuse by using different models (e.g., MaxEnt, BRT, MARS, GLM, and Random Forest). Comparisons between the results obtained by using these models were carried out, sensitivity to the dataset width and covariates' selection was investigated, and accuracy measures were analysed. The results were provided by thematic maps showing the suitability of the plants' presence at different bioclimatic conditions. The outcomes of this study are relevant for decision support of companies and territorial administrations in land use planning.

Keywords Vistrail:SAhm · Citrus · Spatial Distribution · Geostatistical Software

G. A. Catalano · F. Maci · F. Valenti · P. R. D'Urso (✉) · C. Arcidiacono
Department of Agriculture, Food and Environment, University of Catania, Via S. Sofia N.100,
95123 Catania, Italy
e-mail: provvidenza.durso@phd.unict.it

© The Author(s), under exclusive license to Springer Nature Switzerland AG 2023
V. Ferro et al. (eds.), *AIIA 2022: Biosystems Engineering Towards the Green Deal*,
Lecture Notes in Civil Engineering 337,
https://doi.org/10.1007/978-3-031-30329-6_114

1107

1 Introduction

It is widely understood that climate changes are one of the drivers responsible for considerable effects on agriculture due to temperature variation and change in weather patterns. To counteract these changes, a transition towards sustainable food and agriculture requires implementing different actions through a reduction of environmental impacts. Therefore, environmental monitoring is of utmost importance in the identification of these actions as it allows resources protection, impacts mitigation, ensuring a sustainable use of natural resources.

In this field, novel techniques applied to species distribution prediction (Species Distribution Models - SDM) have recently captured the interest of scientists [1, 2, 3, 4] and have been coupled with Geographical Information System (GIS) and remote sensing technologies in order to fulfil the requirements of those forecast analyses. The application of these techniques and technologies, combined with the acquisition of proper information, allows monitoring the suitability of a specific vegetation over time in a territory. Moreover, this knowledge is useful to optimise farm management by modifying the most influencing variables and mitigating the impacts of climate change. The output can be projected onto different spatial layers in order to produce maps of the ecological niche of a species. Among the software tools implementing SDMs, the Software for Assisted Habitat Modeling Package (SAHM) is a promising tool for environmental monitoring, though in the literature few studies have been applied to the agricultural field. Therefore, the main aim of this study included the assessment of the SAHM tool to monitor the suitability of citrus distribution in a territory based on microclimatic variables.

2 Materials and Methods

2.1 Study Area Selection and Input Data Acquisition

Due to the extensive presence of citrus orchards, the study was carried out in the province of Syracuse in eastern Sicily. The surface area of the province reaches about 2.000 km² and is located in the South of Italy. The landscape of this territory is characterised by the presence of the Hyblaean Mountains.

The first step of the analysis required identification of the presence of the trees in the study area. The presence was obtained by comparing the Sicilian TRC (Technical Regional Cartography) with the IT2000 orthophotos acquired from the Sicilian Land Information System (SITR) on the GIS software. In detail, about 10.000 presence points were considered and used as input data in the VISTRAILS:SAHM. Since the forecast model required considering the parameters that have an influence on the presence of the trees, bioclimatic variables were used as input data in the VISTRAIL:SAHM. In detail, the 19 bioclimatic variables provided by the WorldClim database were acquired, as it was done in previous studies [5, 6], and, by using

the GIS tool, data of the 19 bioclimatic variables from 1970 to 2000 were represented in raster format.

2.2 Modelling Methodology

In this study, the open-source *VisTrails:SAHM* scientific workflow system has been utilised to take advantage of its ability to integrate visualisation systems with different tools, and maintain detailed records of the input used, output generated,

and parameter specifications [6]. *VisTrails:SAHM* is composed of various modules that can be applied during the execution of the global model (Fig. 1). The global model was composed of input data, pre-processing, preliminary model analysis and decision, correlative models, and output routines.

In this study, the model defined by Morisette et al. [7] was applied. In detail, during the *preprocessing* phase, the key module PARC was used to accelerate input data analysis. This module allows projection, aggregation, resampling, and clipping of input covariate geospatial data to match the template layer. During the *preliminary model analysis and decision*, two modules were applied: the *model selection split* and the *covariate correlation and selection*. The first module splits the input points into test and training groups and provides evaluation metrics to select the best models or set of models. The second module shows the scatter plot and correlation between each pair of covariates and the relationship between each covariate and the response.

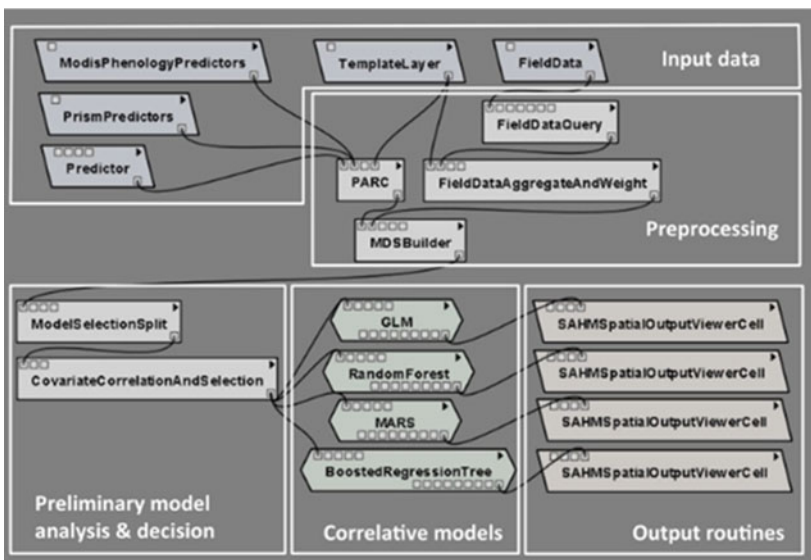


Fig. 1 Modelling scheme of the SDMs implementation. (Source: Morisette et al. 2013)

Based on these elaborations, it is possible to assess the distribution of each variable and to remove those variables highly correlated with others [6]. To this purpose, the maximum values of the *Pearson's coefficient*, *Spearman's coefficient* e *Kendall's coefficient* were computed for each couple of variables. Specifically, the threshold value for the three coefficients is ± 0.8 . In detail, since a high value of the coefficients means there is a strong association between the two variables, in this case one of the two variables was considered and the other was discarded. Then, the models *MaxEnt*, *Boosted Regression Tree (BRT)*, *Multivariate Adaptive Regression Splines (MARS)*, *Generalized Linear Model (GLM)*, and *Random Forest (RF)* were applied in the software *VISTRAILS:SAHM*. By using the default model settings, these models were applied to two groups of data (i.e., *Training* and *Testing*) in order to make comparison among the groups. In the literature, the amount of data in the *training* and *testing* datasets is generally equal to 70% e 30% of the whole data considered, respectively [5], which are the default values in the software. In this study, sensitivity analyses have been performed to test: the model robustness at changing of the training and testing sample width; the covariate selection (SEL) compared to consider all the covariates (ALL).

The evaluation of the accuracy of these models was carried out by computing the *Receiver Operating Characteristic (ROC)* curve and the related metric *Area Under the Curve (AUC)* [3, 4]. Other metrics based on *Specificity* and *Sensitivity* have been considered in this study to compare the different models, such as PCC (Percent Correctly Classified) and TSS (True Skills Stat). *Sensitivity* (TPR – True Positive Rate) evaluates model's ability to predict the percentage of observed presence classified as suitable (true positives) for each available category. *Specificity* (TNR - True Negative Rate) evaluates model's ability to predict the percentage of background classified as unsuitable (true negatives) for each available category.

3 Results

3.1 Comparisons Between Models Operated with Covariate Selection (SEL)

The results of this study were obtained by comparing the output of different SDM models and using data related to the presence of the species in 2000 and climatic data from 1970 to 2000.

Based on the correlation matrix (Fig. 2), the variables Bio_15, Bio_16, Bio_19, Bio_9, Bio_17, Bio_3, and DTM_20 were identified and selected in the module *Covariate Correlation And Selection* as those variables with a cross coefficient of correlation lower than 0.8 [1].

The analysis of the results reported in the maps produced by SDMs application (e.g., Fig. 3 reports MARS and BRT models) showed a similar distribution of the species in the territory; specifically, the highest probability was found in the northern

Fig. 2
 Pearson-Spearman-Kendall
 matrix **a** and biovariables
 influence in percentage **b**

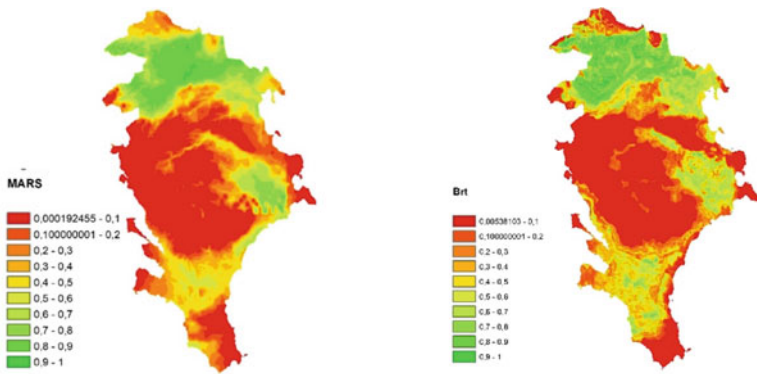
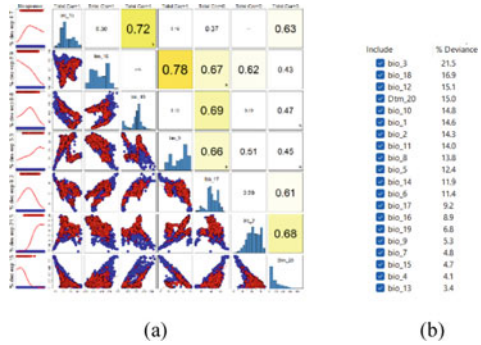


Fig. 3 Current suitability of the plant presence by the application of the models MARS and BRT to the Province of Syracuse

areas of the province, whereas the central areas are considered unsuitable by all models. Of course, there are small differences in the values of the species presence probability produced by the different models, and, therefore, further analysis could evaluate the output of the model by using different model settings, as it was reported by Valavi et al. [8], in order to maximise the model’s metrics.

Based on the results reported in Table 1, the BRT had the highest metrics among the models and, thus, it can be considered as the model with the highest ability to predict the citrus coverage, whereas the MARS model showed the lowest metrics.

3.2 Sensitivity Analyses on Training and Testing Dataset Width

These analyses were carried out to evaluate the model robustness at different percentages of input data for *training* and *testing*. In detail, the percentages of 90% and 10%

Table 1 Model metrics for a dataset composed of 70% Training and 30% Testing

	Model metrics for Training (70%)					Model metrics for Testing (30%)				
	BRT	GLM	MARS	MAXENT	RF	BRT	GLM	MARS	MAXENT	RF
AUC	0.91	0.844	0.832	0.853	0.884	0.825	0.844	0.833	0.847	0.882
PCC	82.5	76.3	75.7	77.5	81	74.8	76.2	75.7	77.4	80.7
TPR	0.824	0.763	0.757	0.766	0.813	0.744	0.76	0.756	0.782	0.81
TNR	0.828	0.763	0.758	0.784	0.808	0.752	0.763	0.752	0.767	0.805
TSS	0.651	0.527	0.514	0.55	0.62	0.496	0.523	0.509	0.548	0.615

Table 2 Model metrics for a dataset composed of 10% training and 90% testing

	Model metrics for Training (10%)					Model metrics for Testing (90%)				
	BRT	GLM	MARS	MAXENT	RF	BRT	GLM	MARS	MAXENT	RF
AUC	0.901	0.836	0.852	0.836	0.842	0.844	0.836	0.816	0.833	0.847
PCC	81.3	75.2	74.6	76.4	75.5	76.1	75.6	75.4	76.5	76.9
TPR	0.811	0.755	0.743	0.753	0.754	0.758	0.759	0.756	0.778	0.769
TNR	0.816	0.748	0.748	0.775	0.756	0.764	0.752	0.752	0.752	0.77
TSS	0.627	0.563	0.491	0.528	0.51	0.522	0.503	0.508	0.53	0.539

were applied for *training* and *testing*, respectively, and vice versa, the percentage of 10% and 90% were applied for *training* and *testing*, respectively. As expected, the metrics for *training* with a 90% input data were higher compared to those computed with a 70% for *training* (Table 1). This is related to the higher input data provided to the model and, therefore, *testing* indices with input data of the 10% were also higher (AUC = 0.902 and TSS = 0.638 for BRT; AUC = 0.852 and TSS = 0.534 for MARS) compared to 70% training-30% testing (Table 1).

The analysis on the indices (Table 2) showed that a lower data input to the *training* reduced the SDM ability to evaluate the model, though it was still adequate due to the high number of presence points. In detail, AUC was always higher than 0.8 for all SDM, PCC greater than 75, and TSS above 0.5. The models with the highest indices were BRT and RF, followed by MaxEnt and GLM; the worst model was MARS. Based on these results, the number of the presence points of the citrus species as well as their distribution on a specific territory are relevant factors for the prediction of the species distribution in a territory.

3.3 Analysis of Covariates' Selection

With the aim of analysing the influence of covariates' number on the outcomes, in this section the comparison between the results obtained from the selection of the covariates (SEL) and that obtained by including all the covariates (ALL) (i.e., the 19 biovariables and the DTM) is described. As expected, in ALL selection, the

software *VISTRAILS:SAHM* required more time to elaborate data compared to SEL selection. Moreover, the metrics related to the *testing* were slightly higher in GLM and MAXENT (AUC = 0.858 and TSS = 0.538; AUC = 0.858 and TSS = 0.567, respectively) and slightly lower in BRT (AUC = 0.826; TSS = 0.638), compared to those in the SEL. In fact, the identification of the optimal compromise between the production of underfitted and overfitted models is a relevant topic in modelling the distribution of species as well as the understanding of the factors that influence these two phenomena. In detail, oversized models with many explanatory variables are extremely complex and can cause random errors in the data; and although complex models may seem more suitable, their predictions can be poorer [9].

4 Discussion

From the comparison with other software tools for SDMs implementation, such as the stand alone MaxEnt software, it is possible to highlight that the *Preprocessing* phase of VisTrails:SAHM reduces time consuming tasks for the operator, such as manually change the reference system of the maps, subset the raster maps based on the study area, and manually convert them in .asc format for MaxEnt use. Two different “runs” of MaxEnt are needed in order to select covariates and the manual computation of Pearson index in between is required, whereas VisTrails:SAHM allows automatic update of Pearson-Spearman-Kendall correlation matrix in relation to variables selection. Moreover, it is possible to analyse intermediate results. Indeed, the reduced number of tasks required by automated phases decreases the number of possible errors performed by the operator [4].

The results of this research work showed that *BRT*, *RF*, and *MaxEnt* are models with the best metrics for the case study analysed, as confirmed in other studies [10]. Based on the analyses carried out in this study, it is relevant to have a high number of presence points of the species. In fact, the *sensitivity analysis* carried out for different widths of *training* and *testing* datasets showed that a wide data input makes the presence suitability model more robust. In fact, the elaborations showed that although the training data were reduced at the 10% of the sample, the accuracy indices of the testing were not lower than the thresholds of significance. This result is corroborated by the findings of Piekielek et al. [5], who obtained weak presence predictions for *Pinus flexilis* due to a low presence of the species in the territory. Further sensitivity analyses [11] modified the main models parameters to optimise the simulation of the citrus distribution probability. In detail, it was found that a high accuracy is achieved when the input presence points of the species were reduced.

5 Conclusions

In this study, the application of the SDM models to citrus were analysed in relation to the dataset width and covariates selection. The outcomes proved that the BRT

and RF, as well as MaxEnt, were the best models for the specific conditions. Having several SDMs in a single software allows careful comparison and modelling of the various processes and results, although further analyses are needed at varying the model settings. A great potentiality of uses and applications in agriculture is expected for this open-source software, suitable to perform decision support for farmers and for planning authorities in their territorial management activity.

Acknowledgements The research study was carried out within the project: ‘PON “RICERCA E INNOVAZIONE” 2014 – 2020, Azione II – Obiettivo Specifico 1b – Progetto “Miglioramento delle produzioni agroalimentari mediterranee in condizioni di carenza di risorse idriche – WATER4AGRI FOOD”, Cod.progetto: ARS01_00825, cod.CUP: B64I20000160005’; and it is in line with the project ‘Piano incentivi per la ricerca di Ateneo 2020-2022 – ‘Engineering solutions for sustainable development of agricultural buildings and land’ (ID: 5A722192152) coordinated by Professor Claudia Arcidiacono.

References

1. Leanza, P.M., Valenti, F., D’Urso, P.R., Arcidiacono, C.: A combined MaxEnt and GIS-based methodology to estimate cactus pear biomass distribution: application to an area of southern Italy. Wiley Online Library. *Biofuels, Bioprod. Bioref.* **16**, 54–67 (2021) <https://doi.org/10.1002/bbb.2304>
2. Leanza, P.M., Valenti, F., D’Urso, P.R., Arcidiacono, C.: EPI GIS- based model to estimate prickly pear biomass potential availability for biogas production: an application to a Mediterranean area. *Agronomy J.* **114**(6), 3206–3224 (2022). <https://doi.org/10.1002/agj2.21192>
3. West, A.M., Evangelista, P.H., Jarnevich, C.S., et al.: Integrating remote sensing with species distribution models; mapping tamarisk invasions using the software for assisted habitat modeling (SAHM). *J. Vis. Exp.* **116**, 54578 (2016a). <https://doi.org/10.3791/54578>. PMID: 27768080; PMCID: PMC5092193
4. West, A.M., Kumar, S., Brown, C.S.: Field validation of an invasive species maxent model. *Eco. Inform.* **36**, 126–134 (2016). <https://doi.org/10.1016/j.ecoinf.2016.11.001>
5. Piekielek, N.B., Hansen, J., Chang, T.: Using custom scientific workflow software and GIS to inform protected area climate adaptation planning in the greater yellowstone ecosystem. *Ecol. Inf.* **40–48** (2015). <https://doi.org/10.1016/j.ecoinf.2015.08.010>
6. Talbert, C., Talbert, M.: User Documentation for the Software for Assisted Habitat Modeling (SAHM) package in VisTrails, USGS (U.S. Geological Survey), *Ecography*. **36**. c. (2001)
7. Morisette, J.T., Jarnevich, C.S., Holcombe, T.R., et al.: VisTrails SAHM: visualization and workflow management for species habitat modelling. *Ecography* **36**, 129–135 (2012). <https://doi.org/10.1111/j.1600-0587.2012.07815.x>
8. Valavi, R., Elith, J., Lahoz-Monfort, J.J., Guillera-Aroita, G.: Modelling species presence-only data with random forests, bioRxiv 2020.11.16.384164, (2020). <https://doi.org/10.1101/2020.11.16.384164>
9. Heikkinen, R.K., Luoto, M., Araújo, M.B., et al.: Methods and uncertainties in bioclimatic envelope modelling under climate change. *Phys. Geogr.* **30**, 751–777 (2006)
10. Catalano, G.A., Maci F., D’Urso P.R., Arcidiacono C.: GIS and SDM-based methodology for resource optimisation: feasibility study for citrus in Mediterranean area. *Agronomy*, MDPI. <https://www.preprints.org/manuscript/202211.0502>
11. Catalano, G.A., D’Urso, P.R., Maci, F., Arcidiacono, C.: Influence of parameters in SDM application on citrus presence in mediterranean area. *Sustainability* **15**, 7656 (2023). <https://doi.org/10.3390/su15097656>

Simulation of the Heating Load in a NZEB Winery Building



Antonino Ciappa, Giovanni Puglisi, Fabiana Convertino, Ileana Blanco, Giuliano Vox, and Evelia Schettini

Abstract The study concerns the design of a Nearly Zero-Energy Building (NZEB) in the agro-industry sector, intended for production, aging and marketing of wine. The building was designed integrating architectural and plant engineering solutions for the purpose of containing thermal need and obtaining low CO₂ emission. The building is divided into three different areas: commercial, production and seasoning. The cellar is placed underground. A model was developed for obtaining the heat load profiles of the building in winter. The software simulation was performed both in steady state UNI-TS 11300 and in dynamic hourly regime, according to UNI EN ISO 52016. The study reports the values of the thermal need of the winery built with the criteria of NZEB, considering the use of glass walls. Due to the different exposure of the glass wall, the office with South-East exposure showed a thermal energy need for heating lower than that of the meeting room with North-West exposure.

Keywords agro-industry efficiency · energy saving · bioclimatic architecture · winter climate control

A. Ciappa

ENEA - Italian National Agency for New Technologies, Energy and Sustainable Economic Development, Technical Unit Energy Efficiency CCEI, Via Principe Di Granatelli 24, 90100 Palermo, Italy

A. Ciappa · F. Convertino · G. Vox · E. Schettini (✉)

Department of Agricultural and Environmental Science (DISAAT), University of Bari Aldo Moro, Via Amendola 165/A, 70126 Bari, Italy
e-mail: evelia.schettini@uniba.it

G. Puglisi

ENEA - Italian National Agency for New Technologies, Energy and Sustainable Economic Development, Technical Unit Energy Efficiency, CR Casaccia (Rome), Via Anguillarese 301, SM di Galeria, 00123 Rome, Italy

I. Blanco

Department of Biological and Environmental Sciences and Technologies (DiSTeBA), University of Salento, SP 6 Lecce - Monteroni, 73100 Lecce, Italy

1 Introduction

In recent years, the agri-food sector has moved towards production with high energy consumption and CO₂ emissions [1]. This has led to particular attention on the energy efficiency of the productive processes, and to the use of renewable energy sources, aimed at reducing energy consumption and CO₂ emissions [2–10].

Wineries can be considered buildings requiring innovations in terms of energy saving. A particular aspect of energy efficiency concerns the control of the microclimate inside the premises where the production activities take place, such as the cellar rooms used for the aging of wine, and the commercial area whose air conditioning represents a significant part of the energy consumption.

Wineries, like other agricultural buildings for food production, differ from standard buildings. The main differences concern the need to guarantee specific air temperature and relative humidity suitable for the production processes and for people working [11]. Also very important is the dynamic interaction between inside air temperature and humidity, building thermal dynamics and outside air temperature [12]. Temperature has a crucial role in wine aging and conservation. High temperatures are certainly a problem, especially in warm Mediterranean areas, and in general low temperature are desirable, but it is also true that long periods of low temperatures represent a problem since they prolong the time of aging [13]. Unlike traditional buildings, the most recent buildings for wine production have been built without particular attention to the thermal performance. Consequently, it has been necessary to make up for this lack with the installation of conditioning systems, with high energy demand. Energy needs vary widely with the location, the technology, and the building dimensions. For example, it was observed that in the English and Welsh wine production the 40% of the energy expended is related to heating, cooling, and ventilation and, due to the northerly cool climate conditions, the energy demand for heating is the highest [14]. Given the importance of the environmental and economic sustainability, there is a strong need for new solutions, including both high performing building design and energy saving facilities [15–17]. Finally, there is another aspect to consider, that in the last years there have been important changes in winery design and new spaces for tasting, cultural and leisure events are often realized, requiring air conditioning and thus new thermal loads [18].

The Energy Performance of Buildings Directive 2010/31/EU (EPBD Directive) is the main legislative instrument at European level for improving the energy efficiency of buildings [19]. EPBD directive supports the concept of Nearly Zero-Energy Buildings (NZEB), identified as very high energy performance buildings, whose needs, very low or almost zero, should be covered to a very significant extent by renewable energy sources.

The Italian Ministerial Decree of 26 June 2015, the so-called “Ministerial Decree minimum requirements”, which defines the methodology for calculating energy performance and the use of renewable sources in buildings, defines the requirements for Nearly Zero-Energy Buildings (NZEB) [20].

The definition of NZEB is often linked not to calculations, but to a vision that involves both the design of energy-efficient buildings and the use of renewable energy sources, also integrated with the productive activities.

This research concerns the design of a NZEB winery located in the South of Italy. The research was conducted using a commercial software for building efficiency energy interventions. The value of the energy needs for winter air conditioning was evaluated, when the commercial and production activities take place.

2 Materials and Methods

A model of winery located in a rural area in the province of Bari, southern Italy, was designed. The winery was designed to reduce energy needs as much as possible according to the criteria of the energy efficiency of buildings.

The winery consists of (Figs. 1 and 2):

- Commercial Area: arranged in three separate rooms (reception room, meeting room, and office) where administrative and promotional activities take place.
- Production Area: a single building, characterized by a single thermal zone, in which there are the various departments for grapes processing, from the delivery of the harvest to the bottling of the wine. Part of this is an unheated cargo handling

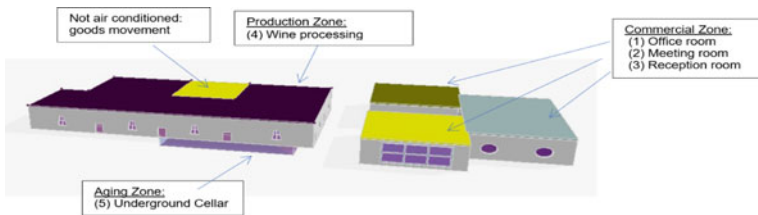


Fig. 1 The winery model: identification of the various zones

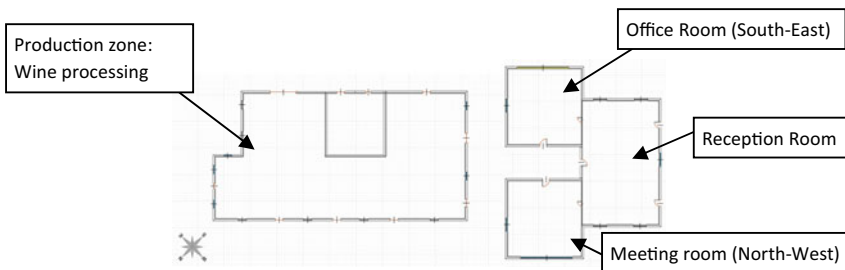


Fig. 2 Floor plan of the winery: production and commercial areas

room. This production area has a seasonal production activity from September to November.

- Aging area: the cellar, therefore the area dedicated to the refinement of wines. It is designed underground, to limit heat exchanges with the external environment, and is located under the production buildings. The cellar is a temperature and humidity controlled thermal zone.

All the opaque and transparent construction elements have been sized in compliance with the legal requirements and regulations on building energy efficiency [21]. Concerning the constructive characteristics, the winery buildings are characterized by walls made of an internal layer of plaster 1.5 cm thick, with a thermal resistance of $0.021 \text{ m}^2 \text{ K W}^{-1}$; porized bricks with a thickness of 35.0 cm and a thermal resistance of $2.174 \text{ m}^2 \text{ K W}^{-1}$, and an external layer of plaster 2.0 cm thick having a thermal resistance of $0.022 \text{ m}^2 \text{ K W}^{-1}$. Thus, the walls have an overall thickness of 35.5 cm and an overall thermal resistance of $2.217 \text{ m}^2 \text{ K W}^{-1}$. Buildings' roofs have a thickness of 26.0 cm and an overall thermal resistance of $3.157 \text{ m}^2 \text{ K W}^{-1}$. Roofs are characterized by an internal layer of plaster (2.0 cm thick with a thermal resistance of $0.029 \text{ m}^2 \text{ K W}^{-1}$), a lightened screed (6.0 cm thick, having a thermal resistance of $0.103 \text{ m}^2 \text{ K W}^{-1}$), an extruded polystyrene foam insulation layer (10.0 cm, with a thermal resistance of $2.941 \text{ m}^2 \text{ K W}^{-1}$), a concrete layer (6.0 cm thick, with a thermal resistance of $0.064 \text{ m}^2 \text{ K W}^{-1}$) and a tiled floor (2.0 cm thick, with a thermal resistance of $0.020 \text{ m}^2 \text{ K W}^{-1}$). Both the office room (exposed to South-East) and the meeting room (exposed to North-West) have a glass wall with motorized movable screens. These are managed by a dedicated system that gives additional thermal resistance by reducing the transmittance at night and consequently the cooling of the rooms. The production building is also equipped with highly insulated shutters.

The winter air conditioning, according to the Italian national legislation, is scheduled from November 15th to March 31st.

Each area is characterized by a temperature function of the intended use. According to the Italian legislation, the commercial area should have a temperature equal to $20 \text{ }^\circ\text{C}$, and the production area equal to $18 \text{ }^\circ\text{C}$. For the cellar an optimal temperature of $9 \text{ }^\circ\text{C}$ is considered.

For each area, the air conditioning energy requirements were considered. The energy analysis of the models was performed according to UNI TS 11300, for assessments based on average monthly values (asset rating and tailored), and to UNI EN ISO 52016, for assessments based on dynamic hourly calculation [21, 22]. The simulations were performed by using Termolog software (Logical Soft, Milan, Italy). The climatic and microclimatic data considered in the study are those provided by the Termolog database. Based on these data and on the buildings' constructive characteristics, the hourly thermal loads were calculated for the winter season.

The air conditioning of the commercial area is carried out by switching on the heating system between 6 a.m. and 5 p.m., to guarantee the set point temperature of $20 \text{ }^\circ\text{C}$ during the occupancy hours of the premises. At night, for the glass walls, additional insulating screens are used to limit the heat loss from inside to outside. The system is turned off on weekend for the commercial area.

3 Results and Discussion

Figure 3(a) shows the external and the internal air temperature together with the energy supplied by the heating system for the meeting room with North-West exposition of the Glass Wall. Given its thermal relevance, the solar radiation is shown too (Fig. 3(b)).

Figure 4 shows the external and the internal air temperature, the energy supplied by the heating system and the solar radiation for the office with South-East exposition of the Glass wall.

At daytime, the office and the meeting room benefit from solar gain due to the presence of glass walls, depending on their exposure. This reduced the thermal energy required by the heating system, especially in the hours of highest insolation. In these hours it is also possible for rooms to overheat above 20 °C. On days with mild temperatures and more solar radiation, the heat requirement tends to decrease to zero.

Figure 5 shows the thermal need of the office and of the meeting room and the solar irradiance as a function of the exposure. It has been noted that for the meeting room, compared to the office, greater thermal energy is required to maintain the set

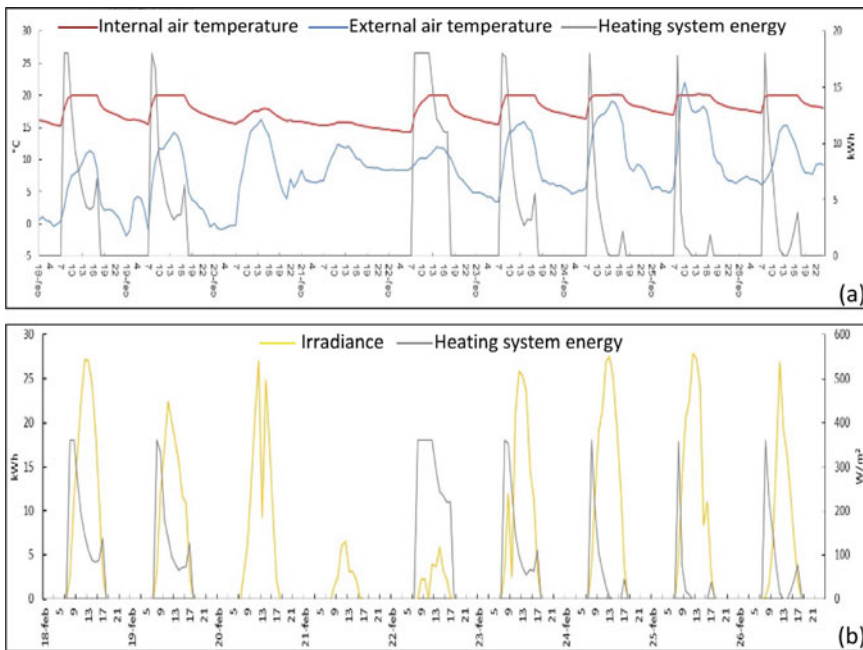


Fig. 3 Meeting room, with North-West exposition of the Glass Wall: external and internal air temperature and energy provided by the heating system **a**; solar radiation and energy provided by the heating system **b**; 18–26 February

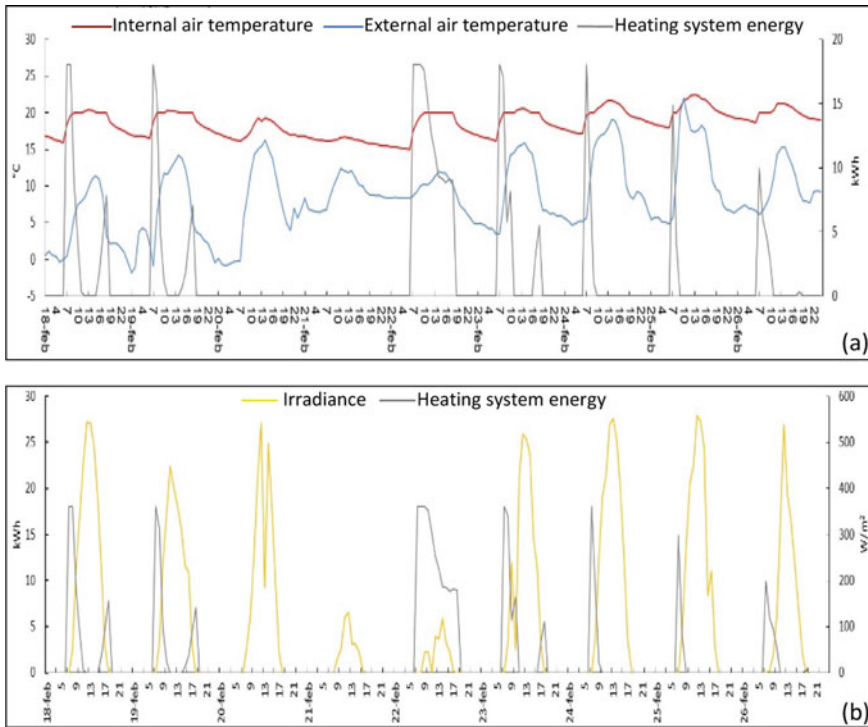


Fig. 4 Office with South-East exposition of the Glass wall: external and internal air temperature and energy provided by the heating system **a**; solar radiation and energy provided by the heating system **b**; 18–26 February

point temperature. This is due to the lower incoming radiation related to the different exposure of the Glass Wall.

Figure 6 shows the comparison between the thermal need of the office (with South-East exposition of the Glass wall) and the meeting room (with North-West exposition of the Glass wall), in the cases in which, in the evening and at night, the heating system is switched off (Fig. 6(a)) or kept at set-back temperatures of 18 °C (Fig. 6(b)). The results in Fig. 6 show lower values of the thermal needs when the setback temperature is not applied both for the meeting room and for the office. Due to the different exposure of the glass wall, offices have a heating energy requirement lower than that of the meeting room.

The hourly calculation carried out according to the UNI EN ISO 52016 standard resulted in hourly thermal need estimates for the whole winery (Figs.7 and 8).

An increase in the peak of energy need in the period 15–30 November was pointed out (Fig. 7). This was due to the activation of the air conditioning system in the production department, when the activities planned to produce wine begin.

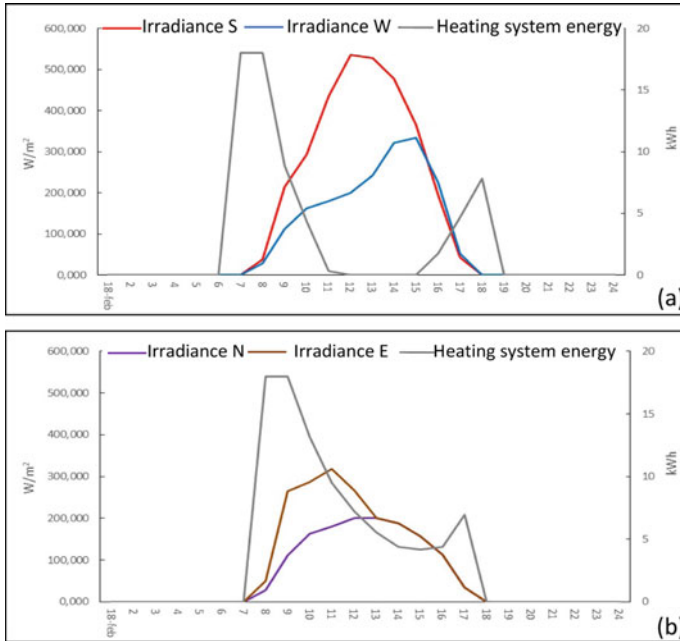


Fig. 5 Energy provided by the heating system and solar irradiance for the different exposures (N, E, S, W): office **a** and meeting room **b**; 18 February

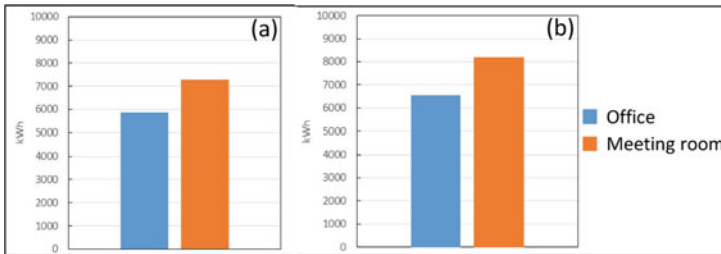


Fig. 6 Comparison of the thermal need of the office and of the meeting room without **a** and with the setback temperature of 18 °C **b**

In December the production sector is not active, therefore the thermal energy needs refer only to the commercial area and to the cellar (Fig. 8). The intermittent air conditioning system operate only in the 5 a.m.–6 p.m. time slot.

The negative values of thermal energy need, when the air conditioning system in the production and commercial area is off, refer to the cellar hourly thermal needs. This must be maintained, all year round, at a constant temperature of 9 °C.

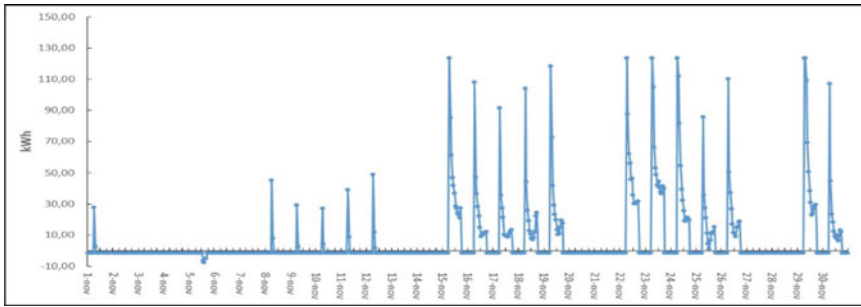


Fig. 7 Hourly thermal need for the winery, November

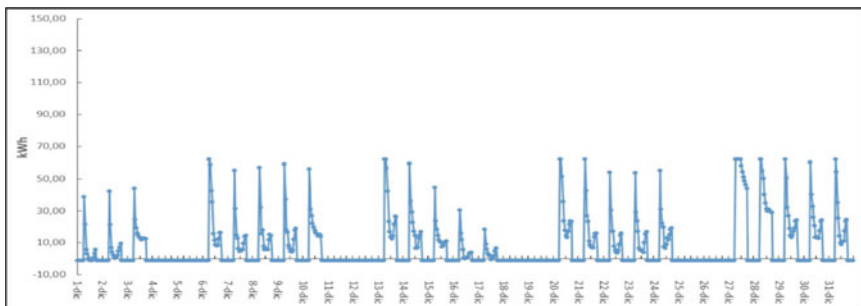


Fig. 8 Hourly thermal need for the winery, December

4 Conclusions

Through proper design choices and the integration of renewable energy-driven polygeneration systems NZEB, a transition to greater energy efficiency in the agro-industrial sector can be achieved.

By choosing energy-efficient buildings, it is possible to obtain significant results in the decarbonisation process and thus in reducing fossil fuels use. The use and the accurate management of the glass walls in relation to their exposure can contribute to energy saving in winter air conditioning. This is accordance with the principles of Bioclimatic Architecture.

This research is the first step for the design of high energy-efficient buildings that must be integrated with renewable energy-driven polygeneration systems. Further developments of the study will deal with the thermal behaviour in summer and thus with the energy requirements for cooling.

Acknowledgements The contribution to programming and conducting this research was equally shared between the Authors.

The present work was carried out under the “Piano Triennale di Realizzazione 2019-2021 della Ricerca di Sistema Elettrico Nazionale- Progetto 1.5 Tecnologie, tecniche e materiali per l’efficienza

energetica ed il risparmio di energia negli usi finali elettrici degli edifici nuovi ed esistenti”, Accordo di Programma Ministero dello Sviluppo Economico – ENEA funded by the Italian Ministry of Economic Development.

This research has been developed in the framework of the activities of the “Centro Interdipartimentale di Ricerca per la Cooperazione allo Sviluppo” (CPS) of the University of Bari, Italy.

References

1. Campiotti, C., Viola, C., Scoccianti, M., Alonzo, G.: Agroalimentare e sviluppo economico sostenibile: energia, efficienza energetica, ambiente e cibo. Riv. Studi sulla Sostenibilità, suppl. 2, 69–86 (2012) <https://doi.org/10.3280/RISS2012-SU2006>
2. Allouhi, A., Kousksou, T., Jamil, A., Bruel, P., Mourad, Y., Zeraoui, Y.: Solar driven cooling systems: an updated review. *Renew. Sustain. Energy Rev.* **44**, 159–181 (2015). <https://doi.org/10.1016/j.rser.2014.12.014>
3. Al-Alili, A., Islam, M.D., Kubo, I., Hwang, Y., Radermacher, R.: Modeling of a solar powered absorption cycle for Abu Dhabi. *Appl. Energy* **93**, 160–167 (2012). <https://doi.org/10.1016/j.apenergy.2010.11.034>
4. Ghaddar, N.K., Shihab, M., Bdeir, F.: Modeling and simulation of solar absorption system performance in Beirut. *Renew. Energy* **10**(4), 539–558 (1997). [https://doi.org/10.1016/S0960-1481\(96\)00039-0](https://doi.org/10.1016/S0960-1481(96)00039-0)
5. Ghafoor, A., Munir, A.: Worldwide overview of solar thermal cooling technologies. *Renew. Sustain. Energy Rev.* **43**, 763–774 (2015). <https://doi.org/10.1016/j.rser.2014.11.073>
6. Puglisi, G., Morosinotto, G., Emmi, G.: Development of an advanced simulation model for solar cooling plants. *Energy Procedia* **70**, 495–503 (2015). <https://doi.org/10.1016/j.egypro.2015.02.153>
7. Hasanuzzaman, M., Malek, A.B.M.A., Islam, M.M., Pandey, A.K., Rahim, N.A.: Global advancement of cooling technologies for PV systems: a review. *Sol. Energy* **137**, 25–45 (2016). <https://doi.org/10.1016/j.solener.2016.07.010>
8. Hwang, Y., Radermacher, R., Al Alili, A., Kubo, I.: Review of solar cooling technologies. *Hvac R Res.* **14**(3), 507–528 (2008). <https://doi.org/10.1080/10789669.2008.10391022>
9. Kalkan, N., Young, E.A., Celiktas, A.: Solar thermal air conditioning technology reducing the footprint of solar thermal air conditioning. *Renew. Sustain. Energy Rev.* **16**(8), 6352–6383 (2012). <https://doi.org/10.1016/j.rser.2012.07.014>
10. Mussard, M.: Solar energy under cold climatic conditions: a review. *Renew. Sustain. Energy Rev.* **74**, 733–745 (2017). <https://doi.org/10.1016/j.rser.2017.03.009>
11. Boulton, R.: A self-sustainable winery, an advanced passive building and remote monitoring of environments in wineries. *J. Agric. Eng.* **48**, 53–58 (2017). <https://doi.org/10.4081/jae.2017.735>
12. Barbaresi, A., Dallacasa, F., Torreggiani, D., Tassinari, P.: Retrofit interventions in non-conditioned rooms: calibration of an assessment method on a farm winery. *J. Build. Perform. Simul.* **10**, 91–104 (2017). <https://doi.org/10.1080/19401493.2016.1141994>
13. Torreggiani, D., Barbaresi, A., Dallacasa, F., Tassinari, P.: Effects of different architectural solutions on the thermal behaviour in an unconditioned rural building. The case of an Italian winery. *J. Agric. Eng.* **49**, 52–63 (2018). <https://doi.org/10.4081/jae.2018.779>
14. Smyth, M., Nesbitt, A.: Energy and English wine production: a review of energy use and benchmarking. *Energy Sustain. Dev.* **23**, 85–91 (2014). <https://doi.org/10.1016/j.esd.2014.08.002>
15. Benni, S., Torreggiani, D., Barbaresi, A., Tassinari, P.: Thermal performance assessment for energy-efficient design of farm wineries. *Trans. ASABE* **56**, 1483–1491 (2013). <https://doi.org/10.13031/trans.56.10259>

16. Navia-Osorio, E.G., Porras-Amores, C., Mazarrón, F.R., Cañas, I.: Impact of climate change on sustainable production of sherry wine in nearly-zero energy buildings. *J. Clean. Prod.* **382**, 135260 (2023). <https://doi.org/10.1016/j.jclepro.2022.135260>
17. Tinti, F., Barbaresi, A., Torreggiani, D., Brunelli, D., Ferrari, M., Verdecchia, A., Bedeschi, E., Tassinari, P., Bruno, R.: Evaluation of efficiency of hybrid geothermal basket/air heat pump on a case study winery based on experimental data. *Energy Build.* **151**, 365–380 (2017). <https://doi.org/10.1016/j.enbuild.2017.06.055>
18. Barbaresi, A., Torreggiani, D., Tinti, F., Tassinari, P.: Analysis of the thermal loads required by a small-medium sized winery in the Mediterranean area. *J. Agric. Eng.* **48**, 9–20 (2017). <https://doi.org/10.4081/jae.2017.670>
19. Energy Performance of Buildings Directive 2010/31/EU (EPBD Directive)
20. Decreto 26 giugno 2015: Applicazione delle metodologie di calcolo delle prestazioni energetiche e definizione delle prescrizioni e dei requisiti minimi degli edifici
21. UNI TS 11300: Prestazioni energetiche degli edifici
22. UNI EN ISO 52016: Energy performance of buildings - Energy needs for heating and cooling, internal temperatures and sensible and latent heat loads

Green Façade to Improve Building Energy Performance in Summer and Winter



Fabiana Convertino, Ileana Blanco, Giuliano Vox, and Evelia Schettini

Abstract Greenery systems are passive technologies which allow increasing buildings thermal control making them less energy intensive. Among greenery systems for buildings, green façades seem to be a particular feasible solution. An experimental test was carried out at the University of Bari, under Mediterranean climate conditions. An evergreen double skin green façade was tested together with an unvegetated wall to grasp their different energy behavior. The experiment was conducted to study both the summer and winter functioning. Experimental data were used to compare micro-climatic conditions characterizing the covered and the bare wall and to analyze the thermal energy transfer at the two walls. The green façade provided benefits during both summer and winter. In summer, the main positive effects concern the cooling of the wall surface and of the nearby air. Sensible reduction of the energy input, thanks to solar shading and plant evapotranspiration was recorded too. In winter, warming of the wall surface and nearby air and lower air velocity near the wall were the most relevant effects. The reduction of radiative and convective losses, thanks to the thermal and wind barrier role played by vegetation, provided further advantages. The improved thermal performance of the building achieved through the green façade positively affects the building's energy requirements for cooling and heating. The findings of this research aid in increasing the knowledge on the performance of green façades in both warm and cold periods and the specific benefits provided.

Keywords Green Infrastructure · Heat Transfer · Shading · Thermal Barrier · Energy saving

F. Convertino · G. Vox (✉) · E. Schettini
Department of Agricultural and Environmental Science (DISAAT), University of Bari "Aldo Moro", Via Amendola 165/A, 70126 Bari, Italy
e-mail: giuliano.vox@uniba.it

I. Blanco
Department of Biological and Environmental Sciences and Technologies (DiSTeBA),
University of Salento, S.P. 6 Lecce - Monteroni, 73100 Lecce, Italy

© The Author(s), under exclusive license to Springer Nature Switzerland AG 2023
V. Ferro et al. (eds.), *AIIA 2022: Biosystems Engineering Towards the Green Deal*,
Lecture Notes in Civil Engineering 337,
https://doi.org/10.1007/978-3-031-30329-6_116

1125

1 Introduction

In recent decades, there has been a rapid growth in population and urbanization, resulting in large amounts of green spaces being diverted from urban areas. Globally, 55% of the world's population lived in cities in 2018, and it is projected to reach 68% by 2050 [1]. Increased urbanization impacted negatively on energy consumption, environmental pollution, and greenhouse gas emissions, as well as temperatures in urban areas, which are higher than in surrounding areas (urban heat island effect) [2]. Vertical green systems (VGSs) are solutions for greening the walls of buildings. They have been suggested as a viable solution to alleviate climate change effects, decrease air pollution levels, and enhance biodiversity in urban areas [3]. A green façade (GF) is a typology of VGSs. GFs are characterized by climbing or hanging plants that grow vertically on the walls of the building; the plants can use the façade itself as support (direct GFs) or modular trellises, wired, and mesh structures (indirect or double-skin GFs) [4, 5]. Plants can be planted in the ground directly at the bottom of the building, or in planters positioned at different levels of the façade [4].

GFs can enhance the energy performance of buildings by facilitating the creation of comfort conditions and reducing energy consumption for air conditioning. In areas characterized by a Mediterranean climate GFs can lead to energy savings in the cooling season. The vegetation layer acts as a solar shading device intercepting solar radiation and reducing solar heat gain. Significant reductions in external wall surface temperature behind the green layer were found [6–8]. GFs are also recognized for their ability to create milder microclimatic conditions within the air gap between the wall and vegetation such as lower temperatures than the external air [9, 10]. GFs exhibit a warming effect for the covered wall in the cold season and at night, due to the thermal mass effect of the substrate and plants and the reduction of the radiative and convective losses [11–14]. Reductions in heat fluxes in GFs compared with a bare wall were assessed, notably in warm periods [12, 14]. The water evapotranspiration process from the plants and substrates provides a further cooling effect [6, 15].

The aim of this study is to analyze the energy performance of a GF application compared with a traditional unvegetated envelope in the winter and summer seasons. A multi-year experimental study concerning an evergreen indirect GF on a south-oriented wall under Mediterranean climate conditions was carried out. The microclimatic conditions characterizing the covered and bare walls, and the thermal energy flux at the two walls were analyzed. The ultimate purpose is to deepen knowledge on the GFs ability to deliver energy saving in buildings in the Mediterranean region.

2 Materials and Methods

A long-term experimental test was carried out at the experimental centre of the University of Bari, in Valenzano (Italy). The site, having latitude 41.0199° N, longitude 16.9048° E and elevation 124 m a.s.l., has a Mediterranean climate (classified as Cfa [16]).

The experimental prototype consists of a block, having a plan of $4.20\text{ m} \times 1.50\text{ m}$ and a height of 2.00 m. The studied wall was south-facing, made of hollow bricks held together with cement mortar, finished externally with a layer of white plaster and without any thermal insulation. The wall has an overall thickness of 0.21 m and a thermal resistance of $0.87\text{ K m}^2\text{ W}^{-1}$. It was realized as many of the external envelopes characterizing the Mediterranean building heritage, with the aim of assessing if greenery systems can improve their thermal performance.

The wall is characterized by a bare part (BW), without vegetation, and a GF part (CW), thermally separated by interposed panels of extruded polystyrene. The realized GF is indirect, made up of evergreen plants of *Rhynchospermum Jasminoides* placed 0.15 m from the wall and supported by an iron net.

The prototype is provided with a measurement equipment consisting of three data loggers (two CR10X and one CR1000 Campbell, Logan, USA) and several sensors. Measurements were taken every 60 s, averaged every 15 min and stored in the data loggers. The measured parameters were: solar radiation on the horizontal plane (measured by a pyranometer, model 8–48, Eppley Laboratory, Newport, RI, USA), wind speed and direction (measured by a wind Sentry anemometer, model 03,002, R.M. Young Company, USA), external air temperature and relative humidity (measured by HygroClip-S3 sensors, Rotronic, Zurich, Switzerland), wall surface temperature (measured by thermistors, Tecno.el s.r.l. Formello, Rome, Italy), canopy temperature (measured by radiometers, Apogee SI 400, Logan, UT, USA), incoming long-wave radiation (measured by a pyrgeometer, PIR, Eppley Laboratory, Newport, RI, USA), solar radiation hitting the CW (measured by a pyranometer, PIR02, Geoves s.n.c., Conegliano, Italy), air speed and direction in front of and behind vegetation (measured by ultrasonic anemometers, ATMOS 22, METER Group, Inc., Pullman, WA, USA).

The prototype was provided with an air conditioning system, consisting of a portable heat pump (Ellisse hp, Olimpia Splendid, Cellatica, Italy) working during warm periods and a fan heater (CH 7000 TURBO Aspira, Fantini Cosmi, Milan, Italy) in cold periods. A room chronothermostat (C804, Fantini Cosmi, Milan, Italy) was used to manage the internal air temperature. The temperature set point was 20°C in winter and 26°C in summer.

Data were collected over two years. A representative winter day, 7 January 2020, and a summer day, 31 July 2020, were analyzed in this paper.

These days were characterized by the climatic parameters shown in Table 1.

Thermal performance of the GF was investigated in both the winter and summer days by focusing on the overall heat transfer at the external surface of the BW and CW and on the achievable energy saving.

Table 1 Main climatic parameters of the site: daily cumulative solar radiation on the horizontal plane (HSR_{cum}), external air temperature (EAT), external air relative humidity (ERH) and wind speed (W); 7 January and 31 July 2020

Day	HSR_{cum} [MJ m ⁻²]	EAT [°C]			ERH [%]			W [m s ⁻¹]		
		Min	Max	Mean	Min	Max	Mean	Min	Max	Mean
7 January	7.7	1.8	11.5	6.9	48.8	89.9	68.6	0.3	2.9	1.7
31 July	24.9	22.3	35.9	29.6	29.2	61.1	42.2	0.0	3.1	1.5

The heat flux (HF , W m⁻²) at the external surface of the walls was calculated by considering all heat transfer mechanisms:

$$HF = E + R + CV \quad (1)$$

where: E [W m⁻²] is the solar radiative flux, R [W m⁻²] is the long-wave radiative energy exchange and CV [W m⁻²] is the convective energy exchange, calculated according to Convertino et al. [11, 17].

The energy saving (ES , W m⁻²) was calculated by:

$$ES = HF_{BW} - HF_{CW} \quad (2)$$

where HF_{BW} and HF_{CW} [W m⁻²] are the overall heat fluxes at the BW and CW, respectively. In winter, GF allowed to obtain ES if the energy flow incoming in the CW was higher than that entering the BW. In summer, ES was achieved if energy flow outgoing from the CW was higher than that from the BW.

3 Results and Discussion

The analysis of the data collected in the two days is indicative of the different behaviors of the BW and CW (Fig. 1). Qualitatively, the external surface of the CW was colder than the BW in the central hours of the days and warmer in the rest of the day. On average, the CW temperature was 0.5 °C higher than that of the BW in winter and 0.2 °C lower in summer. The highest differences between the BW and the CW temperature were recorded in winter, in fact the maximum positive difference was 5.8 °C (at 13:45) and the maximum negative difference was -3.6 (at 2:00). In summer, the maximum positive difference was 5.0 °C, recorded at 13:45, and the maximum negative was -1.7 °C, recorded at 0:45.

The presence of the GF affected the boundary conditions and the thermal parameters of the system compared to the BW case. This impacted the heat transfer at the CW, highlighting differences compared with the BW (Fig. 2). In the winter day, the CW mainly lost energy, while the BW gained energy even in the morning as this was not shaded by vegetation. However, on average, the CW lost less energy than the BW,

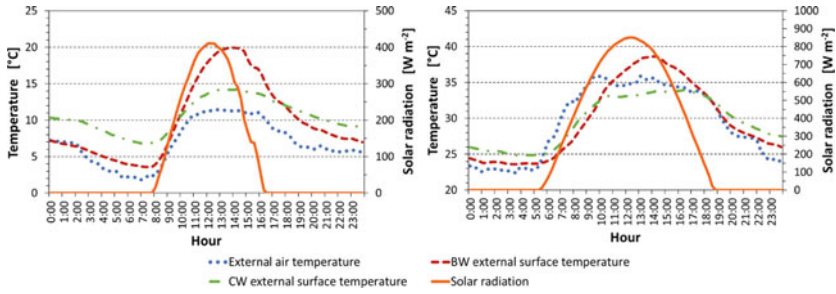


Fig. 1 External air and external surface temperature at the BW and CW (primary axis) and solar radiation (secondary axis), 7 January (left) and 31 July 2020 (right)

especially in the second half of the day. In that period, the BW temperature dropped abruptly, while that of the CW decreased less and later thanks to the greenery acting as a thermal barrier and reducing convective heat losses. In summer, the BW gained more energy than the CW. This difference was much higher in the morning. The GF prevented the CW from absorbing high amount of energy by shading the wall and providing cooling through evapotranspiration.

The difference in heat transfer through the CW and the BW can be read in terms of energy saving or penalty provided by the GF (Fig. 3). In winter, an energy penalty was recorded in the first half of the day and an ES in the second half. In summer, ES was achieved almost all day long and especially in the morning. Overall, the daily ES amounted to 0.07 MJ m⁻² on the 7 January and to 1.70 MJ m⁻² on the 31 July. These findings show that the application of an evergreen GF on a traditional uninsulated building envelope successfully manages to improve its thermal performance in both summer and winter, although to a different extent. This inevitably affects the whole building thermal behavior, allowing a reduction of energy demand for air conditioning and thus energy saving.

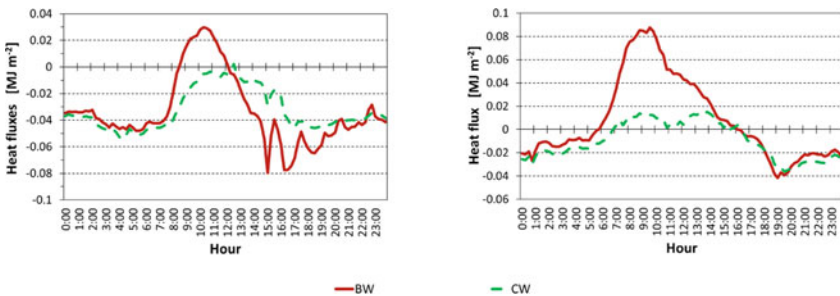


Fig. 2 Heat fluxes at the external surface of the BW and CW, 7 January (left) and 31 July 2020 (right). Positive values indicate energy gains, negative values are energy losses for the wall

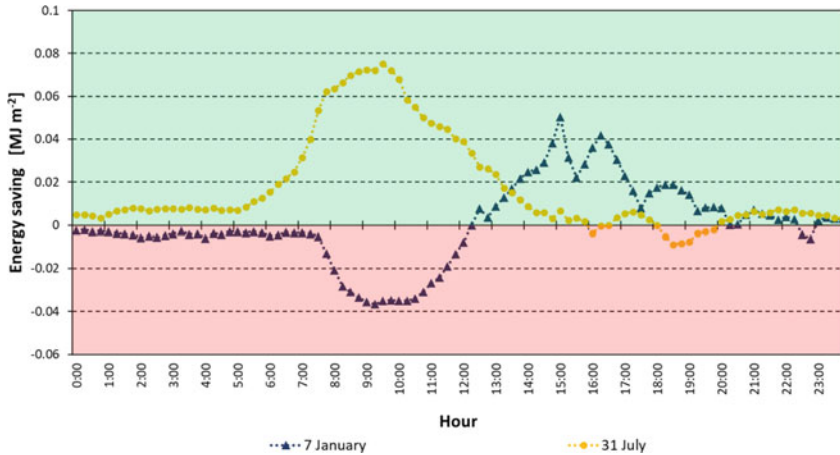


Fig. 3 Energy saving on 7 January and 31 July 2020

4 Conclusions

Green façades are a type of greenery system applied to buildings which can be an answer to the need for a more sustainable and responsible approach to urban planning and construction.

This research showed the energy benefits of applying green façade in comparison with a traditional unvegetated envelope. The outputs came from a multi-year experimental campaign concerning an evergreen green façade on a south-oriented wall under Mediterranean climate conditions. Winter and summer energy behavior were analyzed. The results showed that the application of an evergreen green façade can improve the envelope thermal performance in both cold and warm periods. The highest contribution to energy saving was obtained in the summer day, but a certain advantage was also provided in the winter day.

The findings of this research can enrich the knowledge of green façades, of their energy behavior and of the extent of their contribution to pursuit energy saving in buildings.

Acknowledgements The contribution to programming and conducting this research was equally shared between the Authors.

This research has been developed in the framework of the activities of the “Centro Interdipartimentale di Ricerca per la Cooperazione allo Sviluppo” (CPS) of the University of Bari, Italy.

References

1. United Nations Department of Economic and Social Affairs Population Division: World Urbanization Prospects: The 2018 Revision (ST/ESA/SER.A/420). United nations, New York (2018)
2. Besir, A.B., Cuce, E.: Green roofs and facades: a comprehensive review. *Renew. Sustain. Energy Rev.* **82**, 915–939 (2018). <https://doi.org/10.1016/j.rser.2017.09.106>
3. Bustami, R.A., Belusko, M., Ward, J., Beecham, S.: Vertical greenery systems: a systematic review of research trends. *Build. Environ.* **146**, 226–237 (2018). <https://doi.org/10.1016/j.buildenv.2018.09.045>
4. Pérez, G., Rincón, L., Vila, A., González, J.M., Cabeza, L.F.: Green vertical systems for buildings as passive systems for energy savings. *Appl. Energy.* **88**, 4854–4859 (2011). <https://doi.org/10.1016/j.apenergy.2011.06.032>
5. Manso, M., Castro-Gomes, J.: Green wall systems: a review of their characteristics. *Renew. Sustain. Energy Rev.* **41**, 863–871 (2015). <https://doi.org/10.1016/j.rser.2014.07.203>
6. Wong, N.H., et al.: Thermal evaluation of vertical greenery systems for building walls. *Build. Environ.* **45**, 663–672 (2010). <https://doi.org/10.1016/j.buildenv.2009.08.005>
7. Cuce, E.: Thermal regulation impact of green walls: an experimental and numerical investigation. *Appl. Energy.* **194**, 247–254 (2017). <https://doi.org/10.1016/j.apenergy.2016.09.079>
8. Lee, L.S.H., Jim, C.Y.: Subtropical summer thermal effects of wire-rope climber green walls with different air-gap depths. *Build. Environ.* **126**, 1–12 (2017). <https://doi.org/10.1016/j.buildenv.2017.09.021>
9. Pérez, G., Rincón, L., Vila, A., González, J.M., Cabeza, L.F.: Behaviour of green facades in Mediterranean Continental climate. *Energy Convers. Manag.* **52**, 1861–1867 (2011). <https://doi.org/10.1016/j.enconman.2010.11.008>
10. Lee, L.S.H., Jim, C.Y.: Transforming thermal-radiative study of a climber green wall to innovative engineering design to enhance building-energy efficiency. *J. Clean. Prod.* **224**, 892–904 (2019). <https://doi.org/10.1016/j.jclepro.2019.03.278>
11. Convertino, F., Vox, G., Schettini, E.: Thermal barrier effect of green façades: long-wave infrared radiative energy transfer modelling. *Build. Environ.* **177**, 106875 (2020). <https://doi.org/10.1016/j.buildenv.2020.106875>
12. Djedjig, R., Belarbi, R., Bozonnet, E.: Experimental study of green walls impacts on buildings in summer and winter under an oceanic climate. *Energy Build.* **150**, 403–411 (2017). <https://doi.org/10.1016/j.enbuild.2017.06.032>
13. Jim, C.Y., He, H.: Estimating heat flux transmission of vertical greenery ecosystem. *Ecol. Eng.* **37**, 1112–1122 (2011). <https://doi.org/10.1016/j.ecoleng.2011.02.005>
14. Yang, F., Yuan, F., Qian, F., Zhuang, Z., Yao, J.: Summertime thermal and energy performance of a double-skin green facade: a case study in Shanghai. *Sustain. Cities Soc.* **39**, 43–51 (2018). <https://doi.org/10.1016/j.scs.2018.01.049>
15. Hoelscher, M.-T., Nehls, T., Jänicke, B., Wessolek, G.: Quantifying cooling effects of facade greening: shading, transpiration and insulation. *Energy Build.* **114**, 283–290 (2016). <https://doi.org/10.1016/j.enbuild.2015.06.047>
16. Peel, M.C., Finlayson, B.L., McMahon, T.A.: Updated world map of the Köppen-Geiger climate classification. *Hydrol. Earth Syst. Sci.* **11**, 1633–1644 (2007). <https://doi.org/10.5194/hess-11-1633-2007>
17. Convertino, F., Vox, G., Schettini, E.: Convective heat transfer in green façade system. *Biosyst. Eng.* **188**, 67–81 (2019). <https://doi.org/10.1016/j.biosystemseng.2019.10.006>

Assessing Setups of a Multigas Analyser for Noxious Gas Monitoring in an Open Dairy Barn



D'Urso Provvidenza Rita, Arcidiacono Claudia, and Cascone Giovanni

Abstract The measurements of gas concentrations represent a relevant step for the estimation of emission rate of ammonia and greenhouse gases from livestock buildings. Based on previous research studies, the strategy applied for gas monitoring in open and semi-open dairy houses is central for optimising data collection and the reliability of the measurements.

Since the photo-acoustic spectroscopy system INNOVA (by LumaSense Technologies A/S, Denmark) is commonly used for scientific purposes in the context of gas concentration monitoring in livestock buildings, this research study aimed at refining knowledge on the measurement setup of the instrument by performing in-field experiments. Data of gas concentrations (NH_3 , CH_4 , and CO_2) acquired at different sampling locations (SLs) and setups were continuously recorded in a semi-open dairy barn. Two different datasets were selected to compute the variability associated to different setups of the instrument related to the Sample Integration Time (SIT) and the number of repetitions for each SLs. For the assessment, the one-way analyses of variance were applied to evaluate significant differences for the groups of data.

Based on the results, the INNOVA setup affected the measurement strategy as well as the localisation of sampling locations (SLs). In detail, the SIT setup of INNOVA influenced the duration of a measurement cycle of the device. Moreover, there was not a significant difference between the variability on concentrations with SIT5 and SIT20 ($P > 0.05$). Therefore, the setup with SIT5 is more suitable than SIT20 since it allowed completing a measurement cycle in less than one hour with 12 SLs and 3 repetitions. Consequently, the number of repetitions executed for each measurement had a significant influence on the design of the sampling strategy.

Keywords Gas monitoring · Open livestock buildings · Measurement campaign · Instrument setup · Measuring strategy · Photo-acoustic spectroscopy

D. P. Rita · A. Claudia (✉) · C. Giovanni

Department of Agriculture, Food and Environment (Di3A), Building and Land Engineering Section, University of Catania, Via Santa Sofia 100, 95123 Catania, Italy
e-mail: carcidi@unict.it

1 Introduction

The livestock sector is responsible for negative impacts on both human health and natural systems due to the production of ammonia (NH_3) and greenhouse gases (GHGs), such as methane (CH_4) and carbon dioxide (CO_2) [1]. The main method applied to estimate emissions from naturally-ventilated livestock housing is the CO_2 mass balance method [2, 3]. Based on this method, the most relevant parameter in order to estimate the emission rate of NH_3 and greenhouse gases is gas concentration. Scientific studies on how to collect data, for emission estimation, can optimise gas monitoring in open and semi-open dairy houses and, consequently, improve the estimation of pollutants and the mitigation strategies to reduce their impacts on the environment [4, 5].

In the literature [6–9], various studies have been carried out by using infrared photo-acoustic multigas spectrometers INNOVA (by LumaSense Technologies A/S, Denmark); they are devices for scientific purposes that measure gas concentrations by using the photo-acoustic principle. In detail, an air sample is acquired from the environment and moved into the measurement chamber, sealed by valves. Then, the radiation from an IR-source goes through a chopper and an optical filter into the chamber. The light absorbed by the gas sample in the chamber is proportional to the gaseous concentration. This light is converted into heat, which generates pressure waves. Then, microphones detect these pressure waves and the signal is digitised and converted into gaseous concentration.

Based on the literature, few studies have investigated methods for data collection as well as how to acquire reliable measurements in dairy houses. In detail, the design of the measurement setup (e.g., sequence of the measurements, duration of the measurement) was investigated in the study by Rom & Zhang [10]. They gave hints with regard to measurements carried out in laboratory conditions. Further information about experiment design (e.g., sampling point repetitions, tube length, heating, filter, reliability, device starting) was proposed by Brehme [11]. Although the analyses were carried out in a duck farm during 20 months of observation, the methods applied to define the suggestions for the experiment design were not described. On the contrary, recent studies [12, 13] applied statistics in order to optimise the localization of sampling measurement points and the number of repetitions for each measurement in open dairy barns. In the research study carried out by Hassouna et al. [14], the detection of interference bias and the reduction of uncertainty during the measurement of gas concentrations were assessed. Zhuang et al. [15] studied five gas analysers, including the INNOVA. These five devices were compared and validated in a poultry barn and a pig barn, following the procedure of VERA protocol. The outcomes showed the equivalence between wet chemistry (reference method) and photoacoustic spectroscopy (INNOVA). In other studies [7, 16, 17], the photoacoustic spectroscopy was the reference system in order to evaluate the performance of other devices for measuring gas concentrations.

Among the main parameters involved in the acquisition of gas concentrations, the sample integration time (SIT) represents a relevant parameter that influences

acquisition time for each sample. The SIT is related to the speed and accuracy of the measurement. In detail, it provides greater accuracy when the times are longer [18]. In the literature, specific information about the SIT setup has not been investigated yet.

Based on the main evidences from the literature, the goal of this research study was to provide useful suggestions to optimise the monitoring of gas concentrations of NH_3 , CH_4 and CO_2 in field experiments. In detail, this work aimed at comparing different SIT setups to collect gas concentrations in an open dairy barn by using an INNOVA device.

2 Materials and Methods

2.1 Description of the Dairy Barn

The research study was carried out in a cubicle free-stall dairy barn located in South Italy ($37^{\circ}01'N$, $14^{\circ}32'E$) within the province of Ragusa. The building has an open structure (i.e., about 55.50 m long and 20.80 m wide), characterised by three sides completely open (i.e. SE, NE, and NW sides). The roof is symmetric with a central ridge vent. The roof has a ridge height of 7 m and an eave height of 4 m. The open structure provides natural ventilation within the structure. The barn is equipped with 64 head-to-head cubicles organised in two rows and subdivided into three pens by passages connecting the feeding alley to the service alley (Fig. 1). The cubicles are made of concrete kerbs covered with sand. The natural ventilation system is integrated by two cooling systems composed of a fogging system with fans in the resting area, and a sprinkler system with fans in the feeding alley.

2.2 Design of the Monitoring System and Data Collection

Concentrations of NH_3 , CH_4 and CO_2 were continuously measured by an INNOVA photo-acoustic analyser composed of a Multigas Monitor mod 1412i and a multi-point sampler 1409/12 (Lumasense Technology A/S, Denmark). The sampler system was made of AISI-316 stainless steel and PTFE (poly-tetrafluoroethylene) tubing to minimise adsorption of samples. The system had 11 inlet channels with a tube that connect each channel in the multipoint sampler 1409/12 to the respective sampling location (SL). An air-filter was attached to the end of each sampling tube to keep the 1409 free of particles. The 11 inlet channels converge into one; a three-way valve then directs the gas sample to the gas Monitor for the analysis.

Measurements were performed at eleven SLs (Fig. 1), located at 20 cm from the barn floor in the animal occupied zone (AOZ) according to the findings of Arcidicono et al. [19]. In the analyses, the SLs were subdivided into three areas based

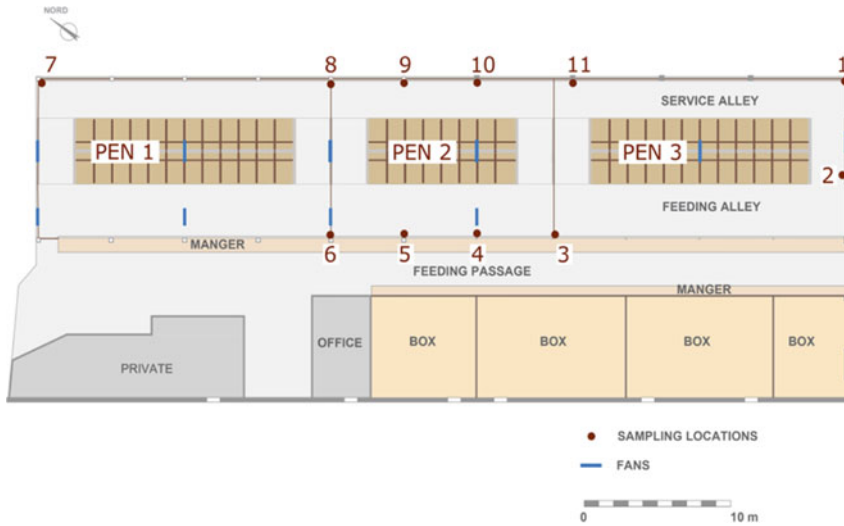


Fig. 1 Farm site layout and representation of the measurement points

on the localisation within the barn: central SLs (SL03-SL04-SL05-SL06); perimeter SLs (SL 08-SL09-SL10-SL11); corner SLs (SL01-SL02-SL07). The central and perimeter SLs were located in PEN2 in order to study different repetitions in space in the same pen. The distance between two SLs of central and perimeter areas of PEN2 was about 5 m. Gas concentrations were continuously acquired according to a measurement cycle, established before the experiment. Based on the evidence reported in the study by Rom and Zhang [10], the measurement cycle (i.e., composed by the numerical sequence of the SLs) was optimised to reduce bias related to detection of very different concentrations (i.e., high and low concentrations) between two adjacent SLs.

INNOVA device is able to perform some repetitions for each SL before switching to the next SL. In this study, INNOVA was set up to perform three repetitions for each SL before switching to the next SL. For each repetition, INNOVA measured the gas concentration of all the gases under study.

A relevant parameter that influences acquisition time for each repetition is the SIT. The SITs used for the experiments were Normal (5 s) and Low (20 s). When the SIT is 5, the detection limits, declared by the manufacturer, are the following: 0.2 ppm for NH_3 , 0.4 ppm for CH_4 , and 1,5 ppm for CO_2 . When the SIT is 20, detection limits are halved.

2.3 Periods of Data Collection and Related Measuring Setup

The measurements were carried out during two periods in May and June 2018. The first period, named Period 1, was from 10/05/18 to 20/05/18, whereas the second period, named Period 2, from 21/05 to 1/06. The SIT was 20 and 5 in Period 1 and Period 2, respectively. In detail, the SIT5 required about 1 min 15 s for each repetition, about 4 min for each SL and less than one hour to complete a measurement cycle ($1.25 \times 3RsSL \times 11 SLs$), whereas the SIT20 required about 2 min and 30 s for a repetition, about 7 min and 30 s for each SLs, and more than one hour for a measurement cycle.

2.4 Data Processing

Based on data acquired during Periods 1 and Period 2, a new dataset for each gas was implemented by starting from the computation of two main parameters: the first parameter was the mean value of gas concentration \bar{x} obtained by averaging concentration values measured in the three repetitions considered in a specific SL; the second was the variability $s_{x,n}$, expressed in percentage as the ratio between the standard deviation s_x and the mean value of the three repetitions \bar{x} in the SL considered. In the construction of the dataset, all the outliers were removed. In detail, it was verified that the mean values of the gas concentrations \bar{x} was not an outlier for both the observation period and the daily trend. As a consequence, each mean value \bar{x} that was classified as outlier for both the observation period and the daily trend was excluded from the dataset. Then, the s_x (ppm) was computed by using the equation of the standard deviation (SD) applied to the three repetitions for each SL:

$$s_x = \sqrt{\frac{\sum_{i=1}^n (x_i - \bar{x})^2}{n - 1}} \equiv SD$$

where n is the number of data points (i.e., 3), x_i was the gas concentration corresponding to the i -th value of the measured data and \bar{x} was the mean value of all x_i . The quantification of the variability $s_{x,n}$ (%) was done by normalising the values of the s_x by the mean value of gas concentration:

$$s_{x,n} = \frac{s_x}{\bar{x}} * 100$$

The resulting dataset was composed of rows that included the following elements: gas type (i.e., NH_3 , CH_4 , CO_2); SLs group (i.e., central, perimeter, corner); SIT group (i.e., SIT 20, SIT 5); \bar{x} ; s_x ; and $s_{x,n}$.

2.5 Statistical Analyses

Based on data analyses, the different setups of the INNOVA measurement device were assessed. In order to carry out statistical analyses, the same number of measurements for SIT 5 and SIT 20 in each group of SLs (i.e., central SLs, perimeter SLs, and corner SLs) was randomly selected. Then, the one-way analysis of variance (ANOVA) was applied to statistically test the differences between the variability of the measurements with SIT5 and SIT20 for each group of SLs (i.e., central SLs, perimeter SLs, and corner SLs). The analysis was carried out for all gas monitored (i.e., NH_3 , CH_4 , CO_2). In each post-hoc analysis the mean values were separated by Tukey's honestly significant difference at $P < 0.05$.

3 Results and Discussion

The results of the statistical analyses carried out on the two groups of SIT (Table 1) showed that there was no significant difference ($P > 0.05$) between the variability of gas concentrations acquired by using SIT20 and SIT5 in different areas of the barn. The only exception was represented by CH_4 measurements at corner SLs which showed significant difference ($p < 0.001$) between SIT5 and SIT 20. This result could be attributed to the position of the SLs at the corner and the high variability of the gas.

In Table 1, the results showed no significant differences between SIT5 and SIT20. Consequently, the setup with SIT5 is more suitable than SIT20 for a continuous monitoring of the gas concentrations inside the barn since it is possible to acquire the same data in all SLs in less than one hour. This is significant for the advancement of the research because when gas concentrations are measured in a SL, gas concentrations in the other eleven SLs were not available because they were not measured at the same time. The result of these analyses agrees with the study of Rom & Zhang [10] which underlines that shortening the SIT, SD could increase but measurement would be completed in a suitable time length. Moreover, Rom & Zhang [10] proposed to design the measuring strategy with a minimum of 12.5 up to 25 min on each position. In field conditions, this requisite could not be applied because the gas concentrations is not constant due to the influence of climatic factors and barn management with effects also on the emission estimation [5, 8, 20, 21]. Moreover, the evaluation of gas emissions is generally based on hourly values, as it was done in several studies [22–24]. In detail, the recent VERA Protocol [2] requires hourly values of NH_3 for continuous measuring methods. Therefore, in this barn typology the setup of INNOVA with SIT 5 made it possible to halve the time needed for each measurement cycle (i.e., less than one hour) compared to SIT 20 (i.e., about one hour and 30 min), and acquiring data in all 11 SLs.

Based on the outcome of this study, the setup of the SIT did not influence data variability. Therefore, the measurement strategy should prefer SIT5 to SIT 20 in

Table 1 Outcomes of the ANOVA and post-hoc test for the variability of gas concentrations of NH₃, CO₂ and CH₄ at SIT 5 and SIT 20 in each zone of the barn

<i>Gas</i>	<i>Zone</i>	<i>SIT</i>	<i>Mean $s_{x,n}$ (%)</i>	<i>Tukey post hoc test</i>	
NH₃	Corner SLs	20		P = 0.12	
		5			
	Perimeter SLs	20		P = 0.18	
		5			
	Central SLs	20		P = 0.24	
		5			
CO₂	Corner SLs	20		P = 0.37	
		5			
	Central SLs	20		P = 0.70	
		5			
	Perimeter SLs	20		P = 0.450	
		5			
CH₄	Corner SLs	5	34.74	A	
		20	27.33		B
	Central SLs	5		P = 0.48	
		20			
	Perimeter SLs	20		P = 0.538	
		5			

order to have a higher frequency of data acquisition. Time required by SIT 5 allowed to optimise time for monitoring and perform measurement repetitions for each SL. In a recent study [12] more than three repetitions for each SLs could be carried out to acquire NH₃ concentrations. For example, up to 4 repetitions for the maximum of 12 SLs could allow monitoring gas concentration at least once per hour. However, the number of repetitions for each SLs is related to the number of SLs in the barn and, consequently, the planning of the measurements should take into account, besides the SIT, both the number of SLs and the number of repetitions. These latter parameters are strictly related to barn dimensions and typology. Reduced plant dimensions allow decreasing the number of SLs and increasing the number of repetitions RsSL with a significant improvement of the quality of data collected.

4 Conclusions

A field experiment was carried out by using the INNOVA photo-acoustic analyser in an open naturally ventilated dairy barn. Different setups of the sample integration time (SIT) were used to acquire concentrations of NH₃, CO₂ and CH₄ and, on these values,

the variability of the data was statistically assessed to provide useful information for the setup of the INNOVA device. The results of this work highlighted that SIT setups affect overall time for acquiring data and, consequently, frequency of sampling.

Based on the advancement in measuring gas concentrations from open dairy barns, the following step is to evaluate the different positions of the sampling points in the monitoring of gas concentrations and related emission estimation in these open structures.

Acknowledgements The authors are grateful to the farm ALPA S.S. for giving the opportunity of carrying out the tests.

Funding The research study was funded by the University of Catania through the ‘Piano incentivi per la ricerca di Ateneo 2020–2022 – Linea 2’ project on ‘Engineering solutions for sustainable development of agricultural buildings and land’ (ID: 5A722192152) coordinated by Prof. Claudia Arcidiacono; and by the University of Catania through the ‘Piano incentivi per la ricerca di Ateneo 2016–2018 – Linea 1’ CHANCE project (ID: 5A722192143) coordinated by Prof. Claudia Arcidiacono. INNOVA device was funded by the project “Centro per l’innovazione dei sistemi di qualità tracciabilità e certificazione dell’agroalimentare” – AGRIVET (ID: G46D15000170009).

References

1. Baldini, C., Borgonovo, F., Gardoni, D., Guarino, M.: Comparison among NH₃ and GHGs emissive patterns from different housing solutions of dairy farms. *Atmos. Environ.* **141**, 60–66 (2016). <https://doi.org/10.1016/j.atmosenv.2016.06.047>
2. VERA: Vera test protocol: For livestock housing and management systems (2018)
3. D’Urso, P.R., Arcidiacono, C., Cascone, G.: Environmental and animal-related parameters and the emissions of ammonia and methane from an open-sided free-stall barn in Hot Mediterranean climate: a preliminary study. *Agronomy* **11**, 1772 (2021). <https://doi.org/10.3390/agronomy11091772>
4. Mendes, L.B., Pieters, J.G., Snoek, D., Ogink, N.W., Brusselman, E., Demeyer, P.: Reduction of ammonia emissions from dairy cattle cubicle houses via improved management- or design-based strategies: a modeling approach. *Sci. Total. Environ.* **574**, 520–531 (2017)
5. D’Urso, P.R., Arcidiacono, C., Valenti, F., Cascone, G.: Assessing influence factors on daily ammonia and greenhouse gas concentrations from an open-sided cubicle barn in hot Mediterranean climate. *Animals* **11**, 1400 (2021). <https://doi.org/10.3390/ani11051400>
6. Saha, C.K., et al.: Seasonal and diel variations of ammonia and methane emissions from a naturally ventilated dairy building and the associated factors influencing emissions. *Sci. Total Environ.* **468–469**, 53–62 (2014). <https://doi.org/10.1016/j.scitotenv.2013.08.015>
7. Wang, X., et al.: Reliable low-cost devices for monitoring ammonia concentrations and emissions in naturally ventilated dairy barns. *Environ. Pollut.* **208**, 571–579 (2016). <https://doi.org/10.1016/j.envpol.2015.10.031>
8. D’Urso, P.R., Arcidiacono, C.: Effect of the milking frequency on the concentrations of ammonia and greenhouse gases within an open dairy barn in hot climate conditions. *Sustainability* **13**, 9235 (2021). <https://doi.org/10.3390/su13169235>
9. Rong, L., Liu, D., Pedersen, E.F., Zhang, G.: Effect of climate parameters on air exchange rate and ammonia and methane emissions from a hybrid ventilated dairy cow building. *Energy Build.* **82**, 632–643 (2014). <https://doi.org/10.1016/j.enbuild.2014.07.089>
10. Rom, H.B., Zhang, G.: Time Delay for Aerial Ammonia Concentration Measurements in Livestock Buildings. *Sensors* **10**, 4634–4642 (2010). <https://doi.org/10.3390/s100504634>

11. Brehme, G.: True measuring with “Innova”. *Measur. Technol.* 58 *Landtechnik* **3**, 196–197 (2003)
12. D’Urso, P.R., Arcidiacono, C., Valenti, F., Janke, D., Cascone, G.: Measuring ammonia concentrations by an infrared photo-acoustic multi-gas analyser in an open dairy barn: Repetitions planning strategy. *Comput. Electron. Agric.* **204**, 107509 (2023). <https://doi.org/10.1016/j.compag.2022.107509>
13. D’Urso, P.R., Arcidiacono, C., Cascone, G.: Analysis of the horizontal distribution of sampling points for gas concentrations monitoring in an open-sided dairy barn. *Animals* **12**, 3258 (2022). <https://doi.org/10.3390/ani12233258>
14. Hassouna, M., Robin, P., Charpiot, A., Edouard, N., Méda, B.: Infrared photoacoustic spectroscopy in animal houses: effect of non-compensated interferences on ammonia, nitrous oxide and methane air concentrations. *Biosys. Eng.* **114**(3), 318–326 (2013). <https://doi.org/10.1016/j.biosystemseng.2012.12.011>
15. Zhuang, S., Brusselman, E., Sonck, B., Demeyer, P.: Validation of five gas analysers for application in ammonia emission measurements at livestock houses according to the VERA test protocol. *Appl. Sci.* **10**(15), 5034 (2020). <https://doi.org/10.3390/app10155034>
16. Li, H., Zhang, C., Xin, H.: Performance of an infrared photoacoustic single gas analyzer in measuring ammonia from poultry houses. *Appl. Eng. Agric.* **31**(3), 471–477 (2015). <https://doi.org/10.13031/aea.31.10826>
17. D’Urso, P.R., Arcidiacono, C., Cascone, G.: Assessment of a low-cost portable device for gas concentration monitoring in livestock housing. *Agronomy* **13**, 5 (2023). <https://doi.org/10.3390/agronomy13010005>
18. LumaSenseTechnologies: Instruction manual. *Int. Bus.* **2003**, 1–183 (2003)
19. Arcidiacono, C., Porto, S.M.C., Cascone, G.: On ammonia concentrations in naturally ventilated dairy houses located in Sicily. *Agric. Eng. Int. CIGR J.* **2015**, 294–310 (2015)
20. D’Urso, P.R., Arcidiacono, C., Cascone, G.: Spatial variability of ammonia concentrations in an open-sided dairy barn. In: Biocca, M., Cavallo, E., Cecchini, M., Failla, S., Romano, E. (eds.) *Safety, Health and Welfare in Agriculture and Agro-food Systems LNCE*, vol. 252, pp. 76–84. Springer, Cham (2022). https://doi.org/10.1007/978-3-030-98092-4_9
21. D’Urso, P.R., Arcidiacono, C., Cascone, G.: The effect of microclimatic conditions on ammonia emissions from an open-sided dairy barn during spring. In: Biocca, M., Cavallo, E., Cecchini, M., Failla, S., Romano, E. (eds.) *Safety, Health and Welfare in Agriculture and Agro-food Systems: Ragusa SHWA 2021*, pp. 85–94. Springer International Publishing, Cham (2022). https://doi.org/10.1007/978-3-030-98092-4_10
22. Saha, C.K., Ammon, C., Berg, W., Loesbin, C., Fiedler, M., Brunsch, R., von Bobrutzki, K.: The effect of external wind speed and direction on sampling point concentrations, air change rate and emissions from a naturally ventilated dairy building. *Biosyst. Eng.* **114**(3), 267–278 (2013). <https://doi.org/10.1016/j.biosystemseng.2012.12.002>
23. Hempel, S., Saha, C.K., Fiedler, M., Berg, W., Hansen, C., Amon, B., Amon, T.: Non-linear temperature dependency of ammonia and methane emissions from a naturally ventilated dairy barn. *Biosyst. Eng.* **145**, 10–21 (2016). <https://doi.org/10.1016/j.biosystemseng.2016.02.006>
24. D’Urso, P.R., Arcidiacono, C., Cascone, G.: Uncertainty in determining ammonia and methane emissions at different sampling locations in an open-sided dairy barn. In: 2021 IEEE International Workshop on Metrology for Agriculture and Forestry, MetroAgriFor 2021 - Proceedings, 2021, pp. 145–150 (2021). <https://doi.org/10.1109/MetroAgriFor52389.2021.9628493>
25. Ngwabie, N., Jeppsson, K.-H., Gustafsson, G., Nimmermark, S.: Effects of animal activity and air temperature on methane and ammonia emissions from a naturally ventilated building for dairy cows. *Atmos. Environ.* **45**, 6760–6768 (2011). <https://doi.org/10.1016/j.atmosenv.2011.08.027>

Agricultural By-Products for Biomethane Production: Opportunities for a Sustainable Bioenergy Conversion



Giovanni Ferrari, Francesco Marinello, and Andrea Pezzuolo

Abstract The use of agricultural and livestock by-products for bioenergy production can contribute to the achievement of sustainable development goals. In the areas where there are already anaerobic digestion plants fed with energy crops, it may be cost-effective to maintain existing plants while changing the diet. In this case, it is necessary to study how this feed change will affect energy production. To evaluate this potential, in this work a biomass distribution model for biogas production was developed. This work aims to develop a scenario for the reconversion of the feeding of biogas plants in the Veneto region to use only agricultural by-products and livestock manure. Considering the existing plants, without installing new facilities, it was calculated that 46.6% of the plants can maintain or increase their power using only by-products, while the remaining 53.4% need to reduce their installed power. With this analysis, it was also possible to identify the 46 plants most suitable for the installation of biomethane upgrading systems.

Keywords By-products · Livestock waste · Biogas plants · GIS · Biomethane

1 Introduction

Many national and international institutions have placed the environment and sustainable development at the core of their political and administrative actions [1]. More and more resources, both economic and technological, have been devoted to the pursuit of cheap and clean sources of energy. These two items constitute the new paradigm of energy policies in developed countries. Access to energy should be guaranteed to all communities, possibly through self-generation, and also assured to future generations, safeguarding environmental resources. With this in mind, bioenergy is one of the most promising sources of energy from the perspective of sustainable development [2].

G. Ferrari (✉) · F. Marinello · A. Pezzuolo
Department of Land, Environment, Agriculture and Forestry, University of Padova, 35020
Legnaro, PD, Italy
e-mail: giovanni.ferrari.7@studenti.unipd.it

© The Author(s), under exclusive license to Springer Nature Switzerland AG 2023
V. Ferro et al. (eds.), *AIIA 2022: Biosystems Engineering Towards the Green Deal*,
Lecture Notes in Civil Engineering 337,
https://doi.org/10.1007/978-3-031-30329-6_118

1143

The use of biomass for energy production is already a widely reliable and proven sector [3]. Various types of biomass can be used: municipal and industrial organic waste, energy crops, agricultural by-products, and forest biomass. The choice of biomass type depends mainly on the spatial context [4]. In agriculture, the bioenergy sector has mainly developed around energy crops: corn silage, sugar beet, sorghum [5]. This mode, although it provides a significant supply of energy at a relatively low cost, requires the use of large areas of agricultural land for dedicated crop production, competing with food production [6]. To cope with this problem, one solution is the use of agricultural and livestock by-products [7]. The use of these biomasses does not conflict with food production, and allows for the exploitation of products that would otherwise have to be disposed of as waste, thus incurring additional costs. In addition, anaerobic digestion of livestock waste allows the production of a more chemically stable digestate that can be used as a fertilizer, reducing the expense of nitrogen management [8]. However, this system must consider the lower energy content of by-products and their greater dispersion over land. For this reason, careful spatial analysis is necessary in order to optimize the logistics of biomass transportation and the location of production facilities [9].

The processes for energy production depend on the type of biomass available and the type of energy required: electricity, heat, biofuels. The predominant use of agricultural resources (both energy crops and by-products) has been the production of electricity in generation systems powered by biogas, which in turn is obtained from the anaerobic digestion of biomass. This system has made it possible to build numerous plants and feed a fair amount of electricity from renewable sources into the grid. However, the only electric power generation is a very low-efficiency process (35% [10]); therefore, there is a large loss of energy [11]. Moreover, if biogas is used consistently, without taking into account the energy peaks demanded by the market, one of the advantages of bioenergy over other renewable sources is lost: the possibility of obtaining a manageable energy source that is not subject to unpredictable natural elements [12]. For this reason, national regulations and research interest are increasingly directed toward the production of biomethane, a gas that can be fed into the grid and stored for very long periods of time, unlike electricity. Biomethane production, however, requires the construction of large and expensive upgrading plants to purify the biogas of carbon dioxide. It is necessary to carefully identify the location of these plants in order to reduce the cost of infrastructure to connect them to the natural gas grid [13].

In this paper, the energy crop-byproduct transition and biogas-biomethane upgrading are addressed. Currently, the biomass supply for anaerobic digestion is mainly energy crops (mainly maize silage) and livestock waste. The objective of this study is to evaluate the effects of replacing energy crops with agricultural by-products and increasing the share of livestock waste. Based on the current location of biogas plants, a supply conversion scenario with 100% by-product-based and livestock manure feed is proposed. In this way, the new theoretically achievable powers in the plants are calculated. In addition, candidate plants for upgrading systems are identified, based on location relative to the natural gas distribution grid and potential installed power. This work is addressed on the spatial and management aspect of

biomass supply to plants. Some important considerations are not considered: changes in the size of the plants due to the change in diet, and the management of a different diet from the current one, resulting in the need to use different pretreatments. These fundamental evaluations, are reserved for more in-depth studies devoted to individual plants. Another aspect is the increased energy demand for the upgrading process. Although the different technologies require different amounts of energy, studies have shown that these values are still lower than those required by anaerobic digestion. In addition, analysis of data provided by plant operators shows that to date much of the heat produced is not used within the plant (about 70%); for these reasons it is assumed that this heat can be used for upgrading processes.

2 Materials and Methods

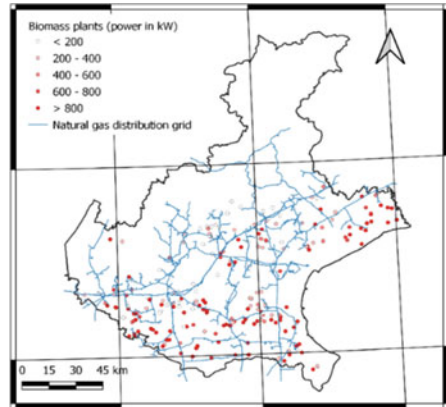
2.1 Data Collection

To calculate the amount and distribution of livestock biomass, the number of animals obtained from the National Livestock Register [15], which provides the number of animals by type and production orientation for each municipality, was considered. Only farms with a minimum size of 20 cattle, 20 pigs or 4,000 poultry were considered. Farming methods that do not allow manure collection (e.g., wild, transhumant) were excluded. Finally, not all farming methods, production technologies and farm sizes allow profitable utilization of livestock manure; therefore, an availability coefficient of 60% was applied to estimate the actual contribution of these biomasses [14].

Data on crops used for the agricultural biomass calculations were provided by AGEA, the Agricultural Disbursement Agency [14], which collects cultivation data for every landholding in the country. Agricultural by-products considered for the analysis of available biomass were: wheat straw, oats, barley, sorghum, ryegrass, triticale, sugar beet processing waste, and corn stover. In order to simulate the production phases, a number of coefficients were applied to ensure that the calculation adhered to the real situation. First, only fields of at least 2,000 m², resulting in single properties not joined with larger ones, were considered; smaller properties are considered economically disadvantageous in terms of mechanization and labor efficiency to collect by-products to be sent to the digester. In addition, a sustainable removal rate (SRR) of 40%-50% [15] was applied to ensure adequate organic matter supply to the field, avoiding soil depletion and maintaining soil fertility [16]. Finally, by-product potential was further reduced by 84% to account for competing uses, such as livestock feed production.

The anaerobic digestion of biomass must occur in plants already in operation to minimize the economic and environmental costs of constructing new digesters. The support of the GSE (Energy service manager) (GSE, 2021) [16], has allowed obtaining the distribution of existing biogas plants with diet and installed power. GSE

Fig. 1 Biogas plants currently operating in Veneto region and natural gas grid distribution



is the agency responsible for the promotion and development of renewable energy sources in Italy. Through the dedicated web portal, it is possible to visualize and download data regarding renewable energy plants in Italy. The database provides the administrative entities where the plants are located, geographic coordinates, types of plants (biogas, biofuels, waste), and installed capacity. The subsequent analysis considered only biogas plants (Fig. 1).

Finally, the natural gas distribution network was acquired from the Veneto Region web portal. The distribution network is needed to determine which plants are in the best location for the installation of upgrading systems.

2.2 Data Analysis

In the first part of the analysis an availability map was created consisting of a grid with 1 km meshes based on the potential energy values of agro-livestock by-products. Each mesh is associated with its energy availability value; this value is the result of the sum of energy from crop by-products and potential energy from waste from livestock activities. A model has been created on QGIS software to associate by-product productions with digestion facilities. This model allowed to simulate a random distribution of by-products, with the attractiveness of the plants inversely proportional to the distance from the biomass production areas. This algorithm considers the statistical possibility of biomasses too be sent to all the plants, and not just to the nearest one, based on commercial contracts or technical requirements. The calculation provided the energy potential from by-products associated with each plant. The potential energy of by-products for each plant was compared to the energy currently produced. This comparison allowed to determine which plants, based on the spatial production of by-products, have the potential to maintain their power, increase it, or need to reduce it.

Table 1 Biomethane potential of by-products and wastes considered in the analysis

By-product	Dry material (%)	Volatile solid (%)	Methane yield (Nm ³ CH ₄ /t VS)
Maize	87	95	239
Wheat	85	93	200
Sugarbeet	27	90	300
Oats	80	93	200
Barley	66	93	200
Sorghum	87	95	239
Ryegrass	45	90	400
Triticale	30	92	440
Cattle manure	8	80	200
Pig manure	5	80	300
Poultry manure	20	80	300

In the last phase, the most suitable plants for the installation of upgrading systems were selected, based on their size and location. Specifically, the plants should be located close to the natural gas distribution grid to reduce the cost, both economic and social, of constructing connections to inject biomethane into the grid. In addition, larger plants should be favored in order to take benefit of the economies of scale generated by the construction of large upgrading plants.

The main physical characteristics and methane productivity of agricultural by-products and livestock manure used for the present study are shown in Table 1.

3 Results and Discussion

The distribution of energy potential was consistent with the distribution of agro-livestock activities in the region. agricultural by-products in the Po Valley in the southern part of the region; livestock waste in areas near the mountainous part in the northwest of the region. Overall, the estimated potential of plant byproducts reached 8,923,811 GJ/year, equal to 867,662 MWh/year of potential CH₄. A total of 67.9% of this potential is represented by corn stalks, and 17.9% is represented by wheat straw. The remaining area, just 14.2%, is made up of all other crops: ryegrass (5.4%), barley (2.4%), sugarbeet (1.4%), sunflower (1.0%), and others (3.9%). Most of the energy potential from livestock activities derives from cattle farms, 3,166,708 GJ/year, or 58.7% of the total, with a population of 734 thousand heads. Swine farms produce 1,313,821 GJ/year of energy potential, 24.4%, with a population of 637 thousand heads. The remainder, 910,172 GJ/year, comes from poultry farms, representing 43,698 thousand heads.

The potential energy of each quadrant of the grid was attributed to biogas plants proportionally to the proximity of the grid to the plants. Only plants within 20 km of each grid were considered; in this way, a maximum transport threshold was imposed, corresponding to a road distance between 25 and 35 km. Results indicate that 23% of facilities cannot maintain their current energy production and must decrease their installed capacity by more than 50%. This result mainly affects larger plants distributed in areas with high plant density and high grain production. The result is explained by the high dependence of digesters on energy crops. 67% of the dry plant material used in the plants comes from corn silage. Its substitution can cause serious supply problems for some plants. A smaller reduction is expected for 30% of the plants, ranging from -50% to 0%. Based on the model, 9% of plants could increase their installed capacity by a small amount, less than 50%, while for 37% of them, the potential increase is higher than 50%. The high potential of agricultural and livestock by-products should be carefully verified; in particular, data on actual availability should be supplemented to consider the specific characteristics of the study area. In general, it appears that by-products can supply the bioenergy system, and can be a viable alternative to energy crops. The latter result is particularly concerning for small plants, isolated or near areas of high livestock production (Figs. 2 and 3).

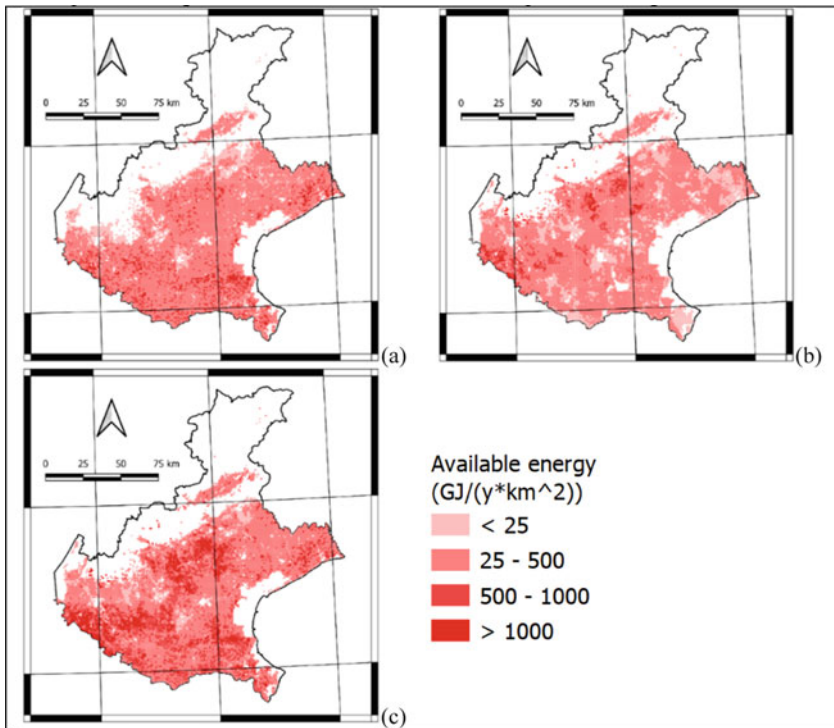
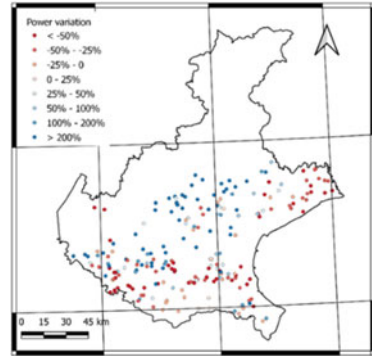


Fig. 2 Biomass availability: agricultural by-products a, livestock waste b, total c

Fig. 3 Power variation of biomass plants



Previous results are particularly influenced by plant size. Small plants, with power outputs less than 500 kW, can all maintain their current powers, and in many cases increase them. Power reductions almost exclusively affect larger plants: 61.5% of plants with power between 500 and 600 kW, 78.6% of plants with power between 600 and 700 kW, 97.1% of plants with power greater than 700 kW (Fig. 4).

Once the powers achievable with the supply of by-products were calculated, plants with a capacity of more than 600 kW and distance of less than 1 km from the natural gas distribution grid were selected. Forty-six plants were identified as suitable for the upgrading of biogas upgrading systems. These plants are located in proximity to the natural gas distribution grid, so the cost of building the infrastructure needed to feed biomethane into the grid is low. These plants can work as hubs, so biogas produced in other plants can be transported to them for the upgrading process (Fig. 5).

Some of these plants, if they operated independently, would not be able to achieve economically profitable biomethane production. Therefore, the idea being proposed is to identify them as collection plants for biogas produced in neighboring plants; they should therefore work as district upgrading plants.

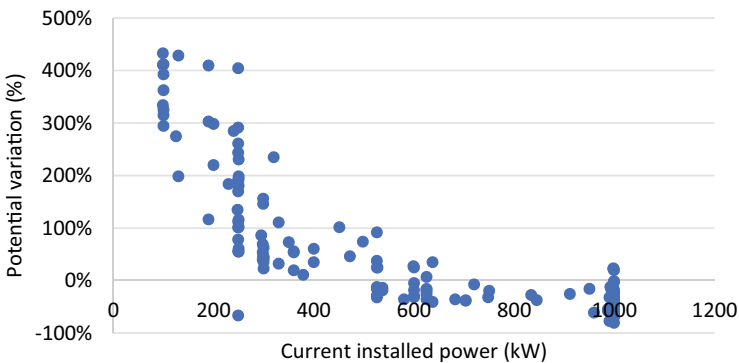
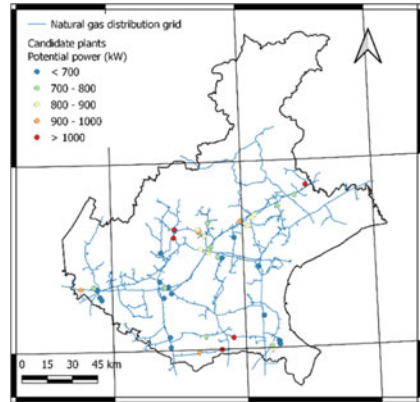


Fig. 4 Power variation compared with current installed power

Fig. 5 Biomass plants candidates to become bio-methane production hubs



4 Conclusions

These results demonstrate the potential of agricultural by-products for energy production and the possibility of converting the production system with low costs for plant owners. Further analysis will determine where it is most cost-effective to install upgrading facilities for biomethane production. This analysis will consider the existing methane distribution network, the potential capacity of the plants and the transport system on the territory. The biomethane produced can be fed into the grid or used as fuel for vehicles. An interesting opportunity is the possibility of selling the biomethane produced in one or more digesters directly to a local company. In this way an energy community logic is developed, which is able to provide, at least in part, for the self-production of the energy it needs. Future and more specific research may move in this direction.

References

1. European Parliament Directive (EU): 2018/2001 of the European Parliament and of the Council on the promotion of the use of energy from renewable sources. *Off. J. Eur. Union* **2018**, 82–209 (2018)
2. Scarlat, N., Dallemand, J.F., Fahl, F.: Biogas: developments and perspectives in Europe. *Renew. Energy* **129**, 457–472 (2018). <https://doi.org/10.1016/j.renene.2018.03.006>
3. Ferrari, G., Pezzuolo, A., Nizami, A.-S., Marinello, F.: Bibliometric analysis of trends in biomass for bioenergy research. *Energies* **13**, 3714 (2020). <https://doi.org/10.3390/en13143714>
4. Ferrari, G., Ai, P., Marinello, F., Pezzuolo, A.: Where and how? A comprehensive review of multicriteria approaches for bioenergy plant siting. *J. Clean. Prod.* **346**, 131238 (2022). <https://doi.org/10.1016/j.jclepro.2022.131238>
5. Jacobs, A., et al.: Greenhouse gas emission of biogas production out of silage maize and sugar beet – An assessment along the entire production chain. *Appl. Energy* **190**, 114–121 (2017). <https://doi.org/10.1016/j.apenergy.2016.12.117>

6. Ignaciuk, A.M., Dellink, R.B.: Biomass and multi-product crops for agricultural and energy production-an AGE analysis. *Energy Econ.* **28**, 308–325 (2006). <https://doi.org/10.1016/j.eneco.2006.01.006>
7. Ferrari, G., Ioverno, F., Sozzi, M., Marinello, F., Pezzuolo, A.: Land-use change and bioenergy production: soil consumption and characterization of anaerobic digestion plants. *Energies* **14**, 4001 (2021). <https://doi.org/10.3390/en14134001>
8. Provolo, G., Perazzolo, F., Mattachini, G., Finzi, A., Naldi, E., Riva, E.: Nitrogen removal from digested slurries using a simplified ammonia stripping technique. *Waste Manag.* **69**, 154–161 (2017). <https://doi.org/10.1016/j.wasman.2017.07.047>
9. Valenti, F., Porto, S.M.C., Dale, B.E., Liao, W.: Spatial analysis of feedstock supply and logistics to establish regional biogas power generation: a case study in the region of Sicily. *Renew. Sustain. Energy Rev.* **97**, 50–63 (2018). <https://doi.org/10.1016/j.rser.2018.08.022>
10. Scarlat, N., Fahl, F., Dallemand, J.F., Monforti, F., Motola, V.: A spatial analysis of biogas potential from manure in Europe. *Renew. Sustain. Energy Rev.* **94**, 915–930 (2018). <https://doi.org/10.1016/j.rser.2018.06.035>
11. Bernotat, K., Sandberg, T.: Biomass fired small-scale CHP in Sweden and the Baltic States: a case study on the potential of clustered dwellings. *Biomass Bioenerg.* **27**, 521–530 (2004). <https://doi.org/10.1016/j.biombioe.2003.10.010>
12. Ferrari, G., Holl, E., Steinbrenner, J., Pezzuolo, A., Lemmer, A.: Bioresource technology environmental assessment of a two-stage high pressure anaerobic digestion process and biological upgrading as alternative processes for biomethane production. *Bioresour. Technol.* **2022**, 360 (2022). <https://doi.org/10.1016/j.biortech.2022.127612>
13. Sharara, M.A., OwusuTwum, M.Y., Runge, T.M., Larson, R.: Planning methodology for anaerobic digestion systems on animal production facilities under uncertainty. *Waste Manag.* **104**, 262–269 (2020). <https://doi.org/10.1016/j.wasman.2020.01.028>
14. Meyer, A.K.P., Ehimen, E.A., Holm-Nielsen, J.B.: Future European biogas: Animal manure, straw and grass potentials for a sustainable European biogas production. *Biomass Bioenerg.* **111**, 154–164 (2018). <https://doi.org/10.1016/j.biombioe.2017.05.013>
15. Scarlat, N., Martinov, M., Dallemand, J.F.: Assessment of the availability of agricultural crop residues in the European Union: potential and limitations for bioenergy use. *Waste Manag.* **30**, 1889–1897 (2010). <https://doi.org/10.1016/j.wasman.2010.04.016>
16. Sahoo, K., Mani, S., Das, L., Bettinger, P.: GIS-based assessment of sustainable crop residues for optimal siting of biogas plants. *Biomass Bioenerg.* **110**, 63–74 (2018). <https://doi.org/10.1016/j.biombioe.2018.01.006>
17. AGEA (2020). <https://www.agea.gov.it/portal/page/portal/AGEAPageGroup/HomeAGEA/home>
18. Anagrafe Nazionale Zootechnica (2020). https://www.vetinfo.it/j6_statistiche/#/
19. GSE: Atlaimpianti (2021). <https://www.gse.it/dati-e-scenari/atlaimpianti>

Heating from Biogas Plants: An Areal Approach for Enhanced Environmental Sustainability



Giovanni Ferrari, Lorenzo Guerrini, and Andrea Pezzuolo

Abstract The availability of renewable energy sources and highly efficient technologies are two critical aspects in evaluating a sustainable low-carbon energy supply. The efficiency of power generation in anaerobic digestion plants is around 35%. The remaining portion of the energy is heat produced in biogas combustion. This heat is usually used to supply the plant itself and the production facilities where it is embedded. However, this supply is only a fraction of the heat produced, lost mainly as waste. To recover the excess heat produced in biogas plants, this research aims to quantify the thermal needs of the buildings around the anaerobic digestion plants in one province of the Veneto Region (Italy) that can be supplied by the plants through district heating systems. District heating systems are an experienced and reliable technology that can validly be used to exploit the economies of scale of centralized heat production. The analysis found that the plants can provide up to 775 MWh/d of heat, saving 25.5–106 m³ of CH₄, and reducing emissions by 127 t of CO₂ each day.

Keywords Bioenergy · Anaerobic digestion · Heat valorization · District heating · Rural areas

1 Introduction

Over the past few years, many national and international institutions have set increasingly ambitious goals for sustainable development and many researches have been conducted in the field of bioenergy [1, 2]. Numerous approaches have been deployed to achieve the expected results, both on the supply side, with ever-increasing production of energy from renewable sources [3, 4], and on the demand side, reducing the energy requirement and increasing the efficiency of utilization systems [5, 6]. Reducing energy consumption is the only truly zero-impact system [7–9], going to

G. Ferrari · L. Guerrini · A. Pezzuolo (✉)
Department of Land, Environment, Agriculture and Forestry, University of Padova, 35020
Legnaro, PD, Italy
e-mail: andrea.pezzuolo@unipd.it

decrease any kind of environmental impact. The fields of action are many: improvement of materials [10], efficient organization of production activities [11, 12], reduction of soil consumption [13] and reduction of energy waste [14]. It is precisely the reduction of thermal energy waste, in the civil and industrial sector, that is one of the areas where action is most needed.

In Italy, the main sources used to meet energy consumption for space heating are natural gas (60%) and biomass (26%) while oil products now play a marginal role (9%) [15]. This system, while providing better environmental results than the use of other fossil fuels, is still highly vulnerable to product availability and price. In addition, natural gas is still a fossil fuel, and as such causes an increase in the concentration of CO₂ in the atmosphere [16]. In this context, the use of alternative and sustainable systems for the production of thermal energy in buildings appears to be as high a priority as ever.

One of the systems that achieves significant energy savings is district heating, which is the supply of hot water to buildings from a single heating center [17]. These centers usually are biomass power plants, which burn municipal solid waste or forest biomass. To achieve the efficiency goals mentioned above, one of the possible sources to be used is heat produced in biogas cogeneration plants. The use of heat produced in electric biogas plants for district heating is a system that several authors believe should be used whenever conditions permit [18]. For this reason, it would be necessary to carefully consider where to locate the plants to promote the optimal utilization of even the heat produced [19].

In Italy, national legislation has encouraged the emergence of many medium- and small-scale electric biogas plants fueled by agricultural products. Nowadays, legislation has strongly favored the use of agro-livestock by-products, particularly straw and livestock manure. These plants have a very low efficiency, about 35% [20], which therefore leads to the loss of energy in the form of heat. This heat is usually used for the needs of the biogas production process, as well as for the supply of thermal energy to the production-farm site where the plant is located [21].

The aim motivating this research is to estimate the possibility of using this heat to supply thermal energy through hot water to the civil, agricultural and industrial buildings located near the anaerobic digestion plant. Usually, these plants are placed in agricultural areas characterized by intensive farming and livestock farming; therefore, they are located near agricultural buildings - stables, barns, product processing facilities, areas used for sheltering vehicles. In many cases, however, the highly anthropized environment means that other industrial facilities and many buildings for civilian use are also located in the vicinity of the plant. Therefore, a careful spatial analysis on the distribution of housing is necessary to achieve an adequate result, as these plants are not built for the purpose of producing and distributing heat, and therefore the definition of a distribution network may present considerable difficulties.

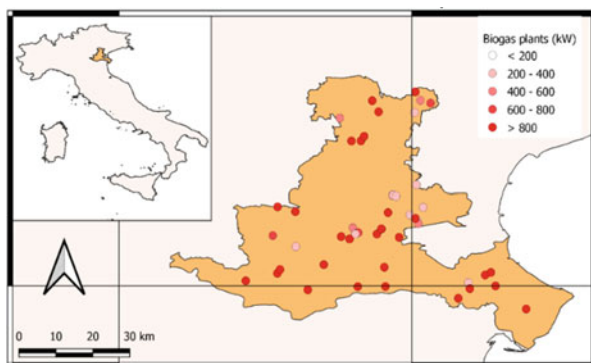


Fig. 1 Biogas plant distribution in the study area

2 Materials and Method

2.1 Availability of Thermal Energy

The study area for this analysis is two provinces (NUTS 3) in the Veneto region of Italy: Padua and Rovigo. In the first phase of the work, data on biogas plants in the study area have been collected. For each plant, the coordinates, the installed electric power, the produced thermal power, the days of effective work during the year have been collected. Biogas plants data were provided by the agricultural office of the Veneto Region [22]. These data have been loaded on the analysis software QGIS. In this way, it was possible to determine the location and potential of the heat sources. A total of 48 facilities were involved in the analysis (Fig. 1).

The heat produced by the plants and available for district heating was provided as an average annual value from the plants. To cope with increases and decreases in heat demand and production, district heating systems are equipped with heat storage tanks. This technology does not prevent there from being less heat availability in winter, when the plant requires more thermal energy to heat the digester.

A thermal conductivity value of the pipe insulation (Polyethylene, HDPE) of $0.025 \text{ W}/(\text{m}\cdot\text{K})$ was assumed to estimate the heat lost in the path [23].

2.2 Facilities and Energy Demand

Data on the buildings present in the study area were collected in the second phase. Building data were provided by the regional cadaster office. The dataset consisted of a shape file in which the perimeters of all buildings in the region were reported, with associated height and use. Therefore, each structure was described with its size, location, height and intended use. A heat consumption per cubic meter of building

Table 1 Properties and energy demand by building class use

Building Class use	Average height (m)	Standard deviation (m)	Min considered height (m)	Energy consumption (kWh/(m ³ ·y))
Housing	5.594	1.824	2.5	53.4
Public Administration	9.719	2.327	2.5	27.0
Public building	7.736	3.402	2.5	27.0
Commercial	6.435	2.262	2.5	27.0
Industrial	6.009	2.754	1.5	27.6
Agricultural	4.616	1.613	1.5	27.6

per year was defined for each use category [19] by “Eq. (1)”:

$$E_{tc} = S_p \cdot h_t \cdot E_{sc} \quad (1)$$

where: E_{tc} is the total energy consumption of the building (kWh/y); S_p is the plan surface (m²); h_t is the total height (m); E_{sc} is the specific energy consumption (kWh/(m³·y)). Using the proximity criterion, it was possible to relate the heat production in the facilities to the heat demands of the buildings. In particular, proximity represent as the road distance, calculated trough the QGIS tool Shortest path and the category of buildings considered are shown in Table 1. These represent the most common categories and those most easily reached by a district heating system. Table 1 also shows the average building height and energy consumption per cubic meter.

2.3 Temporal Trend of Energy Demand

To calculate the flow of thermal energy required by buildings, natural gas flows by sector of use were analyzed [24] (Fig. 2). These flows are very substantial, as Italy bases its energy system on this fossil fuel. There are three sectors of use: industrial production, power generation in thermal power stations, and heat generation in civil buildings. Industrial production and power generation are essentially constant throughout the year. The sector that shows the greatest variability is the civil sector, with high demands in the winter months and a marked decrease in the summer months. These data make it possible to estimate the heat demand of buildings throughout the year, allowing a more correct estimate of the amount of heat needed.

Methane distribution data does not distinguish between residential, administrative, public service, and commercial users. Hence, the trend was applied to all the above categories, although it would be conceivable that some categories, such as health care facilities, have more constant consumption throughout the year. For others, such as homes, the difference between winter and summer consumption is even more

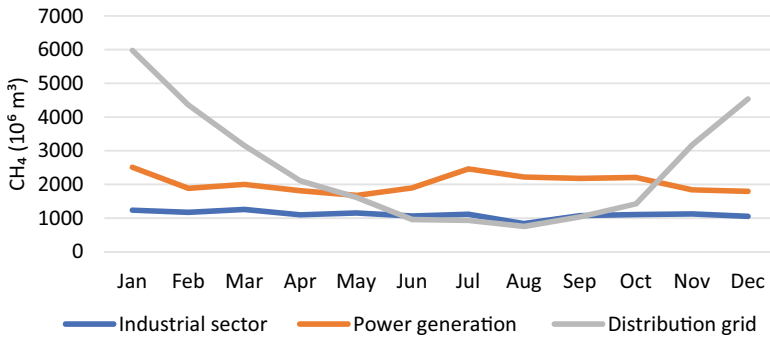


Fig. 2 Monthly trend of energy demand per sector in Italy

pronounced than shown on the graph. For the latter, the consumption of methane for cooking, which does not vary substantially throughout the year and cannot be replaced by the district heating system, was also not considered.

3 Results and Discussion

3.1 Theoretical Supply Distance

A heat availability of 775 MWh per day resulted from the 48 facilities considered in the study. On average, the systems can satisfy the heat demands of all buildings within a radius of 988 m. This parameter changes considerably throughout the year; the lowest value occurs in January, 729 m, when heat demand is greatest, while the highest value occurs in August, 1285 m, when buildings consume the least heat (Figs. 3 and 4).

The number of plants that can meet the heat demands of all buildings within a radius of 2000 m were estimated. The lowest value is 3, and is recorded in all months from November to March, while in June, July and August the value increases to 11.

Observing the supply distances shown in Fig. 4 and comparing them with the heat energy demand trend shown in Fig. 2, it should be noted that the heat consumption of the area served is not proportional to the size of the area. This apparently counter-intuitive result is due to the fact that the plants are generally in rural areas, so there are generally not many buildings in the immediate vicinity. Moving away from the plant increases the possibility of finding settlements, even small ones, that rapidly increase the demand for energy.

To ensure heat supply even during periods of higher demand (e.g. winter), agricultural district heating can be combined with a conventional natural gas-fired generation system. An alternative is to identify priority users/categories, such as hospitals and industries, who can access heat year-round, while for other smaller private users,

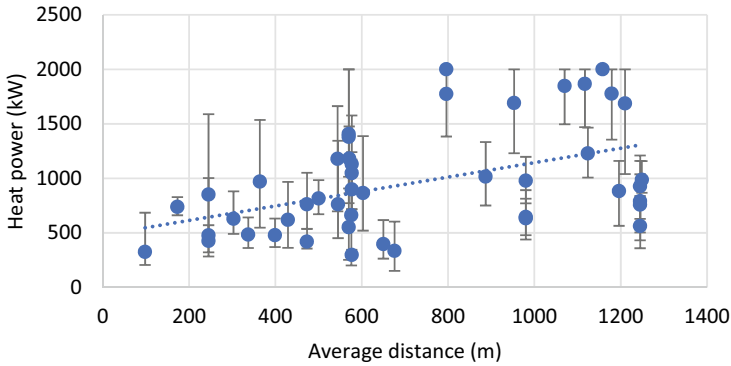


Fig. 3 Distribution of anaerobic digestion plants with the available heat power (kW) and the average supply distance; error bars represent the monthly maximum/minimum distance

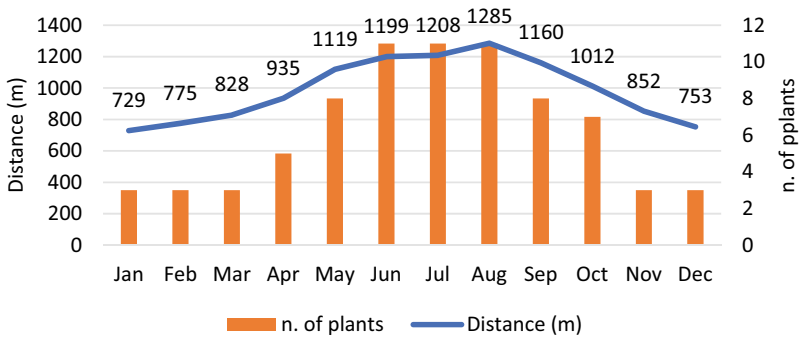


Fig. 4 Monthly variation of theoretical heat supply distance by anaerobic digestion plants and number of plants that can supply all buildings within a radius of 2000 m

this possibility is guaranteed only during certain periods (e.g. spring to autumn). Considering the very short heat transport distances, losses along the way were very small. This point will be developed in future analysis.

3.2 Heat Supply Capacity and CO₂ Saved

In all the environments considered, space and water heating are obtained predominantly by burning methane. Assuming that in these environments methane is the only source of heat for heating, it was possible to calculate the amount of natural gas saved by distributing hot water with the district heating system. As a result, it was possible to calculate the amount of CO₂ equivalent saved with this system. The

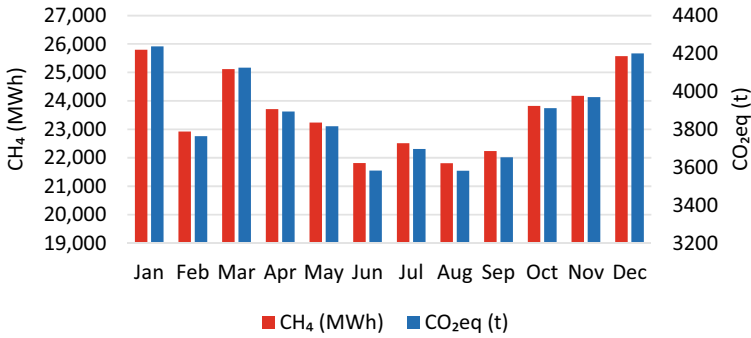


Fig. 5 Monthly trend of supplied energy (in MWh of CH₄) and ton of CO₂ saved (assuming conventional heat with CH₄)

results show that it is possible to save about 282.7 GWh of methane per year, equivalent to $25.5 \cdot 10^6$ m³ of CH₄. This results in emission savings of about 46,400 t of CO₂ per year (127 t of CO₂ every day).

Methane and CO₂ savings also vary throughout the year. In January, CO₂ savings reach 136.7 t CO₂eq per day, while CH₄ consumption is reduced by 75,300 m³ CH₄ per day. The result is particularly significant given that it is precisely in the winter months that the largest volume of imported methane occurs (Fig. 5).

4 Conclusions

In this research, the possibility of using the heat produced in biogas anaerobic digestion-fueled electric plants in rural areas for district heating systems was investigated. Forty-eight biogas plants in two provinces in Italy were evaluated. The plants produce and could distribute up to 282.7 GWh of thermal energy. On average, the system can supply all buildings up to 988 m. Such a system could reduce CO₂ emissions by an average of 127 t_{eq} per day. The use of this energy is important in developing a circular economy that takes advantage of an available resource and allows for a reduction in CO₂ emissions. In addition, this system can provide an additional source of income for farmers by optimizing resources and incentivizing the production of renewable energy from biomass. Future developments can optimize the network coverage in order to maximize the number of buildings supplied.

References

1. European Commission: Directive of the european parliament and of the council as regards the promotion of energy from renewable sources, and repealing Council Directive (EU) 2015/652. COM(2021) 557 Final 2021;2021/0218:12–26.

2. Ferrari, G., Holl, E., Steinbrenner, J., Pezzuolo, A., Lemmer, A.: Environmental assessment of a two-stage high pressure anaerobic digestion process and biological upgrading as alternative processes for biomethane production. *Bioresour. Technol.* **360**, 127612 (2022). <https://doi.org/10.1016/j.biortech.2022.127612>
3. Resch, B., Sagl, G., Trnros, T., Bachmaier, A., Eggers, J.B., Herkel, S., et al.: GIS-based planning and modeling for renewable energy: challenges and future research avenues. *ISPRS Int. J. Geo-Inf.* **3**, 662–692 (2014). <https://doi.org/10.3390/ijgi3020662>
4. Jin, K., Pezzuolo, A., Gouda, S.G., Jia, S., Eraky, M., Ran, Y., Ai, P.: Valorization of bio-fertilizer from anaerobic digestate through ammonia stripping process: a practical and sustainable approach towards circular economy. *Environ. Technol. Innov.* **27**, 102414 (2022). <https://doi.org/10.1016/j.eti.2022.102414>
5. Lange, S., Pohl, J., Santarius, T.: Digitalization and energy consumption. Does ICT reduce energy demand? *Ecol. Econ.* **176**, 106760 (2020). <https://doi.org/10.1016/j.ecolecon.2020.106760>
6. Pezzuolo, A., Chiumenti, A., Sartori, L., Da Borso, F.: Automatic feeding system: evaluation of energy consumption and labour requirement in north-east Italy dairy farm. In: *Proceedings of Engineering for Rural Development, Jelgava, Latvia*, pp. 882–887 (2016)
7. Raadal, H.L., Gagnon, L., Modahl, I.S., Hanssen, O.J.: Life cycle greenhouse gas (GHG) emissions from the generation of wind and hydro power. *Renew. Sustain. Energy Rev.* **15**, 3417–3422 (2011). <https://doi.org/10.1016/j.rser.2011.05.001>
8. Steen, M.: Greenhouse gas emissions from fossil fuel fired power generation systems. *Eur. Comm. Jt Res. Cent* (2001)
9. Nugent, D., Sovacool, B.K.: Assessing the lifecycle greenhouse gas emissions from solar PV and wind energy: a critical meta-survey. *Energy Policy* **65**, 229–244 (2014). <https://doi.org/10.1016/j.enpol.2013.10.048>
10. Maddalena, R., Roberts, J.J., Hamilton, A.: Can Portland cement be replaced by low-carbon alternative materials? A study on the thermal properties and carbon emissions of innovative cements. *J. Clean Prod.* **186**, 933–942 (2018). <https://doi.org/10.1016/j.jclepro.2018.02.138>
11. Inkinen, T., Hämäläinen, E.: Reviewing truck logistics: solutions for achieving low emission road freight transport. *Sustainability* **12**, 1–11 (2020). <https://doi.org/10.3390/SU12176714>
12. Ferrari, G., Ai, P., Alengebawy, A., Marinello, F., Pezzuolo, A.: An assessment of nitrogen loading and biogas production from Italian livestock: a multilevel and spatial analysis. *J. Clean Prod.* **317**, 128388 (2021). <https://doi.org/10.1016/j.jclepro.2021.128388>
13. Ferrari, G., Ioverno, F., Sozzi, M., Marinello, F., Pezzuolo, A.: Land-use change and bioenergy production: soil consumption and characterization of anaerobic digestion plants. *Energies* **14**(13), 4001 (2021). <https://doi.org/10.3390/en14134001>
14. Zhang, M., Yan, T., Wang, W., Jia, X., Wang, J., Klemeš, J.J.: Energy-saving design and control strategy towards modern sustainable greenhouse: a review. *Renew. Sustain. Energy Rev.* **164**, 112602 (2022). <https://doi.org/10.1016/j.rser.2022.112602>
15. GSE: Valutazione del potenziale nazionale e regionale di applicazione della coenerazione ad alto rendimento e del teleriscaldamento efficiente (2016). https://ec.europa.eu/energy/sites/default/files/documents/ca_art.14_eed_ita_update_dec2016_corrected.pdf
16. UK Government: Government conversion factors for company reporting of greenhouse gas emissions (2021). <https://www.gov.uk/government/collections/government-conversion-factors-for-company-reporting>
17. Buffa, S., Cozzini, M., D'Antoni, M., Baratieri, M., Fedrizzi, R.: 5th generation district heating and cooling systems: a review of existing cases in Europe. *Renew. Sustain. Energy Rev.* **104**, 504–522 (2019). <https://doi.org/10.1016/j.rser.2018.12.059>
18. Bernotat, K., Sandberg, T.: Biomass fired small-scale CHP in Sweden and the Baltic States: a case study on the potential of clustered dwellings. *Biomass Bioenerg.* **27**, 521–530 (2004). <https://doi.org/10.1016/j.biombioe.2003.10.010>
19. Ferrari, G., Ai, P., Marinello, F., Pezzuolo, A.: Where and how? A comprehensive review of multicriteria approaches for bioenergy plant siting. *J. Clean Prod.* **346**, 131238 (2022). <https://doi.org/10.1016/j.jclepro.2022.131238>

20. Scarlat, N., Fahl, F., Dallemand, J.F., Monforti, F., Motola, V.: A spatial analysis of biogas potential from manure in Europe. *Renew. Sustain Energy Rev.* **94**, 915–930 (2018). <https://doi.org/10.1016/j.rser.2018.06.035>
21. Weinand, J.M., McKenna, R., Karner, K., Braun, L., Herbes, C.: Assessing the potential contribution of excess heat from biogas plants towards decarbonising residential heating. *J. Clean Prod.* **238**, 117756 (2019). <https://doi.org/10.1016/j.jclepro.2019.117756>
22. AVEPA. <https://www.avepa.it/agenzia>
23. Duquette, J., Rowe, A., Wild, P.: Thermal performance of a steady state physical pipe model for simulating district heating grids with variable flow. *Appl. Energy* **178**, 383–393 (2016). <https://doi.org/10.1016/j.apenergy.2016.06.092>
24. SNAM. Dati operativi relativi al bilanciamento del sistema post del. 312/2016/R/GAS. https://www.snam.it/it/trasporto/dati-operativi-business/8_dati_operativi_bilanciamento_sistema/

Plant Factory with Artificial Lighting: Innovation Technology for Sustainable Agriculture Production



Luigia Mandriota, Ileana Blanco, and Giacomo Scarascia-Mugnozza

Abstract A healthy and safe diet today is increasingly threatened by climate change and economic crises; the rapid growth of the world population and urbanization will lead to an increase in global food needs and highly complex supply chains. Plant factories with artificial lighting (PFAL) give optimal answers to these critical issues, according to the United Nations Sustainable Development Goals, as opposed to conventional agricultural production systems which have reduced the availability of land per capita, generating negative environmental impacts. This work aims to provide a holistic assessment of the PFAL production processes, for efficient use of resources, according to the food-energy-water nexus. The productive yields of the cultivated plant species, the soilless cultivation technologies and fertigation systems, the thermo-hygrometric conditions, the CO₂ level and the artificial lighting conditions are defined, as well as energy sources and automation for production management. PFALs can be implemented in abandoned urban buildings, with a sustainable approach and a view to zero agricultural land consumption, to zero-mile food production and to the circular economy. The analysis shows that many PFALs are installed in countries with high density of urban populations, such as China, the USA, Japan and Northern Europe, to produce mainly herbs and leafy vegetables. Finally, a proposal for the reuse of abandoned industrial and tertiary sector buildings in Mediterranean peri-urban sites for sustainable urban farming is provided.

Keywords Food-energy-water nexus · Soilless culture systems · Leafy vegetables · Artificial intelligence · Urban agriculture

L. Mandriota

Department of Agricultural and Environmental Science DISAAT, University of Bari, Via G. Amendola 165/a, 70126 Bari, Italy

I. Blanco (✉)

Department of Biological and Environmental Sciences and Technologies DiSTeBA, University of Salento, S.P. 6 Lecce - Monteroni, 73100 Lecce, Italy
e-mail: ileana.blanco@unisalento.it

G. Scarascia-Mugnozza

Department of Civil, Environmental, Land, Building Engineering and Chemistry DICATECh, Polytechnic University of Bari, Via Edoardo Orabona, 4, 70125 Bari, Italy

1 Introduction

Food security and a healthy diet, already heavily threatened by climate change and conflict, have been even more neglected in recent years due to COVID-19 and the resulting economic instability. According to the latest FAO report in the last year there has been an increase in malnutrition (PoU) of 1.5% and the UN indicates that world food needs will increase strongly in the coming years according to the growth trend of the world population, which will reach about 2 billion more than the current one. Furthermore, it is estimated that in 2050 over 70% of humanity will migrate to cities, increasing the phenomenon of urbanization [1]. In these circumstances, food production and supply chains will become increasingly complex, generating negative environmental and management impacts on urban areas, in terms of both flow and balance of global energy and matter.

Conventional agricultural production systems, in recent decades, have led to the degradation of the soil used for crops and the loss of natural soil, with very worrying environmental impacts [2], as well as a decrease in the availability of land per capita. In fact, assuming a minimum consumption of 1500 cal per capita per day, to meet food needs with standard agricultural practices based on world population growth, global agricultural production should be increased by 70% by 2050. Furthermore, these systems produce “fossil food”, as defined by the United Nations as they are too based on fossil fuels and excessive consumption of drinking water and soil, generating about a third of greenhouse gas emissions and thus contributing to global warming.

It becomes important to rethink the management of agricultural production in the territories by seeking new methods of cultivation that are more sustainable, for the entire world population, in adequate quantity and quality, compared to traditional soil-based agricultural production [3].

Therefore, in the field of urban agriculture, the Plant Factories with artificial lighting (PFAL) are among the most technologically advanced agricultural plants in a controlled environment (CEA). They are based on vertical soilless cultivation systems placed on shelves, whose environmental conditions are managed by automatic control systems, to optimize spaces, resources, energy and time. They promote a positive environmental impact through a reduction of the food carbon footprint, more efficient land management, employment and diversification of the food market. They offer stable agri-food production all year round, and above all when localized in urban areas, can contribute to zero agricultural land consumption and to the de-carbonization of transport thanks to zero-mile production.

The aim of this work is to carry out holistic and comparative evaluations of various existing PFALs, on a global level, both of a commercial and experimental type. Thermo-hygrometric, lighting and building parameters, cultivation and fertigation technologies, control methodologies, energy sources and automation systems were retrieved and analyzed.

2 Materials and Methods

PFALs are almost all closed vegetables production systems, with an opaque envelope, isolated from the outside and with limited ventilation. A qualitative 4-step approach was chosen to retrieve and evaluate current PFAL practices:

1. List of existing PFALs, carried out through research on scientific literature and on the web: 10 different companies were found and detected also with regards to the economic, climatic and social context. Only developed countries were considered. The data gathered could be not complete and statistically representative; however, the research's purpose is to show the present development of innovative PFAL buildings.
2. Definition of the optimal cultivation parameters of leafy vegetables and fruit vegetables usually grown in the PFALs: the thermo-hygrometric conditions, the carbon enrichment, the light intensity and the spectrometric fractions, the photoperiod and the cultivation period duration.
3. Detection of qualitative and quantitative analysis parameters: geographical location, area of the lot, cultivation area, crop production, daily yield, cultivation technique, type of artificial lighting, soilless technology, level of automation, irrigation water, building envelope.
4. Proposal of a PFAL building typology: following the analysis of the various commercial and experimental companies, a proposal of PFAL building typology system in the Mediterranean area context for vegetable production was defined.

3 Results and Discussion

The selected analyzed PFAL buildings are located in the following countries and quantity, five in Japan, two in China, two in the United States, one in Denmark (Table 1). It emerges that this innovative and high-tech cultivation system is beginning to spread in urban areas of developed countries with a high population density, where food security and land scarcity are emerging issues [3].

Table 2 shows the most common types of plants grown in PFALs, namely fruit vegetables, such as tomatoes, cucumbers, strawberries and peppers, as well as leafy vegetables, especially for the fourth range products, for aromatic herbs and for micro-greens. Indoor cultivation requires high level of climate parameters control. Air temperatures generally varies in the range 15–26 °C for leafy vegetables, with minimum values of 15 °C in the night-time for lettuce, rocket and nasturtium, while a day temperature of 26 °C for basil is the optimum. For fruit vegetables, optimum temperature ranges in 13–28 °C, with minimum values of 13 °C in the nighttime for strawberry, and a daytime temperature of 28 °C for cucumber and pepper. Air relative humidity ranges from 50 to 80% for leafy vegetables and 55–90% for fruit vegetables.

Table 1 Descriptive data of existing PFALs

Company and location	Cultivation area/lot area (m ²)	Crops	Daily production	Cultivation shelves	Cultivation technique	Light source	Automation	Building and enclosures
Fujian Sanan Sino-Science Photobiotech co., Ltd Anxi, Fujian, China [4]	28,700/NA	leafy vegetables and medicinal plants	3096 kg d ⁻¹ for the vegetables (0.2 kg d ⁻¹ m ⁻²)	h level 0.2–0.3 m	NFT, no substrate	LEDs	Sowing, transplanting, harvesting, packaging	Opaque enclosure
Anhui Sanan, Biological co., Ltd., Jinzhai, Anhui, China [4]	11,000/NA							
Sino-Science, North America Photobiotech Inc., Las Vegas, USA [4]	5000/NA							
808 Factory, PFAL1, Yaizu, Shizuoka, Japan [5]	1000/10,000	curly lettuce, green leaf lettuce, romaine lettuce	1600 kg d ⁻¹ (0.8 kg d ⁻¹ m ⁻²)	20 shelves, 10 levels; h level 0.3 m	DFT, urethane foam substrate	FLs, LEDs	Transplanting, packaging	Insulated, hermetic building; opaque enclosure
808 Factory, PFAL2, Yaizu, Shizuoka, Japan [5]	1000/10,000	lettuce		16 shelves, 12 levels; h level 0.4 m	NFT, urethane foam substrate	LEDs	Transplanting, packaging, transport system	
Nordic harvest, Copenhagen, Denmark [6]	7000 / NA	salad, herbs	2740 kg d ⁻¹ (0.4 kg d ⁻¹ m ⁻²)	14 levels	DFT	LEDs	Harvesting, packaging	Opaque enclosure

(continued)

Table 1 (continued)

Company and location	Cultivation area/lot area (m ²)	Crops	Daily production	Cultivation shelves	Cultivation technique	Light source	Automation	Building and enclosures
University of Chiba, experimental PFAL, Kashiwa, Japan [7]	338/406	lettuce, herbs	170 kg d ⁻¹ (0.5 kg d ⁻¹ m ⁻²)	NA	Hydroponic system, urethane foam substrate	FLs	Lighting, nutrient solution, environmental parameters, energy consumption	NA
Spread, Kameoka plant, Kameoka, Japan [8]	2868/4780	lettuce	2000 kg d ⁻¹ (0.7 kg d ⁻¹ m ⁻²)	28 shelves, 12–16 levels	DFT	FLs, LEDs	Packaging	NA
Spread, Techno farm Keihanna, Kizugawa, Japan [8]	3950/11,550		4800 kg d ⁻¹ (1.2 kg d ⁻¹ m ⁻²)	NA	NA	LEDs	Sowing, transplanting, harvesting	NA
9th AeroFarms, Newark, USA [9]	3716/14,000	mustard, kale, rocket, cress, romaine lettuce	2500 kg d ⁻¹ (0.7 kg d ⁻¹ m ⁻²)	h level 0.8–0.9 m	Aeroponics, textile substrate	LEDs	Sowing, harvesting, packaging	Existing disused buildings

NFT: Nutrient Film Technique; DFT: Deep Flow Technique; LED: light-emitting diode; FL: fluorescent lamp; NA: not available.

Table 2 Vegetables optimal growing parameters data [10–21]

Plant species	Temperature [°C]	Relative humidity [%]	Photosynthetic Photon Flux Density (PPFD) [$\mu\text{mol m}^{-2} \text{s}^{-1}$]	Photo-period [h]	CO ₂ [ppm]	Cultivation period [days]
Lettuce	15 (night)–20 (day)	60–80	200, 70%R;30%B	16	1000	49
Rocket	15 (n)–20 (d)	50–70	100–250, 75%R; 25%B	16	1000	30
Basil	22 (n) –26 (d)	75	300, 75%R,25%B	16	1000	25
Nasturtium	15 (n)–20 (d)	50–80	200–400	16	500–1000	21
Broccoli, cabbage, radish microgreens	15 (n)–20 (d)	70	200, 50%R, 50%B	16	500–800	7–21
Tomato	16 (n)–26 (d)	55–60	200	18	800–1500	90
Cucumber	20 (n)–28 (d)	70–90	100, 85% R, 15% B	16	600–1000	55–65
Pepper	18 (n)–28 (d)	65–70	200	14	500–1000	50–65
Strawberry	13 (n)–22 (d)	60–70	200, 30%R,70%B	16	1000	94

Artificial lighting is supplied on average for 14–18 h per day, and the optimal range of light intensity is $100\text{--}300 \mu\text{mol m}^{-2} \text{s}^{-1}$, with spectral monochromatic emissions concentrated in the red and blue light in order to maximize the photosynthetic activity.

CO₂ enrichment in the range of 500 – 1500 ppm is used as a fertilizer for crop yield increase. Cultivation period lasts around one to two weeks for microgreens, on average one month for leafy vegetables and two to three months for fruit vegetables.

Table 1 shows the main characteristics of the PFAL analyzed buildings. The lot area varies between 5000 m² (Kameoka, Japan) and 14,000 m² (Newark, USA), while the inside cultivation area is managed on vertically stacked shelves having a cumulative surface of about 3000 to 29,000 m². The inside installation of shelves is distributed on 10–16 levels of soilless system growing rack, in which the distance between the shelves varies between 0.2 m and 0.9 m (Fig. 1), with an average of 0.3–0.4 m. Both the nutrient film technique (NFT) and the deep water culture system technique (DFT) are mainly used for soilless cultivation in the PFALs. The roots of the plants are fastened in a substrate or suspended in the nutrient solution that provides nutrient-rich water and oxygen to the root system, and then it is collected and reused, carrying out continuous microbiological monitoring and refurbishment. It

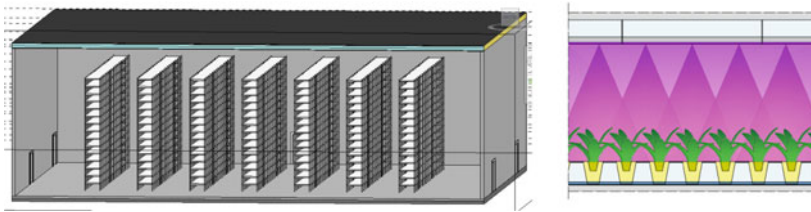


Fig. 1 PFAL axonometric cross section of the cultivation room (left); single level of a vertical racking system (right)

is necessary to continuously monitor the oxygen and nutrient concentrations, salinity and pH, to optimize the growth conditions. Among the investigated PFALs, soilless culture is adopted: four use the NFT system, four the DFT or substrate system, and in one case the aeroponic system is installed [22].

Groundwater, rainwater collected from the roof and domestic or industrial treated wastewater can be used for crop irrigation [23].

Lighting equipment is generally realized with light-emitting diode (LED), and in one case with only fluorescent lighting devices: lamps are anchored in the lower surface of the shelving levels (Fig. 1). LEDs do not emit the broad electromagnetic spectrum but only narrowband adjustable combinations to provide diversified quality, intensity and duration of light at different stages of plant growth. Compared to other lighting devices, LEDs have greater energy savings, greater physical robustness, smaller size and the greater lifespan, up to 100,000 h [24].

Automation in the PFALs optimize processes such as sowing, harvesting, packaging and transport, as well as the control of environmental parameters in order to enhance energy, water and nutrient consumption, reduce labor cost, and increase crop quality and yield. Monitoring sensors and equipment control/regulation systems are present in all the production plants. The automation of the following work processes is retrieved: packaging in six PFALs, harvesting and transplanting in four cases, sowing in three.

The yield of agricultural production is measured in weight in relation to the area used and the time. PFALs allow reaching the highest values of daily yield per unit area among the various forms of CEA [3]. The daily yield per unit area varies from 0.2 to 1.2 kg d⁻¹ m⁻², and the maximum daily production is 4800 kg d⁻¹.

Finally, in one case among the investigated ones, an abandoned building was recovered and reused to install a Plant factory.

4 Proposal for a PFAL in a Mediterranean Context

In many peri-urban Mediterranean sites, abandoned industrial and tertiary sector buildings can be reused for a sustainable agricultural production and shortened food supply chain, contributing to zero agricultural land consumption and to zero-mile production for local communities' food supply. Existing buildings to be



Fig. 2 Layout proposal for a PFAL

recovered as PFALs should generally have, for economic viability, a ground area approximately of 5000 m² to 20,000 m² properly designed for the different functional zones (Fig. 2), whereas a four times larger lot area is required for material product movements, storage, parking, marketing, energy systems. The recommended height of the building with shelving for vegetable cultivation varies between 10.0 and 15.0 m. Recovery design will be implemented considering high-performance building envelopes and high energy efficient equipment systems.

In order to increase sustainability reuse of local resources, such as water and CO₂, and the use of renewable energy must be planned. Irrigation demand can be satisfied by harvesting rainwater from building rooftop as well as building's greywater and urban wastewater after purification; CO₂ for carbon enrichment can be obtained from exhaust fumes of heating or energy generating plants; energy production obtained by integrated building photovoltaics, by industrial waste heat and by organic waste biomass from cultivations harvesting and packaging.

5 Conclusions

Agricultural production in controlled environments and especially in PFALs is of fundamental importance to meet the food needs of urban communities, trying to contain the ecological carbon footprint generated.

The PFALs are the most sophisticated agricultural systems enabling sustainable food production in dense urban areas, exploiting local waste resources like water, energy, CO₂ and biomass. The PFALs have particularly advanced research and development departments, especially where agricultural productivity is the most important.

This research, carried out retrieving the building, equipment and cultivation characteristics of 10 PFALs in different economic, climatic and social context, shows the present development of innovative PFAL buildings and provides useful highlights for the reuse of abandoned industrial and tertiary sector buildings in Mediterranean peri-urban sites for sustainable urban farming.

References

1. United Nations: Sustainable development goals. <https://www.un.org/>. Accessed 29 July 2022
2. Kozai, T., Niu, G.: Chapter 2 - Role of the plant factory with artificial lighting (PFAL) in urban areas. In: Kozai, T., Niu, G., Takagaki, M. (eds.) *Plant Factory (Second Edition)*, pp. 7–34. Academic Press (2020)
3. Benke, K., Tomkins, B.: Future food-production systems: vertical farming and controlled-environment agriculture. *Sustain. Sci. Pract. Policy* **13**(1), 13–26 (2017)
4. SANANBIO homepage. <https://www.sananbio.com/>. Accessed 29 July 2022
5. 808factory homepage. <https://www.808factory.jp/company/>. Accessed 29 July 2022
6. Nordic Harvest homepage. <https://www.nordicharvest.com/>. Accessed 29 July 2022
7. Kikuchi, Y., Kanematsu, Y., Yoshikawa, N., Okubo, T., Takagaki, M.: Environmental and resource use analysis of plant factories with energy technology options: a case study in Japan. *J. Clean. Prod.* **186**, 703–717 (2018)
8. Spread Co. homepage. <https://spread.co.jp/en/>. Accessed 29 July 2022
9. AeroFarms homepage. <https://www.aerofarms.com/>. Accessed 29 July 2022
10. Chen, X.-l., Li, Y.-l., Wang, L.-C., Guo, W.-Z.: Red and blue wavelengths affect the morphology, energy use efficiency and nutritional content of lettuce (*Lactuca sativa* L.). *Sci. Rep.* **11**(1), 8374 (2021)
11. Pennisi, G., Orsini, F., Landolfo, M., Pistillo, A., Crepaldi, A., Nicola, S., Fernández, J.A., Marcelis, L.F.M., Gianquinto, G.: Optimal photoperiod for indoor cultivation of leafy vegetables and herbs. *Eur. J. Hortic. Sci.* **85**(5), 329–338 (2020)
12. Larsen, D.H., Woltering, E.J., Nicole, C.C., Marcelis, L.F.: Response of basil growth and morphology to light intensity and spectrum in a vertical Farm. *Front. Plant Sci.* **11**, 597906 (2020)
13. Xu, W., Lu, N., Kikuchi, M., Takagaki, M.: Continuous lighting and high daily light integral enhance yield and quality of mass-produced nasturtium (*Tropaeolum majus* L.) in Plant Factories. *Plants (Basel)* **10**(6), 1203 (2021)
14. Demir, K., Sankamış, G., Çakırer Seyrek, G.: Effect of LED lights on the growth, nutritional quality and glucosinolate content of broccoli, cabbage and radish microgreens. *Food Chem.* **401**, 134088 (2023)
15. Palmitessa, O.D., Paciello, P., Santamaria, P.: Supplemental LED increases tomato yield in Mediterranean semi-closed greenhouse. *Agronomy* **10**, 1353 (2020)
16. Pan, T., et al.: Interaction of supplementary light and CO₂ enrichment improves growth, photosynthesis, yield, and quality of tomato in autumn through spring greenhouse production. *HortScience* **54**, 246–252 (2019)
17. Madsen, E.: The effect of CO₂-concentration on development and dry matter production in young tomato plants. *Acta Agric. Scand.* **23**, 235–240 (1973)
18. Liang, Y., Kang, C., Kaiser, E., Kuang, Y., Yang, Q., Li, T.: Red/blue light ratios induce morphology and physiology alterations differently in cucumber and tomato. *Sci. Hortic.* **281**, 109995 (2021)
19. Liu, Y., et al.: Blue light increases anthocyanin content and delays fruit ripening in purple pepper fruit. *Postharv. Biol. Technol.* **192**, 112024 (2022)

20. Choi, H.G., Moon, B.Y., Kang, N.J.: Effects of LED light on the production of strawberry during cultivation in a plastic greenhouse and in a growth chamber. *Sci. Hortic.* **189**, 22–31 (2015)
21. Tesi, R.: *Mezzi di protezione per l'ortoflorofrutticoltura e il vivaismo*. Edagricole (2010)
22. Alipio, M.I., Dela Cruz, A.E.M., Doria, J.D.A., Fruto, R.M.S.: On the design of Nutrient Film Technique hydroponics farm for smart agriculture. *Eng. Agric. Environ. Food* **12**(3), 315–324 (2019)
23. Cifuentes-Torres, L., Mendoza-Espinosa, L.G., Correa-Reyes, G., Daesslé, L.W.: Hydroponics with wastewater: a review of trends and opportunities. *Water Environ. J.* **35**(1), 166–180 (2021)
24. Xu, Y.: Chapter 2.1 - Nature and source of light for plant factory. In: Anpo, M., Fukuda, H., Wada, T. (eds.) *Plant Factory Using Artificial Light*, pp. 47–69. Elsevier (2019)

Multispectral UAV-Based Monitoring of Behavior of Different Wheat and Barley Varieties



Gaetano Messina , Giuseppe Badagliacca , Salvatore Praticò ,
Giovanni Preiti , Michele Monti , and Giuseppe Modica 

Abstract Multispectral (MS) remote sensing is a powerful tool for crops monitoring in precision agriculture framework. Due to the high accuracy level requested in this application, unmanned aerial vehicles (UAVs) are the most suitable choice for MS surveys. UAVs allow monitoring crops obtaining data in very high resolution and the possibility to have daily-based surveys. Cereals are the most widely cultivated species in the Mediterranean basin, supporting food chains for bread and pasta as well as livestock production. In these agroecosystems, the development of precision farming techniques is essential to make production more efficient and sustainable, also in order to secure supplies despite volatile food commodity prices characteristic of this post-Covid19 period. The main object of this study was monitoring the behavior of several different wheat and barley varieties, taking into account their spectral aspects and in situ measurements of grain yields. For this purpose, a field experiment, laid out as a randomized block design with three replications for wheat and four for barley, was conducted in San Marco Argentano (CS, Calabria - Italy). In particular, the spectral response of thirty wheat and nineteen barley varieties was compared during different stages of plant growth. UAV surveys were conducted by DJI Phantom 4 Multispectral equipped with a MS sensor, obtaining vigor maps. Several vegetation indices (VIs) were tested to monitor differences between varieties.

Keywords Remote Sensing (RS) · Precision Agriculture (PA) · Crops Monitoring · Cereals

G. Messina (✉) · G. Badagliacca · S. Praticò · G. Preiti · M. Monti
Dipartimento Di Agraria, Università Degli Studi 'Mediterranea' Di Reggio
Calabria, Reggio , Italy
e-mail: gaetano.messina@unirc.it

G. Modica
Dipartimento di Scienze Veterinarie, Università degli studi di Messina, Viale G. Palatucci s.n.,
I-98168 Messina , Italy

1 Introduction

In the framework of precision agriculture (PA), remote sensing (RS) techniques for aerial monitoring provide several solutions to collect data and map production. The tools and methods that are part of PA can play an important role in fulfilling European 2030 targets related to the sustainability of food production, like chemical contamination and nutrient losses limitation and pesticides and fertilizers reduction [1]. Among arable crops, durum wheat and barley represent in Mediterranean areas two strategic commodities for human and animal nutrition being the basis for the production of many typical specialties of the area, such as pasta, couscous and burghul, and for the production of animal feed. Therefore, as part of climate change adaptation strategies, it is necessary to increase their resources use efficiency.

Among aerial RS platforms, unmanned aerial vehicles (UAVs) equipped with multispectral (MS) sensors could offer several benefits over ground-based systems, such as greater efficiency and accuracy through increased spatial and temporal resolution providing images at very high resolution on a daily basis. Combining the different MS bands, the obtained vegetation indices (VIs) allow monitoring, analyzing and mapping temporal and spatial variations of vegetation [2, 3]. For example, a high value of the Normalized Difference Vegetation Index (NDVI) in wheat crop can be associated with a faster growth rate, a high bio-mass accumulation in the vegetative phase with a delay in leaf senescence and an increase in yield [4, 5]. This paper aims to explore the potential use of MS UAV RS to monitor differences between different wheat and barley varieties by testing several different VIs assessing their reliability to predict yield variations and discriminating among varieties.

2 Materials and Methods

2.1 Study Site

The field experiment was carried out in 2021/22 cropping season at the agricultural experimental centre “Caselle” of the Regional Agency for Agriculture “ARSAC” located in San Marco Argentano (CS), Calabria, Italy (39° 38' N, 16° 13' E, 100 m a.s.l.) (Fig. 1) on a sandy-clay-loam soil, classified as Fluventic Haploxerepts, coarse silty, mixed, thermic (Soil Survey Staff). Main soil properties, referred to the 0–20 cm top layer (Ap horizon), are as follows: 21% clay, 24% silt and 55% sand, pH 7.67 (1:2.5 KCl), EC 0.21 dS m⁻¹ (1:2), CEC 26.2 cmol₊ kg⁻¹, total inorganic C (CaCO₃) 18.0 g kg⁻¹, total organic C (Walkley–Black) 9.81 g kg⁻¹, total N (Kjeldahl) 0.95 g kg⁻¹, available P (Olsen) 16.95 mg kg⁻¹. The climate of the experimental site is Mediterranean characterized by mild and rainy winters and warm and dry summers (Warm Mediterranean Climate, Csa according with Koppen's classification). Mean annual rainfall is 706 mm (30-years average), mostly in the autumn and winter (68%) and in the spring (22%) while the mean yearly air temperature is 14.7 °C (30-years

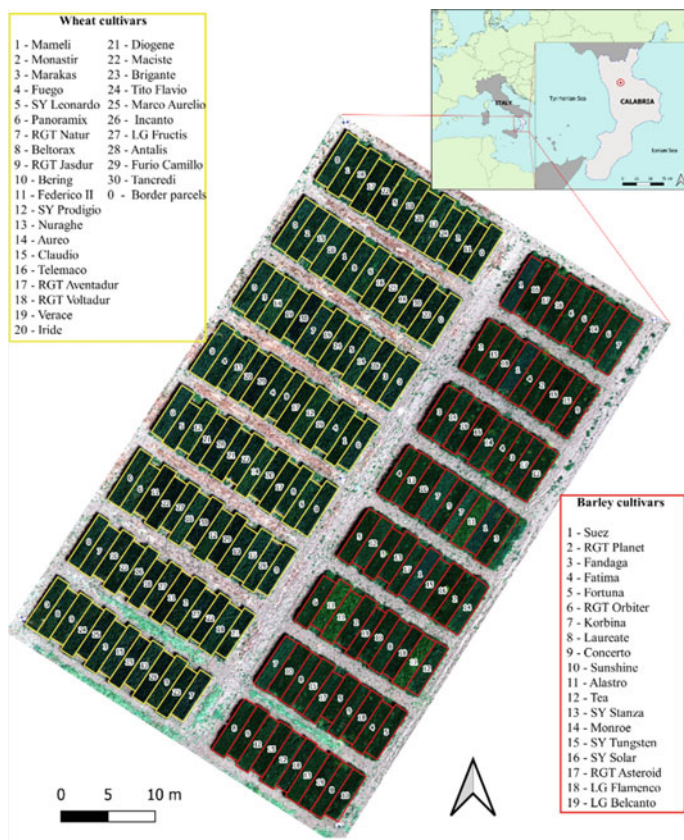


Fig. 1 Above, the location of the experimental site; below, the RGB orthomosaic of field plots. At the left were the wheat plots (variety listed in the yellow table) while at the right were the barley plots (variety listed in the red table)

average) with 17.0 °C in autumn, 8.8 °C in winter, 13.3 °C in spring and 24.6 °C in summer. The average minimum and maximum annual temperatures are 6.8 °C and 27.9 °C.

2.2 Experimental Design and Crop Management

The field trial was set up as a completely randomized block design (RCBD) with three replications for wheat and four replications for barley.

Thirty and nineteen different cultivars of durum wheat and barley respectively, were tested. The wheat cultivars were: Marneli, Monastir, Marakas, Fuego, SY Leonardo, Panoramix, RGT Natur, Beltorax, RGT Jasdur, Bering, Federico II, SY

Prodigio, Nuraghe, Aureo, Claudio, Telemaco, RGT Aventador, RGT Voltador, Verace, Iride, Diogene, Maciste, Brigante, Tito Flavio, Marco Aurelio, Incanto, LG Fructis, Antalis, Furio Camillo, Tancredi; the barley cultivars were: Suez, RGT Planet, Fandaga, Fatima, Fortuna, RGT Orbiter, Korbina, Laureate, Concerto, Sunshine, Alastro, Tea, SY Stanza, Monroe, SY Tungsten, SY Solar, RGT Asteroid, LG Flamenco, LG Belcanto.

In October 2021, the soil was prepared by mouldboard ploughing to a depth of 30 cm followed by one shallow harrowing operation in December 2021, at 15 cm soil depth. For each cultivar of both species, the plot area was of about 10 m⁻² (1.44 × 7.0 m). Durum wheat and barley were sown in rows spaced 18 cm apart at the density of 350 and 300 viable seeds m⁻², respectively for wheat and barley, by using a precision line plot seeder. Fertilization at sowing was provided by broadcasting 200 kg ha⁻¹ of diammonium phosphate (DAP, 18–46–0) at both species while fertilization in top dressing was performed at tillering stage with urea (46–0–0) at 130 kg ha⁻¹ for wheat and 100 kg ha⁻¹ for barley. During the cropping cycle heading time, plant height and the number of spikes per square meter were recorded. Harvest was carried out at full maturity state in early July 2022, by means of a plot combine.

2.3 UAV surveys and image data acquisition

The MS surveys were carried out between the beginning of April and the middle of June. During this period, the UAV flights were carried out three times: 5 April 2022, 3 May 2022 and 14 June 2022. UAV flights were carried out in correspondence of the following wheat and barley stages: late tillering, 25 BBCH-scale phase (5 April 2022); heading, 55 BBCH-scale phase (3 May 2022); early senescence, 91 BBCH-scale phase (14 June 2022).

Surveys were carried out using the multirotor UAV DJI Phantom 4 Multispectral (P4M) (DJI Ltd., Shenzhen, China) (Fig. 2). The P4M is equipped with six 1/2.9-inch CMOS sensors, one RGB sensor for visible imagery and five monochrome sensors for multispectral imagery. The six sensors, all with a global 2 MP shutter, shoot simultaneously, generating six images of 1600 × 1300 pixels. The investigated bands are Blue (450 nm ± 16 nm), Green (560 nm ± 16 nm), Red (650 nm ± 16 nm), Red Edge (730 nm ± 16 nm), Near infrared (NIR) (840 nm ± 26 nm). All flights were conducted at a speed of 2 ms⁻¹, under constant scene illumination and cloud-free conditions and at an altitude of 20 m a.g.l. In the field were placed ground control points (GCPs) to obtain a high-quality geolocated output. GCPs were made using 50 cm × 50 cm black and white polypropylene panels (Fig. 2). GCPs' position coordinate (WGS 84/ETRF 1989 UTM 33N) was georeferenced using a Leica GS12 RTK GNSS (Fig. 2) with planimetric and altimetric accuracy of ± 2.5 cm and ± 5 cm, respectively.



Fig. 2 Ground control point (GCP) and Leica GS12 RTK GNSS (left). The UAV DJI Phantom 4 Pro RTK (DJI Ltd., Shenzhen, China) (right)

2.4 Image processing

Images were aligned, stacked, and radiometrically corrected using Pix4D mapper Pro (version 4.3 – Pix4D SA, Switzerland). Reflectance values, measured on a grey calibration panel placed in the field, were extracted in correspondence of each central band and used to calibrate images. Finally, reflectance orthomosaics, with a ground sample distance of 1 cm, were generated for each band and stacked into a single multiband orthomosaic for each of the five MS bands. For the purpose of evaluating the correlation of the different indices tested with production data and calculating the average values of each index in each wheat and barley variety, only the part of the image occupied by the plots was considered, excluding the surrounding bare soil. In order to eliminate soil surrounding the experimental plots, one mask of each plot was delimited by creating a mask on QGIS 3.22 per MS band at each date of acquisition as shown in Fig. 1. To monitor the growth and the vegetation vigor of the crop, several VIs were tested combining different bands of reflectance maps: Chlorophyll Vegetation Index (CVI), Green Normalized Difference Red Edge Index (GNDRE), Green Normalized Difference Vegetation Index (GNDVI), Modified Chlorophyll Absorption Ratio Index (MCARI2), Modified Triangular Vegetation Index (MTVI), Modified Triangular Vegetation Index 2 (MTVI2), Normalized Difference Red Edge (NDRE), Normalized Difference Vegetation Index (NDVI), Optimized Soil Adjusted Vegetation Index (OSAVI), Renormalized Difference Vegetation Index (RDVI), Red Edge Triangulated Vegetation Index (RTVI), Simple Ratio (SR) and Simple Ratio Red Edge (SR RED EDGE) [6, 7]. For each index, the average value for each plot was obtained using QGIS.

3 Results and Discussion

NDRE vigor maps of the entire field are shown in Fig. 3 for the two surveyed dates 5 April and 3 May 2022. Considering the image of April, in the late tillering phase,

NDRE's value ranged from -0.2 to 0.55. In May, in the heading phase, NDRE's value ranged from -0.10 to 0.59 with the negative values and those of 0 referring to the portion of the field occupied by bare soil (that was subsequently excluded). At the late tillering and heading phases in wheat an average NDRE value of 0.31 and 0.38 were respectively observed. In a study of Adeel et al. (2019) a significant relationship between VIs and crop can be observed at the late tillering phase [8]. On the other hand, previous studies showed that the heading phase is the optimal one for RS of several agronomic traits, including grain yield [9]. In our study slightly higher values of NDRE were found in barley with 0.35 in the April survey and 0.40 in May. The choice of the NDRE for the preparation of the vigor map is motivated by the significant correlation between NDRE and crop yield data observed in wheat with r equal to 0.52*** and 0.55*** in April and 0.62*** and 0.63*** in May respectively. The same values were obtained from correlations with the SR Red Edge index with which the NDRE shares the same bands (NIR and Red Edge) in its formula. Slightly lower r values in May were found in the correlation with the GNDVI (0.60*** and 0.59***) and NDVI indices (0.56*** and 0.55**). Our results partly agree with Walsh et al. [10] that observed similar trend in NDVI, CVI and SR Red Edge for plant vigor estimation and with Marino and Alvino [11] and Adeel et al. [8] in NDVI for yield prediction. With regard to barley, however, no significant correlation was observed for the indices tested with grain yield. This evidence agrees with Herzig et al. [12] and Kefauver et al. [13] that observed a low yield prediction for single VI in barley suggesting a more efficient modelistic approach for this crop. As compared to durum wheat, barley showed positive correlations between MCARI2, MTVI with plant height ($r = 0.67***$ and $r = 0.73***$ respectively).

With regard to the survey period/time, emerged that April VIs images at late tillering, allowed a better discrimination among varieties compared with other periods. Among the tested indices, CVI (April and May), GNDRE (April), NDRE (April and May), NDVI (April and May), RDVI (April), and SR (April) showed a different response among durum wheat varieties (Fig. 4). Specifically, higher difference on VIs response among wheat cultivars was observed by using GNDRE, NDVI and RDVI (Fig. 4). Similar results with regard to NDVI were observed by Marino and Alvino [11] and GNDRE and RDVI by Yang et al. [14]. Also in this case, the study of the spectral and VIs response of barley plots did not reveal any significant results regarding discrimination between the different varieties. These results agree with Kefauver et al. [13] and Di Gennaro et al. [15] did not observed significant differences among barley cultivars testing several VIs. However, it is difficult to determine a single VI suitable for predicting the same biophysical parameters of crops at different growth stages, and it is therefore advisable to use several VIs to better monitor crop characteristics, given the variety of VIs at different growth stages [16].

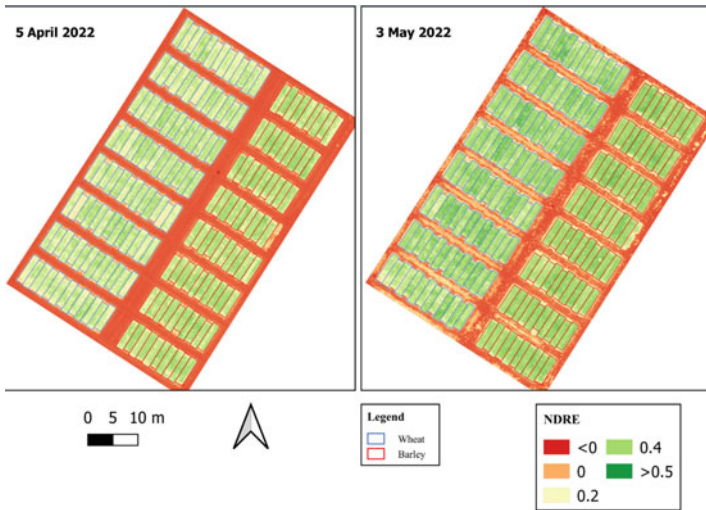


Fig. 3 Vegetative vigor maps of the field derived from UAV images in two dates surveyed 5 April 2022 (on the right) and 3 May 2022 (on the left) based on the Normalized Difference Red Edge index (NDRE). The wheat plots are highlighted in light blue while the barley plots are highlighted in red

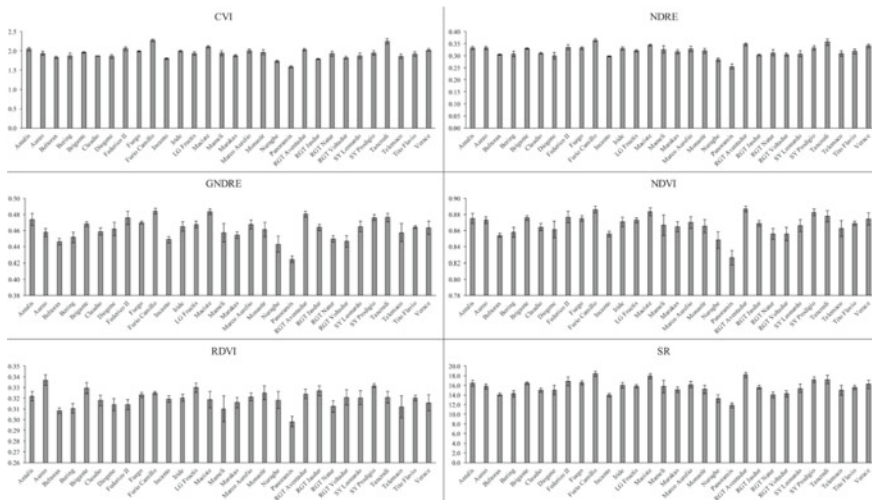


Fig. 4 Specific durum wheat varieties VIs responses at CVI, NDRE, GNDRE, NDVI, RDVI and SR derived from UAV image of 5 April 2022

4 Conclusions

The UAV detection of VIs is a powerful tool for crop monitoring and precision agriculture implementation in order to improve cereal sustainability and predict yields. The results of the present researched showed a good yield prediction, over thirty different durum wheat varieties with different adaptation to the environment and productivity, provided by NDRE and SR Red Edge indices. Conversely, a better discrimination among cultivar were retrieved by GNDRE, NDVI and RDVI when early survey was carried out. With regard to the barley, further studies are needed in order to identify better survey epoch and VIs or VIs model indicators in order to assess varieties adaptability, differences and predict yields.

References

1. European Union Farm to Fork Strategy: For a fair, healthy and environmentally-friendly food system Available online: https://food.ec.europa.eu/horizontal-topics/farm-fork-strategy_en (Accessed Sep 9, 2022).
2. Messina, G., Praticò, S., Badagliacca, G., Di Fazio, S., Monti, M., Modica, G.: Monitoring onion crop “cipolla rossa di tropea calabria igr” growth and yield response to varying nitrogen fertilizer application rates using uav imagery. *Drones*, 5 (2021). <https://doi.org/10.3390/drones5030061>
3. Modica, G., Messina, G., De Luca, G., Fiozzo, V., Praticò, S.: Monitoring the vegetation vigor in heterogeneous citrus and olive orchards. A multiscale object-based approach to extract trees’ crowns from UAV multispectral imagery. *Comput. Electron. Agric.* (2020). <https://doi.org/10.1016/j.compag.2020.105500>
4. Cabrera-Bosquet, L., Molero, G., Stellacci, A., Bort, J., Nogués, S., Araus, J.: NDVI as a potential tool for predicting biomass, plant nitrogen content and growth in wheat genotypes subjected to different water and nitrogen conditions. *Cereal Res. Commun.* **39**, 147–159 (2011)
5. Babar, M.A., Reynolds, M.P., van Ginkel, M., Klatt, A.R., Raun, W.R., Stone, M.L.: Spectral Reflectance Indices as a Potential Indirect Selection Criteria for Wheat Yield under Irrigation. *Crop Sci.* **46**, 578–588 (2006)
6. Xue, J., Su, B.: Significant remote sensing vegetation indices: a review of developments and applications. *J. sensors* **2017**, 17p (2017)
7. Cao, X., Liu, Y., Yu, R., Han, D., Su, B.: A Comparison of UAV RGB and Multispectral Imaging in Phenotyping for Stay Green of Wheat Population. *Remote Sens.* **13**, 1–21 (2021)
8. Adeel, M., Yang, M., Rasheed, A., Yang, G.: A rapid monitoring of NDVI across the wheat growth cycle for grain yield prediction using a multi-spectral UAV platform. *Plant Sci.* **282**, 95–103 (2019)
9. Pavuluri, K., Chim, B.K., Griffey, C.A., Reiter, M.S., Balota, M., Thomason, W.E.: Canopy spectral reflectance can predict grain nitrogen use efficiency in soft red winter wheat. *Precis. Agric.* **16**, 405–424 (2015)
10. Walsh, O.S.; Shafian, S.; Marshall, J.M.; Jackson, C.; Mcclintick-chess, J.R.; Blanscet, S.M.; Swoboda, K.; Thompson, C.; Belmont, K.M.; Walsh, W.L. Assessment of UAV Based Vegetation Indices for Nitrogen Concentration Estimation in Spring Wheat. 71–90 (2018)
11. Alvino, A.; Marino, S. Remote sensing for irrigation of horticultural crops. *Horticulturae*, 3 (2017).

12. Herzig, P., Borrmann, P., Knauer, U., Klück, H.-C., Kiliyas, D., Seiffert, U., Pillen, K., Maurer, A.: Evaluation of RGB and Multispectral Unmanned Aerial Vehicle (UAV) Imagery for High-Throughput Phenotyping and Yield Prediction in Barley Breeding. *Remote Sens.* **13**, 2670 (2021)
13. Kefauver, S.C.; Vicente, R.; Vergara-Díaz, O.; Fernandez-Gallego, J.A.; Kerfal, S.; Lopez, A.; Melichar, J.P.E.; Serret Molins, M.D.; Araus, J.L. Comparative UAV and Field Phenotyping to Assess Yield and Nitrogen Use Efficiency in Hybrid and Conventional Barley. *Front. Plant Sci.* **8** (2017).
14. Yang, M.; et al.: Assessment of Water and Nitrogen Use Efficiencies Through UAV-Based Multispectral Phenotyping in Winter Wheat. *Front. Plant Sci.* **11** (2020).
15. Di Gennaro, S.F., Rizza, F., Badeck, F.W., Berton, A., Delbono, S., Gioli, B., Toscano, P., Zaldei, A., Matese, A.: UAV-based high-throughput phenotyping to discriminate barley vigour with visible and near-infrared vegetation indices. *Int. J. Remote Sens.* **39**, 5330–5344 (2018)
16. Hatfield, J.L., Prueger, J.H.: Value of Using Different Vegetative Indices to Quantify Agricultural Crop Characteristics at Different Growth Stages under Varying Management Practices. *Remote Sens.* **2**, 562–578 (2010)

Physical and Mechanical Characterization of a Low-Quality Sheep Wool Fiber



Monica C. M. Parlato, Giusi Midolo, Simona M. C. Porto,
and Francesca Valenti

Abstract Worldwide, building sector is the leading cause of environmental degradation, global warming, and climate change with the 50% of carbon emissions, 20–50% of consumption of energy and natural resources, and 50% of total solid wastes production. Several studies were carried out by investigating eco-friendly materials that could be involved and integrated into building process with the aim of replacing conventional building materials, e.g., concrete, steel, plastic components. Totally in accordance with the circular economy statements, sustainable materials could be obtained by the reconversion of wastes, e.g., solid wastes coming from urbanized area and agricultural wastes. This research stems from the need to exploit wastes coming from livestock processes, i.e., sheep wool fibers (SWF), and their potential reuse as reinforcement for rammed earth building components. To this aim, experimental trials were performed to get useful information on the mechanical properties of SWF in wet environments like those present in lime mixes. Then, compressive, and flexural tests have been performed on raw earth adobes by incorporating SWF. The obtained results encourage the use of sheep wool fiber as reinforcement for raw earth composite materials.

Keywords green building · natural fibers · sheep wool fiber · raw earth material

M. C. M. Parlato · G. Midolo · S. M. C. Porto (✉) · F. Valenti
Department of Agriculture, Food and Environment (Di3A), University of Catania, Via Santa Sofia, 100 – 95123 Catania, Italy
e-mail: simona.porto@unict.it

M. C. M. Parlato
e-mail: monica.parlato@unict.it

F. Valenti
e-mail: francesca.valenti@unict.it

© The Author(s), under exclusive license to Springer Nature Switzerland AG 2023
V. Ferro et al. (eds.), *AIIA 2022: Biosystems Engineering Towards the Green Deal*,
Lecture Notes in Civil Engineering 337,
https://doi.org/10.1007/978-3-031-30329-6_122

1183

1 Introduction

Several studies are focused on the use of natural fibers as substitutes of synthetic ones like reinforcement fibers into soil matrix composites [1–4]. Addition of fibers, natural or synthetic one, is suitable to avoid drying shrinkage, and improve the mechanical strengths and ductility of the composite material [5, 6].

Natural fibers are of vegetable or animal origin, characterized by lignocellulose or protein structure, respectively.

The replacement of synthetic fibers for natural ones increases environmental sustainability of building sector. Natural fibers have good availability, low cost, renewability, biodegradability; furthermore, they have generally lower density compared to synthetic ones, (i.e., natural fiber density ranges between 1.2–1.6 [g/cm³] glass fiber density is 2.4 [g/cm³]) [7].

Animal fibers could be silk fibers from silkworms, collagen fibers extracted from animal skins, pig hair, wool fibers deriving from sheep shorn, etc.

Several researches focused on the use of sheep wool fibers for building purpose, e.g., thermal, and acoustic insulation and as additive for composite materials [8–10].

Generally, raw wool deriving from shorn sheep is not suitable for textile use, and it is a special waste contaminated with impurities, with high disposal costs for breeders.

For this reason, often sheep wool is illegally disposed of, e.g., burned or buried, with a severe environmental impact.

In Europe are widespread dairy-sheep race breeds to produce meat or milk. These sheep genotypes produce a low-quality wool, unsuitable for textile industry, with diameter ranged between 20–70 μm [11].

However, wool could be considered an environmentally friendly material because its reuse could reduce both environmental pollution and energy consumption.

In this work, mechanical and physical behaviors of a low-quality sheep wool, coming from dairy sheep of *Valle del Belice* race, have been assessed. The aim was to evaluate the possible use of this livestock waste as strengthening system for earthen materials, by simulating the real wet condition of the fiber inside the matrix.

2 Materials and method

2.1 Sheep Wool Fiber

Sheep wool is an animal natural fiber with a semi-crystalline chemical structure. Sheep wool is an α -keratin fiber, with a very complex multilayer structure, composed of 60% animal protein fibers, 15% moisture, 10% fat, 10% sheep sweat and 5% impurities. The natural fiber considered in this research comes from raw wool of “*Valle del Belice*” dairy sheep, race highly widespread in Sicily. This wool is totally useless for textile industry because of the thickness and medium length of fibers.

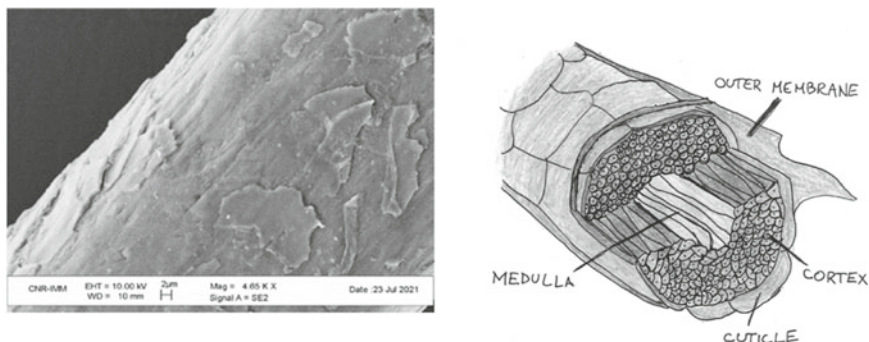


Fig. 1 **a** SEM image of the longitudinal of Valle del Belice wool fiber, **b** transversal section scheme of wool fiber

Figure 1a presents a Scanning Electron Microscope (SEM) image of the wool fiber, and Fig. 1b shows a transversal section scheme of wool fiber.

2.2 Experimental Trial

2.2.1 Physical and Mechanical Properties

To evaluate physical and mechanical behaviors of sheep wool fibers deriving from “Valle del Belice” race, 180 fibers were randomly selected among the raw material, by choosing fibers having around the same initial length (i.e., ranged from 160 to 220 mm). Before performing experimental and measurement trials, fibers were washed by using cold water and only natural soap, i.e., Marseille soap. Then, fibers were dried for 1 week in environment condition (i.e., $T = 20^{\circ}\text{C}$ – RHU = 50%), and trimmed to 150 mm. Firstly, physical behaviors such as diameter, mass, and density, were evaluated. The diameter was measured by using a Zeiss Microscope, (software LAS Core, LEICA application suite Version 3.70) (Fig. 2).

The mass was evaluated by a precision balance Sartorius - model CP124S (Fig. 3). Furthermore, to obtain the apparent density of each sample the mass was divided by the volume.

By following the prescription of ASTM D 2256 – 10 standard the mechanical tests were carried out on each single wool fiber. The tensile tests were performed by using an apparatus designed properly for the purpose, with a gage length of 50 mm. To avoid the gravity effects the fiber assembly was horizontally placed in the apparatus. One edge of the fiber was fixed to the testing machine, and, on the other side of the apparatus, the other edge was kept free to slide.

The mounting of single fiber in the tensile testing machine has been done with great carefully and slowly, to avoid any fiber damages, misalignment of the load, and to prevent premature failure and errors in measurement.

Fig. 2 Diameter measurement of a single fiber

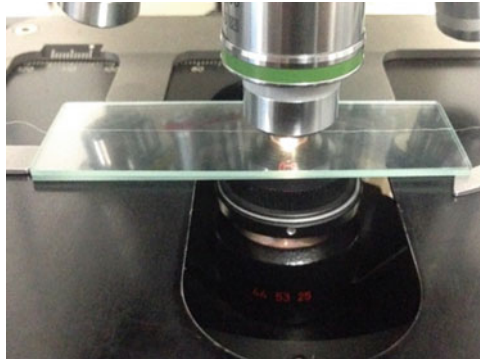


Fig. 3 Mass measurement of a single fiber



Mechanical Test conditions:

1st condition: wet condition. Fibers were immersed for ten minutes in distilled water. Ten minute was found to be a sufficient time for wool to reach saturation.

2nd condition: controlled environment. SWF were immersed in distilled water for ten minutes, then were left to dry for 24 h in a controlled environment with set temperature and humidity (i.e., 20° C and HR 50%).

3rd condition: oven-dried condition. Fibers were put in oven at 80° C for thirty minutes. After this time the fibers reached constant mass.

Due the high hygroscopicity of wool, the authors decided to perform tensile tests under the three above-reported mechanical test conditions to evaluate differences on mechanical behaviors of the fiber, depending on the quantity of water.

During the tests, load stress and elongation were directly measured. While, after performing the tests, secant stiffness modulus, stress and strain at the yield (estimated as intersection between linearized trends in the initial phase and in the plateau region), elongation at break, and stress at break have been evaluated.

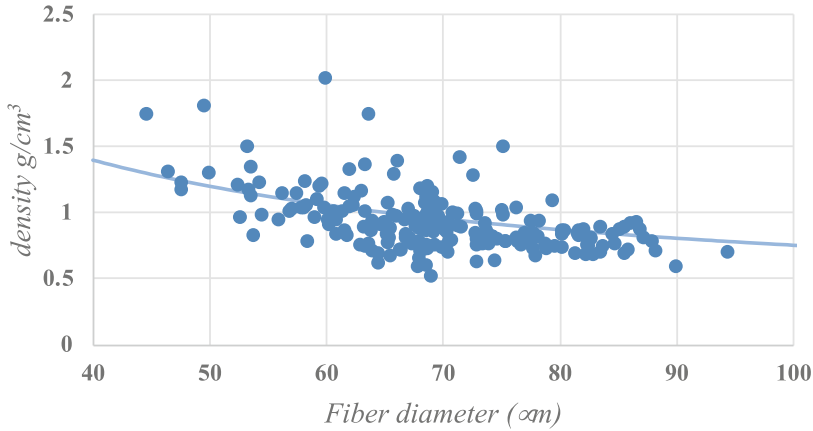


Fig. 4 Correlation between fibers density and fibers diameter

3 Results

3.1 Diameter and Density Measurements

A clear dependency among density and diameter has been detected from the obtained test results. In detail, the smaller the density the larger is the diameter. In Fig. 4 is shown this typical behaviour with a core and fibril internal structure of the fiber.

Moreover, the observed average density is significantly lower than synthetic fibers' density (e.g., glass fiber), 0.94 [gr/cm³] and 2.5 [gr/cm³], respectively.

3.2 Mechanical Properties

Table 1 reports the obtained mechanical values, that are, stress at break, elongation at break, stress and strain at the yield, secant stiffness modulus. Obtained results are dispersed and this is typical of natural materials, i.e., natural fibers with a dependence with the fibers' diameter. Measured breakage tensile stress ranged between 261.50 – 74.01 [MPa].

Table 1 Mechanical test results. Average values and standard deviation.

	σ at break [MPa]		Elongation at break [%]		σ at yield [MPa]		ϵ at yield		E_s [MPa]	
	μ	σ	μ	σ	μ	σ	μ	σ	μ	σ
1	134.57	34.10	42.00	0.11	75.37	21.92	0.04	0.02	2057.06	584.53

(continued)

(continued)

	σ at break [MPa]		Elongation at break [%]		σ at yield [MPa]		ϵ at yield		E_s [MPa]	
	μ	σ	μ	σ	μ	σ	μ	σ	μ	σ
2	144.02	41.61	43.00	0.11	84.70	23.31	0.05	0.02	1903.59	621.32
3	133.65	47.22	43.00	0.19	85.97	33.59	0.07	0.03	1367.38	381.40
4	137.31	41.37	42.00	0.14	81.44	27.15	0.05	0.02	1739.41	755.44

*1: saturated specimens; 2 normal conditioning; 3 dry specimens; 4 entire population.

By starting from the values reported in Table 3, the average trilateral stress–strain curves, for all the performed testing conditions, has been developed (Fig. 5). This schematic representation has been plotted by joining the value of σ and ϵ detected at yield, plateau, and failure phases.

By observing the curves reported Fig. 5, it is possible to affirm that the thermal and hygrometric conditions do not significantly affect the results.

The tensile strength average value was 137.31 MPa, comparable with those reported in literature for similar fibers ranging between 120–174 MPa [12], but lower than the tensile strength of *Merino* wool, an high quality wool used in textile sector [13].

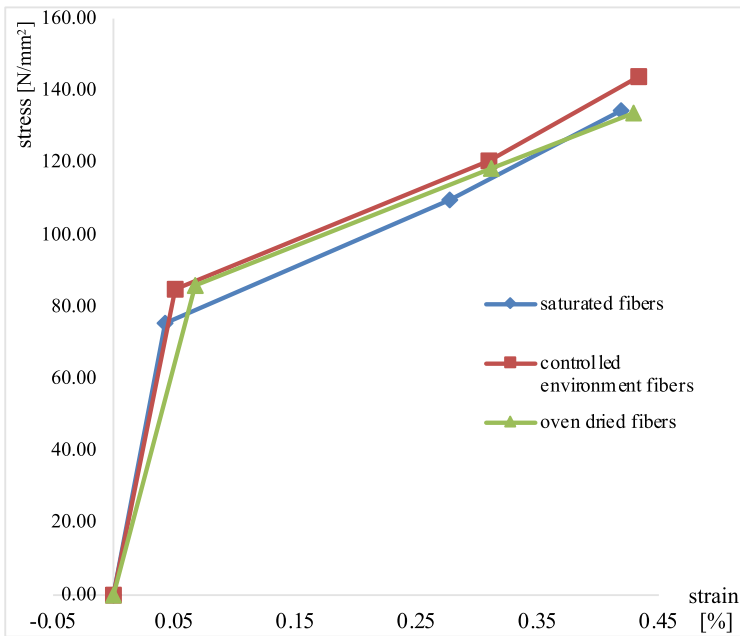


Fig. 5 - Schematic representation of the stress–strain curve ([N/mm²], [%]) under 3 different test conditions

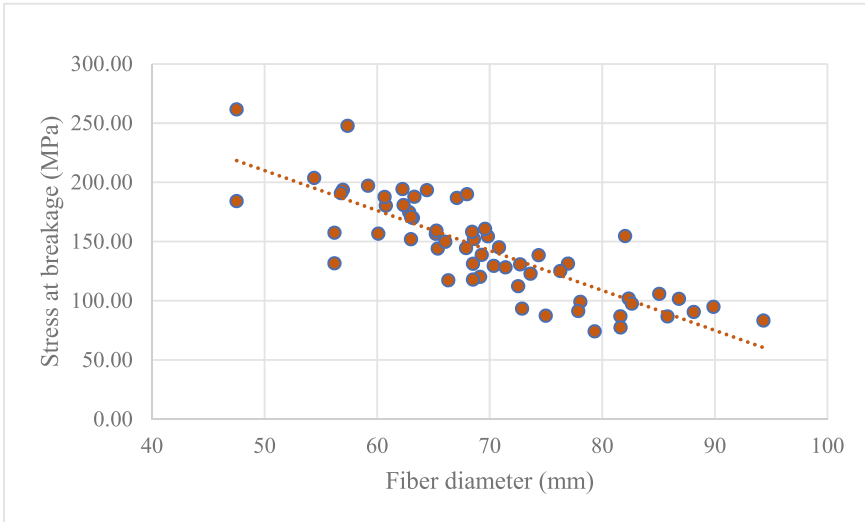


Fig. 6 - Correlation between breakage tensile stress and diameter

In this work a possible correlation between breakage tensile stress and diameter has been also evaluated. In detail, Fig. 6 shows the tensile strength fiber *vs.* diameter fiber. A clear tendency of the breakage stress to decrease with the increase of the diameter has been observed.

The elongation at break computed for *Valle del Belice* wool ranged between 45 and 50%, higher than other natural fibers, e.g., juta, kenaf, etc.

All obtained results appears to encourage the use of this kind of fiber as strengthen system for earthen materials.

4 Discussion

The values of the strength, elongation at break, and initial stiffness are close to those reported in the literature for SWF. Compared to the properties of vegetable fibers, most used for reinforcement, the strength is lower, but the elongation at break resulted higher. Similarly, wool fibers are less stiff than most vegetable fibers. Obtained results demonstrates that the use of SWF as reinforcement fiber within raw earth-based composites could improve their ductility and fracture energy. Indeed, further tests are required to confirm that the addition of wool fibers to raw earth mixes could increase the ductility of the composite. The mechanical results appear quite dispersed, this is a typical result for natural fibers mainly due to the correlation between diameter and mechanical and physical behaviors, i.e., fiber strength and fiber density, respectively. To deep investigate this aspect in the future, tailored analyses, by considering a micromechanical point of view, are required.

5 Conclusions

The aim of this study was the physical and mechanical characterization of *Valle del Belice* wool fibers to evaluate its possible use as strengthening system for earthen building components.

The mechanical results, i.e., average tensile strength of 137.31 MPa, and initial secant modulus of 1.74 GPa, confirm the suitability of these fibers as a reinforcement for composite earth building materials.

Moreover, despite results are quite dispersed, some trends clearly emerged. A correlation between physical and mechanical properties and fibers' diameter was investigated.

The results achieved by performing this experimental trial encourage the possible use of raw wool for building purpose. The conversion of this waste in a real resource for building sector could decrease environmental pollution, by contemporary reducing economic cost for breeders.

References

1. Kandemir, A., Pozegic, T.R., Hamerton, I., Eichhorn, S.J., Longana, M.L.: Characterisation of natural fibres for sustainable discontinuous fibre composite materials. *Materials (Basel)*. **2020**, 13 <https://doi.org/10.3390/ma13092129>.
2. Sharma, V., Marwaha, B.M., Vinayak, H.K.: Enhancing durability of adobe by natural reinforcement for propagating sustainable mud housing. *Int J Sustain Built Environ* **5**, 141–155 (2016). <https://doi.org/10.1016/j.ijbsbe.2016.03.004>
3. Hejazi, S.M., Sheikhzadeh, M., Abtahi, S.M., Zadhoush, A.: A simple review of soil reinforcement by using natural and synthetic fibers. *Constr Build Mater* (2012)
4. Imanzadeh, S., Jarno, A., Hibouche, A., Bouarar, A., Taibi, S.: Ductility analysis of vegetal-fiber reinforced raw earth concrete by mixture design. *Constr Build Mater* **239**, 117829 (2020). <https://doi.org/10.1016/j.conbuildmat.2019.117829>
5. Araya-Letelier, G., Concha-Riedel, J., Antico, F.C., Valdés, C., Cáceres, G.: Influence of natural fiber dosage and length on adobe mixes damage-mechanical behavior. *Constr. Build Mater* (2018). <https://doi.org/10.1016/j.conbuildmat.2018.04.151>
6. Sangma, S., Tripura, D.D.: Experimental study on shrinkage behaviour of earth walling materials with fibers and stabilizer for cob building. *Constr. Build Mater*, 256 (2020). <https://doi.org/10.1016/j.conbuildmat.2020.119449>.
7. Mulenga, T.K., Ude, A.U., Vivekanandhan, C.: Techniques for modelling and optimizing the mechanical properties of natural fiber composites: A review. *Fibers* **9**, 1–17 (2021). <https://doi.org/10.3390/fib9010006>
8. Alyousef, R., et al.: Effect of Sheep Wool Fiber on Fresh and Hardened Properties of Fiber. *Int J Civ Eng Technol* **10**, 190–199 (2019)
9. Fantilli, A.P., Sicardi, S., Dotti, F.: The use of wool as fiber-reinforcement in cement-based mortar. *Constr Build Mater* **139**, 562–569 (2017). <https://doi.org/10.1016/j.conbuildmat.2016.10.096>
10. Klarić, S., Klarić, E., Zametica, M., Gazdić, M.: Building Thermal Insulation Material Based on Sheep Wool. In *Lecture Notes in Networks and Systems*; Springer, 2020; Vol. 76, pp. 698–711. https://doi.org/10.1007/978-3-030-18072-0_82

11. Ganci, M.; Biondi, L.; Parlato, M.C.M.; Porto, S.M.C. Methodology for the Localization of Wool Collecting Centers: The Case Study of Sicily. *Sustainability*, 14 (2022) <https://doi.org/10.3390/su141610378>.
12. Cheung, Y.-H., Ho, M.-P., Lau, T.K., Cardona, F., Hui, D. Natural fibre-reinforced composites for bioengineering and environmental engineering applications. *Compos Part B Eng*, 40, 655–663 (2009) <https://doi.org/10.1016/j.compositesb.2009.04.014>
13. HEARLE, J.W.S.4 - Physical properties of wool. In *Wool*; Simpson, W.S., Crawshaw, G.H., Eds.; Woodhead Publishing Series in Textiles; Woodhead Publishing, ISBN 978–1–85573–574–3, pp. 80–129 (2002).

Historic Agricultural Landscape Characterization: First Attempt of Historic Landscape Characterization (HLC) to Costa Viola Terraced Landscape (Calabria, Italy)



Salvatore Praticò , Francesco Solano , Salvatore Di Fazio ,
and Giuseppe Modica 

Abstract By its own definition, the landscape is a constantly changing entity because of the continuous interactions between nature and human factors. These interactions are synthetically represented by land use land cover (LU/LC) changes. The main object of this study is to analyze changes that occurred for almost 60 years, from 1955 to 2014. The study object is the historic agricultural terraced landscape of the Costa Viola (Southern Italy). This landscape is important because of its status as a protected landscape, listed by UNESCO. The resulting landscape configuration was analyzed, highlighting how yesterday's landscape influenced the current landscape. Several different years have been analyzed and LU/LC maps have been digitalized for each investigated year. In order to highlight the steps that led to the development of today's landscape, the obtained polygons have been overlapped, obtaining a vector with all occurred changes. The proposed approach wants to identify the time when this LU/LC appears for the first period, the so-called first occurrence, highlighting how the past influences landscape composition. This is the common approach of the historic landscape characterisation (HLC) and historic land-use assessment (HLA), two very similar methods whose aim is to study today's landscape and how it has originated.

Keywords Change detection · Historic Land-Use Assessment (HLA) · Agricultural Terraces · Multi-Temporal Remote Sensing · GIS · Overlay mapping

S. Praticò (✉) · S. Di Fazio
Dipartimento di Agraria, Università Degli Studi 'Mediterranea' di Reggio Calabria, Loc. Feo di Vito S.N.C., 89122 Reggio Calabria, Italy
e-mail: salvatore.pratico@unirc.it

F. Solano
Department of Agriculture and Forest Sciences (DAFNE), University of Tuscia, Via S. Camillo de Lellis, 01100 Viterbo, Italy

G. Modica
Dipartimento di Scienze Veterinarie, Università Degli Studi di Messina, Viale G. Palatucci s.n., 98168 Messina, Italy

1 Introduction

By its own definition, the landscape is a constantly changing entity because of the continuous interactions between nature and human factors [1]. Rural landscapes are among the most important and representative of European landscapes. These kind of landscapes are characterized by the simultaneous existence of functional aspects, mainly related to land use/land cover (LU/LC), and cultural aspects, related to the modification and adaptation of the landscape by humans to meet their needs [2]. In this framework, the study of LU/LC changes occurred during the years, assumes a predominant role [3]. Recently, there has been a growing interest, both for stakeholders and decision makers, in understanding the processes by which modern landscapes were created, studying how landscape was step-by-step altered by LU/LC changes and natural resources utilization [4–6]. Historic Landscape Characterization (HLC) and Historic Land-Use Assessment (HLA) are two similar tools for understanding the historical development of landscapes through the study of the changes occurred in their components [7–9]. At the basis of HLC and HLA methods there is the key concept that all aspects of the landscape that we can recognize at the present are shaped through historic processes occurred in the past [10].

The main aim of this still ongoing research is to test the applicability of HLC/HLA methods to historical terraced agricultural landscapes analyzing changes that occurred for almost 60 years, from 1955 to 2014. The Costa Viola agricultural terraced landscape, in the province of Reggio Calabria (Southern Italy) was chosen as study area.

2 Materials and Methods

2.1 Study Area

The Costa Viola area (Fig. 1) is an agricultural terraced area listed in the Italian national register of historic landscapes [11]. It is a narrow coastal strip located in Tyrrhenian side of Calabria Region, facing the Strait of Messina and falling into five municipalities' administrative border. The total surface of the considered area is about 24.1 km² and covers a length of 20 km running from the sea to 1–2 km inland. The area is characterized by very steep slope, so to allow agriculture activities, after the earthquakes occurred in the area between 1783 and 1784, a dry-stone made terraced system was built [12]. The main crops cultivated in the area are vineyards and olive and citrus growths. The originated agricultural terraced landscape is now subject to an abandonment trend [13], in line with the general abandonment of the agricultural activities in mountain zones [14, 15] and reflecting in an ever-increasing

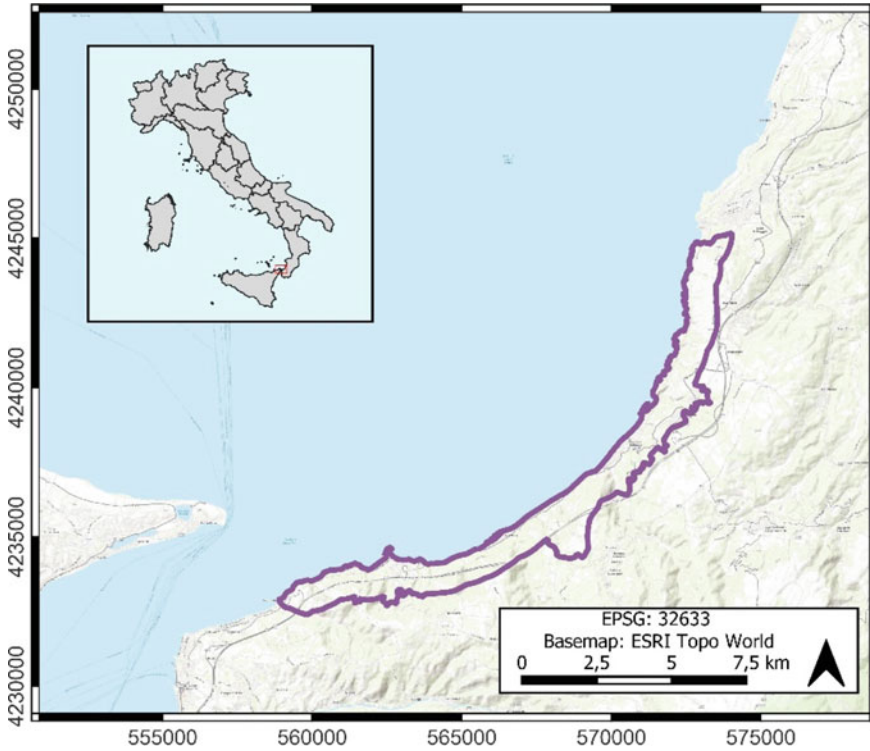


Fig. 1 Costa Viola study area (purple boundary) location

fragmentation of landscape components [16, 17]. Although the decrease of the agricultural importance of the Costa Viola terraced landscape, its cultural significance is gradually increasing. It is now widely recognized the need to reconcile the original agricultural function (which needs a new economic interest) with its recognized cultural value in order to find a new way to manage this landscape.

2.2 Methodology

Through a manual digitalization and a photointerpretation process, a LU/LC vector layer was constructed for each investigated years (i.e., 1955, 1976, 1998 and 2014). Digitalization was performed in GIS environment using different basemaps (Table 1). More details about this process are reported in our already published papers [13, 18].

Table 1 Basemaps used for each investigated year

Frame Data	Source	Year
B/W aerial photos	Italian Military Geographic Institute (IGMI)	1955
		1976
RGB WMS service	National geoportals of the Italian Ministry of the Environment, Land, and Sea	1998
RGB digital orthomosaic	DigitalGlobe WorldView-2 satellite	2014

Table 2 The adopted 26 HLC/HLA types and 8 HLC/HLA zones

HLC/HLA types	HLC/HLA zones
Residential settlements; Historic settlements; Service areas; Dock; Roads & Infrastructures; Construction sites	Built-up areas
Arable fields; Vineyards; Fruit trees; Olive groves	Non-Terraced agricultural areas
Terraced crops; Terraced vineyards; Terraced fruit trees; Terraced olive groves	Terraced agricultural areas
High tree wood; Mediterranean sclerophyllous wood; Transitional areas	Non-Terraced woodlands
Terraced high tree wood; Terraced Mediterranean sclerophyllous wood; Terraced transitional areas	Terraced woodlands
Sparsely vegetated areas; Burned areas	Sparse vegetation
Sands; Rocks	Sands & Rocks
Rivers; Sea	Water bodies

The driven idea behind this step is to map the entire analyzed landscape based on its distinctive characters resulting from known historical processes [19]. The geodatabase associated to each vector layer was constructed in order to easily identify HLC types and HLC zones, based on scale level. On one hand, HLC types identify the most detailed representation of the landscape character, used for a fine level of analysis. On the other hand, HLC zones represent a simplified and generalized version of types, useful for a broader level of analysis [20]. In this research, 26 HLC/HLA types have been taken into account, synthetized in 8 HLC/HLA zones (Table 2). Considering that the main object of the HLC/HLA methodology is the study and characterization of the present landscape, each digitalized map have been overlapped with the most recent one (i.e., 2014 map) obtaining a single vector layer with all types and zone of all investigated years and all changes occurred during the examined time period. Through the study of this data, it was possible to create a final map highlighting the steps that went into the formation of the landscape as we know it today, the so-called “time-depth” [21].

3 Results and Discussions

The photointerpretation process led to the creation of a HLC types map and a HLC zones map (Fig. 2) for each investigated year. Considering the HLC Types, “terraced transitional areas” was the most representative one, occupying a surface of 493.38 ha. The same HLC type was the most representative in 1998 and in 1976, with a surface of 677 ha and 513.79 ha respectively. In 1955, the most representative type was “terraced vineyards”, showing a total surface of 708.14 ha. Considering HLC zones, in 2014 the most representative one was “non-Terraced woodlands” with a total surface of 955.40 ha. In 1998, the HLC zone occupying more surface was “Terraced woodlands” with a surface 1069.63 ha. The same zone was the most representative in 1976, with a surface of 791.70 ha. In 1955 instead, the most represented zone was “Terraced agricultural areas”, occupying a total surface of 813.25 ha. This data highlight an abandonment trend of agricultural practices on terraced fields that led to the abandonment of terraces allowing a re-naturalization by potential forest communities. This findings are in line with those of similar studies conducted for the same area or similar ones [13, 22, 23].

Considering the map of the time-depth (Fig. 3), can be noticed as 959.47 ha, representing the 39.74% of the entire analyzed landscape, occurred before 1955. Changes occurred between 1955 and 1976 led to the formation of 630.11 ha of the today’s landscape, representing the 26.11% of the total. 212.35 ha were shaped between 1976 and 1998, representing the 8.80% of the entire landscape. Finally, 612.25 ha are recently formed in the last 16 years, from 1998 to 2014, representing the 25.36% of the analyzed area. These data show the importance of the past in the today’s landscape, which for the most part, almost 40%, was shaped before the first considered year. Then a decrease of percentage of occurrence can be noticed between 1955 and 1976 and between 1976 and 1998. At the end, a rapid increase can be highlighted in the last time-interval analyzed, from 1998 to 2014, mostly due to human-made transformation of the landscape.

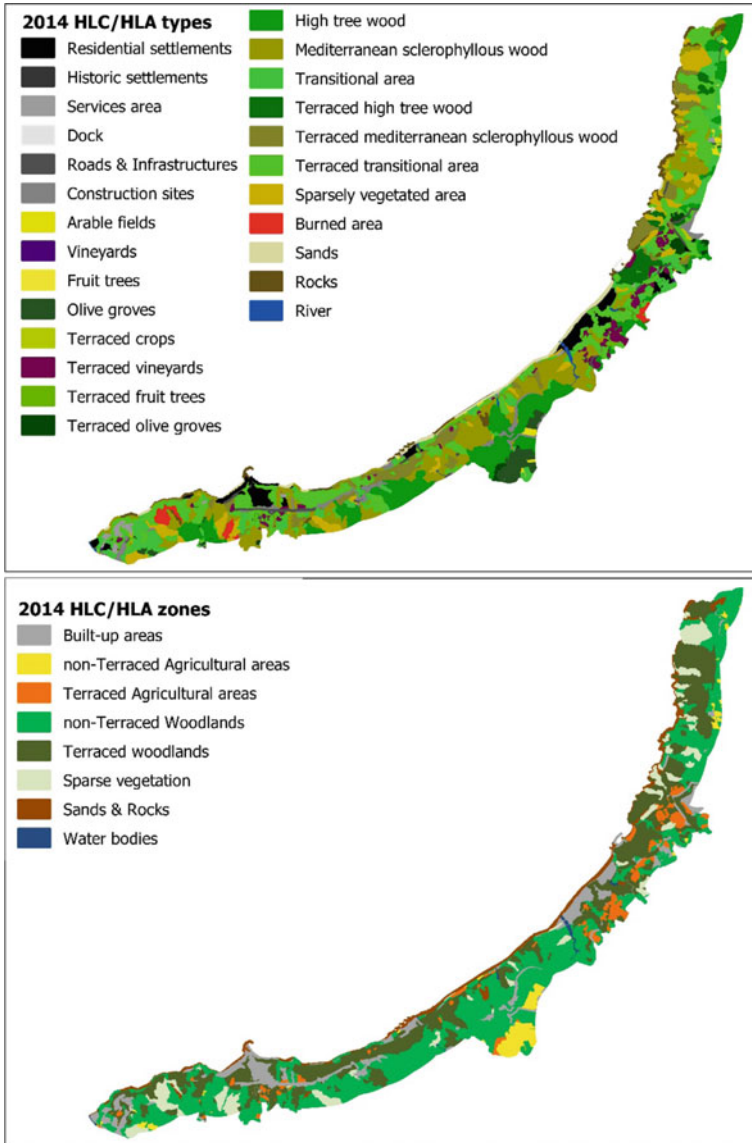


Fig. 2 HLC/HLA types and HLC/HLA zones maps for 2014

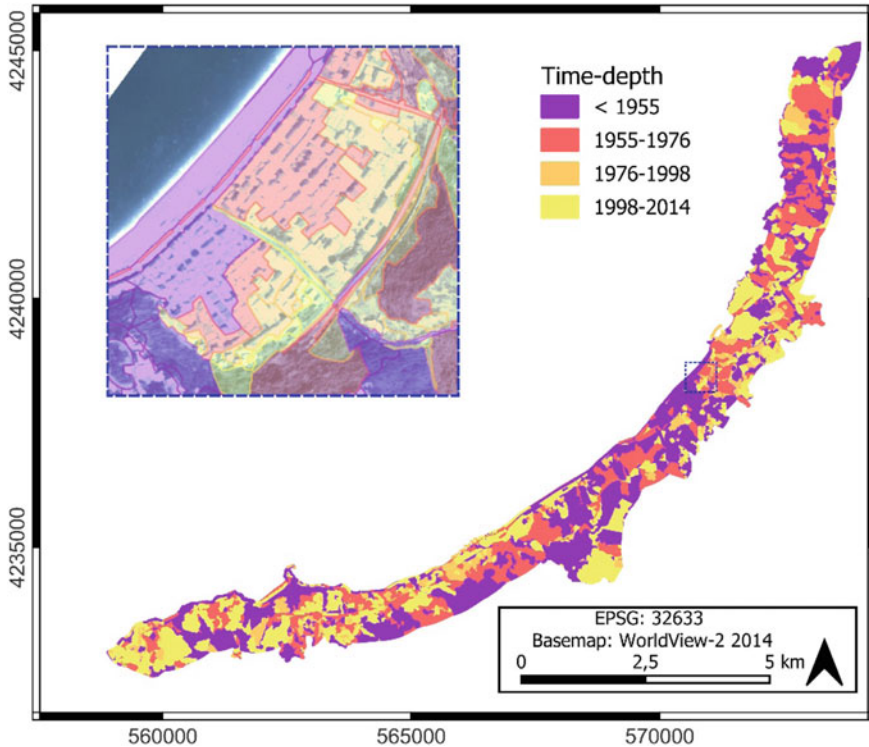


Fig. 3 Time-depth map. The dotted blue square shows a particular zooming of the urbanized area of the ‘Marinella’ neighborhood, in the municipality of Bagnara Calabria

4 Conclusions

This work is part of a still ongoing research and it was aimed to perform a first test about the applicability of HLC and HLA methods to a terraced agricultural landscape. The adopted approach allowed us to highlight how the today’s landscape was influenced by several modifications occurred in the past. The time-depth map allows showing the steps that went into the formation of the landscape as we know it today. Furthermore, the obtained results show the potential applicability of HLC/HLA methodology also in relatively close context like the Costa Viola agricultural terraced landscape. The main limitation of the proposed approach is the need of available ancient basemaps to go back in time detecting the signs of landscape characters and the availability of newer ones to have a constant update of the today’s framework. Moreover, the activities of photointerpretation and digitalization, which should be conducted by specialized research units, resulting to be time-consuming. As future development, a supervised semi-automatic classification approach could be tested.

This method, integrated with other GIS-based approaches, could be a useful tool for stakeholders and decision makers in landscape planning and management activities. Moreover, HLC/HLA could be considered as a starting step in the development of deeper interdisciplinary researches.

References

1. Antrop, M.: Why landscapes of the past are important for the future. *Landsc. Urban Plan.* **70**, 21–34 (2005)
2. Di Fazio, S., Modica, G.: Historic rural landscapes: sustainable planning strategies and action criteria. The Italian experience in the global and European context. *Sustainability* **10**, 3834 (2018). <https://doi.org/10.3390/su10113834>
3. Solano, F., Praticò, S., Piovesan, G., et al.: Characterising historical transformation trajectories of the forest landscape in Rome's Metropolitan area (Italy) for effective planning of sustainability goals. *L Degrad Dev.* **32**, ldr.4072 (2021). <https://doi.org/10.1002/ldr.4072>
4. Solano, F., Colonna, N., Marani, M., Pollino, M.: Geospatial analysis to assess natural park biomass resources for energy uses in the context of the Rome metropolitan area. In: *New Metropolitan Perspectives*, pp. 173–181 (2019). https://doi.org/10.1007/978-3-319-92099-3_21
5. Cillis, G., Statuto, D., Picuno, P.: Historical GIS as a tool for monitoring, preserving and planning forest landscape: a case study in a Mediterranean Region. *Land.* **10**, 851 (2021)
6. Lanucara, S., Praticò, S., Modica, G.: Harmonization and interoperable sharing of multi-temporal geospatial data of rural landscapes. In: *Smart Innovation, Systems and Technologies*, pp. 51–59 (2019). https://doi.org/10.1007/978-3-319-92099-3_7
7. Turner, S.: Historic landscape characterisation: a landscape archaeology for research, management and planning. *Landsc Res.* **31**, 385–398 (2006)
8. Herring, P.C.: Framing perceptions of the historic landscape: historic landscape characterisation (HLC) and historic land-use assessment (HLA). *Scottish Geogr J.* **125**, 61–77 (2009)
9. Fairclough, G., Macinnes, L.: *Guidance for England and Scotland Understanding Historic Landscape*. Landscape (2002)
10. Turner, S.: Historic landscape characterisation. An archaeological approach to landscape heritage. *Routledge Handbook Landscape Character Assess.* In: *Routledge Handbook of Landscape Character Assessment*, pp. 37–50. Routledge, Abingdon (2018)
11. Agnoletti, M., Santoro, A., Gardin, L.: *Italian Historical Rural Landscapes*. Springer, Dordrecht (2013)
12. Graziani, L., Maramai, A., Tinti, S.: A revision of the 1783–1784 Calabrian (southern Italy) tsunamis. *Nat. Hazards Earth Syst. Sci.* **6**, 1053–1060 (2006)
13. Modica, G., Praticò, S., Di Fazio, S.: Abandonment of traditional terraced landscape: a change detection approach (a case study in Costa Viola, Calabria, Italy). *L Degrad Dev.* **28**, 2608–2622 (2017)
14. MacDonald, D., Crabtree, J., Wiesinger, G., et al.: Agricultural abandonment in mountain areas of Europe: environmental consequences and policy response. *J. Environ. Manage.* **59**, 47–69 (2000)
15. Molinillo, M., Lasanta, T., García-Ruiz, J.M.: Managing mountainous degraded landscapes after farmland abandonment in the central Spanish Pyrenees. *Environ. Manage.* **21**, 587–598 (1997)
16. Praticò, S., Solano, F., Di Fazio, S., Modica, G.: A multitemporal fragmentation-based approach for a dynamics analysis of agricultural terraced systems: the case study of Costa Viola Landscape (Southern Italy). *Land.* **11**, 482 (2022)

17. Praticò, S., Solano, F., Di Fazio, S., Modica, G.: A Fragmentation-based analysis of Costa Viola (Southern Italy) agricultural terraces. In: La Rosa, D., Privitera, R. (eds) *Innovation in Urban and Regional Planning*. INPUT 2021. LNCE, vol. 242, pp. 152–159. Springer, Cham (2021). https://doi.org/10.1007/978-3-030-96985-1_17
18. Modica, G., Praticò, S., Pollino, M., Di Fazio, S.: Geomatics in analysing the evolution of agricultural terraced landscapes. In: *Computational Science and Its Applications – ICCSA 2014*. ICCSA 2014, LNCS, vol. 8582, pp. 479–494. Springer, Cham (2021). https://doi.org/10.1007/978-3-319-09147-1_35
19. Millican, K., Dixon, P., Macinnes, L., Middleton, M.: Mapping the historic landscape: historic land-use assessment in Scotland. *Landscapes (United Kingdom)*. **18**, 71–87 (2017)
20. Herring, P.C.: *Cornwall's Historic Landscape: Presenting a Method of Historic Landscape Character Assessment*. Cornwall County Council (1998)
21. Van Eetvelde, V., Antrop, M.: Indicators for assessing changing landscape character of cultural landscapes in Flanders (Belgium). *Land Use Policy* **26**, 901–910 (2009)
22. Petanidou, T., Kizos, T., Soulakellis, N.: Socioeconomic dimensions of changes in the agricultural landscape of the Mediterranean Basin: a case study of the abandonment of cultivation terraces on Nisyros Island. Greece. *Environ Manage.* **41**, 250–266 (2008)
23. Kizos, T., Dalaka, A., Petanidou, T.: Farmers' attitudes and landscape change: evidence from the abandonment of terraced cultivations on Lesvos Greece. *Agric. Hum. Values* **27**, 199–212 (2010)

Recycled Plastics Used in the Production of Agricultural Nets for Crop Protection



Roberto Puglisi, Giuseppe Cillis, Dina Statuto, and Pietro Picuno

Abstract The sustainability of agricultural systems is essential for protecting the rural environment, as well as for feeding the future generations. The creation of efficient closed-cycle farming systems, would lead agricultural production to have less impact on the rural environment. In this framework, the use of plastic nets for crop protection is increasing more and more, hence adding benefits not only to agricultural production, but also to farmers and to the surrounding ecosystems. In fact, thanks to the use of nets for crop protection, it is possible to control the main production parameters inside a greenhouse or a tunnel. In addition, these nets may significantly contribute to energy saving, helping to protect the crop by reducing and optimizing the use of fossil fuels and agro-chemicals, thus limiting their impact on the environment. The purpose of the present experimental work has been to analyze the eco-sustainable innovations coming from plastic nets produced with partially recycled material. Some of these nets, have been subjected to tensile tests in longitudinal and transverse direction, as well as to spectro-photometric analysis, aimed to verify the transmittance and reflectance of the fabric in the UV/PAR/NIR spectrum (200 nm to 2500 nm) and shading effect. The results allowed evaluating and discussing the potential use of partially recycled nets in agriculture that would contribute to reducing the plastic footprint of agriculture.

Keywords Crop protection; Plastic Nets · Energy Saving · Recycled Plastics · Mechanical Properties · Tensile Tests

1 Introduction

Since the middle of the last century, extensive and steadily expanding use of plastic materials in agriculture has been reported worldwide. Plastic materials have revealed essential for the protection and sustainable development of herbaceous, tree, food and

R. Puglisi (✉) · G. Cillis · D. Statuto · P. Picuno
Forestry, Food and Environmental Sciences - SAFE,, University of Basilicata, Potenza, Italy
e-mail: roberto.puglisi@unibas.it

© The Author(s), under exclusive license to Springer Nature Switzerland AG 2023
V. Ferro et al. (eds.), *AIIA 2022: Biosystems Engineering Towards the Green Deal*,
Lecture Notes in Civil Engineering 337,
https://doi.org/10.1007/978-3-031-30329-6_124

1203

ornamental crops. The use of plastic nets has made it possible to prevent the passage of insects that could severely damage plants, while reducing the transmission of diseases (e.g. virosis). At the same time, nets positively contribute to regulate internal thermal conditions within the protected environment and, most importantly, to achieve higher yields, to sharply reduce the use of agro-chemicals, and to achieve significant water savings [1–3]. Compared to crops in open fields, thanks to plastic materials, it is possible to protect crops from climatic adversities, which are currently harmfully increasing. The market of plastics used for these purposes in Europe regards hundreds of thousands of hectares, involving hundreds of thousands of tons of plastic material employed every year. Indeed, according to the FAO [4], farms use 12.5 million tons of plastic products annually in the World. Another 37.3 million tons are used in food packaging. The agricultural production and livestock sectors were found to be the largest users, accounting for a total of 10.2 million tons per year, followed by fisheries and aquaculture with 2.1 million tons and forestry with 0.2 million tons. Asia is estimated to be the largest user of plastics in agricultural production, accounting for nearly half of global use. In the absence of viable alternatives, demand for plastics in agriculture is likely to increase. According to FAO [4], global demand for greenhouse, mulch and silage films will increase by 50 percent, from 6.1 million tons in 2018 to 9.5 million tons in 2030. These trends make it essential to balance the costs and benefits of plastics but, mostly, it is critical to ensure a second life for the plastic material with the use of recycled plastics, in the framework of a circular economy approach. The use of plastic materials causes a high amount of waste, that should be properly disposed of, so as not to cause harm to the environment [5–7]. So far, there is no specific legal framework in Europe ensuring an environmentally friendly, economically feasible and socially accepted system for agricultural plastic waste disposal [8].

Much of agricultural plastic waste can be recycled. Many studies consider mechanical recycling as an appropriate system for post-consume agricultural plastic film recovery [5, 9–13]. In order to be able to reduce the problem of plastic waste, recycling and reuse of different plastic materials is essential, to reduce environmental pollution. One of the basic goals of recycling is to improve the different properties of recycled plastic [14]. It can also lead to interesting benefits, from a technical and economic point of view, through the creation of new products, the improvement of existing ones, and the development of new applications, with decreased costs of the whole process, when mechanical recycling of heterogeneous plastic material is possible, where the need to separate different polymers may be avoided [15].

Picuno et al. [16] discussed ways to improve greenhouse-roofing properties, by introducing a three-layer film, whose middle layer is a recycled PE-LD film. Unfortunately, even today, most agricultural plastic waste in several European countries, and in many countries around the World, is left in the field. In other cases, farmers uncontrollably burn it, hence releasing substances harmful to human health, agricultural product safety and the environment rural. The research presented by Briassoulis et al. [8], has experimentally discussed all the critical parameters that affect the quality characteristics of agricultural plastic wastes regarding their recyclability, or their ability to be used for energy recovery - particularly in cement kilns.

The purpose of this paper is to present research results on a crop protection net made partially from recycled plastic. The basic mechanical and spectro-radiometric characteristics of the crop protection net obtained by using recycled plastics, have been here analyzed. This option may be considered today as innovative, but tomorrow it would be considered as a current practice, so that plastics with enhanced working life and lower environmental impact would be more extensively employed.

2 Materials and Methods

A plastic screen made with 30% of films from recycled PET plastic bottles has been considered in the present analysis, *i.e.*, the “LUXOUS 1147 ECO” (Ludvig Svensson[®]) thermal screen, used to promote energy conservation inside the greenhouse, both day and night. The use of this type of screen allows the greenhouse to retain during nighttime more heat inside, so the use of fossil energy for heating the greenhouse can be reduced. Moreover, by controlling the temperatures inside the greenhouse, it is also possible to minimize the presence of fungal diseases, which are quite harmful to the crops inside the greenhouse.

The producing company reports that the application of the screen is recommended inside the greenhouse in suspended or sliding mechanized systems, which allow for an opening and closing of the screen according to the needs of the farmer.

In addition, the company claims a shading rate on diffuse light of 25%, while shading on direct light of 15% and UV transmission at 12%. The screen looks transparent at the human eye. The shading factor makes the screen suitable for greenhouses especially located in northern Europe, because of the harsh climates. The manufacturer describes it as a warp-knitted screen.

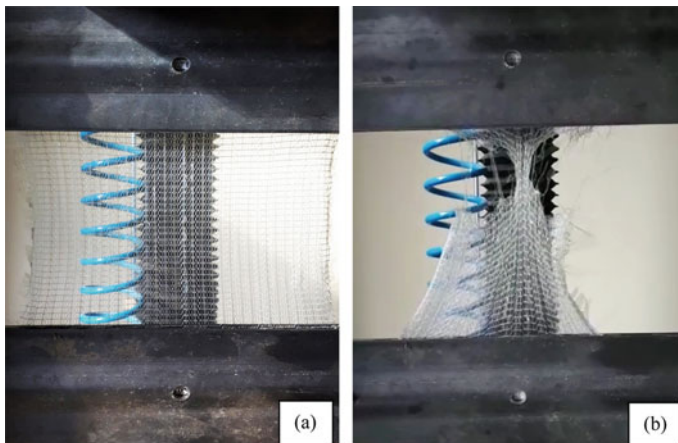


Fig. 1 Screen images before a and after the tensile test b

Table 1 General properties of the LUXOUS 1147 ECO declared By the producing Company (*Ludvig Svensson*[®])

Properties	Value	Unit	Test method
Shading level in diffused light PAR	25	[%]	Protocol NEN 2675
Shading level in direct light PAR	15	[%]	Protocol NEN 2675
Width of strips	4	[mm]	
Weight	57	[g/m ²]	

Table 1 summarizes the physical and mechanical properties of the described screen, with the test methods used by the manufacturer.

The experimental tests have been conducted at the Materials Testing Laboratory of the SAFE School of the University of Basilicata (Italy), through the determination of mechanical properties – *i.e.*: longitudinal and transverse tensile properties - and radiometric properties – *i.e.*: transmittance, reflectance and shading factor. The mechanical properties of the screen were obtained, according to UNI 9405 / EN ISO 13934–1 [17], under the following environmental conditions: Average temperature = 20 °C Relative humidity = 65%.

During the tensile tests, the specimen was pulled with a tensile force along its axis, at a fixed speed, until it broke. A computerized universal testing machine (Galdabini PMA 10® - maximum load = 10 KN) was used (Fig. 1). Ten specimens in the warp direction and ten specimens in the weft direction were tested according to UNI 9405 / EN ISO 13934–1 [17].

The radiometric tests of the screen were obtained through the use of spectrophotometers (Jasco V-570®), which allowed the different specimens to be analyzed for all wavelengths of UV, PAR and NIR (up to 2500 nm).

3 Results and Discussion

3.1 Tensile Test Results

The results of mechanical tests are also summarized in Table 2, where the mean maximum load (F_m) and mean elongation at break (A%) are respectively reported.

The experimental results show specific mechanical behavior for this type of material. Comparing the results with the experimental work of Picuno et al. [13] shows that the screen exhibits, both in weft and warp direction, a significantly lower maximum

Table 2 Tensile tests on LUXOUS 1147 ECO FR, weft/machine direction and warp/transversal direction

Sample	F _m (N)	A (%)
WEFT	531.41 ± 61.94	41.05 ± 12.30
WARP	515.83 ± 180.27	49.99 ± 21.45

load (Fm) than the anti-insect and windbreak nets tested at that time (showing differences of around 270% for the anti-insect nets and 178% for the previously tested windbreak nets). A similar result has been detected with reference to the elongation at break A (%), which has revealed significantly lower, both in weft and warp direction, when compared to the plastic nets tested at that time.

In Figs. 2 and 3, the results obtained from the tensile tests of the tested screen are shown. In these diagrams, it is possible to infer the differences between the different traction tests in both normal (weft) and transverse (warp) direction. In both cases, anyway, it is possible to deduce that the screen is characterized by a trend in which the maximum force is reached almost immediately before the collapse of the material, characterized by a downward and straight trend. This result is produced by the progressive failure of the warp threads. After a semi-collapse of the tensile strength, the material anyway shows some residual resistance before the definitive breakage.

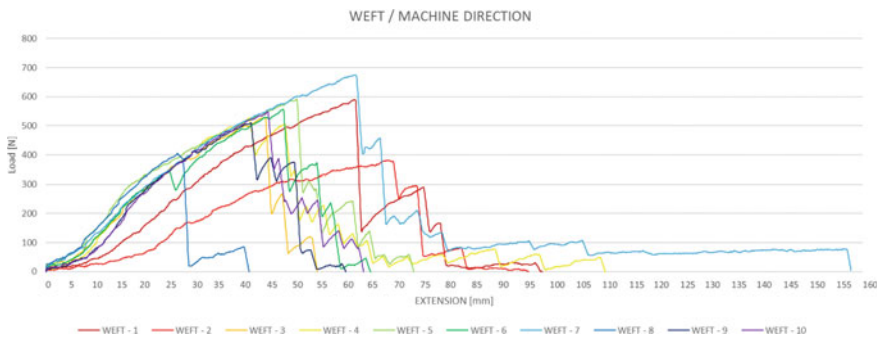


Fig. 2 LUXOUS 1147 ECO FR weft direction

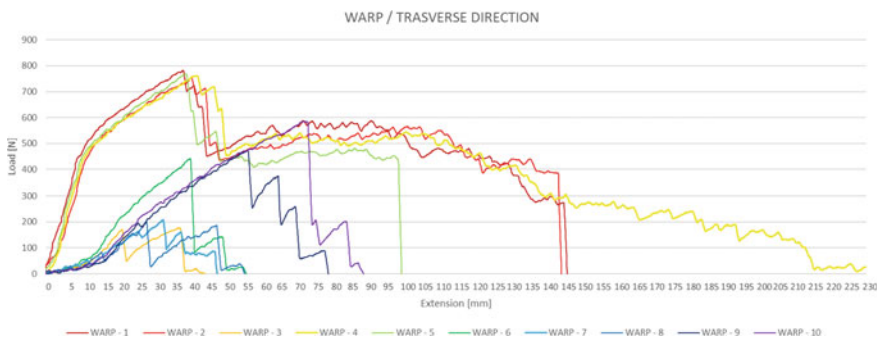


Fig. 3 LUXOUS 1147 ECO FR warp direction

Table 3 Results of spectro-radiometric analysis of the LUXOUS 1147 ECO FR

Range	Wavelength (nm)	Transmittance (%)	Reflectance (%)	Shading effect (%)
Solar	200 - 2500	72.64	17.13	27.36
PAR	400 - 700	81.29	17.39	18.71
Solar-IR	700 - 2500	78.40	18.06	21.40
UV	280 - 400	12.54	6.44	87.46
UVA	315 - 400	2.48	6.24	97.52
UVB	280 - 315	0.21	7.05	99.79

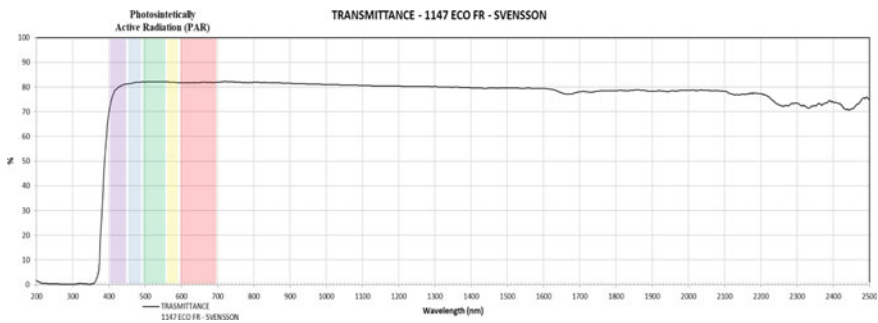


Fig. 4 Transmittance in the UV-VIS-NIR of the screen LUXOUS 1147 ECO FR

3.2 Spectro-Radiometric Analysis

The results of spectro-radiometric analysis on the screen used in the experimental tests showed a uniform behavior, both in transmittance and reflectance, comparable to the performance of a plastic film (Table 3). The UV transmittance was found to be slightly higher (12.54%) than that claimed by the screen manufacturer (12.00%). The spectro-radiometric analysis showed that the shading percentage is higher (18.71%) than the figure stated on the product data sheet (15.00%). Figure 4 and 5 show the plot respectively of the solar transmittance and reflectance along the entire UV–VIS–NIR wavelength 200–2500 [nm] of the tested plastic net.

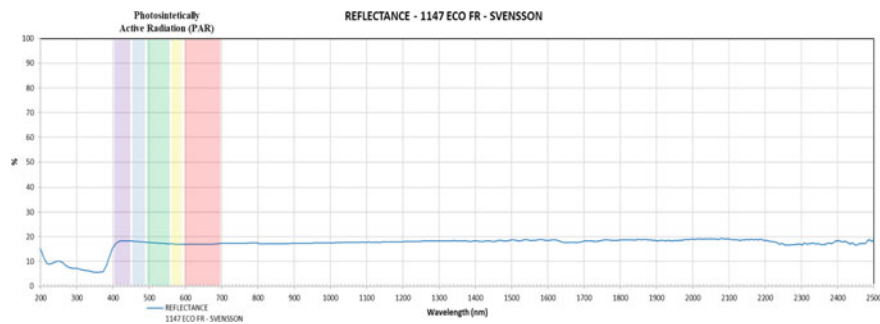


Fig. 5 Reflectance in the UV-VIS-NIR of the screen LUXOUS 1147 ECO FR

4 Conclusions

The development of materials that promote environmental sustainability is one of the keys to reducing the environmental impact of protected agricultural crops. The objective of this study has been the evaluation of the mechanical and radiometric characteristics of a screen produced with 30% recycled PET plastic.

The mechanical and radiometric analyses for this new type of material are essential to improve its performance in agriculture, in compliance with specific certification standards.

The new technologies based on the results obtained from the experimental trial have shown interesting results, that could reveal promising for future applications on the market. In this view, however, further research work and technological innovations are needed. An evaluation of the mechanical and radiometric properties of the screen should also take into account economic and agronomic analyses during the period of use, even to enable the selection of the most suitable material in relation to the specific needs of farmers.

Acknowledgements The Authors wish to thank the screen producer Ludvig Svensson[®] for the kind supply of the plastic screen that were tested in this experimental trial.

Many thanks to Mr. Cosimo Marano - technical staff at the SAFE School of the University of Basilicata - for his support into performing the spectro-radiometrical laboratory analysis and field tests.

This research has been partially supported by the Italian Ministry for University and Research (MIUR) - PON - R&I 2014-2020 – Innovative Industrial Doctorates – Cycle XXXV – Code: DOT1338191.

References

1. Briassoulis, D.; The effects of tensile stress and the agrochemical vapam on the ageing of low density polyethylene (LDPE) agricultural films. Part I. Mechanical Behaviour. *Polymer Degradation and Stability*. 88, 489–503 (2005). <https://doi.org/10.1016/j.polymdegradstab.2004.11.021>

2. Briassoulis, D., Mistrionis, A., Eleftherakis, D.: Mechanical behaviour and properties of agricultural nets — Part I: Testing methods for agricultural nets. *Polym. Testing* **26**, 822–832 (2007). <https://doi.org/10.1016/j.polymertesting.2007.05.007>
3. Immirzi, B., Santagata, G., Vox, G., Schettini, E.: Preparation, characterisation and field-testing of a biodegradable sodium alginate-based spray mulch. *Biosys. Eng.* **102**, 461–472 (2009). <https://doi.org/10.1016/j.biosystemseng.2008.12.008>
4. FAO; Assessment of Agricultural Plastics and Their Sustainability: A Call for Action; FAO: Rome, Italy, 2021; ISBN 978–92–5–135402–5.
5. Sica, C., Dimitrijević, A., Scarascia, G., Picuno, P.: Technical Properties of Regenerated Plastic Material Bars Produced From Recycled Agricultural Plastic Film. *Polym.-Plast. Technol. Eng.* **54**, 150826121339001 (2015). <https://doi.org/10.1080/03602559.2014.1003228>
6. Blanco, I.; Loisi, R.; Sica, C.; Schettini, E.; Vox, G.; Agricultural Plastic Waste Mapping Using GIS. A Case Study in Italy. *Resources Conservation and Recycling*, **137**, 229–242 (2018). <https://doi.org/10.1016/j.resconrec.2018.06.008>
7. Puglisi, R.; Statuto, D.; Picuno, P.; Effects of greenhouse lime shading on filtering the solar radiation. In: *Proceedings of the 48th International Symposium, ATAE 2021 - Actual Tasks on Agricultural Engineering*, 2 - 4 March 2021, Opatija, Croatia, 131–140 (2021).
8. Briassoulis, D., Hiskakis, M., Babou, E., Antiohos, S.K., Papadi, C.: Experimental investigation of the quality characteristics of agricultural plastic wastes regarding their recycling and energy recovery potential. *Waste Manage.* **32**, 1075–1090 (2012). <https://doi.org/10.1016/j.wasman.2012.01.018>
9. Briassoulis, D., Hiskakis, M., Babou, E.: Technical specifications for mechanical recycling of agricultural plastic waste. *Waste Manage.* **33**, 1516–1530 (2013). <https://doi.org/10.1016/j.wasman.2013.03.004>
10. Picuno, P.; Innovative Material and Improved Technical Design for a Sustainable Exploitation of Agricultural Plastic Film. *Polymer-Plastics Technology and Engineering*, **53** (2014) <https://doi.org/10.1080/03602559.2014.886056>
11. Turner, A.; Filella, M.; Lead in plastics – recycling of legacy material and appropriateness of current regulations. *J. Hazardous Materials*, **404** (2021). <https://doi.org/10.1016/j.jhazmat.2020.124131>
12. Batista, T.: Dealing with plastic waste from agriculture activity. *Agronomy*, **12**, 134, (2021).
13. Picuno, P., Tortora, A., Sica, C.: Mechanical characterization of plastic nets for protected cultivation. *Acta Hort.* **801**, 91–98 (2008). <https://doi.org/10.17660/ActaHortic.2008.801.4>
14. Deka, B.K., Maji, T.K., Mandal, M.: Study on properties of nanocomposites based on HDPE, LDPE, PP, PVC. Wood and Clay. *Polym. Bull.* **67**, 1875–1892 (2011). <https://doi.org/10.1007/s00289-011-0529-5>
15. Sica, C., Picuno, P.: Spectro-Radiometrical characterization of plastic nets for protected cultivation. *Acta Hort.* **801**, 245–252 (2008). <https://doi.org/10.17660/ActaHortic.2008.801.23>
16. Picuno, P., Sica, C., Laviano, R., Dimitrijević, A., Scarascia-Mugnozza, G.: Experimental tests and technical characteristics of regenerated films from agricultural plastics. *Polym. Degrad. Stab.* **97**, 1654–1661 (2012). <https://doi.org/10.1016/j.polymdegradstab.2012.06.024>
17. UNI EN ISO 13934-1:2013 - UNI Ente Italiano Di Normazione.
18. Available online: https://store.uni.com/p/UNI21012390/uni-en-iso-13934-12013-114644/UNI21012390_EEN (accessed on 17 August 2022).

Efficiency of Plastic Nets for Greenhouse Shading



Roberto Puglisi, Marco Lippolis, Giuseppe Starace, Paolo Arrigoni,
and Pietro Picuno

Abstract Agricultural production is influenced by extreme weather phenomena, accompanied by major global changes, such as the increasingly sudden and frequent appearance of new types of insects, the transformation of eating habits (e.g., “smart/super foods”), etc. Thus, the concept of crop protection under greenhouse, conceived as a mere passive defense, is gradually being overcome: no longer a shelter “against” or “protecting”, but rather an intelligent structure “for” or “proacting”. Plastic materials used to cover a greenhouse for the purpose of crop protection can play a crucial role on the quality of light hitting crops, controlling radiation in different ways, especially in the PAR wavebands. Covering materials and shading strategies can be suitably selected and implemented in many mild climate areas, as well as in warm regions where spring/summer solar radiation levels are often too high. To study the shading effect, in the present research some field trials have been performed, by covering different small-scale tunnels with a plastic film and protecting them with an outer plastic net (PRISMA HDF®), fixed at different distance from the plastic film for each tunnel. Temperature of air and of soil covered with a layer of black mulching fabric have been measured, together with solar radiation. The results confirmed that the thickness of the gap between shading net and plastic film plays a role on the internal microclimate, which may differently improve the thermal efficiency of the greenhouse and its overall thermodynamic behavior.

Keywords Plasticulture · Plastic Nets · Energy Saving · Windbreak · Radiometric Properties · Shading effect

R. Puglisi (✉) · P. Picuno

School of Agriculture, Forestry, Food and Environmental Sciences – SAFE, University of Basilicata, Potenza, PZ, Italy
e-mail: roberto.puglisi@unibas.it

M. Lippolis · P. Arrigoni

SACHIM S.R.L, Via Mastricale 07, 70017 Putignano, BA, Italy

G. Starace

Dipartimento di Management, Finanza e Tecnologia, Università LUM “Giuseppe Degennaro”, Strada Statale 100 Km 18, 70010 Casamassima, BA, Italy

1 Introduction

Using protected crops, to date, is essential to limit extreme weather phenomena. Studying new solutions for covering greenhouses is essential for the defense against hail, excessive solar radiation, strong wind, rain and harmful pests. The new greenhouse aims to be high-tech, able to guarantee total control of the internal environment and the crops cultivated inside. Temperature control is essential in extreme conditions, both if hot or cold. In the Mediterranean environment, for example, it is important to reduce solar radiation in order to cool the greenhouse, while in northern Europe it is important to retain as much heat generated by solar radiation as possible, to minimize the consumption of fossil fuel [1]. The use of nets for crop protection allows to protect crops from various risks. New technologies are leading to more and more performing materials to make higher yields, healthier and more vigorous fruits, reduce the consumption of agro-chemicals for the control of insects and fungi. The most important factor to check inside the greenhouse – even, at the same time, the more complex one – concerns the light. The new agricultural nets make it possible to fully exploit solar radiation based on the type of cultivation. The cladding materials used to cover a greenhouse intended for crop protection are able to filter solar radiation in different ways, especially within the Photosynthetically Active Radiation - PAR 400–700 [nm] wavebands [2–5]. PAR is essential for crop development. Plants have different needs in terms of light and heat to require, in most cases, nets “*customized*” for the specific type of that cultivation. In addition to the PAR, it is essential to check the filtering of Ultra-Violet (UV) radiation. Filtering the UV reduces the activity of pollinating insects, causing a lowering of yields, especially in crops such as tomatoes [6–9]. Coating materials and shading strategies can therefore be proactively selected and implemented in many Mediterranean areas, as well as in other regions (*e.g.*, arid regions) where incident solar radiation during the spring/summer season is often too much high. A plastic net could play, if used as an autonomous cover, or in synergy with a plastic coating film, a fundamental role in creating more favorable microclimatic conditions during crop growth [5, 10–13]. It could combine the shadow effect with some specific characteristics useful for creating suitable conditions for plants and guaranteeing health conditions for workers as well. In many cases, the farmer is almost obliged to protect the crops. For example, in the cultivation of Cherry, it is essential to use anti-rain nets, to avoid cracking phenomena on the fruit or anti-hail nets to avoid total loss of the yield [14]. With the aim of analyzing the effectiveness of different shading techniques of a greenhouse, Statuto and Picuno [15] conducted an experimental test, comparing two commercial plastic nets characterized by different shading effects. These two plastic nets were tested in the laboratory, where their radiometric characteristics were determined. The same plastic nets were then installed in two different small tunnels located in Southern Italy, in which the indoor air and relative humidity were measured in some days of late spring. The results obtained through these experimental tests enabled to adopt a comparative analysis of the performance of the two shading nets tested, highlighting the role that a correct selection of the suitable net can play on the results in terms

of burns. Further analysis of different shading strategies was conducted by Statuto et al. [16], where the effectiveness of the shading effect of plastic nets in different climates was determined and experimental tests were conducted on some identical small tunnels installed in two different locations, one in the Mediterranean area (Acerenza - Southern Italy) and one in arid conditions (Riyadh - Saudi Arabia). In the current research work report the results of several experimental tests carried out in the Mediterranean (Apulia Region – Southern Italy), conducted on the basis of some previous experimental tests [16, 17] are reported.

2 Materials and Methods

Four small identical tunnels (Fig. 1) were built in the experimental area of the company SACHIM S.r.l. located in the municipality of “Putignano” (Southern Italy - 40°50'17.9"N–17°05'36.9"E). All these tunnels have a length of 4 m. The support structure of each tunnel consists of three arches positioned inside (in RED line Fig. 1) plus as many arches positioned outside (in BLUE line Fig. 1).

The dimensions of the internal structure of the small tunnels (red line) are the same for all tunnels with an internal arch width of 1.08 m and an internal structure height of 1.70 m. The outer structure (blue line) was built to test a double outer cover at four different distances (10, 15, 20, 25 cm) from the inner layer (Fig. 2). A common *Patilux*® plastic film on the inner layer covers the small tunnels, while a *PRISMA HDF*® plastic net has been positioned on the outside; it is a semi-transparent milky white mesh, with a light shielding factor of 57% and a weight of 95 g/m². A black mulching plastic film was applied to the ground inside each tunnel that, after various sensor-setting tests, was covered with a 5 cm layer of soil above - thus resulting in the creation of an impermeable membrane inside the soil. A shading net in contact with plastic film has been considered as a control tunnel. The outdoor and indoor air and ground temperatures were recorded by the CS500-L probes (modified version of the 50Y Humitter from Vaisala, Campbell Scientific Inc., Utah, USA). The solar radiation was recorded by the *LPPYRA02* pyranometers (Delta OHM s.r.l.) The relevant data were recorded by an *HD32MTlog data-logger* (Delta OHM s.r.l.). Measurements of the environmental parameters of the tunnels began last July 2021 until August this year, generating results in terms of temperature differences between the different tunnels. Monthly data were verified and analyzed. Due to the limited number of electronic devices, some sensors were moved between the different tunnels to take measurements. Measurements of the environmental parameters chosen for the present analysis were taken from July 15, 2022 to July 28, 2022.

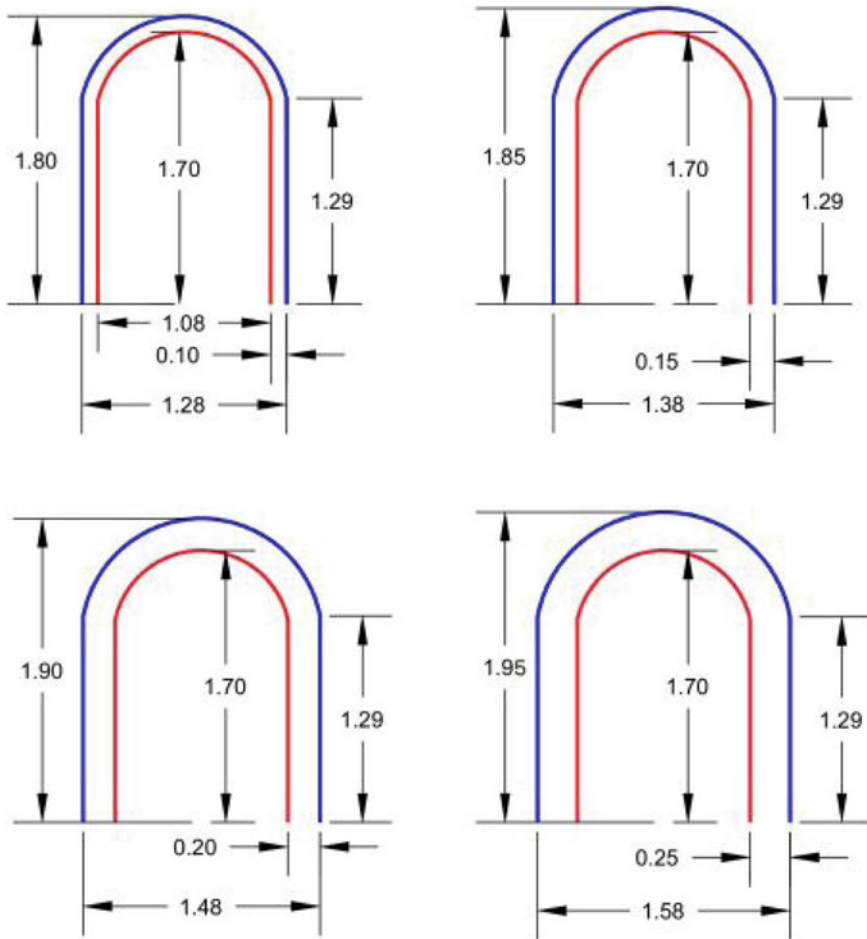


Fig. 1 Descriptive outline of the experimental trial (all dimensions in m)

3 Results and Discussion

The results of the experimental trial show that the use of a 25 cm gap has showed, if compared to other cases (20, 15, 10 cm) and referring to the control tunnel, to significantly limit the temperatures inside the tunnel. Indeed, Fig. 3 shows the temperature difference between the different spaces, which is nearly 3.5 °C at noon when comparing the tunnel with a 25 cm gap with the tunnel with the net in contact with the plastic film (last graph in Fig. 3). The net seems to absorb most of the blocked solar energy when it is in contact with the plastic covering film. In this case, the absorbed radiation is transferred, by conduction, to the film, increasing the temperature of the film, thus the emission of thermal radiation in the tunnel (Fig. 3). During

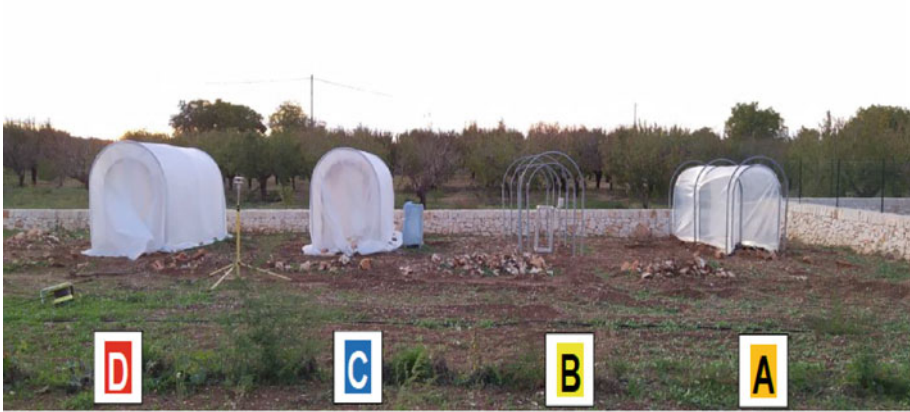


Fig. 2 Tunnel at the start of experimental activities

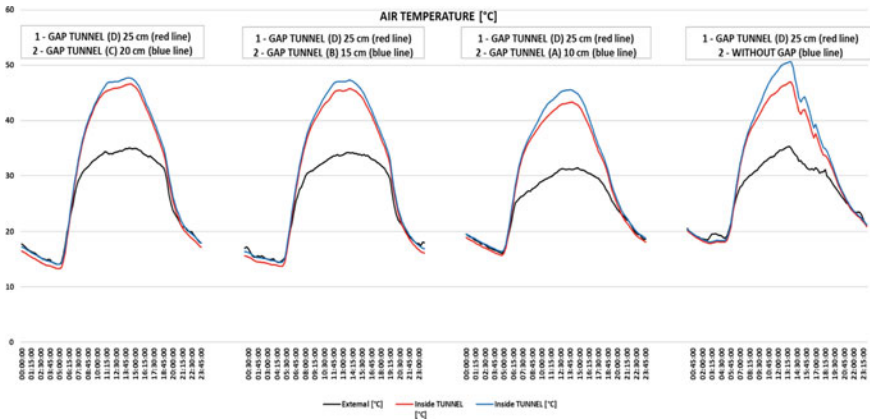


Fig. 3 Air temperature in the trial tunnels measured on different days for each trial

the night, however, the phenomenon is reversed and the temperature recorded in the tunnels covered by the net seems to be slightly higher than in the others (Fig. 3). The trend is also confirmed for the soil temperatures (Fig. 4), in this case the temperature inversion at night was found, *i.e.*, the tunnel with the wider gap is warmer than the control (shading net attached to the plastic film). It can be seen from Fig. 5 that all tunnels have the same absorption in solar radiation. The results of the experimental tests show that the mesh in contact with the covering film increased the temperatures of the film and the internal air more than those of the mesh placed several cm away (25, 20, 15, 10). From these results, we would hence conclude that the wider the thickness of the cavity, the better is the control effect on temperature, among tunnels provided with a air gap between the plastic film and the shading net. An explanation of this phenomenon may be directly connected to the wider surface of exchange by

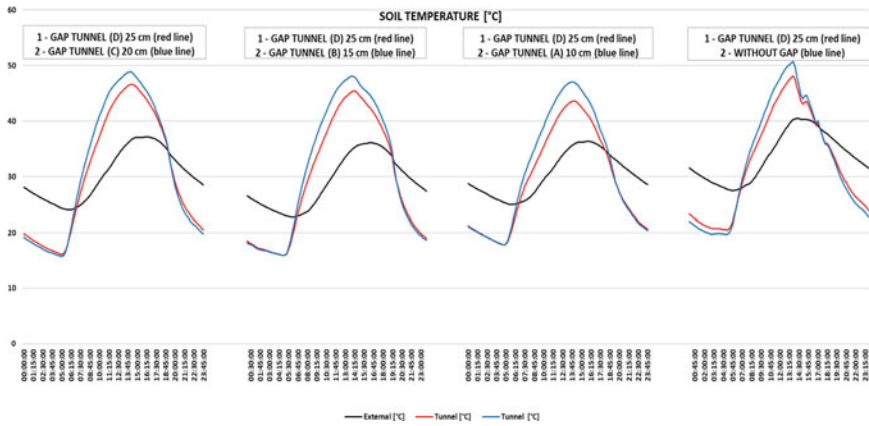


Fig. 4 Soil temperature detected at 5 cm depth in the trial tunnels measured on different days for each trial

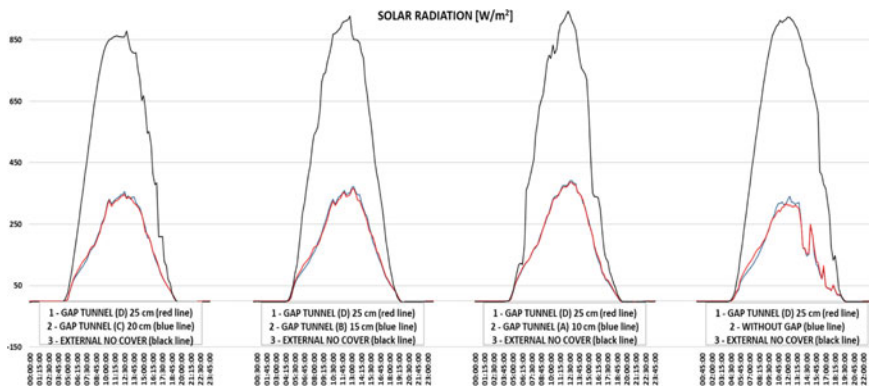


Fig. 5 Radiation inside the small tunnels measured on different days for each trial

convection with the external air, which grows in direct proportion with the thickness of the air gap between film and net.

4 Conclusions

The use of shade nets showed to effectively control the temperatures inside the tunnels. In addition, the position of the shading net, relating to the plastic film, plays a key role in controlling solar radiation and air and soil temperatures inside the tunnel. The ability to control and maintain optimal temperatures inside the tunnels plays a key role in crop growth, the well-being of agricultural operators.

Therefore, it is an indispensable tool that can make the cover material crucial in relation to the microclimatic parameters of the protected environment. When there is an intense flow of solar radiation, external shielding is recommended, and it is suggested to keep the mesh separate from the cover film to achieve a cooling effect in summer days.

Further research is anyway needed to quantify the consequences of the shading effect on the indoor greenhouse climate, to investigate the selective filtering of solar radiation by the plastic net and relevant crop response, as well as to analyze the durability of a plastic net, depending on the site and application conditions.

Acknowledgements The authors would like to thank the netting producer SACHIM s.r.l. - ARRIGONI S.p.A. for kindly providing the plastic nets, instruments for measurements, and the experimental area for carrying out the experimental tests.

We would like to thank Mr. Cosimo Marano - a technician from the SAFE School of the University of Basilicata – for his support in carrying out the field trials.

This research has been partially supported by the Italian Ministry for University and Research (MIUR) - PON - R&I 2014-2020 – Innovative Industrial Doctorates – Cycle XXXV – Code: DOT1338191

References

1. Baeza, E., Breugel, A.J.B., Hemming, S., Stanghellini, C., Smart greenhouse covers: a look into the future. *Acta Hort.* 213–224 (2020). <https://doi.org/10.17660/ActaHortic.2020.1268.28>.
2. Schettini, E., Salvador, F.R.D., Scarascia-Mugnozza, G., Vox, G.: Radiometric properties of photosensitive and photoluminescent greenhouse plastic films and their effects on peach and cherry tree growth. *J. Hortic. Sci. Biotechnol.* **86**, 79–83 (2011). <https://doi.org/10.1080/14620316.2011.11512729>
3. Vox, G., Maneta, A., Schettini, E.: Evaluation of the radiometric properties of roofing materials for livestock buildings and their effect on the surface temperature. *Biosys. Eng.* **144**, 26–37 (2016). <https://doi.org/10.1016/j.biosystemseng.2016.01.016>
4. Abdel-Ghany, A.M., Picuno, P., Al-Helal, I., Alsadon, A., Ibrahim, A., Shady, M.: Radiometric characterization, solar and thermal radiation in a greenhouse as affected by shading configuration in an arid climate. *Energies* **8**, 1–10 (2015)
5. Picuno, P., Abdel-Ghany, A.M.: Spectro-radiometrical analysis of plastic nets for greenhouse shading under arid conditions. In: *Proceedings of the 44th International Symposium on Agricultural Engineering: Actual Tasks on Agricultural Engineering*, Opatija, Croatia, 23–26 February, pp. 469–477 (2016)
6. Guldberg, L.D., Atsatt, P.R.: Frequency of reflection and absorption of ultraviolet light in flowering plants. *Am. Midl. Nat.* **93**, 35–43 (1975)
7. Mori, S., et al.: Biocommunication between plants and pollinating insects through fluorescence of pollen and anthers. *J. Chem. Ecol.* **44**, 591–600 (2018). <https://doi.org/10.1007/s10886-018-0958-9>
8. Diaz, B., Fereres, A.: Ultraviolet-blocking materials as a physical barrier to control insect pests and pathogens in protected crops. *Pest Technol.* **1** (2007)
9. Ben-Yakir, D., Antignus, Y., Offir, Y., Shahak, Y.: Photosensitive nets and screens can reduce insect pests and diseases in agricultural crops. *Acta Hort.* 95–102 (2014). <https://doi.org/10.17660/ActaHortic.2014.1015.10>.

10. Castellano, S., Starace, G., De Pascalis, L., Lippolis, M., Scarascia Mugnozza, G.: Test results and empirical correlations to account for air permeability of agricultural nets. *Biosys. Eng.* **150**, 131–141 (2016). <https://doi.org/10.1016/j.biosystemseng.2016.07.007>
11. Ahemd, H.A., Al-Faraj, A.A., Abdel-Ghany, A.M.: Shading greenhouses to improve the microclimate, energy and water saving in hot regions: a review. *Sci. Hortic.* **201**, 36–45 (2016)
12. Moreno-Teruel, M., et al.: Effects of cover whitening concentrations on the microclimate and on the development and yield of tomato (*Lycopersicon Esculentum* Mill.) inside Mediterranean greenhouses. *Agronomy* **10**, 237 (2020). <https://doi.org/10.3390/agronomy10020237>.
13. Puglisi, R., Statuto, D., Picuno, P.: Effects of greenhouse lime shading on filtering the solar radiation. In: Proceedings of the 48th International Symposium, ATAE 2021 - Actual Tasks on Agricultural Engineering, 2–4 March 2021, Opatija, Croatia, pp. 131–140 (2021)
14. Meland, M., Skjervheim, K.: Rain cover protection against cracking for sweet cherry orchards. *Acta Hortic.* 441–448 (1998). <https://doi.org/10.17660/ActaHortic.1998.468.54>
15. Statuto, D., Picuno, P.: Micro-climatic effect of shading nets for crop protection in Mediterranean areas. In: Proceedings of the 45th Symposium on “Actual Tasks on Agricultural Engineering – ATAE 2017, Opatija (Croatia), 21–24 February 2017. UDC 502.7:631.95, pp. 613–622 (2017)
16. Statuto, D., Abdel-Ghany, A.M., Starace, G., Arrigoni, P., Picuno, P.: Comparison of the efficiency of plastic nets for shading greenhouse in different climates. In: Coppola, A., Di Renzo, G., Altieri, G., D’Antonio, P. (eds.) *Innovative Biosystems Engineering for Sustainable Agriculture, Forestry and Food Production. MID-TERM AIIA 2019*. LNCE, vol. 67, pp. 287–294. Springer, Cham (2019). https://doi.org/10.1007/978-3-030-39299-4_33
17. Statuto, D., Picuno, P., Abdel-Ghany, A.M.: Shading methods for crop protection under greenhouse in Mediterranean areas. In: Proceedings of the 47th International Symposium, Actual Tasks on Agricultural Engineering, 5–7 March 2019, pp. 297–306. Opatija, Croatia (2019)

Multi-Temporal Satellite Imagery for Monitoring Productivity Trend in Mediterranean Coastal Forest Ecosystems: The Study Case of the State Natural Reserve "Duna Feniglia" (Italy)



Francesco Solano , Salvatore Praticò , Giuseppe Modica ,
Giovanni Quilghini, and Gianluca Piovesan 

Abstract Health forests are recognized as a strategic solution for climate change mitigation and biodiversity conservation, allowing to achieve the goals of sustainable development (2030 Agenda). Those within protected areas represent a natural and cultural landscape asset and learning opportunity in many areas of the Mediterranean basin, especially in the coastal zones. Other than the transformations made by humans in the past, many factors influence the ecological dynamics of these forest ecosystems, such as an increase in the pressure of wild animals or the impact of global warming. This study aims to detect the changes in the Mediterranean vegetation growth rate over 21 years, from 2000 to 2020, by a satellite remote sensing multi-temporal monitoring approach. The proposed framework was applied in the state natural reserve “Duna Feniglia” in the province of Grosseto (central Italy), a restored forest ecosystem dominated by the stone pine (*Pinus pinea* L.), a forest type characteristic of the Italian coastal landscape. A multispectral vegetation index was evaluated as a proxy of forest productivity by means of trend curves analysis. Forest functionality (vigor) was also evaluated by developing a productivity state indicator, allowing for the

F. Solano (✉)

Dipartimento Di Scienze Agrarie E Forestali (DAFNE), Università degli studi della Tuscia, Via S. Camillo de Lellis, 01100 Viterbo, Italy
e-mail: f.solano@unitus.it

S. Praticò

Dipartimento di Agraria, loc. feo di Vito s.n.c, Università degli studi ‘Mediterranea’ di Reggio Calabria, 89122 Reggio Calabria, Italy

G. Quilghini

Reparto Carabinieri Biodiversità di Follonica, Via Emilio Bicchocci, 2, 58022 Follonica, Italy

G. Piovesan

Dipartimento di Scienze Ecologiche e Biologiche (DEB), Università degli studi della Tuscia, Largo dell’Università, 01100 Viterbo, Italy

G. Modica

Dipartimento di Scienze Veterinarie, Università degli Studi di Messina, viale G. Palatucci s.n., 98168 Messina, Italy

detection of current changes in primary productivity as compared to a medium-term baseline period. The presented monitoring data can support decision-making tool for an ecological management of the reserve, identifying potential areas of high vulnerability where to conduct new restoration action aimed to stop or prevent ecosystem degradation.

Keywords Vegetation Dynamic Assessment · Multi-Temporal Remote Sensing · Forest Management sustainability · Multispectral Vegetation Indices · Browning · Greening · Divergence

1 Introduction

Forests ecosystems play a fundamental role in the global carbon cycle, for mitigating future climate change and in providing essential ecosystem services for the social well-being. Those placed in protected area can contribute more to the new green deal goals as they can best perform their ecosystem functions [1] especially when stands recover from past disturbances. Studies remarks how high resilient forest could withstand and recover from environmental perturbations and be less sensitive to irreversible shift [2]. Meantime a global decline in recovery rates due to the critical slowing down (CSD) of system processes has been recently highlighted [3]. In this context, gain importance investigate how forest resilience is evolving in response to global change in different biomes. A first step is to increase knowledge of the dynamics of short- and long-term forest growth trend, in terms of productivity. The use of remote sensing-derived data has been widely adopted in these investigations because they have proven to be effective in assessing chlorophyll content [4], being a good proxy of vegetation productivity, and can guarantee long observational records of many parts of the world.

This study wants to be a first step to future explore the temporal variation in forest resilience by analyzing the productivity trajectory in the protected area of “Duna Feniglia”, in central Italy. This coastal forest ecosystem represents a semi-natural and cultural landscape component of the Italian Tyrrhenian coast, which is in an ongoing ecological recovery dynamic from an historical reforestation project [5]. Trend analysis was performed on satellite derived NDVI time series over the past 21 years (2000–2020) and recent productivity state was derived by comparison with an historical reference baseline. Results could help understanding the underlying mechanisms of forest resilience that are of paramount importance to develop ecological management and conservation plans.

2 Materials and Methods

2.1 Study Area

The state natural reserve “Duna Feniglia” is a protected natural area established in 1971 and managed by Italian Carabinieri Forestali. This area (Fig. 1), located in the municipality of Orbetello, in the province of Grosseto, is a “Tombolo” (i.e., a sandbar) that connects the Ansedonia hill to the east and the Mount Argentario to the west. It develops for about 6 km in length for a total area of ~ 500 hectares. The prevailing environment is the tombolo that delimits the nearby lagoon to the south and is almost entirely occupied by a stone pine (*Pinus pinea* L.) forest mixed with Mediterranean maquis and other broadleaved species. The southern edge consists of a sandy coast with typical dune vegetation, while the lagoon edge is occupied by more or less large expanses of vegetation of the brackish marshes [5]. For its different habitats of European interests and the presence of threatened nesting bird species, a site of the Natura 2000 ecological network was established following European Union’s Habitats Directive (Council Directive 92/43/EEC).

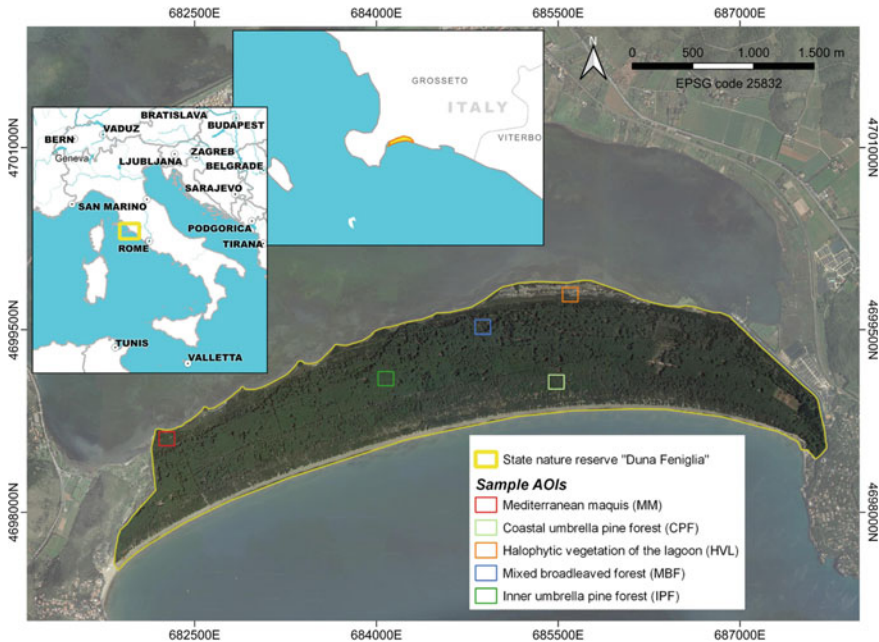


Fig. 1 State nature reserve “Duna Feniglia” study area. The colored squares represent the sample areas of interest (AOIs) for the deepening of the NDVI trend behavior

2.2 Data Collection

To explore the vegetation growth rate trajectory of the reserve we used the normalized difference vegetation index (NDVI) derived from satellite spectral reflectance data, as a proxy of vegetation productivity [6]. NDVI data acquired from the NASA Landsat 7 (L7) and Landsat 8 (L8) satellites were used for the period 2000–2020. In detail we processed the Landsat 7 Collection 1 Tier 1 NDVI Composite (for the period 2000–2012) and the Landsat 8 Collection 1 Tier 1 NDVI Composite (for the period 2013–2016) created from all the scenes in each 32-day period over the year. Both datasets were accessed via Google Earth Engine cloud computing platform [7] and the NDVI are calculated from Tier 1 orthorectified scenes, using the computed top-of-atmosphere (TOA) reflectance [8]. For the period 2017–2020 we used the single L8 images (with cloud cover less than 5%) which we then averaged to get the annual image on which the index was calculated.

2.3 Data Preprocessing

To visualize the presence of a trend in the data the raw NDVI time-series (2000–2020) was smoothed with the locally weighted scatterplot smoothing (LOWESS) function [9] which uses locally-weighted polynomial regression to fit a curve that matches the data points. The original L7 and L8 raw NDVI data were further smoothed to remove noise in the trend signal using the Savitzky-Golay (S-G) filtering method [10]. Then we averaged the NDVI value of each pixel, for each year, obtaining a raster images stack of the mean annual NDVI value for the considered time span for further processing. Prior to trend analysis we checked for serial correlation (autocorrelation) by the autocorrelation function (ACF) and the partial autocorrelation function (PACF) for a lag- k autocorrelation, that is the correlation between values in the time-series that are k time periods apart. All the analysis were performed with R statistical software [11].

2.4 NDVI Trend Analysis

To test the slope and the significance of the long-term NDVI trend on the annual NDVI raster stack, we computed an ordinary least square (OLS) regression at the pixel level to identify areas experiencing changes in primary productivity. A Mann-Kendall [12] non-parametric significance test was then applied, considering as significant only those changes that showed a p -value < 0.05 . Positive significant trends in NDVI would indicate potential improvement in vegetation condition, and negative values potential reduction in productivity. Statistical analyses were conducted in R environment.

Based on the trend analysis for the whole study area we selected 5 sample areas (Fig. 1) to be representative of the major different habitat and trend behavior, for further investigations. We collected our long-term NDVI reference data in a GIS environment via vector polygon, covering different area of interests (AOIs), after verification with field surveys and ground truth acquisition. The AOIs belongs to the umbrella pine forest of the inner part of the reserve (IPF), the coastal umbrella pine forest (CPF), the mixed broadleaved forest (MBF), the Mediterranean maquis (MM) and the halophytic vegetation of the lagoon (HVL).

For each AOI we implemented a productivity state indicator as proposed by the UNCCD [13] for the detection of recent changes in primary productivity trajectories with respect to a baseline period. We first set the baseline period for the comparison with recent productivity from 2000 to 2014 and the target period from 2015 to 2020. We used the last 5 years to avoid annual fluctuations related to climate. For the baseline period we computed a frequency distribution curve of the annual NDVI values that was used to define the 10 percentile classes cut-off values, from 1 to 10 (lowest to highest class). For each mean NDVI value of the baseline period we determined the percentile class it belongs to. We iterated this calculation also for the target period and the difference in class number between the comparison and the baseline period was then calculated. If the difference in the NDVI percentile class between the baseline and the target period was ≥ 2 , then we assumed there was a potential recent improvement in vegetation productivity. If the difference was ≤ 2 it would indicate a recent potential degradation in terms of productivity. Values between -1 to + 1 were considered as stable trend.

3 Preliminary Results and Discussion

The spatialization of the annual mean NDVI trend values shows divergent behavior (Fig. 2). Significantly increasing values are found in all internal parts, while significantly decreasing values are located along the coastal strip and the border with the lagoon. The trend analysis applied to the annual NDVI data, whose potential errors due to the failure of the L7 Scan Line Corrector (occurred on May 31, 2003) we have assumed negligible, showed a general increase in photosynthetic activity during the 21 years considered, with two minima in 2002 and 2014. The trend is growing until it reaches its highest peak in 2019 (Fig. 3).

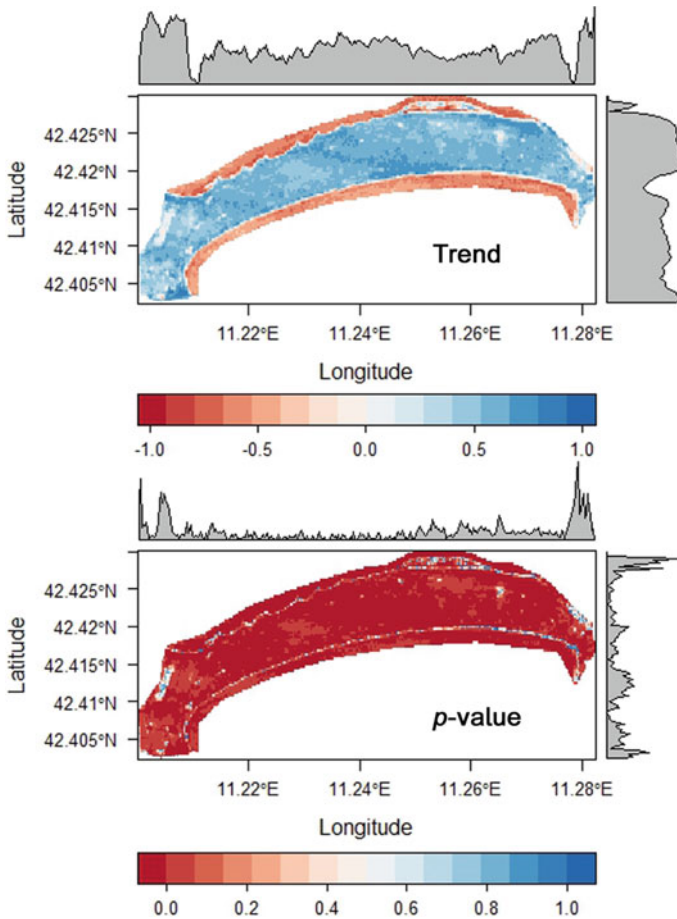


Fig. 2 Mann–Kendall trend test (above) and its significance (below) distribution at pixel level in the state nature reserve “Duna Feniglia” study area, derived from NDVI time series

The in-depth analyzes of the individual AOIs (Tab.1) show a common significant increasing trend for the pine forest habitats (IPF and CPF) with a higher rate in the inner pine forest (Fig. 4). Lower values are found in the vegetation of the Mediterranean maquis from 2000 to 2014, with the last five years up to levels of productivity similar to pine forests (Fig. 4). A decreasing long-term NDVI trend is visible for the lagoon habitat which would suggests a potential browning of this vegetation, while the broadleaved stand remain stable over the time considered.

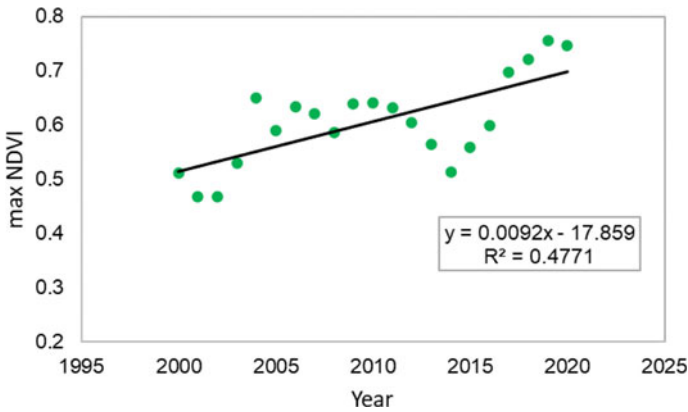


Fig. 3 NDVI trajectory of the state nature reserve “Duna Feniglia” study area, derived from maximum annual NDVI value fitted with an OLS regression

Table 1 Summary table of the Mann–Kendall test for the detection of a monotonic trend in the NDVI time series in each sample area of interest (AOI). Interior pine forest (IPF), costal pine forest (CPF), mixed broadleaved forest (MBF), Mediterranean maquis (MM), halophyte vegetation of the lagoon (HVL)

AOI	Kendall’s tau	Score	2-sided p-value	Denominator
IPF	0.629	132	< 0.001	210
CPF	0.600	126	< 0.001	210
MBF	0.138	29	0.397	209
MM	0.532	111	< 0.001	208
HVL	-0.610	128	< 0.001	210

The results of long-term trends are confirmed by the productivity state indicator referring to the last five years (Fig. 4). Recent improvements were detected for IPF, CPF, and MM while the potential degradation for HVL emerged as a long-term trend.

The overall changes of NDVI in the state nature reserve of Duna Feniglia is thus dominated by positive trends, confirming the overall pattern of greening of vegetation in southern Europe [14, 15] and the role of protected areas to protect biodiversity and ecosystem functionality [16]. Similar widespread greening NDVI trends after 1980 were reported in various studies conducted continentally and globally [17]. Despite the overall positive trend, the localized browning highlight the presence of factors that affect the vitality of vegetation such as coastal dynamics or saltwater intrusion [18].

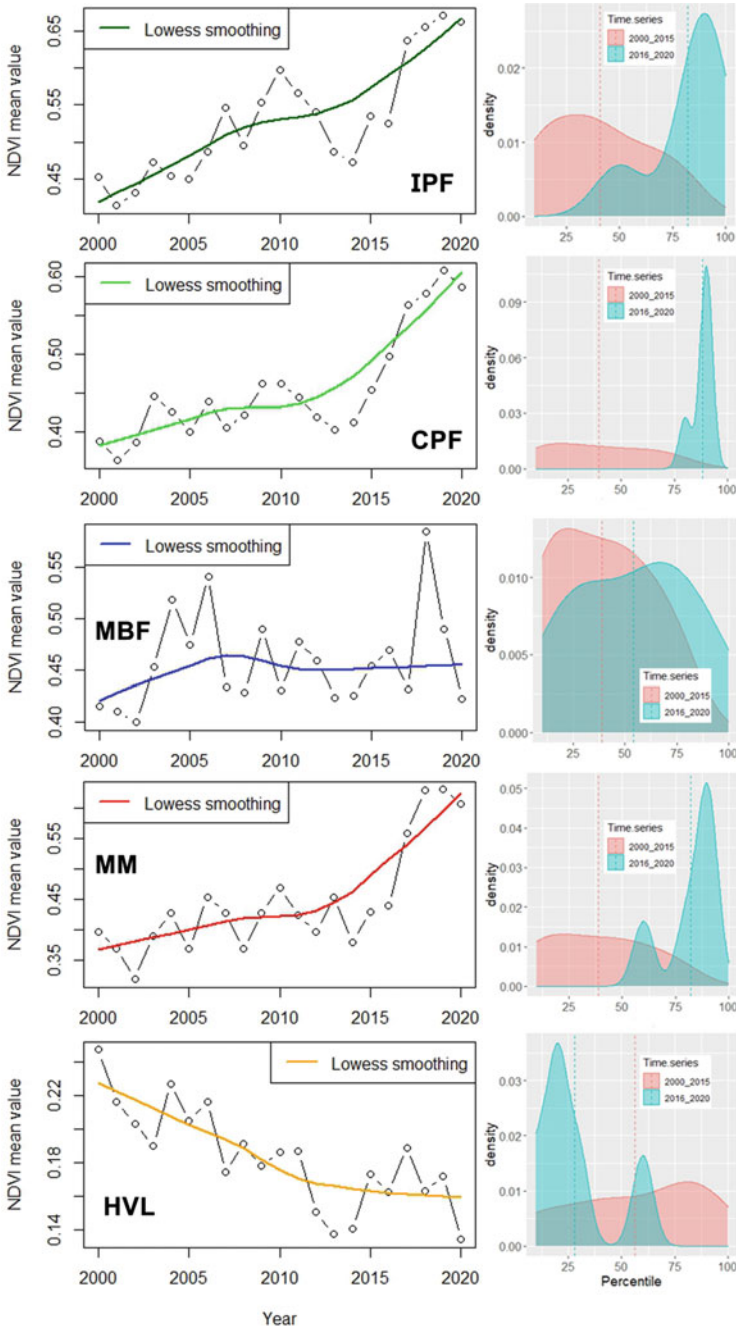


Fig. 4 Time series of mean annual NDVI value (left) of each AOI, fitted with a lowess smoothing function for visualization purpose. Frequency distribution of percentile class (right) of NDVI value of the baseline period (2000–2014) compared with the target period (2015–2020). Vertical dotted line represents the mean value

4 Conclusions

Forests within protected areas play an important role for countering the effects of global climate change and represent an effective natural based solution to preserve biodiversity and ecosystem services in many areas of the Mediterranean basin, especially in the coastal zones. Mediterranean area is a hotspot of biodiversity but also of climate change. Here, it is important to monitor ecosystem responses to withstand or recover from perturbations as their functionality and associated ecosystem services depends on health and resilient forests. This study detected divergent long-term trends in the productivity of vegetation in the state natural reserve “Duna Feniglia” in central Italy. Satellite remote sensing based NDVI series over 21 years, from 2000 to 2020, were collected and evaluated as a proxy of forest productivity. In general, a positive growing trend was observed in the productivity especially in stands dominated by stone pine (*Pinus pinea* L.), a forest type characteristic of the Italian coastal landscape. The establishment of a protected area have favored greening processes but local disturbances - such as those in the dune areas close to the sea or to the lagoon -, can cause browning and ecosystem degradation. Future studies are needed to validate the remote sensing data with dendrochronological analysis and investigate the main drivers of such divergent dynamics. This work represents a first step in monitoring a historical restored dune ecosystem to support an ecological management of the reserve and identify potential areas of high vulnerability, in which to decode and apply restoration programs to promote ecosystem resilience.

References

1. Solano, F., Praticò, S., Piovesan, G., Chiarucci, A., Argentieri, A., Modica, G.: Characterising historical transformation trajectories of the forest landscape in Rome’s Metropolitan area (Italy) for effective planning of sustainability goals. *Land Degrad. Dev.* **32**, 4708–4726 (2021). <https://doi.org/10.1002/ldr.4072>
2. Scheffer, M., et al.: Early-warning signals for critical transitions. *Nature* **461**(7260), 53–59 (2009). <https://doi.org/10.1038/nature08227>
3. Forzieri, G., Dakos, V., McDowell, N.G., Alkama, R., Cescatti, A.: Emerging signals of declining forest resilience under climate change. *Nature* **608**, 534–539 (2022). <https://doi.org/10.1038/s41586-022-04959-9>
4. Haboudane, D., Miller, J.R., Pattey, E., Zarco-Tejada, P.J., Strachan, I.B.: Hyperspectral vegetation indices and novel algorithms for predicting green LAI of crop canopies: modeling and validation in the context of precision agriculture. *Remote Sens. Environ.* **90**, 337–352 (2004)
5. Bellarosa, R., Codipietro, P., Piovesan, G., Schirone, B.: Degradation, rehabilitation and sustainable management of a dunal ecosystem in central Italy. *Land Degrad. Dev.* **7**(4), 297–311 (1996)
6. Camps-Valls, G., et al.: A unified vegetation index for quantifying the terrestrial biosphere. *Sci. Adv.* **7**(9), eabc7447 (2021)
7. Gorelick, N., Hancher, M., Dixon, M., Ilyushchenko, S., Thau, D., Moore, R.: Google earth engine: planetary-scale geospatial analysis for everyone. *Remote Sens. Environ.* **202**, 18–27 (2017). <https://doi.org/10.1016/j.rse.2017.06.031>

8. Chander, G., Markham, B.L., Helder, D.L.: Summary of current radiometric calibration coefficients for Landsat MSS, TM, ETM+, and EO-1 ALI sensors. *Remote Sens. Environ.* **113**(5), 893–903 (2009). <https://doi.org/10.1016/j.rse.2009.01.007>
9. Moran, G.W.: *Locally-Weighted-Regression Scatter-Plot Smoothing (LOWESS): a graphical exploratory data analysis technique*. Naval Postgraduate school, Monterey CA (1984)
10. Jönsson, A.M., Eklundh, L., Hellström, M., Bähring, L., Jönsson, P.: Annual changes in MODIS vegetation indices of Swedish coniferous forests in relation to snow dynamics and tree phenology. *Remote Sens. Environ.* **114**, 2719–2730 (2010)
11. R Core Team.: *R: A language and environment for statistical computing*. R Foundation for Statistical Computing, Vienna, Austria (2022). <https://www.R-project.org/>
12. Wessels, K.J., van den Bergh, F., Scholes, R.J.: Limits to detectability of land degradation by trend analysis of vegetation index data. *Remote Sens. Environ.* **125**, 10–22 (2012). <https://doi.org/10.1016/j.rse.2012.06.022>
13. Sims, N.C., et al.: *Good Practice Guidance. SDG Indicator 15.3.1, Proportion of Land That Is Degraded Over Total Land Area. Version 2.0*. United Nations Convention to Combat Desertification, Bonn, Germany (2021)
14. Pausas, J.G., Millán, M.M.: Greening and browning in a climate change hotspot: the Mediterranean Basin. *BioScience*. **69**(2), 143–151. (2019). <https://academic.oup.com/bioscience/article/69/2/143/5254231>
15. Gemitzi, A., Banti, M. A., Lakshmi, V.: Vegetation greening trends in different land use types: natural variability versus human-induced impacts in Greece. *Environ. Earth Sci.* **78**(5), 1–10 (2019). <https://doi.org/10.1007/s12665-019-8180-9>.
16. Solano, F., Modica, G., Praticò, S., Box, O.F., Piovesan, G.: Unveiling the complex canopy spatial structure of a Mediterranean old-growth beech (*Fagus sylvatica* L.) forest from UAV observations. *Ecol. Indic.* **138**, 108807 (2022). <https://doi.org/10.1016/j.ecolind.2022.108807>
17. Feng, X., Fu, B., Zhang, Y., Pan, N., Zeng, Z., Tian, H., Penuelas, J.: Recent leveling off of vegetation greenness and primary production reveals the increasing soil water limitations on the greening Earth. *Sci. Bull.* **66**(14), 1462–1471 (2021)
18. Barbarella, M., De Giglio, M., Greggio, N.: Effects of saltwater intrusion on pinewood vegetation using satellite ASTER data: the case study of Ravenna (Italy). *Environ. Monit. Assess.* **187**, 166 (2015). <https://doi.org/10.1007/s10661-015-4375-z>

Assessing Differences in Land Productivity Trends to Climatic Data in Arid and Semi-arid Zones: A Study Case in Northern Mozambique



Francesco Solano , Salvatore Praticò , Maria Nicolina Ripa ,
and Giuseppe Modica 

Abstract In recent years many efforts have been made to locate and measure land degradation worldwide to reach the target to reduce its progress, reduce poverty and increase food security and nutrition, following the United Nation Convention to combat desertification (UNCCD) and the Land degradation neutrality (LDN) initiative of the Sustainable Development Goals (SDG) of 2030 Agenda. Several international reports provide different guidance on the most suitable land degradation indicators, and methodological approach in measuring and monitoring them. Among all, land productivity indicator raised interest because it can be easily quantified and spatialized using remote sensing data and techniques, and influence that the various limiting factors have on its performance can be verified. Focusing on the land productivity trajectories, the objective of this study is to analyze how different climatic datasets and trend calculation methods may affect productivity analysis. Analysis was tested and validated in the northern part of Mozambique, as it is a climatically vulnerable zone whose natural resources are rapidly depleting in recent years due to deforestation actions and reduction of soil fertility. Long-term normalized difference vegetation index (NDVI) time series were used as a proxy of land potential productivity from 2001 to 2020. Results were tested for trend significance using different calculation methods and climatic dataset to analyze the effect of data to trend responses. Rainfall dataset was used for climatic signal as the rain is the main limiting factor in arid and semi-arid zones.

F. Solano (✉) · M. N. Ripa
Dipartimento di Scienze Agrarie e Forestali (DAFNE), Università degli Studi della Tuscia, Via S. Camillo de Lellis, 01100 Viterbo, Italy
e-mail: f.solano@unitus.it

S. Praticò
Dipartimento di Agraria, Università degli studi 'Mediterranea' di Reggio Calabria, loc. feo di Vito s.n.c., 89122 Reggio Calabria, Italy

G. Modica
Dipartimento di Scienze Veterinarie, Università degli Studi di Messina, viale G. Palatucci s.n., 98168 Messina, Italy

Keywords Land Degradation · NDVI Time Series · Trend Analysis · Multi-Temporal Remote Sensing · SDG

1 Introduction

In the last years, several national governments have signed agreement and commitments over global and regional targets to stop or slow down and reverse land degradation as well as restoring degraded lands [1]. These events pushed towards several initiatives to reduce land degradation in the near future, but despite that there is still a lack of clear and agreed rules on the measurement and assessment of degraded land, and the debate is still ongoing. With the latest “Good Practice Guidance” of the United Nations Convention to Combat Desertification (UNCCD) [2] about methodological indication on measuring and monitoring degradation indicators, a big step forward has been made in bringing together different theoretical backgrounds. The UNCCD suggests expressing land degradation based on the status of three main indicators that can be derived, quantified, and spatialized also using Earth observations data, giving a more practical approach to monitoring and reporting progress. Several countries are invited to adopt such methodologies as well as to implement them or designing new for planning policies for a sustainable future, contrasting land degradation. That’s how it gains interest to investigate how certain parameters can influence results. In this study we focused on one of the three indicators for estimating degradation, the land productivity, because vegetation indices time series, based on long-term satellite observation, are widely accepted as a proxy of net primary productivity (NPP) [3], allowing the development of several analysis techniques. We explored how different calculation methods and climatic dataset for calibration can affect trend significance responses. The analysis was tested in four of the northern provinces of the Republic of Mozambique (southeast Africa). In this climatically vulnerable zone, whose most of the national population is concentrated [4], natural resources are rapidly depleting in recent years due to deforestation actions and reduction of soil fertility, induced principally by agriculture and urban expansion [5].

2 Materials and Methods

2.1 Study Area

The Republic of Mozambique, located in southeast Africa, occupies a land surface of about 800,000 km² (Fig. 1). It is divided into 11 provinces of which four make up the study area: Cabo Delgado, Niassa, Nampula and Zambesi. This northern part contains most of the country’s population [4]. It is characterized by a diverse landscape including mountains, woodlands, savannah, and coastal plains. The climate

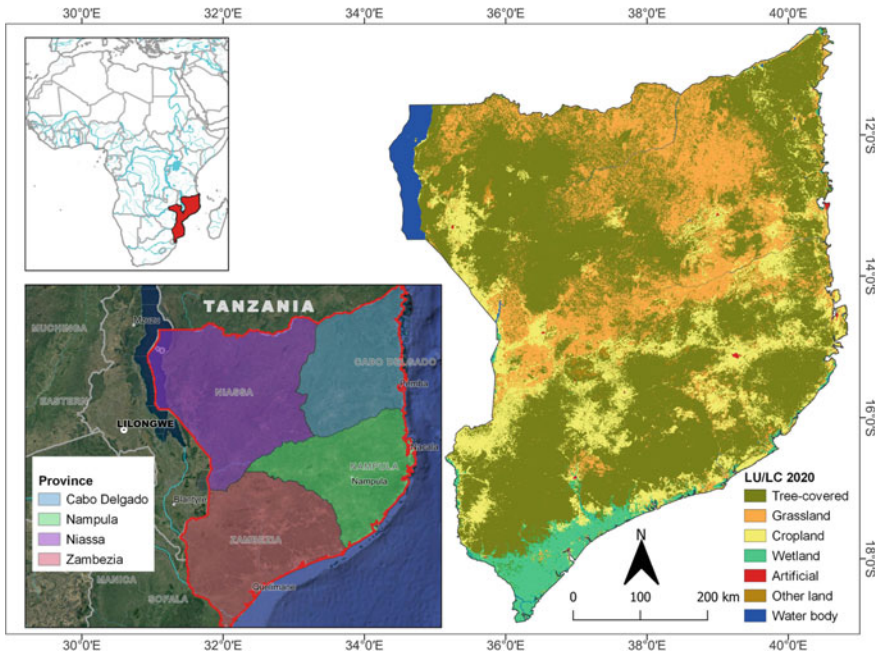


Fig. 1 Study area localization. Land Use/Land Cover (LU/LC) map is derived from the ESA CCI-LC product (<https://www.esa-landcover-cci.org/?q=node/164>), customized for visual purpose

is tropical (to subtropical), with a semiarid region in the southern part of the provinces and two seasons, a dry cool season and a rainy hot one. In this area, protected areas are interspersed with numerous large-scale agricultural investments [6, 7] which, in the last decade have meant that natural resources are rapidly depleting in this part of Mozambique [8].

2.2 Productivity and Climatic Datasets

Land productivity was estimated from satellite derived normalized difference vegetation index (NDVI) time series as a surrogate for deriving productivity information [3]. We used raw NDVI imagery from the 16-day MODIS NDVI products (MOD13Q1 V061) at a 250 m of spatial resolution [9], for the period 2001–2020. Data were collected via Google Earth Engine cloud computational platform [10]. To reduce the residual signal noise, the NDVI time-series was smoothed with a Savitzky–Golay filter [11]. Then we calculated the mean annual NDVI value for each pixel averaging the bi-monthly NDVI image over each year.

As the rain is the main limiting factor in arid and semi-arid zones, four different rainfall datasets were used for climatic signal covering the 2001–2020 period. The

Climate Hazards Group InfraRed Precipitation with Station data (CHIRPS) [12] at 0.05° spatial resolution, the Precipitation Estimation from Remotely Sensed Information using Artificial Neural Networks – Climate Data Record (PERSIANN-CDR) at 0.25° resolution, the Global Precipitation Climatology Centre (GPCC v7) at 1° resolution and the Global Precipitation Climatology Project (GPCP v2.3.1) at 2.5° resolution. Rainfall time series were downloaded and cumulated over each year using R statistical software [13] and were resampled at 250 m resolution allowing the analysis with the MODIS NDVI data.

2.3 Trend Analysis and Responses to Data

Land productivity was analyzed using three different methods on annual MODIS NDVI time series. An ordinary-least square (OLS) regression model was first fitted on the annual NDVI at pixel level. A Mann-Kendal (M–K) non-parametric test [14] was applied to examine the significance of the trend slope for p-value < 0.05. Each pixel was then classified as a significant positive or negative trend (hereafter NDVI trend). To separate the climatic effects on changes in productivity from other causes (i.e., human-induced land degradation) we used the widely accepted residual trend analysis (hereafter RESTREND) [15] that fits an OLS regression between the annual NDVI and the annual rainfall datasets at pixel level. Then another OLS regression is performed on the residuals (difference between the observed and the predicted NDVI value from the linear model) against time and the trend is tested via M–K test. Lastly, we used the rainfall use efficiency method (hereafter RUE) [16] calculated as the relation between annual NDVI and rainfall pixel values for each year under investigation. Then an OLS regression and a M–K test was applied to the RUE trend.

To investigate the sensitivity to the time window, we calculated the NDVI trend, RESTREND and RUE over two 15-year period, from 2001 to 2015 and from 2006 to 2020. We used CHIRPS data as default rainfall data for this analysis. We considered RESTREND using CHIRPS data as reference method to finally test the effect of the other three-monthly rainfall datasets to trend responses.

3 Results and Discussion

All the three methods show moderate significant increasing trends for the 2001–2015 period (between 8.4% and 14.5%) with higher detection rate with the RUE approach (Table 1, Fig. 2).

For NDVI trend and RESTREND, the negative trends are higher than the positive ones, especially during the 2001–2015 period with 23.1% and 19.5% respectively (Table 1). These first results, indicate that land conditions have been worsened during the first decade, also accentuated by unfavorable rainfall conditions for vegetation productivity [17].

Table 1 Proportion of land with significant annual productivity trends, calculated with three different methods, for the 2001–2015 and 2006–2020 periods

Trend slope	NDVI trend (%)		RESTREND (%)		RUE (%)	
	01–15	06–20	01–15	06–20	01–15	06–20
decrease ($p < 0.05$)	23.1	14.9	19.5	13.3	2.1	6.8
increase ($p < 0.05$)	8.4	21.7	11.3	26.8	14.5	25.7
stable	68.6	63.4	69.2	60.0	83.4	67.5

Confirming this is the fact that in all configurations the NDVI trend and the RESTREND showed always higher positive trend values than negative ones in the 2015–2020 period (Fig. 2). Only RUE shows a reverse trend. RUE may fail down because other factors than water are growth limiting, as in the case of very low-cover area [18], or where the growth response is too low to register a significant change. Results highlighted the high sensitivity of the methods to the period of analysis. Such differences may derive from the uneven assessment of land degradation estimations [19].

The annual trends calculated with RESTREND analysis with different rainfall datasets, for the period 2001–2020 (Fig. 3), showed that these northern provinces are characterized by significant trends due to other factors than rainfall. Values are very different ranging from 30.5% to 21% for significant increasing productivity and from 18.5 to 15% for land productivity decline.

The different rainfall datasets used in the RESTREND analysis had an impact on the significant trend's detection. In some cases, their impact was even larger than the climate calibration itself. Determining the best climate calibration methods is a challenging matter. Several calibration methods are available, each of which may be suitable only for detecting certain types or magnitudes of degradation, depending on certain vegetation types or climatic regions [20]. Due to their variation at different rates and spatial scales, some are better represented in existing datasets than others. Comprehensive correction may require advanced modelling approaches that are not described in this document.

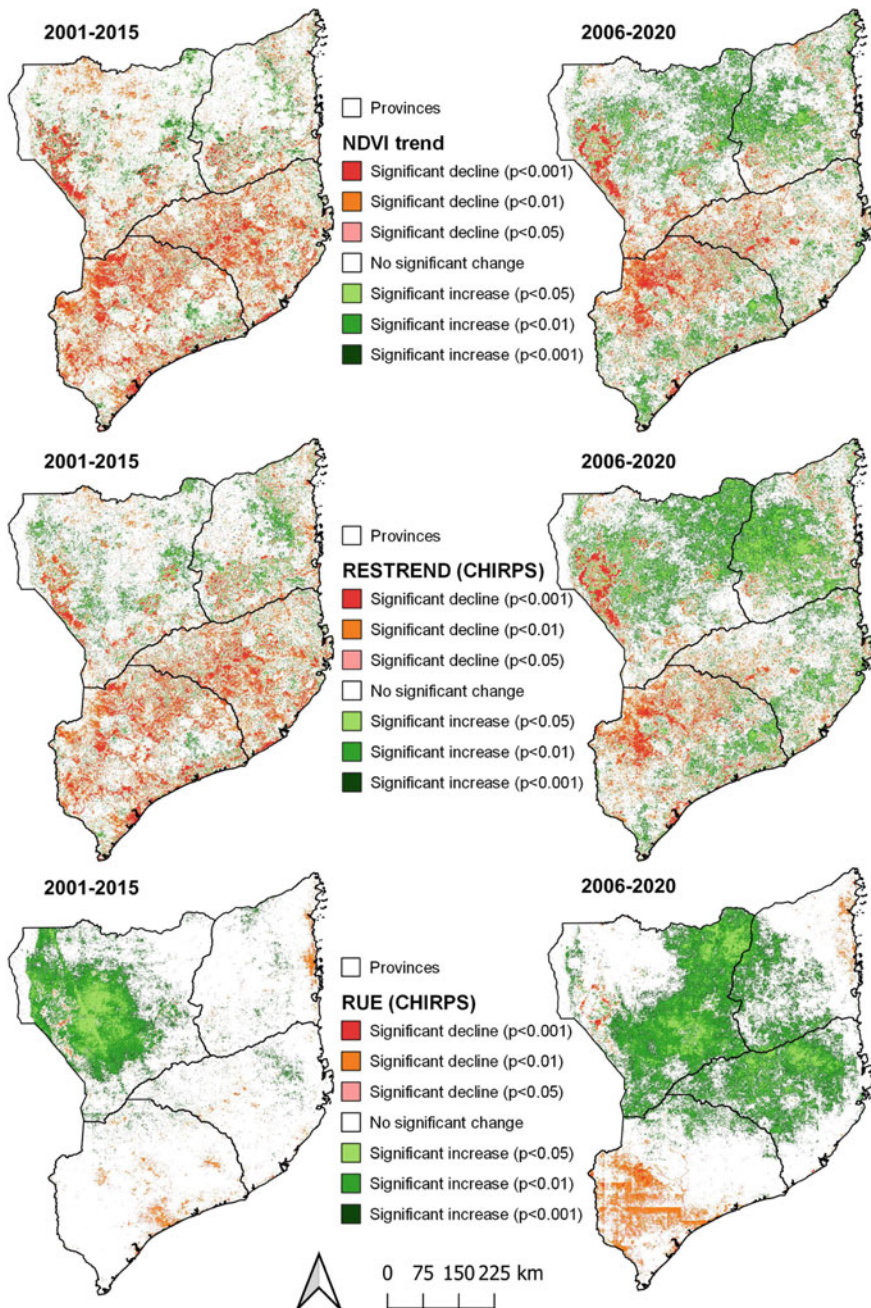
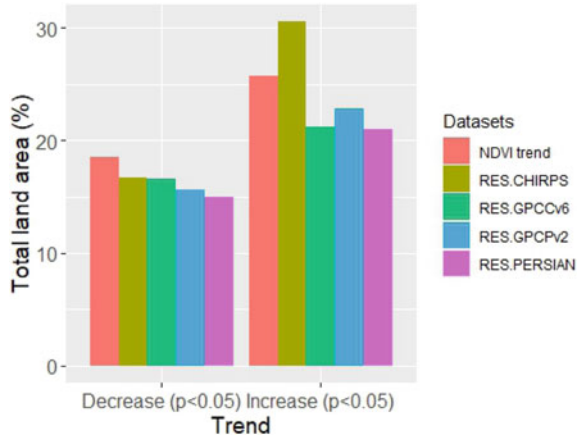


Fig. 2 Maps of the NDVI trajectory significance, calculated with NDVI trend, RESTREND and RUE methods, for the period 2001–2015 and 2006–2020

Fig. 3 Percentage of detected significant positive and negative NDVI trends and RESTREND, calculated with different rainfall datasets, over the 2001–2020 period in the study area



4 Conclusion

Following the United Nation Convention to combat desertification (UNCCD) and the Land degradation neutrality (LDN) initiative of the Sustainable Development Goals (SDG) of 2030 Agenda, several actions pushed towards to reduce land degradation. In this framework international reports provide guidance on the most suitable land degradation indicators, and methodological approach in measuring and monitoring them. Land productivity indicator raised interest because it can be easily inferred using remote sensing data. In this study we focused on how different climatic datasets and trend calculation methods may affect productivity indicator analysis using long-term normalized difference vegetation index (NDVI) time series. The northern part of Mozambique was used as study area as it is a climatically vulnerable zone whose natural resources are rapidly depleting in recent years. We showed that the land productivity indicator was sensitive to the period of analysis and the rainfall dataset used for RESTREND analysis. Rainfall dataset derived from remote sensing observations should be compared with local rain gauge data when available. A prior analysis of the best dataset and parameter for each country to perform RESTREND analysis should be encouraged as well as define a unique framework to make land degradation results and mitigation measures comparable.

References

1. UN Agenda 2030: Transforming our world: The 2030 Agenda for Sustainable Development. UN Publications, Paris (2015)
2. Sims, N.C., et al.: Good Practice Guidance. SDG Indicator 15.3.1, Proportion of Land That Is Degraded Over Total Land Area. Version 2.0. United Nations Convention to Combat Desertification, Bonn, Germany (2021)

3. Sims, N.C., Barger, N., Metternicht, G., England, J.R.: A land degradation interpretation matrix for reporting on UN SDG indicator 15.3.1 and land degradation neutrality. *Environ. Sci. Policy* **114**, 1–6 (2020)
4. Temudo, M.P., Silva, J.M.: Agriculture and forest cover changes in post-war Mozambique. *J. Land Use Sci.* **7**(4), 425–442 (2012)
5. GoM: Mozambique's Forest reference emission level for reducing emissions from deforestation in natural forests (p. 50). Retrieved from Ministério da Terra, Ambiente e Desenvolvimento Rural. República de Moçambique (2018). https://redd.unfccc.int/files/2018_frel_submission_mozambique.pdf
6. Mucova, S.A.R., Leal Filho, W., Azeiteiro, U. M., Pereira, M. J.: Assessment of land use and land cover changes from 1979 to 2017 and biodiversity & land management approach in Quirimbas National Park, Northern Mozambique, Africa. *Global Ecol. Conserv.* **16**, e00447 (2018).
7. Zaehring, J.G., Atumane, A., Berger, S., Eckert, S.: Large-scale agricultural investments trigger direct and indirect land use change: new evidence from the Nacala corridor. Mozambique. *J. Land Use Sci.* **13**(3), 325–343 (2018). <https://doi.org/10.1080/1747423X.2018.1519605>
8. Montfort, F., Bégué, A., Leroux, L., et al.: From land productivity trends to land degradation assessment in Mozambique: effects of climate, human activities and stakeholder definitions. *Land Degrad. Dev.* 1–17 (2020). <https://doi.org/10.1002/ldr.3704>
9. Didan, K.: MODIS/Terra Vegetation Indices Monthly L3 Global 0.05Deg CMG V061. distributed by NASA EOSDIS Land Processes DAAC (2021). <https://doi.org/10.5067/MODIS/MOD13C2.061>
10. Praticò, S., Solano, F., Di Fazio, S., Modica, G.: Machine learning classification of Mediterranean forest habitats in google earth engine based on seasonal sentinel-2 time-series and input image composition optimisation. *Remote Sens.* **13**(4), 586 (2021). <https://doi.org/10.3390/rs13040586>
11. Savitzky, A., Golay, M.J.E.: Smoothing and differentiation of data by simplified least squares procedures. *Anal. Chem.* **36**(8), 1639–1643 (1964). <https://doi.org/10.1021/ac60214a048>
12. Funk, C., et al.: The climate hazards infrared precipitation with stations - A new environmental record for monitoring extremes. *Scientific Data* **2**, 1–21 (2015). <https://doi.org/10.1038/sdata.2015.66>
13. R Core Team.: R: A language and environment for statistical computing. R Foundation for Statistical Computing, Vienna, Austria, (2022). <https://www.R-project.org/>
14. Warren, J., Gilbert, R.O.: Statistical methods for environmental pollution monitoring. *Technometrics* **30**(3), 348 (1988). <https://doi.org/10.2307/1270090>
15. Wessels, K.J., Prince, S.D., Malherbe, J., Small, J., Frost, P.E., VanZyl, D.: Can human-induced land degradation be distinguished from the effects of rainfall variability? A case study in South Africa. *J. Arid Environ.* **68**(2), 271–297 (2007). <https://doi.org/10.1016/j.jaridenv.2006.05.015>
16. Le Houerou, H.N.: Rain use efficiency: a unifying concept in arid-land ecology. *J. Arid Environ.* **7**(3), 213–247 (1984)
17. Masih, I., Maskey, S., Mussá, F.E.F., Trambauer, P.: A review of droughts on the African continent: a geospatial and long-term perspective. *Hydrol. Earth Syst. Sci.* **18**, 3635–3649 (2014)
18. Fensholt, R., et al.: Greenness in semi-arid areas across the globe 1981–2007—an earth observing satellite-based analysis of trends and drivers. *Remote Sens. Environ.* **121**, 144–158 (2012). <https://doi.org/10.1016/j.rse.2012.01.017>
19. Wessels, K.J., van den Bergh, F., Scholes, R.J.: Limits to detectability of land degradation by trend analysis of vegetation index data. *Remote Sens. Environ.* **125**, 10–22 (2012)
20. Kumar, L., et al.: Relationship between vegetation growth rates at the onset of the wet season and soil type in the Sahel of Burkina Faso: implications for resource utilisation at large scales. *Ecol. Model.* **149**, 143–152 (2002)

Impact of Agricultural Plastics on Rural Landscape: A Case Study in the “Metapontino” Agri-Food District (Southern Italy)



Dina Statuto, Giuseppe Cillis, and Pietro Picuno

Abstract Over the past century, the agricultural production has benefited from several factors that have exponentially increased its efficiency. One of the most significant aspects has been the growing use of novel materials, such plastics, which have made it possible to increase manufacturing in a straightforward and cost-effective manner. Different polymer kinds are utilized at various stages of the agricultural production cycle, but when their use is improperly controlled, it can have a variety of negative effects on the environment. In the present study, a practical and summarized system for managing agricultural plastics monitoring and planning has been proposed. The adopted methods are based on the quantification of areas covered by plastics for crop protection, deduced by various datasets of observed data (orthophotos and satellite pictures). Then, through an inductive approach - based on farmer interviews and statistical data – these two approaches have been cross-linked, and an agricultural plastic coefficient (APC) has been proposed, implemented and spatialized in a GIS environment, to produce a database of Agricultural Plastic Wastes (APWs).

Keywords GIS · Remote sensing · Agricultural Plastic Surface · Agricultural Plastic Waste · plastic management

1 Introduction

The increase in agricultural productivity has greatly enlarged in recent decades, due to various factors and technologies that have provided much benefit. Plastics, and new materials in general, have certainly been the most widely used technologies, as they allow for increased production, but at the same time they are easy to use and do not represent an excessive cost for producers [1]. Plastic polymers find use

D. Statuto (✉) · G. Cillis · P. Picuno

SAFE School of Agriculture, Forestry, Food and Environmental Sciences, University of Basilicata, Viale Dell'Ateneo Lucano, n.10, 85100 Potenza, Italy

e-mail: dina.statuto@unibas.it

in different stages of agricultural activity, from fertilization to irrigation, to storage of the final product. Each stage obviously involves the use of a different plastic product, but among the most widely used applications, there is mainly soil and crop protection through plastics for mulching, greenhouses, tunnels etc. [2]. Indeed, this use determines the largest percentage of plastic consumption in agriculture, which reached about 1.7 million tons in 2017 in the EU [3].

However, the use of plastics in agriculture causes significant environmental issues, as those associated with the improper management of significant amounts of post-consume waste. Frequent plastic replacement generates enormous amounts of post-consume materials. As a result, it's possible that macro-, micro-, and nanoplastics would be released into the air, surface and deep waters, and agricultural soil, hence migrating to cultivated crops [4] as well. Scientists are particularly interested in microplastics, since their existence and influence on agroecosystems are still poorly understood and because criteria for quantification are currently being researched. A large portion of these residues is caused by Agricultural Plastic Waste (APW), which is frequently handled carelessly and incorrectly dumped in landfills, being illegally burned in open fields, deposited along rivers or in marginal lands, or even incorporated in the soil. The improper management of APW results in severe environmental and economic issues, including ecosystem degradation, contamination of the soil and water, emission of hazardous pollutants into the air, contamination of food, etc. [5]

In the scientific community, this problem is currently quite prominent. The Sustainable Development Goals (SDGs) make numerous references to plastic pollution, as well as to its responsible usage and recycling. Although there are numerous alternatives to using plastics, it is still required to define approaches and procedures for proper monitoring and management at the local level, because this sector is still in its experimental stages. In this situation, efforts taken before managing APW after use, are crucial for implementing environmentally friendly planning strategies for disposal and recycling [6].

The first step in the way for a proper management is that of quantifying and locating plastics used in agriculture. To do this, GIS is the technology best suited for this purpose, as it provides the tools for both quantifying plastic surfaces and waste and the tools for their proper management and disposal.

In fact, with a GIS approach it is possible, in a first step, to spatialize plastics used in agriculture using different remote sensing data, such as the latest generation satellite images freely available online (for example, those from the Landsat or Sentinel-2 mission) or orthophotos produced by the various regional or national Authorities [7]. Subsequently, other types of statistical or descriptive data can be integrated, in order to quantify the actual amount of plastic present in a given portion of land. In addition, the geodata management capabilities of GIS software allows the implementation of spatial analysis for complex assessments of the impact of plastics on the surrounding environment [8].

In this paper, data produced with different deductive and inductive methodologies in two previous articles [9, 10] have been cross-linked, in order to quantify APW at the local scale in the “Metapontino” agri-food district (Basilicata region – Southern Italy).

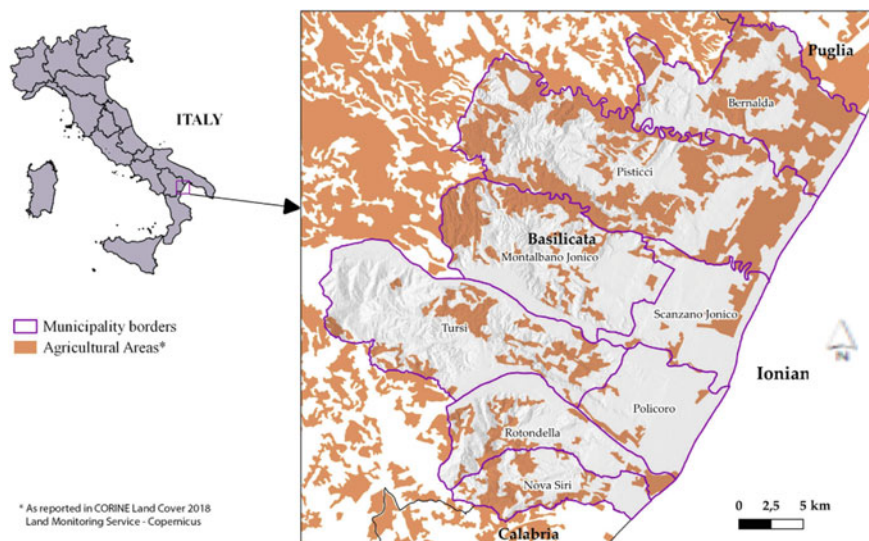


Fig. 1 Study area with agricultural areas as reported in Corine Land Cover 2018

2 Materials and Methods

2.1 Study Area

The eight municipalities in Basilicata region (*i.e.*: Bernalda, Montalbano Jonico, Nova Siri, Pisticci, Policoro, Rotondella, Scanzano Jonico, and Tursi) that are part of the “Metapontino” agri-food district, have been considered as a case study. This study area (Fig. 1) covers around 35 km of the Ionian Sea’s shoreline.

Currently, 26% of the active population in this area works in agriculture, which also generates more than 25% of the whole regional agricultural added value, with a value per hectare of € 2,314 - although only making up 9.4% of the UAA (Utilized Agricultural Area) of the whole Basilicata region. The primary agricultural activity in this region, which is also among the most significant in southern Italy, is the production of fruits and vegetables. In this region, plastic is frequently used, mostly for soil mulching, low- and medium- tunnels, greenhouse coverings, and other crop protection strategies (Fig. 2).

2.2 Agricultural Plastic Surface (APS) Quantification

In order to speed up the process of manually digitizing orthophotos, the use of satellite images has made it possible to detect APSs for the first time quickly and accurately

Fig. 2 Plastic types for strawberry production in the study area



[11]. The Sentinel-2 images that are available for free online download were chosen, because of their optimal spatial, temporal, and spectral resolution.

A Retrogressive Plastic Greenhouse Index (RPGI) proposed by Yang et al. [12], that can be useful for a more quick and practical methodology, was chosen to be tested for the current study. In addition, this can offer helpful information for a preliminary (even if incomplete) screening of locations containing APSs. The RPGI is an indicator that offers a binary classification (presence, absence of greenhouse plastics) and is heavily reliant on the vegetation growing under plastic, as it is higher when crops inside the greenhouse are flourishing. According to some Authors [11] and earlier studies [12], the RPGI (Eq. 1) was in fact calculated for regions where the Normalized Difference Vegetation Index - NDVI (Eq. 2) is less than 0.73. The Sentinel-2 bands B2, B3, B4 and B8 have 10 m spatial resolution and the central wavelengths (λ) measure, respectively, 492.4, 559.8, 664.6, and 832.8 nm.

$$RPGI = B2/1 - \text{mean}(B4 + B3 + B8) \quad (1)$$

$$NDVI = B8 - B4/B8 + B4 \quad (2)$$

The outcome of the previous process was vectorized using a GIS software (QGIS), and this served as the basis for fully digitizing the APS remains (Fig. 3) with the help of 2017 orthophotos at a resolution of 50 cm, which enabled the correction and integration of them in the appropriate way.

2.3 Agricultural Plastic Waste (APW) Estimation

The strategy outlined in this paper has been implemented in two different phases.

In one previous work [10], a coefficient was implemented to calculate the amount of plastic (Agricultural Plastic Coefficient - APC) per year [13]. The plastic greenhouse film ($\text{Kg hectare}^{-1} \text{ year}^{-1}$), mulch films ($\text{Kg} \cdot \text{hectare}^{-1} \cdot \text{year}^{-1}$), and irrigation pipes ($\text{Kg} \cdot \text{m}^{-1}$) were examined for the computation of APC, in view of type of

Fig. 3 Example of APS mapping for a portion of the study area



considered crops. These structures were primarily used to shelter crops from weathering, control growing conditions, reduce weed growth, and use less water [14]. The sum of the contributions due to the different types of agricultural plastics defined the total amount of plastic. From the product of this coefficient with data from the Italian Institute of Statistics (ISTAT) regarding horticultural cultivations, it is possible to calculate the amount of plastic (tons per year) with respect to the different Italian provinces. Then, in view of the fact that the study area notoriously represents almost all the fruit and vegetable agricultural areas in the whole province of Matera, it was possible to calculate the APW per unit area, by carrying out the product with the APSs identified by remote sensing.

The second phase is about testing a methodology to be able to clusterize the APS of a specific cultivation (strawberry cultivation in greenhouses) using the APCoeff. The coefficient is then applied and examined (in a GIS environment) through spatial join operations to create a database of APW amounts for the study area. In order to test the methodology, the 32% of plastic areas were chosen based on the statistical information and field surveys previously conducted, assuming that a strawberry crop is present under cover. This crop was chosen because it is the most representative of the considered study area and the percentage value is derived from the elaborations made for the inductive method [10]. By doing so, although not responsive to reality, it was possible to apply the developed techniques which, thanks to the ease of modulation and updating in the QGIS environment, can be immediately modified.

In Table 1, the calculation of coefficients with respect to different characteristics of plastics used in greenhouse strawberry cultivation is shown.

Then, using the basic tools of QGIS software, a join was made between the APC and APS data, in order to map the amounts of APW through the product between the area cultivated with strawberries in greenhouse and the relevant calculated APC. Additional spatial operations and specific tools were carried out after quantification. The APWs were combined and interpolated using a regular hexagonal grid for more effective management, in order to simplify geographic mapping processes or to minimize the subjectivity introduced by aggregations based on administrative boundaries [14].

Table 1 Technical properties of plastics and calculation of APCoeff for greenhouse strawberry cultivation. In this table, $\text{kg} \cdot \text{m}^{-2} \cdot \text{years}^{-1}$ have been converted to $\text{Kg} \cdot \text{ha}^{-1} \cdot \text{years}^{-1}$

Crops	Plastic tipology	Thickness ^a (μm)	Density ^b ($\text{Kg} \cdot \text{m}^{-3}$ or $\text{Kg} \cdot \text{m}^{-2}$)	Years (n.)	CACorr (adim.)	APC ($\text{Kg} \cdot \text{ha}^{-1} \cdot \text{years}^{-1}$)
Strawberry in Greenhouse	Plastic films	160	1250	2	1.5	1,500
	Mulch films	20	1300	2	0.77	100
	Irrigation pipes		0.008	2	1.1	40
	Tot [APC_tot]					1,64

^aFor the calculation of the APC, the value was converted to meters

^bAs stated in the article, $\text{kg} \cdot \text{m}^{-2}$ refer to irrigation pipes only

3 Results and Discussion

Related to the year 2017, accurate plastics mapping was made possible by the used methodologies, which combine manual and semiautomatic mapping. From the deductive methodology based on remote sensing data [9], it emerges that there are 2,062.23 ha of APS in the study area. Instead, from the inductive methodology, about 1875 tons of APW were quantified [10] so from their ratio it can be estimated that about 900 kg per hectare of APW were produced in the considered study area.

The selection, which covered about 32% of the total APS, allowed the proposed methodologies to be tested in a fully illustrative manner (Fig. 4).

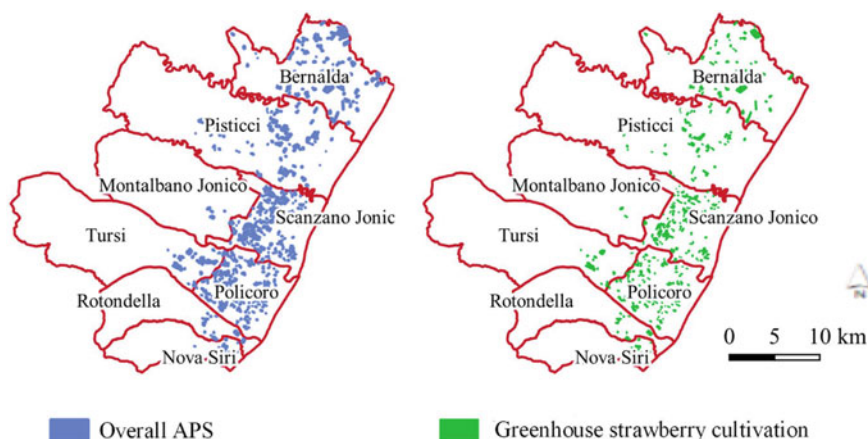


Fig. 4 Overall APS and selection of APS identified as greenhouse strawberry cultivation

The further application has enabled the quantification of APW within the study area. However, the interpolation of the APW within the hexagonal grid, made it feasible to identify the locations with the greatest APW concentration, allowing for a more accurate investigation of the distribution of the quantity of APW present in the research area. A maximum value of 75% was identified, when the APW concentration in cells was separated into percentage groups (Fig. 5). The proposed methodology, which is pivotal to the use of a GIS approach, represents a step forward in quantifying potential plastic waste generated by agricultural activities [15]. The ease of implementation, updating and modeling allow the applicability of these techniques at different scales of investigation. In this study, a hypothetical distribution of strawberries grown in greenhouses was considered, but in the future, combining the remote sensing approach with census data at the municipal level will allow the actual study of APW at the local level and thus provide usable data for decision support tools aimed at agricultural waste management [16].

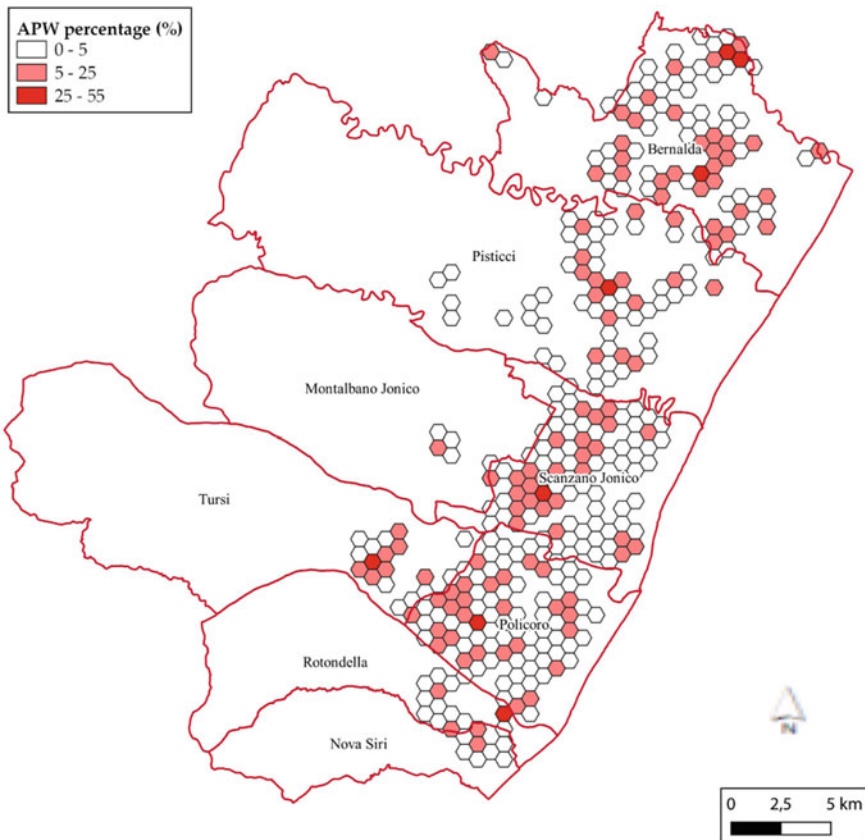


Fig. 5 For every hexagonal cell, the APW is reported as a percentage

4 Conclusions

In order to effectively reuse or dispose of agricultural plastics, it is therefore possible to quantify the amount of agricultural plastics present and analyze their spatial distribution in relation to the territorial context using a GIS environment. The findings of this study has been to provide an initial methodology to estimate at local level the APS by taking benefit from both the methodology of localization of plastics in a remote sensing manner (deductive approach) and that based on statistical data (inductive approach). Future applications, mostly through cross-linking these two different but convergent approaches, may enable the definition of a reliable system for the estimation of geographical distribution of agricultural plastics, so as to make easy and economically convenient their collection, transportation and recycling, so contributing to reduce the plastic footprint of agriculture.

Acknowledgements This research was funded by the Project “Plastic in Agricultural Production: Impacts, Lifecycles and Long-term sustainability—PAPILLONS”, financed by the European Union—Topic: SFS-21-2020 emerging challenges for soil management—Sub-Topic B [2020]: emerging challenges for soil management: use of plastic in agriculture (RIA)—grant agreement ID: 101000210.

References

1. Food and Agriculture Organization of the United Nations (FAO). Food and Agriculture: Driving Action across the 2030 Agenda for Sustainable Development. Rome, Italy (2017). <http://www.fao.org/3/a-i7454e.pdf> Accessed 5 Aug 2022
2. Picuno, P.: Innovative material and improved technical design for a sustainable exploitation of agricultural plastic film. *Polym. Technol. Eng.* **53**, 1000–1011 (2014)
3. Plastics Europe. Plastics—The Facts (2018). <https://plasticseurope.org/wp-content/uploads/2021/10/2018-Plastics-the-facts.pdf> Accessed 1 Aug 2021
4. Kumar, M., et al.: Microplastics as pollutants in agricultural soils. *Environ. Pollut.* **265**, 114980 (2020)
5. Picuno, C., Godosi, Z., Kuchta, K., Picuno, P.: Agrochemical plastic packaging waste decontamination for recycling: Pilot tests in Italy. *J. Agric. Eng.* **50**, 99–104 (2019)
6. de Sousa, F.D.B.: The role of plastic concerning the sustainable development goals: the literature point of view. *Clean. Responsible Consum.* **3**, 100020 (2021)
7. Parlato, M.C., Valenti, F., Porto, S.M.: Covering plastic films in greenhouses system: a GIS-based model to improve post use sustainable management. *J. Environ. Manag.* **263**, 110389 (2020)
8. Blanco, I., Loisi, R.V., Sica, C., Schettini, E., Vox, G.: Agricultural plastic waste mapping using GIS. A case study in Italy. *Resour. Conserv. Recycl.* **137**, 229–242 (2018)
9. Cillis, G., Statuto, D., Schettini, E., Vox, G., Picuno, P.: Implementing a GIS-based digital atlas of agricultural plastics to reduce their environmental footprint; Part I: a deductive approach. *Appl. Sci.* **12**(3), 1330 (2022)
10. Cillis, G., Statuto, D., Schettini, E., Vox, G., Picuno, P.: Implementing a GIS-based digital atlas of agricultural plastics to reduce their environmental footprint: Part II, an inductive approach. *Appl. Sci.* **12**(15), 7545 (2022)

11. Ibrahim, E., Gobin, A.: Sentinel-2 recognition of uncovered and plastic covered agricultural soil. *Remote. Sens.* **13**, 4195 (2021)
12. Yang, D., Chen, J., Zhou, Y., Chen, X., Chen, X., Cao, X.: Mapping plastic greenhouse with medium spatial resolution satellite data: development of a new spectral index. *ISPRS J. Photogramm. Remote Sens.* **128**, 47–60 (2017)
13. Briassoulis, D., et al.: Review, mapping and analysis of the agricultural plastic waste generation and consolidation in Europe. *Waste Manag. Res. J. Sustain. Circ. Econ.* **31**, 1262–1278 (2013)
14. Dharmawan, R.D., Suharyadi, P., Farda, N.M.: Geovisualization using hexagonal tessellation for spatiotemporal earthquake data analysis in Indonesia. *Robotics* **788**, 177–187 (2017)
15. Duque-Acevedo, M., Belmonte-Ureña, L.J., Cortés-García, F.J., Camacho-Ferre, F.: Agricultural waste: review of the evolution, approaches and perspectives on alternative uses. *Glob. Ecol. Conserv.* **22**, e00902 (2020)
16. Zhai, Z., Martínez, J.F., Beltran, V., Martínez, N.L.: Decision support systems for agriculture 4.0: survey and challenges. *Comput. Electron. Agric.* **170**, 105256 (2020)

Geospatial Tools Applications for the Analysis of Attractive Sources Related to Airport Wildlife Strike



Triflò Domenico, D.'Urso Provvidenza Rita, and Arcidiacono Claudia

Abstract Variation in attractive sources around airports deriving from territorial development and landscape transformations may have an effect on the increase of risks for aviation as well as on wildlife protection. In both the rural and urban environments, the presence of wildlife attractive sources in the airport surroundings increases the risk of collision between a wild animal and an aircraft, named 'Wildlife Strike'. The main objective of this study involved the acquisition of basic knowledge useful to control this risk around airports in different seasons. To this aim, supervised classification of open-source remote sensing imagery made available within the ESA Copernicus program was considered as an easy and low-cost solution to the problem of information updating. The integration of this information into a GIS allowed localisation of vegetation and water surfaces bodies in relation to airport 'Obstacle Limitation Surfaces' (OLS), 'Rete Natura 2000' (SIC/ZSC and ZPS) areas, and the 'Important Bird Areas' (IBA) that play a key role in birdlife protection. The case study was related to the 13-km territorial area surrounding the airport of Catania, Italy. In detail, the vegetation coverage was found to increase to about 40% of the total investigated area from summer to early spring. The monitoring of these attractive sources for wildlife, in different seasons of the year made it possible to obtain information about the periods in which it is most useful to reduce the risk. Further geostatistical analyses of kernel density performed by using GIS tools have defined the areas of greatest importance in relation to the weight of their suitability and proximity to the airport considered.

Keywords Wildlife strike · Sustainable management · Remote sensing · GIS · Automated classification · Heatmap

T. Domenico · D. P. Rita · A. Claudia (✉)

Department of Agriculture, Food and Environment, University of Catania, Via S. Sofia N.100,
95123 Catania, Italy

e-mail: *claudia.arcidiacono@unict.it

T. Domenico

e-mail: domenicotrifilo@gmail.com

1 Introduction

In territorial development, the presence of airport infrastructures on the territory plays an essential role for long-haul transportation. It affects landscape transformations as the location of the main national and international airports is usually on the edge of urban areas, so that they are close enough to the most densely populated centres to serve, but remaining in areas adjacent to them.

Therefore, the identification of the environmental risks that affect airport activity need to be carried out at airport surroundings. This implies that a unique situation for each airport comes out in relation to the resources that exist in its catchment area.

Specifically, obstacles and hazards to aviation constitute a serious threat for aviation safety deriving from the surrounding territory, which has to be monitored and handled by airport operators. Among those risks, Wildlife Strike (i.e., the collision between an aircraft and a wild animal; Bird strike in the specific case of birds) is a highly relevant occurrence during aircraft take-off or landing.

In this field, since aircraft collisions with wildlife pose a serious and growing threat to civil aviation safety, the aviation authorities at the different levels, i.e., national and international, have ruled on this issue and produced specific norms and guidelines.

In detail, ICAO (International Civil Aviation Organization) reported that: “Airports should conduct an inventory of bird/wildlife attracting sites within a 13 km circle centred on the ARP, paying particular attention to sites close to the airfield and the approach and departure corridors”. And: “An analysis of this data reveals that approximately ninety per cent (90%) of bird/wildlife strikes occur on or in the immediate vicinity of airports” [1]. Also, ENAC (Italian Civil Aviation Authority) states that “about 90% of the reported impacts for civil aviation occur inside or near airports, especially during take-off and landing. This is due, among other reasons, also to the fact that the air stations constitute an ideal habitat for many ornithic species, including gulls (*Larus spp.*), lapwings (*Vanellus spp.*), birds of prey and starlings (*Sturnus vulgaris*) or some of the most dangerous species for air navigation” [2].

Based on these prescriptions, the airport operators have to collaborate with aviation authorities and the other actors involved and competent in the land management, in order to counteract Wildlife strike phenomenon in the airport surroundings, in full respect of the priority habitats existing in the area. The success of this collaboration, and of the specific interventions to lower the risk, is strictly related to the information on the level of contribution that habitats have in attracting birds, in relation to the season [3].

It is recognised that factors influencing bird strike events depends to some extent on their spatial distribution, but few previous studies have focused on this issue [3–5]. Shao et al. [6] and Pfeiffer et al. [4] have utilised a multi-temporal and multiscale approach, respectively, to analyse the main attractive sources for birdlife, which have been identified as specific land uses within buffer zones by Robinson et al. [7]. Based on these previous experiences, the main aim of this study was the analysis of attractive

sources related to airport Bird strike through the application of geospatial tools, such as those available in GIS and remote sensing systems, in order to define a multi-temporal model suitable to monitor attractive sources during time and constituting a decision tool for the stakeholders involved in the territorial governance. Innovative aspects of the research include:

- Implementation of supervised classification of open-source satellite images and use of open-source software for atmospheric correction with the aim of localisation and monitoring over time of the main attractive sources for birdlife.
- application of a decision-making model of suitability, created on an open-source GIS basis, which allowed geostatistical analyses aimed at identifying the habitats and priority corridors most frequented by wild species in relation to attractive sources, relating them to the main high-value naturalistic areas in the airport surroundings and to the airport Obstacle Limitation Surfaces (OLS).

2 Materials and Methods

2.1 *The Study area Localisation*

In accordance to aviation norms [1], the study area has been identified as the area within 13 km from ARP (Aerodrome Reference Point) of Catania International Airport in Sicily (Italy), which is located south of Catania metropolitan city (Fig. 1). Within this 13-km buffer from the ARP, both the urban center of Catania and the towns that are part of the external metropolitan area fall in the north, while the rural and agricultural areas are located in the south and south-west; to the east the buffer encompasses a portion of the coast on the Ionian Sea.

2.2 *Imagery Acquisition and Elaboration, Data Processing, and Image Classification*

With reference to environmental risks affecting airport activity, the land use data used in this study were extracted from the satellite multispectral sensors of the Copernicus program, the platform created by the European Union to monitor the Earth and its ecosystems, which is based on a family of dedicated satellites named “*Sentinel*”.

In detail, the multispectral images utilised were acquired by Sentinel-2, polar-orbiting satellites of the imaging mission at high multispectral resolution, which is aimed at monitoring land surface conditions (e.g., vegetation, soil, and coastal areas). Each satellite is equipped with a single payload: the Multispectral Instrument (MSI). Through MSI, Sentinel 2 is capable of acquiring 13 spectral bands with wavelengths between 443 and 2190 nm at various spectral resolutions: 10 m (4 bands in the visible and near infrared – bands 2, 3, 4, and 8), 20 m (6 bands in the infrared – bands 5,

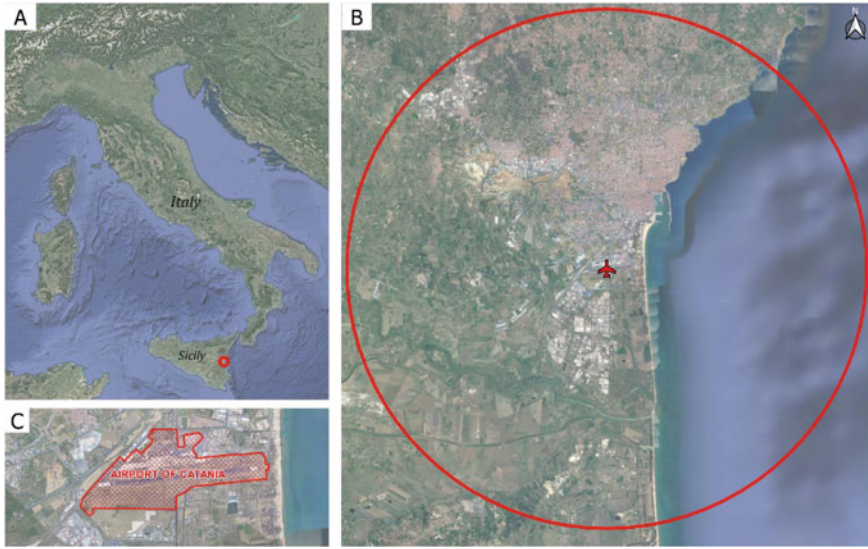


Fig. 1 Localisation of the study area: **a** area within Sicily (Italy); **b** area within 13 km from the ARP (Aerodrome Reference Point) of the Catania International Airport in Sicily (Italy); **c** airport grounds area

6, 7, 8A, 11, and 12), and 60 m (3 bands for atmospheric correction, one in the blue interval, and two in the infrared – bands 1, 9, and 10).

The selection of data collected and analysed for the model proposed in this study regarded three days belonging to three periods of the year that are significant for bird strike: summer period, and spring and autumn migrations [8]. These days were selected, in relation to the satellite revisit period, among those in which the percentage of cloud cover was the lowest of the period. The Sentinel 2 imagery were downloaded from the Copernicus “Open Access Hub” and then elaborated by using the software “SNAP” (Sentinel Application Platform) version 6.0, made available by ESA (European Space Agency). In detail, the elaboration of the multispectral images required the application of the “Sentinel-2 Toolbox” and the “Sen2Cor” Plugin, which performs the atmospheric correction from BOA (Bottom Of Atmosphere) to TOA (Top Of Atmosphere) thus producing Sentinel-2 Level 2A products, named L2A hereafter, that constituted the basis of the subsequent elaborations.

The requirement of standardisation for the multispectral bands having different spatial resolutions was fulfilled by using an additional Plugin, named “Sen2Res”. It allowed improving the spatial resolution of Sentinel-2 products to 10 m/pixel still preserving their reflectance. In detail, the bands 2, 4, 8, 11, and 12 were utilised in this study in the combinations Agriculture, Shortwave infrared, and Geology.

The classification of L2A images was carried out through the following three phases: Training, Classification, Assessment, according to the supervised classification method [9]. In the Training phase, the spectral signatures of the considered

land use classes (i.e., water, uncultivated areas, urban areas, and vegetation) were defined by selecting the representative pixel samples (areas of interest - AOI) for each class by visual analysis on the orthophotos of the area. In the SNAP software, training and testing points were derived each from 50% of the samples. In the Classification phase, the software classified the image based on the spectral signatures of the samples. The methodology proposed in this study included the application of the supervised classification by using the Maximum Likelihood Classifier (MLC), according to studies in the field [11]. In the Assessment phase, the accuracy of the thematic map produced after the supervised classification was assessed through the computation of metrics (Accuracy, Precision, Correlation and Error Rate) calculated on *testing* samples.

2.3 Data Acquisition and Elaboration Through Gis Analyses

After the classification process, the produced thematic maps of the attractive sources considered, i.e., vegetation and surface water, were elaborated in the QGIS open source software for the three days considered. Besides these layers, in the GIS project other naturalistic data were added in order to support the subsequent analyses related to the complex territorial framework. These data included “Rete Natura 2000 (SIC/ZSC and ZPS)” and “Important Birds Areas – IBA”. These areas represent protected priority habitats of high naturalistic and faunal value, which make it possible for the model to consider and highlight the location of the environments to be protected and their position with respect to the attractive sources and the airport considered.

The methodology proposed in this study included geostatistical analyses aimed at identifying the main naturalistic corridors in the airport surroundings in relation to the main areas of high naturalistic value present (SIC/ZSC, ZPS, and IBA). To this end, Heatmaps were produced, i.e., a graphical representation where density of points and their associated weight define the colour of the area. To obtain the Heatmap, the centroid of each pixel was computed by applying the specific GIS tool, and different weights were associated based on their presence in the various surfaces (Table 1). The weight was defined by attributing an increasing value in relation to the naturalistic value of the area.

Table 1 Table of weights associated to surfaces for the geostatistical analysis

Weight	Surfaces
1	No Data
2	Attractive Areas (vegetation and water)
3	attractive areas + high nature value areas (IBA and Natura 2000)

3 Results

The results related to the attractive sources quantification, obtained by the supervised classification of the study area in the three periods considered, are described in Table 2. It shows a summary of the percentages calculated as the ratio between the surface of the attractive sources and the total surface of the area.

This analysis proved that the attractive areas located within the area showed a different pattern: a significant increase in vegetation cover over time, from summer to early spring migration, increasing from 9.7% up to 40% was found; whereas the surface areas of water showed a low variation in the three periods. Hence, it can be highlighted how, although in summer a greater risk of bird strike is generally expected [8], the vegetated surfaces in the investigated area show a ratio of 1:3–1:4 compared to those recorded during the autumn and spring migrations. Therefore, the periods in which it is most useful to reduce the risk in this study area are also migration periods. Actually, the ENAC/BSCI Wildlife Strike annual report [12] for the airport of Catania proves that there has been an increase in the birdlife monitored in the airport grounds from 2015 to 2017 and highlights how in the spring and summer periods the highest number of bird strikes has been recorded. Therefore, the importance of the airport location is crucial and specific for the analysis of its relation with the environment [8].

Further outcomes can be derived from the results of the statistical analyses, through Heatmap production, obtained by weighting the importance of the surfaces in relation to the areas with high naturalistic value, reported in Fig. 2 for the autumn migration period.

In Fig. 2, the density of the attractive areas is depicted at different scales of detail, from 1:200,000 to 1: 50,000.

Moreover, the images of Fig. 2 emphasised how the highest values are registered in the sea areas near the coast compared to the inner areas of the territory. This is due to the higher density of the points in the coastal area. Finally, although kernel analysis highlighted how the areas with high naturalistic value are places of potential risk, however the analysis shows that there are also other attractive vegetational sources on which attention should be focused, particularly in the airport surroundings.

Table 2 Surface area [km²] of attractive sources and percentage over the 13-km area in different periods of the year

	Summer (km ²)	% over 13-km area	autumn migration (km ²)	% over 13-km area	spring migration (km ²)	% over 13-km area
Vegetation cover	51.24	9.7	162.41	30.6	212.10	40.0
Surface water	179.37	33.8	177.61	33.5	178.42	33.6

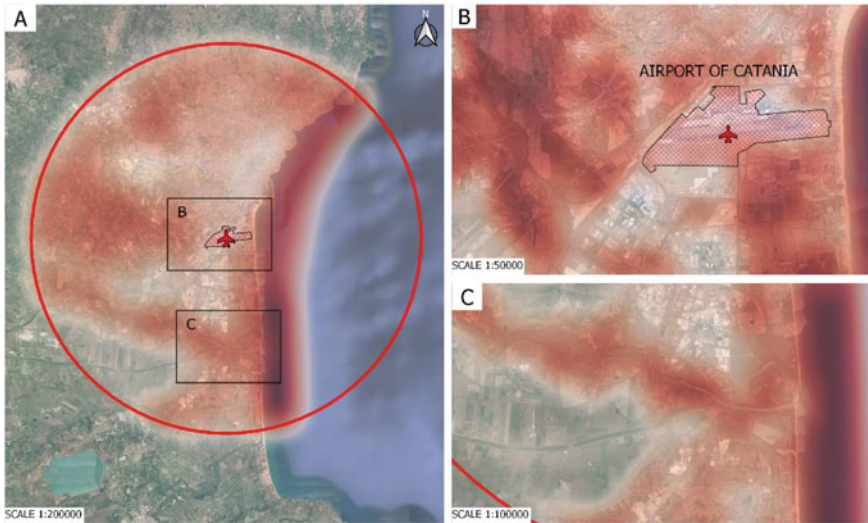


Fig. 2 Autumn migration Heatmap, at different scales of detail: **a** 13-km radius area at 1:200,000; **b** detail of the area surrounding the airport grounds at 1:50,000; **c** detail of the Simeto river area at 1:100,000

4 Discussion

In this study, a research methodology has been proposed to contribute to the improvement and optimisation of the management of the risk linked to the “Wildlife Strike” in the airport environment, from the point of view of both monitoring airport surroundings to increase flight safety and to protect the priority habitats used by the fauna species living in the airport surroundings. The overall aim of this study was to support the improvement of a more sustainable bird strike risk management from the point of view of increasing ecosystems protection around airports.

It is recognised that the landscape structure and composition around the airports has an influence on bird strike [4]. Recently, the spatial and seasonal variations around airports has been considered in bird strike research [3, 13]. In detail, an increase in bird strike at heights greater than 153 m has been observed and the elimination of bird attractors within a 5 km radius from the airport is suggested. Moreover, farmland and wetlands are primary reason for the increase of bird number and risk of bird strike, and risk was found to be lower in winter when landfills are more attractive for birds, while risk was higher in spring and autumn migration [14] when agricultural fields and wetlands were preferred. This is in line with the outcomes of the results reported in this paper, which analysed the distribution of vegetation and water in the landscape in the 13-km area around the airport.

Moreover, in this specific case study, the presence of the Simeto river protected area, south of the airport, is likely to produce a higher presence of flocks crossing the airport grounds due to the migration towards northern areas in spring migration

and towards south areas in autumn migration. This effect is strictly related to the latitude of the site and to the localisation of the airport, including its altitude. In fact, in plain airports the altitude plays a significant role in reducing the risk of bird strike compared to high plateau airports where it influences larger regions [6]. For both conditions, however, the influence of vegetation coverage in space and time in the airport surroundings has been revealed as a crucial ‘driver’ for this kind of risk.

Therefore, the methodology proposed in this study has made it possible to obtain useful results for a better planning of actions aimed at coping with the Wildlife Strike issue and performing environmental protection of the surrounding priority habitats. This methodology constitutes an effective tool for territorial and airport stakeholders, useful for monitoring the attractive sources for the avifauna, which are hazard sources for aviation, and carrying out actions aimed at safeguarding and protecting natural habitats. For this purpose, geostatistical analyses were carried out aimed at identifying the most critical areas, in order to build a decision-making tool aimed at identifying attractive sites. Further on, this methodology could be improved by including in the analysis the airport surfaces (OFZ), the distance from the airport and acquiring further data relating to the interaction between birds and airport activity.

5 Conclusions

The research methodology, described in this study, had the objective to carry out localisation and monitoring over time of the main attractive sources for birds in the airport surroundings, mainly identified in surface waters and vegetation, as well as the development of a model that analyses the relationships between the attractive sources and the sites of high naturalistic value, through the use of geospatial tools.

The research findings showed that the complexity and uniqueness characterising each territory are crucial factors to be analysed and proved that they can profit from in-deep analyses performed through the application of GIS tools coupled with automated classification of remote sensing images. The final objective achieved by this study was to provide a decision-making tool that allows identification of the habitats and priority corridors most frequented by wild species in relation to the attractive sources detected, thus contributing to the land planning governance of the surrounding area in order to limit the presence of attractive sources for wildlife in the airport surroundings yet at the same time protect the priority habitats used by them.

Acknowledgements The research study was carried out within the project: *Piano incentivi per la ricerca di Ateneo 2020-2022* – ‘Engineering solutions for sustainable development of agricultural buildings and land’ (ID: 5A722192152) coordinated by Professor Claudia Arcidiacono; and it is in line with the project on *Individuazione di un modello di gestione informatizzata delle infrastrutture di volo italiane destinate all’aviazione civile e della loro interazione con il territorio*, funded by ENAC.

References

1. ICAO. Airport Services Manual, Part 3 — Wildlife Control and Reduction, 4th edn. International Civil Aviation Organisation, Montreal, QC (2012)
2. ENAC: Flight Safety/Wildlife strike/Che cos'è il wildlife strike (2013). <https://www.enac.gov.it/sicurezza-aerea/flight-safety/wildlife-strike/che-cose-il-wildlife-strike>. Accessed 31 Aug 2022
3. Coccon, F., Zucchetto, M., Bossi, G., Borrotti, M., Torricelli, P., Franzoi, P.: A land-use perspective for birdstrike risk assessment: the attraction risk index. *PLoS UNO* **10**(6), e0128363 (2015). <https://doi.org/10.1371/journal.pone.0128363>
4. Pfeiffer, M.B., Kougher, J.D., DeVault, T.L.: Civil airports from a landscape perspective: a multi-scale approach with implications for reducing bird strikes. *Landsc. Urban Plan.* **179**, 38–45 (2018)
5. Shao, Q., Zhou, Y., Zhu, P., Ma, Y., Shao, M.: Key Factors assessment on bird strike density distribution in airport habitats: spatial heterogeneity and geographically weighted regression model. *Sustainability* **12**(18), 7235 (2020). <https://doi.org/10.3390/su12187235>
6. Shao, Q., Zhou, Y., Zhu, P.: Spatiotemporal analysis of environmental factors on the Birdstrike risk in high plateau airport with multi-scale research. *Sustainability* **12**, 9357 (2020). <https://doi.org/10.3390/su12229357>
7. Robinson, L., Mearns, K., McKay, T.: Oliver Tambo International Airport, South Africa: land-use conflicts between airports and wildlife habitats. *Front. Ecol. Evol.* **9**, 715771 (2021). <https://doi.org/10.3389/fevo.2021.715771>
8. ENAC: Wildlife Strike: un rischio comune e diverso per ogni aeroporto, ENAC - Bird Strike Committee Italy (2016). <https://www.enac.gov.it/pubblicazioni/wildlife-strike-un-rischio-comune-diverso-per-ogni-aeroporto>. Accessed 31 Aug 2022
9. Arcidiacono, C., Porto, S.M.C.: Image processing for the classification of crop shelters. *Acta Hort.* **801**, 309–316 (2008). ISSN: 0567-7572
10. Arcidiacono, C., Porto, S.M.C.: Classification of crop-shelter coverage by RGB aerial images: a compendium of experiences and findings. *J. Agric. Eng.* **XLI**, 1–11 (2010). ISSN:1974-7071
11. Modica, G., Pollino, M., Solano, F.: Sentinel-2 Imagery for Mapping Cork Oak (*Quercus suber* L.) Distribution in Calabria (Italy): Capabilities and Quantitative Estimation. In: International Symposium on New Metropolitan Perspectives ISHT 2018: New Metropolitan Perspectives, pp. 60–67 (2019)
12. ENAC/BSCI: Bird Strike Committee Italy: Relazione Annuale Wildlife Strike 2017 (2017). <https://www.enac.gov.it/pubblicazioni/wildlife-strike-relazione-annuale-2017>. Accessed 31 Aug 2022
13. Dolbeer, R.A.: Increasing trend of damaging bird strikes with aircraft outside the airport boundary: implications for mitigation measures. *Hum. Wildl. Interact.* **5**, 1235–1248 (2011)
14. Metz, I.C., Ellebroek, J., Mulhausen, T., Kugler, D., Hoekstra, J.M.: The bird strike challenge. *Aerospace* **7**, 26 (2020). <https://doi.org/10.3390/aerospace7030026>

Contribute of Digital Information Modelling to Territorial Governance and Airport Safety Interaction Management



Trifilò Domenico, Ragusa Eliana, Alessandro Di Graziano, and Arcidiacono Claudia

Abstract As part of the relationship between airport infrastructure and the surrounding area, at both urban and rural levels, orography of the land and vegetation as well as the artefacts inside or outside the aerodrome's boundary constitute important limiting and risk factors to aviation.

Methods to assess the impact of any existing or potential obstacle or hazard to navigation on airport airside or in the surroundings involves definition of Obstacle Limitation Surfaces, in relation to the type of runway and use.

In Italy, areas in the airport surroundings are identified and the related restrictions are specifically established, then graphically represented and published in specific constraints maps (Obstacle Free Zones) approved by ENAC (Italian Authority for Civil Aviation). Local authorities, in the exercise of their competences with regard to the planning and governance of the territory, adapt their planning tools to the requirements of the constraint maps.

This study investigates the relationships between territorial governance and airport safety, in the light of sector regulations, highlighting the contribution deriving from the use of digital information modelling. The management of obstacles and hazards through their representation in GIS considerably increases knowledge of their impact on the territory. Furthermore, models acquire even more applicative value by integrating the data using BIM tools. In fact, the definition of a management information model of obstacles and hazards to aviation based on the integration of GIS and BIM modelling represents an effective decision-making tool for an aware, efficient, resilient and sustainable territorial management in the airport surroundings.

Keywords GIS · BIM · Obstacles and hazards · Assessment procedures · Land-use planning

T. Domenico (✉) · A. Claudia
Department of Agriculture, Food and Environment, University of Catania, Via S. Sofia N.100,
95123 Catania, Italy
e-mail: domenico.trifilo@unict.it

R. Eliana · A. Di Graziano
Department of Agriculture, Food and Environment, University of Catania, Via S. Doria n.6, 95123
Catania, Italy

1 Introduction

Transport is an essential activity for providing connections between centres, ensuring trade and increasing the tourist attractiveness of a territory. Among all the transport nodes, the airport is a powerful pole of attraction for the territory it serves, as it widens the offer of commercial exchanges and the tourist flows with the rest of the world [1]. These types of nodes become essential because they bring investment into the territory itself.

The development of airport infrastructures must take place in synergy with the territory, mutually respecting their specificities, maintaining both airport safety and urban expansion, and minimising interference with ecosystems, in view of safeguarding the territory and the landscape.

The current Italian legislation provides for the identification of specific areas to be subjected to well-defined airport constraints in order to safeguard the safety of aerodromes. In order to create a synergistic airport model, based on the main territorial regulations for safety around the aerodromes, it is necessary to analyse the procedures and flows that are established between the various actors acting in the system and the products (e.g., documents, and maps) which are drafted and exchanged between them.

This work aims at analysing the main regulations and procedures in force in Italy, which have been issued in order to identify the areas to be subjected under airport constraint, and at analysing actors and products of the system as well as the flows that are established among them. To this aim, the use of the 'Geographic Information System' (GIS) as a decision-support and management tool, fed by airport constraint data and morphological geodata of the territory, is suitable to build a model for conscious, efficient, resilient and sustainable land management. In addition, the study aims to analyse how the GIS-based model can be integrated with the 'Building information model' (BIM) amplifying its potential on particular territorial elements, located in the airport surroundings, to which particular attention should be given during their life cycle since they could represent obstacles or hazards to air navigation.

2 Materials and Methods

The civil aviation sector provides the highest degree of safety among the various transport systems, through advanced international standards for technologies and specific procedures. At the national level, the reference standards for airport safety are the Air Navigation Code [2] and the Airport Construction and Operation Regulations [3].

2.1 Code of the Air Navigation

The Italian Navigation Code regulates the maritime, internal and air navigation, in territorial waters and in the national airspace. More precisely, the regulation of air navigation concerns articles 687 to 1079. Specifically, paragraph 1 of Art. 707 states: *'In order to ensure aviation safety, ENAC identifies the areas to be restricted in the areas adjacent to airports and establishes restrictions on obstacles to aviation and its potential hazards'*. It also states that: *'Local authorities, in the exercise of their powers with regard to territorial planning and governance, adapt their planning tools to provisions required by ENAC'*. In the same article, it is stated that: *'The areas referred to in the first paragraph and their limitations are indicated by ENAC on special maps published by deposit in the office of the municipality concerned'*. Finally, it states that: *'In the directions of landing and take-off, works or activities can be authorised if compatible with the appropriate risk plans, which the territorially competent municipalities adopt, also on the basis of any regional directives, in compliance with the regulation of ENAC on the construction and management of airports, implementing the Annex XIV ICAO (International Civil Aviation Organization)'*.

2.2 Regulation for the Construction and Operation of Airports

This regulation establishes the requirements for the safety of operations, and for issuing and maintaining aerodrome certification. In Chapter 9, Prevention and Risk Management, specifically in Paragraph 6, the following requirements are provided for new settlements falling within the protection areas:

- *Protection Zone A: The anthropogenic load must be kept to a minimum. No new residential developments should therefore be planned in this area. Non-residential activities may be envisaged, with low building rates, which entail the discontinuous permanence of a limited number of people.*
- *Protection Zone B: There may be a modest residential function, with low building rates, and non-residential activities, with average building rates, involving a limited number of persons.*
- *Protection Zone C: There may be a reasonable increase in residential use, with average construction indices, and new non-residential activities.*
- *Protection Zone D: in this area, which is characterised by a minimum level of protection and aimed at ensuring the development of the territory in an appropriate manner and coordinated with the operation of the airport, the implementation of targeted and highly crowded measures must be avoided, such as shopping centres, congresses and high concentration sports, intensive construction, etc....'*

The process that the municipality must follow to adopt the risk plan is regulated by the paragraph 6.7 of Art.9 that states: *‘The risk plan is drawn up by the Municipality whose territory is affected by the protection areas and, if these areas involve the territories of several Municipalities, the plan is drawn up in a coordinated manner’*. *‘The ENAC, having received the risk plan from the Municipalities, expresses its opinion on the basis of aeronautical assessments’*. *‘In its assessments, ENAC considers the aeronautical data that characterise the airport in the current and future scenario as outlined in the development plan, indicating any adaptation needs’*. *‘Significant changes in these parameters, if they have an impact on the risk plans adopted, are communicated by ENAC to the Municipalities in order to assess the effects on the territory and to proceed with any update of the plan’*.

2.3 Norms on Airport Management

The management system prior to Law n. 537/93 established that national civil airports, including all buildings and equipment for aviation, were part of the Aviation State property, which is assigned to ENAC free of charge for the subsequent concession to the airport manager (art. 693 of the Navigation Code). Prior to the enactment of this rule, airport management was carried out according to three models:

1. Direct management by the State: in this management model, the State carried out and provided for the maintenance of all airport assets and flight infrastructure and the management of the airport, collected revenue, and bore all operating costs;
2. Partial management: essentially provided for the concession of part of the airport (passenger terminal, freight and related equipment) while the management of the flight infrastructure remained under the responsibility of the State;
3. Total management: in this form of management, the concessionaire was responsible for the management of all the services that take place in the entire airport system, including the flight infrastructure. The total management was entrusted by special laws to subjects constituted mostly in the form of consortia, joint stock companies, economic public bodies and chambers of commerce.

With Law n. 537/93, the model of total management was indicated as the prevailing regime. The Regulation implementing that law, i.e., D.M. 521/97, in art. 2, established that the airport managers should be exclusively in the form of joint stock companies, and that regions and provinces, municipalities, local authorities and chambers of commerce could also participate, without the obligation of majority ownership.

2.4 Norms Overview for Territorial Governance

The regulation of territorial governance is one of those reserved to the Regions by art. 117 of the Constitution, except for the determination of fundamental principles,

reserved to the legislation of the State. Among the reference norms, which originate from L. 1150/42 and subsequent amendments, the D.P.R. 380/01 (consolidated text) contains the fundamental and general principles and provisions for the discipline of construction activity. In relation to landscape norms (D.Lgs. 42/04 and subsequent amendments), landscape protection is an overriding interest over any other public and private interest, therefore urban plans must comply with territorial landscape plans (Council of State, sentence 27 October 1988, n. 1179).

In this national context, the Regions and local authorities exercise concurrent legislative power in the field of construction, in compliance with the fundamental principles of state legislation derived from the provisions contained in the consolidated text, through their own regional laws. The Municipalities, instead, within their own autonomy deriving from Art. 3 of D. Lgs. n. 267/00, regulate the building activity with its Building Regulations.

In Sicily region the Regional Law n. 19/20, *Rules for the government of the territory*, has recently been issued; it is an example of legislation for the government of the territory in which the objectives of the territorial information system (SITR) are described which collects georeferenced spatial data (Art.14) and mandates local authorities to identify appropriate technical structures that make use of the SITR in the performance of their tasks of spatial planning and town planning (Art.17).

2.5 Territorial Governance through Geographic Information System and Integration with the Building Information Model

From the current regulations described in paragraph 2.1, there is evidence that in Italy areas identified in the airport surroundings are subjected to restrictions in order to achieve aviation safety. This process leads to the construction of special constraint maps (Obstacle Free Zones) by airport managers which, approved by ENAC, are a valid tool for territorial governance by local authorities that will adapt their urban plans in relation to these requirements. Therefore, the definition of a working model that involves the construction of appropriate constraint maps in the GIS environment, would bring considerable advantages. Through GIS models, it is possible to carry out spatial analysis on the information layers and associated attributes [4], creating new usable information and identifying the areas to be subjected to constraints and the protection zones.

This study proposes the integration of geospatial tools, such as GIS, with BIM in order to perform territorial governance. BIM represents a methodology of digital representation of the physical and functional characteristics of a structural asset during its entire life cycle. In the life cycle of an asset, the two systems come into contact and therefore they need to be interoperable mainly in the phases of planning and successive management of the work [5]. BIM-GIS integration can be implemented in three modes [6]: BIM lead and GIS support, GIS Leads and BIM Supports

and BIM and GIS equally involved. In each of these modes, GIS and BIM are involved in different ways according to the final goal. Other hypotheses for future BIM-GIS integration include [7]: the technology hypothesis where GIS and BIM as independent systems are partially applied together to address specific problems; the Science hypothesis in which integration primarily relies on BIM development; and the data source hypothesis that considers BIM as a data source for GIS analyses.

At the international level, the BIM reference standard was introduced by ISO 19650 [8] which establishes an international standard for the management of information on the entire life cycle of an asset built using BIM.

On a national level, the D.L. n. 50/16 - Code of public contracts, which regulates public administrations' contracts to perform works and provide services also through concessions, also identifies the principles of entrustment, and introduces in Italy the BIM, based on the European Procurement Directive (D 2014/24/EU), which had introduced the use of BIM (art.22, paragraph 4) in member states. In addition, thanks to the introduction of D.M. 560/17, which provides for the progressive mandatory nature of BIM from 2019 to 2025, and the technical regulation UNI 11,337 [9], which outlines the concepts, content, the types of information and their storage formats as well as the stakeholders involved in data management and modelling, BIM is going to be used in a systematic way in Italy.

2.6 Standards for GIS-BIM Interoperability

To date, the interaction between BIM and GIS is not always automated. Geospatial modelling usually focuses on the spatial scale and adopts broad perspectives on the surrounding environment, including a multitude of resources scattered over it. BIM, on the other hand, is more focused on modelling the components of a single built element. Over time the information models of both are becoming more and more linked to each other as each built element has a well-defined geographical position within the existing environment and the data is managed in information layers linked together.

Currently, geospatial information modelling is based on international standards developed and maintained by ISO/TC 211 and Open Geospatial Consortium, Inc. (OGC) while the modelling of the constructed resources is based on standards developed and maintained by ISO/TC 59/SC 13 and buildingSMART International (BSI). ISO/TR 23,262:2021 [10] aims, instead, to identify measures for interoperability between GIS and BIM, examining the criticalities and aiming to align the GIS standards developed by ISO/TC 211 and the BIM standards developed by ISO/TC 59/SC 13.

3 Results and Discussion

In this study, 4 actors are identified as taking part in the regulation of activities compatible with air navigation: ENAC, airport manager, Municipality involved, citizens and stakeholders. The schemes shown in Fig. 1 are an example of the actions taken by the actors concerned in regulating activities compatible with air navigation, and the products leading to the definition of constraint maps and the subsequent risk plan. These schemes also highlight actions that may benefit from the use of GIS or the GIS-BIM combination.

The GIS model implemented for the definition and analysis of the main territorial constraints in the airfield, is a valid tool available to territorial stakeholders. It allows the query of geodata and data represented by the aeronautical constraints to allow strategic planning of the territory by local authorities. In the model, the main Obstacle Free Zones must be represented; parameterised according to the ICAO regulations, they give essential information to plan the main constraints that exist in the territory.

In addition, the model must also include the presence of the main obstacles and hazards to aviation in order to better and timely describe some particular elements of the territory.

The model could be expanded by using specific geodata such as cadastral data and the main urban and territorial constraints that exist in the analysed territory. These elements, also related to auxiliary data of the attribute type, would facilitate the description of the characteristics of the territory, and would help performing queries in the GIS system to derive further spatial information and attributes.

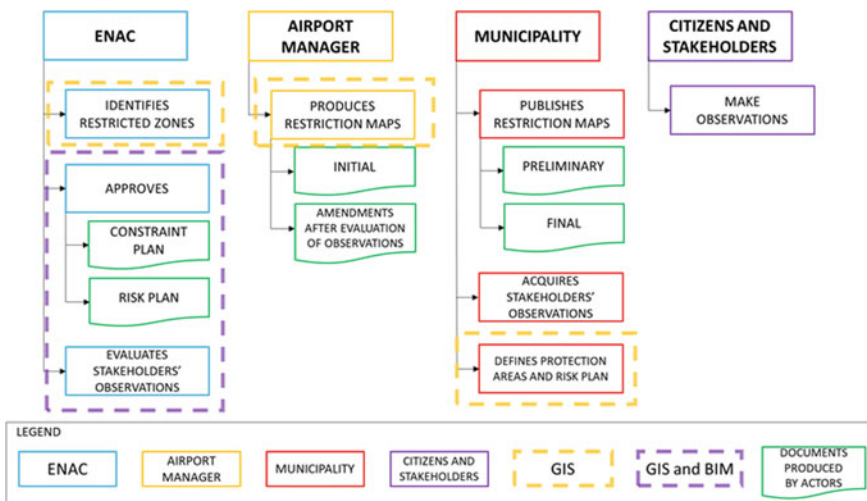


Fig. 1 Schemes of actions and products relating to actors concerned with the regulation of air navigation compatible assets

The integration of GIS and BIM environments will bring significant benefits for spatial planning. In the specific case, the BIM would be suitable for specifically defining those airport structures or infrastructures that, in the vicinity of the runway and the airport grounds, are to be controlled during their life cycle because they constitute potential obstacles or hazards to aviation. Currently, the orientation of the international community is to systematically use the ‘digital twin approach’ for the management of assets, in order to have the geometric support, data sheets, the various components of the work but also the GIS data related to the territorial context in which it will be built.

The shared point of the two systems is constituted by the data. In fact, albeit having different characteristics, the two systems are both created for data query from a database. It is therefore essential that the basic data are as relevant as possible to the reality being investigated. This will make it possible to enhance the information data as a central element of the entire process, allowing the construction of interpretative models of the territorial context that will act as a decision support to public administrations for the planning of the territory itself.

The innovative approach of the integrated use of GIS-BIM systems consists in enclosing a large amount of data in an interoperable information system, in order to be able to make queries to the systems at different information levels and analyse the data by creating scenarios representative of the reality. The impact of the GIS-BIM integration for the management of the interaction between territorial governance and airport safety, in the regulatory context presented in this study, will have significant consequences, such as greater sustainability of the assets, the possibility to conduct more in-depth analyses and to implement a participatory design policy, thus reducing costs and time of constructions and achieving greater control over their life cycle design.

The concept of sustainability will play a key role in the coming years for airport infrastructure, as outlined in the current National Airport Plan [11], which proposes a path of “transformative resilience” that does not reflect the previous conditions but that must constitute a new context more flexible than the needs of the community that lives it, through targeted development policies. In particular, the Plan proposes the adoption of interventions linked to technological innovation that would make it possible to develop a different and greater operational capacity in full compliance with the needs of sustainable growth. This concept will support spatial planning to assess the future transport needs that an area will develop, such as the presence of advanced ultralight aircrafts (VDS): it could have a significant impact on the airport because the flight heights would be lower and the presence of obstacles and hazards to aviation will have to be adapted to this new need.

In the above context, in view of the data exchange between GIS and BIM systems, it is recognised as crucial to create an interoperable data format for the two systems that would not lead to a loss of information levels and standardised. At present, however, this exchange capacity between the two systems is very limited, due to differences in the data format and the scale.

4 Conclusions

The contribute of digital information modelling to the management of the interaction between territorial governance and airport safety has been described in this study to highlight the potentialities of GIS and BIM application and their synergistic effect. BIM-GIS integration would be beneficial at various levels in the life cycle of an asset, would produce enhancement of work quality, would contribute to time optimisation and operating costs reduction.

In this work, it is highlighted how these tools, if well integrated in their use within the various phases of regulation of the activities compatible with aviation, are suitable to produce remarkable advantages for the stakeholders involved, not only in the field of information exchanges with the internal actors of the process but also in the interaction with the public administrations or other external actors that during the life cycle of an asset may be involved at various levels. Although there is such potential for synergy between the two systems, the information exchange is currently limited and lacking. It is therefore believed that further developments in the data exchange between the two systems would greatly improve this process by simplifying use on a large scale and also in sectors other than aeronautical or urban planning.

Acknowledgements The research study was carried out within the project: *Piano incentivi per la ricerca di Ateneo 2020-2022 - 'Engineering solutions for sustainable development of agricultural buildings and land'* (ID: 5A722192152) coordinated by Professor Claudia Arcidiacono; and it is in line with the project *Individuazione di un modello di gestione informatizzata delle infrastrutture di volo italiane destinate all'aviazione civile e della loro interazione con il territorio*, funded by ENAC.

References

1. Ragusa, E., Costa, A., Di Graziano, A.: Exploring new computational strategies for managing maintenance activities of airport pavement systems. *Int. J. Pavement Res. Technol.* (under publication)
2. R.D. 30 March 1942, n. 327. Navigation Code, second part. updated by Legislative Decree 15 March 2006, n.151
3. ENAC: Rules for the construction and operation of airports, Ed.2 of 21 October 2003
4. Arcidiacono, C., Porto, S.M.C.: A model to manage crop-shelter spatial development by multi-temporal coverage analysis and spatial indicators. *Biosyst. Eng.* **107**(2), 107–122 (2010). <https://doi.org/10.1016/j.biosystemseng.2010.07.007>
5. Di Graziano, A., Ragusa, E., Trifilò, D., Triaca, L.M., Trombetti, M., Arcidiacono, C.: interaction between airport facilities and the surrounding area within the GIS and BIM interoperability. *Transp. Res. Proc.* **69**, 273–280 (2023). <https://doi.org/10.1016/j.trpro.2023.02.172>
6. Wang, H., Pana, Y., Luo, X.: Integration of BIM and GIS in sustainable built environment: a review and bibliometric analysis. *Autom. Constr.* **103**, 41–52 (2019)
7. Song, Y., Wang, X., Tan, Y., Wu, P., Sutrisna, M., Cheng, J.C.P., Hampson, K.: Trends and opportunities of BIM-GIS integration in the architecture, engineering and construction industry: a review from a spatio-temporal statistical perspective. *ISPRS Int. J. Geo-Inf.* **6**, 397 (2017)

8. ISO 19650: Organization and digitization of information about buildings and civil engineering works, including building information modelling (BIM), part 1–2–3–4–5 (2018/2022)
9. UNI 11337: Building and civil engineering works - Digital management of building information processes (2017–2021)
10. ISO/TR 23262:2021: GIS (geospatial)/BIM interoperability
11. ENAC: National Airport Plan, February 2012

Correction to: Can a Variable-Rate Sprayer Be Efficient and Economic? Testing and Economic Analysis in Viticulture



Andrea Pagliai, Daniele Sarri, Carolina Perna, and Marco Vieri

Correction to:
Chapter “Can a Variable-Rate Sprayer Be Efficient and Economic? Testing and Economic Analysis in Viticulture” in: V. Ferro et al. (eds.): *AIIA 2022: Biosystems Engineering Towards the Green Deal*, Lecture Notes in Civil Engineering 337,
https://doi.org/10.1007/978-3-031-30329-6_82

The original version of this chapter unfortunately contained a mistake. The first and last names of the chapter authors were interchanged. The correct names should read: Andrea Pagliai, Daniele Sarri, Carolina Perna, Marco Vieri. This has been corrected.

The updated original version of this chapter can be found at
https://doi.org/10.1007/978-3-031-30329-6_82

© The Author(s), under exclusive license to Springer Nature Switzerland AG 2023
V. Ferro et al. (eds.), *AIIA 2022: Biosystems Engineering Towards the Green Deal*,
Lecture Notes in Civil Engineering 337,
https://doi.org/10.1007/978-3-031-30329-6_131

C1